ELSEVIER
ACADEMIC
PRESS

The Science and Technology of RUBBER

THIRD EDITION

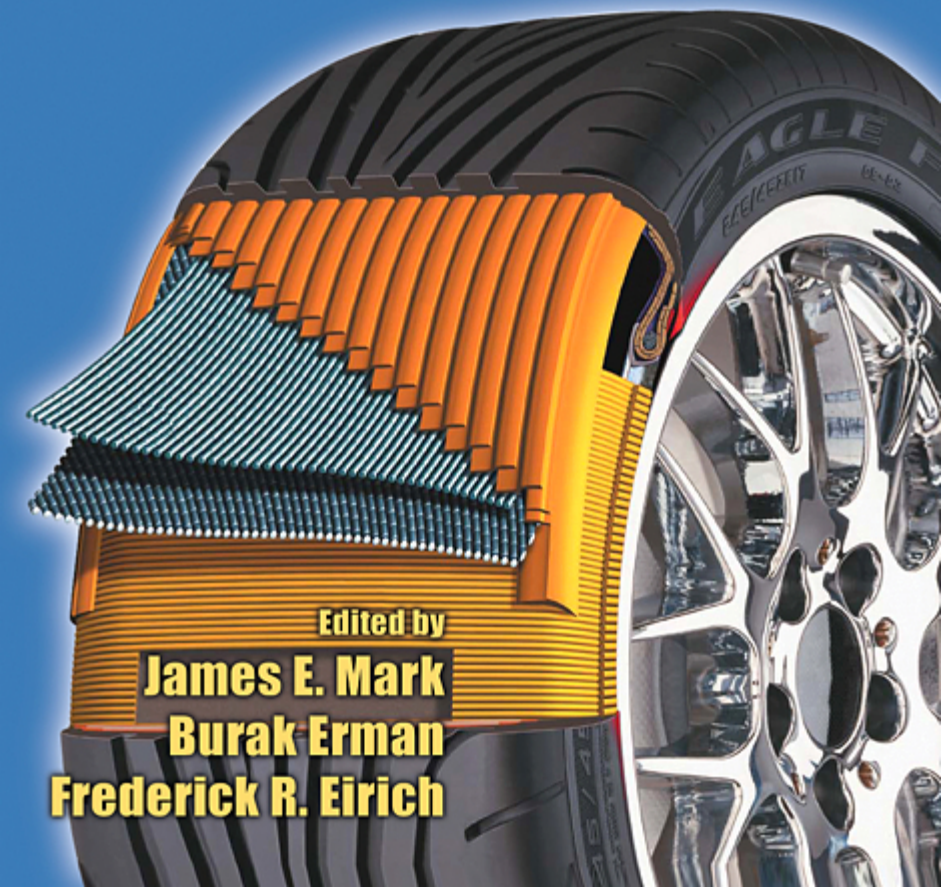

Edited by
James E. Mark
Burak Erman
Frederick R. Eirich

Science and Technology of RUBBER

Third Edition

Science and Technology of RUBBER

Third Edition

Edited by

James E. Mark

Department of Chemistry
The University of Cincinnati
Cincinnati, Ohio

Burak Erman

Department of Chemical and Biological Engineering
Koc University
Istanbul, Turkey

Frederick R. Eirich

Polytechnic University
Brooklyn, New York

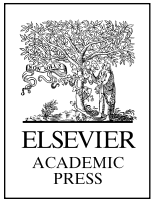

AMSTERDAM • BOSTON • HEIDELBERG • LONDON
NEW YORK • OXFORD • PARIS • SAN DIEGO
SAN FRANCISCO • SINGAPORE • SYDNEY • TOKYO

Academic Press is an imprint of Elsevier

Elsevier Academic Press
30 Corporate Drive, Suite 400, Burlington, MA 01803, USA
525 B Street, Suite 1900, San Diego, California 92101-4495, USA
84 Theobald's Road, London WC1X 8RR, UK

This book is printed on acid-free paper. ♾

Library of Congress Cataloging-in-Publication Data
Science and technology of rubber / [edited by] James E. Mark, Burak Erman.
p. cm.
Includes bibliographical references and index.
ISBN 0-12-464786-3
1. Rubber. I. Mark, James E., 1934– II. Erman, Burak.
TS1870.S35 2005
678′.2–dc22 2005042048

British Library Cataloguing in Publication Data
A catalogue record for this book is available from the British Library

ISBN: 0-12-464786-3

For all information on all Elsevier Academic Press publications
visit our Web site at www.books.elsevier.com

Printed in the United States of America
05 06 07 08 09 10 9 8 7 6 5 4 3 2 1

Contents

Contributors

Numbers in parentheses indicate the pages on which the authors' contributions begin.

R. J. Ceresa (497), Chemistry and Polymer Technology Department, Polytechnic of South Bank, London, England

Stuart L. Cooper (555), Department of Chemical and Biomolecular Engineering, The Ohio State University, Columbus, Ohio 43210

Aubert Y. Coran (321), A. Y. Coran Consulting, Longboat Key, Florida 34228

Emmanuel Custodero (367), Manufacture Française des Pneumatiques Michelin, 63040 Clermont-Ferrand Cedex, France

Sudhin Datta (529), ExxonMobil Chemical Co., Baytown, Texas 77520

Jean-Baptiste Donnet (367), ENSCMu-UHA, 68093 Mulhouse Cedex, France

Burak Erman (157), Department of Chemical and Biological Engineering, Koc University, Rumelifeneri Yolu, Sariyer 34450, Istanbul, Turkey

A. N. Gent (1, 455), The University of Akron, Akron, Ohio 44325-3909

Brian P. Grady (555), School of Chemical Engineering and Materials Science, The University of Oklahoma, Norman, Oklahoma 73019

A. F. Halasa (497), Research and Development, The Goodyear Tire & Rubber Company, Akron, Ohio 44305

Avraam I. Isayev (663), Institute of Polymer Engineering, The University of Akron, Akron, Ohio 44325-0301

James E. Mark (157), Department of Chemistry, The University of Cincinnati, Cincinnati, Ohio 45211-0172

Jean Marie Massie (497), Lexmark International, Lexington, Kentucky 40511

K. L. Ngai (183), Naval Research Laboratory, Washington, D.C. 20375-5320

Deanna L. Gomochak Pickel (29), Research Laboratories, Eastman Chemical Company, Kingsport, Tennessee 37662-5150

Donald J. Plazek (183), University of Pittsburgh, Pittsburgh, Pennsylvania 15261

Roderic P. Quirk (29), The Maurice Morton Institute of Polymer Science, The University of Akron, Akron, Ohio 44325-3909

Brendan Rodgers (401, 619), ExxonMobil Chemical Company, Houston, Texas 77520-2101

C. M. Roland (105), Naval Research Laboratory, Chemistry Division, Code 6120, Washington, D.C. 20375-5342

Walter Waddell (401, 619), ExxonMobil Chemical Company, Houston, Texas 77520-2101

James L. White (237), Department of Polymer Engineering, University of Akron, Akron, Ohio 44325-0301

Preface to the Third Edition

The basic purpose of this new edition is to update the material in the second edition, which is now more than 10 years old. As a result, the 14 chapters in that earlier edition have been revised and expanded, and a new chapter on the recycling of rubbers has been added.

It is again hoped that this book will provide the type of broad overview of elastomers and their mechanical properties that will be useful to the polymer science and engineering community in general.

Preface to the Second Edition

The goals of the new edition of this book are much the same as those described in the Preface to the First Edition, namely a broad overview of elastomers and rubberlike elasticity. Again, the emphasis is on a unified treatment, ranging from chemical aspects such as elastomer synthesis and curing, through theoretical developments and characterization of equilibrium and dynamic properties, to final applications (including tire manufacture and engineering).

Although the material has been divided into the same 14 chapters, advances in the field since the first edition appeared in 1978 required the addition of a great deal of new material. As a result of this extensive updating, the chapters are now generally 20 to 30% longer.

During the past 15 years, a number of the original contributors passed away, retired, or moved into different areas of research or into entirely different nonresearch areas. Of the 23 authors contributing to this second edition, nearly half are new to this editorial project.

The editors, coauthors, and publishers all hope this new edition will find an enthusiastic response from readers in the polymer science and engineering community in general, and from those in the elastomers area in particular.

Preface to the First Edition

The continuing success of the American Chemical Society Rubber Division's correspondence course, based on Professor Morton's "Rubber Technology" persuaded the Division's Educational Committee to introduce a second, more advanced course. This editor was commissioned to assemble a number of chapters on the graduate to postgraduate level, stressing the continuous relation between ongoing research in synthesis, structure, physics, and mechanics and rubber technology and industry. This collection of chapters covering, to various depths, the most important aspects of rubber science and technology, and the list of authors, all leading authorities in their fields, should be of vital interest not only to those who want to expand their formal education or update and supplement their experience in the field, but to anyone interested in the unusual chemistry and physics and the outstanding properties and farflung usefulness of elastomers. The intermediate level of presentation, a mixture of theory, experiment, and practical procedures, should offer something of value of students, practitioners, and research and development managers.

It has been the bias of this editor, based on many years of teaching at Polytechnic's Institute of Polymer Chemistry, that the most successful way of teaching and learning polymer subjects is to refer continually to the special features of macromolecules. For elastomers, in particular, it is most instructive to derive the unique features of high elasticity from those of long flexible chain molecules in their matted and netted state and the changes imposed by large deformations, including the key role played by the internal viscosity as a function of temperature and rate. Swaying the authors to lean to this approach inevitably caused some overlap but, at the same time, allowed synthesis and structure, elasticity and flow, blending, filling, and crosslinking to be treated in different contexts; a more integral composition without too frequent a need for cross references to other chapters became possible. For the same reason, some variation in nomenclature was allowed, especially if it reflected differing uses in the literature.

Particular concerns in preparing this composite book have been the combination of information and instruction, and the sequence and correlation of the chapters' contents. The first 10 chapters take the reader from an introduction through synthesis characterization, mechanical behavior, and flow to

the major processing steps of filling, compounding, and vulcanization and to the theories and measurement of elastomeric performance, leaning strongly on the "materials" approach. The next three chapters deal with the ever broadening fields of blended, modified, and thermoplastic elastomers, while the last chapter, for reasons of space, is the only representative of the chapters originally planned on manufacturing, possibly the forerunner of another volume. All chapters, while presenting theory, mechanism, and the author's overview of the internal consistency of the material's pattern of behavior, serve also as substantial sources of data and as guides to the relevant literature and to further self study. As such, this book should be suitable not only as a basis for the new course, but also as an instrument of instruction for students, teachers, and workers in all fields of polymer and, indeed, of material science.

This, in any case, was the intent of all the authors whose extensive, conscientious, and patient cooperation made this book possible. Special thanks are due to Dr. A. Gessler and the Exxon Corporation, Linden, New Jersey, and Dr. E. Kontos, Uniroyal Chemical Division, who conceived the idea of a second course and of the nature of this book, and to Dr. H. Remsberg, Carlisle Tire and Rubber Company, then Chairman of the Division's Educational Committee, without whose firm backing and continuous understanding this effort could not have been concluded. Drs. Gessler, Kontos, and Remsberg were further instrumental in gathering many of the authors and offering a number of early revisions of the manuscripts.

1 Rubber Elasticity: Basic Concepts and Behavior

A. N. GENT
The University of Akron
Akron, Ohio

I. INTRODUCTION

The single most important property of elastomers—that from which their name derives—is their ability to undergo large elastic deformations, that is, to stretch and return to their original shape in a reversible way. Theories to account for this characteristic high elasticity have passed through three distinct phases: the early development of a molecular model relating experimental observations to the known molecular features of rubbery polymers; then generalization of this approach by means of symmetry considerations taken from continuum mechanics which are independent of the molecular structure; and now a critical reassessment of the basic premises on which these two quantitative theories are founded. In this chapter, the theoretical treatment is briefly outlined and shown to account quite successfully for the observed elastic behavior of rubbery materials. The special case of small elastic deformations is then discussed in some detail because of its technical importance. Finally, attention is drawn to some aspects of rubber elasticity which are still little understood.

Science and Technology of Rubber, Third Edition

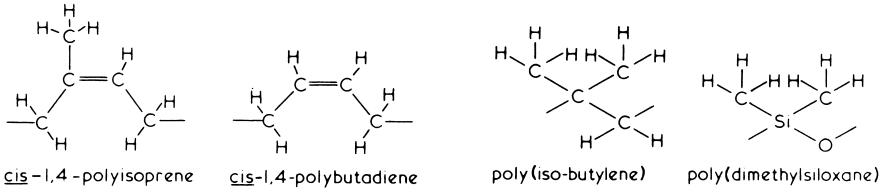

FIGURE 1 Repeat units for some common elastomer molecules.

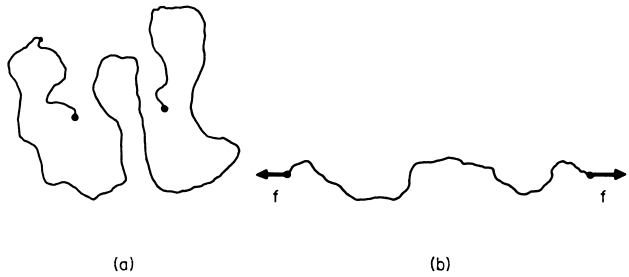

FIGURE 2 (a) Random chain and (b) oriented chain. (From Gent [37].)

II. ELASTICITY OF A SINGLE MOLECULE

The essential requirement for a substance to be rubbery is that it consist of long flexible chainlike molecules. The molecules themselves must therefore have a "backbone" of many noncolinear single valence bonds, about which rapid rotation is possible as a result of thermal agitation. Some representative molecular subunits of rubbery polymers are shown in Fig. 1; thousands of these units linked together into a chain constitute a typical molecule of the elastomers listed in Fig. 1. Such molecules change their shape readily and continuously at normal temperatures by Brownian motion. They take up random conformations in a stress-free state but assume somewhat oriented conformations if tensile forces are applied at their ends (Fig. 2). One of the first questions to consider, then, is the relationship between the applied tension f and the mean chain end separation r, averaged over time or over a large number of chains at one instant in time.

Chains in isolation take up a wide variety of conformations,[1] governed by three factors: the statistics of random processes; a preference for certain

[1]Although the terms *configuration* and *conformation* are sometimes used interchangeably, the former has acquired a special meaning in organic stereochemistry and designates specific steric structures. *Conformation* is used here to denote a configuration of the molecule which is arrived at by rotation of single-valence bonds in the polymer backbone.

sequences of bond arrangements because of steric and energetic restraints within the molecule; and the exclusion of some hypothetical conformations which would require parts of the chain to occupy the same volume in space. In addition, cooperative conformations are preferred for space-filling reasons in concentrated solutions or in the bulk state.

Flory [1] has argued that the occupied-volume exclusion (repulsion) for an isolated chain is exactly balanced in the bulk state by the external (repulsive) environment of similar chains, and that the exclusion factor can therefore be ignored in the solid state. Direct observation of single-chain dimensions in the bulk state by inelastic neutron scattering gives values fully consistent with unperturbed chain dimensions obtained for dilute solutions in theta solvents[2] [2], although intramolecular effects may distort the local randomness of chain conformation.

Flory has again given compelling reasons for concluding that the chain end-to-end distance r in the bulk state will be distributed in accordance with Gaussian statistics for sufficiently long chains, even if the chains are relatively stiff and inflexible over short lengths [1]. With this restriction to long chains it follows that the tension–displacement relation becomes a simple linear one,

$$f = Ar \tag{1}$$

where f is the tensile force, r is the average distance between the ends of the chain, and A is inversely related to the mean square end-to-end distance r_0^2 for unstressed chains,

$$A = 3kT/r_0^2 \tag{2}$$

where k is Boltzmann's constant and T is the absolute temperature.

If the real molecule is replaced by a hypothetical chain consisting of a large number n of rigid, freely jointed links, each of length l (Fig. 3), then

$$r_0^2 = nl^2 \tag{3}$$

In this case r_0^2 is independent of temperature because completely random link arrangements are assumed. The tension f in Eq. (1) then arises solely from an entropic mechanism, i.e., from the tendency of the chain to adopt conformations of maximum randomness, and not from any energetic preference for one conformation over another. The tension f is then directly proportional to the absolute temperature T.

[2]These are (poor) solvents in which repulsion between different segments of the polymer molecule is balanced by repulsion between polymer segments and solvent molecules.

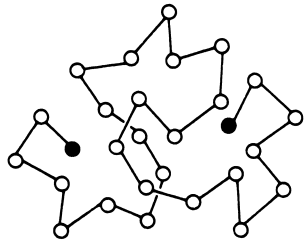

FIGURE 3 Model chain of freely jointed links.

For real chains, consisting of a large number n of primary valence bonds along the chain backbone, each of length l,

$$r_0^2 = C_\infty n l^2 \tag{4}$$

where the coefficient C_∞ represents the degree to which this real molecule departs from the freely jointed model. C_∞ is found to vary from 4 to 10, depending on the chemical structure of the molecule and also on temperature, because the energetic barriers to random bond arrangements are more easily overcome at higher temperatures [1]. $C_\infty^{1/2} l$ may thus be regarded as the effective bond length of the real chain, a measure of the "stiffness" of the molecule.

Equation (1) is reasonably accurate only for relatively short distances r, less than about one-third of the fully stretched chain length [2]. Unfortunately, no good treatment exists for the tension in real chains at larger end separations. We must therefore revert to the model chain of freely jointed links, for which

$$f = (kT/l)L^{-1}(r/nl) \tag{5}$$

where L^{-1} denotes the inverse Langevin function. An expansion of this relation in terms of r/nl,

$$f = (3kTr/nl^2)\left[1 + (3/5)(r/nl)^2 + (99/175)(r/nl)^4 + (513/875)(r/nl)^6 + \cdots\right] \tag{6}$$

gives a useful indication of where significant departures from Eq. (1) may be expected.

Equation (5) gives a steeply rising relation between tension and chain end separation when the chain becomes nearly taut (Fig. 4), in contrast to the Gaussian solution, Eq. (1), which becomes inappropriate for $r > \frac{1}{3} nl$. Rubber shows a similar steeply rising relation between tensile stress and elongation at high elongations. Indeed, experimental stress–strain relations closely resemble those calculated using Eq. (5) in place of Eq. (1) in the network theory

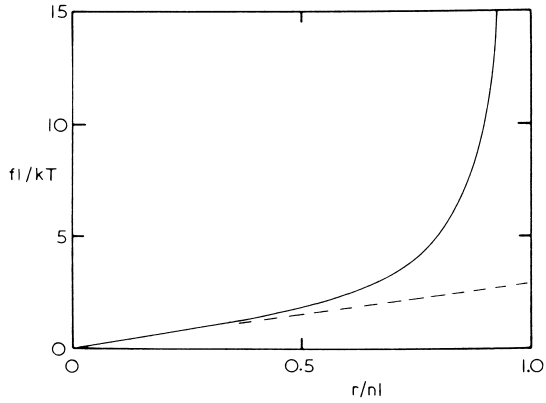

FIGURE 4 Tension–displacement relation for a freely jointed chain [Eq. (5)], ---, Gaussian solution [Eq. (1)]. (From Gent [37].)

of rubber elasticity (outlined in the following section). The deformation at which a small but significant departure is first found between the observed stress and that predicted by small-strain theory, using Eq. (1), yields a value for the effective length l of a freely jointed link for the real molecular chain. This provides a direct experimental measure of molecular stiffness. The values obtained are relatively large, of the order of 5–15 main-chain bonds, for the only polymer which has been examined by this method so far, *cis*-1,4-polyisoprene [3].

Equation (5) has also been used to estimate the force at which a rubber molecule will become detached from a particle of a reinforcing filler, for example, carbon black, when a filled rubber is deformed [4]. In this way, a general semiquantitative treatment has been achieved for stress-induced softening (Mullins effect) of filled rubbers (shown in Fig. 5).

III. ELASTICITY OF A THREE-DIMENSIONAL NETWORK OF POLYMER MOLECULES

Some type of permanent structure is necessary to form a coherent solid and prevent liquidlike flow of elastomer molecules. This requirement is met by incorporating a small number of intermolecular chemical bonds (crosslinks) to make a loose three-dimensional molecular network. Such crosslinks are generally assumed to form in the most probable positions, so that the long sections of molecules between them have the same spectrum of end-to-end lengths as a similar set of uncrosslinked molecules would have. Under Brownian motion each molecular section takes up a wide variety of conformations, as before, but now subject to the condition that its ends lie at

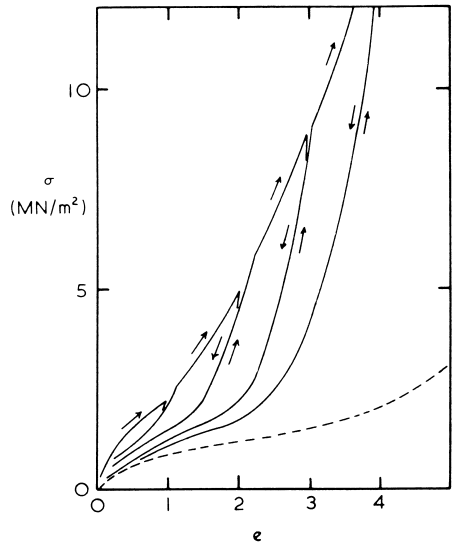

FIGURE 5 Stress-induced softening of a carbon black-filled vulcanizate of a copolymer of styrene and butadiene (25:75); ---, stress–strain curve of a corresponding unfilled vulcanizate. (From Tobolsky and Mark [5].)

the crosslink sites. The elastic properties of such a molecular network are treated later. We consider first another type of interaction between molecules.

High-molecular-weight polymers form entanglements by molecular intertwining, with a spacing (in the bulk state) characteristic of the particular molecular structure [6]. Some representative values of the molecular weight M_e between entanglement sites are given in Table I. Thus, a high-molecular-weight polymeric melt will show transient rubberlike behavior even in the absence of any permanent intermolecular bonds.

In a crosslinked rubber, many of these entanglements are permanently locked in (Fig. 6), the more so the higher the degree of crosslinking. If they are regarded as fully equivalent to crosslinks, the effective number N of network chains per unit volume may be taken to be the sum of two terms N_e and N_c, arising from entanglements and chemical crosslinks, respectively, where

$$N_e = \rho N_A / M_e , \qquad N_c = \rho N_A / M_c$$

and ρ is the density of the polymer, N_A is Avogadro's number, and M_e and M_c denote the average molecular weights between entanglements and between crosslinks, respectively. The efficiency of entanglements in constraining the participating chains is, however, somewhat uncertain, particularly when the number of chemical crosslinks is relatively small [7–9]. Moreover, the

TABLE I Representative Values of the Average Molecular Weight M_e between Entanglements for Polymeric Melts[a]

Polymer	M_e	Polymer	M_e
Polyethylene	4,000	Poly(isobutylene)	17,000
cis-1,4-Polybutadiene	7,000	Poly(dimethylsiloxane)	29,000
cis-1,4-Polyisoprene	14,000	Polystyrene	35,000

[a]Obtained from flow viscosity measurements.

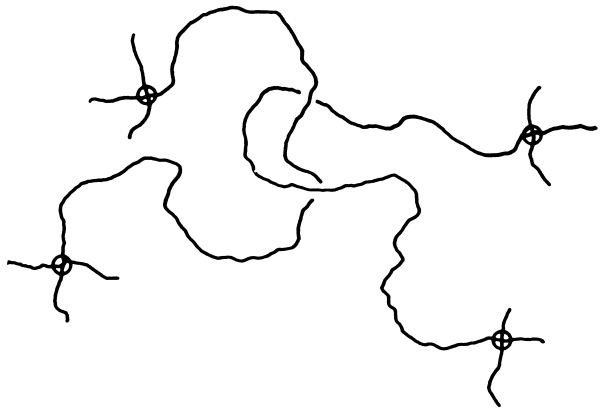

FIGURE 6 Sketch of a permanent entanglement. (From Gent [37].)

force–extension relation for an entangled chain will differ from that for a crosslinked chain [10], being stiffer initially and nonlinear in form. The effective number N of molecular chains which lie between fixed points (i.e., crosslinks or equivalent sites of molecular entanglement) is therefore a somewhat ill-defined quantity, even when the chemical structure of the network is completely specified.

It is convenient to express the elastic behavior of the network in terms of the strain energy density W per unit of unstrained volume. The strain energy w for a single chain is obtained from Eq. (1) as

$$w = Ar^2/2 \tag{7}$$

For a random network of N such chains under a general deformation characterized by extension ratios $\lambda_1, \lambda_2, \lambda_3$ (deformed dimension/undeformed dimension) in the three principal directions (Fig. 7), W is given by [11]

$$W = NAr_f^2(\lambda_1^2 + \lambda_2^2 + \lambda_3^2 - 3)/6 \tag{8}$$

where r_f^2 denotes the mean square end-to-end distance between chain ends (crosslink points or equivalent junctions) in the undeformed state. The close similarity of Eqs. (7) and (8) is evident, especially since $r^2 = (r_f^2/3)(\lambda_1^2 + \lambda_2^2 + \lambda_3^2)$.

For random crosslinking r_f^2 may be assumed to be equal to r_0^2, the corresponding mean square end-to-end distance for unconnected chains of the same molecular length. Because A is inversely proportional to r_0^2 [Eq. (2)], the only molecular parameter which then remains in Eq. (8) is the number N of elastically effective chains per unit volume. Thus, the elastic behavior of a molecular network under moderate deformations is predicted to depend only on the number of molecular chains and not on their flexibility, provided that they are long enough to obey Gaussian statistics.

Although r_f^2 and r_0^2 are generally assumed to be equal at the temperature of network formation, they may well differ at other temperatures because of the temperature dependence of r_0^2 for real chains [Eq. (4)]. Indeed, the temperature dependence of elastic stresses in rubbery networks has been widely employed to study the temperature dependence of r_0^2, as discussed elsewhere [1, 9].

Another way in which r_f^2 and r_0^2 may differ is when the network is altered after formation. For example, when the network imbibes a swelling liquid, r^2 for the swollen network will be increased by a factor λ_s^2 in comparison to its original value, where λ_s is the linear swelling ratio. At the same time the number of chains per unit volume will be decreased by a factor λ_s^{-3}. Thus, the strain energy density under a given deformation will be smaller for a swollen network by a factor λ_s^{-1}.

From the general relation for strain energy, Eq. (8), the elastic stresses required to maintain any given deformation can be obtained by means of virtual work considerations (Fig. 7),

$$\lambda_2 \lambda_3 t_1 = \partial W / \partial \lambda_1$$

with similar relations for t_2 and t_3. Because of the practical incompressibility of rubbery materials in comparison to their easy deformation in other ways, the original volume is approximately conserved under deformation. The extension ratios then obey the simple relationship

$$\lambda_1 \lambda_2 \lambda_3 = 1 \tag{9}$$

As a result, the stress–strain relations become

$$t_1 = \lambda_1 (\partial W / \partial \lambda_1) - p, \qquad \text{etc.}$$

where p denotes a possible hydrostatic pressure (which has no effect on an incompressible solid). Thus, only stress differences can be written explicitly

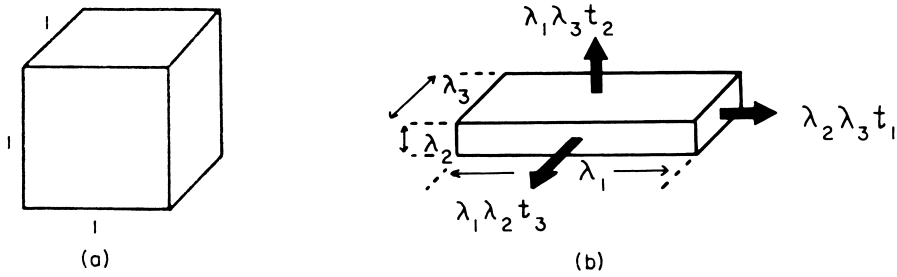

FIGURE 7 (a) Undeformed and (b) deformed states.

$$t_1 - t_2 = (NAr^2/3)(\lambda_1^2 - \lambda_2^2) \tag{10}$$

For a simple extension, say in the 1-direction, we set $\lambda_1 = \lambda$, and $\lambda_2 = \lambda_3 = \lambda^{-1/2}$ [from Eq. (9)], and $t_2 = t_3 = 0$. Hence,

$$t(= t_1) = (NAr^2/3)(\lambda^2 - \lambda^{-1}) \tag{11}$$

It is customary to express this result in terms of the tensile force f acting on a test piece of cross-sectional area A_0 in the unstrained state, where

$$f/A_0 = t/\lambda$$

The corresponding relation is shown in Fig. 8. It illustrates a general feature of the elastic behavior of rubbery solids: although the constituent chains obey a linear force–extension relationship [Eq. (1)], the network does not. This feature arises from the geometry of deformation of randomly oriented chains. Indeed, the degree of nonlinearity depends on the type of deformation imposed. In simple shear, the relationship is predicted to be a linear one with a slope (shear modulus G) given by

$$t_{12} = G\gamma, \qquad G = NAr^2/3 \tag{12}$$

where γ is the amount of shear, e.g., dx/dy.

Because rubbery materials are virtually incompressible in bulk, the value of Poisson's ratio is close to 0.5. Young's modulus E is therefore given by $3G$ to good approximation; however, the predicted relation between stress and tensile strain (extension), $e(= \lambda - 1)$, is linear only for quite small extensions (Fig. 8), so that Young's modulus is applicable only for extensions or compressions of a few percent.

All of the stress relations given above are derived from Eq. (8). They are therefore valid only for moderate deformations of the network, i.e., for deformations sufficiently small for the chain tensions to be linearly related to their

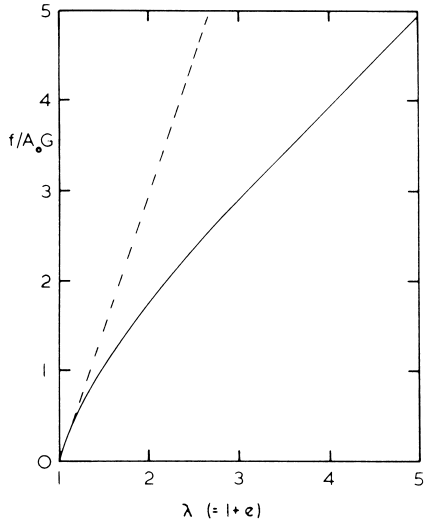

FIGURE 8 Force–extension relation for simple extension. ---, Linear relation obtaining at infinitesimal strains. (From Gent [37].)

end-to-end distances r [Eq. (1)]. Unfortunately, no correspondingly simple expression can be formulated for W using Eq. (5), the relationship for large strains of the constituent chains, in which the molecular stiffness parameter reappears. Instead, a variety of series approximations must be used, as in Eq. (6), to give close approximations to the behavior of rubber networks under large strains [12].

IV. COMPARISON WITH EXPERIMENT

Although the treatment of rubber elasticity given in the preceding section is generally rather successful, certain discrepancies are found to occur. The first consists of observed stresses higher than predicted, e.g., by Eq. (11), and is often expressed by an additional contribution referred to as the C_2 term. This contribution is relatively large at small strains (although it is always the smaller part of the observed stress) and decreases in importance as the strain increases. It also decreases as the network is dilated by swelling with an inert liquid becoming zero at a swelling ratio of about 5. Thus, the "C_2 stress" appears to reflect a non-Gaussian characteristic of network chains, which is important only at small values of the chain end-to-end distance r. Indeed, Thomas [13] has shown that the magnitude of the C_2 stress and its complex dependence on type and degree of strain, and on degree of swelling, can all be accurately described by a simple additional term in the relation for the strain energy w for a single network chain, Eq. (7), which becomes

$$2w = Ar^2 + Br^{-2} \tag{13}$$

The second term clearly becomes insignificant at large values of r.

Further evidence bearing on the physical nature of the discrepancy is provided by two other observations: C_2 does not appear to be strongly dependent on temperature and therefore does not appear to be associated with the energetics of chain conformations; and it is closely correlated with the tendency of the polymer chains to form molecular entanglements. For example, those polymers that have a high density of entanglements in the bulk state (Table I) yield rubbery networks with a relatively high C_2 stress component [9].

Finally, there is no evidence that isolated chains in theta solvents fail to conform to Gaussian statistics, so that the C_2 discrepancy appears to arise only when the molecular chains are tied into a network.

These varied aspects of the C_2 stress suggest that it is associated with entangled chains in networks (Fig. 6) and specifically that it arises from restrictions on the conformations available to entangled chains, different from those operating at crosslink sites [7–9]. Prager and Frisch [10] have pointed out that chains involved in model entanglements are governed by different statistics; their conclusions are quite consistent with what is known of the C_2 stress.

A second discrepancy between theory and experiment is found when the Gaussian part of the measured stresses is compared with the theoretical result for an ideal network. Numerical differences of up to 50% are obtained between the density of effective chains calculated from the observed stresses and that calculated from the chemistry of crosslinking. This discrepancy may be due to an error in the theoretical treatment as given here. James and Guth [14] arrived at stresses only half as large as those given in Eq. (10), from a somewhat different theoretical standpoint.

A third and major discrepancy, already referred to, is found at large deformations when the network chains fail to obey Gaussian statistics, even approximately. Considerable success is achieved in this case by using Eq. (5) in place of Eq. (1) for chain tensions in the network.

Notwithstanding these discrepancies, the simple treatment of rubber elasticity outlined in this chapter has proved to be remarkably successful in accounting for the elastic properties of rubbers under moderate strains, up to about 300% of the unstrained length (depending on the length and flexibility, and hence the extensibility, of the constituent chains). It predicts the general form of the stress–strain relationships correctly under a variety of strains, the approximate numerical magnitudes of the stresses for various chemical structures, and the effects of temperature and of swelling the rubber with an inert mobile liquid on the elastic behavior. It also predicts novel second-order stresses, discussed later, which have no counterpart in classical elasticity theory. In summary, it constitutes a major advance in our understanding of the properties of polymeric materials.

V. CONTINUUM THEORY OF RUBBER ELASTICITY

A general treatment of the stress–strain relations of rubberlike solids was developed by Rivlin [15, 16], assuming only that the material is isotropic in elastic behavior in the unstrained state and incompressible in bulk. It is quite surprising to note what far-reaching conclusions follow from these elementary propositions, which make no reference to molecular structure.

Symmetry considerations suggest that appropriate measures of strain are given by three strain invariants, defined as

$$\mathrm{J}_1 = \lambda_1^2 + \lambda_2^2 + \lambda_3^2 - 3$$
$$\mathrm{J}_2 = \lambda_1^2\lambda_2^2 + \lambda_2^2\lambda_3^2 + \lambda_3^2\lambda_1^2 - 3$$
$$\mathrm{J}_3 = \lambda_1^2\lambda_2^2\lambda_3^2 - 1$$

where λ_1, λ_2, λ_3 are the principal stretch ratios (the ratios of stretched to unstretched lengths, Fig. 7). Moreover, for an incompressible material, J_3 is identically zero, and hence only two independent measures of strain, J_1 and J_2, remain. It follows that the strain energy density W is a function of these two variables only:

$$W = f(J_1, J_2) \tag{14}$$

Furthermore, to yield linear stress–strain relations at small strains, W must be initially of second order in the strains e_1, e_2, e_3. Therefore, the simplest possible form for the strain energy function is:

$$W = C_1J_1 + C_2J_2 \tag{15}$$

where C_1 and C_2 are elastic coefficients with a sum $2(C_1 + C_2)$ equal to the small-strain shear modulus G. Equation 15 was originally proposed by Mooney [17] and is often called the Mooney-Rivlin equation. It is noteworthy that the first term corresponds to the relation obtained from the molecular theory of rubber elasticity, Eq. (8), if the coefficient C_1 is identified with $Nar^2/6 = \frac{1}{2}NkT\,(r/r_0)^2$.

On expanding Eq. (15) as a power series in strains e, where $e = \lambda - 1$, it is found to include all terms in e^2 and e^3. Thus it necessarily gives good agreement with experiment at small strains, say for values of e up to 10 to 20%, where higher powers of e are negligibly small. However considerable confusion has arisen from its application at larger strains, for values of e of 100% or more, when it no longer holds. It is rather unfortunate that experimental stress–strain relations in simple extension appear to be in accord with Eq. (15) up to moderately large strains. This fortuitous agreement arises because the particular strain energy function obeyed by rubber, discussed later, depends

on strain in such a way that the two stress–strain relations in tension are similar in form. Relations for other types of strain are quite different, even at modest strains [18].

A. Stress–Strain Relations

Stresses can be obtained from the derivatives of the strain energy function W:

$$t_1 = \lambda_1(\partial W/\partial \lambda_1) - p \tag{16}$$

Rewriting Eq. (16) in terms of the generic derivatives $\partial W/\partial J_1$ and $\partial W/\partial J_2$ yields

$$t_1 = 2[\lambda_1^2 \partial W/\partial J_1 - (1/\lambda_1^2)\partial W/\partial J_2] - p, \qquad \text{etc.} \tag{17}$$

The functions $\partial W/\partial J_1$ and $\partial W/\partial J_2$ are denoted W_1 and W_2 hereafter.

Experimental measurements indicate that W_1 is approximately constant. However, the second term is far from constant even at moderate strains. Good agreement is obtained when it is expressed as a logarithmic function of J_2 [19]:

$$W = C_1 J_1 + C_2' Ln[(J_2 + 3)/3] \tag{18}$$

where C_2' is a constant. This form of the second term is in reasonably good numerical agreement with the predictions of Thomas's additional term in the strain energy function for a single chain, Eq. (13), and simpler in form.

Values of C_1 and C_2' are similar in magnitude, 0.25 to 0.5 MPa, for typical soft rubber vulcanizates. However, whereas C_1 is approximately proportional to the number of network strands per unit volume, C_2' appears to be rather constant, independent of the degree of crosslinking, and thus it is relatively more important for lightly crosslinked materials. As mentioned earlier, it appears to reflect physical restraints on molecular strands like those represented in the "tube" model of restricted configurations in the condensed state [9]—restraints that diminish in importance as the deformation increases or the strands become more widely separated.

Strain-Hardening at Large Strains

Rubber becomes harder to deform at large strains, probably because the long flexible molecular strands that comprise the material cannot be stretched indefinitely. The strain energy functions considered up to now do not possess this feature and therefore fail to describe behavior at large strains. Strain-hardening can be introduced by a simple modification to the first term in Eq. (18), incorporating a maximum possible value for the strain measure J_1, denoted J_m [20]:

$$W = -C_1 J_m Ln(1 - J_1/J_m) + C_2' Ln[(J_2 + 3)/3] \tag{19}$$

Equation 19 reduces to Eq. (18) when the strains are relatively small, i.e., the ratio J_1/J_m is small. Thus Eq. (19) is probably the simplest possible strain energy function that accounts for the elastic behavior to good approximation over the entire range of strains [21]. It requires three fitting parameters, two of which are related to the small-strain shear modulus G:

$$G = 2[C_1 + (C_2'/3)] \tag{20}$$

The molecular theory of rubberlike elasticity predicts that the first coefficient, C_1, is proportional to the number N of molecular strands that make up the three-dimensional network. The second coefficient, C_2', appears to reflect physical restraints on molecular strands like those represented in the "tube" model [9] and is in principle amenable to calculation. The third parameter, J_m, is not really independent. When the strands are long and flexible, it will be given approximately by $3\lambda_m^2$, where λ_m is the maximum stretch ratio of an average strand. But λ_m^2 is inversely proportional to N for strands that are randomly arranged in the unstretched state [11]. J_m is therefore expected to be inversely proportional to C_1. Thus the entire range of elastic behavior arises from only two fundamental molecular parameters.

Considerable success has also been achieved in fitting the observed elastic behavior of rubbers by strain energy functions that are formulated directly in terms of the extension ratios λ_1, λ_2, λ_3 instead of in terms of the strain invariants I_1, I_2 [22]. Although experimental results can be described economically and accurately in this way, the functions employed are empirical and the numerical parameters used as fitting constants do not appear to have any direct physical significance in terms of the molecular structure of the material. On the other hand, the molecular elasticity theory, supplemented by a simple non-Gaussian term whose molecular origin is in principle within reach, seems able to account for the observed behavior at small and moderate strains with comparable success.

At moderate strains, the value of J_2 is often large enough for terms involving W_2 to be neglected. Some stress–strain relations are now derived using this approximation to illustrate how such calculations are carried out and to deduce under what conditions the deformations become unstable. Instabilities are interesting from a theoretical point of view because they occur suddenly, at a well-defined deformation, and they are often unexpected on the basis of classical elasticity theory. Moreover, a comparison of the observed onset of instability with the predictions of various strain energy functions W provides, at least in principle, a critical test for the validity of a proposed form for W. From a practical standpoint, unstable states are quite undesirable because the deformation becomes highly non-uniform, leading to premature failure.

Inflation of a Thin-Walled Tube

Inflation of a tube is described by extension ratios of λ_1 in the circumferential direction and λ_2 in the axial direction, with the wall thickness h becoming $h/\lambda_1\lambda_2$ because the rubber volume remains constant. The inflation pressure P gives rise to stresses in the circumferential and axial directions:

$$t_1 = \lambda_1^2\lambda_2 r\,P/h$$
$$t_2 = \lambda_1^2\lambda_2 r\,P/2h \tag{21}$$

where r is the tube radius in the unstrained state.

From Eq. (21), on putting the stress $t_3 = 0$, the undefined pressure p is obtained as:

$$p = -2W_1/\lambda_1^2\lambda_2^2 \tag{22}$$

[In a thin-walled tube of large radius the inflating pressure P is much smaller than the stresses t_1 and t_2 that it generates, and thus P can be neglected in comparison with the stress t_3 in determining p.] Inserting this result for p in Eqs. (21) and (22) yields a relation between the extension ration λ_2 and the expansion ratio v (= $\lambda_1^2\lambda_2$) of the internal volume of the tube:

$$2\lambda_2^3 = (v^2+1)/2v^2 \tag{23}$$

The relation between inflating pressure P and internal volume of the tube is then obtained as:

$$Pr/hC_1 = 2(v^2-1)[2v/(v^2+1)]^{1/3}/v^2[1-(J_1/J_m)] \tag{24}$$

This relation is plotted in Fig. 9 for various values of the limiting strain measure J_m. The inflating pressure is seen to pass through a maximum at a volume expansion ratio between about 58 and 66%, depending on the value assumed for J_m. This feature suggests that larger expansions will be unstable. Indeed, thin-walled tubes undergo a strikingly non-uniform deformation at a critical inflation pressure, shown schematically in Fig. 10. One portion of the tube becomes highly-distended as a bubble or aneurysm while the rest is lightly inflated. The two stable deformations that can coexist at the same inflation pressure after the critical state is reached are shown schematically by the horizontal broken line in Fig. 9. However, when J_m is infinitely large, the aneurysm is unbounded and failure would then occur immediately on reaching the critical pressure.

Inflation of a Thin-Walled Spherical Balloon

In this case, if the balloon radius expands by a factor λ, equibiaxial extensions of ratio λ will be set up in the balloon, with a shrinkage ratio $1/\lambda^2$ of the

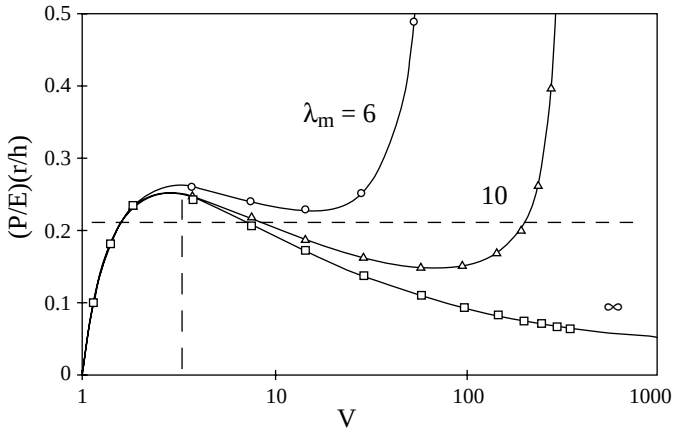

FIGURE 9 Pressure–volume relations for a thin-walled tube from Eq. (24) using various values for the maximum possible extension ratio λ_m. The vertical broken line denotes the onset of instability. ($E = 6\ C_1$.)

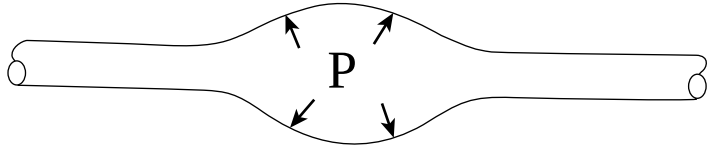

FIGURE 10 Sketch of an aneurysm in an inflated tube.

wall thickness to maintain the rubber volume constant. The circumferential stresses t_1 and t_2 are equal and given by:

$$t_1 = t_2 = 2W_1(\lambda^2 - \lambda^{-4})/[1-(J_1/J_m)] \tag{25}$$

from Eq. (17), when the stress $t_3 = 0$ and $W_2 = 0$. The inflation pressure P is then given by:

$$Pr/hC_1 = 4(\lambda^{-1} - \lambda^{-7})/[1-(J_1/J_m)] \tag{26}$$

where r and h are the unstrained radius and wall thickness of the balloon. In this case the potential instability occurs even earlier, at a radial expansion ratio between 38 and 50% depending on the value chosen for J_m. In practice, the deformation becomes quite complex (Fig. 11). The balloon remains roughly spherical in shape but one part is lightly stretched while the remainder is highly stretched. The two states of strain resemble the two deformations that are predicted at a given pressure after the critical point is reached.

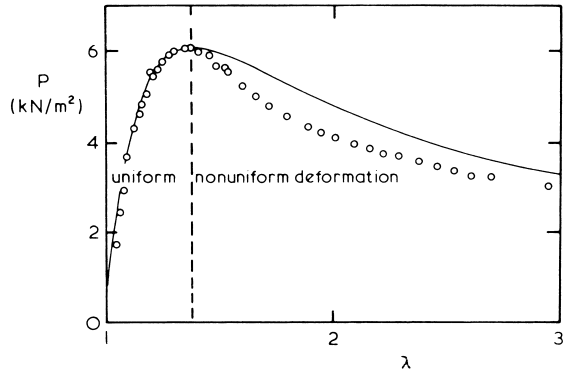

FIGURE 11 Inflation of a thin-walled spherical rubber balloon. Solid curve: Eq. (26) with $J_m = \infty$. (From Gent [37].)

Inflation of a Thick-Walled Spherical Shell

The internal pressure P required to inflate a small spherical cavity in the center of a thick block can be obtained by integrating the contributions from concentric shells (thin-walled balloons) given in the preceding section. The result is [23]

$$P/C_1 = 4\lambda_0^{-1} + \lambda_0^{-4} - 5 \tag{27}$$

for an infinitely extensible rubber ($J_m = \infty$), where λ_o is the biaxial stretch ratio at the surface of the cavity. This relation does not exhibit a maximum and thus does not indicate that the deformation is unstable. However, at high values of λ_o the pressure P asymptotes to a constant value of about $5C_1$, i.e., about $5G/2$, where G is the small-strain shear modulus. For typical rubbery materials where G is about 0.5 MPa, the maximum pressure is thus about 1.2 MPa, or about 12 bar. Any small cavity will expand greatly at this rather modest inflation pressure. Internal fracture is therefore likely to occur in soft rubbery solids at inflation pressures or equivalently, triaxial tensions, of this amount. In practice, all rubbery solids are found to develop internal fractures when supersaturated with gases or liquids at pressures or triaxial tensions about equal to $5G/2$ [23, 24].

Note that the initial radius of the spherical cavity does not appear in Eq. (27). Thus, cavities of all sizes are predicted to inflate equally. However, we have neglected surface energy contributions that will tend to stabilize small cavities. When they are taken into account it appears that only cavities having radii greater than about 100 nm will expand dramatically at the low pressures predicted by Eq. (27). Internal fractures suggest that vulcanized rubber must contain many precursor cavities of this effective size or larger.

Surface Instability of Compressed or Bent Blocks

Biot [25] showed that the surface of an elastic half-space will become unstable at critical values of strain ratios λ_1, λ_3 set up in two perpendicular directions in the surface. The critical condition is

$$\lambda_1^2 \lambda_3 = 0.2956 \tag{28}$$

When the block is subjected to unidirectional compression parallel to the surface, with free expansion permitted in the other two directions, then $\lambda_3 = 1/\lambda_1^{1/2}$ and Eq. (28) yields a critical value for λ_1 of 0.444. A large block of rubber in simple compression is therefore predicted to show a surface instability at a compression of 55.5%. (Beatty [26] noted that various buckling and bulging modes of deformation are generally encountered before this, depending on the slenderness of the block.) If the block is subjected to equi-biaxial compression parallel to the surface, then $\lambda_3 = \lambda_1$ and the critical compression becomes 33.3%.

When a thick elastic block (cuboid) is bent, the inner surface becomes compressed while the extension ratio λ_3 along the width is largely unchanged (at unity). Thus, from Eq. (28) an instability would be expected on the inner surface when λ_1 is 0.544, i.e., when the surface is compressed by about 46%. Experimentally, sharp folds or creases appear suddenly in the inner surface of a bent block at a critical degree of bending [27], see Fig. 12. However, the critical compression of the inner surface was considerably smaller than predicted by Biot's theory, 35% instead of 46%. It is not known why the instability occurred so much sooner than expected. Although rubber follows a more complex strain energy function than the simple form assumed here, it is unlikely that the difference would have such a large effect.

Rubber articles are often subjected to rather severe bending deformations, for example, in tires. Folds and creases in the interior may pass undetected. Nevertheless, they represent lines of high stress concentration and sites of possible failure. Folds ("Schallamach waves") also appear when soft rubber slides over a rigid countersurface [28]. They appear to be Biot creases caused by frictional compression of the surface.

Resistance of a Compressed Block to Indentation

When a block is subjected to a sufficiently large equibiaxial compression in the surface plane it becomes unstable to small indentations. Green and Zerna [29] expressed the relation between indentation force N and amount of indentation d as:

$$N/G = (8/3)R^{1/2} d^{3/2} f(\lambda) \tag{29}$$

where G is the shear modulus of the half-space material, R is the radius of the indentor, and $f(\lambda)$ is a function of the equibiaxial compression ratio λ, given by

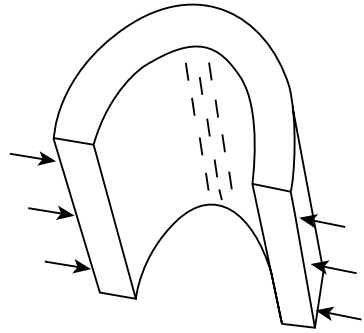

FIGURE 12 Sketch of a bent block showing creases that appear on the inner surface where the compressive strain is greatest.

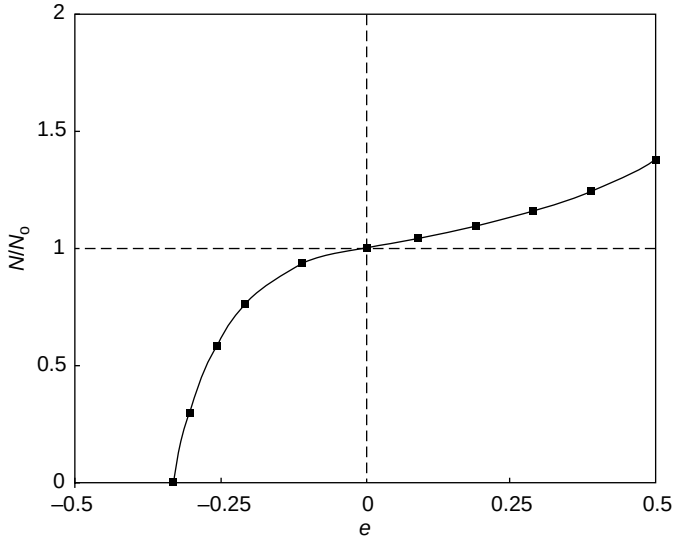

FIGURE 13 Force N for a small indentation vs. equibiaxial strain e parallel to the surface of a half-space. N_o denotes the force when $e = 0$. (From Green and Zerna [29].)

$$f(\lambda) = (\lambda^9 + \lambda^6 + 3\lambda^3 - 1)/\lambda^4(\lambda^3 + 1) \tag{30}$$

Values of indentation force N for a given small indentation, from Eq. (27), are plotted in Fig. 13 against the equibiaxial strain e parallel to the surface, where $e = \lambda - 1$. [N_0 denotes the value for an initially unstrained block, when $f(\lambda) = 2$.] The resistance to indentation is seen to decrease sharply as the compressive strain is increased, becoming zero at a compressive strain of 0.333, in agreement with Biot's result.

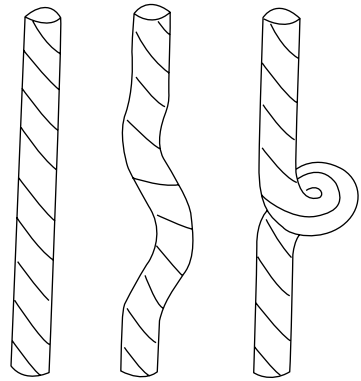

FIGURE 14 Sketch of a "kink" that appears on twisting a stretched rubber rod (From Gent and Hua [30].)

Torsional Instability of Stretched Rubber Rods [30]

Another unstable state is encountered when a stretched rubber rod is subjected to large torsions. A kink suddenly appears at one point along the rod, Fig. 14, and more kinks form on twisting the rod further.

Minimization of the total elastic strain energy suggests that the rod will become unstable at a critical amount of torsion: part of the rod will unwind and form a tight ring while the remainder of the rod will become slightly more stretched. A simple criterion can be derived on this basis for the onset of "kinks." For a neo-Hookean material, Eq. (8), the condition for forming a kink becomes:

$$4(1-1/\lambda^3) = -(a^2\phi^2/\lambda) + 2\pi(a^2\phi^2/\lambda)/[\pi - (a\phi/\lambda^{1/2})] \tag{31}$$

where ϕ is the critical amount of torsion at which uniform torsion becomes unstable, in terms of the imposed extension ratio λ and the rod radius a. Measured values for rods of different radius, stretched to extensions of up to 250%, were found to be in reasonably good agreement with Eq. (31), indicating that the sudden formation of kinks in twisted rubber rods is, indeed, a consequence of an elastic instability.

VI. SECOND-ORDER STRESSES

Because the strain energy function for rubber is valid at large strains, and yields stress–strain relations which are nonlinear in character, the stresses depend on the square and higher powers of strain, rather than the simple pro-

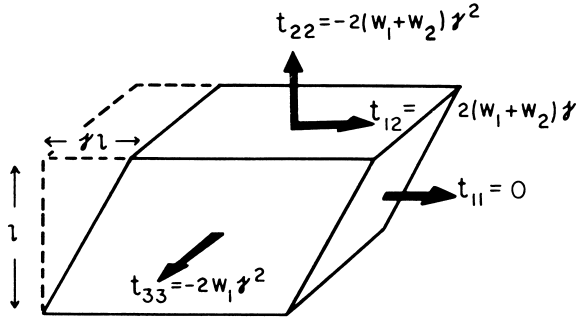

FIGURE 15 Stresses required to maintain a simple shear deformation of amount γ. The normal stress t_{11} is set equal to zero. (From Gent [37].)

portionality expected at small strains. A striking example of this feature of large elastic deformations is afforded by the normal stresses t_{11}, t_{22}, t_{33} that are necessary to maintain a simple shear deformation of amount γ (in addition, of course, to simple shear stresses) [15, 16]. These stresses are predicted to increase in proportion to γ^2.

They are represented schematically in Figs. 15 and 16 for two different choices of the arbitrary hydrostatic pressure p, chosen so as to give the appropriate reference (zero) stress. In Fig. 15, for example, the normal stress t_{11} in the shear direction is set equal to zero; this condition would arise near the front and rear surfaces of a sheared block. In Fig. 16, the normal stress t_{33} is set equal to zero; this condition would arise near the side surfaces of a sheared block. In each case a *compressive* stress t_{22} is found to be necessary to maintain the simple shear deformation. In its absence the block would tend to increase in thickness on shearing.

When the imposed deformation consists of an inhomogeneous shear, as in torsion, the normal forces generated (corresponding to the stresses t_{22} in Figs. 15 and 16) vary from point to point over the cross-section (Fig. 17). The exact way in which they are distributed depends on the particular form of strain energy function obeyed by the rubber, i.e., on the values of W_1 and W_2 which obtain under the imposed deformation state [31].

VII. ELASTIC BEHAVIOR UNDER SMALL DEFORMATIONS

Under small deformations rubbers are linearly elastic solids. Because of high modulus of bulk compression, about 2000 MN/m^2, compared with the shear modulus G, about 0.2 to 5 MN/m^2, they may be regarded as relatively incompressible. The elastic behavior under small strains can thus be described by a single elastic constant G. Poisson's ratio is effectively 1/2, and Young's modulus E is given by $3G$, to good approximation.

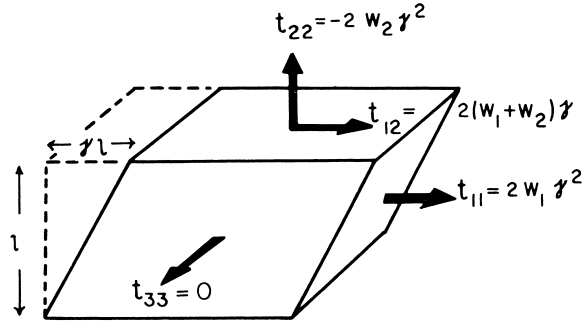

FIGURE 16 Stresses required to maintain a simple shear deformation of amount γ. The normal stress t_{33} is set equal to zero. (From Gent [37].)

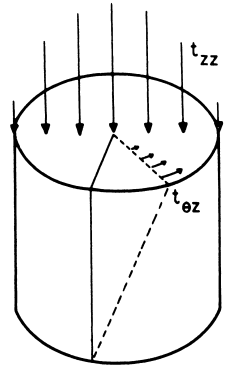

FIGURE 17 Sketch of a cylindrical rod under torsion showing the distribution of normal stress t_{zz} (corresponding to $-t_{22}$ in Figs. 10 and 11) over the cross-section of the rod. (From Treloar [11].)

A wide range of values for G can be obtained by varying the composition of the elastomer, i.e., by changing the chemistry of crosslinking, oil dilution, and filler content; however, soft materials with shear moduli of less than about $0.2\,\mathrm{MN/m^2}$ prove to be extremely weak and are seldom used. Also, particularly hard materials made by crosslinking to high degrees prove to be brittle and inextensible. The practical range of shear modulus, from changes in degree of crosslinking and oil dilution, is thus about 0.2 to $1\,\mathrm{MN/m^2}$. Stiffening by fillers increases the upper limit to about $5\,\mathrm{MN/m^2}$, but those fillers, which have a particularly pronounced stiffening action, also give rise to stress-softening effects like those shown in Fig. 5, so that the modulus becomes a somewhat uncertain quantity.

It is customary to characterize the modulus, stiffness, or hardness of rubbers by measuring their elastic indentation by a rigid die of prescribed size and shape under specified loading conditions. Various nonlinear scales are

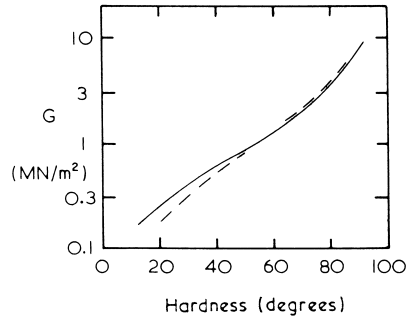

FIGURE 18 Relations between shear modulus G and indentation hardness: —, Shore A Scale; ---. International Rubber Hardness Scale. (From Tobolsky and Mark [5].)

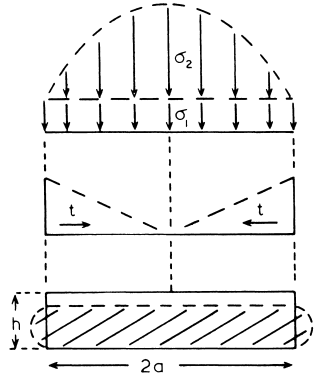

FIGURE 19 Sketch of a bonded rubber block under a small compression. The distributions of normal stress σ and shear stress t acting at the bonded surfaces are represented by the upper portions of the diagram. (From Tobolsky and Mark [5].)

employed to derive a value of hardness from such measurements [32]. Corresponding values of shear modulus G for two common hardness scales are given in Fig. 18.

Many rubber products are normally subjected to fairly small deformations, rarely exceeding 25% in extension or compression or 75% in simple shear. A good approximation for the corresponding stresses can then be obtained by conventional elastic analysis assuming linear relationships. One particularly important deformation is treated here: the compression or extension of a thin rubber block, bonded on its major surfaces to rigid plates (Fig. 19). A general treatment of such deformations has been reviewed [34].

It is convenient to assume that the deformation takes place in two stages: a pure homogeneous compression or extension of amount e, requiring a

uniform compressive or tensile stress $\sigma_1 = Ee$, and a shear deformation restoring points in the planes of the bonded surfaces to their original positions in these planes. For a cylindrical block of radius a and thickness h, the corresponding shear stress t acting at the bonded surfaces at a radial distance r from the cylinder axis is given by

$$t = Eer/h$$

This shear stress is associated with a corresponding normal stress or pressure σ_2, given by

$$\sigma_2 = Ee(a^2/h^2)[1-(r^2/a^2)] \tag{32}$$

These stress distributions are shown schematically in Fig. 19. Although they must be incorrect right at the edges of the block, because the assumption of a simple shear deformation cannot be valid at these points of singularity, they appear to provide satisfactory approximations over the major part of the bonded surfaces [42].

By integrating the sum of the normal stresses $\sigma_1 + \sigma_2$ over the bonded surface, the total compressive force F is obtained in the form [33]

$$F/\pi a^2 e = E[1+(a^2/2h^2)] \equiv E' \tag{33}$$

Clearly, for thin blocks of large radius the effective value of Young's modulus E' [given by the right-hand side of Eq. (33)] is much larger than the real value E because of the restraints imposed by the bonded surfaces. Indeed, for values of the ratio a/h greater than about 10, a significant contribution to the observed displacement comes from volume compression or dilation because E' is now so large that it becomes comparable to the modulus of bulk compression [33] (Fig. 20).

A more accurate treatment of the compression of bonded blocks has been given by Horton *et al.* [34] without invoking the assumption that a simple shear deformation holds right up to the bonded edges. They obtained a result of the same form as Eq. (33) but with the bracketed term on the right-hand side replaced by $[1.2 + (a^2/2h^2)]$. However, this term does not yield the correct value of unity for tall blocks, i.e., when a/h is small, and it is equivalent to Eq. (33) for thin blocks of large radius, when a/h is large. It should therefore be regarded as a better approximation for blocks of intermediate size.

When a thin bonded block is subjected to tensile loading, a state of approximately equal triaxial tension is set up in the central region of the block. The magnitude of the stress in each direction is given by the tensile stress, or negative pressure, σ_2 at $r = 0$, i.e., Eea^2/h^2, from Eq. (32). Under this outwardly directed tension a small cavity in the central region of the block will expand indefinitely at a critical value of the tension, of about $5E/6$. Thus,

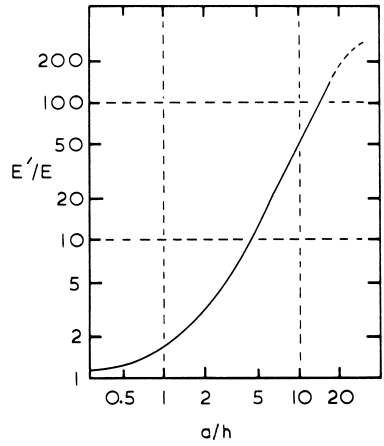

FIGURE 20 Effective value of Young's modulus E' for bonded blocks versus ratio of radius to thickness a/h. (From Tobolsky and Mark [5].)

if cavities are present in the interior of a bonded block, they are predicted to expand indefinitely, i.e., rupture, at a critical tensile strain e_c, given approximately by

$$e_c = 5h^2/6a^2$$

and at a corresponding critical value of the applied tensile load, obtained by substituting this value of e in Eq. (33). To avoid internal fractures of this kind it is thus necessary to restrict the mean tensile stress applied to thin bonded blocks to less than about $E/3$.

In compression, on the other hand, quite large stresses can be supported. A stress limit can be calculated by assuming that the maximum shear stress, developed at the bonded edges, should not exceed G; i.e., the maximum shear deformation should not exceed about 100%. This yields a value for the allowable overall compressive strain of $h/3a$, corresponding to a mean compressive stress of the order of E for disks with a/h between about 3 and 10. This calculation assumes that the approximate stress analysis outlined earlier is valid right at the edges of the block, and this is certainly incorrect. Indeed, the local stresses in these regions depend strongly on the detailed shape of the free surface in the neighborhood of the edge.

VIII. SOME UNSOLVED PROBLEMS IN RUBBER ELASTICITY

We turn now to some features of the elastic response of rubbery materials which are still not fully understood.

As normally prepared, molecular networks comprise chains of a wide distribution of molecular lengths. Numerically, small chain lengths tend to predominate. The effect of this diversity on the elastic behavior of networks, particularly under large deformations, is not known. A related problem concerns the elasticity of short chains. They are inevitably non-Gaussian in character and the analysis of their conformational statistics is likely to be difficult. Nevertheless, it seems necessary to carry out this analysis to be able to treat real networks in an appropriate way.

It is also desirable to treat network topology in greater detail, i.e., to incorporate the functionality of crosslinks, their distribution in space, and loop formation. The effect of mutual interaction between chains in the condensed state appears to be accounted for satisfactorily by the "tube" model for uncrosslinked polymers, but its application to networks seems incomplete. But the problem in greatest need of attention is the response of highly filled elastomers to stress. Filled elastomers are not really elastic; their stress–strain relations are irreversible (see Fig. 5), and it is therefore inappropriate to describe their response to stress by a strain energy function. Moreover, they appear to become anisotropic on stretching and to some degree after release. At present, the molecular processes that occur on deformation and the mathematical framework suitable for describing them are both unclear.

ACKNOWLEDGMENTS

The reader is referred to the classic survey of rubber elasticity by Treloar [11] and to three recent reviews that give fuller accounts of the molecular theory [9, 35, 36]. The author thanks Mr. R. A. Paden for drawing several of the figures.

REFERENCES

1. P. J. Flory, "Statistical Mechanics of Chain Molecules," Wiley-Interscience, New York, 1969.
2. J. P. Cotton, B. Farnoux, and G. J. Jannink, *J. Chem. Phys.* **57**, 290 (1972).
3. M. C. Morris, *J. Appl. Polm. Sci.* **8**, 545 (1964).
4. F. Bueche, *J. Appl. Polym. Sci.* **4**, 107 (1960); **5**, 271 (1961).
5. A. V. Tobolsky and H. F. Mark (Eds.), "Polymer Science and Materials," Wiley, New York, 1971, Chap. 13.
6. L. J. Fetters, D. J. Lohse, and W. W. Graessley, *J. Polym. Sci.*: Part B: *Polym. Phys.* **37**, 1023 (1999).
7. N. R. Langley, *Macromolecules* **1**, 348 (1968).
8. T. A. Vilgis, in "Elastomeric Polymer Networks," J. E. Mark and B. Erman (Eds.), Prentice-Hall, Englewood Cliffs, NJ, 1992, Chap. 5.
9. W. W. Graessley, "Polymeric Liquids and Networks: Structure and Properties," Taylor and Francis Books, New York, 2004.
10. S. Prager and H. L. Frisch, *J. Chem. Phys.* **46**, 1475 (1967).
11. L. R. G. Treloar, "The Physics of Rubberlike Elasticity," 3rd ed., Clarendon Press, Oxford, 1975.

12. E. M. Arruda and M. C. Boyce, *J. Mech. Phys. Solids* **41**, 389 (1993).
13. A. G. Thomas, *Trans. Faraday Soc.* **51**, 569 (1955).
14. H. M. James and E. Guth, *J. Chem. Phys.* **11**, 455 (1943); *J. Polym. Sci.* **4**, 153 (1949).
15. R. S. Rivlin, *Philos. Trans. Roy. Soc. (London) Ser. A* **241**, 379 (1948).
16. R. S. Rivlin, in "Rheology, Theory and Application," F. R. Eirich (Ed.), Academic Press, New York, Vol. 1, 1956, Chap. 10.
17. M. Mooney, *J. Appl. Phys.* **11**, 582 (1940).
18. R. S. Rivlin and D. W. Saunders, *Philos. Trans. Roy. Soc. (London) Ser. A* **243**, 251 (1951).
19. A. N. Gent and A. G. Thomas, *J. Polym. Sci.* **28**, 625 (1958).
20. A. N. Gent, *Rubber Chem. Technol.* **69**, 59 (1996).
21. E. Pucci and G. Saccomandi, *Rubber Chem. Technol.* **75**, 839 (2002).
22. R. W. Ogden, "Non-Linear Elastic Deformations," Ellis Harwood, Chichester, UK, 1984; Dover Publications, Mineola, NY, 1997, Chap. 7.
23. A. N. Gent and P. B. Lindley, *Proc. Roy. Soc. (London) A* **249**, 195 (1958).
24. A. N. Gent and D. A. Tompkins, *J. Appl. Phys.* **40**, 2520 (1969).
25. M. Biot, "Mechanics of Incremental Deformations," Wiley, New York, 1965.
26. M. F. Beatty, in "Finite Elasticity," R. S. Rivlin (Ed.), AMD Vol. 27, American Society of Mechanical Engineers, New York, 1977, p. 125.
27. A. N. Gent and I. S. Cho, *Rubber Chem. Technol.* **72**, 253 (1999).
28. A. Schallamach, *Wear* **17**, 301 (1971).
29. A. E. Green and W. Zerna, "Theoretical Elasticity," 2nd ed., Clarendon Press, Oxford, 1975, Section 4.6, p. 135.
30. A. N. Gent and K. C. Hua, *Int. J. Non-Linear Mech.* **39**, 483 (2004).
31. R. S. Rivlin, *J. Appl. Phys.* **18**, 444 (1947).
32. A. L. Soden, "A Practical Manual of Rubber Hardness Testing," Maclaren, London, 1952.
33. A. N. Gent, *Rubber Chem. Technol.* **67**, 549 (1994).
34. J. M. Horton, G. E. Tupholme, and M. J. C. Gover, ASME, *J. Appl. Mech.* **69**, 836 (2002).
35. J. E. Mark and B. Erman, "Rubberlike Elasticity: A Molecular Primer," John Wiley & Sons, New York, 1988.
36. J. E. Mark and B. Erman (Eds.), "Elastomeric Polymer Networks," Prentice-Hall, Englewood Cliffs, NJ, 1992.
37. A. N. Gent, *J. Polym. Sci. Poly. Symp.* **28**, 625 (1958).

2 Polymerization: Elastomer Synthesis

RODERIC P. QUIRK
The Maurice Morton Institute of Polymer Science
The University of Akron
Akron, Ohio

DEANNA L. GOMOCHAK PICKEL
Research Laboratories
Eastman Chemical Company
Kingsport, Tennessee

I. INTRODUCTION

The development of synthetic rubber played a special role in the history of polymerization chemistry. This was due primarily to the fact that attempts to synthesize rubber were made long before there was even the faintest idea of the nature of polymerization reactions. Such attempts began very soon after the elegant analytical work of Williams [1] in 1860, which clearly demonstrated that *Hevea* rubber was "composed" of isoprene. Thus, Bouchardat [2] in 1879 was actually able to prepare a rubberlike substance from isoprene (which he obtained from rubber pyrolysis), using heat and hydrogen chloride. Tilden [3] repeated this process in 1884 but used isoprene obtained from pyrolysis of turpentine to demonstrate that it was not necessary to use the "mother substance" of rubber itself. These explorations were soon followed by the work of Kondakow (1900) [4] with 2,3-dimethylbutadiene, that of Thiele (1901) [5]

Science and Technology of Rubber, Third Edition

with piperylene, and finally that of Lebedev (1910) [6] on butadiene itself. Mention should also be made of the almost simultaneous, and apparently independent, discoveries in 1910 by Harries [7] in Germany and Matthews and Strange [8] in England of the efficient polymerization in isoprene by sodium.

Although all of these attempts had a noble purpose indeed, the means used could hardly be considered a contribution to science, as the transformation of the simple molecules of a diene into the "colloidal" substance known as rubber was then far beyond the comprehension of chemical science. As a matter of fact, the commercial production of synthetic rubber was already well established, at least in Germany and Russia, *before* Staudinger laid the basis for his macromolecular hypothesis during the 1920s [9]. Even such relatively modern synthetic elastomers as polychloroprene and the poly(alkylene sulfides) were already in commercial production by 1930–1931. This was, of course, also before Carothers and coworkers' pioneering studies on the polymerization of chloroprene [10]!

Hence, it is apparent that it was not the development of an understanding of polymerization that led to the invention of synthetic rubber, but perhaps the reverse. In contrast, it was the new science of organic macromolecules, whose foundations were established by Staudinger, which expanded rapidly during the 1930s and 1940s, and pointed the way to the synthesis of a vast array of new polymeric materials, including synthetic fibers and plastics and even new elastomers. This new science included the classical studies of polycondensation by Carothers and Flory and the establishment of the principles governing free radical chain addition reactions by Schulz, Flory, Mayo, and others [11, 12].

Thus it was that the paths of synthetic rubber and macromolecular science finally crossed and became one broad avenue [13]. Hence today the design of a new elastomer or the modification of an old one requires the same kind of molecular architecture which applies to any other polymer and is based on an understanding of the principles of polymerization reactions.

II. CLASSIFICATION OF POLYMERIZATION REACTIONS AND KINETIC CONSIDERATIONS

Historically polymers have been divided into two broad classes: *condensation* polymers and *addition* polymers [11, 14, 15]. Flory [11, p. 37] has defined these as follows:

> condensation polymers, in which the molecular formula of the structural unit (or units) lacks certain atoms present in the monomer from which it is formed, or to which it may be degraded by chemical means, and addition polymers, in which the molecular formula of the structural unit (or units) is identical with that of the monomer from which the polymer is derived.

Thus, an example of a condensation polymer would be a polyester, formed by the condensation reaction between a glycol and a dicarboxylic acid (with the evolution of water), whereas an addition polymer is exemplified by polystyrene, formed by the self-addition of styrene monomers.

Although these earlier definitions were based on the chain structure of the polymers, they were closely related, as just described, to the *mode of formation* as well. It soon became apparent that such a classification has serious shortcomings, as so-called polycondensates could result from "addition" polymerization reactions. For example, although Nylon 6 can be prepared by the polycondensation reaction of ε-aminocaproic acid [16], it is now synthesized by the ring-opening addition polymerization of ε-caprolactam [17], and this process has a profound effect on the properties of the resulting polymer. This is, of course, due basically to the magnitude of the molecular weight of the final polymer.

Because it is the extraordinarily large size of the macromolecules which leads to their unusual properties, it would be most sensible to classify polymerization reactions in accordance with *the way in which they affect the molecular size and size distribution of the final product*, i.e., in terms of the mechanism of polymerization. On this basis, there appear to be only two basic processes whereby macromolecules are synthesized [18–24]: (1) step-growth polymerization (polycondensation and polyaddition) and (2) chain-growth (chain) polymerization.

A. Polyaddition/Polycondensation

The distinguishing mechanistic feature of step-growth polymerization [18–24] is that all molecular species in the system can react with each other to form higher-molecular-weight species as shown in Eq. (1), where P_i is a species with a number-average number of monomer units per chain equal to i, P_j is a species with a number-average number of monomer units per chain equal to j, and P_{i+j} is a species with a number-average number of monomer units per chain equal to $i + j$. The kinetic consequence of this mechanism of polymer growth is that chain length increases monotonically with extent of reaction, i.e., with time of reaction, as shown in Fig. 1(A).

$$P_i + P_j \rightarrow P_{i+j} \tag{1}$$

These step-growth polymerization reactions fall into two classes [23, 24]:

Polycondensation: growth of polymer chains proceeds by condensation reactions between molecules of all degrees of polymerization. A low-molar-mass by-product (AB) is also formed.

$$\text{A-R-A} + \text{B-R-B} \rightarrow \text{A-R-R-B} + \text{AB} \tag{2}$$

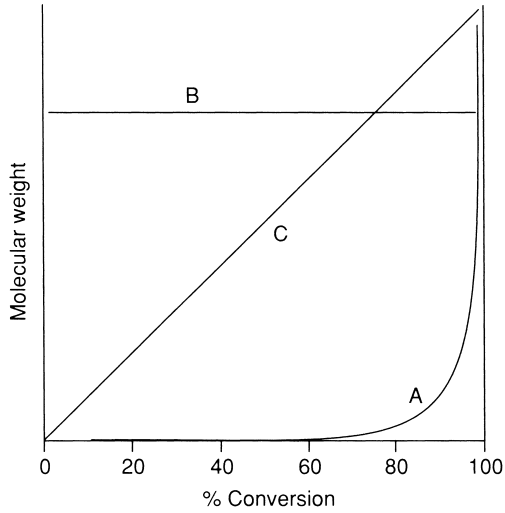

FIGURE 1 Variation of molecular weight with % conversion for (A) step-growth polymerization, (B) chain-growth polymerization, and (C) living chain-growth polymerization with no chain transfer and no chain termination.

Polyaddition: growth of polymer chains proceeds by addition reactions between molecules of all degrees of polymerization.

$$\text{A-R-A} + \text{B-R-B} \rightarrow \text{A-R-AB-R-B} \tag{3}$$

Here A and B are the functional end groups which react with each other. Examples of polycondensation can be seen in the formation of (1) polyesters and (2) polyamides, where the A and B groups would be (1) hydroxyl and carboxyl and (2) amine and carboxyl, respectively, which would combine and split off a molecule of water [16–19]. On the other hand, a polyaddition reaction [Eq. (2)] would be exemplified by the reaction of diisocyanates with glycols to form polyurethanes. In that case, of course, no by-products are formed.

The polymerizations shown in Eqs. (2) and (3) actually represent well-known reactions of small molecules, the only distinction being the minimum requirements of *difunctionality* of each molecule for polymer formation, which makes it possible for the product of each reaction to participate in further reactions. As a rule, the functional groups retain their reactivity regardless of the chain length [11, p. 75], so that these reactions follow the same kinetic rules as for simple molecules; however, in contrast to polyaddition reactions, polycondensations suffer from the serious problem of reversibility (e.g., hydrolysis, or "depolymerization") as a result of the possible accumulation of the by-product (e.g., water), and this must be taken into account. In general, because of the unfavorable equilibrium constant for polycondensation reac-

tions [20], the formation of high polymer requires removal of the small molecule by-products [18].

In both of the foregoing types of reactions, two factors which govern the molecular weight of the polymer are the stoichiometry and the extent of reaction [22]. Thus, it is obvious that an excess of one type of end group will control the maximum chain length attainable, and this can be predicted if the initial molar ratio of functional groups is known. On the other hand, with equivalent amounts of the two types of end groups, the final chain length is theoretically limitless, i.e., infinite in size.

B. Chain Polymerization

The distinguishing mechanistic feature of chain-growth or chain polymerization [21, 22–24] is that chain growth (propagation) occurs only by addition of monomer to reactive sites present on the growing polymer molecules as shown in Eq. (4), where P_n^* is a polymer chain with a reactive site (*) and degree of polymerization of n, M is a monomer unit and P_{n+1}^* is a polymer chain with a reactive site (*) and a degree of polymerization of $n + 1$.

$$P_n^* + M \rightarrow P_{n+1}^* \tag{4}$$

This type of polymerization involves the successive addition of monomers to a growing chain, which is initiated by some reactive species (initiation). Such addition reactions may involve either multiple bonds or rings. The reactive species which initiate such chain reactions must be capable of opening one of the bonds in the monomer and may be either a radical, an electrophile, a nucleophile, or an organometallic species. Hence these polymerizations may proceed by a variety of possible mechanisms depending on the electronic nature of the chain-carrying species, viz., free radical, cationic, anionic, and coordination, as illustrated by the following equations for reactions of double bonds with various types of initiating species:

Free radical

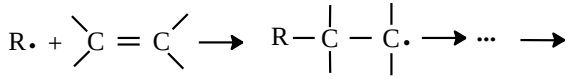

Cationic

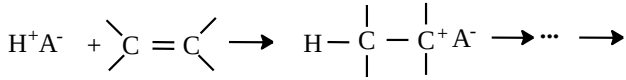

Anionic

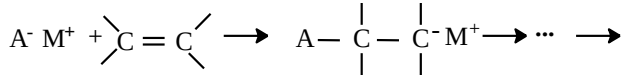

Coordination

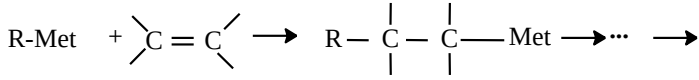

In these equations, the exact nature of the initiating and chain-carrying species can vary from essentially covalent for transition-metal organometallic species in coordination polymerization to ion pairs or free ions in ionic polymerizations, depending on the structure of the chain-carrying species, the counterion, the solvent, and the temperature.

A significant distinction between step polymerization and chain polymerization is that in the latter, each macromolecule is formed by a "chain reaction" which is initiated by some activation step. Thus, at any given time during the polymerization, the reacting species present consist only of *growing chains and monomer molecules*, in addition to the "dead" polymer chains formed earlier by chain termination reactions. These growing chains may be very short-lived (e.g., free radicals or free ions) but may attain very long chain lengths during their brief lifetimes as illustrated in Fig. 1(B). On the other hand, they may have very long lifetimes (e.g., living polymers [22–24]), in which case the chain lengths may increase as a direct function of time of reaction as shown in Fig. 1(C). Hence, unlike the case of step polymerizations, the molecular weights in chain addition polymerization systems may or may not be directly related to time or extent of reaction [see Fig. 1(A)].

III. Polyaddition/Polycondensation

Although, as indicated earlier, polyaddition and polycondensation did not figure prominently in the early explorations of rubber synthesis, it was one of the earliest general methods used for polymerization, because of its relative simplicity. It is thus not surprising that the earliest truly synthetic resins and plastics were of the polycondensate type, such as phenol formaldehyde and polyester. The concept of linking together reactive end groups to build large molecules is fairly simple to comprehend and also lends itself to a relatively simple mathematical analysis.

As stated previously, the kinetics of polyadditions and polycondensations follow the same rules as the simple monofunctional reactions [18, 20, 22, 25], as the reactivity of the functional groups is maintained [11, p. 75] regardless of chain length. The only new feature is, of course, the growth in molecular size, and this has been amenable to a mathematical analysis [11, p. 91]. Considering the type of reactions defined in Eqs. (2) and (3), in the normal case, where the number of A and B groups are equal, the chain lengths are easily predictable as a function of the extent of reaction. Thus, if p represents the *fraction of end groups consumed* at any given time, then the number-average number of units per chain (X_n) is given by $1/(1 - p)$. Thus,

$$M_n = M_o/(1-p) \tag{5}$$

where M_n is the number-average molecular weight of the polymer and M_o is the molecular weight of a chain repeating unit. The consequences of this simple relationship are profound. For example, when 50% of the functional groups have reacted, the number-average degree of polymerization is only 2. To prepare polymers with useful properties, molecular weights of at least 10,000 are required; this means that the degree of conversion of the functional groups must be greater than 99% for a repeating unit with a molar mass of 100 g ($X_n = 100$). It is obvious that relatively few reactions will qualify in terms of this rigorous requirement because of side reactions.

Because this type of polymerization is a completely random process, with all molecules having equal probability of reacting, the *distribution of molecular weights* corresponds to the most *probable, or binomial, distribution*, which is related to the extent of polymerization as follows [11, p. 318].

$$W_x = xp^{x-1}(1-p)^2 \tag{6}$$

$$N_x = p^{x-1}(1-p) \tag{7}$$

where W_x is the weight fraction of x-mers (chains having x units) and N_x is the mole fraction of x-mers. This distribution function can be used to calculate M_w, the weight-average molecular weight, as $M_w = M_o \Sigma x W_x$. It can be shown that the foregoing summation leads to the relation

$$M_w = \frac{(1+p)}{(1-p)}(M_o) \tag{8}$$

which then means that

$$M_w / M_n = 1 + p \tag{9}$$

Hence the weight/number ratio of chain lengths in these systems undergoes a *steady increase with extent of reaction*, approaching an ultimate value of 2.

Thus, we see that polyaddition and polycondensation are characterized by the following features:

1. All molecules have equal probability of reacting.
2. The polymerization rates are essentially described by the concentrations and reactivity of the functional groups.
3. The chain lengths are monotonic functions of the extent of reaction and hence of time of reaction.
4. The attainment of high molecular weights requires a high degree of conversion ($p \to 1$).

In those cases where at least one of the monomers has *more than two* functional groups, the added feature of branching chains is introduced, eventually leading to the formation of molecular networks [11, p. 347], i.e., gelation. This,

of course, complicates the molecular size distribution but does not affect the kinetics of the polymerization.

The foregoing relationships of chain length to extent of reaction would then be expected to apply to such step polymerizations as are involved in the synthesis of poly(alkylene sulfides) from a dihalide and sodium polysulfide (polycondensation) or in the formation of the urethane polymers from glycols and diisocyanates (polyaddition). The polysulfide reaction is actually carried out in a suspension of the dihalide in an aqueous solution of the polysulfide, using a surfactant to stabilize the resulting polymer suspension.

The urethane polymers offer an interesting illustration of the characteristic molecular weights to be expected in this type of polymerization, which can be written as

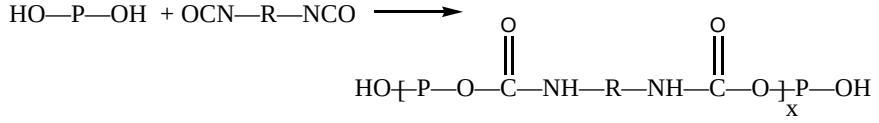

(10)

It should be noted that the P in Eq. (10) represents a low-molecular-weight polymer of a polyester or polyether type (MW 2000), so that this is really a "chain extension" reaction. It turns out that the reaction between an isocyanate group and a hydroxyl goes to a high conversion, i.e., to approximately 98% ($p = 0.98$). Hence the value of x in Eq. (10) is about 50, and the final molecular weight of the urethane polymer is about 100,000. Such high molecular weights are, of course, due solely to the fact that this reaction goes so far toward completion, i.e., where the reactive functional groups can be reduced to concentrations of the order of 10^{-2} M.

IV. CHAIN POLYMERIZATION BY FREE RADICAL MECHANISM

A. General Kinetics

The general kinetics for this mechanism [26] involve the usual three primary steps of any chain reaction, i.e., initiation, propagation, and termination, as shown below. Initiation generally occurs by the formation of free radicals through the homolytic dissociation of weak bonds (e.g., in peroxides or azo compounds) or by irradiation. Termination reactions for vinyl polymers can occur either by combination (coupling), by disproportionation, or by a combination of both reactions (discussed next).

Initiation

$$\mathrm{I} \xrightarrow{k_i} 2\,\mathrm{R}\cdot$$

$$\mathrm{R}\cdot + \mathrm{M} \longrightarrow \mathrm{R\text{-}M}\cdot$$

Propagation

$$M_j\cdot + M \xrightarrow{k_p} M_{j+1}\cdot$$

Termination

$$M_j\cdot + M_k\cdot \xrightarrow[(k_{tc} + k_{td})]{k_t} \text{dead chains}$$

where I = initiator, M = monomer, R = initial free radical, and $M_j\cdot$ = propagating free radical.

Combination

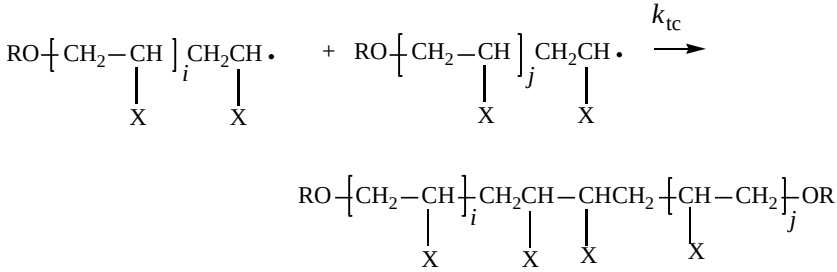

Disproportionation

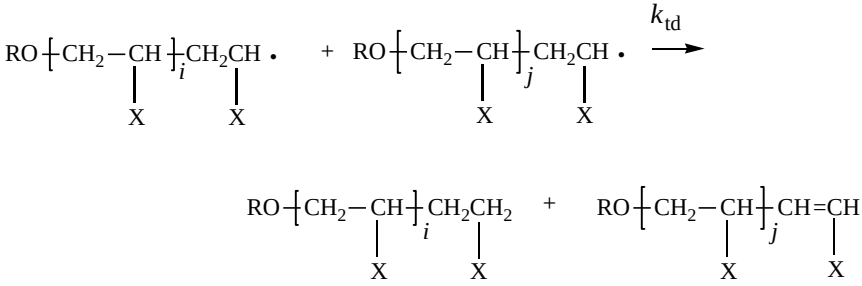

This sequence of steps then leads to the following simple kinetic treatment [26]:

Rate of initiation $R_i = 2k_i[I]$ (11)

Rate of propagation $R_p = k_p[M_j\cdot][M]$ (12)

Rate of termination $R_t = 2k_t[M_j\cdot]^2$ (13)

Assuming a *steady-state condition* where the rate of formation of radicals is equal to their rate of disappearance, i.e., $R_i = R_t$,

$$[M_j \bullet] = k_i^{1/2} k_t^{-1/2} [\mathrm{I}]^{1/2} \tag{14}$$

and

$$R_p = k_p k_i^{1/2} k_t^{-1/2} [\mathrm{M}][\mathrm{I}]^{1/2} \tag{15}$$

Equation (15) thus illustrates the dependency of the overall rate of polymerization on the concentrations of initiator and monomer. The half-power dependence of the rate on the initiator concentration appears to be a universal feature of the free radical mechanism and has been used as a diagnostic test for the operation of this mechanism.

Another important aspect of free radical polymerization is the dependency of the number-average degree of polymerization on initiator and monomer concentrations as shown in Eq. (16). Comparison with Eq. (15) shows that increasing the rate of initiation, by increasing the initiator concentration, increases the rate of polymerization but decreases the degree of polymerization, X_n, which corresponds to the number-average number of units per chain.

$$X_n = k_p k_i^{-1/2} k_t^{-1/2} [M][I]^{-1/2} \tag{16}$$

The general nature of free radical chain polymerization deserves some special attention. Because of the high reactivity of the propagating chain radical, it can only attain a very short lifetime, several seconds at best. This results in a very low stationary concentration of propagating chain radicals (about 10^{-8} M in a homogeneous medium). During this short lifetime, however, each growing radical may still have the opportunity to add thousands of monomer units. Hence the chain length of the macromolecules formed in these systems has no direct relation to the extent of reaction, i.e., to the degree of conversion of monomer to polymer [see Eq. (16) and Fig. 1]. At all times during the polymerization, the reaction mixture contains only monomer, a very small concentration of propagating chains, and dead (nonpropagating) polymer, the latter usually of high molecular weight.

To illustrate more clearly the nature of free radical polymerization, it is instructive to examine the values of the individual rate constants for the propagation and termination steps. A number of these rate constants have been deduced, generally using nonstationary-state measurements such as rotating sector techniques and emulsion polymerization [26]. Recently, the IUPAC Working Party on "Modeling of kinetics and processes of polymerization" has recommended the analysis of molecular weight distributions of polymers produced in pulsed-laser-initiated polymerization (PLP) to determine values of

TABLE I Propagation and Termination Rate Constants in Radical Polymerization[a]

Monomer	k_p at 60°C (liters mole^{-1} sec^{-1})	k_t at 60°C ($\times 10^{-7}$) (liters mole^{-1} sec^{-1})
Styrene	176 (340)[b]	3.6
Methyl methacrylate	367 (830)[c]	1.0
Methyl acrylate	2100	0.5
Vinyl acetate	3700	7.4
Butadiene	100 (320)[d]	~100 (700)[d]
Isoprene	50	—
Chloroprene	(1270)[e]	—

[a]Data taken from Refs. [30–32]; data in parentheses determined by pulsed-laser-initiated polymerization. [b]Ref [29], [c]Ref [33], [d]Ref [34], [e]Ref [35].

propagation rate constants [27, 28]. Illustrative values of propagation and termination rate constants are listed in Table I [29–35]. Thus, although the chain growth step can be seen to be a very fast reaction (several orders of magnitude faster than the rates of the step reactions of the end groups discussed in Section III), it is still several orders of magnitude slower than the termination step, i.e., the reaction of two radicals. It is this high ratio of k_t/k_p which leads to the very low stationary concentration of growing radicals (~10^{-8} M) in these systems.

Although the three individual steps which combine to make up the chain reaction act as the primary control of the chain lengths [see Eq. (16)], "chain transfer" reactions can occur whereby one chain is terminated and a new one is initiated, without affecting the polymerization rate: such reactions will also, of course, affect the chain length. Chain transfer usually involves the homolytic cleavage of the most susceptible bond in molecules of solvent, monomer, impurity, etc., by the propagating radical, e.g.,

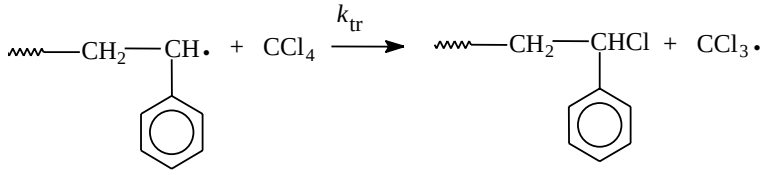

and can be designated as follows:

$$\text{Monomer transfer} \qquad M_j\bullet + M \xrightarrow{k_{trM}} M_j + M\bullet \tag{17}$$

$$\text{Solvent transfer} \qquad M_j\bullet + S \xrightarrow{k_{trS}} M_j + S\bullet \tag{18}$$

$$S\bullet + M \xrightarrow{k'_p} SM\bullet \tag{19}$$

Hence the chain length of the polymer being formed at *any given instant* can be expressed as the ratio of the propagation rate to the sum of all the reactions leading to termination of the chain as

$$X_n = \frac{k_p[M_j\bullet][M]}{(k_{tc} + 2k_{td})[M_j\bullet]^2 + k_{trM}[M_j\bullet][M] + k_{trS}[M_j\bullet][S]}$$

or

$$\frac{1}{X_n} = \frac{(k_{tc} + 2k_{td})R_p}{k_p^2[\mathrm{M}]^2} + \frac{k_{trM}}{k_p} + \frac{k_{trS}[\mathrm{S}]}{k_p[\mathrm{M}]} \tag{20}$$

where X_n is the number-average number of units per chain, k_{tc} the rate constant for termination by combination, and k_{td} the rate constant for termination by disproportionation.

B. Molecular Weight Distribution

The chain length distribution of free radical addition polymerization can also be derived from simple statistics. Thus, for polymer formed at any given instant, the distribution will be the "most probable" and will be governed by the ratio of the rates of chain growth to chain termination,

$$W_x = xp^{x-1}(1-p)^2 \tag{21}$$

where p is the probability of propagation, and $1 - p$ the probability of termination (by disproportionation or transfer). This expression is of course identical to Eq. (6), except for the different significance of the term p. Unlike Eq. (6), however, it expresses only the *instantaneous* chain length for an increment of polymer, not the cumulative value for the total polymer obtained.

From Eq. (21) it follows that the number- and weight-average chain lengths X_n and X_w are expressed by

$$X_n = \frac{1}{1-p} \quad \text{and} \quad X_w = \frac{1+p}{1-p} \sim \frac{2}{1-p} \tag{22}$$

as p must always be close to unity for high polymers. Hence it follows again that

$$X_w / X_n = 2 \tag{23}$$

The value of X_w/X_n for the *cumulative polymer* may, of course, be much higher, depending on the changes in the value of p with increasing conversion. It should be noted, however, that this is valid only where the growing chains ter-

minate by disproportionation or transfer, *not* by combination. It can be shown in the latter case [11, p. 335, 336] that the increment distribution is much narrower, i.e.,

$$X_w / X_n = 1.5 \tag{24}$$

Thus, in summary, the kinetics of free radical polymerization are characterized by the following features:

1. Rate is directly proportional to the half-power of the initiator concentration.
2. Molecular weight is inversely proportional to the half-power of initiator concentration.
3. The lifetime of the growing chain is short (several seconds) but a high molecular weight is obtained, leading to formation of high polymer at the outset of reaction.
4. No direct relation exists between extent of conversion and chain length.
5. Instantaneous chain length is statistical, but the cumulative value can be considerably broader because of changes in relative rates of propagation and termination.

C. Special Case of Diene Polymerization

As polydienes still constitute the backbone of the synthetic rubber industry, it is important to consider the special features which dienes exhibit in free radical polymerization. Despite the fact that this type of polymerization has played and is still playing the major role in industrial production of various polymers, it has never been successful in bulk or solution polymerization of dienes. This is an outcome of the kinetic features of the free radical polymerization of dienes, as indicated in Table I. Thus, the relatively high k_t/k_p ratio (as compared with the other monomers shown) leads to very low molecular weights and very slow rates for polydienes prepared in homogeneous systems, as illustrated in Table II. It can be seen from these data that even in the case of these thermal uncatalyzed polymerizations, where the molecular weight would be at a maximum compared with catalyzed systems, it is still too low by at least an order of magnitude. These systems are also complicated by a competitive Diels-Alder reaction, leading to low-molecular-weight compounds, i.e., "oils."

It is therefore not surprising that the early investigators saw no promise in this mechanism of polymerization of butadiene, isoprene, etc., either by pure thermal initiation or by the use of free radical initiators, such as the peroxides. Instead they turned to sodium polymerization, which, although also rather slow and difficult to reproduce, at least yielded high-molecular-weight rubbery polymers from the dienes. Later, in the 1930s, when emulsion polymerization was introduced, it was found that this system, even though it involves the free

TABLE II Thermal Polymerization of Dienes[a]

Temperature (°C)	Time (hr)	Isoprene			2,3-Dimethylbutadiene		
		Yield (%)		MW, rubber	Yield (%)		MW, rubber
		Oil	Rubber		Oil	Rubber	
85	100	7.9	16.3	4600	—	—	—
85	250	—	—	—	2.7	19.6	3500
85	900	—	35.3	5700	—	49.7	3500
145	12.5	54.7	15.6	4000	11.1	15.6	2100

[a]Data taken from Ref. [37].

radical mechanism, leads to both fast rates and high molecular weights, conducive to the production of synthetic rubber. The special features of emulsion polymerization which lead to such surprising results are discussed in Section V.

D. Controlled Radical Polymerization

There has been a revolution in free radical polymerization chemistry that began in the 1980s with the seminal patent of Solomon, Rizzardo, and Cacioli [38]. These scientists found that it was possible to obtain controlled radical polymerization of monomers such a styrene and alkyl (meth)acrylates by effecting free radical polymerization in the presence of stable nitroxyl radicals as shown below. It has been found that these controlled polymerizations carried out

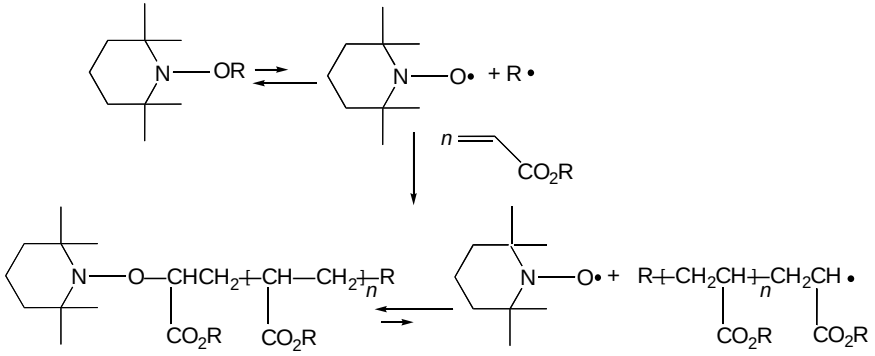

in the presence of stable nitroxyl radicals, such as the tetramethylpyridinyloxy radical (TEMPO) shown above, lead to the synthesis of polymers with con-

trolled molecular weight, narrow molecular weight distributions, end-group functionality, architecture, and block copolymer composition [38–42]. The key requirements for this type of controlled polymerization are (a) a thermally labile bond that undergoes homolysis reversibly to form reactive radicals capable of initiating or propagating polymerization of vinyl monomers, (b) simultaneous formation of a stable radical that rapidly and reversibly combines with propagating radicals but which does not add to vinyl monomers, and (c) an equilibrium constant between radicals and covalent, dormant species that favors the dormant species. In order for a system of this type to be useful, the ratio of the concentration of active radical species to dormant species must be less than 10^{-5} [43]. This implies that the majority of the lifetime of the chain is spent in the dormant stage. Successful systems must maintain an optimum amount of nitroxide such that polymerization can occur at an appreciable rate [44]. It should be noted that radical-radical coupling can still occur, but it is minimized by the low concentration of propagating radicals (e.g., 10^{-8} M). Because termination still occurs, it is obviously inappropriate to call these polymerizations living, although these types of controlled radical polymerizations are often referred to as living in the literature. The kinetics of the stable free radical polymerization are controlled by the persistent radical effect which has been clearly elucidated by Fischer [45, 46].

Careful and extensive investigations of these nitroxide-mediated polymerizations (also referred to as stable free radical polymerization) have established optimum conditions for controlled radical polymerization of a variety of vinyl monomers [47, 48]. Variables examined include the structure of the nitroxide and the presence of other additives to control spontaneous polymerization of monomers such as styrene. It is noteworthy that in place of alkoxyamine initiators, a mixture of a normal free radical initiator such as an azo compound or a peroxide can also be used.

The application of these procedures to 1,3-dienes has presented problems. The rates of polymerization were observed to decrease and then stop due to a buildup of excess free nitroxide [44]. An effective procedure for the controlled polymerization of isoprene at 145°C involved the addition of a reducing sugar such as glucose in the presence of sodium bicarbonate to react with the excess nitroxide [44]. After four hours, polyisoprene with $M_n = 21{,}000$ and $M_w/M_n = 1.33$ was obtained in 25% yield. The reaction of TEMPO-terminated polystyrene with either butadiene or isoprene resulted in the formation of the corresponding diblock copolymers that were characterized by ^{1}H NMR and SEC [49]. No evidence for either polystyrene or polydiene homopolymers was reported.

An alternative procedure to reduce the concentration of excess nitroxide radicals has been reported by Hawker and coworkers [50]. They used the initiator shown below to successfully effect the controlled polymerization of isoprene. It was reported that the corresponding nitroxide has α-hydrogens that can decompose via disproportionation, thereby preventing buildup of excess

nitroxide. Using this initiating/nitroxide system, it was possible to prepare a

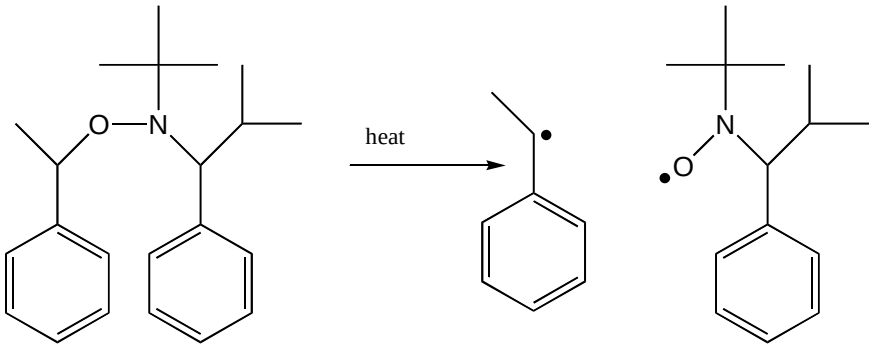

variety of polyisoprenes with controlled molecular weight, high 1,4 microstructure, and polydispersities that ranged from 1.07 for low molecular weights (e.g., M_n = 5,000) to 1.20 for number average molecular weights of 100,000. However, the required reaction conditions were 130°C and reaction times up to 48 hours. Well-defined copolymers of isoprene and styrene or (meth)acrylates were also prepared at 120°C ($M_n \approx$ 17,000; M_w/M_n = 1.1–1.2).

Several other methods for controlled radical polymerization have been developed and should be applicable to elastomer synthesis [47, 48]. One of the other most important systems for controlled radical polymerization is atom transfer radical polymerization (ATRP) [51]. A transition metal (Mt) catalyst participates in an oxidation-reduction equilibrium by reversibly transferring an atom, often a halogen, from a dormant species (initiator or polymer chain) as shown below.

$$P_n\text{—X} + \text{M}t^{\text{m}}(\text{ligand}) \rightleftharpoons P_n\cdot + \text{X-M}t^{\text{m+1}}(\text{ligand})$$

$$P_n\cdot \xrightarrow{k_p[\text{M}]} P_n\cdot$$

Although a variety of transition metal salts are effective, copper salts have been most extensively investigated.

V. EMULSION POLYMERIZATION

A. Mechanism and Kinetics

Polymerization in aqueous emulsions, which has been widely developed technologically, represents a special case of free radical chain polymerization in a heterogeneous system [52–58]. Most emulsion polymerization systems

comprise a water-insoluble monomer in water with a surfactant and a free radical initiator. Although it might be thought that polymerization of water-insoluble monomers in an emulsified state simply involves the direct transformation of a dispersion of monomer into a dispersion of polymer, this is not really the case, as evidenced by the following features of a true emulsion polymerization:

1. The polymer emulsion (or latex) has a much smaller particle size than the emulsified monomer, by several orders of magnitude.
2. The polymerization rate is much faster than that of the undiluted monomer, by one or two orders of magnitude.
3. The molecular weight of the emulsion polymer is much greater than that obtained from bulk polymerization, by one or two orders of magnitude.

It is obvious from the foregoing facts that the mechanism of emulsion polymerization involves far more than the mere bulk polymerization of monomer in a finely divided state. In fact, the very small particle size of the latex, relative to that of the original monomer emulsion, indicates the presence of a special mechanism for the formation of such polymer particles.

The mechanism of emulsion polymerization, as originally proposed by Harkins [59], can best be understood by examining the components of this system, as depicted in Fig. 2, for a typical "water-insoluble" monomer such as styrene (solubility = 0.07 g/L [60]). The figure shows the various loci in which monomer is found, and which compete with each other for the available free radicals. Thus, in the initial stages, the monomer is found in three loci: dissolved in aqueous solution, as emulsified droplets, and within the soap micelles. Both the dissolved monomer and the relatively large monomer droplets represent minor loci for reaction with the initiator radicals (except, of course, in the case of highly water-soluble monomers). The large number of soap micelles containing imbibed monomer, however, represents a statistically important locus for initiation of polymerization. It is thus not surprising that most of the polymer chains are generated within the monomer-swollen soap micelles. The very large number ($\sim 10^{15}$/ml) of very small polymer particles thus formed which are stabilized by adsorbing monolayers of soap deplete the available molecularly dissolved soap, thus destroying the soap micelles at an early stage of the polymerization (~10% conversion in the usual recipe). As all the available soap is distributed, and redistributed, over the surface of the growing particles, the amount of soap is the main factor controlling latex particle size.

During the second stage of the emulsion polymerization, therefore, the loci for available monomer consist of the dissolved monomer, the free monomer droplets, and the monomer imbibed by the numerous polymer particles. As before, the first two of these loci make a minor contribution, whereas the polymer-monomer particles provide a major locus for reaction with the initiator radicals diffusing from the aqueous phase. The major portion of the

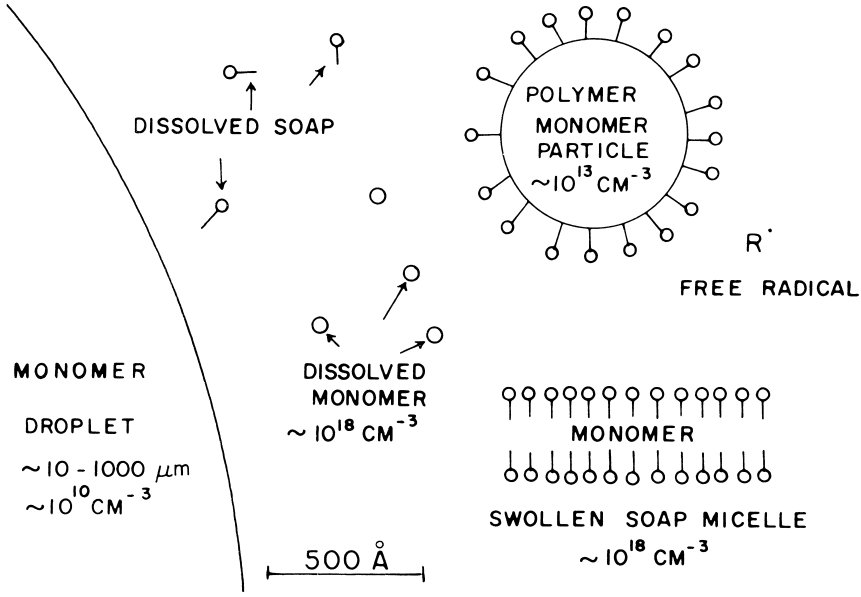

FIGURE 2 Loci in mechanism of emulsion polymerization.

polymerization reaction apparently occurs within this large number of latex particles which are isolated from each other by electrostatic repulsion and kept saturated [61] with monomer diffusing from the monomer droplets. It is this aspect which leads to the unique characteristics of this system [62]. Thus, once an initiator radical enters a polymer monomer particle and initiates a chain, the latter must continue to propagate with the available monomer until *another* radical enters the same particle. In this way, the rate of chain termination is actually controlled by the *rate of entry* of radicals into the particles, and this generally increases the lifetime of the growing chains, and hence the chain length. Furthermore, because the growing chains are all located in *different* particles, they are unable to terminate each other, leading to a higher *concentration* of growing chains and a hence faster rate.

In this way, emulsion polymerization systems can simultaneously achieve a much faster rate and a much higher molecular weight than homogeneous systems. A comparison of the kinetic features of bulk and emulsion polymerization of styrene is given in Table III. It is obvious at once that the main difference lies in the fact that the emulsion system is capable of raising the steady-state concentration of growing chain radicals by two to three orders of magnitude but *not* at the expense of increasing the termination rate which occurs in homogeneous solution (see Eq. [16])!

The situation described earlier, i.e., where radicals entering individual latex particles successively initiate and terminate growing chains, is referred

TABLE III Comparison of Free Radical Polymerization Methods of Styrene

	Homogeneous	Emulsion
Monomer concentration (M)	5	5[a]
Radical concentration (M)	10^{-8}	10^{-6}
Rate of polymerization at 60°C (%/hr)	~2	100
Molecular weight (M_n)	10^5	10^7

[a]Within latex particles.

to as *ideal emulsion polymerization*, as defined by the Smith-Ewart theory [62]. Under these conditions, the concentration of growing chains per unit volume of latex is easily predictable, because at any given time, *half of the particles will contain a growing chain*. In other words, the number of growing chains will be one-half the number of particles. As the latter is of the order of 10^{18} per liter, the concentration of growing chains is of the order of 10^{-6} M compared with 10^{-8} M for homogeneous polymerization systems. Because such growing chains are in an environment rich in monomer (within the monomer-polymer particles), it is not surprising that emulsion polymerization rates are one or two orders of magnitude higher than those of bulk polymerization, as shown in Table III. Furthermore, this high radical concentration does not affect the radical lifetime, i.e., the chain size, which is governed solely by the availability of another free radical for termination and, thus, by the period between successive entries of radicals into particles. For a given rate of initiation, the time between radical entry depends on the number of latex particles; i.e., the radical lifetime (and molecular weight) increases with increasing numbers of particles. According to the theory of Smith and Ewart [62], the number of polymer particles depends on both the initiator concentration and the surfactant concentration,

$$N \propto [I]^{2/5}[S]^{3/5} \tag{25}$$

where $[I]$ is the concentration of initiator and $[S]$ is the concentration of surfactant.

The foregoing situation, of course, holds only for the ideal case, as defined earlier. If the growing chain within the latex particle undergoes some side reaction which transfers the radical activity out of the particle before the next radical enters, or if termination is not rapid when two radicals occupy the same particle, then the number of growing chains at any given time will be, respectively, either smaller or larger than one-half the number of particles. The latter case (more than one radical per particle) can occur, for example, if the particle size is sufficiently large and the termination rate too slow. The rate and

molecular weight will then also be governed by other considerations than the interval between entry of successive radicals. Diagnostically, these situations can be distinguished from the ideal case by the effect of added initiator on the rate of polymerization after formation of particles is complete. Thus, in either case, an increase in initiator concentration will lead to a faster rate of entry of radicals into particles and hence an increase in the number of radicals per particle, leading to an increase in polymerization rate. In contrast, in the ideal case, an increase in frequency of radical entries into particles should not affect the rate, as the particles will still contain a radical only half the time, even though the periods of chain growth will be shorter, leading to a lower molecular weight.

The ideal case of the Smith-Ewart treatment actually proposes a rather elegant method for obtaining the absolute value of the propagation rate constant k_p from emulsion polymerization systems, as shown in Eq. (26), where N is the number of particles per unit volume.

$$R_p = k_p[M]N/2 \tag{26}$$

Equation (26) leads to a solution for k_p from available knowledge of the rate R_p, the concentration of monomer in the monomer-polymer particles $[M]$, and the number of particles, N. This method has been applied to several monomers and has been especially useful in the case of the dienes, where the classical method of photoinitiation poses difficulties. Some of these results are shown in Table IV in the form of the usual kinetic parameters. The results obtained for styrene by photoinitiation techniques are included for comparison. It can be seen that the agreement is remarkably good, considering the widely different experimental methods used. Recent studies of the emulsion polymerization of butadiene have shown that the rate constant for propagation is even higher than previously estimated (see Table I) [34].

The data in Table IV provide evidence that the slow rates and low molecular weights obtained in homogeneous free radical polymerization of these dienes are *not* due to a low rate constant for propagation but rather must be caused by a high rate constant for termination (as indicated in Table I). Hence, under the special conditions of emulsion polymerizations, where the termina-

TABLE IV Propagation Rate Constants from Emulsion Polymerization

Monomer	k_p (liters mole^{-1} sec^{-1}) at 60°C	E_p (kcal mole^{-1})	A_p ($\times 10^{-7}$) (liters mole^{-1} sec^{-1})	Ref.
Butadiene	100	9.3	12	[31]
Isoprene	50	9.8	12	[31]
2,3-Dimethylbutadiene	120	9.0	9	[63]
Styrene	280	7.9	4	[31]
Styrene	176	7.8	2.2	[30]

tion rate is controlled by the rate of entry of radicals into particles, it becomes possible to attain both faster rates and higher molecular weights. It is this phenomenon which led to the rise of the emulsion polymerization system for the production of diene-based synthetic rubbers.

B. Styrene-Butadiene Rubber

1. Kinetics and Molecular Weights

The most successful method developed for the production of a general-purpose synthetic rubber was the emulsion copolymerization of butadiene and styrene (SBR), which still represents the main process in use today [54, 64–69]. The general principles of copolymerization will be discussed in a later section, but it is instructive at this point to examine the other main features of this system. The types of recipes used are seen in Table V [67]. The recipes shown are to be considered only as typical, as they are subject to many variations. It should be noted that the initiator in the 50°C recipe (hot rubber) is the persulfate, whereas in the 5°C recipe (cold rubber) the initiator consists of a redox system comprising the hydroperoxide-iron(II)-sulfoxylate-EDTA. In the latter case, the initiating radicals are formed by the reaction of the hydroperoxide with the ferrous iron, whose concentration is controlled by the EDTA complexing agent; the sulfoxylate is needed to convert the oxidized ferric(III) back to ferrous iron. The phosphate salt serves as a stabilizing electrolyte for the latex.

In both recipes, the thiol acts as a chain transfer agent to prevent the molecular weight from attaining the excessively high values possible in emulsion polymerization systems (see Table VI). It acts in an analogous fashion to the solvent in Eqs. (18) and (19), except that the sulfur-hydrogen bond is extremely susceptible to attack by the growing chain radical, which is thus terminated by a hydrogen atom, forming the RS**.** radical which initiates growth of a new chain:

$$\mathrm{P}\bullet + \mathrm{RS-H} \xrightarrow{k_{\mathrm{tr}}} \mathrm{P-H} + \mathrm{RS}\bullet \tag{27}$$

$$\mathrm{RS}\bullet + \mathrm{M} \xrightarrow{k_j'} \mathrm{RS-M}\bullet \tag{28}$$

These thiols, which are known as "regulators," have transfer constants greater than 1, e.g., k_{tr}/k_p may be 3–4, so that only a small proportion is needed to reduce the molecular weight from several million to several hundred thousand. Diene-based polymers can undergo crosslinking reactions during the polymerization, which leads to the formation of insoluble "gel" rubber when the molecular weight becomes too high. Hence, thiol is used as "modifier" to prevent gel formation and keep the rubber processible. It is also necessary to stop the reaction at intermediate levels of conversion to minimize undesirable gel formation (see Table VII).

TABLE V Typical SBR Emulsion Polymerization Recipes[a]

	SBR-1000[b]	SBR-1500[b]
Polymerization temperature (°C)	50	5
Time (hr)	12	12
Conversion (%)	72	60–65
Ingredients		
Butadiene	71	71
Styrene	29	29
Water	190	190
Soap (fatty or rosin acid)	5	4.5–5
Potassium persulfate	0.3	—
n-Dodecanethiol	0.5	—
t-Dodecanethiol	—	0.2
p-Menthane hydroperoxide[c]	—	0.08
Trisodium phosphate ($Na_3PO_4 \cdot 10H_2O$)	—	0.5
Ferrous sulfate ($FeSO_4 \cdot 7H_2O$)	—	0.4
Sodium formaldehyde sulfoxylate	—	0.10
Tetrasodium salt of ethylenediamine tetraacetic acid (EDTA)	—	0.06

[a]Parts by weight. Data taken from Ref. [67].
[b]Commercial grade numbers assigned by the International Institute of Synthetic Rubber Producers to "hot" and "cold" SBR, respectively.
[c]Or pinane hydroperoxide.

TABLE VI Typical Properties of Emulsion-Polymerized SBR[a]

Property	Hot SBR	Cold SBR
Styrene content	24	24
Molecular weight		
Viscosity average	$1.5–4.0 \times 10^5$	2.8×10^5
Weight average	—	5×10^5
Number average	$0.3–1.0 \times 10^5$	$1.1–2.6 \times 10^5$

[a]Data taken from Ref. [67].

Shortly after Word War II, the American synthetic rubber industry began production of "cold" SBR, from which, it was found, superior tire rubber, especially as regards tread wear, could be prepared. Subsequent studies showed that the reduction in temperature from 50 to 5°C had little or no effect on the microstructure of the polydiene units (*cis*-1,4 versus *trans*-1,4 versus 1,2), or on the comonomer composition, but did exert a marked influence on the molecular weight distribution (Table VI). It was also shown [70] that the

TABLE VII Crosslinking Parameters for Polybutadiene[a]

Temperature (°C)	Relative crosslinking rate, r_x ($\times 10^4$)[b]	χ_w of primary chains at gel point ($\times 10^4$)
60	1.98	2.15
50	1.36	3.13
40	1.02	4.18
0 (cal.)	0.16	26.3

[a]Data taken from Ref. [20].
[b]$r_x = k_x/k_p$, where k_x is the crosslinking rate constant and k_p is the propagation rate constant.

crosslinking reaction i.e., addition of growing chains to polymer double bonds (mainly with 1,2 side chain units), was substantially reduced at these lower temperatures, thus reducing the tendency for gel formation at any given molecular weight.

Table VII shows the maximum molecular weights of polybutadiene attainable at different polymerization temperatures, prior to gelation, expressed as the critical weight-average chain length, x_w, of the primary chains at the gel point. Thus it can be seen that it is possible to increase the chain length by a factor of 9, without forming gel, by decreasing the polymerization temperature from 50 to 0°C. Hence, the amount of thiol chain transfer agent can also be reduced, and this improves the overall chain length distribution by avoiding the formation of the very low molecular weight fraction which results from the rapid reaction of the thiol in the early stages of the polymerization. Furthermore, this possibility of producing gel-free higher molecular weight SBR at reduced polymerization temperature enabled the preparation of a high Mooney viscosity (~100) polymer which could be plasticized by low-cost petroleum oils ("oil-extended" rubber), and still retain its advantageous mechanical properties. As a result, the cold SBR process accounts for more than 85% of the emulsion SBR produced [68].

2. Chain Microstructure

As might be expected, the emulsion polymerization system does not alter the basic mechanism of free radical polymerization as regards the chain unit structure. The latter is, of course, independent of the type of free radical initiator used, in view of the "free" nature of the growing chain end radical. The temperature of polymerization does exert some influence, as shown by the data in Table VIII, but not to a very great extent. It can be seen that the 1,2 side-chain vinyl content is rather insensitive to the temperature, whereas the *trans*-1,4 content increases with decreasing temperature, at the expense of the *cis*-1,4 content. The latter almost vanishes, in fact, at low temperatures and

TABLE VIII Chain Structure of Emulsion Polybutadiene and SBR[a]

Polymerization temperatures (°C)	Isomer (wt%)		
	cis-1,4	*trans*-1,4	1,2
		POLYBUTADIENE	
–33	5.4	78.9	15.6
5	13.0	69.9	16.5
50	19.0	62.7	18.8
70	20.8	59.4	19.8
		SBR	
–33	5.4	80.4	12.7
5	12.3	71.8	15.8
50	18.3	65.3	16.3
70	20.0	63.0	17.3
100	22.5	60.1	17.3

[a]Data taken from Ref. [71].

the polymer then attains its highest *trans*-1,4 content of about 80%. Hence this type of polybutadiene is sufficiently stereoregular to undergo a substantial amount of crystallization on cooling [72, 73]. However, the introduction of the styrene comonomer is sufficient to destroy the chain regularity necessary for crystallization. Furthermore, it is the high-*cis*-1,4 polybutadiene which is desirable and not the *trans*-1,4 form, since the latter has a crystalline melting point of about 150°C and is not an elastomer at ambient temperature. As can be seen from Table VIII, the possibility of attaining a high *cis*-1,4 content at a reasonably high polymerization temperature is quite remote.

Hence, it appears that these minor effects of temperature on the microstructure of the butadiene units cannot be expected to have any real influence on the properties of SBR.

C. Emulsion Polymerization of Chloroprene

1. Kinetics

The only other diene that has been used extensively for commercial emulsion polymerization is chloroprene (2-chloro-1,3-butadiene) [64, 74–77]. The chlorine substituent apparently imparts a marked reactivity to this monomer, since it polymerizes much more rapidly than butadiene, isoprene, or any other dienes (see Tables I and IV); $k_p(35°C) = 595\,L\,mol^{-1}\,sec^{-1}$ [35]. In fact, chloroprene is even more susceptible to spontaneous free radical polymerization than styrene, and requires a powerful inhibitor for stabilization [78]. It poly-

TABLE IX Basic Recipe for Neoprene GN[a]

Ingredient	Parts by weight
Chloroprene	100
Water	150
N wood rosin	4
Sulfur	0.6
Sodium hydroxide	0.8
Potassium persulfate	0.2–0.1
Latex stabilizer[b]	0.7

[a]Temperature, 40°C; time, several hours; conversion, 90%. Data taken from Ref. [81].
[b]A sodium salt of naphthalenesulfonic acid-formaldehyde condensation product.

merizes extremely rapidly in emulsion systems, so that its rate must be carefully controlled.

Various recipes [79, 80] can be used for emulsion polymerization of chloroprene, with potassium persulfate as a popular initiator. A basic recipe [81] which illustrates several interesting features about this monomer is shown in Table IX. Two aspects of this recipe are especially noteworthy: the use of a rosin soap, and the presence of elemental sulfur. Rosin soaps are notorious as retarders in emulsion polymerization, as are most *polyunsaturated* fatty acids. Yet complete conversion can be attained within a few hours. With *saturated* fatty acid soaps, the reaction is almost completed [79] within *one hour* at 40°C!

Sulfur copolymerizes [81, 82] with the chloroprene, forming di- and polysulfide linkages in the chain [as illustrated in Eq. (29)]. The latex is

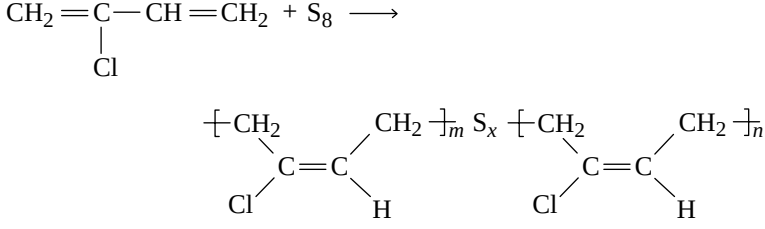

(29)

then treated with the well-known vulcanization accelerator, tetraethyl thiuram disulfide, which, by sulfur–sulfur bond interchange, degrades the crosslinked polychloroprene "gel" and renders it soluble and processible as schematically shown in Eq. (30). In this way it serves a purpose analogous to the thiol chain

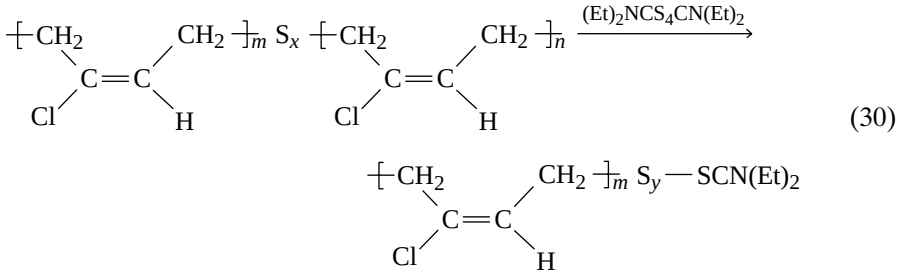

(30)

transfer agents in SBR polymerization. As a matter of fact, the newer grades of polychloroprene are prepared [75, 77, 83] with the use of thiols and other chain transfer agents. The thiols have been found [80] to yield narrower molecular weight distributions for chloroprene than for butadiene or isoprene, due to their much slower rate of disappearance in the presence of chloroprene. These mercaptan grades represent the most common, standard grades [77].

2. Chain Structure

Another feature of the emulsion polymerization of chloroprene that distinguishes it from that of the other dienes is the fact that it leads to a predominantly *trans*-1,4 chain microstructure. Thus, even at ambient polymerization temperature, the polychloroprene contains over 90% *trans*-1,4 units, as shown in Table X, which illustrates the effect of polymerization temperature on stereoregularity of the chain [87]. As expected, lower polymeriza-

TABLE X Effect of Polymerization Temperature on Polychloroprene Chain Microstructure[a]

Temperature (°C)	Isomeric chain microstructure (%)					
	trans-1,4		Isomerized			
	Total	Inverted[b]	1,2	1,2[c]	3,4	*cis*-1,4
–150	~100	2.0	—	—	—	—
–40	97.4	4.2	0.8	0.6	0.5	0.8
–20	97.1	4.3	0.9	0.6	0.5	0.8
0	95.9	5.5	1.2	1.0	1.1	1.8
20	92.7	8.0	1.5	0.9	1.4	3.3
40	90.8	9.2	1.7	0.8	1.4	5.2
90	85.4	10.3	2.3	0.6	4.1	7.8

[a]Data taken from Refs. [75, 84–86].
[b]4,1 enchainment.
[c]—CH_2—C(Cl)=$CHCH_2$Cl.

tion temperatures lead to a more stereoregular *trans*-1,4-polychloroprene. Because of the higher crystal melting point of the *trans*-1,4-polychloroprene (T_m = 105°C [88]), as compared with that of the *cis*-1,4-polyisoprene in Hevea rubber (~20°C), even the polymer containing as little as 80% *trans* units crystallizes readily on cooling, or on stretching. The melting point of emulsion polychloroprene is generally in the range of 40–50°C [75]. Hence emulsion polychloroprene is the only latex polymer which resembles natural rubber, in that it is sufficiently stereoregular to exhibit strain-induced crystallization [74, 75]. This, then, results in high tensile strength in gum vulcanizates, without the need of reinforcing fillers, just as in the case of Hevea rubber. This makes possible the use of polychloroprene in a variety of gum rubber products, endowing them with superior oil and solvent resistance (because of its polarity), as well as high strength.

VI. COPOLYMERIZATION

A. Kinetics

Copolymerization involves the simultaneous chain polymerization of a mixture of two or more monomers [89–92]. Aside from the general kinetic considerations which govern these chain reactions, as described earlier, there is imposed an additional feature, i.e., the relative participation of the different monomers during the growth of the chain. This new parameter is most important, since it controls the composition of the copolymer. Systems involving more than two monomers are difficult to resolve in this respect, but it has been found possible to treat the case of a pair of monomers with relative ease [91, 93–95].

In the chain addition polymerization of *two* monomers, *regardless of the mechanism involved*, the growing chain always must make a choice of reacting with one of the two monomers. Furthermore, there are *two* kinds of growing chains, depending on which type of monomer unit occupies the growing end. Thus, *four* types of propagation steps can be written as follows for any chain copolymerization of two monomers assuming that the reactivity of the chain end depends only on the chain end monomer unit (terminal model [89]):

$$M_1^* + M_1 \xrightarrow{k_{11}} M_1^* \tag{31}$$

$$M_1^* + M_2 \xrightarrow{k_{12}} M_2^* \tag{32}$$

$$M_2^* + M_2 \xrightarrow{k_{22}} M_2^* \tag{33}$$

$$M_2^* + M_1 \xrightarrow{k_{21}} M_1^* \tag{34}$$

where M_1^* and M_1 refer to the growing chain and the monomer, respectively, as before, while the *subscripts* refer to the two kinds of monomer in the mixture. It can be seen that these four propagation reactions lead to *four* propagation rate constants, as shown. Hence the rate of consumption of each monomer may be expressed by the following equations:

$$d[M_1]/dt = k_{11}[M_1^*][M_1] + k_{21}[M_2^*][M_1] \tag{35}$$

$$d[M_2]/dt = k_{12}[M_1^*][M_2] + k_{22}[M_2^*][M_2] \tag{36}$$

Since it is the *relative rate* of consumption of the two monomers which will decide the composition of the chain, it can be expressed by dividing Eq. (35) by Eq. (36) leading to Eq. (37).

$$\frac{d[M_1]}{d[M_2]} = \frac{k_{11}[M_1^*][M_1] + k_{21}[M_2^*][M_1]}{k_{12}[M_1^*][M_2] + k_{22}[M_2^*][M_2]} \tag{37}$$

It is obvious at once that Eq. (37) is quite intractable for direct use. However, it is possible to simplify it considerably by utilizing the "steady-state" treatment, analogous to the one previously described. This is done by assuming the rate of *Eq.* (*32*) *to be equal to that of Eq.* (*34*), and this leads to the equivalence

$$[M_2^*] = \left(\frac{k_{12}}{k_{21}}\right)[M_1^*]\frac{[M_2]}{[M_1]}$$

which, when inserted into Eq. (37), yields Eq. (38), after appropriate rearrangements are made,

$$\frac{d[M_1]}{d[M_2]} = \frac{[M_1]}{[M_2]}\left[\frac{r_1[M_1] + [M_2]}{r_2[M_2] + [M_1]}\right] \tag{38}$$

where $r_1 = k_{11}/k_{12}$ and $r_2 = k_{22}/k_{21}$. The parameters r_1 and r_2 are known as the monomer reactivity ratios, since they express the *relative* reactivity of each of the two kinds of growing chain ends with their "own" monomer as compared with the "other" monomer. They may in fact be considered as expressing the "homopolymerization" tendency of each type of monomer relative to crossover with the comonomer.

Equation (38), which relates the instantaneous composition of the copolymer ($d[M_1]/d[M_2]$) to the prevailing monomer concentrations, can be used to determine the values of r_1 and r_2. Many such values have been recorded [91, 94, 96, 97]. Typical values of these parameters for styrene copolymerizations are shown in Table XI, which illustrates the wide variations that prevail. The *relative reactivity* actually expresses the relative reactivity of each of the monomers shown toward the styrene radical compared to the reaction with styrene monomer.

TABLE XI Monomer Reactivity Ratios for Free Radical Copolymerizations with Styrene (M_1)[a]

Monomer (M_2)	r_1	r_2	Relative reactivity ($1/r_1$)
Maleic anhydride	0.097	0.001	10.3
2,5-Dichlorostyrene	0.268	0.810	3.73
Methyl methacrylate	0.585	0.478	1.71
Methyl acrylate	0.871	0.148	1.15
Vinylidene chloride	1.839	0.087	0.54
Diethyl maleate	6.07	0.01	0.16
Vinyl acetate	18.8	0.02	0.05

[a]Data taken from Ref. [96].

Thus, the r_1 and r_2 values permit some conclusions about the expected composition of the copolymer obtained at any given monomer ratio.

For example, it can be deduced from Table XI that a copolymer of styrene and maleic anhydride ($r_1 r_2 \Rightarrow 0$) would be strongly "alternating" [90] , since it would be *improbable* to have a sequence of two styrene unit, and highly improbable to have a sequence of two maleic anhydride units. Also, it would obviously be extremely difficult to prepare a copolymer of styrene and vinyl acetate, since the latter monomer would be virtually excluded from the styrene polymerization.

It is also obvious, from Eq. (38), that the copolymer composition would not necessarily correspond to the comonomer charge, depending on the values of r_1 and r_2. A desirable system would, of course, be one in which this were the case, i.e., where the comonomers enter into the copolymer in the ratio of their concentrations; i.e., where

$$\frac{d[M_1]}{d[M_2]} = \frac{[M_1]}{[M_2]} \tag{39}$$

This is defined as an "azeotropic" copolymerization [90], by analogy to the distillation of two miscible liquids. Equation (37) would apply under the conditions where

$$\frac{r_1[M_1]+[M_2]}{r_2[M_2]+[M_1]} = 1 \tag{40}$$

and this would be valid, for example, where $r_1 = r_2 = 1$. In that case, Eq. (39) could apply for *all charge ratios*, i.e., the two types of growing chains show no particular preference for either of the two monomers; this is described as a *random copolymerization* [90]. Also Eq. (40) would be valid when $r_1 = r_2$ and

$[M_1] = [M_2]$, i.e., an azeotropic copolymerization would result *only at equimolar* charge ratios. *In general*, Eq. (40) is valid when

$$\frac{[M_1]}{[M_2]} = \frac{(r_2 - 1)}{(r_1 - 1)} \tag{41}$$

This means that any copolymerization will be of an azeotropic type at the particular comonomer charge ratio indicated by Eq. (41). However, it also means that an azeotropic copolymerization is only possible when *both* r_1 and r_2 either greater than 1 or less than 1.

It is important to emphasize that this kinetic treatment is valid for any chain polymerization mechanisms, i.e., free radical, cationic, anionic, and coordination. However, in the case of the ionic mechanisms, the type of initiator used and the nature of the solvent medium may influence the r_1 and r_2 values. This is due to the fact that the growing chain end in ionic systems is generally associated with a counterion, so that the structure and reactivity of such chain ends can be expected to be affected by initiator and the solvent. This will be discussed in Section VIII C.

B. Emulsion Copolymerization of Dienes

The three cases which involve copolymerizations leading to commercial synthetic rubbers are styrene-butadiene (SBR), butadiene-acrylonitrile (NBR), and chloroprene with various comonomers.

1. Styrene-Butadiene (SBR)

A large number of studies have been made of the reactivity ratios in this copolymerization, both in homogeneous and emulsion systems, and the average *r* values have been computed [69, 98, 99] for butadiene and styrene, respectively, as

$$r_B = 1.6, \qquad r_S = 0.5$$

These values apply to solution and emulsion polymerization, presumably because neither monomer is particularly soluble in water, and both are quite insensitive to temperature. It appears, therefore, that the butadiene must enter the chain substantially faster than its charging ratio, and that each increment of polymer formed contains progressively more styrene. This is confirmed by the change in composition of the copolymer with conversion, as shown in Table XII. It can be seen that, at high conversion, the increment, or differential, composition becomes quite high in styrene content with concomitant loss of rubbery properties, even though the cumulative, or integral, composition still shows a low styrene content. This indicates the advisability of stopping the reaction at conversions not much higher than 60% [64].

TABLE XII Comonomer Composition of SBR[a]

Conversion (%)	Styrene in copolymer (wt%)	
	Differential	Integral
0	17.2	—
20	18.8	17.9
40	20.6	18.7
60	23.3	19.7
80	29.5	21.2
90	36.4	22.5
95	45.0	—
100	(100)	(25.0)

[a]Charge weight ratio, 75/25 butadiene/styrene; 50°C. Data taken from Ref. [99].

It should be noted, too, that the r values for this system do not permit an azeotropic polymerization, as predicted by Eq. (39). With respect to the distribution of styrene monomer units in the copolymer, the monomer reactivity ratio product, $r_B r_S = 0.8$, is close to a value of 1.0, which would correspond to an "ideal" copolymerization [90] which would correspond to a random distrubution of styrene units along the chain. For an "ideal" copolymerization, the relative rates of incorporation of the two monomers are independent of the chain end unit as predicted by Eq. (42).

$$r_B = \frac{1}{r_S} \qquad \text{therefore} \quad \frac{k_{BB}}{k_{BS}} = \frac{k_{SB}}{k_{SS}} \tag{42}$$

It is reported that the number average number of styrene units in a sequence is 1.2 as determined by high resolution gel permeation chromatography of ozonolysis products [100]. The observed sequence distribution of monomer units was in accord with calculated values based on the monomer reactivity ratios [101].

2. Butadiene-Acrylonitrile (Nitrile Rubber)

According to Hofmann [102], the reactivity ratios of this pair of monomers at 50°C in *emulsion* polymerization are

$$r_B = 0.4, \qquad r_{AN} = 0.04$$

and they decrease somewhat at lower temperatures, but not to a great extent. These ratios are no doubt influenced by the marked water solubility of the acrylonitrile compared to that of butadiene.

The foregoing *r* values lead to the following situation. In accordance with Eq. (39), an azeotropic copolymer is formed when the acrylonitrile charge is

35 to 40% by weight (or by mole), so that a constant composition is maintained throughout the polymerization. If the acrylonitrile charge is *below* this value, the initial copolymer is relatively rich in acrylonitrile, which progressively *decreases* with increasing conversion. However, if the acrylonitrile charge is higher than the "azeotrope," the initial copolymer contains less acrylonitrile than charged, but the acrylonitrile content *increases* with conversion. Since the commercial nitrile rubbers have nitrile contents from 10 to 40%, these considerations have a very practical significance. With respect to the distribution of comonomer units in the copolymer, the monomer reactivity ratio product, $r_B r_{AN} = 0.016$, is close to zero, which would correspond to an alternating distribution of comonomer units [90].

3. Chloroprene

Polychloroprene is generally prepared commercially as a homopolymer, although small amounts of a comonomer are included in several grades of these elastomers. There are two good reasons for the paucity of chloroprene-based copolymers. In the first place, the homopolymer, as stated previously, has a high *trans*-1.4 chain structure and is therefore susceptible to strain-induced crystallization, much like natural rubber, leading to excellent tensile strength. It also has other favorable mechanical properties. Furthermore, chloroprene is *not* very susceptible to copolymerization by the free radical mechanism, as indicated by the r values in Table XIII. Thus, except for 2,3-dichloro-1,3-butadiene, chloroprene does not efficiently undergo copolymerization with other monomers. Hence, it is not surprising that the few copolymers of chloroprene available commercially contain only minor amounts of comonomers, which are included for their moderate effects in modifying the properties of the elastomers.

TABLE XIII Monomer Reactivity Ratios in Copolymerization of Chloroprene[a]

Monomer M_2	r_1	r_2
Styrene	5.98	0.025
Isoprene	2.82	0.06
Acrylonitrile	5.38	0.056
Methyl methacrylate	6.33	0.080
2,3-Dichloro-1,3-butadiene	0.31	1.98

[a]Data taken from Refs. [96, 103].

VII. Chain Polymerization by Cationic Mechanism

A. Mechanism and Kinetics

In these chain addition reactions, the active species is cationic in nature, initiated by strong acids, either of the protic or Lewis variety [21, 104–111]. Since most of these ionic polymerizations are carried out in nonaqueous solvents with low dielectric constants [109], it is unlikely that the active species is a "free" ion, analogous to a free radical. A multiplicity of active species may be involved as propagating species as shown below by the spectrum of cationic species, one or more of which may be involved as active propagating species, especially in more polar solvents [112]. Unfortunately, very little information

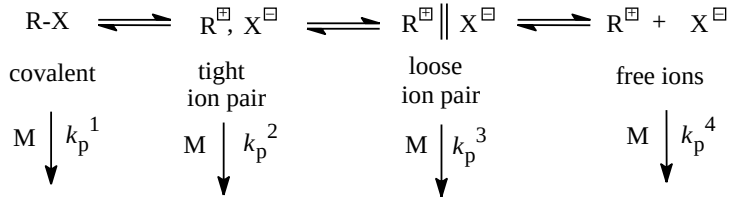

is available about the exact nature of the propagating species in cationic systems. This is mainly due to the inherent experimental difficulties, caused by high reactivity and sensitivity to impurities, especially to traces of water.

The most common initiators of cationic polymerization are Lewis acids, such as $AlCl_3$, BF_3, $SnCl_4$, and $TiCl_4$, although strong protic acids such as H_2SO_4 may also be used. Cationic polymerization is restricted to vinyl monomers with electron-donating or electron-delocalizing substituents, e.g., isobutylene, vinyl alkyl ethers, vinyl amines, styrene, and other conjugated hydrocarbons. These polymerizations are characterized by rapid rates at very low temperatures, e.g., isobutylene is polymerized almost instantaneously at –100°C by $AlCl_3$. The presence of a hydrogen donor, such as water or a protic acid, as a cocatalyst, is usually a prerequisite, as has been shown [113] in the case of isobutylene. On this basis, the Evans-Polanyi mechanism [114] proposed the following reaction sequence for the polymerization of isobutylene by BF_3 monohydrate:

Initiation

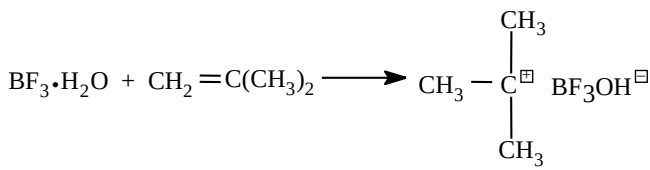

(43)

Propagation

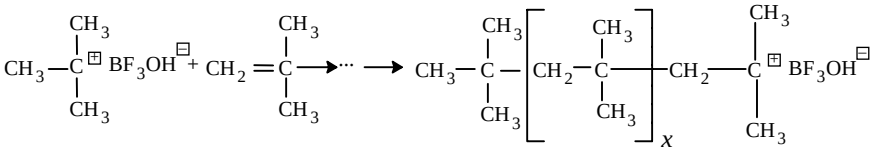

(44)

Termination

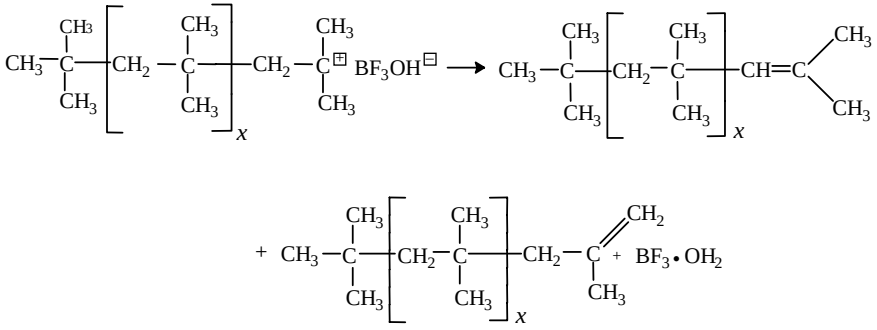

(45)

Chain-transfer to monomer is also an integral step in the cationic polymerization of isobutylene, and it is this reaction which controls the molecular weight [116]:

Chain Transfer

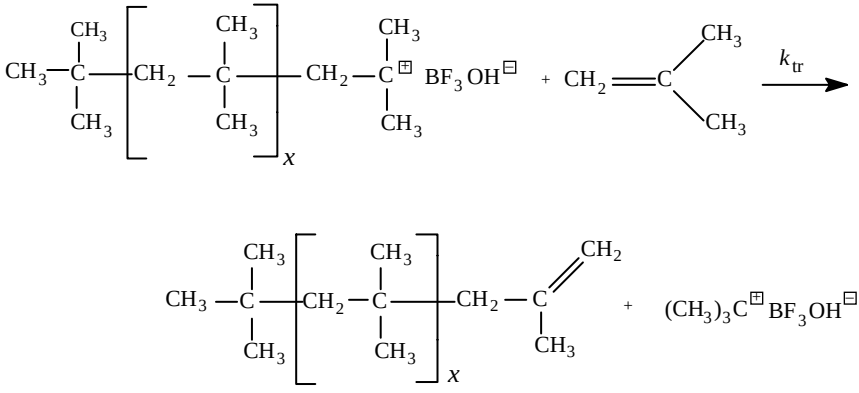

(46)

This mechanism has been supported by infrared and ^{1}H NMR spectroscopic data which provided evidence for the presence of the polymer end groups proposed by this mechanism [105, 106, 117–119], i.e.,

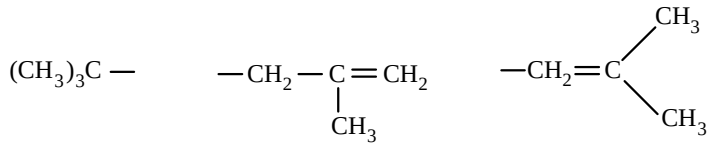

Furthermore, the use of the tracer complex $BF_3 \cdot D_2O$ showed [118] that the polymer contained deuterium while the initiator became converted to $BF_3 \cdot H_2O$.

This mechanism actually involves initiation by addition of a proton [Eq. (43)], from the Bronsted acid formed by the Lewis acid and a coinitiator, to the monomer and subsequent termination of chain growth by loss of a proton to the initiator anion [Eq. (45)] or by chain transfer to monomer [Eq. (46)]. The chain growth, therefore, occurs during the brief lifetime of the carbenium ion, and the initiator or a new carbenium ion is constantly regenerated. The chain transfer step would be expected to have no effect on rate, since the trimethylcarbenium ion should rapidly reinitiate chain growth, but the chain length will decrease. It should be pointed out again, at this point, that it is improbable, in view of the low dielectric constants of the solvents employed, that the active propagating species in these systems are free ions; therefore, the counterion has been depicted as being associated with the carbenium ion in each mechanistic step. This simplified mechanism does not consider the actual nature of the propagating cationic species [112].

The foregoing simplified mechanism is amenable to kinetic analysis, using the steady-state method, as in the case of the free radical mechanism. Using the notation HA to designate the acid initiator, we can write

Initiation

$$\mathrm{HA} + \mathrm{M} \xrightarrow{k_\mathrm{j}} \mathrm{HM^+A^-} \tag{47}$$

Propagation

$$\mathrm{HM^+A^-} + \mathrm{M} \xrightarrow{k_\mathrm{p}} \cdots \rightarrow \mathrm{H[M]}_x\mathrm{M^+A^-} \tag{48}$$

Termination

$$\mathrm{H[M]}_x\mathrm{M^+A^-} \xrightarrow{k_\mathrm{t}} \mathrm{M}_{x+1} + \mathrm{HA} \tag{49}$$

Transfer

$$\mathrm{H[M]}_x\mathrm{M^+A^-} + \mathrm{M} \xrightarrow{k_\mathrm{tr}} \mathrm{M}_{x+1} + \mathrm{HM^+A^-} \tag{50}$$

Rate of initiation

$$R_\mathrm{i} = k_\mathrm{i}[\mathrm{HA}][\mathrm{M}] \tag{51}$$

Rate of termination

$$R_\mathrm{t} = k_\mathrm{t}[\mathrm{HM}_x\mathrm{M^+A^-}] \tag{52}$$

Rate of propagation

$$R_{\mathrm{p}} = k_{\mathrm{p}}[\mathrm{HM}_x\mathrm{M}^+\mathrm{A}^-][\mathrm{M}] \tag{53}$$

Rate of transfer to monomer

$$R_{\mathrm{tr}} = k_{\mathrm{tr}}[\mathrm{HM}_x\mathrm{M}^+\mathrm{A}^-][\mathrm{M}] \tag{54}$$

Here R_{t} has been assumed to be a first-order reaction, since the counterion A^- is considered to be specifically associated with the carbenium ion as shown in Eq. (45) and not as a separate species. Using the steady-state assumption, we equate R_i and R_t and thus obtain Eq. (55) for the steady-state concentration of growing chains.

$$[\mathrm{HM}_x\mathrm{M}^+\mathrm{A}^-] = (k_i/k_t)[\mathrm{HA}][M] \tag{55}$$

Hence,

$$R_p = -d[M]dt = (k_p\, k_i/k_t)[\mathrm{HA}][M]^2 \tag{56}$$

Here again, the propagation rate is virtually the polymerization rate, since the consumption of monomer by the initiation step is negligible. Unlike the free radical case, the rate here is *first-order in initiator concentration*, obviously due to the first-order termination step.

Experimental verification of the foregoing kinetic scheme has been obtained in the case of the cationic polymerization of styrene [120] and vinyl alkyl ethers [121], where the polymerization rate was indeed found to be dependent on the first power of the initiator and on the square of the monomer concentration. However, it should be noted that this simple kinetic scheme is not general for cationic polymerizations; even the steady-state assumption is not valid in many cationic polymerizations [108].

The molecular weight of the polymer can again be expressed in terms of X_{n}, the number-average number of units per chain, which can be defined here as the ratio of the propagation rate to the sum of the rates of all processes leading to chain termination (including transfer). Hence from Eqs. (52–54),

$$X_n = \frac{R_p}{R_{\mathrm{t}} + R_{\mathrm{tr}}} = \frac{k_p[\mathrm{HM}_x\mathrm{M}^+\mathrm{A}^-][M]}{k_t[\mathrm{HM}_x\mathrm{M}^+\mathrm{A}^-] + k_{\mathrm{tr}}[\mathrm{HM}_x\mathrm{M}^+\mathrm{A}^-][M]}$$

or

$$1/X_n = k_{\mathrm{tr}}/k_p + k_t/k_p[M] \tag{57}$$

Equation (57) provides a means of determining the relative contribution of the termination and transfer steps. Thus, if k_{tr} is largely relative to k_t, the molecular weight will be virtually independent of monomer concentration, but if the reverse is true, X_n will be directly proportional to $[M]$. Hence this relation lends itself to a simple experimental test, i.e., a plot of $1/X_n^o$ (the reciprocal of the *initial* X_n value) against $1/[M]^o$ (the reciprocal of the initial monomer concentration). It has actually been found that the polymerization of styrene

by $SnCl_4$ in ethylene dichloride [120], and of vinyl alkyl ethers by $SnCl_4$ in *m*-cresol [121], showed a dominance of termination over transfer, i.e., X_n α [M]; however, for isobutylene polymerization catalyzed by $TiCl_4$ in *n*-hexane [122], the observed polymer molecular weights were independent of monomer concentration, i.e., transfer appeared to predominate.

It is interesting to compare the nature of the individual steps in cationic polymerization with those of the free radical mechanism. Thus, unlike the situation in the latter case, the termination step in cationic polymerization may be expected to require a greater energy than that of propagation, since it involves σ-bond rupture compared to the low-energy attack of the growing carbenium ion on the π bond of the monomer. If indeed the termination step has a higher activation energy than that of propagation, then a rise in temperature should lead to an increase in termination relative to propagation and thus to a lower steady-state concentration of growing chains. The net result would thus be a *decrease* in polymerization rate and molecular weight, i.e., an apparent "negative" overall activation energy for polymerization. This might, of course, be partially or wholly offset if the activation energy of the initiation step were sufficiently high. However, in the majority of cases it appears that this is not the case, so that faster rates (and higher molecular weights) are indeed obtained at reduced temperatures (about –100°C) [115]. Kinetic studies have shown that the ion pair propagation rate constant is $(5–6) \times 10^8$ $Lmol^{-1}sec^{-1}$ for the polymerization of isobutylene with $EtAlCl_2$ in hexanes/methyl chloride (60/40, vol/vol) at –80°C [123].

B. Butyl Rubber

The only important commercial elastomer prepared by a cationic polymerization is butyl rubber, i.e., a copolymer of isobutene and isoprene. The latter monomer is incorporated in relatively small proportions (~1.5 mole % [76]) in order to introduce sufficient unsaturation for sulfur vulcanization. The slurry process with aluminum chloride at –98 to –90°C in methyl chloride diluent can be described by the accompanying "flow sheet" [115, 116, 124]. In this process the polymerization is almost instantaneous and extensive cooling by liquid ethylene is required to control the reaction.

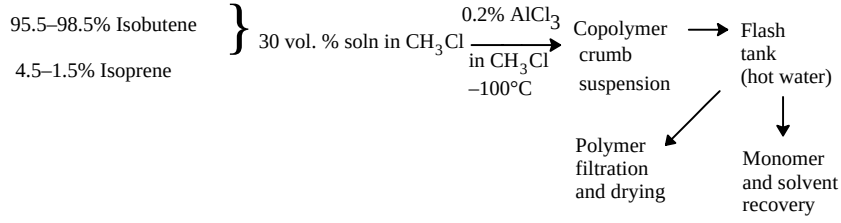

The molecular weights of butyl rubber grades are in the range of 300,000–500,000, and they are very sensitive [124] to polymerization temperature above –100°C. For example, a rise in polymerization temperature of 25°C

can result in a fivefold or 10-fold *decrease* in molecular weight, presumably due to the kinetic factors discussed previously [115]. The molecular weight distribution of butyl rubbers can be as high as M_w/M_n = 3–5 [115], presumably because of the heterogeneous nature of the polymerization process.

Isoprene is used as the comonomer in butyl rubber (0.5–2.5 mol %) [115] because the isobutene-isoprene reactivity ratios are more favorable for inclusion of the diene than those of the isobutene-butadiene pair [124]. Thus, for the former pair, the r(isobutene) = 2.5, and r(isoprene) = 0.4 [124]. It should be noted, however, that as discussed previously, such r values can be markedly influenced by the nature of the initiator and solvent used in the polymerization. The values just quoted are applicable to the commercial butyl rubber process, as described earlier. It has been shown that the isoprene unit enters the chain predominantly in a 1,4-configuration [125].

C. Living Cationic Polymerizations

The controlled/living polymerization of alkyl vinyl ethers was reported in 1984 using the HI/I_2 initiating system in nonpolar solvents [126]. These polymerizations produced polymers with controlled molecular weights, narrow molecular weight distributions, and number average molecular weights that increased linearly with conversion. Shortly thereafter, Faust and Kennedy [127] reported the discovery of the living cationic polymerization of isobutylene by initiation with cumyl acetate/boron trichloride in mixtures of chlorinated solvents plus *n*-hexane to obtain a homogeneous polymerization. Subsequent investigations have discovered a variety of living cationic polymerization systems [123, 128, 129]. For controlled/living polymerization of isobutylene, tertiary halides are generally used in conjunction with strong Lewis acid co-initiators (BF_3, $SnCl_4$, $TiCl_4$, $EtAlCl_2$, and Me_2AlCl) [123, 128, 129]. A key ingredient in many of these systems is a proton trap, such as 2,6-di-*tert*-butylpyridine, to suppress initiation by protons. The general features of living polymerization systems are analogous to those of controlled radical polymerization, i.e., a predominant, unreactive dormant species (covalent species, R-X or P-X) in equilibrium with a small concentration of reactive, propagating species (cationic ion pairs, P^+X^-) as shown below.

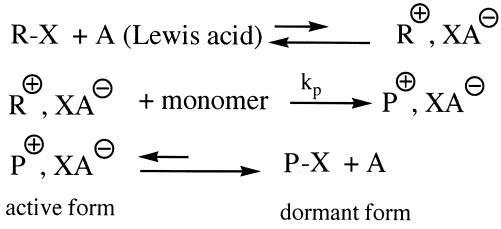

D. Other Cationic Polymerizations: Heterocyclic Monomers

Although butyl rubber is by far the most important commercial elastomer to be synthesized by cationic polymerization, several heterocyclic monomers provide useful elastomeric materials via this mechanism also. Epichlorohydrin can be polymerized to high molecular weight using a complex catalyst formed from a trialkylaluminum compound and water as shown in Eq. (58) [64, 130–132]. For copolymerizations with ethylene oxide, a catalyst formed from a trialkylaluminum compound, water, and acetylacetone is useful [64, 130]. The mechanism proposed for these polymerizations is

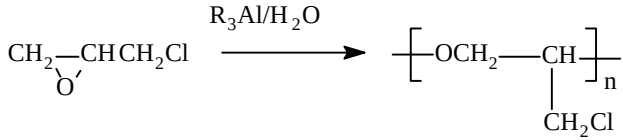

(58)

illustrated in Eq. (59), where coordination to two aluminum sites has been invoked to explain the stereochemical course of these polymerization [132]. The average molecular weight of the homopolymer is 500,000, while the equimolar copolymer with ethylene oxide has molecular weights approaching 1,000,000 [64].

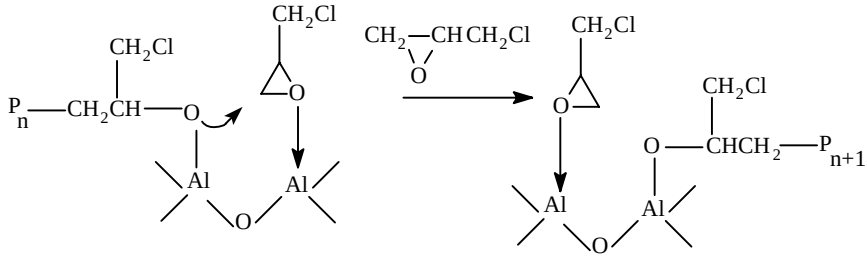

(59)

The cationic polymerization of tetrahydrofuran is used commercially to produce α,ω-dihydroxypoly(tetramethylene oxide) (PTMO glycol). Although this polymer is not used by itself as an elastomer, it is used as one of the elastomeric block components for preparation of segmented thermoplastic polyurethane [133] and thermoplastic polyester [134] elastomers. The cationic polymerization of tetrahydrofuran (THF) is a living polymerization under proper experimental conditions [135–139], i.e., it does not exhibit any termination step, very much like the analogous anionic polymerizations which are discussed in Section VIII. However, these polymerizations are complicated by the fact that the ceiling temperature, where the free energy of polymerization is equal to zero, is estimated to be approximately 83 ± 2°C in bulk monomer solution [140]; therefore, the polymerization is reversible and incomplete conversion is often observed, especially in the presence of added solvent. For

example, at equilibrium in the bulk at 30°C, conversion is 72%; in a mixture of 37.5 vol % CH_2Cl_2, conversion is only 27% [136]. These factors limit the ability to prepare polytetrahydrofurans with controlled molecular weight and narrow molecular weight distributions which are often associated with living polymerizations. To the extent that equilibrium is approached, the polymer molecular weight distribution would broaden towards a statistical value of 2.

The most commonly used catalyst for the commercial polymerization of tetrahydrofuran is fluorosulfuric acid as shown in Eq. (60) [139]. The mecha-

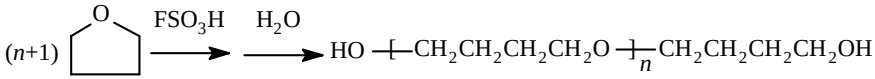

(60)

nism of this cationic polymerization is quite different from the polymerization of isobutene [Eqs. (43–46)] in that the growing chain end is an oxonium ion intermediate in which the positive charge is located on oxygen atom rather than on carbon as shown in the following [136, 139, 141]:

Initiation

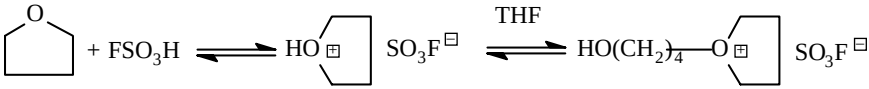

(61)

Propagation

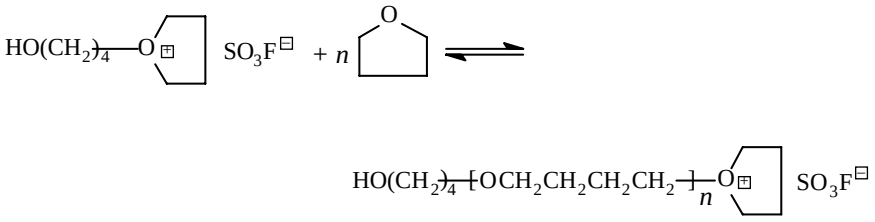

(62)

Another interesting aspect of this polymerization is the observation that the covalent ester is in equilibrium with the oxonium ion [Eq. (63)] and that both of these species can participate in propagation by reaction with monomer [142].

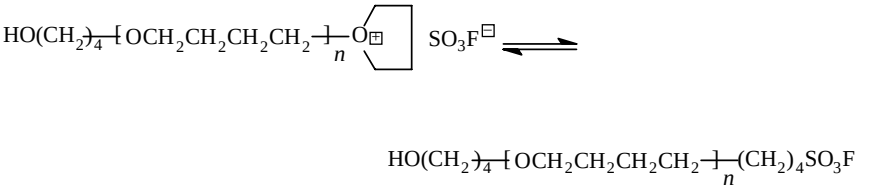

(63)

The commercial α,ω-dihydroxypoly(tetramethylene oxide) (PTMO glycol) polymers have molecular weights in the range of 600–3,000 with molecular weight distributions in the range of 1.2–1.6 which is consistent with the equilibrium nature of these polymerizations [139].

VIII. CHAIN POLYMERIZATION BY ANIONIC MECHANISM

A. Mechanism and Kinetics

An anionic mechanism is proposed for those polymerizations initiated by alkali metal organometallic species, where there is good reason to assume that the metal is strongly electropositive relative to the carbon (or other) atom at the tip of the growing chain [21, 143–151]. However, analogous to the discussion of the active species in cationic polymerization, a multiplicity of active species may be involved as propagating species in anionic polymerization as shown below [150]. In contrast to cationic polymerization, however, there is experimental evidence for the involvement of many of these species under certain experimental conditions [145, 147, 148].

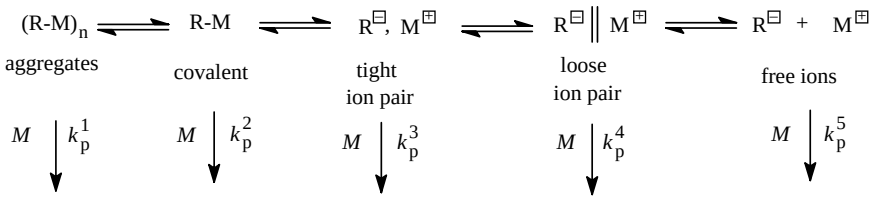

Although the ability of alkali metals, such as sodium, to initiate polymerization of unsaturated organic molecules has long been known (the earliest record dating back to the work of Matthews and Strange [8] and of Harries [7], around 1910, on polymerization of dienes), the mechanism had remained largely obscure due to the heterogeneous character of this type of catalysis. The pioneering work of Higginson and Wooding [152] on the homogeneous polymerization of styrene by potassium amide in liquid ammonia, and that of Robertson and Marion [153] on butadiene polymerization by sodium in toluene, merely showed the important role of the solvent in participating in chain transfer reactions.

The true nature of homogeneous anionic polymerization only became apparent through studies of the soluble aromatic complexes of alkali metals, such as sodium naphthalene. These species are known to be radical anions [154–158], with one unpaired electron stabilized by resonance and a high solvation energy, and are therefore chemically equivalent to a "soluble sodium." They initiate polymerization by an "electron transfer" process [145, 148], just as in the case of the metal itself, except that the reaction is homogeneous and therefore involves a much higher concentration of initiator. The mechanism

of polymerization initiated by alkali metals (or their soluble complexes) can therefore be written as follows, using styrene as an example [145, 148]:

Initiation

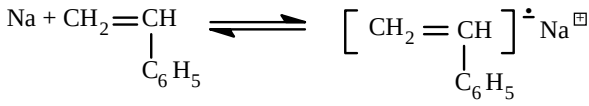

(64)

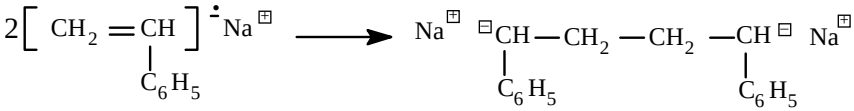

(65)

Propagation

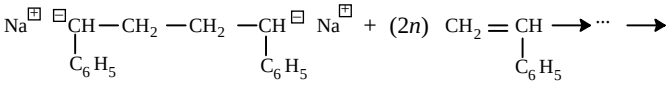

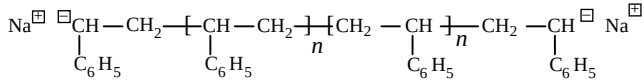

(66)

Thus the first step in the initiation reaction [Eq. (64)] involves a reversible electron transfer reaction from the alkali metal to the styrene monomer to form the styryl radical anion; in a rapid subsequent reaction, two radical anions couple to form a di-anion which can grow a polymer chain at both ends. In the case of the soluble alkali metal aromatic complexes, the overall initiation reaction is extremely fast, due to the high concentrations of radical anion (~10^{-3} M) and monomer (~1 M), and so is the subsequent propagation reaction. However, in the case of the alkali metal initiators, the electron transfer step [Eq. (64)] is very much slower, due to the heterogeneous nature of the reaction, so that the buildup of radical anions is much slower. In fact, there is evidence [153] that, in such cases, a second electron transfer step can occur between the metal and the radical anion to form a di-anion, rather than coupling of the radical anions. In either case, the final result is a di-anion, i.e., a difunctional growing chain.

However, it was investigations of the homogeneous systems initiated by sodium naphthalene in polar solvents which demonstrated the special nature of anionic polymerization, i.e., the fact that a termination step may be avoided under certain circumstances, leading to the concept of "living" polymers [159]. Since these are homogeneous systems, the stoichiometry of the reaction becomes apparent, i.e., two molecules of sodium naphthalene generate one

chain. Furthermore, since all the chains are initiated rapidly and presumably have an equal opportunity to grow, their molecular weight distribution becomes very narrow, approximating the Poisson distribution [160]. These aspects are obscured in the metal-initiated polymerizations owing to the continued slow initiation over a long period of time, leading to a great difference in the "age" of the growing chains and hence in their size distribution.

Polymerization initiated by electron transfer from a metal, or by an aromatic radical anion, represents only one of the anionic mechanisms. It is, of course, possible to consider separately those polymerizations initiated directly by organometallic compounds. Of the latter, the organolithium compounds are probably the best examples, since they are soluble in a wider variety of solvents and are relatively stable. Furthermore, it is these organometallic compounds which are used commercially for the preparation of synthetic elastomers [161, 162]. The mechanism of these polymerizations is somewhat simpler than in the case of sodium napthhalene, since there is no electron transfer step; thus

Initiation

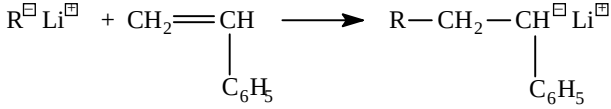

(67)

Propagation

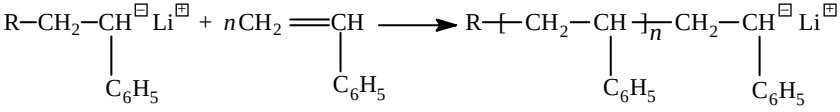

(68)

Termination by impurity or deliberate termination

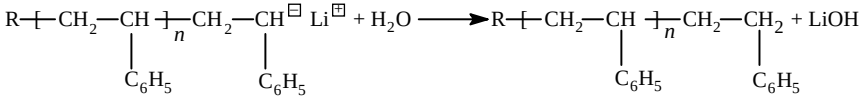

(69)

Hence each organolithium molecule generates one chain, and there is no termination of the growing chains or chain transfer reactions in the absence of adventitious impurities, such as water and acids, and if higher temperatures are avoided to prevent side reactions.

Unlike sodium naphthalene, which requires the presence of highly solvating solvents, such as tetrahydrofuran (THF), the organolithium systems can operate in various polar and nonpolar solvents such as ethers or hydrocarbons. However, the rates are much slower in the latter than in the former solvents.

Hence, if the initiation reaction [Eq. (67)] is very much slower than the propagation reaction, the molecular weight distribution may be considerably broadened [163]. This does not, of course, vitiate the "living" polymer aspect of the polymerization, which has been shown [164] to operate in these systems, regardless of type of solvent, if side reactions do not intervene.

The absence of chain termination and chain transfer reactions in homogeneous anionic polymerization can lead to many novel synthetic routes. Thus, since each chain continues to grow when additional monomer is added, it is possible to synthesize block polymers by sequential addition of several monomers [165, 166]. Another possibility is the synthesis of linear chains with various functional end groups, by allowing the anionic polymer chain end to react with various electrophilic agents, e.g., with CO_2 to form-COOH groups [167]. In addition, linking reactions of polymer chains with multifunctional electrophilic reagents leads to the formation of "star-branched" polymers [168–171]. These possibilities are, of course, of considerable industrial interest.

In view of the unusual mechanism of anionic polymerization, especially the absence of termination and chain transfer reactions, the kinetics of these systems can be treated quite differently than for the other mechanisms. Thus it is possible, by suitable experimental techniques, to examine separately the rates of the initiation and propagation reactions [172, 173], since the stable organometallic chain ends are present in concentrations [$10^{-3} - 10^{-5}$ M] which are easily measured by ultraviolet-visible spectroscopy [174]. The propagation reaction is, of course, of considerable main interest and can be studied by making sure that initiation is complete. In this way, the kinetics of homogeneous anionic polymerization have been extensively elucidated with special reference to the nature of counterion and role of the solvent.

It has been found universally that, in accordance with Eqs. (66) and (68), the propagation rate is always first order with respect to monomer concentration, regardless of solvent system or counterion. However, in contradiction to the foregoing equations, the propagation rate dependency has generally been found to be *lower* than first order with respect to the concentration of growing chains, and the order was found to be strongly dependent on the nature of the solvent and counterion [148, 172–175]. Strongly solvating solvents, such as ethers and amines, lead to much faster rates than nonpolar solvents and affect the kinetics of these polymerizations quite differently than the hydrocarbon media, because more dissociated ionic species such as loose ion pairs and free ions are involved as propagating species [148]. However, since the anionic synthesis of elastomers requires the use of lithium as counterion in hydrocarbon media, the following discussion will focus on the kinetics of these processes.

It would be expected that the kinetics of organolithium-initiated polymerization in hydrocarbon solvents would be simplified because of the expected correspondence between the initiator concentration and the concentration of propagating anionic species, resulting from the lack of termination and chain transfer reactions. However, in spite of intensive study, there is

no general agreement on many kinetic aspects of these polymerizations. The complicating feature is that organolithium compounds are associated into aggregates in hydrocarbon solution, and the degree of aggregation depends on the structure of the organolithium compound, the concentration of organolithium compound, the solvent, and the temperature [147, 176–178]. In general, simple alkyllithium compounds are associated into hexamers or tetramers in hydrocarbon solution.

The kinetics of initiation for styrene and diene polymerization by alkyllithium compounds generally exhibit a fractional kinetic order dependence (e.g., $\frac{1}{4}$ or $\frac{1}{6}$) on the concentration of alkyllithium initiator. This can be rationalized in terms of the following steps:

Initiation

$$(\mathrm{RLi})_n \underset{}{\overset{K_n}{\rightleftharpoons}} n\,\mathrm{RLi} \tag{70}$$

$$\mathrm{RLi} + \mathrm{CH_2{=}CH(C_6H_5)} \xrightarrow{k_i} \mathrm{R{-}CH_2{-}CHLi(C_6H_5)} \tag{71}$$

Thus, it is assumed that only the unassociated alkyllithium compound [formed by dissociation of the aggregate, Eq. (70)] reacts with monomer in the initiation step [Eq. (71)] so the the rate of initiation can be expressed by Eq. (72).

$$R_i = k_i[\mathrm{RLi}][M] \tag{72}$$

The equilibrium concentration of unassociated alkyllithium can be expressed in terms of Eq. (73).

$$[\mathrm{RLi}] = K^{1/n}[(\mathrm{RLi})_n]^{1/n} \tag{73}$$

When this expression for [RLi] is substituted into Eq. (72), Eq. (74) is obtained.

$$R_i = k_i K^{1/n}[(\mathrm{RLi})_n]^{1/n}[M] \tag{74}$$

A good example of this kinetic behavior was found in the study of the *n*-butyllithium-styrene system in benzene, in which a $\frac{1}{6}$ kinetic order dependency on *n*-butyllithium concentration was observed, consistent with the predominantly hexameric degree of association of *n*-butyllithium [179]. However, this expected correspondence between the degree of association of the alkyllithium compound and the fractional kinetic order dependence of the initiation reaction on alkyllithium concentration was not always observed [147]. One source of this discrepancy is the assumption that only the unassociated alkyllithium molecule can initiate polymerization. With certain reactive initiators, such as *sec*-butyllithium in hexane solution, the initial rate of initiation exhibits approximately a first order dependence on alkyllithium concentration, suggesting that

the aggregate can react directly with monomer to initiate polymerization [180]. A further source of complexity is the cross-association of the initiator with the initiated polymer chain; in general, the cross-associated species exhibits a different degree of association and reactivity from the alkyllithium initiator [181, 182]. As a result of cross-association, only the initial rates of initiation can be used to to determine the kinetic order dependence on initiator concentration. Unfortunately, these considerations have not always been recognized. It is interesting to note that the general reactivity of alkyllithiums as initiators is inversely related to the degree of aggregation [183], i.e., *sec*-butyllithium (tetramer) > *n*-butyllithium (hexamer) [180].

The kinetics of the propagation reaction in organolithium polymerization of styrenes and dienes in nonpolar solvents (i.e., hydrocarbons) have also been subjected to intensive study. For styrene polymerizations, a $\frac{1}{2}$ kinetic order dependence on chain-end concentration is observed [Eq. (75)]. Since it has been

$$R_p = k_p K_n^{1/2}[(\mathrm{PsLi})_2]^{1/2}[M] \tag{75}$$

determined that poly(styryl)lithium is associated predominantly into dimers in hydrocarbon solution [147], the observed kinetic order can be explained in terms of Eqs. (76, 77), using the same reasoning as delineated for the initiation kinetics [Eqs. 70–74)]. This explanation is based on the assumption that *only* the dissociated chain ends are active.

$$(\mathrm{PsLi})_2 \overset{K_n}{\rightleftharpoons} 2\ \mathrm{PsLi} \tag{76}$$

$$\mathrm{PsLi} + \mathrm{CH_2{=}CH(C_6H_5)} \xrightarrow{k_p} \mathrm{Ps{-}CH_2{-}CHLi(C_6H_5)} \tag{77}$$

The propagation kinetic order dependence on poly(dienyl)lithium chain end concentration for alkyllithium-initiated polymerization of dienes varies from $\frac{1}{4}$ to $\frac{1}{6}$ for butadiene and from $\frac{1}{2}$ to $\frac{1}{4}$ for isoprene [147, 172, 173, 184]. However, attempts to relate these kinetic orders to proposed higher states of association of poly(dienyl)lithium chain ends have proven to be complicated, because conflicting physical measurements using the same techniques by different groups have shown that such chain ends are associated into dimers and tetramers in hydrocarbon media [150]. These physical measurements include solution viscosity, cryoscopy, and light scattering measurements [185]. Hence, these findings bring into question the whole theory of the nonreactivity of the associated complex, and suggest that a direct interaction between the monomer and the associated polymer chain end may be contributing [186–192; 144, p. 128]. Further complicating this situation are the results of Fetters and coworkers indicating that higher-order aggregates are in equilibrium with dimers [193].

In conclusion, it should be noted that the molecular weights and their distribution follow the rules originally discussed under living polymers [194]. This means that, regardless of the solvents and counterions used, if no termination, chain transfer, or side reactions occur, and if the initiation reaction is fast relative to the propagation reaction, then the molecular weight distribution will approach the Poisson distribution, i.e.,

$$X_w / X_n = 1 + 1/X_n \tag{78}$$

where X_n is the number average number of monomer units and X_w is the weight average number of monomer units. This means that, in principle, a polymer chain of 100 units should have an X_w/X_n ratio of 1.01. This is, of course, impossible to prove experimentally, and it can be assumed that the real distribution would be somewhat broader, due for one thing to imperfect mixing in the reaction mixture. However, values of 1.05 for X_w/X_n are commonly found in these systems [185, 195].

B. Chain Microstructure of Polydienes

Although the alkali metals, unlike the Ziegler Natta systems, do not generally polymerize unconjugated olefins and are not known to lead to any tacticity, they do affect the chain microstructure of polydienes. Thus, the proportion of *cis*-1,4 and *trans*-1,4 addition versus the 1,2 (and 3,4 for polyisoprene) mode can be markedly affected by the nature of the counterion as well as the solvent. Ever since the discovery that lithium polymerization of isoprene can lead to a high *cis*-1,4 structure [196], close to that of natural rubber, there have been many studies of these effects [147, 197–200]. Table XIV shows some of these results for anionic polymerization of isoprene and butadiene. It is obvious from these data that the stereospecific high *cis*-1,4 polyisoprene is obtained only in the case of lithium in hydrocarbon solvents; the highiest cis microstructure is also favored by high ratios of monomer to chain end [199–201]. Other solvents and/or counterions exert a dramatic effect in altering the chain microstructure to form 1,2 and 3,4 enchainments. Similar effects are observed with butadiene and other dienes [147, 150, 197]. However, in the case of butadiene, the maximum *cis*-1,4 content attainable is much less than for isoprene; typical commercial polybutadienes prepared in hydrocarbon solution with butyllithium initiators have microstructures in the range of 36–44% *cis*-1,4, 48–50% *trans*-1,4, and 8–10% 1,2 microstructure [198]. The effect of polar solvents, or of the more electropositive alkali metals, is to produce a high-1,2 polybutadiene.

This marked sensitivity of the stereochemistry of anionic polymerization to the nature of the counterion and solvent can be traced to the structure of the propagating chain end. The latter involves a carbon-metal bond which can have variable characteristics, ranging all the way from highly associated species

TABLE XIV Microstructure of Polydienes Prepared by Anionic Polymerization

Solvent	Cation	Chain microstructure (mole %) *cis*-1,4	*trans*-1,4	1,2	3,4	Ref.
Butadiene						
Hexane[a]	Li^+	30	62	8	—	[200]
Cyclohexane[b]	Li^+	68	28	4	—	[200]
None	Li^+	86	9	5	—	[200]
Tetrahydrofuran (THF)	Li^+	6	6	88	—	[202]
Pentane	Na^+	10	25	65	—	[202]
THF	Na^+	0	9.2	90.8	—	[203]
Pentane	K^+	15	40	45	—	[202]
Pentane	Rb^+	7	31	62	—	[202]
Pentane	Cs^+	6	35	59	—	[202]
Isoprene						
Cyclohexane[b]	Li^+	94	1	—	5	[201]
Cyclohexane[a]	Li^+	76	19	—	5	[201]
None	Li^+	96	0	—	4	[200]
THF	Li^+	12[c]		29	59	[204]
Cyclohexane	Na^+	44[c]		6	50	[199]
THF	Na^+	11[c]		19	70	[199]
Cyclohexane	K^+	59[c]		5	36	[199]
Cyclohexane	Cs^+	69[c]		4	27	[199]

[a] At monomer/initiator ratio of ~17.
[b] At monomer/initiator ratio of 5×10^4.
[c] Total of *cis* and *trans* forms.

with covalent character to a variety of ionic species [150]. The presence of a more electropositive metal and/or a cation-solvating solvent, such as ethers, can effect a variety of changes in the nature of the carbanionic chain end: (a) the degree of association of the chain ends can decrease or be eliminated; (b) the interaction of the cation with the anion can be decreased by cation solvation; (c) a more ionic carbon-metal bond will increase delocalization of the π electrons; and (d) polar solvents will promote ionization to form ion pairs and free ions. Direct evidence for these effects has been obtained from concentrated solution measurements [205, 206], ^1H and ^{13}C NMR spectroscopy [147, 207], ultraviolet-visible spectroscopy [147, 184, 208] and electrolytic conductance [145] measurements.

The control of chain structure and molecular weight afforded by the organolithium polymerization of dienes, has, of course, been of great technological interest [161, 162, 209]. Such product developments have been mainly in the form of (1) polybutadiene elastomers of various chain structures [162, 198, 209] and functional end groups [210], (2) liquid polybutadienes [211], (3) butadiene-styrene copolymers (solution SBR) [69, 161, 162, 209], and (4) styrene-diene triblock copolymers (thermoplastic elastomers) [212].

TABLE XV Monomer Reactivity Ratios for Organolithium Copolymerization of Styrene and Dienes

Monomer 1	Monomer 2	Solvent	r_1	r_2	Ref.
Styrene	Butadiene	Toluene	0.004	12.9	[213]
Styrene	Butadiene	Benzene	0.04	10.8	[214]
Styrene	Butadiene	Triethylamine	0.5	3.5	[214]
Styrene	Butadiene	Tetrahydrofuran	4.0	0.3	[214]
Styrene	Isoprene	Benzene	0.26	10.6	[215]
Styrene	Isoprene	Tetrahydrofuran	9.0	0.1	[216]
Butadiene	Isoprene	Hexane	1.72	0.36	[217]

C. Copolymers of Butadiene

The possibilities inherent in the anionic copolymerization of butadiene and styrene by means of organolithium initiators, as might have been expected, have led to many new developments. The first of these would naturally be the synthesis of a butadiene-styrene copolymer to match (or improve upon) emulsion-prepared SBR, in view of the superior molecular weight control possible in anionic polymerization. The copolymerization behavior of butadiene (or isoprene) and styrene is shown in Table XV. As indicated earlier, unlike the free radical type of polymerization, these anionic systems show a marked sensitivity of the reactivity ratios to solvent type (a similar effect is noted for different alkali metal counterions). Thus, in nonpolar solvents, butadiene (or isoprene) is preferentially polymerized initially, to the virtual exclusion of the styrene, while the reverse is true in polar solvents. This has been ascribed [144] to the profound effect of solvation on the structure of the carbon-lithium bond, which becomes much more ionic in such media, as discussed previously. The resulting polymer formed by copolymerization in hydrocarbon media is described as a tapered block copolymer; it consists of a block of polybutadiene with little incorporated styrene comonomer followed by a segment with both butadiene and styrene and then a block of polystyrene. The structure is schematically represented below:

[butadiene]-[B/S]-[styrene]

The data in Table XV illustrate the problems encountered in such copolymerizations, since the use of polar solvents to assure a random styrene-diene copolymer of desired composition will, at the same time, lead to an increase in side vinyl groups (1,2 or 3,4) in the diene units (see Table XIV). This is of course quite undesirable, since such chain structures result in an increase in the glass transition temperature (T_g) and therefore to a loss of good rubbery properties. Hence, two methods are actually used to circumvent this problem: (1) the use of limited amounts of polar additives such as tetrahydrofuran to

accomplish a reasonable compromise between diene structure and monomer sequence distribution [218]; and (2) the addition of small amounts of potassium *t*-alkoxides [219].

As mentioned earlier, the "living" nature of the growing chain in anionic polymerization makes this mechanism especially suitable for the synthesis of *block* copolymers, by sequential addition of *different* monomers. Since such copolymers have markedly different properties than simple copolymers, they will be discussed separately (in Section X).

D. Terminally Functional Polydienes

Another characteristic of these homogeneous anionic polymerizations, as mentioned earlier, is their potential for the synthesis of polymer chains having reactive end groups. It was recently reported that chain-end functionalization of high molecular weight polybutadiene and solution styrene-*co*-butadiene elastomers (SBR) with a derivative of Michler's ketone, 4,4′-bis(diethylamino)benzophenone, leads to tire tread formulations which have lower rolling resistance and good wet-skid resistance [210]. These effects were observed in spite of the low concentration of chain ends in these polymers (molecular weights > 100,000) [162].

The production of liquid short-chain *difunctional* polymers by anionic polymerization is of considerable technological interest and importance, and has attracted much attention in recent years, since it offers an analogous technology to that of the polyethers and polyesters used in urethane polymers. Such liquid "telechelic" polydienes could thus lead, by means of chain extension and crosslinking reactions, directly to "castable" polydiene networks [161, 162].

The most direct method of preparing telechelic polydienes utilizes a dilithium initiator which is soluble in hydrocarbon solution [220, 221]. The most expedient method of preparing such a dilithium initiator is to react two moles of an alkyllithium compound with a divinyl compound which will not homopolymerize. Unfortunately, because of the association behavior of organolithium compounds in hydrocarbon media [176–178], many potential systems fail because they associate to form an insoluble network-like structure [221]. Expediencies such as addition of Lewis bases can overcome solubility problems of dilithium initiators, however, such additives tend to produce high amounds of 1,2- and 3,4-microstructures (see Table IV). One exception is the adduct formed from the addition of two equivalents of *sec*-butyllithium to 1,3-*bis*(1-phenylethenyl)benzene as shown in Eq. (79) [222, 223]. Although this is a hydrocarbon-soluble, dilithium initiator, it was found that biomodal molecular weight distributions are obtained; monomodal distributions can be obtained in the presence of lithium alkoxides or by addition of Lewis base additives [224, 225]. This initiator has also been used to prepare telechelic polymers in high yields [226].

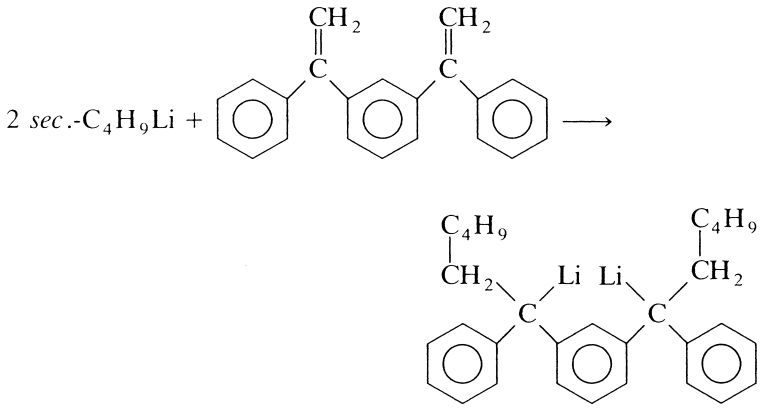

(79)

IX. STEREOSPECIFIC CHAIN POLYMERIZATION AND COPOLYMERIZATION BY COORDINATION CATALYSTS

A. Mechanism and Kinetics

The term "Ziegler-Natta catalysts" refers to a wide variety of polymerization initiators generally formed from mixtures of transition metal salts of Group IV to VIII metals and base metal alkyls of Group II or III metals [21, 227, 228]. It arose from the spectacular discovery of Ziegler *et al.* [229] that mixtures of titanium tetrachloride and aluminum alkyls polymerize ethylene at low pressures and temperatures; and from the equally spectacular discovery by Natta [230] that the Ziegler catalysts can stereospecifically polymerize monoolefins to produce tactic, crystalline polymers. As can be imagined, these systems can involve many combinations of catalyst components, not all of which are catalytically active or stereospecific. However, we shall be concerned here only with polymerizations involving the commercial elastomers, principally polyisoprene, polybutadiene [231–233], and the ethylene-propylene copolymers [234–238].

The mechanism of polymerization of alkenes using Ziegler-Natta-type catalysts is described as a coordination [239] or insertion [240] polymerization process. The coordination terminology assumes that the growing polymer chain is bonded to a transition metal atom and that insertion of the monomer into the carbon-metal bond is preceded by, and presumably activated by, the coordination of the monomer with the transition metal center. Since coordination of the monomer may or may not be a specific feature of these polymerizations, the insertion terminology focuses on the proposal that these reactions involve a stepwise insertion of the monomer into the bond between the transition metal atom and the last carbon atom of the growing chain. It is important to note that the bonding of carbon atoms and transition metals is

described as substantially covalent [240], in contrast to anionic organometallic species, such as organoalkali metal species, which are highly ionic.

Typical soluble catalysts for copolymerization of ethylene and propylene are formed from mixtures of vanadium salts with alkylaluminum chlorides, e.g., VCl_4 with either AlR_2Cl or $AlRCl_2$ where R = alkyl group [236]. A possible hexacoordinated metal structure for the resulting active catalyst is shown below.

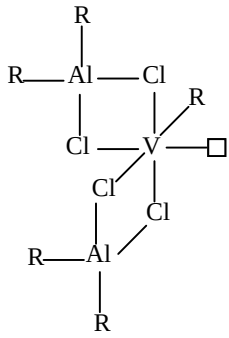

The important features of the active center in accord with the general model of Arlman and Cossee [241] are: (1) an alkylated vanadium center, i.e., an R-V bond; and (2) an empty orbital on vanadium, represented by — □ in the structure, which can be used to bond to the incoming monomer; and an oxidation state of +3 for vanadium [242–244].

The formation of the active catalytic center from the reaction of the transition metal compound and an organoaluminum derivative is shown schematically in Eq. (80). Reduction to a lower valence state may accompany this alkylation reaction since it is generally considered that the active catalytic center has an oxidation state of +3 [236].

Active center formation

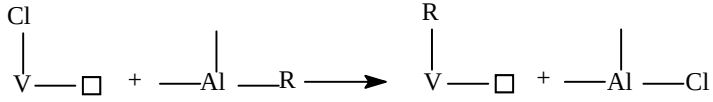

(80)

The steps involved in the chain polymerization of alkenes using this type of catalyst are shown in Eqs. (81–85) [236].

Initiation

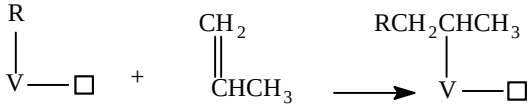

(81)

Propagation

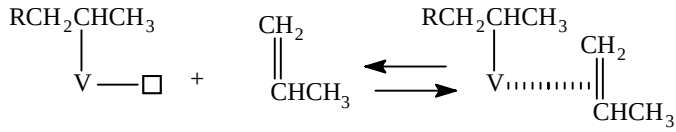

(82)

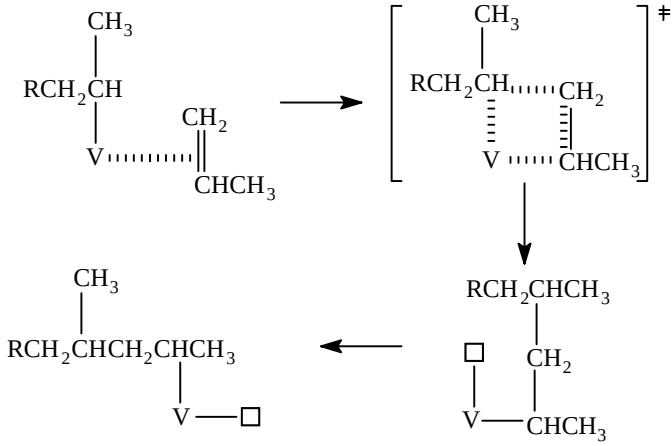

(83)

Termination

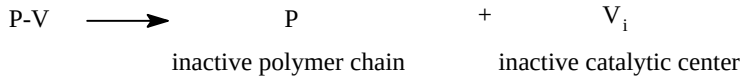

(84)

Spontaneous transfer

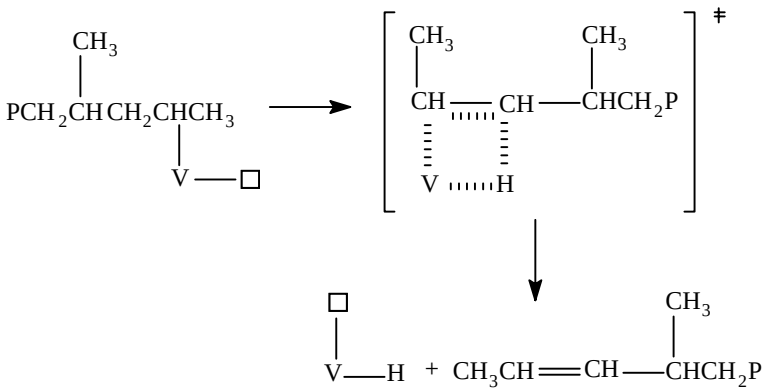

(85)

It should be noted that the monomer coordination step shown in Eq. (82) may not be a distinct step as discussed previously. An important feature of this mechanism which affects the stereospecificity of olefin polymerizations using

these types of soluble catalysts is the fact the the insertion of the monomer into the transition metal-carbon bond involves a secondary insertion reaction, i.e., the more substituted carbon of the double bond in the monomer becomes bonded to the transition metal [245]. In contrast, a primary insertion mechanism to form a transition metal bond to the less substituted carbon on the double bond of the monomer [Ti-CH_2CHR-P] is involved in polymerizations using typical heterogeneous catalysts, e.g., from titanium halides and alkylaluminum compounds [228].

One of the models proposed to explain the stereospecificity for soluble vanadium-based catalysts postulates that it is the minimization of steric effects in the four-center transition state for monomer insertion [see Eq. (83)] which is responsible for the stereospecificity of the polymerization [244, 245]. Thus, it is considered that the *trans*-configuration minimizes steric effects in the transition state and this leads to a syndiotactic configuration of the polymer chain as shown below. In general, the kinetics

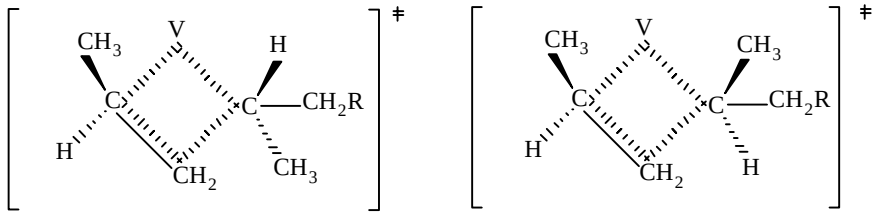

favored *trans* configuration

more hindered *cis* configuration

of alkene polymerizations using Ziegler-Natta-type catalysts are complicated by the multiplicity of active species, catalyst aging and deactivation effects, multiplicity of chain transfer processes, and often by the relatively rapid rates of polymerization [228, 234].

B. Ethylene-Propylene Rubbers

The copolymerization of propylene with ethylene is complicated by the very unfavorable monomer reactivity ratios for propylene and other monomers with ethylene as shown in Table XVI. In general, the less hindered ethylene monomer is favored in Ziegler-Natta copolymerizations by as much as two orders of magnitude for certain catalyst combinations. To obtain homogeneous copolymers, continuous processes are required utilizing incomplete conversions of the propylene comonomer [236]. A further aspect of the commercial preparation of ethylene-propylene rubbers is the inclusion of a third diene comonomer which introduces unsaturation into the final polymer to facilitate peroxide crosslinking reactions and to permit sulfur vulcanization; these terpolymers are called EPDM in contrast to the binary copolymers, which are designated as EPM. The following nonconjugated diene monomers

TABLE XVI Monomer Reactivity Ratios for Copolymerization of Ethylene (M_1) and Propylene (M_2) with Ziegler–Natta Catalysts

Catalyst	Cocatalyst	Temperature (°C)	r_1	r_2
VCl_4	$Al(C_2H_5)_2Cl$	–10	13.7	0.021
		21	3.0	0.073
$VOCl_3$	$Al(i\text{-}C_4H_9)_2Cl$	30	16.8	0.052
$V(acac)_3^a$	$Al(i\text{-}C_4H_9)_2Cl$	30	16	0.04
γ-$TiCl_3$	$Al(C_2H_5)_2Cl$	60	~8	0.05

[a]Vanadium acetylacetonate.

are used commercially because they generate side-chain unsaturation rather than in-chain unsaturation which could lead to oxidative chain scission:

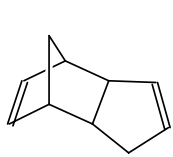

Dicyclopentadiene

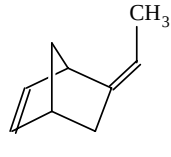

Ethylidene norbornene

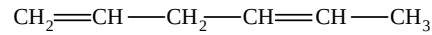

1,4-Hexadiene

The compositions for the more than 150 grades of EPDM elastomers are in the ranges of 40 to 90 mole % ethylene and 0 to 4 mole % diene [236]. Thus, the structure of a typical EPDM elastomer with ethylidene norbornene as termonomer can be represented by the following structure:

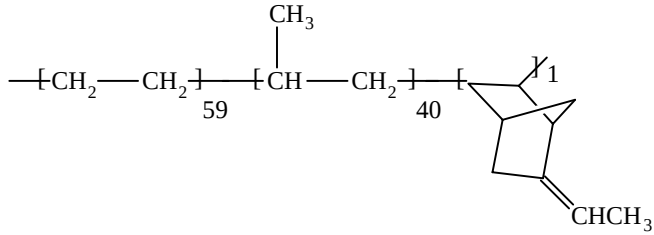

The compositions of EPDM elastomers are controlled by using the appropriate monomer feed ratio [see Eq. (38)] to obtain the desired composition in a continuous polymerization process. In general the excess propylene required is recycled. The molecular weights of EPDM polymers are controlled primarily by chain transfer reactions with added molecular hydrogen [Eqs. (86, 87)], as is common with other Ziegler-Natta polymerizations [228].

$$\text{P-V} + \text{H}_2 \xrightarrow{k_{tr}} \text{P-H} + \text{V-H} \tag{86}$$

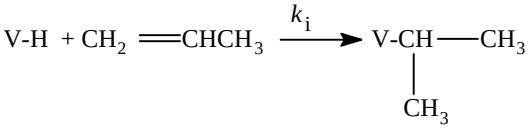

(87)

In the past 20 years, there has been a revolution in the field of Ziegler-Nata and related catalysts for olefin polymerization. This revolution has resulted from the discovery of single-site, homogeneous metallocene catalysts that exhibit higher activity and the ability to readily incorporate more hindered comonomers with ethylene more uniformly along the polymer chain [246, 247]. Metallocene catalysts contain one or two cyclopentadienyl rings coordinated to a transition metal such as titanium, zirconium, or hafnium. The higher activity of metallocene catalysts means that processes can be designed without the need for a catalyst removal step. The structure of a high activity, single-site, metallocene catalyst is shown below. It is noteworthy that a metallocene cation is the proposed catalytically active species. For this type of catalyst generated with a different counterion, the monomer reactivity ratios for copolymerization of ethylene and propylene are r(ethylene) = 1.35 and r(propylene) = 0.82, indicating an almost random copolymerization behavior [248]. These results can be compared with the copolymerization parameters for standard Ziegler-Natta catalysts in Table XVI.

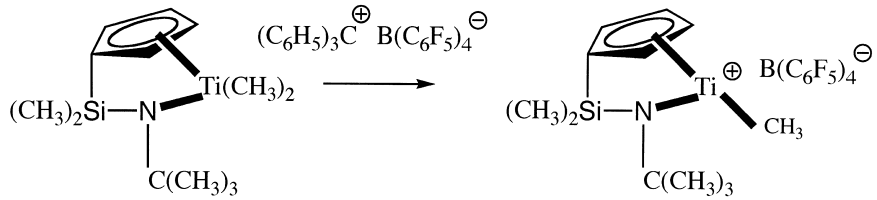

C. Polydienes

Shortly after the discovery of the Ziegler-Natta catalysts, it was found that analogous transition metal catalysts could also effect the stereospecific polymerization of dienes [249]. The wide range of stereoregular polybutadienes which can be prepared with these catalysts is indicated in Table XVII. The stereochemistry of polymerization is dependent upon the transition metal salt, the metal alkyl, temperature, additives, and the stoichiometry of the components. Commercial polybutadienes with high *cis*-1,4-microstructure are prepared using a wide range of transition metal catalysts, of which the most important are those derived from cobalt, nickel, neodymium, and titanium, analogous to those listed in Table XVII.

The mechanism of stereospecific polymerization of 1,3-dienes is also categorized as an insertion polymerization and simplified representations of the

TABLE XVII Microstructure of Polydienes from Transition Metal-Initiated Polymerization[a]

Transition metal salt/metal alkyl	Chain microstructure (mole %)			
	cis-1,4	*trans*-1,4	1,2	3,4
		Isoprene		
$TiCl_4/AlR_3$(1/1)	97			3[b]
α-$TiCl_3/Al(C_2H_5)_3$		98–100		
$Ti(OR)_4/AlR_3$(1/7–8)	36			
		Butadiene		
$TiI_4/Al(i\text{-}C_4H_9)_3$(1/4–5)	92–93	2–3	4–6	
$Ni(octanoate)/Al(C_2H_5)_3/BF_3$ (1/17/15)	96–97	2–3		
$CoCl_2/Al(C_2H_5)_2Cl$/pyridine · H_2O (1/1000/100)	98	1	1	
$NdCl_3/Al(i\text{-}C_4H_9)_3 \cdot nL$[c]	97	2.7	0.3	
$VCl_3/Al(C_2H_5)_3$		99–100		
$Co(acac)_3/AlR_3/CS_2$			99–100[d]	

[a]Data taken from Ref. [231].
[b]Ref. [250].
[c]L = Electron donor such as tetrahydrofuran or pyridine.
[d]Syndiotactic.

stereoselectivity for *cis* [Eq. (88)] and *trans* [Eq. (89)] enchainments are shown below [231].

cis-*stereospecificity*

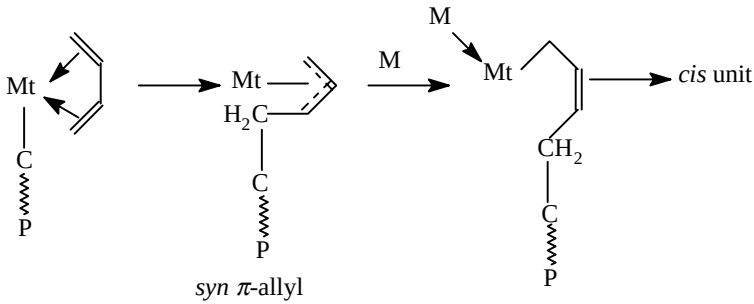

(88)

As indicated in these equations, the main factor determining the stereochemistry of enchainment is the mode of coordination of the transition metal center with the monomer to form either a syn or anti π-allyl type of intermediate. In general, the coordination with two double bonds of the 1,3-diene in an *s-trans* configuration [see (b) Eq. (89)] is less common than the coordination in an *s-cis* configuration shown in Eq. (88) [231]. This interpretation is complicated by the fact that the syn and anti π-allyl complexes are in equilibrium. These simple

trans-*stereospecificity*

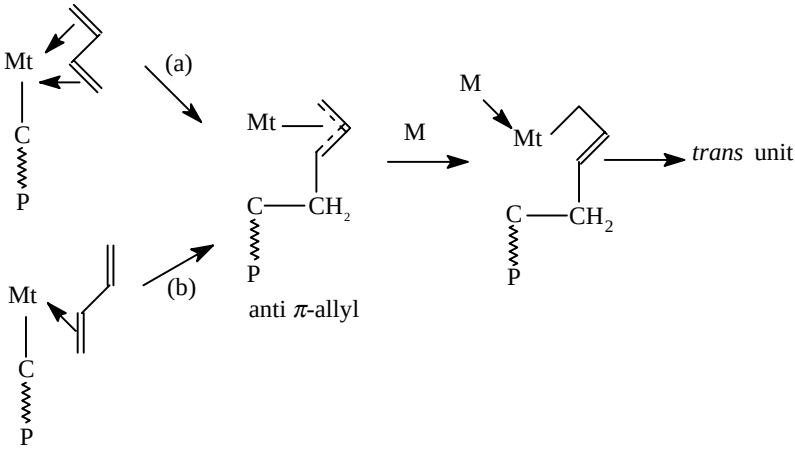

(89)

mechanistic representations are reinforced by the observations that the stereochemistry of diene polymerizations can be altered by the addition of electron donors such as $N(C_2H_5)_3$, $P(OC_6H_5)_3$, or C_2H_5OH. Thus, addition of these electron donors changes the stereochemistry from highly *cis*-stereospecific to highly *trans*-stereospecific for butadiene with catalysts such as $Co(acac)_2/Al(C_2H_5)_2Cl$ [231]. This is explained by assuming that the electron donor occupies one of the two coordination sites required for *cis*-enchainment [see Eq. (88)] which forces the monomer to only coordinate with one site [(b) in Eq. (89)].

The most recent developments in catalysts for stereospecific polymerization of dienes have been in the area of the rare earth or Lanthanide catalysts, specifically the neodymium complexes [251, 252]. The advantages of these systems are high stereospecificity, high activity, control of molecular weight, and no gel formation [251].

D. Polyalkenamers

Cyclic olefins undergo a very unusual type of ring-opening polymerization in the presence of certain transition metal catalysts [253–257]. This is illustrated in Eq. (90) for the ring-opening metathesis polymerization (ROMP) [255] of cyclooctene to form polyoctenamer. Quite surprisingly, the double bond is maintained in the polymer, i.e., it is not a normal addition polymer. The generally accepted mechanism for these

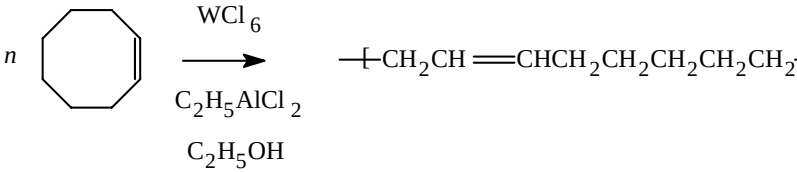

(90)

polymerizations proposes that the active propagating species is a metal carbene intermediate which undergoes a cycloaddition reaction with the cycloalkene to form a four-membered ring intermediate, i.e., a metallocyclobutane [256]. The metallocyclobutane then undergoes ring-opening to form a new metallocarbene propagating species as shown in the scheme below for polymerization of cyclopentene, where *Mt* represents the transition metal center, — □ represents an empty orbital which is available for coordination with the double bond of the monomer, and P_n is the growing polymer chain with number-average number of monomer units equal to *n*. As indicated, these are reversible polymerizations, and an equilibrium distribution of monomer, cyclic oligomers, and high molecular weight polymer is produced.

Scheme for Metathesis Ring Opening Polymerization:

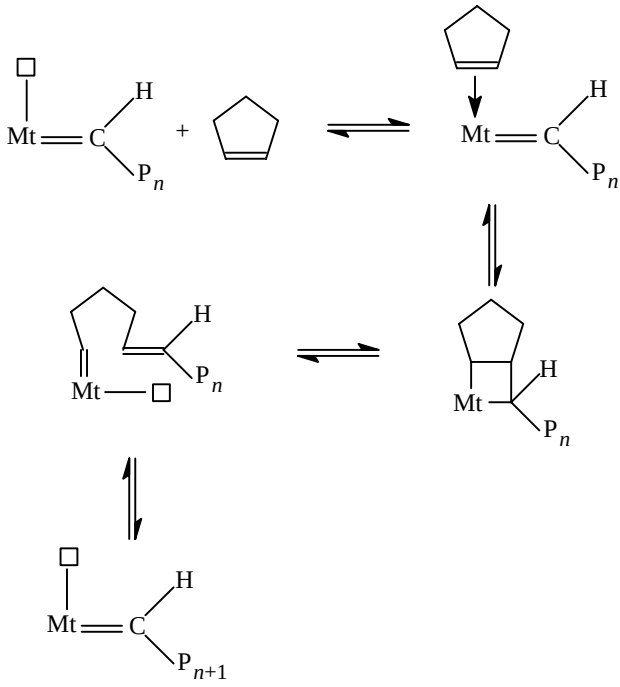

A possible reaction sequence for formation of the metal carbene is shown in Eq. (91), where [W] represents a tungsten catalyst center with its attendant ligands not specifically shown [256].

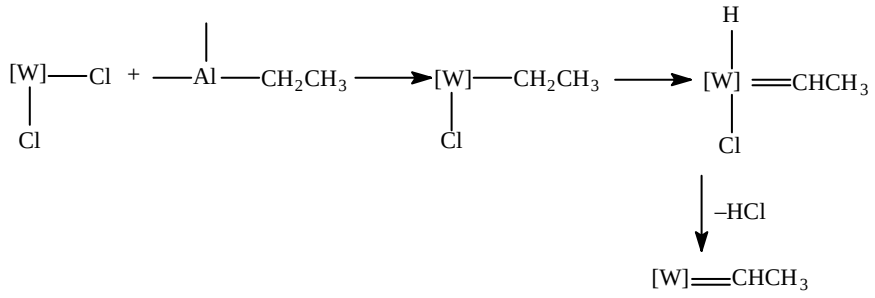

(91)

Although a variety of transition metal compounds can catalyze these ring-opening polymerizations, the most active catalysts are based on molybdenum, tungsten, and rhenium derivatives. These compounds are often used with organometallic cocatalysts, analogous to other transition metal catalysts for olefin and diene polymerization described in previous sections. The $WCl_6/EtAlCl_2/EtOH$ catalyst system has been described as a commercially useful type of catalyst [253]. In general, the stereochemistry of the polymerization varies with the catalyst and reaction time. Polymerizable monomers of importance for elastomer synthesis include cyclopentene, cyclooctene, and 1,5-cyclooctadiene; it is noteworthy that cyclohexene is not polymerizable by this method, presumably because there is no ring strain to drive the polymerization [257]. Another monomer of commercial significance is norbornene, which is very reactive; however, the resulting polymer has a relatively high glass transition temperature [T_g = 35°C for 80% *trans* polymer) [254], but the glass transition temperature can be lowered to –60°C with plasticizers [258].

Since the ring-opening metathesis polymerization is a reversible polymerization, an equilibrium molecular weight distribution of cyclic oligomers and high molecular weight polymer is ultimately obtained [256]; for example, polyoctenamer generally consists of 10 to 15% cyclic oligomer and 85 to 90% polymer [253]. At short reaction times and high monomer concentrations, relatively high molecular weight polymer is formed as a result of kinetic control; the molecular weight decreases with increasing reaction time. The equilibration process also equilibrates the configuration of the double bonds in the polymer such that eventually an equilibrium distribution of configuration results also. Molecular weight control in ring-opening methathesis polymerization is achieved by addition of acyclic alkenes, which react with the growing chain to terminate chain growth and generate a new metal carbene initiator as shown in Eq. (92). Commercially available polyoctenamers (Vestenamers, Hüls, AG) have weight-average molecular weights of approximately 10^5 g/mole, variable *trans*-double bond contents (62 to 80%) and glass transition temperatures of –75 to –80°C [253]. An interesting aspect of the physical pro-

perties of polyoctenamers is that they undergo stress-induced crystallization [254]. The commercial polymers described above have approximately 8 and 30% crystallinity for samples with 62 and 80% *trans*-double bond contents, respectively [253].

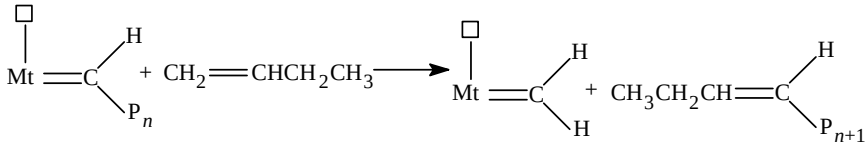

(92)

X. GRAFT AND BLOCK COPOLYMERIZATION*

The idea of graft [259–261] or block [262] copolymerization probably first arose as a means of modifying naturally occurring polymers, such as cellulose (cotton), rubber, or wool. Graft copolymerization, by analogy to the botanical term, refers to the growth of a "branch" of different chemical composition on the "backbone" of a linear macromolecule. In contrast, the related term, block copolymerization, refers to the specific case of growth of a polymer chain from the *end* of a linear macromolecule, thus leading to a composite linear macromolecule consisting of two or more "blocks" of different chemical structure. The importance of these types of polymer structures is basically due to the fact that polymer chains of different chemical structure, which are normally incompatible and form separate phases (because the small entropy of mixing is insufficient to overcome the mostly positive enthalpy of mixing), are chemically bonded to each other. This leads to the formation of microheterogeneities, which can have a profound effect on the mechanical properties of these heterophase systems when compared with the two homopolymers or with a physical mixture of the two polymers [263].

As one might expect, graft and block copolymerization can be accomplished by means of each of the three known mechanisms, i.e, radical, cationic, and anionic, each of which shows its own special characteristics [264]. Hence these mechanisms have been used wherever appropriate for the polymer and monomer involved. The examples quoted in the following discussions will deal primarily with elastomers.

A. Graft Copolymerization by Free Radical Reactions

This has been the most widely applied system for the formation of graft copolymers, since it provides the simplest method and can be used with a wide variety of polymers and monomers. It has not been very useful in the synthesis of block copolymers, as will become obvious from an examination of the methods used. These can be listed as follows.

*See also Chapters 12 and 13.

1. Chemical Initiation

This is still the most popular method for graft copolymerization of elastomers via free radicals. Free radicals (I•) are generated from the same types of initiators which are used for free radical polymerization and copolymerization (see Section IV). In general, these radicals are formed in the presence of a polydiene elastomer and a monomer; therefore, there are several possible reactions of these initiator-derived radicals which can occur as shown in Eqs. (93–96). The competition between initiation of monomer polymerization [Eq. (93)] and reactions to form polymer-derived radicals [Eqs. (94–96)] is dependent on the reactivity of the initiating radical. Thus, no graft copolymer formation with styrene monomer is observed for either polybutadiene or polyisoprene when azobisisobutryonitrile is used to generate radicals, although good grafting efficiency was observed for benzoyl peroxide–generated radicals [265, 266].

$$\mathrm{I} \longrightarrow \mathrm{I}\cdot \qquad (93)$$

$$\mathrm{I}\cdot + \mathrm{M} \xrightarrow{k_1} \mathrm{I{-}M}\cdot$$

$$\mathrm{I}\cdot + \text{—}[\mathrm{CH_2CH{=}CHCH_2}]\text{—} \xrightarrow{k_2} \mathrm{I{-}H} + \text{—}[\mathrm{\underset{\cdot}{C}HCH{=}CHCH_2}]\text{—} \qquad (94)$$

$$\mathrm{I}\cdot + \text{—}[\mathrm{CH_2CH{=}CHCH_2}]\text{—} \xrightarrow{k_3} \text{—}[\mathrm{CH_2CH(I){-}\underset{\cdot}{C}HCH_2}]\text{—} \qquad (95)$$

$$\mathrm{I}\cdot + \text{—}[\mathrm{CH_2CH}(\mathrm{CH{=}CH_2})]\text{—} \xrightarrow{k_3} \text{—}[\mathrm{CH_2CH}(\mathrm{\cdot CH{-}CH_2{-}I})]\text{—} \qquad (96)$$

This result also indicates that growing polystyryl radicals do not abstract hydrogen from these polydienes to generate polymer-derived radicals. The competition between addition of initiator radicals to the double bonds in the polydiene [Eqs. (95, 96)] and hydrogen abstraction [Eq. (94)] is also dependent on the initiator [267]. Thus, *t*-butoxy radicals [$(CH_3)_3CO\cdot$] exhibit an unusual preference for hydrogen abstraction compared to alkyl radicals as shown in Table XVIII. For radicals derived from benzoyl peroxide, the competition between the rate of hydrogen abstraction from polydiene [Eq. (94)] compared to addition of the initiator radical to styrene monomer [Eq. (93)], e.g., k_{abstr}/k_{ad}^{S}, was found to be 1.2 for polyisoprene and 0.63 for polybutadiene [265]. With respect to the addition of initiating radicals to the double bond of the polydiene, it is reported that grafting is favored by higher 1,2-microstructure in the polydiene [268, 269]; the

TABLE XVIII Radical Reactivity Toward Hydrogen Abstraction versus Addition to Double Bonds[a]

Radical	$k_{abstraction}/k_{addition}$[b]
t-$(CH_3)_3CO\cdot$	30
ROO·	1.0
$H_3C\cdot$	0.25
RS·	Exclusive addition

[a]Data taken from Ref. [267].
[b]Ratio of rate constant for hydrogen abstraction [see Eq. (94)] versus addition to a double bond [see Eqs. (95) and (96)].

rate of addition to a vinyl side chain [Eq. (96)] is faster than addition to an in-chain double bond [Eq. (95)].

The formation of graft copolymer from the polymer-derived radicals generated in Eqs. (93–96) are shown in Eqs. (97, 98), where P• represents the polymeric backbone radicals. Finally, in order to control the molecular weight of the graft chains, chain transfer agents such as long chain alkyl thiols can be added [see Eq. (27)] [270].

$$\mathrm{P}\cdot + n\,\mathrm{M} \longrightarrow \underset{\text{graft copolymer}}{\mathrm{P}-[\mathrm{M}]_n-\mathrm{M}\cdot} \tag{97}$$

$$\mathrm{P}\cdot + \mathrm{I}-[\mathrm{M}]_n-\mathrm{M}\cdot \longrightarrow \text{graft copolymer} \tag{98}$$

Since all of these reactions are occurring simultaneously during the graft copolymerization, there is always the possibility of formation of *homopolymer* during the grafting reaction, via reaction of the initiator radical with monomer [Eq. (93)] and also by chain transfer of the growing chain with species *other* than the polymer backbone (e.g., monomer, solvent, initiator). Therefore, in general, the graft copolymer will be contaminated with both the original backbone homopolymer as well as the monomer-derived homopolymer [259].

This type of graft copolymerization has been applied to the grafting of monomers like styrene and methyl methacrylate to natural rubber [271], directly in the latex [272, 273]. Similar methods have been developed for grafting the foregoing monomers, and many other vinyl monomers, to synthetic rubbers like SBR, leading to a variety of plastic-reinforced elastomers and rubber-reinforced high-impact plastics [270, 274]. In this case, grafting can also occur by the "copolymerization" of the monomer with the unsaturated bonds (mainly vinyl) in the polymer as described previously [see Eq. (96)]; thus

$$\mathrm{RM}_x\cdot + \sim\mathrm{CH_2}-\underset{\displaystyle \mathrm{CH_2}=\mathrm{CH}}{\underset{|}{\mathrm{CH}}}\sim \longrightarrow \sim\mathrm{CH_2}-\underset{\displaystyle \mathrm{RM}_x-\mathrm{CH_2}-\mathrm{CH}\cdot}{\underset{|}{\mathrm{CH}}}\sim \longrightarrow \cdots \longrightarrow$$

This reaction can, of course, also lead to crosslinking of the polymer chains, and this must be controlled.

2. Other Methods

Other methods of generating free radicals can also be used to initiate graft polymerization with elastomers, both natural and synthetic. These include irradiation of polymer-monomer mixtures by ultraviolet light [275], high-energy radiation [276, 277], and mechanical shear. The latter is of particular interest because of its unique mechanism, and has been extensively investigated.*

Thus it has been convincingly demonstrated that elastomers, when subjected to several mechanical shearing forces, undergo homolytic bond scission to form free chain radicals. The latter, when in the presence of oxygen, may then undergo various reactions, either becoming stabilized ruptured chains or reacting with other chains to form branched or crosslinked species [278, 279]. When blends of different elastomers are masticated, "interpolymers" are formed by the interaction of the radicals formed from the copolymers [280]. A further extension of such mechanochemical processes occurs when elastomers are masticated in the presence of polymerizable monomers, the chain radicals initiating polymerization and leading to formation of block and graft structures. This was clearly demonstrated in the case of natural rubber [274] and of other elastomers [281, 282]. It should be noted that living anionic polymerizations [283] and controlled/living radical polymerizations such as atom transfer radical polymerization (ATRP) [284] have been used to make well-defined graft copolymers. A very useful method is to copolymerize a well-defined macromonomer bearing a polymerizable chain end group with another monomer to generate a graft copolymer with a random distribution of well-defined graft branches [285].

B. Block Copolymers by Anionic Mechanism

It is, of course, the anionic mechanism which is most suitable for the synthesis of block copolymers, since many of these systems are of the living polymer type, as described previously [144, 150, 165, 194, 262, 263]. Thus it is possible to use organoalkali initiators to prepare block copolymers in homogeneous solution by sequential addition of monomers, where each block has a prescribed molecular weight, based on monomer-initiator stoichiometry, as well as a very narrow molecular weight distribution (Poisson) [185]. As would be expected, such block copolymers are very "pure," due to the absence of any side reactions during the polymerization (e.g., termination, monomer transfer, branching).

Organolithium initiators have been particularly useful in this regard, since they are soluble in a variety of solvents [178] and since they can initiate the polymerization of a variety of monomers, such as styrene and its homologs,

*See also Chapter 11.

the 1,3-dienes, alkyl methacrylates, vinylpyridines, cyclic oxides and sulfides, and cyclic siloxanes [143, 144, 150, 262]. Various block copolymers of these monomers have been synthesized, some commercially, but the outstanding development in this area has been in the case of the ABA type of triblock copolymers, and these deserve special mention [263].

The ABA triblocks which have been most exploited commercially are of the styrene-diene-styrene type, prepared by sequential polymerization initiated by alkyllithium compounds as shown in Eqs. (99–101) [263, 286]. The behavior of these block copolymers illustrates the special characteristics of block (and graft) copolymers, which are based on the general *incompatibility* of the different blocks [287]. Thus for a typical "thermoplastic elastomer" (263), the polystyrene end blocks (~15,000–20,000 MW) aggregate into a separate phase, which forms a microdispersion within the matrix composed of the polydiene chains (50,000–70,000 MW) [288–290]. A schematic representation of this morphology is shown in Fig. 3. This phase separation, which occurs in the melt (or swollen) state, results, at ambient temperatures, in a network of

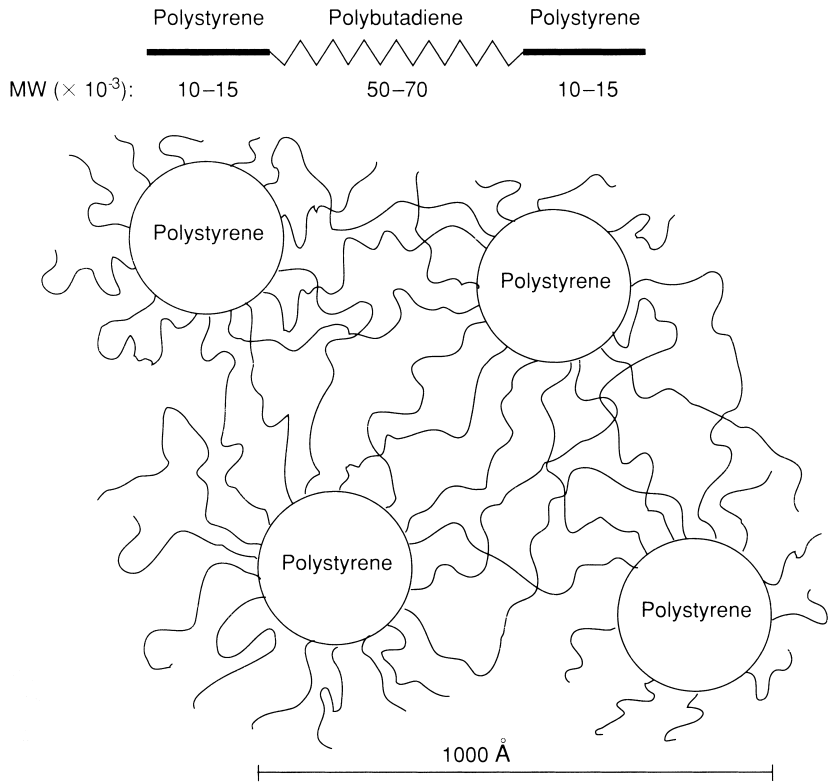

FIGURE 3 Structure of thermoplastic elastomers from ABA triblock copolymers. (From Morton [291].)

elastic polydiene chains held together by glassy polystyrene microdomains. Hence these materials behave as virtually crosslinked elastomers at ambient temperatures, but are completely thermoplastic and fluid at elevated temperatures.

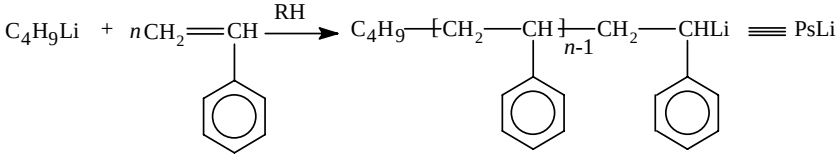

(99)

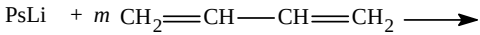

(100)

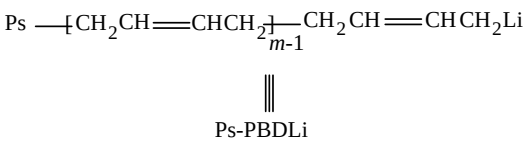

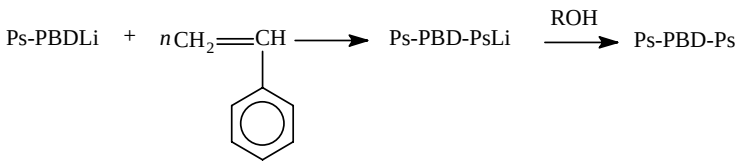

(101)

It is important to note that the morphology of ABA block copolymers is dependent primarily on the relative composition of the block components [165, 287]. For example, as the styrene content increases, the morphology changes from spherical polystyrene domains to cylindrical; further increases in styrene content result in lamellar arrays of both phases and eventually phase inversion to form a continuous polystyrene phase. The properties of the ABA triblock copolymers are dependent and vary with the composition.

Such "thermoplastic elastomers" are very attractive technologically, since they can be heat-molded like thermoplastics, yet exhibit the behavior of rubber vulcanizates. As would be expected, their structure, morphology, and mechanical properties have been studied extensively [291–294]. An electron photomicrograph of a typical styrene-isoprene-styrene (SIS) triblock film is shown in Fig. 4, while the tensile properties of a series of such triblock copolymers are shown in Fig. 5. The unusually high tensile strength of these elastomers, better than that of conventional vulcanizates, is ascribed both to the remarkable regularity of the network, as illustrated in Fig. 5, and to the energy-absorbing characteristics of the polystyrene domains, which yield and distort under high stress [291].

This interesting behavior of the ABA triblock copolymers is not a unique feature of the styrene-diene structure, but can be found in the case of other

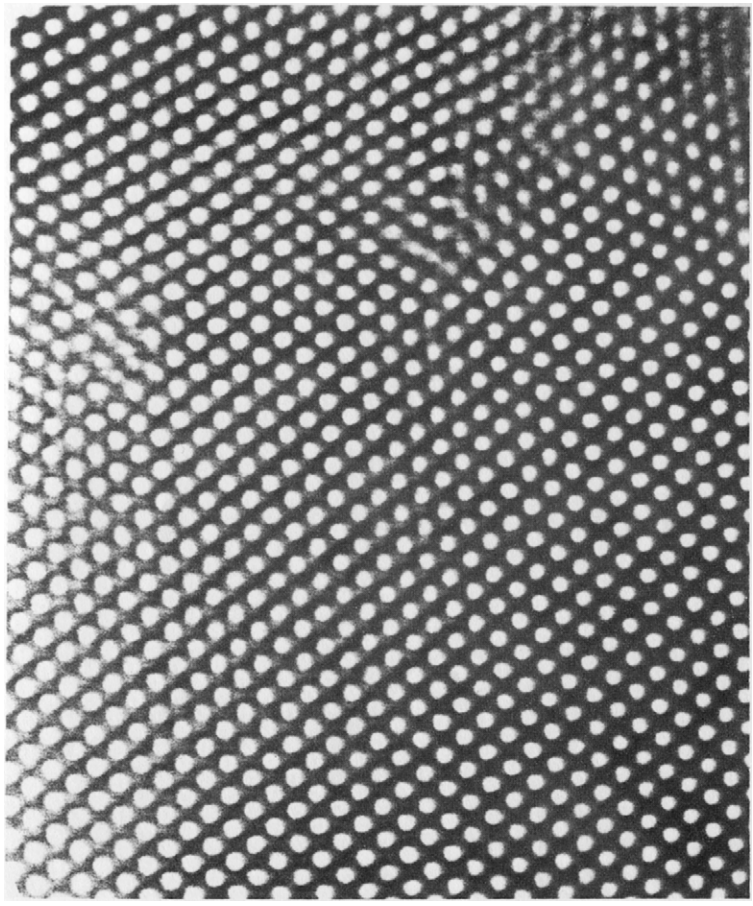

FIGURE 4 Transmission electron photomicrograph of an ultrathin film of a styrene-isoprene–styrene triblock copolymer (MW 16,200–75,600–16,2000). ×100,000.

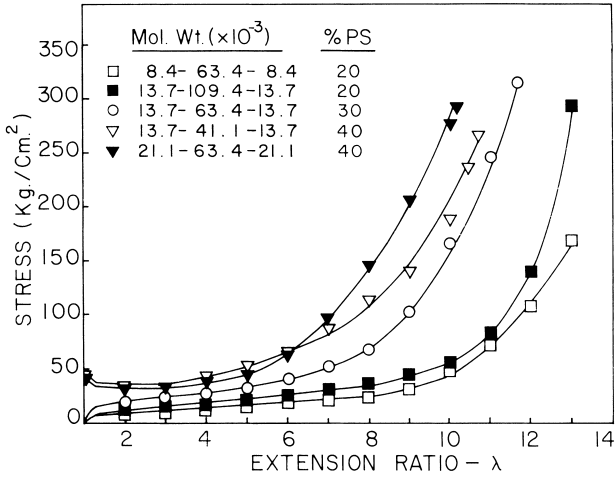

FIGURE 5 Tensile properties of styrene–isoprene–styrene triblock copolymers. (From Morton [291].)

analogous chemical structures. Thus thermoplastic elastomers have been obtained from other triblock copolymers, where the dienes have been replaced by cyclic sulfides [295], cyclic siloxanes [296], or alkyl acrylates [297]; poly(alkyl methacrylate) end blocks have also been investigated [297]. Furthermore, the advent of a number of different types of living polymerization with transition metal, cationic, and radical propagating centers provides new mechanisms for synthesis of ABA-type block copolymers utilizing a wide variety of monomer types [263].

It is important to note that any molecular architecture that provides a thermoplastic block chemically bonded to an elastomeric block, which is in turn bonded to another thermoplastic segment, should exhibit the properties of a thermoplastic elastomer. For example, grafting thermoplastic branches onto an elastomeric backbone produces thermoplastic elastomer behavior [285, 298]. Other examples are the segmented-type polymers—$[AB]_n$—with alternating hard and soft segments; thus, a variety of segmented polyesters and polyurethanes with polyether or polyester soft segments exhibit properties of thermoplastic elastomers [263, 298, 299].

REFERENCES

1. G. Williams, *Proc. R. Soc. London* **10**, 516 (1860).
2. G. Bouchardat, *C. R. H. Acad. Sci.* **89**, 1117 (1879).
3. W. A. Tilden, *J. Chem. Soc.* **45**, 411 (1884).
4. I. Kondakow, *J. Prakt. Chem.* **62**, 66 (1900).
5. J. Thiele, *Justus Liebig's Ann. Chem.* **319**, 226 (1901).
6. S. V. Lebedev, *Zh. Russ. Fiz.-Kim. Ova. Chast.* **42**, 949 (1910).
7. C. D. Harries, *Justus Liebig's Ann. Chem.* **383**, 190 (1911).
8. F. E. Matthews and E. H. Strange, British Patent 24,790 (1910).
9. H. Staudinger, *Chem. Ber.* **53**, 1073 (1920).
10. W. H. Carothers, J. Williams, A. M. Collins, and J. E. Kirby, *J. Am. Chem. Soc.* **53**, 4203 (1931).
11. P. J. Flory, "Principles of Polymer Chemistry," Cornell Univ. Press, Ithaca, NY, 1953, Chap. 1.
12. H. Morawetz, "Polymers: The Origins and Growth of a Science," Wiley, New York, 1985.
13. M. Morton, *Rubber Plast. Age* **42**, 397 (1961).
14. W. H. Carothers, *J. Am. Chem. Soc.* **51**, 2548 (1929).
15. W. H. Carothers, *Chem. Rev.* **8**, 353 (1931).
16. D. Braun, H. Cherdron, and W. Kern, "Practical Macromolecular Organic Chemistry," Harwood Academic Publishers, New York, 1984, p. 255.
17. S. R. Sandler and W. Karo, "Polymer Syntheses," 2nd ed., Academic Press, San Diego, 1992, p. 127.
18. G. C. Eastmond, A. Ledwith, S. Russo, and P. Sigwalt (Eds.), "Comprehensive Polymer Science," Vol. 5: "Step Polymerization," Pergamon Press, Oxford, 1989.
19. J. A. Moore (Ed.), "Macromolecular Synthesis, Collective Volume 1," Wiley, New York, 1978.
20. J. H. Saunders and F. Dobinson, in "Comprehensive Chemical Kinetics," C. H. Bamford and C. F. H. Tipper (Eds.), Elsevier, New York, Vol. 15, 1976, Chap. 7.
21. G. C. Eastmond, A. Ledwith, S. Russo, and P. Sigwalt (Eds.), "Comprehensive Polymer Science," Vol. 3: "Chain Polymerization I;" Vol. 4: "Chain Polymerization II," Pergamon Press, Oxford, 1989.
22. G. Odian, "Principles of Polymerization," 4th ed. Wiley-Interscience, New York, 2004.

23. S. A. Penczek, *J. Polym. Sci.: Part A: Polym. Chem*. **40**, 1665 (2002).
24. A. D. Jenkins, P. Kratochvil, R. F. T. Stepto, and U. W. Suter, *Pure Appl. Chem*. **68**, 2287 (1996).
25. D. H. Solomon (Ed.), "Step-Growth Polymerizations," Dekker, New York, 1972.
26. G. C. Eastmond, in "Comprehensive Chemical Kinetics," Vol. 14A: "Free Radical Polymerization," C. H. Bamford and C. F. H. Tipper (Eds.), Elsevier, New York, 1976, p. 1.
27. R. G. Gilbert, *Pure Appl. Chem*. **64**, 1563 (1992).
28. R. G. Gilbert, *Pure Appl. Chem*. **68**, 1491 (1996).
29. M. Buback, R. G. Gilbert, R. A. Hutchinson, B. Klumperman, F. D. Kuchta, B. G. Manders, K. F. O'Driscoll, G. T. Russell, and J. Schweer, *J. Macromol. Chem. Phys*. **196**, 3267 (1995).
30. M. S. Matheson, E. E. Auer, E. B. Bevilacqua, and E. J. Hart, *J. Am. Chem. Soc.* **71**, 497, 2610 (1949); ibid., **73**, 1700, 5395 (1951).
31. M. Morton, P. Salatiello, and H. Landfield, *J. Polym. Sci.* **8**, 215 (1952).
32. M. Morton and S. D. Gadkary, 130th Meet., Am. Chem. Soc., Atlantic City, N.J., 1956; S. D. Gadkary, M. S. Thesis, Univ. of Akron, Akron, Ohio, 1956.
33. S. Beuermann, M. Buback, T. P. Davis, R. G. Gilbert, R. A. Hutchinson, O. F. Olaj, G. T. Russell, J. Schweer, and A. M. van Herk, *Macromol. Chem. Phys.* **198**, 1545 (1997).
34. P. A. Weerts, A. L. German, and R. G. Gilbert, *Macromolecules* **24**, 1622 (1991).
35. R. A. Hutchinson, M. T. Aronson, and J. R. Richards, *Macromolecules* **26**, 6410 (1993).
36. G. V. Schulz, *Z. Phys. Chem.*, Abt., B **43**, 25 (1939).
37. G. S. Whitby and R. N. Crozier, *Can. J. Res.* **6**, 203 (1932).
38. D. H. Solomon, E. Rizzardo, and P. Cacioli, U.S. Patent 4,581,429 (1986).
39. M. K. Georges, R. P. N. Veregin, P. M. Kazmeier, and G. K. Hamer, *Macromolecules* **29**, 5245 (1993).
40. C. J. Hawker, *J. Am. Chem. Soc.* **116**, 11185 (1994).
41. T. Fukuda, T. Terauchi, A. Goto, Y. Tsuhii, T. Miyamoto, and Y. Shimizu, *Macromolecules* **29**, 3050 (1996).
42. C. J. Hawker, A. W. Bosman, and E. Harth, *Chem. Rev.* **101**, 3661 (2001).
43. T. Fukuda and A. Goto, in "Controlled/Living Radical Polymerization," K. Matyjaszewski (Ed.), ACS Symposium Series 768, American Chemical Society, Washington, D.C., 2000, p. 27.
44. B. Keoshkerian, M. Georges, M. Quinlan, R. Veregin, and B. Goodbrand, *Macromolecules* **31**, 7559 (1998).
45. H. Fischer, *Macromolecules* **30**, 5666 (1997).
46. H. Fischer, *J. Polym. Sci., Part A: Polym. Chem*. **37**, 1885 (1999).
47. K. Matyjaszewski (Ed.), "Controlled/Living Radical Polymerization," ACS Symposium Series 768, American Chemical Society, Washington, D.C., 2000.
48. K. Matyjaszewski (Ed.), "Controlled/Living Radical Polymerization," ACS Symposium Series 685, American Chemical Society, Washington, D.C., 1998.
49. M. K. Georges, G. K. Hamer, and N. A. Listigovers, *Macromolecules* **31**, 9087 (1998).
50. D. Benoit, E. Harth, P. Fox, R. M. Waymouth, and C. J. Hawker, *Macromolecules* **33**, 363 (2000).
51. K. Matyjaszewski and J. Xia, *Chem. Rev*. **101**, 2921 (2001).
52. G. W. Poehlein, in "Encyclopedia of Polymer Science and Engineering," J. I. Kroschwitz (Ed.), Wiley-Interscience, New York, Vol. 6, 1986, p. 1.
53. I. Piirma (Ed.), "Emulsion Polymerization," Academic Press, New York, 1982.
54. D. C. Blackley, "Emulsion Polymerization," Applied Science Publishers, London, 1975.
55. D. H. Napper and R. G. Gilbert, in "Comprehensive Polymer Science," G. C. Eastmond, A. Ledwith, S. Russo, and P. Sigwalt (Eds.), Pergamon, Oxford, Vol. 4, 1989, p. 171.
56. R. G. Gilbert, "Emulsion Polymerization: A Mechanistic Approach," Academic Press, San Diego, 1995.
57. K. Tauer, in "Encyclopedia of Polymer Science and Technology," J. I. Kroschwitz (Ed.), Wiley-Interscience, New York, Vol. 6, 2003, p. 410.
58. P. A. Lovell and M. S. El-Aasser (Eds.), "Emulsion Polymerization and Emulsion Polymers," Wiley, New York, 1997.

59. W. D. Harkins, *J. Am. Chem. Soc.* **69**, 1428 (1947).
60. J. L. Gardon, in "Polymerization Processes," C. E. Schildknecht (Ed.), Wiley-Interscience, New York, 1977, Chap. 6.
61. M. Morton, S. Kaizerman, and M. W. Altier, *J. Colloid Sci.* **9**, 300 (1954).
62. W. V. Smith and R. H. Ewart, *J. Chem. Phys.* **16**, 592 (1948).
63. M. Morton and W. E. Gibbs, *J. Polym. Sci., Part A* **1**, 2679 (1963).
64. W. Hofmann, "Rubber Technology Handbook," Hanser Publishers, Munich, West Germany, 1989.
65. C. M. Blow (Ed.), "Rubber Technology and Manufacture," Hewnes-Butterworths, London, 1971.
66. J. A. Brydson, in "Developments in Rubber Technology-2," A. Whelan and K. S. Lee (Eds.), Applied Science Publishers, London, 1981, p. 21.
67. R. G. Bauer, in "Kirk-Othmer Encyclopedia of Chemical Technology," 3rd ed., Wiley, New York, Vol. 8, 1979, p. 611.
68. H. N. Sun and J. P. Wusters, in "Kirk-Othmer Encyclopedia of Chemical Technology," 4th ed., J. I. Kroschwitz (Ed.), Wiley-Interscience, New York, Vol. 4, 2004, p. 365.
69. M. Demirors, in "Encyclopedia of Polymer Science and Technology," J. I. Kroschwitz (Ed.), Wiley-Interscience, New York, Vol. 4, 2003, p. 229.
70. M. Morton and P. P. Salatiello, *J. Polym. Sci.* **6**, 225 (1951).
71. J. L. Binder, *Ind. Eng. Chem.* **46**, 1727 (1954).
72. K. E. Beu, W. B. Reynolds, C. F. Fryling, and H. L. McMurry, *J. Polym. Sci.* **3**, 465 (1948).
73. A. W. Meyer, *Ind. Eng. Chem.* **41**, 1570 (1949).
74. P. R. Johnson, *Rubber Chem. Tech.* **49**, 650 (1976).
75. C. A. Stewart, Jr., T. Takeshita, and M. L. Coleman, in "Encyclopedia of Polymer Science and Engineering," J. I. Kroschwitz (Ed.), Wiley, Vol. 3, 1985, p. 441.
76. D. C. Blackley, "Synthetic Rubbers: Their Chemistry and Technology," Applied Science Publishers, Essex, 1983, p. 175.
77. R. Musch and H. Magg, in "Polymeric Materials Encyclopedia," J. C. Salamone (Ed.), CRC Press, Boca Raton, FL, Vol. 2, 1996, p. 1238.
78. D. I. Christie, R. G. Gilbert, J. P. Congalidis, J. R. Richards, and J. H. McMinn, *Macromolecules* **34**, 5158 (2001).
79. M. Morton, J. A. Cala, and M. W. Altier, *J. Polym. Sci.* **19**, 547 (1956).
80. M. Morton and I. Piirma, *J. Polym. Sci.* **19**, 563 (1956).
81. A. M. Neal and L. R. Mayo, in "Synthetic Rubber," G. S. Whitby (Ed.), Wiley, New York, 1954, p. 770.
82. W. E. Mochel and J. H. Peterson, *J. Am. Chem. Soc.* **71**, 1426 (1949).
83. C. A. Hargreaves, in "Polymer Chemistry of Synthetic Elastomers," J. P. Kennedy, E. Tornqvist (Eds.), Wiley-Interscience, New York, 1968, p. 233.
84. M. M. Coleman and E. G. Brame, Jr., *Rubber Chem. Tech.* **51**, 668 (1978).
85. M. M. Coleman, D. L. Tabb, and E. G. Brame, Jr., *Rubber Chem. Tech.* **50**, 49 (1977).
86. J. R. Ebdon, *Polymer* **19**, 1232 (1978).
87. R. Petiaud and Q. T. Pham, *J. Polym. Sci., Polym. Chem. Ed.* **23**, 1333 (1985).
88. R. R. Garrett, C. A. Hargreaves, and D. N. Robinson, *J. Macromol. Sci. Chem. A* **4**, 1679 (1970).
89. A. E. Hamielec, J. F. MacGregor, and A. Penlidis, in "Comprehensive Polymer Science," G. C. Eastmond, A. Ledwith, S. Russo, P. Sigwalt (Eds.), Pergamon, Oxford, Vol. 3, 1989, p. 17.
90. G. Odian, "Principles of Polymerization," 4th ed., Wiley-Interscience, New York, 2004, Chap. 6.
91. G. E. Ham (Ed.), "Copolymerization," Wiley-Intersceince, New York, 1964.
92. D. A. Tirrell, in "Encyclopedia of Polymer Science and Engineering," 2nd ed., J. I. Kroschwitz (Ed.), Wiley, New York, Vol. 4, 1986, p. 192.
93. D. A. Tirrell, in "Comprehensive Polymer Science," G. C. Eastmond, A. Ledwith, S. Russo, and P. Sigwalt (Eds.), Pergamon, Oxford, Vol. 3, 1989, p. 195.
94. F. R. Mayo and C. Walling, *Chem. Rev.* **46**, 191 (1950).

95. F. R. Mayo and F. M. Lewis, *J. Am. Chem. Soc.* **66**, 1594 (1944).
96. R. Z. Greenley, in "Polymer Handbook," 4th ed., J. Brandrup and E. H. Immergut (Eds.), Wiley-Interscience, New York, 1999, II-181.
97. G. C. Eastman and E. G. Smith, in "Comprehensive Chemical Kinetics," C. H. Bamford and C. F. H. Tipper (Eds.), Elsevier, New York, Vol. 14A, 1976, p. 333.
98. C. A. Uraneck, in "Polymer Chemistry of Synthetic Elastomers," Part I, J. P. Kennedy and E. Tornqvist (Eds.), Wiley-Interscience, New York, 1968, p. 158.
99. C. F. Fryling, in "Synthetic Rubber," G. S. Whitby (Ed.), Wiley, New York, 1954, p. 257.
100. Y. Tanaka, H. Sato, and J. Adachi, *Rubber Chem. Tech.* **59**, 16 (1986).
101. Y. Tanaka, H. Sato, Y. Nakafutami, and Y. Kashiwazaki, *Macromolecules* **16**, 1925 (1983).
102. W. Hofmann, *Rubber Chem. Tech.* **37**, 1 (1964).
103. R. Greenley, *J. Macromol. Sci. Chem.* **14**, 445 (1980).
104. J. P. Kennedy and B. Ivan, "Designed Polymers by Carbocationic Macromolecular Engineering: Theory and Practice," Hanser Publishers, Munich, 1992.
105. J. P. Kennedy and E. Marechal, "Carbocationic Polymerization," Wiley-Interscience, New York, 1982.
106. J. P. Kennedy, "Cationic Polymerization of Olefins: A Critical Inventory," Wiley-Interscience, New York, 1975.
107. M. Sawamoto and T. Higashimura, in "Encyclopedia of Polymer Science and Engineering," J. I. Kroschwitz (Ed.), Wiley-Interscience, New York, 1989, Supplemental Volume, p. 399.
108. G. Odian, "Principles of Polymerization," 4th ed., Wiley-Interscience, New York, 2004, Chap. 5.
109. A. Gandini and H. Cheradame, in "Encyclopedia of Polymer Science and Engineering," J. I. Kroschwitz (Ed.), Wiley-Interscience, New York, Vol. 2, 1985, p. 729.
110. K. Matyjaszewski (Ed.), "Cationic Polymerizations: Mechanisms, Synthesis, and Applications," Marcel Dekker, New York, 1996.
111. J. E. Puskas and G. Kaszas, in "Encyclopedia of Polymer Science and Technology," J. I. Kroschwitz (Ed.), Wiley-Interscience, New York, Vol. 5, 2003, p. 382.
112. S. Winstein, E. Clippinger, A. H. Fainberg, and G. C. Robinson, *J. Am. Chem.* Soc. **76**, 2597 (1954).
113. R. G. W. Norrish and K. E. Russell, *Trans. Faraday Soc.* **48**, 91 (1952).
114. A. G. Evans and M. Polanyi, *J. Chem. Soc.* 252 (1947).
115. E. N. Kresge, R. H. Schatz, and H. C. Wang, in "Encyclopedia of Polymer Science and Engineering," J. I. Kroschwitz (Ed.), Wiley-Interscience, New York, Vol. 8, 1987, p. 423.
116. R. N. Webb, T. D. Shaffer, and A. H. Tsou, in "Encyclopedia of Polymer Science and Technology," J. I. Kroschwitz (Ed.), Wiley-Interscience, New York, Vol. 5, 2003, p. 356.
117. D. C. Pepper, *Sci. Proc. R. Dublin Soc.* **25**, 131 (1950).
118. F. S. Dainton and G. B. B. M. Sutherland, *J. Polym. Soc.* **4**, 347 (1949).
119. I. Puskas, E. M. Banas, and A. G. Nerheim, *J. Polym. Sci., Symp.* **56**, 191 (1976).
120. D. C. Pepper, *Trans. Faraday Soc.* **45**, 404 (1949).
121. D. D. Eley and A. W. Richards, *Trans. Faraday Soc.* **45**, 425, 436 (1949).
122. P. H. Plesch, *J. Chem. Soc.* 543 (1950).
123. L. Sipos, P. De, and R. Faust, *Macromolecules* **36**, 8282 (2003).
124. J. P. Kennedy, in "Polymer Chemistry of Synthetic Elastomers," J. P. Kennedy and E. Tornqvist (Eds.), Wiley-Interscience, New York, 1968, Part I, p. 291.
125. H. Y. Che and J. E. Field, *J. Polym. Sci., Part B* **5**, 501 (1957).
126. M. Miyamoto, M. Sawamoto, and T. Higashimura, *Macromolecules* **17**, 265 (1984).
127. R. Faust and J. P. Kennedy, *Polym. Bull. (Berlin)* **15**, 317 (1986).
128. S. Hadjikyriacou, M. Acar, and R. Faust, *Macromolecules* **37**, (2004) *in press*.
129. K. Matyjaszewski (Ed.), "Cationic Polymerizations: Mechanisms, Synthesis, and Applications," Dekker, New York, 1996.
130. R. W. Body and V. L. Kyllingstad, in "Encyclopedia of Polymer Science and Engineering," J. I. Kroschwitz (Ed.), Wiley-Interscience, New York, Vol. 6, 1986, p. 307.

131. E. J. Vandenberg, *J. Polym. Sci.* **7**, 525 (1969).
132. E. J. Vandenberg, in "Coordination Polymerization," C. C. Price and E. J. Vandenberg (Eds.), Plenum Press, New York, 1983, p. 11.
133. W. Meckel, W. Goyert, W. Wieder, and H. G. Wussow, in "Thermoplastic Elastomers," 3rd ed., G. Holden, H. R. Kricheldorf, and R. P. Quirk (Eds.), Hanser Publishers, Munich, 2004, p. 15.
134. R. K. Adams, G. K. Hoeschele, and W. K. Witsiepe, in "Thermoplastic Elastomers," 3rd ed., G. Holden, H. R. Kricheldorf, and R. P. Quirk (Eds.), Hanser Publishers, Munich, 2004, p. 183.
135. S. Inoue and T. Aida, in "Ring-Opening Polymerization," K. J. Ivin and T. Saegusa (Eds.), Elsevier, New York, Vol. 1, 1984, p. 185.
136. P. Dreyfuss, "Poly(tetrahydrofuran)," Gordon and Breach, New York, 1982.
137. S. Penczek, P. Kubisa, and K. Matyjaszewski, *Adv. Polym. Sci.* **68/69**, 1 (1985).
138. S. Penczek and P. Kubisa, in "Comprehensive Polymer Science," G. C. Eastmond, A. Ledwith, S. Russo, and P. Sigwalt (Eds.), Pergamon Press, Oxford, Vol. 3, 1989, p. 751.
139. P. Dreyfuss, M. P. Dreyfuss, and G. Pruckmayr, in "Encyclopedia of Polymer Science and Engineering," J. I. Kroschwitz (Ed.), Wiley-Interscience, New York, Vol. 16, 1989, p. 649.
140. M. P. Dreyfuss and P. Dreyfuss, *J. Polym. Sci. A-1* **4**, 2179 (1966).
141. G. Pruckmayr and T. K. Wu, *Macromolecules* **11**, 662 (1978).
142. K. Matyjaszewski, P. Kubisa, and S. Penzcek, *J. Polym. Sci., Polym. Chem. Ed.* **13**, 763 (1975).
143. R. P. Quirk, in "Encyclopedia of Polymer Science and Technology," 3rd ed., J. I. Kroschwitz (Ed.), Wiley-Interscience, New York, Vol. 5, 2003, p. 111.
144. M. Morton, "Anionic Polymerization: Principles and Practice," Academic Press, New York, 1982.
145. M. Szwarc, "Carbanions, Living Polymers and Electron Transfer Processes," Interscience, New York, 1968.
146. P. Rempp, E. Franta, and J. E. Herz, *Adv. Polym. Sci.* **86**, 145 (1988).
147. R. N. Young, R. P. Quirk, and L. J. Fetters, *Adv. Polym. Sci.* **56**, 1 (1984).
148. M. Szwarc, *Adv. Polym. Sci.* **49**, 1 (1983).
149. M. van Beylen, S. Bywater, G. Smets, M. Szwarc, and D. J. Worsfold, *Adv. Polym. Sci.* **86**, 87 (1988).
150. H. L. Hsieh and R. P. Quirk, "Anionic Polymerization," Dekker, New York, 1996.
151. M. Szwarc, "Ionic Polymerization Fundamentals," Hanser, Cincinnati, 1996.
152. W. C. E. Higginson and N. W. Wooding, *J. Chem. Soc.* 760 (1952).
153. R. E. Robertson and L. Marion, *Can. J. Res., Sect. B.* **26**, 657 (1948).
154. D. E. Paul, D. Lipkin, and S. I. Weissman, *J. Am. Chem. Soc.* **78**, 116 (1956).
155. B. J. McClelland, *Chem. Rev.* **64**, 301 (1964).
156. M. T. Jones, in "Radical Ions," E. T. Kaiser and L. Kevan (Eds.), Wiley, New York, 1968.
157. M. Szwarc and J. Jagur-Grodzinski, in "Ions and Ion Pairs in Organic Reactions," M. Szwarc (Ed.), Wiley, 1974, p. 1.
158. N. L. Holy, *Chem. Rev.* **74**, 243 (1974).
159. M. Szwarc, M. Levy, and R. Milkovich, *J. Am. Chem. Soc.* **78**, 2656 (1956).
160. P. J. Flory, *J. Am. Chem. Soc.* **62**, 1561 (1940); see also Ref. 11, p. 336.
161. H. L. Hsieh, R. C. Farrar, and K. Udipi, *CHEMTECH* **626** (1981).
162. I. G. Hargis, R. A. Livigni, and S. L. Aggarwal, in "Developments in Rubber Technology-4," A. Wheland and K. S. Lee (Eds.), Elsevier, Essex, UK, 1987, p. 1.
163. H. L. Hsieh and O. F. McKinney, *J. Polym. Sci., Polym. Lett.* **4**, 843 (1966).
164. M. Morton, A. Rembaum, and J. L. Hall, *J. Polym. Sci. A* **1**, 461 (1963).
165. R. P. Quirk, D. J. Kinning, and L. J. Fetters, in "Comprehensive Polymer Science," G. Allen and J. C. Bevington (Eds.), Pergamon Press, Oxford, Vol. 7, 1989, p. 1.
166. N. Hadjichristidis, S. Pispas, and G. A. Floudas, "Block Copolymers: Synthetic Strategies, Physical Properties, and Applications," Wiley-Interscience, New York, 2003.
167. R. P. Quirk, in "Comprehensive Polymer Science," First Supplement, S. L. Aggarwal and S. Russo (Eds.), Pergamon Press, Oxford, 1992, p. 83.
168. H. L. Hsieh, *Rubber Chem. Tech.* **49**, 1305 (1976).

169. B. J. Bauer and L. J. Fetters, *Rubber Chem. Tech.* **51**, 406 (1978).
170. S. Bywater, *Adv. Polym. Sci.* **30**, 89 (1979).
171. N. Hadjichristidis, M. Pitsikalis, S. Pispas, and H. Iatrou, *Chem. Rev*. **101**, 3747 (2001).
172. S. Bywater, in "Comprehensive Chemical Kinetics," C. H. Bamford and C. F. H. Tipper (Eds.), Elsevier, New York, Vol. 15, 1976, p. 1.
173. A. H. Müller, in "Comprehensive Polymer Science," Vol. 3: "Chain Polymerization I," G. C. Eastmond, A. Ledwith, S. Russo, and P. Sigwalt (Eds.), Pergamon Press, Oxford, 1989, p. 387.
174. S. Bywater, A. F. Johnson, and D. J. Worsfold, *Can. J. Chem.* **42**, 1255 (1964).
175. M. Morton, in "Vinyl Polymerization," Part II, G. Ham (Ed.), Marcel Dekker, New York, 1969, p. 211.
176. J. L. Wardell, in "Comprehensive Organometallic Chemistry: The Synthesis, Reactions and Structures of Organometallic Compounds," G. Wilkinson, F. G. A. Stone, and E. W. Abel (Eds.), Pergamon Press, Oxford, Vol. 1, p. 43.
177. T. L. Brown, *Acc. Chem. Res.* **1**, 23 (1968).
178. B. L. Wakefield, "The Chemistry of Organolithium Compounds," Pergamon Press, Oxford, 1974.
179. D. J. Worsfold and S. Bywater, *Can. J. Chem.* **38**, 1891 (1960).
180. S. Bywater and D. J. Worsfold, *J. Organomet. Chem.* **10**, 1 (1967).
181. F. Schue and S. Bywater, *Macromolecules* **2**, 458 (1969).
182. M. Morton, R. A. Pett, and L. J. Fetters, *Macromolecules* **3**, 333 (1970).
183. C. M. Selman and H. L. Hsieh, *J. Polym. Sci., Polym. Lett. Ed.* **9**, 219 (1971).
184. S. Bywater and D. J. Worsfold, in "Recent Advances in Anionic Polymerization," T. E. Hogen-Esch and J. Smid (Eds.), Elsevier, New York, 1987, p. 109.
185. L. J. Fetters and M. Morton, *Macromolecules* **7**, 552 (1974).
186. J. B. Smart, R. Hogan, P. A. Scherr, M. T. Emerson, and J. P. Oliver, *J. Organomet. Chem.* **64**, 1 (1974).
187. P. D. Bartlett, S. J. Tauber, and W. P. Weber, *J. Am. Chem. Soc.* **91**, 6362 (1969).
188. P. D. Bartlett, C. V. Goebel, and W. P. Weber, *J. Am. Chem. Soc.* **91**, 7425 (1969).
189. R. N. Young, L. J. Fetters, J. S. Huang, and R. Krishnamoorti, *Polym. Int*. **33**, 217 (1994).
190. S. Bywater, *Polym. Int*. **38**, 325 (1995).
191. L. J. Fetters, J. S. Huang, and R. N. Young, *J. Polym. Sci.: Part A: Polym. Chem*. *Ed.* **34**, 1517 (1996).
192. S. Bywater, *Macromol. Chem. Phys*. **199**, 1217 (1998).
193. J. Stellbrink, J. Allgaier, L. Willner, D. Richter, T. Slawecki, and L. J. Fetters, *Polymer* **43**, 7101 (2002).
194. R. P. Quirk and B. Lee, *Polym. Int.* **27**, 359 (1992).
195. M. Morton and L. J. Fetters, *J. Polym. Sci., Macromol. Rev.* **2**, 71 (1967).
196. F. W. Stavely and coworkers, *Ind. Eng. Chem.* **48**, 778 (1956).
197. L. E. Foreman, in "Polymer Chemistry of Synthetic Elastomers," Part II, J. P. Kennedy and E. Tornqvist (Eds.), Wiley, New York, 1968, p. 491.
198. E. W. Duck and J. M. Locke, in "The Stereo Rubbers," W. M. Saltman (Ed.), Wiley-Interscience, New York, 1977, p. 139.
199. S. Bywater, in "Comprehensive Polymer Science," Vol. 3: "Chain Polymerization I," G. C. Eastmond, A. Ledwith, S. Russo, and P. Sigwalt (Eds.), Pergamon Press, Oxford, 1989, p. 433.
200. M. Morton and J. R. Rupert, in "Initiation of Polymerization," F. E. Bailey, Jr. (Ed.), ACS Symposium Series 212, American Chemical Society, Washington, D. C., 1983, p. 283.
201. D. J. Worsfold and S. Bywater, *Macromolecules* **11**, 582 (1978).
202. A. V. Tobolsky and C. E. Rogers, *J. Polym. Sci.* **40**, 73 (1959).
203. A. Rembaum, *et al.*, *J. Polym. Sci.* **61**, 155 (1962).
204. S. Bywater and D. J. Worsfold, *Can J. Chem.* **45**, 1821 (1967).
205. M. Morton and L. J. Fetters, *J. Polym. Sci., Part A* **2**, 3311 (1964).
206. M. Morton, L. J. Fetters, R. A. Pett, and J. F. Meier, *Macromolecules* **3**, 327 (1970).
207. E. R. Santee, Jr., L. O. Malotky, and M. Morton, *Rubber Chem. Tech.* **46**, 1156 (1973).

208. T. Hogen-Esch, *Adv. Phys. Org. Chem.* **15**, 153 (1977).
209. A. Halasa, *Rubber Chem. Tech.* **54**, 627 (1981).
210. N. Nagata, T. Kobatake, H. Watanabe, A. Ueda, and A. Yoshioka, *Rubber Chem. Tech.* **60**, 837 (1987).
211. R. Luxton, *Rubber Chem. Tech.* **54**, 596 (1981).
212. G. Holden and D. R. Hansen, in "Thermoplastic Elastomers" 3rd ed., G. Holden, H. R. Kricheldorf, and R. P. Quirk (Eds.), Hanser Publishers, Munich, 2004, p. 45.
213. R. Ohlinger and F. Bandermann, *Makromol. Chem.* **181**, 1935 (1980).
214. M. Morton and L. K. Huang, unpublished data; L. K. Huang, Ph.D. Dissertation, The University of Akron, Akron, Ohio, 1979; cited in Ref. [144].
215. F. R. Ells, Ph.D. Dissertation, The University of Akron, Akron, Ohio, 1963; cited in [144].
216. Y. L. Spirin, A. A. Arest-Yakubovich, D. K. Polyakov, A. R. Gantmakher, and S. S. Medvedev, *J. Polym. Sci.* **58**, 1161 (1962).
217. D. J. T. Hill, J. H. O'Donnell, P. W. O'Sullivan, J. E. McGrath, I. C. Wang, and T. C. Ward, *Polym. Bull.* **9**, 292 (1983).
218. T. A. Antkowiak, A. E. Oberster, A. F. Halasa, and D. P. Tate, *J. Polym. Sci.*, *Part A-1* **10**, 1319 (1972).
219. C. F. Wofford and H. L. Hsieh, *J. Polym. Sci., Part A-1* **7**, 461 (1969).
220. M. Fontanille, in "Comprehensive Polymer Science," Vol. 3: "Chain Polymerization I," G. C. Eastmond, A. Ledwith, S. Russo, and P. Sigwalt (Eds.), Pergamon Press, Oxford, 1989, p. 376.
221. F. Bandermann, H. D. Speikamp, and L. Weigel, *Makromol. Chem.* **186**, 2017 (1985).
222. L. H. Tung and G. Y. Lo, in "Advances in Elastomers and Rubber Elasticity," J. Lal and J. E. Mark (Eds.), Plenum Press, New York, 1986, p. 129.
223. T. E. Long, A. D. Broske, D. J. Bradley, and J. E. McGrath, *J. Polym. Sci., Polym. Chem. Ed.* **27**, 4001 (1989).
224. R. P. Quirk and J. J. Ma, *Polym. Inter.* **24**, 197 (1991).
225. R. P. Quirk, T. Yoo, Y. Lee, J. Kim, and B. Lee, *Adv. Polym. Sci.* **153**, 67 (2000).
226. Unpublished work of R. P. Quirk and D. Xu, The University of Akron.
227. F. Ciardelli, in "Comprehensive Polymer Science," First Supplement, S. L. Aggarwal and S. Russo (Eds.), Pergamon Press, Oxford, 1992, p. 67.
228. J. Boor, Jr., "Ziegler-Natta Catalysts and Polymerizations," Academic Press, New York, 1979.
229. K. Ziegler, E. Holzkamp, H. Breil, and H. Martin, *Angew. Chem.* **67**, 541 (1955).
230. G. Natta, *J. Polym. Sci.* **16**, 143 (1955).
231. L. Porri and A. Giarrusso, in "Comprehensive Polymer Science," Vol. 4: "Chain Polymerization II," G. C. Eastmond, A. Ledwith, S. Russo, and P. Sigwalt (Eds.), Pergamon Press, Oxford, 1989, p. 53.
232. W. Cooper, in "The Stereo Rubbers," W. M. Saltman (Ed.), Wiley-Interscience, New York, 1977, p. 21.
233. Ph. Teyssie, P. Hadjiandreou, M. Julemont, and R. Warin, in "Transition Metal Catalyzed Polymerizations," R. P. Quirk (Ed.), Cambridge University Press, Cambridge, UK, 1988, p. 639.
234. P. J. T. Tait and I. G. Berry, in "Comprehensive Polymer Science," Vol. 4: "Chain Polymerization II," G. C. Eastmond, A. Ledwith, S. Russo, and P. Sigwalt (Eds.), Pergamon Press, Oxford, 1989, p. 575.
235. F. P. Baldwin and G. Ver Strate, *Rubber Chem. Tech.* **42**, 709 (1972).
236. G. Ver Strate, in "Encyclopedia of Polymer Science and Engineering," J. I. Kroschwitz (Ed.), Wiley-Interscience, New York, Vol. 6, 1986, p. 522.
237. S. C. Davis, W. Von Hellens, H. A. Zahalka, and K. P. Richter, in "Polymeric Materials Encyclopedia," J. C. Salamone (Ed.), CRC Press, Boca Raton, 1996, p. 2264.
238. J. W. M. Noordermeer, in "Encyclopedia of Polymer Science and Technology," J. I. Kroschwitz (Ed.), Wiley-Interscience, New York, Vol. 6, 2003, p. 178.
239. E. J. Vandenberg, in "Encyclopedia of Polymer Science and Engineering," J. I. Kroschwitz (Ed.), Wiley-Interscience, New York, Vol. 4, 1986, p. 174.

240. P. Pino, U. Giannini, and L. Porri, in "Encyclopedia of Polymer Science and Engineering," J. I. Kroschwitz (Ed.), Wiley-Interscience, New York, Vol. 8, 1987, p. 147.
241. E. J. Arlman and P. Cossee, *J. Catal.* **3**, 103 (1964).
242. P. Corradini, G. Guerra, and R. Pucciariello, *Macromolecules* **18**, 2030 (1985).
243. A. Zambelli and G. Allegra, *Macromolecules* **13**, 42 (1980).
244. A. Zambelli and C. Tosi, *Adv. Polym. Sci.* **15**, 31 (1974).
245. P. Corradini, V. Busico, and G. Guerra, in "Comprehensive Polymer Science," Vol. 4: "Chain Polymerization II," G. C. Eastmond, A. Ledwith, S. Russo, and P. Sigwalt (Eds.), Pergamon Press, Oxford, 1989, p. 29.
246. H. H. Brintzinger, D. Fischer, R. Mulhaupt, B. Rieger, and R. M. Waymouth, *Angew. Chem. Int. Ed. Engl.* **34**, 1143 (1995).
247. E. P. Wasserman, in "Encyclopedia of Polymer Science and Technology," J. I. Kroschwitz (Ed.), Wiley-Interscience, New York, Vol. 7, 2003, p. 35.
248. M. Galimberti, N. Mascellani, F. Piemontesi, and I. Camurati, *Macromol. Rapid Commun*. **20**, 214 (1999).
249. S. E. Horne, Jr., J. P. Kichl, J. J. Shipman, V. L. Folt, and C. T. Gibbs, *Ind. Eng. Chem.* **48**, 784 (1956).
250. S. Horne, Jr., in "Transition Metal Catalyzed Polymerizations: Alkenes and Dienes," Part B, R. P. Quirk (Ed.), Harwood, 1983, p. 527.
251. H. L. Hsieh and H. C. Yeh, *Rubber Chem. Tech.* **58**, 117 (1985).
252. M. Kerns, S. Henning, and M. Rachita, in "Encyclopedia of Polymer Science and Technology," J. I. Kroschwitz (Ed.), Wiley-Interscience, Vol. 5, 2003, p. 317.
253. A. Dräxler, in "Handbook of Elastomers," 2nd ed., A. K. Bhowmick, H. L. Stephens (Eds.), Marcel Dekker, New York, 2001, p. 697.
254. E. A. Ofstead, in "Encyclopedia of Polymer Science and Engineering," J. I. Kroschwitz (Ed.), Wiley-Interscience, New York, Vol. 11, 1988, p. 287.
255. B. M. Novak, W. Risse, and R. H. Grubbs, *Adv. Polym. Sci.* **102**, 47 (1992).
256. K. J. Ivin, "Olefin Metathesis," Academic Press, New York, 1983.
257. A. J. Amass, in "Comprehensive Polymer Science," G. C. Eastmond, A. Ledwith, S. Russo, and P. Sigwalt (Eds.), Pergamon Press, Oxford, Vol. 4, 1989, p. 109.
258. A. K. Bhowmick, C. Stein, and H. L. Stephens, in "Handbook of Elastomers," 2nd ed., A. K. Bhowmick and H. L. Stephens (Eds.), Dekker, New York, 2001, p. 775.
259. P. Dreyfuss and R. P. Quirk, in "Encyclopedia of Polymer Science and Engineering," J. I. Kroschwitz (Ed.), Wiley-Interscience, New York, Vol. 62, 1986, p. 551.
260. P. F. Rempp and P. J. Lutz, in "Comprehensive Polymer Science," G. C. Eastmond, A. Ledwith, S. Russo, and P. Sigwalt (Eds.), Pergamon Press, Oxford, Vol. 6, 1989, p. 403.
261. R. P. Quirk, *Rubber Chem. Tech.* **57**, 557 (1984).
262. G. Riess and G. Hurtrez, in "Encyclopedia of Polymer Science and Engineering," J. I. Kroschwitz (Ed.), Wiley-Interscience, New York, Vol. 2, 1985, p. 324.
263. G. Holden, H. R. Kricheldorf, and R. P. Quirk (Eds.), "Thermoplastic Elastomers," Hanser Publishers, Munich, Germany, 2004.
264. G. Odian, "Principles of Polymerization," 4th ed., Wiley-Interscience, New York, 2004, p. 752.
265. G. G. Cameron and M. Y. Qureshi, *J. Polym. Sci., Chem. Ed.* **18**, 2143 (1980).
266. A. Brydon, G. M. Burnett, and G. G. Cameron, *J. Polym. Sci., Chem. Ed.* **11**, 3255 (1973).
267. C. Walling, *Pure Appl. Chem.* **15**, 69 (1967).
268. D. J. Stein, G. Fahrbach, and H. J. Adler, *Angew. Makromol. Chem.* **38**, 67 (1974).
269. B. J. Schmitt, *Angew. Chem. Int. Ed. Engl.* **18**, 273 (1979).
270. D. M. Kulich, P. D. Kelley, and J. E. Pace, in "Encyclopedia of Polymer Science and Engineering," J. I. Kroschwitz (Ed.), Wiley-Interscience, New York, Vol. 1, 1985, p. 388.
271. C. S. L. Baker, in "Handbook of Elastomers," A. K. Bhowmick and H. L. Stephens (Eds.), Marcel Dekker, New York, 2001, p. 61.
272. D. S. Campbell, in "Natural Rubber Science and Technology," A. D. Roberts (Ed.), Oxford University Press, Oxford, 1988, p. 679.

273. P. W. Allen, in "Chemistry and Physics of Rubberlike Substances," L. Bateman (Ed.), MacLaren, London, 1963, p. 97.
274. H. A. J. Battaerd and G. W. Tregear, "Graft Copolymers," Wiley-Interscience, New York, 1967.
275. W. Cooper, P. R. Sewell, and G. Vaughan, *J. Polym. Sci.* **41**, 167 (1959).
276. E. G. Cockbain, T. D. Pendle, and D. J. Turner, *J. Polym. Sci.* **39**, 419 (1959).
277. B. Gupta and N. Anjum, *Adv. Polym. Sci.* **162**, 35 (2003).
278. R. J. Ceresa, "Block and Graft Copolymers," Butterworth, London, 1962, p. 65.
279. M. Pike and W. F. Watson, *J. Polym. Sci.* **9**, 229 (1952).
280. D. J. Angier and W. F. Watson, *J. Polym. Sci.* **18**, 129 (1955); *Trans. Inst. Rubber Ind.* **33**, 22 (1957).
281. D. J. Angier, R. J. Ceresa, and W. F. Watson, *J. Polym. Sci.* **34**, 699 (1959).
282. R. J. Ceresa and W. F. Watson, *J. Appl. Polym. Sci.* **34**, 699 (1959).
283. N. Hadjichristidis, S. Pispas, M. Pitsikalis, H. Iatrou, and D. J. Lohse, in "Encyclopedia of Polymer Science and Technology," J. I. Kroschwitz (Ed.), Wiley-Interscience, New York, Vol. 6, 2003, p. 348.
284. K. A. Davis and K. Matyjaszewski, *Adv. Polym. Sci.* **159**, 1 (2002).
285. R. P. Quirk, D. L. Gomochak Pickel, and G. O. Schulz, in "Thermoplastic Elastomers," G. Holden, H. R. Kricheldorf, and R. P. Quirk (Eds.), Hanser Publishers, Munich, Germany, 2004, p. 323.
286. N. R. Legge, *Rubber Chem. Tech.* **60**, G83 (1987).
287. F. S. Bates and G. H. Fredrickson, *Annu. Rev. Phys. Chem.* **41**, 525 (1990).
288. D. J. Meier, *J. Polym. Sci., Part C* **26**, 81 (1969).
289. E. Helfand, *Acc. Chem. Res.* **8**, 295 (1975).
290. L. Leibler, *Macromolecules* **13**, 1602 (1980).
291. M. Morton, in "Encyclopedia of Polymer Science and Technology," N. Bikales (Ed.), Wiley, New York, Vol. 15, 1971, p. 508.
292. G. Holden, E. T. Bishop, and N. R. Legge, *J. Polym. Sci., Part C* **26**, 37 (1969).
293. T. L. Smith and R. A. Dickie, *J. Polym. Sci., Part C* **26**, 163 (1969).
294. I. W. Hamley (Ed.), "Developments in Block Copolymer Science and Technology," Wiley, New York, 2004.
295. M. Morton, R. F. Kammereck, and L. J. Fetters, *Br. Polym. J.* **3**, 120 (1971).
296. M. Morton, Y. Kesten, and L. F. Fetters, *Polym. Prepr., Am. Chem. Soc., Div. Polym. Chem.* **15**, 175 (1974).
297. R. Jerome, in "Thermoplastic Elastomers," G. Holden, H. R. Kricheldorf, and R. P. Quirk (Eds.), Hanser Publishers, Munich, Germany, 2004, p. 444.
298. A. K. Bhowmick and H. L. Stephens (Eds.), "Handbook of Elastomers," 2nd ed., Marcel Dekker, New York, 2001.
299. S. Abouzahr and G. L. Wilkes, in "Processing, Structure and Properties of Block Copolymers," M. J. Folkes (Ed.), Elsevier, London, 1985, p. 165.

3 Structure Characterization in the Science and Technology of Elastomers

C. M. ROLAND
Naval Research Laboratory
Chemistry Division, Code 6120
Washington, D.C.

I. INTRODUCTION

Early structural characterization of polymers focused on solution properties and their relationship to molecular weight [1–4]. Subsequently spectroscopic and chromatographic techniques were developed, and reviews are widely available [5–10]. In this chapter, various characterization techniques are described. The two prior editions discussed in some detail procedures for the analysis of elastomers. Much of this information is not otherwise available in the open literature, at least not in self-contained fashion. Thus, in preparing the third edition, a significant amount of the previous text was retained, especially that specific to elastomers. Discussion of the classical methods of analysis is largely unchanged, although the text and references have been updated. The coverage of NMR, SANS, and secondary relaxations has been expanded, and several new topics, including orientation, defects, and blends, have been added.

Knowledge of chemical composition, compositional and sequence distribution, molecular weight and its distribution, and the degree and type of

Science and Technology of Rubber, Third Edition

branching allows inferences to be drawn concerning the mechanical properties (Chapters 4, 10), the rheology (Chapters 5, 6), curing behavior (Chapter 7), filler reinforcement (Chapter 8), and chemical reactivity (Chapter 11) of rubber. However, relationships between fundamental molecular variables and the properties of condensed matter are semiquantitative at best, and correlation never guarantees causation. Following the earlier editions, methods for molecular weight determination are discussed at greater length than spectroscopic methods. This bias is based on the idea that areas in which common problems might arise, with individuals making their own data interpretation, should receive greater attention.

II. CHEMICAL COMPOSITION

The chemical *elemental analysis* of polymers can often be carried out by the methods used for low molecular weight organic compounds [1, 2, 9, 11–14]. This is particularly true when combustion of the sample is involved. Thus, C, H, and N can be determined on milligram samples by complete combustion followed by gas chromatographic analysis of the gases evolved. Accuracy is about 0.3%. Sulfur and halogens are also easily determined after combustion, by titration of sulfate or SO_2 for S, and by potentiometric titration with $AgNO_3$ for halogens after treatment of the gases with NaOH and hydrazine sulfate, for example. Interference by nitrogen on sulfur tests must be watched for. Quantities as low as ppm metals can be determined quantitatively and quickly by x-ray techniques.

Elemental analysis only reveals which atoms are present. Determination of the chemical structure can often be addressed using spectroscopic methods. The moieties in the polymer absorb and emit radiation at frequencies which are characteristic of their chemical structure. Skeletal bond transitions can be detected in the infrared and Raman spectra, electronic transitions typical of unsaturated bonds can be detected at ultraviolet and visible wavelengths, and atomic nuclei with magnetic moments can be detected and their positions found by magnetic resonance experiments.

For basic information, *infrared spectroscopy* [8–10, 15, 16] (invariably Fourier transform infrared [FTIR]) is a straightforward technique, accessible to the nonspecialist. Thin films of elastomers can be measured directly, and obtained by casting or molding 20 to 30 mg of sample between polyester or aluminum foil (preferably Teflon-coated). Care must be taken to minimize oxidation if the molding is done at elevated temperature. Most analyses make use on the mid-infrared region at 4000 to 400 cm^{-1}, with sample identification made through comparison, using widely available spectral libraries [8, 17]. If the polymer is crosslinked, sample-forming is more restricted. Microtomed specimens can be used, or the spectra obtained in reflection, most commonly using

attenuated total reflection (ATR) [18–22], or less often, photoacoustic FTIR [23, 24]. The latter refers to the measurement of sound arising from the selective absorption of modulated light. The sample surface is heated by the absorption, which in turns heats the adjacent air, thus producing an alternating pressure wave. Sub-milligram-sized samples can be analyzed using infrared microscopy [16, 25–36].

Raman spectroscopy yields analogous information, but is complementary to infrared absorption, in that vibrations which are infrared inactive are generally Raman active, and vice versa. For example, carbon-sulfur bonds are easily detectable via Raman measurements [5, 10]. Since the detected light is scattered from the sample, spectra are readily obtained on crosslinked specimens. Interferences due to fluorescence are avoided by using a longer wavelength source [37]. Raman microscopy has potential for spatially resolved analyses [38].

Whereas Raman and infrared are useful for "fingerprinting" (i.e., identifying chemical structure), extension of the spectroscopic measurements into the *visible and ultraviolet* (UV) regions are done primarily for quantitative analyses [39–41]. Extinction coefficients for conjugated unsaturated structures are very large.

Although the spectral absorption methods just discussed can be used in a quantitative fashion, calibration is required. With *nuclear magnetic resonance spectroscopy* (NMR) [9, 10, 42–44], particularly proton NMR, the absorption intensity is directly proportional to the number of hydrogen atoms present; consequently, ratios of absorption intensities can be used to determine the number of chemically distinct protons in a sample. Protons resonate at characteristic frequencies (e.g., "chemical shifts") depending on their chemical environment, and therefore the specific chemical nature of the proton can be identified.

Chemical information can also be obtained using carbon-13 NMR. Whereas ^{1}H and ^{13}C NMR are usually done in solution (e.g., "liquid state NMR") in order to improve resolution, ^{13}C spectra can also be obtained on neat specimens, such as rubbers, using these techniques. This is possible as long as there is sufficient molecular motion to average the orientation-dependent variation in chemical shift of chemically identical atoms (chemical shift anisotropy, [CSA]). Chemical shifts in ^{13}C NMR spectra span a much wider range than in proton NMR, and therefore the former provides better spectral resolution. However, the Nuclear Overhauser effect (NOE) and other nuclear relaxation processes cause the ^{13}C absorption intensities to deviate from direct proportionality to the number of carbon atoms. Thus, unless specific techniques are utilized, ^{13}C NMR spectral intensities using standard liquid-state NMR acquisition methods are not quantitative.

This is also true when applying solid-state NMR techniques [43] to obtain high resolution ^{13}C spectra of rigid, nonrubbery samples. Using a combination

of magic angle spinning (MAS) and proton decoupling (via high power radiofrequency irradiation of proton resonances), the line-broadening effects of CSA and ^{13}C-proton dipole–dipole interactions can be removed. Relatively high resolution ^{13}C NMR spectra can be obtained, but absorption intensities will not be proportional to the number of carbon atoms in the sample. NMR not only yields chemical information, but also can be used to analyze polymer tacticity, sequence lengths, short-chain branching, and crystallinity.

Using elemental analyses, infrared, and NMR methods, evaluation of repeat unit structures in a polymer is generally feasible. In some cases, such as low concentration of a monomer unit or *functional group*, or for atoms other than C and H, quantitative estimation is more difficult. An alternative analysis is based on the chemical reactivity of the particular group [45]. For example, acid groups can be titrated accurately with base; olefins will add ozone and halogens quantitatively in some cases; hydroxyl groups can be esterified with anhydrides, with back titrations to evaluate hydroxyl content. In many cases, procedures established for small molecules can be utilized. Of course, slow reaction rates, due to low concentration, or the availability of an appropriate solvent for both the reagents and polymers can pose problems. Brief studies to assess the results as a function of time or temperature can usually establish the reliability of a technique.

Pyrolysis [46–50] of samples can lead to the production of characteristic fragments, which may be analyzed by *gas chromatography* (GC) [9] or *mass spectrometry* (MS) [51]. Since the relationship between fragments and the original polymer is often complex, this technique is a last recourse, for insoluble polymers or samples not amenable to more facile and reliable characterization methods. Combined GC/MS has been used to analyze the volatile components in natural rubber [52]. In *ozonolysis* [9], an unsaturated sample is reacted to form an unstable intermediate, ozonide, which is then further reacted for chemical identification. Ozonolysis of rubber is usually combined with GC analysis [53–56]. In *secondary ion mass spectrometry* (SIMS), the sample surface is irradiated with an ion beam, followed by mass spectrometry of the emitted secondary ions [57, 58]. SIMS has found various applications in rubber, including surface analysis [59–61] and studies of carbon black interaction [62, 63]. Pyrolysis can also serve as a fingerprinting technique for routine analyses. In *thermogravimetric analysis* (TGA) [64, 65], the polymer degradation by-products volatize, whereby the residue provides a measure of the carbon black or other filler content.

Electron paramagnetic resonance (EPR), or electron spin resonance (ESR), can be used to detect types and quantities of free radicals. Such information is of value in studying the chemistry occurring during degradation and fracture of polymeric materials [66–71]. EPR can also be applied to study carbon black and other fillers in polymers [72–74].

III. SEQUENCE DISTRIBUTION OF REPEAT UNITS

Most elastomers are comprised of many additives (a typical formulation includes more than a dozen ingredients), as well as possible impurities. Additionally, the polymer itself may be a copolymer of different monomer units, or the rubber may be a blend of two or more polymers. In order to determine whether the elastomer contains additives or impurities, or is itself heterogeneous, the components of the mixture must be separated, i.e., fractionated. Many methods are available to separate components, with the latter then identified by techniques such as in Table I. Precipitation and/or dissolution methods simply rely on differences in solubility of the components [75]. If the molecular weight distribution is broad, a fractionation scheme is combined with one of the more sophisticated analyses described in the following text. If there is intramolecular heterogeneity, "cross" or "orthogonal" fractionation, which require at least two fractionation mechanisms, may be needed.

The technique of *temperature rising elution fractionation* (TREF) [76, 77] has been developed to measure the compositional distribution of semicrystalline polymers. Polymer is dissolved off a substrate as temperature is raised through the melting region, so that discrimination is based on differences in crystallizability of the fractions. A similar method uses supercritical fluids [78]. TREF can also provide information about the sequence distribution, since longer sequences of a monomer unit are more crystallizable.

Size exclusion chromatography (SEC) [9, 79–81], also referred to as gel permeation chromatography, utilizes differences in hydrodynamic volume.

TABLE I Characterization of Chemical Composition

Technique	Principle of operation
Elemental analysis	Analysis of products of decomposition
Infrared absorption $1 < \lambda\ (\mu m) < 16$	Characteristic vibrational frequencies
Raman scattering	Characteristic vibrational frequencies
Nuclear magnetic resonance (NMR)	Characteristic transition energies of any nucleus with a magnetic moment (^{1}H, ^{2}H, ^{13}C, ^{129}Xe, etc.)
Ultraviolet (UV) and visible light absorption $0.2 < \lambda\ (\mu m) < 0.8$	Characteristic energies of electronic transitions
Functional group analysis	Analyze for known reactions of chemical moiety
Pyrolysis/ozonolysis	Pyrolysis with chromatographic or mass spectrographic identification of fragments
Electron paramagnetic resonance (EPR)	Energy of unpaired electron spin transitions, which depends on chemical environment
Thermogravimetric analysis (TGA)	Weight loss due to temperature-dependent decomposition and evaporation
Mass spectrometry (MS)	Mass of fragments reflects chemical composition
Secondary ion mass spec (SIMS)	Characteristic ions emitted from surface

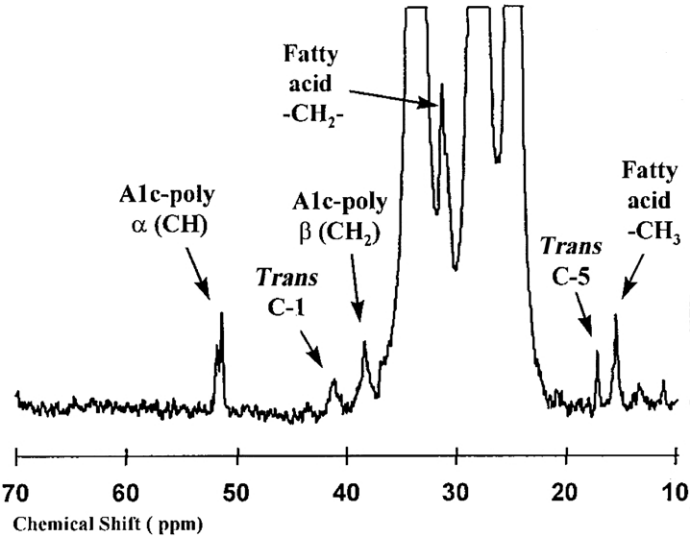

FIGURE 1 Magnified portion of ^{13}C NMR spectrum of natural rubber vulcanized to half its maximum torque. The peak at 16 ppm arises due to *cis*-to-*trans* isomerization. (From Mori and Koenig [92].)

It is discussed in more detail below. The most basic chromatographic technique is adsorption chromatography [82, 83], in which separation arises from variation in the retention of the chain units or functional groups, due to their interaction with a stationary surface. Other techniques rely on rates of sedimentation [84, 85], and diffusion-adsorption phenomena (thin layer chromatography [TLC]) [86, 87]. Thermal diffusion is the basis for thermal field flow fractionation (TFFF) [88–91], discussed later.

Different arrangements of the monomer units give rise to different chemical shifts and scalar couplings (splittings) in the NMR spectra. Using selection rules and empirical knowledge of chemical shifts, chemical structures can be assigned. Since chemical shifts in ^{13}C NMR spectra are larger than in proton spectra, subtle structural differences can be seen for carbon atoms separated by up to five bonds from the point of reference. Thus, ^{13}C NMR can be very useful for determining the distribution of chain units in the polymer backbone. An example of this is seen in Fig. 1, which shows ^{13}C NMR spectra of sulfur-cured natural rubber (NR) reinforced with carbon black [92]. There is a small peak reflecting the trans isomer content, which grows in intensity as the vulcanization proceeds. Thus, the NMR measurements yield quantitative information about the extent of *cis-trans* isomerization accompanying the curing of NR. Similar results are found for *cis*-1,4-polybutadiene rubber [93–95]. Figure 2 illustrates the plethora of changes in the NMR spectrum accompanying curing.

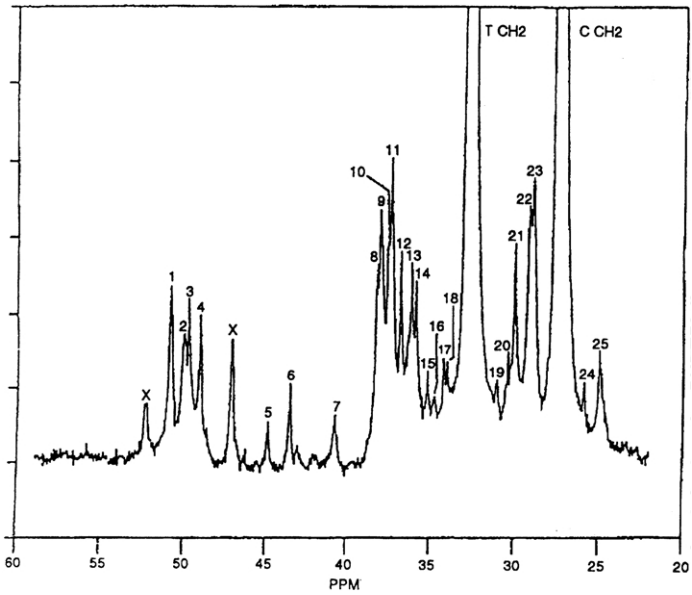

FIGURE 2 Magnified ^{13}C NMR spectrum of *cis*-1,4-polybutadiene after curing. The arrows designate new peaks appearing due to the vulcanization. The first 7 represent methine carbons and the other 18 are due to methylene carbons. (From Clough and Koenig [94].)

Differences in the arrangement of monomer units along the chain backbone is another form of heterogeneity. Chemically different monomer units may occur in sequences of varying length, while identical monomer units can have different geometrical arrangement (stereoisomers), yielding different properties. The stereo-regularity of the polymer can often be determined using the same techniques employed for chemically distinct units, with NMR and infrared the most useful.

When the sequences in the copolymer are longer than six to eight carbons, techniques other than NMR are needed to directly determine their length. The use of pyrolysis followed by GC-MS analysis has been proposed to find the long sequences as fragments in the pyrolyzate, but the data produced are complicated and difficult to interpret [96–99].

IV. CHAIN ARCHITECTURE

The viscoelastic response of amorphous polymers at elevated temperatures is governed to a significant extent by the average molecular weight, M_w, the presence of any long chain branching, and the MWD [100–105]. Even the

properties of cured elastomers may reflect the length of the original chains, since chain ends, whose concentration is inversely proportional to the number-average molecular weight M_n, represent defects.

A. Molecular Weight and Its Distribution

The chain length distribution is usually presented as a plot of the mole fraction or weight average of molecules versus molecular weight. The various average molecular weights represent the moments of the chain length distribution

$$\overline{M}_j = \sum_{i=1}^{\infty} N_i M_i^j \Big/ \sum_{i=1}^{\infty} N_i M_i^{j-1} \tag{1}$$

where $i = 1, 2$, and 3 yields the number average M_n, weight average M_w, and z average M_z, respectively. For a uniform distribution of chain lengths, $M_n = M_w = M_z$. The common random MWD gives $M_w/M_n = 2$ and $M_z/M_w = 1.5$, while for the Schulz-Zimm distribution, $M_n + M_z = 2M_w$ and $1 < M_z/M_w < 2$. Fig. 3 shows a typical molecular weight distribution.

The number average molecular weight determines the colligative properties (i.e., those which depend only on the number of dissolved molecules) of polymer solutions. Measurements of freezing point depression (*cryoscopy*) or

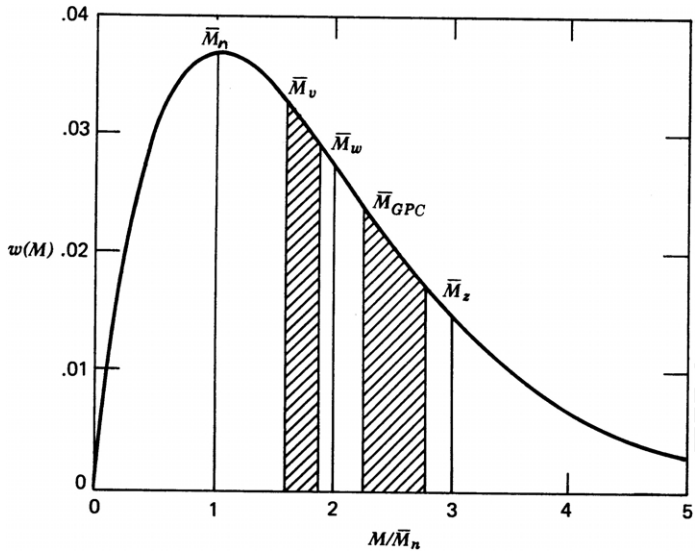

FIGURE 3 Representative molecular weight distribution. $M_{GPC} = \sum w_i M_i^{1+a} \big/ \sum w_i M_i$, where a is the Mark-Houwink exponent. (From Collins, Bares, and Billmeyer [13].)

boiling point elevation (*ebulliometry*) will, in principle, yield the same information for macromolecules as for small molecules [106–108]. These are absolute techniques, which do not require calibration. The change in (melting or boiling) temperature, ΔT, follows a relationship of the form

$$\Delta T/kc = M_n^{-1} + A_1 c + A_2 c^2 + \cdots \quad (2)$$

where c is the concentration, A_i the virial coefficients, and k is a constant that depends on the solvent, temperature, and the instrument. The number of moles of macromolecules present at mass concentrations sufficiently low to obtain ideal solutions is very small. Therefore, the anticipated change, ΔT, in boiling or freezing points are correspondingly small; for $M_n = 10^5$ g/mol, $\Delta T \sim 10^{-5}$ to 10^{-4}°C. Thus, these classical techniques are not used above $M_n \sim 10^4$ g/mol. Moreover, cryoscopy and ebulliometry are time consuming and have poor accuracy.

For low molecular weight samples, the preferred method is by *vapor pressure osmometry (VPO)* [107, 108]. This technique is based on the decrease of vapor pressure of a solvent due to the presence of dissolved polymer. The different equilibrium vapor pressures cause a difference in condensation rate on two matched thermistors, contained in a chamber saturated with solvent vapor. One thermistor is coated with solvent and the other with a solution of the polymer. More solvent condenses on the solution, raising its temperature. The consequent temperature difference is measured, and by calibration, M_n can be determined. VPO is fast and can yield M_n as high as about 5×10^4 g/mol. Commercial vapor pressure osmometers are available.

Membrane osmometry [107–109] relies on the lowering of the acti-vity (free energy) of the solvent by dissolution of a solute, to yield an direct determination of M_n. When a polymer solution is brought in contact with pure solvent, the concentration gradient induces mixing by diffusion. If a semipermeable membrane is placed between the pure solvent and solution, the polymer is trapped but solvent can pass. Equilibrium cannot be attained, but if the polymer solution is in a closed cavity, a pressure develops on the solution side, which eventually stops the solvent flow. The magnitude of this "osmotic" pressure, Π, will depend only on the number of polymer molecules present, at least in the absence of polymer-polymer interactions (i.e., at low concentrations). The equation relating these quantities is analogous to the relation above for the change in melting and boiling points. Measurements at several concentrations with extrapolation of Π/c to $c = 0$ yields M_n. Even for high molecular weight materials, the osmotic pressure is significant. For a 1% solution of a material of $M_n = 10^5$ g/mol, the pressure is about 250 Pa at 25°C. Generally, the technique is useful for molecular weights in the range from 10^4 to almost 10^6 g/mol.

A frequent difficulty with the method is that Π/C may become nonlinear in c for higher concentrations. If this is due to agglomeration, solvent or temperature changes can sometimes eliminate the problem. To get measurable

osmotic pressures for larger M_n, the range of c must be increased. A_2 decreases with M_n in good solvents ($A_2 \sim M^{-0.2}$), but not as fast as c must be increased. Therefore, nonlinear plots are often encountered when studying high M_n samples. In order to linearize the data, $(\Pi/c)^{1/2}$ can be plotted versus c. The greatest difficulties with this method relate to imperfections in the membrane. Sometimes the polymer can diffuse through the membrane, with steady-state values indicating permeation of molecules having $M < 5 \times 10^3$ g/mol. This can lead to significant errors, about 10%, or even larger for distributions skewed to low molecular weights.

Light scattering is another absolute technique for the determination of molecular weights (>10^3 g/mol) [9, 107, 108, 110–116]. (We are only concerned with static light scattering for structural information; however, inelastic light scattering is a powerful technique for studying polymer dynamics. From calibration, it can also yield molecular weight determinations [111].) Light passing through a medium is scattered due to regions of different refractive index, n; thus, polymer molecules dissolved in a solvent having a refractive index different from the polymer will scatter light. Ignoring the contribution from the solvent (which is small compared to the macromolecular scattering), isolated molecules (no interparticle interference), which are much smaller than the wavelength of the light (no intramolecular interferences), will scatter light with an intensity given by

$$I(q) = I_0\left[\frac{4\pi^2 n_o^2}{\lambda^4 N_A}\left(\frac{\partial n}{\partial c}\right)_T^2\right]Mc \tag{3}$$

where $q\left(\equiv \frac{4\pi}{\lambda}\sin\left(\frac{\theta}{2}\right)\right)$ is the momentum transfer and θ the scattering angle, I_0 is intensity scattered at $q = 0$, λ the wavelength, N_A is Avagadro's number, and n_0 and n are the respective solvent and solution refractive indices. The change in the refractive index with concentration is approximately equal to the ratio of the relative refractive index and the polymer mass density, $(\partial n/\partial c)_T = (n_{poly} - n_0)/\rho$. Generally, $\partial n/\partial c|_T < 0.2$ mL/g for polymer solutions.

In a given experiment, the quantity in brackets in Eq. (3) is a constant, K, so

$$R(q) \equiv I(q)/I_0 = KMc \tag{4}$$

where $R(q)$ is the Rayleigh ratio. Polymer chains are large enough (>$\lambda/10$) that light scattered from different parts of the molecule have different phase shifts; thus, Eq. (4) is modified by the molecular structure factor, $P(q)$

$$R(q) = KMc\,P(q) \tag{5}$$

This structure factor can be approximated at small scattering angles as

$$P(q) \approx 1 - \frac{1}{3}q^2 S_g^2 + \cdots \tag{6}$$

which is valid for particles of any shape. S_g is the root-mean-square radius of gyration of the polymer, and small angle is defined by the condition $q << S_g^{-1}$. A plot of $R(q)$ versus q^2 at small q is a straight line whose intercept yields the molecular weight, and the ratio of slope to intercept yields the radius of gyration. Since the reciprocal of the Rayleigh ratio is more sensitive to small variations than R itself, Eq. (5) is usually rewritten (using the fact that $1 + x = [1 - x]^{-1}$ for small x)

$$\frac{Kc}{R(q)} = M^{-1}\left(1+\frac{1}{3}q^2S_g^2\right) \tag{7}$$

Thus, $R(q)^{-1}$ is plotted versus q^2, with the molecular weight and S_g obtained via extrapolation to $q = 0$.

The foregoing assumes independent scattering from each particle. At the usual polymer concentrations, even though the visual turbidity remains negligible, waves scattered from different chains interfere. This interparticle interference causes the scattering intensity to deviate from a linear dependence on c. To correct for the concentration effect, a power series expansion is assumed

$$\frac{Kc}{R(q)} = M_w^{-1}\left(1+\frac{1}{3}q^2\langle S_g\rangle^2\right)+2A_2c+\cdots \tag{8}$$

where A_2 is called the second virial coefficient. Note that in consideration of a distribution of molecular masses, M is now the weight average and the obtained radius of gyration is the mean square z-average. Application of Eq. (8) requires extrapolation to $c = 0$, in addition to the extrapolation to zero angle. These two extrapolations are carried out simultaneously via a Zimm plot (Fig. 4). A proper Zimm plot yields both the radius of gyration and the virial coefficient, consistent with the M_w obtained for the polymer. Deviations from linearity at lower angles indicate artifacts, such as aggregates, gel, dust, etc. [117]. With rubbers, clarification problems can be especially serious due to the possibility of removing some of the polymer along with the contaminants. Using a laser beam having a small cross-sectional area, it is sometimes possible to see "between" gel or dust particles, which are then only detected intermittently as "spikes" of large scattering intensity. This may alleviate to some extent the need for solution clarification. Supplementing the data with dynamic light scattering measurements has been proposed as a means to correct for the contribution from large impurities [118].

Multiple detectors, from 3 to as many as 18, facilitate the extrapolation to zero angle. In principle, a scattering detector can be placed at sufficiently low angles, such that extrapolation of the scattering intensity to $q = 0$ becomes unnecessary, at least if the molecular weights are not too large. When a light scattering detector is attached to a chromatograph, the concentration of polymer is low, to some extent minifying the need for extrapolation to zero concentration. Of course, the radius of gyration and virial coefficient are not

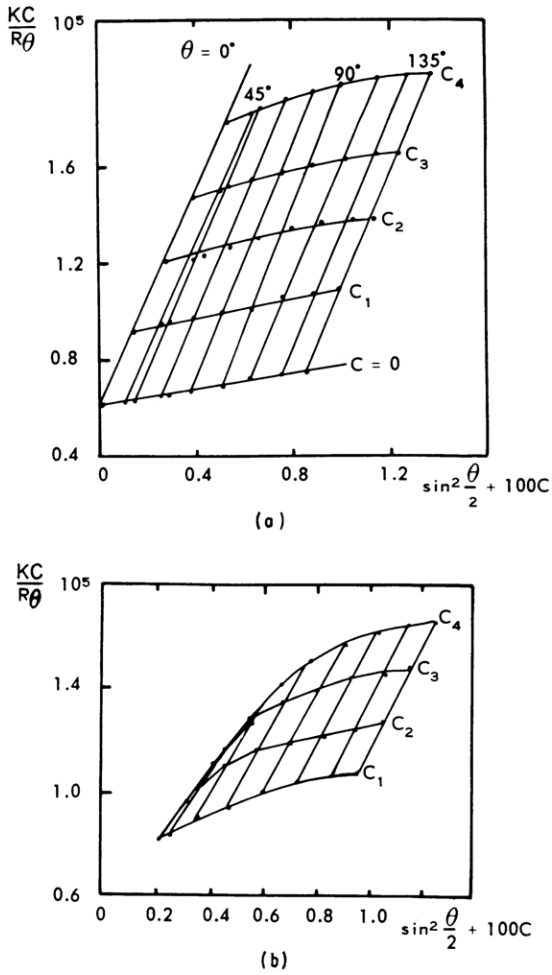

FIGURE 4 Zimm plots of commercial polyvinylchloride in THF: (a) purified solution with expected linear variation of $R(q)^{-1}$, (b) as received material, showing curvature due to aggregation. (From Vavra, Lapcik, and Sabados [117].)

obtained. However, in this manner, a molecular weight determination by light scattering can be completed expeditiously.

Structural information can also be obtained from measurements of *small angle neutron scattering* (SANS) [119–121]. Scattering of neutrons is due to their interaction with nuclei. It differs from light scattering, in that contrast arises from differences in neutron scattering length, rather than refractive index differences. Neutron cross-sections are commonly expressed in terms of the relevant correlation function. Elastic, coherent scattering is proportional to the spatial Fourier transform of the pair-correlation function. The angular

distribution of coherent scattering is reinforced by constructive interference, and thus yields structural and conformational information. Dimensions in the range from 1 nm to 1 μm can be resolved, making the method complementary to electron microscopy.

Inelastic coherent and incoherent scattering are proportional to the space and time Fourier transforms of, respectively, the pair-correlation and the self-correlation functions. Analogous to dynamic light scattering, these are used to probe polymer dynamics [122–125].

The neutron scattering cross-sections of carbon and oxygen are completely coherent. ^{1}H has a very large incoherent scattering cross-section and a small coherent cross-section, while the opposite is true for deuterium. One advantage of SANS is that isotopic labeling (usually the replacement of hydrogen by deuterium) can be used to provide selective contrast. Such labeling has minimal chemical effect, enabling $<S_g>$ and M_w to be determined in situations when light scattering cannot be used. Dust is also not a problem with SANS. An obvious disadvantage of the method is the greater cost of preparing labeled materials.

One important area in which SANS has yielded information not otherwise available is determining chain dimensions in bulk polymers. Samples can be a couple mm in thickness, with up to 50% of the incident neutrons scattered. The mean square radius of gyration and M_w can be determined for a deuterated version of a polymer mixed with its unlabeled analog. No Zimm analysis is required, despite overlap and interpenetration of the chain molecules. The only requirement is that both isotopic species have the same M_w and MWD. A model-independent analysis of the scattering uses the Gunier approximation

$$I(q) = I_0 \exp\left(-\frac{1}{3}q^2 S_g^2\right) \tag{9}$$

valid at small angles. Rubber is usually comprised of flexible chains, so that the single chain structure factor is expected to have the Debye form for a Gaussian coil [see Eq. (6)] [111].

$$P(q) = \frac{2}{q^2 R_g^2}[\exp(-q^2 R_g^2) - (1 - q^2 R_g^2)] \tag{10}$$

This result is shown for polyisoprene in Fig. 5 [126]. Direct SANS measurements of the size of chains in the melt validated Flory's original hypothesis that polymers behave ideally in the bulk. Other applications of SANS to elastomers include investigations of microscopic aspects of network deformation [127–129] and the effect of fillers, such as carbon black and silica, on network deformation [130–132].

The two sources of neutrons are nuclear reactors and particle accelerators (spallation sources). Neutron scattering facilities in North America include the

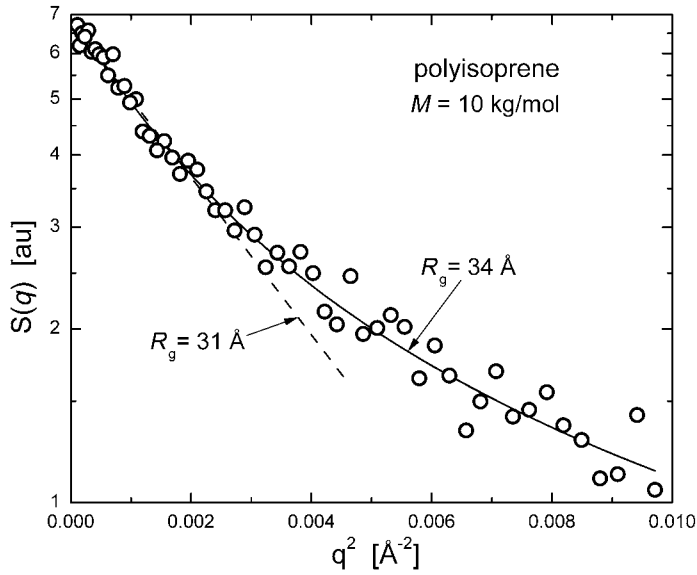

FIGURE 5 SANS from blend of deuterated and conventional polyisoprene (M_w = 10^4 g/mol), plotted in the Gunier form [Eq. (9)] yielding a straight at small angles. The solid line is the fit to the Debye form factor for Gaussian coils [Eq. (10)]. (From Akcasu, Summerfield, Jahsan *et al.* [126].)

National Institute of Standards and Technology, Oak Ridge National Laboratory, the Los Alamos Neutron Science Center, Argonne National Laboratory, Chalk River (Canada) Neutron Beam Laboratory, and the University of Missouri (Columbia). Generally, access involves a proposal system for nonproprietary work, with proprietary studies on a fee basis. There are also SANS facilities in Europe, Asia, and Australia.

In addition to the scattering methods, techniques such as cryoscopy, ebulliometry, and membrane osmometry give absolute molecular weight determinations, with the results independent of branching. Methods which depend on the size of the molecule in solution, such as the *intrinsic viscosity*, *size exclusion chromatography* (SEC), *sedimentation*, etc., require calibration, and the results are a function of polymer geometry, in particular long chain branching (LCB).

Another parameter that can be related to molecular weight is the relative viscosity, defined as the ratio of the viscosity of a polymer solution η to the viscosity of the solvent η_0 (Table II). Reliable for molecular weights $>10^3$ g/mol, the viscosities can be determined by measuring flow times through capillary tubes (diameters ~1 mm), usually with gravity as the driving force for the flow. Automated instrumentation is widely available. Rotational and oscillatory type viscometers are used where a uniform, well-defined, or low shear

TABLE II Solution Viscosity Definitions ($\eta \equiv$ solution viscosity; $\eta_0 \equiv$ solvent viscosity)

Viscosity Definition	Relative $\eta_{rel} = \eta/\eta_0$	Specific $\eta_{sp} = \eta_{rel} - 1$	Reduced $\eta_{red} = \eta_{sp}/C$	Inherent $\eta_{inh} = \ln(\eta_{rel})/C$	Intrinsic $[\eta] = \lim_{C \to 0} \eta_{red}$

rate is required. The ratio of the two viscosities, η/η_0, is called the relative viscosity, and the difference between that number and unity is the "specific" viscosity. Extrapolation to zero concentration of the specific viscosity divided by the concentration yields the *intrinsic viscosity* $[\eta]$. The intrinsic viscosity is related to molecular weight M as [4]

$$[\eta] = \Phi \langle r^2 \rangle^{3/2} / M \tag{11}$$

in which $\langle r^2 \rangle$ is the mean square end-to-end distance and Φ is a constant ($= 2.6 \times 10^{21}$ for r in cm). Equation 11 can be written as

$$[\eta]_\Phi = KM^{1/2} \tag{12}$$

where Θ refers to Theta conditions, and K ($= \Phi(\langle r^2 \rangle / M)^{3/2}$ is constant for sufficiently high molecular weight (~5000 g/mol). Working at Θ conditions is not always feasible, since the temperature control is exacting and there is a tendency for precipitation due to the limited solubility. A convenient alternative is to use the Mark-Houwink relation [107, 108, 133, 134]

$$[\eta] = KM_v^a \tag{13}$$

where $M_n < M_v < M_w$ (see Fig. 3), and a ranges from 0.5 to about 0.8 for rubbery polymers. Both K and a depend on polymer, solvent, and temperature, and must be determined empirically using polymers of known molecular weight. For good solvents, $[\eta]$ for a polymer varies only $\pm 30\%$, and it can be estimated empirically with reasonable accuracy [135, 136].

A convenient and very common method of molecular weight determination ($<10^7$ g/mol) is *size exclusion chromatography (SEC)*, or the more specific term, *gel permeation chromatography (GPC)* [9, 79–81, 137]. A dilute solution of the polymer is passed through a column packed with small (e.g., 5 μm) porous articles. The pore diameters are of the order of the size of the dissolved polymer chains. As the polymer solution passes through the column, polymer molecules diffuse into and out of pores. The accessibility of a given pore is determined by the hydrodynamic volume of the dissolved molecules. Since small molecules fit into more pores, their elution time from the column is longer. The flow can actually be stopped for minutes with little distortion of the chromatogram. The measured parameter is the elution volumes, V_e, which is a function of the molecular sizes in the solution. Based on calibration under identical conditions of the column, using narrow MWD standards, the molecular weight is directly related to V_e.

Empirically, it is known that that if different polymers have the same elution volume from a given GPC column, the product $[\eta]M$ will be constant, where $[\eta]$ is determined under the same conditions (T and solvent). This follows from the Einstein-Simha relation, whereby the quantity $[\eta]M$ is proportional to the hydrodynamic volume. The hydrodynamic volume depends on temperature and solvent, and is roughly half the volume calculated from S_g. Using the "universal calibration method," molecular weight determinations can be made for a polymer using known standards of a different polymer [138–140]. These molecular weight standards are commercially available for various polymers. From Eq. (13)

$$M_U = \left[\frac{K_S}{K_U}\right]^{1/(a_U+1)} M_S^{\frac{a_s+1}{a_U+1}} \tag{14}$$

where the subscripts U and S refer to the unknown and standard samples, respectively.

The resolution of a calibration curve becomes poorer at very high and low molecular weights; that is, large differences in molecular weight are reflected in small changes in elution volume. Note that additives, such as antioxidants, will also elute, so that these may be confused with a low molecular weight fraction of the polymer. Various aspects of the SEC experiment can be adjusted to improve resolution for a given determination [107, 108, 141]. The resolution problem is minimized with modern SEC columns, although smaller particles in the column increase the potential for shear degradation of the sample. The presence of sample heterogeneity, such as blends or branching, exacerbates the resolution problem. SEC detectors include differential refractometers and UV/visible detectors, which give a signal proportional to the polymer concentration, as well as viscometric and light scattering detectors, whose signal depends on both the concentration and the molar mass (discussed earlier). Multiple detectors are employed to facilitate deconvolution of overlapping retention volumes (Fig. 6) [142–146]. For example, the effluent from the column can pass through a light scattering cell or a viscometer, and then through a differential refractometer. The latter serves as a concentration detector and is usually last in line, since it is most easily disrupted by downstream back pressure.

A potentially serious error in the SEC analysis comes from peak broadening, due to nonuniformities in the pore structure of the GPC and inherent to the flow behavior through the column. The resolution of a column can be characterized by the ratio of the spread of the elution volume for a monodisperse sample to the peak of the retention volume. At the extremes of the range for a broad MWD sample, a given elution volume can shift by as much as 50% in molecular weight when the sample is rerun through the same instrument. This type of peak broadening is due to diffusion, mixing and concentration effects, and perhaps in part to a dependence of the hydrodynamic volume on

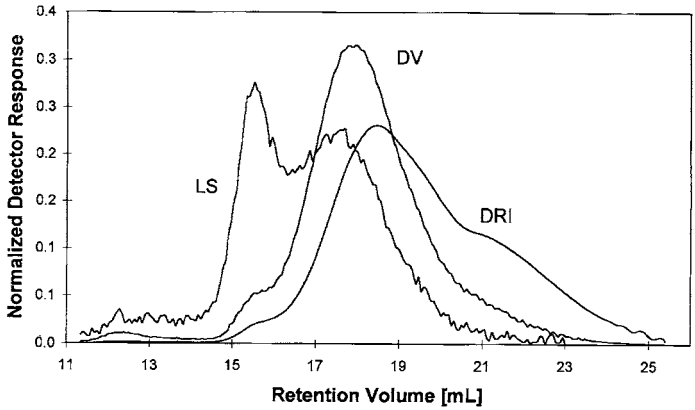

FIGURE 6 Chromatograms of a blend of linear and branched polyesters for light scattering (LS), viscometric (DV), and differential refractive index (DRI) detectors. The response of the LS is superior for larger molecular weights, while the DRI extends the sensitivity to larger retention volumes. (From Balke and Mourey [146].)

concentration. Another source of error for very high molecular weight samples (e.g., $M \sim 10^6$ g/mol or higher) is mechanical degradation (chain scission), transpiring during transport through the column [141, 147].

The classical method of solvent–nonsolvent fractionation according to MWD and compositional distribution depends on solubility differences among the various species. The method is empirical and tedious, involving characterization of phase-separated "cuts" as they are recovered. However, fractionations can be carried out with minimal equipment, and for some polymers are the only source of narrow compositional and MWD standards for techniques like SEC or $[\eta]$. TREF, described earlier, is an automated implementation of the fractionation procedure.

The term *field flow fractionation* (FFF) [107, 108, 148–150] refers to a family of one-phase chromatographic techniques, carried out in thin flow channels. In principle, FFF yield absolute molecular weights, although in practice calibrations similar to SEC are used. An external field is applied perpendicular to the laminar flow of solvent in a channel. The parabolic velocity profile of the flow causes separation according to the position of molecules with respect to the wall. Molecules having weaker interaction with the field remain further from the walls of the channel, thereby eluting sooner. The external field may be a flow field, an electric or magnetic field, or a thermal field. In *thermal field flow fractionation* [88–91], a temperature gradient of tens of degrees is imposed, causing migration and accumulation of the solute polymer at the cold wall, in competition with Brownian motion. The transport coefficient governing the thermal diffusion depends on chemical composition, as well as molecular weight. For a given solute, smaller molecules, having the larger diffusion

coefficients, migrate more toward the center, and are thus eluted first by the flow. In addition to discrimination according to molecular size, TFFF can be used to measure thermal diffusion coefficients of chain molecules [151, 152].

FFF is fast and provides good mass resolution. One of the attractive features that there is no substrate and the channel is too large to be plugged by gel. Thus, it can be especially useful for polymers containing gel. The method is useful for molecular weights up to about 10^7 g/mol, and commercial instrumentation is available.

An absolute method for molecular weight determination is matrix-assisted laser desorption ionization time-of-flight mass spectrometry (MALDI-TOF) [153–155]. The sample is dispersed in a UV-absorbing matrix (e.g., *trans*-cinnamic acid or 2,5-dihydroxybennzoic acid). Irradiation with a UV-laser induces evaporation of ionized polymer chains, which are then detected using TOF. The technique requires relatively narrow MWD samples. Commercial MALDI-TOF instruments are available. Alternative ionization methods have been employed, such as electrospray ionization mass spectrometry (ESI-MS), which may have advantages for certain polymer end groups [156]. TFFF and MALDI-TOF have been coupled to analyze polydisperse samples and polymer mixtures [157].

While sedimentation relies on gravity to drive the separation, rotating the sample at high speeds (up to 70,000 rpm) accelerates the process [9]. *Ultracentrifugation* involves determining the concentration profile by optical means [158]. In equilibrium ultracentrifugation, in which slower rotation speeds are used ($<10^4$ rpm), absolute molecular weight averages ($>5 \times 10^2$ g/mol) can be determined. However, the equilibration time can be as long as days, and so the technique is rarely used. In the biological field, nonequilibrium sedimentation velocity measurements are employed, which are quicker but less rigorous. Ultracentrifugation is one of few techniques yielding the z-average molecular weight, and it can also provide information concerning sample homogeneity. Analytical ultracentrifuges are commercially available.

The methods discussed heretofore involve polymer solutions. Neat samples are analyzed directly via *melt viscosity* measurements. At shear rates low enough (relative to Brownian motion of the chain modes), the melt viscosity becomes independent of shear rate ("Newtonian behavior"), $\eta = \eta_0$. Thus, the viscosity-M_w relationship for a particular temperature can provide an accurate M_w determination (Fig. 7 shows related dielectric data). Given the high molecular weight of elastomers, the main difficulty is attaining zero-shear-rate conditions. At ambient temperatures, $\eta_0 > 10^7$ Pa s. Note that "cold flow" of unvulcanized rubber usually requires weeks or longer. The obvious way to reduce the viscosity is to make measurements at elevated temperatures. However, especially for unsaturated rubbers, degradation may occur before steady-state conditions can be attained. The situation is worse if the polymer has long chain branching.

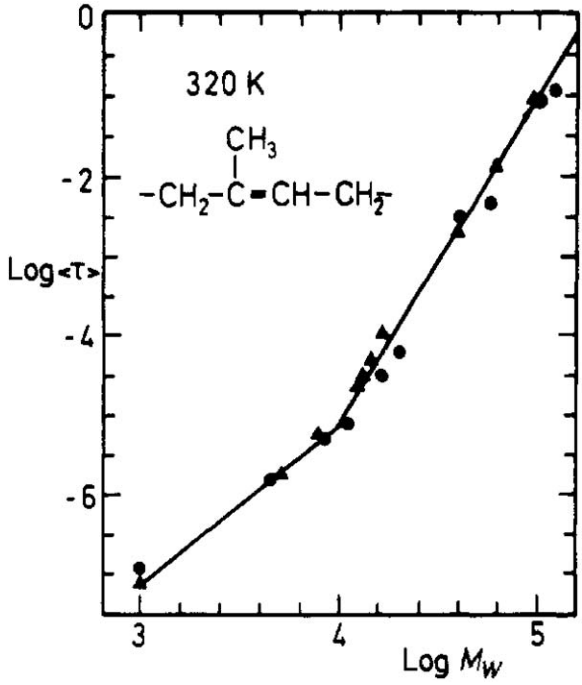

FIGURE 7 Normal mode relaxation time (which is proportional to the melt viscosity) of *cis*-1,4-polyisoprene as a function of molecular weight. The initial Rouse proportionality to molecular weight changes to a $M_w^{3.7}$ dependence beyond $M_w \sim 10{,}000$ g/mol. (From Boese and Kremer [158a].)

B. Long Chain Branching

Long chain branching (LCB), defined as branches having molecular weights of at least a few times the entanglement molecular weight, is common in rubbers. Its most important effect is increasing the viscosity; LCB is present in some commercial rubbers in order to reduce cold flow (i.e., the room temperature creep of rubber during storage). Substantial LCB may require use of a low M_n polymer, in order to retain a viscosity low enough for processing; however, the consequent plethora of chain ends may entail sacrifice of cured properties, especially those relating to heat buildup or strength. Branching affects other properties, affording a means to characterize the degree of branching [159]. For example, the nature of the branching affects the geometry and size of the chain molecule (Fig. 8).

The *intrinsic viscosity* is reduced by branching [viz. Eq. (11)]. The reduction is characterized by the ratio of the respective mean-square radii of gyration of branched and unbranched polymers having the same M_w

TABLE III Characterization of Molecular Weight and Its Distribution

Technique	Variables measured	Principle of operation	Range (g/mol)
Membrane osmometry (MO)	Number average molecular weight; virial coefficient	Osmotic pressure due to diffusion of solvent through membrane impermeable to polymer	
Vapor pressure osmometry	Number average molecular weight	Vapor pressure lowering	$<5 \times 10^4$
Cryoscopy	Number average molecular weight	Freezing point depression	$<10^4$
Ebulliometry	Number average molecular weight	Boiling point elevation	$<10^4$
Light scattering (LS)	Weight average molecular weight Virial coefficient Radius of gyration	Light scattering intensity from solution is proportional to the molecular weight of the solute. Angular dependence related to particle size.	$>10^3$
Neutron scattering	Weight average molecular weight Virial coefficient Radius of gyration	Scattering intensity is proportional to nuclear cross section.	
Intrinsic viscosity	Intrinsic viscosity Viscosity average molecular weight	Solution viscosity depends on polymer molecular weight.	$>10^3$
Size exclusion (SEC) or gel permeation (GPC) chromatography	Molecular weights and distribution	Permeation of polymer from a flowing solution into a porous stationary phase	$<10^7$
Field flow fractionation (FFF)	Molecular weights and distribution	External field effects separation of flowing solute	$<10^7$
Ultracentrifugation	Molecular weight averages	Concentration gradient in a large gravitational field is related to molecular weights.	$>5 \times 10^2$
Sedimentation	Molecular weights Sedimentation coefficient	Rates of diffusion in a gravitational field related to molecular weights	$>5 \times 10^2$
Melt viscosity	Dynamic or steady-state viscosity	Empirical correlation of viscosity and M_w	—

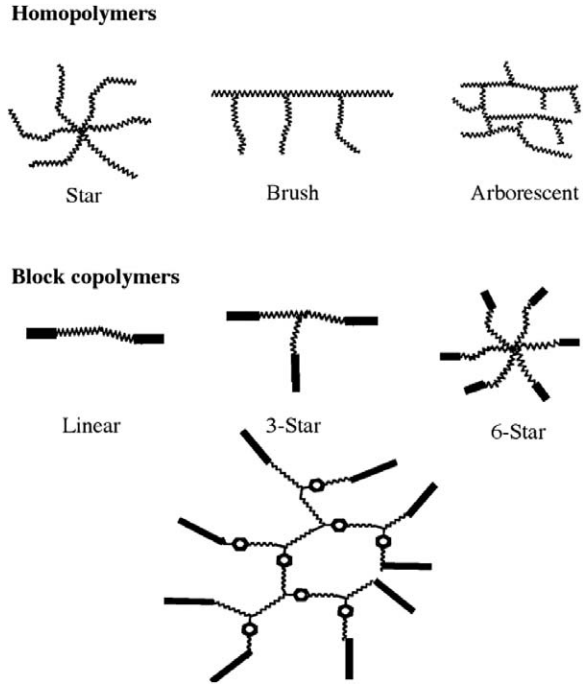

FIGURE 8 Spatial extent of polymer chains depends on the nature and extent of the molecular architecture. (From Puskas [159a].)

$$g = \frac{\langle S^2 \rangle_{br}}{\langle S^2 \rangle_{lin}}, g' = \frac{[\eta]_{br}}{[\eta]_{lin}} \tag{15}$$

The parameter g, which is less than unity for polymers with LCB, is sometimes defined as the ratio of the root-mean-square values, $S_{g,br}/S_{g,lin}$. The calculation of g for a given branch structure is straightforward, but radii of gyration are hard to measure experimentally. Intrinsic viscosities are readily measurable, but relating g' to g, and thus to branch structure is difficult. Calculations of g' involves dilute solution theory with the type of branching explicitly considered. Alternatively, g may be evaluated using model polymers. Determination of absolute levels of branching from intrinsic viscosity measurements is not possible, since it depends on the nature of the branching, including the junction functionality and branch architecture (random, star-branched, dendrimeric, etc.). However, relative values of g' can reflect relative degree of branching.

With light scattering measurement of the radius of gyration [see Eq. (6)], direct comparisons of g values can be made. In Θ solvents, the experimental g values generally agree with calculations, with some notable exceptions [160].

SEC can be used to detect branching [161–170]. Using online detectors that yield absolute molecular weights, comparison standards can be made to assess LCB [171]. Advantage can also be taken of the fact that the product $M[\eta]$ is constant for a fixed value of the SEC elution volume. Thus, SEC data is obtained for a homogeneous fraction of a sample of unknown branching, and the ratio of its intrinsic viscosity to $[\eta]$ for the linear polymer having the same elution volume is calculated. From this, M for the unknown is evaluated and compared to M calculated from its intrinsic viscosity. Note the method requires homogenous fractions.

An empirical relationship for broad MWD samples gives an average value

$$g'' = \frac{M_{V,lin}}{M_{w,LS}} \times \left(\frac{M_w}{M_v}\right)_{GPC} \tag{16}$$

in which $M_{V,lin}$ is the molecular weight calculated from the intrinsic viscosity assuming the polymer is linear, $M_{w,LS}$ is from light scattering measurements, and $\left(\frac{M_w}{M_v}\right)_{GPC}$ is taken from the elution volumes assuming no branching. As an example, for NBS 1476 (a branched polyethylene standard), $g'' = 0.4$, using $[\eta] = 1.04$ dl/g in decalin, $(M_w/M_v)_{\mathrm{SEC}} = 1.16$, $M_{w,LS} = 125{,}000$ g/mol. The number of branches yielding a branching parameter of 0.4 depends on the nature of the branching. For random tetrafunctional branches, $g = 0.4$ corresponds to 20 chain ends per weight average chain.

Advanced SEC analytical techniques take advantage of online *light scattering* and *viscometry* [IV A]. With the SEC calibrated for the product of $[\eta]$ times M versus elution time for a particular polymer species, together with $[\eta]_{\mathrm{Br}}$ or $M_W{}^{Br}$ measurements, one can calculate g factors as the ratio of the measured intrinsic viscosity to the value of $[\eta]$ calculated for the corresponding linear polymer (i.e., linear polymer that would have eluted at the same time).

If well-characterized samples are available, a calibration of viscoelastic properties for the neat material can be used to assess branching. The melt viscosity, as well as the modulus, and other viscoelastic properties of the neat polymer, are influenced by branching. Below a certain molecular weight (which is a few times the entanglement molecular weight), branching reduces the melt viscosity, since the molecular size is smaller for fixed molecular weight. However, for branches long enough to be well-entangled, the dependence of the melt viscosity on branching increases markedly, so that a branched polymer becomes more viscous than its linear counterpart of equal M_w [159, 172–174].

For rubbers such as NR (or synthetic 1,4-polyisoprene) [175] and polybutadiene (both 1,2- and 1,4-isomers) [176], LCB increases the temperature-sensitivity of the viscosity and terminal relaxation time. Thus, by comparing apparent activation energies, or, in the more usual case where the behavior is

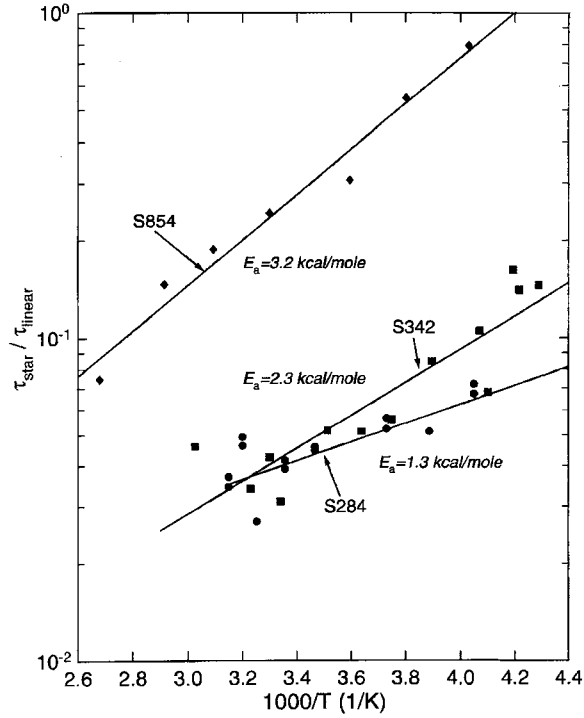

FIGURE 9 Terminal relaxation times of 3-arm star 1,4-polyisoprenes having M_w(g/mol) = 284,000 (S284), 342,000 (S342), and 854,000 (S854), normalized by the relaxation time for linear 1,4-polyisoprene. The excess activation energy due to the LCB is ~400 J per mole of branch entanglements. (Reprinted from Santangelo and Roland [175].)

non-Arrhenius, the temperature dependence of the ratio of relaxation times for an unknown and a linear sample of the same polymer, inferences can be drawn concerning LCB (Fig. 9). For polymers such as 1,4-polyisoprene (see Fig. 7), which have a dipole moment parallel to the chain, dielectric measurements of the normal mode can be used to measured the temperature dependence and thus assess the presence of LCB.

Note that LCB does not enhance the T-dependence of all rubbers. For example, the temperature dependence is the same for linear and branched polyisobutylene [174, 177], polydimethysiloxane [178], and hydrogenated 1,2-polybutadiene [176].

C. Gel

Where the presence of gel is suspected, true viscous flow is not possible (the material is effectively a solid). In such cases, *gel-sol studies* can

be revealing. If crosslinks can be introduced in a controlled fashion (e.g., using peroxide or ionizing radiation), then the initial molecular weight can be determined from the gel dose. However, this requires knowledge of the rates of both crosslinking and chain scission. As crosslinking proceeds beyond the gel point, the partition between gel and sol is governed by the MWD of the sample, which in principle can be used to measure MWD [179].

Networks with crosslink densities only slightly beyond the gel point have minimal mechanical strength. Thus, care must be taken in dissolution of the soluble fraction to avoid damaging the network. If the gel fraction data extrapolate to a negative amount of crosslinking for gelation, the implication is that the original material contained gel. Although gelled material cannot undergo homogenous flow under linear viscoelastic conditions, a lightly crosslinked rubber can be milled, mixed in an internal mixer, and have a measurable Mooney viscosity. Additionally, dissolved polymers can associate, to yield rather permanent aggregates [180, 181]. This phenomenon is common with polymers that can crystallize (e.g., EPDM, polyvinylchloride, polyurethanes). The reversible association, which usually varies with solvent or temperature, is quite distinct from gel formed from covalent crosslinks.

V. GLASS TRANSITION AND SECONDARY RELAXATION PROCESSES

When a measurement of polymer dynamics is made (using, for example, mechanical or dielectric spectroscopy, or dynamic light or neutron scattering), a maximum in the susceptibility (absorption peak) is observed for molecular motions transpiring on the timescale of the experimental variable (e.g., frequency of the applied stress or voltage). In the limit of small perturbations (for which the material response is linear), the relaxation directly reflects the equilibrium Brownian motion. Such correspondence follows from fluctuation-dissipation theory, originally developed to explain Johnson noise in electrical conductors. The gigantic size of polymer molecules provides for an enormous number of degrees of freedom, and thereby motion encompassing many decades of time overly a broad range of length scales (Fig. 10). The longest relaxation processes involve transport of the chain center of mass, and these are termed the terminal or global dynamics. At shorter times, relaxation involves motion of progressively smaller portions of the chain molecule. The rubbery plateau reflects the transient entanglement network, whose dissolution gives rise to a peak in the loss modulus (and also in the dielectric loss for polymers having a dipole moment parallel to the chain) [182]. At frequencies beyond the rubbery plateau, chain motions are unaffected by entanglements. In the softening zone, the modulus is a strong function of frequency, with the behavior referred to as Rouse dynamics. (The Rouse theory was originally developed for dilute polymer solutions, but with small modification can be applied to unentangled polymer melts.) At the highest frequencies prior to the

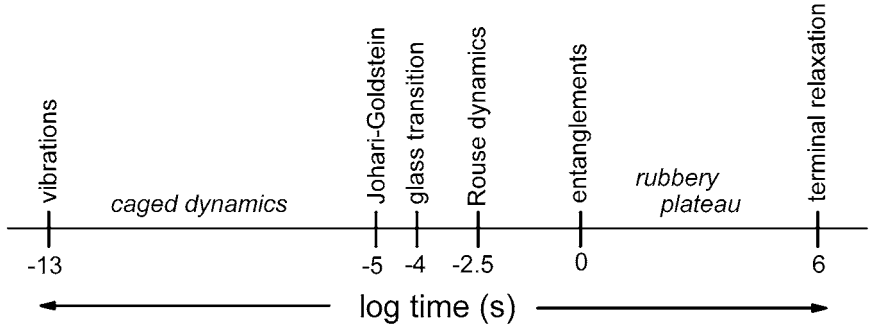

FIGURE 10 Schematic indicating range of motions and corresponding frequencies for 1,4-polyisoprene (M_w = 500,000 g/mol) at –40°C.

glass transition, the portion of chain involved in the relaxation is too short for Gaussian behavior (that is, its end-to-end distance does not have a Gaussian distribution). These "sub-Rouse modes" segue at higher frequencies into the local segmental dynamics.

The local segmental dynamics are associated with the rubber-glass transition, occurring at T_g. It is only in the glass transition zone of the viscoelastic spectrum that both chain modes and local segmental modes can be measured simultaneously at the same temperature, using conventional techniques. Since the chain modes and the local segmental dynamics have different temperature dependences [183–185], a breakdown of the time-temperature superposition principle is observed in the glass transition zone. Thus, master curves for the chain dynamics can be constructed, which extend from the end of the softening zone through the terminal relaxation, and master curves of the local dynamics are possible. However, in the softening zone, the shape of the viscoelastic spectrum changes with temperature (Fig. 11).

While all relaxation times depend on temperature and pressure, only the global motions (viscosity, terminal relaxation time, steady state recoverable compliance) are functions of M_W (and to a lesser extent MWD). An example of the various dynamics of 1,4-polyisoprene are illustrated in Fig. 10. At frequencies beyond the local segmental relaxation, or at temperatures below T_g, secondary relaxation processes can be observed, especially in dielectric spectra. In polymers, many of these secondary processes involve motion of pendant groups. However, the slowest secondary relaxation, referred to as the Johari-Goldstein process, involves all atoms in the repeat unit (or the entire molecule for low M_w materials). This Johari-Goldstein relaxation serves as the precursor to the prominent glass transition.

The T_g of an elastomer is below room temperature, typically lower than –30°C. Otherwise, at ambient temperature, the material would lack the flexibility associated with rubbery behavior. The glass transition is a second-order

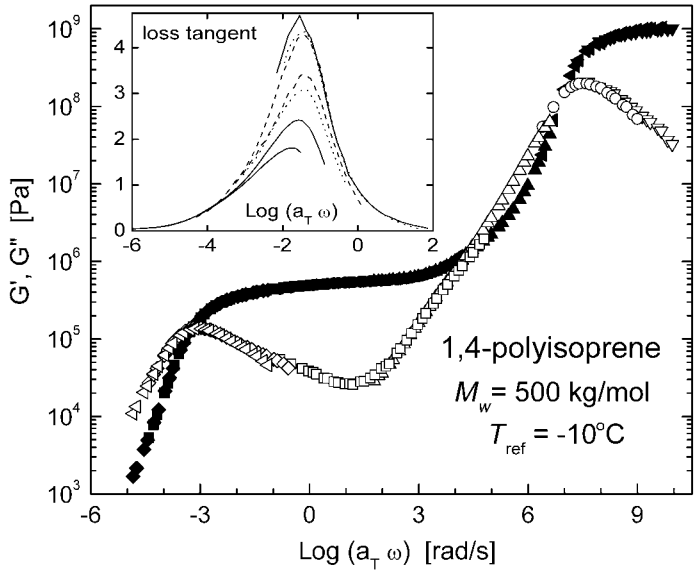

FIGURE 11 Apparent master curves (reference temperature = –10°C) for the storage (solid symbols) and loss (hollow symbols) moduli of *cis*-1,4-polyisoprene (M_w = 500,000 g/mol). The breakdown of time-temperature superpositioning, barely evident in the softening zone, is seen clearly in the loss tangent peak, shown in the inset for temperatures from –66°C to –48°C (the peak height decreases with increasing temperature). (From Santangelo and Roland [183].)

transition because, unlike melting or boiling, there is no discontinuity in the volume at T_g, but only a discontinuous change in the rate of change (i.e., in the thermal expansion coefficient (Fig. 12) [186]. Experimentally, T_g simply reflects the temperature at which local segmental motions become slow relative to the experimental timescale. Thus, values for T_g are a function of both the measurement frequency and the particular relaxation process under observation. There exist a host of properties which can serve as indicators of T_g. T_g is affected by the presence of comonomers in the chain backbone, and of course by nonpolymeric ingredients in the formulation. Both plasticization (lowering of T_g) and antiplasticization (increase of T_g) are known.

In nonisothermal measurements, it is preferable to approach T_g from the equilibrium state (i.e., by cooling), since the properties in the glassy state change due to physical aging. Physical aging refers to structural relaxation far enough below T_g, that the local segmental motion cannot contribute. It is associated with the slow approach of the density to its equilibrium value, with consequent variation in physical properties, including a shift of the glass transition temperature. A measure of this departure from equilibrium is gleaned from the fictive temperature, T_f. Also known as the structural or equilibrium tem-

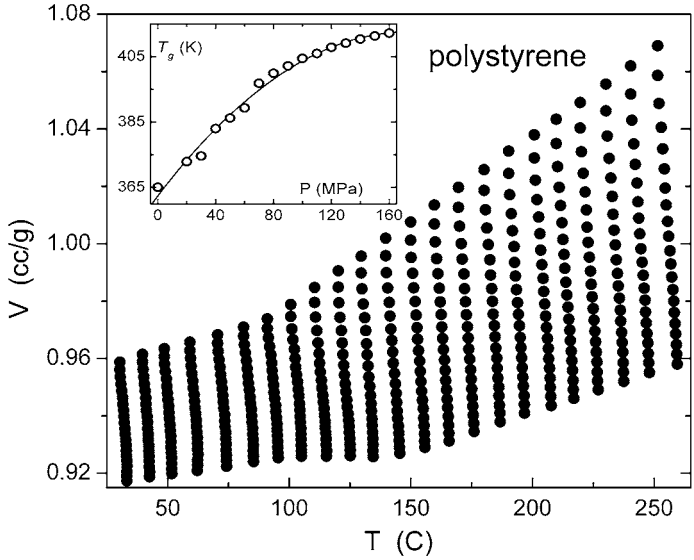

FIGURE 12 Specific volume of polystyrene (M_w = 110,000 g/mol) as a function of temperature at various pressures. The inset shows the variation of T_g with pressure. (From Roland and Casalini [186].)

perature, T_f is the temperature at which the enthalpy of the material would be its equilibrium value; thus, the difference between the fictive temperature and the actual temperature is a measure of the extent of structural relaxation.

The most common means to assess T_g is via heat capacity (C_p) measurements, usually carried out in a differential scanning calorimeters (DSC). The temperature of the sample changes at a fixed rate, with the heat flow monitored. An older, and less useful, variation is differential thermal analysis (DTA), in which heat flow is programmed, and the consequent rate of temperature change is measured. With either method, a discontinuity in the differential response evidences a thermal transition. In a DSC experiment, T_g is commonly identified with the midpoint of the change in heat capacity. This is nearly equal to an alternative definition, the temperature of the intersection of the extrapolated baseline with the tangent of the maximum slope [65]. As stated, DSC measurements should be made during cooling, so that equilibrium is maintained. Otherwise, substantial physical aging can cause the appearance of an endothermic peak at the glass transition. In this situation, the fictive temperature is more informative than the apparent transition temperature. A graphical method for determining T_f is illustrated in Fig. 13.

Modulated (or alternating) DSC (MDSC) [187–189] is a technique in which a modulated heating (or cooling) rate is superimposed on the usual constant heating (or cooling) rate. The measured heat flow is separated into the

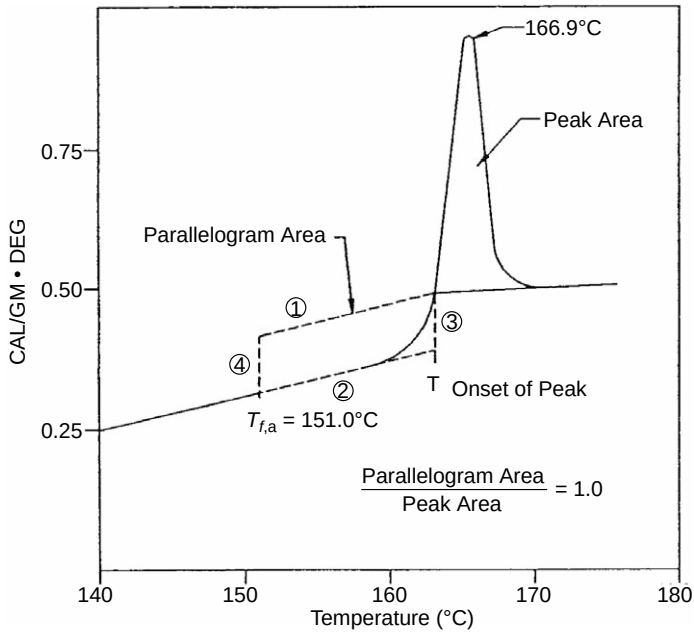

FIGURE 13 DSC of a cured epoxy resin. To determine the fictive temperature, a parallelogram is constructed to the low temperature side of the enthalpy peak, with horizontal sides parallel to the measured heat capacity. The onset of the peak defines the high temperature boundary, while the low temperature boundary (i.e., T_f) is chosen such that the area of the parallelogram equals the peak area. (From Plazek and Frund [186a].)

reversing (time-independent) component, which is proportional to the heat-capacity, and a nonreversing (time-dependent) component, resulting from kinetic effects. This distinguishes reversible thermal processes like the glass transition from irreversible processes, such as enthalpy relaxation and crystallization. MDSC is useful for studying transitions too weak to be detected by conventional DSC, analysis of multiple endotherms, and separating pre-existing crystallinity in the sample from that occurring during the DSC measurement. It also can provide accurate heat capacity measurements under quasi-isothermal conditions.

VI. MORPHOLOGY

Analyzing the morphology of an elastomer includes not only the characterization of the molecular structure of the polymer itself and of the compounding ingredients, but may also extend to the supermolecular scale. Such a characterization includes filler network structure (see Chapter 8), the phase

morphology in heterogeneous blends and thermoplastic elastomers, and any aggregates (clusters) in rubbers containing ionic groups (e.g., carboxylated rubber). A survey of experimental techniques is given in Fig. 14. A few selected aspects of rubber morphology are discussed below.

A. Orientation

Rubber elasticity arises from the orientation of chain segments, and the degree of this orientation underlies the mechanical properties. The most facile way to quantify the orientation is from the (optical) birefringence, defined as the difference in refractive indices for two perpendicular directions, $\Delta n = n_{\parallel} - n_{\perp}$. This birefringence depends on the optical anisotropy of the chain units, as well as their degree of orientation

$$\Delta n = \Delta n_0 f_2(\phi) \tag{17}$$

For birefringence, the orientation function is the second Legendre polynomial of the orientation angle ϕ, $f_2(\phi) = \langle 3\cos^2\phi - 1\rangle/2$, where the brackets denote an average over all chains. The birefringence of perfectly ordered chains, Δn_0 (sometimes called the intrinsic birefringence), must be calculated from the optical polarizabilities of the chain units, and in practice birefringence measurements usually only provide a relative measure of $f_2(\phi)$. The fact that the mechanical stress, σ, is proportional to this same orientation factor gives the stress optical rule

$$\Delta n = C\sigma \tag{18}$$

where C is the stress optical coefficient [190]. This relation is useful for measuring stress in amorphous polymers undergoing flow. Since C is independent of crosslink density, the stress optical rule has application to networks, although it may not be valid at very large strains due to non-Gaussian behavior (finite extensibility). Deviations from Eq. (18) also occur in the glass-transition zone, because of the differing contributions to Δn from the chain modes and the local segmental motion [191]. Since birefringence is fundamentally related to strain, not stress, the stress optical rule necessarily breaks down during creep recovery [192]. The stress becomes zero but there is still orientation within the rubber, hence C becomes unbounded. As shown in Fig. 15, this same phenomena occurs with double networks, formed by further crosslinking of a strained network [193, 194].

When a material is semicrystalline, the observed birefringence is the sum of the Δn from the oriented amorphous phase and the crystalline regions. There is also a contribution due to form birefringence, arising from distortion of the light wave transversing the refractive index boundary between the amorphous and crystalline phases.

Another standard method of measuring polymer orientation is infrared dichroism, which refers to the ratio of the IR absorption for light having

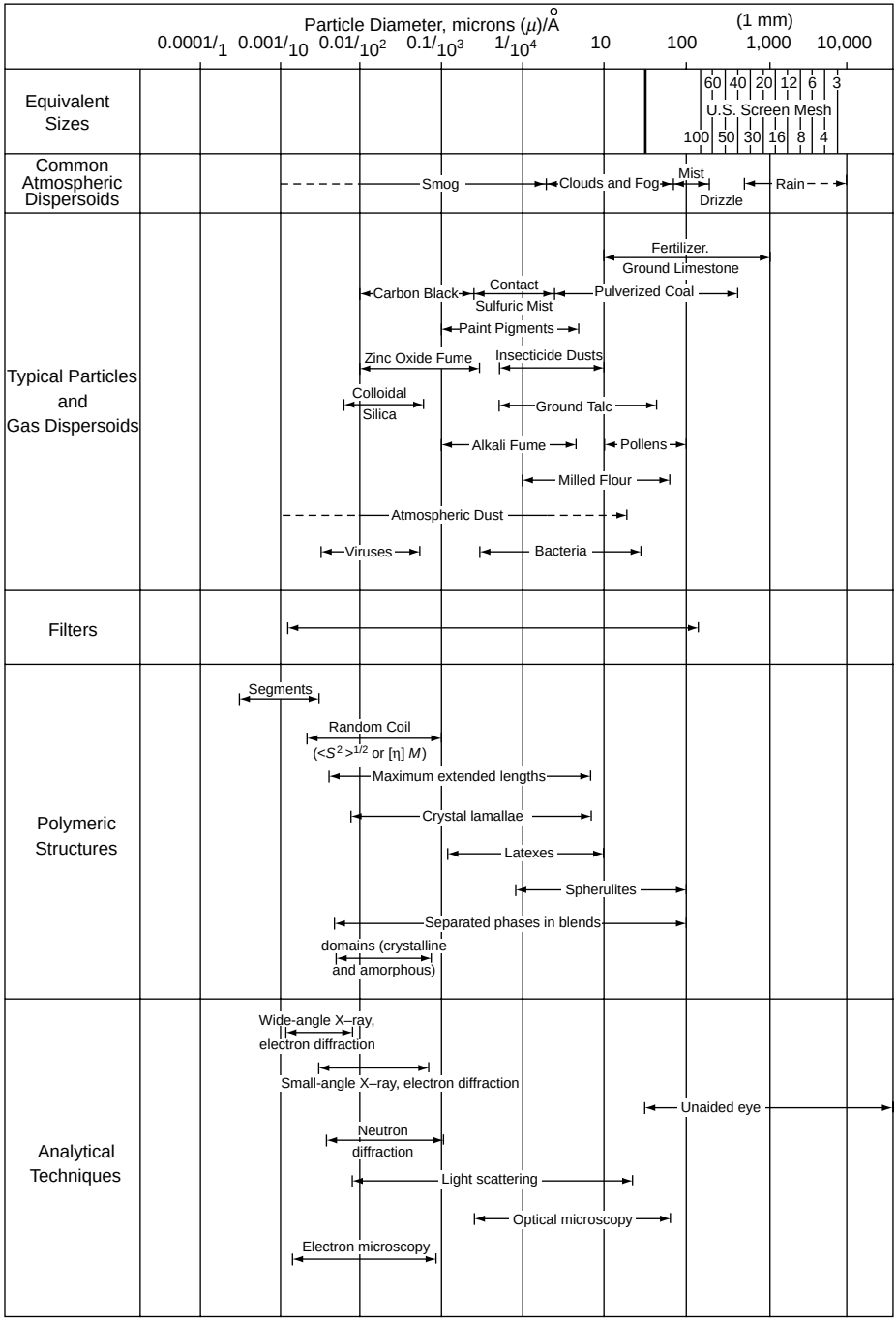

FIGURE 14 Characterization of particles.

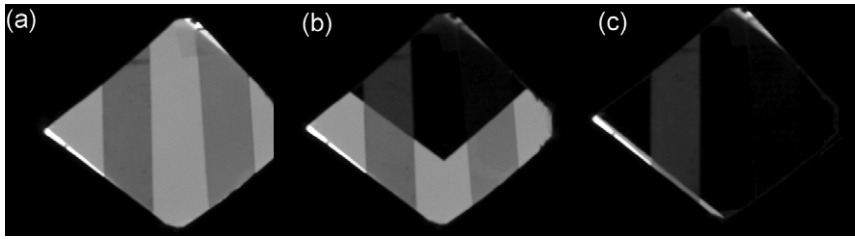

FIGURE 15 Natural rubber sample on left is double network and on right is a conventional NR elastomer (a, b). Both are in a state of mechanical equilibrium (stress = 0). Nevertheless, as seen in (c), the double network transmits light through crossed polarizers, due to its inherent orientation. This is a violation of the stress optical rule, similar to that observed during creep recovery of uncrosslinked rubber.

orthogonal polarizations. IR dichroism yields the same information as birefringence measurements [i.e., $f_2(\phi)$], but with the major advantage of chemical selectivity. The orientation of specific groups can be determined, as well as the orientation of the components in mixtures [195–197]. Analysis requires knowledge of the orientation of the vibrational transition moment with respect to the chain axis. Obviously, combination bands should be avoided. A few percent of deuterated polymer can be added to the sample, so that the infrared measurements can be carried out on thick samples, while still conforming to Beer's law (absorbance < ~0.7). This enables simultaneous measurement of the stress [198]. The complementary technique, polarized Raman spectroscopy, is also used to characterize orientation [199–201].

In polarized fluorescence measurements, the sample is illuminated with polarized light, and the emitted intensity is measured for polarization parallel and perpendicular to the excitation radiation. The experiment yields both $f_2(\phi)$ and the 4th Legendre polynomial, $f_4(\phi) = \langle 35\cos^4\phi - 30\cos^2\phi + 3\rangle/8$. The latter is a more strongly decreasing function of ϕ than is $f_2(\phi)$, so that it weights more the more oriented end of the orientation distribution function. For uniaxial distributions, these two functions alone are adequate to describe the orientation [202].

Another method to characterize orientation is deuterium NMR. Deuterons have a spin quantum number equal to 1, and therefore a nuclear quadrupole moment. Coupling between the quadrupole moment and the two possible NMR transitions (resulting from the three Zeeman levels of the spin = 1 nucleus) yields differences in the energy levels of the two transitions, giving rise to a doublet. The separation of this doublet is proportional to $f_2(\phi)$ (which depends on the orientation of the chemical bond axis of the deuteron relative to the applied external magnetic field); thus, the magnitude of the observed splitting yields directly the orientation.

Orientation in crosslinked elastomers primarily reflects the configurational entropy and intramolecular conformational energy of the chains.

However, as first shown by deuterium NMR experiments on silicone rubber [203, 204], unattached probe molecules and chains become oriented by virtue of their presence in a deformed network. This "nematic coupling" effect is caused by intermolecular interactions (excluded volume interactions and anisotropic forces) [195, 205]. The orientation is only locally effective, so it makes a negligible contribution to the stress [206], and the chains retain their isotropic dimensions [204].

Wide-angle x-ray scattering can be used to evaluate orientation, but it is more suited to semicrystalline polymers. In principle, scattering methods can yield all orientation functions, although experimental limitations restrict determinations to $f_4(\phi)$. Using high flux synchrotron x-ray sources, transient orientations can be measured. This has been used to study the behavior of the amorphous phase during stretching of NR (Fig. 16) [207, 208].

B. Blends

Although many rubbers can be mixed to form an ostensibly homogeneous blend, the overwhelming majority of such mixtures have phase-separated morphologies. To form a useful elastomer, the components need only be sufficiently compatible that a satisfactory dispersion is attained. Actual thermodynamic miscibility, implying segmental mixing of the components, is rare, although it is important to recognize when is achieved. The phase size in a heterogeneous blend will depend on the compatibility of the components and, to a lesser extent, on the mixing conditions. The particle size distribution can be determined from electron micrographs, using image analysis software [209, 210]. If the image contrast is poor, some underestimation of the domain sizes can result, due to poorly discerned peripheries. For microtomed samples, errors can arise if the section thickness is less than the particle size [211]. In principle, the dispersed phase size distribution can be determined from small-angle scattering experiments, using either x-rays or neutrons. Since a comparatively large volume is sampled by the incident beam, scattering methods are less subject to bias than micrography. However, an inherent problem in obtaining structural information from scattering experiments is that only a limited range of reciprocal space is probed. Moreover, the size distribution cannot be uniquely determined from the scattering curve. Only "scattering equivalent" distributions are obtained, based on assumptions about the particle shape and the functional form of the distribution. In Fig. 17 the dispersed particle size of 1,4-polybutadiene in polychloroprene is shown, as determined by transmission electron microscopy (TEM) and small-angle scattering measurements [212]. Scanning transmission x-ray microscopy, based on the chemical specificity of near edge x-ray absorption, has potential for investigating heterogeneous morphologies, although it requires a synchrotron source [213]. Figure 18 demonstrates its utility for resolving blend morphologies without the requirement for staining.

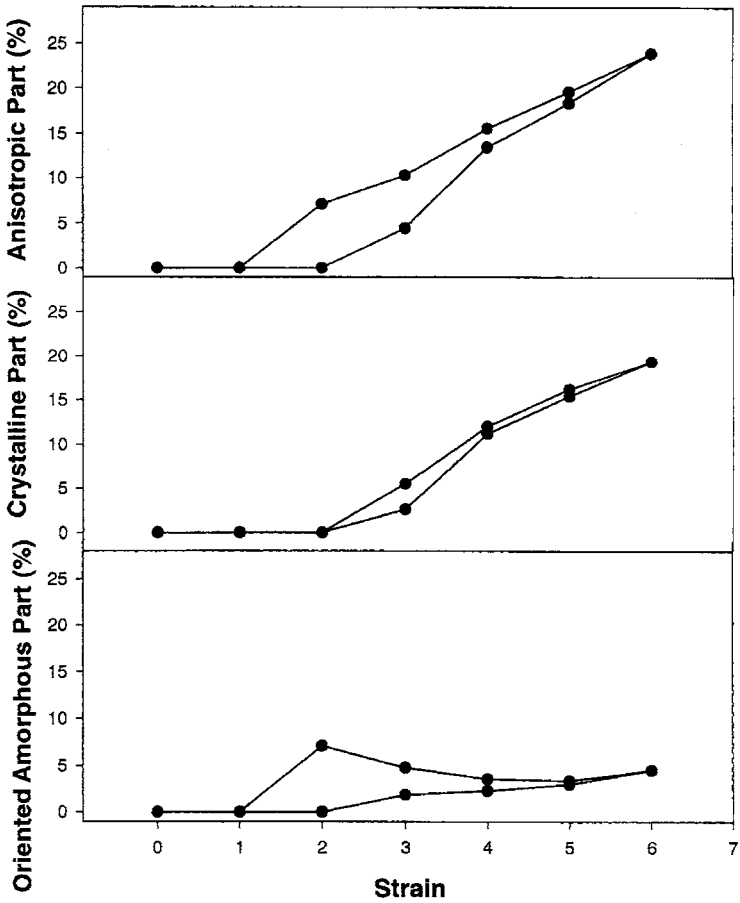

FIGURE 16 Total anisotropic fraction, crystal fraction, and oriented amorphous fraction of sulfur vulcanized NR stretched slowly at ambient temperature. The upper points correspond to extension, and the lower to retraction. For strains >200%, crystallization is induced, resulting in a decrease in the amorphous phase orientation. (From Toki, Sics, Ran *et al.* [208].)

The simplest method of determining whether the phase morphology is homogeneous is by calorimetry. The observation of two transitions, corresponding to the respective T_g of each component, indicates a phase-separated morphology. However, a single transition does not guarantee thermodynamic miscibility, especially if the component T_g's are close. On the other hand, spectroscopic measurements can reveal two distinct relaxation peaks, even for a thermodynamically miscible blend [214–217]. Referred to as "dynamic heterogeneity," this arises when the components have very different intrinsic mobilities. The motion of each component is determined both by its chemical

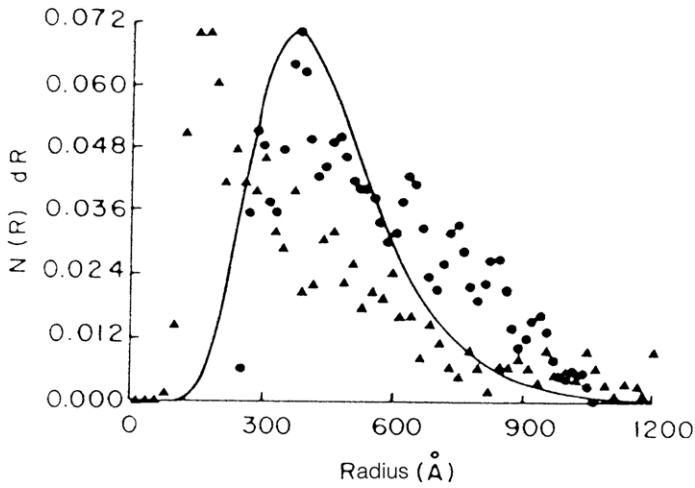

FIGURE 17 Size of dispersed phase in blend of 5% 1,4-polybutadiene in polychloroprene, as determined by analysis of TEM images (triangles), numerical transformation of combined SAN, and SAXS data (circles), and best-fit to scattering curves assuming log normal distribution for particle sizes (solid line). (From Roland and Böhm [212].)

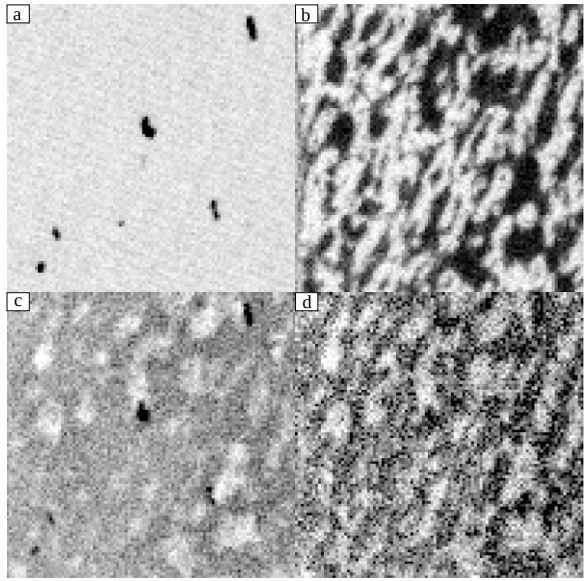

FIGURE 18 Scanning transmission X-ray micrographs ($10\,\mu m^2$) of polybutadiene/poly(isobutylene-co-4-methylstyrene) (30/70) blend containing 20 phr carbon black, at increasing photon energies: (a) lowest energy—only carbon black structure evident; (b) higher energy—unsaturated polymer also evident; (c) and (d) highest photon energies—polyisobutylene now apparent with reversed contrast. Darker regions in the images depict locations of higher absorbing material and lighter regions are more transparent. (From Winesett, Ade, Smith *et al.* [213].)

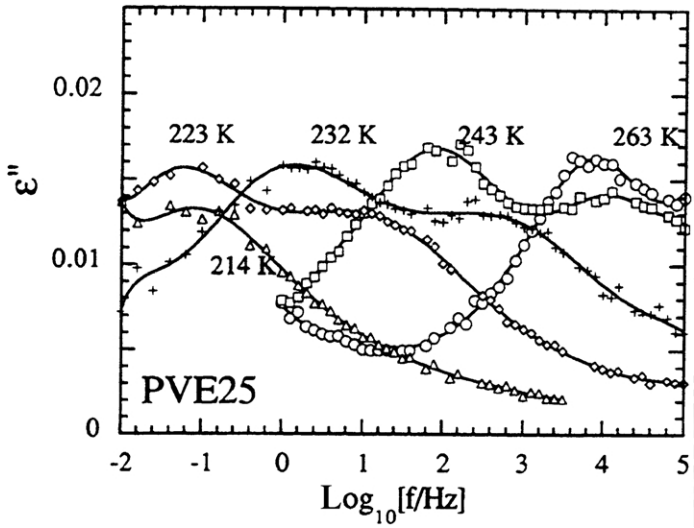

FIGURE 19 Isothermal dielectric loss curves for a thermodynamically miscible blend of 25% 1,2-polybutadiene with natural rubber. Notwithstanding the homogenous morphology, the respective mobilities of the components differ, whereby two peaks are observed in the spectrum. (Reprinted from Alegria, Colmenero, Ngai *et al.* [216].)

composition and by its local environment. The latter is averaged out when the phase morphology is homogenous, which usually results in a single blend T_g. However, when the intrinsic mobilities are very different, two transitions can result, as shown in Fig. 19. Calorimetric T_g's of dynamically heterogeneous, miscible blends are usually quite broad [218].

When the respective component glass transition temperatures are close, the blend T_g is not a useful measure of blend homogeneity. In fact, excess mixing volumes and specific interactions can cause anomalous behavior. The T_g of such a blend can be lower (as seen in polychloroprene/epoxidized polyisoprene blends [219]) or higher (as seen in polylepichlorohydrin/polyvinylmethylether blends [220]), than T_g of either neat component. In blends of polymers having nearly equivalent T_g, ^{129}Xe NMR has proven useful [221]. Xenon is highly polarizable, so that even van der Waals interactions produce large changes in its NMR chemical shift. When dissolved in a heterogeneous polymer blend, two ^{129}Xe NMR lines are observed, if the domains are large (relative to the diffusion time of the xenon). On the other hand, a single resonance is consistent with miscibility and yields an upper bound on the domain size. The technique is most useful for rubbery materials so that the spectral lines are sharp. Various groups have used ^{129}Xe NMR to investigate the phase morphology of blends [222–226]. Figure 20 shows the changes in the ^{129}Xe NMR spectrum during redissolution of a blend of 1,4-polyisoprene and

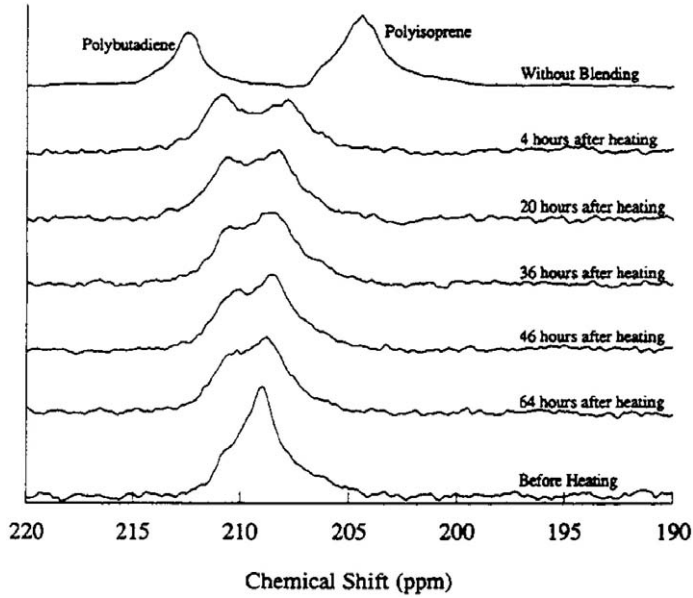

FIGURE 20 NMR spectra of ^{129}Xe dissolved in a homogeneous blend (bottom), and at various times after heating above the LCST, whereby phase separation transpires. The uppermost curve was measured on the pure polymers, simultaneously in the NMR tube but physically separated. (From Walton, Miller, Roland *et al.* [224].)

1,4-polybutadiene after heating above the lower critical solution temperature (LCST).

A problem with phase-separated blends is obtaining a uniform dispersion of the compounding ingredients. For example, the distribution of curatives can be skewed by diffusion from one phase into the other. This problem is more significant when the component polymers have substantially different solubility parameters. Various methods have been proposed to assess the crosslink distribution in rubber blends [227]. Since the glass transition behavior is affected by vulcanization, especially for high degrees of crosslinking, measurement of T_g [228, 229] or the local segmental relaxation [230] of the components can yield information about crosslink distributions. However, the method is insensitive to low degrees of crosslinking and requires the components to have significantly different T_g's. If the crosslinking is low enough that a substantial fraction of the polymer remains soluble, analysis of the respective sol and gel fractions can potentially enable the relative crosslinking of the phases to be assessed [231]. There have been attempts to use TEM of swollen rubber blends to investigate crosslink distributions [227]. NMR imaging can detect spatially varying crosslink densities. Although the technique has been applied to study oxidation of rubber [232], the spatial resolution is too coarse (>10 μm) for blend studies.

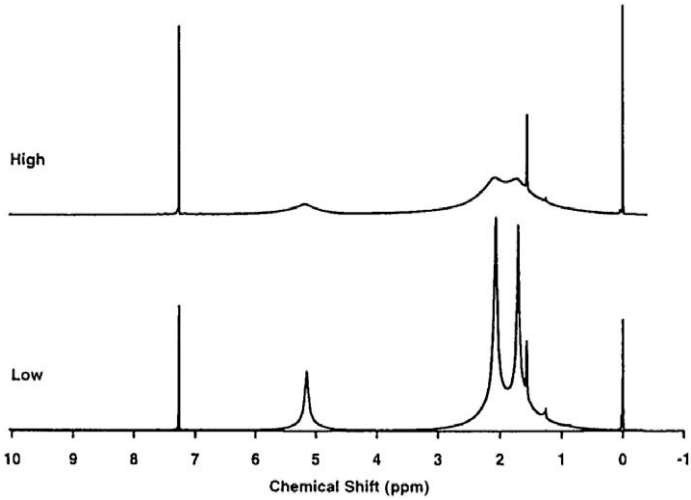

FIGURE 21 ^{1}H NMR spectra of swollen NR elastomers. The spectrum in the upper panel is for a sample having a crosslink density 4.5 times larger than that for the lower panel. The resonance at 5.2 ppm, due to the olefinic protons, can be utilized to determine relative crosslink densities. (From Tinker [227].)

NMR of swollen rubber has been used to determine crosslink distributions in blends [233, 234]. Swelling enhances chain mobility, and the isotropic motion of nuclei averages local fields, thereby narrowing the spectral lines. This allows individual resonances to be characterized. Crosslinking constrains motion and makes it more anisotropic, and thereby the incoherent averaging is less complete, broadening line widths (Fig. 21). Empirical correlations with crosslink density are required for quantitative results.

Crystallization in miscible blends can occur with rejection of the noncrystallizing component, so that its concentration in the amorphous phase increases. Alternatively, if it can be accommodated in the unit cell, it may be entrapped, with consequent alteration in the mean unit cell volume [235]. In NR, there is also a shift from α-lamellae to the β-lamellar form [236] (Fig. 22). These crystal structures have the same unit cell, but the latter has a greater fold-surface free energy. Thus, the noncrystallizing blend component is more readily accommodated into the fold plane at the crystal surface.

C. Crystallinity

Rubbery behavior—large, reversible extensibility—implies an absence of crystallinity, and this is usually the case for undeformed elastomers. However, small extents of crystallization may be present at ambient temperature in some

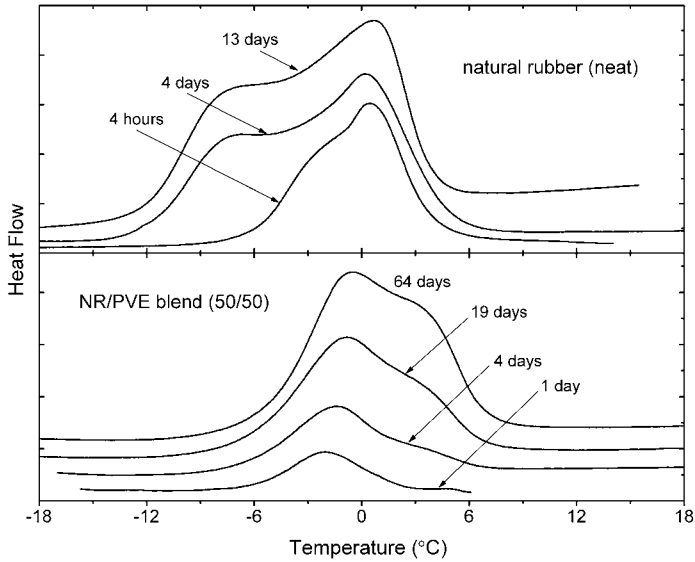

FIGURE 22 DSC melting endotherms in NR, pure (upper panel) and blended 50/50 with 1,2-polybutadiene (lower panel), after crystallization at –25°C for the indicated time periods. The neat rubber initializes crystallizes into the more stable α-lamellae, with substantial β-lamellae only forming at higher extents of crystallization. Miscible blending causes preferential crystallization of the lower melting β-lamellae. (From Zemel and Roland [236].)

elastomers, including EPDM with high ethylene content, epichlorohydrin rubber, and polypropylene oxide rubber. The crystallites in these materials can act as reinforcing agents. Many thermoplastic elastomers have crystalline domains which function as reversible crosslinks [237].

If there is sufficient regularity of their backbone structure, amorphous rubbers crystallize at lower temperatures. This mainly affects storage behavior. Unoriented NR crystallizes through lamellar growth into radial spherulites, having two morphologically differing forms, the more stable α-lamella and the slower forming β-lamella [245]. Both lamellar types have the same crystal unit cell, but differ with respect to growth rates, lamellar thicknesses, and morphologies. As mentioned, the β-lamella have a higher fold surface free energy. In order to accommodate the presence of *trans* units, synthetic *cis*-1,4-polyisoprene tends to crystallize more in the β-form, since the fold surface better tolerates noncrystallizing units [238]. This is similar to the alteration in the crystal morphology of 1,4-polyisoprene caused by miscible blending (see Fig. 22) [236].

Although elastomers are usually amorphous, strain-induced crystallization occurs in rubbers such as *cis*-1,4-polybutadiene, butyl rubber, and NR. Crystallization under stress, discovered 200 years ago [239], increases the modulus and most failure properties of rubber and is essential to performance in many

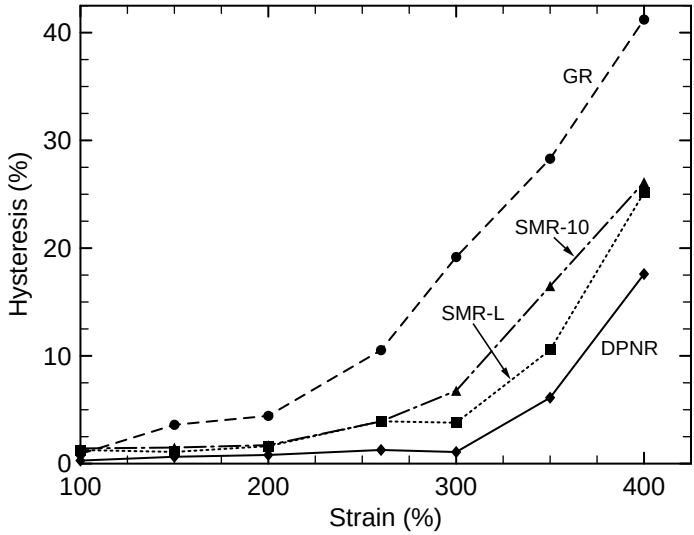

FIGURE 23 The mechanical energy dissipated relative to the total input strain energy for four grades of NR, stretched at RT to various extent. Strain crystallization at ~250% or higher results in more marked hysteresis. (From Choi and Roland [262].)

applications [240–243]. For NR, the propensity for strain-crystallization correlates directly with the failure properties [244]. Crystallization of natural rubber under strain transpires through row nucleation of lamellae, whose growth proceeds perpendicular to the strain direction [238, 245]. The latter, secondary crystallization, can be quite slow [246], and its rate is unaffected by strain [245]. However, the row nucleation rate is greatly enhanced by orientation, effecting rapid initial crystallization [247–250]. The time for strain-induced crystallization of NR is less than 60 ms at RT [246], which makes it difficult to measure strain-induced crystallization rates for different compounds.

A prerequisite for high levels of strain-crystallization is steric purity of the polymer backbone, and this accounts for the better performance of NR in comparison to synthetic *cis*-1,4-polyisoprene [251, 252]. Reinforcing filler influences the crystallization behavior [253–256], as do the other compounding ingredients. The denatured proteins and other hydrocarbon-insoluble contaminants in NR primarily affect the rate of crystallization. For example, it has been shown that acetone extraction [257] and deproteinization of natural rubber [258] both reduce the isotropic crystallization rate, presumably by reducing nucleation sites. In contrast, the degree of crystallinity attained in the absence of orientation is governed by the backbone microstructure, specifically the length of *cis*-1,4 sequences, not by the non-rubber constituents [259].

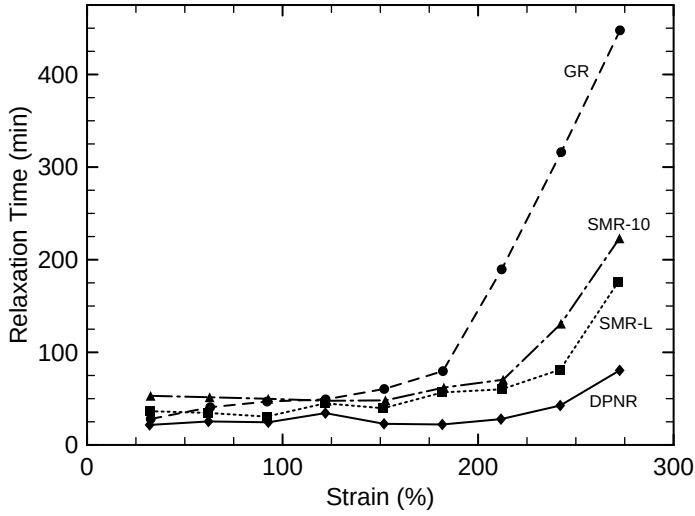

FIGURE 24 The time over which stress decay was observed for four NR elastomers. Initially viscoelasticity governs the relaxation time; at higher strains crystallization commences. (From Choi and Roland [262].)

Since the presence of impurities primarily affects crystal nucleation rather than growth [260, 261], the degree of crystallinity and its dependence on strain is of less interest in accounting for the failure properties of rubber. However, the minimum strain required for crystallization determines the stress concentration necessary to induce crystallization in the vicinity of a crack, as well as its spatial extent. Thus, this minimum strain plays a governing role in mechanical performance. Among the various grades of NR, the greater the purity, the higher the strain required to induce crystallization [262].

Methods to study crystallization of deformed elastomers include x-ray diffraction [207, 208, 263–265], optical birefringence [266, 267], infrared or Raman spectroscopy, electron microscopy [268], dilatometry [269, 270], NMR [271], and mechanical measurements [193, 262, 272]. Strain-induced crystallization is manifested in the latter by both greater hysteresis (Fig. 23) and a longer time for stress decay (Fig. 24). However, the shape of the stress-strain curve during extension does not obviously reveal the onset of crystallization [207, 208, 262].

D. Defects

It is well known that elastomers, like virtually all solid materials, have preexisting, "naturally occurring," flaws [273]. By intensifying local stresses, such flaws exert an influence on the failure properties of elastomers. More recently, interest in these flaws has increased, due to concerns about their potential for reducing the barrier performance of rubber films. This performance is crucial

in the use latex rubber products, such as surgical gloves and condoms, to block transmission of the submicron-sized particles responsible for AIDS, hepatitis, and other viral diseases [274].

The passage of viral-sized particles through ostensibly intact NR latex films has been directly observed in the laboratory [275, 276], and indirectly observed in the field [277]. Evidence for such flaws in NR comes from microscopic observations [278], as well as water absorption measurements, wherein the initial rapid uptake suggests the existence of capillary channels [279].

Since failure properties are affected by the intrinsic defects in rubber, they offer a means to characterize these flaws. The strength of rubber is influenced by the presence of defects having an apparent size in the range between 5 and 70 microns [280–283]. Thus, a means to estimate the size of the largest inherent flaw is by measuring the strength of samples after the introduction of cuts of varying size. The data are extrapolated to the strength of the uncut material, to yield the inherent crack size. If the rubber strain-crystallizes, the precuts must be small so that crystallization of the bulk material transpires prior to failure [284]. For a linearly elastic material, the strength will vary as the square-root of the flaw size [282], while more generally, the strain energy to break is proportional to the flaw size [285]. In Table IV the flaw size deduced from the strain energy to break is listed for various grades of NR [244].

Since fatigue failure of rubber is envisioned as growth of intrinsic flaws, measurement of fatigue lifetimes (e.g., deformation cycles to failure) can provide a measure of the intrinsic flaw size [286–288]. Included in Table IV are the flaw sizes determined from the fatigue life of these NR compounds [244].

The values determined for the inherent flaws only represent effective sizes, corresponding to a given degree of stress concentration [289]. This stress concentration also depends on the shape of a crack (e.g., bluntness), as well as the dissipative capacity of the material itself [290]. While compounding variables such as crosslink density strongly affect the failure properties of rubber, their influence on the intrinsic defect size is more modest [287, 288, 291]. The measured flaw size is unaffected by temperature [281], although it can vary with carbon black type

TABLE IV Intrinsic Flaw Size of Natural Rubber

	Intrinsic flaw size (μm)	
NR grade	**Strain energy**	**Fatigue life**
Guayule rubber	29	26
SMR-10	29	31
SMR-L	26	17
Deproteinized NR	16	10

[292]. The degree of dispersion of compounding ingredients influenced the strength of rubber, apparently by a flaw-initiation mechanism [293].

E. Entanglements

The elastic behavior of rubber for large strains reflects the effect of topological interactions known as entanglements. Entanglements constrain the chains, suppressing lateral motions. The pseudo-network of entanglements gives rise to the characteristic plateau in the time-dependence of the mechanical response of uncrosslinked rubber. While the length (extent over time or frequency) of the rubbery plateau is determined by the molecular weight, its height, G_N^0, reflects the concentration and effectiveness of the entanglements. The storage modulus varies only weakly with frequency, and is approximately proportional to the entanglement concentration, ν_e. Such proportionality in the melt is purely entropic, and is not affected by energy differences between the conformers. The molecular weight between entanglements, $M_e = \rho/G_N^0$ (where ρ is the mass density), depends on chemical structure, and thus is characteristic of the polymer species. The entanglement interactions govern the rheology of uncrosslinked polymers, influencing the viscosity, the dynamic modulus, and the recoverable compliance. Entanglements also affect the mechanical properties of cured rubber, with their role being one of the central issues in the development of accurate rubber elasticity theories (see Chapter 4). The fracture properties of flexible-chain plastics are also influenced by the degree of chain entanglement.

There are various methods of determining M_e and other characteristic molecular weights arising from entanglement interactions. Since the dynamic storage modulus in the plateau region is not strictly invariant to frequency, its magnitude provides only an order of magnitude estimate of G_N^0. Simple relationships, either empirically based [294]

$$G_N^0 = 3.56 G_{\max} \tag{19}$$

or obtained from phenomenological theory [295]

$$G_N^0 = 4.83 G_{\max} \tag{20}$$

have been proposed between G_N^0 and the maximum in the loss modulus. Unfortunately, both approaches seriously underestimate the magnitude for polydisperse polymers, since the dispersion is inhomogeneously broadened. A more reliable assessment of G_N^0 comes from integration of the dispersion in the loss modulus, demarcating the onset of viscous flow

$$G_N^0 = \frac{2}{\pi}\int_{-\infty}^{\infty} G''(\omega) d\ln\omega \tag{21}$$

where on the high frequency side the data is extrapolated (for example, by assuming a power law dependence [296, 297]) to eliminate the contribution from the overlapping transition region.

As described above, NMR can be used to measure chemical crosslink concentrations; however, the spectra are unaffected by physical entanglements. Since these entanglements contribute to the elastic response of cured rubber (see Chapter 4), the difference between crosslink determinations from NMR and modulus measurements can be used to quantify the entanglement concentration. Most applications of this method have been directed toward assessing the role of filler-polymer interaction on the stiffness of elastomers [95].

The physical origin of entanglements and their dependence on chemical structure have been addressed by many investigators. Scaling arguments are commonly employed to conclude that the chain contour length per unit volume governs the magnitude of the topological constraints [298–301]. However, since there are two relevant length scales, the interchain distance (or packing length) and the Kuhn step length, scaling approaches alone can not yield a unique solution to the problem [302]. Some idea concerning the nature of an entanglement must be introduced, leading to some quantitative relationship between chemical structure and the plateau modulus. Various definitions of an entanglement coupling have been proposed, including a fixed number of binary contacts per entanglement [303], a fixed number of binary contacts per entanglement volume [304], and a fixed number of strands per entanglement volume [305, 306]. Although differing quantitatively, these approaches all correctly predict the experimental fact that increases in chain bulkiness and chain flexibility will reduce the plateau modulus [300]. Results from a recent computer simulation are shown in Fig. 25.

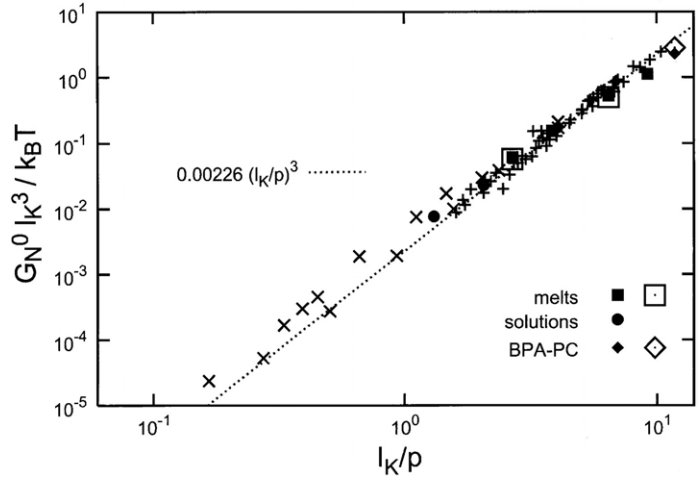

FIGURE 25 Dimensionless plateau modulus versus the ratio of the Kuhn step length, l_K, to the packing length, p. Experimental data for melts (+) and semidilute solutions (×) are included, along with various calculated values (squares, circles, and diamonds). (From Everaers, Sukumaran, Grest *et al*. [307].)

ACKNOWLEDGMENTS

I am grateful to D. J. Lohse, and G. Ver Strate for making available in electronic form the second edition of this chapter, which served as the basis for some of the text herein. This work was supported by the Office of Naval Research.

REFERENCES

1. J. V. Dawkins (Ed.), "Developments in Polymer Characterization," Vol. 1–5, Elsevier, New York, 1986.
2. C. Booth and C. Price (Eds.), "Comprehensive Polymer Science," Vol. 1: "Polymer Characterization," Pergamon, New York, 1989.
3. H. Yamakawa, "Modern Theory of Polymer Solutions," Harper, New York, 1971.
4. P. J. Flory, "Statistical Mechanics of Chain Molecules," Oxford Univ. Press, New York, 1969.
5. Y. Tanaka, *Rubber Chem. and Technol.* **64**, 325 (1991).
6. D. Campbell and J. White, "Polymer Characterization," Chapman and Hall, New York, 1989.
7. F. P. Baldwin and G. Ver Strate, *Rubber Chem. Technol.* **44**, 709 (1972).
8. S. L. Hsu, "Handbook of Vibrational Spectroscopy: A Companion for Polymer Scientists," Wiley, New York 2004.
9. B. H. Stuart, "Polymer Analysis," Wiley, New York, 2002.
10. J. L. Koenig, "Spectroscopy of Polymers," 2nd ed., Elsevier, New York, 1999.
11. D. Braun, "Simple Methods for Identification of Plastics," 3rd ed., Hanser, New York, 1996.
12. J. Mitchell (Ed.), "Applied Polymer Analysis and Characterization," Vol. 2, Hanser, New York, 1992.
13. E. Collins, J. Bares, and F. Billmeyer, "Experiments in Polymer Science," Wiley, New York, 1973.
14. W. Tyler, *Rubber Chem. Technol.* **40**, 238 (1967).
15. H. Ishida, *Rubber Chem. Technol.* **60**, 497 (1987).
16. R. Messerschmidt and M. Harthcock (Eds.), "Infrared Microspectroscopy," Practical Spectroscopy Series, Vol. 6, Marcel Dekker, New York, 1988.
17. http://www.spectroscopynow.com
18. I. Fuhrmann and J. Karger-Kocsis, *J. Appl. Polym. Sci.* **89**, 1622 (2003).
19. S. R. Shield and G. N. Ghebremeskel, *J. Appl. Polym. Sci.* **88**, 1653 (2003).
20. K. D. McCarley and A. L. Bunge, *Internat. J. Pharmaceutics* **250**, 169 (2003).
21. F. H. A. Rodrigues, E. F. Santos, J. P. A. Feitosa, N. M. P. S. Ricardo, and R. C. M. de Paula, *Rubber Chem. Technol.* **74**, 57 (2001).
22. S. Sen, C. Mabuni, and D. Walsh, *J. Appl. Polym. Sci.* **82**, 672 (2001).
23. M. C. P. Peckj, M. A. Samus, R. C. Killgoar, and R. O. Carter, *Rubber Chem. Technol.* **64**, 610 (1991).
24. W. H. Waddell and J. R. Parker, *Rubber Chem. Technol.* **65**, 836 (1992).
25. L. Stebounova, B. B. Akhremitchev, and G. C. Walker, *Rev. Sci. Instr.* **74**, 3670 (2003).
26. F. Keilmann, *J. Biol. Phys*. **29**, 195 (2003).
27. P. J. de Dumas, *Phys. IV* **104**, 359 (2003).
28. F. Keilman, *Vibr. Spect*. **29**, 109 (2002).
29. D. L. Wetzel and S. M. LeVine, *Science* **285**, 1224 (1999).
30. D. V. Palanker, D. M. Simanovskii, P. Huie, and T. I. J. Smith, *Appl. Phys*. **88**, 6808 (2000).
31. K. D. Kempfert, B. Coel, P. Troost, and D.S. Lavery, *Amer. Lab.* **33**, 22 (2001).
32. C. A. Froud, I. P. Hayward, and J. Laven, *Appl. Spect.* **57**, 1468 (2003).
33. A. Ghanbari-Siahkali, K. Almdal, and P. Kingshott, *Appl. Spect.* **57**, 1482 (2003).
34. A. Szep, B. Marosfoi, G. Bertalan, P. Anna, and G. Marosi, *Macromol. Symp.* **202**, 269 (2003).

35. Y. Maeda, H. Yamamoto, and I. Ikeda, *Macromolecules* **36**, 5055 (2003).
36. L. Berger, H. H. Kausch, and C. J. G. Plummer, *Polymer* **44**, 5877 (2003).
37. J. F. Rabolt and D. B. Chase (Eds.), "Fourier Transform Raman Spectroscopy: From Concept to Experiment," Academic Press, New York, 2000.
38. T. W. Zerda, G. Song, and W. H. Waddell, *Rubber Chem. Technol.* **76**, 769 (2003).
39. F. Grum, in "Visible and Ultraviolet Spectrophotometry," A. Weissberger and B. Rossiter (Eds.), Physical Methods of Chemistry, Part IIIB, Vol. 1, Wiley (Interscience), New York, 1972, p. 207.
40. V. M. Raubner, R. Jordan, O. Nuyken, T. Lippert, M. Hauer, B. Schnyder, and A. Wokaun, *Applied Surface Science* **197**, 786 (2002).
41. D. Braun, R. Rettig, and W. Rogler, *Angewandte Makromolekulare Chemie* **211**, 165 (1993).
42. H. Cheng, in "Modern Methods of Polymer Characterization," H. Barth and J. Mays (Eds.), Chemical Analysis, Vol. 113, Wiley, New York, 1991, p. 409.
43. R. Kinsey, *Rubber Chem. Technol.* **63**, 407 (1990).
44. H. T. Wang, T. Bethea, and H. Harwood, *Macromolecules* **26**, 715 (1993).
45. W. T. Smith and J. Patterson, *Anal. Chem.* **58**, 102R (1986).
46. T. Hammond and R. Lehrie, *Brit. Polym. J.* **21**, 23 (1989).
47. D. Vitalini and E. Scamporrino, *Polymer* **33**, 4597 (1992).
48. G. N. Ghebremeskel, J. K. Sekinger, J. L. Hoffpauir, and C. Hendrix, *Rubber Chem. Technol.* **69**, 874 (1996).
49. T. Yamada, T. Okumoto, H. Ohtani, and S. Tsuge, *Rubber Chem. Technol.* **64**, 708 (1991).
50. H. R. Schulten, B. Plage, and R. P. Lattimer, *Rubber Chem. Technol.* **62**, 698 (1989).
51. R. Lattimer, *Rubber Chem. Technol.* **63**, 298 (1990).
52. V. P. Hoven, K. Rattanakaran, and Y. Tanaka, *Rubber Chem. Technol.* **76**, 1128 (2003).
53. S. Kawahara, Y. Inomata, T. Kakubo, Y. Tanaka, K. Hatada, K. Ute, and N. Miyatake, *Rubber Chem. Technol.* **71**, 277 (1998).
54. Y. Tanaka, H. Sato, and J. Adachi, *Rubber Chem. Technol.* **60**, 25 (1987).
55. Y. Tanaka, H. Sato, and J. Adachi, *Rubber Chem. Technol.* **59**, 16 (1986).
56. G. H. Miller and R. H. Tobias, *Rubber Chem. Technol.* **51**, 977 (1978).
57. http://www.simsworkshop.org/default.nclk
58. A. Benninghoven, F. G. Rüdenauer, and H. W. Werner, "Secondary Ion Mass Spectrometry: Basic Concepts, Instrumental Aspects, Applications, and Trends," Wiley, New York, 1987.
59. W. J. Van Ooij, M. Nahmias, and A. Brown, *Surface and Interface Analysis* **61**, 539 (1988).
60. W. J. Van Ooij and V. Rangarajan, *Rubber Chem. Technol.* **61**, 594 (1988).
61. D. Briggs, *Brit. Polym. J.* **21**, 3 (1989).
62. P. Betrand, L. T. Weng, W. Lauer, and R. Zimmer, *Rubber Chem. Technol.* **75**, 627 (2002).
63. P. Betrand and L. T. Weng, *Rubber Chem. Technol.* **72**, 384 (1999).
64. A. K. Sircar, *Rubber Chem. Technol.* **65**, 503 (1992).
65. A. K. Sircar, in "Thermal Characterization of Polymeric Materials," 2nd ed., E. A. Turi (Ed.), Academic Press, New York, 1997.
66. S. Capancioni, K. Schwach-Abdellaoui, W. Kloeti, W. Herrmann, H. Brosig, H. H. Borchert, J. Heller, and R. Gurny, *Macromolecules* **36**, 6135 (2003).
67. D. Hauck, G. Fink, C. Chwatinski, P. Blumler, B. Blumich, and K. Unseld, *Kauch. Gummi Kunstat.* **50**, 392 (1997).
68. O. Hinojosa, J. C. Arthur, and Y. Nakamura, *J Polym. Sci. C Polym. Symp.* **37**, 27 (1972).
69. K. L. Devries, *J. Polym. Sci. C Polym. Symp.* **32**, 325 (1971).
70. R. Partridge, M. C. R. Symons, and J. L. Wyatt, *J. Chem. Soc.—Faraday Trans.* **89**, 1285 (1993).
71. M. D. Pace and C. M. Roland, *Polymer* **32**, 1027 (1991).
72. C. Brosseau, P. Molinie, F. Boulic, and F. Carmona, *J. Appl. Phys.* **89**, 8297 (2001).
73. H. Tang, Z. Y. Liu, J. H. Piao, X. F. Chen, Y. X. Lou, and S. H. Li, *J. Appl. Polym. Sci.* **51**, 1159 (1994).
74. H. Hommel, A. Touhami, and A. P. Legrand, *Makromol. Chem.—Macro. Chem. Phys.* **194**, 879 (1993).

75. G. Ver Strate, C. Cozewith, and S. Ju, *Macromolecules* **21**, 3360 (1988).
76. L. Gilet, M. Loustalot, and J. Bounoure, *Polymer* **33**, 4605 (1992).
77. L. Wild, *Adv. Polym. Sci*. **98**, 1 (1991).
78. A. Dekmezian, T. Morioka, and C. Campo, *J. Pol. Sci. Phys*. **28**, 1908 (1990).
79. T. Zimina, A. Fell, and J. Castledine, *Polymer* **33**, 4129 (1992).
80. A. Dekmezian, T. Morioka, and C. Campo, *J. Polym. Sci. Polym. Phys.* **28**, 1908 (1990).
81. Z. Grubsic-Gallot, J. P. Lingelser, and Y. Gallot, *Polymer Bull*. **23**, 389 (1990).
82. G. Glockner, in "Comprehensive Polymer Science," C. Booth and C. Price (Eds.), Vol 1: "Polymer Characterization," Pergamon, New York, 1989, p. 313.
83. S. H. Xu, P. S. Wells, Y. M. Tao, K. S. Yun, and J. F. Parcher, *ACS Symp. Series* **748**, 96 (2000).
84. H. Yamada, I. Manas-Zloczower, and D. L. Feke, *Powder Technol.* **92**, 163 (1997).
85. C. B. Stanley and H. H. Strey, *Macromolecules* **36**, 6888 (2003).
86. J. Tacx, J. Ammerdorffer, and A. German, *Polymer* **29**, 2087 (1988).
87. S. Mori and M. Mouri, *Anal. Chem*. **61**, 2171 (1989).
88. G. Stegeman, A. C. Vanasten, J. C. Kraak, H. Poppe, and R. Tijssen, *Anal. Chem.* **66**, 1147 (1994).
89. S. H. Lee and A. Molnar, *Macromolecules* **28**, 6354 (1995).
90. L. Lewandowski, M. S. Sibbald, E. Johnson, and M. P. Mallamaci, *Rubber Chem. Technol.* **73**, 731 (2000).
91. J. Janca, I. A. Ananieva, A. Y. Menshikova, and T. G. Evseeva, *J. Chromatography B* **800**, 33 (2004).
92. M. Mori and J. L. Koenig, *J. Appl. Polym. Sci.* **70**, 1391 (1998).
93. A. M. Zaper and J. L. Koenig, *Macromol. Chem.* **189**, 1239 (1988).
94. R. S. Clough and J. L. Koenig, *Rubber Chem. Technol.* **62**, 908 (1989).
95. J. L. Koenig, *Rubber Chem. Technol.* **73**, 385 (2000).
96. C. Tosi, *Adv. Polym. Sci.* **5**, 451 (1968).
97. T. Yamada, T. Okumoto, H. Ohtani, and S. Tsuge, *Rubber Chem. Technol.* **63**, 191 (1990).
98. J. Tulisalo, J. Seppala, and K. Hastbacka, *Macromolecules* **18**, 1144, (1985).
99. J. C. Hu, *Anal. Chem.* **53**, 942 (1981).
100. W. Tuminello, W. Buck, and D. Kerbow, *Macromolecules* **26**, 499 (1993).
101. W. Graessley and G. Ver Strate, *Rubber Chem. Technol.* **53**, 842 (1980).
102. M. Doi, in "Structure and Properties of Polymers," E. L. Thomas (Ed.), Wiley-VCH, Weinheim, Germany, 1993.
103. K. L. Ngai and D. J. Plazek, *Rubber Chem. Technol.* **68**, 376 (1995).
104. S. H. Wasserman, *J. Rheology* **39**, 601 (1995).
105. J. C. Majeste, C. Carrot, and P. Stanescu, *Rheo. Acta.* **42**, 432 (2003).
106. R. U. Bonnar, M. Dimbat, and F. H. Stross, "Number-Average Molecular Weights: Fundamentals and Determination," Interscience, New York, 1958.
107. H. Barth and J. Mays, "Modern Methods of Polymer Characterization," Wiley, New York, 1991.
108. A. Cooper (Ed.), "Determination of Molecular Weight," Chemical Analysis Series, Vol. 103, J. Wiley, New York, 1989.
109. J. Brown and P. Verdier, *J. Res. Natl. Bur. Stand. A* **76**, 161 (1972).
110. T. Tanaka (Ed.), "Experimental Methods in Polymer Science," Academic Press, San Diego, 1999.
111. B. J. Berne and R. Pecora, "Dynamic Light Scattering," Wiley, New York, 1976, Chap. 8.
112. A. Boothroyd and L. J. Fetters, *Macromolecules* **24**, 5215 (1991).
113. G. V. Schulz, K. Altgelt, and H. J. Cantow, *Rubber Chem. Technol.* **30**, 805 (1957).
114. E. Casassa, *Polym. J*. **3**, 517 (1972).
115. A. R. Shultz and W. H. Stockmayer, *Macromolecules* **2**, 178 (1969).
116. H. Suzuki, C. Leonis, and M. Gordon, *Makromol. Chem.* **172**, 227 (1973).
117. J. Vavra, J. Lapcik, and J. Sabados, *J. Polym. Sci. A-2* **5**, 1305 (1967).
118. H. Lindner and O. Glatter, *Macromol. Symp.* **162**, 81 (2000).

119. J. S. Higgins and H. C. Benoit, "Polymers and Neutron Scattering," Clarendon Press, Oxford, 1997.
120. G. D. Wignall, in "Physical Properties of Polymers Handbook," J. E. Mark (Ed.), Amer. Inst. Phys., Woodbury, NY, 1996, Chap. 22.
121. D. J. Lohse, *Rubber Chem. Technol.* **67**, 367 (1994).
122. A. Arbe, J. Colmenero, B. Farago, M. Monkenbusch, U. Buchenau, and D. Richter, *Chem. Phys.* **292**, 295 (2003).
123. D. Richter, *J. Appl. Cryst.* **36**, 389 (2003).
124. P. Stepanek, T. L. Morkved, K. Krishnan, T. P. Lodge, and F. S. Bates, *Physica A* **314**, 411 (2002).
125. B. K. Annis, M. H. Kim, R. Alamo, and M. Pyda, *J. Polym. Sci. Polym. Phys.* **39**, 2852 (2001).
126. A. Z. Akcasu, G. C. Summerfield, S. N. Jahsan, C. C. Han, C. Y. Kim, and H. Yu, *J. Polym. Sci. Polym. Phys.* **18**, 863 (1980).
127. W. Gronski, F. Forster, W. Pyckhout-Hintzen, and T. Springer, *Makromolekulare Chemie—Macromol. Symp.* **40**, 121 (1990).
128. G. Boue, J. Bastide, M. Buzier, A. Lapp, J. Herz, and T. A. Vilgis, *Coll. Polym. Sci.* **269**, 195 (1991).
129. S. Westerman, W. Pyckhout-Hintzen, D. Richter, E. Straube, S. Egelhaaf, and R. May, *Macromolecules* **34**, 2186 (2001).
130. A. Botti, W. Pyckhout-Hintzen, D. Richter, V. Urban, E. Straube, and J. Kohlbrecher, *Polymer* **44**, 7505 (2003).
131. S. Westermann, M. Kreitschmann, W. Pyckhout-Hintzen, D. Richter, E. Straube, B. Farago, and G. Goerigk, *Macromolecules* **32**, 5793 (1999).
132. Y. M. Zhang, S. Ge, B. Tang, T. Koga, M. H. Rafailovich, J. C. Sokolov, D. G. Peiffer, Z. Li, A. J. Dias, K. O. McElrath, M. Y. Lin, S. K. Satija, S. G. Urquhart, H. Ade, and D. Nguyen, *Macromolecules* **34**, 7056 (2001).
133. Y. Du, Y. Xue, and H. L. Frisch, in "Physical Properties of Polymers Handbook," J. E. Mark (Ed.), Amer. Inst. Phys., Woodbury, NY, 1996, Chap. 17.
134. M. Kurata and Y. Tsunashima, in "Polymer Handbook," 4th ed., J. Brandrup, E. H. Immergut, and E. A. Grulke (Eds.), Wiley, New York, 1999, Chap. 7.
135. D. Van Krevelen, "Properties of Polymers," 3rd ed., Elsevier, Amsterdam, 1990.
136. C. Y. Kuo, T. Provder, and M. E. Koehler, *J. Liq. Chromatography* **13**, 3177 (1990).
137. C. Y. Kuo and T. Provder, *ACS Symp. Series* **352**, 2 (1987).
138. Z. Grubisic, P. Rempp, and H. Benoit, *J. Polym. Sci.* **21**, 753 (1967).
139. J. E. Puskas and R. Hutchinson, *Rubber Chem. Technol.* **66**, 742 (1993).
140. C. Kuo, T. Provder, and M. E. Koehler, *ACS Symp. Series* **521**, 231 (1993).
141. J. G. Rooney and G. Ver Strate, in "Liquid Chromatography of Polymers and Related Materials III," J. Cazes (Ed.), Marcel Dekker, New York, 1981.
142. T. Provder, M. W. Urban, and H. G. Barth (Eds.), "Chromatographic Characterization of Polymers: Hyphenated and Multidimensional Techniques," *Adv. Chem. Series* **247**, Amer. Chem. Soc., Washington, D.C., 1995.
143. Y. Brun, *J. Liq. Chromatography & Related Technol.* **21**, 1979 (1998).
144. D. J. Nagy, *Amer. Lab.* **35**, 38 (2003).
145. B. L. Wang, S. Mukataka, E. Kokufuta, M. Ogiso, and M. Kodama, *J. Polym. Sci. Polym. Phys.* **38**, 214 (2000).
146. S. T. Balke and T. H. Mourey, *J. Appl. Polym. Sci.* **81**, 370 (2001).
147. E. Meehan, J. A. McConville, and F. P. Warner, *Polym. Internat.* **26**, 23 (1991).
148. M. Nguyen and R. Beckett, *Polymer International* **30**, 337 (1993).
149. M. E. Schimpf, K. Caldwell, and J. C. Giddings, "Field-Flow Fractionation Handbook," Wiley, New York, 2000.
150. S. Lee, C. H. Eum, and A. R. Plepys, *Bull. Korean Chem. Soc.* **21**, 69 (2000).
151. A. C. van Asten, W. T. Kok, R. Tijssen, and H. Poppe, *J. Polym. Sci. Polym. Phys.* **34**, 297 (1996).
152. M. Nguyen, R. Beckett, L. Pille, and D. H. Solomon, *Macromolecules* **31**, 7003 (1998).

153. H. Creel, *Trends Polym. Sci.* **1**, 336 (1993).
154. M. W. F. Nielsen, *Mass. Spectrom. Rev.* **18**, 309 (1999).
155. D. Cho, S. Park, K. Kwon, T. Chang, and J. Roovers, *Macromolecules* **34**, 7570 (2001).
156. P. Vana, L. Albertin, L. Barner, T. P. Davis, and C. Barner-Kowollik, *J. Polym. Sci. Polym. Polym. Chem.* **40**, 4032 (2002).
157. G. E. Kassalainen and S. K. R. Williams, *Anal. Chem.* **75**, 1887 (2003).
158. T. M. Laue, in "Concise Encyclopedia of Polymer Science and Engineering," J. I. Kroschwitz (Ed.), Wiley, New York, 1990, p. 1225.
158a. D. Boese and F. Kremer, *Macromolecules* **23**, 829 (1990).
159. G. S. Grest, L. J. Fetters, J. S. Huang, and D. Richter, in "Advances in Chemical Physics" XCIV, I. Prigogine and S. A. Rice (Eds.), Wiley, New York, 1996.
159a. J. E. Puskas, *Polymer News* **27**, 325 (2002).
160. P. A. Small, *Adv. Polym. Sci.* **18**, 1 (1975).
161. S. Podzimek, T. Vlcek, C. Johann, *J. Appl. Polym. Sci.* **81**, 1588 (2001).
162. S. Grcev, P. Schoenmakers, and P. Iedema, *Polymer* **45**, 39 (2004).
163. E. Zagar and M. Zigon, *Macromolecules* **35**, 9913 (2002).
164. M. Jayakannan, J. L. J. Van Dongen, G. C. Behera, and S. Ramakrishnan, *J. Polym. Sci. Polym. Chem.* **40**, 4463 (2002).
165. A. Lederer, D. Voigt, C. Clausnitzer, and B. Voit, *J. Chromatography A* **976**, 171 (2002).
166. M. Parth, N. Aust, and K. Lederer, *Macromol. Symp.* **181**, 447 (2002).
167. L. Hong, X. L. Wang, and X. Z. Tang, *J. Appl. Polym. Sci.* **85**, 2445 (2002).
168. P. J. DesLauriers, D. C. Rohlfing, and E. T. Hsieh, *Polymer* **43**, 159 (2002).
169. S. Podzimek and T. Vlcek, *J. Appl. Polym. Sci.* **82**, 454 (2001).
170. A. M. Striegel and M. R. Krejsa, *J. Polym. Sci. Polym. Phys.* **38**, 3120 (2000).
171. S. T. Balke and T. H. Mourey, *J. Appl. Polym. Sci.* **81**, 370 (2001).
172. G. Kraus and J. T. Gruver, *J. Polym. Sci. A* **3**, 105 (1965).
173. K. L Ngai and C. M. Roland, *J. Polym. Sci. Polym. Phys.* **35**, 2503 (1997).
174. C. G. Robertson, C. M. Roland, C. Paulo, and J. E. Puskas, *J. Rheol.* **45**, 759 (2001).
175. P. G. Santangelo and C. M. Roland, *J. Non-Cryst. Solids* **235**, 709 (1998).
176. J. M. Carella, J. T. Gotro, and W. W. Graessley, *Macromolecules* **19**, 659 (1986).
177. P. G. Santangelo, C. M. Roland, and J. E. Puskas, *Macromolecules* **32**, 1972 (1999).
178. C. M. Roland and P. G. Santangelo, *J. Non-Cryst. Solids* **307**, 835 (2002).
179. G. G. A. Böhm and J. O. Tveekrem, *Rubber Chem. Technol.* **55**, 575 (1982).
180. M. Okabe, K. Mitsui, H. Oranaka, M. Jahahashi, and H. Masuda, *Polymer J*. **24**, 653 (1992).
181. J. Horsky and M. Bohdanecky, *Eur. Pol. J.* **26**, 1190 (1990).
182. J. P. Runt and J. J. Fitzgerald (Eds.), "Dielectric Spectroscopy of Polymeric Materials," American Chemical Society, Washington, D.C., 1997.
183. P. G. Santangelo and C. M. Roland, *Macromolecules* **31**, 3715 (1998).
184. D. J. Plazek, I. C. Chay, K. L. Ngai, and C. M. Roland, *Macromolecules* **28**, 6432 (1995).
185. C. M. Roland, K. L. Ngai, P. G. Santangelo, X. H. Qiu, M. D. Ediger, and D. J. Plazek, *Macromolecules* **34**, 6159 (2001).
186. C. M. Roland and R. Casalini, *J. Chem. Phys.* **119**, 1838 (2003).
186a. D. J. Plazek and Z. N. Frund, *J. Polym. Sci. Polym. Phys.* **28**, 431 (1990).
187. R. Androsch and B. Wunderlich, *J. Polym. Sci. Polym. Phys.* **41**, 2039 (2003).
188. J. M. Hutchinson, *J. Therm. Anal. Calorimetry* **72**, 619 (2003).
189. K. Kanari and T. Ozawa, *Thermochimica Acta* **399**, 189 (2003).
190. E. Riande and E. Saiz, "Dipole Moments and Birefringence of Polymers," Prentice-Hall, Englewood Cliff, NJ, 1992.
191. P. H. Mott and C. M. Roland, *Macromolecules* **31**, 7095 (1998).
192. P. H. Mott, A. Rizos, and C. M. Roland, *Macromolecules* **34**, 4476 (2001).
193. C. M. Roland and M. L. Warzel, *Rubber Chem. Technol.* **63**, 285 (1990).
194. P. H. Mott and C. M. Roland, *Macromolecules* **33**, 4132 (2000).
195. I. S. Zemel and C. M. Roland, *Polymer* **33**, 4522 (1992).

196. D. Keroack, Y. Zhao, and R. E. Prud'homme, *Polymer* **40**, 243 (1999).
197. A. K. Kalkar, H. W. Siesler, F. Pfeifer, and S. A. Wadekar, *Polymer* **44**, 7251 (2003).
198. R. M. Kannan and J. A. Kornfield, *J. Rheol.* **38**, 1127 (1994).
199. M. J. Citra, D. B. Chase, R. M. Ikeda, and K. H. Gardner, *Macromolecules* **28**, 4007 (1995).
200. L. A. Archer and G. G. Fuller, *Macromolecules* **27**, 7152 (1994).
201. D. I. Bower, E. L. V. Lewis, and I. M. Ward, *Polymer* **36**, 3473 (1995).
202. D. I. Bower, *J. Polym. Sci. Polym. Phys.* **19**, 93 (1981).
203. B. Deloche and E. T. Samulski, *Macromolecules* **14**, 575 (1981).
204. P. Sotta, B. Deloche, J. Herz, A. Lapp, D. Durand, and J. C. Rabadeux, *Macromolecules* **20**, 2769 (1987).
205. J. F. Tassin, A. Baschwitz, J. Y. Moise, and L. Monnerie, *Macromolecules* **23**, 1879 (1990).
206. M. Doi and H. Watanabe, *Macromolecules* **24**, 740 (1991).
207. S. Toki, I. Sics, S. F. Ran, L. Z. Liu, and B. S. Hsiao, *Polymer* **44**, 6003 (2003).
208. S. Toki, I. Sics, S. F. Ran, L. Z. Liu, B. S. Hsiao, S. Murakami, K. Senoo, and S. Kohjiya, *Macromolecules* **35**, 6578 (2002).
209. M. H. Y. Cheng and E. B. Nauman, *J. Polym. Sci. Polym. Phys.* **42**, 603 (2004).
210. X. W. Qu, S. R. Shang, G. D. Liu, S. W. Zhang, Y. Zhang, and L. C. Zhang, *J. Appl. Polym. Sci.* **91**, 1685 (2004).
211. E. R. Weibel, in "Principles and Techniques of Electron Microscopy," M. A. Hoyat (Ed.), Van Nostrand, New York, Vol. 3, 1973, Chap. 6.
212. C. M. Roland and G. G. A. Böhm, *J. Poly. Sci. Poly. Phys.* **22**, 79 (1984).
213. D. A. Winesett, H. Ade, A. P. Smith, S. G. Urquhart, A. J. Dias, and P. Stevens, *Rubber Chem. Technol.* **76**, 803 (2003).
214. J. B. Miller, K. J. McGrath, C. M. Roland, C. A. Trask, and A. N. Garroway, *Macromolecules* **23**, 4543 (1990).
215. C. M. Roland and K. L. Ngai, *Macromolecules* **24**, 2261 (1991).
216. A. Alegria, J. Colmenero, K. L. Ngai, and C. M. Roland, *Macromolecules* **27**, 4486 (1994).
217. K. L. Ngai and C. M. Roland, *Macromolecules* **28**, 44033 (1995).
218. C. M. Roland, *Macromolecules* **20**, 2557 (1987).
219. K. J. McGrath and C. M. Roland, *Rubber Chem. Technol.* **67**, 629 (1994).
220. A. Alegria, C. Elizetxea, I. Cendoya, and J. Colmenero, *Macromolecules* **28**, 8819 (1995).
221. J. B. Miller, *Rubber Chem. Technol.* **66**, 455 (1993).
222. S. K. Brownstein, J. E. L. Roovers, and D. J. Worsfold, *Magn. Reson. Chem.* **26**, 392 (1988).
223. M. Tomaselli, B. H. Meier, P. Robyr, U. W. Suter, and R. R. Ernst, *Chem. Phys. Lett.* **205**, 145 (1993).
224. J. H. Walton, J. B. Miller, C. M. Roland, and J. B. Nagode, *Macromolecules* **26**, 4052 (1993).
225. J. H. Walton, J. B. Miller, and C. M. Roland, *J. Polym. Sci. Polym. Phys.* **30**, 527 (1992).
226. K. J. McGrath and C. M. Roland, *Rubber Chem. Technol.* **67**, 629 (1994).
227. A. J. Tinker, *Rubber Chem. Technol.* **68**, 461 (1995).
228. Y. F. Shutilin, *Polym. Sci. USSR* **27**, 2386 (1985).
229. A. J. Tinker, *Rubber Chem. Technol.* **63**, 503 (1990).
230. C. M. Roland, *Macromolecules* **27**, 4242 (1994).
231. N. P. Shvydkaya, L. A. Shumanov, L. P. Semenova, and A. S. Lykin, *Kauch. Rezina* **11**, 19 (1980).
232. P. Blumler and B. Blumich, *Rubber Chem. Technol.* **70**, 468 (1997).
233. M. J. R. Loadman and A. J. Tinker, *Rubber Chem. Technol.* **62**, 234 (1989).
234. P. S. Brown, M. J. R. Loadman, and A. J. Tinker, *Rubber Chem. Technol.* **65**, 744 (1992).
235. D. W. Tomlin and C. M. Roland, *Polymer* **34**, 2665 (1993).
236. I. S. Zemel and C. M. Roland, *Polymer* **33**, 3427 (1992).
237. A. K. Bhowmick and H. L. Stephens (Eds.), "Handbook of Elastomers," 2nd ed., Marcel Dekker, New York, 2001.
238. B. C. Edwards, *J. Polym. Sci., Polym. Phys.* **13,** 1387 (1975).
239. J. Gough, *Proc. Lit. and Phil. Soc. Manchester, 2nd Ser.* **1**, 288 (1805).

240. J. H. Magill, *Rubber Chem. Technol.* **68**, 507 (1995).
241. A. N. Gent and L. Q. Zhang, *Rubber Chem. Technol.* **75**, 923 (2002).
242. G. R. Hamed and N. Rattanasom, *Rubber Chem. Technol.* **75**, 935 (2002).
243. P. G. Santangelo and C. M. Roland, *Rubber Chem. Technol.* **74**, 69 (2001).
244. I. S. Choi and C. M. Roland, *Rubber Chem. Technol.* **69**, 591 (1996).
245. E. H. Andrews, P. G. Owen, and A. Singh, *Proc. Royal Soc. London A* **324**, 79 (1971).
246. J. C. Mitchell and D. J. Meier, *J. Polym. Sci. Polym. Phys.* **6**, 1689 (1968).
247. W. R. Krigbaum and R. J. Roe, *J. Polym. Sci. A* **2**, 4391 (1964).
248. A. Ziabicki and L. Jarecki, *Coll. Polym. Sci.* **256**, 332 (1978).
249. G. K. Elyashevich, *Adv. Poly. Sci.* **43**, 205 (1982).
250. C. M. Roland and M. F. Sonnenschein, *Polym. Eng. Sci.* **31**, 1434 (1991).
251. M. J. Brock and M. J. Hackathorn, *Rubber Chem. Technol.* **45**, 1301 (1972).
252. W. Cooper and R. K. Smith, *J. Polym. Sci. A* **1**, 159 (1963).
253. S. Trabelsi, P. A. Albouy, and J. Rault, *Macromolecules* **36**, 9093 (2003).
254. J. E. Mark, *Prog. Polym. Sci.* **28**, 1205 (2003).
255. M. A. Sharaf, A. Kloczkowski, and J. E. Mark, *Rubber Chem. Technol.* **68**, 601 (1995).
256. G. R. Hamed and B. H. Park, *Rubber Chem. Technol.* **72**, 946 (1999).
257. A. N. Gent, *J. Polym. Sci.* **18**, 321 (1955).
258. D. R. Burfield, *Polymer* **25**, 1823 (1984).
259. D. R. Burfield and Y. Tanaka, *Polymer* **28**, 907 (1987).
260. A. N. Gent, *J. Polym. Sci.* **18**, 321 (1955).
261. A. N. Gent, *Inst. Rubb. Ind.* **30**, 139 (1954).
262. I. S. Choi and C. M. Roland, *Rubber Chem. Technol.* **70**, 202 (1997).
263. G. R. Mitchell, *Polymer* **25**, 1562 (1984).
264. R. Oono, K. Miyasaka, and K. Ishikawa, *J. Polym. Sci.* **11**, 1477 (1973).
265. S. Trabelsi, P. A. Albouy, and J. Rault, *Macromolecules* **36**, 7624 (2003).
266. L. R. G. Treloar, *Trans. Faraday Soc.* **43**, 284 (1947).
267. G. R. Taylor and S. R. Darin, *J. Appl. Phys.* **20**, 1075 (1955).
268. T. Shimizu, M. Tsuji, and S. Kohjiya, *Mat. Sci. Res. Internat.* **4**, 117 (1998).
269. A. N. Gent and L. Q. Zhang, *Rubber Chem. Technol.* **75**, 923 (2002).
270. A. N. Gent and L. Q. Zhang, *J. Polym. Sci. Polym.* **39**, 811 (2001).
271. T. Kameda and T. Asakura, *Polymer* **44**, 7539 (2003).
272. A. N. Gent, *Trans. Faraday Soc.* **50**, 521 (1954).
273. C. M. Roland and C. R. Smith, *Rubber Chem. Technol.* **58**, 806 (1985).
274. C. M. Roland, *Rubber World* **208**, 15 (1993).
275. R. F. Carey *et al*., *Sexually Transmitted Diseases* **19**, 230 (1992).
276. V. Kiernan, *New Scientist*, March 23, p. 7 (1996).
277. *The New York Times*, March 22, 1994, p. C3.
278. S. G. Arnold, J. E. Whitman, C. H. Fox, and M. H. Cottler-Fox *Nature* **335**, 19 (1988).
279. K. F. Gazeley, A. D. T. Gorton, and T. D. Pendle, in "Natural Rubber Science and Technology," A. D. Roberts (Ed.), Oxford Univ. Press, Oxford, 1988, Chap. 3.
280. F. Bueche, *Rubber Chem. Technol.* **32**, 1269 (1959).
281. M. Braden and A. N. Gent *J. Appl. Poly. Sci.* **3**, 100 (1960).
282. A. N. Gent, in "Science and Technology of Rubber," F. R. Eirich (Ed.), Academic Press, New York, 1978, Chap. 10.
283. C. M. Roland and J. W. Sobieski, *Rubber Chem. Technol.* **62**, 683 (1989).
284. A. G. Thomas and J. M. Whittle, *Rubber Chem. Technol.* **43**, 222 (1970).
285. C. L. M. Bell, D. Stinson, and A. G. Thomas, *Rubber Chem. Technol.* **55**, 66 (1982).
286. A. N. Gent, P. B. Lindley, and A. G. Thomas, *J. Appl. Poly. Sci.* **8**, 455 (1964).
287. G. J. Lake and P. B. Lindley *J. Appl. Poly. Sci.* **9**, 1233 (1965).
288. G. J. Lake *Prog. Rubber Technol.* **45**, 89 (1983).
289. H. W. Greensmith *J. Appl. Polym. Sci.* **8**, 1113 (1964).
290. G. R. Hamed, H. J. Kim, and A. N. Gent, *Rubber Chem. Technol.* **69**, 807 (1996).

291. G. R. Hamed, *Rubber Chem. Technol.* **56**, 244 (1983).
292. E. S. Dizon, A. E. Hicks, and V. E. Chirico, *Rubber Chem. Technol.* **46**, 231 (1973).
293. W. May, *Trans. Inst. Rubber Ind.* **40**, T109 (1964).
294. V. R. Raju, E. V. Menezes, G. Marin, and W. W. Graessley, *Macromolecules* **14**, 1668 (1981).
295. R. S. Marvin and J. Oser, *J. Res. Natl. Bur. Stand. B* **66**, 171 (1962); **67**, 87 (1963).
296. R. H. Colby, L. J. Fetters, W. G. Funk, and W. W. Graessley, *Macromolecules* **24**, 3873 (1991).
297. C. M. Roland, J. K. Kallitsis, and K. G. Gravalos, *Macromolecules* **26**, 6474 (1993).
298. W. W. Graessley and S. F. Edwards, *Polymer* **22**, 1329 (1981).
299. L. J. Fetters, D. J. Lohse, and W. W. Graessley, *J. Polym. Sci. Polym. Phys.* **37**, 1023 (1999).
300. N. Heymans, *Macromolecules* **33**, 4226 (2000).
301. L. J. Fetters, D. J. Lohse, C. A. Garcia-Francok, P. Brant, and D. Richter, *Macromolecules* **35**, 10096 (2002).
302. D. Richter, B. Farago, R. Butera, L. J. Fetters, J. S. Juang, and B. Ewen, *Macromolecules* **26**, 795 (1993).
303. F. Brochard and P. G. de Gennes, *Macromolecules* **10**, 1157 (1977).
304. R. H. Colby, M. Rubinstein, and J. L. Viovy, *Macromolecules* **25**, 996 (1992).
305. T. A. Kavassalis and J. Noolandi, *Macromolecules* **21**, 2869 (1988); **22**, 2709 (1989).
306. Y. H. Lin, *Macromolecules* **20**, 3080 (1987).
307. R. Everaers, S. K. Sukumaran, G. S. Grest, C. Svaneborg, A. Sivasubramanian, and K. Kremer, *Science* **303**, 823 (2004).

4 The Molecular Basis of Rubberlike Elasticity

BURAK ERMAN
Department of Chemical and Biological Engineering
Koc University
Rumelifeneri Yolu, Istanbul, Turkey

JAMES E. MARK
Department of Chemistry
The University of Cincinnati
Cincinnati, Ohio

I. INTRODUCTION

Rubberlike materials consist of relatively long polymeric chains having a high degree of flexibility and mobility, which are joined into a network structure. The requirement of flexibility and mobility is associated with the very high deformability. As a result of an externally imposed stress, the long chains may alter their configurations, an adjustment which takes place relatively rapidly because of the high chain mobility. The requirement of having the chains linked into a network structure is associated with solidlike features, where the chains are prevented from flowing relative to each other under external stresses. As a result, a typical rubber may be stretched up to about 10 times its original length. On removal of the external force, it rapidly recovers its original dimensions, with essentially no residual or nonrecoverable strain. As a result of these unique mechanical properties, rubbers find important usage ranging from automobile tires to heart valves, gaskets in jet planes, and space vehicles.

Science and Technology of Rubber, Third Edition

In ordinary solids such as crystalline or amorphous glassy materials, an externally applied force changes the distance between neighboring atoms, resulting in interatomic or intermolecular forces. In these materials, the distance between two atoms should only be altered by no more than a fraction of an angstrom if the deformation is to be recoverable. At higher deformations, the atoms slide past each other, and either flow takes place or the material fractures. The response of rubbers on the other hand is almost entirely intramolecular.

Externally applied forces transmitted to the long chains through the linkages let their extremities change the conformations of the chains, and each chain acts like a spring in response to the external stress. The molecular mechanisms relating to rubberlike elasticity were recognized in the early 1930s. Rigorous statistical mechanical theories describing the mechanical behavior of rubbers were given by Guth and James [1], Wall [2], Flory [3], and Flory and Rehner [4]. The present understanding of the molecular basis of rubber elasticity owes much to these early theories. They give an idealized picture of rubber elasticity, but at the same time form the basis of more advanced molecular theories of such elasticity, which describe the effects of intermolecular entanglements observed in real networks. Developments in the field from the beginning up to the present have been reviewed in several monographs (see for example Treloar [5], Mark and Erman [6], and the more recent monograph by Erman and Mark [7]).

In this review we first discuss the structural features of networks that contribute to the stress upon deformation. We discuss the simple classical models of elasticity and the departures from these simple models. Specifically, we differentiate between two classes of models, (1) the constraint models, which assume that the total elastic energy of the network equals the sum of the individual network chain energies, and (2) the trapped entanglement models, which assume that entanglements that are trapped during the crosslinking stage contribute additionally to the network elastic energy. We also give the molecular interpretation of coefficients obtained from the phenomenological theories. Swollen gels and responsive gels are among the most widely studied systems over the past several years, and recent work in this area is discussed. We then discuss the thermoelastic (force-temperature) behavior of networks. The final topics involve neutron scattering experiments (that allow the direct determination of chain dimensions in undeformed and deformed networks), and some recent experimental studies on the elasticity of single polymer chains.

II. STRUCTURE OF A TYPICAL NETWORK

A network is obtained by linking polymer chains together, and this linkage may be either physical or chemical. Physical linking can be obtained by (1) absorption of chains onto the surface of finely divided particulate fillers, (2) formation of small crystallites, (3) coalescence of ionic groups, or (4) coalescence

of glassy sequences in block copolymers. These physical crosslinks are, in general, not permanent and may disappear on swelling or increase in temperature. The corresponding networks are referred to as "physical" or "thermoreversible" and are not considered in the present review. The reader may refer to Burchard and Ross-Murphy [8] for further information on such materials.

Chemical crosslinks may be obtained by randomly joining segments in already formed chains, by random copolymerization, or by end-linking functionally terminated chains. Sulfur cures, peroxide cures, and high-energy irradiations are familiar methods of random crosslinking. Copolymerization of monomers where at least one type has three or more reactive sites also leads to randomly crosslinked networks. Formation of networks by end-linking individual chains by ϕ-functional linkages is the most appropriate method of forming well-defined structures, where the functionality ϕ of a linkage is defined as the number of chains meeting at the junction. A network is called perfect if its junctions have a functionality of at least 3, it has no dangling chains (chains attached to the network only at one of their ends), and it has no loops (chains with both ends meeting at the same junction). Properties of perfect networks are discussed in this chapter. The reader may refer to Erman and Mark [7] and to the original work by Flory [9, 10] for the structure and properties of imperfect networks.

The structure of a perfect network may be defined by two variables, the cycle rank ξ and the average junction functionality ϕ. Cycle rank is defined as the number of chains that must be cut to reduce the network to a tree. The three other parameters used often in defining a network are (1) the number of network chains (chains between junctions) ν, (2) the number of junctions μ, and (3) the molecular weight M_c of chains between two junctions. They may be obtained from ξ and ϕ using the relations

$$\nu = \frac{\xi}{\left(1 - \frac{2}{\phi}\right)} \tag{1}$$

$$\mu = \frac{2\nu}{\phi} \tag{2}$$

$$M_c = \frac{\left(1 - \frac{2}{\phi}\right)\rho N_A}{\frac{\xi}{V_0}} \tag{3}$$

where ρ is the density, V_0 is the reference volume of the network, and N_A is Avogadro's number.

The cycle rank completely defines the connectivity of a network and is the only parameter that contributes to the elasticity of a network, as will be

discussed further in the following section on elementary molecular theories. In several other studies, contributions from entanglements that are trapped during crosslinking are considered in addition to the chemical crosslinks [11]. The trapped entanglement model is also discussed below.

In a typical elastomer, the number of skeletal bonds in a network chain range from about 100 to 700 [12]. Networks with chains shorter than 100 bonds have low extensibilities. Those having chains much larger than 700 bonds may have very high extensibilities but are too weak to serve as load-carrying materials. It is possible to prepare bimodal networks, however, by end-linking very short and very long chains to form networks of significant toughness [13].

III. ELEMENTARY MOLECULAR THEORIES

The basic postulate of elementary molecular theories of rubber elasticity states that the elastic free energy of a network is equal to the sum of the elastic free energies of the individual chains. In this section, the elasticity of the single chain is discussed first, followed by the elementary theory of elasticity of a network. Corrections to the theory coming from intermolecular correlations, which are not accounted for in the elementary theory, are discussed in Section IV.

A. Elasticity of the Single Chain

The chemical structure of a polymer chain determines its statistical properties, such as its average dimensions in space and its flexibility. These parameters, in turn, affect various properties of a network consisting of these chains. A detailed understanding of the single chain is therefore important.

A short sequence of the poly(dimethylsiloxane) (PDMS) chain is shown as an example in Fig. l(a). The silicon and oxygen atoms are located in alternating order along the backbone, with the CH_3's constituting the side groups. The backbone structure between the i − lst and i + 2nd backbone bonds is shown in Fig. l(b). Lengths of the bonds l_i and bond angles ϕ_i, shown in the figure, are approximately constant. Torsional rotations may take place relatively easily, however, about the skeletal bonds. The torsional rotation angle for the ith bond is shown by ϕ in the figure. Large rotations may take place about the skeletal bonds, as a result of which the chain may take different spatial conformations, one of which is shown in Fig. l(c). The quantity **r** represents the instantaneous end-to-end vector of the chain.

In most molecular theories of rubberlike elasticity, the individual chains are approximated by the freely jointed or the freely rotating chain model. In reality, however, rotations about each bond are subject to potentials that arise

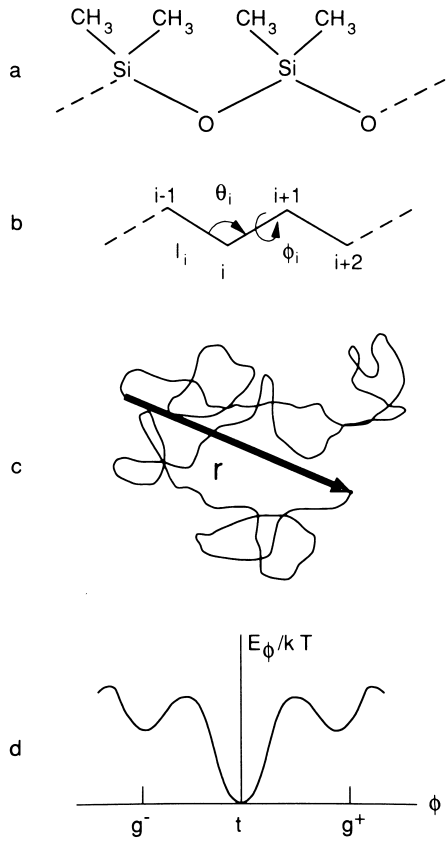

FIGURE 1 (a) A short sequence of the poly(dimethylsiloxane) (PDMS) chain; (b) specification of the backbone structure; (c) typical spatial conformation; (d) typical conformational energy map for different rotational angles ϕ_i.

from the intrinsic torsional potential of the backbone bond and from steric attractive and repulsive forces from neighboring atoms along the chain. The energy to which the bond torsional angle ϕ_i is subject is shown schematically in Fig. 1(d). The "energy map" shown in this figure exhibits three minima, referred to as the three "isomeric states" or "isomeric minima." Of course the numbers of isomeric states may be smaller or larger than 3, depending on the chain architecture. The three minima shown in Fig. 1(d), which are approximately spaced at 120° intervals, are referred to as the *trans* (t), *gauche*+ (g+), and *gauche*– (g–) states. The shape of a chain changes continuously and rapidly as each bond fluctuates about an isomeric minimum, with an amplitude the order of ±60°, and occasionally goes over the energy peak to another isomeric

minimum. The rate of transition from one isomeric minimum to another, which is on the order of one per nanosecond at sufficiently high temperatures, depends primarily on the temperature and on the height of the energy barriers shown in Fig. 1(d). These transitions determine the dynamics of the chain, and determine in part its glass transition temperature. Equilibrium properties of the chain, on the other hand, are influenced by the energy levels of the isomeric minima, as well as their locations. The *trans* state in a randomly configured chain with bond torsional energies as shown in Fig. 1(d) is more populated than the g+ and g– states. The average number of bonds in the t, g+, and g– states is determined according to the Boltzmann distribution of statistical mechanics [14, 15]. According to statistical mechanical arguments, the number of each type of isomeric state in a chain remains essentially the same when the chain is stretched at its two ends. The change in the end-to-end vector takes place by the redistribution of the isomeric states along the chain. As the number of each type of isomeric state remains the same, the total internal energy of the chain remains constant during stretching. The elasticity of the chain resulting from redistribution of isomeric states is referred to as entropic elasticity, and a major part of the elasticity of a network is entropic. If part of the work done in deformation is used to change the relative populations of isomeric states, the bond angles, and the chain lengths, a change in internal energy takes place that results in an "energetic" component of the elasticity. The relationship of the entropic and energetic components to molecular constitution in a network is discussed in the following sections.

The vector **r** joining the two ends of the chain takes different values resulting from rotations about the individual bonds. For chains with more than about 50 skeletal bonds, the probability $W(\mathbf{r})\,dxdydz$ that one end of **r** is at the origin and the other end is in an infinitesimal volume $dV = dxdydz$ is satisfactorily represented by the Gaussian function [16]

$$W(\mathbf{r})dxdydz = \left(\frac{3}{2\pi\langle r^2\rangle_0}\right)^{3/2} \exp\left(-\frac{3r^2}{2\langle r^2\rangle_0}\right)dxdydz \tag{4a}$$

Here, $\langle r^2\rangle_0$ represents the average of the squared end-to-end vectors, and the subscript zero indicates that the chain is in the unperturbed or so-called theta state [9]. It is now well established that chains in the bulk undiluted state are in the unperturbed state. Equation (4a) represents the probability distribution of the vectorial quantity **r**. A less detailed form of representation is the distribution $w(r)$ showing the probability that the magnitude r of **r** has a certain value irrespective of direction. Thus, the probability that the chain end-to-end length is in the range r to $r + dr$ irrespective of its direction is

$$W(\mathbf{r})dr = \left(\frac{3}{2\pi\langle r^2\rangle_0}\right)^{3/2} \exp\left(-\frac{3r^2}{2\langle r^2\rangle_0}\right)4\pi r^2 dr \tag{4b}$$

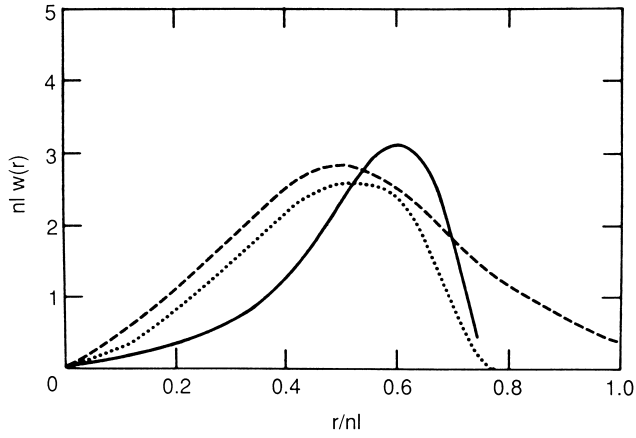

FIGURE 2 Distributions for the end-to-end distance of a PDMS chain having $n = 20$ skeletal bonds of length $l = 1.64$ Å. The Fixman-Alben distribution (dotted curve) and that from a Monte Carlo simulation (solid curve) are compared with the Gaussian approximation (dashed curve).

A schematic representation of the Gaussian function of Eq. (4b) is given by the dashed curve in Fig. 2. The abscissa is normalized by dividing the end-to-end distance by the contour length of the chain, and the ordinate is made nondimensional (unitless) by multiplying $w(r)$ by the contour length.

For chains having fewer than 50 bonds, such as the short chains in a bimodal network for example, the distribution departs markedly from the Gaussian limit. Among various representations of $w(r)$ for short chains are the Hermite series [16], the Fixman-Alben distribution, and Monte Carlo simulations [17]. The Fixman-Alben distribution is given by

$$w(r)dr \propto \exp(-\alpha r^2 + b^2 r^4)4\pi r^2 dr \tag{4c}$$

where a and b are coefficients. This distribution and results of Monte Carlo simulations for a PDMS chain of 20 skeletal bonds are compared with the Gaussian approximation in Fig. 2.

The molecular theories of networks to be presented in the following paragraphs are based on the Gaussian picture of the individual network chains. With reference to the form of the distribution function, these theories are referred to as "Gaussian theories."

The elastic free energy A_{el} of a Gaussian chain is related to the probability distribution $W(\mathbf{r})$ by the thermodynamic expression [7]

$$A_{el} = C(T) - kT \ln W(\mathbf{r}) \tag{5}$$

where $C(T)$ is a function only of temperature T, and k is the Boltzmann constant. Substituting Eq. (4a) into Eq. (5) leads to

$$A_{el} = A^*(T) + \left(\frac{3kT}{2\langle r^2\rangle_0}\right) r^2 \tag{6}$$

Here, $A^*(T)$ is a function of temperature alone. Equation (6) represents the elastic free energy of a Gaussian chain with ends fixed at a separation of r. The average force required to keep the two ends at this separation is obtained from the thermodynamic expression [14]

$$f = \left(\frac{\partial A_{el}}{dr}\right)_T \tag{7}$$

$$= \left(\frac{3kT}{\langle r^2\rangle_0}\right) r \tag{8}$$

where Eq. (8) is obtained by substituting Eq. (6) into Eq. (7). The subscript T denotes differentiation at fixed temperature.

Equation (8) shows that the single chain behaves like a linear spring, with spring constant equal to $3kT/\langle r^2\rangle_0$. Some experimental results on single chains relevant to this prediction are given in Section IX.

B. The Elastic Free Energy of the Network

The total elastic free energy ΔA_{el} of the network relative to the undeformed state is obtained by summing Eq. (6) over the ν chains of the network [6]:

$$\Delta A_{el} = \frac{3kT}{2\langle r^2\rangle_0} \sum_{\nu} (r^2 - \langle r^2\rangle_0) \tag{9}$$

$$= \frac{3\nu kT}{2}\left(\frac{r^2}{\langle r^2\rangle_0} - 1\right) \tag{10}$$

where $\langle r^2\rangle = \Sigma r^2/\nu$ is the average square of the end-to-end vectors of chains in the deformed network. Substituting

$$\langle r^2\rangle = \langle x^2\rangle + \langle y^2\rangle + \langle z^2\rangle \tag{11}$$

into Eq.(10) and using the fact that chain dimensions are isotropic in the undeformed state

$$\langle x^2\rangle_0 = \langle y^2\rangle_0 = \langle z^2\rangle_0 = \frac{\langle r^2\rangle_0}{3} \tag{12}$$

one obtains

$$\Delta A_{el} = \frac{\nu kT}{2}\left[\frac{\langle x^2\rangle}{\langle x^2\rangle_0} + \frac{\langle y^2\rangle}{\langle y^2\rangle_0} + \frac{\langle z^2\rangle}{\langle z^2\rangle_0} - 3\right] \tag{13}$$

The ratios of mean-squared dimensions appearing in Eq. (13) are microscopic quantities. To express the elastic free energy of a network in terms of the macroscopic (laboratory) state of deformation, an assumption has to be made to relate microscopic chain dimensions to macroscopic deformation. Their relation to macroscopic deformations imposed on the network has been a main area of research in the area of rubberlike elasticity. Several models have been proposed for this purpose, which are discussed in the following sections. Before that, however, we describe the macroscopic deformation, stress, and the modulus of a network.

C. The Reduced Stress and the Elastic Modulus

The state of macroscopic deformation may be characterized by considering the deformation of a rectangular prism, with extension ratios λ_x, λ_y, λ_z, along the x, y, and z directions, respectively, as

$$\lambda_x = \frac{L_x}{L_{x0}} \qquad \lambda_y = \frac{L_y}{L_{y0}} \qquad \lambda_z = \frac{L_z}{L_{z0}} \tag{14}$$

where L_{x0}, L_{y0}, L_{z0} are the sides of the prism before deformation and L_x, L_y, L_z are the corresponding sides in the deformed state. For the sake of simplicity, we consider here dry networks, i.e., networks in the absence of a diluent both in the state of formation and during deformation. However, we discuss effects of swelling in Section VI. Also, we consider only the uniaxial case. The true stress τ, i.e., force per unit deformed area, resulting from a uniaxial force acting on a cross-section of the network sample, is obtained by the Treloar relations [5, 7]

$$\tau = 2V^{-1}\left[\lambda_i^2\left(\frac{\partial \Delta A_{\text{el}}}{\partial \lambda_i^2}\right) - \lambda_j^2\left(\frac{\partial \Delta A_{\text{el}}}{\partial \lambda_j^2}\right)\right]_{T,V} \tag{15}$$

where the subscript i denotes the direction of the applied uniaxial force and j denotes one of the other two directions on which only a hydrostatic pressure is acting. The expression in the brackets is evaluated at constant temperature and volume as identified by the subscripts T and V. The reader is referred to Treloar [5] and Ogden [18] for applications to other states of stress.

The engineering stress σ defined as the force per unit undeformed area follows from Eq. (15) as

$$\sigma_i = \frac{\tau}{\lambda} \tag{16}$$

The reduced force $[f^*]$ is defined according to

$$[f^*] = \frac{\tau}{(\lambda^2 - \lambda^{-1})} \tag{17}$$

In the limit of small deformations, the reduced force equates to the shear modulus of the sample, i.e.,

$$G = \lim_{\lambda \to 1}[f^*] \tag{18}$$

The expressions given in this section, which are explained in more detail in Erman and Mark [17], are general expressions. In the next section, we introduce two network models that have been used in the elementary theories of elasticity to relate the microscopic deformation to the macroscopic deformation: the affine and the phantom network models.

1. The Affine Network Model

One of the earlier assumptions regarding microscopic deformation in networks is that the junction points in the networks move affinely (linearly) with macroscopic deformation. It follows that chain end-to-end vectors deform affinely also, and

$$\langle x^2 \rangle = \lambda_x^2 \langle x^2 \rangle_0 \quad \langle y^2 \rangle = \lambda_y^2 \langle y^2 \rangle_0 \quad \langle z^2 \rangle = \lambda_z^2 \langle z^2 \rangle_0 \tag{19}$$

Substituting Eq. (19) into Eq. (13) in conjunction with Eq. (1) leads to

$$\Delta A_{\text{el,affine}} = \frac{1}{2}\left(\frac{\phi}{\phi - 2}\right)\xi kT(\lambda_x^2 + \lambda_y^2 + \lambda_z^2 - 3) \tag{20}$$

A more rigorous statistical analysis [9] gives an additional volume term, $-\mu kT(V/V_0)$ in Eq. (20). This term does not appear in the simplified derivation presented here.

The true stress for the uniaxial case is obtained by substituting Eq. (20) into Eq. (15) as

$$\tau = \left(\frac{\phi}{\phi - 2}\right)\frac{\xi kT}{V_0}(\lambda^2 - \lambda^{-1}) \tag{21}$$

The shear modulus G_{af} of an affine network is obtained from Eqs. (17) and (18) as

$$G_{af} = \left(\frac{\varphi}{\varphi - 2}\right)\frac{\xi kT}{V_0} = \frac{\nu kT}{V_0} \tag{22}$$

where V_0 is the volume during the formation of the network.

2. The Phantom Network Model

The instantaneous vector $\mathbf{r}$ joining two junctions at the extremities of a network chain may be written as the sum of a time-averaged mean $\bar{\mathbf{r}}$ and the instantaneous fluctuation $\Delta\mathbf{r}$ from this mean, i.e.,

$$\mathbf{r} = \bar{\mathbf{r}} + \Delta\mathbf{r} \tag{23}$$

According to the phantom network model, the fluctuations Δr are independent of deformation and the mean $\bar{\mathbf{r}}$ deform affinely with macroscopic strain. Squaring both sides of Eq. (23) and averaging over all chains give

$$\langle r^2 \rangle = \langle \bar{r}^2 \rangle + \left\langle (\Delta r)^2 \right\rangle \tag{24}$$

The average of the quantity $\bar{\mathbf{r}} \cdot \Delta \mathbf{r}$ has been equated to zero in obtaining Eq. (24) inasmuch as this quantity is equally likely to be positive or negative because of the fluctuating term $\Delta \mathbf{r}$, and the average over all possible occurrences vanishes. Equation (24) is valid in both the deformed and undeformed states. It may be written in terms of λ_x, λ_y, and λ_z as

$$\begin{aligned} \langle r^2 \rangle &= \left(\frac{\lambda_x^2 + \lambda_y^2 + \lambda_z^2}{3} \right) \langle \bar{r}^2 \rangle_0 + \left\langle (\Delta r)^2 \right\rangle \\ &= \left[\left(\frac{\lambda_x^2 + \lambda_y^2 + \lambda_z^2}{3} \right) \left(1 - \frac{2}{\phi} \right) + \frac{2}{\phi} \right] \langle r^2 \rangle_0 \end{aligned} \tag{25}$$

Equation (25) is obtained by use of

$$\langle \bar{r}^2 \rangle_0 = \left(1 - \frac{2}{\phi} \right) \langle r^2 \rangle_0 \tag{26}$$

$$\left\langle (\Delta r)^2 \right\rangle_0 = \frac{2}{\phi} \langle r^2 \rangle_0$$

These two relations result from the phantom network model, as shown in derivations given elsewhere [6, 12].

Using Eq. (26) in Eq. (25) and substituting the resulting expression into Eq. (13) leads to

$$\Delta A_{\text{el,phantom}} = \frac{1}{2} \xi kT (\lambda_x^2 + \lambda_y^2 + \lambda_z^2 - 3) \tag{27}$$

Comparison of the expressions for the elastic free energies for the affine and phantom network models shows that they differ only in the front factor. Expressions for the elastic free energy of more realistic models than the affine and phantom network models are given in the following section.

The true stress for the phantom network model is obtained by substituting Eq. (27) into Eq. (15):

$$\tau = \frac{\xi kT}{V_0} (\lambda^2 - \lambda^{-1}) \tag{28}$$

and the shear modulus G_{ph} is obtained from Eqs. (17) and (18) as

$$G_{ph} = \frac{\xi kT}{V_0} \tag{29}$$

Equation (29) shows that the modulus is proportional to the cycle rank ξ, and that no other structural parameters contribute to the modulus. The number of entanglements trapped in the network structure does not change the cycle rank. Possible contributions of these trapped entanglements to the modulus can not therefore originate from the topology of the phantom network.

IV. MORE ADVANCED MOLECULAR THEORIES

The models presented in the previous section are of an elementary nature in the sense that they ignore contributions from intermolecular effects (such as entanglements that are permanently trapped on formation of the network). Among the theories that take account of the contribution of entanglements are (1) the treatment of Deam and Edwards [19] in terms of topological invariants, (2) the slip-link model [20, 21], (3) the constrained-junction and constrained-chain models [22–27], and (4) the trapped entanglement model [11, 28]. The slip-link, constrained-junction, and constrained-chain models can be studied under a common format as can be seen from the discussion by Erman and Mark [7]. For illustrative purposes we present the constrained-junction model in some detail here. We then discuss the trapped entanglement models.

The constrained-junction model was formulated in order to explain the decrease of the elastic moduli of networks upon stretching. It was first introduced by Ronca and Allegra [22] and Flory [23]. The model assumes that the fluctuations of junctions are diminished below those of the phantom network because of the presence of entanglements and that stretching increases the range of fluctuations back to those of the phantom network. As indicated by the second part of Eq. (26), the fluctuations in a phantom network are substantial. For a tetrafunctional network, the mean-square fluctuations of junctions amount to as much as half of the mean-square end-to-end vector of the network chains. The strength of the constraints on these fluctuations is measured by a parameter κ, defined as

$$\kappa = \frac{\left\langle (\Delta R)^2 \right\rangle}{\left\langle (\Delta s)^2 \right\rangle} \tag{30}$$

where $\langle (\Delta R)^2 \rangle$ and $\langle (\Delta s)^2 \rangle$ denote, respectively, the mean-square junction fluctuations in the phantom network and in the entanglement domain. If the range of fluctuations decreases to zero because of entanglements, κ becomes infinitely large. If the effect of entanglements is nil, then $\kappa = 0$. The κ parameter is proportional to the number of junctions in the volume occupied by a given network chain. Thus,

$$\kappa = I \langle r^2 \rangle_0^{3/2} (\mu / V_0) \tag{31}$$

where I is the constant of proportionality. For a network with tetrafunctional junctions, κ may be written

$$\kappa = I(N_A\, d/2)^{3/2}(\langle r^2\rangle_0/M)^{3/2}(\xi/V_0)^{-1/2} \tag{32}$$

where d is the density of the network and M is the molecular weight of chains between two crosslinks.

The elastic free energy of the constrained-junction model is given by the expression

$$\Delta A_{\text{el}} = \frac{1}{2}\xi kT\left\{\sum_{i=1}^{3}(\lambda_i^2 - 1) + \frac{\mu}{\xi}\sum_{i=1}^{3}[B_i + D_i - \ln(1+B_i) - \ln(1+D_i)]\right\} \tag{33}$$

where

$$B_i = \kappa^2(\lambda_i^2 - 1)(\lambda_i^2 + \kappa) \qquad D_i = \lambda_i^2\kappa^{-1}B_i \tag{34}$$

The true stress for the uniaxial case is obtained from Eqs. (15) and (33) as

$$\tau = \frac{\xi kT}{V_0}\left\{(\lambda - \lambda^{-2}) + \frac{\mu}{\xi}[\lambda K(\lambda^2) - \lambda^{-2}K(\lambda^{-1})]\right\} \tag{35}$$

where

$$K(\lambda^2) = B\left[\dot{B}\,(B+1)^{-1} + \kappa^{-1}(\lambda^2\dot{B} + B)(B + \kappa\lambda^{-2})^{-1}\right] \tag{36}$$

$$\dot{B} = \frac{\partial B}{\partial \lambda^2} = B\left[(\lambda^2 - 1)^{-1} - 2(\lambda^2 + \kappa)^{-1}\right] \tag{37}$$

The reduced force is given as

$$[f^*] = \frac{\xi kT}{V_0}\left\{1 + \frac{\mu}{\xi}\left[\frac{\lambda K(\lambda^2) - \lambda^{-2}K(\lambda^{-1})}{\lambda - \lambda^2}\right]\right\} \tag{38}$$

The shear modulus of the constrained-junction model is obtained in the limit of small deformations as

$$G = \left[1 + \frac{\mu}{\xi}\left(\frac{\kappa^2 + 1}{(1+\kappa)^4}\kappa^2\right)\right]G_{ph} \tag{39}$$

which shows that for nonzero values of the parameter κ, the shear modulus of the constrained junction model is larger than the phantom network shear modulus. For the affine limit, $\kappa \to \infty$, the shear modulus is

$$G = \left(1 + \frac{\mu}{\xi}\right)G_{ph} = \frac{\phi}{\phi - 2}G_{ph} \tag{40}$$

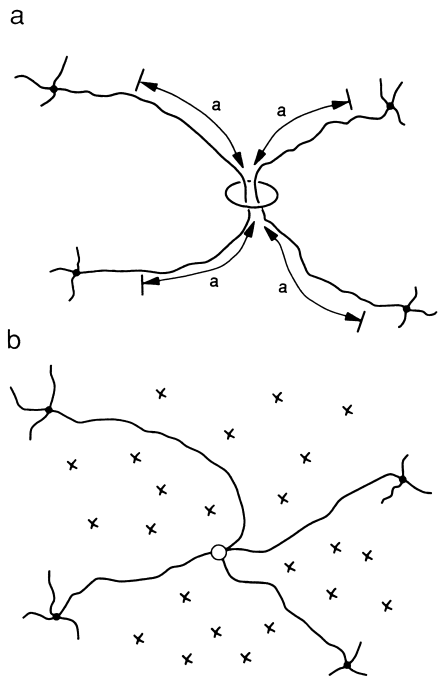

FIGURE 3 Schematic drawing of a slip link, with its possible motions along the network chains specified by the distances a, and its locking into position as a crosslink.

Equation 40 shows that the small deformation shear modulus of an affine network increases indefinitely over the phantom network modulus as junction functionality approaches 2.

The slip-link model incorporates the effects of entanglements along the chain contour into the elastic free energy. According to the mechanism of the slip link, sketched in Fig. 3, a link joins two different chains which may slide a distance a along the contour of the chains. The elastic free energy resulting from this model is

$$A_{\text{el}} = \frac{1}{2} N_c kT \left\{ \sum_{i=1}^{3} \lambda_i^2 + \frac{N_s}{N_c} \sum_{i=1}^{3} \left[\frac{(1+\eta)\lambda_i^2}{1+\eta\lambda_i^2} + \log(1+\eta\lambda_i^2) \right] \right\} \tag{41}$$

where N_c and N_s are the number of chemical crosslinks and slip links, respectively, and $\eta = 0.2343$. The first term on the right-hand side of Eq. (41) is the contribution to the elastic free energy from the phantom network. The effect of entanglements enters as a further contribution and is proportional to the number of slip links.

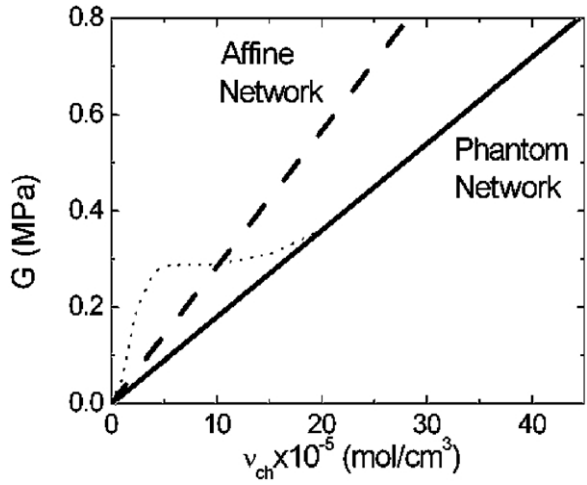

FIGURE 4 Experimental results of Rennar and Oppermann [29] shown by the dotted line. The moduli converge to the phantom network result for high degrees of crosslinking. The results of Erman, Wagner, and Flory [30] fall on the straight line and fully agree with the phantom network model.

The elastic free energy of the constrained-junction model, similar to that of the slip-link model, is the sum of the phantom network free energy and that due to the constraints. Both the slip-link and the constrained-junction model free energies reduce to that of the phantom network model when the effect of entanglements diminishes to zero. One important difference between the two models, however, is that the constrained-junction model free energy equates to that of the affine network model in the limit of infinitely strong constraints, whereas the slip-link model free energy may exceed that for an affine deformation, as may be observed from Eq. (41).

A. Contribution of Trapped Entanglements to the Modulus

The cycle rank ξ of a network denotes the number of chains that have to be cut in order to reduce the network to a tree. The moduli of the phantom, affine, slip-link, and constrained-junction models are all proportional to the cycle rank. The cycle rank is independent of the number of trapped entanglements in the crosslinked system. A network in which chains are highly entangled has the same cycle rank as one with no entanglements. Therefore, the models cited above categorically reject contributions from trapped entanglements to the modulus. However, a large body of experiments have shown that certain fraction of trapped entanglements contribute to the modulus [11, 28]. The contributions to the modulus are given by the widely used Langley equation

$$G = G_{ch} + T_e G_N^0 \tag{42}$$

Here, the modulus G is given as the sum of the modulus G_{ch} due to chemical crosslinks and the trapped entanglement term $T_e G_N^0$, where T_e (called the Langley trapping factor) is the fraction of trapped entanglements that contribute to the modulus, and G_N^0 is the plateau modulus related to the molecular weight M_e between entanglement by the expression

$$G_N^0 = \frac{\rho RT}{M_e} \tag{43}$$

According to the arguments based on the constrained-junction model, the term G_{ch} should equate to the phantom network modulus onto which contributions from entanglements are added.

Experimental determinations of the contributions above those predicted by the reference phantom network model have been controversial. Experiments of Rennar and Oppermann [29] on end-linked PDMS networks, represented by the dotted points in Fig. 4, indicate that contributions from trapped entanglements are significant for low degrees of end-linking but are not important when the network chains are shorter. Experimental results of Erman *et al.* [30] on randomly crosslinked poly(ethyl acrylate) networks fall on the solid line and indicate that the observed high deformation limit moduli are within the predictions of the constrained-junction model.

V. PHENOMENOLOGICAL THEORIES AND MOLECULAR STRUCTURE

The elastic free energy given by the elementary and the more advanced theories are symmetric functions of the three extension ratios λ_x, λ_y, and λ_z. One may also express the dependence of the elastic free energy on strain in terms of three other variables, which are in turn functions of λ_x, λ_y, and λ_z. In phenomenological theories of continuum mechanics, where only the observed behavior of the material is of concern rather than the associated molecular deformation mechanisms, these three functions are chosen as

$$\begin{aligned} I_1 &= \lambda_x^2 + \lambda_y^2 + \lambda_z^2 \\ I_2 &= \lambda_x^2\lambda_y^2 + \lambda_x^2\lambda_z^2 + \lambda_y^2\lambda_z^2 \\ I_3 &= \lambda_x^2\lambda_y^2\lambda_z^2 \end{aligned} \tag{44}$$

$$\Delta A_{\text{el}} = \Delta A_{\text{el}}(I_1, I_2, I_3) \tag{45}$$

The most general form of the elastic free energy may be written as a power series

$$\Delta A_{\text{el}} = \sum_{i,j,k=1}^{\infty} C_{ijk}(I_1 - 3)^i (I_2 - 3)^j (I_3 - 1)^k \tag{46}$$

where C_{ijk} are the phenomenological coefficients. The simple case of the phantom and affine networks is obtained as the first term of the series

$$\Delta A_{\text{el}} = C_{100}(I_1 - 3) \tag{47}$$

The elastic free energy of the so-called Mooney-Rivlin solid is obtained from Eq. (46) as

$$\Delta A_{\text{el}} = C_{100}(I_1 - 3) + C_{010}(I_2 - 3) \tag{48}$$

The reduced force follows from Eqs. (15) and (17) as

$$[f^*] = 2C_1 + \frac{2C_2}{\lambda} \tag{49}$$

where $C_1 = C_{100}/V_0$ and $C_2 = C_{010}/V_0$. For large deformations, the reduced force equates to $2C_1$, which may be identified with the phantom network model modulus. For small deformations, $2C_2$ may be obtained by equating Eq. (49) to Eq. (39) for the constrained-junction model. Thus,

$$2C_1 = G_{ph} \tag{50}$$

$$2C_2 = \frac{\mu}{\xi}\left(\frac{\kappa^2 + 1}{(1+\kappa)^4}\kappa^2\right)G_{ph} \tag{51}$$

Further references to the phenomenological treatment may be found in Treloar [5], Ogden [18], Erman and Mark [7], and Mark [31].

VI. SWELLING OF NETWORKS AND RESPONSIVE GELS

Throughout the preceding discussion, the networks were assumed to be formed in the dry state and tested in the dry state. In recent years, much emphasis has been placed on swelling of networks and their phase transitions under different activities of the network-solvent system. Large scale volume transitions triggered by small changes in environmental variables directed attention to possible uses of swollen gels in the field of responsive materials technologies. The transition involves the gel exuding solvent, for example upon decrease in temperature. The resulting shrinkage ("syneresis") is widely known as "gel collapse," and is shown schematically for such a temperature-induced change in Fig. 5. In the following discussion, charged systems will be considered in particular because the presence of charges facilitates the volume phase transitions in swollen gels.

The change in free energy of a network upon swelling is taken as the sum of the change in the elastic free energy, ΔA_{el}, and the change in free energy of mixing, ΔA_{mix}, and the contributions from ionic groups ΔA_i:

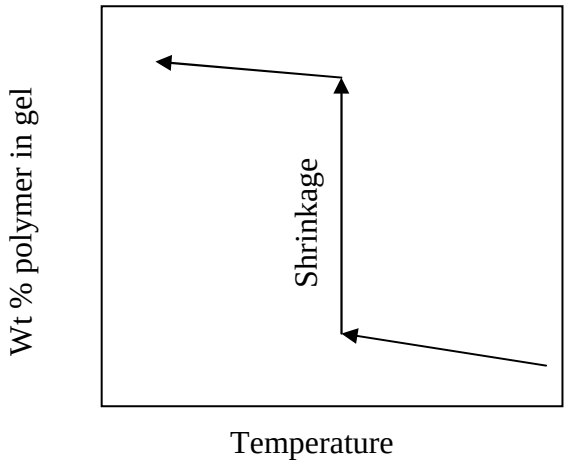

FIGURE 5 A gel exuding solvent upon decrease in temperature, with the shrinkage ("syneresis") generally described as "gel collapse."

$$\Delta A = \Delta A_{\text{el}} + \Delta A_{\text{mix}} + \Delta A_i \tag{52}$$

where, ΔA_{el} may be taken as any of the expressions resulting from a model, ΔA_{mix} is the free energy of mixing, and ΔA_i is the contribution of the ionic groups on the chains. The total chemical potential $\Delta\mu_1$ of solvent in the swollen network is obtained for the constrained-junction model as

$$\frac{\Delta\mu_1}{RT} = \ln(1-v_2) + v_2 + \chi v_2^2 + \frac{1}{\lambda}\frac{\rho V_1}{M_c}\left[1 + \frac{\mu}{\xi}K(\lambda^2)\right] - iv\left(\frac{V_1}{V_0 N_A}\right)\left(\frac{v_2}{v_{20}}\right) \tag{53}$$

where v_2 is the volume fraction of polymer, χ is the Flory interaction parameter, V_1 is the molar volume of solvent, M_c is the molecular weight of a network chain, and λ is the extension ratio, defined for the swelling case as:

$$\lambda = \left(\frac{V}{V_0}\right)^{1/3} = \left(\frac{n_1 V_1 + x V_1 n_2}{V_0}\right) \tag{54}$$

Here, x is the number of repeat units in one network chain, n_1 is the number of solvent molecules, n_2 is the total number of network chains in the system, i is the number of ionic groups on the chains, v is the number of chains, and v_{20} is the volume fraction of chains during the formation of the network.

Equating the chemical potential to zero gives a relationship between the equilibrium degree of swelling and the molecular weight M_c. The relation for $M_{c,ph}$ is obtained for a tetrafunctional phantom network model as

$$M_{c,ph} = -\frac{\frac{1}{2}\rho V_1\left(\frac{v_2}{v_{20}}\right)^{1/3}}{\ln(1-v_2)+v_2+\chi v_2^2-iv\left(\frac{V_1}{V_0 N_A}\right)\left(\frac{v_2}{v_{20}}\right)} \tag{55}$$

where v_2 denotes the equilibrium degree of swelling.

For the affine network model, the molecular weight between crosslinks $M_{c,af}$ is obtained as

$$M_{c,af} = -\frac{\rho V_1\left(v_2^{1/3}-\frac{v_2}{2v_{20}}\right)}{\ln(1-v_2)+v_2+\chi v_2^2-iv\left(\frac{V_1}{V_0 N_A}\right)\left(\frac{v_2}{v_{20}}\right)} \tag{56}$$

Alternatively, the chemical potential expression may be solved for v_2, leading to a value for the degree of swelling of the network. The solution shows that the degree of swelling increases as the chain length between crosslinks increase. The dominant forces that operate in swollen uncharged gels are van der Waals forces, hydrogen bonds, hydrophobic forces, and forces resulting from chain entropy.

When the network chains contain ionic groups, there will be additional forces that affect their swelling properties. Translational entropy of counterions, Coulomb interactions, and ion pair multiplets are forces that lead to interesting phenomena in ion-containing gels. These phenomena were studied in detail by Khokhlov and collaborators [32–35]. The free energy of the networks used by this group is

$$\Delta A = \Delta A_{\text{mix}} + \Delta A_{\text{el}} + \Delta A_{\text{trans}} + \Delta A_{\text{Coulomb}} \tag{57}$$

where ΔA_{trans} and $\Delta A_{\text{Coulomb}}$ are the contributions to the elastic free energy of the networks from the translational entropy of the counterions and the free energy of Coulomb interactions. Several interesting features of gels are obtained through the use of Eq. (57). A network chain of a polyampholyte gel contains both positive and negative charges. The liquid phase in the swollen polyampholyte gel may contain additional counterions. The theoretical and experimental literature on such gels was reviewed recently by Nisato and Candau [36]. In ion-containing gels, when ion containing groups are fully dissociated the gel swells excessively, because of the tendency of the free counterions to occupy as much space as possible. In the other extreme case, called the ionomer regime, counterions are condensed on oppositely charged monomer units, forming ion pairs followed by formation of multiplets. This decreases the osmotic pressure of the gel and results in its collapse. The conditions for ion pair formation and physical and chemical factors leading to gel swelling and collapse have been discussed by Khokhlov and Philippova [37].

VII. ENTHALPIC AND ENTROPIC CONTRIBUTIONS TO RUBBER ELASTICITY: FORCE-TEMPERATURE RELATIONS

The major component of elasticity of a network arises from the "entropic elasticity" of the individual chains. This was the basic assumption of the early molecular theories of rubber elasticity [7]. A closer consideration of the statistics of the single chain shows that the rotational isomeric states allowable to each torsion angle of the chain are not of the same energy, and stretching a chain or changing the temperature may move them from one isomeric minimum to a more favorable one. This results in an energetic contribution to the elasticity of a chain. Thus the total force acting on a network may be written as the sum of an entropic contribution, f_s, and an energetic contribution, f_e

$$f = f_s + f_e \tag{58}$$

Force-temperature relations lead to a quantitative assessment of the relative amounts of entropic and energetic components of the elasticity of the network.

In uniaxial deformation, the energetic contribution to the total elastic force [5–7, 31, 38, 39] is given by the thermodynamically exact relation

$$\frac{f_e}{f} \equiv -T\left[\frac{\partial \ln(f/T)}{dT}\right]_{L,V} \tag{59}$$

The subscripts L and V denote that differentiation is performed at constant length and volume. To carry out the differentiation indicated in Eq. (59), an expression for the total tensile force f is needed. One may use the expression given by Eq. (28) for the phantom network model. Applying the right-hand side of Eq. (59) to Eq. (28) leads to

$$\frac{fe}{f} = \frac{Td\ln\langle r^2\rangle_0}{dT} \tag{60}$$

Equation (60) is important because the right-hand side relates to a microscopic quantity, $\langle r^2\rangle_0$, and the left-hand side is the ratio of the energetic component of the force to the total force, both macroscopic quantities. It should be noted that Eq. (60) is obtained by using a molecular model. Experimentally, the determination of the force at constant volume is not easy. For this reason, expressions for the force measured at constant length and pressure p or constant α and p are used. These expressions are

$$\frac{fe}{f} \equiv -T\left[\frac{\partial \ln(f/T)}{dT}\right]_{L,P} - \frac{\beta T}{(a^3-1)} \tag{61}$$

$$\frac{fe}{f} \equiv -T\left[\frac{\partial \ln(f/T)}{dT}\right]_{a,p} - \frac{\beta T}{3} \tag{62}$$

TABLE I Some Typical Values for f_e/f

Elastomer	f_e/f
Natural rubber	0.18
cis-1, 4-Polybutadiene	0.13
Poly(dimethylsiloxane)	0.20
Elastin	0.26

where β is the thermal expansion coefficient of the network. It should be noted, however, that both of these equations are derived on the basis of the equation of state for simple molecular models and therefore are not quantities based purely on experimental data. Values of the energetic contribution for some typical elastomers are given in Table I.

VIII. DIRECT DETERMINATION OF MOLECULAR DIMENSIONS

Until recently, knowledge of chain dimensions in elastomeric networks (in both undeformed and deformed states) relied on results obtained by measurements at macroscopic length scales and/or the use of a molecular model. The fact that chains take random configurations was based, for example, on the agreement of measured moduli with those predicted by the appropriate theory. Similarly, the fact that the deformations of the chains lie between those of the affine and phantom models followed from the agreement between macroscopically measured moduli and those predicted by theoretical models. Developments in spectroscopic techniques during the last decade, however, shifted the emphasis to a molecular picture of the network. With the help of these experiments, chain dimensions and their transformations under external strain are observed directly at molecular length scales, and inferences from macroscopically measured quantities are no longer necessary. Small-angle neutron scattering is presently the most powerful technique for the determination of chain dimensions and their transformations under strain.

The technique of neutron scattering and its application to polymers in the dilute and bulk states, to blends, and to networks are described in several review articles [40–45]. The major general conclusion of these studies is that the dimensions of chains in a network are identical to their unperturbed dimensions in the bulk uncrosslinked state. These findings were followed by the demonstration [46] that the radii of gyration of PDMS chains in networks are identical to those in the uncrosslinked bulk state. The effects of (1) swelling and (2) uniaxial extension of networks on chain dimensions have been studied extensively since 1980 [46–55], leading in general to the following conclusions: (1) transformations of chain dimensions in general fall between the

predictions of the affine and phantom models, and (2) the effect of the state of dilution during crosslinking on transformations of chain dimensions is very pronounced. Small-angle neutron scattering has also been applied to the analysis of networks that were relaxing after a suddenly applied constant uniaxial deformation [56]. Results of dynamic neutron scattering measurements of Higgins *et al.* [57–59] indicate that segments of network chains diffuse around in a network, and the activation energies of these motions are smaller than those obtained for the center of mass motion of the whole chains. Measurements by Ewen and collaborators [60, 61] on PDMS networks with labeled junctions show that the fluctuations of junctions are substantial and equate approximately to those of a phantom network model. Their results also indicated that the motions of the junctions are diffusive and are similar to those expected from the Rouse model, and that motions of the junctions are much slower than those of deuterated free chain ends.

IX. SINGLE-MOLECULE ELASTICITY

A. Introduction

The only way a single molecule can be deformed is by simply elongating it, by increasing the chain's end-to-end separation. These types of experimental investigations typically focus on stress-strain measurements on single molecules of biopolymers such as proteins or polysaccharides or, in the case of some polynucleotides, on double-stranded chains. Some synthetic polymers have been studied as well. This is a very active area of research, with much of the progress being summarized in regularly appearing review articles [62–68].

Developing techniques for grasping the single chains to be elongated is one of the main challenges in this area, and developing sufficiently sensitive methods for measuring the stresses and strains involved is another. With regard to the required attachments, it is obviously advantageous to have this occur at the *ends* of the chains, and this is accomplished by either having the chains terminate with carefully chosen functional groups or with micrometer-sized beads. In the first case, the functional groups can be bonded onto complementary groups on a probe. In the second approach, the bead can be grasped using a micropipette or a laser beam (acting as an "optical tweezer"). Some less controlled experiments have been carried out by simply having one part of the chain physically or chemically adsorbed onto a surface with another part similarly adsorbed onto a probe. The probe in all these cases is typically the cantilever of what is essentially an atomic force microscope. The degree to which it is moved is a measure of the strain (in the range of nanometers), and its deflection a measure of the force of deformation (generally in the range of piconewtons, pN).

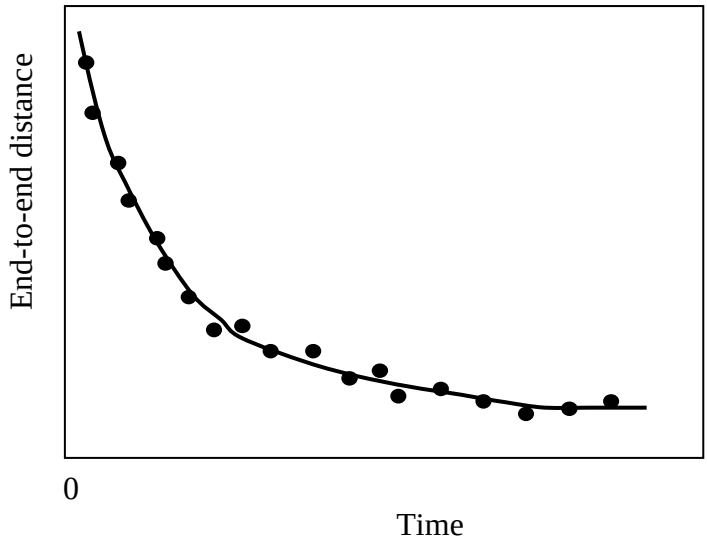

FIGURE 6 Relaxation of a λ-DNA molecule when the maximum extent of stretching is in the Gaussian region. Qualitative sketch based on experimental results presented elsewhere. (From Schroeder, Babcock, Shaqfeh *et al.* [72].)

The utility of such measurements in the area of rubberlike elasticity is illustrated in the following section.

B. Gaussian vs. Non-Gaussian Effects

Such elongation experiments can also provide important information on the retraction of stretched single chains [62, 69–72]. These studies were carried out on chains labeled so as to be directly observable in fluorescence microscopy. Also, the experiments were carried out in a solvent such as water, as was done in the case of the experiments on single λ-DNA molecules illustrated in Fig. 6 [62]. The chains were stretched to desired values of the elongation, and then permitted to relax. The circles represent some experimental results obtained, and the curve shown represents the expected behavior when the retractive force f is proportional to the end-to-end distance r remaining at that stage of the retraction. The results indicate that for moderate extensions the stretched DNA chains are still in the Gaussian region, for which the Eq. (8), $f = (3kT/\langle r^2\rangle_0)r$, predicts the observed proportionality.

In other experiments on this same system, the DNA chains were in fact stretched close to the limits of their extensibility [70]. The results for this more complicated case are shown schematically in Fig. 7. At the higher elongations, the chains are clearly in the non-Gaussian region, as evidenced by a much

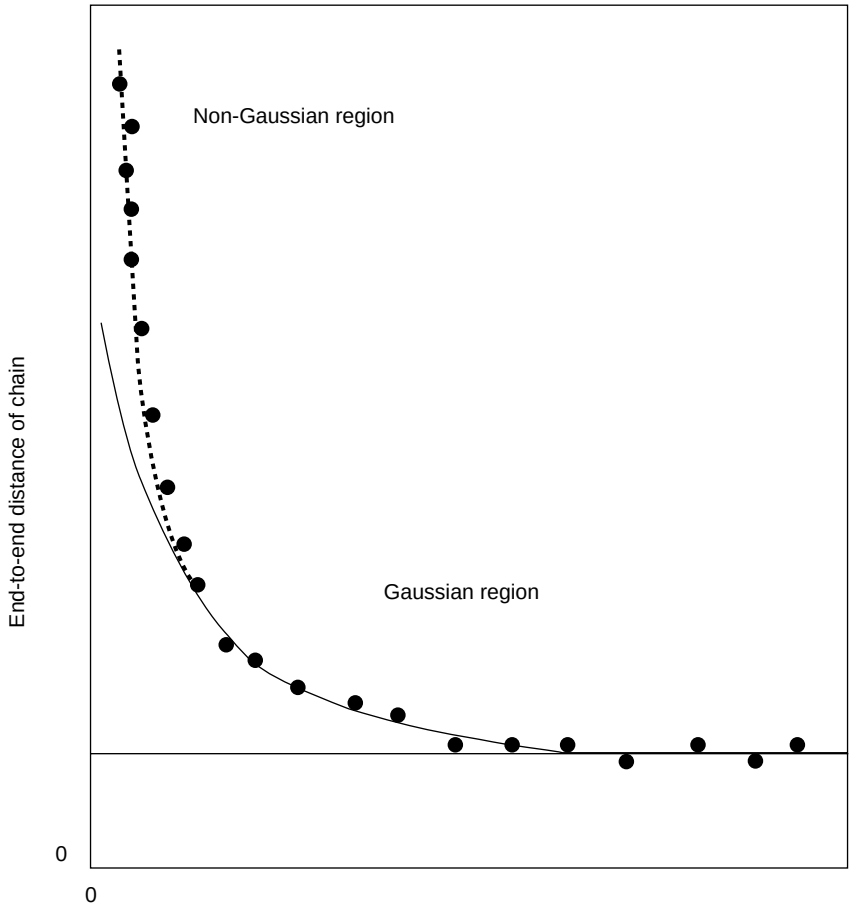

FIGURE 7 Relaxation of the same molecules as in Fig. 6 when the maximum extent of stretching was beyond the Gaussian region. Qualitative sketch based on experimental results presented elsewhere. (From Perkins *et al.* [69–71].)

more pronounced initial drop off in the retractive force. This is then followed by a Gaussian decrease in f once the elongation is sufficiently small to be Gaussian (approximately two-thirds of full extension [7]).

Although such studies are inherently very interesting, it should be noted that they are not directly relevant to the many unresolved questions in the area of rubberlike elasticity that involve the interactions *among the chains* making up an elastomeric network.

REFERENCES

1. E. Guth and H. M. James, *Ind. Eng. Chem*. **33**, 624 (1941).
2. F. T. Wall, *J. Chem. Phys.* **10**, 132 (1942).
3. P. J. Flory, *J. Chem. Phys.* **10**, 51 (1942).
4. P. J. Flory and J. Rehner, *J. Chem. Phys.* **11**, 512, 521 (1943).
5. L. R. G. Treloar, "The Physics of Rubber Elasticity," Clarendon Press, Oxford, 1975.
6. J. E. Mark and B. Erman, "Rubberlike Elasticity. A Molecular Primer," Wiley-Interscience, New York, 1988.
7. B. Erman and J. E. Mark, "Structures and Properties of Rubberlike Networks," Oxford University Press, New York, 1997.
8. W. Burchard and S. B. Ross-Murphy (Eds.), "Physical Networks: Polymers and Gels," Elsevier, London, 1990.
9. P. J. Flory, "Principles of Polymer Chemistry," Cornell Univ. Press, Ithaca, NY, 1953.
10. P. J. Flory, *Macromolecules* **15**, 99 (1982).
11. W. W. Graessley, *Adv. Polym. Sci.* **47**, 67 (1982).
12. P. J. Flory, *Proc. R. Soc. London A* **351**, 351 (1976).
13. J. E. Mark, *Br. Polym. J.* **17**, 144 (1985).
14. P. J. Flory, "Statistical Mechanics of Chain Molecules," Interscience, New York, 1969.
15. W. L. Mattice and U. W. Suter, "Conformational Theory of Large Molecules: The Rotational Isomeric State Model in Macromolecular Systems," John Wiley & Sons, Inc., New York, 1994.
16. P. J. Flory and D. Y. Yoon, *J. Chem. Phys.* **63**, 5358 (1974); D. Y. Yoon and P. J. Flory, *J. Chem. Phys.* **63**, 5366 (1974).
17. B. Erman and J. E. Mark, *J. Chem. Phys.* **89**, 3314 (1988).
18. R. W. Ogden, "Nonlinear Elastic Deformations," Dover Publications, New York, 1997.
19. R. T. Deam and S. F. Edwards, *Philos. Trans. R. Soc. London Ser. A* **280**, 317 (1976).
20. R. C. Ball, M. Doi, S. F. Edwards, and M. Warner, *Polymer* **22**, 1010 (1981).
21. S. F. Edwards and T. Vilgis, *Polymer* **27**, 483 (1986).
22. G. Ronca and G. Allegra, *J. Chem. Phys*. **63**, 4990 (1975).
23. P. J. Flory, *J. Chem. Phys.* **66**, 5720 (1977).
24. P. J. Flory and B. Erman, *Macromolecules* **16**, 800 (1982).
25. A. Kloczkowski, J. E. Mark, and B. Erman, *Macromolecules* **28**, 5089 (1995).
26. A. Kloczkowski, J. E. Mark, and B. Erman, *Comput. Polym. Sci*. **5**, 37 (1995).
27. B. Erman and L. Monnerie, *Macromolecules* **22**, 3342 (1989).
28. N. R. Langley, *Macromolecules* **1**, 348 (1968).
29. N. Rennar and W. Oppermann, *Coll. Polym. Sci.* **270**, 527 (1992).
30. B. Erman, W. Wagner, and P. J. Flory, *Macromolecules* **13**, 1554 (1980).
31. J. E. Mark, *Rubber Chem. Technol.* **46**, 593 (1973).
32. Y. Osada and A. R. Khokhlov (Eds.), "Polymer Gels and Networks," Marcel Dekker, New York, 2002.
33. O. E. Philippova, *Polymer Science Ser. C.* **42**, 208 (2000).
34. A. R. Khokhlov, in "Responsive Gels: Volume Transitions I," K. Dusek (Ed.), Springer Verlag, Berlin, 1992, p. 125.
35. A. R. Khokhlov and O. E. Philippova, in "Solvents and Self-Organization of Polymers," S. E. Webber *et al*. (Eds.), Kluwer Academic Publishers, NATO ASI Series, Vol. 327, 1996, p. 197.
36. G. Nisato and S. J. Candau, in "Polymer Gels and Networks," Y. Osada and A. R. Khokhlov (Eds.), Marcel Dekker, New York, 2002, p. 131.
37. A. R. Khokhlov and O. E. Philippova, in "Polymer Gels and Networks," Y. Osada and A. R. Khokhlov (Eds.), Marcel Dekker, New York, 2002, p. 163.
38. P. J. Flory, *Trans. Faraday Soc.* **57**, 829 (1961).
39. P. J. Flory, A. Ciferri, and C. A. J. Hoeve, *J. Polym. Sci.* **45**, 235 (1960).
40. R. Ullman, *Annu. Rev. Mater. Sci.* **10**, 261 (1980).

41. J. S. Higgins and H. C. Benoit, "Polymers and Neutron Scattering" (Oxford Series on Neutron Scattering in Condensed Matter, 8), Oxford Univ. Press, Oxford, 1997.
42. A. Maconnachie and R. W. Richards, *Polymer* **19**, 739 (1978).
43. C. Picot, in "Static Dynam: Properties Polym. Solid State," Reidel, Dordrecht, 1982, p. 127.
44. L. H. Sperling, *Polym. Eng. Sci.* **24**, 1 (1984).
45. D. J. Lohse, *Polym. News* **12**, 8 (1986).
46. M. Beltzung, C. Picot, P. Rempp, and J. Herz, *Macromolecules* **15**, 1594 (1982).
47. J. A. Hinckley, C. C. Han, B. Moser, and H. Yu, *Macromolecules* **11**, 836 (1978).
48. J. Bastide, R. Duplessix, and C. Picot, *Macromolecules* **17**, 83 (1984).
49. J. Bastide and F. Boue, *Physica A* **104**, 251 (1986).
50. J. Bastide, M. Buzier, and F. Boue, *Polym. Motion Dense Syst*. **112** (1988).
51. J. Bastide, F. Boue, and M. Buzier, in "Molecular Basis of Polymer Networks," A. Baumgartner and C. Picot (Eds.), Springer Verlag, Berlin, 1989, p. 48.
52. F. Boue, B. Farnoux, J. Bastide, A. Lapp, J. Herz, and C. Picot, *Europhys. Lett.* **1**, 637 (1986).
53. M. Beltzung, C. Picot, and J. Herz, *Macromolecules* **17**, 663 (1984).
54. S. B. Clough, A. Maconnachie, and G. Allen, *Macromolecules* **13**, 774 (1980).
55. H. Yu, T. Kitano, C. Y. Kim, E. J. Amis, T. Chang, M. R. Landry, J. A. Wesson, and C. C. Han, in "Advances in Elastomers and Rubber Elasticity," J. Lal and J. E. Mark (Eds.), Plenum Press, New York, 1986, p. 407.
56. F. Boue, J. Bastide, M. Buzier, A. Lapp, J. Herz, and T. A. Vilgis, *Coll. Polym. Sci.* **269**, 195 (1991).
57. G. Allen, P. N. Brier, G. Goodyear, and J. S. Higgins, *Faraday Symp. Chem. Soc.* **6**, 169 (1972).
58. G. Allen, J. S. Higgins, and C. J. Wright, *Faraday Symp. Chem. Soc.* **7**, 348 (1973).
59. G. Allen, M. J. Kirkham, J. Padget, C. Price, *Trans. Faraday Soc*. **67**, 1278 (1971).
60. B. Ewen and D. Richter, *Festkoerperprobleme* **27**, 1 (1987).
61. R. Oeser, B. Ewen, D. Richter, and B. Farago, *Phys. Rev. Lett.* **60**, 1041 (1988).
62. S. Chu, *Science* **253**, 861 (1991).
63. A. Janshoff, M. Neitzert, Y. Oberdorfer, and H. Fuchs, *Angew. Chem. Int. Ed.* **39**, 3213 (2000).
64. H. L. Granzier and G. H. Pollack (Eds.), "Elastic Filaments of the Cell," Kluwer Academic, New York, 2000.
65. T. Hugel and M. Seitz, *Makromol. Rapid Commun.* **22**, 989 (2001).
66. T. Strick, J. F. Allemand, V. Croquette, and D. Benisimon, *Phys. Today* **53**, 46 (2001).
67. W. Zhang and X. Zhang, *Prog. Polym. Sci.* **28**, 1271 (2003).
68. G. W. Slater, Y. Gratton, M. Kenward, L. McCormick, and F. Tessier, *Soft Mater.* **1**, 365 (2003).
69. T. T. Perkins, D. E. Smith, and S. Chu, *Science* **264**, 819 (1994).
70. T. T. Perkins, S. R. Quake, D. E. Smith, and S. Chu, *Science* **264**, 822 (1994).
71. T. T. Perkins, D. E. Smith, R. G. Larson, and S. Chu, *Science* **268**, 83 (1995).
72. C. M. Schroeder, H. P. Babcock, E. S. G. Shaqfeh, and S. Chu, *Science* **301**, 1515 (2003).
73. R. B. Case, Y. P. Chang, S. B. Smith, J. Gore, N. R. Cozzarelli, and C. Bustamante, *Science* **305**, 222 (2004).
74. S. Cui, C. Liu, Z. Wang, X. Zhang, S. Strandman, and H. Tenhu, *Macromolecules* **37**, 946 (2004).

5 The Viscoelastic Behavior of Rubber

K. L. NGAI
Naval Research Laboratory
Washington, D.C.

DONALD J. PLAZEK
University of Pittsburgh
Pittsburgh, Pennsylvania

I. INTRODUCTION

Most rubber is produced from crosslinkable high molecular weight linear polymers with low glass temperatures [1–6]. The high molecular weight is necessary to obtain high extensibility in the ultimate elastomer, and the low glass temperature is required to obtain resilience. These precursors are collections of entangled linear molecules that ultimately are free to flow past one another and hence are viscoelastic liquids [1, 5, 7]. They are viscoelastic by virtue of their time-dependent mechanical response, which reflects the sluggish configurational changes of the molecules. Upon being crosslinked sufficiently, a chemical molecular network (rubber or elastomer) is formed that transforms the polymer into a viscoelastic solid, which does not flow. Like its precursor polymer, the viscoelastic properties are strongly dependent on time or frequency, temperature, pressure, and the presence of swelling solvent or filler. Among viscoelastic solids, rubber has the unique characteristic of preserving material integrity even when subjected to high stresses or strains, although the

Science and Technology of Rubber, Third Edition

viscoelastic behavior is highly dependent on the large stresses or strains [3, 5, 8–10]. However, for sufficiently small stresses and strains, the viscoelastic behavior becomes invariant, and the linear viscoelastic regime prevails [1]. In this chapter, we describe the linear viscoelastic properties of rubber and its dependence on various parameters, including crosslink density, chemical structure, and molecular weight, with experimental data principally coming from measurements on a series of well-characterized and fully cured bisphenol-A-based epoxy resins [11–14] as well as some polybutadienes and fluorinated elastomers [15–17]. Some nonlinear viscoelastic behavior is discussed.

Since rubbers are typically based on amorphous polymers, there is a glass temperature below which the structure falls out of equilibrium. As in other amorphous polymers, the molecular segmental mobility determines the glass temperature of a rubber [1, 5, 7, 18–20]. The change from glassy to rubbery behavior occurs when the randomly oriented polymer chains between crosslinks take over to govern the viscoelastic response. There are common features as well as major differences in the viscoelastic behavior of amorphous polymers and rubbers. A better understanding of both systems is gained by comparing and interpreting them in terms of theoretical models.

II. DEFINITIONS OF MEASURED QUANTITIES, $J(t)$, $G(t)$, AND $G^*(\omega)$, AND SPECTRA $L(\log\lambda)$ AND $H(\log\tau)$

Viscoelastic behavior is a time-dependent mechanical response and is usually characterized with creep compliance, stress-relaxation, or dynamic mechanical measurements. Since time is an additional variable to deformation and force, to obtain unique characterizing functions in these measurements one of the usual variables is held constant.

A. Creep and Recovery

In a shear creep experiment a shearing stress σ_o is created in a previously relaxed material and held constant while the resulting shear strain $\gamma(t)$ increases monotonically with time t.

Given a sufficiently long time of creep, the velocity of creep will decelerate to zero, and $\gamma(t)$ attains an equilibrium limit if a viscoelastic solid is being measured. On the other hand, if the material is a viscoelastic liquid, the velocity of creep will decelerate to a finite constant value. Viscoelastic steady state is achieved, and $\gamma(t)$ increases indefinitely. The creep experiment has a second part when the stress is set to zero after a period of creeping. A portion or all of the strain accumulated during creeping is then recovered as a function of time for a viscoelastic liquid or solid, respectively. For a viscoelastic liquid, the portion that is permanent deformation and irrecoverable reflects the contribution of viscous flow to the total deformation accumulated during creep.

Since a viscoelastic solid does not flow, all of its creep deformation is recoverable.

When the strains or the strain rates are sufficiently small, the creep response is linear. In this case, when the time-dependent strain is divided by the fixed stress, a unique creep compliance curve results; that is, at each time there is only one value for this ratio, which is the compliance; i.e., $\gamma(t)/\sigma_o \equiv J(t)$. The unique shear creep compliance function $J(t)$ (Pa^{-1} or cm^2/dyne, $1\,Pa^{-1} = 0.1\,cm^2$/dyne) obtained for an amorphous polymer, has the usual contributions

$$J(t) = \gamma(t)/\sigma_0 = J_g + J_d\psi(t) + t/\eta \equiv J_r(t) + t/\eta \tag{1}$$

where J_d is a delayed compliance; $\psi(t)$ is a normalized memory function, which is equal to zero when $t = 0$ and is one when $t = \infty$; and η (Pa sec. or poise) is the shear viscosity (10 poise = 1 Pa sec.). J_g is called the glassy compliance, which represents the long time limit of strains that accrue so fast that their time dependence cannot be observed within the usually accessible experimental window, even at the glass temperature, where many molecular motions are very sluggish. The t/η term reflects the permanent viscous deformation. $J_r(t)$ is the recoverable shear compliance, which can be obtained from creep recovery measurements. For a viscoelastic solid η is operationally infinite, since normally a molecular network is present to preclude any permanent deformation. The counterpart of Eq. (1) for a viscoelastic solid is

$$J(t) = \gamma(t)/\sigma_0 = J_g + J_d\psi(t) \tag{2}$$

The creep and recovery experiment is the only characterization of viscoelastic behavior that is readily comprehended, since according to Eq. (1) contributions to the creep compliance are *additive* in the strain. The molecular processes involved are simply short- and long-range configurational orientations and viscous flow reflecting the permanent increasing separation of the centers of gravity of neighboring polymer molecules. It has also been shown that the solvent in polymer solutions contributes additively to the creep strain [21].

With all of the viscoelastic functions it is important to note the limiting values or forms which are qualitatively independent of the molecular structure. For a viscoelastic liquid, $\lim_{t\to 0} J(t) = J_g$, $\lim_{t\to\infty} J(t) = t/\eta$, and $\lim_{t\to\infty} J_r(t) = J(t) - t/\eta = J_g + J_d \equiv J_s$. The last limiting value J_s is called the steady-state recoverable shear compliance. It is the maximum recoverable strain per unit stress, which reflects the maximum configurational orientation achievable at the present stress.

For a viscoelastic solid, $J_r(t) = J(t)$, $\lim_{t\to 0} J(t) = J_g$, and $\lim_{t\to\infty} J(t) = J_g + J_d \equiv J_e$. A different notation J_e is to denote the equilibrium compliance of a solid.

B. Stress Relaxation

After a constant shear strain is created in a previously relaxed material, the resulting shear stress decays with ensuing time to zero for a viscoelastic

liquid and to a finite equilibrium value for a viscoelastic solid. The shear stress relaxation modulus (Pa or dynes/cm^2)

$$G(t) = \sigma(t)/\gamma_0 = G_e + [G(0) - G_e]\varphi(t) \tag{3}$$

Where γ_o is the imposed fixed strain, $\varphi(t)$ is the relaxation function decreasing from $\varphi(0) = 1$ at $t = 0$ to $\varphi(\infty) = 0$ at $t = \infty$, and G_e is the equilibrium modulus, which is finite for a viscoelastic solid and zero for viscoelastic liquid. The time-dependent stresses arising from different molecular mechanisms are *not additive*, and hence it is difficult if not impossible to isolate and characterize each one of them individually. Nevertheless, $G(t)$ is connected to $J(t)$ by the convolution integral equation, $\int_0^t G(s)J(t-s)ds = 1$, from which one function can be calculated from the other by a numerical procedure [22].

C. Dynamic Mechanical Measurements

Sinusoidal stresses or strains of constant frequency are applied to a sample until a steady sinusoidal strain or stress results, with a fixed phase angle between the input and the output. For example, for a sinusoidal shear strain,

$$\gamma(t) = \gamma_0 \sin \omega t \tag{4}$$

where γ_o is the strain amplitude and ω the angular frequency, the stress σ will oscillate sinusoidally as

$$\sigma(t) = \sigma_0 \sin(\omega t + \delta) \tag{5}$$

Since the stress always leads the strain, the phase angle δ is positive. Using the trigonometric formula for the sine of the sum of two angles, Eq. (5) can be rewritten in terms of the shear storage modulus $G'(\omega)$ and the loss modulus $G''(\omega)$ as

$$\sigma(t) = \gamma_0[G'(\omega)\sin(\omega t) + G''(\omega)\cos(\omega t)] \tag{6}$$

where $G'(\omega) = (\sigma_o/\gamma_o)\cos\delta$ and $G''(\omega) = (\sigma_o/\gamma_o)\sin\delta$. G' is a measure of the elastic energy stored and recovered, and G'' is a measure of the energy dissipated as heat in the cyclic deformation. The ratio $G''(\omega)/G'(\omega)$ is $\tan\delta$. Although usually not written out explicitly, δ is a function of ω. The complex dynamics shear modulus $G^*(\omega)$ is defined by

$$G^*(\omega) = G'(\omega) + iG''(\omega) = (\sigma_0/\gamma_0)\exp(i\delta) \tag{7}$$

It can be derived [1] from the general expression of calculating the stress corresponding to any strain history that the G' and G'' are related to the stress relaxation modulus $G(t)$ in Eq. (3) as follows:

$$G'(\omega) = G_e + \omega\int_0^\infty [G(t) - G_e]\sin\omega t \tag{8}$$

$$G''(\omega) = \omega\int_0^\infty [G(t) - G_e]\cos\omega t \tag{9}$$

Again, G_e in Eqs. (8) and (9) is zero for a liquid but is the equilibrium modulus for a viscoelastic solid. For a liquid, it can shown that $\lim_{\omega\to 0}G'(\omega) = \omega^2\eta^2 J_s$ and $\lim_{\omega\to 0}G''(\omega) = \omega\eta$. For the solid, $\lim_{\omega\to 0}G'(\omega) = G_e$, and $\lim_{\omega\to 0}G''(\omega) = \omega\int_0^\infty[G(t) - G_e]dt$.

In an analogous manner, the steady sinusoidal strain in response to the applied sinusoidal stress of constant frequency is expressed in terms of the (in phase) storage compliance $J'(\omega)$ and the (90° out of phase) loss compliance $J''(\omega)$ as

$$\gamma(t) = \sigma_0[J'(\omega)\sin(\omega t) - J''(\omega)\cos(\omega t)] \tag{10}$$

where $J'(\omega) = (\gamma_o/\sigma_o)\cos\delta$ and $J''(\omega) = (\gamma_o/\sigma_o)\sin\delta$. The complex dynamics shear compliance $J^*(\omega)$ is defined by

$$J^*(\omega) = J'(\omega) - iJ''(\omega) = (\gamma_0/\sigma_0)\exp(-i\delta) \tag{11}$$

The minus sign in Eqs. (10) and (11) is the consequence of the strain lagging behind the stress. It can be shown that, for a viscoelastic liquid, the dynamic creep compliances are related to the creep compliance $J(t)$ by the one-sided Fourier transforms:

$$J'(\omega) = J_s - \omega\int_0^\infty [J_s - J(t) + t/\eta]\sin\omega t\, dt \tag{12}$$

$$J''(\omega) = 1/\omega\eta + \omega\int_0^\infty [J_s - J(t) + t/\eta]\cos\omega t\, dt \tag{13}$$

For a viscoelastic solid, the relations are given by

$$J'(\omega) = J_e - \omega\int_0^\infty [J_e - J(t)]\sin\omega t\, dt \tag{14}$$

$$J''(\omega) = \int_0^\infty [J_e - J(t)]\cos\omega t\, dt \tag{15}$$

It follows immediately from Eqs. (7) and (11) that

$$J^*(\omega) = 1/G^*(\omega) \tag{16}$$

For the liquid, the low frequency limits are: $\lim_{\omega\to 0}J'(\omega) = J_s$ and $\lim_{\omega\to 0}J''(\omega) = 1/\omega\eta$. For the solid, they are $\lim_{\omega\to 0}J'(\omega) = J_e$ and $\lim_{\omega\to 0}J''(\omega) = \omega\int_0^\infty[J_e - J(t)]dt$.

D. Retardation Spectra

The retardation spectrum $L(\lambda)$, where λ is the retardation time, characterizes the contribution to the creep compliance $J(t)$, the dynamic storage compliance $J'(\omega)$, and the dynamic loss compliance $J'(\omega)$ according to the following relations (for a viscoelastic liquid; for a viscoelastic solid η is operationally infinite in the following equations),

$$J(t) = J_g + \int_{-\infty}^{\infty} L(1 - e^{-t/\lambda}) d\ln\lambda + \frac{t}{\eta} \tag{17}$$

$$J'(\omega) = J_g + \int_{-\infty}^{\infty} \left[\frac{L}{(1+\omega^2\lambda^2)}\right] d\ln\lambda \tag{18}$$

$$J''(\omega) = \int_{-\infty}^{\infty} \left[\frac{L\omega\lambda}{(1+\omega^2\lambda^2)}\right] d\ln\lambda + \frac{1}{\omega\eta} \tag{19}$$

The integrals involving L deal only with recoverable deformation, which for the most part reflects molecular orientation from various mechanisms. Permanent deformations are accounted for by the terms containing the viscosity coefficient η. From Eq. (17) it can be seen that the long time limit gives the recoverable compliance.

$$J_s = J_r(\infty) \equiv \lim_{t\to\infty}(J(t) - t/\eta) = J_g + \int_{-\infty}^{\infty} L d\ln\lambda \tag{20}$$

Thus the steady state recoverable compliance J_s is the sum of the glassy compliance and the limiting delayed compliance,

$$J_d = \int_{-\infty}^{+\infty} L d\ln\lambda \tag{21}$$

E. Relaxation Spectra

The relaxation spectrum $H(\tau)$, where τ is the relaxation time, characterizes the contribution to the shear modulus $G(t)$, the dynamic storage modulus $G'(\omega)$, and the dynamic loss modulus $G''(\omega)$ according to the following relations (for a viscoelastic solid; for a viscoelastic liquid $G_e = 0$ in the following equations),

$$G(t) = G_e + \int_{-\infty}^{\infty} H e^{-t/\tau} d\ln\tau \tag{22}$$

$$G'(\omega t) = G_e + \int_{-\infty}^{\infty} \left[\frac{H\omega^2\tau^2}{(1+\omega^2\tau^2)}\right] d\ln\tau \tag{23}$$

$$G''(\omega) = \int_{-\infty}^{\infty} \left[\frac{H\omega\tau}{(1+\omega^2\tau^2)}\right] d\ln\tau \tag{24}$$

In the limit of $\omega \to \infty$, Eq. (23) yields the relation,

$$G_g = G_e + \int_{-\infty}^{\infty} H d\ln\tau \tag{25}$$

where G_g is the glassy modulus.

F. Tensile (Bulk) Compliance, Tensile (Bulk) Modulus

Although the viscoelastic functions and their interrelations have been given above for shear deformation, they apply to tensile and bulk deformations as well. The analogues of $J(t)$, $J'(\omega)$, $J''(\omega)$, $G(t)$, $G'(\omega)$, and $G''(\omega)$, for tensile deformation are the tensile compliance $D(t)$, the tensile storage compliance $D'(\omega)$, the tensile loss compliance $D''(\omega)$, the tensile modulus $E(t)$, the tensile storage modulus $E'(\omega)$, and the tensile loss modulus $E''(\omega)$ respectively. For bulk deformation the corresponding quantities are the bulk compliance $B(t)$, the bulk storage compliance $B'(\omega)$, the bulk loss compliance $B''(\omega)$, the tensile bulk modulus $K(t)$, the bulk storage modulus $K'(\omega)$, and the bulk loss modulus $K''(\omega)$. All equations in the preceding text hold for tensile (bulk) deformation after all quantities have been changed in connotation from shear to tensile (bulk). It can be shown that the three compliances and moduli are related by the following equations:

$$D(t) = \frac{J(t)}{3} + \frac{B(t)}{9} \tag{26}$$

$$E(t) = \left[\frac{1}{3G(t)} + \frac{1}{9K(t)}\right]^{-1} \tag{27}$$

If the specimen is highly incompressible such that $K(t) > > G(t)$, and $B(t) < < J(t)$, we have the simpler relations:

$$E(t) = 3G(t) \tag{28}$$

$$D(t) = J(t)/3 \tag{29}$$

These relations enable one to relate the shear viscoelastic functions to their tensile counterparts. At high compliance levels, rubbers are highly incompressible, and the proportional relation between the tensile and shear moduli and compliances holds. However, at lower compliances approaching J_g, the Poison ratio μ (which in an elongational deformation is $-d\ln w/d\ln l$, where w is the specimen's width and l is its length) is less than $\frac{1}{2}$. Eqs. (28) and (29) are then no longer exact. For a glass $\mu \sim \frac{1}{4}$. When $G(t) = K(t)$, $E(t) = 2.25\ G(t)$.

III. THE GLASS TEMPERATURE

The glass temperature T_g is a function of the rate of cooling and the pressure at which it was determined. At a specified a rate of cooling and pressure, T_g is a corresponding state variable for the viscoelastic properties and applications of noncrystalline polymers [5, 20]. It is a material characterizing parameter. For example, if T_g is much higher than the temperature of application, the polymer is a hard glass and may be suitable for applications as engineering plastics. If T_g is sufficiently lower, the polymer is rubbery and may be used in the rubber industry. Although references are made to "the transition from the rubbery state to the glassy state," no such transition occurs because the rubber and the glass are in the same thermodynamic state; only the molecular mobility is different. The kinetic change from rubbery to glassy behavior is reflected in the change in enthalpy H or volume V. For example, as seen in Fig. 1 at a fixed rate of cooling Q_1 a liquid's H and V decreases along an equilibrium line until the liquid's approach to its equilibrium configuration becomes so slow that it cannot keep up with the diminishing temperature. At all lower temperatures the specific volume is greater than its equilibrium value

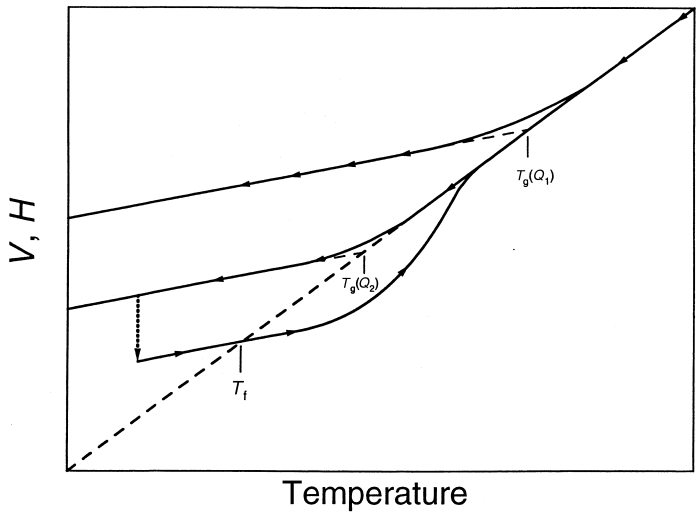

FIGURE 1 Schematic plots of the variation of volume V and enthalpy H with temperature. The uppermost line represents cooling from equilibrium liquid at a more rapid rate Q_1. The line in the middle represents cooling at a slower rate Q_2. The thin lines are extrapolations of the glass lines to higher temperatures. Their intersections with the equilibrium liquid line (thicker dashed line) define the glass temperatures, $T_g(Q_1)$ and $T_g(Q_2)$. The downward pointing arrow indicates isothermal physical aging for a period of time. The low-lying line represents heating at the rate Q_2 of the aged glass to restore thermal equilibrium at some higher temperature.

and glassy behavior is observed. At a slower rate of cooling Q_2 equilibrium can be approximated to a lower temperature, and a lower T_g is observed. The intersection of the equilibrium liquid line with the nonequilibrium glass line is defined as T_g. Thus T_g is a decreasing function of the cooling rate Q.

Upon cessation of cooling below T_g, the enthalpy and volume slowly but incessantly decrease toward their equilibrium values. During this decrease, other kinetic properties, such as the rate of creep, slow down. This deceleration of kinetic processes is called physical aging and is reflected in Fig. 1 by the dotted line. These effects are reversible, in that these changes are erased when the material is taken to temperatures above T_g where equilibrium properties are readily achieved [23–27]. The rate of volume contraction greatly decelerates as the temperature is decreased, and it becomes impossible to wait for the achievement of equilibrium at temperatures below about $T_g - 25°C$. If physical aging is terminated after a time t_{age} and the annealed glass is heated at a constant rate, V initially increases along a denser glass line, undershoots the equilibrium volume line, and finally returns to equilibrium at some temperature higher than $T_g(Q_2)$. Explanation of this behavior is beyond the scope of this chapter but can be found in other texts [5, 26, 27]. The temperature at which the glass line intersects the equilibrium line is called the fictive temperature T_f of the annealed glass.

IV. VOLUME CHANGES DURING CURING

A polymer, whether the chains are entangled or not, is a viscoelastic liquid. In order to make it into a viscoelastic solid, the polymer chains can be chemically linked together by curing agents to form a molecular network. The process is called curing or vulcanization. The volume contracts during curing because van der Waals "bonds" are replaced by shorter covalent bonds. Since T_g strongly depends on volume, it is instructive to know exactly how volume changes as curing proceed, the volume reached when the material is fully cured, and its dependence on the density of crosslinks and other parameters. In addition to volume shrinkage, the changes as a function of the time of curing, t_{cur}, of other properties, including (1) the rise of the fictive temperature T_f [25–28], (2) the increase of degree of cure and gel fraction, (3) the increase of the viscosity, and (4) the decrease of the equilibrium compliance J_e, are also of interest. Such a demonstration by measurements is rare. Hence it is worthwhile to present the results from a detailed experimental study of curing a series of epoxy resins derived from diglycidyl ethers of bisphenol A with differing initial linear molecular chain lengths [11–14]. Some characterization parameters of these Epon Resins 828, 1001F, 1004F, and 1007F are shown in Table I.

Their structures are represented by

TABLE I Epoxy Resin Properties

Material	M_n (g/mol)	n	T_g (°C)	f	Soluble fraction (% wt/wt)	M_x
Epon 828	380	0.14	–14	2.0	0.3	420
Epon 1001F	996	2.31	31	1.9	1.3	910
Epon 1002F	1342	3.52	40	1.8	1.9	1130
Epon 1004F	1450	4.85	56	1.7	2.8	1520
Epon 1007F	2600		70	1.4	9.0	2870

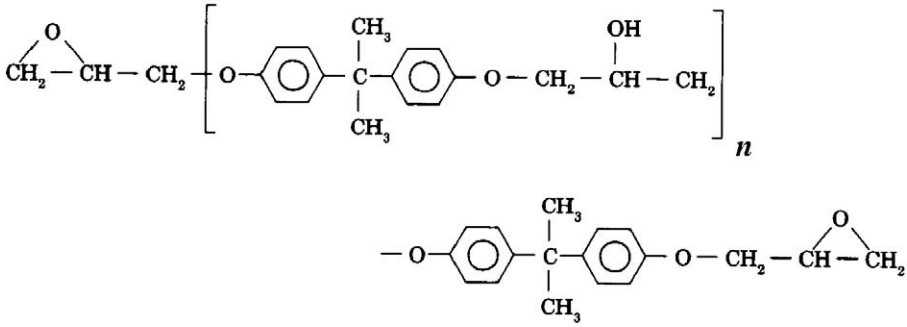

where n is the average number of repeat units in the epoxy resin molecule, and f is the functionality.

The curing agents are the diamines 4,4′-methylene dianiline (MDA)

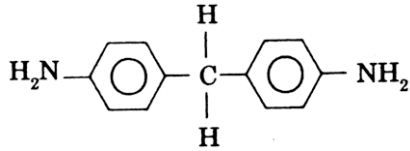

and 4,4′-diamino diphenyl sulphone (DDS).

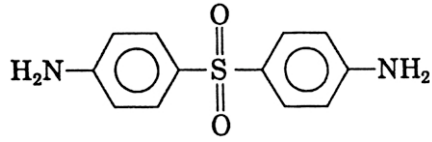

The shrinkage of EPON 1001F as it reacts with a stoichiometric ratio of the diamine DDS in a two-stage cure is presented in Fig. 2. The reaction mixture was first heated at a rate of 5°C/min up to 142°C under a pressure of 5 MPa. Following the attainment of a constant curing temperature, T_{cur} = 142°C, the decrease in volume due to curing of the epoxy resins was monitored for over 2 days (50 h). During this first stage, the specific volume decreased by 3.5%. In the following second stage, the curing temper-

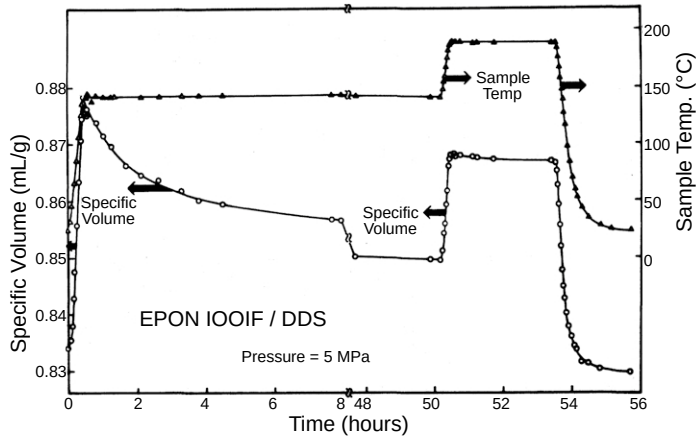

FIGURE 2 Specific volume and temperature history of the 1001F/DDS epoxy resin during curing under a pressure of 5 MPa.

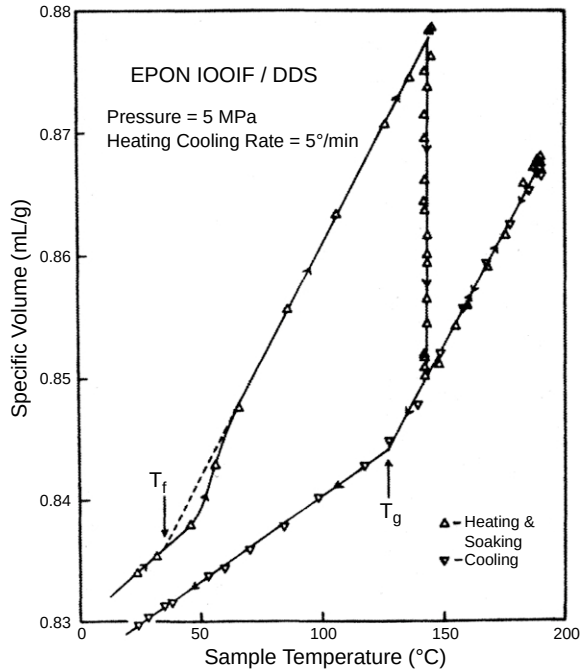

FIGURE 3 Specific volume data from Fig. 2 plotted as a function of the temperature.

ature was increased to 190°C for 3 hours to approach a complete cure, where an additional 0.1% of shrinkage occurred.

The specific volume history data of the curing 1001/DDS are cross-plotted in Fig. 3, where the specific volume is shown as a function of temperature. The

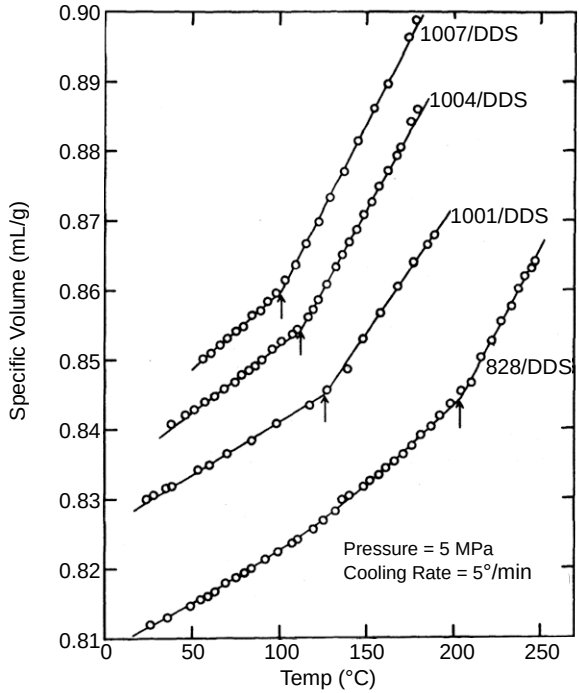

FIGURE 4 The specific volume–temperature cooling curves obtained on the fully cured 1007, 1004, 1001, and 828/DDS resins.

mixed reactants start as a glass at room temperature. During the heating to T_{cur} = 142°C, a fictive temperature T_f of 35°C is seen to be bypassed with the specific volume increases in the same manner as illustrated in Fig. 1. Thereafter the volume of the reactant mixture is seen to increase linearly as the temperature is increased to T_{cur}. The isothermal volume contraction caused by the curing at T_{cur} is seen in Fig. 3 as the vertical drop. This is followed by the equilibrium volume–temperature line of the cured 1001/DDS, first traversed when temperature is raised from T_{cur} to 190°C in the second stage. Upon cooling at 5°C/min, the equilibrium volume–temperature line is retraced in the opposite direction until the glass temperature T_g of the fully cured 1001/DDS is reached, where the volume breaks off to follow the glass line as illustrated in Fig. 1.

The specific volume–temperature cooling curves obtained on the fully cured 1007, 1004, 1001, and 828/DDS resins are shown together in Fig. 4. The systematic decrease in specific volume with increasing crosslink density is clearly depicted as is the increase of T_g with crosslink density. The glass temperatures for the fully cured 1007, 1004, 1001, and 828/DDS resins are 101, 112, 127, and 204°C respectively.

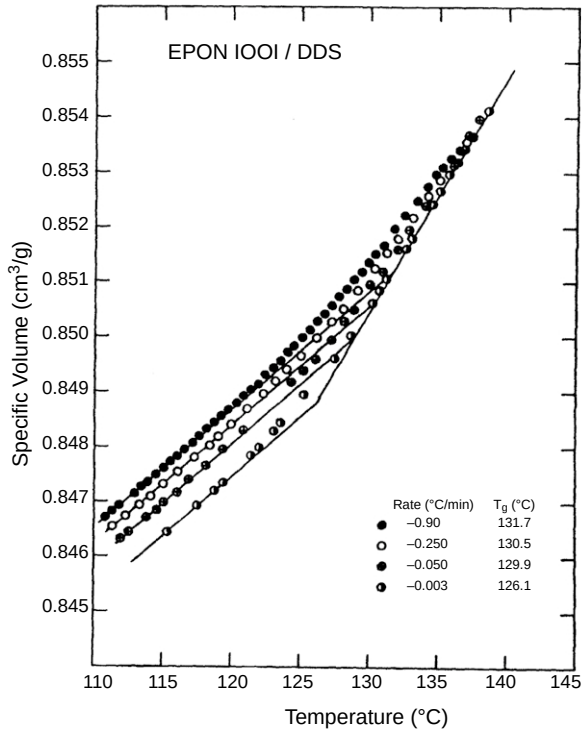

FIGURE 5 The specific volume–temperature cooling curves obtained on the fully cured 1001/DDS resin for different cooling rates.

The dependences of specific volume and glass temperature on cooling rates have been elucidated in general by Fig. 1. A glass transition temperature, T_g, is determined from the intersection of the equilibrium line with the glass line extrapolated to higher temperatures. This procedure of obtaining T_g's is explicitly demonstrated in Fig. 5 on specific volume–temperature cooling curves for the fully cured epoxy resin 1001/DDS. The dependence of T_g on Q is shown in Fig. 5.

V. VISCOELASTIC BEHAVIOR ABOVE T_g

A. Isothermal Measurements of Time or Frequency Dependence

The viscoelastic response of equilibrium rubber networks can be obtained by measuring the shear and tensile moduli or compliances as a function of time, or the corresponding dynamic moduli and compliances as a function of frequency. As discussed in Section II, the measurements of any viscoelastic function can be converted to another viscoelastic function.

The Epons 828, 1001, 1002, 1004, and 1007 fully cured with stoichiometeric amounts of DDS are examples of well-characterized networks. Therefore, mechanical measurements on them offer insight into the viscoelastic properties of rubber networks. The shear creep compliance $J(t)$ of these Epons were measured above their glass temperatures [11, 12, 14]. From the statistical theory of rubber elasticity [1–5, 29–33] the equilibrium modulus G_e is proportional to the product $T\rho$, where ρ is the density at temperature T, and hence the equilibrium compliance J_e is proportional to $(T\rho)^{-1}$. Thus $J(t)$ is expected to be proportional to $(T\rho)^{-1}$, and $J(t)T\rho$ is the quantity which should be compared at different temperatures. Actually the reduced creep compliance

$$J_p(t) = J(t)T\rho/T_0\rho_0 \tag{30}$$

is the quantity of choice in plotting against time, where T_0 is a reference temperature and ρ_0 is the density at T_0. This is used so that one can read off from such a plot the actual magnitudes of $J(t)$ measured at the reference temperature T_0. Illustrative results are shown in Fig. 6, where $J_p(t)$ determined on Epon 1007/DDS at seven temperatures between 99.8 and 127.3°C with $T_0 = 100.7$°C are presented. The measured $J_p(t)$ extends from the glassy level slightly above 10^{-10} cm^2/dyn up to a firm rubbery compliance close to 10^{-7} cm^2/dyn.

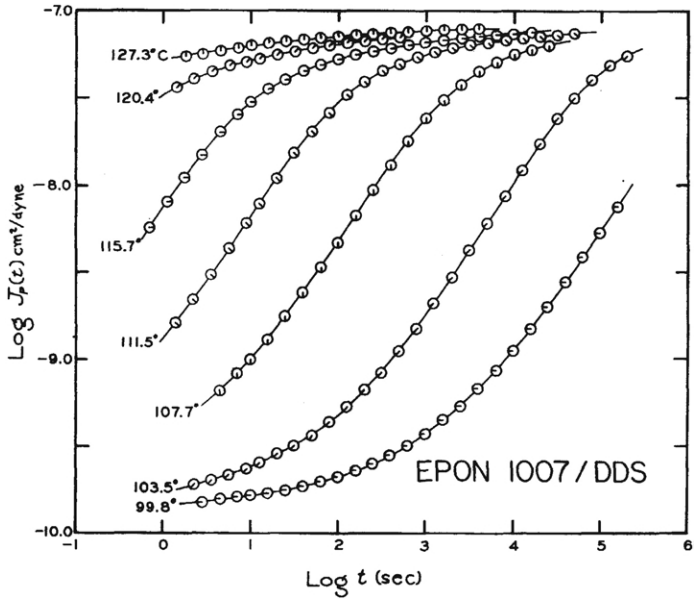

FIGURE 6 Reduced shear creep compliance curves $J_p(t)$, cm^2/dyne, determined on Epon 1007/DDS at seven temperatures, as indicated, presented logarithmically as a function of logarithmic time t.

B. Temperature Dependence

Traditionally it is assumed that the temperature dependences of the retardation times of all viscoelastic modes or mechanisms of polymers are proportional to one and the same monomeric friction coefficient ζ_0 [1, 5, 7, 34]. For rubber networks, the viscoelastic modes include those with shorter retardation times responsible for volume change and the glass temperature, and the longer retardation times of polymer strands between crosslinks contributing to rubbery deformation and J_e. Thus the retardation times $\lambda(T)$ of all the viscoelastic modes contributing to $J_p(t)$ at any temperature T are related to that at a chosen reference temperature T_0 by the same multiplicative factor given by

$$a_T = \zeta_0(T)/\zeta_0(T_0) \tag{31}$$

This means that the measured $J_p(t)$ at (T, t) is equivalent to that at $(T_0, t/a_T)$, as seen in Fig. 6 by the measured compliance moving horizontally to shorter times along the logarithmic time-scale with increasing temperature. This time–temperature equivalence of the viscoelastic function is referred to as thermorheological simplicity. In practice, the test of time–temperature equivalence of experimental data is carried out by successively shifting the data measured at T, first for T closest T_0, along the $\log(t)$ axis by a displacement $-\log a_T$ to overlap with each other to form a reduced curve. Measurements for $T > T_0$ are shifted to longer times, while measurements for $T < T_0$ are shifted to shorter times. A well-defined reduced curve means the viscoelastic response is thermorheologically simple [35]. It represents $\log J_p(t)$ at T_0 over an extended time range. The time-scale shift factors a_T that were used in the reduction of the creep compliance curves to obtain the reduced curve constitute the temperature dependence. a_T is fitted to an analytical form, which is often chosen to be the Williams-Landel-Ferry (WLF) equation [1],

$$\log a_T = -C_1(T - T_0)/(C_2 + T - T_0) \tag{32}$$

or equivalently the Vogel-Fulcher-Tammann-Hesse (VFTH) equation [1],

$$a_T = A \exp[C/(T - T_\infty)] \tag{33}$$

For the chosen reference temperature T_0, $A = \exp[-C/(T_0 - T_\infty)]$. The parameter $C/2.303$ is equal to the product, C_1C_2, of the two constants in the WLF equation, and $T_\infty = T_0 - C_2$. From the WLF or the VFTH equation for the temperature dependence of a_T, the reduced data curve can be constructed for another choice of the reference temperature T_0.

The procedure was carried out on the measured $J_p(t)$ of Epon 1007/DDS in Fig. 6. The reduced curve extending over 10 decades of time with the choice

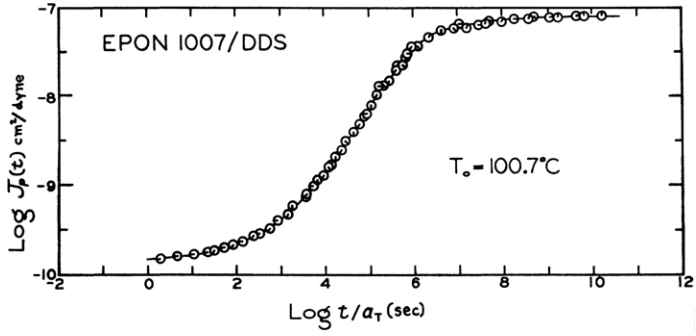

FIGURE 7 Reduced shear creep compliance curves $J_p(t)$ of Epon 1007/DDS shifted to superimpose with the curve at the reference temperature 100.7°C shown logarithmically versus the logarithm of the reduced time t/a_T.

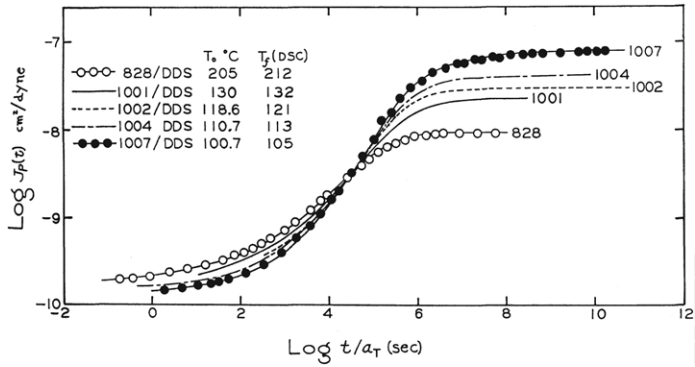

FIGURE 8 Comparison of reduced shear creep compliance curves of Epon 828, 1001, 1002, 1004, and 1007/DDS plotted logarithmically against time at the reference temperatures indicated, which are close to the respective T_g's.

T_0 of 100.7°C is shown in Fig. 7. This test of time–temperature equivalence is eminently successful as found in other molecular network polymers [14–16].

The measured $J_p(t)$ curves of the other epoxy resins studied, Epon 1004, 1002, 1001, and 828/DDS, were successfully reduced at chosen reference temperatures, and the results are shown in Fig. 8 as functions of the reduced time t/a_T in a double logarithmic plot. This comparison plot was constructed by requiring all the reduced curves to cross at a compliance level of log $J_p(t) = -8.5$. The choice of T_0 is 100.7, 110.7, 118.6, 130, and 205 for the DDS crosslinked 1007, 1004, 1002, 1001, and 828 Epons respectively.

The time-scale shift factors a_T that were determined in the reduction of the creep compliance curves to obtain the reduced curves shown in Fig. 8 are presented in Fig. 9. The logarithm of a_T are plotted as a function of the reciprocal absolute temperature. The temperature dependence data can be fitted

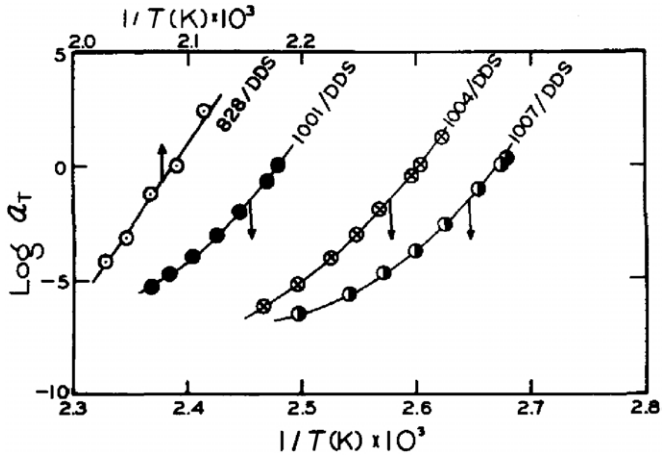

FIGURE 9 Logarithmic temperature shift factors $\log a_T$ plotted as functions of the reciprocal absolute temperature T/K for the four indicated epoxy resins that were obtained from the reduction process used in producing the curves in Fig. 8.

to either the WLF Eq. (32) or the VFTH Eq. (33), except for the tightest network 828/DDS, which appears to be Arrhenius.

C. The Equilibrium Compliance J_e

It can seen from Fig. 8 that the equilibrium compliance J_e decreases uniformly from the 1007/DDS to the 828/DDS as expected on the basis of the kinetic theory of rubberlike elasticity, since the concentration of network chains increases, and the molecular weight per crosslinked unit, M_x, decreases in the same order. The M_x values calculated as ρRTJ_e are listed in Table I. They are remarkably close to the molecular weight values of the starting epoxy resins.

At all temperatures it is seen (see Fig. 4) that the order of densities is primarily determined by the density of crosslinks. However, the epoxy networks with lower crosslink densities and lower specific densities surprisingly display lower glassy compliance J_g values at their respective T_g's. This is believed to be due to particularly strong dependence of the J_g's, and the large increase of T_g with crosslink density. The strong temperature dependence of J_g is possibly due to the increasing prominence of the secondary relaxation in the epoxy networks in more tightly crosslinked networks. This conjecture can be checked by dielectric relaxation measurements of the secondary relaxation.

D. Retardation Spectra

The viscoelastic retardation spectra $L_p(\ln\lambda)$ have been calculated from the $J_p(t)$ curves presented in Fig. 8. Iterative computer calculations were necessary

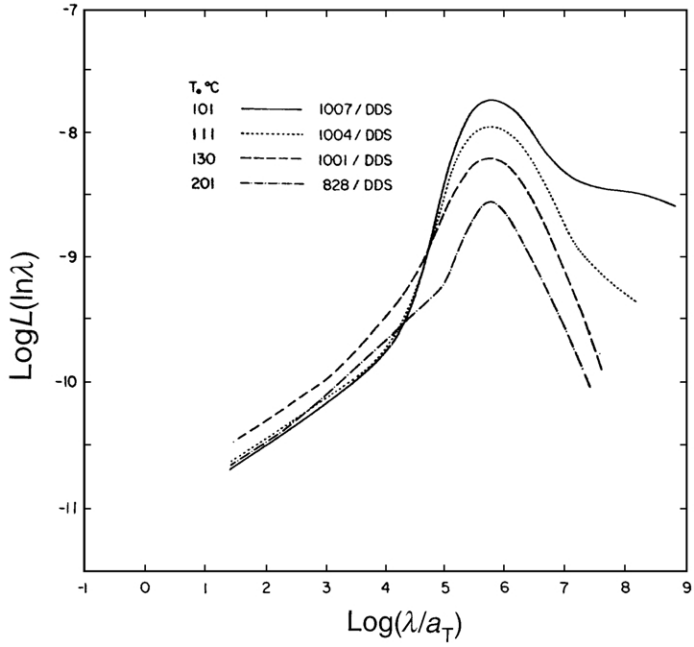

FIGURE 10 Logarithmic presentation of the retardation spectra $L(\ln\lambda)$ versus the logarithm of the reduced time λ/a_{T} of four fully cured epoxy resins as indicated. Temperature at which the spectra are shown were chosen to match the times at the maxima.

to obtain optimized values of $L_p(\ln\lambda)$ [21], which are shown in Fig. 10. The temperatures of presentation of the L_{p}s were chosen to match the positions of the observed maximum. These reference temperatures T_0' are only slightly different from the T_0 values obtained from the common compliance used in preparing Fig. 8. The short time linear variation of $\log\lambda$ with $\log(\lambda/a_T)$ is virtually common to all of the epoxy samples. The $\frac{1}{3}$ slope of each line at short times is a result of the assumed Andrade creep [36, 37], $J(t) \equiv J_{\mathrm{g}} + \beta t^{1/3}$ at short times used to determine J_{g}. One cannot rule out the possibility that the actual slope may differ from one network to another. Nevertheless, beyond the Andrade creep region the various crosslinked resins exhibit a fairly symmetrical maximum in $\log L_p$, which increases in magnitude with the increase in the molecular weight per crosslinked unit, i.e., the length of the molecular network strands. The looser molecular networks, not unexpectedly, are capable of dissipating greater amounts of mechanical energy into heat. The increasing peak in $\log L_p$ clearly indicates that the fracture energy should show a corresponding increase, and it does [38]. The two epoxies with the loosest networks show the beginnings of a second long-time peak in $L_p(\ln\lambda)$, which is expected when both the crosslink and entanglement networks are involved in determining J_{e}.

The crosslink network must be looser than the entanglement network for both peaks to be seen.

VI. VISCOELASTIC BEHAVIOR OF OTHER MODEL ELASTOMERS

The viscoelastic properties of a series of fully cured epoxy resins with different crosslink densities and their trends have been discussed in some details in the previous section. Qualitatively these properties are shared by all crosslinked elastomers, although quantitatively they depend on molecular architecture and the chemical type of the network polymer and the crosslinking agent. Hence it is instructive to show the viscoelastic behavior of other model network systems and compare them.

A. Fluorinated Hydrocarbon Elastomers "Viton" (15)

The starting material is a copolymer of vinylidene fluoride and hexafluoropropylene with molecular weight in the neighborhood of 2.0×10^5. The vulcanization recipe is 100 parts copolymer, 3 parts high activity magnesia, 3 parts calcium hydroxide, and 1 to 4 parts curing agents. Three "Viton" fluoroelastomers with different degrees of crosslinking obtained from DuPont were studied. The average molecular weights of the network chains M_c were estimated to be 2700 for Sample 10-B, 4100 for 10-A, and 7800 for 11-A. These parameters together with some other physical properties of the three samples are listed in Table II.

TABLE II Physical Properties of Fluoroelastomers

Sample	Density 25°C, g/cm^3	$\log G_e$ Pa[a]	$\log G_e$ Pa[b]	M_c, g/mol[a]	M_c, g/mol[c]
11-A	1.837	5.76	5.80	7790	7220
10-A	1.833	6.05	5.94	4060	5220
10-B	1.830	6.22	6.17	2720	3070

Sample	C_1, kPa	C_2, kPa	$\log 2(C_1 + C_2)$[d]	SI, g/g[e]
11-A	150	280	5.93	3.01
10-A	300	200	6.00	2.42
10-B	620	0	6.09	2.13

[a]From compression measurements on swollen samples.
[b]Estimated from compliance curve, $T_0 = -20$°C.
[c]From estimate of J_e (creep).
[d]C_1 and C_2 in Pa. Mooney-Rivlin Equation constants. For the equation, see Ref. 1.
[e]Weight swelling index measured in methyl ethyl ketone at 25°C.

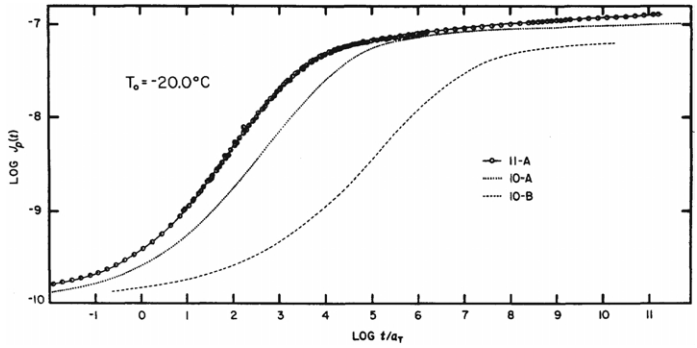

FIGURE 11 Logarithmic plot of the reduced shear creep compliance curves $J_p(t)$ (in cm^2/dyne = $10\,Pa^{-1}$) against the reduced time t/a_T (in seconds). The reference temperature of reduction, T_0, is –20.0°C for all curves. Data points are shown only for Sample 11-A.

1. Creep Compliance Data

Torsional shear measurements yielded isothermal shear creep compliances, $J(t)$, that ranged from the glassy level $10^{-10}\,cm^2$/dyne ($10^{-9}\,Pa^{-1}$) to near equilibrium values in the neighborhood of the usual $10^{-7}\,cm^2$/dyne ($10^{-6}\,Pa^{-1}$). The reduced isothermal shear compliance, $J_p(t)$, calculated by Eq. (30), obey time–temperature superposition, and the well-defined reduced curves are shown logarithmically in Fig. 11 plotted against the reduced time scale, t/a_T, where a_T is the usual time-scale shift factor. The most highly crosslinked sample has the highest T_g, –19.6°C, as expected. In addition to raising T_g, the increasing level of crosslinking depresses the equilibrium compliance, J_e. This depression is, of course, rationalized by the classical kinetic theory of rubberlike elasticity, which concludes that J_e is inversely proportional to the concentration of elastic elements, i.e., the number of polymeric network chains per unit volume. The approach to the different J_e values is clearly seen in Fig. 11 for the three fluoroelastomers studied.

2. Temperature Dependence of the Shift Factors

The horizontal logarithmic time scale shifts that are required to superpose the data obtained at different temperature are the logarithms of the a_T shift factors. The a_T values thus reflect the principal temperature dependence of the viscoelastic process. It was possible to represent the time-scale temperature dependences of the three samples with a single VFTH Eq. (33) in which only one parameter T_∞, which reflects the change in T_g, varies with the level of crosslinking. The fit achieved is shown in Fig. 12. The atmosphere in which the measurements were made is important since samples measured in air contain the moisture absorbed under ambient conditions, whereas those measured in rough vacuum (use about symbol ~ 10^{-2} torr = 1.3 Pa) are at least partially

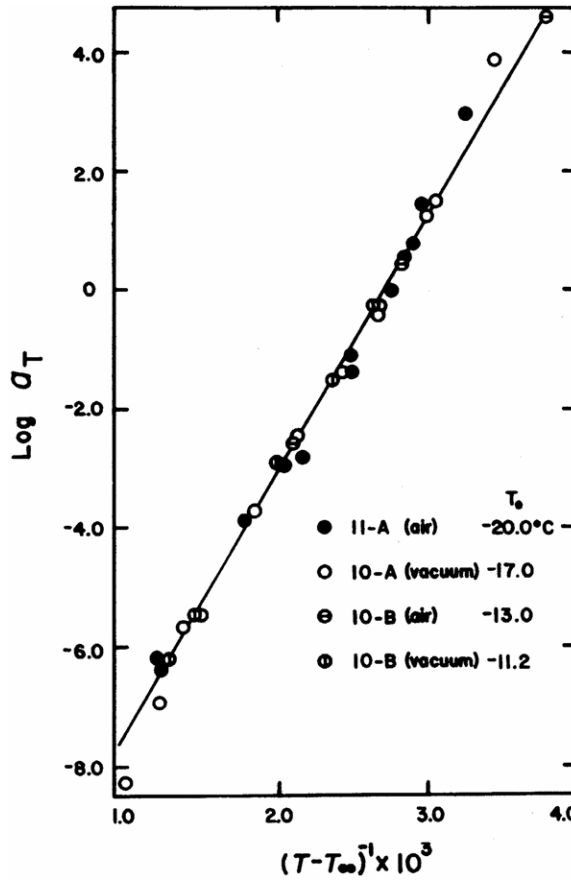

FIGURE 12 Logarithmic plot of the time-scale shift factors against temperature differences. The atmosphere in which the measurements were made is either in air containing the moisture absorbed under ambient condition or in rough vacuum, which is partially dry. $T_\infty = -57, -54, -50, -48°C$, respectively, for Samples 11-A (air), 10-A (vacuum), 10-B (air), and 10-B (vacuum).

dried. The constant C in the VFTH equation is 990°C for all the samples measured. The difference, Δ, between T_g and T_∞ is 32.8°C for 11-A, 31.3°C for 10-A, and 30.4°C for 10-B. Within experimental uncertainty, Δ is thus shown to be constant, as is usually observed for a homologous series of polymers or polymer solutions over sizeable concentration range [37, 39].

3. Retardation Spectra

Retardation spectra L_p were determined from the $J_p(t)$ curves of Fig. 10. The results reduced to $T_o = -20°C$ are shown in Fig. 13, where the principal maximum concentration of retardation mechanisms is shown to be at correspondingly longer times as T_g is increased with additional crosslinking. The

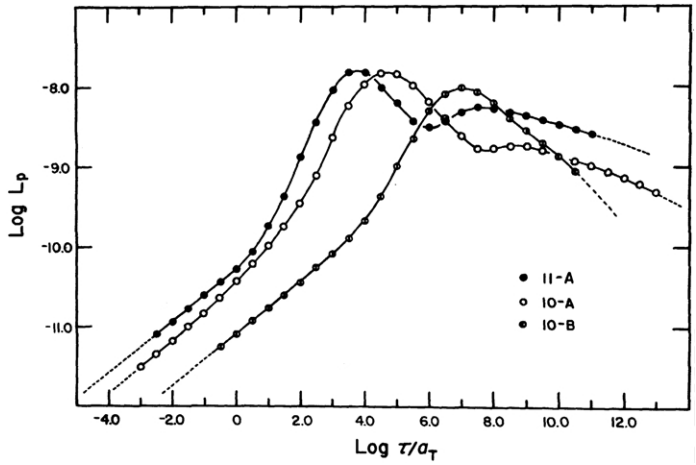

FIGURE 13 Logarithmic plot of the retardation spectra as functions of the logarithmic reduced retardation times, λ/a_T (in seconds). The reference temperature of reduction T_0 is –20.0°C for all curves.

logarithmic curves at shorter reduced times showing a slope of $\frac{1}{3}$ for all three fluoroelastomers are consequences of the assumed Andrade creep [36, 37], $J(t) \equiv J_g + \beta t^{1/3}$ at short times used to determine J_g.

A significant feature to be noted is the presence of the long-time or terminal peak, which grows in size with decreasing crosslink concentration. The Sample 10-B, with the highest crosslink density, exhibits but a slight shoulder at long times, whereas Sample 11-A, with about one-third the crosslink density, exhibits a distinct long-time terminal peak, which reflects greater viscoelastic losses at longer times presumably arising from adjustments of the entanglement network.

The effect is seen in proper perspective when the characteristics of the different networks are viewed at corresponding-state temperatures (usually temperatures equidistant from T_g). Such a comparison of the retardation spectra is made in Fig. 14. When the reference temperatures shown in Fig. 14 are chosen, the difference, $\Delta' = T_o - T_g$, becomes 4.2, 5.3, and 6.1°C for 11-A, 10-A, and 10-B respectively, and the short-time portions of the spectra coincide rather closely. From the difference in the ordinate of the curves in Fig. 14, we can infer that at $\log(\lambda/a_T) = 10$, Sample 11-A would creep approximately 100 times faster than Sample 10-B.

4. Derived Dynamic Mechanical Properties

Once the retardation spectra are known over an extended time scale, it is possible to calculate numerically the components of the complex dynamic

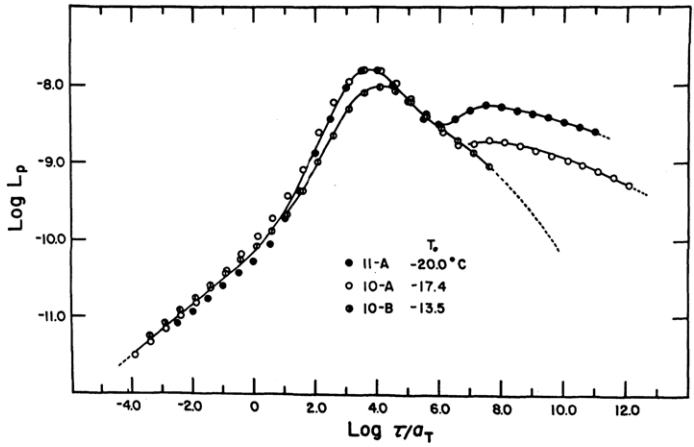

FIGURE 14 Logarithmic plot of the retardation spectra against log λ/a_T reduced to the reference temperature indicated for correspondence at short times in the primary softening dispersion.

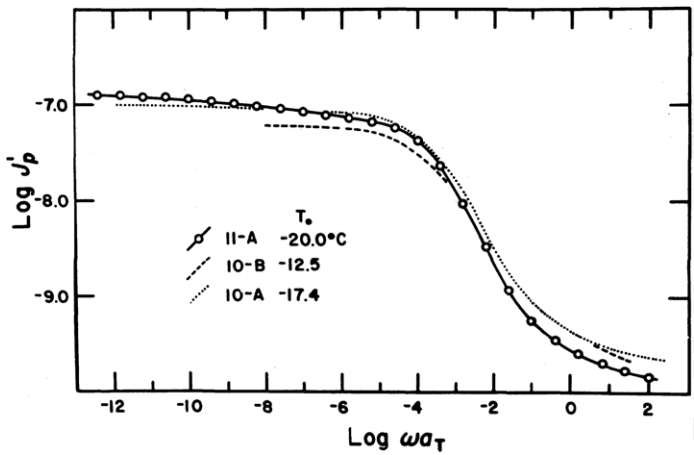

FIGURE 15 Logarithmic comparison plot of the reduced dynamic storage compliance J_p' (in cm^2/dyne = 10 Pa^{-1}) against the logarithm of the reduced frequency ωa_T (s^{-1}). The reduced reference temperature give correspondence in the softening dispersion and match the loss tangent primary maxima.

shear compliance, $J_p'(\omega) - iJ_p''(\omega)$, by Eqs. (18) and (19). With the $J_p'(\omega)$ and $J_p''(\omega)$ values, the storage, $G_p'(\omega)$, and loss, $G_p''(\omega)$, dynamic moduli can be calculated algebraically by Eq. (16). The results for $J_p'(\omega)$ and $G_p''(\omega)$ are shown in Figs. 15 and 16 respectively. The reference temperatures chosen in these plots are the same as those for the presentation of the retardation spectra in Fig. 14 except for a slight (1°) change for Sample 10-B. The $J_p'(\omega)$ curves can

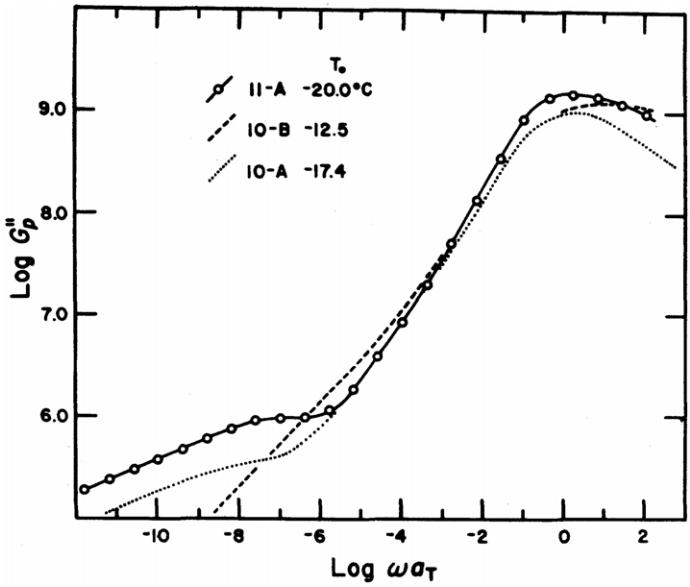

FIGURE 16 Logarithmic comparison plot of the reduced dynamic loss modulus G_p'' (in dyne/cm^2 = 0.1 Pa) against the logarithm of the reduced frequency ωa_T (s^{-1}). The reduced reference temperature give correspondence in the softening dispersion and match the positions of the loss tangent primary maxima.

be seen to be the semiquantitative mirror images of the $J_p(t)$ curves. The limiting low frequency value for $J_p'(\omega)$ is the equilibrium compliance J_e, which is the long time limit of the $J_p(t)$ curve for these viscoelastic solids. The small change in shape of the primary softening dispersion is partly a reflection of a significant effect of the level of crosslinking on the viscoelastic loss in this region of the frequency scale. Since the amount of energy dissipated per cycle of deformation is proportional to G'', the reduced loss modulus $G_p''(\omega)$ is of interest, as well as the loss tangent which is a measure of the relative energy loss. Figure 16 shows that the low frequency losses in the more lightly crosslinked elastomers are significantly greater at corresponding-state temperatures. In the softening dispersion, the three curves superpose roughly, and the distinctions are not clear.

However, the loss tangent curves (Fig. 17) show that Sample 11-A, with the lowest concentration of network chains, exhibits the largest relative energy dissipation in the primary softening dispersion. It is clear that the relative ranking of energy losses is the same in both the primary softening dispersion and in the low frequency region, i.e., Sample 10-B, with the tightest molecular network, shows the least amount of relative energy dissipation.

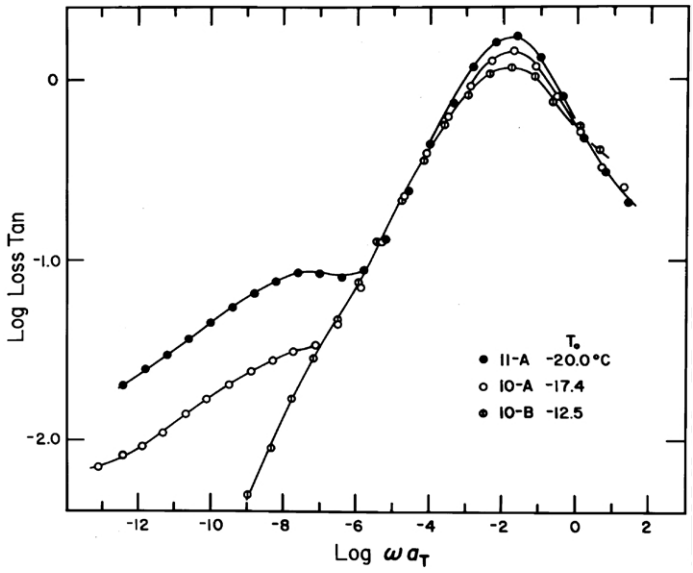

FIGURE 17 Logarithmic plot of the loss tangent against the logarithm of the reduced frequency ωa_T (s^{-1}), reduced to reference temperatures that match the positions of the primary maxima.

B. Urethane-Crosslinked Polybutadiene Elastomers (16)

Three urethane-crosslinked polybutadiene elastomers (TB-1, TB-2, and TB-3) of varying crosslinking levels, along with a similarly crosslinked styrene-butadiene copolymer (HTSBR) and two polybutadiene polymers randomly crosslinked with dicumyl peroxide (PB-1 and PB-2), have been investigated to determine their viscoelastic behavior. Elsewhere, TB-1, TB-2, and TB-3 have been designated as HTPB-1, HTPB-2, HTPB-3 respectively.

Torsional creep measurements were made on the urethane-crosslinked polybutadiene elastomers at temperatures between –68 and 25°C. The average molecular weight of a networks chain, M_c, is 3400, 5200, and 8300 for TB-1, TB-2, and TB-3 respectively. The reduced shear creep compliance $J_p(t/a_T)$ curves obtained for the three samples are shown in Fig. 18. The reference temperatures are chosen to be 7.4, 0.0, and 17.0°C for TB-1, TB-2, and TB-3 respectively so that superposition is achieved at shorter times in the primary softening dispersion. The most loosely urethane-crosslinked TB-3 has the largest $J_e = 2.5 \times 10^{-6}\,Pa^{-1}$. There is a plateau intermediate between the glassy compliance J_g (not reached in these measurements) and J_e, and its level is about $2.0 \times 10^{-7}\,Pa^{-1}$ in all three samples. The network chain density does not affect the form of the time-dependent response up to and including the intermediate plateau in the $J_p(t)$ curves. Only the terminal dispersion, i.e., the approach to J_e, is influenced. The shift factors, a_T, that were used to obtain the

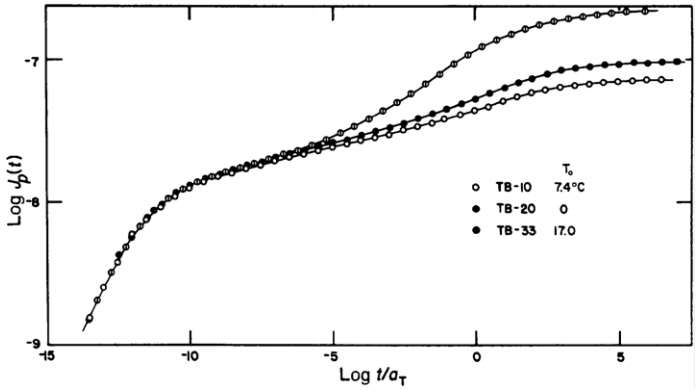

FIGURE 18 Logarithm of the reduced shear creep compliance curves $J_p(t)$ (in Pa^{-1}) for the three urethane-end linked polybutadiene elastomers displayed as a function of the logarithm of the reduced time t/a_T (in seconds). The reference temperatures of reduction are chosen so that superposition is achieved at short times in the primary softening dispersion. (○) TB-1, 74°C, (●) TB-2, 0°C, (Θ) TB-3, 17°C.

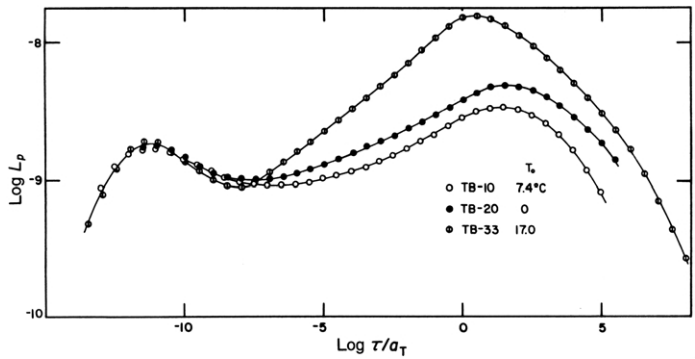

FIGURE 19 The logarithm of the reduced retardation spectrum, L_p, shown as function of the logarithm of the reduced retardation time, λ/a_T, for the three urethane-end linked polybutadiene elastomers. (○) TB-1, (●) TB-2, (Θ) TB-3. The response has been reduced to corresponding state temperatures of 74°C, 0°C, and 17°C, respectively for the primary softening transition.

reduced $J_p(t/a_T)$ curves surprisingly have the Arrhenius temperature dependence for all three samples, and not the WLF form found in the Epons and the Vitons. This departure to the Arrhenius form is attributed to the nature of the crosslinking units [16].

Reduced retardation spectra, L_p, calculated from the creep compliance $J_p(t/a_T)$ curves shown in Fig. 18, are presented logarithmically in Fig. 19 as a function of the logarithm of the reduced retardation time, λ/a_T. The chosen reference temperatures bring the short time spectral contributions together, showing the similarity between the networks of different chain density. The

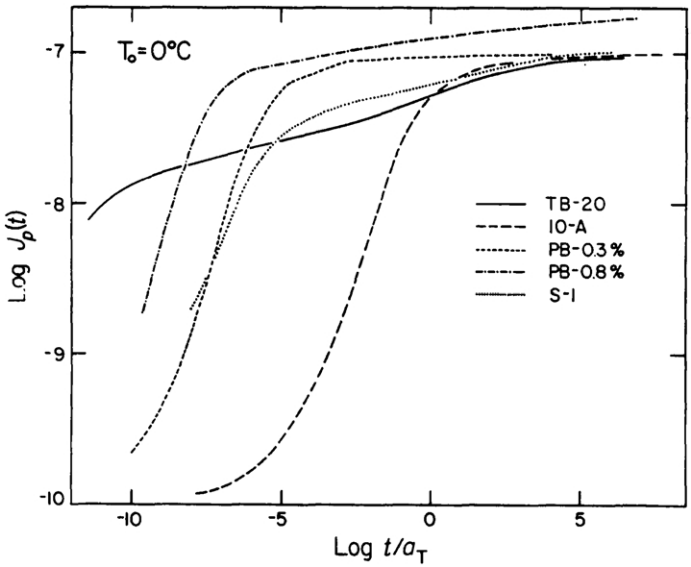

FIGURE 20 Double logarithmic plot of the reduce shear creep compliance curves $J_p(t)$ (in Pa^{-1}) as a function of the logarithm of the reduced retardation time, t/a_T, for five elastomers at $T_0 = 0°C$. Solid line (HTPB-2), long dashed line (Viton), short dashed line (PB-2), dashed-dotted line (PB-1), dotted line (HTSBR).

contributions to the terminal peak do indeed reflect the network topological differences. The more lightly crosslinked networks are markedly more dissipative at relatively longer times; i.e., in the time scale region populated by the mechanisms contributing to the long-time or terminal peak in L_p. The objective measure of the width of the plateaus seen in the $J_p(t/a_T)$ curves is the separation of the peaks in $L_p(\lambda/a_T)$. These terminal peaks and their separation from the softening dispersion peak are remarkably large (12 to 13 decades of time). Usually spectral peaks dominate half a dozen logarithmic units of the time scale, and the separation of the terminal peak from the softening peak is a strong function of the network density [1, 40]. Nevertheless, the inverse relationship of viscoelastic dissipation at long times to network density as first seen in the response of natural rubber networks [1, 41] is confirmed phenomenologically in the urethane-crosslinked polybutadiene elastomers, even if their viscoelastic spectra are not completely understood on a molecular level.

C. Comparisons Between Different Elastomers

The logarithm of the reduced shear creep compliance $J_p(t/a_T)$ of several elastomers are compared at 0°C in Fig. 20 as a function of the logarithm reduced time-scale $\log(t/a_T)$. The elastomers include (1) the urethane-crosslinked polybutadiene elastomer, TB-2, described in Subsection B; (2)

the randomly crosslinked fluorinated hydrocarbon elastomer VITON 10-A, described in Subsection A; (3) two polybutadiene elastomers, PB-1 and PB-2, randomly crosslinked with 0.8 and 0.3 g of dicumyl peroxide for 100 g of polybutadiene [16]; and (4) a styrene-butadiene copolymer [16] similar to the urethane-crosslinked polybutadiene elastomers. However, we shall not review the various viscoelastic functions measured on natural rubbers with varying levels of crosslinking [40–42]. Stress relaxation, dynamic mechanical, and creep measurements were made on the same series of natural rubber samples respectively by Thirion and Chasset [41], Ferry and coworkers [42], and Plazek [40].

The equilibrium shear compliances J_e indicated at long times are all about $1.0 \times 10^{-6}\,\mathrm{Pa}^{-1}$ except for that of the PB-1 sample, which is unexpectedly somewhat higher. The fact that the PB-1 softening dispersion is found at shorter times than that of the PB-2 elastomer has to be attributed to its higher *cis* to *trans* ratio of placements, 0.80 as opposed to 0.67, which reflects a lower T_g. The fact that the rate of creep of the VITON elastomer is approximately five orders of magnitude slower in the softening dispersion than that of the PB-2 is believed to be a reflection of a T_g that is 70°C higher. What is most unexpected is that the softening of dispersion of the urethane-crosslinked elastomers are found at surprising short times; e.g., the intermediate plateau of TB-2 is reached near $\log(t/a_T) = -12$ in spite of the fact that its T_g is some 13°C higher than that of the PB-2 material. Yet the latter's intermediate plateau is approached at about $\log(t/a_T) = -6$; some seven orders of magnitude later. Hence, the material which is further above its T_g creeps slower in the softening zone.

However, if the creep compliance curves are compared at their respective T_g's, we see in Fig. 21 that the softening dispersions are, within experimental

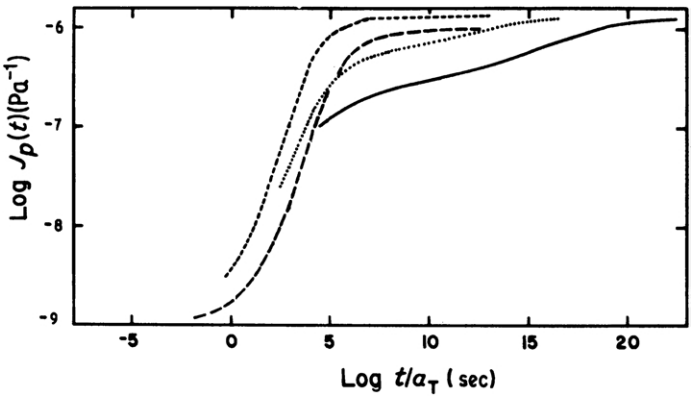

FIGURE 21 Double logarithmic plot of the reduced shear creep compliance, $J_p(t)$, as a function of the reduced retardation time, t/a_T, for four elastomers at $T_0 = T_g$. Solid line (HTPB-2), long dashed line (Viton), short dashed line (PB-2), dotted line (HTSBR).

uncertainty, at the same place in the time scale of response. Specifically, the positions of the four $J_p(t/a_T)$ curves at a compliance level of $1.0 \times 10^{-8}\,\mathrm{Pa}^{-1}$ appears to be spread on a time scale by not much more than one decade of time. Relative uncertainties of T_g values of ±1.5°C can account for this spread in positions. Until more precise relative T_g's can be measured, we can tentatively surmise that at T_g all polymers at the same rate are deep in the softening zone. This conclusion appears reasonable when one considers that short-range chain dynamics should determine both creep rates just above the glassy level as well as changes in the local liquid structure, the kinetics of which determine T_g.

Table III lists some of the parameters that characterize the physical properties of the elastomers. Comparisons of the elastomers can also be made by these parameters.

D. Other Viscoelastic Measurements

Measurements of linear and nonlinear viscoelastic behavior of elastomers have a long history. Instead of reviewing the works done in the past by various workers using different techniques, we choose to present the viscoelastic properties of elastomers through what we believe to be accurate measurements on chemically and physically well-characterized elastomers. We hope these sets of data bring out the generic viscoelastic properties of elastomers and their dependence on variables such as the crosslink density and glass temperature. There are remaining differences from one family of elastomers to another, and they should reflect the influence of other variations in molecular structure of the polymer and the crosslinking agent. Nevertheless, the reader should be aware of the previous works on the same subject. Here we can only cite some of them [40–53].

VII. THE CALCULATION OF THE TEAR ENERGY OF ELASTOMERS FROM THEIR VISCOELASTIC BEHAVIOR

At high temperatures ($T >> T_g$) and slow rates of deformation where near equilibrium deformations are involved, the nature and strength of the polymer chain backbone bonds play a determining role in the failure (tearing) of an elastomer. Lake and Thomas [54] developed a successful theory for the threshold equilibrium tear energy $\tilde{T}_0$ (Jm^{-2}), which is dependent upon the bond energy and the crosslink density of an elastomer. A compilation of such values, where most values fall between 40 and $80\,\mathrm{Jm}^{-2}$, has been presented by Gent and Tobias [55]. At practical rates and temperatures of tearing $\tilde{T}$ values are found to be orders of magnitude higher.

Smith [56], Mullins [57], and Mueller and Knauss [58] have qualitatively related the tear energy of elastomers to their time-dependent mechanical

TABLE III Physical Properties of Model Elastomers

Elastomer	ρ(25°C)	T_g °C	log G_e^b N/m^2	log G_e^c N/m^2	ν_e/V^p $\times 10^4$ cm^{-3}	M_x^d M-R	M_x^e Chem.	M_x^b Sw.	M_x^g	C_1 $\times 10^{-5}$ N/m^2	C_2 $\times 10^{-5}$ N/m^2	log 2(C_1 + C_2)	S.I.^{q}	E_0^r
TB-10	0.9577	–81^n	6.10	6.1_3	5.11	2730	3140	1860	1760	4.25	1.3	6.04	2.95	32.9
TB-20	0.9557	–80^n	5.97	6.0_0	3.69	5230	6200	2590	2370	2.2	3.0	6.02	3.18 3.19	32.9
TB-33	0.9535	–80^n	5.60	5.6_0	1.60	9700		5930	5930	1.20	1.30	5.70	4.53	14.2
PB 0.8% Di-cup 40-50-10^m	0.896	–98^k		5.7_1										
PB 0.3% Di-cup 36-54-10^m	0.904	–93^n	5.96 5.96	6.0_1	3.66 3.71	3780		2600		2.75	3.30	6.08	3.25 3.27	35.0
SBR-1 (S1)	0.962^j (0.955)^n	–65^n	5.96	5.9_0		3750	3740		2980	3.1	1.45	5.96		26.1
Viton 11A	1.837	–24.2^a	5.763	5.8_0	2.36^h			7790	7220	1.5	2.8	5.93	3.01	24.0
Viton 10A	1.833	–22.7^a	6.045	5.9_4	4.54^h			4060	5220	3.0	2.0	6.0	2.42	28.8
Viton 10B	1.830	–19.6^a	6.218	6.1_7	6.76^h			2720	3070	6.2	0	6.09	2.13	37.3

TB (or HTPB) = Hydroxy-terminated polybutadiene; encapped with toluene diisocyanate at an NCO/OH ratio of 2 to 0; extended with 1,4 butane diol and crosslinked with trimethylolpropane.
SBR-1 = Hydroxy-terminated styrene-butadiene copolymer; encapped, extended, and crosslinked as the TB.
PB = Polybutadiene crosslinked with dicumyl peroxide.
Vitons = Fluorinated hydrocarbon elastomers.
[a]DSC 10°/min by In-Chul Chay.
[b]From compression measurements on swollen samples.
[c]Estimated from compliance curve, T_0 = –20°C for Viton's, T_0 = 0°C for other elastomers.
[d]From Mooney-Rivlin C_1's.
[e]From molecular weight of the precursor.
[f]From estimate of J_e (creep).
[h]Measurements carried out by Douglas Adams and Guo-fang Gu.
[k]Estimated from the position of the primary softening dispersion on the time scale.
[m]Cis-trans-vinyl content.
[n]Measured at the Akron Polymer Science Institute, DSC cooling rates of 5°/min.
[p]Effective network chains concentration in moles/cm^3. From compression measurements. C_1 and C_2 in Pa.
[q]S.I. = swelling index = wt., swollen/wt., dry. Vitons in methyl ethyl ketone and all others in toluene.
[r]Young's Modulus from stress–strain curve.

properties. A thorough treatment of elastomeric failure is given in Chapter 10 of this book. Here we wish to show how the rate dependence of the tear energy, which is difficult to determine, can be calculated from the more easily determined creep compliance function. In doing so, all of the structure–viscoelastic property correlations that have been determined for elastomers can be utilized in the development of tougher rubbers.

The contribution of irreversible viscoelastic processes to the tearing energy at the lowest rates of deformation must arise from the slowest long-range coordinated molecular motions. As the rates of deformation are increased, the tearing energy must increase monotonically as faster, shorter-range motions become involved in the advancing tear tip.

Since the distribution function of retardation times (the retardation spectrum L) is a measure of the population of viscoelastic mechanisms along the time scale [17], one of the simplest propositions for obtaining the tear energy $\tilde{T}(C)$ from a material's viscoelastic behavior would be

$$\tilde{T}(C) = f_1 \int_{+\infty}^{c_1/C} L(\ln \lambda) d \ln \lambda \tag{34}$$

where f_1 and c_1 are proportionality constants and C (m/sec) is the rate of tearing. It has been assumed that $c_1/C = \gamma^{-1}$ (sec), where γ is the elongational strain at the tip of the tear. However, there is no a priori reason to expect that all of the viscoelastic mechanisms are equally effective in contributing to the tear energy. Results from the application of Eq. (1) indicate that this is not so. The simple integration over L results in proportional increases of the calculated $\tilde{T}$ at relatively short times (or high rates) that are too small. A weighting function is needed to increase the influence of mechanisms found near the foot of the softening dispersion; see following text.

The best predictive equation that has been found for the tear energy $\tilde{T}(C)$ is

$$\tilde{T}(C) = k f_1 \int_{+\infty}^{c_1/C} L(\ln c_2 \lambda) \left[1 + c_3 \exp(c_4 \ln c_2 \lambda - c_5)^2\right] d \ln \lambda \tag{35}$$

where:

c_1 scales the tear rates to strain rates,
c_2 adjusts the retardation time-scale to the tear-rate scale,
c_3 determines the weighting function magnitude,
c_4 determines the weighting function width,
c_5 determines the location of the weighting function, which depends on the short-time peak location,
f_1 is the primary scaling factor, and
k is a factor depending on the equilibrium compliance of the elastomer which equals $(5.0 - \log J_e)$.

Efforts to optimize the fits of the results calculated from Eq. (35) with temperature-reduced tear energy data yielded $c_1 = 1000$; c_2, 100; c_3, 10; c_4, 0.020; and f_1, 7.5×10^9 for all of the elastomers tested. c_5 varies from polymer to

polymer as shown in Table IV where the characteristics of the elastomers studied are presented. c_5 values were determined by fixing the peak of the weighting function to be 5.0 logarithmic units to longer times than the short-time peak of $L(\ln \lambda)$. Equilibrium compliances and threshold tear energies are also shown in Table IV.

The widely varying retardation spectra of four of the network polymers that have been discussed above are shown in Fig. 22 at their respective T_g's.

TABLE IV Material Characterization Constants of Some Model Elastomers

Epon 28-1 is a Shell Epon 828 resin crosslinked with a stoichiometric amount of methylene dianiline, MDA. The other elastomers are identified in Table III.

Elastomer	$T_{f,g}$, °C	$\log J_e$, Pa^{-1}	$\tilde{T}_e$, J/m^2	ρ (25°C), g/cm^3	M_x	C_5
HTPB-1	–79	–6.14	45	0.9577	1760	25.56
HTPB-2	–79	–6.01	50	0.9557	2370	25.24
HTPB-3	–79	–5.63	60	0.9535	5930	23.35
HTSBR-1	–65	–5.95	60	0.955	2980	25.42
Viton 10B	–17	–6.19	45	1.830	3070	26.53
Viton 10A	–19	–5.98	55	1.833	5220	23.35
Viton 11A	–22	–5.85	75	1.837	7220	23.12
PB (0.3%)	–93	–5.99	45	0.904	2600	24.92
Epon 28-1	164	–7.21	10	1.194	270	29.48

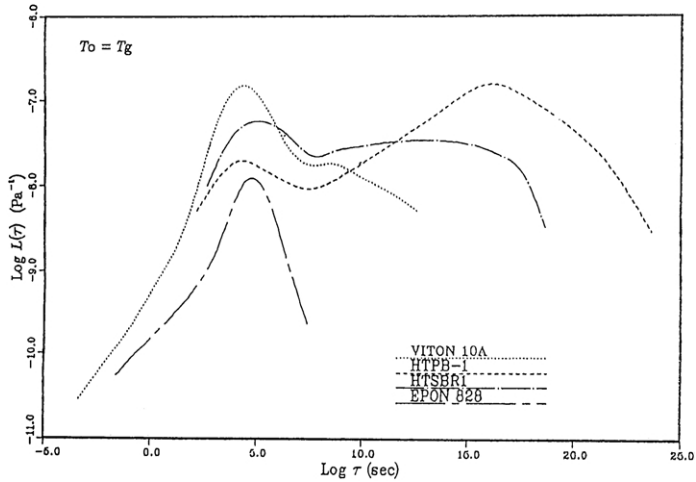

FIGURE 22 Double logarithmic plot of the retardation spectra, $L(\ln \lambda)$ (in Pa^{-1}) for four crosslinked polymers, as indicated, against the retardation time λ (sec). The reference temperature T_0 is T_g for all the materials.

Their short-time behavior is similar, but enormous differences are seen at long reduced-times λ/a_T. The epoxy resin Epon 828 fully cured with a stoichiometric amount of 4.4-mehylene dianiline has the tightest molecular network, $M_x = 270$, which exhibits a single narrow maximum in $L(\lambda)$ and no long-time mechanisms. The fluorinated hydrocarbon elastomer Viton 10A has a substantially looser network M_x and hence a much greater primary maximum in $L(\lambda)$ reflecting a much greater J_e. A slight long-time maximum is seen, indicating that the mesh is loose enough to allow contributions arising from adjustments of the entanglement network. Many very long-time mechanisms are seen in the response of the isocyanate crosslinked hydroxy terminated butadiene and styrene-butadiene copolymer, which reflect the presence of an intermediate plateau in $J(t)$. This behavior has not been seen in other elastomers and is not understood. Microphase separation may be involved, but no evidence has been obtained for this speculation. However, the presence of the population of extremely long-time mechanisms, according to the hypotheses giving rise to Eq. (35), should require large tearing energies at very tearing rates. Indeed, the results of the integration over the weighted $L(\lambda)$'s from long to short times are shown in Fig. 23, and the agreement between the calculated lines and the measured data points is encouraging.

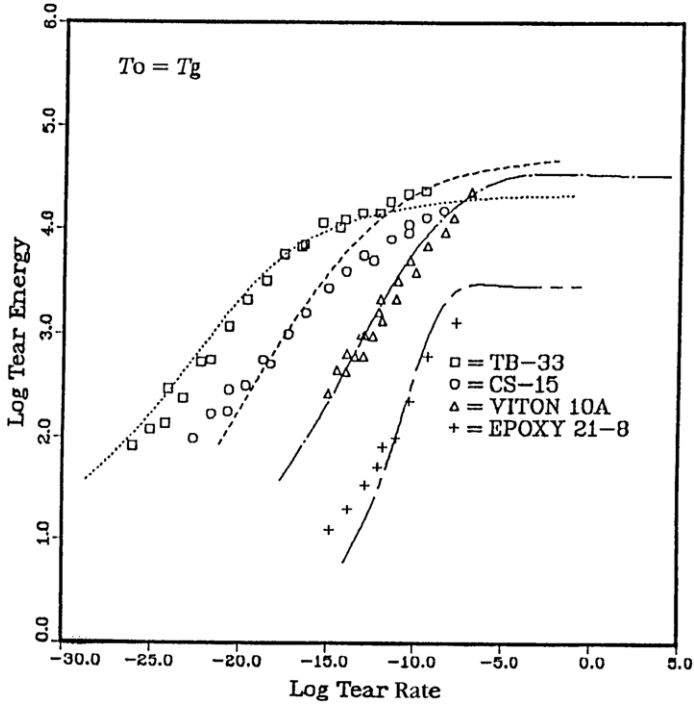

FIGURE 23 The measured (data points) and calculated [line from Eq. (35)] tear energy curves for four amorphous crosslinked materials as indicated in the key. $T_0 = T_g$.

VIII. THEORETICAL INTERPRETATION OF VISCOELASTIC MECHANISMS AND ANOMALIES

A. Breakdown of Thermorheological Simplicity of Low Molecular Weight Polymer

Rubber is a viscoelastic solid formed by crosslinking a polymer, which is initially a viscoelastic liquid. In spite of this difference there still are some common issues in the physics of the glass temperature and the viscoelastic mechanisms in the softening dispersion (i.e., called the glass-rubber transition zone in Ferry [1]. A case in point can be taken by comparing the viscoelastic behavior of the neat epoxy resin Epon 1001F [14] with that of the fully cured network Epon 1001F/DDS discussed in Section V. The glass temperature T_g of Epon 1000F is 31°C, which is significantly lower than the value of 127°C of the fully cured Epon 1000F/DDS. The increase in the T_g in going from the oligomer to the rubber can be rationalized (at least in part) by the decrease in the specific volume, which can be inferred by comparing Figs. 4 and 5. However, it is not so easy to understand the difference in the temperature dependence of the softening dispersion of the two materials. As shown previously in Figs. 6–8, the reduced shear compliance curves $J_p(t)$ measured at different temperatures of Epon 1001F/DDS were reduced to a common curve $J_p(t/a_T)$ at a reference temperature T_o. This thermorheological simplicity of the softening dispersion of Epon 1001F/DDS was not found in neat Epon 1001F. The shear viscosity η was determined in the temperature range 30 to 77°C. The recoverable shear compliance $J_r(t)$ (defined by Eq. [1]) was obtained at nine temperatures from 30.2 to 53.5°C as presented in Fig. 24.

The steady-state recoverable shear compliance $J_s = \lim_{t\to\infty} J_r(t)$ shows a strong temperature dependence. A dramatic 10-fold decrease of J_s is seen in Fig. 24 to occur with a 20°C decrease in temperature toward T_g. Consequently, the $\log J_r(t)$ curves cannot be reduced to a common curve. The thermorheological complexity exhibited by neat Epon 1001F is similar to that found in many other low molecular weight polymers [18, 19, 37, 59, 60–67]. A good example is the low molecular weight polystyrene of 12,300 molecular weight chosen for comparison because J_s at high temperatures is about the same as neat Epon 1001F. The $J_r(t)$ data of this nearly monodisperse polystyrene sample are shown in Fig. 25. The decrease of J_s when temperature is lowered to approach T_g is quantitatively similar in the two cases. This anomalous but general viscoelastic behavior of low molecular weight polymers certainly contradicts the assumption that the relaxation times of all relaxation mechanisms or modes simply shift along the logarithmic time-scale and are proportional to the monomeric friction factor ζ_o [1]. This assumption, if correct, would mean that the polymer was thermorheologically simple, which is clearly not the case. It should be of fundamental interest in the study of the dynamics of polymers. Unfortunately, possibly because of the difficulty of finding an explanation, it

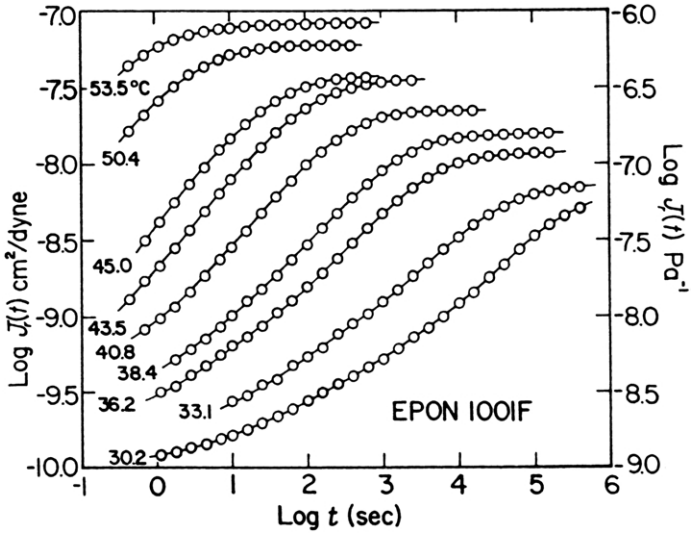

FIGURE 24 Logarithmic presentation of the recoverable shear compliance $J_r(t)$ of Epon 1001F as a function of the logarithm of time t at nine temperatures as indicated. Dramatic loss of long-time viscoelastic mechanisms is evident when temperature is decreased toward T_g.

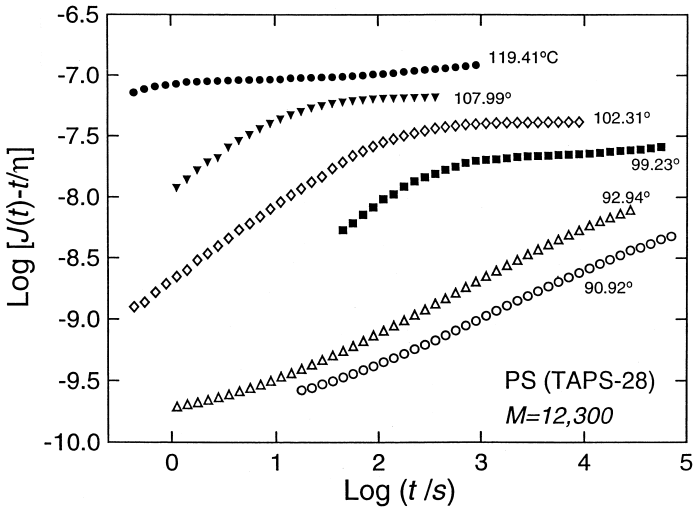

FIGURE 25 Logarithmic presentation of the recoverable shear compliance $J_r(t)$ of a nearly monodisperse polystyrene sample with molecular weight of 12,300 as a function of the logarithm of time t at six temperatures as indicated. Dramatic loss of long-time viscoelastic mechanisms is evident when temperature is decreased toward T_g.

seems to have been ignored in the development of polymer viscoelasticity in the past few decades.

1. The Coupling Model

As far as we know, at present only one explanation has been given for the breakdown of thermorheological simplicity in low molecular weight polymers [18, 19, 61, 68, 69], and that is based on the coupling model [70–77]. It is beyond the scope of this chapter to review in detail this model and the explanation it provides. A brief description of the essential points is given here. The segmental relaxation responsible for "structural relaxation" and the glass behavior moderated by molecular crowding and interaction is a cooperative process involving complex time-dependent motions of many molecules. Although all local segments attempt configurational rearrangements with primitive rate, $\tau_{0\alpha}^{-1}$, and primitive relaxation function,

$$\phi(t) = \exp(-t/\tau_{0\alpha}) \tag{36}$$

not all attempts can be successful due to constraints arising from intermolecular interaction or coupling between the local segments. The initially successful (unsuccessful) ones are appropriately called the fast (slow) local segmental motions. Since the many-molecule dynamics are stochastic, at some later time the fast (slow) motions become slow (fast). Immediate parallel consequences of such complex many-molecules dynamics are: (1) it takes more decades of time for the segmental relaxation to complete its course (time-scale stretching) and the characteristic relaxation time of the relaxation, τ_α, is much longer than $\tau_{0\alpha}$. (2) The relaxation process is dynamically heterogeneous, meaning that at any time there are fast and slow moving molecules and they exchange roles over the time scale, τ_α, of the entire segmental (α) relaxation process [72, 78]. The Kohlrausch's [79] correlation function,

$$\phi(t) = \exp\left[-(t/\tau_\alpha)^{1-n}\right] \tag{37}$$

where the exponent, $(1 - n)$, is a fraction of unity, and τ_α is a characteristic segmental relaxation time, is perhaps one of the functions with the least number of parameters that stretch the course of the segmental relaxation over a number of decades. The time-scale stretching increases with n. Slowing down implies that $\tau_\alpha >> \tau_{0\alpha}$. A priori the relation between τ_α and $\tau_{0\alpha}$ is unknown. However, the coupling model provides a relation between these two relaxation times. At sufficiently short times, primitive relaxation prevails and proceeds unimpeded. It is only after some rather well defined time, t_c, that the many-molecule dynamics slows down the relaxation. Hence the correlation function is Eq. (36) for $t < t_c$, and crossover to Eq. (37) for $t > t_c$, smoothly within a small neighborhood of t_c. The crossover time t_c is temperature independent, and its value is determined by the intermolecular interaction poten-

tial. For polymers $t_c \approx 2 \times 10^{-12} s$ [76, 77, 80]. This crossover is expected on theoretical grounds [70, 72, 73], borne out by rigorous results of simple models [74, 75], and supported by experimental data [77, 80, 81]. Taking advantage of this general crossover property of the correlation function and requiring quasi-continuity of its two parts at t_c, we have the relation,

$$\tau_\alpha = [t_c^{-n} \tau_{0\alpha}]^{1/(1-n)} \tag{38}$$

between the two relaxation times via the "coupling parameter" n, which appears in the fractional exponent of the Kohlrausch correlation function [Eq. (37)]. This relation has been used to explain the anomalous properties of τ_α, due to the complex many-molecule dynamics, from the corresponding normal and transparent properties $\tau_{0\alpha}$ of a simple independent relaxation [18, 77, 81].

In polymers having no side-group, the appearance of a secondary relaxation at higher frequencies than the segmental relaxation is intriguing. Examples include polybutadiene (PB) and even polyisoprene (PI). The existence of a secondary relaxation in PB has been well known [82, 83], but in PI it was found only recently [84]. The dielectric relaxation data of PB and PI showing both the segmental relaxation and the secondary relaxation is presented in Figs. 26 and 27. Equally intriguing is the appearance of secondary relaxation in rigid small molecular glass-formers such as toluene and chlorobenzene

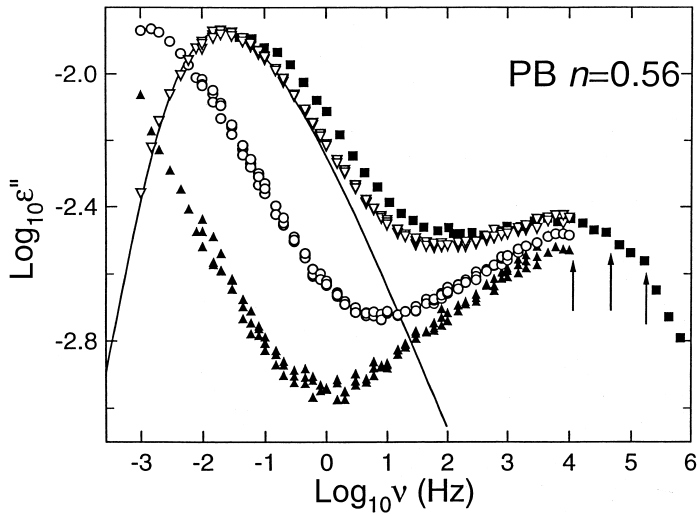

FIGURE 26 Isothermal dielectric loss data of 1,4 polybutadiene that show resolved Johari-Goldstein relaxation in the supercooled liquid state above T_g. Representative KWW fit to the α-relaxation peak are shown as line. The value of n so determined is given in the figures. Each vertical arrow pointing toward certain data taken at some temperature indicates the location of the independent relaxation frequency, $\nu_{0\alpha} = 1/2\pi\tau_{0\alpha}$, where $\tau_{0\alpha}$ is calculated using Eq. (38). ▲, ○, ▽, ■, are data taken at –97.5, –95, –92.5, and –91.2 C, respectively.

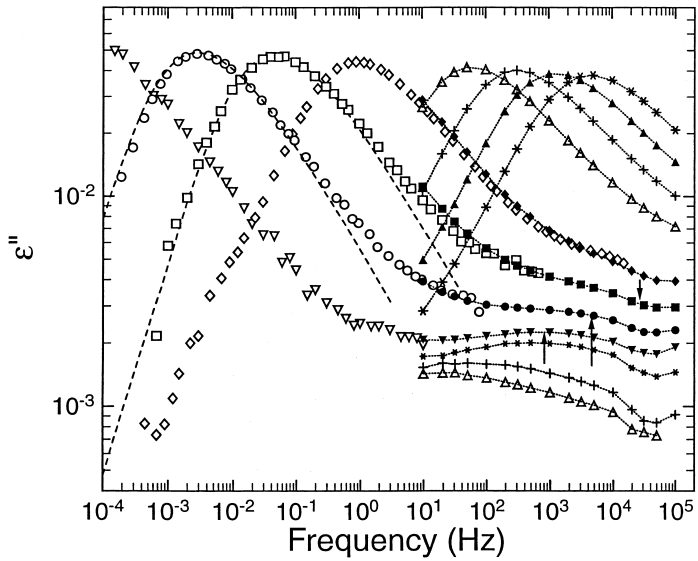

FIGURE 27 Dielectric loss spectra of PI. The data at 216.0 K (◇), 211.15 K (□), 208.15 K (○), and 204.15 K (▽) were obtained using the IMass Time Domain Dielectric Analyzer. All the other data, which start at 10 Hz and continue up to 100 kHz, were taken with the CGA-83 Capacitance Bridge. There is good agreement of the CGA-83 data at 216.7 K (◆), 212.7 K (■), 208.7 (●), and 204.7 K (▼) with the IMass data at 216.0 K (◇), 211.15 K (□), 208.15 K (○), and 204.15 K (▽) respectively, after the latter have been shifted horizontally by an amount determined from the VFTH temperature dependence of the α-relaxation frequency, in order to account for the slight differences in temperature. The other eight spectra were obtained only using the CGA-83. The spectra that show α-loss maxima correspond (from right to left) to T = 236.7 (*), 232.7 (▲), 228.7 (+), and 224.7 K (△). The lower three CGA-83 curves, which show β-loss peaks, were taken (starting from the bottom) at 169.7 (△), 181.7 (+), and 200.7 K (*). The vertical arrows mark the locations of the calculated primitive relaxation frequencies, $\nu_{0\alpha} = 1/2\pi\tau_{0\alpha}$, at (from right to left) 212.7 K (■), 208.7 K (●), and 204.7 K (▼). The locations of these $\nu_{0\alpha}$ should be compared with the secondary relaxation peaks at these temperatures.

[85–87]. Because there is no internal degree of freedom these secondary relaxations must originate from some local motion of the entire molecule. Such secondary relaxations are of the Johari-Goldstein (JG) kind [85–87]. They are supposedly universal, existing in all glass-formers, and are considered to be the precursor of the primary structural relaxation. Some criteria for distinguishing JG relaxation from other garden variety of secondary relaxations have been established based on the close relationship of its properties with the primary relaxation [87]. The primitive or independent relaxation of the coupling model [Eq. (36)] is the precursor of the cooperative (i.e., intermolecularly coupled) α-relaxation [Eq. (37)], and it entails the motion of all parts of the molecule, but is a local process. Thus these attributes of the primitive relaxation are shared with the JG relaxation, and it can be expected that the independent relaxation time, $\tau_0\alpha$, is approximately located near the most probable

relaxation time τ_β of the JG relaxation at all temperatures T and pressures P. The relation complementary to Eq. (38), $\tau_{0\alpha} = (t_c)^n(\tau_\alpha)^{1-n}$, enables $\tau_{0\alpha}$ to be calculated from τ_α and n in the Kohlrausch function, Eq. (37), that fits the time dependence of the α-relaxation. For polymers and small molecular liquids t_c has the approximate value of $2 \times 10^{-12} s$. Remarkably,

$$\tau_{0\alpha}(T, P) \approx \tau_\beta(T, P) \tag{39}$$

is found to hold quantitatively in many glass-formers [87–91]. The correspondence between the two relaxation times is illustrated in Figs. 26 and 27 for PB and PI. The universal JG relaxation brings the primitive relaxation of the coupling model to life.

It is particularly interesting to point out that the JG relaxation was found in the uncrosslinked Epon 828 and its relaxation time τ_β is in good agreement with $\tau_{0\alpha}$ [87, 91].

The relaxation strength, $\Delta_{\varepsilon\beta}$, of the JG relaxation [92] in all these glass-formers is found to change on heating through the glass transition temperature in a similar manner as the changes observed in the enthalpy H, entropy S, and volume V. The derivative of $\Delta_{\varepsilon\beta}$ with respect to temperature, $d\Delta_{\varepsilon\beta}/dT$, is raised from lower values at temperatures below T_g to higher values at temperatures above T_g, mimicking the same behavior of the specific heat C_p and the expansion coefficient, which are the derivatives dH/dT and dV/dT respectively [92]. The angle of rotation of the JG relaxation, and hence $\Delta_{\varepsilon\beta}$, is likely dependent on the specific volume and entropy. Thus the rate of change of $\Delta_{\varepsilon\beta}$ with temperature is similar to the thermodynamic quantities. Moreover, although the relaxation time τ_β of all β-relaxations including the JG kind has Arrhenius temperature dependence in the glassy state, the actual temperature dependence of τ_β at temperatures above T_g at equilibrium volume is not a continuation of the Arrhenius temperature dependence below T_g. It is more like another VFTH temperature dependence that is weaker than that of τ_α. [93–95]. The fact that τ_β has another VFTH temperature dependence above T_g is consistent with Eqs. (38) and (39) because the temperature dependence of $\tau_{0\alpha}$ calculated by Eq. (38) from the VFTH temperature dependence of τ_α is non-Arrhenius.

It is remarkable that the relaxation strength $\Delta_{\varepsilon\beta}$ as well as the relaxation time τ_β of the JG relaxation show changes at T_g, in spite of the fact that the fast JG relaxation has transpired long before the slow α-relaxation. These properties suggest that the JG relaxation senses the specific volume V (or free volume fraction f) and/or entropy S (or configurational entropy S_c). In particular, the friction coefficient of τ_β is dependent on $V(f)$ and/or $S(S_c)$. Because of the correspondence between the two relaxation times [Eq. (39)], the same conclusion can be made on the friction coefficient of $\tau_{0\alpha}$.

2. Explanation of Thermorheological Complexity

With the help of the JG relaxation, we have deduced in the previous section that the primitive local segmental relaxation time $\tau_{0\alpha}$ or its friction

coefficient depends on the specific volume V (or free volume fraction f) and/or entropy S (or the configurational entropy S_c). Since the primitive relaxation as well as the JG relaxation is a local process involving the entire monomer, fittingly their friction coefficient can be identified as the monomeric friction coefficient ζ_o [1], i.e.,

$$\tau_{0\alpha} \propto \zeta_0 \tag{40}$$

We hasten to point out that in the literature [1] ζ_o is commonly associated with the friction coefficient of τ_α and the relaxation times of all other longer time viscoelastic mechanisms (e.g., the entire relaxation or retardation spectrum). This common association of ζ_o with τ_α is not used in the coupling model (CM), which instead identifies ζ_o as the friction coefficient of $\tau_{0\alpha}$ [18, 59–61, 65, 68, 69], although the dependences of ζ_o on V (f) and/or S (S_c) are retained.

The whole purpose of the CM is to take intermolecular coupling of the local segmental relaxation into account, and in the process transform $\tau_{0\alpha}$ to τ_α. It follows from Eqs. (38) and (40) that

$$\tau_\alpha \propto [\zeta_0]^{1/(1-n)} \tag{41}$$

The exponent, $1/(1 - n)$, is larger than one. Hence τ_α has a stronger dependence on V (f) and/or S (S_c), and on temperature and pressure, than $\tau_{0\alpha}$ or τ_β.

The softening dispersions of entangled low molecular weight polymers are often modeled by the Rouse modes modified for undiluted polymers [1]. From their very definition only involving the coordinates of a single chain, the Rouse modes are not intermolecularly coupled, and their relaxation times, τ_{Ri}, are proportional to the monomeric friction coefficient ζ_0 [18], i.e.,

$$\tau_{Ri} \propto \zeta_0 \tag{42}$$

Thus the relaxation time τ_α of the segmental relaxation has stronger temperature dependence than τ_{Ri} of the Rouse modes in the softening dispersion, albeit the former is shorter than the latter. This difference in temperature dependence immediately explains the breakdown of thermorheological simplicity of low molecular weight polymers (see Figs. 24 and 25) [19, 37, 61]. It also leads to an explanation of the observed decrease of J_s when temperature is decreased toward T_g, which was given by Ngai, Plazek, and Bero [69].

The disparity between the temperature dependences of τ_α and τ_{Ri} [Eqs. (41) and (42)] depends on the size of the coupling parameter n. Polystyrene has a larger n (= 0.63) than polyisobutylene (= 0.45) [19, 96, 97]. Hence we expect the degree of breakdown of thermorheological simplicity is lesser in polyisobutylene (PIB) than polystyrene (PS). This expectation, as well as other predicted differences in viscoelastic properties of PIB and PS, were confirmed

by experiments [68, 69]. When a low-T_g diluent is added to PS, the severity of intermolecular coupling in neat PS is mitigated, and the coupling parameter n is decreased. Consequently, in solutions of PS there is lesser breakdown of thermorheological simplicity, and the decrease of the steady state compliance J_s with falling temperature is suppressed. These changes in viscoelastic behavior from neat PS to solutions of PS was found experimentally [98], and the viscoelastic spectrum of PS in solution resembles that of PIB [99]. Later we shall discuss the dynamics of junctions in crosslinked polymers and its changes upon addition of a diluent (swelling). The junction dynamics are also well described by the coupling model, and are characterized by the junction coupling parameter, n_J [100, 101]. Decrease of n_J on dilution was found in the experimental data of junction dynamics [100, 101], in analogy to the change in segmental dynamics of PS upon addition of a diluent.

B. Thermorheological Simplicity of Elastomers

In contrast to the starting neat Epon 1001F (see Fig. 24), the reduced shear compliance curves $J_p(t)$ of elastomer Epon 1001F/DDS were successfully in reduction to a well-defined common curve $J_p(t/a_T)$ at a reference temperature T_o (see Figs. 6–8). The thermorheological complexity and the strong decrease of J_s on lowering temperature found in neat Epon 1001F are absent in Epon 1001F/DDS. Such a change of viscoelastic properties upon crosslinking a polymer is explained as follows.

The polymer strands in Epon 1001F/DDS are tied at both ends to crosslinkers, and obviously their relaxation cannot be modeled by the Rouse modes. Furthermore, the crosslink junctions of a network are highly constrained. These constraints give rise to intermolecular coupling of the junction motions. As shown in section D to follow, the junction dynamics are well described by the coupling model with the Kohlrausch stretched exponential correlation function, $\exp[-(t/\tau_J)^{1-n_J}]$ with a sizeable coupling parameter n_J [100, 101]. τ_J is the slowed-down junction relaxation time cause by intermolecularly coupling. In analogy to Eq. (38) for segmental relaxation, τ_J is related to its primitive junction relaxation time τ_{0J} by

$$\tau_J = \left[t_c^{-n_J}\tau_{0J}\right]^{1/(1-n_J)} \tag{43}$$

In the coupling model all primitive relaxation times, including $\tau_{0\alpha}$ and τ_{0J}, are proportional to the monomeric friction coefficient ζ_0. Hence from Eq. (43) the temperature dependence of τ_J depends on n_J and is given by

$$\tau_J \propto [\zeta_0]^{1/(1-n_J)} \tag{44}$$

Since the junctions are intermolecularly coupled and have significantly large n_J, so is the longer length scale modes i of the polymer strands anchored on

both ends to the junctions, which now have nonzero coupling parameters n_i, and obviously they cannot be modeled by Rouse modes. The temperature dependences of their relaxation times, $\tau_i \propto [\zeta_0]^{1/(1-n_i)}$, is no longer that different from τ_α because n_i is comparable to n_J and n. Thus thermorheologically complexity of the viscoelastic response of crosslinked networks is minimized and cannot be detected by time–temperature superpositioning.

Intuitively, junctions are expected to be more effective in constraining viscoelastic mechanisms having larger length scales (i.e., longer wavelengths and retardation times). The largest effect should occur for the mode whose length scale corresponds to the molecular weight between crosslinks, M_x, which is responsible for the equilibrium compliance of the network. We now examine this by analyzing once more the creep compliance data of the series of fully cured epoxy resins. To facilitate the comparison of the modes of the chain between crosslinks, we subtract off J_g from each of the reduced creep compliance $J_p(t)$ data of Epon 828F/DDS, 1001F/DDS, 1004F/DDS, and 1007F/DDS. The difference $(J_p(t) - J_g)$ is plotted against reduced time in Fig. 28. For compliance levels up to approximately $4\,\mathrm{GPa}^{-1}$, $(J_p(t) - J_g)$ has a power law form, and is entirely due to segmental motion. Note that this power law behavior is consistent at short times with the stretched exponential form,

$$J_P(t) - J_g = \Delta J_\alpha \left[1 - \exp(-t/\tau_\alpha)^{1-n}\right] \tag{45}$$

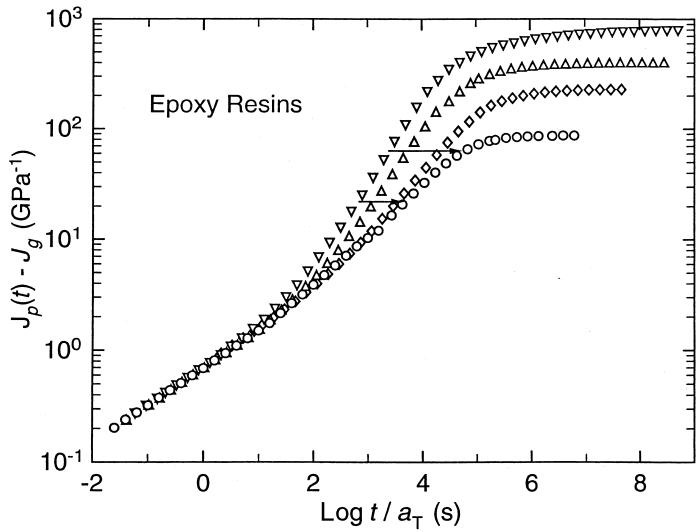

FIGURE 28 Comparison of the $[J_p(t) - J_g]$ curves as a function of the reduced retardation time, t/a_T, of fully cured Epon 828/DDS (O), 1001/DDS (◊), 1004/DDS (△), and 1007/DDS (▽). The shift factors and reference temperature for Epon 828/DDS are identical to the values used in Fig. 8. For the other three elastomers, horizontal shifts of –0.72, –1.18, and –1.5 have been applied to superimpose the data in the short time regime associated with segmental relaxation.

found for the compliance contributed by the segmental retardation of several polymers [61, 96, 98, 102] with ΔJ_α about $4\,\mathrm{GPa}^{-1}$. Values of $(J_p(t) - J_g)$ higher than about $4\,\mathrm{GPa}^{-1}$ are contributed by viscoelastic modes having length scales larger than that of the segmental motion. For networks, the longest length scale of viscoelastic modes is determined by M_x. In Fig. 28, the shift factor and the reference temperature for the 828/DD are identical to that used in Fig. 8. For the other three epoxies, additional horizontal shifts have been applied to superpose their power law regime with that of 828/DDS. Thus, at the revised reference temperatures, all networks have the same segmental retardation time.

The viscoelastic responses of the four networks can now be compared. One obvious difference between them is the decrease of the equilibrium compliance with decrease of M_x, a consequence of the elimination of longer length scale viscoelastic modes. More subtle is the shift of the viscoelastic modes contributing at the same compliance level toward longer times when the crosslink density is increased. The magnitude of the shifts are not uniform, but increases with the compliance (or equivalently the length scale of the viscoelastic modes). The two horizontal arrows in Fig. 28 illustrate this trend. This behavior is readily explained by the coupling model as follows. Viscoelastic mode i of a fixed length scale is more constrained (and hence has a larger coupling parameter n_i) in the tight 828/DDS network than in the loose 1007F/DDS network. It follows from the coupling model relation, $\tau_i \propto [\zeta_0]^{1/(1-n_i)}$, that τ_i in 828/DDS is more sensitive to temperature change than it is in 1007F/DDS.

C. Changes of the Segmental Relaxation Time and the Johari-Goldstein Relaxation Time with Crosslink Density

We have pointed out at the end of Section VIII.1 that the JG relaxation was found in the uncrosslinked Epon 828, and its relaxation time τ_β is in good agreement with $\tau_{0\alpha}$. We have also discussed that the coupling parameters n of the segmental relaxation of the repeat units near the junctions are comparable to the coupling parameter n_J of the junctions (see Section D to follow). As a result there is an increase of the average n of the segmental relaxation with the increase of crosslink density. From Eq. (38), such increase of n gives rise to concomitant increase of the segmental relaxation time τ_α and hence the glass temperature T_g, which experimentally is indeed the case. On the other hand, $\tau_{0\alpha}$ is unchanged if the crosslink density is not too high to have an effect on the specific volume and configurational entropy. We expect then from $\tau_{0\alpha}(T) \approx \tau_\beta(T)$ [Eq. (39)] that, on crosslinking Epon 828, the JG relaxation time should not differ much from that found in neat Epon 828, while τ_α and the glass temperature increases significantly. Isochronal [103] and isothermal [104] dielectric relaxation data of Epon 828 have found that indeed τ_β changes little and have about the same Arrhenius temperature dependence, while T_g increases significantly with time of curing. At T_g, τ_α is the same for all samples

by definition, but the separation distance, $\log[\tau_\alpha(T_g)] - \log[\tau_\beta(T_g)]$, increases with curing time [103, 104]. This trend is predicted by the coupling model through Eq. (38), which shows the increase of $\log[\tau_\alpha(T_g)] - \log[\tau_{0\alpha}(T_g)]$ with n caused by increasing crosslink density, and $\tau_{0\alpha}(T_g) \approx \tau_\beta(T_g)$ [Eq. (39)].

D. Junction Dynamics

1. Experimental Data

The relaxation dynamics of junctions in polymer networks have not been well-known until the advent of solid-state ^{31}P NMR spin-lattice relaxation measurements in a series of poly(tetrahydrofuran) networks with tris(4-isocyanatophenyl)-thiophosphate junctions [100]. The junction relaxation properties were studied in networks with molecular weights between crosslinks, M_c, ranging from 250 to 2900. The dominant mechanism for ^{31}P nuclear spin lattice relaxation times measured over a wide range of temperatures were fit satisfactorily by spectral density functions, $\hat{J}(\omega)$, derived from the Fourier transforms of the Kohlrausch stretched exponential correlation functions

$$C_J(t) = \exp\left[-(t/\tau_J)^{1-n_J}\right] \tag{46}$$

where τ_J and n_J are the junction correlation time and coupling parameter respectively. In the temperature range of measurements high above T_g [100], τ_J was appropriately assumed to have an Arrhenius temperature dependence of

$$\tau_J = \tau_\infty^* \exp\left(E_a^*/RT\right) \tag{47}$$

From these fits Shi *et al.* [100] obtained the coupling parameter n_J, the pre-exponential factor τ_∞^*, and the activation enthalpy E_a^* for the series of networks of different crosslink densities as well as a swollen sample (Fig. 29).

2. Coupling Model Explanation [101, 105]

n_J was found to increase with crosslink density and decrease with addition of a solvent at constant crosslink density [100]. These trends of n_J are in accord with the interpretation of n_J as the coupling parameter because of the increase of intermolecular constraints with the density of crosslinks. There is a significant increase of the activation enthalpy E_a^* with higher crosslink density, which is compensated by a concomitant decrease of the pre-exponential factor τ_∞^*. On the other hand, on swelling the polymer network with M_c = 650, E_a^* decreases while τ_∞^* increases. The experimental data on n_J, E_a^*, and τ_∞^* of the networks are summarily shown in Figs. 30 and 31.

The Arrhenius temperature dependence of τ_J implies the same for the primitive relaxation time of the junction, τ_{0J}, which is written out explicitly as

$$\tau_{0J} = \tau_\infty \exp(E_a/RT) \tag{48}$$

The relation between τ_J and τ_{0J}, the counterpart of Eq. (38), has been given by Eq. (43). The latter spawns two separate relations,

$$E_a^* = E_a/(1-n_J) \tag{49}$$

and

$$\tau_\infty^* = [t_c^{-n_J}\tau_\infty]^{1/(1-n_J)} = \tau_\infty[\tau_\infty/t_c]^{n_J/(1-n_J)} \tag{50}$$

These expressions qualitatively explain the experimentally observed increase of E_a^* and decrease of τ_∞^* with crosslink density through the increase of n_J. Quantitatively one can calculate E_a and τ_∞ by Eq. (49) and Eq. (50) respectively from the experimental values of n_J, E_a^*, and τ_∞^* for each network, and $t_c = 2 \times 10^{-12} s$ [106]. The calculated values of E_a and τ_∞, shown in Fig. 30 and Fig. 31 respectively, are roughly constant ($E_a \approx 27$ kJ/mol and $\tau_\infty \approx 10^{-14} s$), indicating that all the crosslink junctions have about the same mobility had their motion not been slowed down by intermolecular coupling to various degrees depending on the crosslink density. The nearly constant $E_a \approx 27$ kJ/mol can be interpreted as some barrier enthalpy and $\tau_\infty \approx 10^{-14} s$ as the reciprocal of some reasonable attempt frequency.

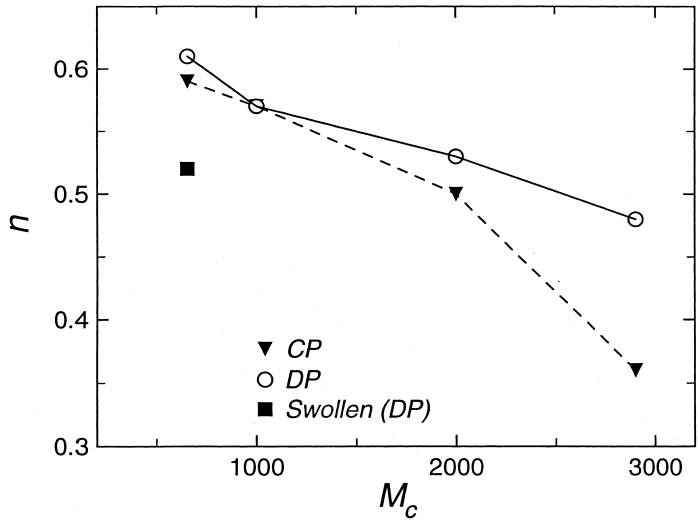

FIGURE 29 Plot of the coupling parameter of junction dynamics n_J determined from experimental data by Shi *et al.* [100] for four polymer networks with different molecular weights between crosslinks, M_c. Solid inverted triangles and open circles are from ^{31}P NMR data taken using cross (CP) and direct (DP) polarization, respectively. The solid square is for a swollen sample with $M_c = 650$. The lines are drawn to guide the eyes.

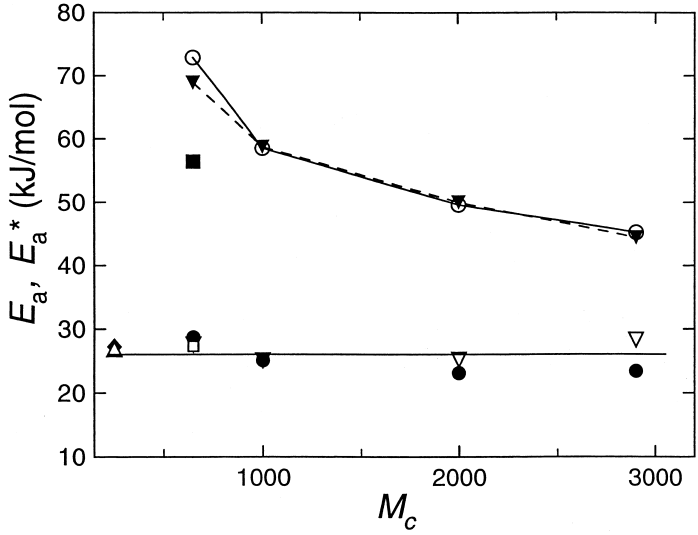

FIGURE 30 Solid inverted triangles and open circles are the apparent activation enthalpy E_a^* obtained from ^{31}P NMR data taken using cross (CP) and direct (DP) polarization, respectively [100]. The solid square is E_a^* for a swollen sample with $M_c = 650$. The open inverted triangles and solid circles are E_a calculated by Eq. (49) from E_a^* and n_J for the cross (CP) and direct (DP) polarization experiments, respectively. The open square is E_a calculated from E_a^* and n_J for the swollen sample. The solid diamond and open triangle are E_a determined directly from experiment for sample with $M_c = 250$ using cross (CP) and direct (DP) polarization, respectively.

3. Similarity of Flory's Constrained Junction Model for Elasticity to the Coupling Model for Junction Dynamics

The application of the coupling model to junction dynamics turns out to be similar in spirit as the application of the constrained junction model of Flory and coworkers [33, 107, 108] to the elasticity of networks. Calculation of the stress–strain relationship for a real network requires analysis of the response of a given chain to the imposition of a bulk deformation, described classically by two extremes, the affine [109] and the phantom [3, 29, 30] model. Real networks exhibit a strain dependence of their elastic stress that is at variance with the predictions of either the affine or the phantom network models. This is not surprising since the junctions in a real polymer network fluctuate away from positions corresponding to affine displacement, while interference from neighboring chains reduces the magnitude of such fluctuations from that available to a phantom network [31, 110]. In the constrained junction model of Flory and coworkers, the fluctuation of the junctions is limited to a domain of constraints imposed by steric hindrances from neighboring segments, with the range and position of these domains changing with deformation. Flory introduced the parameter κ, defined in terms of the number of junctions in the

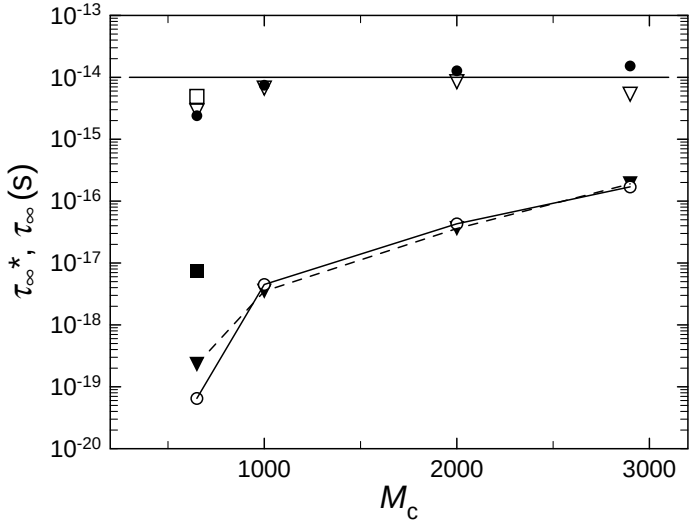

FIGURE 31 Solid inverted triangle and open circles are the apparent pre-exponential factor τ_∞^* determined by Shi *et al.* [100] from their experimental data for four polymer networks with different molecular weights between crosslinks, M_c using cross (CP) and direct (DP) polarization, respectively. The solid square is τ_∞^* for a swollen sample with $M_c = 650$. The open inverted triangles and solid circles are τ_∞ calculated by Eq. (50) from τ_∞^* and n_J for the cross (CP) and direct (DP) polarization experiments respectively with $t_c = 2 \times 10^{-12} s$. The open square is τ_∞ calculated from τ_∞^* and n_J for the swollen sample.

volume occupied by a network chain, as a measure of the severity of the local constraints relative to those imposed by the phantom network. The contribution to the force from the constraints is zero for $\kappa = 0$. Thus the same arguments given by Flory for the importance of considering local constraints on junctions (as caused by interactions with neighboring chains) in his treatment of elasticity of polymer networks justify the need of using models, such as the coupling model, which explicitly considers the effect on the dynamics of these constraints when describing junction relaxation.

Flory's constraint junction model and the coupling model are concerned with the effects of constraints on junctions in polymer networks. They address different manifestations of constraints on network junctions imposed by surrounding chains. Flory was concerned with the consequent restriction on the configurations available to the network, which affects its elastic energy. The coupling model focuses on the manner in which intermolecular constraints slow down the motion of the network junctions and cause the modification of the correlation function of the junctions for a perfect network of phantom chains, $C_{ph}(t)$. From the idea that phantom chains can pass one another, we expect that $C_{ph}(t)$ has an exponential time dependence, $\exp(-t/\tau_{J0})$. Following the general physical principle behind the coupling model, the constraints

on junctions will modify $C_{ph}(t)$ to $C_J(t)$ as given by Eq. (46) at times after $t_c \approx 2 \times 10^{-12} s$.

In the coupling model, the magnitude of n increases with the severity of the constraints relative to those imposed by the phantom network. Thus n bears a similarity to the quantity κ in the constraint junction model. The elastic stress in the constrained junction model, f_c, differs from that for phantom chains, f_{ph}, in a perfect network (no dangling ends). The ratio f_c/f_{ph} is a measure of the contribution to the stress from local constraints on junction fluctuations to that for phantom chains. Similarly, in the coupling model we may use the logarithm of the ratio $\log(\tau_\infty/\tau_\infty^*)$ and the ratio E_a^*/E_a as gauges of modification of the junction relaxation by constraints. Typically τ_∞ is of the order of $10^{-14} s$ (see also Fig. 31). This, together with $t_c \approx 2 \times 10^{-12} s$, indicates that the ratio τ_∞/t_c is much less than unity. Hence from Eqs. (49) and (50), both $\log(\tau_\infty/\tau_\infty^*)$ and the difference $(E_a^*/E_a - 1)$ increase with n or the severity of constraints, and both quantities vanish at $n = 0$ (corresponding to a phantom network). These dependences on n are analogous to the dependence of the quantity f_c in Flory's model.

The proffered analogy is supported by an examination of the dependences on crosslink density, diluent concentration, crosslink functionality, and macroscopic strain on the junction constraints of the Flory model with n, $\log(\tau_\infty/\tau_\infty^*)$, and $(E_a^*/E_a - 1)$ in the coupling model. The results of these comparisons of the Flory model and the coupling model are summarized in Table V.

IX. APPENDIX: NOMENCLATURE

A	empirical constant in VFTH equation
a_T	shift factor
B	bulk compliance
B^*	complex dynamic bulk compliance
B'	bulk storage compliance
B''	bulk loss compliance
C	empirical constant in VFTH equation, or rate of tearing
C_1, C_2	coefficient in WLF equation
C_p	specific heat
$C_{ph}(t)$	correlation function of junction for a perfect network of phantom chains
$C_J(t)$	correlation function of junction
c_1	constant
c_2	constant
c_3	constant
c_4	constant
c_5	constant
D	tensile compliance
D^*	complex dynamic tensile compliance
D'	tensile storage compliance
D''	tensile loss compliance
E	Young's (tensile) modulus

TABLE V Similarity Between Flory's Constrained Junction Model for Elasticity and the Coupling Model for Junction Dynamics

Network feature	Anticipated effect	Flory Model	Coupling Model			^{31}P NMR Experiment		
		f_c	n	$E_a^*/E_a - 1$	$\log(\tau_\infty/\tau_\infty^*)$	n	$E_a^*/E_a - 1$	$\log(\tau_\infty/\tau_\infty^*)$
Higher crosslink density	More firmly embedded junctions	*higher*	*higher*	*higher*	*higher*	*higher*	*higher*	*higher*
Diluent	Reduced severity of constraints	*lower*	*lower*	*lower*	*lower*	*lower*	*lower*	*lower*
Higher crosslink functionality	More constrained junctions	*higher*	*higher*	*higher*	*higher*			
Extension	Alleviation of constraintss	*lower*	*lower*	*lower*	*lower*			

E^*	complex dynamic tensile modulus
E'	tensile storage modulus
E''	tensile loss modulus
E_a	primitive activation energy
E_a^*	measured or apparent activation energy
f	free volume fraction, or functionality
f_1	proportionality constant
f_c	elastic stress in the constrained junction model of Flory
f_{ph}	elastic stress in the phantom chains model
G	shear modulus
$G(t)$	shear relaxation modulus
G^*	complex dynamic shear modulus
G'	shear storage modulus
G''	shear loss modulus
G_e	equilibrium modulus
G_g	glassy shear modulus
H	shear relaxation spectrum, or enthalpy
J	shear compliance
$J(t)$	shear creep compliance
J^*	complex dynamic shear complaince
J'	shear storage compliance
J''	shear loss compliance
J_d	delayed shear compliance
J_e	equilibrium shear compliance
J_g	glassy shear compliance
$J_p(t)$	reduced shear compliance
$J_r(t)$	recoverable shear compliance
J_s	steady state shear compliance
$\hat{J}(\omega)$	spectral density function
K	bulk modulus
K^*	complex dynamic bulk modulus
K'	bulk storage modulus
K''	bulk loss modulus
k	proportionality factor
L	shear retardation spectrum
$L_p(t)$	reduced shear retardation spectrum
M_x	average molecular weight per crosslinked unit
M_c	average molecular weight of a network strand
n	coupling parameter of segmental relaxation
n_i	coupling parameter of the i-th mode of a polymer strand anchored on both ends to the network junctions
n_J	coupling parameter of network junction relaxation
P	pressure
Q	cooling or heating rate
R	gas constant
S	entropy
S_c	configurational entropy
T	temperature
T_f	fictive temperature
T_g	glass temperature
T_0	reference temperature
T_∞	VFTH temperature
$\tilde{T}$	tear energy

$\tilde{T}_0$	threshold equilibrium tear energy
t	time
t_c	crossover time of the coupling model
t_{cure}	time of curing
V	specific volume
β	Andrade coefficient
γ_0	imposed shear strain
$\gamma(t)$	shear strain
$\Delta\varepsilon\beta$	relaxation strength of the JG relaxation
δ	phase angle between stress and strain
ζ_0	monomeric friction coefficient
λ	retardation time
η	shear viscosity
κ	Flory's parameter in the constrained junction model
ρ	density
σ_0	imposed shear stress
$\sigma(t)$	shear stress
τ	relaxation time
τ_J	network junction relaxation time
$\tau\alpha$	segmental relaxation time
$\tau_o\alpha$	primitive relaxation time of the coupling model
$\tau\beta$	Johari-Goldstein secondary relaxation time
τ_{oJ}	primitive relaxation time of the network junction
τ_{Ri}	relaxation time of i-th Rouse mode
τ_∞	prefactor
τ^*_∞	prefactor
ω	frequency in rad/sec

REFERENCES

1. J. D. Ferry, "Viscoelastic Properties of Polymers," 3rd ed., Wiley, New York, 1980.
2. P. J. Flory, "Principle of Polymer Chemistry," Cornell University Press, Ithaca, NY, 1953.
3. L. R. G. Treloar, "The Physics of Rubber Elasticity," 3rd ed., Clarendon, Oxford, 1975.
4. J. E. Mark and B. Erman, "Rubberlike Elasticity: A Molecular Primer," Wiley-Interscience, New York, 1988.
5. J. E. Mark *et al.*, "Physical Properties of Polymers," 3rd ed., Cambridge Univ. Press, Cambridge, 2004.
6. A. N. Gent, in "Science and Technology of Rubber," 2nd ed., Academic Press, New York, 2004, Chap. 10.
7. D. J. Plazek and G. Berry, in "Glass: Science and Technology, Vol. 3, Viscosity and Relaxation," D. R. Uhlmann and N. J. Kreidl (Eds.), Academic Press, New York, 1986, Chap. 7.
8. A. R. Payne and R. E. Whittaker, *Rubber Chem. Technol.* **44**, 340 (1971).
9. L. Mullin, *J. Appl. Polym. Sci.* **2**, 257 (1959).
10. T. L. Smith, in "Treatise on Materials Science and Technology," Academic Press, New York, 1977.
11. I.-C. Choy and D. J. Plazek, *J. Polym. Sci.*: *Part B: Polym. Phys.* **24**, 1303 (1986).
12. D. J. Plazek and I.-C. Choy, *J. Polym. Sci.*: *Part B: Polym. Phys.* **27**, 307 (1989).
13. D. J. Plazek and Z. N. Frund, Jr., *J. Polym. Sci.*: *Part B: Polym. Phys.* **28**, 431 (1990).
14. D. J. Plazek and In-Chul Chay, *J. Polym. Sci.*: *Part B: Polym. Phys.* **29**, 17 (1991).
15. D. J. Plazek, I.-C. Choy, F. N. Kelley, E. von Meerwall, and L.-J. Su, *Rubber Chem. Technol.* **56**, 866 (1983).

16. D. J. Plazek, G.-F. Gu, R. G. Stacer, L.-J. Su, E. von Meerwall, and F. N. Kelley, *J. Mater. Sci.* **23**, 1289 (1988).
17. D. J. Plazek and M. Rosner, *Rubber Chem. Technol.* **71**, 679 (1998).
18. K. L. Ngai, D. J. Plazek, and R. W. Rendell, *Rheol. Acta* **36**, 307 (1997).
19. K. L. Ngai and D. J. Plazek, *Rubber Chem. Technol. Rubber Reviews* **68**, 376 (1995).
20. D. J. Plazek and K. L. Ngai, in "Glass Transition Temperatures," in "Handbook of Polymer Properties," J. E. Mark (Ed.), American Institute of Physics, College Park, MD, 1996, p. 139.
21. E. Riande, H. Markovitz, D.J. Plazek, and N. Raghupathi, *J. Poly. Sci. Symp*. **50**, 405 (1995).
22. I. L. Hopkins and R. W. Hamming, *J. Appl. Phys*. **28**, 906 (1957).
23. L. C. E. Struik, "Physical Aging in Amorphous Polymers and Other Materials," Elsevier, Amsterdam, 1978.
24. A. J. Kovacs, J. J. Aklonis, J. M. Hutchinson, and A. R. Ramos, *J. Polym. Sci.: Polym. Phys. Ed.* **17**, 1097 (1979).
25. G. B. McKenna, in "Comprehensive Polymer Science, Vol. 2, Polymer Properties," C. Booth and C. Price (Eds.), Pergamon, Oxford, 1989, p. 311.
26. I. M. Hodge, *Macromolecules* **16**, 898 (1983).
27. C. T. Moynihan *et al*. *Ann. N.Y. Acad. Sci.* **279**, 15 (1976).
28. A. Q. Tool, *J. Am. Cer. Soc.* **29**, 240 (1946).
29. H. M. James and E. Guth, *J. Chem. Phys.* **15**, 669 (1947).
30. H. M. James and E. Guth, *J. Chem. Phys.* **21**, 1039 (1953).
31. P. J. Flory, *Proc. Roy. Soc. London A* **351**, 351 (1976).
32. P. J. Flory, *Polymer* **20**, 1317 (1979).
33. P. J. Flory and B. Erman, *Macromolecules* **15**, 800 (1982).
34. M. Doi and S. F. Edwards, "The Theory of Polymer Dynamics," Clarendon Press, Oxford, 1986.
35. F. R. Schwarzl and A. J. Staverman, *J. Appl. Phys*. **23**, 838 (1952).
36. D. J. Plazek, *J. Colloid Sci*. **15**, 40 (1960).
37. D. J. Plazek and V. M. O'Rourke, *J. Polym. Sci., A-2* **9**, 209 (1971).
38. J. D. LeMay, B. J. Swetlin, and F. N. Kelley, in "Characterization of Highly Crosslinked Polymer," ACS Series No. 243, American Chemical Society, Washington, D.C., 1984, p. 177.
39. G. C. Berry and T. G. Fox, *Adv. Polym. Sci*. **5**, 261 (1968).
40. D. J. Plazek, *J. Polym. Sci., A-2* **4**, 745 (1966).
41. P. Thirion and R. Chasset, in "Proceedings of the Conference on Physics of Non-Crystalline Solids," North Holland, Amsterdam, 1965; *Rev. Gen. Caoutchouc*. **41**, 271 (1964).
42. J. D. Ferry, R. G. Manke, E. Maekawa, Y. Oyanagi, and R. A. Dicke, *J. Phys. Chem.* **68**, 3414 (1964).
43. H. Leaderman, *J. Polym. Sci.* **16**, 261 (1955).
44. A. R. Payne, *J. Appl. Polym. Sci*. **3**, 127 (1960).
45. H. Leaderman, *J. Polym. Sci.* **59**, S42 (1962).
46. R. A. Dicke and J. D. Ferry, *J. Phys. Chem.* **70**, 2594 (1966).
47. R. H. Valentine, J. D. Ferry, T. Homma, and K. Ninomiya, *J. Polym. Sci.: Part A-2* **6**, 479 (1968).
48. A. R. Payne and R. E. Whittaker, *Rubber Chem. Technol.* **44**, 340 (1971).
49. J. F. Saunders and J. D. Ferry, *Macromolecules* **7**, 681 (1974).
50. A. N. Gent, in "Science and Technology of Rubber," J. E. Mark and B. Erman (Eds.), Academic Press, New York.
51. Y. Isono and J. D. Ferry, *Rubber Chem. Technol.* **57**, 925 (1984).
52. K. Arai and J. D. Ferry, *Rubber Chem. Technol.* **59**, 592 (1986).
53. K. Arai and J. D. Ferry, *Rubber Chem. Technol.* **59**, 605 (1986).
54. G. J. Lake and A. G. Thomas, *Proc. Roy. Soc., London* **300**, 108 (1967).
55. A. N. Gent and R. H. Tobias, *J. Polym. Sci. Polym. Phys. Ed.* **20**, 2051 (1982).
56. T. L. Smith, *J. Polym. Sci., A-2* **1**, 3597 (1963).
57. L. Mullins, *Trans. Inst. Rubber Ind*. **35**, 213 (1959).
58. H. K. Mueller and W. G. Knauss, *J. Appl. Mech*. **38**, 483 (1971).

59. K. L. Ngai, D. J. Plazek, and S. S. Deo, *Macromolecules* **20**, 3047 (1987).
60. K. L. Ngai, A. Schönhals, and E. Schlosser, *Macromolecules* **25**, 4915 (1992).
61. D. J. Plazek, C. Bero, S. Neumeister, G. Floudas, G. Fytas, and K. L. Ngai, *J. Colloid Polymer Sci*. **272**, 1430 (1994).
62. R. W. Gray, G. Harrison, and J. Lamb, *J. Polym. Sci. Polym. Phys. Ed.* **14**, 1361 (1976).
63. R. W. Gray, G. Harrison, and J. Lamb, *Proc. R. Soc. London* **356**, 77 (1977).
64. J. Cochrane, G. Harrison, J. Lamb, and D. W. Phillips, *Polymer* **21**, 837 (1980).
65. K. L. Ngai, A. Schönhals, and E. Schlosser, *Macromolecules* **25**, 4915 (1992).
66. A. Schönhals and E. Schlosser, *Physica Scripta* **T49A**, 233 (1993).
67. D. J. Plazek, *J. Rheology* **40**, 987 (1996).
68. D. J. Plazek, X. D. Zheng, and K. L. Ngai, *Macromolecules* **25**, 4920 (1992).
69. K. L. Ngai, D. J. Plazek, and C. Bero, *Macromolecules* **26**, 1065 (1993).
70. K. L. Ngai, *Comments Solid State Phys*. **9**, 127 (1979).
71. K. L. Ngai, A. K. Rajagopal, and S. Teitler, *J. Chem. Phys*. **88**, 5086 (1988).
72. K. L. Ngai and R. W. Rendell, in "Relaxation in Complex Systems and Related Topics," Ian A. Campbell and C. Giovannella (Eds.), NATO ASI Series, Vol. 222, Plenum, New York, 1990, p. 309.
73. K. L. Ngai, S. L. Peng, and K. Y. Tsang, *Physica A* **191**, 523 (1992).
74. K. Y. Tsang and K. L. Ngai, *Phys. Rev. E* **54**, 3067 (1997).
75. K. L. Ngai and K. Y. Tsang, *Phys. Rev. E* **60**, 4511 (1999).
76. K. L. Ngai and R. W. Rendell, in "Supercooled Liquids, Advances and Novel Applications," J. T. Fourkas, D. Kivelson, U. Mohanty, and K. Nelson (Eds.), ACS Symposium Series, Vol. 676, American Chemical Society, Washington, D.C., 1997, p. 45.
77. K. L. Ngai, *IEEE Transactions in Dielectrics and Electrical Insulation* **8**, 329 (2001).
78. K. Schmidt-Rohr and H. W. Spiess, *Phys. Rev. Lett.* **66**, 3020 (1991).
79. R. Kohlrausch, *Pogg. Ann. Phys*. **12**, 393 (1847); *Pogg. Ann. Phys.* **91**, 56, 179 (1854).
80. J. Colmenero, A. Arbe, G. Coddens, B. Frick, C. Mijangos, and H. Reinecke, *Phys. Rev. Lett.* **78**, 1928 (1977).
81. K. L. Ngai, in "Disorder Effects on Relaxational Properties," R. Richert and A. Blumen (Eds.), Springer Verlag, Berlin, 1994, Chap. 3.
82. A. Kudlik, S. Benkhof, T. Blochowicz, C. Tschirwitz, and E. Rössler, *J. Mol. Structure* **479**, 210 (1999).
83. R. Casalini, K. L. Ngai, C. G. Robertson, and C. M. Roland, *J. Polym. Sci. Polym. Phys. Ed.* **38**, 1841 (2001).
84. C. M. Roland, M. J. Schroeder, J. J. Fontanella, and K. L. Ngai, *Macromolecules* **37**, 2630 (2004).
85. G. P. Johari and M. Goldstein, *J. Chem. Phys*. **53**, 2372 (1970).
86. G. P. Johari, *Annals New York Acad. Sci*. **279**, 117 (1976).
87. K. L. Ngai and M. Paluch, *J. Chem. Phys.* **120**, 2857 (2004).
88. K. L. Ngai, *J. Phys.: Condens. Matter* **15**, S1107 (2003).
89. K. L. Ngai and M. Paluch, *J. Phys. Chem. B* **107**, 6865 (2003).
90. S. Correzi, M. Beiner, H. Huth, K. Schröter, S. Capaccioli, R. Casalini, D. Fioretto, and E. Donth, *J. Chem. Phys.* **117**, 2435 (2002).
91. K. L. Ngai and S. Capaccioli, *Phys. Rev. E* **69**, 03150 (2004).
92. G. P. Johari, G. Power, and J. K. Vij, *J. Chem. Phys.* **116**, 5908 (2002); G. P. Johari, G. Power, and J. K. Vij, *J. Chem. Phys.* **117**, 1714 (2002); G. Power, G. P. Johari, and J. K. Vij, *J. Chem. Phys.* **119**, 435 (2003).
93. M. Paluch, C. M. Roland, S. Pawlus, J. Ziolo, and K. L. Ngai, *Phys. Rev. Lett.* **91**, 115701 (2003).
94. J. Köplinger, G. Kasper, S. Hunklinger, *J. Chem. Phys.* **113**, 4701 (2001).
95. A. Arbe, J. Colmenero, D. Richter, J. Gomez, and B. Farago, *Phys. Rev. E*. **60**, 1103 (1999).
96. K. L. Ngai, D. J. Plazek, and I. Echeverria, *Macromolecules* **29**, 7937 (1996).
97. K. L. Ngai, D. J. Plazek, and A. K. Rizos, *J. Polym. Sci. Polym. Phys.* **35**, 599 (1997).
98. K. L. Ngai, D. J. Plazek, and V. M. O'Rourke, *Macromolecules* **30**, 5450 (1997).

99. K. L. Ngai and D. J. Plazek, *Macromolecules* **35**, 9136 (2002).
100. J.-F. Shi, L. C. Dickinson, W. J. MacKnight, and J. C. W. Chien, *Macromolecules* **26**, 5908 (1993).
101. K. L. Ngai and C. M. Roland, *Macromolecules* **27**, 2454 (1994).
102. B. E. Read, *J. Non-Cryst. Solids* **131**, 408 (1991).
103. I. Alig and G. P. Johari, *J. Polym. Sci. Part B: Polym. Phys.* **31**, 299 (1993).
104. M. Beiner and K. L. Ngai, to be published.
105. K. L. Ngai, C. M. Roland, and A. F. Yee, *Rubber Chem.& Tech*. **66**, 817 (1993).
106. At the time of writing Reference 101, this value of t_c has not yet been determined directly by experiment, and values about 10 times longer were used.
107. P. J. Flory, *Rubber Chem. Technol.* **52**, 110 (1979).
108. P. J. Flory, *Polym. J*. **17**, 1 (1985).
109. L. G. R. Treloar, *Rep. Prog. Phys.* **36**, 755 (1973).
110. G. Ronca and G. Allegra, *J. Chem. Phys.* **63**, 4990 (1975).

6 Rheological Behavior and Processing of Unvulcanized Rubber

JAMES L. WHITE
Department of Polymer Engineering
University of Akron
Akron, Ohio

I. INTRODUCTION

A. Overview

The fabrication of rubber parts generally involves the mixing and processing of bulk unvulcanized compounds and sometimes solutions and emulsions through complex equipment. The ease or difficulty of fabrication depends on how these rubber systems respond to applied stresses and deformations, their *rheological* (from *rheos*: "to flow," and *logos*: "science of") properties. It is the purpose of this chapter to describe both rheological properties and the processing of unvulcanized elastomers and their compounds. We also consider some of the implications of rheology for processing. The subject of this chapter, processing technology and engineering science, has been treated in much more detail in the author's book [W16].

B. Rheological Properties

The study of the rheological properties and processing of elastomers and their solutions and compounds dates to the origins of the industry in the 1820s. The patent literature, memoirs, and reviews of the early 19th century contain

Science and Technology of Rubber, Third Edition

numerous discussions of the flow and fabrication of natural rubber and gutta percha [B17, B29, C6, C7, G12–14, H4–11]. The fundamental properties and methods of processing rubber are associated with Thomas Hancock, Charles Macintosh, Edwin Chaffee, Charles Goodyear, Richard Brooman, Charles Hancock, and others, many long forgotten. It was not, however, until the development of three-dimensional linear viscoelasticity by Ludwig Boltzmann [B26] at the University of Vienna in 1874 that the understanding of the rheological properties of rubbery materials became sophisticated enough to allow rational study. Furthermore, it was another half-century before Bruno Marzetti [M8–11] of Pirelli SpA in Italy and (in the 1930s) J. R. Scott [S5, S6] of the British Rubber Manufacturers Research Association (BRMRA), John H. Dillon [D7–9] of the Firestone Tire and Rubber Company, and Melvin Mooney [M40, M41, M46] of the U.S. Rubber Company (the last two in the United States) undertook the study of the deformation and flow of unvulcanized rubber. In each case the motivation seems to have been the development of quality control instrumentation to ensure satisfactory processibility. Fortunately, each of the four was a careful, observant, and thoughtful scientist. Marzetti interpreted the extrusion of rubber through a cylindrical die in terms of the flow of a fluid with a shear rate-dependent viscosity. This view was confirmed by Scott, Dillon, and Mooney. Scott [S5] was the first to realize that rubber compounded with large quantities of small particles exhibited a yield stress below which there was no flow. This view was supported by Dillon and Johnston [D9]. Mooney [M41] obtained both the first quantitative viscosity–shear rate data on rubber and the first measurements of elastic recoil, and Dillon and Cooper [D8] reported the first investigations of stress transients at the beginning of flow.

Post–World War II studies of the rheological properties of unvulcanized elastomers have been dominated by the idea that these materials are viscoelastic. Research along these lines was initiated by Leaderman [L4, L5], at the Textile Research Institute of Princeton University, who rediscovered the work of Boltzmann [B26] cited earlier. In the late 1940s, Tobolsky and his coworkers [A2, A3, D11, T5] at Princeton University made extensive stress relaxation measurements on polyisobutylene. In succeeding years, linear viscoelastic measurements were performed on a wide variety of polymers in temperature regions in which they exhibited rubbery behavior. Tobolsky devised a program to relate the viscoelastic behavior to molecular parameters, such as molecular weight and glass transition temperature. This work carried out in the late 1940s and 1950s was reviewed in a 1959 monograph by Tobolsky [T5]. In the 1960s, Bernstein, Kearsley, and Zapas [B14, B15] made extensive studies of large strain nonlinear viscoelastic properties of polyisobutylene and proposed a three-dimensional constitutive equation to represent its behavior. In later years, non-linear transient experiments on polyisobutylene and natural rubber were similarly interpreted [M24, M34].

The hypothesis of Scott [S5] that highly filled elastomers exhibited yield values was confirmed by Zakharenko and his coworkers [Z1] as well as

by Vinogradov *et al.* [V3, V4] (both in Moscow) and later by others [M33, M37, O10, S11, T7, W28]. Yield values were also found to occur by subsequent researchers for thermoplastics filled with a wide variety of particles including talc [C8], titanium dioxide [M2, M29, T1], calcium carbonate [M2, S25, T1], as well as carbon black [L14, M3, T1]. Mullins and Whorlow [M51, M52] of the BRMRA found highly filled rubber–carbon black compounds to exhibit strong time-dependent (thixotropic) characteristics. Their results were confirmed and extended by others [M37]. Since the late 1970s, there have been efforts [I5, L10, M34–36, S26, W9, W22, W24] to develop three-dimensional constitutive equations representing the yield value, thixotropic and viscoelastic characteristics of these compounds.

C. Quality Control Instrumentation

The first 40 years of the 20th century saw an enormous increase in the production of rubber products especially in the tire industry. The horrendous nonuniformity of the wild rubber used in the 19th century was reduced by the introduction of plantation rubber from Malaya in 1910 (see the discussion of Litchfield [L14]). From the 1920s, efforts were made by various industrial and plantation-related scientists to develop improved quality control. Here we may cite the efforts notably of Marzetti [M8–11] of Pirelli, Williams [W29] of Firestone, Griffiths [G18] of the Dunlop Rubber Company, van Rossem and van der Meijden [V1] of the Netherlands Government Rubber Institute (NGRI), Karrer [K2, K3] of the B. F. Goodrich Company, Dillon [D7–9] of Firestone, Mooney [M40, M46] of U.S. Rubber, Hoekstra [H18] also of the NGRI, and Baader [B1] of Continental Gummiwerke. These efforts involved using capillary instruments [D7, D8, G18, M8–11], compressional flow between parallel disks [B1, H18, K2, K3, V1], and shearing disk rotational rheometers [M40, M46].

In the late 1930s, the I.G. Farbenindustrie began commercial production of emulsion-polymerized butadiene–styrene copolymer (SBR) synthetic rubber under the designation Buna S. [K10]. They adopted, after a comparison of many instruments [H1], the Defo compressional flow instrument devised by Baader [B1] of Continental Gummiwerke. This instrument was used from the 1930s until the end of World War II to test and qualify the German Buna S. [B2–7]. In the American government synthetic rubber program [W4] to develop SBR, termed by them GR-S, the Mooney shearing disk viscometer [M40] was adopted [M42, M44, M46, T3, T4, W4].

In the post–World War II period, the Mooney viscometer has tended to maintain its dominance, though it has been increasingly challenged by new generations of instruments which seek to measure viscoelastic characteristics. Mooney [M42, M46] himself had urged the use of elastic recovery measurements following flow in his shearing disk rheometer and Baader [B1] had included recovery measurements in his original Defo test. Little attention was given to viscoelastic effects in processing until the 1960s. Researchers with U.S.

Rubber/Uniroyal [T8, T9, W25] and B. F. Goodrich independently came to realize the importance of stress relaxation behavior. The B. F. Goodrich Company in the 1970s introduced a practical male–female biconical shear stress relaxation instrument known as the DSR [H14, M31]. Subsequently the Rubber and Plastics Research Association (RAPRA, successor to the BRMRA) developed a modified compression plastometer for this purpose [B16, N7].

In the 1980s, Bayer AG, successor to I. G. Farbenindustrie synthetic rubber activities, devised two new instruments in a program led by Koopmann (K13–18). These were both a Mooney viscometer with stress relaxation measurement capability [K17] and an improved Baader Defo instrument [K13–18]. The Bayer researchers preferred the improved Defo. The Mooney viscometer with stress relaxation is now manufactured by Alpha Technologies [G21]. The new Defo was made by Haake [S7] under Bayer license.

Alpha Technologies manufactures an instrument that measures linear viscoelastic dynamic mechanical properties.

D. Processing

The earliest successful rubber processing technology was that of Charles Macintosh [H11, M4, W7] devised in the 1820s which prepared solutions of rubber in a volatile solvent and coated it onto textile fabrics for the purpose of waterproofing. Macintosh's firm in Manchester and Thomas Hancock's in London were the two major early manufactures. In the 1830s, the Americans Edwin Chaffee [C6, G14, W16, W31] and Charles Goodyear [G12, G14] developed the mill, calender, and vulcanization molding technologies. This brought companies such as Farrel Foundry and Machine and the Birmingham Iron Foundry (from 1927 combined into Farrel Birmingham later Farrel Corp.) into the business of manufacturing mills and calenders [F1, W11, W13]. This technology was exported to Europe. By the 1870s, the Harburger Eisen and Bronzewerke [M5] (from the 1960s part of Krupp) began manufacturing calender rolls. The introduction of the screw extruder for gutta percha and rubber in the 1870s [G15, H15, S4] led to creation of new machinery firms, notably Francis Shaw and Company [W14] in Manchester, England, and John Royle in Paterson, New Jersey. Germany's rubber industry became concentrated in the city of Hannover [M5], with the major firm (from 1870) being Continental Gummiwerke. Two important firms concentrating on manufacture of rubber processing equipment including extrusion and calendering developed in Hannover. These were Paul Troester Maschinenfabrik (in 1892) [M5, W12] and Hermann Maschinenbau [M5] (in 1896), both created in the last decade of the 19th century.

The 20th century saw the rise of the tire industry and the development of organic accelerators. These were coupled with the demands of the automotive industry and led to the development of the internal mixer to replace the two-

roll mill. Originally, Werner and Pfleiderer was the leading firm [H16, K4, W13, W15], but their unwillingness to prosecute the patent of Fernley H. Banbury led to the development of his internal mixer technology [B12, B13, H16, K4, W13] by the Birmingham Iron Foundry and, after 1927, by Farrel-Birmingham (now Farrel Corp.) [K4, W11, W13].

The factory system based on internal mixers, screw extruders, calenders, and vulcanization presses has remained basically unchanged in the past half-century. Internal mixers have had major improvements, e.g., intermeshing rotors proposed by Francis Shaw and Company [C16] and Werner and Pfleiderer [L3], and variable intermeshing clearance rotors [P1] proposed by Pomini–Farrel SpA. Sophisticated computer control systems have been introduced. The early single hot-feed extruders have been replaced by cold-feed extruders with increasingly sophisticated design including pin barrel extruders [G7, H12, H13, M18, W16] as well as complex control systems.

E. Flow Simulation of Processing

The origins of flow simulation of processing should probably he traced to the establishment of the Navier–Stokes equations [S22] and its early solutions [L1, S24]. Reynolds' 1886 simulation [R6] of the flow of lubricating oil in bearings has had enormous influence on succeeding flow simulations of viscous fluids moving through small clearances. Specific studies relating to the flow of rubber in processing operations and the implications of non-Newtonian flow behavior date to the 1930s with the work of Mooney [M39] and Dillon and Johnston [D9] or flow-through tubes. These papers though are closely related to viscometry and a better beginning may be Ardichvili's 1938 analyses of flow between [A10] and bending of [A11] calender rolls, followed by Gaskell's [G2] 1950 non-Newtonian flow modeling of the former problem.

In the 1950s considerable attention was given to simulation of the screw extrusion process by researchers with the Goodyear Tire and Rubber Company [P10], DuPont [C1], and Bayer AG [M20, M21]. By the 1960s, rather sophisticated models of nonisothermal non-Newtonian flow in metering regions of extruder screws were published by Griffith [G17] and Zamodits and Pearson [Z2]. Simulation of polymer processing in the 1960s was dominated by J. R. A. Pearson of Cambridge University whose early activities in screw extrusion we have just cited. Pearson [P2–6] showed in a series of papers published in the early 1960s how hydrodynamic lubrication theory may be applied to die design. He subsequently showed how membrane theory could be applied to simulate processing operations such as tubular film extrusion and blow molding [P5, P6].

In the 1970s, attention turned to simulation of injection molding of thermoplastics, with the first papers concerned with either isothermal mold filling [R8, W8] or nonisothermal filling very simple molds [K1]. From the late 1970s, commercial computer software for simulating nonisothermal injection

molding was developed by both C. Austin and his firm Moldfow Australia and by K. K. Wang and his coworkers at Cornell University.

The 1970s also saw the first application of finite-element computational techniques to polymer processing operations, with Tanner and his coworkers [C3, T2] playing a key early role with applications to extudate swell and wire coating. Subsequently, commercial computer software based on finite-element analysis of Newtonian/non-Newtonian fluid mechanics was developed by various entrepreneurs, notable among which was M. Crochet of the University Louvain-le-Neuve and his Polyflow. Crochet [C22] reviewed the progress of finite-element analysis in solving viscoelastic fluid problems.

Until the 1980s, most simulations of polymer operations related to thermoplastics problems. The special processing machinery of the rubber industry had receive little attention. It is only in the late 1980s that realistic simulations appeared for internal mixers [C10, C11, H20, H21, K6–8, W19] and pin barrel extruders [B31, B32, B34, K22]. These have used primarily lubrication theory-based simulations.

II. BASIC CONCEPTS OF MECHANICS

In this section we develop the basic ideas of classical rheological thought. We presume elastomers to deform as continuous media and to be subject to the formalism of continuum mechanics [T10]. We begin by developing the idea of the nature of applied forces and the stress tensor.

The idea of the stress tensor in a material arises from the necessity of representing the influence of applied forces on deformation. The applied forces **F** acting on a body may be represented as the sum of contact forces acting on the surface and body forces **f**, such as gravitation, which act directly on the elements of mass. We may write [T10] (Fig. 1)

$$\mathbf{F} = \sum_i \mathbf{t}_i \Delta a_i + \sum_t \mathbf{f}_j \Delta m_j = \oint \mathbf{t} da + \oint \rho \mathbf{f} dV \tag{1}$$

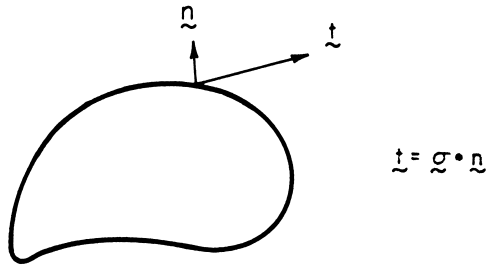

FIGURE 1 Stress vector.

where **t** is the force per unit area (stress vector) acting on the surface area elements Δa_i, and the $\oint$ indicates the integration exists over the entire surface.

The idea of the stress tensor comes from relating **t** to the unit normal vector **n** to the surface through

$$\mathbf{t} = \sigma \cdot \mathbf{n} \tag{2}$$

where $\boldsymbol{\sigma}$ is an array of nine quantities

$$\boldsymbol{\sigma} = \begin{vmatrix} \sigma_{11} & \sigma_{12} & \sigma_{13} \\ \sigma_{21} & \sigma_{22} & \sigma_{23} \\ \sigma_{31} & \sigma_{32} & \sigma_{33} \end{vmatrix} \tag{3}$$

known as the stress tensor or matrix. $\boldsymbol{\sigma}$ may be considered as a second-order tensor or a Gibbs dyadic

$$\boldsymbol{\sigma} = \sum_i \sum_j \sigma_{ij} \mathbf{e}_i \mathbf{e}_j \tag{4}$$

The concepts of the stress vector and stress tensor were developed during the 1820s by Cauchy. The direction of the stress component is *i*. When the direction of the stress component *i* is perpendicular to the plane ($\sigma_{ij} i = j$), the stress is called the normal stress. When the direction *i* is tangent to the plane *j* ($\sigma_{ij} i \neq j$), the stress is called the shear stress.

Applying the divergence theorem to Eq. (1) gives

$$\oint \mathbf{t} da = \oint \boldsymbol{\sigma} \cdot \mathbf{n} da = \int \nabla \cdot \boldsymbol{\sigma} dV \tag{5}$$

$$\mathbf{F} = \int [\nabla \cdot \boldsymbol{\sigma} + \rho \mathbf{f}] dV \tag{6}$$

where ∇ is the del operator

$$\nabla = \mathbf{e}_1 \frac{\partial}{\partial x_1} + \mathbf{e}_2 \frac{\partial}{\partial x_2} + \mathbf{e}_3 \frac{\partial}{\partial x_3} \tag{7}$$

The complete dynamics of a deforming body requires including the contact forces, the body (gravitational) forces $\rho \mathbf{f}$ with inertial forces. For a macroscopic mass *M*

$$\mathbf{F} = \frac{d}{dt} \int \rho \mathbf{v} dV = \int [\nabla \cdot \boldsymbol{\sigma} + \rho \mathbf{f}] dV \tag{8}$$

while for a macroscopic fixed-space "control volume" through which the mass may move [T10]

$$\int \frac{\partial}{\partial t}(\rho \mathbf{v})dV + \oint \rho \mathbf{v}(\mathbf{v}\cdot\mathbf{n})da = \int [\nabla\cdot\boldsymbol{\sigma} + \rho\mathbf{f}]dV \tag{9}$$

It follows that at a point within the body [T10]

$$\rho\left[\frac{\partial \mathbf{v}}{\partial t} + (\mathbf{v}\cdot\nabla)\mathbf{v}\right] = \nabla\cdot\boldsymbol{\sigma} + \rho\mathbf{f} \tag{10}$$

Equation (10), which establishes the balance of forces at a point within the body, is known as Cauchy's law of motion.

The components of the stress tensor are not independent of each other. By a balance of torques and angular moments similar to that leading to Eq. (10) it may be shown that the stress tensor is symmetric [T10]; i.e.,

$$\boldsymbol{\sigma} = \boldsymbol{\sigma}^{\mathrm{T}} \qquad \text{or} \qquad \sigma_{\mathrm{ij}} = \sigma_{ji} \tag{11}$$

Thus, the off-diagonal components of Eq. (4), which are the shear stresses, are related through

$$\sigma_{12} = \sigma_{21}, \qquad \sigma_{13} = \sigma_{31}, \qquad \sigma_{23} = \sigma_{32}$$

The basic problem of rheology is the development of expressions for $\boldsymbol{\sigma}$ in terms of the deformation and kinematics of materials. The deformation behavior of continuous materials may then be determined through solutions of Eq. (10).

If a body is not subjected to applied forces, the stress components reduce to equal normal hydrostatic pressure components

$$\boldsymbol{\sigma} = -p\mathbf{I}, \qquad \mathbf{I} = \begin{vmatrix} 1 & 0 & 0 \\ 0 & 1 & 0 \\ 0 & 0 & 1 \end{vmatrix} \tag{12}$$

where p is the pressure. More generally, when forces are applied, we may express the stress tensor in terms of the pressure and an extra stress tensor $\mathbf{P}$ through the relation

$$\boldsymbol{\sigma} = -p\mathbf{I} + \mathbf{P} \tag{13a}$$

Specifically for normal stresses

$$\sigma_{-ii} = -p + P_{-ii} \tag{13b}$$

and for shear stresses

$$\sigma_{ij} = P_{ij} \qquad (i \neq j) \tag{13c}$$

and we need not distinguish between σ_{ij} and P_{ij} when $i \neq j$.

III. RHEOLOGICAL PROPERTIES

A. Gums

1. Overview

In this section we begin by reviewing experimental studies of the rheological behavior of unvulcanized elastomers and related materials. We then seek to correlate this behavior in terms of the theory of viscoelasticity. First, the linear theory of viscoelasticity in which there is broad consensus of agreement in the rheological community is discussed. We then describe the nonlinear theory, where the level of consensus is much less.

2. Experimental Studies

The experimental literature largely divides between studies of behavior in small strain and studies in steady shear flow. Much of the emphasis has been to relate such behavior to molecular structure.

a. Small-Strain Studies

During the 1940s and early 1950s, Leaderman [L4, L5], Tobolsky [A2, A3, D11, T5], Ferry [F3], and others made extensive studies of the small-strain behavior of elastomers and related polymers. These studies involved creep (deformation under applied stress), stress relaxation following applied stresses, and imposed oscillatory strains. These and other experimental techniques used have been described in special detail in the monograph of Ferry [F3]. These studies showed that all of these deformations could be represented in terms of the superposition principle of Boltzmann [B26] [see Eq. (43)].

Tobolsky and his coworkers made extensive efforts to characterize the stress relaxation characteristics of elastomers, notably polyisobutylene. The stress would decay over time to zero at a rate dependent on temperature and molecular weight (Fig. 2). They expressed the relaxation through a series of exponentials or a spectrum of relaxation times. Consider the shear stress decay $\sigma(t)$ following an shear imposed strain γ_0. This may be used to define a shear relaxation modulus $G(t)$ through

$$\frac{\sigma(t)}{\gamma_0} = G(t) = \sum_{i=1}^{m} G_i e^{-t/\tau_i} \tag{14}$$

$$G(t) = \int_0^\infty H(\tau) e^{-t/\tau} d \ln \tau$$

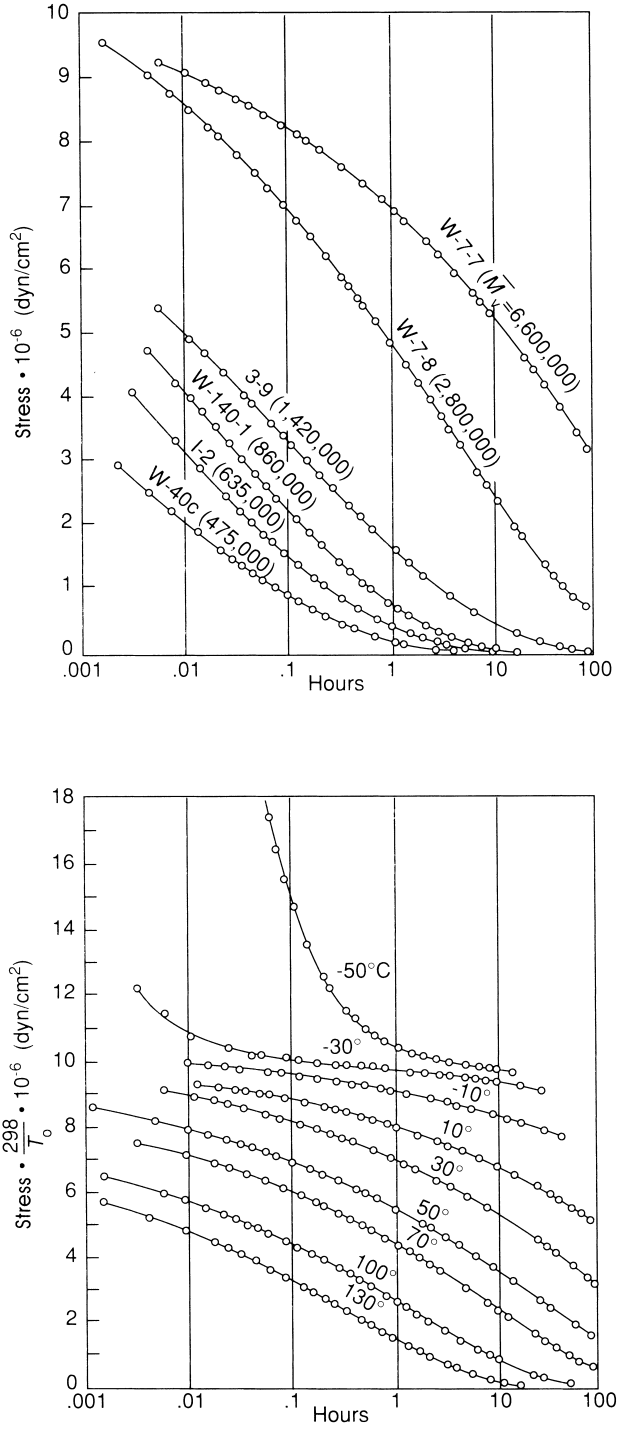

FIGURE 2 Stress relaxation from the measurements of Andrews *et al.* [A2, A3].

TABLE I Linear Viscoelastic Representation for $G(t)$ of SMR5-NR (100°C)

i	G_i (Pa)	τ_i (sec)
m	2,199	230
$m-1$	9,166	37.7
$m-2$	33,290	7.31
$m-3$	59,200	0.925
$m-4$	59,000	0.095

From Montes and White [M34].

Table I summarizes the G_i, τ_i relaxation times obtained for natural smoked sheet at 100°C.

Tobolsky and his coworkers found they could study $G(t)$ over a very wide range of times by constructing "master curves" from data obtained at different temperatures. Specifically they found that:

$$G(t,T) = \frac{\rho T}{\rho_s T_s} G(t/a_T) \tag{15}$$

which interrelates stress relaxation data at different temperatures T where a_T is a temperature-dependent shift factor applied to the time. Here ρ is density, and ρ_s and T_s are values at a standard temperature unique to each polymer. The shift factor a_T may be represented as a universal function of $T - T_s$. The value of T_s is related to the glass transition temperature. This was established by Tobolsky and Ferry and their respective coworkers, but is associated primarily with Williams, Landel, and Ferry [W30].

Tobolsky and his coworkers found that the $H(\tau)$ relaxation spectrum function for polyisobutylene may be represented by the combination of a wedge and box, i.e., as

$$H(\tau) = \frac{A}{\sqrt{\tau}} \qquad \tau < \tau_1 \tag{16a}$$

$$H(\tau) = H_0 \qquad \tau_2 < \tau < \tau_m \tag{16b}$$

H_0 and A were independent of molecular weight, but τ_m exhibited a strong dependence. Specifically

$$\tau_m = CM_w^{3.4} \tag{17}$$

Oscillatory strain experiments were also studied in this period, notably by Ferry and his coworkers [F3]. These were found to produce both "in-phase"

and "out-of-phase" stress components. These were interpreted in terms of the expression

$$\sigma(t) = G'(\omega)\gamma(t) + \eta'(\omega)\frac{d\gamma}{dt} \tag{18}$$

where the term $\eta'(\omega)$ is known as the dynamic viscosity. We may also define a complex viscosity $\eta^*(\omega)$:

$$\eta^*(\omega) = \sqrt{[G'/\omega]^2 + (\eta')^2} \tag{19}$$

In later years, the $G(t)$ and $H(\tau)$ functions have been further investigated by various researchers including Ninomiya [N4], Bogue *et al*. [B23], and notably Masuda *et al.* [M12, M13] with respect to the influence of molecular weight distribution. The effect of the presence of high-molecular-weight polymer in a blend was to make $G(t)$ relax more slowly. The effect on $H(\tau)$ was to make $H(\tau)$ decrease more slowly at large τ. They found that at large times for narrow molecular weight distribution samples, the box of Eq. (16b) is replaced by a more complex function which includes a spike. Ninomiya [N4] and Bogue *et al.* [B23] seek to develop functional forms to represent the effect of the breadth of the molecular weight distribution of $H(\tau)$.

b. Shear Viscosity and Normal Stresses

Shear viscosity measurements on elastomers and polymer melts began with Mooney [M41] in 1936 and continued in the 1940s. Early measurements focused on molecular weight dependence and the dependence of the shear viscosity on shear rate.

The shear viscosity was found to be a decreasing function of shear rate (Fig. 3) but to have an asymptotic viscosity, η_0, at lower shear rates. Fox and Flory [F5] found the zero shear viscosity of η_0 of linear polymer chains to depend on the 3.4 power of molecular weight. This was subsequently confirmed by various researchers [B39, F6, G20, P13, P14]. It was at first found that the zero shear viscosity for branched polymers was lower than that for linear polymers of the same molecular weight [S2]; however, subsequently Kraus and Gruver [K20] showed that above a molecular weight, characteristic of the molecular topology, η_0 for carefully prepared cruciform and Y-shaped polymers actually increases more rapidly perhaps with the sixth power.

The viscosity–shear rate dependence at higher shear weight also has a dependence on molecular weight distribution. In the mid 1960s, Vinogradov and Malkin [V6] found that plots of η/η_0 versus $\eta_0\dot{\gamma}$ were independent of temperature for all polymers. They also argued that this was a universal plot valid for all polymers. This was, however, found not to be the case. In succeeding years, various laboratories [M30, O9, Y3] have found that such plots are strongly dependent on the molecular weight distribution. η/η_0 falls off more

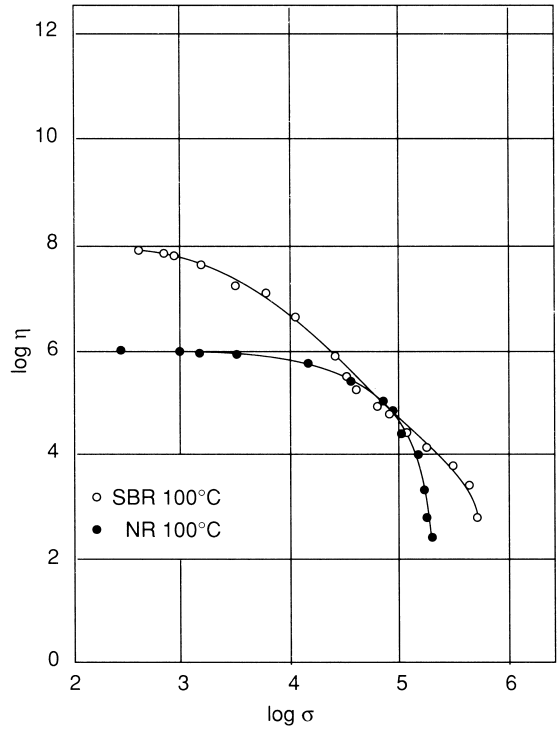

FIGURE 3 Shear viscosity of rubber gums: SMR natural rubber and SBR (Bridgestone-Firestone Duradene 706) as a function of shear stress.

rapidly as molecular weight distribution narrows. Yamane and White (Y3) correlated data on a wide range of polymers including polystyrene, polypropylene, and polybutene-1 to produce a master plot, which allows prediction of breadth of molecular weight distribution for viscosity–shear rate data.

Correlations of the type described in the preceding paragraph are limited to linear hompolymers and have no validity for long-chain branched polymers such as low-density polyethylene.

Cox and Merz [C20] have made the remarkable experimental observation that the non-Newtonian shear viscosity function of flexible chain polymers has the same form as the complex viscosity–frequency function, i.e.,

$$\eta(\dot{\gamma}) = \eta^*(\omega) \tag{20}$$

Normal stresses originally recognized by Weissenberg [W3] through observation of rod climbing effects in soap–hydrocarbon liquid suspensions and polymer solution systems began to be measured on thermoplastics in the 1960s [C9, K9]. White and Tokita [W24] noted their occurrence in gum

elastomers sheared in a Mooney disk rheometer. These were recognized by Weissenberg [W3] from the beginning to be associated with melt elasticity and to be sensitive to breadth of molecular weight distribution. White and Kondo [W20] addressed the dependence of the low-shear-rate principal normal stress difference coefficient Ψ_1 and its dependence on molecular weight. They argued that the dependence should be of order 6.5 to 7.0 which was consistent with their own experiments and other results in the literature. In a 1978 paper, Oda, White, and Clark [O2] correlated normal stresses for polystyrenes with varying molecular weight distribution with shear stress. It was found that the principal normal stress difference N_1, when treated as a function of shear stress, was independent of temperature:

$$N_1 = A\sigma_{12}^a \tag{21}$$

N_1 was larger at the same σ_{12} for broad molecular weight distributions but increased less rapidly with shear stress (i.e., A was large and a was smaller).

2. Theory of Linear Viscoelasticity

By the late 1940s, experimental researchers led by Leaderman and Tobolsky found that the small-strain properties of elastomers and thermoplastic melts were described by the theory of linear viscoelasticity developed by Boltzmann [B26] in the 1870s. This view is made clear in the monographs of Leaderman [L5] and Mark and Tobolsky [M7], which were published in this period. In the next two decades, this subject was developed in monographs by Tobolsky [T5] and, later, Ferry [F3].

Boltzmann's formulation is based on linear materials with incomplete memory. Consider a material which when subjected to strain ε at time zero exhibits a stress.

$$\sigma = G(t)\gamma \tag{22}$$

where $G(t)$ is a modulus function that decays with time. If the response of this material is linear, the stress σ developed for a series of sequential deformations $\gamma_1, \gamma_2, \gamma_3, \ldots$ at times $t_1, t_2, t_3, \ldots$ will be at time t

$$\sigma = G(t-t_1)\gamma_1 + G(t-t_2)\gamma_2 + G(t-t_3)\gamma_3 + \ldots \tag{23}$$

$$= \int_{-\infty}^{t} G(t-s)d\gamma(s) = \int_{-\infty}^{t} G(t-s)\frac{d\gamma}{ds}ds \tag{24}$$

where the integral, refers to the limit for which the applied deformation in continuous. Equation (21) is known as Boltzmann's superposition integral.

If a constant shear rate is imposed at time zero, the stress will be given by

$$\sigma = \left[\int_0^t G(s)ds\right]\dot{\gamma} \tag{25}$$

For long times the integral corresponds to the zero shear viscosity η_0, i.e.,

$$\eta_0 = \int_0^\infty G(s)ds \tag{26}$$

Another deformation of interest is to impose a sinusoidal shear strain $\gamma_0 \sin \omega t$. The stress σ is now found to be expressible as

$$\sigma = \omega\left[\int_0^\infty G(s)\sin\ \omega s\ ds\right]\gamma_0 \sin \omega t + \omega\left[\int_0^\infty G(s)\cos\ \omega s\ ds\right]\gamma_0 \cos \omega t \tag{27}$$

i.e., there are in-phase and out-of-phase components [compare Eq. (18)]. Equation (27) is often rewritten

$$\sigma(t) = G'(\omega)\gamma_0 \sin \omega t + G''(\omega)\gamma_0 \cos \omega t \tag{28}$$

where

$$G'(\omega) = \omega\int_0^\infty G(s)\sin\ \omega s\ ds \tag{29}$$

$$G''(\omega) = \omega\int_0^\infty G(s)\cos\ \omega s\ ds \tag{30}$$

$G'(\omega)$ is known as the storage modulus and $G''(\omega)$ as the loss modulus. Equation (28) is often rewritten in the form

$$\sigma(t) = G^*(\omega)\sin(\omega t + \delta) \tag{31}$$

where δ is a phase angle and $G^*(\omega)$ is known as the complex modulus. Clearly,

$$G'(\omega) = G^*(\omega)\cos\delta \tag{32a}$$

$$G''(\omega) = G^*(\omega)\sin\delta \tag{32b}$$

which leads to

$$G^* = \sqrt{(G')^2 + (G'')^2} \tag{33}$$

$$\tan\delta = G''/G' \tag{34}$$

The quantity $\tan\delta$ is known as the loss tangent.

The "loss modulus" and "loss tangent" expressions for the terms $G''(\omega)$ and $\tan\delta$ suggest that the $G''(\omega)$ term in Eq. (28) is associated with a dissipative process. This should be apparent from the input $\gamma_0 \sin \omega t$ and the output stress component in $\cos \omega t$ of Eq. (18) where a dynamic viscosity $\eta'(\omega)$ is introduced

$$\eta' = \frac{G''(\omega)}{\omega} = \int_0^\infty G(s) \cos \omega s \, ds \tag{35}$$

It has become customary to represent $G(t)$ as a series or continuous spectrum of exponential terms as expressed in Eq. (14). Historically the reason for representations using exponentials is that a single exponential term represents the form of a model that had been proposed by Maxwell [M14] in the 1860s prior to the publication of Boltzmann [B26]. This model has the form of a differential equation which is equivalent to

$$\frac{d\sigma}{dt} = G\frac{d\gamma}{dt} - \frac{1}{\tau}\sigma \tag{36}$$

The solution of Eq. (36) is

$$\sigma = \int_0^\infty G e^{-(t-s)/\tau} \gamma(s) ds \tag{37}$$

This suggests that $G(t)$ could he expressed as a sum of exponentials, i.e., as presented in Eq. (14). The use of Eq. (14) for $G(t)$ leads to a zero shear viscosity of

$$\eta_0 = \int_0^\infty G(s) ds = \sum G_i \tau_i = \int_0^\infty H(\tau) d\tau \tag{38}$$

For sinusoidal oscillations, the storage and loss moduli are found to be

$$G'(\omega) = \sum \frac{\omega^2 \tau_i^2 G_i}{1 + \omega^2 \tau_i^2} \tag{39a}$$

$$G''(\omega) = \sum \frac{\omega \tau_i G_i}{1 + \omega^2 \tau_i^2} \tag{39b}$$

and the dynamic viscosity $\eta'(\omega)$ is

$$\eta'(\omega) = \sum \frac{\tau_i G_i}{1 + \omega^2 \tau_i^2} \tag{39c}$$

We also define $\eta^*(\omega)$, the complex viscosity.

$$\eta^*(\omega) = \frac{1}{\omega}\left[(G'(\omega))^2 + (G''(\omega))^2\right]^{1/2} \tag{39d}$$

When $\omega \to 0$, $\eta'(\omega)$, and $\eta^*(\omega)$ have the same form as the steady shear viscosity and

$$\eta_0 = \eta(0) = \eta'(0) = \eta^*(0) \tag{40}$$

The formulation described above is one dimensional and expressed in terms of a shear stress. It is possible to obtain a three-dimensional representation. Indeed this was done in the original paper of Boltzmann [B26]. Equation (21) may be written in terms of a stress tensor $\boldsymbol{\sigma}$ and pressure p as

$$\boldsymbol{\sigma} = -p\mathbf{I} + 2\int_{-\infty}^{t} G(t-s)\mathbf{d}(s)ds \tag{41}$$

with

$$\mathbf{d} = \frac{1}{2}\left[\nabla\mathbf{v} + (\nabla\mathbf{v})^T\right] \tag{42}$$

d is known as the rate of deformation tensor and **I** a unit tensor. This may be shown by "integration by parts" to be equivalent to

$$\boldsymbol{\sigma} = -p\mathbf{I} + 2\int_{-\infty}^{t} \Phi(t-s)\boldsymbol{\gamma}(s)ds \tag{43}$$

where

$$\Phi(t) = -\frac{dG(t)}{dt} \qquad \textit{and} \qquad G(\infty) = 0 \tag{44a}$$

We may write $\Phi(t)$ as

$$\Phi(t) = \sum \frac{G_i}{\tau_i} e^{-t/\tau_i} \tag{44b}$$

and $\boldsymbol{\gamma}$ is the infinitesimal strain tensor measure from the instantaneous state, i.e.,

$$\boldsymbol{\sigma} = -p\mathbf{I} + 2\int_{0}^{\infty} \Phi(z)\boldsymbol{\gamma}(z)dz \tag{45}$$

4. Theory of Nonlinear Viscoelasticity

A proper formulation of a special theory of nonlinear viscoelasticity was developed by Zaremba [Z5] in 1903, roughly 30 years after the classic paper of Boltzmann [B26]; however the modern period, when there was general acceptance of such formulations, begins with the work of Oldroyd [O6] in 1950. In the 1950s, various special theories of nonlinear viscoelastic behavior were developed by Oldroyd [O7, O8], deWitt [D6], Rivlin and Ericksen [R10], and Noll [N5]. Lodge [L16] and Yamamoto [Y2] sought to develop nonlinear theory using molecular arguments. A totally general formulation of large strain viscoelastic behavior was presented by Green and Rivlin [G16] and Noll [N6] at the end of the decade. This general formulation was then applied to model various special types such as viscometric laminar shear flows [C16, C20, R9] and wave propagation [C14].

Although consensus had rapidly developed around the Boltzmann formulation of linear viscoelasticity, this was not to be the case for the specific forms of the nonlinear theory to use. The general formulation of nonlinear theory devised notably by Green, Rivlin, Noll, Coleman, Ericksen, and Truesdell has not been further developed by newer generations of researchers. Rather, since the mid 1960s, it has declined in influence. From 1960 on, we have increasing numbers of new theories being published. Some of these theories are phenomenological, others based to varying extents on molecular models.

From the early 1970s, powerful numerical tools and high-capacity computers have become increasingly available. In Newtonian fluid dynamics, this led to great increases in our knowledge. For nonlinear viscoelastic fluids where there has been no consensus on constitutive equations, we have instead simulations being carried out for many different models, with a maze of differing predictions of flow behavior and numerical instabilities associated with particular models. By the 1990s, nonlinear viscoelasticity theory and fluid mechanics had taken on many aspects of farce as opposed to science.

It is, however, necessary that we try to weave some rational web that allows us to describe a rational nonlinear theory. The general formulation of Green and Rivlin [G16] took the position that the stress tensor is a general hereditary function of the strain history. The stress tensor was expressed as infinite series of integrals:

$$\boldsymbol{\sigma} = -p\mathbf{I} + \int_0^\infty \Phi(z)\mathbf{e}(z)dz + \int_0^\infty \int_0^\infty [\Psi(z_1, z_2)\mathbf{e}(z_1)\mathbf{e}(z_2) + \sum(z_1, z_2)[\text{tr } \mathbf{e}(z_1)]\mathbf{e}(z_2)]dz_1 dz_2 + \ldots \tag{46}$$

where $\mathbf{e}(z)$ is a nonlinear strain measure and $\Phi(z)$, $\Psi(z_1, z_2)$, and $\Sigma(z_1, z_2)$ are memory functions. Here z is a time measured backward from the present. The strains $\mathbf{e}$ are also measured backward in time. $\Phi(Z)$ is the linear viscoelasticity

relaxation function of Eq. (45). The experiments of Zapas and Craft [Z4], among others, indicate that there is only one stress relaxation function. White and Tokita [W26] show that this is equivalent to reducing Eq. (46) to

$$\boldsymbol{\sigma} = -p\mathbf{I} + \int_0^\infty m(z)[\mathbf{c}^{-1} - \kappa\mathbf{c}]\,dz \tag{47}$$

where $m(z)$ depends on the invariants of $\mathbf{c}^{-1}$, the Finger deformation, tensor, or $\mathbf{c}$, the Cauchy deformation tensor. This type of constitutive equation was arrived at by various authors including Bernstein, Kearsley, and Zapas [B14, B15] and Wagner [W1], among others, using different reasoning. Other authors [B20, B22, B24, C2] arrived at similar constitutive forms but used different invariants such as those of the rate of deformation tensor. The general form of Eq. (47) is often referred to as a BKZ fluid (for Bernstein, Kearsley, and Zapas, who were the earliest proponents).

One particular form of Eq. (47) which has been successfully used for representing the nonlinear viscoelastic behavior of elastomers is due to Bogue and coworkers [B22, B24, C9]. Both Middleman [M24] and Montes and White [M34] have used the form

$$m(z) = \sum_i \frac{G_i}{\tau_{\text{ieff}}} e^{-z/\tau_{\text{ieff}}} \tag{48}$$

with

$$\tau_{\text{ieff}} = \frac{\tau_i}{1 + a\tau_i \overline{\Pi_{\text{d}}^{1/2}}} \tag{49a}$$

$$\overline{\Pi_{\text{d}}^{1/2}} = \frac{1}{t}\int_0^t \Pi_{\text{d}}^{1/2}\,dz \tag{49b}$$

$$\Pi_{\text{d}} = 2\,\text{tr}\,d^2 = 2d_{ij}d_{ij} \tag{49c}$$

d is the rate of deformation tensor of Eq. (43) for gum elastomers. In the work of the latter authors the linear viscoelastic behavior through $G(t)$ for an SMR-5 natural rubber sample at 100°C was fit with the parameters given earlier in Table I. The parameter a of Eq. (49a) was taken as 0.7. A comparison of Eqs. (47)–(49) with steady-state shear viscosity data, transient shear viscosity data, transient shear viscosity at the startup of flow, and stress relaxation following flow is given in Fig. 4. The agreement is quite good.

Criminale, Ericksen, and Filbey [C21] (see also White [W5]) have shown that for long duration shearing flows the general constitutive equations of form Eqs. (46) and (47) reduce to the form

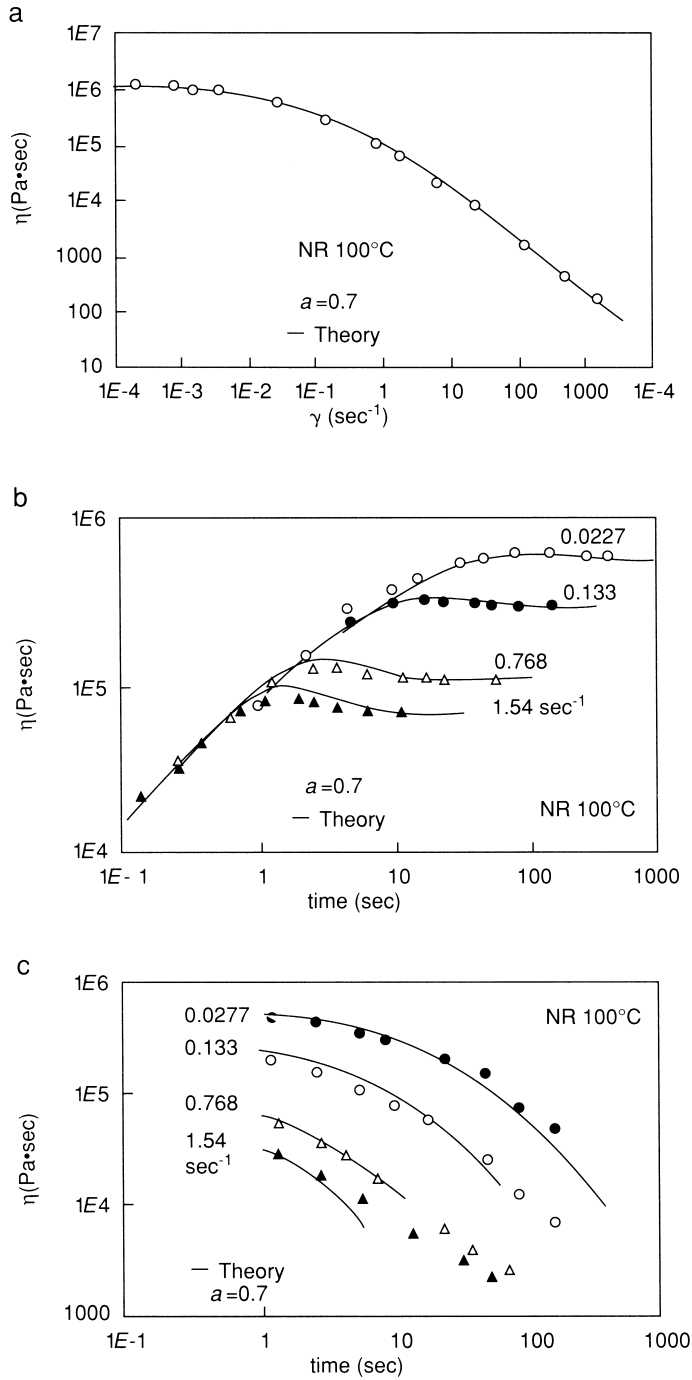

FIGURE 4 Comparison of rheological model of Eqs. (47)–(49) with experiment for natural rubber. (a) Steady-state shear viscosity. (b) Transient shear viscosity at beginning of flow. (c) Stress, relaxation following now.

$$\boldsymbol{\sigma} = -p\mathbf{I} + 2\eta\mathbf{d} + 4\Psi_2\mathbf{d}^2 - \Psi_1\frac{\delta\mathbf{d}}{\delta t} \tag{50a}$$

where:

$$\frac{\delta\mathbf{d}}{dt} = \frac{\partial}{\partial t}\mathbf{d} + (\mathbf{v}\cdot\nabla)\mathbf{d} - \nabla\mathbf{v}\cdot\mathbf{d} - \mathbf{d}\cdot\nabla\mathbf{v} \tag{50b}$$

Here η is the shear viscosity, and Ψ_1 and Ψ_2 are the first and second normal stress difference coefficients. These are functions of tr $\boldsymbol{d}^2$, the trace or sum of the diagonal components of $\boldsymbol{d}\cdot\boldsymbol{d}$ [see Eq. (49c)],

$$\eta = \eta(\text{tr}\,\mathbf{d}^2)\Psi_1 = \Psi_1(\text{tr}\,\mathbf{d}^2)\Psi_2 = \Psi_2(\text{tr}\,\mathbf{d}^2) \tag{51}$$

At low values of $\mathbf{d}$ and tr $\mathbf{d}^2$, the shear viscosity of Eq. (51) goes to the linear viscoelastic value [C15, W5], i.e.,

$$\eta \to \int_0^\infty G(s)ds \tag{52a}$$

and the quantity Ψ_1 goes to its first moment:

$$\Psi_1 \to 2\int_0^\infty sG(s)ds \tag{52b}$$

For a simple shear flow, i.e.,

$$v_1 = \dot{\gamma}x_2\mathbf{e}_1 + 0\mathbf{e}_2 + 0\mathbf{e}_3 \tag{53}$$

Eq. (50) predicts the stress field, i.e.,

$$\sigma_{12} = \eta\dot{\gamma} \tag{54}$$

$$\sigma_{11} - \sigma_{22} = \Psi_1\dot{\gamma}^2, \qquad \sigma_{22} - \sigma_{33} = \Psi_2\dot{\gamma}^2$$

where η, Ψ_1, and Ψ_2 are dependent on $\dot{\gamma}^2$. Thus both shearing stresses and normal stresses are predicted. The results of this paragraph are important because they represent the basis of interpretation of shear flow viscometry of viscoelastic polymer melts and elastomers.

There is a major literature associated with a second class of theories based on generalizing Maxwell's Eq. (36). This was the approach of Zaremba [Z5], Oldroyd [O6–8], deWitt [D6], and Noll [N5] and predates the formulation of Eq. (46). Further papers by White and Metzner [W22], Johnson and Segalman

[J1], and Phan-Tien and Tanner [P7, P8] have developed this approach. This class of constitutive equations is generally of the form

$$\boldsymbol{\sigma} = -p\mathbf{I} + \mathbf{P} \tag{55}$$

$$\frac{\delta \mathbf{P}}{\delta t} + \sum_j a_j(\nabla \mathbf{v}, \mathbf{P}) + b(\mathbf{P}) = 2\eta(\text{tr } \mathbf{d}^2)\mathbf{d} + c(\text{tr } \mathbf{d}^2)\frac{\delta \mathbf{d}}{\delta t}$$

P is an extra stress tensor and a_j, b, η, and c are functions of tr d^2 as indicated. These formulations are much more arbitrary in character than the approach of Eqs. (46) and (47).

The formulations of (47) and (55) have been criticized by Leonov [L9, L11], among others, as not being tested for consistency with the second law of thermodynamics. For Newtonian fluids, such testing requires a positive shear viscosity. For a linear viscoelastic material, one may show that the relaxation modulus function must be always positive to satisfy the second law. The requirements for Eqs. (47) and (55) are not so clear. Leonov has sought to develop nonlinear viscoelastic rheological models based on thermodynamic arguments.

B. Compounds

1. Overview

Although experimental studies of the flow of rubber compounds date to the 1930s [D9, S5], it was only in the late 1980s that there were extensive experimental studies. Reasonable rheological models also date to the 1980s; however, there have been relatively few investigations in this area and little consensus has been reached. In this section we first review the experimental literature. We then turn to rheological models that have been used. The central thrust of the rheological data is the existence of yield values and thixotropic characteristics in rubber compounds.

2. Experimental

We begin this section by first describing steady-state shear flow behavior. We then turn to the discussion of time-dependent characteristics.

In 1931, Scott [S5] on the basis of compression plastomer studies suggested that rubber–particulate compounds at high loadings exhibited yield values; further, he suggested the expression

$$\sigma = Y + K\dot{\gamma}^n \tag{56}$$

to represent the shear stress–shear rate behavior at shear stresses higher than yield value Y. This view was supported by a subsequent study of Dillon and Johnston [D9] using a capillary rheometer. Dillon and Johnston also used

Eq. (56). Equation (56) is usually named for Herschel and Bulkley [H17], who used (or rather misused) this formulation earlier for polymer solutions. Scott-Herschel Bulkley is a better name for Eq. (56).

There was little discussion of this perspective during the next 25 years, and only in the 1960s was there renewed attention. In 1962, Zakharenko *et al.* [Z1] in Moscow reported shear flow measurements of rubber–carbon black compounds. In 1972, Vinogradov *et al.* [V8], also in Moscow, reported similar results for other rubber–carbon black compounds and indicated the occurence of yield values. At the same time similar behavior was reported for talc–polypropylene compounds by Chapman and Lee [C8] of Shell and for titanium dioxide–polyethylene compounds by Minagawa and White [M29].

From about 1980, there have been extensive investigations of the shear viscosity of rubber–carbon black compounds and related filled polymer melts. Yield values in polystyrene–carbon black compounds in shear flow were found by Lobe and White [L15] in 1979 and by Tanaka and White [T1] in 1980 for polystyrene with calcium carbonate and titanium dioxide as well as carbon black. From 1982, White and coworkers found yield values in compounds containing butadiene–styrene copolymer [M1, M37, S12, S18, T7, W29], polyisoprene [M33, M37, S12, S18], polychloroprene [S18], and ethylene–propylene terpolymer [O10, S18]. Typical shear viscosity–shear stress data for rubber–carbon black compounds are shown in Figs. 5(a) and (b). White *et al.* [S12, S18, W28] fit these data with both Eq. (56) and the expression

$$\sigma = Y + \frac{A}{1 + B\dot{\gamma}^{1-n}}\dot{\gamma} \tag{57}$$

Generally it was found that 0.15 volume fraction small particles seem to be required to produce yield values. The yield value Y and viscosity level increase with both increasing particle loading (Figs. 5[a], [b]) and decreasing particle size (Fig. 5[c]). Note: Y is largest for the ISAF compounds and lower for the FEF. It is lowest for the SRF compounds. This is the same order as the particle size (ISAF has the smallest particles). Larger yield and viscosities are also found for calcium carbonate compounds [S25]. For rubber compounds the yield value is of order 50 to 100 kPa and the power law exponent n about 0.2. In Table II, we present values Y, A, B, K, and n of Eqs. (56) and (57).

Recently, Osanaiye *et al.* [O10] have made extensive measurements of creep in rubber–carbon black compounds at very low stresses. It was found that there were stresses below which there was no flow. The yield values determined by these authors were somewhat lower than those reported earlier.

The results of Osanaiye *et al.* [O10] were subsequently confirmed for various polymer melt/elastomer-particle compounds [A10, K8a, L13].

Studies of transient behavior of rubber–carbon black compounds were first reported by Mullins and Whorlow [M51, M52] in 1950. They found that there were strong time-dependent thixotropic effects in rubber–carbon black

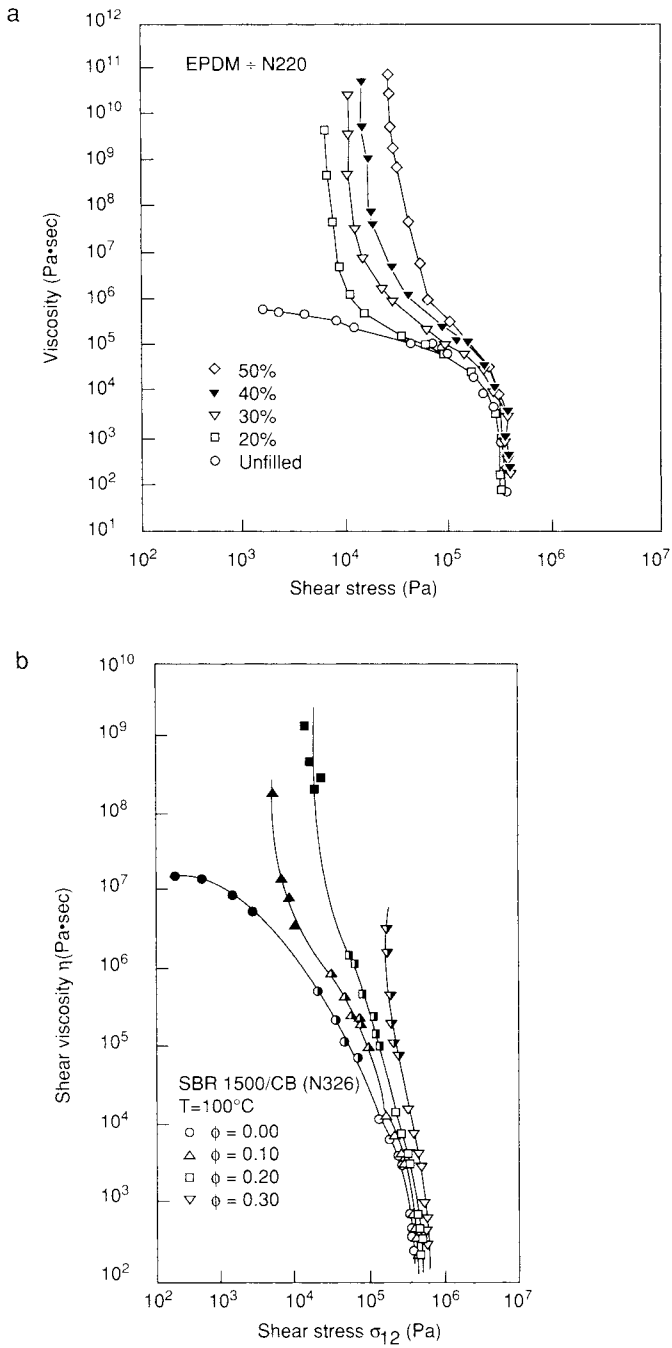

FIGURE 5 (a) Shear viscosity–stress rate data for EPDM rubber compound. Percentages are for volume percent. (b) Shear viscosity–shear rate for SBR rubber compound. ϕ is volume fraction. (c) Shear viscosity–shear stress rate showing effect of particle size.

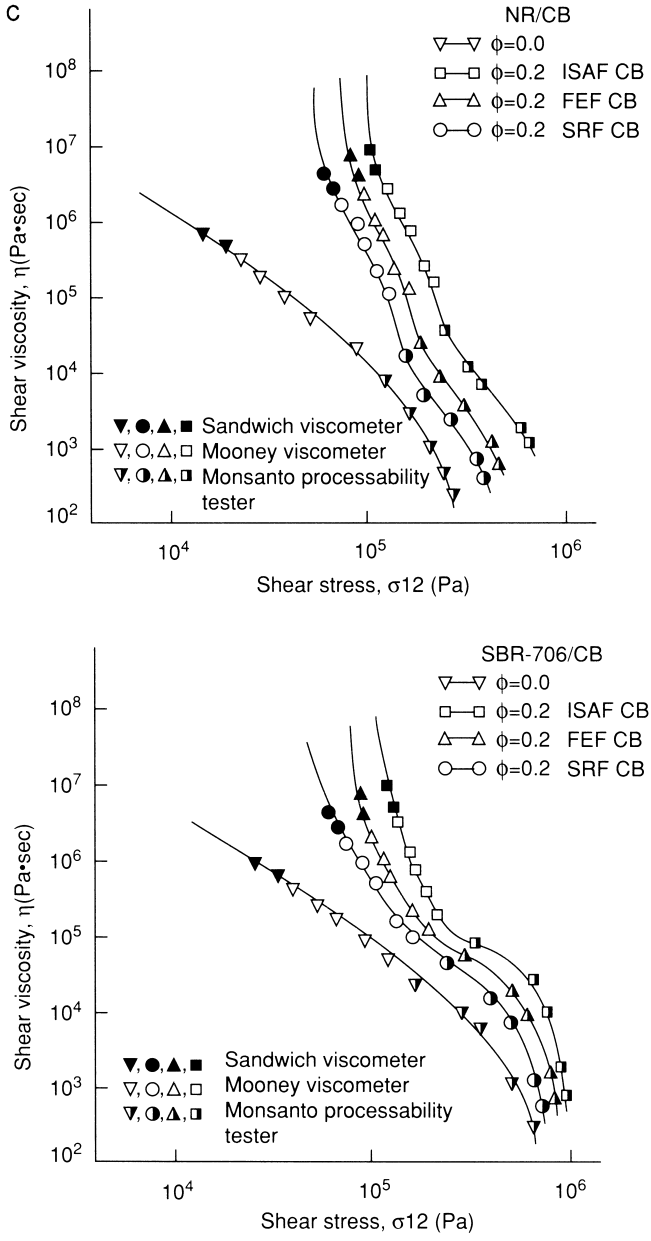

FIGURE 5 (*Continued*).

TABLE II Parameters Y, A, B, K, and n of the Scott–Herschel–Bulkley [Eq. (56)] and White *et al.* [Eq. (57)] Models for Rubber Compounds[a]

Material	Carbon black type	Volume fraction	Y (kPa)	$K = A/B$ (kPa·sec^n)	A (kPa·sec)	B (sec^{1-n})	n
NR	N 220	0.2	119	134.5	73	0.54	0.21
	N 550	0.2	79	105	97	0.93	0.20
	N 762	0.2	62	89	1,268	1.43	0.20
SBR	N 220	0.2	130	200	1,770	8.85	0.225
	N 550	0.2	82	187	7,130	3.82	0.21
	N 762	0.2	62	140	12,970	92.65	0.255
NR	N 330	0.2	63	103	587	5.68	0.175
	N 330	0.3	138	104	330	3.17	0.18
	N 326	0.2	65	108	4,500	41.5	0.2
SBR-1500	N 330	0.2	60.3	132	704	5.32	0.22
	N 330	0.3	158	141	1,030	7.31	0.19
	N 326	0.2	13	142	586	41.33	0.195
CR	N 330	0.2	56	113	178	15.8	0.22
EPDM	N 330	0.2	57.5	176	500	31.3	0.17

[a]From Shin *et al.* [S12].

compounds that were not found in gum elastomers. If one (1) sheared a gum elastomer, time (2) then halted the flow and (3) started up the flow again, within a short period the material would remember its earlier deformation history and respond with stresses lower than it had when it was sheared in the virgin state. If the period of rest was more than 1 minute, all previous history would be forgotten, and the stress response of the gum would be as a virgin material. This was not found in carbon black compounds. Following flow, at first, as with gums, their stress responses would be milder. Again, but now requiring a much longer time, the compounds would gradually gain back their apparent virgin response. However, unlike gums, the compounds would continue to build up a "structure" indefinitely. The longer the storage, the higher the stress transients required to break up the structure and induce steady shear flow. This same problem has been investigated by Montes *et al.* [M37]. Typical examples of storage effects on stress transients at the beginning of flow are shown in Fig. 6. As the storage time increases, the stress overshoot transients become larger and larger. With sufficient storage times they exceed the initial sample.

Lobe and White [L15] studied stress relaxation following imposed strains in polystyrene–carbon black compounds and found that the stresses did not decay to zero, but to a finite value of stress roughly equal to the yield value of Eqs. (56) and (57). Montes *et al.* [M37] have found similar effects in rubber–carbon black compounds. This is shown in Fig. 7. Montes *et al.* found similar effects in stress relaxation following shear flow.

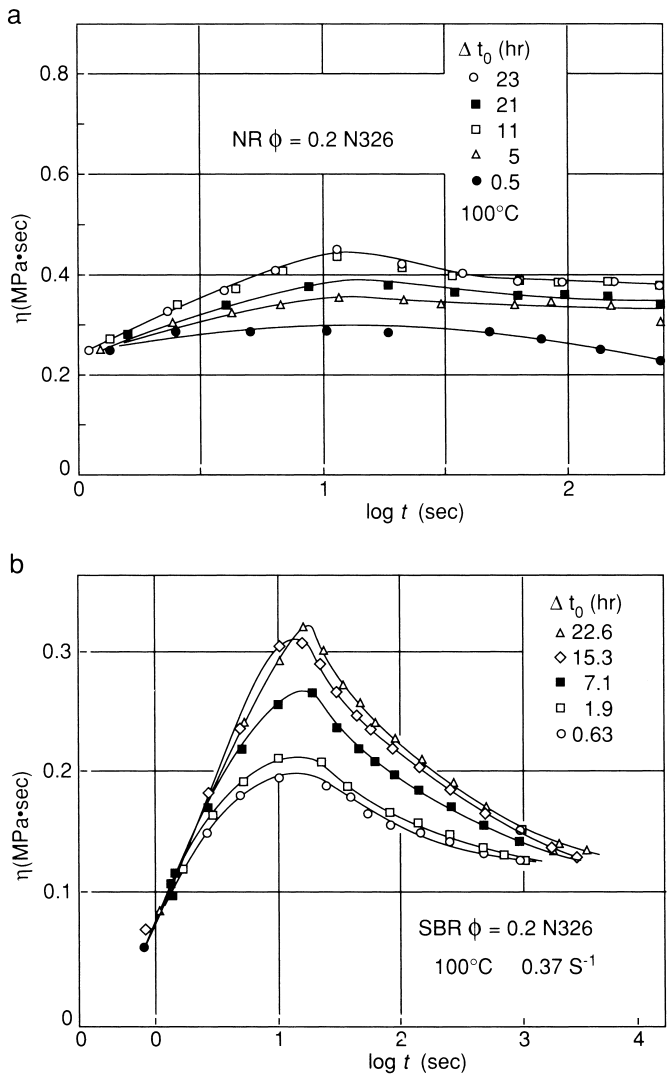

FIGURE 6 Storage effects on stress transients at beginning of flow. (a) Transient shear viscosity of NR with 0.2 volume fraction N 326 black, $T = 100°C$. (b) Transient shear viscosity of SBR with 0.2 volume fraction N 326 black, $T = 300°C$.

There have been many studies of the dynamic viscosity $\eta'(\omega)$ and complex viscosity $\eta^*(\omega)$ of rubber–carbon black compounds and other filled systems. Nakajima *et al.* [N2] and later researchers found that the Cox–Merz [C19] rule mentioned earlier for flexible chain polymer melts is not valid for filled polymer melts or elastomcr. Generally, one has the inequality $\eta^*(\omega) > \eta(\dot{\gamma})$. The complex viscosity is considerably larger.

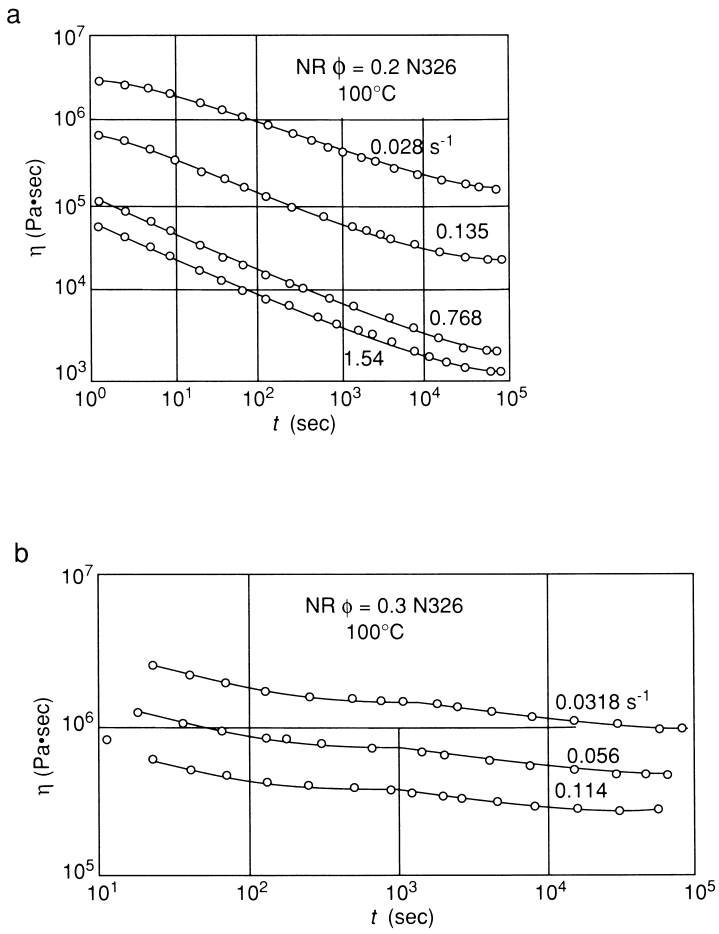

FIGURE 7 Stress relaxation in natural rubber–carbon black compound following flow. (a) NR $\phi = 0.2$. (b) NR $\phi = 0.3$.

3. Theory of Plastic Viscous Fluids

The theory of flow of materials with yield values dates to the work of Schwedoff [S8] of the University of Odessa in 1890. Schwedoff designed and built a coaxial cylinder instrument to measure the shear viscosity of gelatin suspensions. For steady shear flows he correlated his data with

$$\sigma = Y + \eta_B \dot{\gamma} \tag{58}$$

a result later rediscovered by Bingham [B18, B19] and usually named after him.

A three-dimensional formulation of the Bingham plastic was developed by Hohenemser and Prager [H19] in 1932 using the von Mises yield criterion (see Reiner [R4] and Prager [P15]). This employs a deviatoric stress tensor **T** and has the form

$$\boldsymbol{\sigma} = -p_1\mathbf{I} + \mathbf{T} \tag{59a}$$

with

$$\text{tr } \mathbf{T} = T_{11} + T_{22} + T_{33} = 0 \tag{59b}$$

Accepting the von Mises yield surface

$$\text{tr } \mathbf{T}^2 = 2Y^2 \tag{60}$$

T has the form above the yield stress defined by Eq. (60):

$$\mathbf{T} = \frac{Y}{\sqrt{\frac{1}{2}\,\text{tr } \mathbf{T}^2}}\mathbf{T} + 2\eta_B\mathbf{d} \tag{61}$$

tr $\mathbf{T}^2$ is the trace of the scalar product of $\mathbf{T}\cdot\mathbf{T}$, and **d** is the rate of deformation tensor of Eq. (29b). Oldroyd [O3] has shown that Eq. (49) may be written in the simpler form

$$\mathbf{T} = \frac{2Y}{\sqrt{2\,\text{tr } \mathbf{d}^2}}\mathbf{d} + 2\eta_B\mathbf{d} \tag{62}$$

Oldroyd [O5] first envisaged viscous fluids with yield values and non-Newtonian viscosities. He wrote

$$\mathbf{T} = \frac{2Y}{\sqrt{2\,\text{tr } \mathbf{d}^2}}\mathbf{d} + 2\eta_B(\text{tr } \mathbf{d}^2)\mathbf{d} \tag{63}$$

where η_B depends on tr $\mathbf{d}^2$. The Scott–Herschel–Bulkley equation, Eq. (56), may be expressed

$$\mathbf{T} = \frac{2Y}{\sqrt{2\,\text{tr } \mathbf{d}^2}}\mathbf{d} + 2K[2\,\text{tr } \mathbf{d}^2]^{(n-1)/2}\mathbf{d} \tag{64}$$

and Eq. (57) as

$$\mathbf{T} = \frac{2Y}{\sqrt{2\,\text{tr } \mathbf{d}^2}}\mathbf{d} + \left[\frac{A}{1 + B[2\,\text{tr } \mathbf{d}^2]^{(1-n)/2}}\right]\mathbf{d} \tag{65}$$

Parameters for the constitutive equations of Eqs. (64) and (65) for rubber compounds are contained in Table II.

4. Plastic Viscoelastic Fluid Models

The concept of a material with a yield value that behaved in a differentially viscoelastic manner above the yield value was also due to Schwedoff [S8]. He reported transient experiments and concluded that the gelatin material responded as a viscoelastic material above its yield value. This led him to modify the one-dimensional Maxwell model into the form

$$\frac{d\sigma}{dt} = G\frac{d\gamma}{dt} - \frac{t}{\tau}(\sigma - Y) \tag{66}$$

and proposed it would represent the rheological properties of gelatin suspensions.

There was no follow-up to the work of Schwedoff as there had been to Maxwell. During most of the century following Schwedoff's paper, his work was remembered only through the monographs of Reiner [R2, R3]. It is only with the publication of Hohenemser and Prager [H19] and more especially White [W9] and in 1979 that the approach initiated by Schwedoff was revived. Specifically, it was pointed out that Eq. (66) is a differential equation whose solution is

$$\sigma = Y + \int_0^\infty Ge^{-(t-s)/\tau}\frac{d\gamma}{ds}(s)ds \tag{67}$$

This could be considered a special case of a more general form:

$$\sigma = Y + \int_0^\infty G(t-s)\frac{d\gamma}{ds}ds \tag{68}$$

Using the analog of Eq. (61), White proposed that for a material responding as a viscoelastic material above the yield value,

$$\mathbf{T} = \frac{Y}{\sqrt{\frac{1}{2}\,\mathrm{tr}\,\mathbf{T}^2}}\mathbf{T} + \mathbf{H} \tag{69}$$

where $\mathbf{H}$ is a memory functional. This was shown to be equivalent to

$$\mathbf{T} = \frac{2Y}{\sqrt{2\,\mathrm{tr}\,\mathbf{H}^2}}\mathbf{H} + \mathbf{H} \tag{70}$$

Three-dimensional formulations for **T** including nonlinear viscoelastic integral forms are contained in the papers of White [W9], White and Tanaka [W23], and White and Lobe [W21]. These all have the general form of Eq. (70) with [compare Eq. (47)]

$$\mathbf{H} = \int_0^\infty m(z)\left[\mathbf{c} - \frac{1}{3}(\text{tr } \mathbf{c}^{-1})\mathbf{I}\right]dz \tag{71}$$

where $m(t)$ is a memory function. Isayev and Fan [I5] have also proposed a formulation of the type of Eq. (70), but using the Leonov model [L9] as the basis of **H**.

5. Thixotropic Plastic Viscoelastic Fluid

The problem of constitutive equations involving thixotropy is an old one. In the 1930s, Freundlich and Jones [F9], among others, associated thixotropy in suspensions of small particles with the occurrence of yield values.

The formulations described in the previous section show yield values coupled with viscous and viscoelastic flow, but not with thixotropy. It is possible to introduce thixotropy into plastic fluid behavior by allowing Y to depend on the history of tr $\mathbf{d}^2$. This approach was applied to fluids with viscoelastic response above the yield value by Suetsugu and White [S26] and later by Montes and White [M35].

Alternate approaches to represent thixotropy rates of structural breakdown and re-formation may be developed involving the stresses, deformation rate, and internal structure. Linear theories of this type date to Goodeve and Whitfield [G10, G11].

The most recent study of this type, that of Montes and White [M35], compares its predictions with the rheological behavior of rubber compounds and we cite it here. Montes and White write the yield function [compare Eq. (49c)]

$$Y(\Pi_\text{d}, t) = Y_\text{f} + \left(\beta_1 \Pi_\text{d}^{1/2} + \beta_2 \Pi_\text{d}\right) \int_{-\infty}^{t} \alpha \Pi_\text{d}^{1/2} e^{-\alpha \Pi_\text{d}^{1/2}} (t - s) ds \tag{72}$$

$m(z)$ is taken to have same form as Eqs. (48a) and (49). The modulus G_i was taken to have the same value as G_i^0, the value for the gum, and τ_i was taken to be $f(\phi)\tau_i^0$, where τ_i^0 is the value for the gum and $f(\phi)$ the magnitude of the increases of τ_i^0 for a noninteractive filler.

The formulation of Eqs. (70)–(72) was compared with experiment for an SMR-5 nature rubber with 0.2 volume fraction N-326 carbon black. The steady-state viscosity is compared with experiment in Fig. 8(a), and the transient shear stress buildup at the start of flow is considered in Fig. 8(b). The shear flow–rest–shear flow data are contained in Fig. 8(c). The agreement is, in general, good.

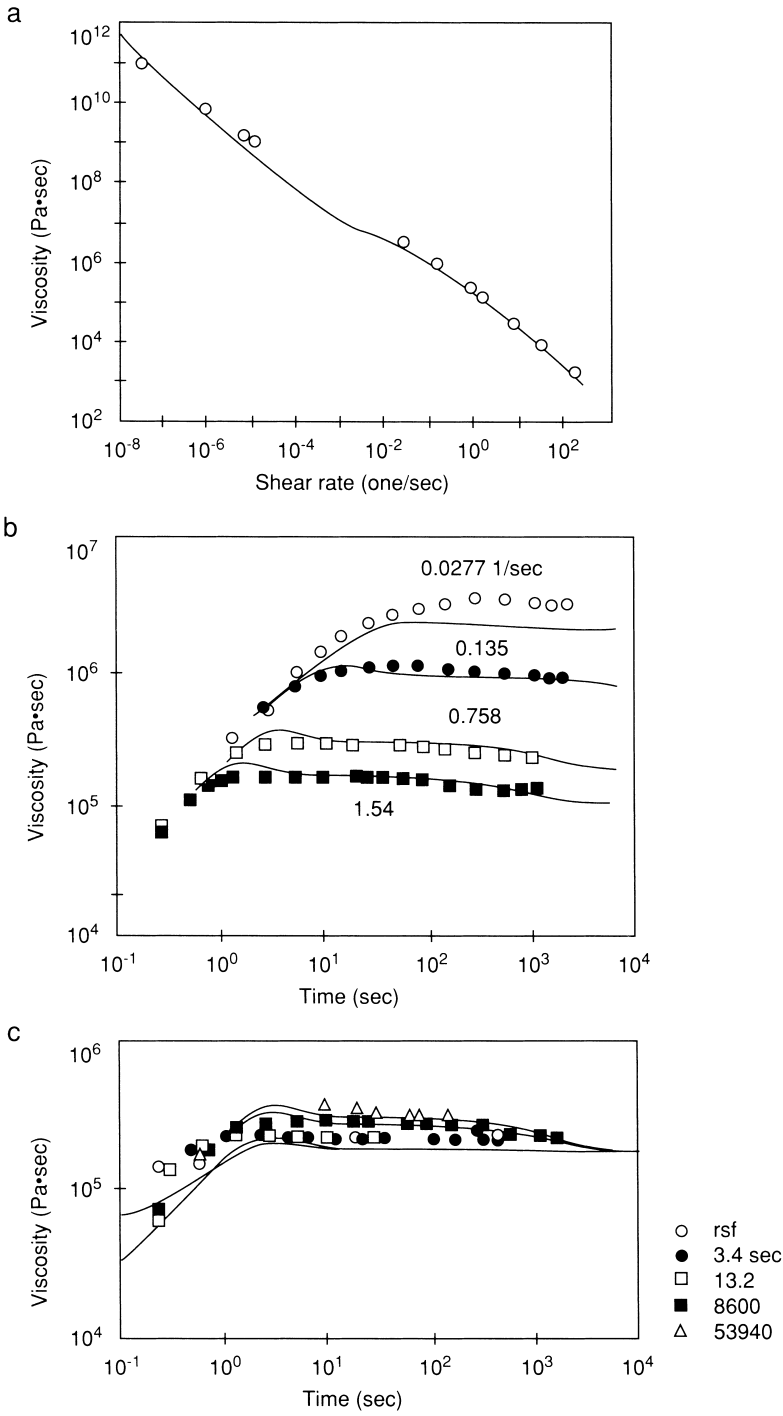

FIGURE 8 Comparison of rheological model of Eqs. (70)–(72) with experiment on rubber–carbon black compound. (a) Steady shear viscosity. (b) Transient. (c) Shear–rest-shear flow behavior.

An alternate formulation rather different from that of this section has been given by Leonov [L10]. It also combines thixotropic behavior and a yield value and is based on thermodynamic arguments.

IV. BOUNDARY CONDITIONS

It is now well accepted that Newtonian liquids adhere to solid surfaces as pointed out by Goldstein [G9]. It was a very controversial subject as late as the 1840s, as may be seen by reading the writings of Stokes [S22–24] in this period.

There is a long history of concerns about the boundary conditions of rubber and rubber compounds on steel and other metal surfaces. Melvin Mooney described in his Goodyear Medal Address [M46] that the potential slippage of rubber on steel surfaces was his first concern when he was assigned by the U.S. Rubber Company to work on the processability of unvulcanized rubber in 1928. Indeed, it concerned him throughout his career and was also the subject of a paper published [M45] in the year that he retired, 1959. Mooney's experiences with rubber caused him to be the first scientist to seek to develop experimental techniques to measure slippage of materials during flow. In a paper published in 1931 [M39], he described methods of determining slippage in both capillary and coaxing cylinder rheometers. We describe Mooney's often-quoted capillary analysis in Section VI, D. In a 1936 paper [M41] devoted to determining the shear viscosity of natural rubber in a coaxial cylinder viscometer, Mooney carefully put grooves into both the stationary cylinder and rotor to prevent slippage on either surface. This was also done in his 1934 shearing disk instrument intended for quality control [M40]. Mooney was not the only one in this early period concerned with slippage. Similar concerns were expressed by Garner [G1] in regard to the Williams compression plastomer.

In the 1940s, little attention was given to this subject, but in the 1950s, we find Mooney with Black [M47] discussing slippage in extrusion through slit dies. In a 1954 paper, Decker and Roth [D4] described several experiments in a Mooney shearing disk viscometer. They found that the measured shear viscosity depended on the depth of the serrations on the shearing disk and on the type of metal which was coated onto the surface. Mooney [M43, M45] made extensive studies of slippage in the 1950s generally by comparing the results of serrated and smooth steel rotors in a Mooney viscometer. He found that slip was induced by adding soap to rubber, especially emulsion-polymerized butadiene–styrene copolymer. He reported experiments on polytetrafluroethylene-coated rotors, which showed greatly reduced torques apparently associated with slippage. In a 1958 review paper on the rheology of elastomers, Mooney [M44] presents "slippage" as if it is a well-established fact and describes the work cited earlier in which he seeks to quantify his results in terms of slip velocities.

In the two decades following Mooney's retirement, there was little in the literature referring to this phenomenon; however, in 1980, Turner and Moore [T12] of Avon Rubber returned to this subject. These authors constructed a controlled-pressure rotational rheometer to study the rheological and slip flow characteristics of rubber and its compounds. It was thus possible to compare behavior at the same pressures. They first compared a gum butyl rubber in this apparatus and then showed that the torque rotor speed data are the same for all three rotors; however, when a fully compounded nitrile rubber (NBR) with high levels of plasticizers and fillers was investigated, it was found that the torques on the ground and polished rotors were significantly lower than that on the ground rotors. This was taken as evidence of slip. Slip was similarly found in an ethylene–propylene terpolymer highly filled with carbon black and oil. It was found that the slip velocity increased with temperature and was suppressed by applied pressure.

Ahn and White [A1] have shown that carbooxylic acids and amides induce slip in polyethylene and polypropylene melts presumably by exuding to the surface and forming a low viscosity layer. This was also found to be the case with carbon black compounds, but the situation with compounds containing polar particles was more complex.

In 1988, Montes and his coworkers [M37] at the University of Akron described experiments on a rebuilt multispeed Mooney viscometer which had been pressurized in the manner described by Turner and Moore [T12]. Torque–rotor speed sweeps were made at various applied pressure for both gums and compounds. It was found that at applied pressures below 0.5 MPa (500 kPa), the torque was greatly reduced, indicating the occurrence of slippage (Fig. 9). If a low pressure were initially applied and then a substantial pressure imposed, the torque would suddenly increase as shown in Fig. 10. This indicated the rapid occurrence of adhesion of polymer on the rotor. If the pressure were removed, the torque would slowly decay away (see Fig. 10). The onset of slippage could be observed from the rubber caps removed from the rotors; it would begin on the outer radius and propagate inward. These studies have been extended by Han *et al*. [H3] and White *et al.* [W18] from the same laboratories. These authors noted that the critical pressure for the onset of slippage, which seemed to be about 0.2 MPa, was independent of the metal of construction with the exception of polytetrafluorethylene (PTFE) in which it was most serious. When, however, one operated at low applied pressures, brass and copper gave rise to the highest shear stresses, followed by aluminum, then different steels, and finally PTFE. Generally, slippage occurs at about the same critical pressure with smooth and serrated rotors, but in the region of slip, there are higher stresses with serrated rotors.

Brzoskowski *et al*. [B30, B33, B35] at the University of Akron have described experiments involving extrusion through dies made out of porous metal. When air pressures are at a level of 0.2 MPa, there is an enormous decrease in pressure gradient along the die axis. Such decreases can be more

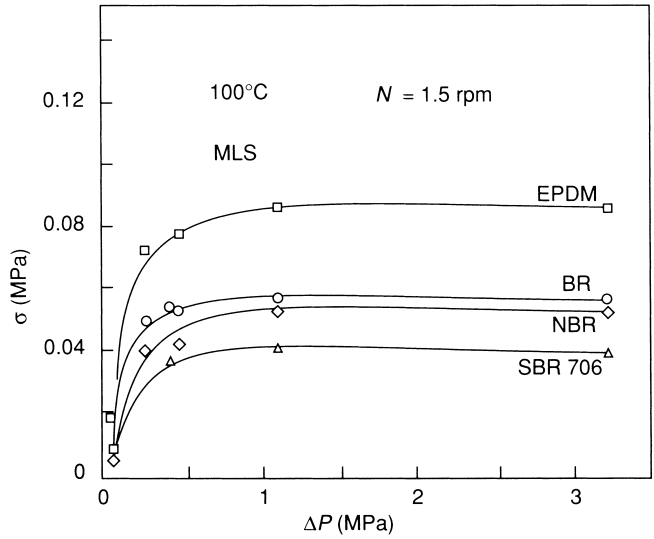

FIGURE 9 Effect of pressure level on torque in biconical rheometer.

than 90%. An experimental study showing the influence of decreasing the imposed air pressure on a rubber compound in steps is shown in Fig. 11. When the pressure decreases below 0.2 MPa, the axial pressure drop increases drastically. These results strongly imply the development of slippage.

V. MECHANOCHEMICAL BEHAVIOR

A. Degradation of Individual Elastomers

Mastication softening of natural rubber was discovered around 1820 by Hancock [H11], who also found that at any concentration level, solutions of masticated rubber would possess a lower viscosity than the initial polymer. It was not, however, until the acceptance of the macromolecular hypothesis and the work of Cotton [C17] and Busse and Cunningham [B37, B38] in the 1930s that the importance of oxygen (as well as the mechanism involved) in the mastication process came to light. The results of these researchers were subsequently verified by Pike and Watson [P11]. Essentially it is thought that the natural rubber degrades to form free radicals under the action of stresses and that the radicals are stabilized through reaction with oxygen:

$$\mathrm{R{-}R'} \xrightarrow{\text{stress}} \mathrm{R^{\bullet} + R_{\bullet}}$$

$$\mathrm{R^{\bullet} + O_2 \longrightarrow RO_{2\bullet}}$$

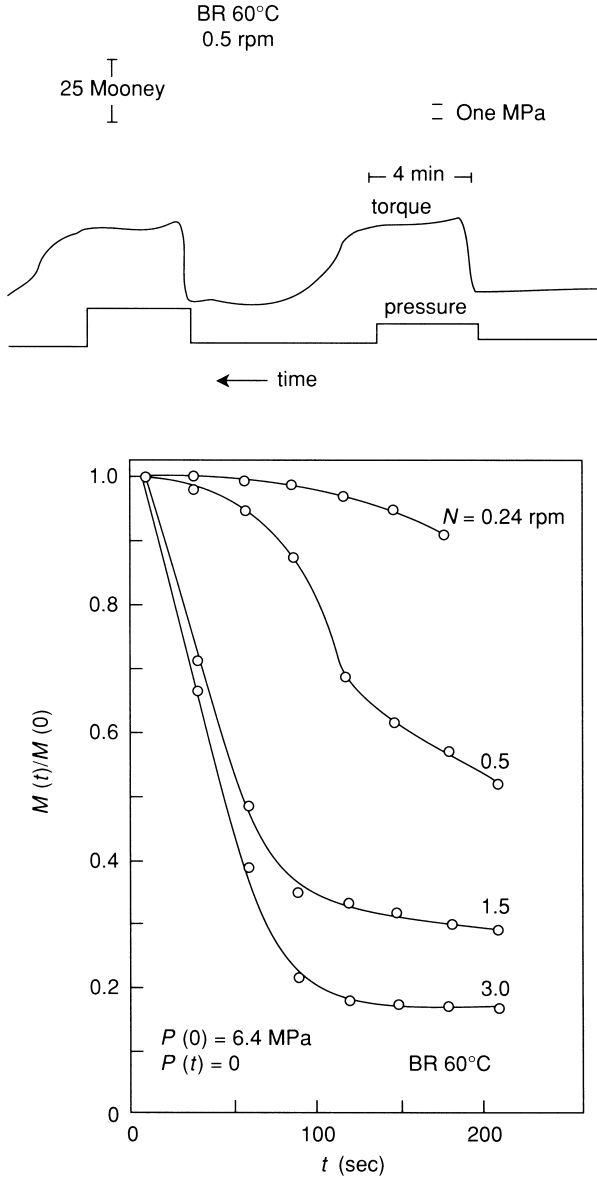

FIGURE 10 Influence of pressure history on torque history in a rotational rheometer.

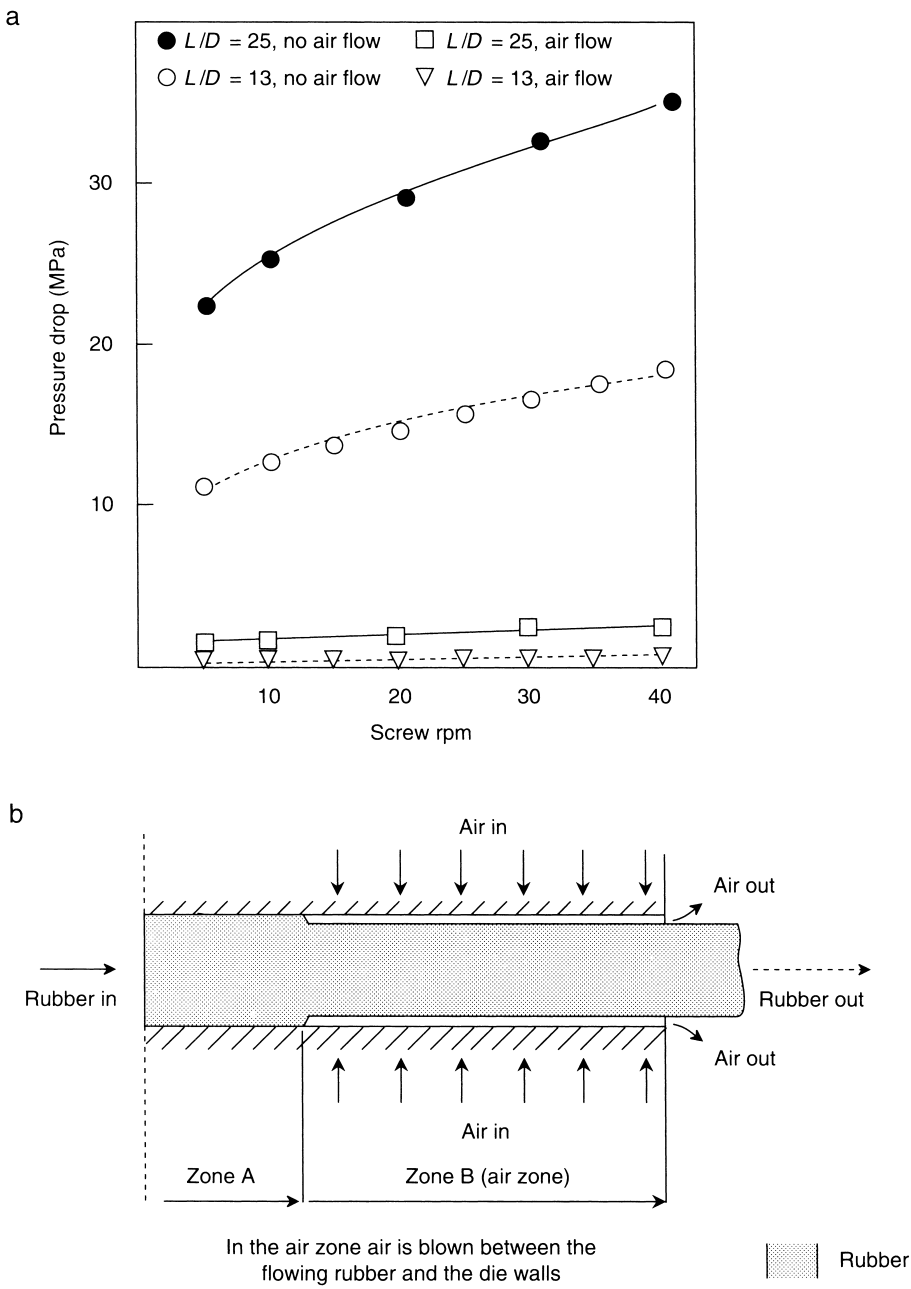

FIGURE 11 Effect of air pressure in porous metal air-lubricated die.

One of the major points made, notably by Busse, was that the temperature has a peculiar influence on breakdown. At low temperatures, degradation is induced by applied stresses, and if the temperature is increased while the kinematics of mastication are unchanged, the rate of polymer degradation will decrease. If the temperature continues to be raised, the rate of degradation will pass through a minimum and begin to increase again. This is due to the interaction of the simultaneous decrease in viscosity and increase in rate of oxidative attack with temperature.

Generally it is found that there is little reduction in molecular weight when mastication is carried out in nitrogen. Busse and Cunningham [B38] and Pike and Watson [P11] have found that addition of free radical acceptors to natural rubber masticated in nitrogen leads to molecular weight reduction. Pike and Watson suggest that the free radical acceptors play a role similar to that of oxygen. Quantitative verification of this has been obtained by Ayrey *et al.* [A13] who related spectral and radiochemical determination of end groups to molecular weight reduction.

The influence of mastication on molecular weight distribution has been studied by Angier *et al.* [A5] and later investigators. It was found that high-molecular-weight species are preferentially degraded and narrower-molecular-weight-distribution materials are formed.

Although most investigations of stress-induced degradation have been carried out on natural rubber, studies on other elastomers (synthetic *cis*-1,4-polyisoprene, *cis*-1,4-polybutadience, butadiene–styrene copolymer) have appeared [B27, F4]. Folt [F4] has studied the influence of mastication-induced degradation on the rheological properties of elastomers, especially polybutadienes and polyisoprenes. The greatest breakdown rates are found in *cis*-1,4-polyisoprene, a fact attributed to (1) stress-induced crystallization occurring during the deformation process, which results in especially high stresses, and (2) resonance stabilization of the radicals produced.

B. Rubber Blends

Angier and Watson [A7, A9] found that graft copolymers could be prepared by masticating elastomer blends in the absence of oxygen. The systems studied included natural rubber/polychloroprene, natural rubber/butadiene–styrene copolymer, and polychloroprene/butadience–styrene copolymer. The mechanism hypothesized was

$$\mathrm{A{-}A'} \xrightarrow{\text{stress}} \mathrm{A\cdot + A'\cdot},$$

$$\mathrm{B{-}B'} \xrightarrow{\text{stress}} \mathrm{B\cdot + B'\cdot}$$

$$\mathrm{A\cdot + B\cdot} \longrightarrow \mathrm{A{-}B}$$

C. Elastomers Swollen with Monomers

It has been shown by Angier and Watson [A8, W2] that if an elastomer is swollen with a vinyl monomer (styrene, chlorostyrene, acrylic acid, methyl acrylate, methacrylic acid, methyl methacrylate, vinyl pyridine, methyl vinyl ketone, etc.), mastication in the absence of oxygen can lead to the formation of block copolymers. This would seem to occur through the mechanism

$$\mathrm{R{-}R'} \xrightarrow{\text{stress}} \mathrm{R\cdot + R\cdot}$$

$$\mathrm{R\cdot + M} \longrightarrow \mathrm{RM\cdot}$$

$$\mathrm{RM\cdot + M} \longrightarrow \mathrm{RMM\cdot}$$

$$\mathrm{RMM\cdot + M} \longrightarrow \mathrm{RM_{n+1}M\cdot}$$

Angier *et al*. [A4, C4] have shown that this process may also be applied to glassy vinyl plastics if they are processed in a rubbery state.

VI. RHEOLOGICAL MEASUREMENTS

A. Parallel Plate and Sandwich Rheometer

Perhaps the conceptually simplest type of rheometer can be constructed by sandwiching a material to be tested between two or three parallel plates that are separated by a distance H, and moving one plate parallel to the others at a velocity V (Fig. 12). The shear rate $\dot{\gamma}$ is V/H. For normal liquids this is not practical, but for elastomers and compounds it is very much so. Apparatus of this type have been designed and used by Zakharenko *et al*. [Z1],

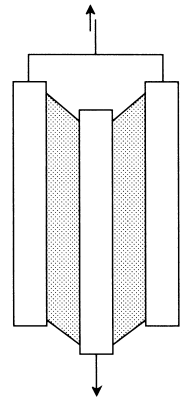

FIGURE 12 Sandwich rheometer.

Middleman [M24], Goldstein [G8], Furuta *et al.* [F11], Lobe and White [L14], Toki and White [T7], Montes *et al.* [M37], Osanaiye *et al.* [O10], and K. J. Kim and White [K8a]. The apparatus (with constant-temperature chamber) may be placed in a tensile tester and operated in a mode with a fixed velocity V giving a constant shear rate. It may, on the other hand, be used in a creep mode with hanging weights. This provides constant stress experiments. At low stress levels one needs to compensate for the weight of the central member which exerts a gravitational stress [O10]. At very low stresses one may accurately determine the yield value of rubber–carbon black compounds. Osanaiye *et al.* [O10] have made measurements at shear stresses below the yield value.

The shear rate $\dot{\gamma}$ is the ratio of the velocity of the moving member V to the perpendicular distance between the plates, i.e.,

$$\dot{\gamma} = V/H \tag{73}$$

The shear stress σ_{12} is

$$\sigma_{12} = \frac{F}{2A} = \frac{F}{2(A_0 - VWt)} \tag{74}$$

The term VWt accounts for the decreasing active surface of the sandwich face. W is the width of the sandwich and t is experimental time.

B. Biconical Rheometer

The concepts of the cone-plate and biconical rheometers developed in the 1940s (Fig. 13). The cone-plate instrument is due to Freeman and Weissenherg [F10] and intended for modest-viscosity fluids. It has the basis of his "rheogoniometer" which also measured normal stresses. The biconical rheometer was developed in the same period by Piper and Scott [P12] of the BRMRA and was from the beginning intended for rubber. Similar instruments are discussed by Turner and Moore [T12] and Montes *et al.* [M37, M38]. In the latter instruments, the pressure is controlled by charging the rubber into the rheometer by an attached pressure-driven device.

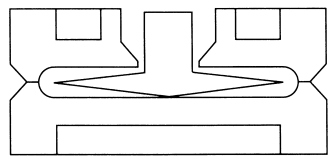

FIGURE 13 Biconical rheometer.

The great advantage of cone-plate geometries occurring in both instruments is that for small-cone angles, the shear rate is constant throughout the gap between the cone and the plate. It is given by

$$\dot{\gamma} = \frac{\Omega}{h(r)} = \frac{\Omega}{r\tan\alpha} = \frac{\Omega}{\tan\alpha} \tag{75}$$

where $h(r)$ is the vertical distance from the plate to the cone and α is the angle between the cone and plate.

The shear stress in a biconical instrument may be computed from the torque M through the expression

$$M = 2\int_0^R 2\pi r^2 \sigma_{12} dr = \frac{4\pi R^3}{3}\sigma_{12} \tag{76}$$

The instruments of Turner and Moore [T12] and Montes *et al.* [M38] are pressurized by an external reservoir. This allows shear flow measurements to be carried out at constant shear rates and conditions for the development of slippage in individual compounds to be determined.

C. Shearing Disk Viscometer

The shearing disk viscometer introduced in 1934 by Mooney [M40] has played a very important role in the rubber industry because of its utilization for monitoring and control of rubber samples (Fig. 14). It is related to the parallel disk type shear flow instrument that has been widely used for polymer solutions and melts.

The shear rate between the two disks at radial position r is

$$\dot{\gamma}(r) = r\Omega/h \tag{77}$$

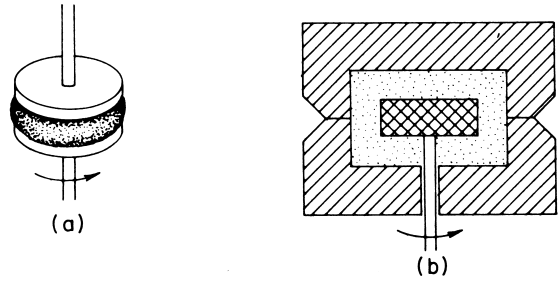

FIGURE 14 Shear disk viscometers: (a) parallel disk, (b) Mooney.

where h is the distance between the disks and Ω is the rotation rate of the moving disk. The torque M in this geometry is given by

$$M = \int_0^R 2\pi r^2 \sigma_{12} dr \tag{78}$$

where σ_{12} varies with radius r. As has been shown by several researchers, Eq. (77) may be substituted into Eq. (78) and the integral differentiated with respect to the shear rate, $\dot{\gamma}(R)$, at the outer perimeter of the disk to yield

$$\sigma_{12}(R) = \left(\frac{S+3}{4}\right)\left(\frac{2M}{\pi R^3}\right) \tag{79}$$

where

$$S = d \log M / d \log \Omega$$

For a power law fluid $S \sim n$.

In a shearing disk viscometer, the torque M on the disk may be expressed as

$$M = 2\left[\underbrace{\int_0^R 2\pi r^2 \sigma_{\theta z} dr}_{\text{surface}}\right] + \underbrace{2\pi R^2 H(\sigma_{\theta r})_R}_{\text{periphery}} \tag{80}$$

where H is the thickness of the disk. Equation (80) may be solved for the torsional shear stress at the outer radius of the disk and an expression analogous to Eq. (73) obtained:

$$\sigma_{\theta z}(R) = \frac{S+3}{4}\left(\frac{2M}{\pi R^3}\right) F \tag{81}$$

Where, the function F is given by Nakajima and Harrel [N3].

The quality-control shearing disk viscometer has always had only a single rotor speed (2 rpm), though Mooney [M42] as early as the 1940s built a multispeed unit. The use of Eq. (81) to determine $\sigma_{\theta z}(R)$ and shear viscosity implies a multispeed instrument.

There has long been interest in making measurements of viscoelastic properties in this instrument. Mooney [M42] described measurements of elastic recoil, and Koopmann and Kramer [K16] of Bayer AG developed a Mooney viscometer allowing stress relaxation after flow. Such an instrument was later discussed by Montes *et al.* [M37]. Monsanto [G21] and later Alpha Technologies have commercialized a quality-control instrument similar to that of Koopmann and Kramer.

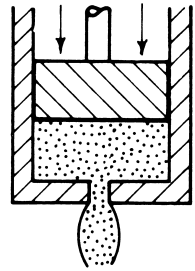

FIGURE 15 Capillary rheometer.

D. Capillary Rheometer

The capillary rheometer, one the oldest and most widely applied experimental tools for measuring the viscosity of fluids (Fig. 15), was used extensively on almost all classes of complex fluids by the founders of modern rheology during the 1920s and 1930s. Its application to rubber dates to the work of Marzetti [M8–11] and Dillon and coworkers [D7–9], and it has been widely used through the years.

The basic idea of the instrument is to relate the pressure loss for extrusion through a small-diameter tube of diameter D and length L to the shear stress at the capillary wall and the extrusion rate to a wall shear rate. The total pressure drop p_T through a die is the sum of a pressure loss within the die Δp and a second pressure drop Δp_e at the ends (i.e., at the entrance and the exit):

$$p_T = \Delta p_e + \Delta p \tag{82}$$

We may relate Δp to the wall shear stress $(\sigma_{12})_w$ by a simple force balance

$$\pi D L (\sigma_{12})_w = (\pi D^2/4)\Delta p \tag{83}$$

which allows us to write

$$(\sigma_{12})_w = D\Delta p/4L \tag{84a}$$

$$p_T = \Delta p_e + 4(\sigma_{12})_w L/D \tag{84b}$$

As noted by Mooney and Black [M47] and subsequently Bagley [B8], ΔP_e can he large relative to Δp. By using a series of dies with varying L/D, one may determine $(\sigma_{12})_w$ from the slope of a graph of p_T versus L/D, which is called a Bagley plot [B8]. The wall shear rate must be kept constant, but this may be ensured by using dies of constant diameter and maintaining Q.

Implicit in Eq. (84) is the idea that the diameter of the reservoir preceding the die is much greater than the die. If this is the case, reservoir pressure

losses need to be considered. This correction has been considered by Metzger and Knox [M22].

The capillary wall shear rate may be obtained in a manner devised by Weissenberg and coworkers [E4] (see also Mooney [M39]). Noting that Eq. (83) applies to a telescoping flow at each radius, we see that the shear stress varies linearly with the radius

$$\sigma_{12}(r) = (\sigma_{12})_{\mathrm{w}}(r/R) \tag{85}$$

This allows us to rewrite the extrusion rate as

$$Q = \int_0^R 2\pi r v_1 dr = \frac{\pi D^3}{8(\sigma_{12})_{\mathrm{w}}} \int^{(\sigma_{12})_{\mathrm{w}}} z^2 \left(-\frac{dv_1}{dr}\right) dz \tag{86}$$

where we have integrated by parts and presumed the material to adhere to the wall. Differentiation of $32Q/\pi D^3$ with respect to $(\sigma_{12})_{\mathrm{w}}$ and application of the Leibnitz rule for the differentiation of integrals allow us to solve for the capillary wall shear rate:

$$\dot{\gamma}_{\mathrm{w}} = \left(-\frac{dv_1}{dr}\right)_{\mathrm{w}} = \left(\frac{3n'+1}{4n}\right)\frac{32Q}{\pi D^3} \tag{87a}$$

with

$$n' = \frac{d\ln(\sigma_{12})_{\mathrm{w}}}{d\ln(32Q/\pi D^3)} \tag{87b}$$

Application of Eqs. (84) and (87b) allows the evaluation of the viscosity function $\eta(\dot{\gamma})$.

Mooney [M39] modified Eqs. (86) to allow for slip and has shown how slip at the capillary wall may be determined. Basically, in place of Eq. (86), one has

$$Q = \int_0^R 2\pi r v_1 dr = \frac{\pi R^2}{4} v_{\mathrm{s}} + \frac{\pi D^3}{8(\sigma_{12})_{\mathrm{w}}} \int_0^{(\sigma_{12})_{\mathrm{w}}} \left(-\frac{dv_1}{dr}\right) dz \tag{88a}$$

$$\frac{8Q}{\pi D^3} = \frac{2v_s}{D} + \frac{1}{(\sigma_{12})_{\mathrm{w}}} \int^{(\sigma_{12})_{\mathrm{w}}} z^2 \left(-\frac{dv_1}{dr}\right) dz \tag{88b}$$

The integral in Eq. (88b) depends only on the die wall shear stress so that

$$v_{\mathrm{s}} = \left[\frac{\partial(4Q/\pi D^3)}{\partial(1/D)}\right]_{(\sigma_{12})_{\mathrm{w}}} \tag{89}$$

This requires experiments at constant $D\Delta p/4L$ with varying diameter D, which means variable pressure.

Capillary rheometers have been widely used for quality control in the rubber industry since the 1920s [D7, D8, G18, M8–11]. As late as the 1970s, they were advocated by Monsanto. The major problem with the instrument is that it gives values at high shear rates where the viscosity is relatively insensitive to molecular weight and its distribution. Furthermore, gum elastomers are often in an unstable flow region in such instruments.

E. Compression Rheometer

The basic theory of flow of a non-Newtonian fluid in a compressional rheometer is due to Scott [S5], whose analysis is in terms of a power law fluid (Fig. 16). One presumes the flow is basically laminar shearing, with the fluid being driven radially outward from the approaching disks. By continuity at any radius r

$$\pi r^2\left(-\frac{dH}{dt}\right)=\int_0^H 2\pi r v_r(z)dz \tag{90}$$

A pressure field exists between the disks with the maximum pressure at the center. The pressure gradient is related to the shear stress through

$$\sigma_{rz}(r)=\left(z-\frac{H}{2}\right)\frac{\partial p}{\partial r} \tag{91}$$

for z greater than $H/2$. In Scott's model as stated earlier, a power law model is presumed between shear stress and shear rate:

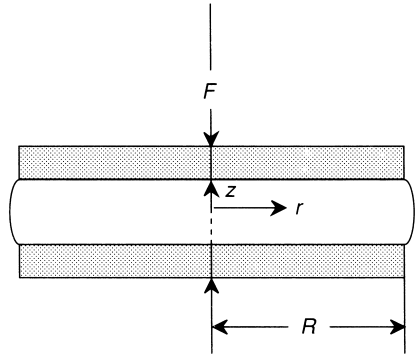

FIGURE 16 Compression rheometer.

$$K\left(-\frac{dv_r}{dz}\right)^n = \left(z - \frac{H}{2}\right)\frac{\partial p}{dr} \tag{92}$$

The velocity field $v_r(z)$ was determined. Using Eq. (90), this may be converted to the rate of downward platen movement $(-dH/dt)$.

The compression force F is related to $p(r)$ through

$$F = -\int_0^R 2\pi r p(r) dr \tag{93}$$

This leads to

$$F = 2r\left(\frac{2n+1}{n}\right)^n K \frac{R^{n+3}}{n+3}\frac{1}{H^{2n+1}}\left(-\frac{dH}{dt}\right)^n \tag{94}$$

The shear rate and shear stress at the outer radius of the disk are

$$\dot{\gamma}(R) = -\frac{dv_r}{dz} = \left[\frac{2n+1}{n}\right]\left(\frac{R}{H}\right)\left(-\frac{1}{H}\frac{dH}{dt}\right) \tag{95}$$

$$\sigma_{12}(R) = \sigma_{rz}(R) = \frac{n+3}{4}\left(\frac{H}{R}\right)\frac{F}{\pi R^2} \tag{96}$$

Compressional flow rheometers have been studied since the time of Williams *et al*. [W29] and van Rossem and van der Meijden [V1]. In the 1920s, the Firestone Tire and Rubber Company (W29) and the B. F. Goodrich Company (K2, K3) used the compression plastometer as a quality-control instrument. Subsequently in the 1930s, Baader [B1–7] and Continental Gummiwerke [B1–7] developed a similar instrument called the Defo for quality control which was used by the I. G. Farbenindustrie during World War II to test Buna S. synthetic rubber. After the war interest in the Defo fell off and the Mooney viscometer (Section VI, C) of the victorious side came to be generally accepted. Koopmann and his coworkers at Bayer AG [K14–17] have developed a much improved Defo which is manufactured by Haake Messetechnik in Karlsruhe.

F. Elongational Rheometer

A wide range of instruments have been developed as elongational rheometers. The earliest instrument of this type was by Ballman [B11] and involved inserting a vertical specimen and stretching it at an accelerating crosshead speed. The stretch rate is

$$\dot{\gamma}_E = \frac{1}{L}\frac{dL}{dt} \tag{97}$$

where L is the sample length. If this is to be constant in time, $L(t)$ must increase as

$$L(t) = L(0)e^{\dot{\gamma}_E t} \tag{98}$$

The stress is

$$\sigma = F(t)/\pi R^2(t) \tag{99}$$

where R is the sample radius. A second type of experiment was devised in which samples were floated on a silicone bath and clamped at one end and drawn out at the other end by a weight [C12], moving clamp [V5], or rollers [I1]. In one version, two sets of rollers are used [M17]. In the experiment with the weight, a cam is used so as to lead to constant stress. In the experiments with a fixed clamp and one set of rollers, the stretch rate is

$$\dot{\gamma}_E = \frac{V}{L} \tag{100a}$$

and if two sets of rollers are used,

$$\dot{\gamma}_E = \frac{V}{L/2} \tag{100b}$$

If an accelerating clamp is used with a bath, then Eq. (98) must be reproduced.

All of the experiments just described are intended for thermoplastics. Only Cotton and Thiele [C19] have developed a uniaxial elongational flow instrument intended for elastomers. In this instrument an extruded rubber strand is placed over two pulleys. The two ends descend between a pair of knurled pulleys which draws the strand ends downward.

VII. PROCESSING TECHNOLOGY

A. Internal Mixers

1. General

The first step of rubber processing is combining the ingredients of a compound in a mixing device. In the early years of the industry, this was done on a two-roll mill open to the environment [C7, G14]. From the second decade

of the century there was a transition [K4, W13], now long completed, to carrying out this mixing in an internal mixer of a design basically developed by Banbury [B12, B13] (see also White [W13] and pioneered by the new Farrel Corp. [W11]). The modern internal mixer consists of a mixing chamber containing two counterrotating rotors. At the center of the top of the mixing chamber is a shaft through which compounding ingredients gain access. During most of the mixing cycle, the shaft contains a ram which presses the compounding ingredients into the chamber. At the bottom of the mixing chamber is a door which opens at the end of the cycle and dumps the mixed compound. This machine is shown in Fig. 17.

The rotors of the internal mixer in the original design of Banbury [B12] were separated and had two curved flights which tended to pump in opposite direction. In subsequent years, there were many efforts to improve the design of internal mixers. Lasch and Frei [L2], of Werner and Pfleiderer, Tyson and Comper [T13] of Goodyear, and Sato *et al*. [S1] of Bridgestone/Kobe Steel have described internal mixers with rotors having four rather than two flights. These give better dispersing character than two-flight rotors. Today most internal mixers with separated rotors contain four flights (Fig. 18).

Internal mixers with a much different mixing chamber design were proposed by Cooke [C17] of Francis Shaw and Company and by Lasch and Stromer [L3] of Werner and Pfleiderer. These internal mixers possess intermeshing counterrotating rotors (Fig. 1.9). In these internal mixers, both rotors must move at the same angular velocity. The Francis Shaw mixer, the "Intermix," was marketed first and received considerable attention. In time, the intermeshing mixers dominated the mechanical rubber goods industries in Europe and Japan.

Passoni [P1] of Pomini has developed an intermeshing rotor design where the rotors may be moved transverse to their axes to control the interrotor clearance.

Separated rotor internal mixers are produced by Farrel Corp. in the United States and England. Kobe Steel and its Kobelco–Stewart Bolling subsidiary make these machines in Japan and the United States. Werner and Pfleiderer Gummitechnik (recently a wholly owned Krupp firm) make internal mixers in Germany and Techint-Pomini in Italy. Mitsubishi Heavy Industries, a licensee of Werner and Pfleiderer Gummitechnik, produce separated rotor internal mixers in Japan. Intermeshing rotor internal mixers are produced by Francis Shaw and Company in England (now owned by Farrel). Werner and Pfleiderer Gummitechnik (and their licensee Mitsubishi Heavy Industries) produces such internal mixers in Germany and Japan. Pomini manufactures a variable-clearance intermeshing internal mixer in Italy.

2. Basic Studies

There was little basic study of the internal mixer until relatively recently. In 1979, Freakley and Wan Idris [F8] published the first flow visualization

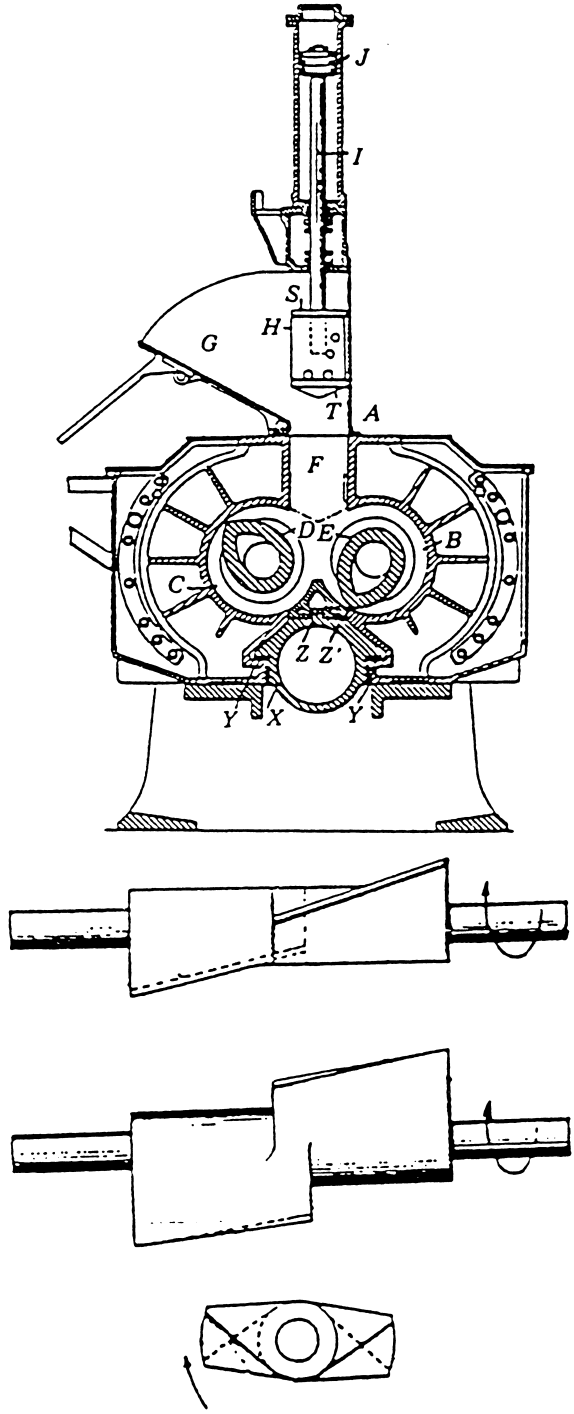

FIGURE 17 F. H. Banbury's internal mixer and rotor design. (From Banbury [B12, B13].)

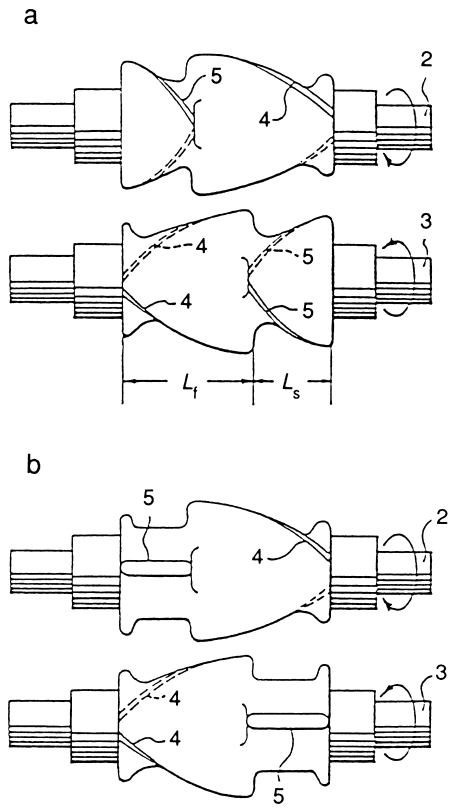

FIGURE 18 Internal mixer rotors from the designs of Sato *et al.* [S1] of Bridgestone and Kobe Steel.

investigation of a nonintermeshing rotor internal mixer using a glass window normal to the rotor axes. A more extensive study was subsequently reported by Bridgestone and Kobe Steel [A12, S1] for the purpose of optimizing rotor design. This investigation used adjustable rotors in a transparent polycarbonate chamber. An aqueous polymer solution was used as a process fluid. Later studies by Min and White [M27, M28], Morikawa *et al.* [M48–50], and Kim and White [K5, K6, W19] using apparatus similar to those. Freakley and Wan Idris focused not only on the material motions inside of the internal mixer but on comparing different elastomers and following the mixing cycle (Fig. 20). Cho *et al.* (*C12*) have compared two-wing Banbury rotors and four-wing Tyson-Comper rotors in flow visualization experiments. The four-wing rotors mix more rapidly. A more recent investigation of flow visualization was published by Toh *et al.* [T6].

Basically it is found that material in the internal mixer chamber for double- and four-flight rotors circulated around the mixing chamber (Fig. 21).

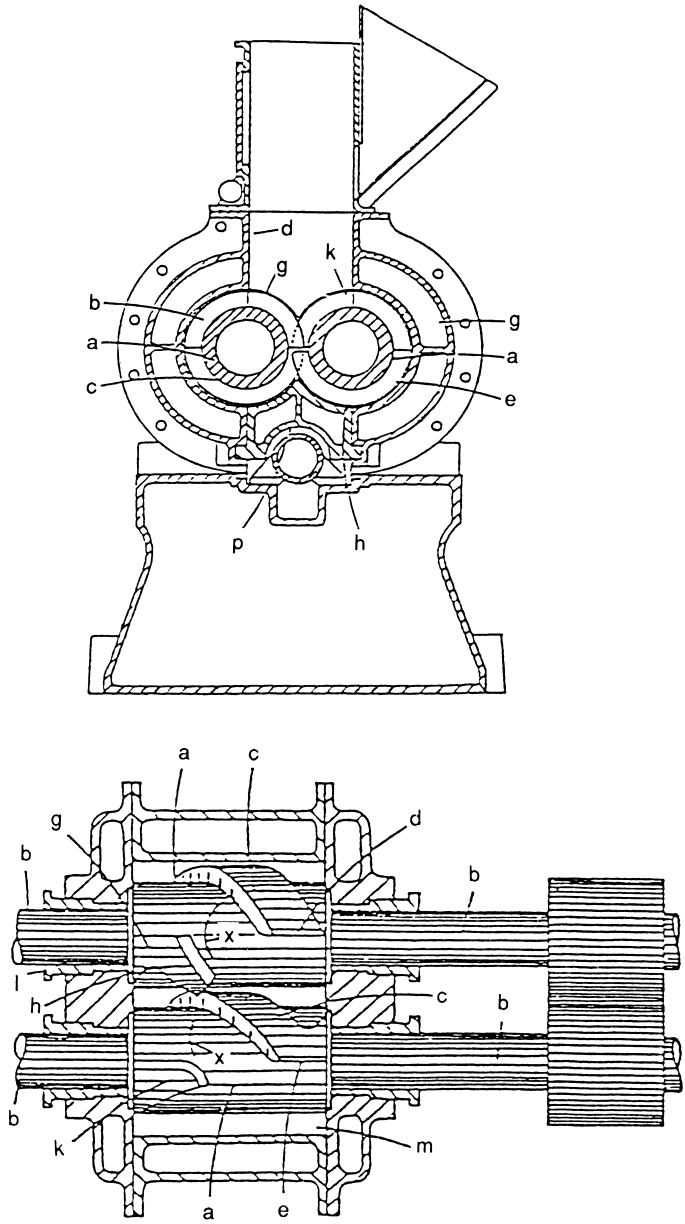

FIGURE 19 Intermeshing internal mixer design of Cooke. (From Coleman and Noll [C16].)

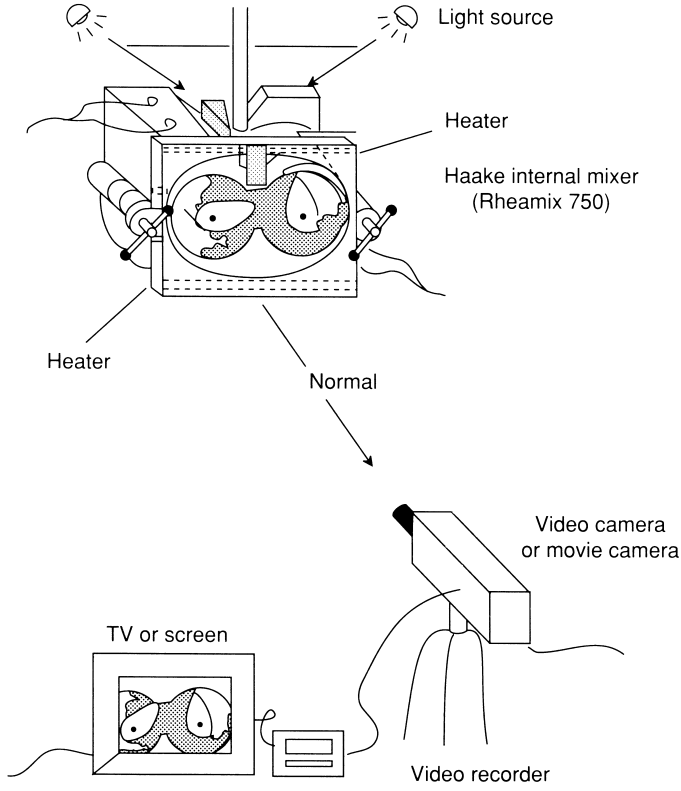

FIGURE 20 Flow visualization in internal mixer.

Natural rubber tends to cling to rotors, and most synthetic rubbers are torn into chunks. The addition of carbon black and oil to an internal mixer has been studied by flow visualization techniques for a wide range of elastomers. The tearing of elastomers into crumbs disrupts the mixing of carbon black, which proceeds more surely with natural rubber. The rate of oil absorption depends on available surface area of the elastomer and proceeds more rapidly with torn rubber crumbs and slowly with natural rubber.

More recently, P. S. Kim and White [K9] compared mixing in R. T. Cooke design [C17] intermeshing and separated rotor internal mixers using flow visualization. Bale homogenization, black incorporation, and oil absorption were found to be more rapid in intermeshing rotor mixers. Koolihiran and White [K19] compare the mixing in double-flighted Banbury rotors and Cooke intermeshing rotors of silica, talc, and carbon black into SBR. The intermeshing rotors are much better for dispersive mixing.

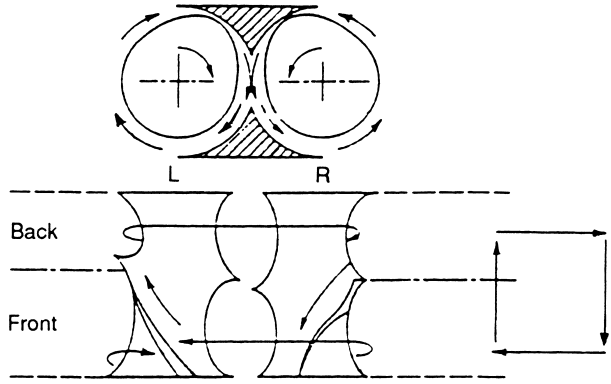

FIGURE 21 Circulation of material in internal mixer.

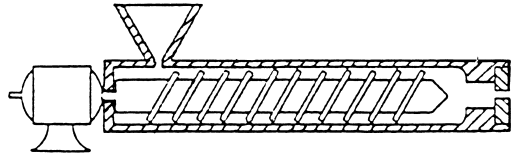

FIGURE 22 Screw extruder.

B. Screw Extrusion

1. General

Screw extruders were first introduced into the rubber industry in the late 19th century by Francis Shaw, John Royle, and Paul Troester and became the basis of the machinery companies they created (Fig. 22). The original rubber extruders were hot-feed screw extruders, for which strips of rubber compound preheated on a two-roll mill were added to the extruder. The screws had deep channels and short length/diameter ratios.

In the 1930s, Paul Troester Maschinenfabrik [W12] introduced the cold-feed screw extruder to which cold strips of rubber compound were added.

The cold-feed extruder had shallow screw channels and a much longer length/diameter ratio. The original cold-feed extruder produced extrudates which had large temperature distributions and became distorted as they emerged from the die. The issue in cold-feed extrusion of rubber was to produce a thermally homogenized product in the extruder screw which would yield thermally uniform extrudate that does not distort. From the 1960s, there have been several improvements in cold-feed extruders. First, Maillefer [M6]

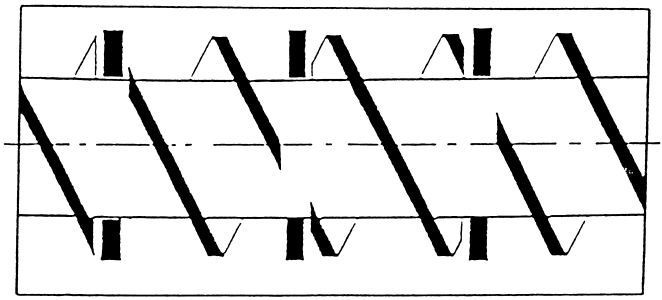

FIGURE 23 Pin barrel screw extruder.

and Geyer [G3] (of Uniroyal Inc.) introduced the barrier screw design. This introduces a second flight which isolates the less easily flowing material and prevents it from emerging from the screw until it softens. This was commercialized in the United States by NRM (under Uniroyal license) as the Plastiscrew. Designed for the purpose of controlling the melting of the solid bed in thermoplastics by Maillefer and for isolating scorched rubber compound by Geyer, this screw, when used in cold-feed rubber extruders, gave more uniform extrudates but with relatively high temperatures.

Subsequently many new designs of special sections for cold-feed screw extruders, such as the Troester shear section and the various designs of Lehnen and Menges [L8, M19], gave further improvements.

In the 1970s, Menges and Harms [H12, H13, M18] of the Institut für Kunststoffverarbeitung and of Uniroyal, proposed the use of a pin barrel cold-feed extruder (Fig. 23). This was found to give greatly improved extrudate uniformity. The machine was first licensed to Paul Troester Maschinenfabrik and subsequently to other machinery firms including Hermann Berstorff Maschinenbau and Krupp Gummitechnik in Germany, Techint-Pomini SpA in Italy, Nakatazoki in Japan, and Farrel Corp. in the United States.

2. Basic Studies

The earliest studies of the flow of elastomers in screw extruders is found in the work of Vila [V3] and Pigott [P10]. The observations of Pigott are especially interesting. There were relatively few basic investigations in succeeding years. The characteristics of flow and starvation in devolatilizing screw extruders were considered by Brzoskowski *et al.* [B36] and by Vergnes *et al.* [V2]. A more substantial study of starvation cold-feed rubber screw extruders was given by Kubota *et al.* [K21], who showed that the extent of fill was proportional to the die pressure.

Flow marker studies in screw extruders for rubber compounds were initiated by Menges and Lehnen [M19] to evaluate the mixing and homogenizing characteristics of various screw designs. These studies feed equal-viscosity

pigmented and white strips containing curatives into the extruder. After a steady state is achieved, the extruder is shut down, heated up, and cured in place. The screw is then removed, and the rubber compound strip peeled off and sectioned.

Flow marker studies in a cold-feed rubber pin barrel extruder were first reported by the inventors Menges and Harms [M18] and in more recent years by Yabushita *et al.* [Y1] and Shin and White [S11]. It was generally found that pin barrel sections do a much superior job of homogenizing (mixing pigmented and white strips) than ordinary screw sections (Fig. 24). In the investigations of Yabushita *et al.* [Y1] and Shin and White [S11] comparisons are also made with screws containing grooves on their flights but possessing no pins. These are found to be intermediate in homogenizing character. The latter authors [S11, Y1] found that introducing slices into screw flights reduces screw pumping characteristics. They also found that introducing pins has little effect on pumping. Shin and White compare a range of rubber compounds and show that although introduction of a pin always improves homogenization, the level of homogenization varies considerably from compound to compound. It is apparently this homogenizing character, as related to temperature fields in large extruders, which allows pin barrel extruders to produce uniform extrudates to higher outputs.

C. Die Extrusion

1. General

The design of dies has been a problem since the beginning of extrusion technology. The mid-19th-century patent literature [B17, B29, G15] gives considerable attention to the development of cylindrical, annular, and wire coating dies for ram and later screw extruders. In this century, much emphasis has been on the development of sheeting dies including the invention of various control systems to maintain thickness uniformity [L6, L12, P9, R1, R7]. Such dies have either (1) converging/diverging sections, which convert the cylindrical orifice at the end of the extruder to a slit shape, or (2) a manifold, which distributes melt across the die, providing a uniform feed of polymer melt to the die (Fig. 25). They are often called "T" and coathanger dies.

Die systems which may coextrude tread and sidewall or tread/sidewall/liner have received considerable attention since the 1930s [E3, F2, L7, S3, S14] (Fig. 26). Generally today several screw extruders are constructed in a "piggyback" design. These feed the various individual components to the die system.

There have been many advances in the development of profile dies. Techniques have been developed which allow the extrusion of curved sections [G5, M25, M26]. The work of Goettler [G5] and Miller *et al.* [M25, M6] describe different technologies for extruding curved tubes and profiles.

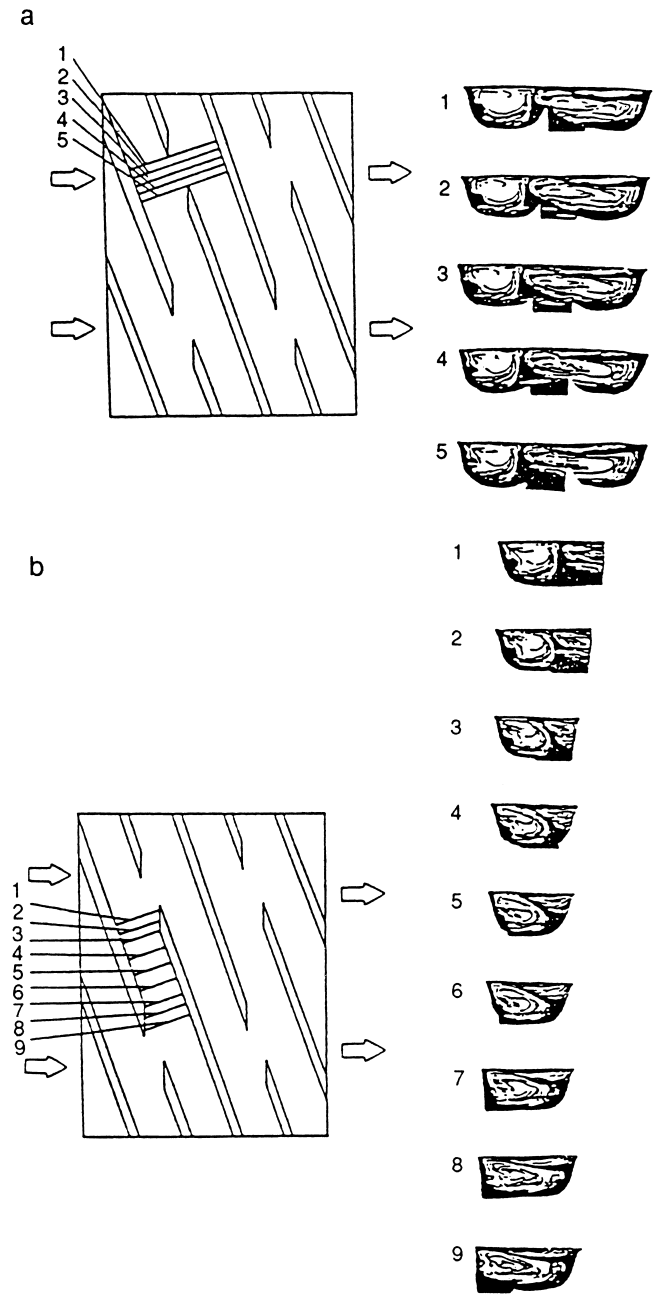

FIGURE 24 Flow marker experiments for pin barrel extruder of Yabushita *et al.* [Y1]. (a) Cross sections of vulcanized rubber strip removed from the area between the first and second grooves (extruder run without pin application). Operating conditions $T_b = 80°C$, $T_s = 80°C$, $N = 10\,min^{-1}$. (b) Cross-section of vulcanized rubber strip removed from the area of the first groove (extruder run without pin application). Operating conditions: $T_b = 80°C$, $T_s = 80°C$, $N = 10\,min^{-1}$.

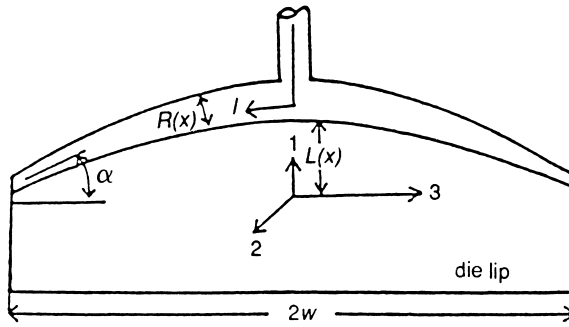

FIGURE 25 Coathanger die design to produce slit extrudate.

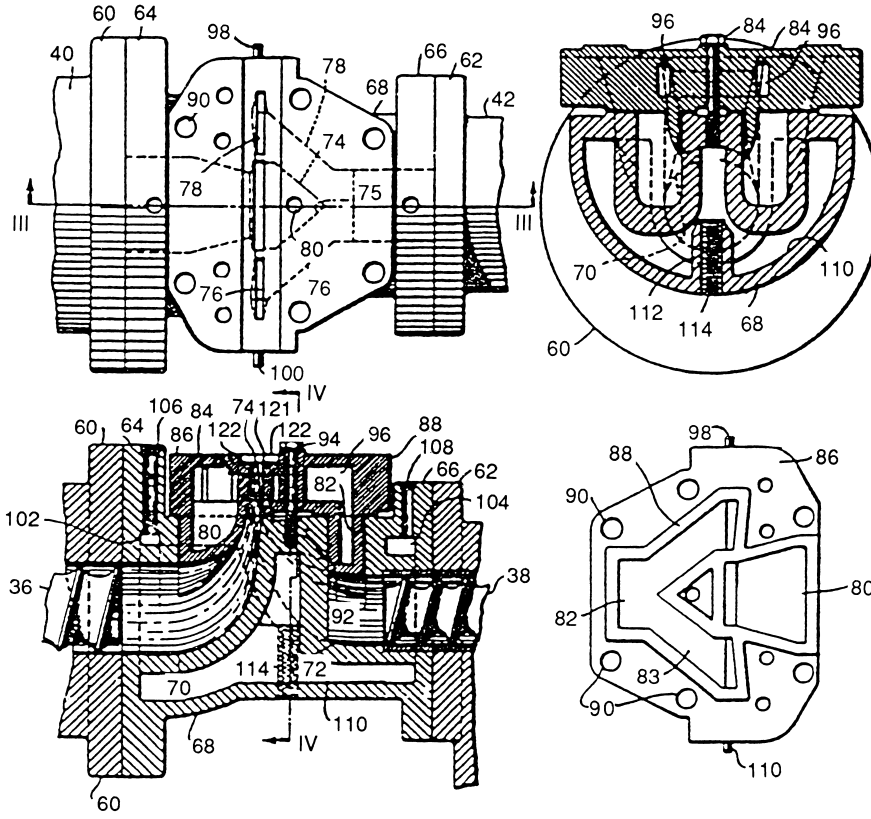

FIGURE 26 Coextrusion dies for tread/sidewall.

Rubber compounds often contain chopped fibers. It is important to control the orientation of fibers in extrudates emerging through dies. An example is in rubber tubing/hose where fibers should be circumferential not axial. Various methods have been developed to achieve this. These include various dies with rotating mandrels [C5, D10], and a die with a diverging section developed by Goettler *et al.* [G4, G6] of Monsanto has been devised for the same purpose.

2. Basic Studies

Experimental studies of flow of elastomers through dies date to the work of Marzetti [M8–11] in the 1920s. Any reasonable review of the present state of knowledge must note the very extensive literature in this area developed for thermoplastics. Investigations for thermoplastics have included both studies of extrudate swell and quality and flow marker/birefringence investigations of fluid motions within dies. The studies of Bagley and Birks [B9], Ballenger and White [B10], and Han and Drexler [H2] are typical of the latter activities, which have yielded information on the occurrence of circulating flows inside dies, stress fields in flowing melts, and mechanisms of extrusion instabilities. Low-density polyethylene (LDPF) is the most promient of polymer melts showing large circulating flows in the die entrance. The effect is also found, however, in polystyrene [B10].

Generally, rubber is processed in the form of highly filled compounds and is opaque. This has tended to suppress activities on rubber compounds except for observations of extrudate swell and quality. It is, however, important to say what has been done which is relevant.

The first study of pertinence of flow of rubber compounds within dies is that of Mooney and Black [M47] who noted the occurrence of large die entrance pressure losses (see the discussion in Section VI, D). Similar observations for thermoplastics were subsequently made by Bagley [B8]. White and Crowder [W17] reported extensive die end pressure losses for rubber compounds. Their results suggest the effects may be larger than for thermoplastics.

Experimental studies by Ma *et al.* [M3] have shown that addition of small particles including carbon black suppresses the large circulating vortices found in LOPE. Studies by Ma *et al.* [M1] and Song *et al.* [S18] on rubber compounds have found no evidence of circulating flow in the die entrance.

A most important effect of the addition of carbon black and other fillers to elastomers and thermoplastics is to reduce extrudate swell and shrinkage and improve extrudate surface quality, i.e., the tendency to eliminate extrudate distortion [S12, W17].

D. Molding

1. General

Molding represents not a single technology but a host of them (Fig. 27). These range from *compression molding*, where chunks or sheets are placed in an open mold which is then closed around it. After the part is formed (and, for rubber, vulcanized), the mold is opened and the part removed. In *injection molding*, material is injected under pressure into a closed mold. After the part is formed and vulcanized, the mold is again opened. *Transfer molding* represents a combination of injection and compression molding in which rubber is injected from a reservoir into a compression mold. *Blow molding* involves the preparation of a preform which is inserted into a mold. This is subsequently inflated (by hot air/steam or some other fluid perhaps contained in a bag) to fill out the mold.

These technologies date to the first half of the 19th century and were developed by the Hancock brothers (Thomas and Charles in England) and the Goodyear brothers (Charles and Henry in the United States). Much of this development can be read in the autobiographies and patents of Thomas Hancock [H11] and Charles Goodyear [G14] published in the mid-l9th century. In 1846–1847 patents, Hancock [H4–7] described the process technologies for injection molding, blow molding (including using a flexible bag made of vulcanized rubber to contain the pressurized hot air), and molding of foams using gutta percha, natural rubber, and their blends.

The 20th century has seen the clear development of two distinct types of rubber molding technology. One of these involves the molding of tires; the second involves mechanical goods. Tire manufacturing technology involves two processes in its shaping step. The first is building tire preforms on a drum [F17, G19, M16], and the second, the molding of the preform into a final tire with associated vulcanization [D1, S9, T11].

In rubber mechanical goods production one sees a wide range of manufacturing operations including compression molding, transfer molding, and screw injection molding.

2. Basic Studies

Basic studies of flow mechanisms in molding have been lacking for rubber compounds. Almost all published studies have been for thermoplastics. Most of these investigations involve injection mold filling.

It has been long realized that there are two regimes of injection mold filling. These involve a slowly expanding front or jetting into a mold. Oda *et al.* [O1] have shown that jetting into a mold is the result of the polymer or compound having a low extrudate swell. The often complex occurrence of this swell is associated with the melt temperature and its variations in runners. Isayev and his coworkers [I3, I4, I6] have extensively studied pressure

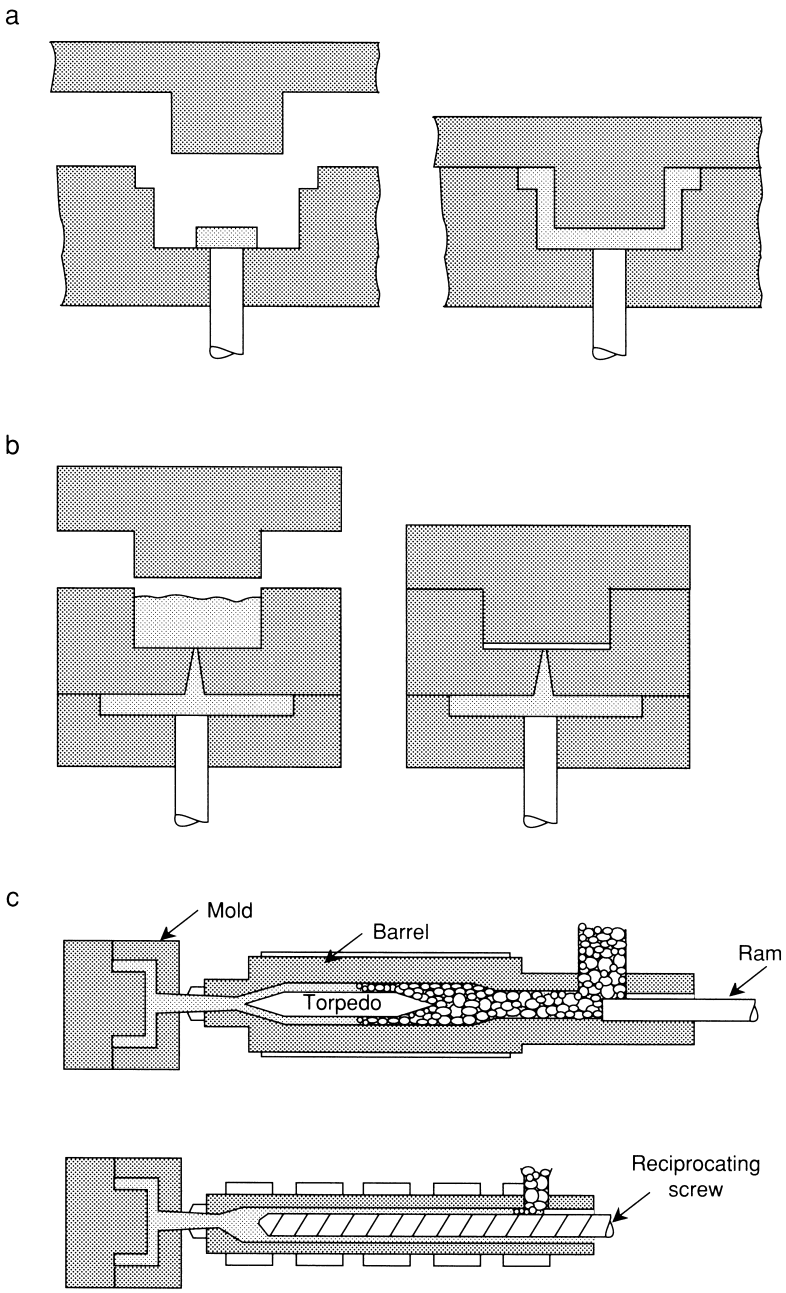

FIGURE 27 Different types of molding technologies. (a) Compression molding. (b) Transfer molding. (c) Injection molding. (d) Blow molding. [(d) is reprinted with permission from W. A. Holmes Walker, "Polymer Conversion." Halsted Press, London, 1975.]

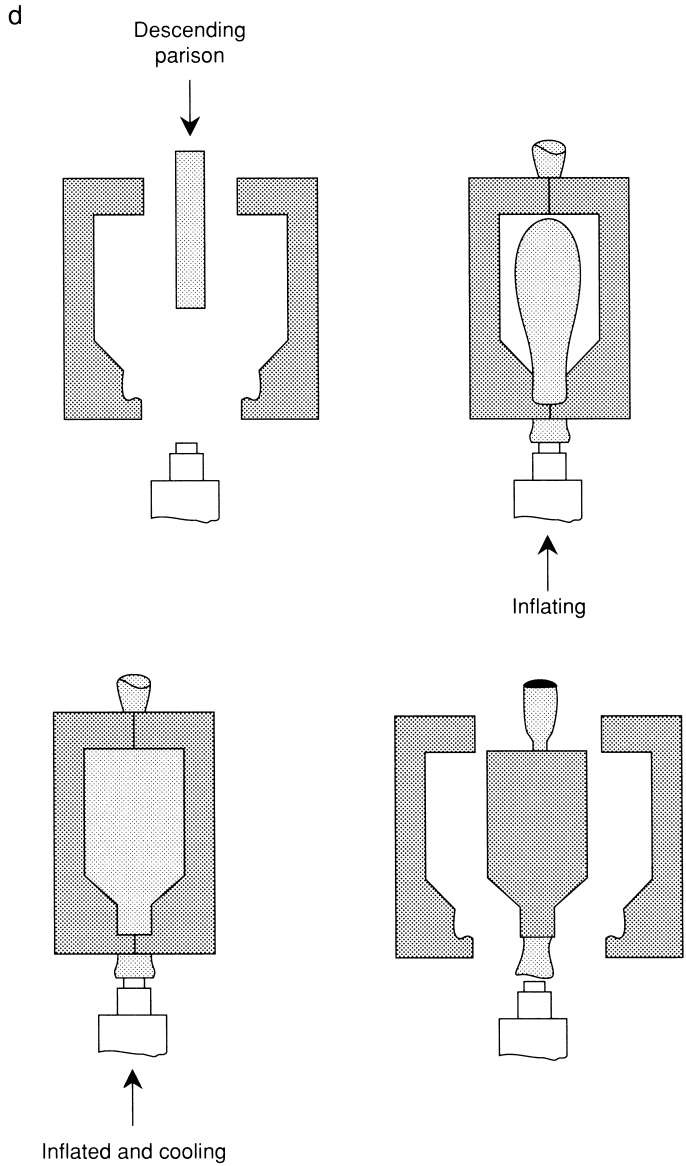

FIGURE 27 (*Continued*).

development and injection mold filling by rubber compounds when the front is slowly expanding in the mold.

VIII. ENGINEERING ANALYSIS OF PROCESSING

A. General

There are many ways in which elastomer rheology may be applied to processing operations. This is because processing is in large part simply flow and shaping of compounds. The most obvious use is in determining the sources of problems when difficulties arise in factory production. Frequently the breakdown of regular production, can be traced to some cause such as high viscosity levels or elastic memory of compounds. This is, of course, how the early rubber rheologists were first employed and, to a good extent, is what they do to this day.

B. Dimensional Analysis

1. General

One of the most useful ideas for the industrial polymer rheologist is dimensional analysis. In this traditional method of engineering analysis, the conservation laws (force–momentum, energy, etc.) are placed in dimensionless form, and the dimensionless groups that arise are interpreted. There were applications of this approach to the development of model basins for ships and to the flow of liquids in pipes and the 19th century. Indeed, the general philosophy of dimensional analysis in engineering was developed by Osborne Reynolds for the latter application. These ideas were extended in the early years of the 20th century by Wilhelm Nusselt. The dimensionless correlations developed by these authors can be used as a guide in the design of pipelines, heat exchangers, and packed columns. Numerous texts describe this subject matter and are an integral part of university engineering education [B21, E2].

Unfortunately, the Reynolds–Nusselt dimensional analysis studies are not directly applicable to polymer melt and rubber processing for two important reasons. First, they are based on Newtonian fluid behavior, and second, they do not include viscous dissipation heating.

The earliest considerations of the dimensional analysis of isothermal viscoelastic fluids were by Karl Weissenberg during the period from 1928 to 1948. Weissenberg [W3] suggested that the recoverable elastic strain represents fluid elasticity in the same way that the Reynolds number represents inertia. A large recoverable strain represents high viscoelastic forces. Reiner [R4] later suggested that the basic dimensionless group correlating viscoelastic phenomena was a "Deborah number," which may be represented as a ratio of the charac-

teristic relaxation time τ_{ch} to a residence time t. A large t value of τ_{ch} or a small value of t will, according to Reiner, accentuate viscoelastic response. A more quantitative formulation of the intuitive ideas of Weissenberg and Reiner resulted after the modern theory of nonlinear viscoelasticity had been developed. White [W6], White and Tokita [W26], and Metzner *et al.* [M23] published analyses that have brought these ideas together into a formal scheme. This approach would be expected to be valid for thermoplastics and most applications of elastomer gums but not compounds.

We begin with Cauchy's law of motion, Eq. (10), and a general constitutive equation such as Eq. (47), which yields

$$\rho\left[\frac{\partial \mathbf{v}}{\partial t}+(\mathbf{v}\cdot\nabla)\mathbf{v}\right]=-\nabla p+\nabla\cdot\int_0^\infty m(z)[\mathbf{c}^{-1}+\kappa\mathbf{c}]dz+\rho g \tag{101}$$

A characteristic velocity U and length L are introduced into this equation and the entire expression is put in dimensionless form. These dimensionless groups are

$$\frac{LU\rho}{G_m\tau_m},\qquad \frac{U^2}{gL},\qquad \tau_m\frac{U}{L},\qquad \frac{\tau_m}{t},\qquad \frac{\tau_i}{\tau_m},\qquad \frac{G_i}{G_m},\qquad a_j \tag{102}$$

where τ_m is the maximum relaxation time [see Eq. (14)] and G_m the corresponding modulus. Here $LU\rho/G_m\tau_m$ is a Reynolds number signifying the ratio of inertial to viscous forces: U^2/gL is a Froude number representing a ratio of inertial to gravitational forces: $\tau_m U/L$ is known as the Weissenberg number and τ_m/t as the Deborah number, both representing the ratio of viscoelastic to viscous forces. The other groups are viscoelastic ratio numbers representing the detailed character of the functional.

Generally, inertial forces are negligible in polymer melts and elastomers, and gravitational forces need not be considered. This leaves the Weissenberg, Deborah, and viscoelastic ratio numbers. If we consider an application to a processing operating in which the material flows through some equipment, it must be recognized that t is a residence time and

$$\tau_m/\mathrm{t}=[\tau_m/(L_{11}/U)]=\tau_m U/L_{11} \tag{103}$$

L_{11} is a characteristic length in the direction of flow. The Deborah number is equivalent to a Weissenberg number with the characteristic length in the direction of flow. Our dimensionless groups thus reduce to

$$\tau_m U/L,\qquad \tau_i/\tau_m,\qquad G_i/G_m,/G_j \tag{104}$$

The results of the preceding paragraph have some important implications. First, the characteristic velocity and length arise in only one group, and this

occurs in the form of a ratio U/L. This means that for any particular viscoelastic fluid there will be dynamic similarity between large and small geometrically scaled isothermal systems only if velocities are scaled with lengths. Furthermore, if any instabilities or changes in regime occur within such a system, they will occur at a critical value of a dimensionless group of the form $\tau U/L$ where the characteristic time τ is given by

$$\tau = \tau_{\mathrm{m}} F[\tau_i/\tau_{\mathrm{m}}, G_i/G_{\mathrm{m}}, a\gamma] \tag{105}$$

Here the function F may be quite complex, so that τ may differ significantly from material to material (with differing viscoelastic ratio numbers) even if they possess the same τ_{m}.

2. Rubber Compounds

Now we turn to rubber compounds and specifically to plastic viscous and plastic viscoelastic fluids.

Dimensional analysis of plastic fluids with yield values was first considered by Oldroyd [O4] and then subsequently by Prager [P15]. Oldroyd pointed out that a new dimensionless group of form

$$\frac{YL}{\eta U} \tag{106}$$

arises. This group has become known as the Bingham number.

For a plastic viscoelastic fluid, the dimensionless groups of Eq. (102) should be replaced by

$$\frac{YL}{\tau_{\mathrm{m}} G_{\mathrm{m}} U}, \qquad \tau_{\mathrm{m}} \frac{U}{L}, \qquad \frac{\tau_i}{\tau_{\mathrm{m}}}, \qquad \frac{G_i}{G_{\mathrm{m}}}, \qquad a_j \tag{107}$$

As with viscoelastic fluids in Eq. (100) and plastic viscous fluids in Eq. (106), dynamic similarity involves systems with the same U/L. Both viscoelastic and plastic flow phenomena are then associated with dimensionless groups involving U/L.

Attention needs also to be given to thixotropic effects. The preceding dynamic similarity formulation must involve equivalent periods of deformation.

3. Nonisothermal Effects

The discussion of the foregoing paragraphs is limited to isothermal systems, with which, however, we are generally not concerned. We must also consider the energy equation [B21], which we may write as

$$\rho c\left[\frac{\partial T}{\partial t} + (\mathbf{v}\cdot\nabla)T\right] = k\nabla^2 T + \boldsymbol{\sigma}:\nabla\mathbf{v} \tag{108}$$

Introducing characteristic velocity U, length L, and temperature difference θ, we may show that the dimensionless groups arising in this equation are

$$LU\rho c/k, \qquad \eta U^2/k\theta \tag{109}$$

as well as $G_m\tau_m/\eta$ and viscoelasticity-related groups of Eq. (102) or plastic viscoelastic parameters of Eq. (107) as appropriate. Here, $LU\rho c/k$ is known as the Peclet number and signifies the ratio of convective heat flux to heat conduction, whereas $\eta U^2/k\theta$ is the Brinkman number, representing the ratio of viscous heating to heat conduction [B21].

The Brinkman number is of great importance in the interpretation of polymer processing because it represents the ability of the system to conduct away heat produced by viscous dissipation. It is useful to rewrite it in the form

$$\frac{\eta U^2}{k\theta} = L^2\left(\frac{\eta}{k\theta}\right)\left(\frac{U}{L}\right)^2 \tag{110}$$

If we compare small and large systems that have been scaled at constant U/L, as we would expect for dynamic similarity, the Brinkman number increases as L^2. The larger the system, the greater the tendency for viscous heating to override heat conduction and for the temperature to rise. Another way of stating this is that a large system will tend to behave adiabatically. Thus the isothermal dimensional analysis and interpretation are most suitable to systems with small dimensions. For large systems, we have to consider viscous dissipation as well.

The origin of the effect described in the preceding paragraph may he viewed in another way. Viscous dissipation heating is proportional to the volume of the system L^3, whereas heat transfer is proportional to the surface area, which varies as L^2. As one goes to larger systems, surface area per unit volume decreases, making heat transfer more difficult and the system more adiabatic.

A final point of importance, which has already been implied but which should be stated more explicitly, is the inability to scale at both constant Weissenberg number (or Bingham number) and constant Brinkman number, i.e., at constant

$$\frac{Y}{\tau G}\frac{L}{U}, \qquad \tau U/L, \qquad \eta U^2/k\theta \tag{111}$$

The only way one may scale at constant Brinkman number is to maintain the characteristic velocity U constant as L increases, which would decrease the Weissenberg number.

Quite often nonisothermal effects are dominant and one must mainly worry about Eq. (110).

C. Simulations of Internal Mixers

Efforts to model flow in an internal mixer may be traced to the l950s [B25, P16); however, it was not until the late 1980s that there was a substantial effort involving several different independent investigations [C10, C11, D2, D3, H20, H21, K6–8, W19, Y4]. Generally, two different approaches were being used, one presuming hydrodynamic lubrication theory [H20, H21, K6–K8, W19] to be valid and a second based on the complete equations of motion and applying finite-element analysis [C10, C11, Y4).

In the first of these approaches, early work concentrated on simulations in Cartesian coordinates [D2, K6–K8, W19] reminiscent of journal bearing theory. More recently these activities have concentrated on cylindrical coordinate formulations [D3, H20–H22) essentially based on solving the set of equations

$$0 = -\frac{\partial p}{\partial z} + \eta \frac{\partial}{\partial r}\left(r \frac{\partial \upsilon_z}{\partial r} \right) \tag{112a}$$

$$0 = -\frac{1}{r}\frac{\partial p}{\partial \theta} + \eta \frac{1}{r}\frac{\partial}{\partial r}\left(r \frac{\partial \upsilon_\theta}{\partial r} \right) \tag{112b}$$

and integrating the velocity fields to obtain expressions for fluxes q_3 and q_θ defined by

$$q_z = \frac{1}{R^*}\int_{R_1}^{R_2} r\upsilon_z dr \tag{113a}$$

$$q_\theta = \int_{R_1}^{R_2} \upsilon_\theta dr \tag{113b}$$

The fluxes q_z and q_θ are balanced according to

$$\frac{\partial q_z}{\partial z} + \frac{1}{4}\frac{\partial}{\partial \theta}(rq_r) = 0 \tag{114}$$

which is then solved numerically.

It is necessary to solve the preceding equations both with boundary conditions suitable for flow (1) between the chamber wall and the rotor and (2) in the interrotor region, and to match boundary conditions. The solution to Eq. (113) yields a pressure field which may be converted to a flux field. Basically, it is found that the two rotors act as screw pumps, pumping in opposite directions and creating a circulational flow in the mixing chamber. Kim *et al.* [K6–8, W19] and Hu and White [H20–H22] have sought to represent flow patterns by defining mean fluxes F_l, F_c, F_{tr}, F_d which represent flow patterns which respectively represent fractional flows that are longitudinal along the roads

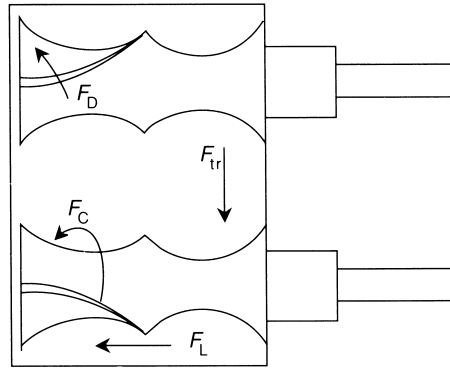

FIGURE 28 Definition of fractional flow fluxes F_l, F_c, F_{tr}, F_D in an internal mixer.

TABLE III Flow Characteristics of Double- and Four-Flight Internal Mixer Rotors from the Patent Literature

Inventor	Company	Year	$F_L + F_{tr}$	F_c	F_d	$\lvert Q_L^-/Q_L^+\rvert$	t_{circ} (min)
Banbury [B12]	W & P Birmingham Iron Foundry	1916	0.321	0.674	0.005	0.31	2.7
Lasch and Frei [L2]	Werner & Pfleiderer	1943	0.295	0.689	0.016	0.21	3.7
Tyson and Comper [T13]	Goodyear Tire & Rubber	1966	0.375	0.615	0.010	0.78	2.3
Sato *et al.* [S1]	Kobe Steel	1981	0.398	0.588	0.014	0.50	2.0

(F_L) and circumferential around the rotors (F_c), transfer flow between rotors (F_{tr}), and "dispersive" flow going over rotor flights F_d (Fig. 28). They have computed these functions for various geometries including many rotors listed in the patent literature. Typical results are summarized in Table III, where Banbury's double-flighted rotors are compared to the four-flighted rotors of Lasch and Frei [L2], Tyson and Comper [T13], and Sato *et al.* [S1]. The Sato *et al.* rotors compared to the old Banbury rotors exhibit a 20% more rapid circulation and a 180% greater flow over flight tips. P. S. Kim and White [K10] have modeled the flow in intermeshing rotor internal mixers.

D. Simulations of Screw Extrusion

Simulations of flow in a single screw extruder date to the 1920s, with early efforts being largely associated with pumps for lubricating oils. In the 1950s, the flow in screw extruders became a subject of interest in flow in many

industrial laboratories. The earliest work was largely repetitive of the activities on screw pumps in the 1920s.

The simplest Newtonian fluid model based on hydrodynamic lubrication theory involves the solution of the equations

$$0 = -\frac{\partial p}{\partial x_1} + \eta \frac{\partial^2 v_1}{\partial x_2^2} \tag{115a}$$

$$0 = -\frac{\partial p}{\partial x_3} + \eta \frac{\partial^2 v_3}{\partial x_2^2} \tag{115b}$$

where direction 1 is along the screw channel, 2 is normal to the screw surface, and 3 is perpendicular to the screw flights. The velocity fields v_1 and v_3 are, if the coordinate system is fixed in the screw,

$$v_1(x_2) = \pi DN \cos\phi \left(\frac{x_2}{H}\right) - \frac{H^2}{2\eta}\left(\frac{\partial p}{\partial x_1}\right)\left[\left(\frac{x_2}{H}\right) - \left(\frac{x_2}{H}\right)^2\right] \tag{116a}$$

$$v_3(x_2) = -\pi DN \sin\phi \left[3\left(\frac{x_2}{H}\right) - 2\left(\frac{x_2}{H}\right)^2\right] \tag{116b}$$

where H is the depth of the screw channel, N screw speed, D screw diameter, and ϕ screw helix angle. $\partial p/\partial x_3$ has been determined by the boundary condition of no screw fight leakage:

$$\int_0^H v_3(x_2)\,dx_2 = 0 \tag{117}$$

The screw throughput is

$$\begin{aligned} Q &= W\int_0^H v_1(x_2)\,dx_2 \\ &= \frac{1}{2}\pi DN\cos\phi - \frac{H^3 W}{12\eta}\frac{\partial p}{\partial x_1} \end{aligned} \tag{118}$$

By the 1960s, there were efforts to simulate flow in screw extruders including both non-Newtonian and nonisothermal character. This is found notably in the work of Griffith [G17] and Zamodits and Pearson [Z2]. They basically formulate in Cartesian coordinates a lubrication-based model with equations of motion of the form

$$0 = -\frac{\partial p}{\partial x_1} + \frac{\partial}{\partial x_2}\left[\eta \frac{\partial v_1}{\partial x_2}\right] \tag{119a}$$

$$0 = -\frac{\partial p}{\partial x_3} + \frac{\partial}{\partial x_2}\left[\eta \frac{\partial v_3}{\partial x_2}\right] \tag{119b}$$

and the energy equation (with neglect of heat convection):

$$0 = k\frac{\partial^2 T}{\partial x_2^2} + \eta\left[\left(\frac{\partial v_1}{\partial x_2}\right)^2 + \left(\frac{\partial v_3}{\partial x_2}\right)^2\right] \tag{120}$$

The non-Newtonian viscosity has the form (as would be expected from the Criminale–Erickson–Filbey theory [C20] [Eqs. (50) and (51)] of

$$\eta = F_1(T) f_2\left[\left(\frac{\partial v_1}{\partial x_2}\right)^2 + \left(\frac{\partial v_3}{\partial x_2}\right)^2\right] \tag{121a}$$

where approximately for a power law fluid

$$\eta = Ae^{-B(T-T_0)}\left[\left(\frac{\partial v_1}{\partial x}\right)^2 + \left(\frac{\partial v_3}{\partial x_2}\right)^2\right]^{\frac{n-1}{2}} \tag{121b}$$

Griffith [G17] and Zamodits and Pearson [Z2] simultaneously solve Eqs. (119), (120), and (121) to obtain the screw pumping characteristics. These show that decreasing power law exponent n and making the material more non-Newtonian reduces pumping characteristics (Fig. 29). Similarly, increasing the viscosity and the temperature dependence of the viscosity by increasing $B(T)$ also reduces pumping characteristics. The above formulation may be improved by adding a term in $\rho c v_1 \partial T/\partial x_1$ on the left-hand side of Eq. (110a).

Rubber compounds have yield values, so the actual behavior in screw extruders must be more complex than indicated by the preceding analysis. If the rubber compound is a plastic material, then Eqs. (119a) and (119b) may be replaced by

$$0 = -\frac{\partial p}{\partial x_1} + \frac{\partial \sigma_{12}}{\partial x_{12}} \tag{122a}$$

$$0 = -\frac{\partial p}{\partial x_3} + \frac{\partial \sigma_{32}}{\partial x_2} \tag{122b}$$

or

$$\sigma_{12} = x_2 \frac{\partial p}{\partial x_1} + C \tag{122c}$$

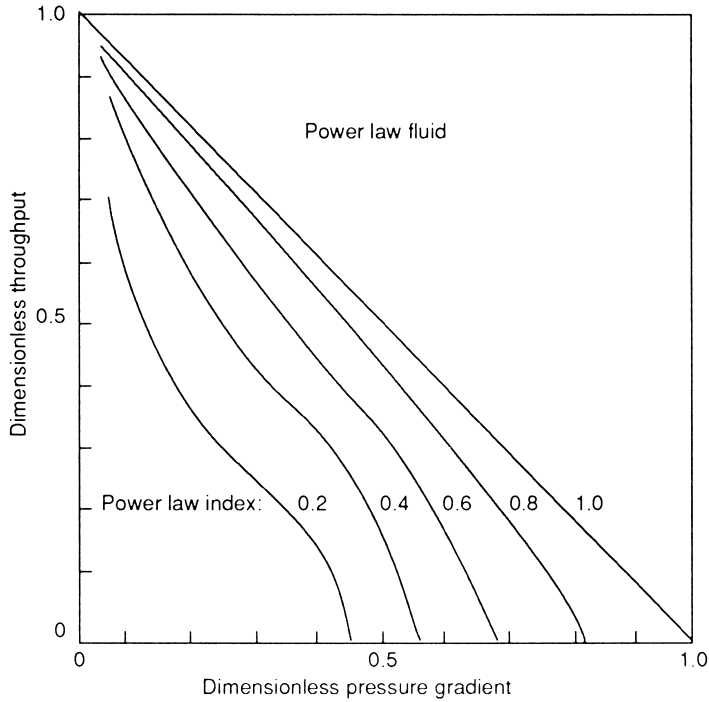

FIGURE 29 Effect of non-Newtonian viscosity on screw pumping characteristics.

$$\sigma_{32} = x_2 \frac{\partial p}{\partial x_3} + C \tag{122d}$$

Consider the case of no die: the pressure gradient $\partial p/\partial x_1$ is zero, and the shear stress σ_{12} is uniform through the screw channel depth. When σ_{12} exceeds Y, a simple shear flow will arise. This will in turn set up a pressure gradient $\partial p/\partial x_3$ induced by the screw flights, and an associated circulational flow will develop. If there is a pressure gradient $\partial p/\partial x_1$, then from Eq. (122c) the shear stress will vary across the channel, reaching a maximum at the barrel, and can reach low values at intermediate values of the cross-section. If these stresses decrease below the yield value, a solid plug will develop at an intermediate position in the cross-section. However, as may be seen from experiments of Merges and Lehnen [M19, L8] and Brzoskowski *et al.* [B36, K17], only circulating flows and no plugs are seen. This is because of the small magnitudes of the yield value.

The flow in pin barrel extruders has been simulated in recent years by Brzoskowski *et al.* [B31, B32, B34] using hydrodynamic lubrication theory methods for a Newtonian fluid. Basically they embed a coordinate system in

the screw channel and set up a flux balance of the form [equivalent to Eq. (114)]

$$\frac{\partial q_1}{\partial x_1} + \frac{\partial q_3}{\partial x_3} = 0 \tag{123}$$

where the fluxes have the form

$$q_1 = \int_0^H v_1(x_2)dx_2 = \frac{1}{2}U_2 H - \frac{H^3}{12\eta}\frac{\partial p}{\partial x_1} \tag{124a}$$

$$q_3 = \int_0^H v_3(x_2)dx_2 = \frac{1}{2}U_3 H - \frac{H^3}{12\eta}\frac{\partial p}{\partial x_3} \tag{124b}$$

Equation (121) is solved numerically by finite-difference methods. Figure 30 shows computed flow fields in the neighborhood of pins.

Kumazawa *et al.* [K22] have determined mean temperature fields in screw extrusion by introducing the heat balance

$$\rho c q_1 \frac{d\overline{T}}{dx_1} = -[U_s(\overline{T} - T_s) + U_b(\overline{T} - T_b)] + (\sigma_{12})_b \pi DN \cos\phi + (\sigma_{32})_b \pi DN \sin\phi - q_1 \frac{dp}{dx_1} \tag{125}$$

where $\overline{T}$ is a "cup mixing" velocity averaged, temperatures T_s and T_b are screw and barrel temperatures, and U_s and U_b are overall screw and barrel heat transfer coefficients.

It is possible to simulate complete velocity and temperature fields through the screw channel cross-section and not simply be limited to mean fluxes. Here one generalizes Eqs. (119a), (119b), and (120) to

$$0 = -\frac{\partial p}{\partial x_1} + \frac{\partial}{\partial x_2}\left[\eta \frac{\partial v_1}{\partial x_2}\right] + \frac{\partial}{\partial x_3}\left[\eta \frac{\partial v_1}{\partial x_3}\right] \tag{126a}$$

$$0 = -\frac{\partial p}{\partial x_3} + \frac{\partial}{\partial x_2}\left[\eta \frac{\partial v_3}{\partial v_2}\right] \tag{126b}$$

$$\rho c\left[v_1 \frac{\partial T}{\partial x_1} + v_3 \frac{\partial T}{\partial x_3}\right] = k\left[\frac{\partial^2 T}{\partial x_2^2} + \frac{\partial^2 T}{\partial x_3^2}\right] + \eta\left[\left(\frac{\partial v_1}{\partial x_2}\right)^2 + \left(\frac{\partial v_3}{\partial x_2}\right)^2 + \left(\frac{\partial v_1}{\partial x_3}\right)^2\right] \tag{126c}$$

This allows evaluation of the effects of the screw flights and pins, but it is a much more difficult problem to solve.

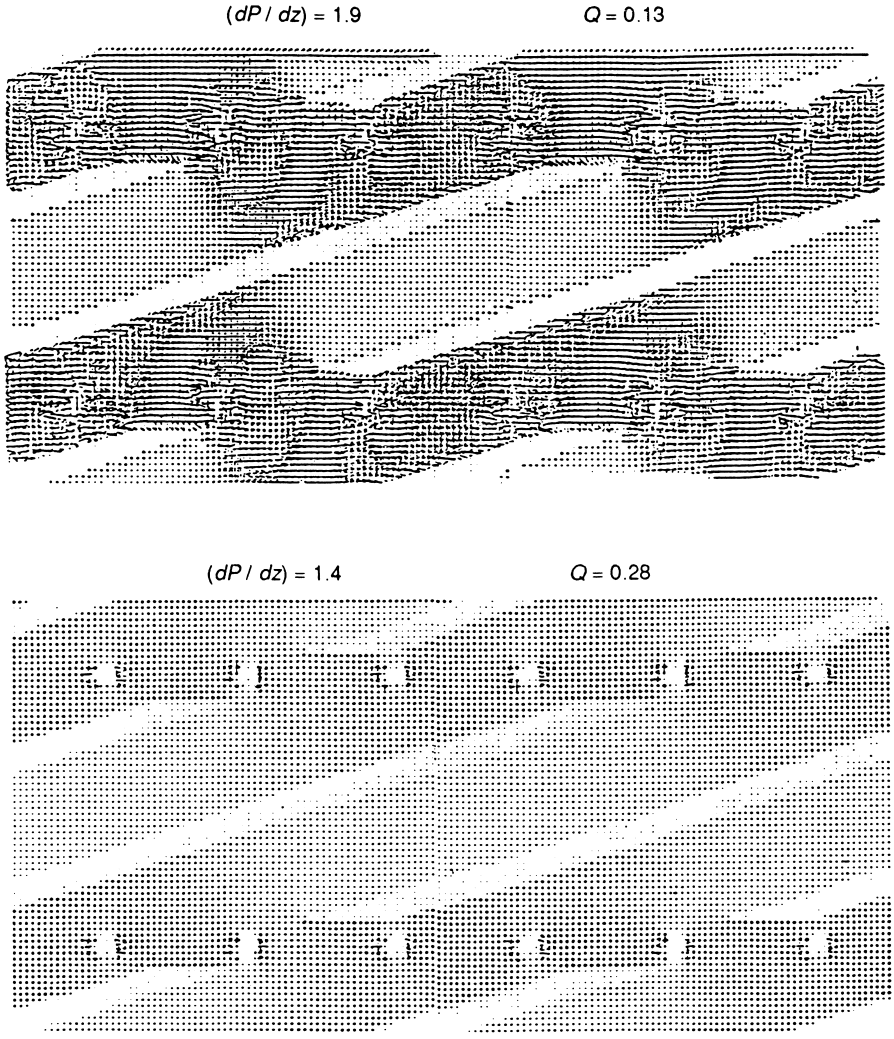

FIGURE 30 Flow patterns in a pin barrel extruder.

E. Simulations of Die Extrusion

Efforts to model flow of polymer melts and rubber compounds in dies are associated with the development of viscometry. The first extended effort at simulation of flow in dies was by Pearson [P2–5] who used the same lubrication theory formulation described in the two previous sections, i.e., basically Eqs. (123a), (123b), (124a), and (124b).

Consider the following simple analysis intended for coathanger and T dies. In dies there is only pressure flow. For a Newtonian fluid, Eqs. (115a) and

(115b) would have the simple solution (if the coordinate system is set in the center of the die channel)

$$\upsilon_1 = \frac{H^2}{2\eta}\left(-\frac{\partial p}{\partial x_1}\right)\left[1-\left(\frac{x_2}{H}\right)^2\right] \tag{127a}$$

$$\upsilon_3 = \frac{H^2}{2\eta}\left(-\frac{\partial p}{\partial x_3}\right)\left[1-\left(\frac{x_2}{H}\right)^2\right] \tag{127b}$$

This leads to fluxes

$$q_1 = 2\int_0^{H/2} \upsilon_1(x_2)dx_2 = \frac{H^3}{12\eta}\left(-\frac{\partial p}{\partial x_1}\right) \tag{128a}$$

$$q_3 = 2\int_0^{H/2} \upsilon_3(x_2)dx_2 = \frac{H^3}{12\eta}\left(-\frac{\partial p}{\partial x_3}\right) \tag{128b}$$

The fluxes may vary with position so that q_1 and q_3 must be balanced as in Eq. (123). This leads to

$$\frac{\partial}{\partial x_1}\left(H^3\frac{\partial p}{\partial x_1}\right)+\frac{\partial}{\partial x_1}\left(H^3\frac{\partial p}{\partial x_1}\right)=0 \tag{129}$$

governing the pressure field in a die and the flux field being obtained from Eqs. (128).

Specifying the geometry of a die is equivalent to specifying $H(x_1, x_3)$. This allows computation of $p(x_1, x_3)$ and $q_j(x_1, x_3)$ for different designs. A common problem might be to determine what functions $H(x_1, x_3)$ will make $q_1(L, x_3)$ a constant, i.e., the die exit flux independent of position along the die lips.

The preceding problem needs to be more formulated generally using Eqs. (119a) and (119b), including non-Newtonian character such as Eq. (121a). The fluxes q_1 and q_3 will depend on H and pressure gradients in a different manner for non-Newtonian fluid systems. Equation (123) will remain valid but Eq. (124) must be replaced by

$$\frac{\partial}{\partial x_1}\left(S\frac{\partial p}{\partial x_1}\right)+\frac{\partial}{\partial x_3}\left(S\frac{\partial p}{\partial x_3}\right)=0 \tag{130}$$

where S is defined by

$$S = \frac{H^3}{12\overline{\eta}} \tag{131}$$

$\overline{\eta}$ is an effective non-Newtonian viscosity.

It should be noted that rubber compounds are plastic materials and that stresses have low values in the center of die cross-sections. When the stresses drop below stress Y, the velocity gradients will go to zero, and there will be a localized solid plug.

It is possible to obtain information on temperature changes as well. To a first approximation, if adiabatic behavior is considered, one may use the logic leading to Eq. (125) to surmise that the increase in temperature in flow through a die is

$$\overline{T} - \overline{T}_0 = \frac{\Delta p}{\rho c} \tag{132}$$

where $\overline{T}$ is a "cup mixing" temperature.

More generally one needs to solve Eq. (130) together with

$$\rho c q_1 \frac{d\overline{T}}{dx_1} = -U(\overline{T} - T_{sn}) + q_1 \frac{dp}{dx_1} \tag{133}$$

while recognizing that the viscosity is temperature independent. Shah and Pearson [S10] have analyzed this type of problem and shown that instabilities are possible leading to q_1 becoming a function of x_3.

Velocity and temperature profiles may be determined through a die cross-section using Eqs. (126), but it is again a difficult problem.

F. Simulations of Molding

The only available literature on simulation of molding of rubber has involved injection mold filling, i.e., the filling of a fixed mold shape from a gate. The approach to simulation is very close to what we have discussed for dies in the previous section. The filling of a mold for an isothermal Newtonian fluid may be mathematically described by Eq. (129), and that for a nonisothermal non-Newtonian fluid, by introducing Eq. (130). This type of problem has been simulated by Isayev and his coworkers [I2–4, I6, S15, S16]. The treatment basically resembles that of injection molding thermoplastics except for the necessity of considering vulcanization kinetics during mold filling. Thermal modeling including heat transfer in the thickness direction must he considered. This requires inclusion of Eq. (120) with heat convection terms.

REFERENCES

A1. S. Ahn and J. L. White, *Int. Polym. Process.* **18**, 243 (2003); *J. Appl. Polym. Sci.* **90**, 1555 (2003); Ibid. **91**, 651 (2004).

A2. R. D. Andrews, N. Hofman-Bang, and A. V. Tobolsky, *J. Polym. Sci.* **3**, 669 (1948).
A3. R. D. Andrews and A. V. Tobolsky, *J. Polym. Sci.* **7**, 221 (1952).
A4. D. J. Angier, R. J. Ceresa, and W. F. Watson, *J. Polym. Sci.* **34**, 699 (1958).
A5. D. J. Angier, W. T. Chambers, and W. F. Watson, *J. Polym. Sci.* **25**, 129 (1957).
A6. D. J. Angier, E. Farlie, and W. F. Watson, *Trans. Inst. Rubber Ind.* **34**, 8 (1958).
A7. D. J. Angier and W. F. Watson, *J. Polym. Sci.* **20**, 235 (1956).
A8. D. J. Angier and W. F. Watson, *J. Polym. Sci.* **25**, 1 (1957).
A9. D. J. Angier and W. F. Watson, *Trans. Inst. Rubber Ind.* **33**, 22 (1956).
A10. T. Araki and J. L. White, *Polym. Eng. Sci.* **38**, 616 (1998).
A11. G. Ardichvili, *Kautschuk* **14**, 23 (1938).
A12. G. Ardichvili, *Kautschuk* **19**, 41 (1938).
A13. T. Asai, T. Fukui, K. Inoue, and M. Kuriyama, Paper III-4 presented at International Rubber Conference, Paris, June 1982.
A14. G. Ayrey, C. G. Moore, and W. F. Watson, *J. Polym. Sci.* **19**, 1 (1956).
B1. Th. Baader, *Kautschuk* **14**, 223 (1938).
B2. Th. Baader, *Kautsch. Gummi* **3**, 159 (1950).
B3. Th. Baader, *Kautsch. Gummi* **3**, 205 (1950).
B4. Th. Baader, *Kautsch. Gummi* **3**, 245 (1950).
B5. Th. Baader, *Kautsch. Gummi* **3**, 279 (1950).
B6. Th. Baader, *Kautsch. Gummi* **3**, 323 (1950).
B7. Th. Baader, *Kautsch. Gummi* **3**, 361 (1950).
B8. E. B. Bagley, *J. Appl. Phys*. **28**, 624 (1957).
B9. E. B. Bagley and A. M. Birks, *J. Appl. Phys.* **31**, 556 (1960).
B10. T. F. Ballenger and J. L. White, *J. Appl. Polym. Sci.* **15**, 1949 (1971).
B11. R. L. Ballman, *Rheol. Acta* **4**, 137 (1965).
B12. F. H. Banbury, U.S. Patent 1,200,070 (1916).
B13. F. H. Banbury, U.S. Patent 1,227,522 (1917).
B14. B. Bernstein, E. A. Kearsley, and L. J. Zapas, *Trans. Soc. Rheol.* **7**, 391 (1963).
B15. B. Bernstein, E. A. Kearsley, and L. J. Zapas, *J. Res. Natl. Bur. Stand.*, *Sect. B* **68**, 103 (1964).
B16. J. P. Berry, R. W. Sambrook, and J. Beasley, *Plast. Rubber Process*. p. 97 (1977).
B17. H. Bewley, English Patent 10,825 (1845).
B18. E. C. Bingham, *J. Wash. Acad. Sci.* **6**, 177 (1916).
B19. E. C. Bingham, "Fluidity and Plasticity," McGraw–Hill, New York, 1922.
B20. R. B. Bird and P. J. Carreau, *Chem. Eng. Sci.* **23**, 427 (1968).
B21. R. B. Bird, W. E. Stewart, and E. N. Lightfoot, "Transport Phenomena," Wiley, New York, 1960.
B22. D. C. Bogue, *IEC Fundam*. **5**, 253 (1966).
B23. D. C. Bogue, T. Masuda, Y. Einaga, and S. Onogi, *Polym. J.* **1**, 563 (1970).
B24. D. C. Bogue and J. L. White, "Engineering Analysis of Non-Newtonian Fluids," NATO Agardograph.
B25. W. R. Bolen and R. E. Colwell, *SPE ANTEC Tech. Pap.* **4**, 1008 (1958).
B26. L. Boltzmann, Sitzungsber, *Kaiserl. Akad. Wiss. Wien* **70**, 275 (1874).
B27. C. Booth, *Polymer* **4**, 471 (1963).
B28. H. H. Bowerman, E. A. Collins, and N. Nakajima, *Rubber Chem. Technol*. **47**, 307 (1974).
B29. R. A. Brooman, English Patent 10,582 (1845).
B30. R. Brzoskowski, S. Montes, J. L. White, and N. Nakajima, *J. Non-Newtonian Fluid Mech.* **31**, 43 (1989).
B31. R. Brzoskowski and J. L. White, *Int. Polym. Process.* **5**, 191 (1990).
B32. R. Brzoskowski and J. L. White, *Int. Polym. Process.* **5**, 238 (1990).
B33. R. Brzoskowski, J. L. White, and B. Kalvani, *Kunststoffe* **80**, 922 (1990).
B34. R. Brzoskowski, J. L. White, W. Szydlowski, N. Nakajima, and K. Min, *Int. Polym. Process*. **3**, 134 (1988).

B35. R. Brzoskowski, J. L. White, W. Szydlowski, F. C. Weissert, N. Nakajima, and K. Min, *Rubber Chem. Technol*. **60**, 945 (1987).
B36. R. Brzoskowski, J. L. White, F. C. Weissert, N. Nakajima, and K. Min, *Rubber Chem. Technol*. **59**, 634 (1986).
B37. W. F. Busse, *Ind. Eng. Chem.* **24**, 140 (1932).
B38. W. F. Busse and R. N. Cunningham, *Proc. Rubber Technol. Conf. London*, p. 288 (1938).
B39. W. F. Busse and R. Longworth, *Trans. Soc. Rheol*. **6**, 179 (1962).
C1. J. F. Carley, R. S. Mallouk, and J. M. McKelvey, *Ind. Eng. Chem*. **45**, 974 (1953).
C2. P. J. Carreau, *Trans. Soc. Rheol*. **16**, 99 (1972).
C3. B. Caswell and R. I. Tanner, *Polym. Eng. Sci*. **18**, 416 (1978).
C4. R. J. Ceresa, *Polymer* **1**, 477 (1960).
C5. L. C. Cessna, U.S. Patent 3,651,187 (1972).
C6. E. M. Chaffee, U.S. Patent 16 (1836).
C7. E. M. Chaffee, U.S. Patent 1939 (1841).
C8. F. M. Chapman and S. L. Lee, *Soc. Plast. Eng. J.* **26**, 37 (1970).
C9. I. J. Chen and D. C. Bogue, *Trans. Soc. Rheol*. **16**, 59 (1972).
C10. J. J. Cheng and I. Manas-Zloczower, *Polym. Eng. Sci*. **29**, 701, 1059 (1989).
C11. J. J. Cheng and I. Manas-Zloczower, *J. Appl. Polym. Sci. Appl. Polym. Symp*. **44**, 53 (1989).
C12. J. W. Cho, J. L. White, and L. Pomini, *Kautsch Gummi Tech* **50**, 496 (1997); J. W. Cho, J. L. White, and L. Pomini, *Kautsch Gummi Tech* **50**, 728 (1997).
C13. F. N. Cogswell, *Plast. Polym.* April, 109 (1968).
C14. B. D. Coleman, M. E. Gurtin, and I. Herrera, *Arch. Rat. Mech. Anal*. **19**, 1, 239, 266 (1965).
C15. B. D. Coleman and H. Markovitz, *J. Appl. Phys*. **35**, 1 (1964).
C16. B. D. Coleman and W. Noll, *Arch. Rat. Mech. Anal*. **3**, 289 (1959).
C17. R. T. Cooke, British Patent 431,012 (1935).
C18. F. H. Cotton, *Trans. Inst. Rubber Ind*. **5**, 487 (1931).
C19. G. Cotton and J. L. Thiele, *Rubber Chem. Technol*. **51**, 749 (1978).
C20. W. P. Cox and E. H. Merz, *J. Polym. Sci*. **28**, 619 (1958).
C21. W. O. Criminale, J. L. Erickson, and G. L. Filbey, *Arch. Rat. Mech. Anal*. **1**, 410 (1958).
C22. M. Crochet, *Rubber Chem. Technol*. **62**, 426 (1989).
D1. B. Darrow, U.S. Patent 1,282,767 (1918).
D2. B. David, T. Sapir, A. Nir, and Z. Tadmor, *Int. Polym. Process*. **7**, 204 (1992).
D3. B. David, A. Nir, and Z. Tadmor, *Int. Polym. Process*. **5**, 155 (1990).
D4. G. E. Decker and F. L. Roth, *India Rubber World* **128**, 399 (1953).
D5. J. S. Deng and A. I. Isayev, *Rubber Chem. Technol*. **64**, 296 (1991).
D6. T. deWitt, *J. Appl. Phys*. **26**, 889 (1955).
D7. J. H. Dillon, *Physics* (*NY*) **7**, 73 (1936).
D8. J. H. Dillon and L. V. Cooper, *Rubber Age* (*NY*) p. 1306 (1937).
D9. J. H. Dillon and N. Johnston, *Physics* **4**, 225 (1933).
D10. H. J. Donald, U.S. Patent 3,279,501 (1966).
D11. R. A. Dunell and A. V. Tobolsky. *J. Chem. Phys.* **17**, 100 (1949).
El. S. Eccher and A. Valentinotti, *Ind. Eng. Chem.* **50**, 829 (1958).
E2. E. R. G. Eckert and R. M. Drake, "Heat and Mass Transfer," McGraw–Hill, New York, 1959.
E3. J. E. Eilersen, U.S. Patent 3,099,859 (1963).
E4. R. Eisenschitz, B. Rabinowitsch, and K. Weissenberg, *Mitt. Deutsch. Materialpruf. Son-derh*, **9**, 9 (1929).
Fl. F. Farrel III, "Solid Men of the Place Gave Strong Roots," Newcomen Society, New York, 1956.
F2. P. Fay, U.S. Patent 2,569,373 (1951).
F3. J. D. Ferry, "Viscoelastic Properties of Polymers," Wiley, New York, 1969.
F4. V. Folt, *Rubber Chem. Technol.* **42**, 1294 (1969).
F5. T. G. Fox and P. J. Flory, *J. Am. Chem. Soc.* **70**, 2384 (1949).

F6. T. G. Fox, S. Gratch, and E. Loeshaek, in "Rheology," Academic Press, New York, Vol. 1, 1956.
F7. L. C. Frazier, U.S. Patent 3,485,692 (1969).
F8. P. K. Freakley and N. Y. Wan Idris, *Rubber Chem. Technol.* **52**, 134 (1979).
F9. H. Freundlich and A. D. Jones, *J. Phys. Chem.* **40**, 1217 (1936).
F10. S. M. Freeman and K. Weissenburg, *Nature* **161**, 324 (1948).
F11. I. Furuta, V. M. Lobe, and J. L. White, *J. Non-Newtonian Fluid Mech.* **1**, 207 (1976).
G1. T. L. Garner, *India Rubber J.* **78**, (1929).
G2. R. E. Gaskell, *J. Appl. Mech.* **73**, 334 (1950).
G3. P. Geyer, U.S. Patent 3,375,549 (1968).
G4. L. A. Goettler and A. J. Lambright, U.S. Patent (filed Feb. 2, 1976) 4,056,591 (1977); U.S. Patent (filed July 25, 1975) 4,057,610 (1977).
G5. L. A. Goettler, A. J. Lambright, R. I. Leib, and P. J. D. Mauro, *Rubber Chem. Technol.* **54**, 277 (1981).
G6. L. A. Goettler, R. I. Leib, and A. J. Lambright, *Rubber Chem. Technol.* **52**, 838 (1979).
G7. H. J. Gohlisch, W. May, F. Ramm, and W. Ruger, Extrusion of Elastomers, in "Plastics Extrusion Technology," F. Hensen (Ed.), Hanser, Munich, 1988.
G8. C. Goldstein, *Trans. Soc. Rheol.* **18**, 357 (1974).
G9. S. Goldstein (Ed.), "Modern Developments in Fluid Dynamics," Clarendon Press, Oxford, 1938.
G10. C. F. Goodeve, *Trans. Faraday Soc.* **35**, 342 (1939).
G11. C. F. Goodeve and G. W. Whitfield, *Trans. Faraday Soc.* **34**, 511 (1938).
G12. C. Goodyear, U.S. Patent 3633 (1844).
G13. C. Goodyear, U.S. Patent 5536 (1848).
G14. C. Goodyear, "Gum Elastic and Its Varieties with a Detailed Account of Its Applications and Uses and the Discovery of Vulcanization," Privately printed, New Haven, CT, 1855.
G15. M. Gray, British Patent 5056 (1879).
G16. A. E. Green and R. S. Rivlin, *Arch. Rat. Mech. Anal,* **1**, 1 (1957).
G17. F. M. Griffith. *Ind. Eng. Chem. Fundam.* **1**, 180 (1962).
G18. R. W. Griffiths, *Trans. Inst. Rubber Ind.* **1**, 308 (1926).
G19. F. F. Grosevnor, U.S. Patent (filed Aug. 17, 1916) 1,254,685 (1918).
G20. J. T. Gruver and G. Kraus, *J. Polym. Sci. A.* **2**, 797 (1964).
G21. H. G. Gurhin and W. Spreutels, *Kautsch. Gummi Kunstst.* **43**, 431 (1990).
H1. H. Hagen, *Kautschuk* **15**, 88 (1939).
H2. C. D. Han and L. H. Drexler, *J. Appl. Polym. Sci.* **17**, 2329 (1973).
H3. M. H. Han, J. L. White, N. Nakajima, and R. Brzoskowski, *Kautsch. Gummi Kunstst.* **43**, 1060 (1990).
H4. C. Hancock, English Patent 11,147 (1846).
H5. C. Hancock, English Patent 11,208 (1847).
H6. C. Hancock, English Patent 11,575 (1847).
H7. C. Hancock, English Patent 11,874 (1847).
H8. T. Hancock, English Patent 4768 (1823).
H9. T. Hancock, English Patent 7344 (1837).
H10. T. Hancock, English Patent 9952 (1843).
H11. T. Hancock, "Personal Narrative of the Origin and Progress of the Caoutchouc or India Rubber Manufacture in England," Longman, Brown, Green, Longmans & Roberts, London, 1857.
H12. E. G. Harms, *Eur. Rubber J.* **6**, 23 (1978); *Kunststoffe* **74**, 33 (1984).
H13. E. G. Harms, G. Menges, and R. Hegele, German Offenlegungsshift 2,235,784 (1974); U.S. Patent 4,178,104 (1979); U.S. Patent 4,199,263 (1980).
H14. E. R. Harrel, J. P, Porter, and N. Nakajima, *Rubber Chem. Technol.* **64**, 254 (1991).
H15. H. Herrmann, "Schneckenmaschinen in der Verfahrenstechnik," Springer, Berlin, 1972.

H16. H. Herrmann, in "Kunststoffe ein Werkstoff macht Karriere," W. Glenz (Ed.), Hanser, Munich, 1985.
H17. W. H. Herschel and R. S. Bulkley, *Proc. ASTM* **26**, 62 (1926).
H18. J. Hoekstra, *Physics* **4**, 295 (1933); *Kautschuk* **9,** 750 (1933).
H19. K. Hohenemser and W. Prager, *Z. AMM* **12,** 216 (1932).
H20. B. Hu and J. L. White, *Int. Polym. Process.* **8**, 18 (1993).
H21. B. Hu and J. L. White, *Rubber Chem. Technol.* **66**, 257 (1993).
H22. B. Hu and J. L. White, *Kautsch Gummi Kunstst* **49**, 285 (1996).
I1. Y. Ide and J. L. White, *J. Appl. Polym. Sci*. **22**, 1061 (1978).
I2. A. I. Isayev, Injection Molding of Rubber Compounds, in "Injection and Compression Molding Fundamentals," A. I. Isayev (Ed.), Dekker, New York, 1987.
I3. A. I. Isayev, Injection Molding of Rubbers, in "Comprehensive Polymer Science," G. Allen, J. C. Bevington, and S. L. Aggarwal (Eds.), Pergamon Press, Oxford, Vol. 7, 1989.
I4. A. I. Isayev and Y. H. Huang, *Adv. Polym. Technol.* **9**, 167 (1988).
I5. A. I. Isayev and X. Fan, *J. Rheol.* **34**, 35 (1990).
I6. A. I. Isayev, M. Sobhanie, and J. S. Deng, *Rubber Chem. Technol.* **61**, 906 (1988).
J1. M. W. Johnson and D. Segalman, *J. Non-Newtonian Fluid Mech.* **2**, 255 (1977).
K1. M. R. Kamal and S. Kenig, *Polym. Eng. Sci.* **12**, 294 (1972).
K2. E. Karrer, *Ind. Eng. Chem. Anal. Ed.* **1**, 158 (1929); *Ind. Eng. Chem.* **21**, 770 (1929).
K3. E. Karrer, J. M. Davies, and E. O. Dieterich, *Ind. Eng. Chem., Anal. Ed.* **2**, 96 (1930).
K4. D. H. Killeffer, "Banbury, The Master Mixer," Palmerton, New York, 1962.
K5. J. K. Kim, International Seminar on Elastomers, *J. Appl. Polym. Sci.*, *Appl. Polym. Symp.* **50**, 145 (1992).
K6. J. K. Kim and J. L. White, *Nihon Reoroji Gakkaishi* **17**, 203 (1989).
K7. J. K. Kim and J. L. White, *Int. Polym. Process.* **6**, 103 (1991).
K8. J. K. Kim, J. L. White, K. Min, and W. Szydlowski, *Int. Polym. Process.* **4**, 9 (1989).
K8a. K. J. Kim and J. L. White, *Polym. Eng. Sci.* **39**, 2189 (1999).
K8b. P. S. Kim and J. L. White, *Rubber Chem. Technol*. **67**, 871 (1994).
K9. P. S. Kim and J. L. White, *Kautsch Gummi Kunstst* **49**, 10 (1996).
K10. P. S. Kim and J. L. White, *Rubber Chem. Technol.* **69**, 686 (1996).
K11. R. G. King, *Rheol. Acta* **5**, 35 (1966).
K12. E. Konrad, *Angew. Chem.* **62**, 491 (1950).
K13. R. Koopmann, *Kautsch. Gummi Kunstst.* **36**, 108 (1983).
K14. R. Koopmann, *Polym. Testing* **5**, 341 (1985).
K15. R. Koopmann, *Kautsch. Gummi Kunstst.* **38**, 281 (1985).
K16. R. Koopmann and H. Kramer, *J. Testing Eval. ASTM* **12**, 407 (1984).
K17. R. Koopmann and J. Schnetger, *Kautsch. Gummi Kunstst.* **39**, 131 (1986).
K18. G. Kraus and J. T. Gruver, *J. Polym. Sci. A* **3**, 105 (1965).
K19. C. Koolihiran and J. L. White, *J. Appl. Polym. Sci.* **78**, 1551 (2000).
K20. K. Kubota, R. Brzoskowski, J. L. White, F. C. Weissert, N. Nakajima, and K. Min, *Rubber Chem. Technol.* **60**, 924 (1987).
K21. T. Kumazawa, R. Brzoskowski, and J. L. White, *Kautsch. Gummi Kunstst.* **43**, 688 (1990).
L1. H. Lamb, "Hydrodynamics," 6th ed., Cambridge University Press, London, 1932.
L2. A. Lasch and K. Frei, German Patent 738,787 (1943).
L3. A. Lasch and E. Stromer, German Patent 641,685 (1937).
L4. H. Leaderman, *Ind. Eng. Chem.* **35**, 374 (1943).
L5. H. Leaderman, "Elastic and Creep Properties of Filamentous Materials and Other High Polymers," Textile Found., Washington, D.C., 1943.
L6. L. J. Lee, J. F. Stevenson, and R. M. Griffith, U.S. Patent 4,425,289 (1984).
L7. P. W. Lehman, U.S. Patent 2,096,362 (1937).
L8. J. P. Lehnen, *Kunststofftechnik* **9**, 3, 90, 114, 198, 352 (1970).
L9. A. I. Leonov, *Rheol. Acta* **15**, 85 (1976).
L10. A. I. Leonov, *J. Rheol.* **34**, 155 (1990).

L11. A. I. Leonov, *J. Non-Newtonian Fluid Mech.* **42**, 343 (1990).
L12. G. H. Lewis, U.S. Patent 1,252,821 (1918).
L13. L. L. Li and J. L. White, *Rubber Chem. Technol.* **69**, 628 (1996).
L14. P. W. Litchfield, "Industrial Voyage," Doubleday, Garden City, NY, 1954.
L15. V. M. Lobe and J. L. White, *Polym. Eng. Sci.* **19**, 617 (1979).
L16. A. Lodge, *Trans. Faraday Soc.* **52**, 120 (1956).
M1. C. Y. Ma, J. L. White, F. C. Weissert, A. I. Isayev, N. Nakajima, and K. Min, *Rubber Chem. Technol.* **58**, 815 (1985).
M2. C. Y. Ma, J. L. White, F. C. Weissert, and K. Min, *Polym. Composites* **6**, 215 (1985).
M3. C. Y. Ma, J. L. White, F. C. Weissert, and K. Min, *J. Non-Newtonian Fluid Mech.* **17**, 275 (1985).
M4. C. Macintosh, English Patent 4804 (1823).
M5. H. Mahn, H. Orth, K. H. Roitzsch, and W. Woeckener, in "Kunststoffe ein Werkstoffe macht Karriere," W. Glenz (Ed.), Hanser, Munich, 1985.
M6. C. Maillefer, Swiss Patent 363,149 (1962).
M7. H. Mark and A. V. Tobolsky, "Physical Chemistry of High Polymeric Systems," 2nd ed., Interscience, New York, 1950.
M8. B. Marzetti, *India Rubber World* **68**, 776 (1923).
M9. B. Marzetti, *Chim. Ind. Appl.* **5**, 342 (1923).
M10. B. Marzetti, *Atti Della Reale Acad. Naz. Lincei* **32**, 399 (1923); *Rubber Age* **19**, 454 (1924).
M11. B. Marzetti, *Rubber Age* **20**, 139 (1925).
M12. T. Masuda, K. Kitagawa, T. Inoue, and S. Onogi, *Macromolecules* **4**, 116 (1970).
M13. T. Masuda, Y. Ohta, and S. Onogi, *Macromolecules* **4**, 763 (1971).
M14. J. C. Maxwell, *Philos. Trans. R. Soc.* **157**, 249 (1866).
M15. J. M. McKelvey, *Ind. Eng. Chem.* **45**, 982 (1953).
M16. F. M. McLaughlin, U.S. Patent 2,325,001 (1943).
M17. J. Meissner, *Rheol. Acta* **8**, 78 (1969).
M18. G. Menges and E. G. Harms, *Kautsch. Gummi Kunstst.* **25**, 469 (1972); **27**, 187 (1974).
M19. G. Menges and J. P. Lehnen, *Plastverarbeiter* **20**, 31 (1969).
M20. W. Meskat, *Kunststoffe* **41**, 417 (1951).
M21. W. Meskat, *Kunststoffe* **45**, 87 (1955).
M22. A. P. Metzger and J. R. Knox, *Trans. Soc. Rheol.* **9**, 13 (1965).
M23. A. B. Metzner, J. L. White, and M. M. Denn, *AIChE J.* **12**, 863 (1966); *Chem. Eng. Prog.* **62**, 12, (1966).
M24. S. Middleman, *Trans. Soc. Rheol.* **13**, 125 (1969).
M25. W. H. Miller, U.S. Patent 3,069,853 (1991).
M26. W. H. Miller, C. C. Lee, and J. F. Stevenson, *Int. Polym. Process.* **6**, 253 (1991).
M27. K. Min and J. L. White, *Rubber Chem. Technol.* **58**, 1024 (1985).
M28. K. Min and J. L. White, *Rubber Chem. Technol.* **60**, 361 (1987).
M29. N. Minagawa and J. L. White, *J. Appl. Polym. Sci.* **20**, 501 (1976).
M30. W. W. Minoshima, J. L. White, and J. E. Spruiell, *Polym. Eng. Sci.* **20**, (1980).
M31. S. R. Moghe, *Rubber Chem. Technol.* **39**, 247 (1976).
M32. W. D. Mohr and R. S Mallouk, *Ind. Eng. Chem.* **51**, 765 (1959).
M33. S. Montes and J. L. White, *Rubber Chem. Technol.* **55**, 1354 (1982).
M34. S. Montes and J. L. White, *Kautsch. Gummi Kunstst.* **44**, 731 (1991).
M35. S. Montes and J. L. White, *Kautsch. Gummi Kunstst.* **44**, 937 (1991).
M36. S. Montes and J. L. White, *J. Non-Newtonian Fluid Mech.,* **49**, 277 (1993).
M37. S. Montes, J. L. White, and N. Nakajima, *J. Non-Newtonian Fluid Mech.* **28**, 183 (1988).
M38. S. Montes, J. L. White, N. Nakajima, F. C. Weissert, and K. Min, *Rubber Chem. Technol.* **61**, 698 (1988).
M39. M. Mooney, *J. Rheol.* **2**, 210 (1931).
M40. M. Mooney, *Ind. Eng. Chem., Anal. Ed.* **6**, 147 (1934).
M41. M. Mooney, *Physics* **7**, 413 (1936).

M42. M. Mooney, *J. Colloid Sci.* **2**, 69 (1947).
M43. M. Mooney, personal communication (ca. 1965); unpublished U.S. Rubber Company report (1953).
M44. M. Mooney, in "Rheology," F. R. Eirich (Ed.), Academic Press, New York, Vol. 2, 1958.
M45. M. Mooney, *Proc. Int. Rubber Conf. (Washington),* p. 368 (1959).
M46. M. Mooney, *Rubber Chem. Technol.* **35**, xxvii (1962).
M47. M. Mooney and S. A. Black, *J: Colloid Sci.* **7**, 204 (1952).
M48. A. Morikawa, K. Min, and J. L. White, *Adv. Polym. Technol.* **8**, 383 (1988).
M49. A. Morikawa, J. L. White, and K. Min, *Kautsch. Gummi Kunstst.* **41**, 1226 (1988).
M50. A. Morikawa, K. Min, J. L. White, *Int. Polym. Process* **4**, 23 (1989).
M51. L. Mullins, *J. Phys. Colloid Chem.* **54**, 239 (1950).
M52. L. Mullins and R. W. Whorlow, *Trans. Inst. Rubber Ind.* **27**, 55 (1951).
N1. N. Nakajima, *Rubber Chem. Technol.* **54**, 266 (1981); **55**, 937 (1982).
N2. N. Nakajima, H. H. Bowerman, and E. A. Collins, *J. Appl. Polym. Sci.* **21**, 3063 (1977).
N3. N. Nakajima and E. R. Harrel, *Rubber Chem. Technol.* **52**, 962 (1979).
N4. K. Ninomiya, *J. Colloid Sci.* **14**, 49 (1959).
N5. W. Noll, *J. Rat. Mech. Anal.* **4**, 3 (1955).
N6. W. Noll, *Arch. Rat. Mech. Anal.* **2**, 197 (1958).
N7. R. H. Norman, *Plast. Rubber Int.* **5**, 243 (1985).
O1. K. Oda, J. L. White, and E. S. Clark, *Polym. Eng. Sci.* **16**, 585 (1976).
O2. K. Oda, J. L. White, and E. S. Clark, *Polym. Eng. Sci.* **18**, 25 (1978).
O3. J. G. Oldroyd, *Proc. Cambridge Philos. Soc.* **43**, 100 (1947).
O4. J. G. Oldroyd, *Proc. Cambridge Philos. Soc.* **43**, 382 (1947).
O5. J. G. Oldroyd, *Proc. Cambridge Philos. Soc.* **45**, 595 (1949).
O6. J. G. Oldroyd, *Proc. R. Soc. A* **200**, 523 (1950).
O7. J. G. Oldroyd, *Q. J. Mech. Appl. Math* **4**, 271 (1951).
O8. J. G. Oldroyd, *Proc. R. Soc. A* **245**, 278 (1958).
O9. S. Onogi, T. Masuda, I. Shiga, and F. Costaschuk, U.S.–Japan Seminar on Polymer Processing and Rheology, *Appl. Polym. Symp.* **20**, 37 (1973).
O10. G. Osanaiye, A. I. Leonov, and J. L. White, *J. Non-Newtonian Fluid Mech.*, **49**, 87 (1993).
P1. G. Passoni, U.S. Patent 4,775,240 (1988).
P2. J. R. A. Pearson, *Trans. J. Plast. Inst.* **30**, 230 (1962).
P3. J. R. A. Pearson, *Trans. J. Plast. Inst.* **31**, 125 (1963).
P4. J. R. A. Pearson, *Trans. J. Plast. Inst.* **32**, 239 (1964).
P5. J. R. A. Pearson, "Mechanical Principles of Polymer Melt Processing," Pergamon Press, New York, 1966.
P6. J. R. A. Pearson and C. J. S. Petrie, *Plast. Polym.* **38**, 85 (1970); *J. Fluid Mech.* **40**, 1 (1970); *J Fluid Mech.* **42**, 609 (1970).
P7. N. Phan Tien, *J. Non-Newtonian Fluid Mech.* **22**, 259 (1978).
P8. N. Phan Tien and R. I. Tanner, *J. Non-Newtonian Fluid Mech.* **2**, 353 (1977).
P9. W. R. Phillips, U.S. Patent 3,195,183 (1965).
P10. W. T. Pigott, *Trans. ASME* **73**, 947 (1951).
P11. M. Pike and W. F. Watson, *J. Polym. Sci.* **9**, 229 (1952).
P12. G. H. Piper and J. R. Scott, *J. Sci. Inst.* **22**, 206 (1945).
P13. R. S. Porter and J. F. Johnson, *Proc. 4th Int. Rheol. Cong.* **2**, 467 (1965).
P14. R. S. Porter and J. F. Johnson, *Chem. Rev.* **66**, 1 (1966).
P15. W. Prager, "Mechanics of Continua," Ginn, Boston, 1961.
P16. W. Prager, in Appendix to the article by J. T. Bergen in "Processing of Thermoplastic Materials," E. C. Bernhardt (Ed.), Reinhold, New York, 1959.
P17. W. Prager and P. Hodge, "Theory of Perfectly Plastic Solids," Wiley, New York, 1951.
R1. V. C. Ratliff, U.S. Patent 2,720,679 (1955).
R2. M. Reiner, "Deformation and Flow," Lewis, London, 1948, and later editions.

R3. M. Reiner, "Lectures on Theoretical Rheology," North Holland, Amsterdam, three editions (1943), (1949), (1960).
R4. M. Reiner, *Phys. Today* **17**, 62 (1964).
R5. O. Reynolds, *Philos. Trans. R. Soc. London, Ser. A* **174**, 935 (1883).
R6. O. Reynolds, *Philos. Trans. R. Soc. London, Ser. A* **177**, 157 (1886).
R7. J. G. Richardson, U.S. Patent 3,761,553 (1973).
R8. S. Richardson, *J. Fluid Mech.* **56**, 609 (1972).
R9. R. S. Rivlin, *J. Rat. Mech. Anal.* **5**, 179 (1956).
R10. R. S. Rivlin and J. L. Ericksen, *J. Rat. Mech. Anal.* **4**, 323 (1955).
S1. N. Sato, M. Miyaoka, S. Yamasaki, K. Inoue, A. Koriyama, T. Fukui, T. Asai, K. Nakagawa, and T. Masaki, U.S. Patent 4,284,358 (1981); U.S. Patent 4,300,838 (1981).
S2. J. R. Schaefgen and P. J. Flory, *J. Am. Chem. Soc.* **70**, 2709 (1948).
S3. G. H. Schanz, U.S. Patent 2,807,833 (1957).
S4. G. Schenkel, "Kunststoffe Extruder-Technik," Hanser, Munich, 1963.
S5. J. R. Scott, *Trans. Inst. Rubber Ind.* **7**, 169 (1931).
S6. J. R. Scott, *Trans. Inst. Rubber Ind.* **10**, 481 (1935).
S7. G. Schramm, *Kaustch. Gummi Kunstst.* **40**, 756 (1987).
S8. T. Schwedoff, *J. Deo Phys.* **9**, 34 (1890); *Phys. Z.* **1**, 552 (1900).
S9. F. A. Seiberling and C. A. Carlton, U.S. Patent 2,032,508 (1936).
S10. Y. T. Shah and J. R. A. Pearson, *Chem. Eng. Sci.* **29**, 1485 (1974).
S11. K. C. Shin and J. L. White, *Rubber Chem. Technol.* **66**, 121 (1993).
S12. K. C. Shin, J. L. White, R. Brzoskowski, and N. Nakajima, *Kautsch. Cummi Kunstst.* **43**, 181 (1990).
S13. A. H. P. Skelland, "Non-Newtonian Fluid and Heat Transfer," Wiley, New York, 1967.
S14. R. W. Snyder and J. I. Haase, U.S. Patent 1,952,469 (1934).
S15. M. Sobhanie, J. S. Deng, and A. I. Isayev; *J. Appl. Polym. Sci., Appl. Polym. Symp.* **44**, 115 (1989).
S16. M. Sobhanie and A. I. Isayev, *Rubber Chem. Technol.* **62**, 939 (1989).
S17. L. E. Soderquist, U.S. Patent 2,296,800 (1942).
S18. H. J. Song, J. L. White, K. Min, N. Nakajima, and F. C. Weissert, *Adv. Polym. Technol.* **8**, 43 (1988).
S19. J. F. Stevenson, *AIChE J.* **18**, 540 (1972).
S20. J. F. Stevenson, Extrusion of Rubber and Plastics, in "Comprehensive Polymer Science," G. Allen, J. C. Bevington, and S. L. Aggarwal (Eds.), Pergamon Press, Oxford, Vol. 7, 1989.
S21. J. F. Stevenson and W. H. Miller, U.S. Patent 5,067,885 (1991).
S22. G. G. Stokes, *Trans. Cambridge Philos. Soc.* **8**, 287 (1845).
S23. G. G. Stokes, "Report on Recent Researches in Hydrodynamics," Report of the British Association (1846).
S24. G. G. Stokes, *Trans. Cambridge Philos. Soc.* **9**, (1851).
S25. Y. Suetsugu and J. L. White, *J. Appl. Polym. Sci.* **28**, 1481 (1983).
S26. Y. Suetsugu and J. L. White, *J. Non-Newtonian Fluid Mech.* **14**, 121 (1984).
T1. H. Tanaka and J. L. White, *Polym. Eng. Sci.* **20**, 949 (1980).
T2. R. I. Tanner, U.S.–Japan Seminar on Polymer Processing and Rheology, *Appl. Polym. Symp.* **20**, 201 (1973).
T3. R. H. Taylor, *India Rubber World* **112**, 582 (1945).
T4. R. H. Taylor, J. H. Fielding, and M. Mooney, "Symposium on Rubber Testing," ASTM, New York, 1947, p. 36.
T5. A. V. Tobolsky, "Properties and Structure of Polymers," Wiley, New York, 1960.
T6. M. Toh, T. Gondoh, T. Mon, S. Haren, and Y. Murakami, International Seminar on Elastomers, *J. Appl. Polym. Sci.*, *Appl. Polym. Symp.* **50**, 133 (1992).
T7. S. Toki and J. L White, *J. Appl. Polym. Sci.* **27**, 3171 (1982).
T8. N. Tokita, personal communication (1975).
T9. N. Tokita and J. L. White, *J. Appl. Polym. Sci.* **10**, 1011 (1966).

T10. C. Truesdell and R. A. Toupin, The Classical Field Theories, in "Handbuch der Physik," Vol. III/1, Springer, Berlin, 1960.
T11. L. G. Turk, U.S. Patent 3,782,871 (1974).
T12. D. M. Turner and M. D. Moore, *Plastic Rubber Proc.*, (Sept./Dec.), 81 (1980).
T13. D. Tyson and L. Comper, U.S. Patent 3,230,581 (1966).
V1. A. van Rossem and H. van der Meijden, *Kautschuk* **3**, 369 (1927); *Rubber Age* (*NY*) **23**, 443 (1928).
V2. B. Vergnes, N. Bennani, and C. Guichard, *Int. Polym. Process.* **1**, 19 (1986).
V3. G. R. Vila, *Ind. Eng. Chem.* **36**, 1113 (1944).
V4. G. V. Vinogradov, *Pure Appl. Chem.* **39**, 115 (1974).
V5. G. V. Vinogradov, V. D. Fikham, R. D. Radushkevich, and A. Ya Malkin, *J. Polym. Sci. A*-2 **8**, 657 (1970).
V6. G. V. Vinogradov and A. Y. Malkin, *J. Polym. Sci. A*-2 **4**, 135 (1966).
V7. G. V. Vinogradov and A. Y. Malkin, "Rheology of Polymers," Mir, Moscow, 1980.
V8. G. V. Vinogradov, A. Y. Malkin, E. P. Plotnikova, O. Y. Sabasi, and N. E. Nikolayava, *Int. J. Polym. Mater.* **2**, 1 (1972).
W1. M. H. Wagner, *Rheol. Acta* **15**, 136 (1976).
W2. W. F. Watson, *Trans. Inst. Rubber Ind.* **34**, 237 (1958).
W3. K. Weissenberg, *Nature* **159**, 310 (1947).
W4. G. S. Whitby (Ed.), "Synthetic Rubber," Wiley, New York, 1954.
W5. J. L. White, *J. Appl. Polym. Sci.* **8**, 1129 (1964).
W6. J. L. White, *J. Appl. Polym. Sci.* **8**, 2339 (1964).
W7. J. L. White, *J. Inst. Rubber Ind. (Rubber Ind.)* **8**, 148 (1974).
W8. J. L. White, *Polym. Eng. Sci.* **15**, 44 (1975).
W9. J. L. White, *J Non-Newtonian Fluid Mech.* **5**, 177 (1979).
W10. J. L. White, International Seminar on Elastomers, *J. Appl. Polym. Sci., Appl. Polym. Symp.* **50**, 109 (1992).
W11. J. L. White, *Int. Polym. Process.* **7**, 2 (1992).
W12. J. L. White, *Int. Polym. Process.* **7**, 110 (1992).
W13. J. L. White, *Rubber Chem. Technol.* **65**, 527 (1992).
W14. J. L. White, *Int. Polym. Process.* **7**, 290 (1992).
W15. J. L. White, *Int. Polym. Process.* **8**, 2 (1993).
W16. J. L. White, "Rubber Processing: Technology, Materials, and Principles," Epic Press, Hanser, Munich, 1995.
W17. J. L. White and J. W. Crowder, *J. Appl. Polym. Sci.* **18**, 1013 (1974).
W18. J. L. White, M. H. Han, N. Nakajima, and R. Brzoskowski, *J. Rheol.* **35**, 167 (1991).
W19. J. L. White and J. K. Kim, *J. Appl. Polym. Sci., Appl. Polym. Symp.* **49**, 59 (1989).
W20. J. L. White and A. Kondo, *J. Non-Newtonian Fluid Mech.* **3**, 41 (1977).
W21. J. L. White and Y. Lobe, *Rheol. Acta* **21**, 167 (1982).
W22. J. L. White and A. B. Metzner, *J. Appl. Polym. Sci.* **7**, 1867 (1963).
W23. J. L. White and H. Tanaka, *J. Non-Newtonian Fluid Mech.* **8**, 1 (1981).
W24. J. L. White and N. Tokita, *J. Appl. Polym. Sci.* **9**, 1921 (1965).
W25. J. L. White and N. Tokita, *J. Appl. Polym. Sci.* **11**, 321 (1967).
W26. J. L. White and N. Tokita, *J. Appl. Soc. Japan* **22**, 719 (1967); **24**, 436 (1968).
W27. J. L. White and N. Tokita, *J. Appl. Polym. Sci.* **12**, 1589 (1968).
W28. J. I. White, Y. Wang, A. I. Isayev, N. Nakajima, F. C. Weissert, and K. Min, *Rubber Chem. Technol.* **60**, 337 (1987).
W29. I. Williams, *Ind. Eng. Chem.* **10**, 324 (1923).
W30. M. L. Williams, R. F. Landel, and J. D. Ferry, *J. Am. Chem. Soc.* **77**, 3701 (1955).
W31. R. F. Wolf, *India Rubber World*, Aug. 1, p. 39 (1936).
Y1. Y. Yabushita, R. Brzoskowski, J. L. White, and N. Nakajima, *Int. Polym. Process.* **6**, 219 (1989).
Y2. M. Yamamoto, *J. Phys. Soc. Japan* **11**, 413 (1956).

Y3. H. Yamane and J. L. White, *Polym. Eng. Rev.* **2**, 167 (1982).
Y4. H. H. Yang and I. Manas-Zloczower, *Int. Polym. Process.* **7**, 195 (1992).
Z1. N. V. Zakharenko, F. S. Tolstukhina, and G. M. Bartenev, *Rubber Chem. Technol.* **35**, 326 (1962).
Z2. H. Zamodits and J. R. A. Pearson, *Trans. Soc. Rheol.* **13**, 357 (1969).
Z3. L. J. Zapas, *J. Res. Natl. Bur. Stand., Sect. A* **70**, 525 (1966).
Z4. L. J. Zapas and T. Craft, *J. Res. Natl. Bur. Stand.*, *Sect. A* **69**, 541 (1965).
Z5. S. Zaremaha, *Bull Acad. Sci. Cracow*, June, p. 594 (1903).

7 Vulcanization

AUBERT Y. CORAN
A. Y. Coran Consulting
Longboat Key, Florida

I. INTRODUCTION

Most useful rubber articles, such as tires and mechanical goods, cannot be made without vulcanization. Unvulcanized rubber is generally not very strong, does not maintain its shape after a large deformation, and can be very sticky. In short, unvulcanized rubber can have about the same consistency as chewing gum.

The first commercial method for vulcanization has been attributed to Charles Goodyear. His process (heating natural rubber with sulfur) was first used in Springfield, Massachusetts, in 1841. Thomas Hancock used essentially the same process about a year later in England. Since those early days, there has been continued progress toward the improvement of the process and in the resulting vulcanized rubber articles. In addition to natural rubber, over the years, many synthetic rubbers have been introduced. Also, in addition to sulfur, many other substances have been introduced as components of curing (vulcanization) systems. This chapter is an overview of the science and technology of vulcanization. Emphasis is placed on the vulcanization of general-purpose "high-diene" rubbers (e.g., natural rubber [NR], styrene-butadiene rubber [SBR], and butadiene rubber [BR]) by sulfur in the presence of organic accelerators.

This paper is adapted from "Vulcanization" by Aubert Y. Coran in the *Encyclopedia of Polymer Science and Engineering, Second Edition, Volume 17*.

The accelerated-sulfur vulcanization of these rubbers along with the vulcanization of other rubbers which are vulcanized by closely related technology (e.g., ethylene-propylene-diene monomer rubber [EPDM], butyl rubber [IIR], halobutyl rubbers, and nitrile rubber [NBR]) comprises more than 90% of all vulcanization. Nevertheless, we give some consideration to vulcanization by the action of other vulcanization agents such as organic peroxides, phenolic curatives, and quinoid curatives.

Dynamic vulcanization (DV) is also considered. DV is the crosslinking of one polymer in a blend of polymers during its mixing therein, all polymers of the blend being in the molten state. The process is used in the preparation of thermoplastic elastomeric compositions from rubber–plastic blends.

II. DEFINITION OF VULCANIZATION

Vulcanization is a process generally applied to rubbery or elastomeric materials. These materials forcibly retract to their approximately original shape after a rather large mechanically imposed deformation. Vulcanization can be defined as a process which increases the retractile force and reduces the amount of permanent deformation remaining after removal of the deforming force. Thus vulcanization increases elasticity while it decreases plasticity. It is generally accomplished by the formation of a crosslinked molecular network (Fig. 1.).

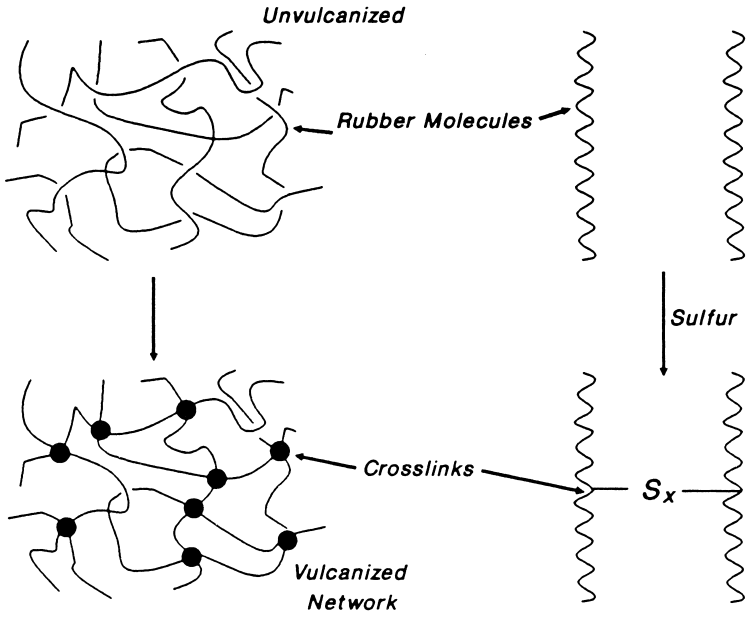

FIGURE 1 Network formation.

According to the theory of rubber elasticity [1], the retractile force to resist a deformation is proportional to the number of network supporting polymer chains per unit volume of elastomer. A supporting polymer chain is a linear polymer molecular segment between network junctures. An increase in the number of junctures or crosslinks gives an increase in the number of supporting chains. In an unvulcanized linear high polymer (above its melting point), only molecular chain entanglements constitute junctures.

Vulcanization, thus, is a process of chemically producing network junctures by the insertion of crosslinks between polymer chains. A crosslink may be a group of sulfur atoms in a short chain, a single sulfur atom, a carbon to carbon bond, a polyvalent organic radical, an ionic cluster, or a polyvalent metal ion. The process is usually carried out by heating the rubber, mixed with vulcanizing agents, in a mold under pressure.

III. EFFECTS OF VULCANIZATION ON VULCANIZATE PROPERTIES

Vulcanization causes profound changes at the molecular level. The long rubber molecules (molecular weight usually between 100,000 and 500,000 daltons) become linked together with junctures (crosslinks) spaced along the polymeric chains, with the average distance between junctures corresponding to a molecular weight between crosslinks of about 4,000 to 10,000 daltons. As a result of this network formation, the rubber becomes essentially insoluble in any solvent, and it cannot be processed by any means which requires it to flow, e.g., in a mixer, in an extruder, on a mill, on a calender, or during shaping, forming, or molding. Thus, it is essential that vulcanization occur only after the rubber article is in its final form.

Major effects of vulcanization [2–4] on use-related properties are illustrated by the idealization of Fig. 2. It should be noted that static modulus increases with vulcanization to a greater extent than does the dynamic modulus. (Here, static modulus is more correctly the equilibrium modulus, approximated by a low strain, slow-strain-rate modulus. Dynamic modulus is generally measured with the imposition of a sinusoidal, small strain at a frequency of 1–100 Hz.) The dynamic modulus is a composite of viscous and elastic behavior, whereas static modulus is largely a measure of only the elastic component of rheological behavior.

Hysteresis is reduced with increasing crosslink formation. Hysteresis is the ratio of the rate-dependent or viscous component to the elastic component of deformation resistance. It is also a measure of deformation energy that is not stored (or borne by the elastic network) but that is converted to heat. Vulcanization then causes a trade-off of elasticity for viscous or plastic behavior. Tear strength, fatigue life, and toughness are related to the breaking energy. Values of these properties increase with small amounts of crosslinking, but they are reduced by further crosslink formation. Properties related to the

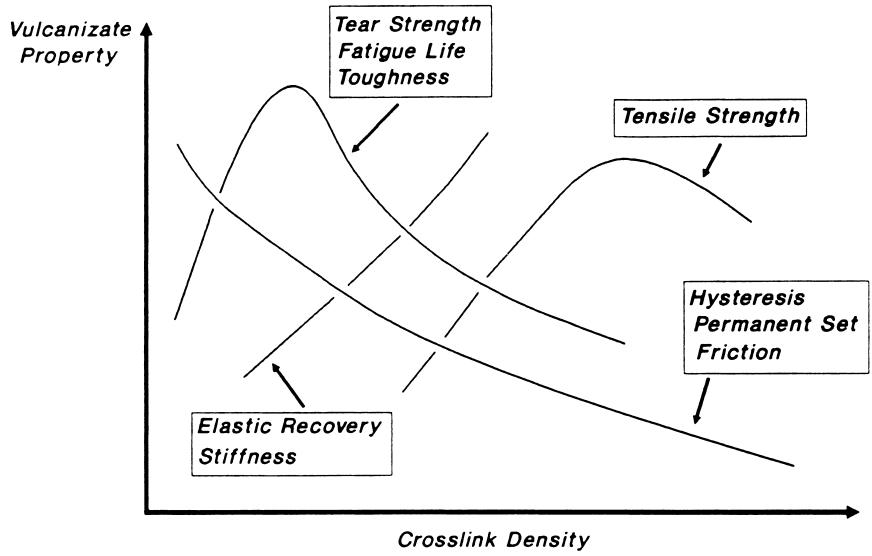

FIGURE 2 Vulcanizate properties as a function of the extent of vulcanization.

energy-to-break increase with increases in both the number of network chains and hysteresis. Since hysteresis decreases as more network chains are developed, the energy-to-break related properties are maximized at some intermediate crosslink density.

It should be noted that the properties given in Fig. 2 are not functions only of crosslink density. They are also affected by the type of crosslink, the type of polymer, and type and amount of filler, etc.

Reversion Reversion is a term generally applied to the loss of network structures by nonoxidative thermal aging. It is usually associated with isoprene rubbers vulcanized by sulfur. It can be the result of too long of a vulcanization time (overcure) or of hot aging of thick sections. It is most severe at temperatures above about 155°C. It occurs in vulcanizates containing a large number of polysulfidic crosslinks. Though its mechanism is complex, a good deal about the chemical changes that occur during the reversion of natural rubber has been deduced [5].

Sometimes the term "reversion" is applied to other types of nonoxidative degradation, especially with respect to rubbers not based on isoprene. For example, thermal aging of SBR (styrene-butadiene rubber), which can cause increased crosslink density and hardening, has been called reversion since it can be the result of overcure.

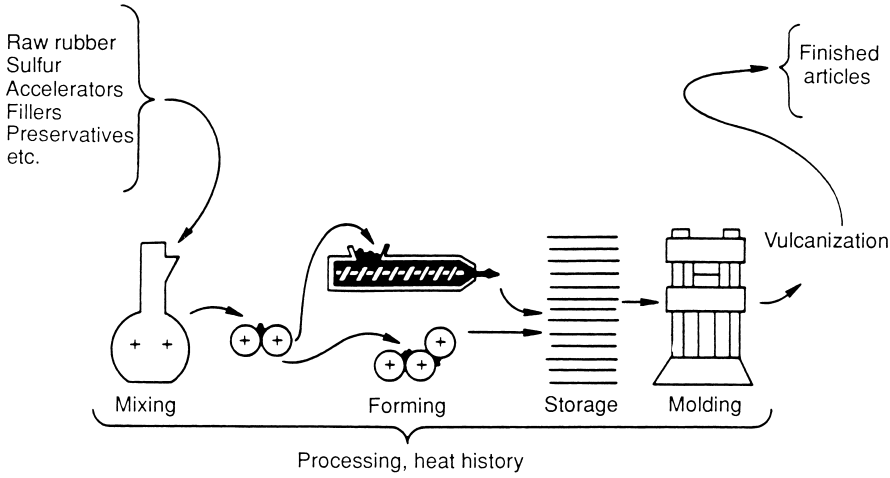

FIGURE 3 The effect of processing on heat history.

IV. CHARACTERIZATION OF THE VULCANIZATION PROCESS

Important characteristics related to the vulcanization process are the time elapsed before crosslinking starts, the rate of crosslink formation once it starts, and the extent of crosslinking at the end of the process. There must be sufficient delay or scorch resistance (resistance to premature vulcanization) to permit mixing, shaping, forming, and flowing in the mold before vulcanization. Then the formation of crosslinks should be rapid and the extent of crosslinking must be controlled (Figs. 3 and 4).

Scorch resistance is usually measured by the time at a given temperature required for the onset of crosslink formation as indicated by an abrupt increase in viscosity. The Mooney viscometer is usually used [4]. During this test, fully mixed but unvulcanized rubber is contained in a heated cavity. Imbedded in the rubber is a rotating disc. Viscosity is continuously measured (by the torque required to keep the rotor rotating at a constant rate) as a function of time. The temperature is selected to be characteristic of rather severe processing (extrusion, calendering, etc.).

Both the rate of vulcanization after the scorch period and the final extent of vulcanization are measured by devices called cure meters. Many workers contributed to this development [6]. Widely used cure meters are oscillating disc rheometers of the type introduced by the Monsanto Company in about 1965. The development of the oscillating disc rheometer, largely through the efforts of R. W. Wise, was the beginning of modern vulcometry, which has become standard practice in the industry. Before the development of the cure meter, it was necessary to measure mechanical properties of many specimens

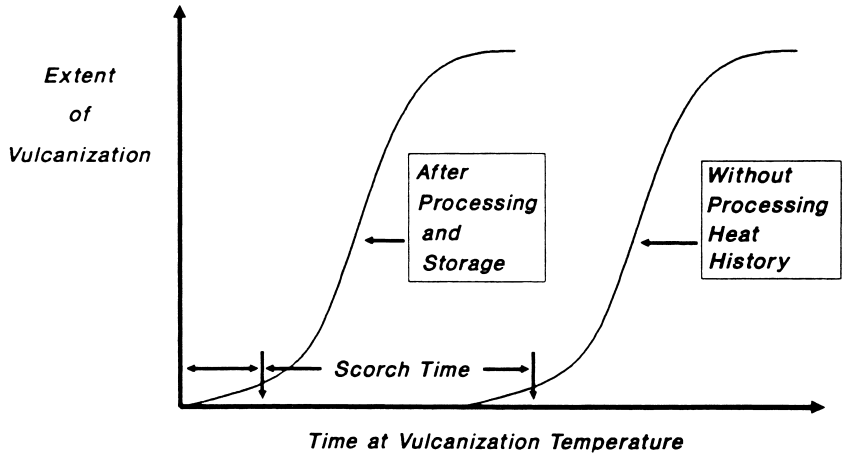

FIGURE 4 The effect of heat history (processing) on scorch safety.

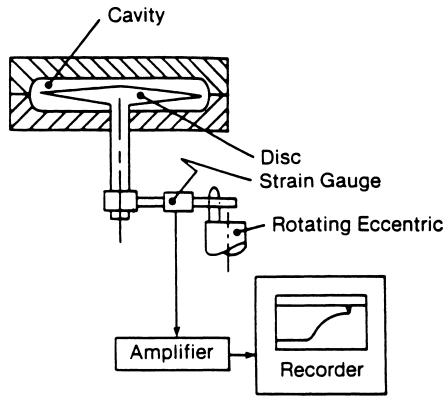

FIGURE 5 Oscillating disc rheometer.

of a rubber sample, each vulcanized for a different length of time at a given temperature.

In order to measure the vulcanization characteristics, the rubber is enclosed in a heated cavity (Fig. 5). Imbedded in the rubber is a metal disc that oscillates sinusoidally in its plane about its axis. Vulcanization is measured by increase in the torque required to maintain a given amplitude (e.g., degrees of arc) of oscillation at a given temperature. The torque is proportional to a low strain modulus of elasticity. Since this torque is measured at the elevated temperature of vulcanization, the portion of it due to viscous effects is minimal. Thus it has been assumed that the increase in torque during vulcan-

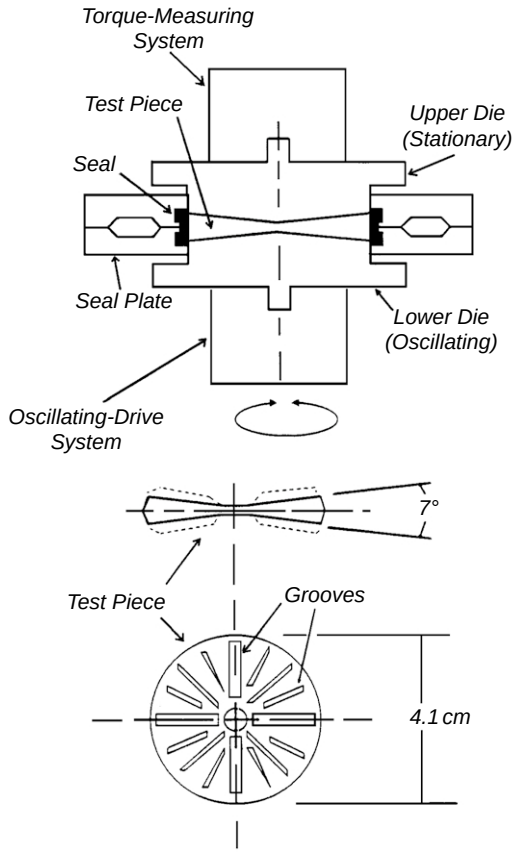

FIGURE 6 Moving-die rheometer.

ization is proportional to the number of crosslinks formed per unit volume of rubber. The torque is automatically plotted against time to give a so-called rheometer chart, rheograph, or cure curve.

Newer versions of the cure meter have been introduced (e.g., Fig. 6). The cavity is much smaller and there is no rotor. In this type of cure meter, one-half of the die (e.g., the upper half) is stationary and the other half oscillates. These instruments are called moving-die rheometers. The sample is much smaller and heat transfer is faster. Also, because there is no rotor, the temperature of the cavity and sample can be changed more rapidly. In either case (oscillating disc or moving die), torque is automatically plotted against time. Such a chart is shown in Fig. 7.

The cure curve gives a rather complete picture of the overall kinetics of crosslink formation and even crosslink disappearance (reversion) for a given rubber mix. In some cases, instead of reversion, a long plateau or marching

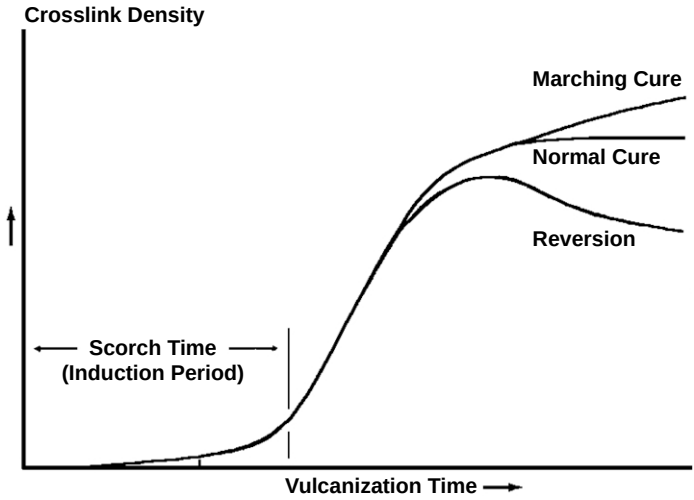

FIGURE 7 Rheometer cure curve.

cure can occur. The cure meter is, therefore, extensively used to control the quality and uniformity of rubber stocks (also called rubber compounds).

Vulcometry started as a research tool to study vulcanization. It was then used to control uniformity of rubber mixed in the factory. Also programmed temperature-profile vulcometry has been used to develop recipes for industrial use. The cure temperature–time profile of an industrial mold can be imposed on the curing cavity of the cure meter. The test sample can then be vulcanized in the cure meter under the same conditions as those encountered in the factory. Both the extent of cure and temperature can be simultaneously displayed as functions of time.

V. VULCANIZATION BY SULFUR WITHOUT ACCELERATOR

Initially, vulcanization was accomplished by using elemental sulfur at a concentration of 8 parts per 100 parts of rubber (phr). It required 5 hours at 140°C. The addition of zinc oxide reduced the time to 3 hours. The use of accelerators in concentrations as low as 0.5 phr has since reduced the time to as short as 1 to 3 minutes. As a result, elastomer vulcanization by sulfur without accelerator is no longer of much commercial significance. (An exception to this is the use of about 30 or more phr of sulfur, with little or no accelerator, to produce molded products of hard rubber or "ebonite.") Even though unaccelerated sulfur vulcanization is not of commercial significance, its chemistry has been the object of much research and study.

The chemistry of unaccelerated vulcanization is controversial. Many slow reactions occur over the long period of vulcanization. Some investigators have felt that the mechanisms involved free radicals [7–9]:

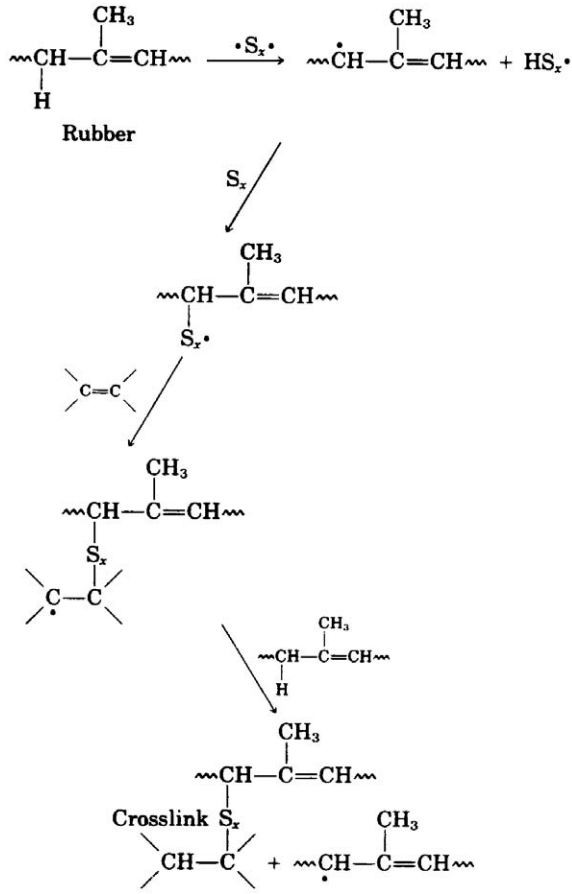

SCHEME 1

Other investigators have promoted ionic mechanisms [10]:

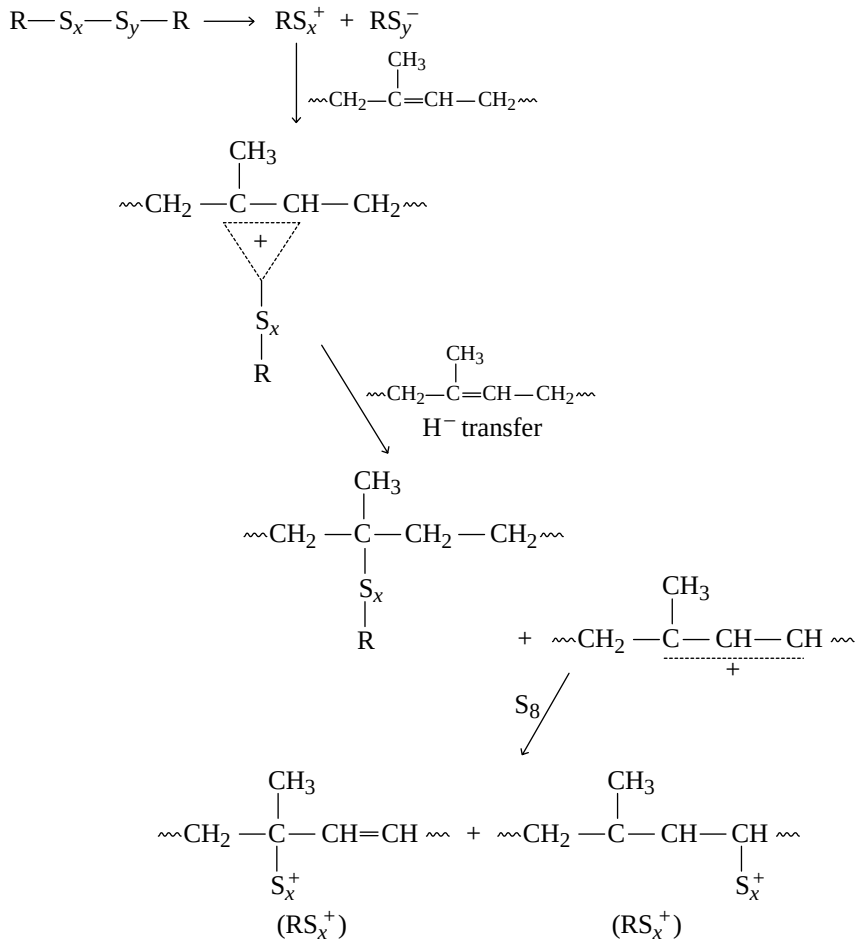

SCHEME 2

The intermediates,

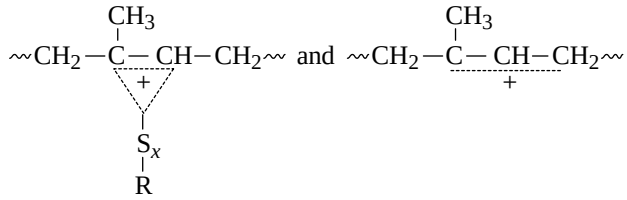

were proposed in Scheme 2 to explain the fact that model compound reactions gave both unsaturated and saturated products, sulfur atoms being connected to both secondary and tertiary carbon atoms.

VI. ACCELERATED-SULFUR VULCANIZATION

Organic chemical accelerators were not used until 1906 (65 years after the Goodyear–Hancock development of unaccelerated vulcanization [Fig. 8]), when the effect of aniline on sulfur vulcanization was discovered by Oenslager [11]. This could have been, at least partially, in response to the development of pneumatic tires and automobiles near the turn of the century. Aniline, however, is too toxic for use in rubber products. Its less toxic reaction product with carbon disulfide, thiocarbanilide, was introduced as an accelerator in 1907. Further developments lead to guanidine accelerators [12]. Reaction products formed between carbon disulfide and aliphatic amines (dithiocarbamates) were first used as accelerators in 1919 [13]. These were and are still the most active accelerators with respect to both crosslinking rate and extent of crosslink formation. However, most of the dithiocarbamate accelerators give little or no scorch resistance and their use is impossible in many factory-processing situations. The first delayed-action accelerators were introduced in 1925 with the development of 2-mercaptobenzothiazole (MBT) and 2-

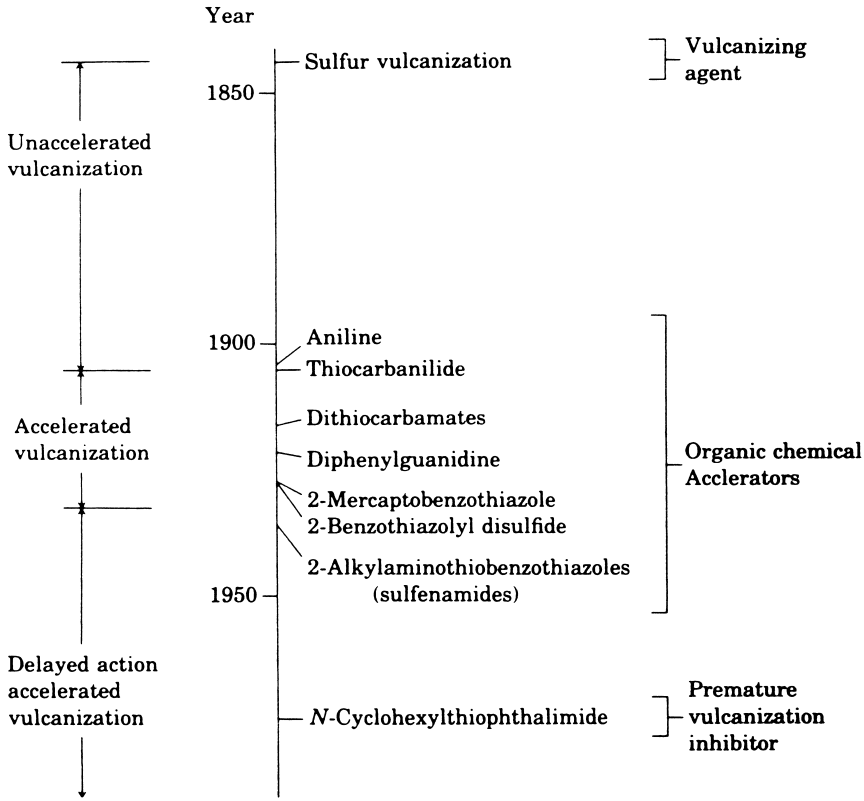

FIGURE 8 The history of vulcanization by sulfur.

benzothiazole di-sulfide (or 2,2′-dithiobisbenzothiazole) (MBTS) [14–16]. This nearly coincided with the deployment of cord-ply construction (1920–1930), which enabled mass production of automobile tires. Even more delayed action and yet faster curing vulcanization were possible in 1937 with the introduction of the first commercial benzothiazolesulfenamide accelerator [17, 18]. Still more delay became possible in 1968 with the availability of an extremely effective premature vulcanization inhibitor (PVI). This compound was N-(cyclohexylthio)phthalimide (CTP), small concentrations of which were used along with benzothiazolesulfenamide accelerators. The history of the progress toward faster vulcanization but with better control of premature vulcanization or scorch is illustrated by Figs. 8, 9, and 10.

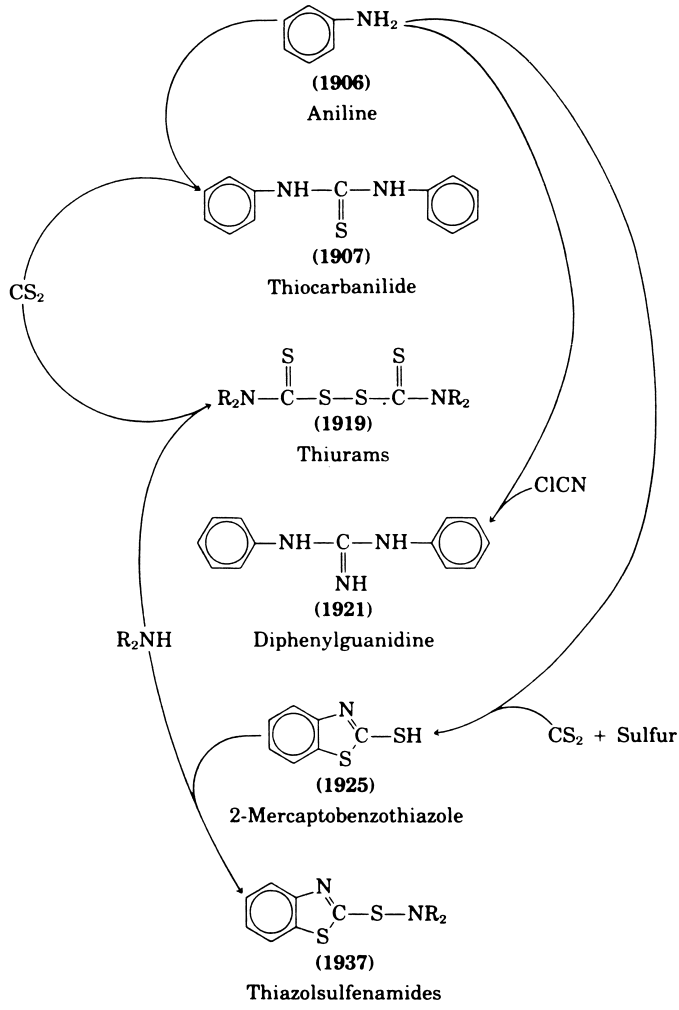

FIGURE 9 The chemistry of accelerator synthesis.

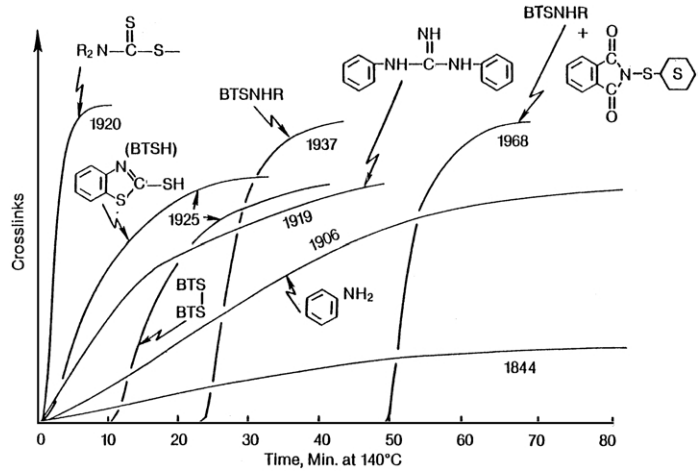

FIGURE 10 Improvements in the accelerated-sulfur vulcanization of natural rubber.

Accelerated-sulfur vulcanization is the most widely used method. For many applications, it is the only rapid crosslinking technique that can, in a practical manner, give the delayed action required for processing, shaping, and forming before the formation of the intractable vulcanized network. It is used to vulcanize natural rubber (NR), synthetic isoprene rubber (IR), styrene-butadiene rubber (SBR), nitrile rubber (NBR), butyl rubber (IIR), chlorobutyl rubber (CIIR), bromobutyl rubber (BIIR), and ethylene-propylene-diene-monomer rubber (EPDM). The reactive moiety for all of these elastomers can be represented by

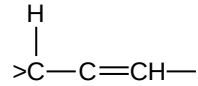

Typically a recipe for the vulcanization system for one of the above elastomers contains 2–10 phr of zinc oxide, 1–4 phr of fatty acid (e. g., stearic), 0.5–4 phr of sulfur, and 0.5–2 phr of accelerator. Zinc oxide and the fatty acid are vulcanization-system activators. The fatty acid with zinc oxide forms a salt that can form complexes with accelerators and reaction products formed between accelerators and sulfur. (Accelerators are classified and illustrated in Table I.)

Frequently, mixtures of accelerators are used. Typically, a benzothiazole type is used with smaller amounts of a dithiocarbamate (thiuram) or an amine type. An effect of using a mixture of two different types of accelerator can be that each activates the other and better-than-expected crosslinking rates can be obtained. Mixing accelerators of the same type gives intermediate or average results.

We should note here that there is urgency to reduce the use of accelerators based on secondary amines, which can react with nitrogen oxides to form

TABLE I Accelerators for Sulfur Vulcanization

Compound	Abbreviation	Structure
Benzothiazoles		
2-Mercaptobenzothiazole	MBT	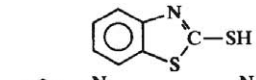
2,2′-Dithiobisbenzothiazole	MBTS	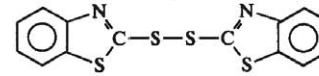
Benzothiazolesulfenamides		
N-Cyclohexylbenzothiazole-2-sulfenamide	CBS	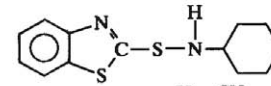
N-t-butyobenzothiazole-2-sulfenamide	TBBS	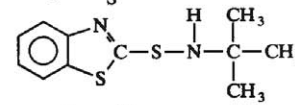
2-Morpholinothiobenzothiazole	MBS	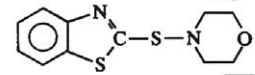
N-Dicyclohexylbenzothiazole-2-sulfenamide	DCBS	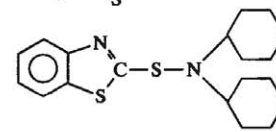
Dithiocarbamates		
Tetramethylthiuram monosulfide	TMTM	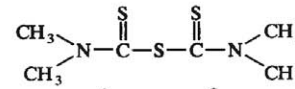
Tetramethylthiuram disulfide	TMTD	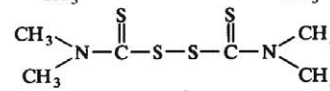
Zinc diethyldithiocarbamate	ZDEC	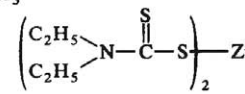
Amines		
Diphenylguanidine	DPG	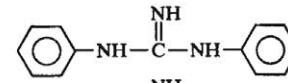
Di-o-tolylguanidine	DOTG	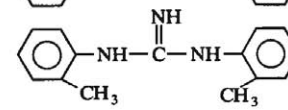

suspected carcinogenic nitrosamines. This is especially a problem with dithiocarbamate-type accelerators. Proposed accelerators, which do not give carcinogenic nitrosamine derivatives, include dibenzylamine-derived dithiocarbamates and those based on sterically hindered amines.

Different types of accelerators impart vulcanization characteristics which differ with respect to both scorch resistance and crosslinking rate. Figure 11 is

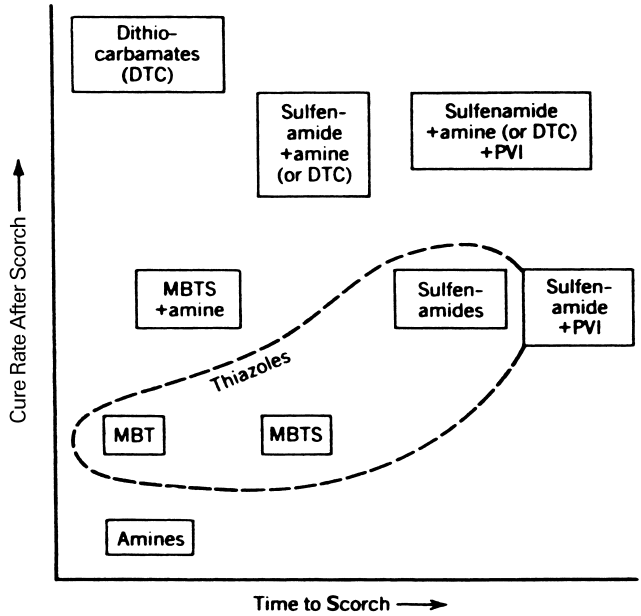

FIGURE 11 Vulcanization characteristics given by various accelerators and combinations.

a map of accelerator system characteristics. Within groups or types, differences can be obtained by choosing the individual accelerators. In the group of benzothiazolesulfenamides, the scorch resistance and vulcanization time increase in the order: TBBS or CBS, MBS, DCBS.

The effect of the addition of small concentrations of the premature vulcanization inhibitor (PVI), N-(cyclohexylthio)phthalimide, is also given by Fig. 11. This retarder [19] is frequently used to independently control scorch resistance with little effect on the rate of crosslinking [4]. Before the development of N-(cyclohexylthio)phthalimide as a PVI, acidic retarders, e.g., salicylic acid, acetylsalicylic acid, phthalic anhydride, and benzoic acid, were used. These additives improved scorch resistance but also gave greatly reduced rates of crosslink formation after the delay. Another retarder of the past was N-nitrosodiphenylamine, which is less active and not now used because of toxicological concerns.

A. The Chemistry of Accelerated-Sulfur Vulcanization

The general reaction path of accelerated-sulfur vulcanization is thought to be as follows [4, 20–24]: Accelerator reacts with sulfur to give monomeric polysulfides of the structure Ac–S_x–Ac where Ac is an organic radical derived from the accelerator (e.g., benzothiazyl-). The monomeric polysulfides

interact with rubber to form polymeric polysulfides, e.g., rubber–S_x–Ac. During this reaction, 2-mercaptobenzothiazole (MBT) is formed if the accelerator is a benzothiazole derivative and if the elastomer is natural rubber. (In SBR the MBT becomes bound to the elastomer molecular chain probably as the thioether rubber–S–Ac.) When MBT itself is the accelerator in natural rubber, it first disappears then reforms with the formation of BT–S–S_x–S–BT and rubber–S_x–Ac. Finally, the rubber polysulfides react, either directly or through an intermediate, to give crosslinks, rubber–S_x–rubber. A reaction scheme can be written as follows:

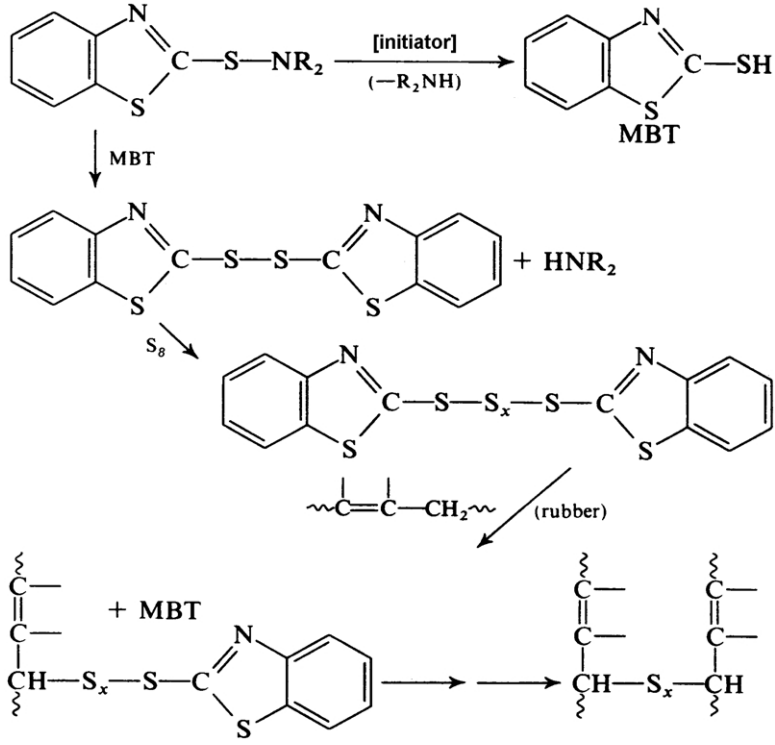

There are obvious differences between accelerated vulcanization and unaccelerated vulcanization. (Greater crosslinking efficiencies and greater crosslinking rates are obtained with accelerated vulcanization.) But there are more subtle differences. Results from model reactions with curing ingredients indicate that sulfur becomes attached to the rubber hydrocarbon almost exclusively at allylic positions [25]. This is not the case with unaccelerated-sulfur vulcanization, thus:

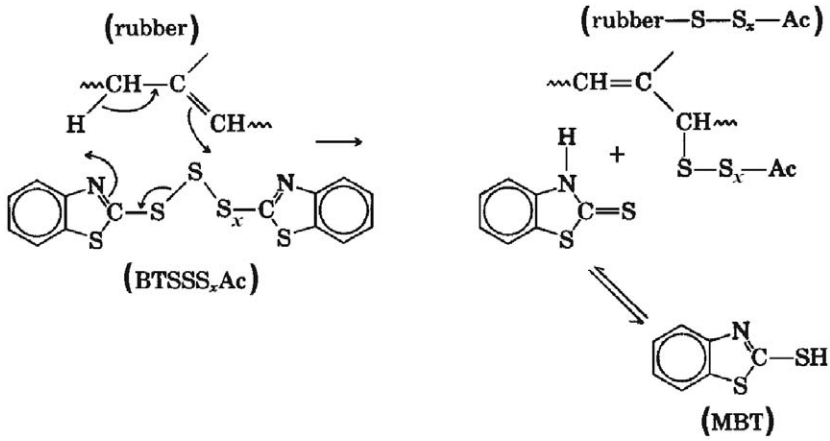

Rather than the eight-member-ring intermediate shown above, one could propose a six-member-ring sulfurization intermediate:

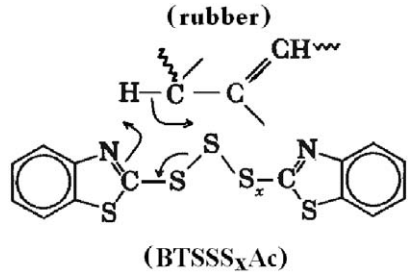

This is similar to what was suggested by Nieuwenhuizen *et al*. with respect to their work on dithiocarbamate acceleration [26]:

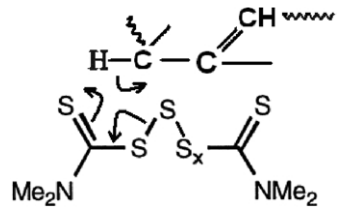

Others have proposed that zinc must be present for sulfuration [27]. At any rate, crosslinks could then form, in a number of ways, e.g.:

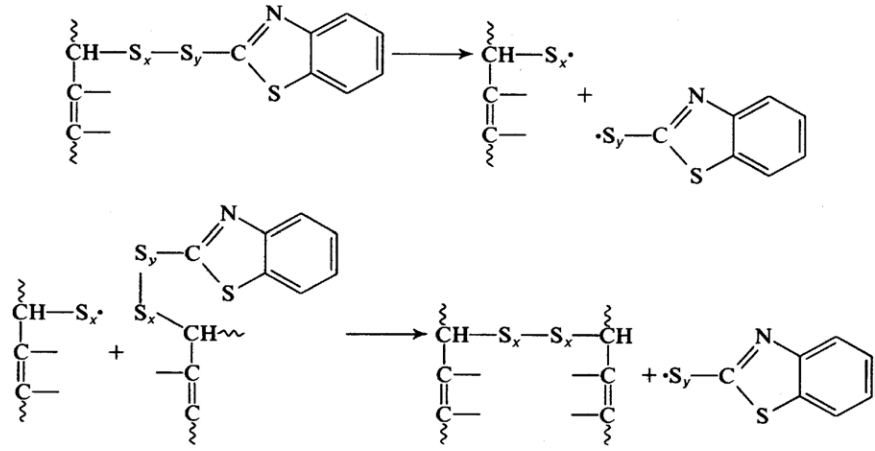

By using solid-state C-13 NMR spectroscopy, Koenig and his group [28] have added much detail to the chemical structure of the sulfurated network backbone. The following diagrams show the types of structures that have been assigned to the attachment points of the sulfur atoms to the rubber molecular backbone:

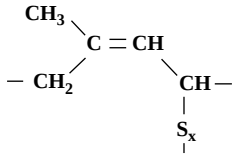

A1c

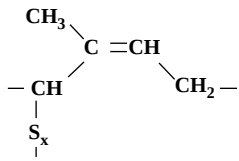

B1c

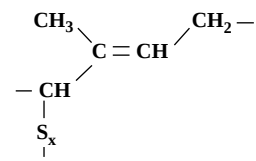

B1t

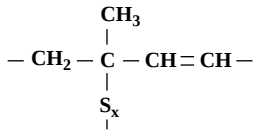

Unsaturated A2

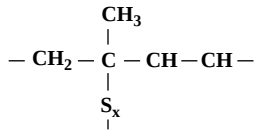

Saturated A2

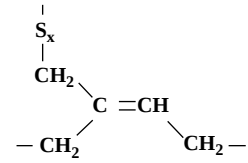

C1c

Koenig's group has done much work on conditions that change the relative amounts of the various types of attachments. For example, both the B1c and B1t type polysulfides increase with the level of carbon black loading (for types N110, N220, N326, N330, N550, and N765) [29].

B. Delayed-Action Accelerated Vulcanization

If crosslink formation is by a free radical mechanism, delayed action could be the result of a quenching action by the monomeric polysulfides formed by reactions between accelerator and sulfur. If the polymeric polythiyl radicals (crosslink precursors) are rapidly quenched by an exchange reaction before they are able to form crosslinks, crosslink formation would be impeded until substantial depletion of the monomeric polysulfides [4]. This is illustrated as follows:

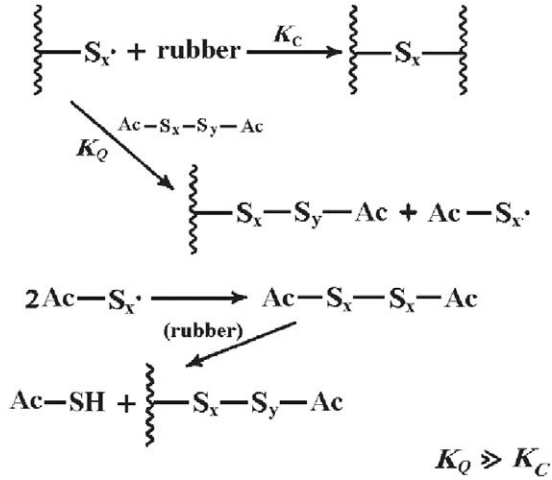

Thus, one theory for delayed action is the quenching of free radical crosslink precursors by monomeric polysulfides. It has been found that if bisalkylpolysulfides are mixed with uncured rubber stocks, more delay results. It is also been shown that the early reaction products formed by the interaction between accelerator and sulfur (Ac–S_x–Ac) are inhibitors of crosslink formation. The very substances which give rise to the formation of the crosslink precursor (rubber–S_x–Ac) inhibit the formation of the crosslinks [25]. We note that other mechanisms for delayed action have been proposed. In the case of acceleration by benzothiazolesulfenamides, the accelerator is depleted in an autocatalytic fashion with the formation of 2-mercaptobenzothiazole (MBT). The rate of this depletion is about proportional to the amount of MBT present. There is strong evidence which indicates that the following reactions occur in sulfenamide-accelerated systems:

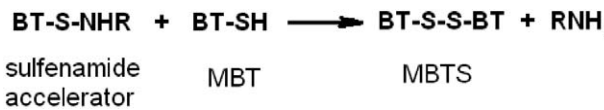

If MBT could be taken out of the system as fast as it forms, substantial increases in processing safety would result. Such is the case when the

premature vulcanization inhibitor, N-(cyclohexylthio)phthalimide (CTP) is present. This compound [19] and others like it react rapidly with MBT to form 2-(alkyldithio)benzothiazoles, R–S–S–BT, which are active accelerators but which do not interact rapidly with the sulfenamide accelerator:

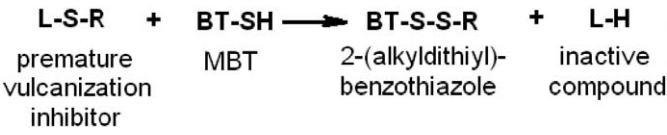

where L is a "leaving group" of the premature vulcanization inhibitor (e.g., N-phthalimido- for CTP).

The importance of scorch control cannot be overemphasized. Present-day tire plants could not compete without good control of scorch resistance or processing safety as it is commonly called. Such safety is necessary in order to rapidly process rubber mixes at high temperatures (through extrusion, calendering, etc.) into preforms for molding (e.g., tire components).

Delayed action mechanisms and reaction kinetics have been discussed and reviewed [24–36].

C. The Role of Zinc in Benzothiazole-Accelerated Vulcanization

An increase in the concentration of fatty acid and hence increases in the concentration of available Zn^{++} causes an increased overall rate in the early reactions (during the delay period), which lead to the formation of rubber–S_x–Ac. However, it gives rise to a decrease in the rate of crosslink formation but an increase in the extent of crosslinking [37]. The increase in the rates of the early reactions has been explained by the interaction:

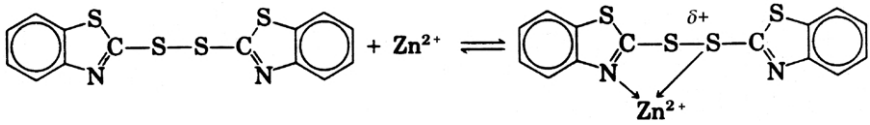

where the chelated form of the accelerator is more reactive than the free accelerator during the early reactions:

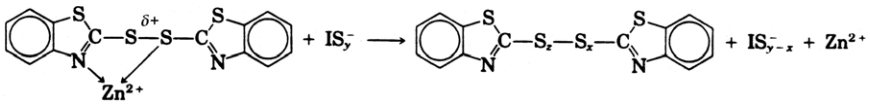

Here, I–S_y– is an ionized form of linear sulfur. It could be rapidly formed in a reaction between sulfur and any of a number of initiating species. Others have proposed that the presence of Zn^{++} can increase the rate of sulfurization through the formation of complexes of the type:

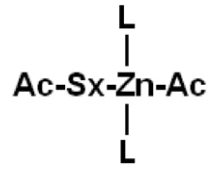

where L is a ligand such as an amine molecule [27, 36].

The decreased specific rate of crosslink formation, and the increased extent of crosslinking due to the presence of Zn^{++} in benzothiazole-accelerated vulcanization, have been explained by the following scheme [37]:

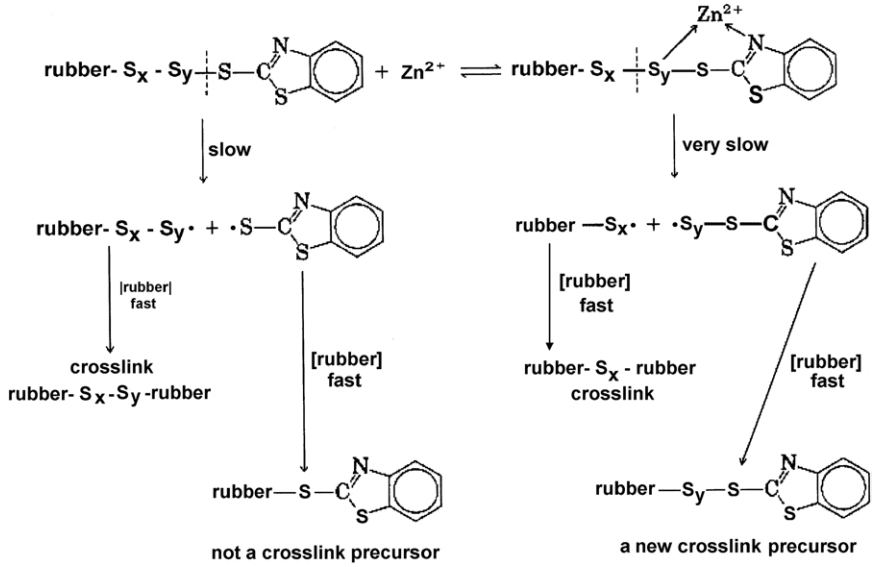

Zinc chelation changes the position of the S–S bond most likely to break. Since a stronger bond must break, the rate is slower. Though the rate of crosslinking is slower, the extent of crosslink formation is increased since less sulfur is used in each crosslink. That is, the crosslinks are of lower sulfidic rank.

The presence of zinc compounds can also promote the reduction the sulfur rank of crosslinks during high-temperature ageing of the vulcanizate, e.g., during reversion [38]. In some cases zinc compounds actually promote the decomposition of crosslinks [23].

D. Achieving Specified Vulcanization Characteristics

For many years, it was difficult to independently control the two main vulcanization characteristics, scorch resistance (processing safety) and rate of crosslink formation. In the case of natural rubber (NR), if one had chosen a

fast accelerator system in order to obtain short curing times in the press, then process safety would have suffered greatly. If one had chosen a delayed action acceleration system, then the rate of vulcanization in the press would have been limited. The development of the highly efficient premature vulcanization inhibitor N-(cyclohexylthio)phthalimide (CTP) changed all of that, since great improvements in scorch resistance with little or no change in crosslinking rate became possible [39]. Thus the rate of crosslink formation can be adjusted by the selection of accelerators. For example, the moderately fast delayed-action accelerator t-butylbenzothiazolesulfenamide (TBBS) can be partially replaced by a small amount of a coaccelerater (e.g., 0.1 to 0.2 phr of tetramethylthiuram disulfide [TMTD] or tetrametnylthiumarm monosulfide [TMTM]) to obtain a greatly increased cure rate; however, the scorch resistance will be significantly reduced. In such a case, the scorch resistance can be regained by the addition of 0.05 to 0.25 phr of CTP, without a noticeable decrease in the rate of crosslinking [4, 40].

It is true that merely increasing the concentration of TBBS will give an increase in cure rate with only a small change in scorch resistance. However, the increase in accelerator concentration will generally be rather large and the concentration of sulfur will be adjusted downward to keep the hardness and stiffness constant (maintaining constant crosslink density). The relatively large change in the concentrations of sulfur and accelerator will cause changes in vulcanizate-performance properties. (See the following section on vulcanizate properties.)

In rubber mixes containing only a synthetic rubber, such as styrene-butadiene rubber (SBR) or butadiene rubber (BR), the effects of cure-system changes may not be as pronounced as they are in the case of NR. However, if even a relatively small amount of NR is present, the effects of cure-system changes on the vulcanization process parameters resemble those obtained with NR alone.

One of the curing characteristics that one would like to control is reversion that can occur in compounds containing natural rubber. There is more than one approach to reducing the amount of reversion. One can use sulfur donors or increase the ratio of accelerator concentration to sulfur concentration. One could carry out the vulcanization at a reduced temperature for a longer period. However, these approaches give rise to effects that will have to be compensated. Another approach is use of additives such as certain bisimides, e.g., N,N′-*m*-phenylene-biscitraconimide and N,N′-*m*-phenylene-bismaleimide [41–43] or trialkoxysilylalkylpolysulfides such as bis-(3-triethoxisilylpropyl)-tetrasulfide [44].

E. Effects on Adhesion to Brass-Plated Steel

The adhesion between rubber and brass-plated steel (e.g., steel tire cords for belted radial tires) has been the subject of much study and speculation.

Brass plating is presently the major method of obtaining adhesion between natural rubber and the steel of tire cords. Over the years there has been much speculation about its mechanism, but there is agreement on one aspect of the adhesion of natural rubber to brass-plated steel: the actual adhesive between the natural rubber and the brass-plated cord, formed *in situ* during the vulcanization process, is an interfacial layer of sulfides and oxides of copper [45, 46].

The adhesive layer between the rubber and cord is generally considered to be formed by the interaction between the copper and the vulcanization system. As a result of this, optimization of the vulcanization system with respect to adhesion is critical. Also, a change in the composition of the brass coating on the steel wires, or a change in the thickness, can require a change in the vulcanization system in order to maintain the optimum level of adhesion.

Reviews on the subject of brass-plated steel cord–natural rubber adhesion have been written by van Ooij who has done much of the work in the field. Van Ooij [46] has given a model for rubber–brass adhesion, in which a copper sulfide layer forms on the brass before the onset of crosslink formation. The thin film of copper sulfide has good adhesion and cohesion. In addition, the film is so porous that rubber molecules can become entangled with it. It is not required that the film forms simultaneously with the formation of crosslinks during vulcanization; but, rather, it is required that the copper sulfide film be completely formed before crosslinking starts. Indeed, adhesion between brass-plated steel and natural rubber can frequently be improved by the use of the retarder, CTP [4] or by using a more delayed action accelerator such as N-dicyclohexylbenzothiazole-2-sulfenamide (DCBS) [47].

Failure rarely occurs between the rubber and the copper sulfide film. It generally occurs cohesively within the sulfide film or adhesively in a layer below the sulfide film.

Sulfidation of the brass surface is not due to its interaction with elemental sulfur, but it is the result of the interaction between the brass surface and accelerator-sulfur reaction products which can be represented by the general structure, Ac–S_y–Ac and Ac–S_y–H, where Ac is an accelerator-derived moiety (e.g., benzothiazolyl group). The value of the subscript, *y*, increases with the ratio of the concentration of sulfur to the concentration of accelerator used in the curing system. Generally, high sulfur levels and high ratios of sulfur concentration to accelerator concentration favor good rubber-to-brass adhesion.

The choice of accelerator also has an effect on the quality of adhesion between cord and rubber. The accelerator should not form a stable copper complex which dissolves in the rubber. This would be quite corrosive to the brass plating. In this respect, benzothiazoles and their sulfenamides are much better than dithiocarbamates. DCBS is a particularly good sulfenamide accelerator for rubber-to-brass adhesion.

F. The Effect on Vulcanizate Properties

Increases in sulfur and accelerator concentrations give higher crosslink densities and, therefore, higher moduli, stiffness, hardness, etc. However, as the ratio of the concentration of accelerator to the concentration of sulfur increases, the proportion of monosulfidic crosslinks increases in natural rubber stocks (also called rubber compounds). Greater amounts of accelerator (with respect to sulfur) also give an abundance of pendent groups of the type, $–S_x–Ac$, which are attached to and "dangle" from the rubber molecular chains. Higher ratios of sulfur concentration to accelerator concentration give both more polysulfide crosslinks and more sulfur combined with the rubber chains to form sulfur-containing six-membered heterocyclic rings along the rubber molecular chains. In addition, conjugated olefinic double bonds appear along the polymer backbone chain. These features are indicated by Fig. 12. Such changes in the vulcanizate network structure, no doubt, are responsible for changes which occur in vulcanizate properties as a result of changes made in the curing-system recipe [48–53].

Effects of changes in the concentrations of accelerator and sulfur on vulcanizate properties have been studied by using the following recipe (parts by weight): natural rubber, 100; N330 carbon black, 50; N-isopropyl-N′-phenyl-p-phenylenediamine (IPPD antidegradant) 2; zinc oxide, 5; stearic acid, 3;

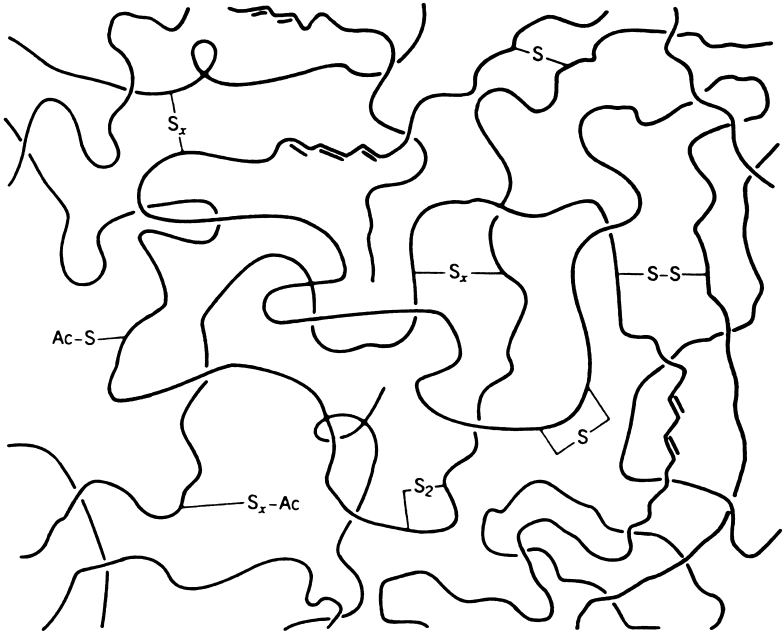

FIGURE 12 Crosslink types and chain modifications.

plasticizer, 3; sulfur, variable; N-cylohexylbenzothiazolesulfenamide (CBS), variable [4].

The effects of changes in the accelerator concentration on 300% modulus (jargon for stress at 300% tensile strain), thermal-oxidative aging, and fatigue life (DeMattia flex crack) are given in Fig. 13. The effects on 300% modulus are indicated by the diagonal contours of negative slope. They are parallel and show that the stress at 300% strain increases with an increase in either sulfur or accelerator concentration. The contours for % retention of ultimate elongation after hot air aging (at 100°C for 2 days) indicate that oxidative aging, in the presence of IPPD, depends only on the concentration of sulfur. Higher concentrations of sulfur give poor aging characteristics in correlation with the higher number of points of chain sulfuration. This suggests that sulfur substitution along the chain can activate chain scission by reactions with oxygen [54].

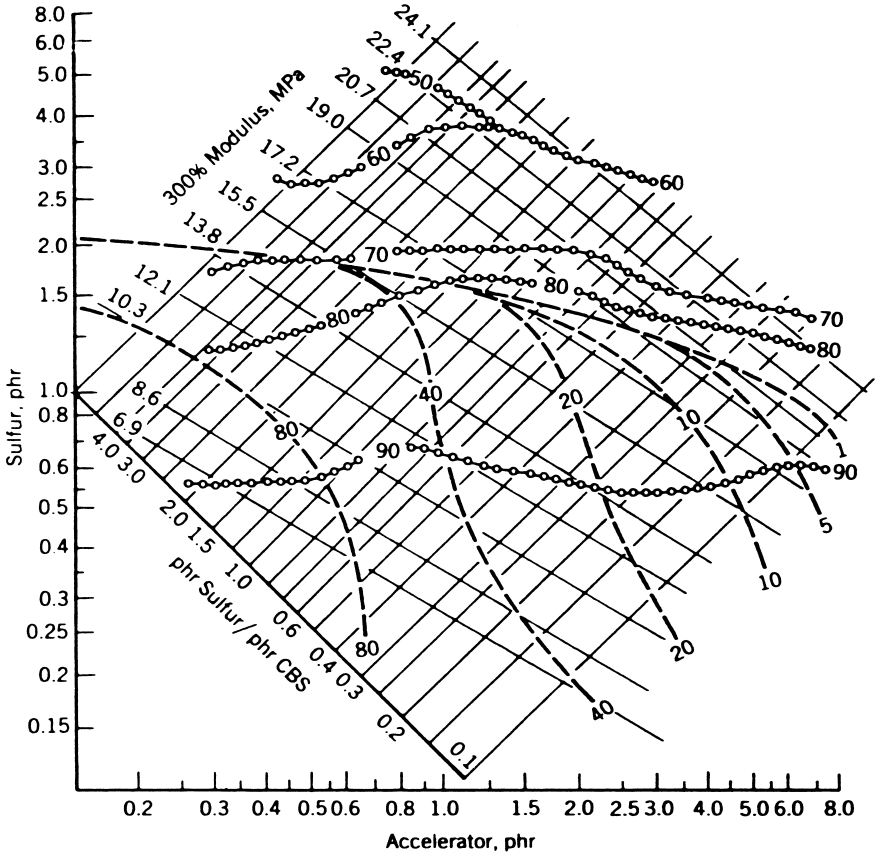

FIGURE 13 Vulcanizate properties: —, 300% modulus (Mpa); – –, De Mattia flex fatigue life (khz $\times 10^{-1}$); -O-O-O-O-, % retention of ultimate elongation after 2 days at 100°C.

TABLE II Fatigue Life at Constant 300% Modulus

phr Sulfur/phr sulfenamide	Flex life (kc)
6	400
5	500
4	530
3	550
2	550
1	400
0.6	350
0.4	270
0.3	250
0.2	190

Another view is that sulfur interferes with the antidegradant activity (in this case with IPPD) [55].

The contours for flex fatigue life are complex. The test is run such that the specimens are about equally strained; however, there is some question as to whether the tests should be run at equal strain or at equal strain energy [56, 57]. For some cases, where strain is restricted by fabric reinforcement, fatigue test data should be compared at equal strain amplitude. For other applications, where the strain is not limited, the tests should be run at equal strain energy. The contours as presented here can be interpreted in terms of either constant strain or constant strain energy: All points on the chart can be compared at an approximately equal strain per cycle; however, if we interpolate between the flex-life contours but only along a constant modulus contour, we can extract values corresponding to approximately equal strain energy per cycle. By choosing higher modulus contours, we are considering higher strain energies.

Considering the group of flex-life contours as a whole, or at approximately constant strain energy per cycle, we may conclude the following: a high level of either sulfur or accelerator gives poor flex life. However, by the selection of the proper ratio of sulfur concentration to accelerator concentration, higher modulus vulcanizates can be obtained with at least some optimization of fatigue life. The flex life at approximately equal strain energy per cycle can be illustrated by extracting values along the 13.8 Mpa modulus contour line. Table II can then be constructed.

For the strain energy corresponding to a 300% modulus of 13.8 Mpa, the maximum flex life (as measured by the DeMattia flex test) is obtained when 2.5 times as much sulfur as accelerator is used. Other optimum ratios for various 300% moduli can be obtained from the contours. Some of these are given in Table III.

These optimum ratios and fatigue life data should not be considered to be universal values. Different recipes, different types of antidegradants, different

TABLE III Optimized Fatigue Life

Stress at 300% strain, 300% Modulus (MPa)	Optimum sulfur conc./accelerator conc. ratio	Optimized flex life (kc)
6.9	3.50	800
10.4	3.00	800
13.8	2.50	550
15.5	1.00	300
17.2	0.45	120
19.0	0.27	70

types of fillers, different concentrations of antidegradants and fillers, different base polymers, different types of fatigue tests, etc., give rise to different optimum sulfur concentration–accelerator concentration ratios and different optimum fatigue life values. Nevertheless, the trends given here have been generally noted.

The low values for fatigue life at low levels of sulfur, but high levels of accelerator, have been attributed to high concentrations of accelerator-terminated appended groups [58] and high concentrations of monosulfidic crosslinks. Monosulfidic crosslinks are not able to exchange, rearrange, or break to relieve stresses without the breakage of main chains.

On the other hand, polysulfidic crosslinks are able to rearrange under stress [2, 4, 59]. The rearrangement of a crosslink occurs in two steps: (1) breaking, (2) reforming. Recent data [60] indicate that only the breaking of the weak polysulfide crosslinks is required for the strengthening of the vulcanizate network. It is only required that enough of the crosslinks be weak (in comparison to backbone bonds) for the rubber to be strong. At any rate, when moderately high concentrations of sulfur (with respect to accelerator) are used, flex life improves, presumably due to the presence of enough weak or rearrangeable polysulfidic crosslinks.

When even higher concentrations of sulfur are used (with the maintenance of constant modulus), flex life decreases. It is possible that this is due to the large amount of cyclic chain modification associated with high levels of sulfur.

Natural rubber compositions, vulcanized by high levels of accelerator and low levels of sulfur, have been called EV and semi-EV vulcanizates. Here, "EV" means efficient vulcanization, since sulfur is used efficiently in the production of crosslinks. On the average, the crosslinks are shorter than in the case of conventional vulcanization; they contain more monosulfidic crosslinks and less polysulfidic ones, or their average sulfur rank is lower. Though EV vulcanizates suffer with respect to fatigue resistance, they are frequently used because of their excellent reversion resistance (resistance to nonoxidative thermal aging or overcure) and good resistance to thermal-oxidative aging. The resistance to reversion or thermally induced loss of crosslinks is thought

to be the result of the greater intrinsic stability of the lower rank (disulfidic and especially monosulfidic) crosslinks. Semi-EV vulcanizates (wherein the sulfur concentration to accelerator-moiety concentration ratio is at an intermediate value) are an advantageous compromise in which fairly good unaged fatigue life is obtained, but maintained after aging.

Rather than using high levels of accelerator to obtain EV and semi-EV vulcanizates, it is sometimes advantageous to replace some of the sulfur with a so-called sulfur donor. Examples of these are tetramethylthiuram disulfide (TMTD) and 4,4′-dithiodimorpholine (DTDM).

This type of vulcanization system design was reported by McCall [57]. He found that by judiciously balancing the levels of accelerator, sulfur, and DTDM, he could obtain good vulcanization characteristics, good thermal stability, good flex life, and superior retention of flex life.

G. Accelerated-Sulfur Vulcanization of Various Unsaturated Rubbers

Over the years, much of the research on accelerated-sulfur vulcanization was done by using natural rubber as a model substrate. Natural rubber was the first elastomer and therefore the search for understanding of vulcanization originated with work on natural rubber. Even in recent years most of the work published on the study of vulcanization has been related to natural rubber. This was because of the tradition of doing research on natural rubber and because of the fact that the largest knowledge base to build upon was with respect to natural rubber. It should be mentioned that a large factor in the establishment of the tradition of research on the vulcanization of natural rubber was the British Rubber Producers Research Association or BRPRA (now called the Malaysian Rubber Producers Research Association or MRPRA). Of course, this institution is essentially devoted to natural rubber.

Most of the work cited in the previous sections is related to natural rubber. However, some studies have been directed to the vulcanization of butadiene 1,4-polymers [51, 61, 62]. Other basic work on the vulcanization of ethylene-propylene-diene-monomer rubber (EPDM) has been carried out [63, 64].

The chemistry of the accelerated vulcanization of BR, SBR, and EPDM appears to have much in common with the vulcanization of natural rubber: Before the formation of crosslinks, the rubber is first sulfurated by accelerator-derived polysulfides (Ac–S_x–Ac) to give macromolecular, polysulfidic intermediates (rubber–S_x–Ac). However, whereas in the case of MBTS- or benzothiazolesulfenamide-accelerated sulfur vulcanization of natural rubber, MBT is given off during the formation of rubber–S_x–BT from the attack of rubber by BT–S_x–BT, in the case of BR and SBR, MBT is not eliminated and remains unextractable presumably because it becomes bound as the macromolecular thioether rubber–S–BT. (BT is a 2-benzothiazolyl group.) As in the case of natural rubber, the average length of a crosslink (its sulfidic rank, the value of x in the crosslink, rubber–S_x–rubber) increases with the ratio of sulfur concentration to accelerator concentration (S/Ac) used in the

compounded rubber mix. However, in the case of BR or SBR, the crosslink sulfidic rank is not nearly as sensitive to S/Ac as it is in the case of natural rubber. Model compound studies of the vulcanization of EPDM (e. g., wherein ethylidenenorbornane was used as a model for EPDM) [50, 51] indicate that the polysulfidic rank of the EPDM crosslinks probably responds to changes in S/Ac in a natural rubberlike fashion. A difference here is that evidence for model monosulfidic crosslinks was lacking while model disulfidic crosslinks were more apparent than in the case of natural rubber vulcanization.

Reversion (when defined as the loss of crosslinks during nonoxidative thermal vulcanizate aging) is a problem associated mainly with natural rubber or synthetic isoprene polymers. It can occur only under severe conditions in butadiene rubber; in SBR, instead of the softening associated with the nonoxidative aging of natural rubber, one can observe hardening (the so-called marching modulus) during extensive overcure. In natural rubber and synthetic isoprene-polymer rubbers, the crosslinks tend to be more polysulfidic than in the case of BR or SBR. The highly polysulfidic crosslinks are more heat-labile than their lower rank cousins in BR and SBR; they are more likely to break and then form cyclic chain modifications. But the reason for the formation of the crosslinks of higher polysulfidic rank in isoprene rubbers than in butadiene polymers is grandly elusive, though it almost has to be related to the methyl groups that are substituents along the isoprene-polymer chains but that are absent from butadiene-polymer chains.

The effect of zinc is much greater in the vulcanization of isoprene rubbers than it is in the vulcanization of BR and SBR. Again, the reason for the difference is not known, but a strong speculation is that this difference is also related to the presence of methyl groups only in the case of the isoprene rubbers.

H. Selected Accelerated-Sulfur System Recipes

Examples of recipes are given in Table IV. These recipes are not intended as ultimate solutions to compounding problems. Variations will undoubtedly be necessary to meet particular requirements.

VII. VULCANIZATION BY PHENOLIC CURATIVES, BENZOQUINONE DERIVATIVES, OR BISMALEIMIDES

Diene rubbers such as natural rubber, SBR, and BR can be vulcanized by the action of phenolic compounds [65–68], which are (usually di-)substituted by -CH2-X groups where X is an -OH group or a halogen atom substituent. A high-diene rubber can also be vulcanized by the action of a dinitrosobenzene that forms *in situ* by the oxidation of a quinonedioxime [69–73] that had been incorporated into the rubber along with the oxidizing agent, lead peroxide.

TABLE IV Recipes for Accelerated Sulfur Vulcanization Systems[a]

	NR	SBR	Nitrile (NBR) 1	Nitrile (NBR) 2	Butyl (IIR)	EPDM
Zinc oxide	5.00	5.00	3.00	2.00	3.00	5.00
Stearic acid	2.00	2.00	0.50	0.50	2.00	1.00
Sulfur	2.50	1.80	0.50	0.25	2.00	1.50
DTDM[b]	—	—	—	1.00	—	—
TBBS[b]	0.60	1.20	—	—	—	—
MBTS[b]	—	—	2.00	—	0.50	—
MBT[b]	—	—	—	—	—	0.50
TMTD[b]	—	—	1.00	1.00	1.00	1.50
Vulcanization conditions[c]						
Temperature (°C)	148	153	140	140	153	160
Time (min.)	25	30	60	60	20	20

[a]Concentrations in phr.
[b]DTDM, 4,4′-dithiodimorpholine; TBBS, *N*-t-butylbenzothiazole-2-sulfenamide; MBTS, 2,2′-dithiobisbenzothiazole (2-benzothiazole disulfide); MBT, 2-mercaptobenzothiazole; TMTD, tetramethylthiuram disulfide.
[c]Conditions change depending on other aspects of the compositions.

The attack upon rubber molecules by the vulcanization system can be visualized in a way similar to that which was postulated for the sulfurization of the rubber molecules by the action of accelerated-sulfur vulcanization systems. Reaction schemes for these two types of vulcanization can be written as follows:

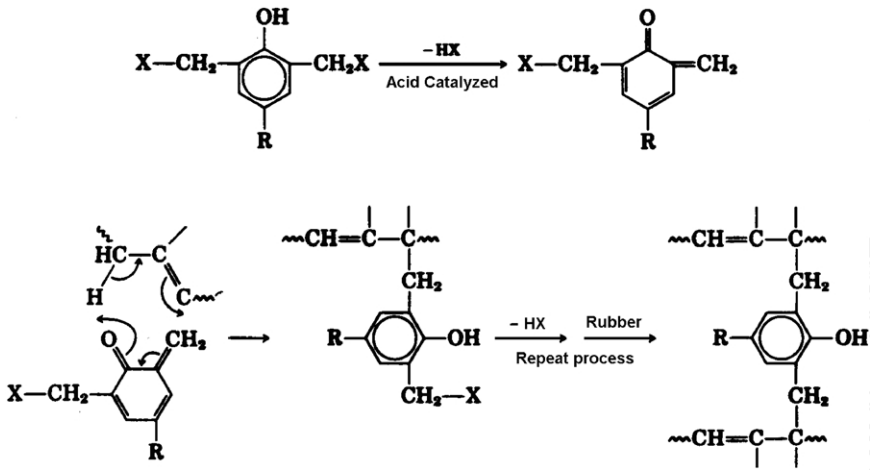

Vulcanization by phenolic curatives.

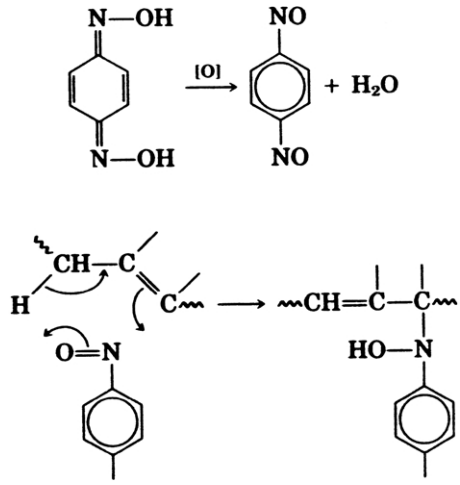

Vulcanization by benzoquinonedioxime.

As shown above, the chemical structural requirements for these types of vulcanization are that the elastomer molecules contain allylic hydrogen atoms. The attacking species from the vulcanization system must contain sites for proton acceptance and electron acceptance in proper steric relationship. This will then permit the following rearrangement, where A is the proton acceptor site and B is the electron acceptor site:

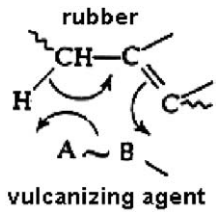

This is an explanation for the fact that this type of vulcanization is not enabled by double bonds per se, without allyic hydrogens in the elastomer molecules [4, 74]. (It should be pointed out that the phenolic curative can also act by a slightly different mechanism to give crosslinks which contain chromane structural moieties [75], the allylic hydrogens still being required.)

Another vulcanizing agent for high-diene rubbers is *m*-phenylenebismaleimide. A catalytic free radical source such as dicumyl peroxide or benzothiazyl disulfide (MBTS) is usually used to initiate the reaction. A reaction scheme for this type of vulcanization, adapted from Kovacic *et al.* [76] is as follows:

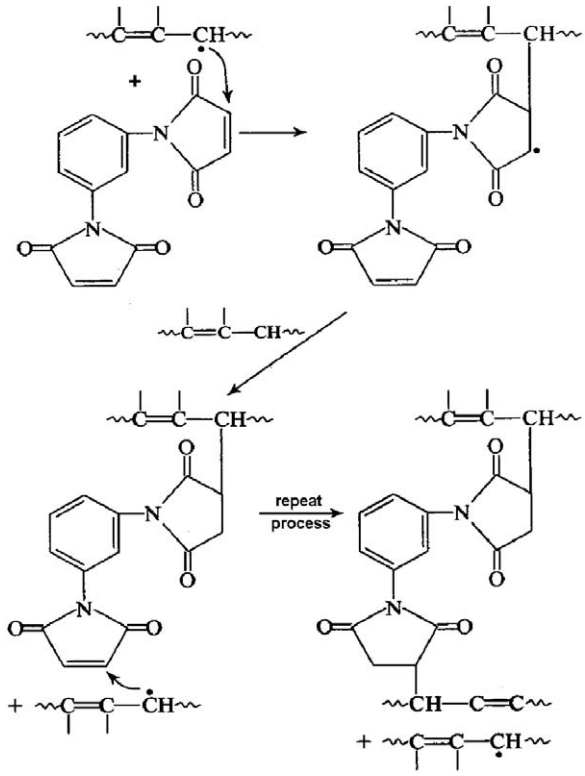

Although a free radical source is frequently used with a maleimide vulcanizing agent, at high enough vulcanization temperatures, the maleimides react with the rubber without the need for a free radical source. This could occur as shown here:

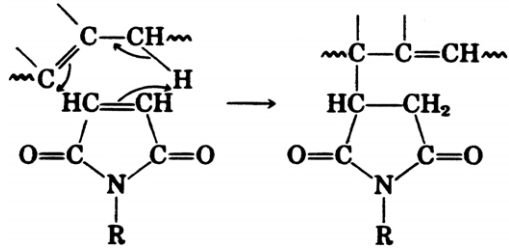

This is another example of what has variously been called a pseudo-Diels-Alder, ene, or "no-mechanism" reaction [77]. It is similar to the reaction written for the attack of rubber molecules by phenolic curatives or the *in situ* formed nitroso derivative of the quinoid (e.g., benzoquinonedioxime) vulcanization system. It is also closely related to the sulfurization scheme written for accelerated-sulfur vulcanization. Comparisons between accelerated sulfur,

phenolic, quinoid, and maleimide vulcanization can then be visualized as follows:

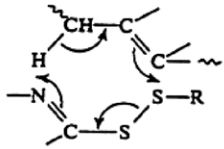

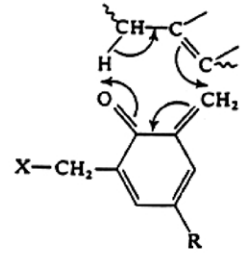

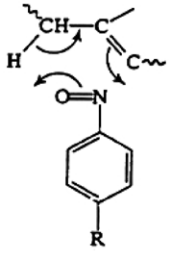

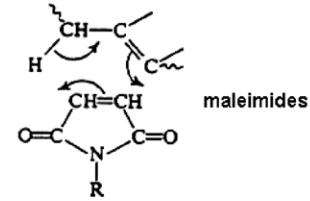

Selected recipes for vulcanization by phenolic curatives, benzoquinonedioxime, or m-Phenylenebismaleimide are given by Table V. Vulcanizates based on these types of curatives are particularly useful in cases where thermal stability is required.

TABLE V Recipes for Vulcanization by Phenolic Curatives, Quinone Derivatives, or Maleimides[a]

	IIR		SBR		
	1	2	1	2	NBR
Zinc oxide	5.00	5.00	—	—	—
Lead peroxide (Pb_3O_4)	—	10.00	—	—	—
Stearic acid	1.00	—	—	—	—
Phenolic curative (SP-1056)[b]	12.00	—	—	—	—
Benzoquinonedioxime (GMF)	—	2.00	—	—	—
m-Phenylenebismaleamide (HVA-2)[c]	—	—	0.85	0.85	3.00
2-Benzothiazyl disulfide (MBTS)	—	—	2.00		
Dicumyl peroxide	—	—	—	0.30	0.30
Vulcanization condition[d]					
Temperature (°C)	180	153	153	153	153
Time (min.)	30	20	25	25	30

[a]Concentrations in phr.
[b]Schenectady chemicals.
[c]Du Pont.
[d]Conditions change depending on other aspects of the compositions.

VIII. VULCANIZATION BY THE ACTION OF METAL OXIDES

Chlorobutadiene or chloroprene rubbers (CR), also called neoprene rubbers, are generally vulcanized by the action of metal oxides. CR can be represented by the structure:

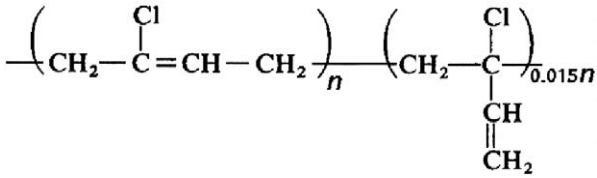

The crosslinking agent is usually zinc oxide, which is used along with magnesium oxide. CR can be vulcanized in the presence of zinc oxide alone; however, magnesium oxide is necessary to give scorch resistance. The reaction is thought to involve the allylic chlorine atom, which is the result of the small amount of 1,2-polymerization:

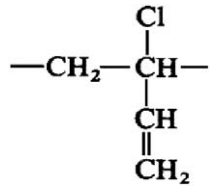

A mechanism that has been written for the vulcanization of CR by the action of zinc oxide and magnesium oxide is as follows [3]:

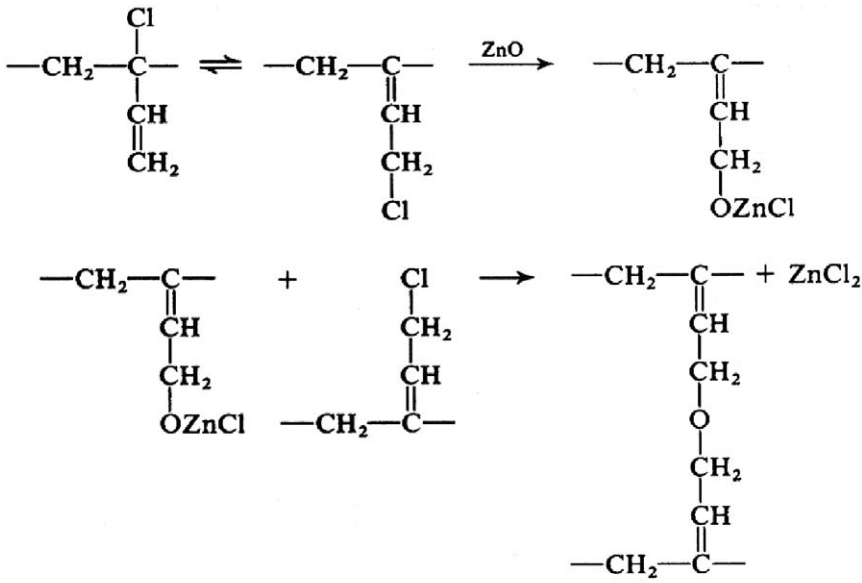

$$ZnCl_2 + MgO \longrightarrow ZnO + MgCl_2$$

Most accelerators used in the accelerated-sulfur vulcanization of other high-diene rubbers are not applicable to the metal oxide vulcanization of neoprene rubbers. An exception to this is in the use of the so-called mixed curing system for CR, in which metal oxide vulcanization is combined with accelerated-sulfur vulcanization. Along with the metal oxides, tetramethylthiuram disulfide (TMTD), N,N′-di-o-tolylguanidine (DOTG), and sulfur are used. This may be desirable for high resilience or for good dimensional stability. The accelerator which has been most widely used with metal oxide cures is ethylenethiourea (ETU) or 2-mercaptoimidazoline. Further extensive use of ETU in the vulcanization of CR is somewhat in doubt since it is a suspected carcinogen. The related compound, thiocarbanalide, an old accelerator for sulfur vulcanization, has been revived for CR vulcanization. Other substitutes for ETU have been proposed [78, 79]. A mechanism for ETU acceleration has been given by Pariser [80]:

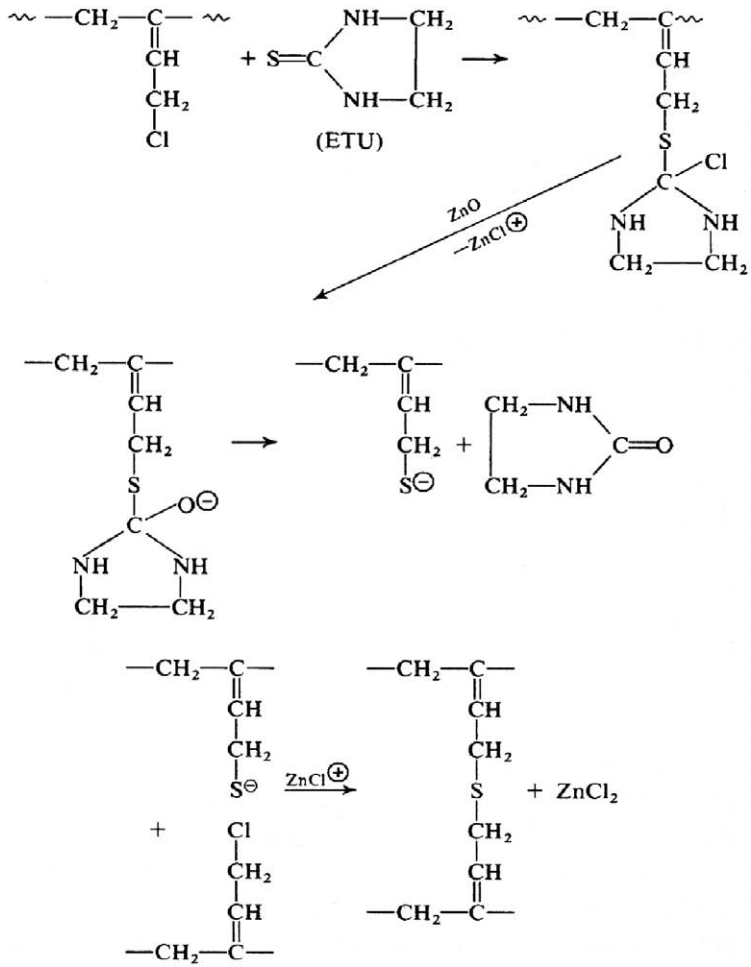

TABLE VI Vulcanization Systems for Chloroprene Rubber[a]

ZnO	5.00	5.00	5.00
MgO	4.00		4.00
Calcium stearate	—	5.50	—
Stearic acid	—	—	1.00
TMTM	—	—	1.00
DOTG	—	—	1.00
ETU	0.5	0.5	—
Sulfur	—	—	1.0
Vulcanization Condition[b]	153	153	153
Temperature (°C)			
Time (min)	15	15	15

[a]Concentrations in parts by weight per 100 parts of neoprene W.
[b]Conditions change depending on other aspects of the compositions.

Examples of recipes for metal oxide vulcanization are given in Table VI. It should be noted that in one case, calcium stearate was used instead of magnesium oxide to obtain better aging characteristics [81].

IX. VULCANIZATION BY THE ACTION OF ORGANIC PEROXIDES

Most elastomers can be vulcanized by the action of organic peroxides [82, 83]. Diacyl peroxides, dialkyl peroxides, and peresters have been used. Dialkyl peroxides and t-butyl perbenzoate give efficient crosslinking. Di-t-butyl peroxide and dicumyl peroxide give good vulcanizates, but the former is too volatile for general use. Dicumyl peroxide is widely used, however its vulcanizates have the odor of acetophenone, which is a byproduct of the vulcanization process. Other nonvolatile peroxides of the same class, which give vulcanizates free of the odor of acetophenone, are 1,1-bis(t-butylperoxy)-3,3,5-trimethylcyclohexane and 2,5-dimethyl-2,5-bis(t-butylperoxy)hexane. This latter compound is particularly good for vulcanization at higher temperatures (as high as 180°C) since it is more thermally stable than the others.

It should be noted that acidic compounding ingredients (fatty acids, certain carbon blacks, and acidic silicas) can catalyze nonradical-generating, wasteful decomposition of peroxides. Other compounding ingredients such as antidegradants can reduce crosslinking efficiency by quenching or altering the free radicals before they can react with the polymeric substrate.

Peroxides are vulcanizing agents for elastomers that contain no sites for attack by other types of vulcanizing agents. They are useful for ethylene-

propylene rubber (EPR), ethylene-vinylacetate copolymers (EAM), certain millable urethane rubbers, and silicone rubbers. They are not generally useful for vulcanizing butyl rubber (poly[isobutylene- co-isoprene]) because of a tendency toward chain scission, rather than crosslinking, when the polymer is subjected to the action of a peroxide.

Elastomers derived from isoprene and butadiene are readily crosslinked by peroxides; but many of the vulcanizate properties are inferior to those of accelerated-sulfur vulcanizates. However, peroxide vulcanizates of these diene rubbers may be desirable in applications where improved thermal ageing and compression set resistance are required.

A. Peroxide Vulcanization of Unsaturated Hydrocarbon Elastomers

The initiation step in peroxide-induced vulcanization is the decomposition of the peroxide to give free radicals, thus

$$\text{Peroxide} \longrightarrow 2\,\text{R}\bullet$$

where R is an alkoxyl, alkyl, or acyloxyl radical, depending on the type of peroxide used. (Dibenzoyl peroxide gives benzoyloxyl radicals but dicumyl peroxide gives cumyloxyl and methyl radicals [84].) If the elastomer is derived from butadiene or isoprene, the next step is either the abstraction of a hydrogen atom from an allylic position on the polymer molecule or the addition of the peroxide-derived radical to a double bond of the polymer molecule [85–87].

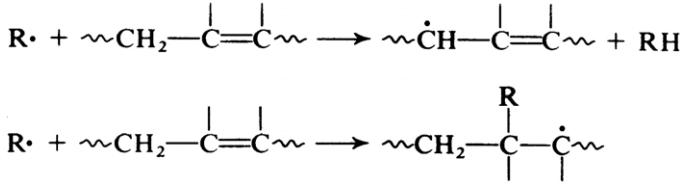

For isoprene rubber, the abstraction route predominates over radical addition. Two polymeric free radicals then unite to give a crosslink.

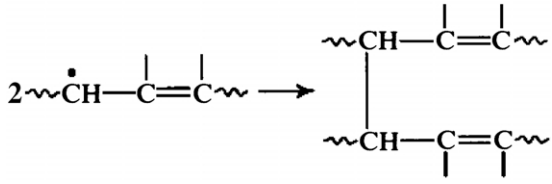

Crosslinks could also form by a chain reaction that involves the addition of polymeric free radicals to double bonds [82, 88].

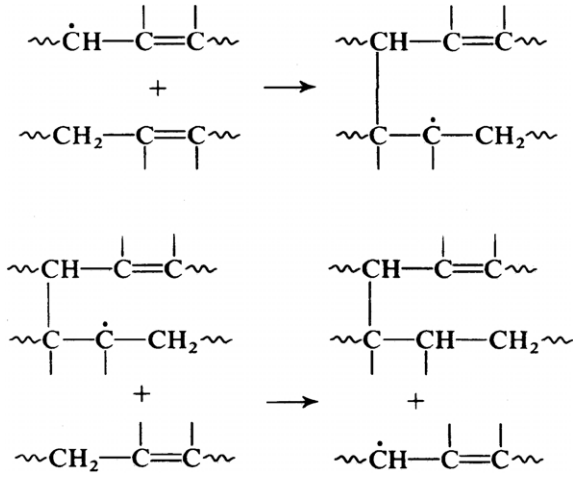

In this case crosslinking occurs without the loss of a free radical so that the process can be repeated until termination by radical coupling. Coupling can be between two polymeric radicals to form a crosslink or by an unproductive processes: a polymeric radical can unite with a radical derived from the peroxide. If a polymeric radical decomposes to give a vinyl group and a new polymeric radical, a scission of the polymer chain is the result.

Few monomeric radicals are lost by coupling with polymeric radicals when dialkyl peroxides are used as the curative. Also, if the elastomer is properly chosen, the scission reaction is not excessive [82–88]. For dicumyl peroxide in natural rubber, the crosslinking efficiency has been estimated at about 1.0. One mole of crosslinks is formed for each mole of peroxide; crosslinking is mainly by the coupling of two polymeric radicals [89, 90]. One peroxide moiety gives two monomeric free radicals, which react with rubber to give two polymeric radicals that couple to form one crosslink.

In the case of BR or SBR, the efficiency can be much greater than 1.0, especially if all antioxidant materials are removed. A chain reaction is indicated here. It might be explained by steric considerations. In butadiene-based rubbers, double bonds are quite accessible. Radical addition to double bonds could give highly reactive radicals that would be likely to add to other polymer double bonds. A chain of additions might be more likely in butadiene rubber than in the presence of hindering methyl groups in isoprene rubbers.

One might expect that nitrile rubber would also be vulcanized with efficiencies greater than 1.0; however, though the double bonds in nitrile rubber are highly accessible, the crosslinking efficiency is somewhat less than 1.0 [88].

B. Peroxide Vulcanization of Saturated Hydrocarbon Elastomers

Saturated hydrocarbon polymers are also crosslinked by the action of organic peroxides, though the efficiency is reduced by branching. Polyethylene is crosslinked by dicumyl peroxide at an efficiency of about 1.0, saturated EPR gives an efficiency of about 0.4, while butyl rubber cannot be cured at all. For polyethylene, the reaction scheme is similar to that of the unsaturated elastomers.

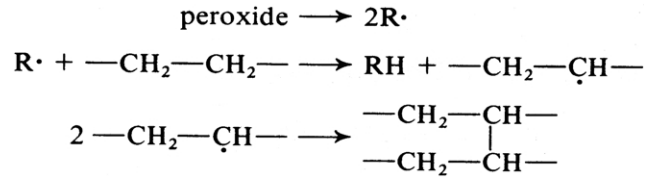

However, branched polymers undergo other reactions.

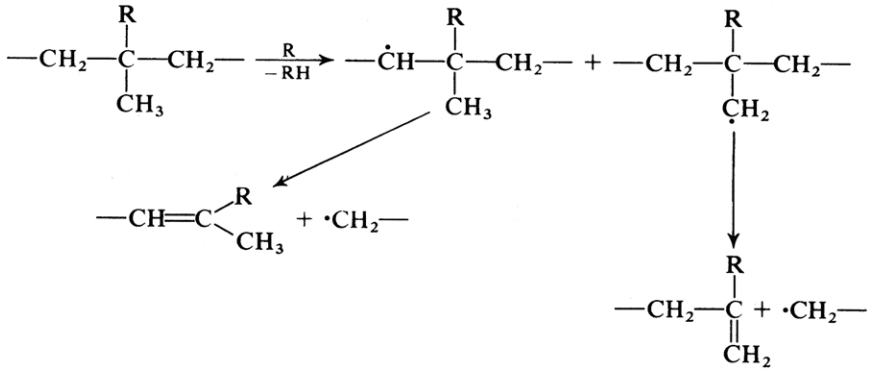

Here, though the peroxide has been depleted, no crosslinks have been formed between polymer chains, and the average molecular weight of the polymer has even been reduced by scission.

Sulfur, or the so-called coagents [88, 91], can be used to suppress scission. Examples of coagents are m-phenylenebismaleimide, high-1,2 (high-vinyl) polybutadiene, triallyl cyanurate, diallyl phthalate, ethylene diacrylate, etc. Their mechanism of action may be as follows:

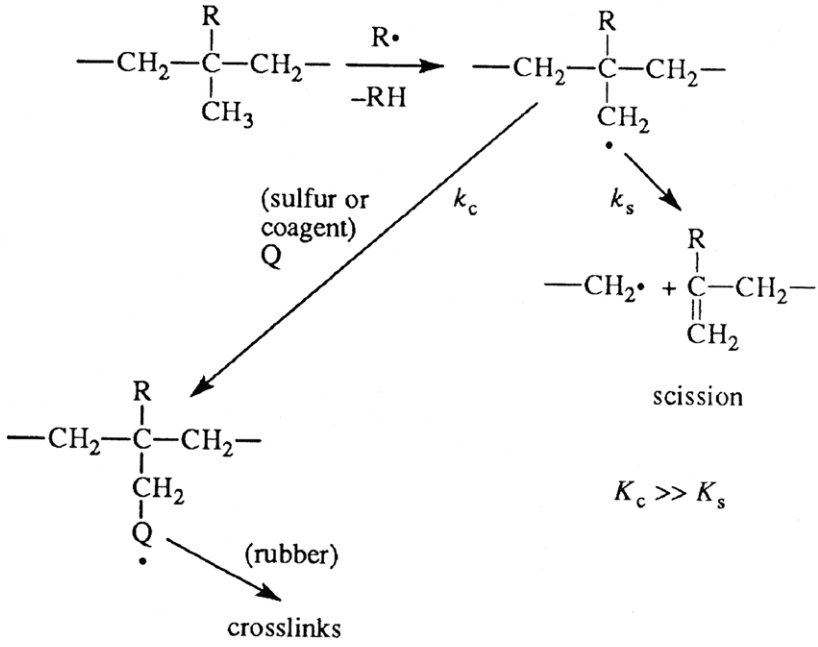

C. Peroxide Vulcanization of Silicone Rubbers

Silicone rubbers can be represented by

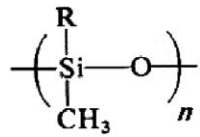

where R can be methyl, phenyl, vinyl, trifluoropropyl, or 2-cyanoethyl. Silicone rubbers that contain vinyl groups can be cured by dialkyl peroxides such as dicumyl peroxide. Saturated silicone rubbers require diacyl peroxides such as bis-(2,4-dichlorobenzoyl) peroxide. In the case of saturated siloxane rubbers, the mechanism is hydrogen atom abstraction followed by polymeric radical coupling to give crosslinks. Nonproductive use of peroxide results from the coupling of the polymeric radicals with the lower-molecular-weight free radicals formed by the decomposition of the peroxide curative. The incorporation of vinyl groups improves the crosslinking efficiency [92, 93].

Vulcanization is frequently done in two steps. After a preliminary vulcanization in a mold, a high-temperature (e.g., 180°C) postcure is carried out in air. The high-temperature postcure removes acidic materials, which can catalyze hydrolytic decomposition of the vulcanizate [94]. Also, the high temperature enables the formation of additional crosslinks of the following type [95]:

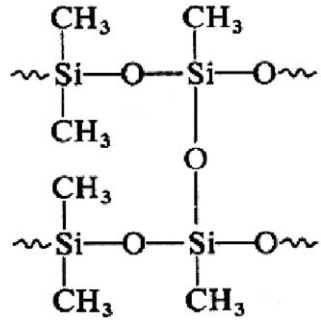

D. Peroxide Vulcanization of Urethane Elastomers

Urethane elastomers suitable for peroxide vulcanization are typically prepared from an hydroxyl-group-terminated oligomeric adipate polyester and 4,4′-methylenediphenylisocyanate (MDI). A typical structural representation is as follows:

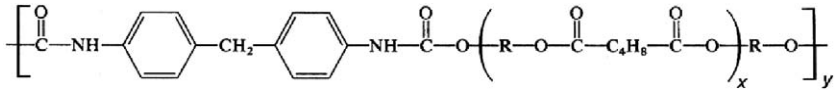

Hydrogen atoms can be abstracted from arylated methylene groups, but hydrogen atoms may also be abstracted from alpha-methylene groups of the adipate moieties. Though they are usually sufficient, vulcanization efficiencies can be increased by the incorporation of urea structures into the polymer chain [96].

E. Recipes for Peroxide Vulcanization

Examples of starting-point recipes are given in Table VII. Outstanding characteristics of peroxide vulcanizates are low permanent set and high thermal stability of the network.

X. DYNAMIC VULCANIZATION

Dynamic vulcanization (DV) is the vulcanizing or crosslinking of one polymer during its molten-state mixing with another polymer or with other polymers. The polymers are first thoroughly mixed and then, during further mixing, *one* of the polymers is obliged to become crosslinked, whereas the remaining other polymeric material remains uncrosslinked. The process produces a dispersion of crosslinked polymer in a matrix or continuous phase of uncrosslinked polymer. If the dispersed crosslinked material is elastomeric and

TABLE VII Recipes for Peroxide Vulcanization[a]

	NR	SBR	EPR	Silicone rubber	Millable urethane
Dicumyl peroxide	1.0	1.0	2.7		2
Bis(2,4-dichlorobenzoyl peroxide	—			1.0	
Triallyl cyanurate			1.5		
Vulcanization conditions[b]					
Temperature (°C)	150	150	160	115,250[c]	153
Time (min.)	45	45	30	141,440[c]	45

[a]Concentrations in phr.
[b]Conditions change depending on other aspects of the compositions.
[c]Temperature and time of postcure in air.

the continuous or matrix material is of a melt-processable plastic, then the composition can be used as an impact-resistant thermoplastic resin, or if there is a large enough proportion of rubber in the composition, it might be suitably used as a thermoplastic elastomer (TPE).

Fischer [97] used the DV process to prepare compositions containing *partially* vulcanized rubber. It has since been found that improved, very strong elastomeric compositions of EPDM and polypropylene could be prepared by dynamic vulcanization provided that the rubber was completely vulcanized [98].

The DV process for thermoplastic elastomers can be described as follows: after sufficient melt-mixing of plastic and rubber, vulcanizing agents are added. Vulcanization of the rubber phase occurs as mixing continues. After removal from the mixer, the cooled blend can be chopped, extruded, pelletized, injection molded, etc. Such a composition is described as a dispersion of very small particles of vulcanized rubber in a thermoplastic resin matrix. Such compositions are prepared commercially by a continuous process by using a twin-screw extruder.

Dynamic vulcanization gives the following improvements, in comparison with blends that have not been dynamically vulcanized: reduced set, improved ultimate properties, improved fatigue resistance, improved resistance to attack by hot oils, greater stability of melt-phase morphology, greater melt strength, etc.

A. EPDM–Polyolefin Compositions

The dynamic vulcanization of blends of EPDM rubber with polyolefins (PP or PE) has been described [98]. The rubber–plastic proportions and the extents of vulcanization were varied. In a few instances the rubber was first

press cured and then ground to various particle sizes. The ground rubber particles were then mixed with molten polypropylene. It was found that the ultimate properties (UE and UTS) varied inversely with rubber particle size. Since the smallest particle sizes of vulcanized rubber were obtained by dynamic vulcanization (not by grinding of cured rubber), the more durable compositions were obtained by dynamic vulcanization.

Only a small amount of crosslink formation is required for a large improvement in tension set. However, tensile strength improves rather continuously as the crosslink density of the rubber phase is increased. Compositions can be vulcanized by accelerated sulfur, methylolphenolic materials (e.g., catalyzed by $SnCl_2$), or other curatives [99].

As the concentration of the polyolefin resin increases, the compositions become less like rubber and more like plastic. Modulus, hardness, tension set, and strength increase.

B. NBR–Nylon Compositions

Excellent elastomeric NBR–nylon compositions have also been prepared by dynamic vulcanization during the melt-mixing of intimate blends of NBR with various nylons. In this case, the effect of curatives was complicated by the fact that some nitrile rubbers tend to self-cure at temperatures of mixing. Sulfur, phenolic, maleimide, or peroxide curatives can be used. The thermoplastic elastomeric compositions prepared by the dynamic vulcanization of nylon–NBR blends are highly resistant to hot oil. As in the case of the EPDM–polyolefin blends, increases in the amount of rubber in the composition reduce stiffness but increase resistance to permanent set.

C. Other Elastomeric Compositions Prepared by Dynamic Vulcanization

In addition to EPDM–Polyolefin and NBR–Nylons combinations, a large number of other rubber–plastic combinations have been used to prepare thermoplastic vulcanizates by dynamic vulcanization [100].

The best compositions are prepared when the surface energies of the rubber and plastic material are matched, when the entanglement molecular length of the rubber molecule is small, and when the plastic material is crystalline. It is also necessary that neither the plastic nor the rubber decompose in the presence of the other at temperatures required for melt-mixing. Also, in each case, a curing system appropriate for the rubber under the conditions of melt-mixing is required.

D. Technological Applications

The lower cost of thermoplastic processing is the motivation for the development of thermoplastic elastomers. However, failure in the achievement of

truly rubberlike properties has impeded the acceptance of thermoplastic–elastomer technology. Nevertheless, relatively recently commercialized compositions based on polypropylene and *completely* vulcanized EPDM have many of the excellent properties of the polyurethane and copolyester-type thermoplastic elastomers and even improved set and fatigue resistance. Applications of these materials can be listed as follows: caster wheels, convoluted bellows, diaphragms, gaskets, seals, tubing, mounts, bumpers, glazing seals, shields, suction cups, torque couplings, vibration isolators, plugs, connectors, rollers, oil-well injection lines, handles, grips, hose covers, vacuum tubing, bushings, grommets, protective sleeves, shock isolators, ducts, various hoses (e.g., hydraulic, agricultural spray, paint spray, plant air-water, mine hose, etc.), wire and cable insulation and strain relief, jacketing, etc.

REFERENCES

1. P. J. Flory, "Principles of Polymer Chemistry," Cornell Univ. Press, Ithaca, NY, 1953, Chap. 11.
2. L. Bateman, C. G. Moore, M. Porter, and B. Saville, in "The Chemistry and Physics of Rubber-Like Substances," L. Bateman (Ed.), John Wiley & Sons, Inc., New York, 1963, Chap. 19.
3. W. Hofmann, "Vulcanization and Vulcanizing Agents," Maclaren and Sons Ltd., London, 1967.
4. A. Y. Coran, in "Science and Technology of Rubber," F. R. Eirich (Ed.), Academic Press, New York, 1978, Chap. 7.
5. N. J. Morrison and M. Porter, *Rubber Chem. Technol.* **57**, 63 (1984).
6. G. E. Decker, R. W. Wise, and D. Guerry, *Rubber Chem. Technol.* **36**, 451 (1963); A. I. Juve, P. W. Karper, L. O. Schroyer, and A. G. Veith, *Rubber Chem. Technol.* **37**, 434 (1964), and references therein.
7. E. H. Farmer and F. W. Shipley, *J. Polym. Sci.* **1**, 293 (1946).
8. E. H. Farmer, *J. Chem. Soc.* p. 1519 (1947).
9. E. H. Farmer, *J. Soc. Chem. Ind.* **66**, 86 (1947).
10. L. Bateman, C. G. Moore, and M. Porter, *J. Chem. Soc.* p. 2866 (1958).
11. G. Oenslager, *Ind. Eng. Chem.* **23**, 232 (1933).
12. M. Weiss, U.S. Patent 1,411,231 (1922).
13. S. Malony, U.S. Patent 1,343,222 (1920).
14. C. Bedford, U.S. Patent 1,371,922–4 (1921).
15. L. Sebrell and C. Bedford, U.S. Patent 1,522,687 (1925).
16. G. Bruni and E. Romani, *India Rubber J.* **62**, 63 (1921).
17. E. Zaucker, M. Bogemann, and L. Orthner, U.S. Patent 1,942,790 (1934).
18. M. W. Harmon, U.S. Patent 2,100,692 (1937).
19. A. Y. Coran and J. E. Kerwood, U.S. Patent 3,546,185 (1970).
20. R. H. Campbell and R. W. Wise, *Rubber Chem. Technol.* **37**, 635 (1964).
21. R. H. Campbell and R. W. Wise, *Rubber Chem. Technol.* **37**, 650 (1964).
22. P. L. Hu and W. Scheele, *Kautsch. Gummi* **15**, 440 (1962).
23. N. J. Morrison and M. Porter, *Rubber Chem. Technol.* **57**, 63 (1984).
24. P. Ghosh, S. Katare, P. Patkar, J. M. Caritjers, V. Venkatasubramanian, and K. A. Walker, *Rubber Chem. Technol.* **76**, 592 (2003).
25. T. D. Skinner, *Rubber Chem. Technol.* **45**, 182 (1972).
26. P. J. Nieuwenhuizen, J. Reedijk, M. Van Duin, and W. J. McGill, *Rubber Chem. Technol.* **70**, 368 (1997).

27. F. Ignatz-Hoover, A. R. Katritzky, V. S. Lobanov, *Rubber Chem. Technol*. **72**, 318 (1999).
28. J. L. Koenig, *Rubber Chem Technol*. **73**, 385 (2000).
29. M. Mori and J. L. Koenig, *Rubber Chem Technol*. **68**, 551 (1995).
30. R. T. Armstrong, J. R. Little, and K. W. Doak, *Rubber Chem. Technol*. **17**, 788 (1944).
31. A. Y. Coran, *Chemtech* **23**, 106 (1983).
32. R. T. Leib, A. B. Sullivan, and C. D. Trivette, *Rubber Chem. Technol*. **43**, 1188 (1970).
33. P. N. Son, *Rubber Chem. Technol*. **46**, 999 (1973).
34. A. B. Sullivan, L. H. Davis, and O. W. Maender, *Rubber Chem. Technol*. **56**, 1061 (1983).
35. R. Ding, A. I. Leonov, and A. Y. Coran, *Rubber Chem. Technol*. **69**, 81 (1996).
36. A. V. Chapman and M. Porter, in "Natural Rubber Science and Technology," A. D. Roberts (Ed.), Oxford University Press, Oxford, 1988.
37. A. Y. Coran, *Rubber Chem. Technol*. **38**, 1 (1965).
38. R. W. Layer, *Rubber Chem. Technol*. **65**, 211 (1992).
39. C. D. Trivette, Jr., E. Morita, and O. W. Maender, *Rubber Chem. Technol*. **50**, 570 (1977).
40. H. Roebuck, K. M. Davies, *Plast. Rubber Process*. p. 63, June (1977).
41. R. N. Datta, A. H. M. Schotman, A. J. M. Weber, F. G. H. Van Wijk, P. J. C. Van Haeren, J. W. Hofstraat, A. G. Talma, and A. G. V. D. Bovenkamp-Bouwman, *Rubber Chem. Technol*. **70**, 129 (1997).
42. R. N. Datta, A. G. Talma, and A. H. M. Schotman, *Rubber Chem. Technol*. **71**, 1073 (1998).
43. R. N. Datta and M. S. Ivan, *Rubber World* **212**, 24 (1995).
44. E.-W. Tan and S. Wolff, U.S. Patent 4,517,336 (1985).
45. S. Buchan, "Rubber to Metal Bonding," Crosby Lockwood & Sons, London, 1959.
46. W. J. van Ooij, *Rubber Chem. Technol*. **52**, 605 (1979); *Rubber Chem. Technol*. **57**, 421 (1984).
47. K. D. Albrecht, *Rubber Chem. Technol*. **46**, 981 (1973).
48. M. L. Studebaker, *Rubber Chem. Technol*. **39**, 1359 (1966).
49. C. G. Moore, L. Mullins, and P. McL. Swift, *J. Appl. Polym. Sci*. **5**, 293 (1961).
40. C. G. Moore and B. R. Trego, *J. Appl. Polym. Sci*. **5**, 299 (1961).
51. T. D. Skinner and A. A. Watson, *Rubber Chem. Technol*. **42**, 404 (1969).
52. R. M. Russell, T. D. Skinner, and A. A. Watson, *Rubber Chem. Technol*. **42**, 418 (1969).
53. P. M. Lewis, *NR Technology* **17**, 57 (1986).
54. C. R. and O. Lorenz, *Ind. Eng. Chem*., *Prod. Res. Dev*. **2**, 279 (1963).
55. C. L. M. Bell and J. I. Cuneen, *J. Appl. Polym. Sci*. **11**, 2201 (1967).
56. A. N. Gent, P. B. Lindley, and A. G. Thomas, *J. Appl. Polym. Sci*. **8**, 455 (1964).
57. E. B. McCall, *J. Rubber Res. Inst. Malaya* **22**, 354 (1969).
58. D. S. Campbell, *J. Appl. Polym. Sci*. **14**, 1409 (1970).
59. W. Cooper, *J. Polym. Sci*. **28**, 195 (1958).
60. P. S. Brown, M. Porter, and A. G. Thomas, "The Role of Crosslink Breakage in Determining the Strength of Vulcanizates," International Rubber Conference, Harrogate, preprint 18a, 1987.
61. J. R. Wolfe, T. L. Pugh, and A. S. Killian, *Rubber Chem. Technol*. **41**, 1329, 1339 (1968).
62. E. C. Gregg, Jr. and S. E. Katrenick, *Rubber Chem. Technol*. **43**, 549 (1970).
63. J. H. M. van den Berg, J. W. Beulen, E. F. J. Duynstee, and H. L. Nelissen, *Rubber Chem. Technol*. **57**, 265 (1984).
64. J. H. M. van den Berg, J. W. Beulen, J. M. H. Hacking, and E. F. J. Duynstee, *Rubber Chem. Technol*. **57**, 725 (1984).
65. S. van der Meer, *Rev. Gen. Caoutch. Plast*. **20**, 230 (1943).
66. C. Thelamon, *Rubber Chem. Technol*. **36**, 268 (1963).
67. A. Giller, *Kaut. Gummi Kunstst*. **19**, 188 (1966).
68. M. Van Duin and A. Souphanthong, *Rubber Chem Technol*. **68**, 717 (1995).
69. J. Rehner and P. J. Flory, *Rubber Chem. Technol*. **19**, 900 (1946).
70. R. F. Martell and D. E. Smith, *Rubber Chem. Technol*. **35**, 141 (1962).
71. A. B. Sullivan, *J. Org. Chem*. **31**, 2811 (1966).
72. C. S. L. Baker, D. Barnard, and M. Porter, *Rubber Chem. Technol*. **35**, 141 (1962).

73. L. M. Gan and C. H. Chew, *Rubber Chem. Technol.* **56**, 883 (1983).
74. F. P. Baldwin, P. Borzel, C. A, Cohen, H. S. Makowski, and J. F. Castle, *Rubber Chem. Technol.* **43**, 522 (1970).
75. A. Greth, *Kunststoffe* **31**, 345 (1951).
76. P. Kovacic and P. W. Hein, *Rubber Chem. Technol.* **35**, 528 (1962).
77. H. M. R. Hoffmann, *Angew. Chem., Int. Ed. Engl.* **8**, 556 (1969).
78. K. Mori and Y. Nakamura, *Rubber Chem. Technol.* **57**, 34 (1984).
79. H. Kato and H. Jujita, *Rubber Chem. Technol.* **55**, 949 (1982).
80. R. Pariser, *Kunststoffe* **50**, 623 (1960).
81. R. O. Becker, *Rubber Chem. Technol.* **37**, 76 (1964).
82. L. D. Loan, *Rubber Chem. Technol.* **40**, 149 (1967).
83. P. R. Dluzneski, *Rubber Chem. Technol.* **74**, 451 (2001).
84. J. Scanlan and D. K. Thomas, *J. Polym. Sci., Part A* **1**, 1015 (1963).
85. E. H. Farmer and S. E. Michael, *J. Chem. Soc.* p. 513 (1942).
86. E. H. Farmer and C. B. Moore *J. Chem. Soc.* p. 131 (1951).
87. E. H. Farmer and C. B. Moore *J. Chem. Soc.* p. 142 (1951).
88. L. D. Loan, *J. Appl. Polym. Sci.* **7**, 2259 (1963).
89. D. K. Thomas, *J. Appl. Polym. Sci.* **6**, 613 (1962).
90. K. W. Scott, *J. Polym. Sci.* **58**, 517 (1962).
91. L. P. Lenas, *Rubber Chem. Technol.* **37**, 229 (1964).
92. F. M. Lewis, *Rubber Chem. Technol.* **35**, 1222 (1962).
93. D. K. Thomas, *Polymer* **7**, 243 (1966).
94. C. W. Roush, J. Kosmider, and R. L. Baufer, *Rubber Age* **94**, 744 (1964).
95. W. Hofmann, "Vulcanization and Vulcanizing Agents," Maclaren and Sons Ltd., London, 1967, p. 242.
96. P. G. Bork and C. W. Roush, in "Vulcanization of Elastomers," G. Alliger and I. J. Sjothun (Eds.), Reinhold, New York, 1964, p. 366.
97. W. Fischer, U.S. Patent 3,758,643 (1973).
98. A. Y. Coran and R. Patel, *Rubber Chem. Technol.* **53**, 781 (1980).
99. A. Y. Coran and R. P. Patel, "Thermoplastic Elastomers," 2nd ed., G. Holden, N. R. Legg, R. Quirk, and H. E. Schroeder (Eds.), Hanser, Munich, 1996, Chap. 7, p. 153.
100. A. Y. Coran, R. Patel, and D. Williams, *Rubber Chem. Technol.* **55**, 116 (1982).

8 Reinforcement of Elastomers by Particulate Fillers

JEAN-BAPTISTE DONNET
ENSCMu-UHA
Mulhouse Cedex
France

EMMANUEL CUSTODERO
Manufacture Française des Pneumatiques Michelin
Clermont-Ferrand Cedex
France

I. INTRODUCTION

The reinforcement of elastomers by particulate fillers has been extensively studied in the past, particularly in the 1960s and 1970s. The first reason is naturally the drastic changes in mechanical properties that induces fillers reinforcement: many of the usual applications of elastomers could not be envisaged without the use of particulate fillers. The other reason seems to us to be of a very different nature, and probably resides in the "mystery" of the reinforcement mechanism that has fascinated many scientists and remains, despite their efforts, mainly not understood today.

It is necessary to define precisely what is *reinforcement*, because this word covers very different meanings when applied to thermoplastics, thermosets, or elastomers. Confusion is mainly due to the fact that reinforcement qualifies an increase in mechanical properties, but what is expected as mechanical properties is very different considering the different matrices and applications.

For plastics, reinforcement results in an increase in modulus and hardness. The effect of particulate fillers is quite clear, they replace a part of the matrix:

Science and Technology of Rubber, Third Edition

so modulus becomes higher, but deformation at break decreases in the same time.

The situation is very different for elastomers: the use of reinforcing fillers induces a simultaneous increase modulus and deformation at break. Curiously, the replacement of a part of the deformable matrix by solid objects doesn't reduce its deformability. The increase of these two antagonistic properties characterizes elastomer reinforcement. This fascinating paradox, despite not being fully understood, explains the ability of reinforced elastomers to provide unique material properties and applications and justify their success in different technological fields.

II. PREPARATION OF FILLERS

A. Nonreinforcing Fillers

As it will be discussed later, the size of the filler is probably one of the most important properties for reinforcement. So, particulate fillers obtained by grinding of minerals or by coarse precipitation are *usually* nonreinforcing fillers because of their size: they are too big. Such fillers can even be used in elastomers but just confer them a very slight increase in modulus and a very significant drop in break properties occurs.

B. Reinforcing Fillers

1. Carbon Black

a) Historical Processes
b) Furnace Process
c) Post Treatments, Surface Modification

The great majority of carbon black post-treatment studies have been conducted to increase strength/quality of reinforcement. So the chemical modifications that have been tested are strongly linked to the different theories envisaged for reinforcement.

In the 1960s, carbon black–elastomer interaction was considered as the result of a *chemical bonding* [1, 2] between acidic surface functions and natural rubber alkaline moieties [3, 4]. So many studies have been conducted to increase carbon black activity by surface oxidation [4]: oxygen at high temperatures, H_2O_2, ozone, nitric acid. The type of oxidation used determines the number and the type of functions obtained; it is interesting to underline that such chemical modifications are used at industrial scale for specialty carbon blacks (inks, pigments).

In the early 1980s, Danneberg proposed the mechanism of molecular slippage [5] and post treatments turned to chemical grafting of polymeric chains onto carbon black surface [6].

More recently, the need for low hysteresis compounds has reactivated chemical modification studies. Many modification processes have been proposed: functionalization [7], surface coating of carbon black by silica [8], and alumina [9].

2. Silicas

The use of silica in rubber mixes can not be considered as new at all, because this filler has been used in rubber formulations since the beginning of the 20th century [10]. Silicas are not reinforcing fillers in the proper sense, because silica-reinforced mixes exhibit much lower mechanical properties, particularly considering modulus at break and abrasion resistance. So silicas weren't used as reinforcing fillers but mainly in association with carbon black.

Two major breakthroughs have transformed this facility product into a reinforcing filler that can achieve all carbon black mixes properties with, in addition, a decreased hysteresis of major interest for tire applications. The first step was made in the 1970s by Wolff, who proposed a specific silane coupling agent, the TESPT [11]. The second step arises in the 1990s with an R. Rauline's patent, which introduces the use of specific precipitation silica, elastomers, and mixing conditions to achieve reinforcement [12].

a. Precipitated Silicas

Silicas used as reinforcing fillers are mainly obtained by precipitation [13, 14]. The process basically consists in the preparation of a silica glass by alkaline fusion of pure sand and an alkaline salt. Then this glass is solubilized in water at high temperature and acid precipitated. The silica suspension obtained is then filtered, washed, and dried.

In order to obtain reinforcing silicas, much care must be taken in precipitation recipes (to obtain small rigid objects) and drying conditions (to maintain high dispersibility) [14–16].

It is also interesting to underline that silicas can be very easily chemically modified by doping or grafting of species during or at the end of their preparation [17].

b. Fumed Silicas

Fumed silicas are obtained by high temperature oxydecomposition of SiH_4, or other methyl hydride precursors ($SiHMe_3$, SiH_2Me_2 . . .):

$$n\ SiH_4 + 2n\ O_2 \rightarrow n\ SiO_2 + 2n\ H_2O$$

Coming out of the furnace, fumed silicas are obtained in a fluffy form, and because of their high temperature of formation, they present a very stable morphology and few surface silanols compared to precipitation silicas. This confers a high dispersibility and reactivity to fumed silicas but, because of their higher price, they are rarely used in the rubber industry.

3. New Reinforcing Fillers

Very recently, many studies have been conducted to identify new reinforcing systems. These systems are similar to silica compounds and characterized by the use of a coupling agent to chemically bond elastomer chains to filler surface. Many reinforcing systems have been patented: alumina oxyhydroxide and oxide [18, 19], titanium oxides [20], and silicon nitride/carbide [21].

III. MORPHOLOGICAL AND PHYSICOCHEMICAL CHARACTERIZATION OF FILLERS

As will be demonstrated later, morphology and physicochemical properties of reinforcing fillers are of crucial importance because they directly define their reinforcement ability. Their characterization formerly was based essentially on morphological properties (surface area and structure), but because of the use of silicas as reinforcing filler, there is now a strong need for dispersibility and surface chemistry characterization.

A. Filler Morphology Characterization

1. Filler Morphology

It is important to emphasize that the actual morphology of carbon blacks has remained unknown for decades, even if it was commonly used in the rubber industry. This is due to the very small size of its constituting objects; they are smaller than 0.1 μm and can only be resolved by transmission electron microscopy.

a. MET

As observed by transmission electron microscopy, carbon blacks appear as irregular chainlike, branched aggregates of partially fused spheres [22].

Aggregates constitute the smallest dispersible unit of carbon black and are virtually unbreakable in usual conditions of use; therefore, aggregates must be considered as the actual reinforcing objects.

The chainlike, branched structure of aggregates makes them very bulky, and their effective volume is much higher than the volume of the aggregate itself. This observation is of primary importance because the effective volume of the aggregate will be more or less its volume in the mixes and define which part of rubber can be deformed and not. This bulkiness is usually called *structure* and generally measured by other methods (see later section on structure); some very interesting studies have been conducted in the past to classify carbon black aggregates in different shape classes (bulk, ellipsoid, linear, etc.) [23].

Even if they are usually called *primary particles*, spheres that constitute aggregate are partially fused together and never exist by themselves. Anyway, their size is of great importance because it defines the actual surface of interaction between carbon black and elastomeric phase: the lower the size of

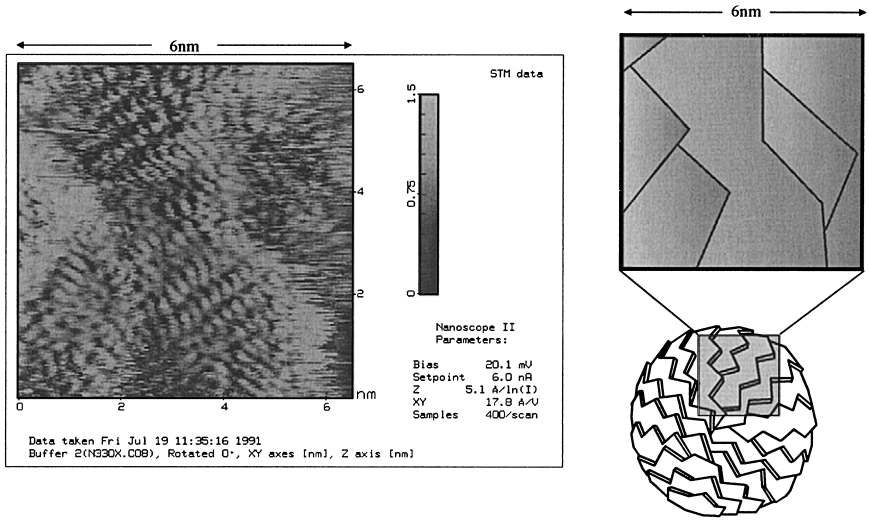

FIGURE 1 STM observation of carbon black surface at atomic scale resolution. (From Bueche [2].)

primary particles, the higher the interface extension. Primary particle size distribution has been estimated by TEM image analysis, but carbon black surface area is usually more efficiently obtained by adsorption methods (see later section on surface area).

At very high magnification, it is possible to observe directly the internal structure of carbon black primary particles. They are constituted by overlapping graphitic layers that locally present a quasi-crystalline *turbostratic* structure with an approximately 0.35 nm interlayer spacing, close to pure graphite (~0.332 nm).

b. STM, AFM

Scanning tunnelling microscopy (STM) [24–26] has been applied to carbon black characterization. As suggested by TEM, carbon black surface morphology consists in the overlapping of graphitic sheets in an onionlike structure (Fig. 1).

Carbon black surfaces appear surprisingly ordered, and graphitic edges should be identified with chemically reactive zones that were previously assigned to "amorphous" zones [27].

Atomic force microscopy (AFM) has also been used for three-dimensional characterization of carbon black aggregates [28].

c. Silicas

Electron transmission microscopy of silicas is much more difficult, particularly for precipitation silicas, which tend to reagglomerate during preparation and are fairly often unstable under high magnification.

Reinforcing silicas observed by TEM present a morphology very close to carbon black; they are constituted by small, chainlike, branched aggregates. However, the identification of silicas' primary particles is much more difficult because they are significantly more fused.

2. Surface Area

a. Introduction

Surface area is probably the most important morphological characterization of reinforcing fillers because it corresponds to the extension of the interface, i.e., the interaction between elastomer and filler surface.

As evidenced by transmission electron microscopy [23, 29], surface area is directly linked to the size of primary particles so that American Society of Testing Materials (ASTM) has chosen this parameter for carbon black nomenclature [30]. More precisely, ASTM nomenclature includes four digits, the first one relates to vulcanization speed (N as *normal* or S as *slow*), then tree numbers, which first correspond to the primary particle diameter [31].

ASTM numbers	Primary particle diameter (nm)	Previous nomenclature
900–999	201–500	MT: Medium Thermal
800–899	101–200	FT: Fine Thermal
700–799	61–100	SRF: Semi-Reinforcing Furnace
600–699	49–60	GPF: General Purpose Furnace
500–599	40–48	FEF: Fine Extrusion Furnace
400–499	31–39	FF: Fine Furnace
300–399	26–30	HAF: High Abrasive Furnace
200–299	20–25	ISAF: Intermediate Super Abrasive Furnace
100–199	11–19	SAF: Super Abrasive Furnace
000–099	1–10	—

Particle size diameter can only be done by TEM characterization and is difficult and costly, so surface area of fillers is usually obtained by different adsorption methods. (From Janzen and Kraus [32] and Janzen [33].)

b. Nitrogen Adsorption/BET

Adsorption of nitrogen and surface area determination by BET method is probably the most widely used method for surface area characterization of reinforcing fillers [34–36]. This method is very sensitive, reliable, and can be applied to all reinforcing fillers because it is either not or very weakly influenced by surface chemistry.

The main drawback of BET characterization is that the surface area obtained includes micropores whose surface can not be reached by elastomeric chains, which are much bigger than nitrogen [37]. So, many are now using the *t-plot* method that allows the determination of the net surface excluding micropores [35].

c. CTAB Adsorption

Cetyl triethyl ammonium bromide (CTAB) adsorption is widely used in carbon black industry [32, 34, 38]. This method consists of making a suspension of a known mass of carbon black into a water CTAB solution of known concentration. Carbon black is then filtered and the quantity of adsorbed CTAB is determined by titration of the remaining CTAB in the filtrate. Surface area of carbon black is then deducted from the amount of CTAB adsorbed, using a previously determined calibration with a reference carbon black.

CTAB surface area characterization is not influenced by micropores because of the size of CTAB molecule, but it can be influenced by surface chemistry and impurities [39]. Hence, it tends to disappear and to be replaced by BET/*t-plot*, which is much more reliable.

d. Iodine Adsorption

Iodine surface characterization proceeds in exactly the same way as CTAB, except that the adsorbed species is I_2 instead of CTAB. This method can only be applied to carbon black characterization [40].

Because iodine probably partly adsorbs and partly reacts with double bonds on the surface, the iodine method is extremely sensitive to any surface functions, modifications, or contaminations [41]. Hence, this method, formerly very widely used in carbon black industry, is now replaced by CTAB or BET/*t-plot*.

3. Structure

If structure is rather easy to define on the basis of MET images, it is much more difficult to measure it quantitatively. Nevertheless, the determination of structure is of primary importance because structure defines the actual volume of the filler in the mix and therefore the level of strain amplification of the deformable phase (see "Mechanical Properties of Filled Rubbers").

a. TEM Measurements

Some attempts have been made to use TEM measurements to determine structure of fillers. But in spite of the well-constructed studies [42, 43], the qualification of TEM images that are two-dimensional do not lead to a three-dimensional image.

b. DBP Absorption

Practically, structure determination of fillers is obtained by a very simple and easy method: dibutyl phtalate absorption (DBPA) [44]. This method consists of filling up the voids in and between aggregates with DBP, which is a viscous liquid. Historically, the DPB volume was determined by making a solid pellet of carbon black and DBP with a spoon. Now, this delicate measurement is made automatically with a couple-monitored Banbury, in which a well-

known quantity of dry carbon black is placed. DBP is then added drop by drop, and the structure value is obtained when torque reaches a given value.

DBP measurements are surprisingly reliable and can be easily and quickly obtained. Nevertheless, DBP measurement can be sensitive to surface chemistry, and values obtained with fillers of different nature can't be directly compared. For silicas, dioctyl phtalate can also be used instead of DBP [14].

DBP values also depend on pelletization/granulation of the filler. This makes sense because DBP measures the *total* void volume: intra-aggregate voids, which are the pertinent parameter, but also inter-aggregate voids, which essentially reflect pelletization/granulation. Thus, fluffy or loosely pelletized black will have higher DBP value; in the same way, spray-dried silicas will have greater DBP value than granulated ones, even if their aggregates are exactly the same.

c. CDBP Absorption

Very frequently, DBP adsorption is made with carbon black previously submitted to very high pressure into a cylinder, for example, 24,000 psi four times [44]. Crushed DBP absorption or CDBPA are equal to DBP (for *low* structure carbon blacks) or significantly lower than DBP (for *high* structure carbon blacks).

The high pressure crush procedure is supposed to reproduce aggregate breakage during mixing, but because DBP measures either intra-aggregates and inter-aggregates voids, it is difficult to settle if the decrease in DBP absorption is due to the compaction of the filler induced by the pressure [45] or to an actual breakage of aggregates.

d. Mercury Porosimetry

Filler structure can also easily be determined by mercury porosimetry [46–48]. Filler is placed in a small chamber and mercury is forced into the voids by increasing pressure. The intrusion curve gives the volume of mercury intruded in pores for each applied pressure. Usually, intrusion curves present a well defined step at high pressure, which corresponds to the filling of the smallest pores (intra-aggregate and inter-primary-particles voids). Step's high gives a structure index which excludes inter-aggregate voids and so is more representative of the intrinsic structure of the filler. In addition, mercury porosimetry allows a direct determination of filler surface area, excluding micropores [49], and can be applied to any particulate filler [50].

4. Aggregate Size Distribution

Aggregate size distribution is the last morphological characterization of reinforcing fillers. This measurement is very rarely used, despite the great interest in knowing the size of aggregates, which directly influences distances between reinforcing objects in the mix, and therefore the strain amplification. This surprising situation is mainly due to the fact that this determination is particularly difficult to make [33].

a. TEM/AI Measurement

Transmission electron microscopy/image analysis (TEM/AI) has been used for a long time to determine aggregate size distribution of carbon black and silicas [51]. Such studies are very costly because they need at least a few thousand aggregate size measurements to determine precisely the size distribution. Nevertheless, using TEM/AI aggregates are measured as two-dimensional projections, which probably maximizes their sizes.

b. Disk Centrifugation

One better method to access aggregate size distribution is probably to use disk centrifugal photo or x-ray sedimentometers [52]. This apparatus consists of a transparent void disk that can be rotated at very high speed. A sedimentation medium is first injected into the rotating disk, and then a very small quantity of filler suspension is injected at its surface. Sedimentation is registered by light or x-ray transmission.

Aggregate size distribution of carbon blacks [53] and silicas can be easily obtained by this method. Its main drawback is that, unlike with EM-AI, aggregate sizes are probably underestimated because they settle following their lowest project area.

c. Tint

Coming from the ink and pigment industry, the tint measurement is a very simple way to evaluate the mean aggregate size of carbon black [54, 55]. This characterization consists of making a paste of known amounts of carbon black, white solid powder (titanium or zinc oxide), and oil (DBP, for example). Then the reflectivity of the paste is measured; it has been demonstrated that tint values will roughly correlate with mean aggregate size and can be considered as an indicator of aggregate size distribution broadness [33, 56].

B. Dispersibility

Even if the relationship between filler dispersion and abrasion resistance is well established, relatively few studies have been done on the characterization of filler dispersibility. This is mainly due to the fact that carbon black dispersibility was commonly judged satisfactory, partly because it is indeed high, but more probably because all mixing apparatuses were designed for dispersing carbon blacks.

The use of silica has given a new light to this domain, because, contrary to carbon black, dispersibility is one of the key properties for achieving silica reinforced mixes [14, 48, 57].

Obviously, filler dispersibility is mainly influenced by interactions between agglomerates and/or aggregates, in other words, the force/energy needed in order to separate two objects. For carbon black, these interactions are mainly due to van der Waals forces, which are very low compared to the hydrogen bonding existing between silica objects.

In addition, pelletization process has a great influence on dispersibility: any action leading to a higher compaction of the filler increases interaction between filler objects and so decreases its dispersibility.

a. Reflectivity

The most commonly used technique to qualify filler dispersibility is to study light reflectivity of clean-cut mixes. Some apparatuses have been developed to evaluate filler dispersion using a calibrated set of reference mixes (Dispergrader). However, such characterization mainly detects dispersion defects of a few tens of microns, and direct comparison of carbon black and silica mixes has to be done cautiously. In any case, it is necessary to make a mix, which means choosing a formula, a mixer, and mixing conditions; thus the result can not be considered as an intrinsic dispersibility measurement of the filler, but just reflect the dispersibility of the filler in one mix with a set of mixing conditions.

b. Laser Granulometry

Recently, a method has been patented to determine filler dispersibility. It consists of measuring continuously the size of the filler by laser granulometry during an ultrasonic desagglomeration [18]. This characterization can be applied to any filler and is an intrinsic property; however, the use of water as a desagglomeration medium can be a problem because of its high polarity compared to elastomers.

C. Filler Physicochemistry

Compared to morphology, filler chemistry has been only slightly studied, partly because of the difficulty of such characterisations and more probably because since the 1970s reinforcement is broadly considered as a physical interaction between elastomer and filler. So carbon black chemical characterizations mainly date from the 1960s, and few new technical methods have been applied to carbon black surface characterization since this time. The situation is somewhat different for silicas, because silica reinforcement is the consequence of a chemical reaction of silane with silica surface. Few studies have been published in the elastomer reinforcement area, probably because silica surface was already well characterized for other applications.

Concerning physicochemical characterization, the studies are limited to surface energy distribution determination, which will be discussed first.

1. Surface Energy

Elastomer reinforcement by carbon black is generally considered as the consequence of the adsorption of polymeric chains onto carbon black surface. Therefore carbon black surface energy knowledge is of primary importance in carbon black characterization. However, very few carbon black surface

energy measurements have been published; this can be easily understood considering the difficulty of such measurements on a highly heterogeneous and tortuous surface.

Immersion calorimetry allows carbon black [58, 59] or silica [60] surface energy determination. This technique can be used with different liquids or solutions of low mass elastomers, but it presents the main drawback of giving a mean surface energy value (~50–70 mJ/m^2), when surface adsorption of polymeric trains probably preferentially occurs on the highest surface energy sites.

This justifies the use of inverse gas chromatography (IGC) for filler surface energy characterization. This technique can be used in two very different modes: "infinite" or "finite" dilution.

In "infinite" dilution, very small quantities of alkanes of growing numbers of carbons are adsorbed onto carbon black [61, 61a, 62] or silica surface [60]; from their retention times, it is possible to calculate the dispersive component of surface energy $\gamma_{s,d}$. Because of the very low surface coverage during characterization, this value corresponds to the highest energetic sites [24]. According to this technique, surface energy grows with carbon black surface area; because high surface area carbon blacks are highly reinforcing, this result should be considered encouraging. Surface energy values obtained can reach values of 300–500 mJ/m^2, which can't be considered as realistic for carbonaceous surfaces. In addition, this determination seems to be also sensitive to chemical modification of carbon black surface even if the probes used should only characterize the dispersive part of surface energy.

"Finite" dilution is a more powerful technique in that it is possible to obtain the complete energetic site distribution for carbon black [24, 63] or silica [64, 65]. In this technique, surface is fully covered by the probe and the distribution is calculated by a specific post treatment of desorption signal. Using this technique, carbon blacks present approximately the same surface energy distribution differing only in the number of adsorption sites. The energetic site distribution is particularly broad, with sites of high (~100 mJ/m^2) to low (~10 mJ/m^2) energy. Mean values are consistent with these obtained by immersion calorimetry.

Finally, it should be mentioned that a procedure similar to IGC, a "finite" dilution, can be applied to nitrogen adsorption isotherm and allow surface nanoroughness characterization of any filler [66].

2. Surface Chemistry

a. Carbon Black

Impurities. Because of its manufacturing process, carbon black surface includes some organic and mineral impurities [67, 68].

Organic impurities are mainly poly aromatic hydrocarbons (PAH) [69]. They correspond to partially unconverted fuel that has been readsorbed onto carbon black. These PAHs are present at a very low content and, because of their firm adsorption on carbon black, the extraction must be conducted in a

Soxhlet apparatus with a strong solvent (toluene) and at high temperature (80°C). However, it has been demonstrated that organic impurities have no significant effect on carbon black reinforcement [24].

Mineral impurities come from quench and pelletization steps in the carbon black production process. As presented before, the decrease in temperature of carbon black and exhaust gases is mainly obtained by injection of a great mass of water. Additional water is also added to carbon black during pelletization. Even if this water is purified, the remaining mineral salts precipitate onto the carbon black surface and, because of the high temperature, are reduced to basic salts. Mineral impurities of carbon blacks can easily be extracted by solubilization in water, as in the so-called "pH of carbon black," in which carbon black is suspended in water and the pH then filtered and the pH of the filtered water measured. Mineral impurities don't seem to alter carbon black reinforcement properties but they have a significant effect on vulcanization speed, which increases with the pH value of carbon black.

Oxygenated Functions. Oxygenated functions on carbon black surface were observed in the early 1950s [70] and completely characterized by H. P. Boehm in the 1960s [71]. At this time, interaction between carbon black and natural rubber was considered the consequence of chemical reactions between the carbon black surface's acidic groups and basic moieties present in the natural rubber structure [71a].

The carbon black surface function characterization consists of suspending a given amount of carbon black in solutions of known normality of basis of different strength: $NaHCO_3$, Na_2CO_3, NaOH in water, and EtONa in ethanol [72]. Then carbon black is filtered and the number of reacted acidic groups obtained by titrating the remaining basis in filtrate (Fig. 2).

In the 1960s, carbon blacks were mainly prepared by *channel* processes, and their acidic functions were present at about 10^{-3} eq/g, which allows relatively easy determinations; but now, with *furnace* blacks, the surface acidic functions are generally of about 10^{-5} eq/g, and specific techniques [73] or drastic reaction conditions must be used [24]. Obviously, such delicate determination must be conducted on previously extracted black, in order to eliminate basic mineral impurities that would hinder any characterization of the rare acidic groups present on carbon black.

This observation allows one to believe that acidic groups on carbon blacks are mainly produced by surface oxidation in the production process, probably during drying following pelletization. Therefore, acidic groups could be considered an alteration of carbon black surface.

This point of view is supported by the fact that oxidized blacks which have an acidic surface group content of about 10^{-2} eq/g exhibit a very low reinforcement ability, even if their slow vulcanization is corrected.

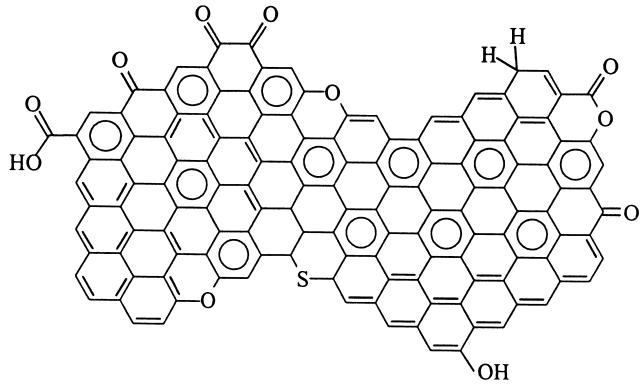

FIGURE 2 Chemical functions on carbon black surface. (From Bueche [2].)

Double Carbon Bonds, Hydrogen Content. All chemical studies done in the past on carbon black have focused on chemical impurities or on functions produced by partial surface oxidation of carbon black, and not on its *own* surface reactivity.

Now carbon blacks can not be considered as chemically inert surfaces. Their reaction with iodine or oxygen, their structure evidenced by STM [24], demonstrates the presence of a great number of reactive double bonds on their surface.

Following Medalia and Kraus [41], such double bonds could react with sulfur [74–76], olefins [77], and radicals [3, 78] to provide chemical bonding between carbon black surface and polymer, but their direct quantitative determination has never been obtained. Several authors have observed a strong correlation between hydrogen content of carbon blacks and their reinforcement ability. The content and reactivity of hydrogen present on graphitic edges have been determined by isotopic exchange and correlated to carbon black reinforcement ability [79, 80]. This characterization is particularly difficult and usually hydrogen mass content is used; these values also are surprisingly well correlated to reinforcement ability of carbon blacks [81].

b. Silica

Silanols. Because of its numerous and longstanding uses in other applications, silica surface chemistry is clearly better known than that of carbon black [13].

Silica surface chemistry is mainly defined by the surface content in silanols Si—OH; silanols can be "isolated," O≡Si—OH, or "geminated," O═Si═$(OH)_2$. They are generally highly associated by hydrogen bonds (Fig. 3).

For *fumed* silicas, silanol content is about 2 Si—OH/nm^2 [82, 83], but for *precipitation* silicas, silanol content can reach values as high as 6 to more than 10 Si—OH/nm^2 [84]. It is essential to emphasize that such high silanol content

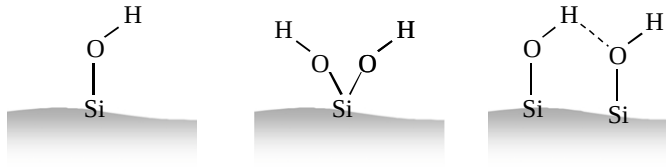

FIGURE 3 "Isolated," "geminated," and associated silanols.

cannot be considered as true per se: considering bond length and silicon–oxygen arrangement, a content of 2–3 Si—OH/nm^2 corresponds to a full coverage of the surface with silanols [13]. Such high values are generally attributed to the existence of polysilicic acid chains, —$[Si(OH)_2]_n$—O—$Si(OH)_3$, and to the fact that BET surface area doesn't take into account pores of very small size in which some silanols are located.

Silanol surface content can not reasonably be considered an indicator for silica reinforcement ability; indeed, because of its size, the coupling agent used to bond silica surface and elastomer can not react with more than two or three silanols of the surface [85, 86]. Moreover, a high number of silanols will induce more associations by hydrogen bonding and so decrease their chemical reactivity.

Other Surface Functions. Silica surface chemistry cannot be used to determine the silanol surface content. Particularly, for silicas synthesized by precipitation, some other chemical species can modify silica's surface reactivity.

For example, because of an incomplete hydrolysis of silicate, ≡ Si—O—Na can be observed; because of an incomplete washing of silica after filtering, sulfate can be adsorpted onto silica surface. In addition, some salts used for silica processing can also be added and modulate its reactivity [17].

Obviously, as discussed earlier in the silica production process, silica surface can also be modified by other chemical species added during and after its preparation. In any case, this modifier only changes silanol reactivity by enhancing [87] or decreasing its acidity.

IV. THE MIX: A NANOCOMPOSITE OF ELASTOMER AND FILLER

Even if the term *nanocomposite* is usually not used in reinforcement by particulate fillers, it would be particularly adapted: mixing of reinforcing solids and elastomers is not limited to the arithmetic "sum" of the properties of both taken independently but gives a synergetic alliance that achieves new properties.

Moreover, the term *filler* is more or less inadequate, because the particulate solid is not used to fill a *void* . . . that is to diminish the cost of the elastomeric product. Indeed, elastomer and reinforcing filler should be considered

as two inseparable parts of equal merit in the composite. As expressed nicely by Papirer, "carbon black and polymer is the wedding of the century."

This introduction is much more than a semantical debate; it underlines the importance of a *global* approach including reinforcing filler *and* elastomeric matrix relationships.

A. Dispersion, Aggregate Sizes, and Distances

1. Dispersion

a. Dispersion of Filler in Rubber Matrix

The quality of particulate filler dispersion in the elastomer matrix is of primary importance for compound mechanical and use properties [88–92].

In very recent years, filler dispersion characterization has been brought again into light because of the difficulties encountered to disperse silica in rubber [93, 94].

Usually, filler dispersion is achieved in a Banbury mixer and is presented to proceed in two different steps. In the first step, filler is distributed in pure polymer in the form of pellets or subpellets (i.e., *agglomerates*) [95] and then, in the second step, subpellets are eroded into aggregates by an "onion peeling" process [96]. This second phase, which eliminates agglomerates and determines inter-actual-aggregate distances is much longer and necessitates higher mechanical energetic input.

As discussed earlier, dispersibility and so dispersion is mainly controlled by the strength of interaction between agglomerates and/or aggregates, which is a direct consequence of their surface energy. The influence of surface energy on dispersion has been clearly demonstrated by the use of different matrices; when matrix surface energy increases and becomes closer to filler surface energy, dispersion is facilitated.

b. Characterization

Filler dispersion characterization is particularly difficult because it must be conducted on a very broad range of scale [97]: from microscopic undispersed agglomerates, which are defects and will decrease a product's life, to nanoscopic distances between aggregate, which will greatly influence reinforcement level [98]. Indeed, filler dispersion characterization has been conducted with a large number of analytical techniques: optical, electronic [30, 99], and atomic force microscopy [100, 101], but also x-rays [23, 102, 103] and neutron diffraction. The main difficulty is to recompose a global image from very different data, because any of these techniques gives directly a complete description of dispersion.

c. Influence of Filler's Properties

In addition to filler's surface energy, which is of major importance, dispersion can also be influenced by filler's morphological properties.

Dispersion is highly influenced by filler surface area: the higher the surface area, the lower the dispersion [104]. This result is probably due to the fact that high surface area usually has smaller aggregates, which will develop more interactions with their neighbors in the dry state.

Filler structure also has a neat influence on dispersion: the higher the structure, the higher the dispersion. This result is well established and likened to the fact that more "open" aggregate structures develop a lower number of contact with their neighbors in the dry state.

2. Object Sizes in the Mix

As discussed earlier, filler occurs as a distribution of different aggregate sizes. This characterization is interesting as a potential, but this final aggregate size distribution could not be achieved in mixes. Indeed, dispersion can be incomplete and some agglomerates can be left in the mix, shifting the actual size of reinforcing objects to a higher value. On the other hand, because of the high shear strengths developed during mixing, some aggregate breakage can also occur and produce an actual size of reinforcing objects lower than expected on the basis of filler characterization. Therefore, considering the possibility of filler in the mix, we will use the term *object*, which can refer to either aggregates *or* agglomerates.

Obviously, aggregate size distribution characterization in the mix is very delicate. Some transmission electron microscopy observations have been conducted on microtome thin cuts, but such characterizations are restricted to a small number of aggregates and can only lead to qualitative conclusions [23]. Direct characterization of object distribution in the mix has also been conducted using x-ray [105] or neutron diffraction, but such approaches are strongly limited by the high concentration of filler objects and their refraction index, which is relatively close to that of rubber. One other way to characterize object size distribution is to extract the filler from the mix by thermal or catalyzed polymer decomposition; these procedures probably greatly affect object size, because of possible reagglomerations.

The characterization of filler object size distributions in the mix mainly remains a domain to develop. In any case, it is generally accepted that aggregate size of carbon black decreases during mixing [29, 106], even if any of the methods used can eliminate possible artifact. About this, it is interesting to recall that crushed DBP, as previously discussed, has been developed to take into account possible aggregate breakage. Considering silica, explicit data has been published considering this problem, but the same possible aggregate breakage seems also possible.

3. Distances

Characterization of interobject distances in the mix is the reciprocal problem of object size determination and involves the same difficulties—and the same lack of experimental data.

However, it should be noted that usual filler loadings used in elastomers, (around 20% in volume), are very close to the maximal fraction that can be incorporated into the elastomeric matrix. This fraction is very low compared to compact spheres arrangement, but, as discussed earlier, filler's aggregates present a highly open structure; moreover, maximum loading is highly dependent on the filler's structure.

Based on simple models, it as been demonstrated that interobject distances are in the range of a few tens of nanometers; this result is consistent with the fact that carbon black mixes are electrically conducting, which implies that interobject distances are low enough to allow tunnel conduction [107].

Moreover, it has been demonstrated that optimum filler loading corresponds to very similar interaggregate distances, without regard to aggregate size or structure [108]. This very interesting result underlines the decisive influence of interaggregate distances in elastomer reinforcement.

B. Filler–Elastomer Interactions

1. Carbon Black

a. Elastomer Adsorption

"Filler Network". Because of carbon black high surface energy, elastomeric chains are strongly adsorbed onto its surface. This adsorption, even if it is limited to a small part of the elastomeric chains, called "trains," drastically slows down their mobility [103, 109, 110].

As a simplified—but slightly incorrect—picture, it can be considered that "trains" have a lowered transition temperature [111, 112]. The exact thickness of this layer remains disputed [109, 112a, 113] but values of 1–5 nm are usually considered [114]. Anyway, it is very noticeable that such thickness corresponds at least to 3 to 15% of total elastomeric phase [114a]. Taking into account carbon black structure/tortuosity, values as high as 30% have been proposed.

A more accurate approach considers that elastomeric chains present a gradient of mobility coming from carbon black surface to bulk.

The high surface areas and loadings of carbon blacks used in elastomer reinforcement induce such small distances between reinforcing objects that almost any elastomeric chain contacts at least one aggregate [108]. In addition, because the statistical size of polymeric chains is in the range of interaggregate distances, close neighboring objects are probably bounded together by chains adsorbed onto both aggregates.

The bonding of carbon black aggregates constitutes the *filler network*.

Bound Rubber. The filler network is clearly evidenced by *bound rubber* measurements [115–117]. *Bound rubber* is a very specific measurement done on green mixes; it consists of determining the part of rubber that can not be extracted by a good solvent [118]. A small part of rubber, previously weighted,

is put in toluene and submitted to extraction at a room temperature. Samples swell but usually not delitate; the surrounding solvent is regularly renewed to ensure an optimal extraction, and samples are weighted to follow extraction progression. After 1 or 2 weeks, extraction is completed and samples are dried and weighted. The weight difference corresponds to the soluble part of elastomer, that is, to the chains that were weakly adsorbed on the carbon black surface.

When the extraction temperature increases, the bound rubber decreases and, above about 80°C, samples completely delitate, indicating the disappearance of the continuous networking of carbon black aggregates by elastomer chains.

Because *bound rubber* measures elastomer adsorption onto filler surface, it is highly dependent on filler loading, specific surface, and structure, which are parameters that can be measured independently [119]. However, at given loading and carbon black surface area and structure, it has been demonstrated that *bound rubber* is also dependent on carbon black surface energy [120].

b. Chemical Surface Bonding

Before the 1970s, carbon black reinforcement of elastomers was generally considered chemical by nature [121]. It was supposed that carbon black surface acidic groups were reacting with natural rubber basic moieties conducting to a strong covalent bond that was responsible for carbon black reinforcement ability.

In the 1970s, *furnace* gradually replaced *channel* technology. But even if *furnace* carbon blacks present ten times less surface acidic groups, their reinforcing ability remains unchanged or increased. On the other hand, synthetic elastomers, which obviously have more basic moieties than natural rubber, were also perfectly reinforced by carbon black. In addition, the preparation of surface-oxidized carbon or grafted blacks [4] leads to a decreased reinforcement ability.

It was then obvious that chemical reaction of carbon black surface acidic groups with natural rubber basic moieties was not responsible for reinforcement. So the newly discovered mechanism of "molecular slippage," proposed by Dannenberg and based on molecular adsorption, was quickly and fully adopted [5, 122].

These observations do not allow the full refutation of chemical reinforcement theory. Chemical bonding by acidobasic reaction is clearly rejected, but, following Medalia and Kraus [41], other chemical reactions could occur in carbon black mixes. For example, elastomeric chain breaking during mixing can lead to radicals that could react with carbon black surface [123]; sulfur-direct bonding of elastomer and carbon black could also be envisaged [77].

2. Silica

a. Silica–Silane Reaction

In contrast to carbon black, it is necessary to use a coupling agent to achieve silica elastomers reinforcement. TESPT, triethoxysilylpropyltetrasulfide, is the most widely used coupling agent.

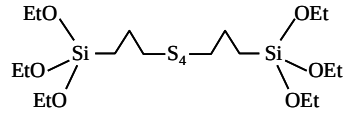

TESPT is a bifunctional molecule with a triethoxysilyl moiety reactive toward silica's silanols and a polysulfidic moiety that reacts with elastomeric chains.

Because reaction temperatures are somewhat different, the reaction of TESPT with silica surface mainly occurs during mixing when the reaction of polysulfidic moiety takes place during curing [85, 86] (Fig. 4).

b. Polymer Adsorption

When a coupling agent is used to generate a covalent bond between silica surface and elastomeric chains, it also limits polymer adsorption because of its shielding effect. So in silica–silane–elastomer compounds, the "filler network" will be much lower than in carbon black–elastomer systems. However, it remains *qualitatively* the same, and elastomer chain mobility is also limited in the close neighboring of silica surface [124].

Obviously, if any coupling agent is used, polymer adsorption will naturally occur [125, 126]; in addition, because of the high polarity of silica, some direct interaction between silica aggregates will also take place and constitute an additional filler–filler network. These effects will not happen in silica-reinforced systems when an appropriate amount of coupling agent is used.

Bound rubber determination is also applied to silica compounds, even if the numerous possible interactions naturally limit the interpretation of the values [127, 128].

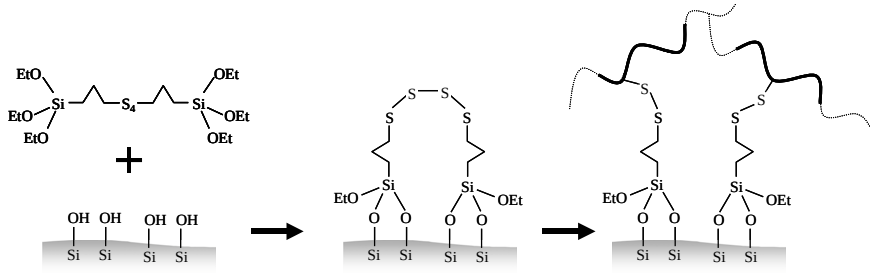

FIGURE 4 TESPT loadings are about one $Si(OEt)_3$ per nm^2, which roughly corresponds to a complete coverage of silica surface. So, for precipitation silicas with content 6 to 10 Si—OH/nm^2, many surface silanols will remain unreacted.

V. MECHANICAL PROPERTIES OF FILLED RUBBERS

A. Mechanical Properties in Green State

The increased life time expected from reinforcement by particulate fillers naturally refers to cured pieces. The incorporation of reinforcing fillers greatly changes the viscosity of green compounds, conducting to a mainly plastic behavior that allows their processing.

1. Viscosity

It is generally reported that elastomers filled with a volume fraction ϕ present a viscosity following [129]:

$$\eta = \eta_0 \cdot (1 + 2.5 + \phi + 14.1 \cdot \phi^2)$$

It is interesting to remember that this relationship has been established for solid spherical objects having any interaction among them and/or with the surrounding medium. As widely discussed earlier in this chapter, reinforcing systems are very far from this: carbon black or silica aggregate are highly structured, and elastomeric chains strongly adsorb onto carbon black surfaces.

2. Occluded Rubber

Elastomer interaction with carbon black or silica is very difficult to estimate and correct. On the other hand, it is much easier to take into account the actual volume of aggregate in the mix, and it has been proposed that a corrected volume fraction ϕ_c be used, which integrates the influence of filler structure as represented by DBP [130–132].

$$\phi_c = \frac{\phi}{2} \cdot \left[1 + \frac{1 + 0.02139 \cdot \mathrm{DBP}}{1.46}\right] \quad \text{et} \quad \eta = \eta_0 \cdot (1 + 2.5 \cdot \phi_c + 14.1 \cdot \phi_c^2)$$

The ϕ_c value represents the "actual" size of filler aggregates in the mix; it includes, naturally, the filler object itself plus a significant volume of polymer that is shielded from deformation by aggregate tortuousity. This part of the polymer that will not be deformed is usually called *occluded rubber* [131, 133, 134].

Nevertheless, occluded rubber must not be confused with the polymer part whose molecular mobility is changed by adsorption. *Occluded rubber*, which is mainly trapped in aggregate fractal sites, only represents a part of the volume of elastomer whose molecular motion is slowed down.

Occluded rubber and viscosity increases with filler structure and loading; on return, specific surface area of the filler has an influence on green mix viscosity.

3. Shear Dependence of Viscosity, Non-Newtonian Behavior

The presence of reinforcing fillers also increases the non-Newtonian behavior of elastomers. This effect is mainly due to the fact that the incorporation of fillers in elastomers decreases the volume of the deformable phase. As discussed in the following text, this decrease is not limited to the actual volume of the filler, but must also include the existence of occluded rubber. So, when filled mixes are submitted to shear forces, because of the lower deformable volume, the actual deformation and speed of deformation are much higher than in unfilled mixes [1, 134]. This phenomenon is usually called *strain amplification effect*; obviously *strain amplification* is not specific to reinforced systems but to any filled polymer.

The influence of filler is not limited to this enhancement of the non-Newtonian behavior of elastomers. At very small shear rates, filled green compounds also exhibit an additional increase of viscosity that can not be explained by *strain amplification*. This effect is usually attributed to the existence of the filler network: the direct bonding of reinforcing objects by adsorbed chains implies a increased force to be broken. Obviously this influence can only be observed at very low strain, because a very small increase of interaggregate distances immediately implies a desorption of the bridging elastomeric chains.

B. Mechanical Properties in Vulcanized State

1. Introduction

As for pure elastomers, the vulcanization step provides sulfur bridges between elastomeric chains and connects them into an infinite network. Vulcanization is supposed to be mainly unaffected by the presence of the reinforcing fillers and transforms the roughly plastic green mixes into viscoelastic vulcanizates.

For silica mixes, the high temperature of the vulcanization step allows the reaction of the polysulfidic moiety of the coupling agent with elastomer, ensuring the chemical covalent bonding of polymer to silica surface.

As in the green state, the *strain amplification*, due to the limited volume of the actually deformable phase, remains the first order result of filler incorporation. For a given macroscopic deformation, the actual deformation of the polymeric matrix will always be much higher, obviously depending on the filler volume and its structure, which defines occluded rubber volume.

The viscosity equation is usually generalized to Young or shear modulus G* [129, 132, 135]:

$$G^* = G_0^* \cdot (1 + 2.5 \cdot \phi_c - 14.1 \cdot \phi_c^2)$$

where G_0^* is the shear modulus of the unfilled vulcanized matrix at the same shear strain. Obviously, it is possible to vary the modulus by changing vulcan-

ization conditions, providing more or fewer sulfur bridges and so higher or lower G* values. Anyway, as evidenced by the equation, vulcanization changes G^*_0 but roughly does not affect reinforcement by itself.

2. Small-Strain Properties, Dynamic Viscoelastic Measurements

a. Payne Effect

Reinforced vulcanized samples generally present a marked viscoelastic behavior that is usually studied by dynamic viscoelastic measurements. In this experiment, a sample is subjected to periodic sinusoidal shear strain γ (at defined frequency ω and temperature T). Its dynamic shear modulus G^* is complex and can be written as the sum of the storage modulus G′, and the loss modulus G″.

$$G^*(\gamma) = G'(\gamma) + i \cdot G''(\gamma)$$

The dynamic storage modulus G′ presents an interesting variation when γ increases: at very low shear strain, G′ is constant (phase 1 in Fig. 5), then strongly decreases (phase 2 in Fig. 5) and reaches a plateau value (phase 3 in Fig. 5). This evolution of G′ is usually described as the *Payne effect* [136].

This change in G′ also corresponds to an important variation of G″ that passes through a maximum value. δ, the phase angle between stress and strain, is given by:

$$\tan(\delta[\gamma]) = \frac{G''(\gamma)}{G'(\gamma)}$$

The evolution of G′ and G″ in the range of 0.1 to 0.5 strain amplitude is of major importance because this domain corresponds to the most common solicitations of filled rubber compounds, for example in tire tread applications [137].

G″, the loss modulus, must not be confused with hysteretic losses of which the expression naturally depends on solicitation mode: hysteretic losses are proportional to G″ (constant strain), or $G''/G^{*2} \sim \tan(\delta)/G'$ (constant stress) or to $\tan(\delta)$ (constant energy).

It is also important to stress that filled elastomers are a very complex thermorheological system: particularly, G′ and G″ variations do not follow the same laws in frequency and temperature [138].

b. Mechanism

The Payne effect is widely accepted as the mechanical consequence of the progressive destruction of the "filler network" under shear strain.

The attribution of the Payne effect to the filler network is strongly supported by the fact that carbon black pastes, made with carbon black and low molecular weight oils, present very similar G* levels at very low shear strain

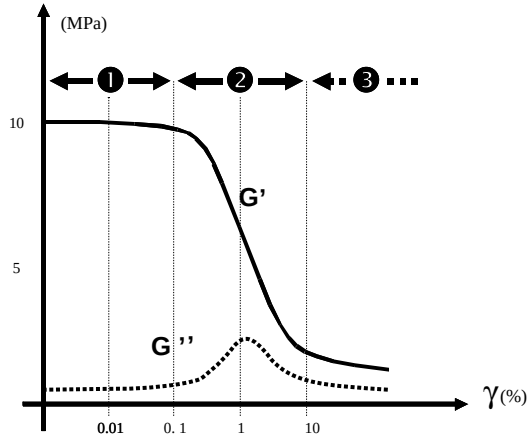

FIGURE 5 Schematic illustration G′ and G″ variation.

[139]. Obviously, when strain increases, G* drops drastically for carbon black pastes and much more slowly for filled rubber compounds, because of the *progressive* desorption of elastomeric chains.

Dannenberg's molecular slippage model, which will be discussed in detail in the next section, gives a good schematic view of the molecular mechanism that is responsible for the Payne effect. Numbers ❶, ❷, and ❸ refer to Fig. 5.

❶ At equilibrium, elastomer chains are adsorbed onto filler surface (state ⓪). When strain increases, it induces a progressive extension of elastomer chain segments that bridges filler particles (state ❶). Obviously, this extension is much greater than macroscopic deformation because of *strain amplification*. At very low strain, the macroscopic deformation energy is stored in elongated chains as elastic energy and so can be fully recovered when strain decreases: G″ is low and constant.

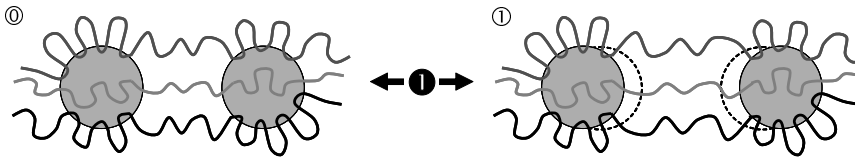

❷ At higher deformation, it is necessary to decompose the solicitation cycle. During the first extension at higher rate, stored elastic energy overpasses adsorption energy, and elastomer chains progressively desorb from filler surface (state ②, ★ sites desorbed).

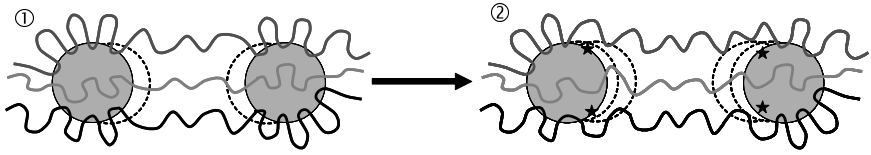

This desorption lengthens the bridging polymer segments that have to direct impacts. First, G′, which is roughly inversely dependent on the length of bridging chains, decreases; second, a part of the initially elastic energy stored in deformed chains is converted into molecular mobility and mechanically lost, which corresponds to an increase in G″.

The decrease of deformation that immediately follows the first extension at the higher rate does not exactly lead to initial state ①; indeed, in the short time of the dynamic deformation cycle, adsorption can not reach equilibrium state and remains imperfect, as illustrated by state ③.

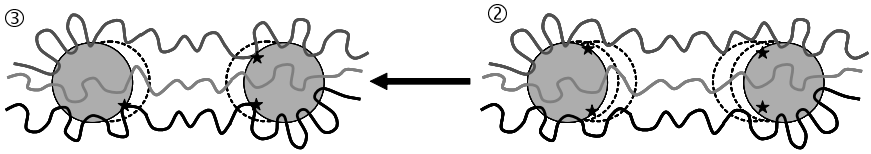

Thus during phase ❷, bridging elastomeric chains undergo adsorption–desorption cycles between "pseudo" equilibrium states ② and ③:

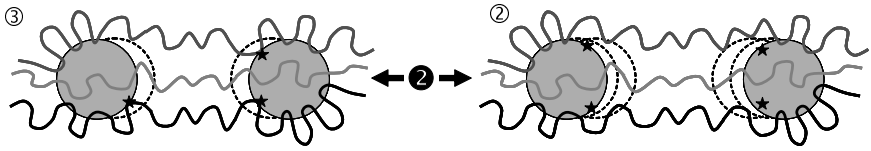

Obviously, elastomer desorption occurs gradually, because of the very broad interaggregate distance distribution that induces an also broad distribution of bridging elastomer segments. This explains the smooth decrease of G′ for mixes and its step shape for shorter molecules such as oils.

❸ Progressively, desorption induces a homogenization of bridging elastomer segment lengths. This homogenization and the stabilization of the modulus will be discussed in detail in the next section.

c. Hysteresis

It appears from the previous mechanism that G′ and G″ variations will be directly influenced by interaggregate distances [108] and the strength of elastomeric chain adsorption on the filler surface.

d. Interaggregate Distances

Any change in mix composition or processing that influences interaggregate distance distribution will change hysteresis: the lower the average distance, the higher the hysteresis and vice versa [140, 141].

Filler loading evidently decreases interaggregate distances. When filler mean aggregate size decreases, at the same loading level, the number of reinforcing objects increases and diminishes mean interaggregate distance. Increased structure provides, at the same loading ratio, lower interaggregate distances. Thus, increasing loading, surface area (i.e., decreasing aggregate size), or structure induces higher hysteresis of mixes.

On the other hand, low hysteresis mixes can be achieved by dispersion methods that increase interaggregate distances; prolonged or two-stage mixing or master-batch techniques have been used in order to decrease hysteresis [23, 104].

e. Adsorption Strength

Coupling agents that mask filler surface strongly reduce elastomer adsorption and thus hysteresis of mixes. This partially explains the low hysteresis value of silica mixes [140].

It is also possible to use functionalized elastomers to reduce mixes hysteresis; such elastomers have specific chemical moieties that react with the filler surface. These reactions lower hysteresis because of the decrease of polymer dangling chains and by shielding of the filler surface [142, 143].

3. Large Strain Properties

a. Observations

At large strain, dynamic viscoelastic measurements can not be made accurately because of the important self-heating of the sample during the experiment. Therefore large-strain properties are usually determined by uniaxial extension [144] (Fig. 6).

As was observed for G* in dynamic shear-strain measurements, a clear decrease of Young's modulus $E + \sigma/\varepsilon$ is observed at low strain ($\varepsilon < 1$). This corresponds to the previously described phases ❶ and ❷, even if phase ❶ is obviously not observable. (see Fig. 5).

At higher extension rates ($\varepsilon > 1$), Young's modulus increases and reaches a "pseudo maximum" just before the sample break.

A very significant observation is the *stress softening effect*, also called the *Mullins effect* [145, 146]. In this experiment, a compound sample is stretched to ε_1 and returned to zero strain, then stretched again. For strain below ε_1, its stress-strain curve is significantly below the first one but rejoins it at ε_1. *Stress softening* is dependent on the initial strain level; it can be partially reduced by thermal treatment but not be totally effaced (Fig. 7).

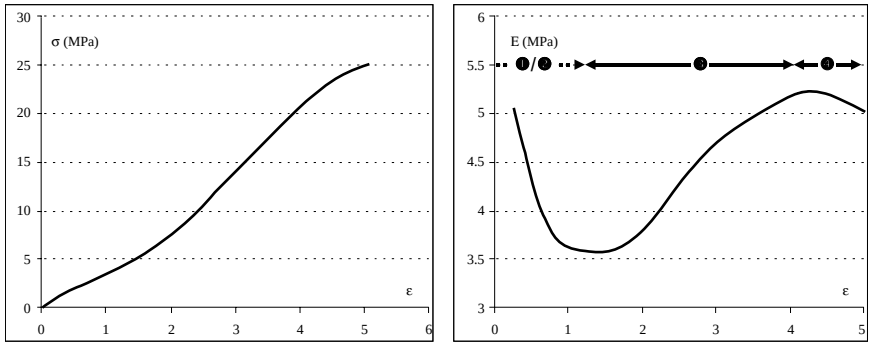

FIGURE 6 Stress and Young's modulus of reinforaced compound. (Data from Medalia and Kraus [41].)

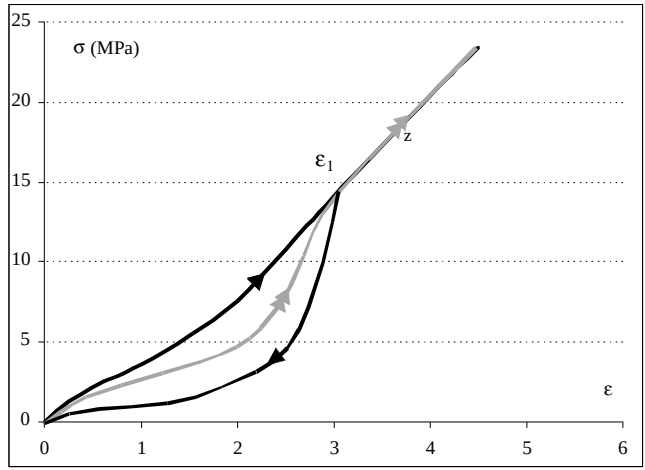

FIGURE 7 Schematical illustration of *stress softening effect.*

b. Interpretation

The *paradox* of reinforcement by particulate fillers is that there is a simultaneous increase of modulus *and* elongation at break. This fact is clearly illustrated by the comparison of stress–strain curves of pure and carbon-black-filled elastomer (Fig. 8).

The modulus increase is the logical consequence of *strain amplification* due to the replacement of a part of elastomeric deformable phase by a particulate rigid filler: for a macroscopic deformation ε, the *local* deformation of

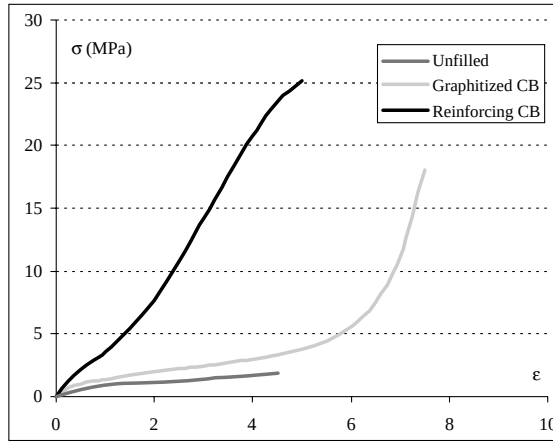

FIGURE 8 Stress–strain curve of unfilled, graphitized, and reinforcing carbon black samples. (Data from Medalia and Kraus [41].)

bridging chains is much higher. Strain amplification should also induce a neat decrease in elongation at break, which is not observed: here is the paradox.

Even if this point clearly remains mainly undecided, one way to surpass this paradox is to consider that fillers allow a locally more cooperative sharing of the stress.

In the early 1960, Bueche was probably the first to consider carbon black as a part of a polyfunctional network [1, 2]. In his model, carbon black aggregates were chemically linked by chains and constitute what Medalia and Kraus describe as a "giant multifunctional crosslink" network [41].

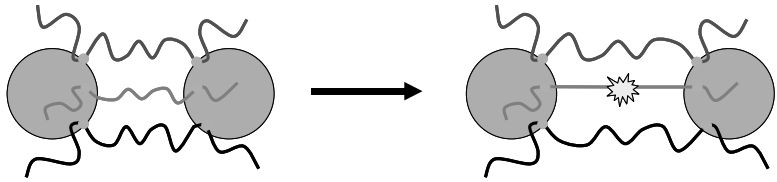

Even if Bueche's model tried to give a molecular origin of reinforcement, it remains difficult to consider that it ensures a massive local sharing of the stress: when the shortest chain reaches its finite extensibility, it is really not evident that a large part of the stress is shared by other bridging chains. Moreover, Bueche's model supposes chemical bonding of elastomeric chains, which is, *a minimo*, debatable (see previous text). In any case, it must be mentioned that chain breaks during extension have been demonstrated using ESR [147].

At the end of the 1960s, Dannenberg completely renewed reinforcement understanding by proposing the "molecular slippage" model that we have previously used to illustrate Payne's effect [5, 118]. In contrast to Bueche, Dannenberg suggested that interaction between elastomer and carbon black was mainly caused by adsorption and not by chemical bonding. Because of its low energy and reversibility, adsorption permits elastomer–filler contacts to change continuously and so allows the homogenization of bridging segment lengths, which ensures the local sharing of stress [41, 122].

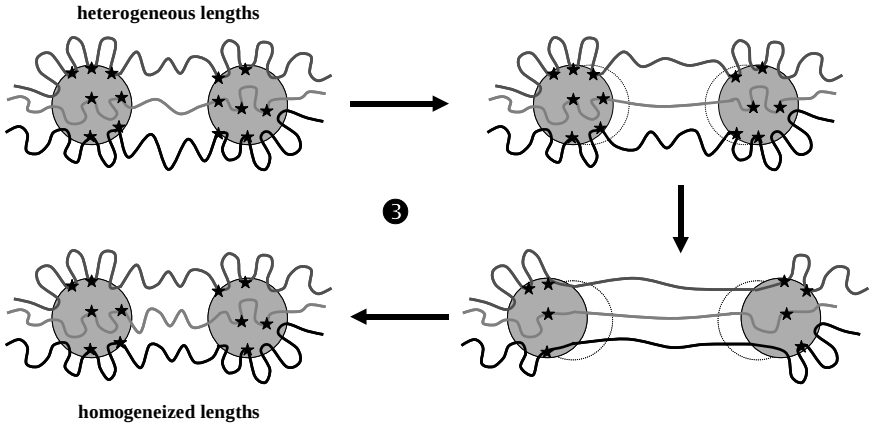

It is noteworthy that the concept of "giant multifunctional crosslink" network associated with the "molecular slippage" model proposes a possible mechanism for length homogenization of bridging chains and gives a rather satisfactory answer to the reinforcement paradox. So the increase of modulus in phase ❸ is due to this stress sharing between bridging chains.

Obviously, the obtained homogenization directly depends on the maximum strain at which the compound has been accommodated. In other words, chain segment lengths are homogenized for any strain below the maximum strain; at higher strains, a new homogenization should occur [148]. This naturally corresponds to the so-called stress softening effect previously described [146].

The stress sharing by segment homogenization is naturally limited by the number of bridging segments between reinforcing objects; when all connecting chains reach approximately the same length, modulus is at its maximum. A further increase of strain produces total chain slippage of the shortest chain; then the number of bridging segments decreases (phase ❹). Each remaining bridging chain must support an increased force that produces their massive dewetting and macroscopic break. The filler dewetting under strain has been evidenced by TEM direct observation [149].

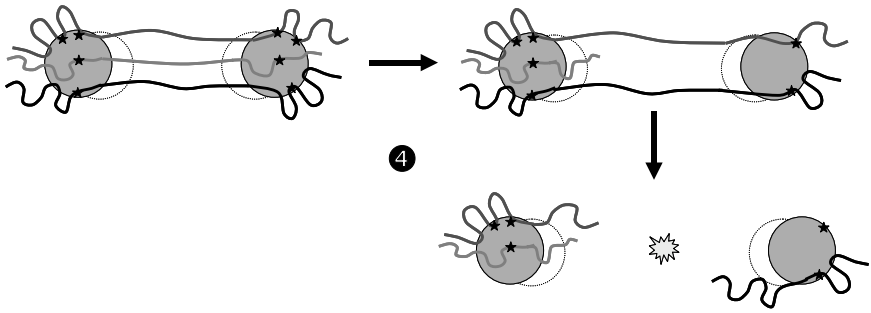

C. Applications

As discussed in the introduction, reinforcement of elastomers can only be considered for a specific application, because it corresponds to an increase of product service life. Hence, in order to give some practical illustration of the different topics discussed earlier, we will present some results about carbon

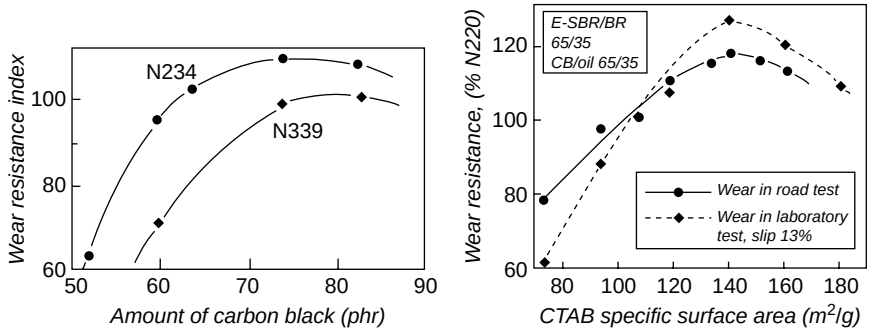

FIGURE 9 Wear resistance index versus carbon black loading and surface area. (From Sone [108].)

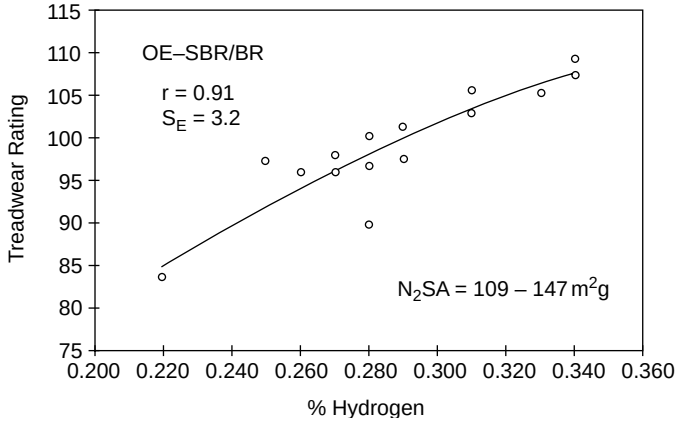

FIGURE 10 Treadwear versus carbon black hydrogen content [81].

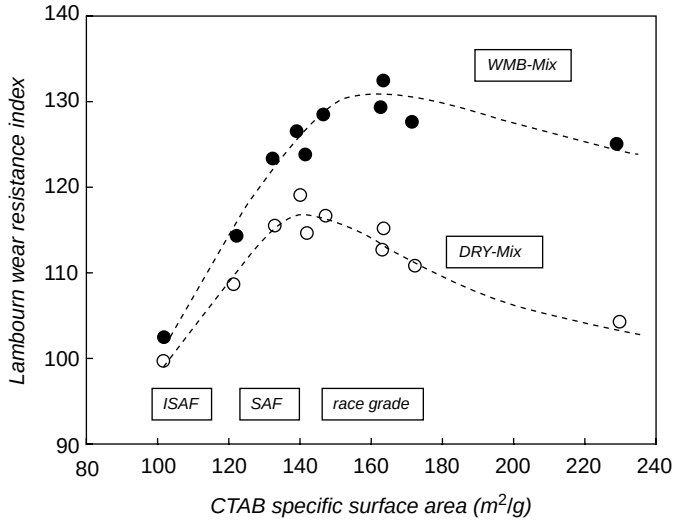

FIGURE 11 Comparision of abrasion resistance for dry mixes and masterbatches. (From Sone, Ishiguro, Akimoto *et al.* [104].)

black reinforcement for materials subjected to wear, for example reinforced compounds used for tire treads.

Carbon black loading, surface area, and structure basically increase wear resistance; for very high loadings or surface area, a significant decrease in wear resistance is observed (Fig. 9); this effect can be attributed to deficient dispersion [108].

Carbon black surface activity, as revealed by hydrogen content, has also a significant influence on wear resistance [81] (Fig. 10).

Carbon black dispersion also influences abrasion resistance, and the maximum observed for high carbon black loadings and surface area can be significantly shifted by using specific dispersion techniques like masterbatching [104, 150] (Fig. 11).

REFERENCES

1. F. Bueche, *J. Appl. Polym. Sci.* **5**, 271 (1961).
2. F. Bueche, *J. Appl. Polym. Sci.* **4**, 107 (1960).
3. J.-B. Donnet and G. Heinrich, *Bull. Soc. Chim. Fr.* p. 1609 (1960).
4. J. Le Bras and E. Papirer, *J. Appl. Polym. Sci.* **22**, 525 (1983).
5. E. M. Dannenberg, *Rubber Chem. Technol.* **48**, 410 (1975).
6. J.-B. Donnet, E. Papirer, and A. Vidal, Grafting of Macromolecules onto Carbon Blacks, "Chem. and Physics of Carbon," P. L. Walker, Jr. and P. A. Thrower (Eds.), Marcel Dekker, New York, 1975.

7. N. Tsubokawa and M. Hosoya, *Reactive Polym.* **14**, 33 (1991); N. Tsubokawa and M. Hosoya, *Reactive Polym.* **14**, 95 (1991).
8. M. J. Wang, T. A. Brown, W. J. Patterson, and R. A. Francis, International Rubber Conference 1997, Kuala Lumpur, 6–9 October 1997.
9. EP1034222, E. Custodero, L. Simonot, and J.-C. Tardivat, Carbon black coated with an aluminous layer and method for obtaining same (1997).
10. A. Voet, J. C. Morawski, and J. B. Donnet, *Rubber Chem. Technol.* **50**, 342 (1977).
11. S. Wolff, International Rubber Conferences, 14–17 October 1975, p. 295; S. Wolff, *Kautchuk Gummi Kunstoffe* **34**, 280 (1981).
12. EP0501227 and R. Rauline, Rubber compound and tires based on such a compound (1991).
13. A. P. Legrand, in "The Surface Properties of Silicas," A. P. Legrand (Ed.), J. Wiley and Sons, New York, Vol. 1, 1998, pp. 1–18.
14. EP0157703, Y. Chevallier, and J. C. Morawski, Precipitated silica with morphological properties, process for producing it and its application, especially as a filler (1984); Y. Chevallier, and J. C. Morawski, *EUCHEM* (1986).
15. N. A. Shabanova and I. V. Silos, *Colloid J.* **58**, 256 (1996).
16. EP0890602, W. L. Hergenrother, J. C. Oziomek, and M. William, Addition of salts to improve the interaction of silica with rubber (1997).
17. Y. Bomal, Y. Chevallier, and P. Cochet, Novel method for preparing precipitated silica, novel aluminium-containing precipitated silicas, and use thereof for reinforcing elastomers, patent WO9630303, (1995).
18. WO9928376, E. Custodero, L. Simonot, and J.-C. Tardivat, Reinforcing aluminous filler and rubber composition comprising such a filler (1997).
19. EP0810258, E. Custodero, and J.-C. Tardivat, Diene rubber composition containing alumina as reinforcing filler and use in tire treads (1996).
20. EP1114092, E. Custodero, L. Simonot, and J.-C. Tardivat, Rubber composition for tyre, based on diene elastomer and a reinforcing titanium oxide (1999).
21. WO2002053634, L. Simonot, T. Chartier, and E. Custodero, Rubber composition made with diene elastomer and a reinforcing silicon carbide (2002); WO2004003067, L. Simonot, A. Lapra, A. Veyland, and E. Custodero, Rubber composition based on diene elastomer and a reinforcing silicon nitride (2002).
22. W. M. Hess, G. C. McDonald, and E. Urban, *Rubber Chem. Technol.* **46**, 204 (1973).
23. W. M. Hess, *Rubber Chem. Technol.* **64**, 386 (1991).
24. E. Custodero, "Caractérisation de la surface des noirs de carbone, nouveau modèle de surface et implications pour le renforcement," Ph.D. Thesis, Université de Haute Alsace, 1992.
25. N. Probst and J. B. Donnet, "Differentiation of Carbon Black Particularities by Scanning Tunneling Microscopy," 2nd International Conference on Carbon Black, 1993, pp. 261–263.
26. J.-B. Donnet and E. Custodero, *C. R. Acad. Sci., Ser. 2* **314**, 579 (1992).
27. J.-B. Donnet and E. Custodero, *Carbon* **30**, 813 (1992).
28. J.-B. Donnet and T. K. Wang, *Analusis* **22**, M24 (1994); J.-B. Donnet, E. Custodero, and T. K. Wang, *Kautsch. Gummi Kunstst.* **49**, 274 (1996).
29. C. R. Herd, G. C. McDonald, and W. M. Hess, *Rubber Chem. Technol.* **65**, 107 (1992).
30. ASTM D2663.
31. ASTM D1765.
32. J. Janzen and K. Kraus, *Rubber Chem. Technol.* **44**, 1287 (1971).
33. J. Janzen, *Rubber Chem. Technol.* **55**, 669 (1982).
34. G. Kraus and J. Jansen, *Kautchuk Gummi Kunstoffe* **31**, 569 (1978).
35. W. A. Wampler, *The Carbon Aggregate* **5**, 2 (1997).
36. R. W. Magee, *Rubber Chem. Technol.* **68**, 590 (1995); R. W. Magee, *The Carbon Aggregate*, **2**, 1 (1995).
37. R. H. Bradley, I. Sutherland, and E. Sheng, *J. Colloid Interface Sci.* **179**, 561 (1996).
38. M. Bele, A. Kodre, J. Grdadolnik, S. Pejovnik, and J. O. Besenhard, *Carbon* **36**, 1207 (1998).

39. W. A. Wampler, M. Gerspacher, and C. P. O'Farrell, *The Carbon Aggregate* **4**, 3 (1997).
40. B. R. Puri and R. C. Bansal, *Carbon* **3**, 227 (1965).
41. A. I. Medalia and G. Kraus, Reinforcement of Elastomers by Particulate Fillers, in "Science and Technology of Rubber," 2nd ed., J. E. Mark, B. Erman, and F. R. Eirich (Eds.), Academic Press, San Diego, 1994.
42. W. M. Hess and G. C. McDonald, *Rubber Chem. Technol.* **56**, 892 (1983).
43. T. C. Gruber, T. W. Zerda, and M. Gerspacher, *Carbon* **37**, 1209 (1993).
44. D. Creeden, *The Carbon Aggregate* **4**, 1 (1997).
45. R. E. Dollinger, R. H. Kallenberg, and M. L. Studebaker, *Rubber Chem. Technol.* **40**, 1311 (1967).
46. R. Pirard, B. Sahouli, S. Blacher, and J. P. Pirard, *J. Colloid Interface Sci.* **217**, 216 (1999).
47. L. Moscou, S. Lub, and O. K. F. Bussemaker, *Rubber Chem. Technol.* **44**, 805 (1971).
48. L. R. Evans and W. H. Waddell, *Kautchuk Gummi Kunstoffe* **48**, 718 (1995).
49. D. R. Milburn, B. D. Adkins, and B. H. Davis, in "Characterization of Porous Solids," K. K. Unger (Ed.), Elsevier, Amsterdam, 1988, pp. 501.
50. I. B. Paul, T. N. Roy, and P. N. Mukherjee, *Indian Journal of Technology* **20**, 441 (1982).
51. D. Göritz, J. Böhm, and B. Freund, International Rubber Conference 1997, Kuala Lumpur, 6–9 October 1997, pp. 201–205.
52. T. Allen, Photocentrifuges, *Powder Technol.* **50**, 193 (1987).
53. A. C. Patel and K. W. Lee, *Elastomerics* **122**, 14 (1990); A. C. Patel and K. W. Lee, *Elastomerics* **122**, 22 (1990).
54. A. I. Medalia and L. W. Richards, *J. Colloid Interface Sci.* **40**, 233 (1972).
55. A. I. Medalia and L. W. Richards, *J. Colloid Interface Sci.* **40**, 233 (1972).
56. A. I. Medalia, E. M. Dannenberg, F. A. Heckmann, and G. R. Cotten, *Rubber Chem. Technol.* **46**, 1239 (1976).
57. P. Cochet, P. Barruel, L. Barriquant, J. Grobert, Y. Bomal, and E. Prat, *Meeting Rubber Div. Amer. Chem. Soc. Orlando*, 26–29 October 1993, pp. 1–43; P. Cochet, P. Barruel, L. Barriquand, J. Grobert, Y. Bomal, and E. Prat, *Rubber World*, pp. 20–24 (1994).
58. R. A. Beebe, M. H. Polley, W. R. Smith, and C. B. Wendell, *J. Am. Chem. Soc.* **69**, 2294 (1947).
59. M. L. Gonzalez-Martin, B. Janczuk, L. Labajos-Broncano, and J. M. Bruque, *Langmuir* **13**, 5991 (1997).
60. J.-B. Donnet, T. K. Wang, Y. J. Li, H. Balard, and G. T. Burns, *Rubber Chem. Technol.* **73**, 634 (2000).
61. S. Wolff, E. H. Tan, and J. B. Donnet, *Kautch. Gummi Kunstoffe* **47**, 485 (1994).

61a. J.-B. Donnet and C. M. Lansinger, *Kautchuk Gummi Kunstoffe* **45**, 459 (1992).

62. S. Wolff and M. J. Wang, *Rubber Chem. Technol.* **65**, 329 (1992).
63. M. J. Wang and S. Wolff, *Meeting Rubber Div. Amer. Chem. Soc.*, Detroit, 8–11 October, (1991); M. J. Wang, S. Wolff, and J. B. Donnet, *Rubber Chem. Technol.* **64**, 714 (1990).
64. M. J. Wang, S. Wolff, and J. B. Donnet, *Rubber Chem. Technol.* **64**, 559 (1991).
65. J. Jagiello, G. Ligner, and E. Papirer, *J. Colloid Interface Sci.* **137**, 128 (1990).
66. A. Lapra, E. Custodero, and N. Simon, *Kautschuk Gummi, Kunststoffe.* **57**, 52 (2004).
67. B. Schubert, F. P. Ford, and F. Lyon, *Encyclopedia of Industrial Chemical Analysis* **8**, 1 (1969).
68. M. L. Deviney, *Adv. Colloid Interf. Sci.* **2**, 237 (1969).
69. G. T. Taylor, T. E. Redington, and M. J. Bayley, *Am. Ind. Hyg. Assoc. J.* **41**, 819 (1980).
70. D. S. Villars, *J. Am. Chem. Soc.* **69**, 214 (1947).
71. H. P. Boehm, *Angew. Chem.* **78**, 617 (1966); H. P. Boehm, *Farbe Lak* **79**, 419 (1973).

71a. J.-B. Donnet, G. Heinrich, and G. Riess, *Rev. Gen. Caoutch. Plast.* **38**, 1803 (1961); J.-B. Donnet, G. Heinrich, and G. Riess, *Rev. Gen. Caoutch. Plast.* **41**, 519 (1964).

72. H. P. Boehm, *Carbon* **32**, 759 (1994).
73. P. Bertrand and L. T. Weng, *Rubber Chem. Technol.* **72**, 384 (1998).
74. D. Rivin, *Rubber Chem. Technol.* **36**, 729 (1963); D. Rivin, *Rubber Chem.Technol.* **44**, 307 (1971).
75. J. E. Lewis, L. R. Deviney, Jr., and C. F. McNabb, *Rubber Chem. Technol.* **43**, 449 (1970).

76. E. Papirer, V. T. Nguyen, and J. B. Donnet, *Carbon* **16**, 141 (1978).
77. D. Rivin, J. Aron, and A. I. Medalia, *Rubber Chem. Technol.* **41**, 330 (1968).
78. W. F. Watson, *Ind. Eng. Chem.* **47**, 1281 (1955).
79. E. Papirer, A. Voet, and P. H. Given, *Rubber Chem. Technol.* **42**, 1200 (1969).
80. E. Papirer, J. B. Donnet, and J. Heinkele, *J. Chim. Phys.* **68**, 581 (1971).
81. W. M. Hess, J. A. Ayala, P. C. Vegvari, and F. D. Kistler, *Kautsch. Gummi Kunstst.* **41**, 1215 (1988); M. Soeda and Y. Kurata, *Nippon Gomu Kyokaishi* **68**, 616 (1995).
82. S. Läufer, *J. Molec. Struct.* **60**, 409 (1980).
83. B. Humbert, *J. Non-Crystalline Solids* **191**, 29 (1995).
84. M. Zaborski, A. Vidal, G. Ligner, H. Balard, E. Papirer, and A. Burneau, *Langmuir* **5**, 447 (1989).
85. A. Hunsche, U. Görl, A. Müller, M. Knaack, and T. Göbel, *Kautchuk Gummi Kunstoffe* **50**, 881 (1997).
86. U. Görl, A. Hunsche, A. Müller, and H. G. Koban, *Rubber Chem. Technol.* **70**, 608 (1997).
87. N. Cardona-Martinez and J. A. Dumesic, *J. Catal.* **125**, 427 (1990); J. Uytterhoeven and J. J. Fripiat, *Bull. Soc. Chim. Fr.* 788 (1962).
88. G. R. Cotten, *Meeting Rubber Div. Amer. Chem. Soc.* Houston, 25–28 October 1983, p. 38.
89. J. M. Funt, *Rubber World* (February), 21 (1986).
90. M. Gerspacher and C. P. O'Farrell, *Rubber Plastics News* **23**, 85 (1993).
91. F. Bomo and J. C. Morawski, *ACS, Rubber Div., Houston*, October, (1983).
92. B. R. Richmond, *IRC 1993 Conference Proceedings*, Orlando, 26–29 October 1993, Paper 158.
93. Y. Bomal, P. Cochet, B. Dejean, I. Gelling, and R. Newell, *Kautchuk Gummi Kunstoffe* **51**, 259 (1998).
94. Y. Bomal, P. Cochet, B. Dejean, and J. Machurat, *Rubber World*, **6**, 33 (1993).
95. B. B. Boonstra and A. I. Medalia, *Rubber Age* **92**, 892 (1963); B. B. Boonstra and A. I. Medalia, *Rubber Age* **93**, 82 (1963).
96. S. Shiga and M. Furuta, *Rubber Chem. Technol.* **58**, 1 (1985).
97. L. Nikiel, M. Gerspacher, H. Yang, and C. P. O'Farrell, *157th ACS Rubber Division Meeting Dallas*, 4–6 April 2000, Paper 31.
98. A. Y. Coran and J. B. Donnet, *Rubber World* **65**, 1016 (1993); A. Y. Coran, and J. B. Donnet, *Rubber Chem. Technol.* **65**, 998 (1993).
99. W. M. Hess, C. R. Herd, and E. B. Sebok, *Kautchuk Gummi Kunstoffe* **47**, 328 (1994).
100. S. Maas and W. Gronski, *Kautchuk Gummi Kunstoffe* **47**, 409 (1994).
101. A. Lapra, "Caractérisation moléculaire et propriétés mécaniques des réseaux élastomères SBR renforcés par la silice," Université Paris VI, 1999.
102. F. Ehrburger-Dolle, M. Hindermann-Bischoff, F. Livet, F. Bley, and C. Rochas, *Langmuir* **17** 329 (2001).
103. A. P. Legrand, N. Lecomte, A. Vidal, B. Haidar, and E. Papirer, *J. Appl. Polym. Sci.: Appl. Polym. Symp.* **46**, 2223 (1992).
104. K. Sone, M. Ishiguro, H. Akimoto, and M. Ishida, *Rubber World* **206**, 29 (1992).
105. R. J. Young, D. H. A. Al-Khudhairy, and A. G. Thomas, *J. Mater. Sci.* **21**, 1211 (1986).
106. G. C. McDonald and W. M. Hess, *Rubber Chem. Technol.* **50**, 842 (1977).
107. A. I. Medalia, *Rubber Chem.Technol.* **59**, 432 (1986).
108. K. Sone, *Int. Polym. Sci. Technol.* **26**, 60 (1999).
109. J. O'Brien, E. Cashell, G. E. Wardell, and V. J. McBrierty, *Macromol.* **9**, 653 (1976); V. J. McBrierty and J. C. Kenny, *Kautchuk Gummi Kunstoffe* **47**, 342 (1994).
110. T. A. Vilgis and G. Heinrich, *Macromol.* **27**, 7846 (1994).
111. S. Kaufmann, W. P. Slichter, and D. D. Davis, *J. Polym. Sci. A* **9**, 829 (1971).
112. F. De Candia, M. Carotenuto, L. Gargani, L. Guadagno, and E. Lauretti, *Kautchuk Gummi Kunstoffe* **49**, 99 (1996).

112a. J. Leisen, J. Breidt, and J. Kelm, *Rubber Chem. Technol.* **72**, 1 (1998).

113. M. E. Semaan, L. Nikiel, and C. A. Quarles, *Carbon* **39**, 1379 (2001).
114. G. Kraus, *Fortschr. Hochpolym. Forsch.* **8**, 155 (1971).
114a. Z. Rigbi, *Kautchuk Gummi Kunstoffe* **46**, 36 (1993).
115. P. B. Stickney and R. D. Falb, *Rubber Chem. Technol.* **37**, 1299 (1964); G. Kraus, *Rubber Chem. Technol.* **38**, 1070 (1965); L. L. Ban, W. M. Hess, and L. A. Papazian, *Rubber Chem. Technol.* **47**, 858 (1974).
116. D. S. Villars, *J. Polym. Sci.* **21**, 257 (1996).
117. L. L. Ban, W. M. Hess, and L. A. Papazian, *Rubber Chem. Technol.* **47**, 585 (1974).
118. E. M. Dannenberg, *Rubber Chem. Technol.* **59**, 512 (1986).
119. B. Meissner, *J. Appl. Polym. Sci.* **18**, 2483 (1974); B. Meissner, *J. Appl. Polym. Sci.* **50**, 285 (1993).
120. S. Wolff, M. J. Wang, and E. H. Tan, *Rubber Chem. Technol.* **66**, 163 (1993).
121. W. B. Wiegand, *Trans. Inst. Rubber Ind.* **1**, 141 (1925).
122. E. M. Dannenberg and J. J. Brennan, *Rubber Chem. Technol.* **39**, 597 (1966); E. M. Dannenberg, *Trans. Inst. Rubber Ind.* **42**, T26 (1966).
123. J. Le Bras and E. Papirer, *Rubber Chem. Technol.* **52**, 43 (1979).
124. H. Hommel, A.-P. Legrand, H. Balard, and E. Papirer, *Makromol. Chem*. **194**, 879 (1993).
125. F. Bomo, *Makromol. Chem., Macromol. Symp.* **23**, 321 (1989).
126. H. G. Killian, H. Schenk, and S. Wolff, *Colloid Polym. Sci.* **265**, 410 (1987).
127. M. Ashida, K. Abe, and T. Watanabe, *Int. Polym. Sci. Technol*. **4**, T42 (1977).
128. M. Strauss, H. G. Killian, B. Freund, and S. Wolff, *Colloid Polym. Sci.* **272**, 1208 (1994).
129. E. Guth and O. Gold, *Phys. Rev.* **53**, 322 (1938).
130. A. I. Medalia, *Rubber Chem. Technol.* **47**, 411 (1974).
131. G. Kraus, *J. Polym. Sci. B* **8**, 601 (1970).
132. A. I. Medalia, *Rubber Chem.Technol.* **46**, 877 (1973).
133. A. I. Medalia, *J. Colloid Interface Sci.* **32**, 115 (1970).
134. A. I. Medalia, *Rubber Chem.Technol.* **47**, 411 (1974).
135. H. M. Smallwood, *J. Appl. Phys.* **15**, 758 (1944).
136. J. A. C. Harwood, L. Mullins, and A. R. Payne, *J. Appl. Polym. Sci.* **9**, 3011 (1965); J. A. C. Harwood and A. R. Payne, *J. Appl. Polym. Sci.* **10**, 315 (1966); J. A. C. Harwood, A. R. Payne, and J. F. Smith, *Rubber Chem. Technol.* **43**, 687 (1970).
137. A. I. Medalia, *Rubber Chem.Technol.* **64**, 481 (1991).
138. B. Duperray and J.-L. Leblanc, *Kautsch. Gummi Kunstst.* **35**, 298 (1982).
139. A. R. Payne, in "Reinforcement of Elastomers," G. Kraus (Ed.), Wiley Interscience, New York, 1965, Chap. 3.
140. J. O. Harris and R. W. Wise, in "Reinforcement of Elastomers," G. Kraus (Ed.), Wiley Interscience, New York, 1965.
141. M. J. Wang, S. Wolff, and E. H. Tan, *Rubber Chem. Technol.* **66**, 178 (1993).
142. N. Nagata, T. Kobatake, H. Watanabe, A. Ueda, and A. Yoshioka, *Rubber Chem. Technol.* **60**, 837 (1987).
143. F. Tsutsumi, M. Sakakibara, and N. Oshima, *Rubber Chem. Technol.* **63**, 8 (1990).
144. I. Soos, *Int. Polym. Sci. Technol.* **9**, T84 (1982); I. Soos, *Int. Polym. Sci. Technol.* **10**, T77 (1983); I. Soos, *Int. Polym. Sci. Technol.* **11**, T4 (1984).
145. L. Mullins and N. R. Tobin, *J. Appl. Polym. Sci.* **9**, 2993 (1965).
146. L. Mullins, *Rubber Chem. Technol.* **42**, 339 (1969).
147. A. B. Sullivan and R. W. Wise, *Proc. 5th Int. Rubber Conf.* 235 (1967).
148. A. N. Gent, *J. Appl. Polym. Sci.* **18**, 1397 (1974).
149. W. M. Hess, F. Lyon, and K. A. Burgess, *Kautsch. Gummi Kunstst.* **20**, 135 (1967).
150. M. J. Wang, P. Zhang, K. Mahmud, T. Lanoye, and V. Vejins, *Tire Technology International* **58**, 54, December 7 (2002).

9 The Science of Rubber Compounding

BRENDAN RODGERS AND WALTER WADDELL
ExxonMobil Chemical Company
Houston, Texas

I. INTRODUCTION

Compounding, a term that has evolved within the tire and rubber industry, is the materials science of modifying a rubber or elastomer or a blend of polymers and other materials to optimize properties to meet a given service application or set of performance parameters. Compounding is therefore a complex multidisciplinary science necessitating knowledge of materials physics, organic and polymer chemistry, inorganic chemistry, and chemical reaction kinetics. The materials scientist, when designing a rubber formulation, has a range of objectives and restrictions within which to operate. Product performance requirements will dictate the initial selection of formula ingredients. These materials must be environmentally safe, meet occupational health and safety requirements, be processable in the product manufacturing facilities, and be cost effective.

Compounded rubber has many unique characteristics not found in other materials, such as dampening properties, high elasticity, and abrasion resistance. Hence rubber has found use in applications such as tires, conveyor belts, large dock fenders, building foundations, automotive engine components, and a wide range of domestic appliances. The ingredients available to the materials scientist for formulating a rubber compound can be divided into five categories:

Science and Technology of Rubber, Third Edition

1. Polymers	Natural rubber, synthetic polymers
2. Filler systems	Carbon blacks, clays, silicas, calcium carbonate
3. Stabilizer systems	Antioxidants, antiozonants, waxes
4. Vulcanization system components	Sulfur, accelerators, activators
5. Special materials	Secondary components such as pigments, oils, resins, processing aids, and short fibers

Each class of materials is reviewed in this chapter.

II. POLYMERS

World rubber usage of around 18 million metric tons is split between natural rubber, which constitutes about 46% of global consumption, and synthetic rubber, of which styrene–butadiene rubber (SBR) accounts for about 18%. The balance of synthetic rubbers (47%) consists of polybutadiene rubber and a range of speciality polymers such as urethanes, halogenated polymers, silicones, and acrylates. Traditionally, the growth of synthetic and natural rubber consumption is virtually in line with the gross national product of, collectively, North America, the European Community, and the northwest Pacific rim [1, 2].

A. Natural Rubber

Global natural rubber consumption is split among tires (75%), automotive mechanical products (5%), nonautomotive mechanical products (10%), and miscellaneous applications such as medical and health-related products (10%). Since the 1960s, the quality and consistency of natural rubber has improved, primarily because of the implementation of standard specifications defining a range of grades of rubber. Natural rubber is available in three basic types: technically specified rubbers, visually inspected rubbers, and specialty rubbers.

The American Society for Testing and Materials (ASTM) describes six basic grades of coagulated technically specified natural rubber which is processed and compacted into 34-kg blocks [3] (Table I). These six general grades of technically specified natural rubber are defined in more detail by the respective producing countries. Standard Malaysian Rubber (SMR), Standard Indonesian Rubber (SIR), and Thai Technical Rubber (TTR) expand the range of rubbers available. For example, two constant-viscosity Standard Malaysian Rubber CV grades are available, SMR CV50 and CV60 [2]. SMR 10 and SMR 20 grades are also available as viscosity stabilized (SMR 10CV and SMR 20CV).

The Rubber Manufacturers Association has a further set of standards for quality and packing of latex natural rubber grades. Table II defines the eight

TABLE I Specifications for Technically Graded Natural Rubber

Property	Rubber grade					
	L	CV	5	10	20	50
Dirt (% maximum)	0.050	0.050	0.050	0.100	0.200	0.500
Ash (% maximum)	0.60	0.60	0.60	0.750	1.00	1.50
Volatile matter (%)	0.80	0.80	0.80	0.80	0.80	0.80
Nitrogen (%)	0.60	0.60	0.60	0.60	0.60	0.60
Plasticity	30	—	30	30	30	30
Plasticity retention index	60	60	60	50	40	30
Color index	6.0	—	—	—	—	—
Mooney Viscosity	—	60	—	—	—	—

TABLE II International Natural Rubber Type and Grade Specification

Type	Natural rubber	Description
1	Ribbed smoked sheet	Coagulated sheets, dried, and smoked latex. Five grades available (RSS1–5)
2	White and pale crepe	Coagulated natural liquid latex milled to produce a crepe
3	Estate brown crepe	Fresh lump and other high-quality scrap generated on the plantation
4	Compo crepe	Lump, tree scrapes, and smoked sheet cuttings are milled into a crepe
5	Thin brown crepe	Unsmoked sheets, wet slab, lump, and other scrap from estates and small holdings
6	Thick blanket crepe	Wet slab, lump, and unsmoked sheets milled to give a crepe
7	Flat bark crepe	All types of scrap natural rubber including earth scrap
8	Pure smoked blanket crepe	Milled smoked rubber derived exclusively from ribbed smoked sheets

types of rubber covered in their specifications. Here, coagulated latex is sheeted, dried, and packed into bales of up to 113.5 kg. Grading is by visual inspection. Quality assurance laboratories have sets of visual standards for inspections [4].

The third category of natural rubbers are the specialty materials, which include liquid low molecular weight rubber, methyl methacrylate grafted polymers, oil-extended natural rubber, deproteinized natural rubber, epoxidized natural rubber, and superior-processing natural rubber.

Natural rubber usage has increased substantially in modern radial tires. Bernard and coworkers [5] compared the natural rubber levels of heavy-duty radial truck tires to those of the equivalent bias tire and noted the following increase:

Natural rubber (%)	Bias	Radial
Tread	47	82
Skim coat	70	100
Sidewall	43	58

The reasons for the increase have been attributed to improved green strength, increase in component-to-component adhesion, improved tear strength, lower tire temperatures generated under loaded dynamic service conditions, and lower tire rolling resistance to improve vehicle fuel efficiency.

The increase in natural rubber usage translates into approximately 21 kg per tire for a radial construction compared with approximately 9 kg found in a bias truck tire. Natural rubber compounds also tend to find use in covers of high-performance conveyor belts where a similar set of performance parameters such as those of a truck tire tread compound are found. Low hysteretic properties, high tensile strength, and good abrasion resistance are required for both products.

B. Synthetic Elastomers

Classification of synthetic rubber is governed by the International Institute of Synthetic Rubber Producers (IISRP). In the case of styrene–butadiene rubber, polyisoprene rubber, and polybutadiene, a series of numbers have been assigned which classify the general properties of the polymer [6]. For example, the IISRP 1500 series defines cold emulsion-polymerized (i.e., below 10°C), nonpigmented SBR. The 1700 series of polymers describes oil extended cold emulsion SBR. Table III illustrates the general numbering used by IISRP. The numbering system for solution-polymerized stereo elastomers is given in Table IV.

Tire production consumes approximately 60% of the global synthetic rubber production. Of this, SBR is the largest-volume polymer, representing over 65% of the synthetic rubber used in tires. Polybutadiene (BR) ranks second in production output [1, 2]. Tables V–VII illustrate the consumption of synthetic rubber by product group. Styrene butadiene rubber finds extensive use in tire treads because it offers wet skid and traction properties while retaining good abrasion resistance. Polybutadiene (BR) is frequently found in treads, sidewalls, and some casing components of the tire because it offers good abrasion resistance, and tread wear performance and enhances resistance to cut propagation. BR can also be blended with natural rubber, and many

TABLE III Classification of Synthetic Rubbers by IISRP

Class number	Description
1000 series	Hot nonpigmented emulsion SBR (polymerized above 38°C)
1500 series	Cold nonpigmented emulsion SBR (polymerized below 10°C)
1600 series	Cold polymerized/carbon black master batch/14 phr oil (max) SBR
1700 series	Oil extended cold emulsion SBR
1800 series	Cold emulsion-polymerized/carbon black master batch/more than 14 phr oil SBR
1900 series	Emulsion resin rubber master batches

TABLE IV IISRP Solution-Polymerized Stereo Elastomers

	Butadiene and copolymers	Isoprene and copolymers
Dry polymer	1200–1249	2200–2249
Oil extended	1250–1299	2250–2299
Black master batch	1300–1349	2300–2349
Oil–black master batch	1350–1399	2350–2399
Latex	1400–1449	2400–2449
Miscellaneous	1450–1499	2450–2499

TABLE V Synthetic Rubber Consumption

Tires	60%
Automotive parts	10%
Nonautomotive mechanical goods	9%
Thermoplastic elastomer composites	6%
Footwear	4%
Construction	3%
Wire and cable	2%
Adhesives	1%
Miscellaneous goods	5%

authors have reported that such compositions give improved fatigue and cut growth resistance [7].

Before reviewing elastomer characteristics required to meet any given set of tire performance parameters, it is appropriate to identify two means by which the materials scientist may describe a polymer: polymer macrostructure

TABLE VI U.S. Consumption of SBR

Product	Percent of total consumption
Passenger tires	50
Retread rubber	13
Truck tires	8
Special tires (aircraft, earthmover, etc)	4
Automotive mechanical goods	7
Miscellaneous use (domestic appliances medical equipment, construction)	18

TABLE VII U.S. Consumption of Polybutadiene

Product	Percent of total consumption
Passenger tires	45
Truck tires	28
Retread rubber	4
Special tires (aircraft, earthmover, etc.)	1
Mechanical goods	2
Miscellaneous applications (polymer blends, polymer modifiers with polystyrene or styrene acrylonitrile butadiene terpolymers)	20

and polymer microstructure. The macrostructure of a polymer defines the molecular weight and also crosslink distribution, polymer chain branching, and crystallite formation. The arrangement of the monomers within a polymer chain constitutes its microstructure. Butadiene can adopt one of three configurations as illustrated in Fig. 1. These molecular configurations or stereochemistry can be described as follows:

vinyl-(1,2) The third and fourth carbon atoms are pendant; the first and second carbon atoms participate in the polymer backbone.

trans-(1,4) The hydrogen atoms attached to the carbon–carbon double bond on the polymer backbone are on opposite sides.

cis-(1,4) The two hydrogen atoms attached to the carbon–carbon double bond in the polymer are on the same side of the double bond.

Table VIII illustrates the effect of the catalyst system on polymer microstructure [10].

TABLE VIII Polybutadiene Microstructure

Catalyst	Isomer level to +/– 1% Cis-%	Trans-%	Vinyl-%
Li	35	55	10
Ti	91–94	2–4	4
Co	96	2	2
Nd	98	1	1
Ni	96–98	0–1	2–4

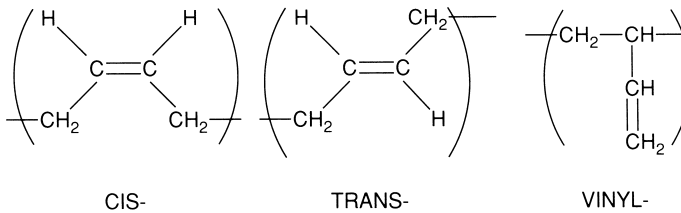

FIGURE 1 Polymer microstructure: possible configurations for butadiene in SBR and BR.

The relative levels of each of the three isomers in a polymer such as BR can have a dramatic effect on the material's performance. For example, lithium-catalyzed solution polymers, with approximately 36% *cis* content, tend to process easily, whereas high-*cis* Ti and Ni polymers (92% *cis*) are more difficult to process at factory processing temperatures but show better abrasion resistance. High-*trans* BR (93% *trans*) tends to be a tough, crystalline material at room temperature. High-vinyl butadiene BR polymers in tire treads tend to show good wet skid and wet traction performance [7–10].

Nordsiek [9] documented a series of empirical guidelines which might be used in designing a polymer for a set of tire performance targets. By preparing various blends of BR and SBR, Nordsiek produced a series of compounds in which the T_g increased from –100 to –30°C. He noted the following points:

1. As the T_g increases there is a near-linear drop in abrasion resistance.
2. Wet grip or traction improves nearly linearly with the increase in compound T_g.
3. Addition of a catalyst modifier during the preparation of solution-polymerized, lithium-catalyzed BR results in an increase in the 1,2-vinyl butadiene level in the polymer and causes an increase in T_g. There is a corresponding drop in abrasion resistance and an increase in wet traction.
4. Inclusion of styrene leads to an increase in traction performance and loss in abrasion resistance. There is a linear relationship between

TABLE IX Characterization of an Idealized Tread Compound: Tan δ Temperature Curve[a]

Temperature zone (°C)	Feature	Performance parameter
–60 to –40	T_g	Abrasion
–20		Low-temperature properties
+20	—	Wet traction
+40 to +60	—	Rolling resistance
+80 to +100	—	Heat buildup

[a]Data taken from Nordsiek [9].

styrene and vinyl-1,2-butadiene. Approximately two vinyl-1,2-butadiene units gave a tire traction performance equivalent to that of one styrene unit.

5. Inclusion of 3,4-isoprene in polyisoprene leads to an increase in T_g and a corresponding increase in traction, and an increase in the percentage incorporation of 1,2- or 3,4-piperylene in polypiperylenes results in a T_g increase, causing a loss in abrasion resistance and an increase in grip.

This allowed the tan δ temperature curve of a tread compound run from –100 to +100°C to be segmented into zones which would characterize that tire tread compound's performance (Table IX). Such property targets enabled development of the concept of "integral rubber"; i.e., a polymer can be designed to meet rolling resistance, traction, and tread wear targets without a drop in overall tire performance.

Day and Futamura [11] evaluated the impact of variation in l,2-butadiene and styrene content in SBR on the properties of a compounded formulation. Briefly, (1) an increase in styrene produced an increase in tensile strength, (2) an increase in vinyl-1,2-butadiene resulted in a drop in both tear strength and ultimate elongation, and (3) at equal T_g, neither vinyl-1,2-butadiene nor styrene level affected the formulation's hysteretic properties.

Brantley and Day then conducted a study to compare the tire performance of emulsion- and solution-polymerized SBR [12]. The authors noted that solution-polymerized polymers, which tend to have a narrower molecular weight distribution and lower T_g than equivalent emulsion-polymerized polymers, have lower hysteretic properties. They then showed that a solution SBR with the same bound styrene as an emulsion SBR will give lower rolling resistance, improved dry traction, and better tread wear. Emulsion SBR, however, tends to show better wet skid, wet traction, and wet handling performance. Kern and Futamura later elaborated on this work by evaluating the impact of

TABLE X Comparison of Emulsion and Solution-Polymerized SBR

Property	Emulsion SBR	Solution SBR
Viscosity (M_L1 + 4 at 100°C)	50	57
Time to optimum cure (min at 150°C)	40	25
Tensile strength (MPa)	26	21
Ultimate elongation (%)	400	300
Rebound (%)	48	61

vinyl-1,2-butadiene level in a solution SBR and again comparing this with an emulsion SBR [13]. Though this work was conducted with passenger tires, many of the principles should be applicable to the range of tires such as light truck and heavy-duty truck tires.

The authors collected the test data shown in Table X. From these data it can be noted that the number-average molecular weight, or M_n, of a commercial emulsion SBR such as IISRP 1500 or 1712 is typically 90,000 to 175,000. The primary molecular weight of a solution-polymerized polymer produced with an anionic lithium catalyst can, in contrast, be increased toward 250,000 without gelation. In addition, emulsion-polymerized SBR contains only about 92% rubber hydrocarbon as a result of the presence of residues from the production process; solution polymers tend to be near 100% hydrocarbon. As a consequence, the authors concluded that the number-average molecular weight can be considered the key parameter of polymer macrostructure, particularly with respect to the hysteretic characteristics of a tread formulation. Hence the differences in macrostructure between emulsion- and solution-polymerized polymers will dictate many of their properties in a tire tread compound.

When considering only solution polymers, polymer microstructure has a greater effect on tire tread compound performance. Table XI illustrates the impact on tire traction, rolling resistance, and tread wear of a polybutadiene tread on which the vinyl-1,2-butadiene level had been increased from 10 to 50% [12]. The corresponding drop in wear and increase in tire rolling resistance are in agreement with the empirical rules presented by Nordsiek [9] who attributed such tire property trends to the polymer T_g.

Table XII shows how polybutadiene microstructure and macrostructure, i.e., molecular weight, Mw, and Mn, polydispersity, and branching can effect the processability of a polymer [14]. A study with both cobalt- and neodenium-catalyzed polybutadiene showed the relationship between polydispersity or molecular weight distribution and increases in stress relaxation. Increases in stress relaxation, as measured by the Mooney viscometer, will infer greater

TABLE XI Effect of Polymer Butadiene Vinyl Level on Tire Performance

Vinyl level	10%	50%
Glass transition temperature	–90°C	–60°C
Tire properties[a]		
Wet traction	100	120
Rolling resistance rating	100	95
Tread wear rating	100	90

[a]Higher rating is better.

TABLE XII Macrostructure and Mooney Viscometry [14]

Catalyst	Polymer sample	M_w	M_n	M_w/M_n	M_L1+4	Mooney stress relaxation
Cobalt	1	338	156	2.17	47	4.50
	2	318	131	2.43	45	7.50
	3	321	125	2.57	46	9.00
	4	303	108	2.81	44	14.00
Neodenium	1	353	186	2.10	50	5.00
	2	381	103	3.70	42	8.00
	3	347	87	3.99	44	9.00
	4	368	86	4.28	42	10.00

difficulty in compound processing, gauge control, "nerve," and extrudate or calendered sheet shrinkage [15].

Halobutyl rubber (HIIR) is used primarily in tire innerliner and white sidewalls. These elastomers are best for tire air retention owing to lower air permeability as well as aging and fatigue resistance. The chlorinated (CIIR) and brominated (BIIR) versions of isobutylene isoprene rubber (IIR) can be blended with other elastomers to improve adhesion between HIIR compounds and those based on general purpose elastomers, and improve vulcanization kinetics [16].

Attempts at using halogenated isobutylene based polymers in tread compounds has been limited, even though such tread compounds display good performance in winter applications and have good traction performance. A new isobutylene polymer modified with *p*-methylstyrene and then brominated is also available that offers a fully saturated backbone to resist aging while improving compatibility with general purpose elastomers such as natural rubber and styrene–butadiene rubbers.

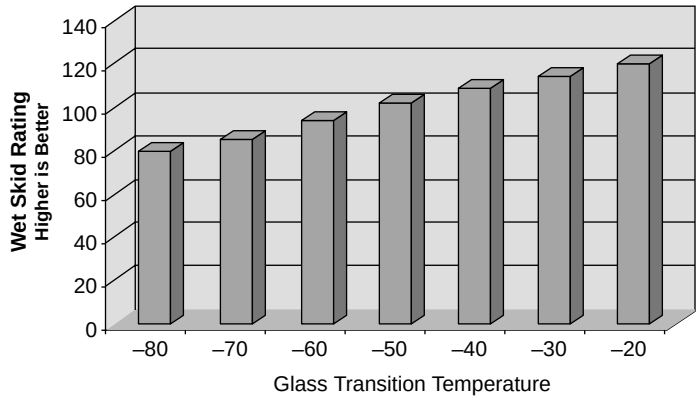

FIGURE 2 Effect of Tg on tire traction performance. (From Saito [18].)

It is common to blend more than one type of rubber within a given tire tread compound. An example of this is the truck drive axle tire tread compounds that must not only possess high strength but must also have good fatigue resistance. In passenger car tires, as many as four different polymers may be used for the tread compound totaling 100 phr; e.g., 25 phr emulsion SBR, 25 phr solution SBR, 30 phr BR, and 20 phr NR. If solution SBR categories can be considered as each one falling with a 10°C T_g range, there are at least nine groups of specialty SSBR polymers commercially available, in addition to the range of proprietary polymers chemical operations produce to support tire manufacturing [7, 16].

Figure 2 shows the effect of Tg on wet skid. If an increase in wet grip is required with minimum impact on rolling resistance, then a change in Tg is best accomplished via an increase in the vinyl–butadiene level rather than in the bound styrene content. Alternatively, if wear is of higher importance, Tg should be adjusted by a change in the bound styrene level. The optimum Tg could therefore be obtained by adjustment of either the vinyl–butadiene or styrene contents to obtain the required wet grip, rolling resistance, and wear performances. It has been demonstrated [17–19] that an increase in wear performance would lead to a trade-off in traction performance (Fig. 3).

High molecular weight commercial polymers are oil extended to facilitate processing and also to enable the production of polymers that will yield compounds with better mechanical properties than those with lower molecular weight polymers of corresponding structure [20]. Table XIII displays a selection of emulsion SBR grades. Aromatic oils can raise the glass transition temperature of the corresponding oil-free polymer. Naphthenic oils will tend to shift the transition temperature below the value of the oil-free rubber.

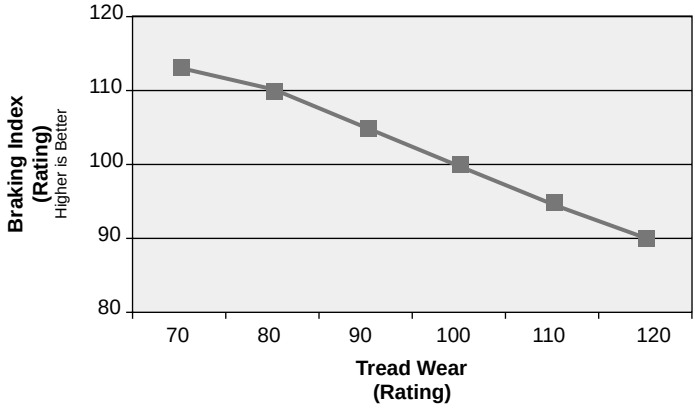

FIGURE 3 Relationship between wear and braking qualities. (From Oberster, Bouton, and Valaites [19].)

TABLE XIII Oil Extended Emulsion SBR [20]

IISRP polymer	Mooney nominal viscosity (M_L1+4)	Styrene (%)	Oil type	Oil level (PHR)
1707	50	23.5	Naphthenic	37.5
1712	50	23.5	Aromatic	37.5
1720	40	23.5	Naphthenic	50.0
1721	55	40.0	Aromatic	37.5

TABLE XIV ASTM and IISRP Classification of Oils for Oil Extended Elastomers [6]

Type	Asphaltenes	Polar compound content (%)	Saturated hydrocarbon content (%)	Category	Viscosity gravity constant
101	0.75	25.0	20.0	Highly Aromatic	>0.900
102	0.50	12.0	20–35	Aromatic	0.900
103	0.30	6.0	35–65	Naphthenic	0.875
104A	0.10	1.0	65.0	Paraffinic	>0.820
104B	0.10	1.0	65.0	Paraffinic	0.820 Max

The primary function of oil in rubber is to facilitate improvement in processing, i.e., the ease of mixing in an internal mixer, to improve mixed compound uniformity such as viscosity, and to improve downstream processing such as in extrusion. The specific oils used in oil-extended elastomers have been categorized into essentially five groups, which are summarized in Table XIV.

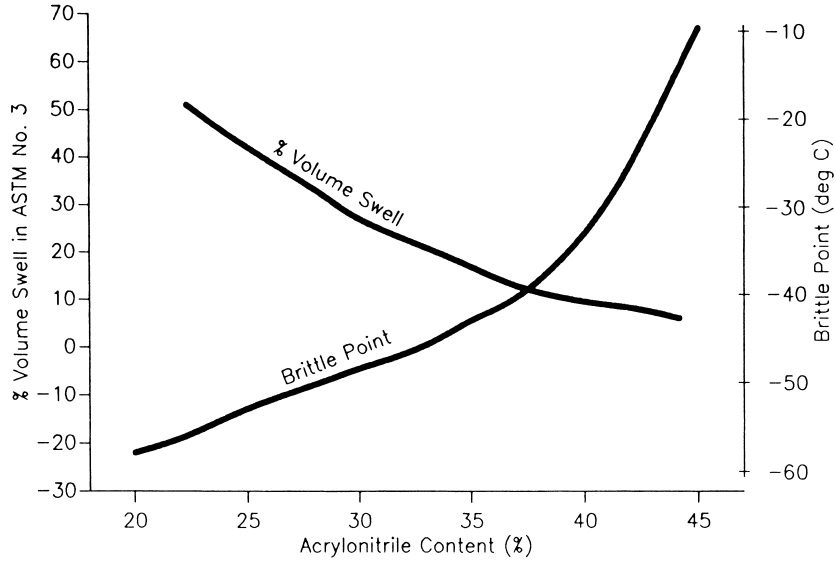

FIGURE 4 Acrylonitrile content and NBR oil absorption.

Though natural rubber, SBR, and BR represent the largest consumption of elastomers, several additional polymers merit a brief discussion because of their economic significance, i.e., nitriles, polychloroprene, butyl, and ethylene–propylene–diene monomer (EPDM) elastomers [2, 6].

Nitrile rubber (NBR) is a copolymer of acrylonitrile and butadiene. Its most important property is resistance to oil absorption; it therefore finds extensive use in such products as hydraulic hose and automotive engine components, where oil resistance is essential. Figure 4 illustrates the effect of acrylonitrile level on oil absorption (IRM 903 oil). Conversely, NBR polymers have poor cold flex properties, which prohibits their use on equipment operating in cold climates.

NBR tends to break down readily on a mill or banbury. Peptizers are not normally required, though antigel agents are needed if mixing temperatures exceed 140°C. Because of the polymer's low green strength, sufficient shear during mixing is not achieved to enable use of SAF or ISAF carbon blacks. It can also result in poor processing qualities such as mill bagging. Antioxidants are essential in NBR compounds as NBR will oxidize readily in hot air. Polymerized 2,2,4-trimethyilihydroquinolene is the most effective antioxidant. Antiozonants and waxes are ineffective with NBR compounds.

Polychloroprene is made either from acetylene:

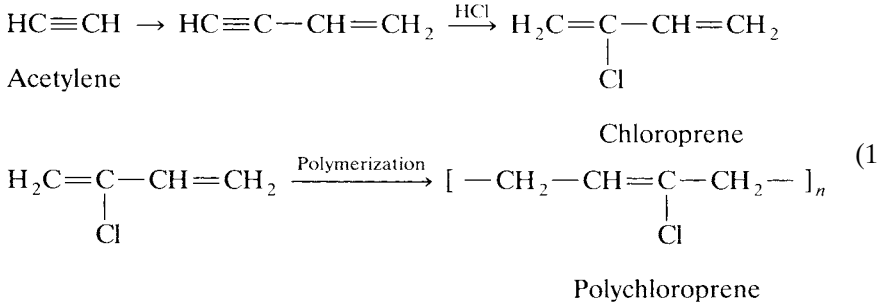

(1)

or butadiene

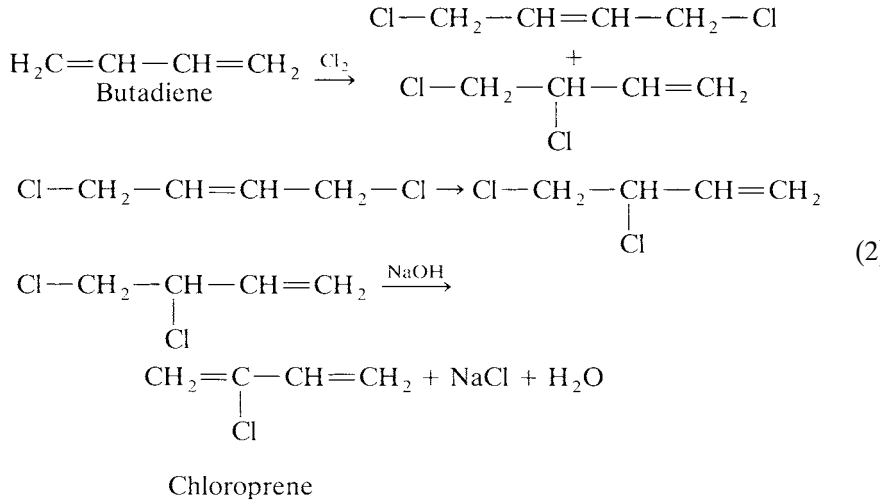

(2)

Acetylene is reacted to form vinyl acetylene, which is then chlorinated to form chloroprene. This can then be polymerized to polychloroprene. Polychloroprene contains approximately 85% *trans*-, 10% *cis*-, and 5% *vinyl*-chloroprene. Because of its high *trans*- content, polychloroprene tends to crystallize readily.

Depending on the grade of polymer, polychloroprene can be vulcanized by zinc oxide or magnesium oxide. Tetramethylthiuram disulfide can serve as a retarder. Polychloroprene is inferior to NBR for oil resistance but is still significantly better than natural rubber, SBR, or BR. Like NBR it also finds extensive use in such products as oil seals, gaskets, hose linings, and automotive engine transmission belts where resistance to oil absorption is important.

Butyl rubbers are a copolymer of isobutylene and isoprene:

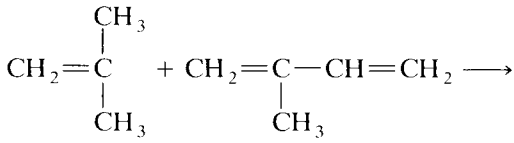

Isobutylene Isoprene

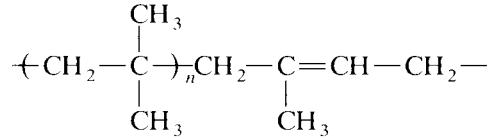

Butyl (3)

Isobutylene and isoprene are in a ratio of approximately 50/1. Chlorobutyl rubber and bromobutyl rubber are produced by the halogenation of butyl rubber. Butyl rubber and halobutyl rubber are highly impermeable to air and show very low water absorption, and good heat and ozone resistance. As noted earlier, they therefore find extensive use in liners of radial tires, covers and insulation of high-voltage electric cables, and automobile engine and radiator hoses.

High-tensile-strength butyl compounds generally use FEF- or GPF-grade carbon blacks. Vulcanization systems tend to be based on thiazole accelerators such as mercaptobenzothiazole disulfide (MBTS) and thiuram accelerators such as tetramethylthiuram disulfide (TMTD). Low-tensile-strength compounds will use a clay or silica reinforcing filler in place of carbon black.

Copolymerization of ethylene and propylene produces an elastomeric polymer which is virtually inert because of the absence of carbon–carbon double bonds (EPM). Such polymers thus tend to be crosslinked with peroxides or by radiation. To improve the reactivity of ethylene–propylene copolymers, 1 to 10% of a third monomer can be added to give a terpolymer or ethylene–propylene–diene monomer (EPDM). The primary diene monomers used in EPDM are 1,4-hexadiene, dicyclopentadiene, and ethylidene norbornene. Introduction of an unsaturated monomer such as ethylidene norbornene will enable use of sulfur-based crosslinking systems.

EPDM tends to show good resistance to ozone attack, oxidation resistance, and moisture resistance. It is therefore used in applications which require good weather resistance and heat stability. Roofing materials, outer covers of high-voltage electric cables, and selected automotive hoses use EPDM.

See Table XV for the abbreviations of selected elastomers.

III. FILLER SYSTEMS

Fillers, or reinforcement aids, such as carbon black, clays, and silicas are added to rubber formulations to meet material property targets such as tensile

TABLE XV Nomenclature for Selected Elastomers [6]

AU	Polyester urethane
BR	Polybutadiene
BIIR	Brominated isobutylene-isoprene (bromobutyl)
CIIR	Chlorinated isobutylene-isoprene (chlorobutyl)
CPE	Chlorinated polyethylene
CR	Chloroprene rubber
CSM	Chlorosulfonyl polyethylene
EAM	Ethylene–vinyl acetate coploymer
EPDM	Terpolymer of ethylene, propylene, and a diene with a residual unsaturated portion in the chain
EPM	Ethylene–propylene copolymer
EU	Polyether urethane
HNBR	Hydrogenated acrylonitrile-butadiene rubber (highly saturated nitrile rubber)
IIR	Isobutylene–isoprene rubber (butyl)
IR	Synthetic polyisoprene
NBR	Acrylonitrile-butadiene rubber
SBR	Styrene–butadiene rubber
E-SBR	Emulsion styrene–butadiene rubber
S-SBR	Solution styrene–butadiene rubber
X-NBR	Carboxylated nitrile–butadiene rubber
X-SBR	Carboxylated styrene–butadiene rubber
YSBR	Block copolymers of styrene and butadiene

TABLE XVI Types of Carbon Blacks

Type	ASTM designation	Particle size (nm)	General use
SRF	N 762	61–100	Nontread components
GPF	N 660	49–60	Nontread components
FEF	N 550	40–48	Nontread components
FF	N 475	31–39	Nontread components
HAF	N 330	26–30	Tread and other components
ISAF	N 220	20–25	Tread
SAF	N 110	11–19	Tread

strength and abrasion resistance. Carbon black technology is as complex as polymer science, and an extensive range of blacks are available, each imparting specific sets of properties to a compound. The correct choice of carbon black is therefore as important as the development of a formulation's polymer system in meeting a product performance specification. Table XVI displays the general classes of rubber-grade carbon blacks as defined in ASTM Standard D1765-04 [21].

TABLE XVII Carbon Black Properties

ASTM designation	Iodine number	DBP	Compressed DBP	NSA Multipoint	STSA	Tint strength
N 110	145	113	97	127	115	123
N 115	160	113	97	137	124	123
N 120	122	114	99	126	113	129
N 121	121	132	111	122	114	119
N 125	117	104	89	122	121	125
N 134	142	127	103	143	137	131
N 219	118	78	75			123
N 220	121	114	98	114	106	116
N 231	121	92	86	111	107	120
N 234	120	125	102	119	112	123
N 299	108	124	104	104	97	113
N 326	82	72	68	78	76	111
N 330	82	102	88	78	75	104
N 339	90	120	99	91	88	111
N 343	92	130	104	96	92	112
N 347	90	124	99	85	83	105
N 351	68	120	95	71	70	100
N 358	84	150	108	80	78	98
N 375	90	114	96	93	91	114
N 472	250	178	114	270	145	
N 550	43	121	85	40	39	
N 630	36	78	62	32	32	
N 650	36	122	84	36	35	
N 660	36	90	74	35	34	
N 762	27	65	59	29	28	
N 772	30	65	59	32	30	
N 990		43	37	8	8	
N 991		35	37	8	8	

A. Carbon Black Properties

Carbon black can be described qualitatively by a series of properties: particle size (and surface area); particle size distribution; structure (particle aggregates); surface activity (chemical functional groups such as carboxyl, and ketones). Key properties describing a carbon black can be listed as follows (Table XVII):

Iodine number	Measure of surface area (particle size). The higher the iodine number, the smaller the particle size.
DBP	Measure of structure or size of carbon black aggregate. The higher the DBP number, the higher the structure.
Tint	Optical absorbance, which increases with smaller particles.
CTAB	Specific surface area measurement corrected for the effect of micropores.

Carbon black terms are defined in Table XVIII. Further reference can also be made to ASTM Standards D1566-04 on general compounding terms [22] and D3053-04 specifically for carbon blacks [23].

As an empirical guide, an increase in a carbon black aggregate size or structure will result in an improvement in cut growth and fatigue resistance. A decrease in particle size results in an increase in abrasion resistance and tear strength, a drop in resilience, and an increase in hysteresis and heat buildup. The impact of carbon black type and loading on tread compound performance has been studied by Hess and Klamp [24], who evaluated 16 types of carbon black in three tread formulations with varying oil levels. The authors documented a number of criteria relating carbon black to the hysteretic properties of rubber compounds. These included loading, aggregate size, surface area, aggregate size distribution, aggregate irregularity (structure), surface activity, dispersion, and phase distribution within a heterogeneous polymer system.

From tire testing of the selected carbon black types, the following points were noted:

1. Reduction of carbon black loading lowers tire rolling resistance. At a constant black loading, an increase in oil level will increase rolling resistance but also improve traction (at low oil levels, an increase in oil level may decrease compound hysteresis by improving carbon black dispersion).
2. Increasing black fineness raises both rolling resistance and traction.
3. An increase in the broad aggregate size distribution decreases the tire rolling resistance with constant surface area and DBP.
4. Tread-grade carbon blacks can be selected to meet defined performance parameters of rolling resistance, traction, wear, etc.

Figure 5 illustrates the general trends for tread-grade carbon black loading and the effect on compound physical properties. As carbon black level increases, there are increases in compound heat buildup and hardness and, in tires, an increase in rolling resistance and wet skid properties. Tensile strength, compound processability, and abrasion resistance, however, go through an optimum after which these properties deteriorate.

To exploit the results of work such as that of Hess and Klamp in improving tire rolling resistance, Swor and coworkers have developed new-technology N 200 series carbon blacks which, they claim, will give a better balance of tire performance properties and the general principles will be applicable to a range of tire designs [24].

In attempting to predict the direction which future research in carbon black technology will follow, a review of the literature suggests that carbon black–elastomer interactions will provide the most potential to enhance compound performance. Le Bras demonstrated that carboxyl, phenolic, quinone,

TABLE XVIII Definition of Carbon Black Terms

Furnace carbon black	Class of carbon blacks produced by injection of defined grades of petroleum feedstock into a high-velocity stream of combustion gases under a set of defined processing conditions, e.g., N 110 to N 762.
Thermal carbon black	Type of carbon black produced by thermal decomposition of hydrocarbon gases, e.g., N 990, N 991.
Microstructure	Carbon black microstructure describes the arrangement of carbon atoms within a carbon black particle.
Particle	Small spherical component of a carbon black aggregate produced by fracturing the aggregate. Particle size is measured by electron microscopy.
Aggregate	Distinct, colloidal mass of particles in its smallest dispersible unit.
Agglomerate	Arrangement or cluster of aggregates.
Structure	Measure of the deviation of the carbon black aggregate from a spherical form.
Iodine number	Weight in grams of iodine absorbed per kilogram of carbon black. Measure of particle surface area. The smaller the particle size, the greater the iodine number.
Carbon black DBP	Volume of dibutyl phthalate in cubic centimeters absorbed by 100 g of carbon black. DBP number is a measure of the structure of the carbon black aggregate.
Tint	Tint is a ratio of the reflectance of a reference paste to that of a sample paste consisting of a mixture of zinc oxide, plasticizer, and carbon black.
CTAB	Measure of the specific surface area corrected for the effect of micropores. CTAB (cetyltrimethylene ammonium bromide) is excluded from the smaller interstices and thus better represents the portion of a particle surface area in contact with the polymer.
Nitrogen surface area	Measure of total particle surface area, due to nitrogen gas being able to cover the full surface including pores without interface from surface organic functional groups.
Compressed DBP	The DBP test, but where the sample undergoes a series of compressions (4 times to 24,000 lb) before testing. This enables a measure of changes the carbon black will undergo during compound processing.
Pellet	Mass of compressed carbon black formed to reduce dust levels, ease handling, and improve flow.
Fines	Quantity of dust present in a pelletized carbon black; should be at the minimum level possible.
Pellet hardness	Measure of the load in grams to crush a defined number of pellets. It is controlled by the quantity of pelletizing agent. For best pellet durability and compound mixing, pellet hardness range should have a narrow distribution. Examples of pelletizing agents are lignosulfonates and molasses.
Ash	Residue remaining after burning carbon black at 550°C for 16 hours; primarily a measure of the quality of plant cooling water.
Toluene discoloration	Hydrocarbons extractable in toluene from carbon black; can be used as a measure of the residence time in a furnace.
Hydrogen and oxygen content	Residual hydrogen and oxygen remaining after carbon black is produced; will be in the form of phenolic lactonic, carboxylic, quinonic, and hydroxyl functional groups. Such groups can have significant effects on vulcanization kinetics and reinforcement potential of the carbon black.

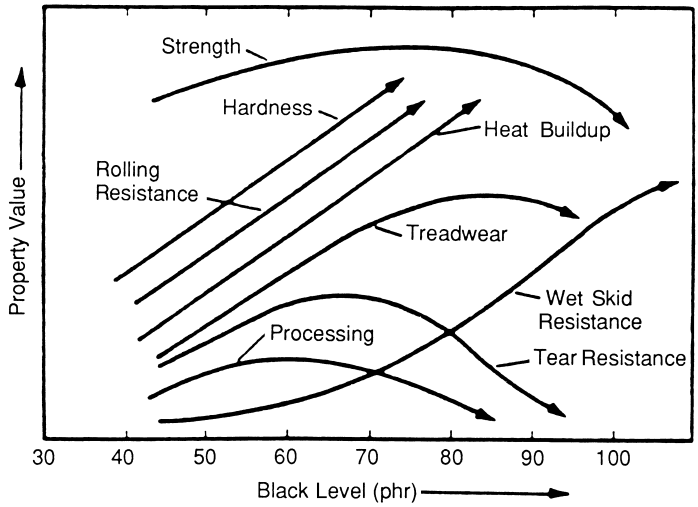

FIGURE 5 Effect of carbon black level on compound properties.

and other functional groups on the carbon black surface react with the polymer and provided evidence that chemical crosslinks exist between these materials in vulcanizates [25]. Ayala and coworkers [26, 27] determined a rubber–filler interaction parameter directly from vulcanizate measurements. The authors identified the ratio σ/n, where σ = slope of the stress–strain curve which relates to the black–polymer interaction, and n = the ratio of dynamic modulus E' at 1 and 25% strain amplitude and is a measure of filler–filler interaction. This interaction parameter emphasizes the contribution of carbon black–polymer interactions and reduces the influence of physical phenomena associated with networking. Use of this defined parameter enabled a number of conclusions to be made:

1. The σ/n values obtained provided a good measure of black–polymer interaction for a range of polymers including SBR, IIR, NR, and NBR.
2. Higher σ/n values were obtained for SBR and NBR, the aromatic structure in SBR and the polar —CN group in NBR clearly influencing black–filler interaction.
3. Analysis of dry carbon black surface indicated the presence of a range of hydrocarbon groups, which is in line with earlier work [25]. These groups are capable of reacting with other functional groups.

Given the establishment of organic functional groups on the carbon black surface, Wolff and Gorl investigated the reactivity of organosilane such as bis(3-triethoxysilylpropyl)tetrasulfane with furnace blacks [28]. The authors deduced that such groups as carboxyl, lactol, quinone, and ketone will react

with the ethoxy group of bis(3-triethoxysilylpropyl)tetrasulfane and which then become pendant on the carbon black surface:

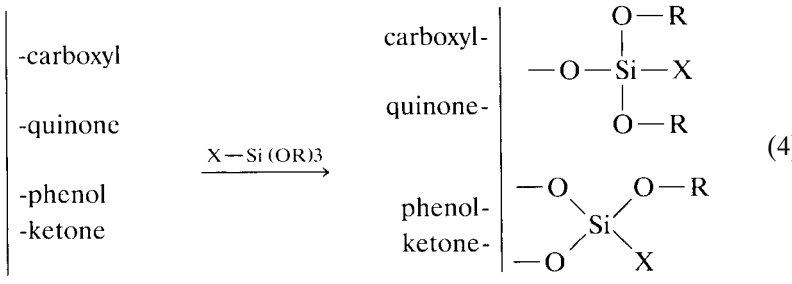

(4)

Carbon black surface — Activated carbon black surface

On the basis of extract analysis and compound properties of organosilane-treated carbon black, Wolff and Gorl concluded:

1. Carbon black is able to bind with a specific amount of trialkoxysilane.
2. The quantity of bound organosilane correlates with carbon black particle surface area and level of oxygen-containing functional groups.
3. The triethoxysilyl group constitutes the reactive part of the silane, forming a covalent bond with the carbon black.
4. Reaction of bis(triethoxysilylpropyl)tetrasulfane with carbon black allows a reduction of compound hysteresis.

This work laid the foundation for many of the newer technology carbon blacks. These fall into two categories, postprocess modification where the surface of the carbon black is treated to improve its properties, and in-process modification where another material is introduced to again enhance the basic properties of the filler [29].

Examples of postprocess systems under evaluation include surface oxidation using ozone, hydrogen peroxide, or nitric acid. Such approaches are used in the production of conductive blacks. Reaction with diazonium salts, plasma treatment, and polymer grafting are also under investigation.

In-process modification includes metal addition, development of inversion blacks or nanostructure blacks, and carbon black–silica dual phase fillers.

B. Silica and Silicates

Addition of silica to a rubber compound offers a number of advantages such as improvement in tear strength, reduction in heat buildup, and increase

in compound adhesion in multicomponent products such as tires. Two fundamental properties of silica and silicates influence their use in rubber compounds: ultimate particle size and the extent of hydration. Other physical properties such as pH, chemical composition, and oil absorption are of secondary importance.

Silicas, when compared to carbon blacks of the same particle size, do not provide the same level of reinforcement, though the deficiency of silica largely disappears when coupling agents are used with silica. Wagner reported that addition of silica to a tread compound leads to a loss in tread wear, even though improvements in hysteresis and tear strength are obtained [30]. The tread wear loss can be corrected by the use of silane coupling agents [31].

The chemistry of silica can be characterized as follows:

1. Silica, which is amorphous, consists of silicon and oxygen arranged in a tetrahedral structure of a three-dimensional lattice. Particle size ranges from 1 to 30 nm and surface area from 20 to 300 m^2/g. There is no long-range crystal order, only short-range ordered domains in a random arrangement with neighboring domains.
2. Surface silanol concentration (silanol groups —Si—O—H) influence the degree of surface hydration.
3. Silanol types fall into three categories—isolated, geminal (two —OH hydroxyl groups on the same silicon atom), and vicinal (on adjacent silicon atoms)—as illustrated in Fig. 6.
4. Surface acidity is controlled by the hydroxyl groups on the surface of the silica and is intermediate between those of P—OH and B—OH. This intrinsic acidity can influence peroxide vulcanization, although in sulfur curing, there is no significant effect. Rubber–filler interaction is affected by these sites.
5. Surface hydration caused by water vapor absorption is affected by surface silanol concentration. High levels of hydration can adversely affect final compound physical properties. Silicas are hydroscopic and thus require dry storage conditions.

To illustrate the influence of surface hydroxyl groups and hydration levels on rubber properties, Wagner [30] took a series of silicas of different surface areas, hydroxylated to different extents, and then added them to an SBR compound at 50 phr (Table XIX). The author concluded that a reduction in silanol level as a result of an increase in absorbed water will decrease cure time, tensile strength, and also abrasion resistance.

In general, silicas produce relatively greater reinforcement in more polar elastomers such as NBR and CR than in nonpolar polymers such as SBR and NR. The lack of reinforcement properties of silica in NR and SBR can be corrected through the use of silane coupling agents. An essential prerequisite for a coupling agent is that the molecule be bifunctional, i.e., capable of reacting

TABLE XIX Effect or Surface Hydration on Silica Properties

	Silica A	Silica B
Surface area (m^2/g)	152.0	152.0
Loss at 105°C (% H_2O)	6.8	0.5
Mooney scorch	14.0	16.0
Rheometer t_{-90}	27.0	47.0
Tensile strength (MPa)	18.3	21.7
Elongation at break	480	480
300% modulus (MPa)	7.0	9.5
Pico abrasion	67.0	103.0

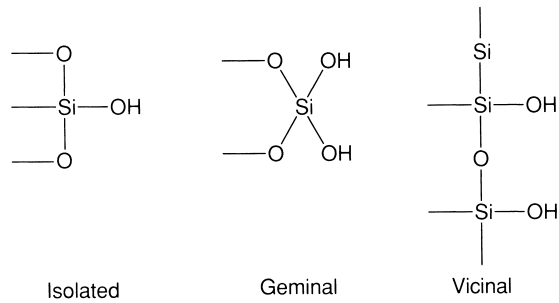

FIGURE 6 Typical silanol groups on silica.

chemically with both the silica and either directly or indirectly with the polymer via participation in the vulcanization reaction or sulfur crosslinking process.

Use of silicas in rubber compounds offers two advantages: reduction in heat buildup when used as a part for part replacement of carbon black and improvement in tear strength, cut, chip, and chucking resistance. When loadings approach 20%, however, the drop in abrasion resistance of, for example, a tread compound renders the formulation no longer practical. Silane coupling agents offer the potential to overcome such drops in compound performance. Therefore, to compound silica effectively, a discussion of the properties and chemistry of coupling agents, and specifically silane coupling agents, is pertinent.

Silicas can be divided into three groups or classes. These include standard or conventional silicas, semi-highly dispersible (semi-HD) or easily-dispersible silica, and the latest group developed is termed highly dispersible silica or HDS (Table XX). The silanol composition on the surface of three types of silicas remains to be elucidated, but it would be anticipated that the HDS silicas would have higher concentrations of geminal groups, whereas the conventional silica would have a greater amount of isolated silanols [10, 31].

TABLE XX **Silica Groups**

Surface Area (m^2/gm)	90–130	130–180	180–220
Conventional	Tire casing. Non-tire internal & external components	Tire treads. Tire casings & non-tire products external components	Tire treads & non-tire external components for abrasion resistance
Semi-highly dispersible	Tire casing. Non-tire products external components	Tire treads. Tire casings	Tire treads
Highly dispersible	Tire casings. Tire treads	Tire treads	High performance tire treads

C. Chemistry of Silane Coupling Agents

There are three silane coupling agents of commercial significance and these have similar properties: mercaptopropyltrimethoxysilane (A189), bis(triethoxysilylethyltolylene)polysulfide (Y9194), and bis(3-triethoxisilylpropyl) tetrasulfane (TESPT). Commercial designations are in parentheses. The coupling agent TESPT has been covered more extensively in the literature than other silane coupling agents; however, the following discussion on the use of silane coupling agents is applicable to all three materials [31].

TESPT, a bifunctional polysulfidic organosilane, was introduced as a coupling agent to improve the reinforcement properties of silicas in rubbers. Use of coupling agents offers the following advantages:

- Lowers heat buildup and hysteresis in silica-loaded compounds
- Increases 300% modulus and tensile strength, again, in silica-loaded compounds
- Improves reinforcing effect of clays and whiting
- Serves as a reversion resistor in equilibrium cure systems
- Improves DIN abrasion resistance

The mechanism of silane coupling agent reinforcement comprises two phases: (1) the hydrophobation reaction in which coupling agent reacts with silica, and (2) the formation of crosslinks between the modified silica and polymer. Silanization of the silica surface can occur quite readily, though with TESPT systems, the reaction is generally carried out *in situ* at between 150 and 160°C in an internal mixer. Though an excess of silanol groups are present on the silica surface and reaction rates are fast, this high temperature is required because of the steric hindrance around the silylpropyl group in TESPT.

As noted earlier, three types of functional silanol groups exist on the silica surface: isolated hydroxyl groups, geminal groups (two —OH groups on one Si atom), and vicinal groups (see Fig. 6). The silanization reaction is illustrated in Eq. 5.

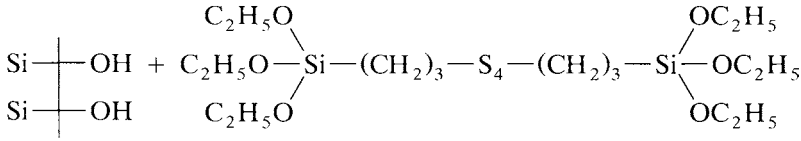

Silica TESPT

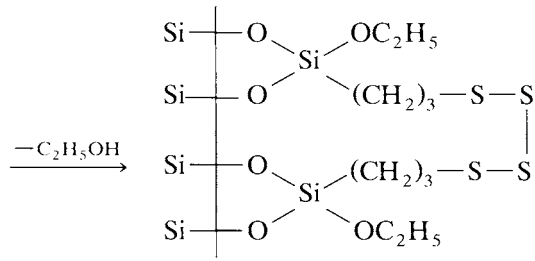

(5)

Silica/TESPT intermediate product

The filler/silane intermediate can now react with the allyl position of unsaturated sites on the polymer chain. The vulcanization of rubber is known to proceed via reaction of an accelerator, such as a sulfenamide, with sulfur, zinc oxide, and stearic acid, to generate a sulfurating agent [32]. Equation 6 gives a somewhat simplistic schematic of the vulcanization reaction. On completion of the reaction, the pendant accelerator will cleave off (i.e., Captax) after generation of a crosslink. This accelerator residue, Captax, is an accelerator in its own right and continues to participate in further crosslinking as vulcanization continues.

In silica reinforcement systems containing TESPT, Wolff has suggested that the reaction is similar when the TESPT/silica intermediate is present instead of sulfur, in which case the crosslinking agent is the polysulfidic sulfur chain. Wolff showed that mercaptobenzothiazyl disulfide (MBTS) reacts with the tetrasulfane group, thus forming 2 moles of the polysulfide:

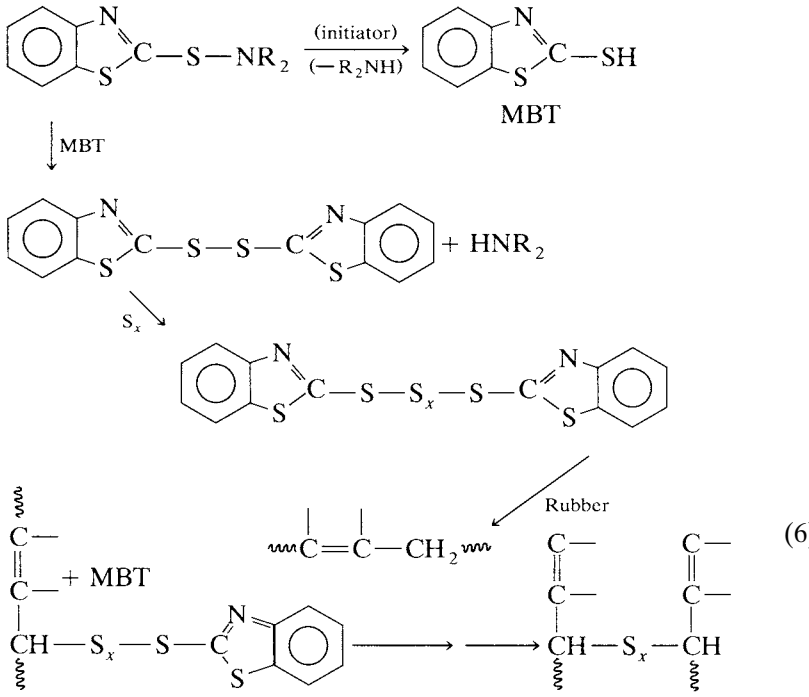

(6)

The silica particle is on one side and the mercaptobenzthiazolyl on the other. This polysulfidic pendant group on the silica surface will now undergo crosslink formation with the polymer in much the same way as occurs in rubber-bound intermediates that convert to crosslinks. Wolff [33] suggested that the MBT entity reacts with the allyl position of a double bond of the rubber, thus releasing MBT and forming the rubber–silica bond.

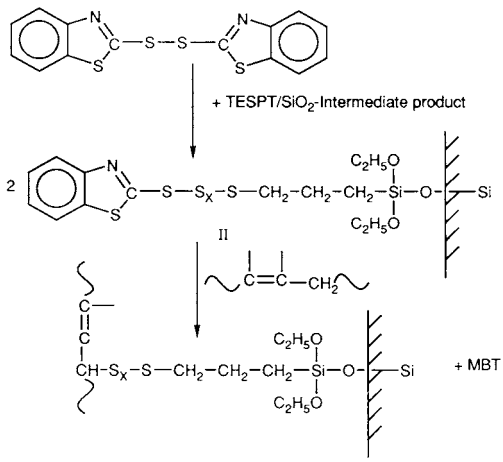

(7)

Proper compounding of silica with coupling agents has permitted the use of such filler systems in applications including shoe soles; engine mounts in which coupling agent/silica NR compounds provide the necessary hysteretic properties; tire treads in which, again, hysteretic properties are important; and a range of other applications such as golf balls [31].

D. Other Filler Systems

A series of additional filler systems merit brief discussion, not because of their reinforcement qualities but because of their high consumption. These include kaolin clay (hydrous aluminum silicate), mica (potassium aluminum silicate), talc (magnesium silicate), limestone (calcium carbonate), and titanium dioxide.

As with silica, the properties of clay can be enhanced through treatment of the surface with silane coupling agents. Thioalkylsilanes can react with the surface to produce a pendant thiol group which may react with the polymer through either hydrogen bonding, van der Waal forces, or crosslinking with other reactive groups:

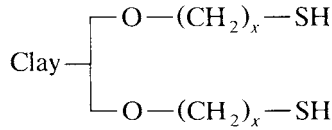

(8)

Such clays show improved tear strength, an increase in modulus, improved component-to-component adhesion in multicomponent products, and improved aging properties.

Calcium carbonate is used as a low-cost filler in rubber products for static applications such as carpet underlay. Titanium dioxide finds extensive use in white products such as white tire sidewalls where appearance is important.

IV. STABILIZER SYSTEMS

The unsaturated nature of an elastomer accounts for its unique viscoelastic properties. However, the presence of carbon–carbon double bonds renders elastomers susceptible to attack by oxygen, ozone, and also thermal degradation. A comprehensive review of elastomer oxidation and the role of antioxidants and antiozonants is available [34].

A. Degradation of Rubber

Oxidation of elastomers is accelerated by a number of factors including heat, heavy metal contamination, sulfur, light, moisture, swelling in oil and solvents, dynamic fatigue, oxygen, and ozone. Three variables in the compound

formulation can be optimized to resist degradation: polymer type, cure system, and antidegradant system.

Thermooxidative stability is primarily a function of the vulcanization system. Peroxide vulcanization or cure systems tend to perform best for reversion resistance as a result of the absence of sulfur and use of carbon–carbon crosslinks. Efficient vulcanization (EV) systems that feature a low sulfur level (0.0–0.3 phr), a high acceleration level, and a sulfur donor similarly show good heat stability and oxidation resistance. Such systems do, however, have poor resistance to fatigue because of the presence of predominantly monosulfidic crosslinks. Conventional cure systems that feature a high sulfur level and low accelerator concentration show poor heat and oxidation resistance because the polysulfidic crosslinks are thermally unstable and readily oxidized. Such vulcanization systems do, however, have better fatigue resistance. Semi-EV cure systems, which are intermediate between EV and conventional systems, are a compromise between resistance to oxidation and required product fatigue performance.

Oxidation proceeds by two fundamental mechanisms.

1. *Crosslinking*: A predominantly di- or polysulfidic crosslink network breaks down into monosulfidic crosslinks. Compound hardness increases, fatigue resistance decreases, and the compound becomes much stiffer. SBR, EPDM, NBR, and polychloroprene tend to show this behavior.
2. *Chain scission*: The polymer chain breaks, causing a softening of the compound and decreased abrasion resistance. Natural rubber tends to show such degradation.

The degradation of unsaturated elastomers is an autocatalytic, free radical chain reaction, which can he broken into three steps:

Initiation

$$\mathrm{RH\ (elastomer)} \xrightarrow[\text{heat}]{\mathrm{O_2,\ light}} \mathrm{R\cdot HOO\cdot\ (free\ radical)} \tag{9}$$

Propagation

$$\begin{aligned}
\mathrm{R\cdot + O_2} &\longrightarrow \mathrm{ROO\cdot} \\
\mathrm{ROO\cdot + R'H} &\longrightarrow \mathrm{ROOH + R'\cdot} \\
\mathrm{ROOH} &\longrightarrow \mathrm{RO\cdot + \cdot OH} \\
\mathrm{RO\cdot + R''H} &\longrightarrow \mathrm{ROH + R''\cdot} \\
\mathrm{\cdot OH + R''} &\longrightarrow \mathrm{R''\cdot + H_2O}
\end{aligned} \tag{10}$$

Termination

$$\begin{aligned} &R\cdot + \cdot R \\ &R\cdot + ROO\cdot \longrightarrow \text{Nonradical products} \\ &ROO\cdot + \cdot OOR \end{aligned} \qquad (11)$$

Like any chemical process, the rate of reaction will increase with temperature. Increase in service temperature will thus accelerate the degradation of rubber, the rate of reaction with oxygen being governed by the Arrhenius equation.

Ultraviolet light initiates free radical oxidation at the exposed surface of an elastomeric product to generate a layer of oxidized rubber. Heat, moisture, or high humidity can then initiate crazing of the surface which subsequently can be abraded off. Such degradation of the surface is more severe with nonblack stocks than with black compounds. Nonblack compounds such as white tire sidewalls thus require higher levels of nonstaining antioxidants than carbon black-loaded formulations.

Heavy transition metals ions such as iron, manganese, and copper catalyze oxidation of elastomers. Compounds of manganese or copper such as oleates and stearates are readily soluble in rubber, enabling rapid oxidation of the polymer. *para*-Phenylenediamine antidegradants are used to hinder the activity of such metal ions.

A major cause of failure in rubber products is surface crack development. The growth of such cracks under cyclic deformation results in fatigue failure. Fatigue-related cracks are initiated at high stress zones. Attack by ozone can induce crack initiation at the surface which then propagates as a result of flexing. Ozone-initiated cracking can be seen as crazing on the sidewalls of old tires. Ozone readily reacts with the carbon–carbon double bonds of unsaturated elastomers to form ozonides. Under strain, ozonides readily decompose, resulting in chain cleavage and a reduction in polymer molecular weight. Such polymer molecular weight reduction becomes apparent as surface crazing and cracking:

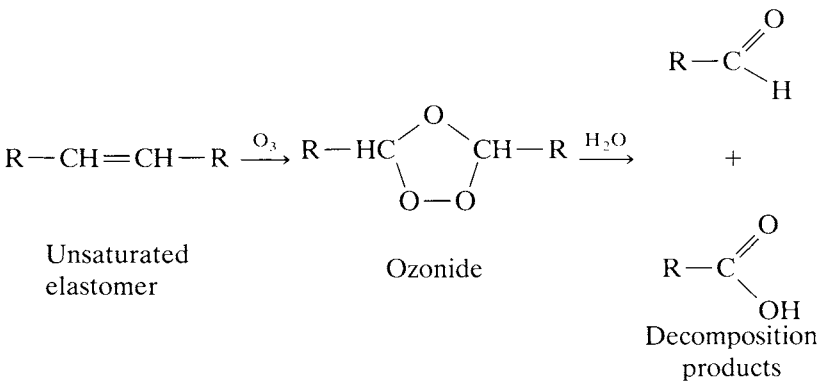

(12)

Polymer blends, in which the constituent polymers are incompatible, tend to improve fatigue resistance. For example, natural rubber and polybutadiene show good resistance to fatigue, crack initiation, and growth because of the formation of heterogeneous polymer phases; a crack growth in one polymer phase is arrested at the boundary with the adjacent polymer phase.

Natural rubber and polybutadiene blends tend to be used in tire side-walls which undergo flexing, and also in tire treads which have a lug pattern and contain high-stress zones at the base of the tread blocks.

In summary, the addition of antidegradants becomes important in order to protect the elastomeric compound from this broad range of enviromental, chemical, and service related aging phenomena.

B. Antidegradant Use

The selection criteria governing the use of antidegradants can be summarized as follows:

1. *Discoloration and staining:* In general, phenolic antioxidants tend to be nondiscoloring and amines are discoloring. Thus for elastomers containing carbon black, more active amine antioxidants are preferred as discoloration is not important.
2. *Volatility:* As a rule, the higher the molecular weight of the antioxidant, the less volatile it will be, though hindered phenols tend to be highly volatile compared with amines of equivalent molecular weight. Thus, correct addition of antioxidants in the compound mix cycle is critical if loss of material is to be avoided.
3. *Solubility:* Low solubility of an antidegradant will cause the material to bloom to the surface, with consequent loss of protection of the product. Therefore, solubility of antidegradants, particularly antiozonants, controls their effectiveness. The materials must be soluble up to 2.0 phr, must be able to migrate to the surface, but must not be soluble in water or other solvents such as hydraulic fluid so as to prevent extraction of the protectant from the rubber.
4. *Chemical stability:* Antidegradant stability against heat, light, oxygen, and solvents is required for durability.
5. *Concentration:* Most antidegradants have an optimum concentration for maximum effectiveness after which the material solubility becomes a limiting factor. *para*-Phenylenediamines offer good oxidation resistance at a loading of 0.5 to 1.0 phr and antiozonant protection in the range 2.0 to 5.0 phr. Above 5.0 phr *para*-phenylenediamines tend to bloom.
6. *Environment, health, and safety:* For ease of handling and avoidance of dust and inhalation, antidegradants should be dust free while free flowing.

C. Antidegradant Types

1. *Nonstaining antioxidants:* This class of antioxidants is subdivided into four groups: phosphites, hindered phenols, hindered bisphenols, and hydroquinones. Hindered bisphenols such as 4,4′-thiobis(6-t-butyl-*m*-cresol) are the most persistent of the four classes of material. Because of their lower molecular weight, hindered phenols tend to be volatile. Phosphites tend to be used as synthetic rubber stabilizers, and hydroquinones such as 2,5-di-*tert*-amylhydroquinone are used in adhesives:

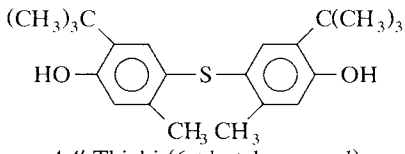

4,4′-Thiobis(6-*t*-butyl-*m*-cresol)

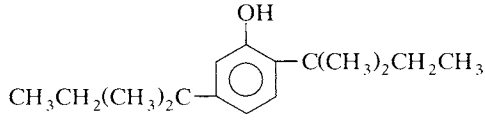

2,5-di-*tert*-amylhydroquinone

2. *Staining antioxidants:* Two classes of staining or discoloring antioxidants find extensive use, polymerized dihydroquinolines and diphenylamines:

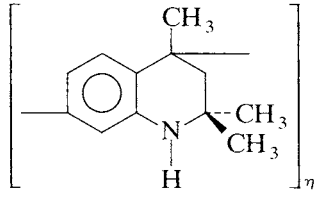

Polymerized 1,2-dihydro-2,2,4-trimethylquinoline

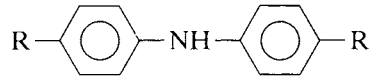

Diphenylamine class antioxidants

Dihydroquinolines differ in the degree of polymerization, thus influencing migratory and long-term durability properties. They are good general antioxidants and also are effective against heavy metal prooxidants such as nickel and copper ions. The polymeric nature of dihydroquinolines results in low volatility and migratory properties in a vulcanizate. Thus, there is minimum loss of protectant through extraction or diffusion, durability is improved, and high-temperature stability is improved. Diphenylamine antioxidants tend to show a directional improvement in compound fatigue resistance.

3. *Antiozonants: para*-Phenylenediamines (PPDs) are the only class of antiozonants used in significant quantities. The general structure is:

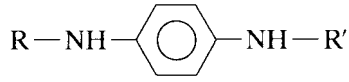

They not only serve to protect rubber products from ozone but also improve resistance to fatigue, oxygen, heat, and metal ions. There are three general categories of paraphenylenediamines and are listed as follows;

i. Dialkyl PPDs: The substituent R groups are both alkyls, as in diisopropyl-*p*-phenylenediamine. The R group can range from C3 up to C9. Dialkyl PPD antidegradants tend to induce higher levels of scorch in a compound than other classes of PPD antidegradants, and tend to migrate faster than other PPD because of their low molecular weight. They lack persistence.
ii. Alkyl-aryl PPDs: One R group is an aromatic ring; the other is an alkyl group. The most widely used PPD in this class is *N*-1,3-dimethylbutyl-*N*′-phenyl-*p*-phenylenediamine. This antiozonant offers good dynamic protection, good static protection when combined with wax, better compound processing safety and scorch safety, and, slower migratory properties, allowing it to be more persistent and suitable for long product life.
iii. Diaryl PPDs: The third class of PPDs contain two aromatic pendant groups, as in diphenyl-*p*-phenylenediamine or di-*β*-naphthyl-*p*-phenylenediamine. They are less active than alkyl-aryl PPDs and also tend to bloom, thus rendering them unsuitable for many applications.

4. *Waxes:* Waxes are an additional class of materials used to improve rubber ozone protection primarily under static conditions. Waxes used in elastomeric formulations fall into two categories: Microcrystalline wax has a melting point in the region 55 to 100°C and is extracted from residual heavy lube stock of refined petroleum. Paraffin wax has melting points in the range 35 to 75°C and is obtained from the light lube distillate of crude oil.

The properties of waxes are listed in Table XXI. Wax protects rubber against static ozonolysis by forming a barrier on the surface. Wax migrates from the bulk of the rubber continuously, maintaining an equilibrium con-

TABLE XXI Composition of Paraffin and Microcrystalline Waxes

	Microcrystalline	Paraffin
Molecular weight	500–800	340–430
Melting point (°C)	55–100	35–75
Mean carbon chain length	C-25	C-60
Features	Branched molecules	Linear molecules

centration at the surface. Microcrystalline waxes migrate to the rubber surface at a slower rate than paraffins because of the higher molecular weight and branching. Furthermore, microcrystalline waxes tend to perform best at high service temperatures, whereas paraffin waxes protect best at low temperatures. This is related to the rate of migration of the wax to the product surface.

It should be noted that under dynamic conditions, the protective wax film breaks down, after which the antiozonant system in the rubber formulation will serve as the primary stabilizer or protection mechanism. Waxes are used to ensure protection against ozone for products in storage, such as tires in a warehouse.

In summary, a number of empirical guidelines can be used to develop an antidegradant system for an elastomeric formulation:

1. Short-term static protection is achieved by use of paraffinic waxes.
2. Microcrystalline waxes provide long-term ozone protection while the finished product is in storage.
3. A critical level of wax bloom is required to form a protective film for static ozone protection.
4. Optimized blends of waxes and PPDs provide long-term product protection under both static and dynamic applications and over a range of temperatures.
5. Excess levels of wax bloom can have a detrimental effect on fatigue resistance, because the thick layer of wax can crack under strain and the crack can propagate into the product.

V. VULCANIZATION SYSTEM

Vulcanization, named after Vulcan, the Roman God of Fire, describes the process by which physically soft, compounded rubber materials are converted into high-quality engineering products. The vulcanization system constitutes the fourth component in an elastomeric formulation and functions by inserting crosslinks between adjacent polymer chains in the compound. A typical vulcanization system in a compound consists of three components: (1) activators; (2) vulcanizing agents, typically sulfur; and (3) accelerators. The chemistry of vulcanization has been reviewed elsewhere in this text. It is appropriate, however, to review each of these components within the context of developing a compound for a defined service application.

A. Activators

The vulcanization activator system consisting of zinc oxide and stearic acid has received much less research effort than other components in the rubber compound. Stearic acid and zinc oxide levels of 2.0 and 5.0 phr, respectively,

TABLE XXII ASTM D3184 Formulations 1A and 2A (ACS 1 and 2)

ACS 1		ACS 2	
Natural rubber	100	Natural rubber	100
Metal oxide	6	Metal oxide	5
Stearic acid	0.5	Stearic acid	2
Sulfur	3.5	Carbon black (IRB 5)	35
MBT	0.5	Sulfur	2.25
		TBBS	0.7

TABLE XXIII Effect of Metal Oxide Type on Compound Properties of ACS 1 Base Formulation

Compound: / Metal oxide:	1 MgO	2 CaO	3 TiO2	4 FeO	5 ZnO	6 PbO
Cation Electronegativity	1.2	1.0	1.5	1.9	1.6	1.8
% Free sulfur	2.69	2.51	2.60	2.74	1.43	1.03
Monsanto rheometer at 150°C, deta torque [M_H-M_L (dN · m)]	14.0	17.0	19.00	24.0	29.0	43.0
Tensile strength (MPa)	4.84	6.37	3.09	4.40	14.80	20.0
Elongation (%)	731	695	817	530	667	634
300% modulus (MPa)	0.90	1.14	0.58	1.85	2.96	2.2
Shore A hardness at 21°C	32	34	26	24	38	42
ASTM tear strength, die B(kN/m)	38	53	11	21.5	68	67

are accepted throughout the rubber industry as being adequate for achievement of optimum compound physical properties when in combination with a wide range of accelerator classes and types and also accelerator-to-sulfur ratios. To clarify why zinc oxide is selected over the other metal oxides, a comparative study was conducted with magnesium oxide, calcium oxide, titanium dioxide, lead oxide, and zinc oxide. All the metal oxides were evaluated in ASTM D3184 [35]; compound numbers 1A (gum stock) and 2A (which contains carbon black), are also referred to as American Chemical Society (ACS) compounds 1 and 2, respectively (Table XXII). Test data are presented in Tables XXIII and XXIV [36].

TABLE XXIV Effect of Metal Oxide Type on Compound Properties of ACS 2 Base Formulation

Compound:	1	2	3	4	5	6
Metal oxide:	MgO	CaO	TiO2	FeO	ZnO	PbO
Cation Electronegativity	1.2	1.0	1.5	1.9	1.6	1.8
% Free sulfur	0.39	0.35	0.72	0.68	0.15	0.15
Monsanto rheometer at 150°C, deta torque [M_H-M_L (dN·m)]	24.0	23.5	18.50	29.5	61.5	54.0
Tensile strength (MPa)	14.21	20.28	12.03	15.41	25.63	26.38
Elongation (%)	631	592	595	565	492	502
300% modulus (MPa)	2.94	4.86	2.91	2.53	11.04	8.9
Shore A hardness at 21°C	39	46	40	39	57	57
ASTM tear strength, die B (kN/m)	30	61	22	31.5	161	140

A plot of the electronegativity of the six metals of the oxides evaluated in the study versus rheometer torque ($M_H - M_L$) indicates that outside a given electronegativity range of 1.6 to 1.8, optimum vulcanizate properties will not be obtained (see Figs. 6–8). Electronegativity is a measure of the metal atom's affinity for electron attraction. Viewing Figs. 6–8 it can be concluded that for metals of electronegativity less than 1.55, a consequent shift to ionic bonding with sulfur induces a reduction in electrophilicity in the penultimate sulfur atoms of complexes:

$$X—S_x—S^- \cdots M^{+2} \cdots S^- —S_x—X$$

$$R—H \cdots S_y—X$$

Conversely, with metals of electronegativity greater than 1.85, such as iron, the greater covalent character of the M + · · S- linkage with reduced charge separation would adversely affect generation of amine or carboxylate ligands to the metal ion as in

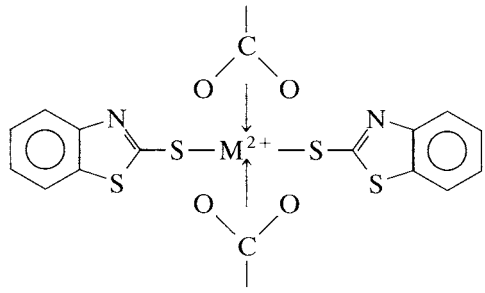

which in turn will reduce the solubility of the sulfurating reagent, consequent drop in sulfurating agent activity, and resultant drop in vulcanizate properties.

In summary, zinc is most suited to participate in formation of the sulfurating complex. Coordination of external ligands (ROO—, R′2 NH:) of the zinc atom causes the bonding between XS—S_x . . . and . . . S_y—SX groups to weaken, thereby increasing the contribution of the polar canonical form:

$$XS-S_x^- - Zn^{2+} - S_y^- - SX$$

This effect is induced by ligands satisfying vacant 4*p* orbitals and distributing positive charge from the metal. The result will be increased nucleophilicity of XSS_x- but decreased electrophilicity of XS_y+ in the sulfurating complex. The same is true for Cd^{2+} and Pb^{2+} complexes which have vacant *p* orbitals to accommodate coordination ligands. In the case of Mg^{2+} and Ca^{2+} complexes, coordination will not readily occur, the reduced ease of formation being further influenced by the inability of the metal to achieve an inert gas configuration as in more stable organometallics. Toxicity of CdO and PbO prohibits their use, and thus ZnO has found virtually universal use in the rubber industry, the ultimate loading in a compound being dependent on the product application.

As part of the metal oxide study, a comparative study of oleic acid and stearic acid, each at 1.0, 2.0, and 3.0 phr, was conducted on ASTM No. 2A (ACS 2) compound.

The data outlined in Table XXV illustrate a number of points:

1. An increase in the fatty acid level reduces vulcanization activation energy, the effect being greater for stearic acid.

TABLE XXV Influence of Fatty Acid Level in Vulcanizates

Compound:	**1**	**2**	**3**	**4**	**5**	**6**
Fatty acid:	**⟨Stearic⟩**			**⟨Oleic⟩**		
phr:	**1.0**	**2.0**	**3.0**	**1.0**	**2.0**	**3.0**
Crosslink density (rating)	100	94	106	75	80	89
Activation energy (kJ $mole^{-1}$)	131.5	101.5	97.6	135.1	114.2	110.5
Tensile strength (MPa)	27.50	26.8	26.9	28.5	28.0	26.4
Elongation (%)	545	535	538	591	576	551
Shore A hardness	52	53	50	50	52	52
Tear strength, ASTM die B (kN/m)	72	112	103	72	94	80
Aged tensile strength (MPa)	17.50	18.1	21.3	15.8	16.8	17.3

2. Stearic acid/ZnO-activated compounds show higher crosslink densities compared with oleic acid systems.
3. Aging and tear strength properties of stearic acid/ZnO compounds are superior to those of oleic acid systems.

The effectiveness of stearic acid in activating vulcanization is a function of its solubility in the elastomer, molecular weight, and melting point.

B. Vulcanizing Agents

Three vulcanizing agents find extensive use in the rubber industry: sulfur, insoluble sulfur, and peroxides. The chemistry of peroxides has been reviewed in Chapter 7. Rhombic sulfur is the most common form of sulfur used in the rubber industry and, other than normal factory hygiene and operational procedures, does not require any special handling or storage. Sulfur is soluble in natural rubber at levels up to 2.0 phr. Above this concentration, insoluble sulfur must be used to prevent migration of sulfur to the compound surface, i.e., sulfur bloom.

C. Accelerators

Accelerators are products which increase both the rate of sulfur crosslinking in a rubber compound and crosslink density. Secondary accelerators, when added to primary accelerators, increase the rate of vulcanization and degree of crosslinking, with the terms primary and secondary being essentially arbitrary. A feature of such binary acceleration systems is the phenomenon of synergism. Where a combination of accelerators is synergistic, its effect is always more powerful than the added effects of the individual components.

Accelerators can be readily classified by one of two techniques:

1. *Rate of vulcanization*: Ultra-accelerators include dithiocarbamates and xanthates. Semiultra-accelerators include thiurams and amines. Fast accelerators are thiazoles and sulfenamides. A medium-rate system is diphenylguanidine. A slow accelerator is thiocarbanilide.
2. *Chemical classifications*: Most accelerators fall into one of eight groups.

Aldehydeamines	Sulfenamides
Thioureas	Dithiocarbamates
Guanidines	Thiurams
Thiazoles	Xanthates

Factors involved in the selection of vulcanization systems must include the type of elastomer, type and quantity of zinc oxide and fatty acid, rate of vulcanization, required resistance to fatigue, and service conditions. It is also recommended that use of nitrosamine-generating accelerators be avoided.

The type of elastomer will influence the rate of cure and also the resultant crosslink network. Natural rubber tends to cure faster than SBR. Cure

systems containing thiuram accelerators such as tetramethylthiuram disulfide will show short induction times and fast cure rates compared with a system containing diphenylguanidine.

Sulfenamide accelerators represent the largest class of accelerators consumed on a global basis:

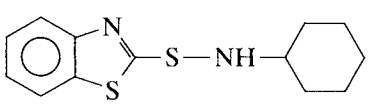

Cyclohexylbenzothiazole sulfenamide (CBS)

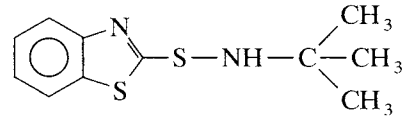

tert-Butyl-2-benzothiazole sulfenamide (TBBS)

The mechanism and chemistry of vulcanization have been reviewed earlier. It is therefore more appropriate to define the general principles governing the activity of an accelerator such as a sulfenamide. Three parameters merit elucidation:

1. *Bond strength of the sulfur-nitrogen bond*: Sulfenamides are cleaved into mercaptobenzothiazole and amine fragments during formation of the sulfurating complex, and the amine forms ligands with the zinc ion. Bond energy must be sufficiently low so as not to prevent generation of active accelerator species or sulfurating reagent.
2. *Stereochemistry of the amine fragment*: The steric bulk of the amine ligand coordinated with the zinc ion, if too large, can hinder the formation of an active sulfurating agent. This is seen as an increase in induction times, change in vulcanization rate, and, ultimately, change in physical properties.
3. *Basic strength of the amine fragment*: An increase in the basicity of the amine fragment of the sulfenamide results in an increase in the rate of vulcanization. More basic amines also tend to induce poor scorch resistance (Table XXVI). Further reference should be made to Chapter 7 on vulcanization.

D. Retarders and Antireversion Agents

The induction time or scorch resistance of a compound can be improved by addition of a retarder. *N*-Cyclohexylthiophthalimide (CTP) is by far the largest-tonnage retarder used in the rubber industry. The reader is referred to the review by Morita for discussion of the mechanism of CTP reactivity and also the chemistry of other special retarders such as the thiosulfonamide class of materials [37].

Resistance to compound reversion, particularly of natural rubber compounds, has received more recent attention because of the broad range of requirements including faster processing of compounds in production,

TABLE XXVI Effect of Sulfenamide Amide Fragment Basicity (pK_b) on Compound Scorch Activity[ab]

R radical	pK_b of free amine	Mooney scorch t^{-10} at 135°C	Cure rate index
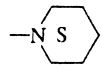	3.3	29.8	1.00
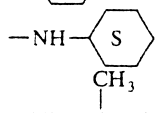	3.7	32.7	2.05
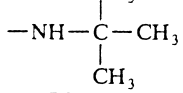	4.2	31.8	2.10
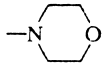	6.2	42.4	2.32
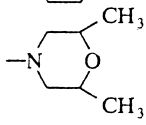	6.2	45.2	2.57

[a]Compound: 100 phr SBR-1500, 50 HAF, 4.0 ZnO, 2.0 stearic acid, 10.0 oil, 1.5 antioxidant, 1.75 sulfur, equimolar accelerator levels.
[b]Cure rate index is $t_{35} - t_{10}$ at 135°C on a Mooney plastimeter [36].

processing at higher temperatures, and, perhaps more important, extension of product service life. Three antireversion agents have been used commercially:

1. As reviewed earlier, a semi-EV system is a compromise designed to produce, in structural terms, a vulcanizate containing a balance of monosulfidic and polysulfidic crosslinks at a defined optimum cure state. If polysulfidic crosslinks are to persist over extended periods, new ones must be created to replace those lost through reversion. With use of normal accelerations systems, there is limited opportunity for such events. Maintenance of a polysulfidic network through the curing process thus dictates utilization of a dual-cure system both of which are independent of each other. This is the principle of the equilibrium cure (EC) system. Here, bis(3-triethoxysilylpropyl)tetrasulfane (TESPT) is added as a slow sulfur donor [38] (Fig. 7).
2. Bis(citraconimidomethyl)benzene, commercial name Perkalink 900, has been introduced which functions exclusively as a reversion resistor. It is understood to react via a Diels–Alder reaction to form a six-membered ring on the polymer chain (Fig. 8). The ultimate crosslink is thermally stable and replaces sulfur crosslinks that disappear during reversion [39].

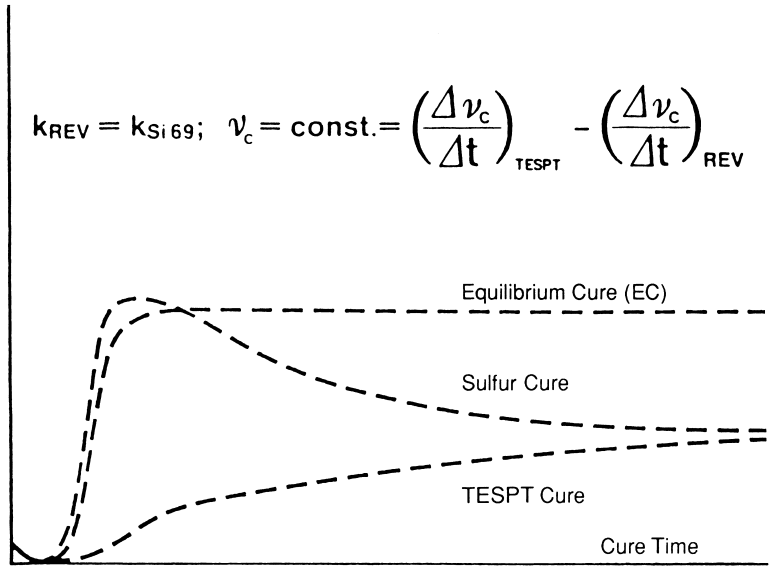

FIGURE 7 Rheometer profile of the EC system.

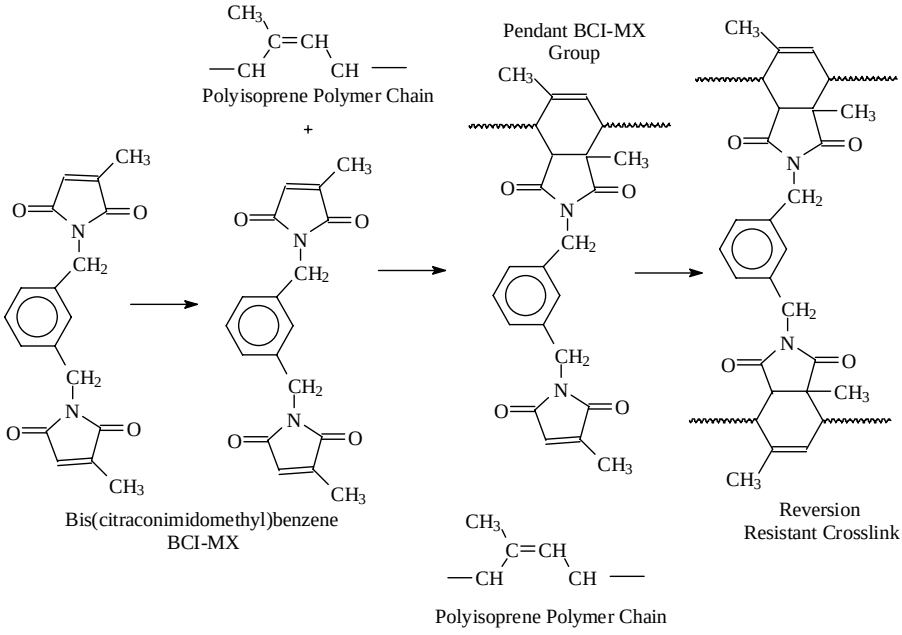

FIGURE 8 Proposed reversion resistance mechanism of bis(citraconimidomethyl)benzene (BCI-MX).

TABLE XXVII Comparison of the Scorch Activity of a Range of Selected Commercial Accelerators[a]

Accelerator	Abbreviation	Scorch time (min)	
		ACS 1	ACS 2
Diisopropylbenzothiazole	DIBS	63	21
Cyclohexyl-2-benzothiazolesulfenamide	CBS	26	15
tert-Butyl-2-benzothiazolesulfenamide	TBBS	60	23
Oxydiethylene benzothiazole-2-sulfenamide	MBS	60	24
Dimethylmorpholine benzothiazole-2-sulfenamide	—	60	27
Benzothiazyl-*N*,*N*-diethylthiocarbamyl sulfide	—	26	15
Mercaptobenzothiazole	MBT	12	9
Benzothiazyl disulfide	MBTS	73	12
Tetramethylthiuram monosulfide	TMTM	25	12
Tetramethylthiuram disulfide	TMTD	13	6
Tetraethylthiuram disulfide	TETD	18	9
Zinc dibutyldithiocarbamate	ZDBC	5	4
Zinc dimethylthiocarbamate	ZDMC	6	4
Diphenylguanidine	DPG	16	10

[a]Data obtained from the formulation ACS 2 (ASTM D3184-89, 2a) but containing 50 phr HAF.
[b]Use of nitrosamine-generating accelerators should be avoided.

3. Sodium hexamethylene-1,6-bisthiosulfide dihydrate, when added to the vulcanization system, breaks down and inserts a hexamethylene-1,6-dithiyl group within a disulfide or polysulfide crosslink. This is termed a hybrid crosslink. During extended vulcanization periods or accumulated heat history due to product service, polysulfidic–hexamethylene crosslinks shorten to produce thermally stable elastic monosulfidic crosslinks. At levels up to 2.0 phr, there is little effect on compound induction or scorch times, nor on other compound mechanical properties [39].

$$^{+}Na^{-}SO_3 — S — (CH_2)_6 — S — SO_3^{-}Na^{+} \cdot 2H_2O$$

Hexamethylene-1,6-bis(thiosulfate)
disodium salt, dihydrate

Table XXVII shows industry recognized abbreviations for various accelerators.

VI. SPECIAL COMPOUNDING INGREDIENTS

In addition to the four primary components in a rubber formulation, i.e., the polymer system, fillers, stabilizer system, and vulcanization system, there are a range of secondary materials such as processing aids, resins, and

TABLE XXVIII Physical Properties of Three Classes of Oils Used in the Rubber Industry

Physical property	ASTM methods	Paraffinic	Naphthanic	Aromatic
Specific gravity	D1250	0.85–0.89	0.91–0.94	0.95–1.0
Pour point (°F)	D97	0.0 to +10	–40 to +20	+40 to +90
Refractive index	D1747	1.48	1.51	1.55
Aniline point	D611	200–260	150–210	95.0–150.0
API gravity	D287	28.0–34.0	19.0–28.0	10.0–19.0
Molecular weight	D2502	320–650	300–460	300–700
Aromatic content (%)		15.0	44.0	68.0

coloring agents (e.g., titanium dioxide used in tire white sidewalls). These are briefly discussed to establish a guideline for the use of the materials in practical rubber formulations.

A. Processing Oils

Process oils in a rubber formulation serve primarily as a processing aid. Oils fall into one of three primary categories: paraffinic, naphthenic, and aromatic. The proper selection of oils for inclusion in a formulation is important. If the oil is incompatible with the polymer, it will migrate out of the compound with consequent loss in required physical properties, loss in rubber component surface properties, and deterioration in component-to-component adhesion, as in a tire. The compatibility of an oil with a polymer system is a function of the properties of the oil such as viscosity, molecular weight, and molecular composition. Table XXVIII defines the physical properties of three typical classes of oils.

Aniline point is a measure of the aromaticity of an oil. It is the point at which the oil becomes miscible in aniline. Thus the lower the aniline point, the higher the aromatic content. All three classes of oils contain high levels of cyclic carbon structures; the differences are in the number of saturated and unsaturated rings. Oils can therefore be described qualitatively as follows:

- Aromatic oils contain high levels of unsaturated rings, unsaturated naphthanic rings, and pendant alkyl and unsaturated hydrocarbon chains. The predominant structure is aromatic.
- Naphthenic oils have high levels of saturated rings and little unsaturation.
- Paraffinic oils contain high levels of naphthenic rings but also higher levels of alkyl pendant groups, unsaturated hydrocarbon pendant

TABLE XXIX Oil Selection Guide for Range of Commercial Elastomers

Oil	Polymer	Examples of product applications
Naphthenic	Ethylene-propylene rubber EPDM Polychloroprene SBR PBD	Sealants, caulking Adhesives General rubber products
Paraffinic	Natural rubber Polyisoprene Butyl SBR Polychloroprene	Textile application Caulking Sealants
Aromatic	Natural rubber SBR Polybutadiene	Tires Automotive components

groups, and, most important, fewer naphthenic groups per molecule. Pure paraffins from refined petroleum condense out as wax.

The selection of an oil for a given polymer depends on the presence of polar groups in the polymer, such as —CN groups in NBR and —Cl in CR. Hydrogen bonding and van der Waals forces impact on the effectiveness of an oil in a compound. Table XXIX presents a general guide for selection of an oil for a given polymer. This selection guide is necessarily brief and there are many exceptions. The key parameters to be noted though are the oil's tendency to discolor the product, the oil's tendency to stain adjacent components in a product, and the solubility of the oil in the polymer [36].

B. Plasticizers

Though processing oils, waxes, and fatty acids can be considered as plasticizers, within the rubber industry the term *plasticizer* is used more frequently to describe the class of materials which includes esters, pine tars, and low-molecular-weight polyethylene.

Phthalates are the most frequently used esters. Dibutylphthalate (DBP) tends to give soft compounds with tack; dioctylphthalate (DOP) is less volatile and tends to produce harder compounds because of its higher molecular weight. Polymeric esters such as polypropylene adipate (PPA) are used when low volatility is required along with good heat resistance.

Though total consumption is tending to fall, pine tars are highly compatible with natural rubber, give good filler dispersion, and can enhance

compound properties such as fatigue resistance and component-to-component adhesion which is important in tire durability. Other low-volume plasticizers include factice (sulfur-vulcanized vegetable oil); fatty acid salts such as zinc stearate, which can also act as a peptizer; rosin; low-molecular-weight polypropylene; and organosilanes such as dimethylpolysiloxane.

C. Chemical Peptizers

Peptizers serve as either oxidation catalysts or radical acceptors, which essentially remove free radicals formed during the initial mixing of the elastomer. This prevents polymer recombination, allowing a consequent drop in polymer molecular weight, and thus the reduction in compound viscosity. This polymer softening then enables incorporation of the range of compounding materials included in the formulation. Examples of peptizers are pentachlorothiophenol, phenylhydrazine, certain diphenylsulfides, and xylyl mercaptan. Each peptizer has an optimum loading in a compound for most efficiency.

Peptizers such as pentachlorothiophenol are generally used at levels between 0.1 and 0.25 phr. This enables significant improvement in compound processability, reduction in energy consumption during mixing, and improvement in compound uniformity. High levels can, however, adversely affect the compound properties, as excess peptizer continues to catalyze polymer breakdown as the product is in service.

D. Resins

Resins fall into one of three functional categories: (1) extending or processing resins, (2) tackifying resins, and (3) curing resins. Resins have been classified in an almost arbitrary manner into hydrocarbons, petroleum resins, and phenolic resins.

Hydrocarbon resins tend to have high glass transition temperatures so that at processing temperatures they melt, thereby allowing improvement in compound viscosity mold flow. They will, however, harden at room temperature, thus maintaining compound hardness and modulus. Within the range of hydrocarbon resins, aromatic resins serve as reinforcing agents, aliphatic resins improve tack, and intermediate resins provide both characteristics. Coumarone-indene resin systems are examples of such systems. These resins provide:

1. Improved tensile strength as a result of stiffening at room temperature
2. Increased fatigue resistance as a result of improved dispersion of the fillers and wetting of the filler surface
3. Retardation of cut growth by dissipation of stress at the crack tip (as a result of a decrease in compound viscosity)

Petroleum resins are a by-product of oil refining. Like hydrocarbon resins, a range of grades are produced. Aliphatic resins which contain oligomers of isoprene tend to be used as tackifiers, whereas aromatic resins, which also contain high levels of dicyclopentadiene, tend to be classed more as reinforcing systems.

Phenolic resins are of two types, reactive and nonreactive. Nonreactive resins tend to be oligomers of alkyl-phenyl formaldehyde, where the *para*-al-kyl group ranges from to C4 to C9. Such resins tend to be used as tackifying resins. Reactive resins contain free methylol groups. In the presence of methylene donors such as hexamethylenetetramine, crosslink networks will be created, enabling the reactive resin to serve as a reinforcing resin and adhesion promoter.

E. Short Fibers

Short fibers may be added to compounds to further improve compound strength. They can be processed just as other compounding ingredients. Short fibers include nylon, polyester, fiberglass, aramid, and cellulose. The advantages of adding short fibers to reinforce a compound depend on the application for which the product is used; however, general advantages include improved tensile strength, improvement in fatigue resistance and cut growth resistance, increase in stiffness, increased component or product stiffness, improved cutting and chipping resistance as in tire treads.

VII. COMPOUND DEVELOPMENT

The preceding discussion reviewed the range of materials which are combined in an elastomeric formulation to generate a defined set of mechanical properties. Elastomeric formulations can be developed by one of two techniques. Model formulations can be obtained from raw material supplier literature or other industry sources such as trade journals. Such formulations approximate the required physical properties to meet the product performance demands. Further optimization might then include, for example, acceleration level determination to meet a required compound cure induction time, and carbon black level evaluation to match a defined tensile strength target. Where more complex property targets must be met and no model formulations are available, a more efficient technique is to use either Taguchi analysis or multiple regression analysis.

A series of components in a formulation can be optimized simultaneously through use of a computer optimization. A number of models are suitable for use in designed experiments [40]. Regardless of the technique or model selected, a series of simple steps are still pertinent before the experimental work is initiated:

TABLE XXX Examples of Tire Compounds

	Tread	Sidewall	Wire coat	Ply coat	Inner liner
Polymer system	NR BR S-SBR E-SBR	NR BR	NR	NR BR	IIR CIIR BIIR NR
Filler system	SAF ISAF HAF	FF FEF GPF	HAF	HAF	GPF
Vulcanization system	Semi-EV	Adapted to polymer system	Conventional system	Conventional system Semi-Ev	Adapted to polymer system
Miscellaneous components	Oils Waxes	Antidegradants Waxes	Adhesion promoters	Adhesion promoters	—

1. Definition of the objective of the work
2. Identification of the variables in the formulation to be analyzed
3. Selection of the appropriate analysis for the accumulated experimental data
4. Analysis of the data within the context of previously published data and knowledge of the activity and characteristics of the raw materials investigated
5. Statistical significance of the data (data scatter, test error, etc.)

The designed experiment will then entail:

1. Define the key property targets, such as tensile strength, fatigue resistance, and hysteretic properties.
2. Select an appropriate design, for example a two-variable factorial or three-, four-, or five-variable multiple regression.
3. Calculate multiple regression coefficients from the accumulated experimental data. The coefficients can be computed from the regression equations which can be either a linear equation,

$$\text{property} = aX + bY + C$$

in the case of a simple factorial design, or a second-order polynomial where interactions between components in a formulation can be viewed:

$$\text{property} = aX + bY + cZ + dX^2 + eY^2 + fZ^2 + gXY + hXZ + jYZ + C$$

TABLE XXXI Model Truck Tire Tread Formulation

Natural rubber	100.00
Carbon black (N 220)	50.00
Peptizer	0.20
Paraffin wax	1.00
Microcrystalline wax	1.00
Aromatic oil	3.00
Polymerized dihydrotrimethylquinoline	1.00
Stearic acid	2.00
Zinc oxide	5.00
Sulfur	1.20
TBBS	0.95
DPG	0.35
Retarder (if required)	0.25

TABLE XXXII Model Sidewall Formulation

Natural rubber	50.00
Polybutadiene	50.00
Carbon black (N 330)	50.00
Peptizer	0.20
Paraffin wax	1.00
Microcrystalline wax	1.00
Aromatic oil	10.00
Polymerized dihydrotrimethylquinoline	1.00
Dimethylbutylphenyl-*p*-phenylenediamine	3.00
Stearic acid	2.00
Zinc oxide	4.00
Sulfur	1.75
TBBS	1.00
DPG	0.35
Retarder (if required)	0.25

Here, a property or the dependent variable might be modulus, and X, Y, and Z are independent variables such as oil level, carbon black level, and sulfur level. The terms a, b, c, d, etc., are coefficients for the respective dependent variables, and C is a constant for the particular model. Clearly, other equations are possible but depend on the objective of the study in question.

4. Construct appropriate contour plots to visualize trends in the data and highlight interaction between components in the formulation.

TABLE XXXIII Model Tire Casing Ply Coat

Natural rubber	70.00
Polybutadiene	30.00
Carbon black (N 660)	55.00
Peptizer	0.20
Paraffin wax	1.00
Microcrystalline wax	1.00
Aromatic oil	7.00
Polymerized dihydrotrimethylquinoline	1.00
Dimethylbutylphenyl-*p*-phenylenediamine	2.50
Stearic acid	2.00
Zinc oxide	4.00
Sulfur	2.50
MBTS	0.80

TABLE XXXIV Model Conveyor Belt Cover

Natural rubber	100.00
Carbon black (N 330)	50.00
Peptizer	0.20
Paraffin wax	1.00
Microcrystalline wax	1.00
Aromatic oil	5.00
Polymerized dihydrotrimethylquinoline	1.00
Dimethylbutylphenyl-*p*-phenylenediamine	2.50
Stearic acid	2.00
Zinc oxide	4.00
Sulfur	2.50
TBBS	1.00

5. Compute an optimization of the ingredients.
6. If required, run a compound confirmation study to verify the computed compound optimization.

A wide range of experimental designs are available, and it is recommended that the attached reference be reviewed for further information [40].

Table XXX to XXXV display a series of model formulations on which further compound optimization can be based. Additional formulations are available in industry publications such as those from the Malaysian Rubber Producer's Research Association [41,42].

TABLE XXXV Carpet Underlay

SBR	100.00
Calcium carbonate	150.00
Reclaim (as filler)	20.00
Clay	25.00
Iron oxide	4.00
Sodium bicarbonate	10.00
Blowing agent	1.00
Peptizer	0.20
Paraffin wax	1.00
Microcrystalline wax	1.00
Aromatic oil	60.00
Stearic acid	1.50
Zinc oxide	3.00
Sulfur	3.00
MBT	1.50
TMTD	0.50
DPG	0.50

VIII. COMPOUND PREPARATION

In a modern tire or general products production facility, rubber compounds are prepared in internal mixers. Internal mixers consist of a chamber to which the compounding ingredients are added. In the chamber are two rotors that generate high shear forces, dispersing the fillers and other raw materials in the polymer. The generation of these shear forces results in the production of a uniform, quality compound. After a defined mixing period, the compound is dropped onto a mill or extruder where mixing is completed and the stock sheeted out for ease of handling. Alternatively, the compound can be passed into a pelletizer.

Depending on the complexity of the formulation, size of the internal mixer, and application for which the compound is intended, the mix cycle can be divided into a sequence of stages. For an all-natural-rubber compound containing 50 phr carbon black, 3 phr of aromatic oil, an antioxidant system, and a semi-EV vulcanization system, a typical Banbury mix cycle will be as follows:

Stage 1 Add all natural rubber; add peptizer if required. Drop into a mill at 165°C.

Stage 2 Drop in carbon black, oils, antioxidants, zinc oxide, stearic acid, and miscellaneous pigments such as flame retardants at 160°C.

Stage 3 If required to reduce compound viscosity, pass the compound once again through the internal mixer for up to 90 seconds or 130°C.

Stage 4 Add the cure system to the compound and mix it up to a temperature not exceeding 115°C.

Computer monitoring of the internal mixer variables such as power consumption, temperature gradients through the mixing chamber, and mix times enables modern mixers to produce consistent high-quality compounds in large volumes. The mixed compound is then transported to either extruders for production of extruded profiles, calenders for sheeting, or injection molding.

Depending on the compound physical property requirements, compounds can be prepared on mills. Mill mixing takes longer, consumes larger amounts of energy, and gives smaller batch weights. The heat history of the compound is reduced, however, and this can be advantageous when processing compounds with high-performance fast acceleration systems. Two-roll mills function by shear created as the two rolls rotate at different speeds (friction ratio). This ratio of rolls speeds is variable and is set dependent on the particular type of compound. The higher the friction ratio, the greater the generated shear and intensity of mixing.

IX. ENVIRONMENTAL REQUIREMENTS IN COMPOUNDING

In addition to developing products to satisfy customers, the environmental implications of the technology must be taken into consideration. The environmental impact on compound development must be viewed in two parts: (1) product use and long-term ecological implications; (2) health and safety, in both product service and product manufacture.

An example of the impact of product usage and the environmental implications is tire rolling resistance and its effect on vehicle fuel consumption. Reduction in tire rolling resistance results in a drop in vehicle fuel consumption. This has an immediate impact on the generation of exhaust gases such as carbon monoxide, carbon dioxide, and nitrous oxides.

The crown area of the tire, which includes the tread and belts, accounts for approximately 75% of the radial passenger tire rolling resistance. Improvements in the hysteretic properties of the tread compound will therefore enable a reduction in tire rolling resistance and consequent improvements in vehicle fuel economy. The crown area and particularly the tread compound also affects the life cycle of the tire. Longer-wearing tires (including retreading) delay the point in time when used tires must enter the solid waste disposal system.

Critical to a tire's life cycle performance is the ability to maintain air pressure. Tire inner liners composed of halobutyl-based compounds exhibit very low air and moisture permeability. Therefore, tires built with the proper selection of compounds can reduce the rate of premature failure, again delaying entry into the scrap tire and solid waste streams.

Table XXXVI illustrates how the incorrect selection of a tire innerliner polymer will lead to more rapid deterioration in tire performance properties. Replacement of chlorobutyl with natural rubber or reclaim butyl will lead to a more rapid loss in tire air pressure and loss in overall tire performance [43].

TABLE XXXVI Relationship Between HIIR/IIR Content and Permeability, ICP, and Step-Load Endurance

Rubber hydrocarbon content in liner	HIIR/IIR, %Vol	Liner permeability (Ox 10^8) at 65 C+	Equilibrium intracarcass pressure (IOF). MPa	FMVSS 109 step-load hours to failure
100 BIIR	65.2	3.0	0.032	61.5
75 BIIR/25 NR	48.3	4.2	0.063	56.9
65 BIIR/35 NR/20 IIR*	42.2	5.9	0.063	40.2
60 SBR/40 NR/20 IIR*	16.1	6.9	0.090	31.5

*IIR via whole tube reclaim, containing ~50% by weight IIR. Treated as filler.

Improved tire designs have enabled reduction in noise levels. This has become an important environmental consideration. Optimum footprint pressures reduce damage to highway pavements and bridges. All of these improvements in tire rolling resistance, life cycle duration, noise generation, and tire footprint pressure have been incorporated into the full range of tires, from small automobile to heavy truck to large earthmover equipment tires. Today's radial tires use 60 to 80% natural rubber as the polymer portion of compounds. Because natural rubber is obtained from trees, it is an ideal renewable resource, and thus as a biotechnology material is preferred to petroleum-based synthetic polymers, when equivalent compound properties can be attained.

Tires are one of the most durable technological products manufactured today. They are a resilient, durable composite of fabric, steel, carbon black, natural rubber, and synthetic polymers. The qualities that make tires or other engineered rubber products a high-value item create a special challenge of disposal. Tires and other rubber products, such as conveyor belts and hydraulic hoses, are not biodegradable and cannot be recycled like glass, aluminum, or plastic. Four potential applications for such products entering the solid waste stream have been identified:

1. The calorific energy of tires is higher (35 MJ/kg) than that of coal (24 MJ/kg). With properly designed equipment, tires can be burned to produce heat in cement kilns.
2. Tires can be burned in furnaces at power-generating facilities to produce electrical energy.
3. Ground up scrap tires are beginning to find use in some special asphalt applications.
4. Tires with the proper installation technology can serve a variety of applications in the construction industry as marine reefs, energy-efficient house construction, highway bank reinforcement, and erosion control.

These four methods of disposal represent the best options for scrap tire and rubber products disposal. It is anticipated that a variety of new applications for disposal of scrap rubber products will emerge in the future.

In summary, materials scientists must consider the implications of their materials choices, from the quantity of energy to manufacture the product, to the performance during its useful life cycle, and finally to disposal methods. The Environmental Protection Agency (EPA) also provides constraints that the materials scientist must consider in the design of compounds. As most rubber compounds contain approximately 6 to 20 different materials, not only the materials themselves must be clean and harmless, but any by-products that form during product tire manufacturing must also be harmless to humans and the environment.

The aromatic content of carbon blacks and oils was once considered hazardous. Data were generated that showed that carbon black was stabilized and did not represent a hazard to workers. Resins for cure or tack, antioxidants, antiozonants, and cure accelerators also must be investigated to ensure that the material and any impurities meet changing health and safety standards. Materials safety data sheets and chemical health and toxicity data must be maintained on all materials.

Nitrosamine-generating chemicals represent an area where suspect materials have been removed from rubber products, even though no governing legislation has yet been drafted. Nitrosamines can be formed when secondary amine accelerators are used to cure rubber. These accelerator changes have a very significant effect on the total rubber industry.

Solvent composition and volatility limits can have significant effects on synthetic rubber production and also tire manufacturing. Limits of exposure to some trace impurities defined in the U.S. Federal Clean Air Act are to be based on the hazard represented, not simply the best available measurement capability.

In conclusion, the materials scientist must continue to adjust to the changes in both the environment and health and safety standards.

X. SUMMARY

This chapter has reviewed both the types and the properties of elastomers, compounding with a range of filler or reinforcement systems such as carbon black, and enhancement of filler performance by novel use of compounding ingredients such as silane coupling agents. Other issues such as antioxidant systems and vulcanization systems were also discussed. The role of the modern materials scientist in the tire and rubber industry is to use materials to improve current products and develop new products. Four key parameters govern this development process:

1. *Performance*: The product must satisfy customer expectations.
2. *Quality*: The product must be durable and have a good appearance, and appropriate inspection processes must ensure consistency and uniformity.
3. *Environment*: Products must be environmentally friendly in manufacturing, use, and disposal.
4. *Cost*: The systems must provide a value to the customer.

In meeting these goals rubber compounding has evolved from a "black art," as it was at the start of the 20th century, to a complex science necessitating knowledge in advanced chemistry, physics, and mathematics.

REFERENCES

1. "Worldwide Rubber Statistics, 2003," International Institute of Synthetic Rubber Producers, Houston, TX, 2003.
2. S. Datta, in "Rubber Compounding, Chemistry and Applications," B. Rodgers (Ed.), Marcel Dekker Inc., New York, 2004.
3. ASTM D2227-96: Standard specification for natural rubber technical grades, 2002.
4. The Rubber Manufacturers Association, "The International Standards of Quality and Packaging for Natural Rubber Grades, The Green Book," The International Rubber Quality and Packaging Conference, Office of the Secretariat, Washington, D.C., January 1979.
5. D. Bernard, C. S. L. Baker, and I. R. Wallace, "NR Technology," Vol. 16, 1985, pp. 19–26.
6. "The Synthetic Rubber Manual," 14th ed., International Institute of Synthetic Rubber Producers, Houston, TX, 1999.
7. S. M. Mezynski and M. B. Rodgers, "Heavy Duty Truck Tire Materials and Performance," Kautschuk Gummi Kunststoffe, Frankfurt, Vol. 46, 1993, pp. 718–726.
8. B. D. Simpson, "The Vanderbilt Rubber Handbook," 12th ed., R. Babbit (Ed.), R. T. Vanderbilt Co., Inc., Norwalk, CT, 1978.
9. K. H. Nordsiek, "The 'Integral Rubber' Concept—An Approach To An Ideal Tire Tread Rubber," Kautschuk Gummi Kunstsoffe, Frankfurt, Vol. 38, 1985, pp. 178–185.
10. M. B. Rodgers, W. H. Waddell, and W. Klingensmith, "Rubber Compounding," in "Kirk-Othmer Encyclopedia of Chemical Technology," 5th ed., John Wiley & Sons, New York, 2004.
11. G. L. Day and S. Futamura, Paper 22 presented at a meeting of the Rubber Division, American Chemical Society, New York, 1986.
12. H. L. Brantley and G. L. Day, Paper 33 presented at a meeting of the Rubber Division, American Chemical Society, New York, 1986.
13. W. J. Kern and S. Futamura, "Solution SBR as a Tread Rubber," ACS Rubber Division, Quebec, Paper 78, 1987.
14. N. Kumar, A. Chandra, and R. Mukhopadhyay, *International J. Polymer Science* **34**, 91 (1996).
15. W. H. Waddell, M. B. Rodgers, and D. S. Tracey, "Natural Rubber," ACS Rubber Division Meeting, Grand Rapids, MI, Paper A, 2004.
16. W. H. Waddell, M. B. Rodgers, and D. S. Tracey, "Tire Applications of Elastomers, Part 1. Treads," Rubber Division Meeting, Grand Rapids, MI, Paper H, 2004.
17. S. M. Mezynski and M. B. Rodgers, "Radial Medium Truck Tire Performance and Materials," ACS Rubber Division, Akron Rubber Group, 1989.
18. A. Saito, *International Polymer Science & Technology* **26**, T/19 (1999).

19. A. E. Oberster, T. E. Bouton, and J. K. Valaites, *Die Angewandte Mackromolekulare Chemie* **29/30** (Nr 367), 291 (1973).
20. W. A. Schneider, F. Huybrechts, and K. H. Nordesik, *Kautschuk Gummi Kunstsoffe* **44**, 528 (1989).
21. ASTM D1795-04. Standard Classification System for Carbon Blacks Used in Rubber Products, 2004.
22. ASTM D1566-04. Standard Terminology Relating to Rubber, 2004.
23. ASTM D3053-04. Standard Terminology Relating to Carbon Black, 2004.
24. W. M. Hess and W. K. Kemp, *Rubber Chem. Technol.* **56**, 390 (1983).
25. J. LeBras and E. Papirer, *Rubber Chem. Technol.* **52**, 43 (1979).
26. J. A. Ayala, W. M. Hess, F. D. Kistler, and G. Joyce, Paper 42 presented at a meeting of the Rubber Division, American Chemical Society, Washington, D.C., 1990.
27. J. A. Ayala, W. M. Hess, A. O. Dotson, and G. Joyce, *Rubber Chem. Technol.* **63**, 747 (1990).
28. S. Wolff and U. Gorl, "The Influence of Modified Carbon Blacks on Viscoelastic Compound Properties," Presented at International Rubber Conference, 1991.
29. W. A. Wampler, T. F. Carlson, and W. R. Jones, in "Rubber Compounding, Chemistry and Applications," B. Rodgers (Ed.), Marcel Dekker Inc., New York, 2004.
30. M. P. Wagner, *Rubber Chem. Technol.* **55**, 703 (1976).
31. A. Blume, H. D. Luginsland, W. Meon, and S. Uhrlandt, in "Rubber Compounding, Chemistry and Applications," B. Rodgers (Ed.), Marcel Dekker Inc., New York, 2004.
32. L. Bateman, C. G. Moore, M. Porter, and B. Saville, in "Chemistry and Physics of Rubber-Like Substances," John Wiley, New York, 1963.
33. S. Wolff, *Rubber Chem. Technol.* **55**, 967 (1983).
34. S. W. Hong, in "Rubber Compounding, Chemistry and Applications," B. Rodgers (Ed.), Marcel Dekker Inc., New York, 2004.
35. ASTM D3184-89. Standard Methods for Evaluation of and Test Formulations for Natural Rubber, 1989.
36. W. W. Barbin and M. B. Rodgers, in "Science and Technology of Rubber," 2nd ed., J. E. Mark, B. Erman, F. R. Eirich (Eds.), Academic Press, New York, 1994.
37. E. Morita, *Rubber Chem. Technol.* **53**, 393 (1980).
38. S. Wolff, Presented at a meeting of the Rubber Division, American Chemical Society, Las Vegas, NV, 1990.
39. "Rubber Chemicals," Flexsys Technical Bulletin, 1998.
40. R. J. DelVecchio, "Understanding Design of Experiments," Hanser, Cincinnati, OH, 1997.
41. Malaysian Rubber Producers' Research Association, "The Natural Rubber Formulary and Property Index," Imprint of Luton, England, 1984.
42. W. H. Waddell, R. S. Bhukuni, W. W. Barbin, and P. H. Sandstrom, in "The Vanderbilt Rubber Handbook," 13th ed., R. F. Ohm (Ed.), R. T. Vanderbilt Company, Norwalk, CT, 1990.
43. A. Niziolek, Nelsen, and R. Jones, *Kautschuk Gummi Kunststoffe*, **53**, 358 (2000).

10 Strength of Elastomers

A. N. GENT
The University of Akron
Akron, Ohio

I. INTRODUCTION

Fracture is a highly selective process: only a small number of those molecules making up a test piece or a component actually undergo rupture; the great majority are not affected. For example, of the 10^{26} chain molecules per cubic meter in a typical elastomer, only those crossing the fracture plane, about $10^{18}/m^2$, will definitely be broken. Moreover, these will not all break simultaneously but successively as the fracture propagates across the specimen at a finite speed.

Thus, the first questions posed in studying the strength of elastomers (and other materials as well) are: where and under what conditions does fracture begin? Also, what laws govern the growth of a crack once it has been initiated? This chapter seeks to answer such questions, first in a general way and then with particular reference to important modes of failure of elastomers in service. It does not deal with the rather complex problem of the strength of composite structures, such as a pneumatic tire, which involves failure of adhesive bonds at interfaces between the components as well as fracture of the components themselves.

We consider first the initiation of fracture from flaws or points of weakness, where the applied stresses are magnified greatly. The rate of development of cracks after initiation is treated next. Naturally, this depends on the local stress levels but also on the way in which these stresses vary with time. For

Science and Technology of Rubber, Third Edition

example, rapid crack growth may take place if stresses are applied and removed frequently, whereas the crack may grow quite slowly, if at all, when the same stresses are held constant and never removed. This phenomenon of accelerated growth under dynamic stressing is termed *mechanical fatigue* or *dynamic crack growth.* It is treated in Sections V(E) and VII.

Because rubber is viscoelastic, or more generally anelastic, to varying extents and because the mechanical properties depend on rate of deformation and temperature, it is not surprising to find that the strength is also dependent on the rate at which stresses are applied and on the temperature of measurement. These effects are discussed in Sections V(B) and VI(A). Other effects of the environment, notably the destructive action of ozone, are discussed in Section VIII. Finally, a brief survey is given of abrasive wear.

II. INITIATION OF FRACTURE

A. Flaws and Stress Raisers

Every solid body contains flaws or points of weakness resulting from heterogeneities of composition or structure. In addition, because of the presence of sharp corners, nicks, cuts, scratches, and embedded dirt particles or other sharp inclusions, applied stresses are magnified (concentrated) in certain regions of the body so that they greatly exceed the mean applied stress. Fracture will begin at such a site where the local stress exceeds a critical level and the small flaw starts to grow as a crack.

The stress concentration factor, i.e., the ratio of the stress at the tip of a sharp flaw σ_t to the applied tensile stress σ, is given by Inglis's relation for elastic solids that obey a direct proportionality between stress and strain [1]:

$$\sigma_t/\sigma = 1 + 2(l/r)^{1/2} \tag{1}$$

where l is the depth of an edge flaw and r is the radius of the tip in the unstressed state. If the flaw is totally enclosed, it is roughly equivalent to an edge flaw of depth $l/2$ (Fig. 1). Thus, edge flaws are more serious stress raisers than enclosed flaws of the same size, and they are more usual sources of fracture than inclusions, but not exclusively so. Heterogeneities of composition have been shown to nucleate fatigue cracks internally [2]. Also, some types of cracks cannot form near a free surface (see Section IV).

When the tip radius is much smaller than the depth of the flaw, as seems probable for the severe stress raisers responsible for fracture, Eq. (1) can be approximated by

$$\sigma = (\sigma_t r^{1/2})/2l^{1/2} \tag{2}$$

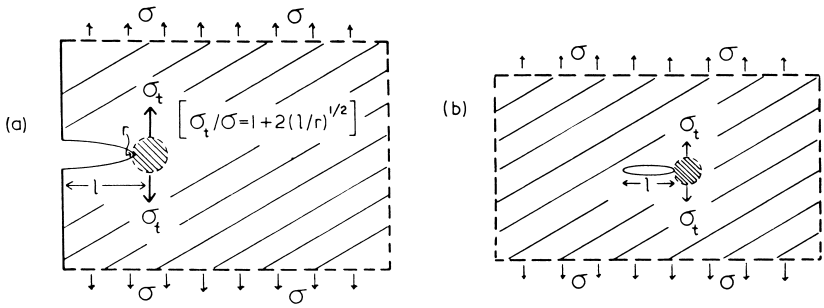

FIGURE 1 Stresses near a crack of depth l and tip radius r.

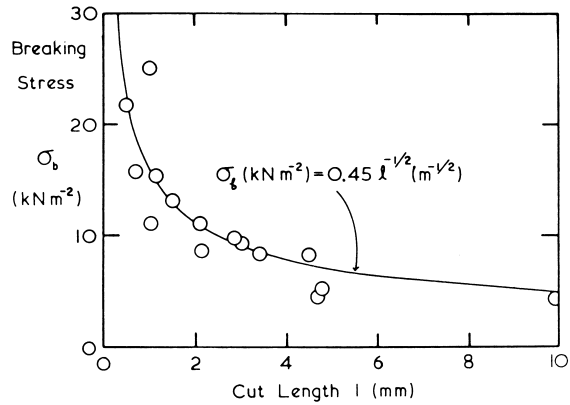

FIGURE 2 Fracture stresses for test pieces having cuts of depth l, exposed to ozone. (From Braden *et al.* [4].)

Thus, the breaking stress, denoted by σ_b, is predicted to vary inversely with the depth of the flaw l, in proportion to $1/l^{1/2}$. This prediction has been tested for brittle polymers, i.e., in the glassy state [3], and for rubbery materials cracked by ozone (Fig. 2). In both cases the breaking stress σ_b was found to vary in accordance with Eq. (2) with the depth of a crack or razor cut made in one edge of the test piece. For elastomers broken by mechanical stress alone, however, elongations at break are generally much too large for the assumption of linear stress–strain behavior to be valid, and Eq. (2) becomes a relatively poor approximation. Even so, by extrapolating measured values of the breaking stress for different depths of edge cut to the breaking stress for a test piece having no cuts introduced at all, the depth of flaw characteristic of the material may be inferred. (Actually, the value obtained is the depth of a cut equivalent in stress-raising power to natural flaws, which may be smaller

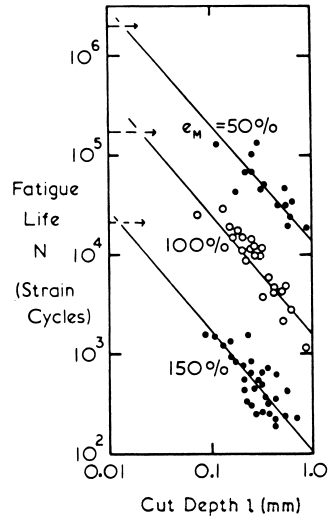

FIGURE 3 Fatigue lives N for test pieces having initial cuts of depth l, subjected to repeated extensions to the indicated strains.

and sharper, or larger and blunter, than knife cuts of equivalent stress–concentration power.)

For both rubbers and glasses the value obtained in this way is about $40 \pm 20\,\mu$m. The same value is also obtained by extrapolating measured stresses for ozone cracking (see Fig. 2) back to that value observed for a test piece having no initial cut in it, and also by extrapolating the fatigue lives of test pieces with cuts introduced in them back to the fatigue life for test pieces with no cuts (Fig. 3). In all these cases, substantially the same value of the natural flaw size is obtained. Moreover, it is largely independent of the particular elastomer or mix formulation used, even though these factors greatly alter the way in which the breaking stress or fatigue life changes with cut size, as discussed later. Thus, a variety of fracture processes appear to begin from a natural flaw equivalent to a sharp edge cut $40\,\mu$m deep.

The exact nature of these failure initiation sites is still not known. They may consist of accidental nicks in molded or cut surfaces, but even if great care is taken in preparing test pieces (e.g., by molding against polished glass), the breaking stress is not greatly increased. Dust or dirt particles or other heterogeneities nearly as effective as mold flaws seem to be present in a sufficient amount to initiate fracture. Only when the test piece size is reduced to about $10^{-8}\,m^3$ or less is a significant increase in strength observed, suggesting that powerful stress raisers are present only in concentrations of $10^8/m^3$ or less. Of course, if a way could be found to eliminate them, or at least reduce the effective sharpness of these natural flaws, substantial increases in strength, and even more striking increases in fatigue life, might be achieved, as discussed later. At

present, however, they appear to be an inevitable consequence of the processes used in making elastomeric materials and components.

B. Stress and Energy Criteria for Rupture

Equations (1) and (2) raise several other questions. What is the radius r of a natural flaw? What is the magnitude of the breaking stress at the tip σ_t when the flaw starts to grow as a crack? From a comparison of experimental relations such as that shown in Fig. 2 with the predictions of Eq. (2), only the product $\sigma_t r^{1/2}$ can be determined and not the two quantities separately. The value of r is, however, unlikely to exceed $1\,\mu$m for a sharp cut, and hence the tip stress σ_t may be inferred to be greater than 200 MPa, taking a value for the product $\sigma_t r^{1/2}$ of $0.2\,\mathrm{MN\,m^{-3/2}}$ as representative of fracture under mechanical stress. For ozone cracking this product takes the value $900\,\mathrm{N\,m^{-3/2}}$ (see Fig. 2), and hence the tip stress in this case is presumably 1 MPa or greater.

We must recognize, however, that a tear that begins to propagate from an initial cut or flaw will soon develop a characteristic tip radius r of its own, independent of the sharpness of the initiating stress raiser [5]. It is therefore more appropriate to treat the product $\sigma_t r^{1/2}$ as a characteristic fracture property of the material. Indeed, Irwin [6, 7] proposed that fracture occurs for different shapes of test piece and under varied loading conditions at a characteristic value of a "stress intensity factor" K_c, defined as

$$K_c = (\pi^{1/2}/2)\sigma_t r^{1/2} = \pi^{1/2}\sigma_b l^{1/2} \tag{3}$$

when expressed in terms of the applied stress σ_b by means of Eq. (2).

An alternative but equivalent view of the critical stress criterion for fracture was proposed by Griffith [8, 9] for elastic solids, and applied by Irwin [6, 7] and Orowan [10] to solids that are globally elastic, even when they exhibit plastic yielding around the crack tip. Griffith suggested that a flaw would propagate in a stressed material only when, by doing so, it brought about a reduction in elastically stored energy W more than sufficient to meet the free energy requirements of the newly formed fracture surfaces. Irwin and Orowan recognized that in practice the energy expended in local plastic deformation during crack growth generally far exceeds the true surface energy; however, provided that the total energy expended is proportional to the amount of surface created by fracture, Griffith's relations may still be employed.

Griffith's fracture criterion takes the form

$$-(\partial W/\partial A) \geq G_c/2 \tag{4}$$

where A is the surface area of the specimen, which increases as the crack grows, and G_c is the amount of energy required to tear through a unit area of the material. The factor 2 arises on changing from the area torn through to the area of the two newly formed surfaces. The derivative is evaluated at constant length of the sample, so that the applied forces do no work as the crack

advances. (An example where this is not appropriate, because the crack will advance only when the applied forces do the necessary work, is given in Section II[D].)

In Griffith's original treatment, the surface free energy per unit area of fracture plane was employed in place of the generalized fracture energy $G_c/2$. His results therefore carried the implication of thermodynamic reversibility. In contrast, G_c merely represents energy dissipated during fracture. Nevertheless, provided that it is dissipated in the immediate vicinity of the crack tip and is independent of the overall shape of the test piece and the way in which forces are applied to its edges, the magnitude of G_c can be employed as a characteristic fracture property of the material, independent of the test method. This expectation has been borne out by critical experiments on a variety of materials, including elastomers, using test pieces for which the relation between the breaking stress σ_b and the rate of release of strain energy on fracture G_c, defined by Eq. (4), can be either calculated or measured experimentally [11, 12]. Two important cases are considered here.

C. Tensile Test Piece

As shown in Fig. 4, a thin strip of thickness t with a cut in one edge of depth l is placed in tension until it breaks. The effect of the cut in diminishing the total stored elastic energy at a given extension may be calculated approximately by considering a small triangular region around the cut (shown shaded in Fig. 4) to be unstrained and the remainder of the test piece to be unaffected by the presence of the cut, with stored strain energy U per unit volume. The reduction in strain energy due to the presence of the cut is thus kl^2tU, where k is a numerical constant whose value depends on the applied strain (k is given

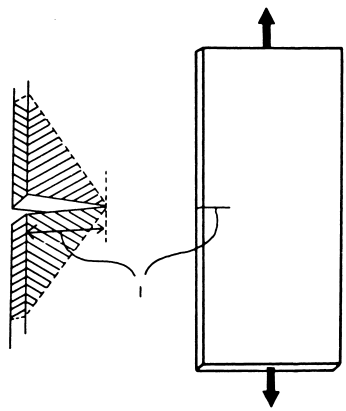

FIGURE 4 Tensile test piece.

approximately by $\pi/(1 + e)^{1/2}$, where e is the tensile strain [13]). Thus, as the tensile strain increases, k decreases from a value of π at small strains, to about 1 at large strains.]

For a tensile test piece, therefore, $-(\partial W/\partial A) = klU$ and $(\partial A/\partial l) = 2t$. Equation (4) becomes [11]

$$2klU \geq G_c \tag{5}$$

We note that the breaking stress σ_b does not appear explicitly in this fracture criterion. σ_b is the stress at which the strain energy density U satisfies Eq. (5). It therefore depends on the elastic properties of the material and the length of the initial cut, as well as on the fracture energy G_c. For a material obeying a linear relation between tensile stress σ and extension e, the stored energy U is given by $Ee^2/2$ or $\sigma^2/2E$, where E is Young's modulus. The stress and extension at break are therefore given by

$$\sigma_b = (G_c E/\pi l)^{1/2} \tag{6}$$

$$e_b = (G_c/\pi l E)^{1/2} \tag{7}$$

where k has been given the value π appropriate to linearly elastic materials. Equations (6) and (7) were obtained by Griffith [9].

On comparing Eqs. (3) and (6), we see that the critical stess intensity factor K_c and the fracture energy, or critical strain energy release rate G_c, are related to each other and to the breaking stress at the crack tip, as follows:

$$K_c^2 = EG_c = (\pi/4)\sigma_t^2 r = (\pi/2)U_t E r \tag{8}$$

where U_t is the strain energy density at the crack tip. Hence,

$$G_c = (\pi/2)U_t r \tag{9}$$

The fracture energy G_c is thus a product of the energy required to break a unit volume of material at the crack tip, i.e., in the absence of nicks or external flaws, and the effective diameter of the tip, as pointed out by Thomas [14]. These two factors can be regarded as independent components of the fracture energy: an "intrinsic" strength U_t and a characteristic roughness or bluntness of a developing crack, represented by r. Because K_c also involves the elastic modulus E, it is not considered as suitable a measure of the fracture strength as G_c for materials, like elastomers, of widely different moduli.

Equation (5) is more generally applicable than Eq. (6) because it is not restricted to linearly elastic materials. It constitutes a criterion for tensile rupture of a highly elastic material having a cut in one edge of length l, in terms of the fracture energy G_c. Two important examples of test pieces of this type are (1) the ASTM "tear" test piece for vulcanized rubber (ASTM D624-54) and (2) a typical tensile test piece that has accidental small nicks caused, for example, by imperfections in the surface of the mold or die used to prepare it.

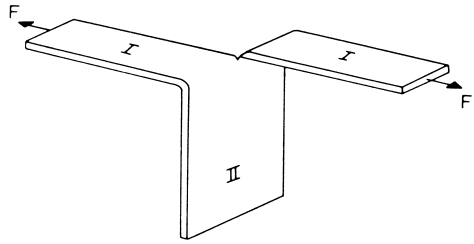

FIGURE 5 Tear test piece.

Several features of Eqs. (6) and (7) are noteworthy. For a given value of fracture energy G_c, stiffer materials with higher values of Young's modulus E will have higher breaking stresses and lower extensions at break than softer materials. These correlations are well known in the rubber industry. Less well known is the effect of the size of an initial cut or flaw on both the breaking stress and elongation at break. Finally, if the fracture criterion, Eq. (5), is met for an initial flaw of depth l, it will be greatly exceeded as fracture proceeds. As a consequence, a crack will accelerate across the specimen catastrophically.

D. Tear Test Piece

This test piece, shown in Fig. 5, has regions I in the arms that are in simple extension and a region II that is virtually undeformed. If the arms are sufficiently wide, or if they are reinforced with inextensible tapes, their extension under the tear force F will be negligibly small. The work of fracture $G_c\Delta A$ is then provided directly by the applied force F acting through a distance $2\Delta l$, where Δl is the distance torn through. The corresponding area torn through is $t\Delta l$, where t is the thickness of the sheet.[1] On equating the work supplied to that required for tearing, the fracture criterion becomes [11]

$$F \geq G_c t/2 \tag{10}$$

Because the tear force in this case is a direct measure of the fracture energy G_c and is independent of the elastic properties of the material and of the length of the tear, this test piece is particularly suitable for studying the effects of composition and test conditions on G_c [17–22].

It is important to recognize that the fracture energy G_c is not a constant value for a particular material; it depends strongly on the temperature and rate of tear, i.e., the rate at which material is deformed to rupture at the tear tip, as discussed in Section V(B). Nevertheless, several critical values may be distinguished. The smallest possible value is, of course, twice the surface free

[1]Actually, the tear tends to run at 45° to the thickness direction, i.e., at right angles to the principal tensile stress, and thus the tear path has a width of about $\sqrt{2}t$ instead of t [15, 16].

energy, about 50 mJ/m^2 for hydrocarbon liquids and polymers [23]. Values of this order of magnitude are indeed observed for fracture induced by ozone, when the function of the applied forces is merely to separate molecules already broken by chemical reaction, as discussed in Section VIII.

Another critical value is that necessary to break all of the molecules crossing a plane, in the absence of any other energy-absorbing processes. This minimum energy requirement for mechanical rupture is found to be about 50 J/m^2; it is treated in the following section. Finally, there are the considerably larger values found in normal fracture experiments, ranging from 100 to 100,000 J/m^2. These are described in Section V.

III. THRESHOLD STRENGTHS AND EXTENSIBILITIES

A threshold value for the fracture energy of elastomers was first pointed out by Lake and Lindley from studies of fatigue crack growth [24]. By extrapolation, they found that a minimum amount of mechanical energy, about 50 J/m^2 of torn surface, was necessary for a crack to propagate at all. Mueller and Knauss measured extremely low tearing energies directly, by employing low rates of tear, high temperatures, and a urethane elastomer composition swollen highly with a mobile fluid [25]. Under these near-equilibrium conditions, they obtained a lower limit of about 50 J/m^2 for the tear energy, similar to Lake and Lindley's extrapolated value. More recently, threshold tear strengths have been measured for several elastomers, crosslinked to varying degrees [20–22]. Again, the values are about 20–100 J/m^2, much smaller than tear energies obtained in conventional tearing experiments, which range from about 10^3 to about 10^5 J/m^2, depending on tear rate, test temperature, and elastomer composition [26]. Indeed, they amount to only about 1 lb of force to tear through a sheet several inches thick.

Nevertheless, they are much larger than would be expected on the basis of C—C bond strengths alone. For example, about 2×10^{18} molecules cross a randomly chosen fracture plane having an area of 1 m^2, and the dissociation energy of the C—C bond is about 5×10^{-19} J. Thus, a fracture energy of only about 1 J/m^2 would be expected on this basis, instead of the observed value of about 50 J/m^2.

This large discrepancy has been attributed by Lake and Thomas [27] to the polymeric character of elastomers: many bonds in a molecular chain must be stressed equally to break one of them. Thus, the greater the molecular length between points of crosslinking, the greater the energy needed to break a molecular chain. On the other hand, when the chains are long, a smaller number of them cross a randomly chosen fracture plane. These two factors do not cancel out; the net effect is a predicted dependence of the threshold fracture energy G_0 on the average molecular weight M_c of chains between points of crosslinking, of the form [27]

$$G_0 = \alpha M_c^{1/2} \tag{11}$$

Two other features of molecular networks can be taken into account, at least in an approximate way: the presence of physical entanglements between chains, at a characteristic spacing along each chain of molecular weight M_e, and the presence of molecular ends that do not form part of the load-bearing network. Equation (11) then becomes

$$G_0 = \alpha[(1/M_c) + (1/M_e)]^{-1/2}[1 - 2(M_c/M)] \tag{12}$$

where M is the molecular weight of the polymer before crosslinking [27]. The constant α involves the density of the polymer, the mass, length, and effective flexibility of a monomer unit, and the dissociation energy of a C—C bond, assumed to be the weakest link in the molecular chain. If reasonable values are taken for these quantities [27], α is found to be about $0.3\,J/m^2$ (g/g-mole)$^{-1/2}$. Thus, for a representative molecular network, taking $M_c = M_e = 15{,}000$ and $M = 300{,}000$, the threshold fracture energy obtained is about $25\,J/m^2$, in reasonable agreement with experiment in view of uncertainties and approximations in the theory. Moreover, the predicted increase in fracture energy with molecular weight M_c between crosslinks appears to be correct; increased density of crosslinking (shorter network chains) leads to lower threshold fracture energies [20–22]. Because, however, the tensile strength σ_b also involves the elastic modulus E [Eq. (6)], and E is increased by crosslinking, the threshold tensile strength shows a net increase with increased crosslinking.

Threshold values of tensile strength and extensibility may be calculated by means of Eq. (6), using an average threshold fracture energy of $50\,J/m^2$, a "natural" flaw size of $40\,\mu m$ (assumed to be independent of composition), and a typical value for Young's modulus E for rubber of 2 MPa (corresponding to a Shore A hardness of about 48°). The results are $\sigma_{b,0} = 0.9$ MPa and $e_{b,0} = 0.45$. These values are indeed close to experimental "fatigue limits," i.e., stresses and strains below which the fatigue life is effectively infinite in the absence of chemical attack [24].

A surprisingly large effect has been found on the tensile strength and, by inference, on the tear strength of rubber as a result of the specific *distribution* of molecular weights M_c in the network [28]. When a small proportion of short chains, about 5 mole%, is combined in a network of long chains, the tensile strength is considerably higher than for other mixtures. It seems likely that the threshold strength is also higher. This remarkable enhancement of strength may be the result of strain redistribution within the network, i.e., the ability to undergo nonaffine deformation, so that internal stress concentrations are minimized. Whatever the cause, the phenomenon is clearly of both scientific and practical interest.

Low values of fracture energy, only about one order of magnitude greater than the threshold level, have been obtained by measuring the resistance of rubber to cutting with a sharp knife, a razor blade. Frictional effects were

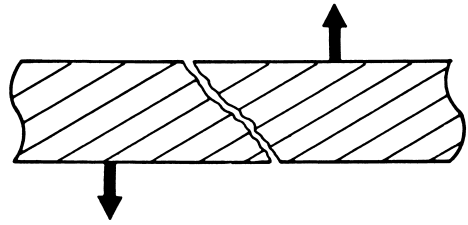

FIGURE 6 Tearing under shear stresses (schematic). (From Knauss [15] and Ahagon *et al.* [16].)

minimized by stretching the sample as it was being cut. By adding the energy supplied by the stretching force to that supplied by the cutter, the total fracture energy was found to be rather constant, and low, of the order of $300\,J/m^2$ [29]. The value was affected by the sharpness of the blade used, being lower for sharper blades, as would be expected from Eq. (9).

IV. FRACTURE UNDER MULTIAXIAL STRESSES

Although relatively few studies have been made of the fracture of elastomers under complex stress conditions, some general conclusions can be drawn regarding fracture under specific combined-stress states, as follows.

A. Compression and Shear

Elastomers do not appear to fail along shear planes. Instead, fractures develop at 45° to the direction of shear (Fig. 6), i.e., at right angles to the corresponding principal tensile stress [15, 16], at a shear stress theoretically equal to the tensile strength [9]. Indeed, the general condition for rupture appears to be the attainment of a specific tensile stress σ_t at the tip of an existing flaw, and this circumstance can arise even when both applied stresses are compressive, provided that they are unequal [9]. When all the compressive stresses are equal, i.e., under a uniform triaxial compression, the elastomer will merely decrease in volume. No case of fracture under such a loading condition is known.

Under a uniaxial compressive stress, the theory of brittle fracture predicts a breaking stress eight times as large as in tension [Eq. (6)] by growth of a crack in an oblique direction [9]. A uniform compressive stress is not, however, readily achieved. Instead, friction at the loaded surfaces of a thin compressed block generally prevents the elastomer from expanding freely in a lateral direction, and a complex stress condition is set up. The outwardly bulging surfaces may split open when the local tensile stress is sufficiently high, but this local fracture does not propagate inward very far because the interior is largely

under triaxial compression. Instead, the tear curves around and eventually causes a ring of rubber to break away from the outside of the block, leaving the remainder of the block intact but with a narrower central cross section [30]. Thus, a rubber block in compression is remarkably resistant to fracture, but its stiffness may be seriously reduced after many load cycles by loss of rubber from the outer regions.

Failure in simple shear is still more complex. An approximate treatment for an interfacial crack, starting at one edge, yields a relation analogous to Eq. (5):

$$G = kUt \tag{13}$$

Here the constant k is 0.4 initially and then varies between 0.2 and 1.0 as the crack length increases [31].

B. Equibiaxial Tension

Quite surprisingly, the breaking stress in equibiaxial tension has been found to be significantly greater than in uniaxial tension [32, 33], by about 20 to 30%. The breaking elongation is lower but the stored elastic energy at fracture is greater. It should be noted that test sheets put into a state of biaxial extension do not have a cut edge at the desired point of failure, in the central region of the sheet, whereas specimens for uniaxial tests are usually cut from sheets in the form of thin strips. Stress raisers caused by cutting will therefore be present only in uniaxial tests.

Experiments with rather brittle rubber sheets that contained deliberately introduced initial cracks of the same size and type in both uniaxial and biaxial specimens have shown that the breaking stress is still about 20 to 30% higher in equibiaxial tension [33]. The results were, however, consistent with a single value for the fracture energy G_c (about $150\,J/m^2$). The difference between the two tests is that when a crack grows in a sheet stretched equibiaxially, only about one-half of the strain energy stored in that area is released, whereas for a crack growing in a uniaxially stretched specimen, all of the energy is released. As a consequence, the strain energy needs to be considerably larger, about twice as large, to cause fracture in equibiaxial stretching.

C. Triaxial Tension

A small spherical cavity within a block of rubber will expand elastically from its original radius r_0 to a new radius λr_0 under the action of an inflating pressure P. In the same way, it will expand to an equal degree when the faces of the block are subjected to a uniform triaxial tension of $-P$, i.e., to a negative hydrostatic pressure (Fig. 7), provided that the rubber is itself undilatable. When the expansion is small, it is proportional to P and given by $\lambda = 1 + 3P/4E$, where E is Young's modulus of the rubber. When the expansion is large, it

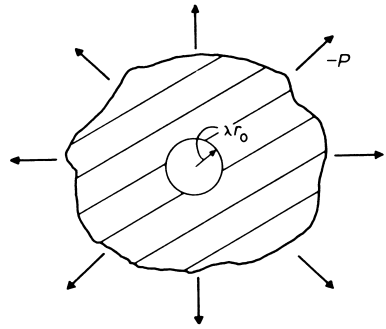

FIGURE 7 Expansion of a cavity under a triaxial tension.

increases more rapidly than in direct proportion. Indeed, for rubber obeying the neo-Hookean constitutive relation for elasticity (see Chapter 1), the expansion becomes indefinitely large at a finite value of the applied tension, given by [34–36]

$$-P = 5E/6 \tag{14}$$

Of course, the original cavity will burst when the expansion of its wall reaches the breaking extension of the rubber, and a large tear will form, governed by an energy requirement for growth. For large precursor voids, the tensile stress for bursting open is much smaller than Eq. (14) predicts [37]. And for small precursor voids, there are two further complexities: the actual surface energy of the void needs to be taken into account [37, 38], and the bursting stresses become so large that the rubber around the cavity will cease to follow elasticity relations valid only for low and moderate strains [39]. However, over a surprisingly wide range of initial radius r_0, from about $0.5\,\mu$m to about 1 mm, Eq. (14) is found to be a close approximation to the predicted fracture stress [39].

Rubber samples are almost invariably found to undergo internal cavitation at the triaxial tensions given by Eq. (14). This phenomenon must therefore be regarded as the consequence of an elastic instability, namely, the unbounded elastic expansion of preexisting cavities, too small to be readily detected, in accordance with the theory of large elastic deformations. It does not generally involve the fracture energy, because it is principally a transformation of potential energy (from the loading device) into strain energy. Apparently, rubber contains many precursor voids lying in the critical range, $0.5\,\mu$m to 1 mm (not larger because they would break open at lower stresses).

The critical stress predicted by Eq. (14) depends only on the elastic modulus and not at all on the strength of the elastomer. In agreement with this, cavitation stresses in bonded rubber blocks under tension (Figs. 8 and 9) [35], and near rigid inclusions, at points where a triaxial tension is set up (Figs.

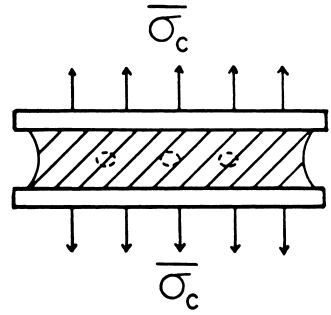

FIGURE 8 Cavitation in a bonded block (schematic).

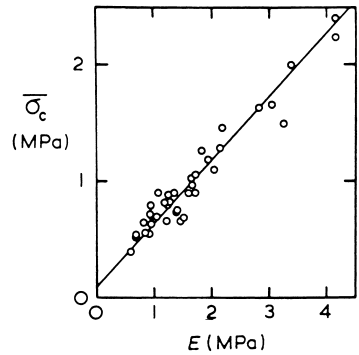

FIGURE 9 Critical applied stress σ_c for cavitation in bonded blocks (see Fig. 8) versus Young's modulus E of the elastomer. (From Gent and Lindley [35].)

10 and 11) [40], are found to be accurately proportional to E and independent of the tear strength of the elastomer, in accordance with the dominant role of an elastic rather than a rupture criterion for failure.

Cavitation near small rigid inclusions is more difficult to induce [41], probably because the volume of rubber subjected to a critical triaxial tension is too small to contain relatively large precursor voids. And larger stresses are necessary to expand small voids less than about 0.5 μm in diameter.

If elastomers could be prepared without any microcavities greater than, say, 10 nm in radius, they would be much more resistant to cavitation. This seems an unlikely development, however, so Eq. 14 remains an important general fracture criterion for elastomers. It predicts a surprisingly low critical triaxial tension, of the order of only a few atmospheres, for soft, low-modulus elastomers. Conditions of triaxial tension should probably be avoided altogether in these cases.

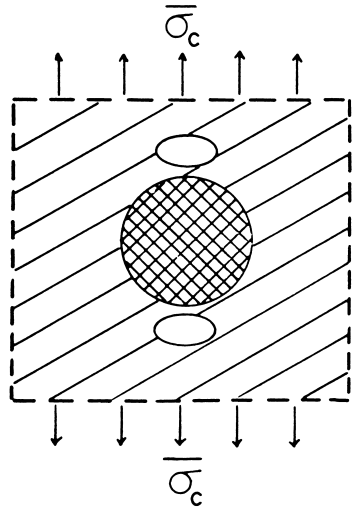

FIGURE 10 Cavitation near a rigid inclusion (schematic).

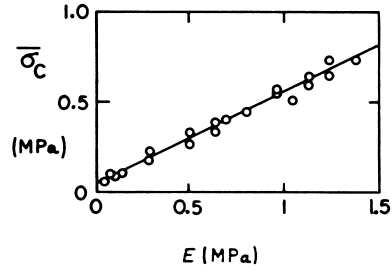

FIGURE 11 Critical applied stress σ_c for cavitation near rigid inclusions (see Fig. 10) versus Young's modulus E of the elastomer. (From Oberth and Bruenner [40].)

Cavitation is an important practical issue when elastomers are used for containing high-pressure gases [42]. If the gas dissolves in the rubber and migrates to fill the precursor voids, it will be at the (high) external pressure. Then, when the outside pressure is released suddenly, the voids break open in accordance with Eq. (14).

V. CRACK PROPAGATION

A. Overview

Whereas the initiation of fracture appears to be a similar process for all elastomers, the propagation of a crack is widely different. Three basic patterns

of crack propagation, or tearing, can be distinguished corresponding to three characteristic types of elastomeric compound:

1. Amorphous elastomers like SBR
2. Elastomers, like natural rubber and Neoprene, that crystallize on stretching, even if only at the crack tip where local stresses are particularly high
3. Reinforced elastomers containing large quantities, about 30% by volume, of a finely divided reinforcing particulate filler such as carbon black

Elastomers in the first category show the simplest tearing behavior and are therefore described first. For these materials, once fracture has been initiated, a tear propagates at a rate dependent on two principal factors: the strain energy release rate G and the temperature T. The former quantity represents the rate at which strain energy is converted into fracture energy as the crack advances. It is defined by a relation analogous to Eq. (4):

$$G = -2(\Delta W/\Delta A) \tag{15}$$

Here W denotes the total strain energy of the specimen and A denotes the surface area (which, of course, increases as the crack advances).

Even if a crack is stationary, because the critical value G_c at which fracture takes place has not been attained, Eq. (15) is still a useful definition of the rate G at which energy would be available from the strained specimen. For a tensile strip with an edge cut, it yields

$$G = 2\pi l U \tag{16}$$

by analogy with Eq. (5), and for a tear test piece,

$$G = 2F/t \tag{17}$$

from Eq. (10).

B. Viscoelastic Elastomers

Experimental relations between the fracture energy G, the rate of tearing, and the temperature of test are shown as a three-dimensional diagram in Fig. 12 for an SBR material. The fracture energy is seen to be high at high rates of tearing and at low temperatures, and vice versa, in a manner reminiscent of the dependence of energy dissipation in a viscous material on rate of deformation and temperature. Indeed, when the rates of tear are divided by the corresponding molecular segmental mobility ϕ_T at the temperature of test, the relations at different temperatures superpose to form a single master curve, as shown in Fig. 13 [43]. In this figure, the rates have been multiplied by the factor

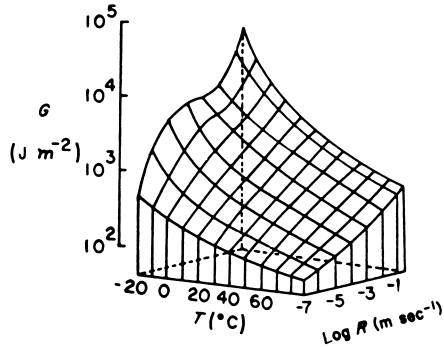

FIGURE 12 Fracture energy G for an unfilled SBR material as a function of temperature T and rate of tearing R. (From Greensmith and Thomas [17].)

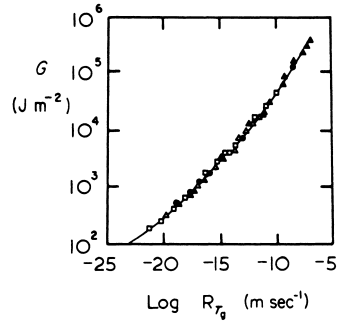

FIGURE 13 Fracture energy G versus rate of tearing R reduced to T_g for six unfilled amorphous elastomers. (From Mullins [43].)

$$a_T = \phi_{T_g} / \phi_T \tag{18}$$

to convert them into equivalent rates of tearing at the glass transition temperature T_g of the polymer, –57°C for the SBR material of Fig. 12.

Furthermore, values of fracture energy G for five other amorphous elastomers, two butadiene–styrene copolymers of lower styrene content (Tg = –72 and –78°C) and three butadiene–acrylonitrile copolymers having Tg values of –30, –38, and –56°C, all fall on a single curve in this representation, increasing with rate of tearing in a similar way to the dissipation of energy internally by a viscous process [43]. We conclude that the fracture energy G is approximately the same for all unfilled amorphous lightly crosslinked elastomers under conditions of equal segmental mobility, and that the dependence of tear strength on temperature arises solely from corresponding changes in segmental mobility.

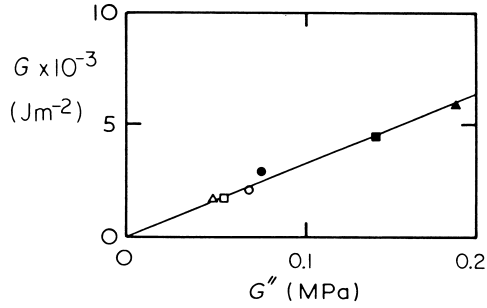

FIGURE 14 Fracture energy G versus shear loss modulus G'' for six unfilled amorphous elastomers. (From Mullins [43].)

Thus, internal energy dissipation determines the tear resistance of such elastomers: the greater the dissipation, the greater the tear strength. This point will also emerge in connection with variations in tensile strength of elastomers (see Section VI). It is demonstrated strikingly in the present case by a proportionality between fracture energy G and a direct measure of energy dissipation, namely, the shear loss modulus G'', for the same six elastomers (Fig. 14) [43].

For simple C—C crosslinked elastomers [44], the reduction factors a_T used to transform tear energy results at different temperatures as in Fig. 12 to yield a master curve as in Fig. 13 are found to correspond closely to the universal form of the WLF rate–temperature equivalence relation [45]:

$$\log a_T = -17.5(T - T_g)/(52 + T - T_g) \tag{19}$$

At low rates of tearing, about 10^{-20} m/s at T_g, the contribution from viscous losses becomes vanishingly small and the tear strength is reduced to the small threshold value, G_o. As the tear rate increases, the tear strength rises, approximately in proportion to $(Ra_T)^{0.24}$, until it becomes about $1000 \times G_o$, i.e., by about three orders of magnitude. Thus, over wide ranges of rate and temperature the strength of simple rubbery solids can be expressed as:

$$G/G_o = 1 + 2.5 \times 10^4 (Ra_T)^{0.24} \tag{20}$$

where G_o is determined by the structure of the molecular network [Eq. (11) and (12)] [44].

At the highest rates of tear, about 1 m/s at T_g the tear strength is extremely high, approaching 10^6 J/m^2. Simultaneously, elastomers become leathery and, eventually, glasslike. Indeed, at still higher rates and lower temperatures they would fracture like typical polymeric glasses, by a failure process in which a narrow craze band forms and propagates, and is followed by a running crack [46]. The fracture energy for this process is relatively small, about 500–1000 J/m^2, in comparison with that for highly viscous but highly deformable

elastomers, so that the curve shown in Fig. 13 turns sharply down at higher rates to level off at this value.

Why is the tear strength so strongly dependent on tear rate and temperature, i.e., on the viscoelastic response of the polymer? This striking feature has been explained by Knauss [47] as a consequence of retarded elasticity. His treatment assumes that the stress intensity factor K_c, given by Eq. (8), is largely unchanged by changes in rate and temperature, so that

$$K_c^2 = E(t)G_o = E(t = \infty)G \tag{21}$$

where $E(t)$ denotes the tensile modulus E at a time t after straining. $E(t = \infty)$ denotes the equilibrium modulus. Energy G obtained from a quasi-equilibrium solid far from the crack tip is expended in breaking material with a time-dependent modulus $E(t)$ at the crack tip. Thus, the fracture energy G is expected to increase with rate of tearing R approximately in proportion to the increase in elastic modulus E with rate of deformation,

$$G/G_o = E(t = \delta/R)/E(t = \infty) \tag{22}$$

where δ is a characteristic distance ahead of the crack tip over which the high stress concentration at the crack tip is built up. This simple picture gives a good representation of the observed increase in fracture energy with rate and temperature, but the value of δ obtained by a direct comparison of G and E is too small, about 1 Å, to be physically reasonable [44]. The discrepancy may arise because tearing is discontinuous on a microscopic scale, i.e., it may take place in a stick-slip fashion. When rubber is cut at a controlled rate with a sharp knife, the variation of cutting resistance with rate of cutting and temperature is found to be accounted for correctly by Eq. (22) using a value for δ about equal to the blade tip diameter [29, 48, 49].

The tear strength of sulfur-crosslinked elastomers is higher and its dependence on temperature is greater than would be expected from Eq. (19) [44]. This has been attributed to fracture of weak polysulfide crosslinks rather than the stronger C–C bonds in network chains. As a result, a second temperature-dependent process is introduced, because the strength of S–S bonds falls as the temperature is raised. The strength of practical rubber compounds thus reflects not only internal dissipation of energy from viscous processes [43] but also in detachment from filler particles, from changes in tear tip radius [48], and from fracture of weak crosslinks [44].

C. Strain-Crystallizing Elastomers

As shown in Fig. 15, the tear strength of strain-crystallizing elastomers is greatly enhanced over the range of tear rates and temperatures at which crystallization occurs on stretching, at the tear tip. At high temperatures, however, crystallization becomes thermodynamically prohibited because even the high melting temperatures of crystallites in highly stretched elastomers have been

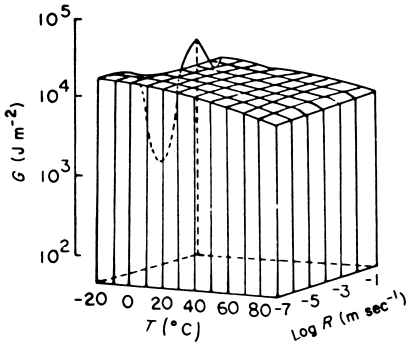

FIGURE 15 Fracture energy G for a strain-crystallizing elastomer, natural rubber, as a function of temperature T and rate of tearing R. (From Greensmith and Thomas [17].)

exceeded. Conversely, at low temperatures and high rates of tear, molecular reorganization into crystallites cannot take place in the short times of stretching as the crack tip advances. Thus, the strengthening effect of strain-induced crystallization is limited to a particular range of tear rates and temperatures, as seen in Fig. 15. Outside this range, the material has only the strength associated with its viscous characteristics, dependent on $T - T_g$.

The high strength of strain-crystallizing materials has been attributed to pronounced energy dissipation on stretching and retraction, associated with the formation and melting of crystallites under nonequilibrium conditions [50]. Reinforcing particulate fillers have a similar strengthening action, as discussed later, and they also cause a marked increase in energy dissipation. Whether this is the sole reason for the strengthening effect of crystallites and fillers, and other strengthening inclusions such as hard regions in block copolymers, hydrogen-bonded segments, etc., is not clear, however.

D. Reinforcement with Fillers

A remarkable reinforcing effect is achieved by adding fine particle fillers such as carbon black or silica to a rubber compound. They cause an increase in tear strength and tensile strength by as much as 10-fold when, for example, 40% by weight of carbon black is included in the mix formulation. But this strengthening action is restricted to a specific range of tear rates and test temperatures—ranges that depend on both the type of filler and the elastomer [17, 51] (Fig. 16). Outside this range of effectiveness, the filler does not enhance the observed strength to nearly the same degree.

The marked enhancement of tear strength in certain circumstances is associated with a pronounced change in the character of the tear process, from relatively smooth tearing with a roughness of the torn surface of the order of 0.1–0.5 mm to discontinuous stick-slip tearing, where the tear deviates from a

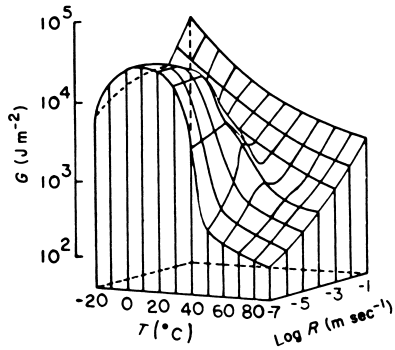

FIGURE 16 Fracture energy G for an amorphous elastomer (SBR) reinforced with 30% by weight FT carbon black. (From Greensmith [18].)

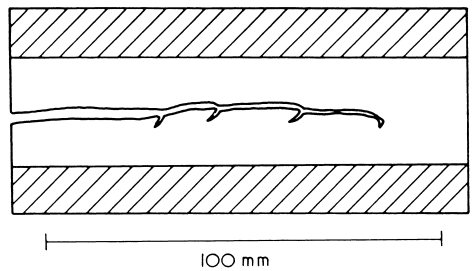

FIGURE 17 "Knotty" tear in a carbon-black-reinforced elastomer. (From Gent and Henry [52].)

straight path and even turns into a direction running parallel to the applied stress, until a new tear breaks through. This form of tearing has been termed *knotty tearing* [17]; an example is shown in Fig. 17. A typical tear force relation is shown in Fig. 18(a); it may be compared with the corresponding relation for an unfilled material in Fig. 18(c). The peak tearing force at the "stick" position reaches high values, but the force during catastrophic "slip" tearing drops to a much lower level, only about twice as large as that for continuous tearing of the unfilled elastomer. Indeed, when the tear is prevented from deviating from a linear path by closely spaced metal guides, or is made to propagate in a straight line by stretching [52] or prestretching [53] the sample in the tearing direction, then the tear force is much smaller, only two to three times that for the corresponding unfilled material (see Fig. 18[b]).

Thus, reinforcement of tear strength by fillers is of two kinds: a small (no more than two- to threefold) increase in intrinsic strength, and a major deviation of the tear path on a scale of several millimeters under special conditions of rate of tearing, temperature, and molecular orientation. The first effect

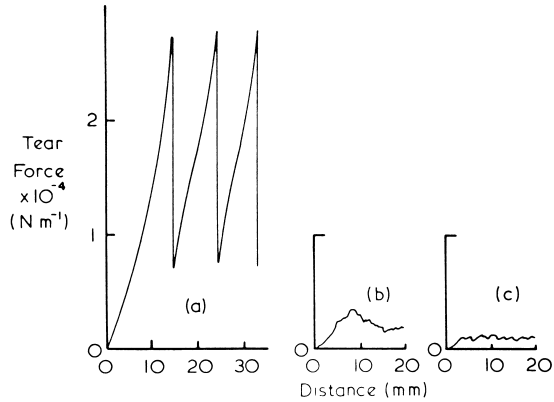

FIGURE 18 Tear force relations for (a) a filled elastomer without constraints; (b) the same material with the tear confined to a linear path; and (c) the corresponding unfilled elastomer, with and without constraints. (From Gent and Henry [52].)

may be attributed to enhanced energy dissipation in filled materials, as discussed in the previous section. The second is attributed to a *lowering* of the tear resistance sideways, parallel to the stretching direction. If the tear resistance is reduced sufficiently in the sideways direction, then the tear will be deflected sideways and rendered relatively harmless. Paradoxically, rubber is reinforced if its strength is lowered in a certain direction—one that does not result in catastrophic fracture. This mechanism of reinforcement is supported by two observations: measurements of tear strength in the stretching direction show a pronounced decrease as the stretch is increased, and calculations reveal that the energy available to turn a crack into this direction is surprisingly large (40% or more of that for continuing in the straight-ahead direction when the sample is highly stretched) [54]. Thus, when the tear strength in the stretching direction falls to 40% or less of that in the straight-ahead direction, the crack is expected to turn sideways.

E. Repeated Stressing: Dynamic Crack Propagation

Although amorphous elastomers are found to tear steadily, at rates controlled by the available energy for fracture G (as shown in Figs. 13 and 14), strain-crystallizing elastomers do not tear continuously under small values of G, of less than about 10^4J/m^2 for natural rubber for example (see Fig. 15). Nevertheless, when small stresses are applied repeatedly, a crack will grow in a stepwise manner by an amount Δl per stress application, even though the corresponding value of G is much below the critical level [5].

Experimentally, four distinct growth laws have been observed (Fig. 19) corresponding to four levels of stressing [55, 56]:

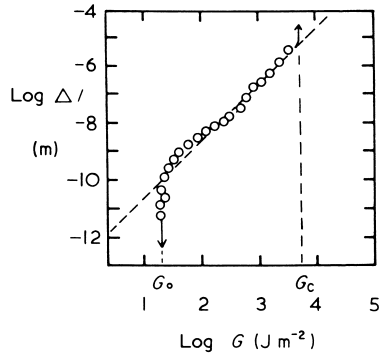

FIGURE 19 Crack growth step Δl per stress application versus energy G available for fracture, for a natural rubber vulcanizate. (From Lake and Lindley [24].)

1. $G < G_0$: no crack growth occurs by tearing, but only by chemical (ozone) attack.
2. $G_0 < G < G_1$: the growth step Δl is proportional to $G - G_0$.
3. $G_1 < G < G_c$: the growth step Δl is proportional to G^{α}.
4. $G \sim G_c$: catastrophic tearing.

The transitional value of G between one crack growth law and another, denoted G_1 above, is found to be about 400 J/m^2. No explanation has yet been advanced either for the form of these experimental growth laws or for the transition between them. They must therefore be regarded for the present as empirical relations for the growth step Δl per stress application.

In practice it is customary to approximate crack growth over a wide range of G values (but greater than the threshold value G_o) by a "Paris Law" relation that can be put in the form:

$$\Delta l = B'(G/G_0)^{\alpha} \tag{23}$$

where the constant B' is found to be about 1 Å per stress application for many rubber compounds and the exponent α takes different values for different elastomers, ranging from 2 for natural rubber compounds, represented by the broken line in Fig. 19, to values of 4 to 6 for noncrystallizing elastomers such as SBR and *cis*-/*trans*-polybutadiene.

Crack growth in natural rubber compounds is brought about only by imposing the deformation; if the deformation is maintained, the crack does not grow further under forces insufficient to cause catastrophic tearing. The reason for this is that a crystalline region develops in the highly stressed material at the crack tip and effectively precludes further tearing. This explains a striking feature of crack growth in strain-crystallizing elastomers: the growth steps under repeated stressing become extremely small if the test piece is not relaxed completely between each stress application [55]. In these

circumstances, the crystalline region does not melt; it remains intact to prevent further crack growth when the stresses are reimposed. As a result the mechanical fatigue life (discussed in the following section) becomes remarkably prolonged if the component is never relaxed to the zero-stress state (see Fig. 33). Indeed, failure in these circumstances is a consequence of chemical attack, usually by atmospheric ozone [55], rather than mechanical rupture.

Amorphous elastomers show more crack growth under intermittent stressing than under a steady stress, and the additional growth step per stress cycle is found to depend on the available energy for fracture G in substantially the same way as for natural rubber. The principal difference is that over region 3, the exponent α in Eq. (23) is about 4 for SBR in place of 2 for NR [56].

Andrews has put forward a general explanation for the slowing down of a crack in an amorphous elastomer (and the complete cessation of tearing in a strain-crystallizing elastomer), after the stresses have been applied, in terms of time-dependent stress changes at the tip of the crack [57, 58]. As a result, the stress concentration at the growing tip is smaller for a viscoelastic material, or for one which is energy-dissipating, than would be expected from purely elastic considerations. Crack growth is correspondingly slowed. This concept has features in common with that of Knauss, described briefly in Section V(B).

Oxygen in the surrounding atmosphere is found to increase crack growth, presumably by an oxidative chain scission reaction catalyzed by mechanical rupture. The minimum energy G_0 is found to be somewhat larger for experiments carried out *in vacuo* [55, 59, 60]. When antioxidants are included in the elastomer formulation, then the results in an oxygen-containing atmosphere approach those obtained *in vacuo*.

F. Thermoplastic Elastomers

Thermoplastic elastomers derive their physical characteristics from the fundamental immiscibility of different polymers. They consist of triblock molecules having the general structure A—B—A, where A denotes a glassy polymeric strand, e.g., of polystyrene, and B denotes a flexible polymeric strand, e.g., of polybutadiene. The end sequences A are immiscible in polymer B and hence they tend to cluster together to form small domains of a glassy polymer isolated within an elastomeric matrix. Moreover, because the sequences A at each end of one triblock molecule generally become part of different glassy domains, a network of elastomeric strands is formed, linked together by small hard domains, 10–30 nm in diameter. Materials of this kind behave in a characteristically rubberlike way, at least at temperatures below the glass temperature of polymer A and above that of polymer B.

The tear strength of a representative thermoplastic elastomer, Kraton 1101 (Shell Chemical Company), is quite comparable to that of a well-

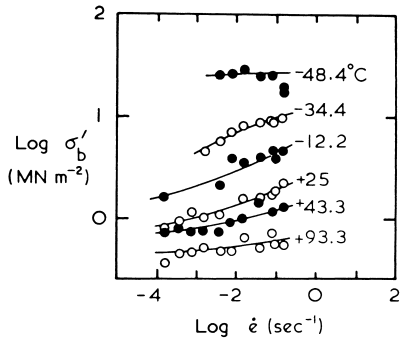

FIGURE 20 Breaking stress σ_b for an SBR vulcanizate versus rate of elongation $\dot{e}$. (From Smith [61].)

reinforced amorphous or strain-crystallizing elastomer, about 20 kJ/m^2 at room temperature. This remarkably high value is attributed to plastic flow of the hard domains under high local stresses, approaching the breaking point. Indeed, such a deformation process seems essential for these materials to have the capacity to dissipate strain energy, as any tough material must do.

VI. TENSILE RUPTURE

A. Effects of Rate and Temperature

In Fig. 20 several relations are shown for the breaking stress σ_b of an unfilled vulcanizate of SBR as a function of the rate of elongation at different temperatures [61]. A small correction factor (T_g/T) has been applied to the measured values to allow for changes in the elastic modulus with temperature. The corrected values are denoted σ_b'.

The experimental relations appear to form parallel curves, superimposable by horizontal displacements. The strength at a given temperature is thus equal to that at another temperature provided that the rate is adjusted appropriately, by a factor depending on the temperature difference. (Using a logarithmic scale for rate of elongation, a constant multiplying factor is equivalent to a constant horizontal displacement.) As in the case of fracture energy G (see V[B]), this factor is found to be the ratio ϕ_{T_g}/ϕ_T of segmental mobilities at the two temperatures [61]. It is readily calculated from the WLF relation [Eq. (19)]. A master curve may thus be constructed for a reference temperature T_s, chosen here for convenience as T_g, by applying the appropriate shift factors to relations determined at other temperatures. The master curve for tensile strength, obtained from the relations shown in Fig. 20, is given in Fig. 21.

The variation of tensile strength with temperature, like the variation in fracture energy, is thus due primarily to a change in segmental mobility.

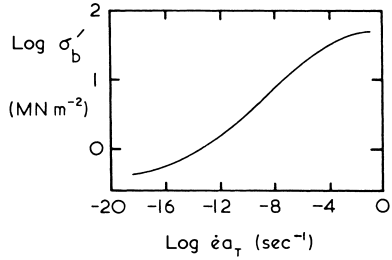

FIGURE 21 Master relations for breaking stress σ_b as a function of rate of elongation $\dot{e}$, reduced to T_g (–60°C) by means of the WLF relation, Eqs. (18) and (19). (From Smith [61].)

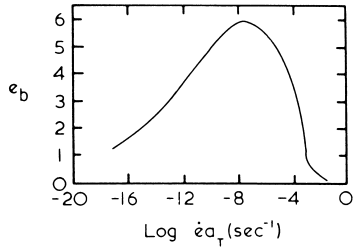

FIGURE 22 Master relations for breaking elongation e_b as a function of rate of elongation $\dot{e}$, reduced to T_g (–60°C). (From Smith [61].)

Moreover, the master curve has the form expected of a viscosity-controlled quantity: it rises sharply with increased rate of elongation to a maximum value at high rates when the segments do not move and the material breaks as a brittle glass [62]. The breaking elongation at first rises with increasing rate of elongation, reflecting the enhanced strength, and then falls at higher rates as the segments become unable to respond sufficiently rapidly (Fig. 22).

Rupture of a tensile test piece may be regarded as catastrophic tearing at the tip of a chance flaw. The success of the WLF reduction principle for fracture energy G in tearing thus implies that it will also hold for tensile rupture properties. Indeed, σ_b and e_b may be calculated from the appropriate value of G at each rate and temperature, using relations analogous to Eqs. (6) and (7). The rate of extension at the crack tip will, however, be much greater than the rate of extension of the whole test piece, and this discrepancy in rates must be taken into account [63].

In addition, it is clear from the derivation of Eq. (5) that U represents the energy obtainable from the deformed material rather than the energy put into deforming it. For a material with energy-dissipating properties, the energy available for fracture is only a fraction of that supplied. Such a material will therefore appear doubly strong in a tensile test or in any other fracture process

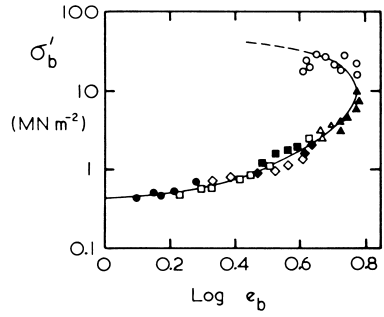

FIGURE 23 Failure envelope for an SBR vulcanizate. (From Smith [64].)

in which the tear energy is supplied indirectly by the relief of deformations elsewhere.

B. The Failure Envelope

An alternative representation of tensile rupture data over wide ranges of temperature and rate of elongation is obtained by plotting the breaking stress σ_b against the corresponding breaking extension e_b [64]. Tensile results on which Figs. 20–22 are based are replotted in this way in Fig. 23. They yield a single curve, termed the *failure envelope*, which has a characteristic parabolic shape. Following around the curve in an anticlockwise sense corresponds to increasing the rate of extension or to decreasing the temperature, although these two variables do not appear explicitly. Thus, at the lower extreme, the breaking stress and elongation are both small. These conditions are found at low rates of strain and at high temperatures. Conversely, the upper extreme corresponds to a high breaking stress and low extensibility. These conditions obtain at high rates of strain and low temperatures, when the material responds in a glasslike way.

The principal advantages of the "failure envelope" representation of data seem to be twofold. First, it clearly indicates the maximum possible breaking elongation $e_{b,max}$ for the material. This is found to be well correlated with the degree of crosslinking, specifically with the molecular weight between crosslinks M_c, as predicted by elasticity theory:

$$\lambda_{max} = 1 + e_{b,max} \propto M_c^{1/2} \tag{24}$$

Second, the failure envelope can be generalized to deal with different degrees of crosslinking, as discussed later. It has therefore been employed to distinguish between changes in crosslinking and other changes that affect the response to rate of elongation and temperature but do not necessarily affect M_c. Examples of this are plasticization and addition of reinforcing fillers [65].

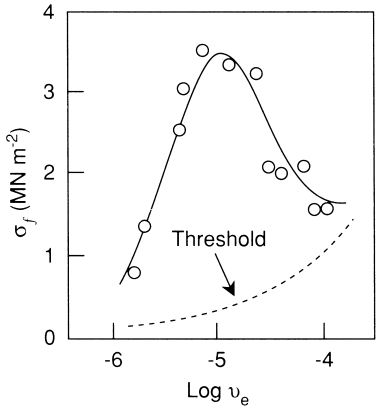

FIGURE 24 Tensile strength of SBR vulcanizates versus degree of crosslinking, represented by v_e. (From Bueche and Dudek [66].) Broken curve: author's estimate of threshold strength under nondissipative conditions.

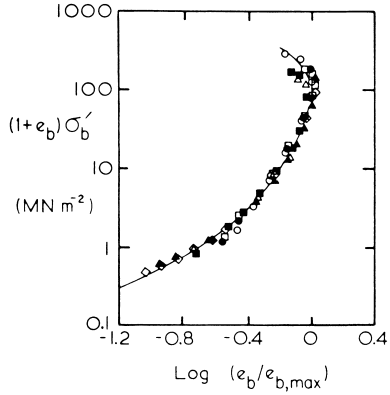

FIGURE 25 Failure envelope for Viton A-HV materials crosslinked to various extents ($e_{b,max}$ ranging from 2.5 to 18). (From Smith [65].)

C. Effect of Degree of Crosslinking

The breaking stress is usually found to pass through a sharp maximum as the degree of crosslinking is increased from zero. An example is shown in Fig. 24. This maximum is due primarily to changes in viscoelastic properties with crosslinking and not to changes in intrinsic strength. For example, it is much less pronounced at lower rates of extension [66], and it is not shown at all by swollen specimens [67]. Bueche and Dudek [66] and Smith and Chu [68] therefore conclude that it would not exist under conditions of elastic equilibrium.

Two different reduction schemes have been employed to construct failure envelopes for materials having different degrees of crosslinking. The first, shown in Fig. 25, consists of scaling the breaking elongation e_b in terms of its

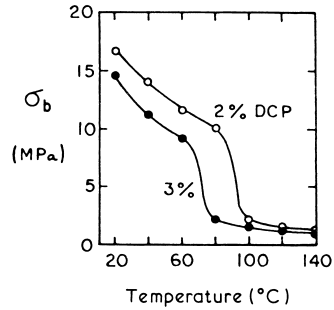

FIGURE 26 Tensile strength of natural rubber crosslinked with dicumyl peroxide (DCP) versus temperature. (From Thomas and Whittle [72].)

maximum value, which is, of course, dependent on the degree of crosslinking [Eq. (24)]. Also, the breaking stress σ_b is converted into a true stress at break, rather than the nominal stress employed until now. (The nominal tensile stress is given by the tensile force divided by the unstrained cross-sectional area of the specimen. It has been commonly used in the literature dealing with deformation and fracture of elastomers.) This reduction scheme is clearly quite successful in dealing with a wide range of crosslinking (see Fig. 25) [65].

The second method consists of scaling the stress axis by dividing the nominal stress at break by a measure of the density of crosslinking [69]. This method also appears to bring data from differently crosslinked materials into a common relationship.

D. Strain-Crystallizing Elastomers

Whereas amorphous elastomers show a steady fall in tensile strength as the temperature is raised (see Fig. 20), strain-crystallizing elastomers show a rather sudden drop at a critical temperature T_c (Fig. 26) [70–73]. This temperature depends strongly on the degree of crosslinking, as shown in Fig. 26. It is clearly associated with failure to crystallize at high temperatures; however, although the bulk of the specimen is amorphous above T_c, the highly strained material at the flaw tip probably continues to crystallize. Thomas and Whittle [72] draw a parallel between the drop in strength at the critical temperature T_c and the similar sharp drop at a critical depth l_c of an edge cut (Fig. 27), for strength measurements made at room temperature.

Two other aspects of the critical temperature are noteworthy. First, it is substantially the same for compounds reinforced with fillers. Second, it depends strongly on the type of crosslinking, being highest for long, polysulfidic crosslinks and lowest for carbon–carbon crosslinks. Apparently, labile crosslinks are an important factor in promoting crystallization.

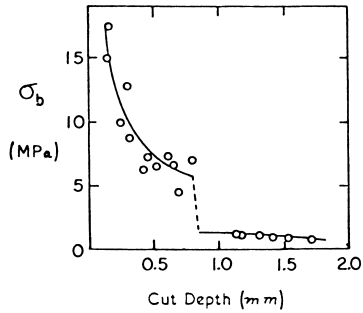

FIGURE 27 Tensile strength of natural rubber crosslinked with 2% dicumyl peroxide versus depth of initial edge cut. (From Thomas and Whittle [72].)

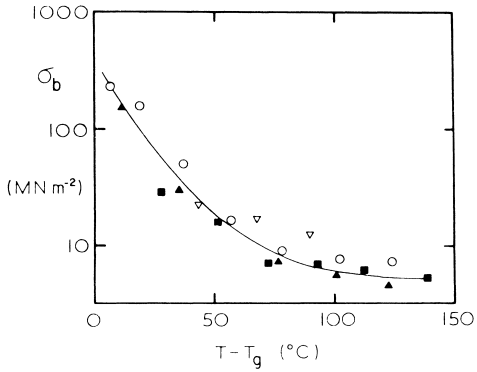

FIGURE 28 Tensile strength of polyurethane elastomers versus $T - T_g$ (T_g ranging from –67 to –17°C). (From Smith [65].)

E. Energy Dissipation and Strength

A general correlation between tensile strength and the temperature interval ($T - T_g$) between the test temperature T and the glass transition temperature T_g has been recognized for many years, as discussed in Section VI(B) [74]. An example is shown in Fig. 28, where the strengths of polyurethane elastomers with T_g values ranging from –67 to –17°C are plotted against $T - T_g$ [65]. All the results fall on a single curve in this representation, indicating once more that segmental viscosity governs the observed strength.

A more striking demonstration of the close connection between energy dissipation and strength has been given by Grosch *et al.* [75]. They showed that a direct relationship exists between the energy density required to break elastomers U_b and the energy density dissipated on stretching them almost to the breaking elongation U_d. This relationship held irrespective of the mechanism of energy loss, i.e., for filled and unfilled, strain-crystallizing and amorphous elastomers (Fig. 29). Their empirical relation is

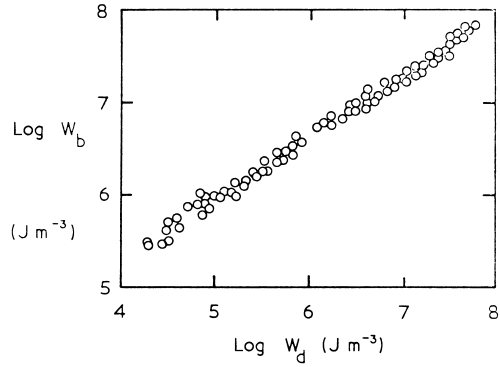

FIGURE 29 Work-to-break (W_b) versus energy dissipated (W_d) on stretching almost to the breaking elongation. (From Grosch, Harwood, and Payne [75].)

$$U_b = 410U_d^{2/3} \tag{25}$$

W_b and W_d are expressed in joules per cubic meter. Those materials that require the most energy to bring about rupture, i.e., the strongest elastomers, are precisely those in which the major part of the energy is dissipated before rupture.

VII. REPEATED STRESSING: MECHANICAL FATIGUE

Under repeated tensile deformations, cracks appear, generally in the edges of the specimen, and grow across it in an accelerating way. This process is known as fatigue failure. It has been treated quantitatively in terms of stepwise tearing from an initial nick or flaw [76, 77], as follows: Every time a deformation is imposed, energy G becomes available in the form of strain energy to cause growth by tearing of a small nick in the edge of the specimen. The value of G for tensile test pieces is given by Eq. (5). The corresponding growth step Δl is assumed to obey Eq. (22), i.e., to be proportional to G^a, so that the crack growth law becomes

$$\Delta l / l^{\alpha} = (2kU)^{\alpha} B' \Delta n \tag{26}$$

where n is the number of times the deformation is imposed and k is a numerical constant, about 2 (see Section II[C]). The depth of the crack after N strain cycles is then obtained by integration,

$$l_0^{(1-\alpha)} - l^{(1-\alpha)} = (2kU)^{\alpha} B' N \tag{27}$$

where l_0 is the initial depth of the nick. An example of crack growth is shown in Fig. 30; it conforms closely to Eq. (27) with $\alpha = 2.0$.

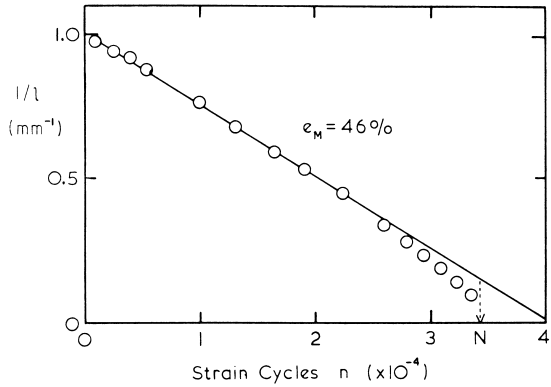

FIGURE 30 Growth of an edge crack in a test piece of a natural rubber vulcanizate stretched repeatedly to 46% extension. (From Greensmith, Mullins, and Thomas [26].)

If the crack grows to many times its original depth, so that $l \gg l_0$ before fracture ensues, then the corresponding fatigue life may be obtained by setting $l = \infty$ in Eq. (27) yielding

$$1/N = (2kU)^{\alpha} B' l_0^{(\alpha-1)} \tag{28}$$

This is a quantitative prediction for the fatigue life N in terms of the strain energy U and two material properties, the crack growth exponent α and the characteristic dimension B', which can be determined in a separate experiment as described earlier (see Section V[E]). Measured fatigue lives for specimens with initial cuts of different length (see Fig. 3) and for imposed deformations of different magnitude have been found to be in good agreement with the predictions of Eq. (28) [55, 76, 77].

Examples of the dependence of fatigue life on initial cut size are shown in Figs. 3 and 31. Lives for test pieces which contain no deliberately introduced cuts, represented by horizontal broken lines in Fig. 3, may be interpreted as stepwise tearing from a hypothetical nick or flaw, about 20 μm deep, as discussed previously. It is particularly noteworthy that closely similar sizes are deduced for natural flaws for both strain-crystallizing and noncrystallizing elastomers by such extrapolations, because for a noncrystallizing elastomer (SBR), the crack growth law is quite different over the main tearing region. The exponent α in the fatigue life relation, Eq. (28), becomes 4 in place of 2. Measured fatigue lives for an unfilled SBR compound have been found to be in good accord with this relation for a wide range of initial cut depths l_0 and deformation amplitudes [55].

The different crack growth laws for strain-crystallizing and noncrystallizing elastomers thus lead to quite different fatigue life relations. For a noncrystallizing elastomer, the fatigue life is much more dependent on the size of

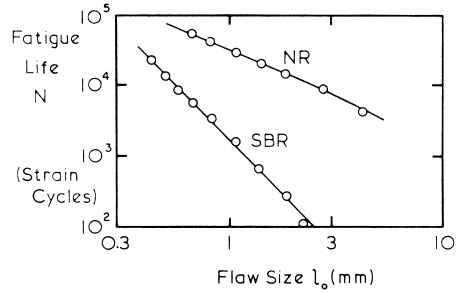

FIGURE 31 Fatigue life versus depth of initial cut for test pieces of natural rubber and SBR stretched repeatedly to 50% extension. (From Lake and Lindley [55].)

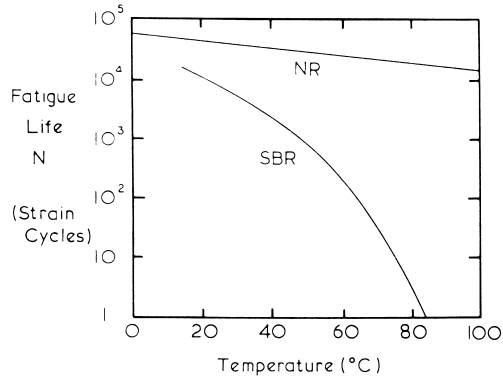

FIGURE 32 Fatigue life versus temperature for test pieces of natural rubber and SBR stretched repeatedly to 175% extension. (From Greensmith, Mullins, and Thomas [26].)

the initial flaw (see Fig. 31) and the magnitude of the imposed deformation, so that such elastomers are generally longer-lived at small deformations and with no accidental cuts, but much shorter-lived under more severe conditions. The fatigue life is also drastically lowered at high temperatures as a result of the sharp increase in cut growth rate as the internal viscosity is decreased (Fig. 32). In contrast, the hysteresis associated with strain-induced crystallization is retained, provided that the temperature does not become so high (about 100°C for natural rubber) that crystallization no longer occurs. The fatigue life for natural rubber is therefore not greatly affected by a moderate rise in temperature.

A more striking difference is found between strain-crystallizing and non-crystallizing elastomers when the stress is not relaxed to zero during each cycle. As shown in Fig. 33, the fatigue life of a natural rubber vulcanizate is greatly increased when the minimum strain is raised from zero to, say, 100% because the crystalline barrier to tearing at the tip of a crack does not then

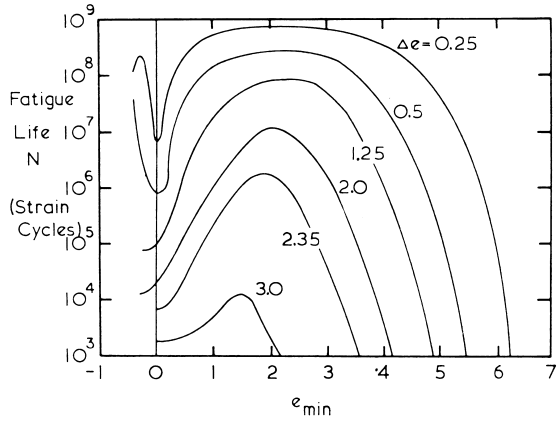

FIGURE 33 Fatigue life for test pieces of natural rubber versus minimum extension e_{min}. Δe denotes the additional strain imposed repeatedly. (From Cadwell *et al.* [78].)

disappear in the minimum-strain state. As a result, the growth of flaws is virtually stopped unless the total applied strain is very large, about 400%. No comparable strengthening effect on raising the minimum strain level is found for noncrystallizing elastomers.

Corresponding to the threshold value G_0 of tearing energy, below which no crack growth occurs by mechanical rupture, there is a minimum tensile strain e_0 below which normal-sized flaws do not grow under fatigue conditions. For typical elastomers, this mechanical fatigue limit is found to be about 50 to 100% extension, by calculation from Eq. (7) and by direct observation [24]. At extensions below this level, the fatigue life is infinite in the absence of chemical attack, for example, by ozone in the surrounding atmosphere.

Reinforcing fillers greatly enhance the tear strength and tensile strength of elastomers but do not cause an equivalent improvement in the crack growth and fatigue properties. At a given strain energy input, the measured lives are appreciably longer, but if compared at equal available energy levels, they are not much increased. The initial flaw size and threshold tear energy G_0 are therefore deduced to be similar to those for unfilled materials. The growth steps are apparently too small for pronounced deviation of the tear, and hence "reinforcement" against fatigue failure by this mechanism is not so pronounced.

VIII. SURFACE CRACKING BY OZONE

In an atmosphere containing ozone, stretched samples of unsaturated elastomers develop surface cracks which grow in length and depth until they eventually sever the test piece. Even when they are quite small, they can cause a

serious reduction in strength and fatigue life. The applied tensile stress necessary for an ozone crack to appear may be calculated approximately from Eq. (6). The fracture energy G is only about 0.1 J/m^2 [4], representing the small amount of energy needed for "fracture" of a liquid medium, i.e., about twice the surface energy for a hydrocarbon liquid [23]. Molecular scission apparently occurs readily by reaction with ozone, and does not require mechanical energy to be induced. Taking a representative value for E for a soft rubber of 2 MPa and a value of 40 μm for the effective depth l of a chance surface flaw, Eq. (6) yields a critical tensile stress for ozone cracking of about 50 kPa and a critical tensile strain of about 5%. These predictions are in reasonably good agreement with experimentally observed minimum values for ozone attack.

As the stress level is raised above the minimum value, numerous weaker stress raisers become effective and more cracks form. Actually, a large number of small, mutually interfering cracks are less harmful than a few widely separated cracks which develop into deep cuts, so that the most harmful condition is just above the critical stress.

The rate at which a crack grows when the critical energy condition is satisfied depends on two factors: the rate of incidence of ozone at the crack tip and the rate of segmental motion in the tip region. When either of these processes is sufficiently slow, it becomes rate controlling. The overall rate R of crack growth is thus given approximately by

$$R^{-1}\,(\mathrm{sec/m}) = 8 \times 10^{13}\phi_T^{-1} + 1.2 \times 10^5 C^{-1} \tag{29}$$

where ϕ_T (sec^{-1}) is the natural frequency of Brownian motion of molecular segments at the temperature T, given by the WLF relation [Eqs. (18) and (19)], in terms of ϕ_{T_g} (where $\phi_{T_g} = 0.1\,\mathrm{sec}^{-1}$ [45]), and C (mg/L) is the concentration of ozone in the surrounding air [79].

For a typical outdoor atmosphere, C is of the order of 10^{-4} mg/L, and the second term in Eq. (30) is then dominant for values of ϕ_T greater than about $10^4\,\mathrm{sec}^{-1}$, that is, at temperatures more than 25°C above T_g [79].

IX. ABRASIVE WEAR

A. Mechanics of Wear

Abrasive wear consists of the rupture of small particles of elastomer under the action of frictional forces, when sliding takes place between the elastomer surface and a substrate. A suitable measure of the rate of wear is provided by the ratio A/μ, where A is the volume of rubber abraded away per unit normal load and per unit sliding distance, and μ is the coefficient of friction. This ratio, termed *abradability*, represents the abraded volume per unit of energy dissipated in sliding. Master curves for the dependence of abradability on the speed of sliding, reduced to a convenient reference temperature by means of the

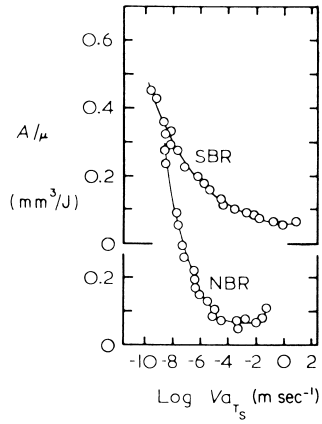

FIGURE 34 Abradability A/μ versus speed of sliding V, reduced to 20°C, for SBR and NBR vulcanizates. (From Grosch and Schallamach [80].)

WLF relation [Eqs. (18) and (19)], are shown in Fig. 34. The abradability is seen to decrease with increasing speed, pass through a minimum, and then rise again at high speeds as the material becomes glasslike in response. This behavior resembles the variation of the reciprocal of the breaking energy U_b with rate of deformation (a reciprocal relationship because high abradability corresponds to low strength). Indeed, Grosch and Schallamach [80] found a general parallel between A/μ and $1/U_b$. For this comparison values of the breaking energy U_b were determined at high rates of extension, about 10,000% per second, to bring them into agreement with measurements of abradability carried out at a sliding speed of 10 mm/sec. This scaling relation indicates that the size of the rubber elements involved in deformation and wear was of the order of 0.1 mm, comparable to the size of the abrasive asperities on the particular track employed in the experiments. Moreover, the coefficient of proportionality C between abradability and breaking energy was found to be similar, about 10^{-3}, for all the unfilled elastomers examined. The magnitude of C represents the volume A of rubber abraded away by unit energy applied frictionally to a material for which unit energy U_b per unit volume is necessary to cause tensile rupture. It may be regarded as a measure of the inefficiency of rupture by tangential surface tractions; large volumes are deformed but only small volumes are removed. Apparently the ratio is similar throughout the rubber-to-glass transition and for a variety of elastomers.

The abradabilities A/μ were found to be generally about twice as large for carbon black-filled elastomers as for corresponding unfilled materials. This surprising observation that "reinforced" materials wear away faster can be partially accounted for in terms of the tear strength measurements referred to in a previous section. Under conditions of relatively smooth tearing, it was concluded that the intrinsic strength of reinforced materials is not particularly high; instead, it was found to be comparable to that of unfilled elastomers. The

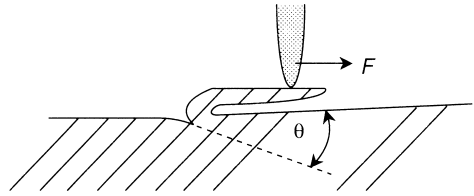

FIGURE 35 Sketch of a single surface ridge subjected to a frictional (tearing) force *F*. (From Southern and Thomas [81].)

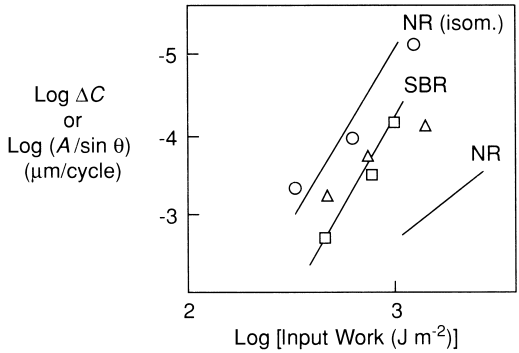

FIGURE 36 Rate of wear *A* versus frictional work input for NR, △; SBR, □; and isomerized (non-crystallizing) NR, ○. Solid lines represent crack growth properties Δl (= ΔC) of the same materials under repeated stressing. (From Southern and Thomas [81].)

measurements of abradability considered here suggest that it is actually somewhat lower under abrasion conditions.

Southern and Thomas [81] have related the rate of wear A to the crack growth resistance of the rubber by a simple theoretical treatment. A pattern of lateral ridges is generated in steady-state wear, known as the Schallamach abrasion pattern. A single ridge is shown in Fig. 35. The frictional force F pulls laterally on the ridge crest and tends to tear the rubber in the direction indicated by a broken line, at an angle θ to the surface. Fracture energy G is made available for tearing in this direction, given by $F(1 + \cos\theta)$. The crack will therefore advance by a distance Δl, given by Eq. (23). This leads to a loss in thickness of rubber of $\Delta l(\sin\theta)$. Thus,

$$A = B' \Big/ G_0^{\alpha} F^{\alpha} (1+\cos\theta)^{\alpha} \sin\theta \tag{30}$$

where α is either 2 or 4, depending on elastomer type. The angle θ may be estimated by direct inspection of the way in which abrasion patterns move over the surface during wear. All other terms in Eq. (30) can be determined from tear growth measurements. Thus, the theory does not involve any fitting constants. In these circumstances, it is remarkably successful in accounting for the rate of wear of several unfilled elastomers under severe conditions of pattern abrasion (Fig. 36).

Two difficulties must be mentioned, however. The agreement is unsatisfactory for unfilled natural rubber, which wears away much more rapidly than crack growth measurements would predict (see Fig. 36). It has been suggested that this material may not undergo strain-induced crystallization under abrasive conditions, i.e., under rapidly applied compressive and shearing stresses, and therefore does not show the high resistance to crack growth associated with crystallization. Also, the wear of reinforced rubber is much slower than would be predicted on the basis of crack growth measurements. Further work is needed to clarify this point, which is of great practical importance.

B. Chemical Effects

Under mild abrasion conditions, chemical changes within the elastomer become important in wear [82–84]. The scale of wearing remains small, but the particles of debris are often sticky and agglutinate to form larger particles, several millimeters in size. Indeed, *cis*-polyisoprene and poly(ethylene–co-propylene), for which molecular rupture under shearing conditions is particularly pronounced, both develop a tarry liquid surface during abrasion. In contrast, *cis*-polybutadiene shows no signs of structural deterioration. The debris appears to be unchanged chemically and nonadhering. Evidently, different chemical changes are undergone by different elastomers and are responsible for the different types of wear.

Two reactions can occur during wear: oxidative degradation as a result of frictional heating in the contact zone and mechanochemical degradation initiated by shear-induced rupture of chemical bonds. Present evidence favors the latter process. For example, in the absence of oxygen, the wear of *cis*-polyisoprene changes to resemble that of *cis*-polybutadiene, whereas the wear of poly(ethylene–co-propylene) is unaltered [84]. These results are in accord with the response of these materials to free radical reactions.

Surprisingly, the products of chemical changes within the elastomer are capable of causing rapid wear of metals used as abraders [85–87]. For example, when a knife blade is used as a scraper to abrade rubber, the blade itself wears away and becomes blunted, and the volume of metal removed is substantially greater when the broken elastomer molecules form relatively stable free radicals [87]. Thus, wear of the metal is attributed to direct chemical attack by reactive polymeric species, probably free radicals, during frictional contact [87]. Similar wear has been observed with polymers in other physical states [88]; it appears to be a quite general phenomenon when molecular rupture takes place during sliding.

ACKNOWLEDGMENTS

This review was initially prepared in the course of a program of research on fracture supported by a grant from the Office of Naval Research (Contract N00014-85-K-0222; Contract

Officer, Dr. R. S. Miller). It is based largely on five earlier reviews [89–93]. The author is indebted to E. H. Andrews, T. L. Smith, A. G. Thomas, and other authors cited in the text for many helpful discussions and to R. A. Paden for preparing many of the diagrams.

REFERENCES

1. C. E. Inglis, *Trans. Inst. Naval Architects* (*London*) **55**, 219 (1913).
2. R. J. Eldred, *J. Polym. Sci. B* **10**, 391 (1972).
3. J. P. Berry, in "Fracture: An Advanced Treatise," Vol. 7: "Fracture of Non-metals and Composites," H. Liebowitz (Ed.), Academic Press, New York, 1972, Chap. 2.
4. M. Braden and A. N. Gent, *Kautsch. Gummi* **14**, WT157 (1961); E. H. Andrews, D. Barnard, M. Braden, and A. N. Gent, in "The Chemistry and Physics of Rubberlike Substances," L. Bateman (Ed.), Wiley, New York, 1963, Chap. 12.
5. A. G. Thomas, *J. Polym. Sci.* **31**, 467 (1958).
6. G. R. Irwin, "Fracturing of Metals," Am. Soc. Metals, Cleveland, 1948.
7. G. R. Irwin, *J. Appl. Mech.* **24**, 361 (1957).
8. A. A. Griffith, *Philos. Trans. R. Soc.* (*London*), *Ser. A* **221**, 163 (1921).
9. A. A. Griffith, "Proceedings, 1st International Congress on Applied Mechanics, Delft, 1924," pp. 55–63.
10. E. Orowan, *Rep. Progr. Phys.* **12**, 185 (1949).
11. R. S. Rivlin and A. G. Thomas, *J. Polym. Sci.* **10**, 291 (1953).
12. A. G. Thomas, *J. Appl. Polym. Sci.* **3**, 168 (1960).
13. H. W. Greensmith, *J. Appl. Polym. Sci.* **7**, 993 (1963); G. J. Lake, in "Proceedings, International Conference on Yield Deformation Fracture Polymers, Cambridge," Institute of Physics, London, 1970, p. 53.
14. A. G. Thomas, *J. Polym. Sci.* **18**, 177 (1955).
15. W. G. Knauss, *Int. J. Fracture Mech.* **6**, 183 (1970).
16. A. Ahagon, A. N. Gent, H.-W. Kim, and Y. Kumagai, *Rubber Chem. Technol.* **48**, 896 (1975).
17. H. W. Greensmith and A. G. Thomas, *J. Polym. Sci.* **18**, 189 (1955).
18. H. W. Greensmith, *J. Polym. Sci.* **21**, 175 (1956).
19. A. G. Veith, *Rubber Chem. Technol.* **38**, 700 (1965).
20. A. Ahagon and A. N. Gent, *J. Polym. Sci.*, *Polym. Phys. Ed.* **13**, 1903 (1975).
21. A. N. Gent and R. H. Tobias, *J. Polym. Sci.*, *Polym. Phys. Ed.* **20**, 2051 (1982).
22. A. K. Bhowmick, A. N. Gent, and C. T. R. Pulford, *Rubber Chem. Technol.* **56**, 226 (1983).
23. H. Tarkow, *J. Polym. Sci.* **28**, 35 (1958).
24. G. J. Lake and P. B. Lindley, *J. Appl. Polym. Sci.* **9**, 1233 (1965).
25. H. K. Mueller and W. G. Knauss, *Trans. Soc. Rheol.* **15**, 217 (1971).
26. H. W. Greensmith, L. Mullins, and A. G. Thomas, in "The Chemistry and Physics of Rubberlike Substances," L. Bateman (Ed.), Wiley, New York, 1963, Chap. 10.
27. G. J. Lake and A. G. Thomas, *Proc. R. Soc.* (*London*) *A* **300**, 108 (1967).
28. J. E. Mark and M.-Y. Tang, *J. Polym. Sci.*, *Polym. Phys. Ed.* **22**, 1849 (1984).
29. G. J. Lake and O. H. Yeoh, *Int. J. Fracture Mech.* **14**, 509 (1978); *Rubber Chem. Technol.* **53**, 210 (1980).
30. A. Stevenson, *Int. J. Fracture Mech.* **23**, 47 (1983).
31. P. B. Lindley and S. C. Teo, *Plast. Rubber Mater. Appl.* **4**, 29 (1979).
32. R. A. Dickie and T. L. Smith, *J. Polym. Sci. A*-2 **7**, 687 (1969).
33. C. W. Extrand and A. N. Gent, *Int. J. Fracture Mech.* **48**, 281 (1991).
34. A. E. Green and W. Zerna, "Theoretical Elasticity," Sect. 3.10. Oxford Univ. Press, London, 1954.
35. A. N. Gent and P. B. Lindley, *Proc. R. Soc.* (*London*) *A* **249**, 195 (1958).
36. G. H. Lindsay, *J. Appl. Phys.* **38**, 4843 (1967).

37. M. L. Williams and R. A. Schapery, *Int. J. Fracture Mech.* **1**, 64 (1965).
38. A. N. Gent and D. A. Tompkins, *J. Polym. Sci. A*-2 **7**, 1483 (1969).
39. A. N. Gent and C. Wang, *J. Mater. Sci.* **26**, 3392 (1991).
40. A. E. Oberth and R. S. Bruenner, *Trans. Soc. Rheol.* **9**, 165 (1965).
41. A. N. Gent and B. Park, *J. Mater. Sci.* **19**, 1947 (1984).
42. B. J. Briscoe and S. Zakaria, *Polymer* **31**, 440 (1990).
43. L. Mullins, *Trans. Inst. Rubber Ind.* **35**, 213 (1959).
44. A. N. Gent and S.-M. Lai, *J. Polym. Sci.: Part B: Polym. Phys.* **32**, 1543 (1994).
45. J. D. Ferry, "Viscoelastic Properties of Polymers," 2nd ed., Wiley, New York, 1970.
46. R. P. Kambour, *J. Polym. Sci.*, *Macromol. Rev.* **7**, 1 (1973).
47. W. G. Knauss, in "Deformation and Fracture of Polymers," H. H. Kausch, J. A. Hassell, and R. I. Jaffee (Eds.), Plenum Press, New York, 1974, pp. 501–540; J. M. Bowen and W. G. Knauss, *J. Adhesion* **39**, 43 (1992).
48. G. J. Lake and O. H. Yeoh, *J. Polym. Sci.* **25**, 1157 (1987).
49. A. N. Gent, S.-M. Lai, C. Nah, and C. Wang, *Rubber Chem. Technol.* **67**, 610 (1994).
50. E. H. Andrews, *J. Appl. Phys.* **32**, 542 (1961).
51. D. De and A. N. Gent, *Rubber Chem. Technol.* **69**, 834 (1996).
52. A. N. Gent and A. W. Henry, in "Proceedings, International Rubber Conference, London, 1967," Maclaren, London, 1968, pp. 193–204.
53. R. Houwink and H. H. J. Janssen, *Rubber Chem. Technol.* **29**, 4 (1956).
54. A. N. Gent, M. Razzaghi-Kashani, and G. R. Hamed, *Rubber Chem. Technol.* **76**, 122 (2003).
55. G. J. Lake and P. B. Lindley, *Rubber J. Int. Plast.* **146**, 24; **146**, 30 (1964).
56. G. J. Lake and P. B. Lindley, *J. Appl. Polym. Sci.* **10**, 343 (1966).
57. E. H. Andrews, *J. Mech. Phys. Solids* **11**, 231 (1963).
58. E. H. Andrews and Y. Fukahori, *J. Mater. Sci.* **12**, 1307 (1977).
59. A. N. Gent and M. Hindi, *Rubber Chem. Technol.* **63**, 123 (1990).
60. A. N. Gent, G. L. Liu, and T. Sueyasu, *Rubber Chem. Technol.* **64**, 96 (1991).
61. T. L. Smith, *J. Polym. Sci.* **32**, 99 (1958).
62. F. Bueche, *J. Appl. Phys.* **26**, 1133 (1955).
63. F. Bueche and J. C. Halpin, *J. Appl. Phys.* **35**, 36 (1964); J. C. Halpin, *Rubber Chem. Technol.* **38**, 1007 (1965).
64. T. L. Smith, *J. Polym. Sci. A* **1**, 3597 (1963).
65. T. L. Smith, "Rheology," F. R. Eirich (Ed.), Academic Press, New York, Vol. 5, 1969, Chap. 4.
66. F. Bueche and T. J. Dudek, *Rubber Chem. Technol.* **36**, 1 (1963).
67. L. M. Epstein and R. P. Smith, *Trans. Soc. Rheol.* **2**, 219 (1958).
68. T. L. Smith and W. H. Chu, *J. Polym. Sci. A*-2 **10**, 133 (1972).
69. R. F. Landel and R. F. Fedors, in "Proceedings 1st International Conference on Fracture, Sendai," Vol. 2, p. 1247, Japan. Soc. Strength and Fracture of Materials, Tokyo, 1966.
70. B. B. S. T. Boonstra, *India Rubber World* **121**, 299 (1949).
71. J. A. C. Harwood, A. R. Payne, and R. E. Whittaker, *J. Appl. Polym. Sci.* **14**, 2183 (1970).
72. A. G. Thomas and J. M. Whittle, *Rubber Chem. Technol.* **43**, 222 (1970).
73. A. N. Gent and L.-Q. Zhang, *Rubber Chem. Technol.* **75**, 923 (2002).
74. A. M. Borders and R. D. Juve, *Ind. Eng. Chem.* **38**, 1066 (1946).
75. K. A. Grosch, J. A. C. Harwood, and A. R. Payne, *Nature* **212**, 497 (1966).
76. P. B. Lindley and A. G. Thomas, in "Proceedings, Fourth International Rubber Conference, London, 1962," pp. 428–442.
77. A. N. Gent, P. B. Lindley, and A. G. Thomas, *J. Appl. Polym. Sci.* **8**, 455 (1964).
78. S. M. Cadwell, R. A. Merrill, C. M. Sloman, and F. L. Yost, *Ind. Eng. Chem.*, *Anal. Ed.* **12**, 19 (1940).
79. A. N. Gent and J. E. McGrath, *J. Polym. Sci. A* **3**, 1473 (1965).
80. K. A. Grosch and A. Schallamach, *Trans. Inst. Rubber Ind.* **41**, 80 (1965).
81. E. Southern and A. G. Thomas, *Plast. Rubber Mater. Appl.* **3**, 133 (1978).

82. G. I. Brodskii, N. L. Sakhnovskii, M. M. Reznikovskii, and V. F. Evstratov, *Sov. Rubber Technol.* **18**, 22 (1960).
83. A. Schallamach, *J. Appl. Polym. Sci.* **12**, 281 (1968).
84. A. N. Gent and C. T. R. Pulford, *J. Appl. Polym. Sci.* **28**, 943 (1983).
85. G. A. Gorokhovskii, P. A. Chernenko, and V. A. Smirnov, *Sov. Mater. Sci.* **8**, 557 (1972).
86. Y. A. Evdokimov, S. S. Sanches, and N. A. Sukhorukov, *Polym. Mech.* **9**, 460 (1973).
87. A. N. Gent and C. T. R. Pulford, *J. Mater Sci.* **14**, 1301 (1979).
88. G. V. Vinogradov, V. A. Mustafaev, and Y. Y. Podolsky, *Wear* **8**, 358 (1965).
89. E. H. Andrews, "Fracture in Polymers," American Elsevier, New York, 1968.
90. A. N. Gent, in "Fracture: An Advanced Treatise," Vol. 7: "Fracture of Non-metals and Composites," H. Liebowitz (Ed.), Academic Press, New York, 1972, Chap. 6.
91. F. R. Eirich and T. L. Smith, in "Fracture: An Advanced Treatise," Vol. 7: "Fracture of Non-metals and Composites," H. Liebowitz (Ed.), Academic Press, New York, 1972, Chap. 7.
92. A. N. Gent and C. T. R. Pulford, in "Developments in Polymer Fracture—1," E. H. Andrews (Ed.), Applied Science Publishers, London, 1979, Chap. 5.
93. G. J. Lake and A. G. Thomas, Strength, in "Engineering with Rubber," 2nd ed., A. N. Gent (Ed.), Hanser Publishers, Munich, 2001, Chap. 5.

11 The Chemical Modification of Polymers

A. F. HALASA
Research and Development
The Goodyear Tire & Rubber Company
Akron, Ohio

JEAN MARIE MASSIE
Lexmark International
Lexington, Kentucky

R. J. CERESA
Chemistry and Polymer Technology Department
Polytechnic of South Bank
London, England

I. INTRODUCTION

The terms *rubber* and *elastomer* embrace those polymers which have useful rubberlike, highly elastic properties at ambient temperatures; however, many polymers which are nonrubbers by themselves can be chemically modified to a relatively small extent to give products with very useful viscoelastic properties. For example, the introduction of a few chlorine atoms and sulfoxide groups into polyethylene changes the macromolecules so that they no longer tend to form crystalline regions, but become elastomers over a wide temperature range. These groups also allow vulcanization so that reversibly

Science and Technology of Rubber, Third Edition

deforming, solvent-resistant products can be formulated. On the other hand, starting with a conventional rubber, it is possible, by means of chemical reactions, to convert the macromolecular chains so that they lose their viscoelasticity and become thermoplastic at ambient temperatures (e.g., the cyclization of polyisoprenes). Quite apart from the question of the temperature at which observations are carried out, the borderline between the viscoelastic and the plastic states is a relatively ill-defined one. The common factor of rubbers and plastics is, of course, their macromolecular nature. Now that we have a better understanding of their structure at a molecular level (not forgetting rubber-modified plastics and "plasticized" rubbers), we are able to say that, with some exceptions, a modification that can be carried out on one polymer species may, under suitable conditions, be carried out on a polymer of a different species. Whether the same type of chemical modification will give us the properties we are seeking without the loss of properties we would wish to retain is a matter, first, for conjecture and, subsequently, for experimental verification.

In the early days of polymer chemistry and technology, a new chemical modification successfully applied to one polymer was quickly evaluated with a whole range of chemically similar reagents (e.g., the esterification of cellulose), and the same type of reaction was attempted with the available range of similar material. Today, the number of homopolymers available runs into the hundreds, and the number of random copolymers runs into the thousands; therefore, the number of possible chemical modifications, including block and graft copolymers, runs into astronomical figures. Only a fraction of these potential systems has been evaluated (and then frequently only in a superficial way to obtain patent coverage) so that the field is wide open for research and development. Because of its breadth and depth, the field of the chemical modification of polymers can be treated only in outline in a single chapter, and only the more important reactions can be described. To serve the interest of the reader, however, this broad survey is punctuated by discussions in greater depth of areas that are of interest to rubber chemists and that, in the opinion of the writer, have considerable potential for further development. The emphasis is on the principles underlying the chemical modification of polymers; specific details of reactions conditions are deliberately omitted. A number of aspects of the chemical modification of rubbers have been covered in detail elsewhere in this book, and the reader is referred to the appropriate chapters on chemistry, vulcanization, characterization, block copolymers, and so on.

II. CHEMICAL MODIFICATION OF POLYMERS WITHIN BACKBONE AND CHAIN ENDS

Polymer properties are dependent on many factors, including chain end interactions with substrates such as carbon black or silica fillers, as well as clay

and calcium carbonate. At this point, there is a large volume of work that has been done on chain end modification, particularly those made by anionic polymerization with group I or group II metals [1, 2, 3], as seen below:

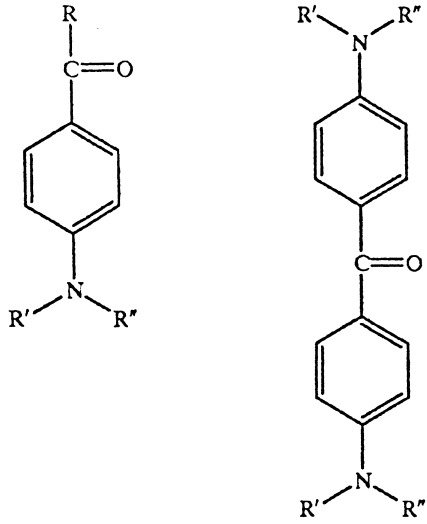

This approach was made possible via the reaction of metallic chain ends with active metal halide as shown on the following page, such as tin tetrachloride and silica terachlorides. These types of reactions led to increased molecular weight as well as improvements in polymer filler interactions that result in improved properties of the polymers [4].

Modification of polymers through the introduction of polar moieties such as amine siloxy groups made by anionic catalysts or so-called "living polymerizations" are made by either functional initiators or by chain functional monomers, as has been reported by several groups. The functional initiators are cyclic amines attached to alkyl groups and the functional monomers are based on styrene and disoproenyl benzene [5–9].

More recently, a U.S. Patent has been issued to the Goodyear Tire and Rubber Company, which claimed that polar functional monomers could be copolymerized with conjugated dienes and vinyl aromatics to chemically modify the polymer chain. Functional monomers, such as 3-(2-pyrrolidinoethyl) styrene:

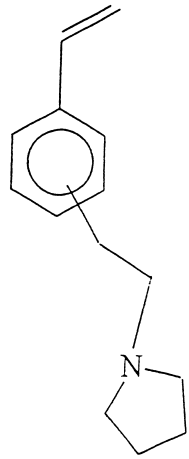

or 3-(pyrrolidino-2-methylethyl) α-methylstyrene:

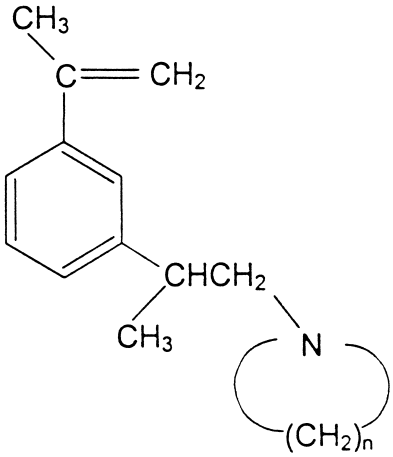

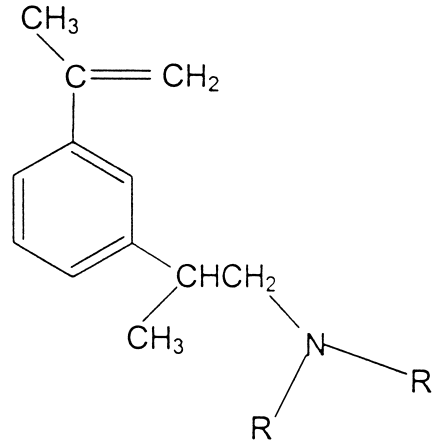

have been copolymerized with solution and emulsion styrene butadiene copolymers in ratios from 1 to 10% and have imparted major improvements in polymer properties resulting in lower hysterisis and better wet grip of tires [10–12].

III. ESTERIFICATION, ETHERIFICATION, AND HYDROLYSIS OF POLYMERS

The chemical modifications discussed in this section are historically and scientifically so closely linked to one polymer, cellulose, that although the

latter occurs primarily as a fiber and not an elastomer, a discussion of this group of cellulose modifications seems appropriate. Apart from the fact that some cellulose derivatives, like ethyl cellulose, when plasticized, can be quite elastomeric, the effects of modification of a basic polymer are particularly well demonstrable on a substance as stiff and highly crystalline as cellulose. Moreover, in view of the expected hydrocarbon shortage, cellulose may soon gain a new role as a polymeric starting commodity.

Cellulose, identified chemically as β-1,4-glucan, is the most widely found natural polymer, constituting the permanent structure of plant cell walls. For the general properties and chemistry of cellulose itself the reader is referred to standard textbooks and recent reviews.

Much of the early history of the chemical modification of cellulose is related to the attempts to find a solvent for it, as its macromolecular structure was not understood at that time. In l844, Mercer discovered and commercialized the interaction of alkali with cellulose fibers, a process still in use under the name *mercerization*. The initial product of the reaction, alkali cellulose, is not a chemical modification but a physical form in which water and sodium ions penetrate the macromolecular structure and reduce the hydrogen bonding, with consequent swelling of the fibers. The initial product, cellulose I, is converted to cellulose II, a complex physicochemical modification, in the final washing stage. The degree and rate of swelling in this process are dependent on the source of the cellulose, and if the fibers are stretched prior to and during the reaction, optimum interaction is achieved. Many other inorganic salt solutions swell cellulose [13], and of these, zinc chloride has found the widest application. Aqueous solutions of thiourea, resorcinol, chloral hydrate, and benzene sulfonates also lead to limited swelling of cellulose. In all cases, the reduction in physical crosslinking can be followed by a study of the x-ray diffraction diagrams of the crystalline content.

The complete solubility of cellulose in cuprammonium solutions, discovered in 1857 by Schweizer, led to the development of the rayon industry, but, as in the case of alkali cellulose, the regenerated polymer is chemically the same as the precursor. Regeneration via cellulose zanthate solutions, invented by Cross and Bevan in 1893, is another process still in use; it forms the basis for the manufacture of Cellophane.

The first "chemical" modification of cellulose was achieved by Braconnot in 1833 with the production of cellulose nitrate from a wide range of cellulosic materials. The products were highly inflammable powders which could be dissolved in concentrated acetic acid to give clear tough varnishes. (Note the conversion of a fiber to a film by chemical modification.) In 1847, highly nitrated cellulose, guncotton, was discovered by Bottger and Schonbein, and in 1870, Schutzenberger produced acetylated cellulose using hot acetic anhydride as the reaction medium. These reactions have a common mechanism [14], namely, the esterification of the hydroxyl groups in the basic cellulose moiety:

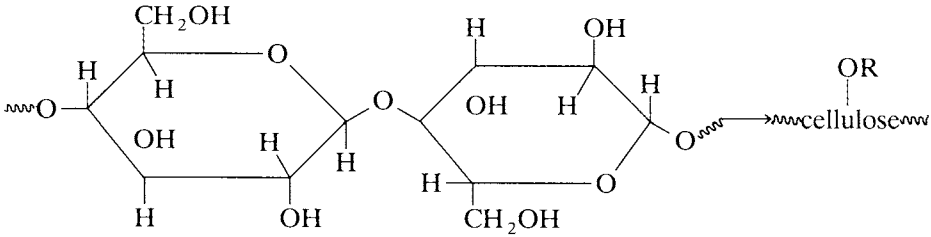

(1)

Since this early work, a very large range of organic acids have been used to prepare cellulose esters, mixed esters, and ether esters [15]. A typical example of considerable commercial importance is the acetylation of cellulose. As in all esterifications of macromolecular materials, the accessibility of the hydroxyl groups to the esterifying acid is of prime importance. Reaction (1) represents complete esterification, a process which is probably never fully achieved. The identification of the esterified products is, therefore, dependent not only on the content of acetyl groups but also on the location of these groups on the macromolecular backbone. Both factors are affected by the method of preparation and the esterification conditions.

Although many esterification reactions [14] are based on inorganic acids, for insoluble hydroxyl compounds like cellulose, xanthation is more important. Sodium hydroxide is normally used to produce the swollen alkali cellulose, which (after aging) is reacted with carbon disulfide to form the sodium salt of cellulose xanthate:

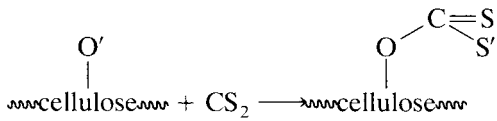

(2)

The cellulose can be regenerated by spinning (or extruding as a film) into an acid bath containing salts such as sodium and zinc sulfate [13]. During spinning or extrusion, the macromolecules are oriented in the direction of flow to give high strength to the viscose fiber or the Cellophane film. The occurrence of macromolecular orientation during spinning is very important, and it is used in the chemical modification of many polymers.

The cellulose ethers constitute another important group of cellulose derivatives prepared from alkali cellulose by standard etherification reactions between the hydroxyl groups and an alkyl halide. The properties of the ethers depend on the extent of the reaction, i.e., the degree of etherification. In general, the ethyl celluloses are water-insoluble thermoplastic materials, whereas methyl ether, ethyl hydroxyethyl cellulose, and carboxymethyl cellulose are soluble in cold water and are used as viscoelastic thickeners and adhesives.

For the preparation of synthetic hydroxy polymers, hydroxyl groups can be introduced by copolymerization of the base monomer with a hydroxy monomer. These groups can then be used for esterification or etherification [16], but the relatively high cost of hydroxy monomers detracts from the wide spread use of direct copolymerization. Instead, one introduces the groups required by the complete or partial hydrolysis of the ester groups in an appropriately hydrolyzable polymer, such as poly(vinyl acetate). Complete hydrolysis yields poly(vinyl alcohol) (PVA), a water-soluble polymer with considerable utility as a stabilizer and viscosity modifier for aqueous systems:

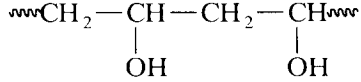
(3)

PVA has a unique use as a strengthening fiber in conjunction with weaker materials such as merino wools in the weaving of delicate fabrics, from which it can afterward be removed by water washing. A major portion of the polymer produced is reacted with aldehydes to form the corresponding poly(vinyl formal), poly(vinyl acetal), and poly(vinyl butyral):

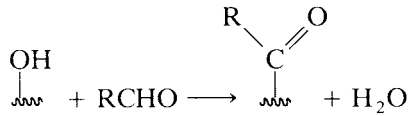
(4)

There are different grades of each of these materials according to the overall molecular weight and the degree of substitution. These polymers are used as components of systems with unique adhesive properties, e.g., in the manufacture of safety glass laminates [poly(vinyl butyral) and mixed derivatives] and of metal-to-metal adhesive [poly(vinyl formal) cured with phenolics and other resins]. Reactions of poly(vinyl alcohol) with acids or anhydrides occur as normal esterifications, a route used to synthesize polymers and copolymers which cannot be readily formed by conventional polymerization (e.g., when the reactivity ratios of the monomers are not suitable).

Natural rubber and synthetic rubbers in general do not have hydroxyl groups in sufficient numbers for them to be used for esterification reactions. Terminal hydroxyl groups may be introduced into synthetic rubbers as terminal catalyst or initiator fragments and used for coupling or extension reactions.

IV. THE HYDROGENATION OF POLYMERS

Any polymer with unsaturated hydrocarbon groups, either in the main chain or as side groups, can be hydrogenated. Early research on the hydrogenation of elastomers focused on destructive hydrogenation with consequent

loss of the macromolecular structure. This is beyond the scope of this chapter so the reader is referred to several references on the subject (12, 17, 18). The most recent work in hydrogenation has produced excellent products, such as linear polyethylene from the hydrogenation of poly(1,4-butadiene) [19, 20] and poly(ethylene–co-propylene) rubber from the hydrogenation of polyisoprene.

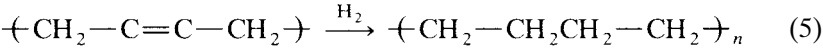

(5)

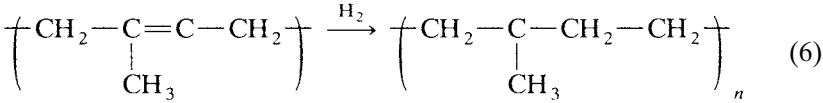

(6)

These reactions were carried out using a heterogenous catalyst.

Homogeneous soluble transition metal catalysts for hydrogenation have been used to create novel polymers. Homogeneous hydrogenation catalysts are usually generated from Ziegler-type catalysts based on nickel or cobalt organic salts reduced in the presence of organoaluminum or organolithium compounds. These catalysts are used to form saturated elastomers by hydrogenating unsatured elastomers. The resulting polymers have vastly different viscoelastic properties than their unsaturated parent polymers. For example, the hydrogenation of a 99% poly(1,2-butadiene) has resulted in the formation of polybutene [21] which has a lower glass transition temperature than its parent elastomer. It is interesting to note that hydrogenation does not affect the polymer molecular weight or backbone architecture.

The ease of hydrogenation and the resultant degree of saturation achieved reflect the microstructure of the polymer. Hydrogenation of unsatured elastomers usually proceeds in a blocky way. This is due to the different reactivities of the various double bonds. In general, double bonds of 1,2 structure are four times more reactive than double bonds of 1,4 structure. *cis*-1,4 units are more reactive than *trans*-1,4 units. Chamberline *et al*. [22] have shown that hydrogenation of 1,2 units is statistically random, whereas the hydrogenation of l,4 units is not.

The complete hydrogenation of poly(l,4-butadiene), *cis* or *trans* structure, forms a polyethylene with a low melting point of about 115°C. It is believed that this linear polyethylene is a low-density material. Unpublished data obtained on the partial hydrogenation of a 99% *cis* poly(1,4-butadiene) showed that the hydrogenation proceeded in a blocky fashion. The 40 to 50% hydrogenation of poly(1,4-butadiene) *(cis* content 98%) made by nickel catalyst gives a polymer with a melt point of +98°C and a crystallization temperature of –13°C as measured by differential scanning calorimetry (DSC). This confirms the fact that hydrogenation of *cis*-poly-1,4-butadiene proceeds in a blocky fashion to produce a block of polyethylene and a block of poly(*cis*-1,4-butadiene).

Polybutadienes made by anionic catalysts in the presence of polar modifiers contain a mixed microstructure of *cis*-1,4, *trans*-1,4, and 1,2 units. Hydrogenation of these polymers leads to interesting products. As mentioned previously, hydrogenation favors the 1,2 units over the 1,4 units by a 3 (or 4?)-to-1 ratio. Because of this mismatch in reactivity, hydrogenation of a polybutadiene containing 40 to 50%, 1,2 units produces a polymer containing a polyethylene portion with a T_m of 85 to 95°C and a rubbery portion with a T_g of –62°C.

Block copolymers can also be hydrogenated to produce unique products. Hydrogenated triblock copolymers of poly(styrene–co-butadiene–co-styrene) (SBS) are commercially available from the Shell Company under the trade name Kraton G. The middle block is usually a mixed microstructure of poly(1,2-butadiene) and poly(1,4-butadiene) units. The resulting product is a hydrogenated unsaturated polymer which exhibits greater thermal and oxidative properties than the parent SBS triblock.

Similar procedures have been used by several workers [23] to hydrogenate poly(1,4-butadiene–co-1,2-butadiene) diblocks [24] and poly(l,4-butadiene–co-1,4-isoprene–co-1,4-butadiene) triblocks. Hydrogenation of these diblock and triblock copolymers forms thermoplastic elastomers with crystalline and amorphous segments. All these materials exhibit crystallinity, glass transition, solubility, and dynamic mechanical loss spectra different from those of their unsaturated counterparts.

Another method of preparing saturated rubbers was developed [25] using the diimide reduction. This method can be used to produce a high degree of saturation dependent on the type of reagent used; however, side reactions can occur in this method. Generation of the diimide from *p*-toluenesulfonyl hydrides leaves an acidic fragment which may cause cyclization in some unsaturated elastomers.

V. DEHALOGENATION, ELIMINATION, AND HALOGENATION REACTIONS IN POLYMERS

A. Dehydrochlorination of Poly(vinyl chloride)

The dehydrochlorination of poly(vinyl chloride) has been the subject of much investigation, particularly with the view of developing greater stability in PVC polymers and copolymers. Like many polymeric reactions, dehydrochlorination is a complex process. The vinylene groups, created by the elimination of HCl from adjacent carbon atoms in the chain,

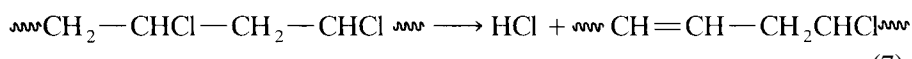

(7)

may be the result of free radical ionic, or ion–radical steps. The presence of a small proportion of head-to-head, tail-to-tail, and other configurational irregularities in the backbone structure of poly(vinyl chloride) leads to more complex elimination steps by thermal degradation (alone or in the presence of catalysts such as aluminum chloride). The introduction of ring structures, a major process during dehydrochlorination, is likewise affected by the distribution of the chlorine atoms along the polymeric backbone. Hydrogen bromide can be effectively eliminated thermally from poly(vinyl bromide), as dehydrohalogenation is a universal thermal reaction, the complexities of which increase from chloride to iodide.

B. Thermal Elimination

The thermal elimination process can be applied to most "substituted" groups in vinyl polymers by controlled pyrolysis at 600 to 700°C, producing polyvinylene compounds, e.g., by the splitting off of acetic acid from poly(vinyl acetate). By careful temperature control, one can achieve bifunctional reactions and/or intramolecular cyclizations. This has been developed commercially at relatively high temperatures, in the case of the polymerization of methacrylamide above 65°C, to yield a polymer with a substantial proportion of imide groups:

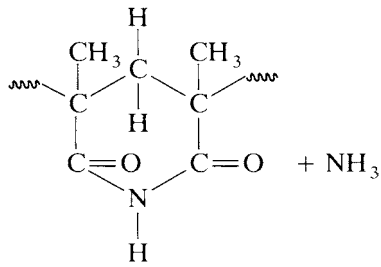

(8)

Polymers and copolymers of multifunctional vinyl monomers (using the term to cover the presence of a halogen or other reactive group in addition to the vinyl group, rather than in the sense of more than one polymerizable group), such as α-chloroacrylic acid, often undergo partial lactonization and hydrolysis during polymerization. Heating in alcohol solution or electrolyzing alcoholic solutions, one obtains, e.g., the introduction of double lactam rings during the acid hydrolysis of poly(α-acetamineoacrylic acid)

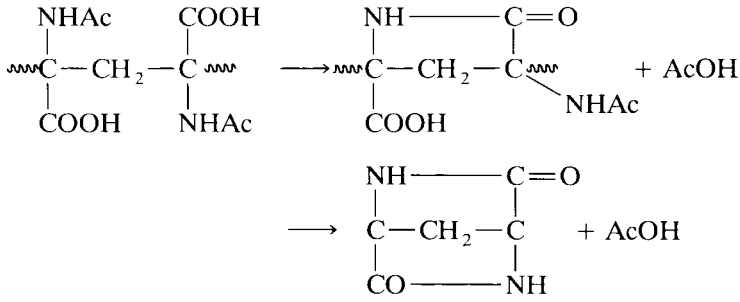

(9)

The discoloration of polyacrylonitrile is due to a similar type of elimination reaction, which in this case occurs intra- as well as intermolecularly to give crosslinked insoluble ring products:

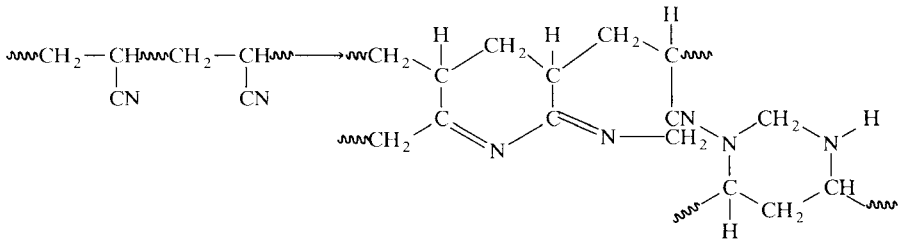

(10)

The controlled heating of polyacrylonitrile fibers under tension also causes an elimination of nitrogenous products to leave a "carbon fiber" of high tensile strength that can be considered as the end product of the line of chemical elimination reactions. Carbon fibers from cellulosic materials, lignin, and various interpolymers and blends have been developed. The structures of these products consist largely of three-dimensional carbon networks, partially crystalline and partially graphitic or amorphous.

C. Halogenation of Polymers

Halogenation and hydrohalogenation of elastomers have been reported extensively in the literature [26]. The main problems with these reactions are the cyclization and chain scission that occur parallel to the halogenation reaction. These introduce difficult problems in the characterization of the resulting products. Despite these problems, several products have been prepared and commercialized. Chlorination of poly(1,4-butadiene) to prepare a product similar to poly(vinyl chloride) has been reported by several workers [27]. This process had extensive side reactions and chain degradation. The chlorination of butyl rubber and conjugated diene–butyl rubbers gives end products that are used in the tire industry as inner liners for air retention.

Ethylene–propylene copolymers (EPDM) are, by their random copolymerization, amorphous in structure and therefore easily halogenated. EPDM has been chlorinated to improve its properties and cocurability with other rubbers. The chlorination was directed toward the termonomer dicyclopentadiene to form the allylic chloride [28]. In this manner, EPDM was chlorinated, and the resulting products had improved properties.

EPDM rubbers are modified by 1,2-addition of *N*-chlorothiosulfonamides to their olefinic sties [29–31]. Such additions may be carried out in solution or without solvent in an internal mixer or extruder. The solventless reactions are facilitated by added carboxylic acids [32, 33] or by certain metal salts of weak acids [34]. The modified EPDMs are of interest because of their ability to covulcanize in ozone-resistant blends with polydiene rubbers [29–31]. Although less fully explored, *N*-chlorothiocarboxamides and imides also react with EPDM to produce modified products which covulcanize in blends with polydienes [35].

In the absence of oxygen, the chlorination of polyethylene, with or without a catalyst, can be controlled to provide products with varying chlorine content. The chlorination process is statistically random so that chlorination of polyethylene to the same chlorine content as poly(vinyl chloride) (60%) gives a product which is chemically different from PVC yet fully compatible with it. This random chlorination of polyethylene destroys its crystallinity. At a degree of chlorination corresponding to the loss of all its crystallinity, the chlorinated product becomes soluble at room temperature. The *p*-bromination of polyethylene follows a similar course to yield a rubberlike polymer at 55% bromine content.

Both chlorination and bromination of polypropylene and isobutylene lead to degradation of the main chain, with the loss of many useful properties. Degradation during chlorination can, however, be avoided at low temperatures by limiting the reaction to a maximum of about 2%. This procedure forms a useful commercial product.

The addition of hydrogen chloride to unsaturated elastomers has also received considerable attention. Extensive work has been done on the hydrochlorination of *Hevea* [poly(*cis*-1,4-1,4-isoprene)] and *Balata* [poly(*trans*-l,4-isoprene)] rubbers since 1940 [36, 37]. Both *cis*-1,4 and *trans cis*-1,4-polyisoprenes readily add hydrogen chloride following Markovnikov's rules with only a small amount of cyclization.

D. Cyclization of Polymers

Cationic cyclization of unsaturated elastomers such as poly(*cis*-1,4-isoprene), poly(3,4-isoprene), poly(1,2-butadiene), and poly(1,4-butadiene) usually leads to the formation of cyclized resinous products of no commercial value. An extensive review on the subject has been published by Schults *et al*. [38]. Cyclization of unsaturated elastomers, such as polyisoprene, can be

carried out in the solid state, in solution, or even in the latex. The process involves the transformation of linear macromolecular chains into much shorter ones consisting of mono-, di-, tri-, and tetrapolycyclic groups distributed randomly along the chain. Cyclization of polyisoprene increases its glass transition temperature by 20 to 30°C. The mechanism of cyclization of elastomers depends on the catalyst employed in the process.

VI. OTHER ADDITION REACTIONS TO DOUBLE BONDS

A. Ethylene Derivatives

Besides the addition of halogens and hydrohalogens "across the double bond" just covered, there are many other reagents which will react similarly with unsaturated polymers by free radical, ionic, or radical–ion mechanisms. Of prime importance is the addition of ethylene derivatives to polydienes. One of the earliest reactions of natural rubber to be studied in detail was the combination with maleic anhydride [39]. Depending on the reaction conditions and the presence or absence of free radical initiators, one or more of four basic reactions may take place, with the products shown (the arrows indicate where the addition has taken place and the new bonds formed).

1. Intramolecular addition to the double bond within polyisoprene chains:

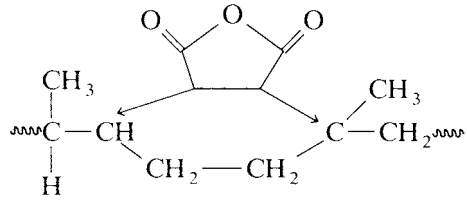

(11)

2. Intermolecular addition to double bonds in different polymer chains. In this group should be included the statistically possible reaction between widely separated double bonds within the same molecule:

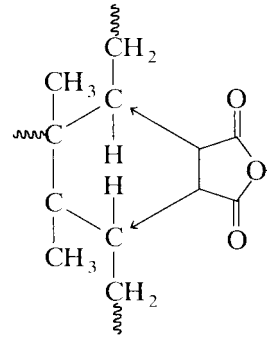

(12)

3. Addition to α-methylenic carbon atoms of a polyisoprene chain:

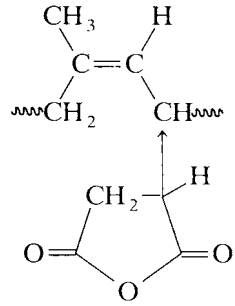

(13)

4. Intermolecular addition to α-methylenic carbon atoms in adjacent chains (or widely spaced α-methylenic carbon atoms in the same macromolecule):

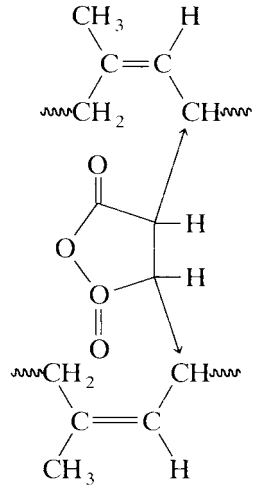

(14)

In general, the overall reaction rates increase with rising temperature and in the presence of oxygen or free radical initiators, but these same conditions promote intermolecular reactions leading to gel formation. Similar reactions take place with gutta-percha, synthetic poly(*cis*-1,4-isoprene), and poly(*cis*-1,4-butadiene). Many workers used two-roll mills and other mastication techniques as convenient ways of blending the maleic anhydride with rubbers at elevated temperatures, but where these techniques have been used, mechanochemical reactions have complicated the overall process. Reaction products of natural rubber containing 5 to 10% combined maleic anhydride can be vulcanized by conventional sulfur cures: of greater interest is the possibility of creating crosslinking by the use of oxides of calcium, magnesium, and zinc.

Other compounds reacting similarly via activated double bonds (excluding here block or graft copolymerization) include maleic acid, *N*-methyl-maleimide, chloromaleic anhydride, fumaric acid, γ-crotonolactone, *p*-benzoquinone, and acrylonitrile. Other polymers with unsaturated backbones, such as polybutadiene, copolymers of butadiene with styrene and with acrylonitrile, and butyl rubber, react in similar ways, but the recorded reaction with poly(vinyl chloride) is largely mechanochemical in nature (discussed later).

B. The Prins Reaction

Another addition to polymers with main-chain unsaturation is the Prins reaction between ethylenic hydrocarbons and compounds containing aldehydic carbonyl groups. Kirchof, in 1923, described the reaction of natural rubber in benzene solution with aqueous formaldehyde in the presence of concentrated sulfuric acid. The general reaction of an aldehyde, RCHO, with a polyisoprene in the presence of an inorganic or organic acid or an anhydrous metal salt is represented by

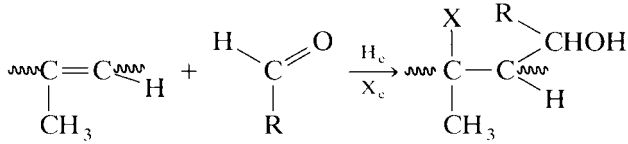

(15)

In the absence of such catalysts, the reaction leads to a shift in the double bond rather than its elimination:

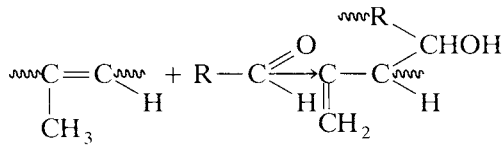

(16)

These reactions can be carried out in solution or in dispersion or by reaction in the solid phase [39]; in the last case it is again difficult to differentiate the Prins reaction from mechanochemical reactions initiated by chain rupture during mastication.

Other aldehydic compounds, such as glyoxal and chloral, also react in a similar way with polyisoprenes and unsaturated rubbers [e.g., poly(*cis*-1,4-isoprenes), poly(*cis*-l,4-butadiene) and copolymers of isobutylene and isoprene]. The use of strong acids, or Lewis acids, causes complications, as the acids themselves, under suitable conditions, catalyze cyclization and *cis–trans* isomerization, and these reactions may occur simultaneously with the addition reactions.

VII. OXIDATION REACTIONS OF POLYMERS

Uncontrolled oxidation of rubber is detrimental to its physical properties. Oxidation reactions take place readily at unsaturated groups in polymers and are often referred to collectively as *epoxidation*; however, oxidation under controlled conditions can lead to useful products such as the epoxidized natural rubber introduced by the Malaysian Rubber Producers Association [38–41]. Natural rubber in the latex form is treated with hydrogen peroxide dissolved in acetic acid. This gives 50% epoxidized natural rubber. This rubber shows very interesting physical properties and excellent carbon black dispersion. Similarly, nonaqueous epoxidizations of synthetic polyisoprene can be achieved using either hydrogen peroxide or hypochloride in t-butanol. The controlled degree of epoxidation usually leads to some interesting products. For example, the 25% epoxidized synthetic polyisoprene is an elastomer with viscoelastic properties similar to those of the unepoxidized material, but has better carbon black dispersion. This gives high modulus and tensile strength, however, higher degrees of epoxidation (60 to 75%) produce a resinous material which is not rubbery.

VIII. FUNCTIONALIZATION OF POLYMERS

Polymers with stable backbones such as polystyrene, polyethylene, and polypropylene can be functionalized. Functionalization of polystyrene has received considerable attention, because it is a unique polymer with aromatic rings which are capable of undergoing many nucleophilic as well as electrophilic reactions. A resin recently introduced on the market is based on sulfonated polystyrene. Applications for this resin include ion-exchange material and catalyst binding materials.

Electrophilic substitution on polystyrene through a chlorometallation reaction yields chlorine functionality. This has opened up the possibilities of making many derivatives of polystyrene. Starting with chlorometallated polystyrene, derivatives such as quaternary, ammonium, or phosphonium salts have been made. Similarly, ethers, esters, sulfonamides, silanes, and ketone derivatives have been made by replacing the chlorine atom on chlorometallated polystyrene. In the case of polystyrene, however, it was discovered that chain end functionalization can be realized if the chain ends were terminated by group I metals such as lithium and potassium.

Both the Japanese Synthetic Rubber Company and Nippon Zeon have reported that anionically prepared elastomers that are functionally terminated by active lithium can be chain terminated with Michler ketone, benzophenone, and a variety of enamide groups. Moreover, these chains can be terminated with silicone or tin metals. Chain end functionalization did not change the

viscoelasticity of the polymer chains but rather dramatically improved the elastomer–filler interaction and, therefore, reduced its hysteretic properties.

IX. MISCELLANEOUS CHEMICAL REACTIONS OF POLYMERS

Direct replacement of the hydrogen atoms of aromatic rings such as styrene or the allylic hydrogen in poly(1,4-butadiene) or poly(1,4-isoprene) can be carried out via metallation with organometallic compounds of group I such as lithium, sodium, and potassium. Usually, the yield tends to be low and the product is insoluble; however, the use of chelating diamines with organolithium compounds has increased the yield, and the products are soluble in cyclohexane. For example, polystyrene has been metallated in high yields to give polylithiated polystyrene in which several functional groups have been successfully introduced. Similarly, polyisoprene and polybutadiene have been successfully metallated with either s-butyllithium or t-butyllithium in the presence of tetramethylethylenediamine (TMEDA) at 50°C. In the case of the polyisoprene, chain scission and reduction in molecular weight resulted at longer metallation temperatures and times. In many cases, these lithiated polymers have been used to prepare graft and block copolymers. These are discussed in more detail in Section IX(B).

X. BLOCK AND GRAFT COPOLYMERIZATION

A. Effects on Structure and Properties of Polymers

Some of the most significant changes in structure and properties of polymers can be brought about by either block or graft copolymerization (see Chapter 13). The term *block copolymer* is applied to macromolecules made up of sequences with different chemical (or physical, i.e., tactic) structures, usually represented by A, B, and C. The sequences are of a molecular weight that would give them polymeric features even if separated. The manner in which these sequences are arranged defines the type of block copolymer prepared. A diblock copolymer is represented by AB, indicating that a segment with chemical composition A is connected to a segment with composition B. Other possible types of block copolymers include triblocks ABA and ABC, for example. They may be linear or branched; the linear structures are called block copolymers,

$$\text{AAAAAA} \cdot \text{BBBB} \cdots \text{BBBBB} \cdot \text{AAAAA} \tag{17}$$

and the branched structures graft copolymers (18),

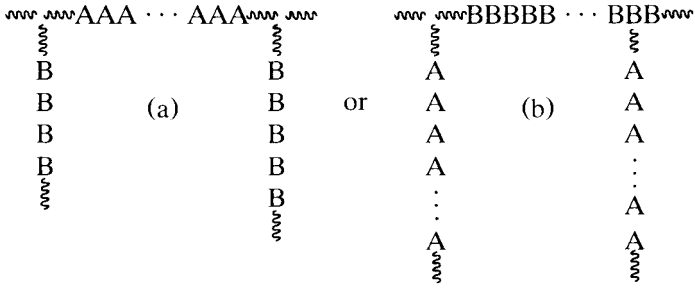

Thus the same polymeric sequences may be put together as block or as graft copolymers, with differing properties, though in the author's experience, the major differences between the properties of block and graft copolymers of the same constituent polymers are pronounced only in solution or in the melt. For example, natural rubber may be block copolymerized with poly(methyl methacrylate), or methyl methacrylate monomer may be grafted onto natural rubber. In an attempt to distinguish by nomenclature one structure from the other, insertion of the letters *b* and *g*, for block and graft, respectively, between the names of the specific sequences was introduced, e.g., natural rubber–*b*-poly(methyl methacrylate) and natural rubber–*g*-poly(methyl methacrylate) in the case of the examples cited. The structures of these two macromolecules would be represented by (17) and (18a), where the . . . AAAA . . . sequences represent natural rubber and the . . . BBBBB . . . sequences represent pply(metyl methacrylate).

The number and order of sequences may be more complicated. Block copolymers are usually made by free radical or living polymerizations. These processes can produce polymers that consist of a pure A block connected to a pure B block, with no interphase zone of mixed A and B structure. The preparation of block copolymers is not limited to monomers A and B, but can also encompass segments of random copolymers. For example, a block of a random copolymer AB can be connected to a block of polymer A or B. Moreover, the point of attachment of the blocks can be either at the end or the middle of the polymer chain. Several examples of the various types of block copolymers possible follow:

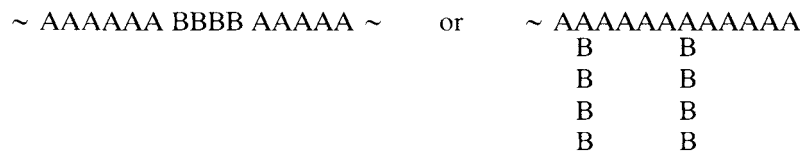

$$\sim \text{ABABAB}\quad \text{AAAAAA} \sim \qquad \text{or} \qquad \sim \text{ABABBABB}\quad \begin{matrix}\text{A}\\ \text{A}\\ \text{A}\\ \text{A}\end{matrix}\quad \begin{matrix}\text{AAAAAAA}\\ \text{B}\\ \text{B}\\ \text{B}\\ \text{B}\end{matrix} \sim$$

$$\sim \text{ABABA}\quad \text{BBBBBBB} \sim \tag{20}$$

When the sequences making up the segments are random copolymers, the prefix *co* may be introduced, with the major component monomer preceding the minor constituent. A backbone polymer of butadiene–styrene rubber grafted with styrene containing a small percentage of acrylic acid would be described as poly[(butadiene–co-styrene)–(styrene–co-acrylic acid)] and could be schematically represented as

$$\begin{matrix}\sim\text{AABABAAABBABAAAABBA}\sim\\ \begin{matrix}\text{B}\\ \text{B}\\ \text{B}\\ \text{C}\\ \text{B}\\ \text{B}\\ \text{B}\\ \text{B}\\ \text{C}\\ \text{B}\end{matrix}\qquad\qquad \begin{matrix}\text{B}\\ \text{B}\\ \text{C}\\ \text{B}\\ \text{B}\\ \text{B}\\ \text{C}\\ \text{B}\\ \text{B}\\ \text{B}\end{matrix}\end{matrix} \tag{21}$$

where A represents butadiene, B, styrene, and C, acrylic acid.

B. Block Copolymer Synthesis

Several methods can be used to synthesize block copolymers. Using living polymerization, monomer A is homopolymerized to form a block of A; then monomer B is added and reacts with the active chain end of segment A to form a block of B. With careful control of the reaction conditions, this technique can produce a variety of well-defined block copolymers. This ionic technique is discussed in more detail in a later section. Mechanicochemical degradation provides a very useful and simple way to produce polymeric free radicals. When a rubber is mechanically sheared [40], as during mastication, a reduction in molecular weight occurs as a result of the physical pulling apart of macromolecules. This chain rupture forms radicals of A and B which then

recombine to form a block copolymer. This is not a preferred method because it usually leads to a mixture of poorly defined block copolymers.

Using living polymerizations, the Shell Company was able to commercialize several poly(styrene–co-butadiene) and poly(styrene–co-isoprene) block copolymers known in the industry as Kraton 1101 and Kraton G. These block copolymers have found many uses in the shoe sole and adhesive industries. The physical properties were dependent on the macrostructure and microstructure of these block copolymers.

C. Examples

As major examples, let us consider the three monomers butadiene, styrene, and acrylonitrile, and see how they can be block copolymerized together by mechanochemical means. From the large number of theoretical possibilities, 11 have been selected for discussion; these may be prepared by mastication of the following:

1. A butadiene–styrene copolymer rubber with acrylonitrile monomer
2. Polyacrylonitrile (plasticized) with a mixture of butadiene and styrene monomers
3. A butadiene–acrylonitrile copolymer rubber with styrene monomer
4. Polystyrene with a mixture of butadiene and acrylonitrile monomers
5. A styrene–acrylonitrile resin with a mixture of styrene and butadiene monomers
6. Polybutadiene with a mixture of styrene and acrylonitrile monomers
7. A butadiene–styrene rubber with polyacrylonitrile (best plasticized)
8. A styrene–acrylonitrile resin with polybutadiene
9. A butadiene–acrylonitrile rubber with polystyrene
10. A high styrene–butadiene resin with acrylonitrile monomer
11. A high styrene–butadiene resin with polyacrylonitrile (plasticized)

(All of the foregoing reactions except 2 and 11 have been reported in the patent literature or are known to have been commercially evaluated.) In each example, the products would be chemically and physically different in terms of the makeup of the structural sequences, and all properties would also depend on the relative proportions of the initial components. In all mechanochemical reactions, some of the starting polymer or copolymer remains unchanged, mainly the low-molecular-weight fraction, which is not effectively sheared, and some homopolymer may be formed from the polymerizing monomers by chain transfer reactions. Varying the mastication conditions greatly influences the yield and rate of reaction; the chemical nature of the products is less affected, except that the presence of butadiene as one of the constituents (either polymer or monomer) will cause increasing gel contents with continued mastication. Processes 3, 5, 6, 8, and 9 are known to give products in which a rubber phase is dispersed in a resinous matrix; i.e., they are alternative methods for producing an A–B–S-type copolymer.[1] The

presence of a proportion of block or graft copolymer in the system assists in stabilizing the dispersion of the rubber phase in the resin matrix by acting at the phase boundary as a "soap," i.e., a compatibilizing agent at the phase boundary.

D. Other Methods of Effecting Mechanicochemical Reactions

Mechanicochemical degradation is the term used in describing chain scission of polymer backbones through the application of shear during a processing operation. It was previously believed that this type of process led to carbon–carbon chain scission, which usually causes a dramatic change in rheological properties. In the early 1950s, Watson and coworkers [41, 42] showed that, in the absence of oxygen, radicals produced by mechanical shear can be used to initiate the polymerization of vinyl monomers to form block copolymers. For example, vibromilling of natural rubber below its glass transition temperature has enabled block copolymerization of natural rubber with methyl methacrylate to be carried out on a small scale, with conversions as high as 86%. Similar results were achieved with styrene and with acrylonitrile.

This type of approach has also been used to attach antioxidants to unsaturated polymers. The novel approach of Scott in the 1970s [43] using the technique employed by Watson enabled the attack of substituted allyl mercaptans and disulfides to olefinic double bonds employing the Kharasch reactions.

Mechanicochemical reactions can occur during processing, when the polymer is converted to a finished product. The chain scission can occur in both saturated and unsaturated polymer backbones. For example, during processing in a screw extruder, backbone scission in polypropylene produces long-tail free radicals which can form macroalkyl radical peroxides. These peroxides are responsible for the observed decrease in melt viscosity. In the absence of oxygen, these monoallyl macroradicals can be used to graft new monomers or such polymers as polypropylene and polyethylene to the backbone. In this manner, maleic adducts of polypropylene have been prepared, giving improved dyeability, hydrophilicity, and adhesion.

E. Ionic Mechanisms

Ionic mechanisms for the preparation of block copolymers are a very important tool of the synthetic polymer chemist. A feature of many homogeneous anionic polymerizations in solution is that termination can be avoided by careful control of experimental conditions. In fact, an infinite life of the active chain end is theoretically possible, and this has led to the term *living polymers*. Polymer carbanions can resume growth after the further addition of monomer. By changing the monomer composition, block copolymerization is readily initiated, and this process can be repeated. A major advantage of this

[1]It has been found in practice that a number of monomers that normally do not polymerize by free radical processes in the temperature range 10 to 50°C can be block copolymerized by cold mastication techniques, indicating ionic initiation via heterolytic scission.

type of synthesis over most free radical processes is the ability to control the chain length of the sequences by adjusting the concentrations of initiating sites and of monomer at each stage of the block copolymerization.

Anionic block copolymerization employs organolithium initiators, which have wider use because of their extended range of solubility, which includes hydrocarbons [44]. Organolithium compounds act as initiators by direct attack of the organic anion on the monomer species, again a fast reaction and, in the absence of compound with active hydrogen atoms, without transfer or termination steps. If carefully executed, the reaction permits one to have precise control over molecular weight and (the narrow) molecular weight distribution.

The convenience of this technique has led to the development of many commercial products, including thermoplastic elastomers based on triblocks of styrene, butadiene, and isoprene. The initiator used in these systems is based on hydrocarbon-soluble organolithium initiators. In some cases, a hydrocarbon-soluble dilithio initiator has been employed in the preparation of multiblock copolymers. Several techniques are used to prepare thermoplastic elastomers of the ABA type. All these are discussed in detail in Chapter 2. A short summary of these techniques is given here.

1. Three-Stage Process with Monofunctional Initiators

In this technique, used, e.g., for the synthesis of block copolymers of poly(styrene–*b*-butadiene–*b*-styrene) (SBS), a polystyrene block is formed by employing *n*-butyllithium as the initiator in an aromatic solvent. Butadiene monomer is then added to react with the polystyrene–lithium chain end to form the poly(butadiene) block. If the reaction was terminated at this stage, a poly(styrene–*b*-butadiene) copolymer would result, which has no thermoplastic properties. Therefore, styrene monomer is added to produce the triblock SBS. The process for the preparation of SBS is very carefully controlled to avoid the formation of a diblock, as the presence of any appreciable amount of SB dramatically reduces the thermoplastic properties of SBS.

2. Two-Stage Process with Difunctional Initiators

Several commercial processes using difunctional initiators based on soluble organolithium compounds have been developed. These compounds can polymerize at both ends. Difunctional initiators are useful in the cases of ABA block copolymers where B can initiate A but A cannot initiate B. These difunctional initiators are useful in the preparation of SBS. The elastomeric butadiene block is polymerized with hexane as a solvent. The added styrene monomer is also soluble in hexane. This method is also useful in preparing triblocks with hydrocarbon middle blocks and polar end blocks such as poly(methacrylonitrile–*b*-isoprene–*b*-methacrylonitrile).

3. Monofunctional Initiation and Coupling

In this two-stage process, B is sequentially polymerized onto A, and then the two chains are coupled to yield an ABBA block copolymer. Triblocks of

SBS have been prepared using this method, with methylene dichloride as the coupling agent. The disadvantage is the formation of radical anions which can lead to contamination of the triblock with multiblock species.

4. Tapered Block Copolymers

This method is used to form a block copolymer which consists of two segments of essentially homopolymeric structure separated by a block of a "tapered" segment of random copolymer composition. These are usually prepared by taking advantage of the differences in reaction rates of the component monomers. When polymerized individually in hexane, butadiene reacts six times more slowly than styrene; however, when styrene and butadiene are copolymerized in a hydrocarbon solvent such as hexane, the reaction rates reverse, and the butadiene becomes six times faster than the styrene. This leads to a tapering of the styrene in a copolymerization reaction. For more details on the synthesis techniques, the reader is referred to Chapters 2 and 13.

F. Graft Copolymer Synthesis

The synthesis of graft copolymers is much more diverse but can nevertheless be divided into groups of related processes: (1) polymer transfer, (2) copolymerization via unsaturated groups, (3) redox polymerization, (4) high-energy radiation techniques, (5) photochemical synthesis, and, most importantly, (6) metallation using activated organolithium with chelating diamines.

1. Polymer Transfer

In a free radical polymerization, chain transfer is an important reaction. Chain transfer to a monomer, solvent, mercaptan, or other growing chain can take place. When a chain transfer reaction to another chain takes place, it creates a radical which acts as a site for further chain growth and grafting (see Chapter 2 for additional details):

$$\begin{aligned} \mathrm{P} + \mathrm{P} &\rightarrow \mathrm{PH} + \mathrm{P}\cdot \\ \mathrm{R}\cdot + \mathrm{P} &\rightarrow \mathrm{RH} + \mathrm{P}\cdot \\ \mathrm{P}\cdot + \mathrm{P}\cdot &\rightarrow \mathrm{PH} + \mathrm{P}\cdot \end{aligned} \tag{22}$$

The reaction proceeds by the transfer of a hydrogen or halogen (in the case of halogenated polymers) atom from a macromolecule P to the growing chains P· (or to an excess initiator free radical R·, thereby "terminating" them). The reactivity is now located on the transfer molecule, which in turn initiates copolymerization, i.e., the growth of a grafted side chain of a newly introduced second monomer. A measure of grafting occurs with most monomer–polymer

systems, especially those initiated by benzoyl peroxide, if the concentrations of polymer and initiator are high.

The simplest technique is to dissolve the polymer in the appropriate solvent; add the peroxide initiator, which abstracts a hydrogen radical and generates a radical on the polymer chain; and then add fresh monomer for grafting onto this site. This technique has been employed in grafting methylacrylate onto natural rubber and synthetic polyisoprene. In this manner, several commercially useful products such as ABS resins have been prepared; however, tire elastomers are not made in this manner because of the generation of micro and macro gel particles, which are detrimental to physical properties. In many cases when latex grafting has been used, the product has usually been targeted toward thermoplastic applications rather than rubber applications.

2. Copolymerization via Unsaturated Groups

Other methods (e.g., most car body repairs) are based on the polyester–styrene copolymerization process (reinforced with various types of inert mesh or glass fabric), a graft copolymerization of styrene onto backbone unsaturated polymer of relatively low molecular weight. In general, for high grafting yields, a reasonably high concentration of pendant vinyl groups is required on the backbone polymer. For glass-reinforced plastics, the polyester resins are selected with this in view. In natural rubber, a few such groups per molecule[2] are always present and these undoubtedly participate during normal grafting. The content of pendant vinyl groups can be increased by mastication of unsaturated rubbers under nitrogen, because the resonance structures recombine as

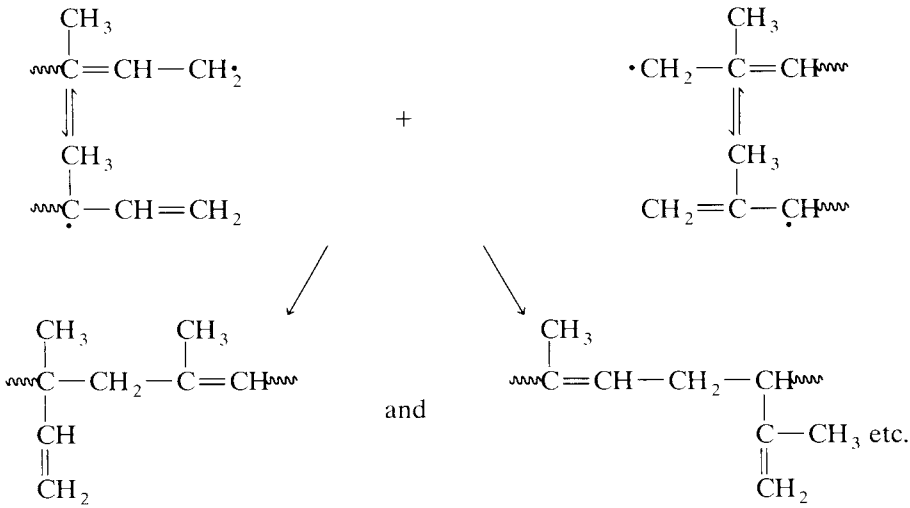

(23)

[2]About 0.4% of the unsaturated groups are pendant vinyl groups in an average sample of acetone-extracted pale crepe rubber.

The direct introduction of peroxide groups into the backbone of polymers, such as poly(methyl methacrylate), has been used to produce macromolecular initiators for the synthesis of block copolymers, e.g., poly(methyl methacrylate–*b*-acrylonitrile) and poly(methyl methacrylate–*b*-styrene). Ozonization can also be used, with careful control of the degree of ozonolysis, to introduce epoxy ring structures into natural rubber:

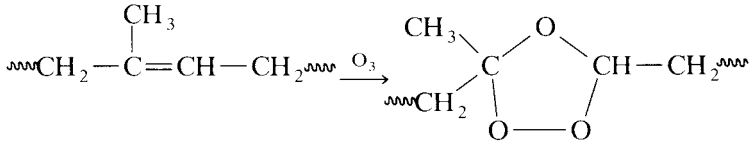

(24)

By carrying out the reaction to about 4% of the available double bonds in a solvent such as toluene at a low temperature followed by a nitrogen purge, grafting can be effected by addition under nitrogen of methyl methacrylate (MMA) monomer (reacting at 80°C in sealed ampules) and formation of two MMA chains attached to the oxygens of the opened —O—O— bridge. This technique should be applicable to isoprene and butadiene copolymers.

3. Redox Polymerization

Redox polymerizations are among the most popular techniques for grafting reactions, and of the possible initiator systems, ferrous ion oxidation and those based on ceric ion reduction are widely used. In a redox polymerization, a hydroperoxide or similar group is reduced to a free radical plus an anion, while the metal ion is oxidized to a higher valency state, and at the same time a monomer is added. When the reducible group is attached to a polymeric chain, the free radical grafting sites thus formed on the macro-molecular backbone act as initiators for graft copolymerization

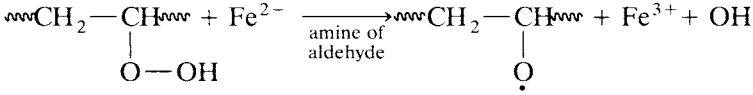

(25)

This method has been used to graft methyl methacrylate to natural rubber latex. (Actually, fresh latex contains a few hydroperoxide groups per macromolecule, which can take part in grafting reactions.) Recentrifuged latex concentrate is mixed with methyl methacrylate and a solution of tetraethylene pentamine is added, followed by a small quantity of ferrous sulfate solution. The homogenized blend is allowed to stand, often overnight [45]. The graft copolymer is isolated by coagulation. As practically all free radical sites are formed on the rubber backbone, there is very little free poly(methyl methacrylate) in the grafted system; on the other hand, some rubber chains are without grafts, as not all chains have hydroperoxy groups. Higher yields of graft copolymer are obtained by allowing the monomer to dissolve in, and equilibrate with,

the latex particles before adding the amine and ferrous ion initiator. It has been claimed that passing oxygen (air) through the latex for several hours reduces the free rubber content of the polymerization product, but nitrogen purging is then necessary to prevent dissolved oxygen from acting as a polymerization inhibitor.

Hydroxy polymers can be grafted by redox polymerization by using a water-soluble peroxide, such as hydrogen peroxide in conjunction with ferrous ions. The OH radicals thus produced abstract H atoms from the hydroxy groups in the polymer, giving free radical grafting sites on the backbone. This method has been used with starch and cellulose derivatives, but considerable quantities of homopolymer are formed from the initial hydroxyl radicals in parallel with the H abstraction. By introducing a few hydroxyl groups into a copolymeric synthetic rubber, grafting can be effected, provided the presence of homopolymer can be tolerated. Mixtures of ferrous ammonium sulfate and ascorbic acid are suitable redox initiation systems. Many patents claim the preferred use of ceric ions, which easily oxidize hydroxyl groups by a radical–ion reaction:

$$\begin{aligned} \mathrm{R{-}OH + Ce^{3+} \rightarrow R{-}\overset{+}{\underset{\bullet}{O}}H + Ce^{2\bullet}} \\ \mathrm{R{-}\overset{+}{\underset{\bullet}{O}}H + OH \rightarrow R{-}O^{\bullet} + H_2O} \end{aligned} \tag{26}$$

The advantage of this reaction lies in the fact that only hydroxyls on the polymer are converted into R—O free radicals, so that no homopolymer can be produced and pure graft is obtained.

4. High-Energy Radiation Techniques

During high-energy irradiation in vacuo, e.g., from a ^{60}Co source, some main-chain degradation of natural rubber and other polyisoprenes occurs:

$$\sim\!\mathrm{CH_2{-}\overset{\mathrm{CH_3}}{\overset{|}{C}}{=}CH{-}CH_2{-}CH_2{-}\overset{\mathrm{CH_3}}{\overset{|}{C}}{=}CH{-}CH_2}\!\sim\!\rightarrow \tag{27}$$

Much of the irradiation energy is also adsorbed by the removal of hydrogen atoms:

$$\begin{aligned} &\sim\!\mathrm{CH_2{-}\overset{\mathrm{CH_3}}{\overset{|}{C}}{=}CH{-}\,CH_2^{\bullet}} + {\bullet}\mathrm{CH_2{-}\overset{\mathrm{CH_3}}{\overset{|}{C}}{=}CH{-}CH_2}\!\sim \\ &\sim\!\mathrm{CH_2{-}\overset{\mathrm{CH_3}}{\overset{|}{C}}{=}CH{-}CH_2}\!\sim \xrightarrow{\text{irrad}} \sim\!\mathrm{CH_2{-}\overset{\mathrm{CH_3}}{\overset{|}{C}}{=}CH{-}\dot{C}H}\!\sim \end{aligned} \tag{28}$$

The irradiation of natural rubber in the presence of a vinyl monomer thus leads primarily to a synthesis of graft copolymers, but some block copolymer is certainly always present. Irradiation syntheses may be carried out in solution, either in contact with liquid monomer (with or without a diluent) or in contact with monomer in the vapor phase, or in emulsion or suspension. The rubber may be preirradiated in the absence of air to produce free radicals for later monomer addition, but the life of these radicals is short as a result of mobility within the rubber matrix. Irradiation at very low temperatures makes it possible to use the trapped radicals technique for a variety of natural and synthetic rubbers. Plastics and polymers with a crystalline phase are more readily preirradiated to initiate later grafting by trapped radicals. Irradiation may also be carried out in air to introduce peroxide groupings:

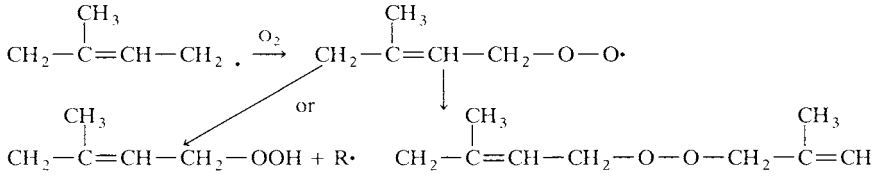

(29)

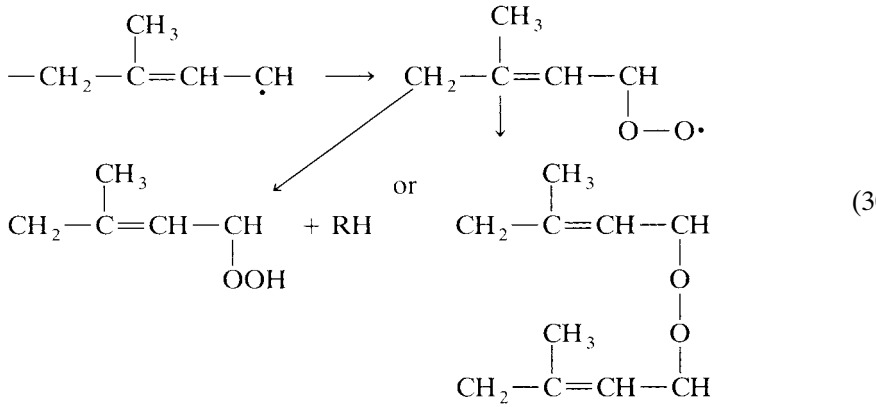

(30)

These groups can then be used to initiate grafting by any of the methods already discussed. Latex phase grafting is generally favored for its simplicity; natural rubber grafts with methyl methacrylate styrene, acrylonitrile, and vinyl chloride have been made in this way [46].

The irradiation of mixed lattices for subsequent combination of the ruptured chains is another approach; it has been carried out with natural rubber and poly(vinyl chloride) lattices to prepare graft (and block) copolymers in fairly high yields without the problem of monomer recovery. The same method has been used to graft polychloroprene onto synthetic polyisoprene dispersions and onto polybutadiene lattices of various compositions.

5. Photochemical Synthesis

Macromolecules containing photosensitive groups which absorb energy from ultraviolet frequencies often degrade by free radical processes. The degradative process as a rule is fairly slow, but by the addition of photosensitizers, such as xanthone, benzyl, benzoin, and 1-chloroanthraquinone, the rate can be speeded up to enable graft copolymerization to take place in the presence of methyl methacrylate or other monomers. This can be done in the case of natural rubber in the latex phase with reasonably high yields of graft copolymer. Natural rubber–*y*-polystyrene and poly(butadiene–*y*-styrene) have both been prepared by ultraviolet irradiation of sensitized latex–monomer dispersions. A combination of photochemical synthesis and redox-type initiation can also be carried out—a process known as one-electron oxidation—to achieve grafting with minimal homopolymer formation.

Bromine atoms on the backbone of a polymer can be liberated readily by ultraviolet irradiation to give free radical sites for grafting reactions. The bromination can be photochemically induced

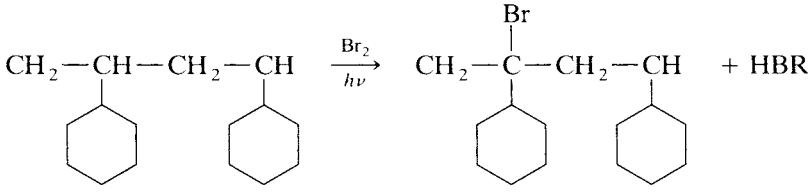

(31)

or a chain transfer agent such as carbon tetrabromide may be used in the polymerization step to introduce the labile groups,

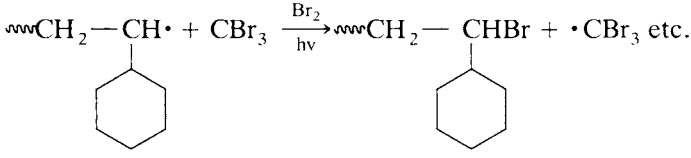

(32)

With the aid of suitable sensitizers, polymers such as brominated butyl rubber, valuable because of their flame retardancy, may act as backbone polymers for a variety of grafting reactions.

An early synthesis of block copolymers was based on the ultraviolet irradiation of poly(methyl vinyl ketone) in the presence of acrylonitrile. The initial degradative step is

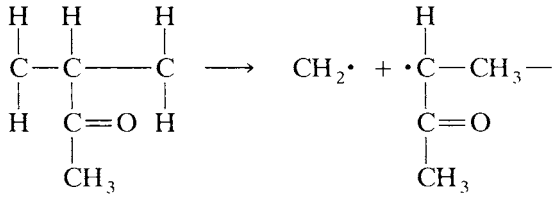

(33)

This degradation reaction, supplemented by various subsequent oxidation steps, has found renewed interest in the form of the introduction of photodegradable plastics as part of the campaign to reduce plastic litter from throwaway packaging. Although as yet there has been no demand for photodegradable rubbers, the incorporation of a small percentage of a vinyl ketone into a rubber copolymer or homopolymer would open the way to a useful synthesis of block copolymers.

Many other syntheses of block and graft copolymers have been reported, but enough has been said to indicate the scope of these reactions and to indicate a potential that has still to be thoroughly explored. Many grafting and block copolymerization systems have only been evaluated for plastic materials but are capable of extension to rubbers.

6. Metallation Using Activated Organolithium with Chelating Diamines

Unsaturated elastomers can be readily metallated with activated organolithium compounds in the presence of chelating diamines or alkoxides of potassium or sodium. For example, polyisoprene, polybutadiene, styrene–butadiene copolymers, and styrene–isoprene copolymers can be metallated with *n*-butyllithium · TMEDA complexes (1/1 or 1/2 ratio) to form allylic or benzylic anions. The resulting allylic anion can be employed as an initiator site to grow certain branched or comb polymer species. These polymers can include polystyrene, which would form hard domains, or polybutadiene, which forms soft domains.

Research in this area has resulted in the preparation of several comb polymers [47, 48]. The metallation technique is a useful and versatile method as it can be used with any polymeric material which contains a few double bonds. For example, ethylene–propylene was successfully grafted with norbornene. Similar reactions were performed on polymeric materials which contain aromatic rings, such as polystyrene, poly-α-methyl styrene, and polyphenylene oxide (PPO).

In general, polymeric materials that contain either side groups or main-chain allylic or acidic hydrogens can be metallated with organolithium compounds in the presence of chelating diamines. They can also be grafted with ionically polymerizable monomers to produce comblike materials [49].

G. Base Polymer Properties

Though the properties of block and graft copolymers are discussed in Chapters 3, 5, and 13, some properties of the copolymer particularly germane to this discussion are briefly mentioned here.

The properties of, say, natural rubber grafted with poly(methyl methacrylate) cannot be evaluated unless the copolymer is isolated from either homopolymer species. The methods used are based on fractional precipitation, selective solution, or a combination of these basic techniques. For details, the reader is referred to Chapter 3. In many cases, though, technologists are

concerned with the materials as manufactured, so we consider in this context also the properties of the block and graft copolymers without homopolymer removed.

The presence of two chemically different polymeric sequences in the same chain causes that macromolecule to act as a soap; i.e., it helps to compatibilize two species of homopolymer in a blend by accumulating at their interface, assisting a more gradual transition from one phase to the other, and thus reducing the interfacial energy. Microphase separation, of course, still occurs, the predominant case in practice, but macrophase separation is thereby usually prevented. In high-impact polystyrene and in A–B–S copolymers prepared by grafting reactions, the dispersed rubber phase in the glassy matrix and the dispersed glassy phase within the rubbery particles are both prevented from forming separate phases by the graft copolymer chains, which on a molecular scale have their rubbery segments associated with the rubber particles and their plastic segments with the glass phase. In this respect, there is little difference in properties between a graft and a linear block copolymer—the essential feature is the presence of the two types of sequences in the same macromolecule.

The block copolymeric thermoelastic polymers owe their properties to this very structure, whereby the polystyrene end blocks (along with any homopolymeric polystyrene) form the microphase, which is dispersed within a continuous phase of polybutadiene formed from the polybutadiene segments of the central sequences in S–B–S-type block copolymers. (For this to happen, the total volume of the polybutadiene segments must exceed the total volume of the polystyrene segments. When the reverse is the case, the product exhibits the properties of a high-impace polystyrene; see again Chapter 13.) Although the polystyrene "structures" act as physical crosslinks at low temperature, at processing temperatures above the softening temperature of polystyrene both segment types exhibit viscoelasticity, allowing the material to be extruded, injection molded, etc. On cooling, the polystyrene domains become rigid again and assert their influence on the material properties.

When block and graft copolymers are dispersed in solvents, the solutions have properties which depend on whether or not the copolymer is eventually fully solvated. If the solvent is a "good" solvent for both sequences, e.g., chloroform in the case of natural rubber graft copolymerized with poly(methyl methacrylate) [50], then both segment types are expanded and films cast from dilute solutions will usually be intermediate in properties to the two homopolymers (in this example the properties of a reinforced rubber film). If the solvent is a good solvent for the rubber but a poor solvent or nonsolvent for poly(methyl methacrylate), e.g., petroleum ether, then the solutions show the typical turbidity of a block or graft copolymer and the cast film is highly elastic. When the solvent is acetone, a good solvent for poly(methyl methacrylate) but a nonsolvent for rubber, the cast films are plastic with high tear strengths. See again Chapter 10.

When grafting is carried out on a polymer under conditions such that the physical form of the substrate polymer is maintained, then the original properties of the substrate usually predominate, and supplementary properties accrue as a result of the grafting. This is invariably the case when the substrate is in fibrous form, e.g., cellulose, nylons, and terylene grafted with various monomer systems. The nature of the grafting reaction to these fibers is usually such as to form a surface coating over the substrate polymer; the surface characteristics, such as dyeing, are therefore usually those of the grafting system.

It is very doubtful that any blends of two polymers, or of chemically different copolymers, can from a thermodynamic point of view ever be fully compatible. Even most block or graft copolymers systems therefore show microphase separation which will be typical for the properties of a given system. Chemical modification, as discussed in the earlier part of this chapter, will in general lead to the formation of polymeric single phases, provided the reaction has been carried out homogeneously. The choice need not be restricted, however, to just these two approaches, as chemical modification can be carried out after block or graft copolymerization or vice versa. Very little has been published on such a consecutive use of these two physically different ways of modifying polymers chemically, so there is considerable scope for developing new modifications of long-established rubbers, as well as generally for changing old into new polymers.

REFERENCES

1. D. M. Bielinsk, L. A. Sulsarki, H. M. Stanley, and R. A. J. Pethrick, *Appl. Plym. Sci.* **56**, 853 (1995).
2. M. Yamato and M. Oahu, *Progress in Organic Coating* **27**, 277 (1996).
3. D. N. Schulz, A. F. Halasa, and A. E. Oberster, *J. Polym. Sci. Chem. Ed.* **12**, 153 (1974).
4. C. A. Urneck and J. N. Short, *J. Appl. Polymer Sci.* **14**, 1421 (1970).
5. A. F. Halasa, *J. Polym. Sci. Polym. Ed.* **19**, 1357 (1981).
6. A. Yoshioka, A. Ueda, H. Watanabe, and N. Nagata, *Nippon Kagaka Kaisha* 341.
7. A. Uda Brain, Proceedings of the International Institute of Synthetic Rubber Producers, 33rd Annual Meeting, 1992, pp. 65–83.
8. G. Bohm and D. Graves, U.S. Patent 4,788, 229 (1988).
9. A. F. Halasa and Wen-ling Hsu (to The Goodyear Tire and Rubber Co.), U.S. Patents 6,693,160 and 6,753,447 (2004).
10. Reference deleted in page proofs.
11. H. L. Hsieh and R. P. Quirk, "Anionic Polymerization: Principles and Practical Applications," Marcel Dekker, New York, 1996.
12. J. E. Hall, T. A. Antikowiak, European Patent 0693 505 (1955).
13. V. C. Haskell, in "Encyclopedia of Polymer Science and Technology," H. S. Mark *et al*. (Eds.), Wiley-Interscience, New York, Vol. 3, 1965, p. 60.
14. G. N. Bruxelles and N. R. Grassie, in "Encyclopedia of Polymer and Technology," H. S. Mark *et al*. (Eds.), Wiley-Interscience, New York, Vol. 3, 1965, p. 307.
15. B. P. Rouse, in "Encyclopedia of Polymer and Technology," H. S. Mark *et al*. (Eds.), Wiley-Interscience, New York, Vol. 3, 1965, p. 325.

16. W. Jarowenko, in "Encyclopedia of Polymer Science and Technology," H. S. Mark *et al*. (Eds.), Wiley-Interscience, New York, Vol. 3, 1965, p. 787.
17. J. Wichlatz, in "Chemical Reaction of Polymers," M. Fetters (Ed.), Interscience, New York, 1964, Chap. 2.
18. A. Yakubchik, B. Tikhominov, and V. Sumilov, *Rubber Chem. Technol.* **35**, 1063 (1962).
19. H. Rachapudy, G. Smith, V. Raju, and W. Graessley, *J. Polym. Sci. Phys. Ed.* **17**, 1211 (1979).
20. A. F. Halasa, *Rubber Chem. Technol.* **54**, 627 (1981).
21. A. F. Halasa and J. M. Massie, "Kirk-Othemer Encyclopedia of Chemical Technology" 4th ed., Vol. 8, John Wiley & Sons, Inc., New York, 1993.
22. Y. Chamberline, J. Pascoult, H. Razzouk, and H. Cheradem, *Makromol. Chem. Rapid Commun* **2**, 322 (1981).
23. A. F. Halasa, L. E. Vescelius, S. Futamura, and J. Hall, "IUPAC Symposium on Macromolecules," Vol. 28, Amherst, MA, 1982.
24. A. F. Halasa (to The Goodyear Tire & Rubber Co.), U.S. Patent 3,872,072 (1985) and U.S. Patent 4,237,245.
25. H. Harwood, D. Russell, J. Verthe, and J. Zymons, *Macromol. Chem.* **163**, 1 (1973).
26. M. Poutsma, in "Methods of Free Radical Chemistry," S. Huyser (Ed.), Dekker, New York, Vol. 1, 1969, Chap. 3.
27. J. Bevington and L. Ratt, *Polymer* **16**, 66 (1975).
28. L. Schoen, W. Raajien, and W. Van'twout, *Br. Polym. J.* **7**, 165 (1975).
29. R. J. Hopper (to The Goodyear Tire & Rubber Co.), U.S. Patent 3,915,907 (1975).
30. R. J. Hooper, *Rubber. Chem. Technol.* **49**, 341 (1976).
31. R. J. Hooper, R. D. Mcquateand, T. G. Hutchin, Preprints, International Conference on Advances in the Stablization and Controlled Degradation of Polymers, Lucerne, Switzerland, May 23–25, 1984.
32. R. J. Hooper (to The Goodyear Tire & Rubber Co.), U.S. Patent 4,820,780 (1989).
33. R. J. Hooper (to The Goodyear Tire & Rubber Co.), U.S. Patent 4,910,266 (1990).
34. D. A. White, R. S. Auda, W. M. Davis, and D. T. Ferrughlli (to Exxon Chemical Co.), U.S. Patent 4,956,420 (1990).
35. R. J. Hooper (to The Goodyear Tire & Rubber Co.), U.S. Patent 4,017,468 (1977).
36. A. Staudinger, *Rubber Chem. Technol.* **17**, 15 (1944).
37. M. Gordon and J. Tyler, *J. Polym. Chem.* **3**, 537 (1953).
38. D. N. Schults, S. Turner, and M. Golub, *Rubber Chem. Technol.* **85**, 809, (1983).
39. J. I. Cunneen and M. Porter, in "Encyclopedia of Polymer Science and Technology," H. S. Mark *et al*. (Eds.), Wiley-Interscience, New York, Vol. 2, 1965, p. 502.
40. R. J. Ceresa, in "Encyclopedia of Polymer Science and Technology," H. S. Mark *et al*. (Eds.), Wiley-Interscience, New York, Vol. 2, 1965, p. 502.
41. C. Avery and W. Watson, *J. Appl. Polym. Sci.* **19**, 1 (1956).
42. R. J. Ceresa and W. Watson, *J. Appl. Polym. Sci.*, **101**, 1 (1959).
43. G. Scott, *Polym. Eng. Sci.* **24**, 1007 (1984).
44. W. H. Janes, in "Block Copolymers," D. C. Allport and W. H. Janes (Eds.), Applied Science Publishers, London, 1973, p. 62.
45. J. E. Morris and B. C. Sekher, Proceedings of the International Rubber Conterence, Washington, D.C., 1959, p. 277.
46. E. G. Cockbain, T. D. Pendle, and D. T. Turner, *J. Polym. Sci.* **39**, 419 (1959).
47. A. F. Halasa, *Adv. Chem. Ser.* **130**, 77 (1974).
48. J. Folk, R. Sclott, D. Hoey, and J. Pendeltor, *Rubber Chem. Technol.* **46**, 1044 (1973).
49. A. F. Halasa, G. Mitchell, M. Stayer, D. P. Tate, and R. Koch, *J. Polym. Sci. Chem. Ed.* **14**, 297 (1976).
50. F. M. Merrett, *Trans. Faraday Soc.* **50**, 759 (1964).

12 Elastomer Blends

SUDHIN DATTA
ExxonMobil Chemical Co.
Baytown, Texas

I. INTRODUCTION

Blends of elastomers are of technological and commercial importance since they allow the user to access properties of the final blended and vulcanized elastomer that are not accessible from a single, commercially available elastomer alone. These potentially improved properties include chemical, physical, and processing benefits. In reality, all blends show compositionally correlated changes in all of these properties compared to the blend components. The technology of elastomer blends is largely focused on the choice of individual elastomers and the creation of the blends to achieve a set of final properties. This chapter shows some of the instances of the uses of elastomer blends. Empirical guidelines for the creation of novel blends of elastomers is a comparatively more difficult proposition.

Blends provide an acceptable technological process for accessing properties not available in a single elastomer. In elastomers composed of a single monomer in a single insertion mode (e.g., 1,2 polybutadiene), there are no other procedures available except blends. In the case of elastomers that are copolymers (e.g., styrene–butadiene rubber [SBR]), changes in intramolecular composition, such as formation of a block polymer instead of random copolymer at the same composition, are effective. However, intramolecular changes are limited by available synthesis processes. Intermolecular changes, in either composition or distribution of monomers, such as in blends, are not limited by such systemic or synthetic limitations.

Theoretically, blends of elastomers can attain a wide variation in properties. Combinations of elastomers can lead to changes in properties due to either intrinsic differences in the constituents or differences in the reinforcement and vulcanization of the constituents. Miscible blends of elastomers that

Science and Technology of Rubber, Third Edition

consist of a single elastomeric phase with microscopically uniform crosslinking and distribution of reinforcing agents reflect a compositionally weighted average of the intrinsic properties of the constituents. Miscible blends are commonly used though they have been very rarely recognized. Analysis of such blends, particularly after vulcanization, is difficult. The current analytical techniques are only slightly more capable than the classical techniques of selective precipitation of the components of an unvulcanized elastomer blend from solution [1].

Common examples of miscible blends are ethylene–propylene copolymers of different composition that result in an elastomer comprising a semicrystalline, higher ethylene content and an amorphous, lower ethylene content components. These blends combine the higher tensile strength of the semicrystalline polymers and the favorable low temperature properties of amorphous polymers. Chemical differences in miscible blends of ethylene–propylene and styrene–butadiene copolymers can also arise from differences in the distribution and the type of vulcanization site on the elastomer. The uneven distribution of diene, which is the site for vulcanization in blends of ethylene–propylene–diene elastomers, can lead to the formation of two distinct, intermingled vulcanization networks.

Immiscible blends show additional, more complex changes due to a microscopically inhomogeneous phase structure of the two component elastomers. The two separate phases typically have differences in the retention of the fillers and plasticizers as well as vulcanization in the presence of the curative. Changing the properties of elastomers by uneven distribution of fillers and vulcanization is, however, the more common use of blends of immiscible elastomers [2]. The engineering properties of elastomers (i.e., tensile strength, hysteresis) in vulcanized compounds depend not only on the elastomer itself but also on the amount and identity of the fillers and plasticizers, as well as on the extent of cure. In an immiscible blend, the amount of these additives in any phase can be modulated by changes in the viscosity and chemical identity of the elastomer, the surface chemistry of the filler, the chemical nature of the plasticizer, and the sequence of addition of the components as well as the details of the mixing procedure. A large body of experimental procedures (*vide infra*) has been developed to attain a thermodynamically metastable, interphase distribution of additives in blends. On vulcanization, this distribution is rendered immobile and leads to desirable engineering properties of the blend.

Two notable reviews of elastomer blends exist. The first, by Hess *et al.* [3], reviews the applications, analysis, and the properties of the immiscible elastomer blends. The second, by Roland [4], has in addition a discussion of the physics of mixing immiscible polymer blends and a more recent account of the analytical methods. Other reviews by Corish [5] and McDonel *et al.* [6] deal with specific aspects of elastomer blends. These reviews are focused on immiscible blends of elastomers. In this review we will complement this with information on miscible blends.

II. MISCIBLE ELASTOMER BLENDS

A. Thermodynamics

The extension of thermodynamics to a blend of elastomers has been discussed by Roland [4]. Miscible blends are most commonly formed from elastomers with similar three-dimensional [7] solubility parameters. An example of this is blends from copolymer elastomers (e.g., ethylene–propylene or styrene–butadiene copolymers) from component polymers of different composition, microstructure, and molecular weights. When the forces between the components of the polymer blend are mostly entirely dispersive, miscibility is only achieved in neat polymers with a very close match in Hansen's three-dimensional solubility parameter [7].

Miscible blends of elastomers differ from corresponding blends of thermoplastics in two important areas. First, the need for elastic properties require elastomers to be high molecular weight polymers with a limited polydispersity. This reduces the miscibility of dissimilar elastomers by interdiffusion of the low molecular components of the blends. Second, elastomers are plasticized in the conventional compounding with process oils. The presence of plasticizers leads to a higher free volume for the blend components and stabilizes, to a small extent, blends of dissimilar elastomers.

B. Kinetics

The formation of miscible rubber blends slows the rate of crystallization [8a, b] when one of the components is crystallizable. This phenomenon accounts for data that shows lower heats of fusion that correlate to the extent of phase homogeneity [9] in elastomer blends. Additionally, the melting behavior of a polymer can be changed in a miscible blend. The stability of the liquid state by formation of a miscible blend reduces the relative thermal stability of the crystalline state and lowers the equilibrium melting point [10a, b]. This depression in melting point is small for a miscible blend with only dispersive interactions between the components.

C. Analysis

1. Glass Transition

The principal effect of miscibility of elastomer blends of dissimilar elastomers is alteration of the glass-transition temperature. Since miscible blends should have negligible changes in the conformation of the polymer chains, the entanglement density of miscible blends should be a compositionally weighted average of entanglement density of the pure components.

2. Magnetic Resonance Imaging

Nuclear magnetic resonance (NMR) has been applied to the study of homogeneity in miscible polymer blends and has been reviewed by Cheng [11a] and Roland [11b]. When the components of a blend have different Tg's, proton NMR can be used to assess the phase structure of the blend by taking advantage of the rapid decrease of proton–proton coupling with nuclear separation [11c]. For blends containing elastomers of almost identical Tg, proton MAS NMR is applied to blends where one of the components is almost completely deuterated [12]. Another technique is crosspolarization MAS ^{13}C NMR [13]. The transfer of spin polarization from protons to the ^{13}C atoms of the deuteriated component can occur if these carbons are in proximity (nanometers) to the protons.

3. Crystallinity

Changes in polymer crystallinity have also been employed to study the homogeneity of elastomer blends [14]. Morris [14a] studied the rate of crystallization of *cis*-1,4-BR in blends with SBR. At any given blend composition, the BR crystallization rate diminishes with greater blend homogeneity. Sircar and Lamond [14b] also studied the changes in BR crystallinity in blends with NR, IR, EPM, CIIR, NBR, and CR (Fig. 1). The nature of the blend component had the greater effect since the more compatible blends (smaller domains) had the greater the loss in BR crystallinity.

4. Interdiffusion

Interdiffusion between a pair of polymers is a demonstration of their thermodynamic miscibility. The adhesion between contacted rubber sheets parallels the extent of any interdiffusion of the polymer chains [15a]. If the contacted sheets are comprised of immiscible rubbers, no interdiffusion occurs. Natural rubber (NR) and 1,2-polybutadiene (1,2-BR) are miscible even at high molecular weights [15b, c]. When NR is brought into contact with 1,2-BR, they interdiffuse spontaneously. When some form of scattering contrast exists between the materials, interdiffusion will enhance the scattering intensity (either x-ray or neutron) measured from the plied sheets. A variety of spectroscopic methods [15d–j] have been used to detect the interdiffusing species.

5. Mechanical Properties

Miscible blends should have greater mechanical integrity than a comparable multiphase structure. Miscible rubber blends that react chemically have a densification and a higher cohesive energy density. This may provide improved mechanical properties but has been observed only below the Tg [16].

D. Compositional Gradient Copolymers

A significant development [17] in the last decade is the use of miscible blends of compositionally different EPDM. The blends are designed to

balance viscoelastic properties such as the rate of extrusion or adhesion with physical properties such as tensile strength by changes in the relaxation characteristics. This is achieved with the components having different average molecular weight or differences in the crystallinity (due to extended ethylene sequences) or both. An example of the components of these blends is shown in Table I. The blends of component A with one of the B polymers are miscible and are made by mixing hexane solutions of the elastomers. Figures 2 and 3 show the effect on tensile strength of the compounded but unvulcanized

TABLE I Ethylene–Propylene Blend Components Differing in Molecular Weight and Crystallinity

Sample	Composition C2 Wt%	Viscosity ML(1 + 4) 125°C
A	60	41
B_1	74	72
B_2	76	247
B_3	78	1900
B_4	68	189
B_5	84	291

Viscosity determined according to ASTM D1646.

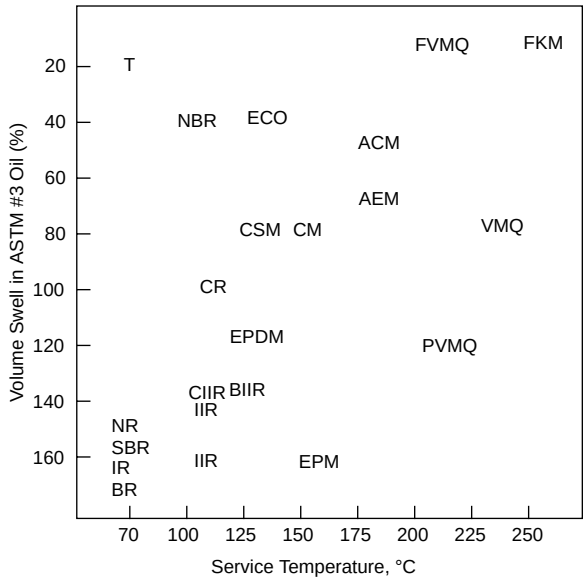

FIGURE 1 Elastomer distribution by resistance to aromatic solvents (ordinate) and temperature (abcissae).

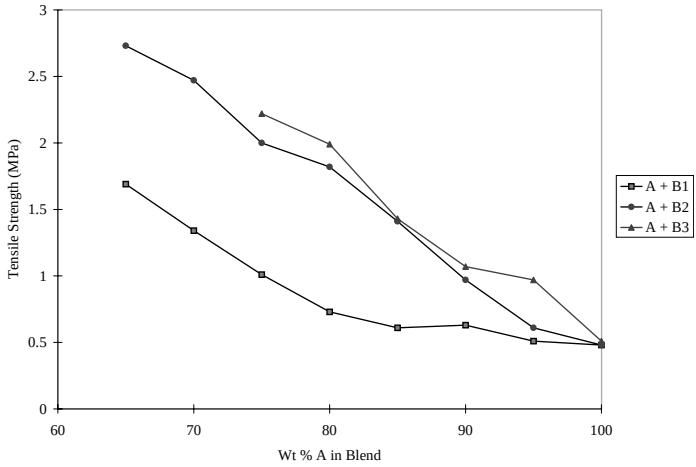

FIGURE 2 Variation in tensile strengh of unvulcanized, compounded blends of ethylene–propylene copolymer due to differences in molecular weight distribution.

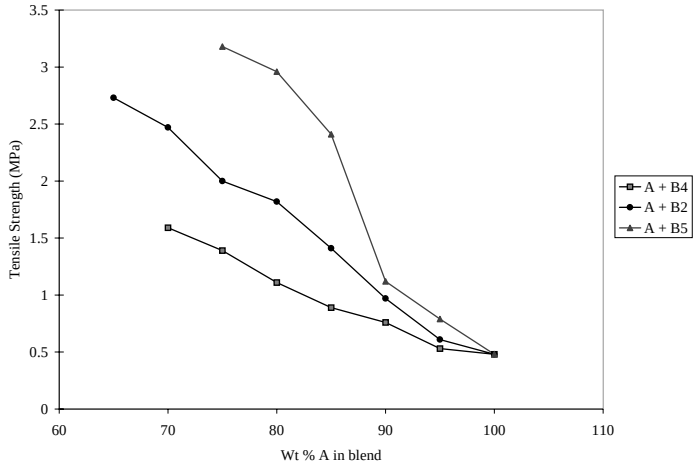

FIGURE 3 Variation in tensile strength of unvulcanized, compounded blends of ethylene–propylene copolymer due to differences in composition and crystallinity distribution.

blends from the components in Table I. The blends in Fig. 2 are different in the molecular weight distribution while in Fig. 3 they are different in composition and crystallinity. This dispersion in molecular weight and crystallinity is apparent in other viscoelastic properties such as peel adhesion. Figures 4 and 5 show self-adhesion measured by the force needed for the failure of a spliced portion in blends identical to those in Fig. 2 and Fig. 3, respectively. Adhesion

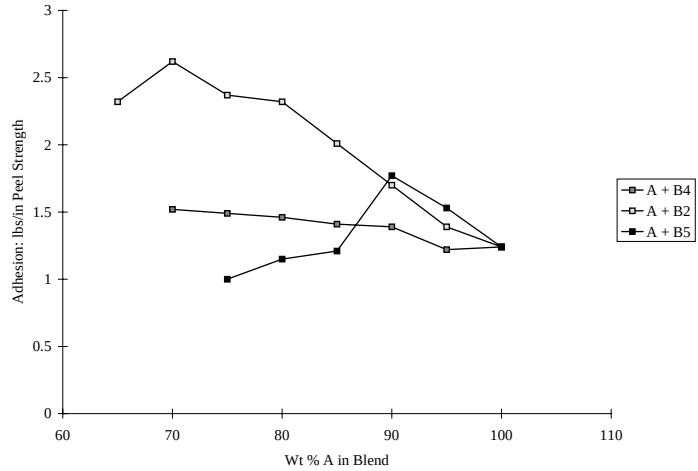

FIGURE 4 Variation in peel adhesion of unvulcanized, compounded blends of ethylene–propylene copolymer due to differences in molecular weight distribution.

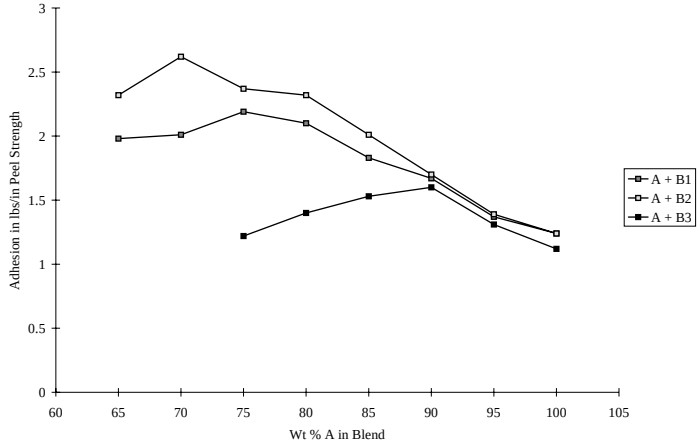

FIGURE 5 Variation in peel adhesion of unvulcanized, compounded blends of ethylene–propylene copolymer due to differences in composition and crystallinity distribution.

increases with increasing molecular weight and compositional dispersity of the blend. This is shown by the comparative data for B1 and B2 in Fig. 4, and B4 and B2 in Fig. 5. Small increases in the cystallinity and molecular weight dispersion by blending promote adhesion by slowing down the latter without substantial effect on the former. Further increases in either severely retard the intermingling of chains necessary for the self-adhesion.

TABLE II Ethylene–Propylene Blend Components Differing in Crosslink Density

Sample	Composition C2 wt%	Composition ENB wt%	Viscosity ML(1 + 4) 125°C
A_1	57.0	3.2	20
A_2	60.2	2.9	32
A_3	60.3	2.8	41
A_4	59.4	2.6	51
A_5	60.5	3.2	67
B	64	0.9	2100

Viscosity determined according to ASTM D1646.

Nonuniform vulcanization networks in miscible blends of elastomers have a strong effect on tensile strength and elongation. These networks have an intermolecular distribution in crosslink density and are composed of different concentrations of crosslinkable sites in the components of the blend. Differences in the level of the enchained diene (5-ethylidene-2-norbornene) for EPDM copolymers [18, 19] or differences in the level of the vulcanizable chain end unsaturation for siloxane polymer define these blends [20]. These networks lead to an increase in both the elongation as well as the tensile strength at high elongation compared to vulcanizates of similar viscosity having a uniform network. In particular, nonuniform networks display a nonlinear increase in the tensile modulus at high elongation. This nonlinearity is due to a nonaffine deformation of the network at the high elongation, which continually reallocates the stress during elongation to the lightly crosslinked component of the blend that is most able to accommodate the strain. Blends of one A and various amounts of polymer B in Table II were blended in hexane solution, compounded, and vulcanized. Both of the polymers are amorphous, and the A polymers differ in the molecular weight and contain approximately 3% of vulcanizable diene (ENB). The B polymer is much lower in diene and has 0.7% ENB. The tensile strength of the blends derived from all of the A with varying amounts of B are shown in Fig. 6. In all cases where small amounts (<25%) of B are included in the blends, the tensile strength is higher for the blends than for the parent A, even though the extent of vulcanization is lower in the blends than in the blend components A due to reduction in the total amount of diene.

E. Distinct Polymers

1. IR–BR Blends

Blends of 1,4-IR with predominantly 1,2-BR are unique since they are miscible, chemically distinct, high-molecular weight homopolymers [21a–e],

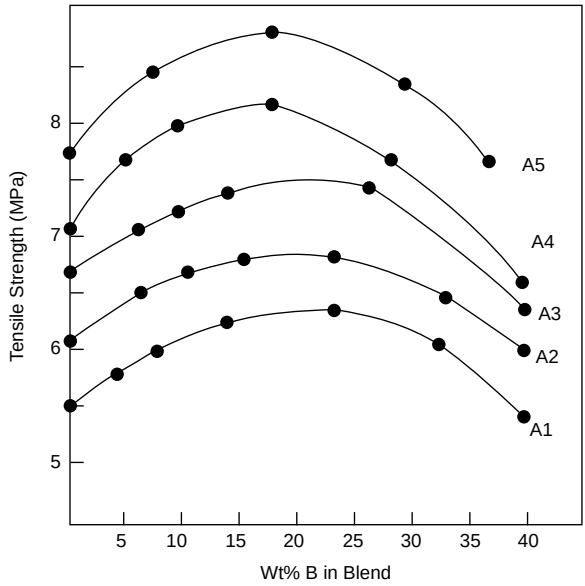

FIGURE 6 Tensile strength of blends in Table II differing in crosslink density.

even though there is no dipole or specific interaction between the components [21c]. As the concentration of 1,4 units in the BR increases, there is a decrease in miscibility with IR. The interaction parameter measured for blends of IR with BR of varying 1,2 and 1,4 geometry indicates that the exchange enthalpy between IR and BR becomes more endothermic as the concentration of 1,4-units increases [21b, d]. Differences in structure are apparent from the thermal expansion coefficients of the components. The difference in thermal expansion coefficients of IR and BR is greatly diminished as the 1,2 content of the latter increases.

2. Epoxidized PI–CPE Blends

The intramolecular epoxidation of 25 mole % of PI leads to miscible blends with CPE containing 25 wt % chlorine [22a, b]. The origin of the miscibility is the specific interactions involving the oxirane of the epoxy ring with the chlorine.

F. Reactive Elastomers

The formation of miscible blends of elastomers by mutual chemical reaction of the blend components has been explored by Coleman *et al.* [23a–d]. Chemical reaction in a miscible blend provides the negative free energy needed to compensate for the unlike i–j contacts between dissimilar

elastomers. Miscible blends were formed by the use of stabilizing weak hydrogen bonding between a 2,3-dimethyl butadiene-4-vinyl phenol copolymer and carbonyl group of polymers such as EVA and poly alkyl methacrylates. The extent of the H-bonding stabilization was modulated by the concentration of the phenol residues in the unsaturated copolymer. The choice of the stabilizing chemical bond between the elastomers is important. A stable, localized chemical bond would lead to a loss of viscoelastic properties characteristic of an unvulcanized elastomer. Weak hydrogen bonding is fluxional and allows flow in response to stress in the elastomer blend.

III. IMMISCIBLE ELASTOMER BLENDS

A. Formation

Immiscible blends can be made from any two dissimilar elastomers. They can be made by *in situ* copolymerization, blending polymer solutions or suspensions, and mechanical mixing. These procedures have been reviewed by Corish [5]. In contrast to blends of other polymers, elastomers can be either "preblended" or "phase mixed" with each other [24]. "Preblended" systems are those where the compounding ingredients (e.g., fillers, plasticizers, and curatives) are added simultaneously to a mixture of the immiscible polymers. In "phase mixed" blends, ingredients are added separately to each of the individual polymers in separate compounding operations. The compounded elastomers are then blended together. Phase mixed blends provide a greater certainty of the initial interphase location of fillers, plasticizers, and curatives than the preblends.

B. Kinetics of Blend Morphology

The kinetics of the formation of the phase morphology is dominated by two competitive factors. First, the viscoelastic flow of elastomers, the presence of plasticizers, the long resting times (days) between mixing and crosslinking as well as low shear processing steps (e.g., calendering) are ideal for the development of the equilibrium morphology. However, the sluggish diffusion of high molecular weight elastomers, the presence of particulate fillers, and the ultimate crosslinking generate persistent nonequilibrium morphologies. Tokita [25a] and Avgeropoulos *et al.* [25b] have studied the mixing of EPDM with the diene rubbers—NR or BR—as a function of relative viscosity.

The detailed morphology of elastomer blends depends on (1) the mixing procedure, (2) the rheology of the blend components, and (3) the interfacial energy. As with other polymer blends, the elastomer of lower viscosity tends to be the continuous phase [26a–b]. Cocontinuous blend morphology is observed only for elastomers with similar viscosities. The viscoelastic forces developed during the formation of the compounded blend from two rheologi-

cally dissimilar elastomers are principally responsible for the morphology. Interfacial tension due to chemical differences between the elastomers is less important [26c].

C. Analysis

1. Microscopy

Phase contrast light microscopy has been applied extensively to the analyses of unfilled binary elastomer combinations. This method is based on differences in the refractive indices of the polymers and has been reviewed by Kruse [27a]. Callan *et al.* [27b–d] have shown the versatility of the method for a wide range of binary blends containing NR, SBR, BR, CR, NBR, EPDM, IIR, and CIIR. The results of these experiments are shown in Table III, which lists the measured areas of the disperse phase in more than 50 combinations of Banbury-mixed 75/25 binary blends containing eight different elastomers. Blends of IIR–CIIR and SBR–BR are excluded since the contrast was low. It can be seen that NBR produced the greatest heterogeneity in all blends except those with CR.

Transmission electron microscopy (TEM) is applicable to both filled and unfilled elastomer blends. However, for most elastomer combinations, there is no contrast between the polymer phases in a TEM. If the polymers differ significantly in unsaturation, osmium tetroxide (OsO_4) or ruthenium tetroxide (RuO_4) staining is the best method for obtaining contrast. The metal oxides selectively oxidize the unsaturation and the location of the metal atoms in the phase with the greater unsaturation provides the electron density contrast for TEM. Contrast for TEM analysis of elastomer blends of diene rubbers is achieved through the sulfur hardening method developed by Roninger [28a]

TABLE III Average Areas (in μm^2) of the Dispersed Phase in 75:25 Pure Elastomer Blends

Disperse phase 25%	Matrix (75%)							
	NR	**CR**	**BR**	**SBR**	**NBR**	**EPDM**	**IIR**	**CIIR**
NR	—	45	1.5	1.2	300	1.5	2.0	3.2
CR	35	—	4.0	2.5	1.5	25	20	15
BR	0.7	4.5	—	—	15	2.2	2.1	2.5
SBR	0.5	2.7	—	—	20	2.1	12	10
NBR	400	1.3	17	30	—	250	100	225
EPDM	3.5	75	2.8	2.6	225	—	2.0	1.5
IIR	3.0	15	3.0	4.2	75	1.0		
CIIR	2.2	25	2.3	2.5	85	1.2		

and utilized by Smith and Andries [28b]. Small rubber specimens are immersed in a molten mixture of sulfur, an accelerator, and zinc stearate. The selective absorption of the zinc salts into the SBR phase renders it darker than the BR in a TEM.

Scanning electron microscopy involves simpler specimen preparations than TEM. Both OsO_4 and RuO_4 staining techniques work with SEM and can be applied to both bulk specimens and films. Atomic force microscopy is an extension of scanning tunneling microscope (STM) and has the potential for atomic resolution. In its simplest form, the AFM [29a–d] acts as a "miniature surface profilometer" and provides topographical images. The potential advantages of these techniques include higher resolution, simplicity of specimen preparation, and greater versatility in varying the mechanisms for achieving image contrast. Digital image analysis has expedited particle size analysis from micrographs [29e–h] at resolution limits of a few Angstroms.

2. Glass Transition Temperature

The most common method of estimating the degree of homogeneity in elastomer blends is by measurement of the temperature of transitions from rubber to glass [30]. For elastomers this is usually at subambient temperatures. Glass transition measurements do not provide any information on blend morphology. The observation of distinct transitions corresponding to the respective components of the blend indicates the existence of a multiphase structure. A potential source of error is that vulcanization tends to raise the Tg due to restricted motion of the chains; this might be interpreted as miscibility.

3. Magnetic Resonance Imaging

NMR imaging of solids has been used to characterize the phase sizes with a spatial resolution of less than $50\,\mu$m in immiscible mixtures containing polybutadiene. Butera *et al*. [31a] have reported improvement over the ^{13}C NMR method by using magic angle spinning (MAS) in polymer blends containing a deuterated and a protonated polymer. More recently, Koenig *et al*. [31b–e] have used NMR for the determination of vulcanization efficiencies in elastomer blends.

4. Light, X-ray, and Neutron Scattering

Roland and Bohm [32a] used both SAXS and SANS in conjunction with TEM to assess the size of butadiene domains (5% by weight) in a CR matrix. Roland *et al*. used different master batches containing deuterated and protonated butadiene, respectively. These were each blended on a two-roll mill to study the coalescence of the polybutadiene phase. Coalescence (measured by SANS) was minimized by low temperature mixing, or by significantly increasing the molecular weight of the disperse or continuous phase to create a greater disparity in viscosity. Some preliminary SANS work on IR blended with deuterated 1,2-BR has been reported [32b, c]. All scattering techniques

are affected by the presence of fillers, which lead to more extensive scattering than the phase morphology. This is a severe limitation to the wide applicability of these techniques to most elastomers.

D. Interphase Distribution of Filler, Curatives, and Plasticizers

At ambient and processing temperatures, elastomers are viscous fluids with persistent transport phenomenon. In immiscible blends, these lead to change in the size and shape of the elastomer phases and migration of the fillers, plasticizers, and curatives from one phase to another. These changes are accelerated by processing and plasticization but retarded by the ultimate vulcanization. Retention of the favorable properties of a metastable blend, which is often attained only at a select interphase morphology and filler/plasticizer distribution, thus requires careful control of both the processing and the vulcanization procedures.

1. Curative and Plasticizer Migration in Elastomer Blends

During mixing, curatives are initially located within the continuous phase [33a]. Since the curatives dissolve in the elastomer, curative migration across phase boundaries can occur [33b–e]. Owing to the higher solubility of sulfur in elastomers containing diene or styrene groups and the greater affinity of many accelerators for polar rubbers, large differences in crosslink density of the different phases result on vulcanization. Further, increased rate of vulcanization in the diene or styrene containing elastomers can cause depletion of the curatives in this component, leading to even greater curative migration (Le Chatelier's principle). For most elastomer blends, these effects are in concert, and the result is a large cure imbalance [33f] between the phases. In addition, the boundary layers of the two elastomers, adjacent to the interface, can be different than the bulk since the greatest migration of curatives and plasticizers occurs in the proximity to this region. The transfer of curatives to one phase at the expense of the other creates a morphology where the boundary layers separates a curative-depleted, slightly crosslinked elastomer near a curative-enriched, tightly crosslinked elastomer.

Amerongen [34a] has an early review on curative migration in heterophasic elastomer blends based on optical and radiochemical analyses. A later, more detailed work by Gardiner [34b–d] used optical analysis to study curative diffusion across the boundaries of elastomer blends consisting of binary combination of polymers of CIIR, IIR, EPDM, CR, SBR, BR, and NR. Gardiner measured a diffusion gradient for the concentration change as a function of distance and time. His measurements for the diffusion of accelerator and sulfur from IIR to other elastomers are listed in Table IV.

2. Cure Compatibility

Adequate properties in a vulcanized rubber blend depend on the covulcanization across the phases. Covulcanization is the formation of a single

TABLE IV Curative Diffusion Coefficients in Elastomer Blends

Curative	From	To	$D \times 10^7$ cm^2/s
Accelerator (TDDC)	IIR	BR	12.66
		EPDM	1.09
		CR	1.08
		SBR	0.58
		NR	0.70
Sulfur	IIR	SBR	4.73
		SBR & 50 PHR N700 CB	17.2
		NR	2.82

network structure including crosslinked macromolecules of both polymers. The degree of vulcanization is at similar levels in both phases with crosslinking across the phase interfaces. Shershnev [35a] and earlier Rehner and Wei [35b] have summarized the experimental requirements for covulcanization of the components of elastomer blends. These are:

1. Phase blending followed by very short, high-temperature cure cycles [35c]
2. Vulcanization agents chemically bound to the elastomer [35d–f]
3. Accelerators similar in solubility parameter to less reactive elastomers [35g–j]
4. Insoluble vulcanizing systems that cannot migrate
5. Nonpolar vulcanizing agents that distribute uniformly and have similar reactivities toward different elastomers (e.g., peroxides and reactive resins)

Gardiner [34b–d] and Woods and Davidson [36] have improved the covulcanization of EPDM–NR and IIR–NR blends by using an insoluble lead-based curative for the less unsaturated elastomer. The blends with soluble curatives from the same elastomers were much inferior. Coran [35f] covulcanized EPDM–NR blends by modifying the EPDM with maleic anhydride. The modified EPDM can be crosslinked with zinc oxide to form an ionic crosslink network. The migration of curatives was investigated by Bhowmick and De [35c] in binary blends of NR, BR, and SBR. Cure rates decreased in that order, and the migration of curatives was the greatest for NR–SBR.

The state of cure of the phases in a blend can be determined from changes in the magnitude of the damping peaks [37a] and from freezing-point-depression measurements on swollen networks. Honiball and McGill [37b] have employed the freezing point depression of solvent-swelled NR–BR blends to determine the crosslink densities of the individual polymer phases.

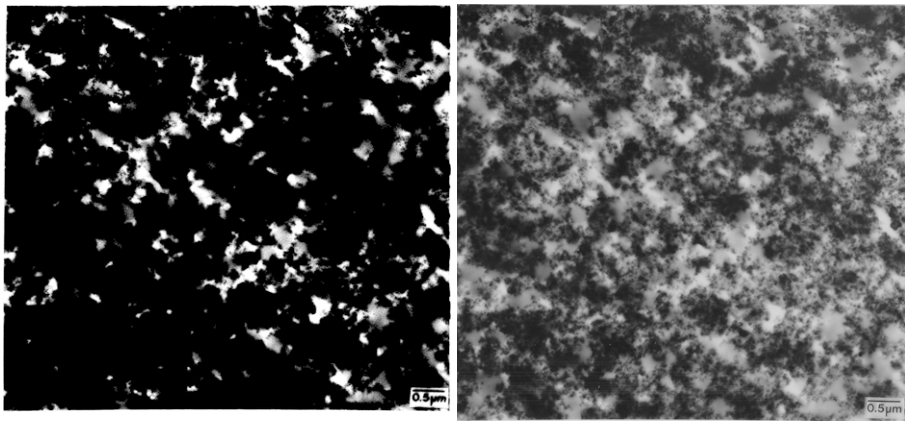

(a) (b)

FIGURE 7 Micrographs of a N234 carbon black distribution in 70:30 blend of NBR and EPR. (a) The EPR is a copolymer of 42 mole % ethylene. (b) The EPR has 43 mole % ethylene and 0.9 mole % primary amine functionality.

The freezing point depression of a solvent in a swollen vulcanizate is dependent on the volume fraction of solvent in the elastomer phase.

3. Interphase Filler Transfer

The distribution of fillers (e.g., carbon black, silica) and various processing aids in heterogeneous elastomer blends can be nonuniform. Interphase transfer of fillers has been observed in blends of both diene and saturated elastomers. This migration is due to the greater solvation between a filler and one of the polymers in the melt-mixed blends. Callan *et al.* [38a] showed significant transfer of carbon black from NR to BR and silica from BR to NR in solution and latex blends. Extensive carbon black transfer from a low unsaturation elastomer (IIR and EPDM) to other high unsaturation (e.g., diene) elastomers occurs regardless of the master batch mixing procedure [38a]. This is seen in blends of EPDM or IIR with NR or SBR. During mechanical mixing, chemisorption of the unsaturated polymer onto the carbon black occurs, thus preventing any subsequent transfer of the carbon black. In all instances, the carbon black was located almost entirely in the NR phase when added to the preblended elastomers. Transfer of carbon black from EPDM to NBR could be reversed if the EPDM was functionalized with a primary amine [38b]. Amines are tenaciously chemisorbed to the surface of carbon black, and the functionalization allows the EPDM phase to retain significant amounts of filler. The carbon black distribution is shown in Fig. 7(a) for the blend of EPDM with NBR and is compared to Fig. 7(b) for the blend of the amine functionalized EPDM with NBR.

TABLE V Effect of Carbon Black on the Distribution in 50:50 Natural-Rubber/SBR Blend Containing 45 Phr Black

Carbon black type	Surface area	Bound rubber, %	Carbon-black loading, in phr	
	(CTAB) m^2/g			
			NR	SBR
N560	43	17.0	41.2	48.8
N347	87	28.0	33.9	56.1
N339	95	30.2	31.1	58.9
N234	120	30.4	30.0	60.0
Vulcan(10H)	136	33.1	27.2	62.8
N326	84	22.5	31.9	68.1
N330	81	25.0	34.0	66.0

Callan *et al*. [38a, b] used the differential swelling technique (*vide infra*) for a ranking of the relative affinity of carbon black to various elastomers. The data was obtained for 50/50 binary blends, and the carbon black was added to about 25 binary elastomer combinations. The carbon black retention in each phase was estimated from TEM micrographs of the blend. The ranking of carbon black affinity for different elastomers was in the order SBR > BR, CR, NBR > NR > EPDM > CIIR, IIR. Cotton and Murphy [38d], in a complementary experiment, have determined the carbon black distribution for seven different carbon blacks in preblended SBR–BR and SBR–NR blends. The data is shown in Table V. The carbon blacks differ in the surface structure and size: they ranged in surface area (CTAB) from 43 to 136 m^2/g. For all cases of SBR–NR blends, the carbon black was preferentially located in the SBR phase.

E. Analysis of Interphase Transfer

1. Microscopy

Electron microscopy is a common technique for determining the filler distribution in a heterogeneous elastomer blends. Dias *et al*. [39] have used time of flight secondary mass spectrometry (TOF-SIMS) to simultaneously determine the morphology as well as curative diffusion in BIMS–diene elastomer blends.

2. Differential Swelling

The method of differential swelling of thin section of blends of EPDM and IIR was first utilized by Callan *et al*. [40a]. In blends with EPDM, the IIR phase absorbs more solvent; therefore, the IIR domains are thinner and

appear lighter in the TEM. Hess *et al*. [40b] applied the same differential swelling method to the analysis of carbon black distribution at low filler loadings. Wang *et al*. [40c] have improved the technique by swelling separately with two solvents—one for each of the phases.

3. Staining

Staining with volatile reactive metal oxides, OsO_4 and RuO_4, is the preferred method for achieving inter-phase contrast for TEM analyses. It is applicable to blends of elastomers with different degrees of unsaturation such as NR–EPDM blends.

4. Differential Pyrolysis

This method is applicable to blends containing polymers with significantly different thermal degradation temperatures. It has been used for analysis of carbon black distribution in NR–SBR and NR–BR blends [41a, b].

5. GC Analysis of Bound Rubber

Bound rubber is the elastomer insoluble in solvents due to chemisorption onto the carbon black during mixing. It is extracted by swelling the unvulcanized polymer in a solvent for an extended period. Any soluble lower molecular weight polymer that is not bound to the carbon black is removed. This method was first used by Callan *et al*. [38a] for a number of elastomer blends.

6. Mechanical Damping

The value of *tan d* (at Tg) is lower for a filled elastomer than the pure elastomer [42a, b]. This is due to the increase in dynamic elastic modulus of the filled compound for the higher temperature side of the Tg peak. The effect is governed by filler concentration and loading. Maiti *et al*. [42c] have used this lowering of *tan d* at Tg to estimate the distribution of filler in an immiscible elastomer blend.

F. Compatibilization

Compatibilization of highly incompatible elastomers has only been used to a limited extent [43a–d]. Compatibilization is the addition of a minor amount of an interfacial agent and serves only to stabilize the extended surface of the dispersed phase in a finely dispersed morphology. The amount and composition of the interfacial agents are not designed to affect the bulk properties of either of the phases. Properties of elastomer blends are determined by intensive properties such as cohesive energy, crosslink densities, and chemisorption of fillers of the components that are unaffected by the addition of compatibilizers. However, in binary blends of elastomers with large differences in solubility parameters, as in polyolefin elastomers with polar elastomers, properties are dominated by the large domain size and the lack of

interfacial adhesion. These elastomer blends are significantly improved by the addition of a compatibilizer.

Setua and White [44a, b] used CM (chlorinated polyethylene) as a compatibilizer to improve the homogeneity of binary and ternary blends of CR, NBR, and EPR. NBR–EPM and CR–EPDM blends homogenize more rapidly when small amounts of CM are added. The presence of the compatibilizer leads to reductions in both the time needed for mixing, observed by flow visualization, and the domain size of the dispersed phase, observed by SEM. Arjunan *et al*. [44c] have used an ethylene acrylic acid copolymer and an EPR-g-acrylate as a compatibilizer for blends of EPDM–CR. The addition of the compatibilizer leads to the reduction in the phase size of the dispersed EPDM phase as well as increase in the tensile tear strength of the blend.

Intensive properties of the blend components that dominate vulcanizate properties of the elastomer are improved if the compatibilizer is the predominant fraction of the elastomer blend. Davison *et al.* [45] describe the formation of compatibilized blends of poly (alkyl acrylates) and preformed EPDM-g-acrylate that on vulcanization are resistant to solvents. The acrylate-grafted EPDM are copolymers of methyl-, ethyl-, or n-butyl acrylate. These vulcanized blends have excellent tensile strength and modulus, similar to a single elastomer. Cotton and Murphy [38d] were able to generate the graft polymer *in situ* during compounding. A primary amine copolymerized EPDM blended with NBR to form a graft polymer by the amidine reaction of the amine with the nitrile. The grafting reaction was catalyzed by the presence of the Lewis acidic phophite plasticizer for the NBR phase. The compatibilizer promotes the formation of very small dispersed phase domains. Figures 8(a) and 8(b) are micrographs of the dispersion of the EPDM and amine functionalized EPDM, respectively, in the NBR matrix. In this case, the previous micrographs (see Fig. 7) also show the retention of carbon black filler in the bulk of the EPDM phase. Vulcanization of the amine functional EPDM and NBR blends with nonpolar peroxides that are expected to distribute equally in both phases lead to blends with excellent solvent and temperature resistance.

G. Properties of Immiscible Blends

While true miscibility may not be required for elastomer properties, adhesion between the immiscible phases is required. Immiscible polymer blends that fulfill this criteria provide a significant opportunity to change the rheological, tensile, and wear properties of elastomer blends compared to miscible blends.

1. Processing

Blends are often used to improve the processability of rubbers. This improvement may consist of either lowering the viscosity or producing a material less prone to melt fracture during flow. Secondary elastic effects such as

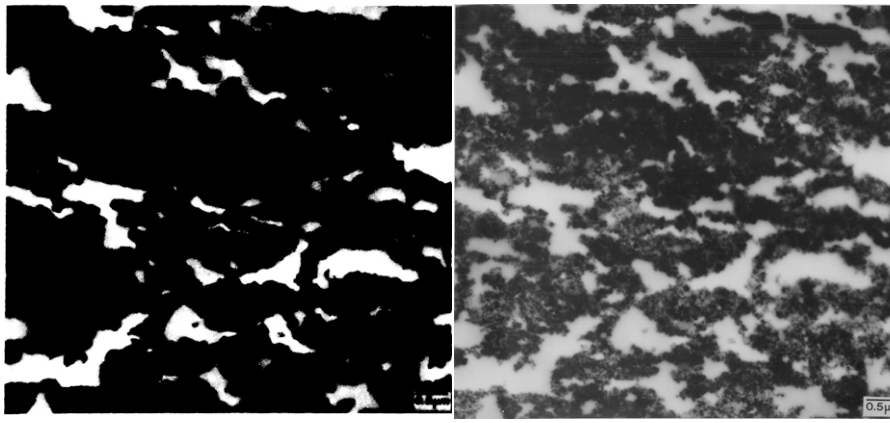

(a) (b)

FIGURE 8 Micrographs of a dispersion of 70:30 blend of NBR and EP elastomer. (a) The EP elastomer is a copolymer of 42 mole % ethylene. (b) The EP elastomer has 43 mole % ethylene and 0.9 mole % primary amine functionality.

die swell can also be affected by blending. Avgeropoulos *et al.* [46a] showed that the low viscosity phase in a binary blend tends to become continuous. The effect is accelerated under shear as the morphology of the blend responds to the applied stresses. In the vicinity of a wall, the shear rates tend to be highest, and the lower viscosity component will accumulate at the surface [46b]. Incorporation of only a few percent of EPDM to a fluoroelastomer or of PDMS into an SBR [46c] was found to reduce steady state viscosities. This is due to the lower viscosity component residing at the interface.

Much of the knowledge in this area is either derived from practical experience or anecdotal. Theoretical predictions of the viscosity of elastomer blends [46f, g] are of limited use since (1) the inhomogeneous phase morphology of an elastomer blend changes easily in response to applied stress, and (2) the nonuniform distribution of fillers and plasticizers in the phases responds to flow. These structural changes in elastomer blends under shear lead to anomalous rheological properties quite different from the expected average of pure components.

2. Modulus

In a heterogeneous blend, the details of the morphology do not generally exert much influence on the stress–strain tensile response. Contrary to expectation that the continuous phase would have more influence, the stress–strain response of unfilled EPDM–BR blends was found to be unaffected by a change in the BR domains from continuous to disperse [47a].

Carbon black distribution has a profound effect on modulus. Meinecke and Taftaf [47b] have shown that an increase in the nonuniformity of this filler

distribution results in a lower blend modulus. The transfer of a portion of the carbon black from one phase lowers its modulus more than the increase in modulus of the phase with the higher carbon black concentration. This effect is related to the nonlinear dependence of rubber modulus on carbon-black loading [47c, d].

3. Tack and Adhesion

Adhesion is a surface phenomenon due to entangling of chains at the surface. Adhesion of different elastomers before (tack) and after vulcanization (co-cure) can often be obtained only through the blending of the dissimilar elastomers with a single component. However, the composition of the surface and thus the adhesion characteristics can be altered without using a high concentration of a particular elastomer in the blend.

Blends with components that differ in viscosity tend to have the lower viscosity rubber concentrated at the surface during processing. The most common procedure for increasing the tack and co-cure of elastomer blends is to have a single elastomer as the predominant phase in each of the blends. Morrisey [48] showed that tack of dissimilar elastomers blended with NR improves monotonically with the amount of NR in the blend. Increasing the proportion of a single elastomer in both blends enables the ability of the plied surfaces to fuse together.

4. Hysteresis

A principal use of elastomer blends is in sidewalls of automotive tires. The reduction of hysteresis losses ("rolling resistance") is a principal design target. Lower hysteresis in a single elastomer requires reduced carbon-black loading or increased crosslink density. These changes adversely affect other aspects of performance. Blending of elastomers provides a lower hysteresis with few of these adverse effects. The hysteresis of a filled elastomer containing zones of different carbon black concentrations is lower than a uniformly filled elastomer. Blends of dissimilar elastomers, with differing ability to retain carbon black, provide an easy experimental process to obtain this nonuniform carbon-black distribution.

5. Failure

Improved failure properties can result from the blending of elastomers, including performance that exceeds either pure component. An important aspect of the structure of a rubber blend is the nature of the interphase bonding. The mechanical integrity of an interphase crosslinked morphology will usually lead to superior performance. In blends of SBR and chlorobutyl rubber, for example, an increase in fatigue life was obtained by the introduction of interphase crosslinking. Similarly, providing for interfacial coupling improves the tensile strength of EPDM/silicone-rubber blends [49a].

There is improved abrasion resistance associated with a preferential carbon black–BR phase distribution in blends of NR–BR and SBR–BR. The first abrasion studies on the effects of carbon black phase distribution in NR–BR blends were reported by Krakowski and Tinker [50a]. Tread wear resistance was found to increase progressively with increasing carbon black in the BR phase, which was determined from TEM analyses. Tse *et al.* [50b] have shown in blends of dispersed BIMS in BR matrix failure due to fatigue can be retarded if the mean distance between the crosslinks of the BIMS is less than 60 nm.

The incidence of cracking due to ozone attack has been investigated for NR–EPDM blends [49b–f]. Andrews [49g] showed that small zones of EPR in an EPR–NR blend provide a barrier that inhibits ozone crack growth. Ambelang *et al.* [49h] found the importance of small EPM domain size in EPDM–SBR blends. Matthew [49b] has shown that carbon black improves the ozone resistance of NR–EPDM. An improvement was obtained in the blends with a balanced carbon-black phase obtained by phase inversion. This is because (1) there is better reinforcement of the EPDM phase and (2) carbon black in the EPDM expands the volume of that phase. In BIMS–BR blends, the ozone failure can be retarded by reducing the size of the BIMS dispersion [50b].

The transport properties of polymer blends are of interest both for the practical application of blends and for providing insight into the morphology of the blend. Measurement of the effect of blend composition on permeability in various rubbers has been described [49i]. The permeability of elastomer blends depends on the concentration of the continuous phase and the morphology of the dispersed phase. Extended disperse phase structures, particularly lying in a stacked or lamellar configuration, can lead to a reduced permeability because of the more tortuous path that must be taken by penetrants [49j].

H. Applications

1. Unsaturated Elastomer Blends

The most common blends of unsaturated elastomers are those used in various sections of automotive tires. Table VI lists the important component of tires and the typical blends used for them. Much of the literature of elastomer blends reflects this important application. It is outside the scope of this chapter to discuss each of the applications. We have outlined most of the important principles used in the generation of the blends.

2. Saturated and Unsaturated Elastomer Blends

The use of blends of polyolefin elastomers, such as IIR and EPDM, as substantial components in blends of unsaturated elastomers is a rapidly developing area. Mouri *et al.* [51] have compared the properties of EPDM–NR and

TABLE VI Elastomer Blends in Automotive Tires [3]

Component	Passenger tires	Commercial vehicle tires
Tread	SBR–BR	NR–BR or SBR–BR
Belt	NR	NR
Carcass	NR–SBR–BR	NR–BR
Sidewall	NR–BR or NR–SBR	NR–BR
Liner	NR–SBR–IIR	NR–IIR

BIMS–NR blends as sidewall components. In many of the applications, the saturated elastomer is considered a polymeric antioxidant for the diene rubber. It is believed that the higher molecular weight polyolefins are better in these applications due to limited interdiffusion and a more stable morphology. Some of the benefits in tensile properties and abrasion resistance of the blends may be due to the interdiffusion of high molecular chains of dissimilar elastomers across the phase interface. Significant advances have been made in modifying the structure of polyolefin elastomers to increase the compatibility to unsaturated elastomers. Tse *et al.* [50b] have shown that uncompatibilized blends of saturated elastomers and unsaturated elastomers are possible if the former contains substantial amounts (>12%) styrene residues. This is expected to be an important area of development in the future with the advent of new synthesis procedures for polyolefins.

IV. CONCLUSION

The formulation and use of elastomer blends is technologically demanding. Miscible blends are widely used but usually not recognized since analytical separation of the vulcanized elastomer is experimentally impossible. Immiscible blends require excellent phase dispersion and interfacial adhesion typical of all polymer blends. In addition, they require control of filler distribution and crosslink density in each component. This is due to the need for mechanical integrity in vulcanized elastomers. The current design criteria of North American automotive tires require treads to last for 80,000 miles with less than 0.4 inch of wear. Vulcanized roofing membranes require 35 years of outdoor exposure with minimal change in elongation and tensile strength. The technical complexity of analysis and use of elastomer blends has lead to secrecy for many of the formulations and uses. In spite of the difficulties of analysis and gaps in understanding, the use of blends containing elastomers continues to be an active and increasing area of research. Part of the impetus is the availability of directed synthesis of many of the older elastomers. These

new synthetic tools include new catalysts ("single sited") and process designs for the manufacture of ethylene-based polyolefin elastomers, group transfer polymerization for acrylates, and anionic polymerization for diene elastomers. The availability of elastomers with a narrow compositional and molecular weight distribution in these syntheses makes the utility of blending more apparent and useful.

V. APPENDIX 1: ACRONYMS FOR COMMON ELASTOMERS

ABR	acrylate–butadiene rubber
ACM	copolymer of ethylacrylate and a comonomer (acrylic rubber)
ANM	ethylacrylate–acrylonitrile copolymer (acrylate rubber)
BIMS	brominated isobutylene paramethyl styrene rubber
BR	butadiene rubber (polybutadiene)
BIIR	bromobutyl rubber
CIIR	chlorobutyl rubber
CFM	polychlorotritluoroethylene (fluoro rubber)
CM	chloropolyethylene (previous designation CPE)
CO	epichlorohydrin homopolymer rubber (polychloromethyloxiran)
CR	chloroprene rubber (polychloroprene)
CSM	chlorosulfonylpolyethylene
EAM	ethylene–ethyl acrylate copolymer (e.g., Vamac)
ECO	copolymer of ethylene oxide (oxiran) and chloromethyloxiran
ENM or H-NBR	proposed code for hydrogenated NBR
ENR	epoxidized NR
EPDM	ethylene–propylene–diene terpolymer
EPM	ethylene–propylene copolymer
EVM	ethylene–vinylacetate copolymer (previous code: EVA or EVAC)
FMQ	methyl silicone rubber with fluoro groups (previous designation FSI)
FPM / FPM	rubber having fluoro and fluoroalkyl or fluoroalkoxy substituent group
IIR	isobutylene–isoprene rubber (butyl rubber)
IR	isoprene rubber (synthetic)
MQ (PVMQ)	methyl silicone rubber (with vinyl and phenyl end groups)
NBR	acrylonitrile–butadiene rubber (nitrile rubber)
NR	isoprene rubber (natural rubber)
PUR	generic code for urethane rubbers
Q	generic code of silicone rubbers
SBR	styrene–butadiene rubber
TM	polysulfide rubbers
TOR	trans-polyoctenamer
VMQ	methyl silicone rubber with vinyl groups

REFERENCES

1. R. German, R. Hank, and G. Vaughan, *Rubber Chem. Technol.* **40**, 569 (1967).
2. The sampling of polymer blends in "Polymeric Compatibilizers" by S. Datta and D. J. Lohse, Hanser-Gardner, 1996, that >93% of polymer blends are combinations of thermoplastic and elastomers. However, automotive tires (5000 kt/yr in 1995), a blend of elastomers, are the largest application for any immiscible polymer blend.

3. W. M. Hess, C. R. Herd, and P. C. Vergari, *Rubber Chem Technol.* **66**, 329 (1993).
4. C. M. Roland, *Rubber Chem. Technol*. **62**, 456 (1989).
5. P. J. Corish, in "Science and Technology of Rubber," F. R. Eirich (Ed.), Academic Press, New York, 1978, Chap. 12.
6. E. T. McDonel, K. C. Baranwal, and J. C. Andries, in "Polymer Blends," D. R. Paul and S. Newman (Eds.), Academic Press, New York, Vol. 11, 1978, Chap. 19.
7. (a) C. M. Hansen, "The Three Dimensional Solubility Parameter and Solvent Diffusion Coefficients," Danish Technical Press, Copenhagen, 1967. (b) C. M. Hansen and A. Beerbower, Solubility Parameters, in "Encyclopedia of Chemical Technology, Supplement Volume," 2nd ed., Wiley, New York, 1971.
8. (a) J. P. Runt and L. M. Martynowicz, *Adv. Chem. Ser.* **211**, 111 (1985). (b) H. D. Keith and F. J. Padden, J. *Appl. Phys.* **36**, 1286 (1964).
9. A. Ghijsels, *Rubber Chem. Technol.* **60**, 278 (1977).
10. (a) T. Nishi and T. T. Wang, *Macromolecules* **8**, 909 (1975). (b) B. Rim and J. P. Runt, *Macromolecules* **17**, 1520 (1984).
11. (a) H. N. Cheng, in "Polymer Analysis and Characterization IV," H. G. Barth and J. Janca (Eds.), John Wiley and Sons, New York, 1992, p. 21. (b) C. M. Roland, *Rubber Chem. Technol.* **62**, 456 (1989). (c) B. Albert, R. Jerome, P. Teyssie, G. Smyth, N. G. Boyle, and V. J. McBrierty, *Macromolecules* **18**, 388 (1985). (d) C. M. Roland and C. A. Trask, *Polym. Mater., Sci. Eng.* **60**, 832 (1989).
12. D. L. Vander Hart, W. F. Manders, R. S. Stein, and W. Herman, *Macromolecules* **20**, 1726 (1987).
13. (a) J. Schaefer, M. D. Sefcik, E. O. Stejskal, and R. A. McKay, *Macromolecules* **14**, 188 (1981). (b) T. R. Steger, J. Schaefer, E. O. Stejskal, R. A. McKay, and M. D. Sefcik, *Annals NY Acad. Sci.* **371**, (1981).
14. (a) M. C. Morris, *Rubber Chem. Technol*. **40**, 341 (1967). (b) A. K. Sircar and T. G. Lamond, *Rubber Chem. Technol.* **46**, 178 (1973).
15. (a) C. M. Roland and G. G. A. Bohm, *Macromolecules* **18**, 1310 (1985). (b) C. M. Roland, *Rubber Chem. Technol.* **61**, 866 (1988). (c) C. M. Roland, *Macromolecules* **20**, 2557 (1987). (d) J. Klein, *Prilos. Mag.* **43**, 771 (1981). (e) J. Klein, D. Fletcher, and L. J. Fetters, *Nature (London)* **304**, 526 (1983). (f) Y. Kumugai, K. Watanabe, T. Miyasaki, and J. Hata, *J. Chem. Eng. Jpn.* **12**, 1 (1979). (g) T. Gilmore, R. Falabella, and R. L. Lawrence, *Macromolecules* **13**, 880 (1980). (h) T. Hashimoto, Y. Tsukahara, and H. Kawai, *Macromolecules* **14**, 708 (1981). (i) J. E. Anderson and J.-H. Jou, *Macromolecules* **20**, 1544 (1987). (j) G. C. Summerfield and R. Ullman, *Macromolecules* **20**, 401 (1987).
16. L. W. Kleiner, F. E. Karasz, and W. J. MacKnight, *Polym. Eng. Sci.* **19**, 519 (1979).
17. (a) S. Datta and E. N. Kresge, U.S. Patent 4,722,971 (1988). (b) S. Datta, L. Kaufman, and P. Ravishankar, U.S. Patent 5,571,868 (1996).
18. F. Morrar, L. L. Ban, W. G. Funk, E. N. Kresge, H.C. Wang, S. Datta, and R. C. Keller, U.S. Patent 5,428,099 (1996).
19. (a) Z. M. Zhang and J. E. Mark, *Polym. Sci. Polym. Phys. Ed.* **20**, 473 (1982). (b) J. E. Mark and A. L. Andrady, *Rubber Chem. Tech.* **54**, 366 (1981).
20. (a) D. I. Livingston and R. L. Rongone, *Proc. 5th, Int. Rubboer Conf.*, Brighton, England, Paper No. 22 (1967). (b) G. M. Bartenev and G. S. Kongarov, *Rubber Chem. Technol.* **36**, 668 (1983). (c) P. A. Marsh, A. Voet, L. D. Price, T. J. Mullens, and L. Kongarov, *Rubber Chem. Technol.* **41**, 344 (1968). (d) R. Couchman, *Macromolecules* **20**, 1712 (1987). (e) T. K. Kwei, E. M. Pearce, J. R. Pennacchia, and M. Charton, *Macromolecules* **20**, 1174 (1987). (f) M.-J. Brekner, H. A. Schneider, and H.-J. Cantow, *Polymer* **29**, 78 (1988). (g) M. Aubin and R. E. Prud'homme, *Macromolecules* **21**, 2945 (1988).
21. (a) C. M. Roland, *J. Polym. Sci., Polym. Phys. Ed.* **26**, 839 (1988). (b) C. A. Trask and C. M. Roland, *Polym. Comm.* **29**, 332 (1988). (c) C. M. Roland, *Macromolecules* **20**, 2557 (1987). (d) C. M. Roland and C. A. Trask, *Rubber Chem. Technol.* **62**, 456 (1989). (e) C. A. Trask and C. M. Roland, *Macromolecules* **22**, 256 (1988).

22. (a) I. R. Gelling, *NR Technol.* **18**, 21 (1987). (b) A. G. Margaritis, J. K. Kallitsis, and N. K. Kalfoglou, *Polymer* **28**, 2122 (1987).
23. (a) M. M. Coleman, G. J. Pehlert, and P. C. Painter, *Macromolecules* **29**, 6820 (1996). (b) G. J. Pehlert, P. C. Painter, B. Veytsman, and M. M. Coleman, *Macromolecules* **30**, 3671 (1997). (c) M. M. Coleman, G. J. Pehlert, X. Yang, J. Stallman, and P. C. Painter, *Polymer* **37**, 4753 (1996). (d) G. J. Pehlert, X. Yang, P. C. Painter, and M. M. Coleman, *Polymer* **37**, 4763 (1996).
24. P. J. Corish and B. D. W. Powell, *Rubber Chem. Technol.* **47**, 481 (1974).
25. (a) N. Tokita, *Rubber Chem. Technol.* **60**, 292 (1977). (b) G. N. Avgeropoulos, R. C. Weissert, P. H. Biddison, and G. G. A. Bohm, *Rubber Chem. Technol.* **49**, 93 (1976).
26. (a) M. Takenaka, T. Izumitani, and T. Hashimoto, *Macromolecules* **20**, 2257 (1987). (b) H. Yang, M. Shibayama, and R. S. Stein, *Macromolecules* **19**, 1667 (1986). (c) J. Kumaki and T. Hashimoto, *Macromolecules* **19**, 763 (1986).
27. (a) J. E. Kruse, *Rubber Chem. Technol.* **46**, 653 (1973). (b) J. E. Callan, W. M. Hess, and C. E. Scott, *Rubber Chem. Technol.* **44**, 814 (1971). (c) C. E. Scott, J. E. Callan, and W. M. Hess, *J. Rubber Res. Inst. Malays.* **22**, 242 (1969). (d) J. E. Callan, B. Topcik, and F. P. Ford, *Rubber World* **161**, 60 (1965).
28. (a) F. H. Roninger, Jr., *Ind. Eng. Chem., Anal. Ed.* **6**, 251 (1933). (b) R. W. Smith and J. C. Andries, *Rubber Chem Technol.* **47**, 64 (1986).
29. (a) E. W. Stroup, A. Pungor, V. Hilady, and J. D. Andrade, *Polym. Prepr. ACS., Div. Polym. Chem.* **34**, 86 (1993). (b) W. Stocker, B. Bickmarm, S. N. Magonov, and H. J. Cantow, *Ultramicroscopy* **42**, 1141 (1992). (c) Y. H. Tsao, S. X. Yang, and D. F. Evans, *Langmuir* **8**, 1188 (1992). (d) E. Hamada and R. Kaneko, *Ultramicroscopy* **42**, 184 (1992). (e) J. E. Sax and J. M. Ottino, *Polymer* **26**, 1073 (1985). (f) T. Nishi, T. Hayashi, and H. Tanaka, *Makromol. Chem., Macromol. Symp.* **16**, 91 (1988). (g) J. Kruse, *Rubber Chem. Technol.* **46**, 653 (1973). (h) D. Vesely and D. S. Finch, *Makromol. Chem., Macromol. Symp.* **16**, 329 (1988).
30. (a) R. Buchdahl and L. E. Nielsen, *J. Polym. Sci.* **15**, 1 (1955). (b) M. C. Morris, *Rubber Chem. Technol.* **40**, 341 (1967). (c) H. K. de Decker and D. J. Sabatine, *Rubber Age* **99**, 73 (1967). (d) L. Bohn, *Rubber Chem. Technol.* **41**, 495 (1968). (e) W. Scheele, *Kautsch. Gummi Kunstst.* **24**, 387 (1971). (f) A. R. Ramos and R. E. Cohen, *Polym. Eng. Sci.* **17**, 639 (1977). (g) K. A. Mazich, M. A. Samus, P. C. Kilgoar, Jr., and H. K. Plummer, Jr., *Rubber Chem. Technol.* **59**, 623 (1986).
31. (a) R. J. Butera, J. B. Lando, and B. Simic-Glavaski, *Macromolecules* **20**, 1724 (1987). (b) M. R. Krejsa and J. L. Koenig, *Rubber Chem. Technol.* **64**, 635 (1991). (c) M. R. Krejsa and J. L. Koenig, *Rubber Chem. Technol.* **65**, 956 (1992). (d) S. R. Smith and J. L. Koenig, *Macromolecules* **24**, 3496 (1991). (e) S. N. Sarkar and R. A. Komoroski, *Macromolecules* **25**, 1420 (1992).
32. (a) C. M. Roland and G. G. A. Bohm, *J. Polym. Sci., Polym. Phys. Ed.* **22**, 79 (1984). (b) C. A. Trask and C. M. Roland, *Macromolecules* **22**, 256 (1989). (c) C. M. Roland and G. G. A. Bohm, *J. Polym. Sci., Polym. Phys. Ed.* **22**, 79 (1984).
33. (a) J. L. Leblanc, *Plast. RubberProcess. Appl.* **2**, 361 (1982). (b) G. J. Van Amerongen, *Rubber Chem. Technol.* **37**, 1065 (1964). (c) V. A. Shershnev, *Rubber Chem. Technol.* **66**, 537 (1982). (d) M. G. Huson, W. J. McGill, and R. D. Wiggett, *Plast. Rubber Process. Appl.* **6**, 319 (1985). (e) R. F. Bauer and A. H. Crossland, *Rubber Chem. Technol.* **61**, 585 (1988). (f) A. K. Bhowmick and S. K. De, *Rubber Chem. Technol.* **63**, 960 (1980). (g) R. L. Zapp, *Rubber Chem. Technol.* **46**, 251 (1973).
34. (a) G. J. Amerongen, *Rubber Chem. Technol.* **37**, 1065 (1964). (b) J. R. Gardiner, *Rubber Chem. Technol.* **41**, 1312 (1968). (c) J. R. Gardiner, *Rubber Chem. Technol.* **42**, 1058 (1969). (d) J. R. Gardiner, *Rubber Chem. Technol.* **43**, 370 (1970).
35. (a) V. A. Shershnev, *Rubber Chem. Technol.* **66**, 537 (1982). (b) J. Rehner, Jr. and P. E. Wei, *Rubber Chem. Technol.* **42**, 985 (1969). (c) A. K. Bhowmick and S. K. De, *Rubber Chem. Technol.* **63**, 960 (1980). (d) K. C. Baranwal and P. N. Son, *Rubber Chem. Technol.* **47**, 88 (1974). (e) K. Hashimoto, M. Miura, S. Takagi, and H. Okamoto, *Int. Polym. Sci. Technol.* **3**, 84 (1976). (f) A. Y. Coran, *Rubber Chem. Technol.* **61**, 281 (1988). (g) R. W. Amidon and R. A. Gencarelli, U.S. Patent 3,674,824 (1972). (h) R. P. Mastromatteo, J. M. Mitchell, and T. J. Brett, *Rubber*

Chem. Technol. **44**, 1065 (1971). (i) Sumitomo Chemical Company, British Patent 1,325,064 (1973). (j) M. E. Woods and T. R. Mass, U.S. Patent 3,830,881 (1974).
36. M. E. Woods and J. A. Davidson, *Rubber Chem. Technol.* **49**, 112 (1976).
37. (a) M. G. Huson, W. J. McGill, and P. J. Swart, *J. Polym. Sci., Polym. Lett. Ed.* **22**, 143 (1984). (b) D. Honiball and W. J. McGill, *J. Polym. Sci., Polym. Phys.* **26**, 1529 (1988). (c) L. D. Loan, *Rubber Chem. Technol.* **40**, 149 (1967).
38. (a) J. E. Callan, W. M. Hess, and C. E. Scott, *Rubber Chem. Technol.* **44**, 814 (1971). (b) J. E. Callan, W. M. Hess, and C. E. Scott, *Rev. Gen. Caoutch. Plast.* **48**, 155 (1971). (c) A. K. Sircar and T. J. Lammond, *Rubber Chem. Technol.* **46**, 178 (1973). (d) G. Cotton and L. J. Murphy, *Rubber Chem. Technol.* **61**, 609 (1988).
39. A. J. Dias and A. Galuska, *Rubber Chem. Technol.* **69**, 615 (1996).
40. (a) J. E. Callan, B. Topcik, and E. P. Ford, *Rubber World* **151**, 60 (1951). (b) W. M. Hess, P. A. Marsh, and F. J. Eckert, presented at a meeting of the Rubber Division, American Chemical Society, Miami Beach, FL, 1965. (c) Y. F. Wang and H. C. Wang, *Rubber Chem. Technol*. **70**, 63 (1997).
41. (a) W. M. Hess, R. A. Swor, and P. C. Vegvari, *Kautsch. Gummi Kunstst.* **38**, 1114 (1985). (b) W. M. Hess and V. E. Chirico, *Rubber Chem. Technol.* **50**, 301 (1977).
42. (a) A. Medalia, *Rubber Chem. Technol.* **51**, 437 (1978). (b) W. P. Fletcher and A. N. Gent, *Br. J. Appl. Phys.* **8**, 1984 (1957). (c) S. Maiti, S. K. De, and A. K. Bhowmick, *Rubber Chem. Technol.* **65**, 293 (1992).
43. (a) M. E. Woods and T. R. Mass, *Adv. Chem. Ser.* **l42**, 386 (1975). (b) E. T. McDonel, K. C. Baranwal, and J. C. Andries, in "Polymer Blends," D. R. Paul and S. Newman (Eds.), Academic Press, New York, Vol. 2, 1978, p. 263. (c) L. Leibler, *Makromol Chem. Macromol Symp*. **16**, 1, (1982). (d) J. Noolandi and K. M. Hong, *Macromolecules* **16**, 482 (1982).
44. (a) D. K. Setua and J. L. White, *Kautsch. Gummi Kunstst.* **44**, 821 (1991). (b) D. K. Setua and J. L. White, *Poly. Eng. & Sci.* **31**, 1742 (1991). (c) P. A. Arjunan, R. B. Kusznir, and A. Dekmezian, *Rubber World* **21** (1997).
45. J. A. Davison, W. Nudenberg, and Y. Rim, U.S. Patent 4,316,971 (1982).
46. (a) G. N. Avgeropoulos, R. C. Weissert, P. H. Biddison, and G. G. A. Bohm, *Rubber Chem. Technol.* **49**, 93 (1976). (b) C. M. Roland and M. Nguyen, *J. Appl. Polym. Sci.* **36**, 141 (1988). (c) A. C. Pipkin and R. I. Tanner, *Ann. Rev. Fluid Mech.* **9**, 13 (1977). (d) W. M. Hess, P. C. Vegvari, and R. A. Swor, *Rubber Chem. Technol.* **68**, 350 (1985). (e) W. M. Hess, R. A. Swor, and P. C. Vegvari, *Kautsch. Gummi Kunstst.* **38**, 1114 (1985). (f) R. F. Heitmiller, R. Z. Maar, and H. H. Zabusky, *J. Appl. Polym. Sci.* **8**, 873 (1964). (g) S. Uemura and M. Takayanagi, *J. Appl. Polym. Sci.* **10**, 113 (1966).
47. (a) H. Yang, M. Shibayama, and R. S. Stein, *Macromolecules* **19**, 1667 (1986). (b) E. A. Meinecke and M. I. Taftaf, *Rubber Chem. Technol.* **37**, 1190 (1988). (c) A. I. Medalia, *Rubber Chem. Technol.* **61**, 437 (1978). (d) E. A. Meinecke and M. I. Taftaf, *Rubber Chem. Technol.* **61**, 534 (1988).
48. R. T. Morrisey, *Rubber Chem. Technol.* **44**, 1029 (1971).
49. (a) J. M. Mitchell, *Rubber Plast. News*, June 3, 1985, p. 18. (b) N. M. Matthew, *J. Polym. Sci. Polym. Lett. Ed.* **22**, 135 (1984). (c) W. von Hellens, Rubber Division, American Chemical Society, Detroit, MI, Fall 1989. (d) F. C. Cesare, *Rubber World* **201**, 14 (1989). (e) W. Hong, *Rubber Plast. News* **19**, 14 (1989). (f) W. von Hellens, D. C. Edwards, and Z. J. Lobos, *Rubber Plast. News* **20**, 61 (1990). (g) E. H. Andrews, *J. Polym. Sci*. **10**, 47 (1966). (h) B. Ambelang, F. H. Wilson, Jr., L. E. Porter, and D. L. Turk, *Rubber Chem. Technol.* **42**, 1186 (1969). (i) J. Barrier, *Rubber Chem. Technol.* **28**, 814 (1956). (j) J. Kinning, E. L. Thomas, and J. M. Ottino, *Macromolecules* **20**, 1129 (1987).
50. (a) F. J. Krakowski and A. J. Tinker, *Elastomerics* **122**, 34; **122**, 24 (1990). (b) M. F. Tse, K. O. McElrath, H.-C. Wang, Y. F. Wang, and A. L. Tisler, Paper 24, 153rd Rubber Division Meeting, ACS, Indianapolis, IN, May 5–8, 1998.
51. H. Mouri and Y. Tonosaki, Paper 65, 152rd Rubber Division Meeting, ACS, Cleveland, OH, October 21–24, 1997.

13 Thermoplastic Elastomers

BRIAN P. GRADY
School of Chemical Engineering and Materials Science
The University of Oklahoma
Norman, Oklahoma

STUART L. COOPER
Department of Chemical and Biomolecular Engineering
The Ohio State University
Columbus, Ohio

I. INTRODUCTION

Thermoplastic elastomers (TPEs) are an extremely fast growing segment of polymer manufacturing. A rate of 5% growth per year is expected until 2007, at which time the total U.S. demand for these materials will reach 1.5 billion lb at a total annual sales of approximately 3 billion dollars per year [1]. The majority of this growth comes in the form of replacements for other types of materials, and the growth of so-called "soft-touch" surfaces. In the approximately 10 years since the second edition of this book appeared, there has been an important technological advancement in this area: the vastly increased production of thermoplastic polyolefin elastomers as a result of the worldwide adoption of metallocene catalysts.

The primary advantage of TPE over conventional rubber is the ease (and therefore low cost) of processing, the wide variety of properties available, and the possibility of recycling and reuse. Besides the obvious environmental benefits of a recyclable raw material, TPE scrap material can be reprocessed. The disadvantage of these materials relative to thermosets is the relatively high cost of raw materials, the general inability to load TPEs with low cost fillers

Science and Technology of Rubber, Third Edition

such as carbon black, and poor chemical and temperature resistance. This last property prevents TPEs from being used in automobile tires.

In order to qualify as a thermoplastic elastomer, a material must have three essential characteristics:

1. The ability to be stretched to moderate elongations and, upon the removal of stress, return to something close to its original shape.
2. Processable as a melt at elevated temperature.
3. Absence of significant creep.

In nearly all cases, thermoplastic elastomers will be a copolymer, i.e., there will be at least two monomers in the polymer chain. A thermoplastic elastomer will generally have the modulus versus temperature curve shown in part (c) of Fig. 1. The plateau region must include the service temperature of the material. Typically through changes in comonomer composition or identity, the plateau can be shifted upward or downward, giving the manufacturer a great deal of flexibility.

Most TPEs have certain similar structural characteristics. The comonomers typically have long runs, making the material a block copolymer. The comonomers are almost always dissimilar, leading to microphase separation on a nanometer length scale, which means these materials are properly termed nanomaterials (these materials were present long before this term became

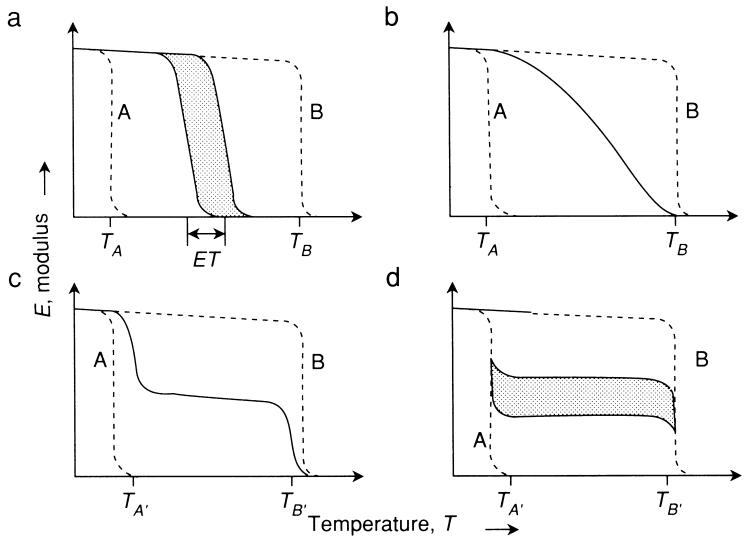

FIGURE 1 Diagram of the dependence of modulus on temperature for copolymers. In all the sketches, the dashed lines refer to the behavior for the pure materials. The hatched area shows that the range of the behavior can vary depending on the relative amounts of A and B. (a) Random A–B copolymer. (b) Block copolymer of A and B with extremely short blocks. (c) Segmented block copolymer with imperfect phase separation. (d) Segmented block copolymer with perfect phase separation. (From Bonart [220].)

fashionable!). The driving force for phase separation is always enthalpic and usually one to two orders of magnitude weaker than primary valence bonds. Crystallinity, hydrogen bonding, ionic, and van der Waals driving forces all have been shown to cause microphase separation in these systems.

The two phases in these systems have different properties. One phase, the soft phase, contains a component that is above its glass transition temperature (T_g) and melting temperature (T_m) so that chains have a high amount of mobility. The other phase, the hard phase, contains chains that are rigidly locked in place, because the service temperature is below either T_m or T_g. The relative amount of the two phases controls the physical properties of the TPE by determining which phase is isolated or continuous. The ability to easily vary these parameters through stoichiometry allows TPEs to be used in the wide variety of applications alluded to earlier.

A large number of structures fall into the category of thermoplastic elastomers. The structures of some common thermoplastic elastomers are shown in Fig. 2. Shell Development Company developed the first commercially available thermoplastic elastomer in the early 1960s, which became the KRATON [2] family of materials. These materials are either poly (styrene-b-butadiene-b-styrene) (SBS), poly (styrene-b-isoprene-b-styrene) (SIS), or poly (styrene-b-ethylenebutylene-b-styrene) (SEBS) triblock copolymers. Phase separation occurs because of the incompatibility between the hard and soft segment. The styrene-rich domains serve as the hard phase since T_g for polystyrene is approximately 100°C. The molecular weight polydispersity is low because these triblocks are typically anionically polymerized. The terminal styrene anchors the polymer, which gives this material the necessary toughness while the flexible soft segment imparts elasticity. Approximately 50% of all thermoplastic elastomers produced are SBS, SIS, or SEBS triblock copolymers.

Another major category of thermoplastic elastomers, accounting for approximately 30% of the thermoplastic elastomer market, are based polyolefins. The three most important materials that comprise this category are copolymers of ethylene and propylene (EP), copolymers of propylene and higher α-olefins such as 1-butene and 1-octene, and copolymers of ethylene and α-olefins. In the latter two cases, the propylene or ethylene is the major component. Two important differences between the ethylene-rich and propylene-rich materials are flexibility and softening point; the ethylene-rich materials are more flexible but also soften at a temperature roughly 50°C below that of the propylene-rich materials. These types of materials are important enough to be given a very common abbreviation, TPO, which stands for thermoplastic elastomer-olefinic. A specific example of these types of TPEs are the Engage [3] family of materials, which are copolymers of ethylene and α-olefins. Metallocene catalysts, mentioned earlier, have allowed better control over the run lengths of the normal EP copolymers. Generally EP copolymers and copolymer blends are slightly higher cost and higher performance than the triblock copolymers.

(a)

m/n ~ 8
n ~ 100

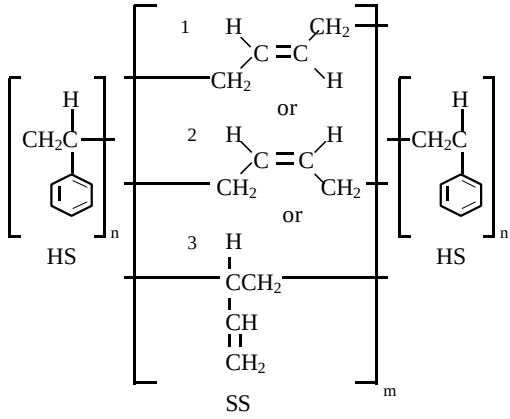

(b)

n = 1–5
m ~ 20
x ~ 20

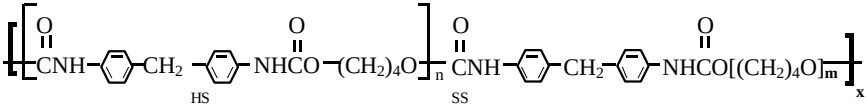

(c)

n = 1–5
m ~ 20
x ~ 20

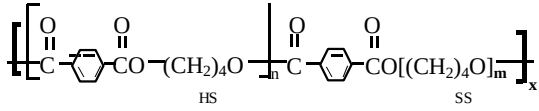

(d)

n = 1–5
m ~ 20
x ~ 20

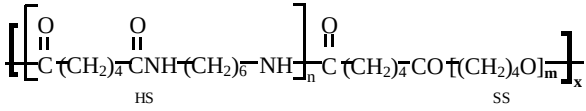

(e)

m/(n + 1) ~ 20
n ~ 1
x ~ 100

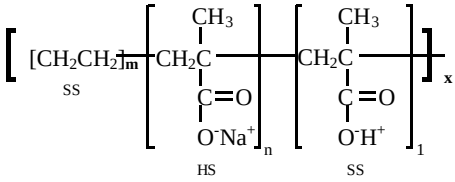

FIGURE 2 Structures of commercially important thermoplastic elastomers; HS = hard segment, SS = soft segment. (a) SBS; (b) MDI–BD–PTMO polyurethane; (c) PTMT and PTMO copolyester; (d) nylon 66 and PTMO copolyamide; (e) random copolymer ionomer E-MAA neutralized with sodium.

The EP thermoplastic elastomers are distinguished from the crosslinked analogues, which are not thermoplastics since reforming is impossible. A very important thermoplastic elastomer is comprised of a blend of an EP copolymer with an ethylene–propylene–diene (EPDM) terpolymer. This latter material is, of course, a crosslinkable thermoset; however, these materials can be processed as thermoplastics if the crosslinkable component is present at low enough concentration to be present as an isolated phase. Melt-processing causes the formation of chemical bonds within the isolated rubber phase, a process called dynamic vulcanization. A commercial example of this type of material is Santoprene [4] manufactured by Advanced Elastomer Systems. Other blends of noncrosslinkable TPEs with crosslinkable materials are used commercially. These materials are classified as elastomer blends and are the subject of Chapter 12.

Polyurethane elastomers are copolymers with a hard segment that contains aromatic rings and a polyether or polyester soft segment. Polyurethane elastomers are part of a family of materials termed segmented block copolymers, which is defined as a material with alternating hard and soft segments that repeat multiple times in a single polymer chain. Microphase separation occurs because of incompatibility between the aromatic rings and the soft segment. In some cases, the hard segment may crystallize as well. Segmented block copolymers have the general formula $(AB)_x$ where a triblock copolymer has the general formula ABA. Polyurethanes are generally manufactured from an aromatic diisocyanate, an oligomeric diol, and a low molecular weight diol. The low molecular weight diol is typically called the chain extender because it links AB segments together. A typical polyurethane based on diphenylmethylene-4,4′ diisocyanate (MDI), poly(tetramethylene oxide) (PTMO), and butanediol (BD) is shown in Fig. 2. A commercial example of a polyurethane is the MDI–BD family of materials manufactured by the Dow Chemical Company under the commercial name Pellethane [5]. Polyurethanes are generally expensive and have found uses in high performance structural applications as well as foams. Approximately 15% of the thermoplastic elastomer market is claimed by polyurethanes.

Another class of segmented block copolymers is segmented block copolymers containing an aromatic polyester hard segment and a polyether or polyester soft segment. Hard segment crystallization provides the driving force for phase separation in this system. A copolyester made from poly (tetramethylene terephtalate) and poly(tetramethylene oxide) (4GT–PTMO), which is a member of the Hytrel [6] high performance thermoplastic elastomers manufactured by DuPont, is also shown in Fig. 2. These materials are oil resistant and stable to higher temperatures than other thermoplastic elastomers, which makes these materials more suitable for applications such as automobile engine parts.

Two other thermoplastic elastomers are shown in Fig. 2. The copolyamide thermoplastic elastomers are comparable to the copolyesters in structure.

Crystallization provides the driving force for phase separation in these materials as well. These materials have especially low chemical permeability and can offer good properties at low temperatures. A commercial example of a copolyamide is PEBAX [7] marketed by Atofina. Copolyamides compete with polyurethanes and copolyesters for market share. Ionomers are the final material that will be discussed. Ionomers are materials where a small mole fraction of monomers, usually less than 10%, contain an ionic functionality. These materials are not segmented like most of the other materials discussed in this chapter, rather the ionic groups are distributed randomly along the polymer backbone. Incompatibility between the ionic groups and the nonpolar polymer backbone leads to the formation of ionic-rich domains. A commercial example of an ionomer is Surlyn [8] manufactured by DuPont, shown in Fig. 2.

This chapter is organized along the following lines: the general synthetic concepts discussed in Chapters 2 and 11 will be augmented by a discussion that is concerned only with synthetic techniques important in TPE synthesis. The bulk of the chapter will be concerned with the TPE morphology, since the morphology determines their physical and mechanical properties. This discussion will be followed by specific examples illustrating the effect of structure on the physical properties. The thermodynamics of phase separation, which includes detailed discussions on morphology as well as thermal behavior, will follow. The rheology and processing of these materials will be discussed next. Finally, some applications for thermoplastic elastomers will be highlighted. Emphasis will be given to those topics that are common to all thermoplastic elastomers; however, some discussion specific to commercially important materials will also be included. Also, the discussions are not meant to be exhaustive; for further information, the interested reader can consult some of the references provided throughout this chapter.

II. SYNTHESIS OF THERMOPLASTIC ELASTOMERS

A. Step-Growth Polymerization: Polyurethanes, Polyether-esters, Polyamides

Polyurethanes, copolyesters, and copolyamides are all produced via step-growth polymerization. In step-growth polymerizations relevant to the production of thermoplastic elastomers, a molecule containing two reactive functional groups of one type (e.g., a diisocyanate) reacts with another molecule containing two reactive functional groups of another type (e.g., a diol) to form a polymer. As discussed more thoroughly in Chapter 2, step-growth polymerizations require extremely high conversions (>99%) to produce high molecular weight product. Generally, TPE properties are only weakly dependent on overall molecular weight, so the breadth of the distribution is usually not very important, although it is important to achieve high molecular weights.

Controlling the ratio of functional reactive groups is critical to achieving high molecular weights as the following formula shows in the case of a stoichiometric imbalance between the two reacting functional groups:

$$\bar{n}_n = \frac{1+r}{1+r-2rp} \tag{1}$$

where r is the ratio of the initial imbalance of the functional groups and is defined to be always less than 1, p is the extent of reaction, and n is the number average degree of polymerization. Even to achieve moderate molecular weights, stoichiometric imbalances of more than a few percent cannot be tolerated.

Before embarking on a short description of the synthesis of polyurethanes, the reader should be aware that polyurethanes are generally divided into three classes: foams, coatings, and TPEs. This chapter concerns only the latter, and the morphological difference between a TPE urethane and others is the fact that the chain is not crosslinked, and the segment lengths are longer. Synthetically, crosslinked materials tend to use water, whereas water must be excluded from a reaction that wishes to produce a TPE polyurethane. Books [9–12] on the subject generally cover all three types of polyurethanes, sometimes without a clear distinction between the different uses.

Polyurethanes can be synthesized in solution [13] or in bulk [14]. Solution polymerized polyurethanes generally have more uniform hard and soft segment distributions. Bulk polymerized polyurethanes generally have higher molecular weights, partially caused by side reactions that cause crosslinking [15]. The majority of industrially produced polyurethanes are made in bulk. Bulk synthesized polyurethanes are reacted at temperatures between 80°C and 120°C. The isocyanate–alcohol reaction is highly exothermic, which means that heat must be removed from the reaction mixture so that the temperature will be kept below the degradation temperature of 140°C. Generally, higher temperatures mean more side reactions and crosslinking. To produce totally linear polyurethanes, temperatures under 50°C should be used [16]. Two methods are used in the bulk, the "one-shot" method and the prepolymer method. In the "one-shot" method, all the ingredients are mixed together; in the prepolymer method, the diisocyanate and oligomeric diol are allowed to react before the chain extender is added. Generally, the oligomeric diol and the diisocyanate are not miscible, so the reaction occurs at the interface between the two components, which can lead to large compositional variations over the course of the reaction. A common solvent for the diols, the diisocyanate, and the polymer is needed for solution polymerization. A relatively polar organic solvent such as N,N-dimethyl acetamide or dimethyl sulfoxide will generally suffice. Usually the analogue of the prepolymer method, described earlier for bulk polymerization, is used for solution polymerized polyurethanes. Unlike the bulk reaction, an organotin catalyst is employed in solution polymerization. Organotin compounds are generally not utilized in

the bulk method since incomplete catalyst removal will lead to poor hydrolytic stability of the final product.

Another common thermoplastic elastomer produced from a step-growth polymerization are the copolyesters. The general reaction scheme is very similar to the polyurethanes except the hard segment reactants are usually diesters rather than diisocyanates, which means that a small molecule by-product must be removed in order to achieve high conversions. Generally, copolyesters are produced in a melt phase transesterification polymerization described by Witsiepe [17]. In the first step, the oligomeric diol, chain extender, and diester are mixed and allowed to react at elevated temperature (~200°C) in the presence of a titanate catalyst in order to produce prepolymer. The high temperature serves to drive the reaction toward completion as well as remove the low boiling byproduct through fractional distillation. Polymers are produced by raising the temperature to 250°C and lowering the pressure to less than 1 mmHg, which causes the second transesterification. The chain extender is removed as a by-product from this second stage. The temperature must be kept below 260°C in order to prevent substantial degradation [18]. Reaction completion is monitored by the viscosity of the reaction mixture. Molecular weights of approximately 25,000 g/mol generally result from this procedure.

Different pairs of functional groups can be reacted to form amide linkages, and all of them have been used to produce copolyamides [19]. These include reactions between carboxylic acids and diamines, acid chlorides and diamines, and carboxylic acids and isocyanates. The latter is especially useful for producing copolyamides with aromatic hard segments. The copolyamides are most commonly produced with either ester or amide linkages between the amide hard segment and soft segment. Again, high temperatures are sometimes needed to produce high molecular weight material.

B. Anionic Polymerization: Styrene–Diene Copolymers

Anionic polymerization is used to produce the styrenic block copolymers and produces a polymer with an extremely narrow block and overall molecular weight distributions. The narrow molecular weight distributions are extremely useful in fundamental studies of polymers, and have led to a great deal of study of anionic polymerization, much more than justified by its commercial importance. In fact, the styrenic-block copolymers are the only polymers produced in large quantities via anionic polymerization. The extremely narrow polydispersity is evident in the following expression for the polydispersity index:

$$\frac{n_w}{n_x} = 1 + \frac{n_x}{(n_x + 1)^2} \tag{2}$$

where n_w is the weight-average degree of polymerization and n_x is the number-average degree of polymerization. This analysis assumes no chain transfer and

no chain termination reactions, which are easily achieved using low temperatures and pure ingredients. An extremely fast initiation rate relative to propagation is also assumed.

The triblock copolymers SBS or SIS are produced using a high vacuum process that serves to eliminate both oxygen and water from the reaction mixture [20]. Besides the general features discussed in Chapter 2 that apply to any anionic synthesis, it is important to produce a polydiene block with a high 1,4 structure so that the glass transition temperature of the soft phase will be sufficiently low. This is generally accomplished by using a relatively nonpolar solvent, e.g., cyclohexane or toluene, which favors 1,4 formation. SEBS is formed through the hydrogenation of SBS.

Generally three anionic polymerization methods can be used to produce the styrene–diene triblock copolymers: a three-stage process with monofunctional initiator, a two-stage process with monofunctional initiator and a difunctional linking agent, and a two-stage process with a difunctional initiator [21]. In all cases, the initiator of choice is an organolithium compound. In the first process, the styrene monomer is anionically polymerized, followed by the butadiene monomer, and then finally more styrene monomer is added to produce a triblock polymer. The butadiene rapidly initiates when added to the styrene blocks; however, a small amount of polar solvent is needed to initiate the final styrene anionic polymerization. In the second process, the styrene and diene blocks are polymerized separately then combined using the difunctional linking agent, which produces symmetric triblocks. The key in this method is to control the stoichiometry exactly so that no diblocks are formed. A small amount of diblock material has an extremely adverse effect on mechanical properties. Finally, a difunctional initiator can be used to initiate the diene block followed by the styrene endblocks. This method suffers from the difficulty in finding an appropriate difunctional initiator.

C. Catalytic Polymerization

Ethylene–propylene copolymer thermoplastic elastomers and other ethylene-α olefin copolymers are produced from either Ziegler-Natta or metallocene processes. Ziegler-Natta polymerizations are reactions catalyzed by a mixture of alkyl metal halides, e.g., $Al(C_2H_5)_2Cl$ and transition metal salts, e.g., $TiCl_4$. These polymerizations typically produce crystallizable stereospecific products. For example, in propylene-α olefin copolymers, polypropylene crystallites provide the hard phase for the TPE. Long blocks of one component, which are necessary for phase separation, result from the inherent reactivity ratios of the components. In spite of the industrial importance of Ziegler-Natta polymerizations, their kinetics are not well understood. This is a result of the often heterogeneous nature of this reaction as well as the possibility of multiple mechanisms. Ziegler-Natta polymerizations are discussed in more detail in Chapter 2. Blends of EP copolymers with isotactic polypropylene are

often made in a two-step reaction process. The first reactor contains only propylene monomer, while the second reactor contains both propylene and ethylene. Other blends are made by mixing the pure components together in the melt. Blending conditions have a large effect on the resulting properties. Compatibilizers, which are often triblock copolymers, can adjust the blend's characteristics.

Metallocene polymerizations have many of the same properties as Ziegler-Natta polymerizations, but as the name implies, the catalyst is very different. Metallocene catalysts have two general properties that lead to stereospecific products: first, the catalyst is rigid, and second, the catalyst is chiral. These properties are obtained by having a metal cation sandwiched between two negatively charged cyclopentadienyl anions. Figure 3 shows a representative metallocene catalyst, 1,1′-ethylenedi-η^5-indenylzirconium dichloride. A modification to this approach is to replace one of the cyclopentadienyl anions with a ring containing a nitrogen atom, and then constraining the ring by bonding the nitrogen via a bridging atom, typically silicon. Just as in the Ziegler-Natta polymerization, a compound with labile alkane groups is required; one typical compound used is methyl alumoxane. Unfortunately for the economics of the process, the amount of aluminum required is much higher in the metallocene materials than in the Ziegler-Natta materials. In spite of the higher cost of these materials, metallocene polymerizations are gaining in market share because of the ability to better control the number of defects, which in turn can be used to tune copolymer properties. Just as with Ziegler-

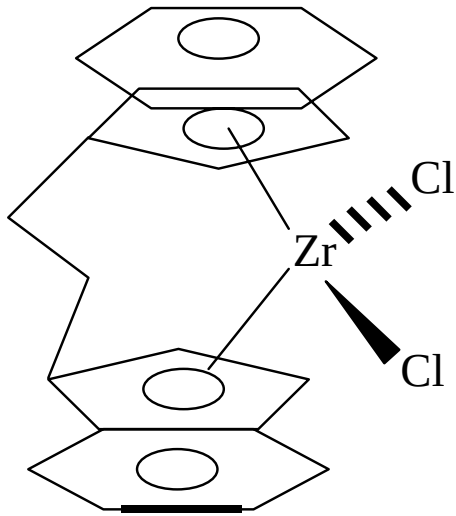

FIGURE 3 Structure of 1,1′-ethylenedi-η^5-indenylzirconium dichloride, a common metallocene catalyst. Only one enantiomer is shown; both enantiomers produce isotactic product for this particular catalyst.

Natta polymerizations, metallocene polymerizations are used to produce non-stereospecific polymers because of changes in molecular weight distribution and reactivity ratios relative to other types of polymerizations.

D. Free Radical Polymerization

Free radical copolymerization is used to produce ionomers that are used commercially as thermoplastics elastomers. There are two types of TPE ionomers, copolymers of ethylene and methacrylic acid, and copolymers of ethylene and acrylic acid. The mole fraction of the acid monomer is typically 5% or less. The property difference between the two types of copolymers are small; copolymers of ethylene and methacrylic acid are slightly more resistant to the formation of anhydrides that can crosslink the polymer. The usual method uses high pressure (~1500 atm) and high temperatures (~130°C) similar to the method used for low density polyethylene. In contrast with Ziegler-Natta polymerizations, the kinetics are well known (see Chapter 2). The neutralizing cation after synthesis is hydrogen; this material does not phase separate into the nanometer-size aggregates required for toughness improvements. Therefore neutralization with an appropriate metal salt occurs industrially by mixing the polymer and the salt together in an extruder or roll mill [22]. In commercial materials, not all the hydrogen atoms are replaced by a metal cation, or else a material with too high a viscosity is produced; typical neutralization levels in most ionomers is around 50%.

E. Molecular Weight and Chain Structure

Determining the molecular weight and the chain microstructure is very difficult for some thermoplastic elastomers. Nearly all molecular weight characterization techniques rely on the ability to dissolve the polymer in a solvent in such a manner that the polymer chains behave individually. Since TPEs are usually composed of two dissimilar components, a good solvent for one of the components may be a poor solvent for the other component, which leads to aggregation of similar components from different chains. Hence the molecular weight is an aggregate molecular weight, rather than a true molecular weight. Even if this problem is overcome, methods that measure molecular weight relative to a standard, such as gel permeation chromatography (GPC), cannot be converted to actual molecular weight because the proportionality constant depends on the copolymer composition.

For polyurethanes and polyesters, end group analysis, either by titration or infrared analysis, can be used to monitor the extent of reaction and the final molecular weight if the reaction stoichiometry is properly controlled. This method only works well if the molecular weight is below about 20,000 g/mol. Membrane osmometry and light scattering can give reliable molecular weights if the appropriate solvent is used; however, a long time is required to make

these measurements. Different solvents must be tested so that data can be collected without significant curvature that indicates aggregation. Ultracentrifugation is almost never used because, among other issues, by definition a theta solvent does not exist for thermoplastic elastomers. The molecular weight calculated from viscosity measurements will also depend on the copolymer composition since the radius of gyration (R_g) of the polymer will generally be a function of composition. Fractionation methods also typically fail because the fractionation efficiency depends not only on molecular weight distribution but also composition distribution. Most often, GPC is used and the molecular weight is usually reported relative to a standard and for a certain solvent.

Molecular weight characterization of polyurethanes using GPC was studied in detail [23]. Three different molecular weight standardization methods were tested, and it was found that a multidetector method using an refractive index and an UV spectrometer in series provided the most accurate results. The UV spectrometer was used to calculate the variation of the derivative of refractive index with respect to concentration at each point in the chromatogram, which accounts for the effect of changing copolymer composition with molecular weight. The authors found that the normal polystyrene standards used to calibrate the GPC give an upper limit on the actual molecular weight. Nevertheless, the authors were hesitant to call these values absolute. A related issue is the molecular weight of the linear prepolymers if a staged reaction scheme is used; a procedure for determining the molecular weight and soft segment–hard segment distribution of end-capped diisocyanates using GPC and a double detection method was given recently [24].

Accurate molecular weights can be easily measured for the triblock copolymers. Because these materials are produced via anionic polymerization, the theoretical molecular weight is usually very close to the actual molecular weight. Depending on the polymerization method, the pure styrene or pure diene block can be removed and the molecular weight measured before making the triblock. Finally, molecular weight standards of polystyrene, polybutadiene, and polyisoprene are commercially available, which means measuring absolute molecular weight of these blocks is easily done using GPC.

The chain microstructure has a very important influence on the properties of TPEs. As mentioned earlier, production of SBS or SIS with a high 1,4 content is necessary. TPO properties also depend quite heavily on any deviations of the microstructure from the ideal head-to-tail, pure isotactic, or syndiotactic microstructure. Properties such as tacticity, *cis*-trans isomerization, and copolymerization content are usually characterized using NMR. Peak positions and peak intensities are used to quantitatively ascertain microstructure to a high degree of accuracy. Copolymer composition can also be determined using NMR. Infrared spectroscopy can also be employed to determine microstructural characteristics in some polymers.

In the segmented block copolymers, the average molecular weight of the hard and soft segments is very important, and the number of studies for the

various types of TPE that have investigated this variable are too numerous to list here, although the anionic block copolymers deserve special mention in this regard because of their importance in elucidating fundamental thermodynamic information. In general, the higher the molecular weight of the blocks, the more complete the phase separation. However, it should be noted that complete phase separation is not always desired, since a decrease in toughness will eventually occur as phase separation becomes more complete. A related parameter, which is particularly important in both segmented block copolymers as well as the TPOs, is the distribution (as opposed to the average) of hard and soft segment lengths. In the latter, the hard segments are typically crystalline domains of either propylene or ethylene, and studies of crystallite size distribution are an important topic not just to TPEs. For the step-growth block copolymers, the distribution of soft segments tends to be fairly trivial to characterize, since the fully formed soft segment is typically one of the ingredients fed to the reaction. The hard segment, on the other hand, is typically formed as part of the polymerization, and more sophisticated approaches are required. Two approaches have been applied to study the effect of the distribution of hard segment lengths: the first is to synthesize hard segments with a known length distribution [25] and the second is to attempt to measure the hard segment lengths. Of course, the latter is necessary for all commercial materials. A number of experimental methods have been used to determine hard segment length distributions. One method is to chemically cleave the structure at the point where the hard segment and the soft segment join and analyze the residual fractions using GPC or HPLC [26–29]. ^{13}C NMR [30] and mass spectroscopy [31] have been used to determine hard segment length in MDI–PTMO polyurethane chains extended with ethylene diamine. Monte Carlo simulations of Markov processes have also been used to derive hard segment molecular weight distributions under ideal and nonideal conditions [32–37].

III. MORPHOLOGY OF THERMOPLASTIC ELASTOMERS

A. General Characteristics

In spite of the wide variety in structure of two-phase thermoplastic elastomers, the number of underlying morphologies in commercially important materials is surprisingly small. If we assume that A is initially the minor component and B the major component, then the seven equilibrium morphologies given in increasing A content are [38]:

1. Isolated spheres of A in a continuous matrix of B
2. Hexagonally packed isolated cylinders of A in a continuous matrix of B
3. Alternating lamellae of A and B

4. Hexagonally packed isolated cylinders of B in a matrix of A
5. Isolated spheres of B in a matrix of A

Other, more complicated morphologies can be generated with anionically synthesized block copolymers; a complete review of this subject is beyond the scope of this chapter, and the interested reader is referred to reviews [39, 40] and monographs on the subject [41, 42]. Transmission electron micrographs are shown in Figs. 4–6 for each of the phases for a SBS block polymer. In general, the morphology in commercial materials are not nearly as well developed as the micrographs imply. Once the general morphology (spheres, cylinders, etc.) has been specified, specific questions remain concerning domain spacing, radii, and arrangement in space. These questions will be dealt with in some detail later in this chapter.

The underlying morphology will have a large effect on the physical properties. The soft phase is usually the continuous phase to maintain the elastomeric behavior of the material. In materials that have crystalline hard segments, such as copolyesters and polyurethanes, both phases are essentially continuous. Thermoplastic elastomers almost never have the soft segment as the isolated phase and the hard segment as the continuous phase. The most

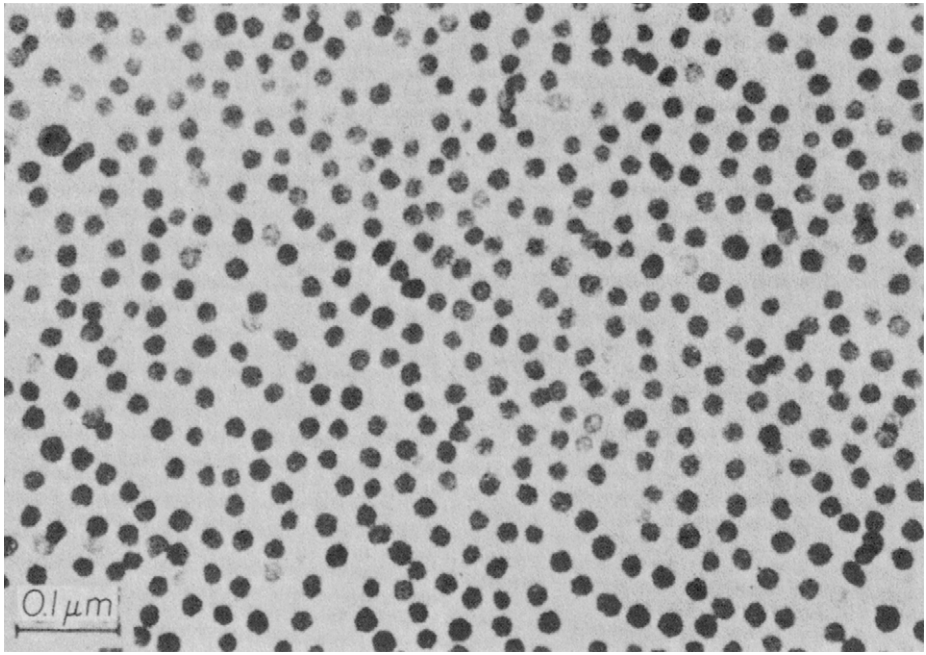

FIGURE 4 TEM of spherical butadiene domains in SBS (80% styrene) film cast from toluene. The same patterns were observed in both normal and parallel sections, confirming the periodicity of butadiene domains. (From Matsuo [221].)

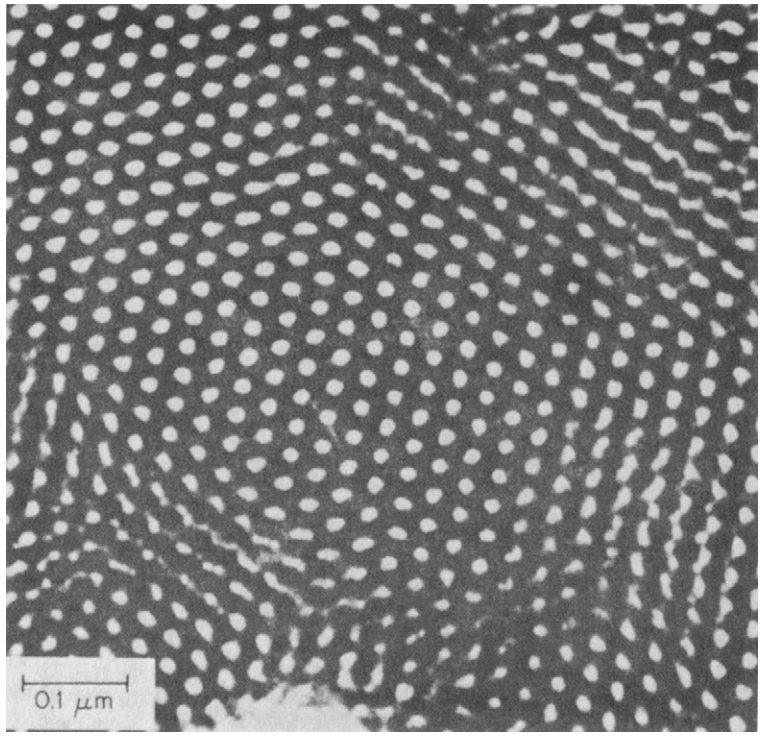

FIGURE 5 TEM of cylindrical microdomains in extruded and annealed SBS sample where the micrograph was taken perpendicular to the extrusion direction. An electron micrograph taken parallel to the extrusion direction had a striated structure. (From Dlugosz *et al*. [222].)

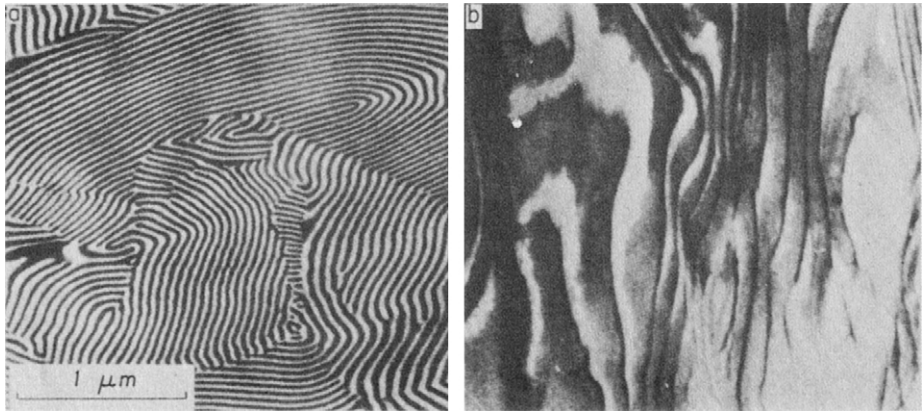

FIGURE 6 TEM of lamellar domains in SBS (40% styrene) film cast from cyclohexane. (a) Normal section; (b) parallel section with lamellar layers orienting their surface parallel to film surface.

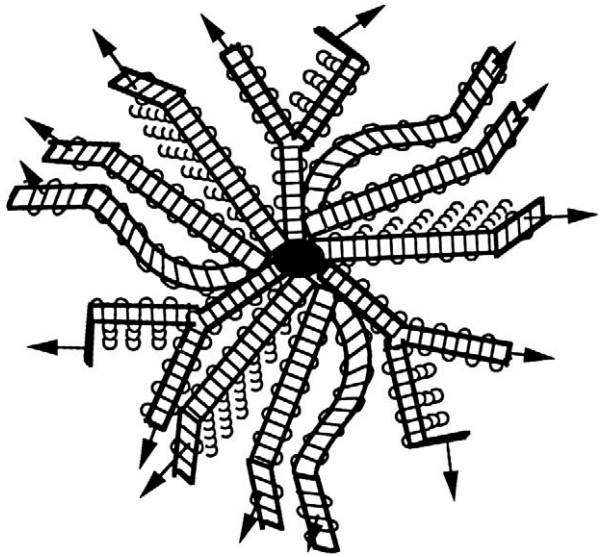

FIGURE 7 Illustration of phase separation in SBS triblock copolymers normally used as a thermoplastic elastomer. The isolated spherical styrene domains form the hard phase, which acts as both intermolecular tie points and filler. The continuous butadiene imparts the elastomeric characteristics to this polymer.

common morphology for TPEs is illustrated in Fig. 7 for SBS triblock copolymers. The isolated hard phase acts as intermolecular tie points for the elastomeric soft phase. Normally the isolated hard domains are between 1 and 20 nm. The ability to crystallize changes the morphology dramatically; the crystalline regions form rectangular thin sheets of material termed lamellae and hence will not be constrained into isolated domains and form more of a continuous structure. As with all polymers, lamellae can organize into spherulites and, a bit surprisingly, the segmented nature of the TPE does not prevent the formation of these large superstructures.

The interface between the hard and soft segment is often considered as a separate phase. The influence of the interface on the properties of TPEs is considered to be very important, although not well understood. The higher cost of TPEs relative to commodity polymers is justified in different ways for different materials, but in general a property worth a high premium is toughness, i.e., a great deal of energy is required for failure. Toughness is achieved by creating stress-relieving processes in a material, and in TPEs much of these processes occur at the hard and soft domain interface resulting in the deflection and bifurcation of cracks [43]. The adhesion between the interface and the polymer matrix is especially important in developing toughness in EP copolymer blends since failure often occurs in blends because of poor interfacial adhesion.

As implied earlier, kinetic considerations play an extremely important role in the morphology of TPEs. Predicting the precise morphology of any TPE without some knowledge of sample history is impossible. To produce a material that is near the equilibrium morphology, the TPE can be annealed above the dissolution transition of the hard segment, but below the order–disorder temperature. Polydispersity in block lengths may also give morphologies that deviate substantially from the underlying morphologies. Finally, many industrially produced parts have oriented microdomains remaining from processing.

The remainder of this section contains an introduction to analytical methods used to characterize the morphology of TPEs. A short description of each method is given, with emphasis on those characteristics relevant to TPEs. Important examples of each method are also discussed, so the reader can understand how each method is used to characterize the morphology of TPEs.

B. Studies of Morphology

1. Transmission Electron Microscopy (TEM)

In transmission electron microscopy (TEM), a sample is bombarded with electrons, and the number of electrons that travel through the sample, which is proportional to the sample thickness and the electron density, is measured as a function of position. If the electron densities are not identical for each phase in a TPE, the number of electrons passing through the two phases may be different and hence contrast will be created. TEM can be used on samples with extremely well ordered morphologies where the length scale of electron density variations is greater than the resolution of the method. If the morphology is not well ordered, then the average number of domains of one type that a single electron passes through does not vary with position. The thickness of the film can be reduced, but a practical limit to thickness reductions exists. Since the electron density difference between atoms that comprise polymers is generally very small, a low molecular weight compound with a high electron density that will preferentially bind or migrate to one of the two phases is almost always added. Typical compounds used for such staining are OsO_4 and RuO_4.

Styrene–diene block copolymers represent the optimum material for TEM. If prepared properly, these materials can be almost 100% phase separated with the staining agent residing almost exclusively in the diene phase. The morphology is generally well ordered, and individual domain sizes tend to be large. Examples of electron micrographs of SBS block copolymers were given in Figs. 4–6. TEM is probably the most important characterization method used for the determination of bulk morphology, so most papers in the field published TEM micrographs of their systems. The review papers and books referenced earlier contain a thorough description of TEM studies of block copolymers.

Copolyesters [44] and polyurethanes [45] have also been imaged. These two materials have not been the focus of electron microscopy studies for many years because of the difficulties in excluding artifacts. In fact, one must cast a very questioning eye on published results of these systems for this very reason. A number of papers by Winey *et al*. [46–48] have appeared in the last 5 years describing results of TEM studies of ionomers. The heavy metal atoms are used to provide the necessary contrast, and high-resolution TEM is used to image these systems. A much wider variety of ion aggregate morphologies have been found than previously thought, including spheres and vesicles.

2. Infrared and Raman Spectroscopy

In infrared spectroscopy, a beam of infrared light is passed through a sample, and light is absorbed if the frequency of the light is the same as the frequency of a normal mode of vibration. This method is sensitive to molecular bonding between atoms. Beer's law relates the absorbance (A) of a vibration to its absolute concentration:

$$A = \varepsilon t c \tag{3}$$

where ε is the absorption coefficient, t is the path length, and c is the concentration. As indicated previously, infrared spectroscopy can be used to explore chain microstructure. Beyond chemical characterization, infrared spectroscopy can aid in describing interchain interactions such as hydrogen bonding or crystallization.

Hydrogen bonding is the secondary bonding of hydrogen atoms to an atom containing unpaired electrons. Hydrogen bonds generally have strengths on the order of 3 kcal/mol, which is a half order of magnitude less than covalent bond strengths but an order of magnitude greater than simple van der Waals interactions [49]. Hydrogen bonding is extremely important in polyurethanes and copolyamides and occurs between the urethane or amide hydrogen and the carbonyl oxygen. Since hydrogen bonding occurs primarily between hard segments, it provides a strong driving force for phase separation and hard segment crystallization.

Hydrogen bonding causes a shift toward lower wave number (lower energy) in the vibration of the bonds involving the hydrogen donating group and the hydrogen accepting group, which indicates that both primary bond strengths have been diminished because of the secondary hydrogen bond. In a typical thermoplastic elastomer that can hydrogen bond, vibrations of functional groups participating in hydrogen bonding are split into bands termed *bonded* and *free*. Table I gives wave numbers that have been assigned to the bonded and free bands for the C = O and N–H vibrations for a variety of polymers. There is a small but noticeable effect of the polymer type on the exact wave number for the vibration. The two vibrations listed for some C = O stretches are due to the ordered (crystalline) and disordered bonded states.

TABLE I Band Assignments of Hydrogen Bonded Functional Groups in TPEs

Material	Free	Bonded	Reference
C = O	1720 cm^{-1}	1685 cm^{-1}	59, 61
Polyurethane: hexamethylene diisocyanate/butanediol.		1700 cm^{-1}	
N—H	3440 cm^{-1}	3320 cm^{-1}	
C = O	1740 cm^{-1}	1700 cm^{-1}	55
Polyurethane: 2,6 toluene diisocyanate/butanediol/PTMO			
N—H	3460 cm^{-1}	3300 cm^{-1}	
C = O	1733 cm^{-1}	1703 cm^{-1}	53, 56
Polyurethane: MDI/butanediol/PTMO			
N—H	3420 cm^{-1}	3320 cm^{-1}	
C = O	1680 cm^{-1}	1636 cm^{-1}	60, 62
Polyamide: Nylon 11	1645 cm^{-1}		
N—H	3450 cm^{-1}	3300 cm^{-1}	

Since hydrogen bonding is extremely important and infrared studies are relatively inexpensive and simple, a large number of papers have been published in this field. Many studies have tried to relate the amount of hydrogen bonding to the degree of phase separation using Beer's law. Harthcock [50] explored the carbonyl stretching region in model polyurethanes with monodisperse hard segment lengths. A detailed morphological model that relates the hard segment order to the infrared vibrational frequency was given and is reproduced in Fig. 8. A similar study was undertaken by Luo *et al.* for polyurethane ureas [51]. Changes in hydrogen bonding due to structural changes such as hard segment [52] and soft segment type [53] have also been studied. FTIR has aided in the discovery of structure–mechanical property relationships for segmented polyurethanes [54]. The thermal behavior of hydrogen bonding has been investigated in some detail [55–57]. A series of papers published by Painter and Coleman [58–62] on polyamides and polyurethanes concluded that many of the studies involving thermal behavior were based on incorrect reasoning concerning the nature of hydrogen bonds. These authors showed that quantitative analysis of the N–H region was impossible because of the large difference in extinction coefficient between the bonded and free bands along with the large change in the bonded N–H extinction coefficient as a function of temperature. The simple analysis [55] normally employed to describe the dependence of the extinction coefficient with temperature could not be used because the vibrational frequency of the N–H bond shifted, which indicated that the hydrogen bond strength changed. Therefore the reader should be very careful interpreting papers that quantitatively analyze the N–H stretching region.

Raman spectroscopy in general gives complementary information to infrared spectroscopy and, because of the historical difficulty in performing

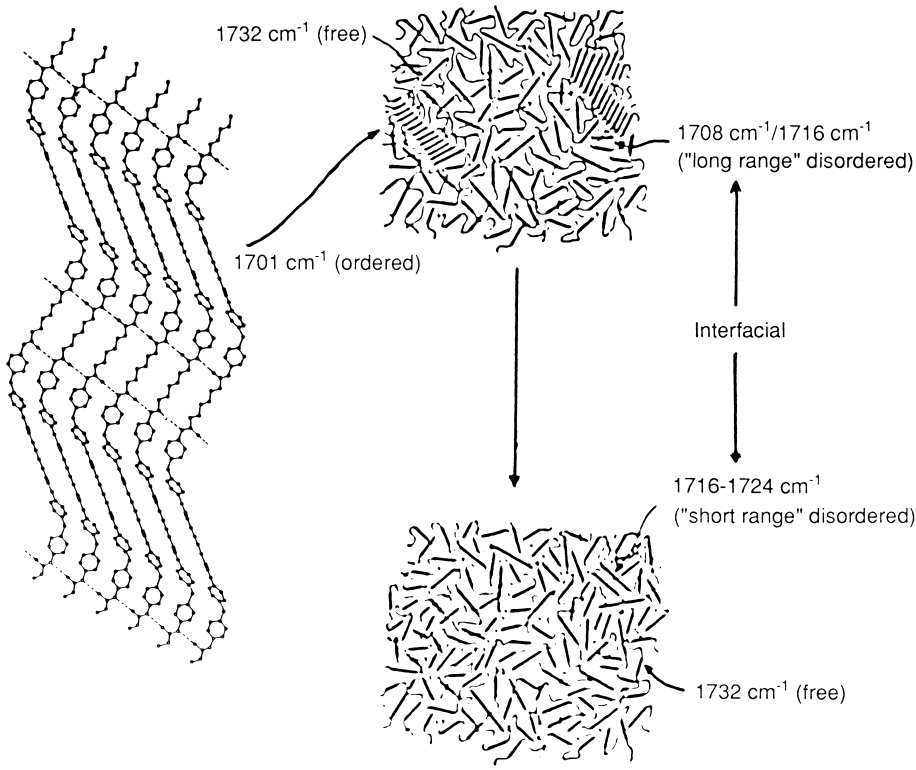

FIGURE 8 Morphological model developed by Harthcock that shows the wave number of the C = O stretching vibration absorbed intensity to the local environment. (From Harthcock [50].)

these experiments, Raman studies of TPEs have been much less frequent than infrared spectroscopy. Raman experiments have become much simpler in the last 10 years with the development of powerful lasers and CCD detection systems, although the cost of a Raman spectrometer is still much more than an FTIR spectrometer. Raman spectroscopy has two distinct advantages to IR spectroscopy: first, the signal can be measured remotely using fiber optics, which makes it possible to use Raman for process control, and second, laser light can be focused to an approximately 1 micron spot, allowing researchers to image very small cross-sectional areas. The spatial-resolving capabilities of micro-Raman has been used to probe the composition heterogeneity in polyurethanes [63].

Another use of infrared spectroscopy uses linearly polarized infrared radiation to determine information about oriented samples, an experiment that has been termed infrared dichroism. The absorbance will be a maximum when the electric field vector and the dipole moment vector are in the same

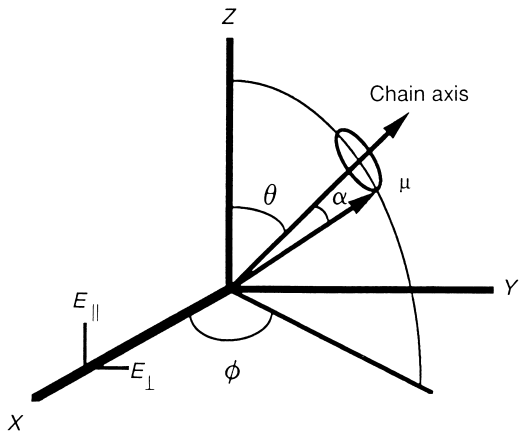

FIGURE 9 Geometry for uniaxial extended sample.

direction, and the absorbance will be zero when the two are perpendicular. Only uniaxial orientation will be considered because this situation is normally found in the literature. R, the dichroic ratio, is defined as follows:

$$R = \frac{A_{\parallel}}{A_{\perp}} \tag{4}$$

where $A_{\parallel}$ is the absorbance when the orientation direction and the polarization direction are parallel to each other and $A_{\perp}$ is the absorbance when the two directions are perpendicular. The relevant geometry is shown in Fig. 9. Let $f(\theta)$ represent the orientation distribution function, i.e., $f(\theta)d\theta$ is the fraction of chain axis that lies within an angle $d\theta$ of θ. This function can be expanded in terms of the Legendre polynomials:

$$f(\theta) = \frac{1}{2\pi} \sum_{n=0}^{\infty} \frac{2n+1}{2} \langle P_n(\cos\theta) \rangle P_n(\cos\theta) \tag{5}$$

Only even number polynomials need to be considered since the assumption of uniaxial symmetry implies that the average values of the odd powers of $\cos\theta$ are zero. From Fig. 9 after rather extensive mathematical manipulation it can be shown that:

$$\langle P_2(\cos\theta) \rangle = \frac{3\langle \cos^2\theta \rangle - 1}{2} = \frac{(R-1)(R_0+2)}{(R+2)(R_0-1)} \tag{6}$$

R_0 is given by $2\cot^2\alpha$, where α is the angle between the dipole moment vector and the chain axis. $\langle P_2(\cos\theta) \rangle$ is the one parameter measure of orientation normally given in the literature for uniaxially oriented samples. α is a function of the vibration in question and is known for a number of vibrations useful in studying thermoplastic elastomers [64].

Infrared dichroism can be used to follow the orientation of each phase independently if nonoverlapping bands can be found in each domain where α is known. For example, in polyurethanes, the bonded carbonyl band is typically used to monitor hard segment orientation, while the free carbonyl band or CH stretching bands are used to follow soft segment orientation [65–67]. The hard segment orientation is almost always less than the soft segment orientation at the same draw ratio. In semicrystalline and more highly ordered polyurethanes, the hard segments are ordered transverse to the stretch direction initially and later become aligned in the elongation direction. Morphologically, at low elongations, the radial arms of the spherulite become oriented in the stretch direction, which means that the chain axes become oriented perpendicular to the stretch direction. At higher elongations, hard segments are physically removed from the arms and align with the elongation. In relaxation experiments, the soft segments tend to relax very quickly to a nearly unperturbed conformation, while hard segments relax much more slowly, especially at high strains. The transverse orientation of the hard segments is reversible, while physically removed hard domains cannot be restored to their previous environment without heating the sample. Dichroism measurements have been made on 4GT–PTMO copolyesters that showed the same negative orientation at low elongations followed by positive orientation at higher elongations [68]. Dichroism measurements at higher temperatures in MDI–BD polyurethanes showed changes in behavior; the onset of positive orientation occurs at a much lower elongation, and the hard segment orientation becomes much greater at a given draw ratio. These results were interpreted as a weakening of hard segment domain cohesion at higher temperatures [69]. The response to elongation is also altered when polyurethanes are hydrolytically degraded [70] or plasticized [71].

3. Wide Angle X-ray Scattering (WAXS)

When an electron density difference occurs periodically over a distance that is the same order of magnitude as the wavelength of x-rays, x-rays will be scattered coherently from a sample. A peak or peaks corresponding to this distance will appear in the scattering pattern if the periodicity occurs enough times. The width and number of the peaks will be proportional to the variation of this repeat distance about its average value, as well as the number of times this periodicity occurs before ending. WAXS measures electron density variations with distances on the order of angstroms, which corresponds to interatomic distances. Therefore, WAXS is utilized to study thermoplastic elastomers with crystalline hard or soft segments.

The fundamental relationship that relates the repeat distance of electron density variation and the scattering angle is Bragg's law [72]

$$n\lambda = 2d \sin\theta \tag{7}$$

where n is an integer, λ is the wavelength of radiation, 2θ is the angle between the incident and exiting radiation, and d is the repeat distance between crystallographic planes. Further details regarding the crystallographic analysis of polymers are quite complicated and beyond the scope of this chapter. The interested reader is referred to the text by Alexander [73].

Detailed crystallographic studies have been performed on copolyesters, copolyamides, and polyurethanes. Regarding the former, hard segment crystallites of 4GT are identical to 4GT homopolymer crystallites in the quiescent state. A different crystalline form is found in the hard segment when the TPE is extended due to the methylene sequences forming an all-trans configuration [74, 75]. Using electron microscopy [76] and SAXS [77], the lamellar thickness has been shown to be smaller than the average hard segment length, which means that chain folding must occur. Although the unit cell is insensitive to soft segment fraction or soft segment composition, the overall amount of hard segment crystallites decreases as the soft segment fraction increases, as shown in Fig. 10. However, the fraction of 4GT units that are crystalline increases as the soft segment fraction increases [78]. These materials will also show strain-induced crystallization under stretching [79].

Copolyamides show many of the same features as the copolyesters in WAXS studies. The crystal structure in the hard segment (nylon) domains is the same as in the homopolymer [80]. Whether chain folded crystals occur depends on the block length of the hard segment, at short block lengths a fringed micelle model was postulated to occur, while at long block lengths chain folding was present [81–83]. At sufficiently low temperatures (below 0°C), the soft segment will crystallize if the soft segment is PTMO [84]. Finally,

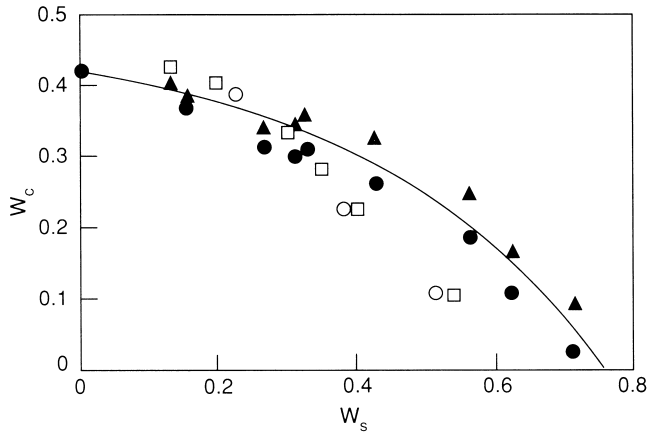

FIGURE 10 Weight fraction of crystallites, W_c, vs. weight fraction of soft segments, W_s, for 4GT–PTMO copolyester. ▲ from density measurements, ● from WAXS, open symbols from differential scanning calorimetry.

the PTMO segments show strain-induced crystallization, which is reversible if the sample is heated slightly above room temperature. The crystallization is great enough so that a permanent set will occur [85].

Polyurethanes show many of the same features as the copolyesters and copolyamides with respect to both hard and soft segment crystallinity. One substantial difference between polyurethanes and the previous two materials is that not all commercial polyurethane TPEs show hard segment crystallinity; MDI-based polyurethanes show crystallinity while TDI-based urethanes do not. Two crystalline structures have been found for MDI–BD hard segments in the unoriented state with another distinct form found in the oriented state [86, 87]. Other studies have examined the effect of chain extender length on the crystal structure [88]. The differences between polyurethanes with chain-folded and chain-extended hard segment crystallites has been extensively studied by Eisenbach *et al.* [89].

Copolymers of isotactic propylene (iPP) with α-olefins also exhibit diffraction peaks due to iPP crystallites. As one would predict, increasing the α-olefin content decreases the percent crystallinity. When the copolymer is blended with iPP homopolymer, the copolymer will cocrystallize with the homopolymer, a phenomena that is rare in polymers. Cocrystallization is believed to substantially contribute to the improved mechanical properties found in the blend [90]. Large spherulites are not generally found in these blends as opposed to the homopolymer, and the crystal form is monoclinic rather than smectic [91].

4. Small-Angle X-ray Scattering (SAXS)

WAXS measures the scattering of x-rays at distances relatively far away from the primary beam, while SAXS measures the scattering very close to the primary beam. Since the scattering distance is inversely related to the distance in real space, SAXS is sensitive to length scales on the order of nanometers rather than angstroms. SAXS is used to probe the two phase morphology in TPEs. In other words, WAXS characterizes intraphase morphology, while SAXS characterizes interphase morphology.

Precise collimation systems are needed to make measurements close to the primary beam. In addition, scattering at small angles is usually very weak. Both pinhole and line collimation has been used; block collimation systems require mathematically transforming the data from line collimation to point collimation. During the last 15 years, the development of synchrotron sources and better area detectors has led to a proliferation of scattering experiments that occur in real time.

The interpretation of SAXS curves is more difficult than WAXS curves. In WAXS, the atoms are so small that they can be considered as point scatterers. In SAXS, however, the individual domains are not insignificant on the length scale of x-rays, and this scattering must be considered. Scattering due to individual domains is called *form factor scattering*, while scattering due to

the spatial arrangement of the domains is called *structure factor scattering*. The total scattering can be considered as the product of structure and form factor scattering if and only if the domains are spherically symmetric. For a spherically symmetric two-phase system with uniform electron densities in each phase and one phase discretely immersed in a sea of the other, the scattered intensity can be written as [92]:

$$\frac{I(q)}{I_e(q)V} = nV_0^2(\rho_1 - \rho_0)^2 \phi^2(qR)S(q) \tag{8}$$

where $I(q)$ is the scattered intensity at the scattering vector q ($q = 4\pi \sin\theta/\lambda$), $I_e(q)$ is the scattering of one electron if it were the sample, V is the irradiated volume, n is the number density of discrete domains, $(\rho_1 - \rho_0)$ is the electron density difference between the two phases, $\varphi(qR)$ is the form factor scattering, and $S(q)$ is the structure factor scattering. $\varphi(qR)$ has been calculated for a number of common shapes [93].

$S(q)$ is generally not a simple function unless the system is very well ordered. If the system is well ordered, then multiple peaks should appear in the SAXS pattern. The relative spacing of these peaks can be used to tentatively identify the domain packing arrangement. The only TPEs that show multiple peaks are the anionically synthesized materials, and typically only if laboratory processing procedures are used. A great many studies in the literature have used SAXS to study these types of materials; an excellent listing is found in the review papers given earlier.

In commercially important TPEs, a much more featureless pattern is typically found; the most common SAXS pattern from a TPE is a very broad single peak. Bragg's law can be used to calculate an interdomain spacing; of course this calculation is convoluted with form-factor scattering. Two more quantitative approaches are typically applied to the analysis of the data. One approach is to develop a morphological model, calculate the scattering pattern, and change adjustable morphological parameters until the predicted pattern matches the experimental pattern. The second approach is to Fourier

TABLE II Relative Peak Positions in Structure Factor for Common Well-Ordered Morphologies

Arrangement	Relative peak positions
Simple cubic packed spheres	1, √2, √3, √4, √5, √6, √8, √9, . . .
Body-centered cubic packed spheres	1, √2, √3, √4, √5, √6, √7, √8, . . .
Face-centered cubic packed spheres	1 ,1.155, 1.633, 1.915, 2, . . .
Diamond packed spheres	1, 1.633, 1.915, 2.309, 3.416, . . .
Hexagonally packed cylinders	1, √3, √4, √7, √9, . . .
Lamellae	1, 2, 3, 4, 5, . . .

transform the data and calculate a radial distribution function for electron density. A description of these approaches is beyond the scope of this review; the interested reader should examine monographs on the subject [94, 95].

SAXS can be used to study the interfacial region between the two phases. SAXS gives a one-parameter measure of the interfacial thickness if some concentration profile is assumed. In a two-phase system with sharp interfaces, the scattering at high angles will be given by (after background subtraction):

$$\lim_{q\to\infty}\left[q^4\frac{I(q)}{I_e(q)V}\right]=2\pi(\rho_1-\rho_0)^2\frac{S}{V} \tag{9}$$

where S is the total interfacial surface area. The presence of a diffuse interface causes the intensity to fall off more rapidly than a q^{-4} dependence predicted above. Ruland [96] has shown that Eq. (9) is modified as shown below:

$$\lim_{q\to\infty}\left[q^4\frac{I(q)}{I_e(q)V}\right]=[H^2(q)]2\pi(\rho_1-\rho_0)^2\frac{S}{V} \tag{10}$$

$H^2(q)$ has been calculated for sigmoidal and linear [97] concentration gradients. Because of the errors associated with background determination, the use of SAXS to study interface properties should be considered to be relative rather than absolute.

TPE investigations that involve SAXS are numerous. Because the information from SAXS is often ambiguous, the most effective studies are often done in conjunction with a different morphological probe such as electron microscopy or small-angle neutron scattering. Because the number of studies that have used SAXS to study TPEs are far too numerous to list, and in order to give the reader some flavor for SAXS experiments on TPEs, three interesting examples will be highlighted.

Deformed SBS triblock copolymers have been extensively investigated with SAXS [98–101]. However, patterns were collected after these samples were allowed to relax, which has been shown to substantially affect the morphology [102]. The use of synchrotron radiation along with two-dimensional detectors enables intensity measurements while the sample is being drawn. In one such study [103], short polystyrene cylinders were imbedded in a continuous polybutadiene phase. The deformation was found to be affine in the meridional direction until an elongation of 3, which corresponds to the inflection point of the stress–strain curve. Above an elongation ratio of 4, it was shown that the cylinders were aligned with their long axis parallel to the stretch direction. The cylinders were not disrupted up to an elongation ratio of 8.

SAXS determinations of interfacial thickness have been used to show that MDI–BD polyether urethanes exhibit narrower interfaces than polyester urethanes [104]. The difficulty of correct background subtraction has been discussed in detail [105, 106], nevertheless the interfacial thickness assuming a

linear gradient profile was approximately twice as large for the polyester versus the polyether soft segments using two different procedures applied in the same way to the patterns. The absolute magnitude of the numbers must be questioned since other authors have found substantially larger values for similar materials [107, 108].

Small-angle x-ray scattering has been used to follow morphological changes in copolyesters as a function of temperature [109–111]. In order to slow down the crystallization kinetics, 4GT was replaced by poly(tetramethylene isophthalate) (4GI) as the hard segment. Similar to the 4GT systems, the crystallization rate was found to only weakly influence the morphology of these copolyesters. At a fixed temperature, the Bragg spacing increased with decreasing hard segment concentration, and the long spacing was roughly proportional to the inverse of the undercooling. Annealing at temperatures near the melting point led to morphological reorganization through the melting of imperfect crystallites and recrystallization into more perfect crystallites, which was accompanied by an irreversible increase in the Bragg spacing.

5. Small-Angle Neutron Scattering (SANS)

The only difference between SAXS and SANS is that the contrast for neutron scattering is a variation in scattering density rather then electron density. Scattering density is a function of the nucleus (not the atomic number!) and varies in a complex way. Because the difference in scattering density between hydrogen and deuterium is large, isotopic substitution is used to create the contrast required for SANS. Perhaps the most famous use of SANS in polymer science was the experimental verification that polymer chains in the bulk assume an unperturbed random coil conformation [112, 113].

SANS can be used to look at the same sorts of things that SAXS is used for, i.e., domain size, distance between adjacent domains, interphase sizes, etc., and a number of studies have used SANS in this manner. However, SANS has a capability unrealizable with SAXS: if a fraction of the chains in the system contain deuterium, with the rest containing hydrogen, or the reverse is true, then it is possible to examine scattering from individual chains. Therefore in two-phase systems with isotopic substitution, scattering will be from two sources: chain scattering, both interchain and single chain, and interphase contrast. By matching the scattering density of the two phases through partial labeling of one or both phases, it is possible to eliminate scattering due to interphase contrast (which gives information similar to SAXS) and study only single-chain scattering. Since the amount of phase mixing is unimportant (assuming no volume change upon mixing) and the compositions of the pure phases are well known in most TPEs, contrast matching is relatively easy to perform. Methods have also been developed for noncontrast matched systems to isolate the single chain scattering by subtracting the interdomain scattering, using either SAXS or unlabeled SANS patterns [114].

For a two-phase system where interphase scattering has been eliminated and only one phase has been partially labeled, the coherent scattering intensity can be written as:

$$I(q) = \left[\frac{(\Delta\beta)^2 m_0}{\rho_m N_A} \right] v_l v_d (1 - v_d) N S(q) \tag{11}$$

where $\Delta\beta$ is the coherent neutron scattering length density difference between the fully hydrogenous and fully deuterous materials, v_l is the volume fraction of the labeled phase, v_d is the volume fraction of deuterous material in the labeled phase, N_A is Avogadro's number, m_0 and N are the monomer molecular weight and number of repeat units respectively, and $S(q)$ is the single-chain scattering function. Further review of SANS theory and experimental studies of polymers is found in monographs on the subject [115–117].

The effect of temperature and composition on chain conformation has been investigated in MDI–BD–PPO polyurethanes [118], 4GT–PTMO copolyesters, and MDI–BD–PTMO polyurethanes [119–122]. At room temperature, R_g, of the soft segments in the polyurethane, TPEs are approximately 25% larger than in bulk, while for the copolyester the increase is only approximately 10%. The soft segment radius of gyration decreased as the temperature increased above room temperature for the all materials except for a MDI–BD–PTMO material at a 7:6:1 mole ratio. Evidence of phase mixing was found when the temperature reached a high enough value for all materials except the 7:6:1 material as evidenced by an increase in R_g of the soft segment with temperature. SANS measurements of the 4GT segments indicate that substantial chain folding occurs in the copolyesters. The hard segment R_g in the copolyester increased dramatically with temperature, which indicated that the amount of chain folding and/or the degree of phase separation was changing. The hard segment R_g decreased as the temperature was raised in the 7:6:1 polyurethane, which the authors were unable to satisfactorily explain. Measurements of the entire chain dimensions in the copolyesters indicated that the chain initially contracted then expanded as the temperature was raised.

In lamellar styrene–diene diblock copolymers, SANS studies showed that the segment R_g contracts to 70% of the unperturbed value parallel to the interface and expands to 160% of the unperturbed value perpendicular to the interface [123, 124]. These values were found for both the styrene and diene blocks. A study of stretching SIS block copolymers having spherical styrene phases showed that the deformation in the direction of stretch was greater than affine, while the deformation perpendicular to the stretch was much less [125].

6. Nuclear Magnetic Resonance (NMR)

Solid-state NMR has the capability of providing information on a wide variety of characteristics in TPEs, encompassing both static and dynamic properties as well as orientation information. As mentioned previously, NMR can

be used to determine chain microstructure information such as tacticity and sequence distributions. NMR has been used in TPEs to investigate spatial interactions between atoms as well as the relative mobility of particular segments. Deuterium labeling significantly expands the capabilities of NMR. Using pulse sequences, relaxation times of segments on different time scales can be probed. Given its capabilities, the information gained from this technique, although significant and important, has not been as great as one might expect because of the extreme difficulty in spectral interpretation.

NMR measures change in the spin magnetic moment of nuclei. A strong magnetic field (~10^5 Gauss) along one axis, usually taken as the z direction, causes a net population distribution of nuclear spins aligned parallel to the magnetic field. Polarized electromagnetic energy in the radiofrequency region (10^2 MHz) with the magnetic field vector perpendicular to the z direction causes transitions to a higher energy spin state. A voltage that is proportional to the relaxation of nuclei from the higher energy state to a lower energy state is measured as a function of electromagnetic radiation frequency in typical NMR experiments. However, chemical shift rather than frequency is reported where chemical shift is defined as

$$\frac{v(sample) - v(standard)}{v(standard)} \tag{12}$$

where v represents frequency and the standard is a material that contains the same atomic species. Only nuclei with nonzero spin quantum numbers can be studied with this technique. In TPEs, the most common nuclei that fulfill this requirement are ^{1}H, ^{2}D, and ^{13}C.

The chemical shift, which is due to electronic shielding by atoms in the surrounding environment, is generally anisotropic in solids. Three other anisotropic interactions can occur in solid-state NMR: dipole–dipole interactions, which is a through-space interaction with other nuclei; spin–spin coupling, which is a through-bond interaction of two spins; and the quadropole interaction, which occurs when the spin quantum number is greater than $\frac{1}{2}$ and generally obscures the spectrum if present. Due to the fast tumbling of the molecules in solution, the dipole–dipole interactions and the quadropole interaction generally vanish, leaving the isotropic chemical shift and the spin–spin interaction. Much of solid-state NMR involves creating experimental conditions that reduce or eliminate some of these inherent complications.

In order to remove anisotropic interactions, a technique called "magic angle spinning" (MAS) is used. Solid interactions have an approximate angular dependence of $(3\cos^2\theta - 1)$, where θ is the angle between the z-direction and the sample. If a sample is spun around its axis and the axis is at the magic angle with respect to the magnetic field ($\theta \approx 54.7°$), then much of the anisotropy is removed. If the rotation frequency is less than the characteristic frequency of the averaged interaction, then spinning sidebands will appear at integral multiples of the spinning speed. Usually, solid-state NMR spectra are

obtained at two or more rotation speeds to identify the true features. Other interactions can be removed using radiofrequency pulses. High-power proton decoupling removes proton dipole–dipole and spin–spin coupling to different nuclei, such as ^{13}C. Cross polarization enhances magnetization of rare spins from abundant spins. ^{13}C nuclei are often enhanced using ^{1}H.

Radiofrequency pulses are also utilized to measure relaxation times. Three relaxation times have been measured in TPEs, and each is sensitive to different phenomena. T_1, the spin–lattice relaxation time in the laboratory frame, is the relaxation from the nonequilibrium population distribution created by the pulse to the equilibrium Boltzmann distribution. T_1 is sensitive to molecular motions that rate in the range of 10^6–10^9 Hz. T_2, the spin–spin relaxation time, is the relaxation caused by the establishment of equilibrium between nuclear spins within the system. Spin–spin relaxation measurements also probe motions with rates in the range of 10^6–10^9 Hz; however, low frequency motions (10^2–10^3 Hz) also affect T_2. Generally, T_2 is one to three orders of magnitude smaller than T_1 in solid polymers. $T_{1\rho}$, the spin–lattice relaxation time in the rotating frame, probes motions with rates on the order of 10^3–10^4 Hz. Cross polarization is usually used in $T_{1\rho}$ measurements.

T_2(H) measurements have been made with a series of SBS block copolymers with styrene contents between 14 and 30% [126]. Three different T_2 relaxation processes were found: a fast relaxation due to hard segment material, an intermediate relaxation due to interfacial material, and a slow relaxation due to soft segment material. T_2 for the interface was approximately two orders of magnitude greater than for the hard segment, while T_2 for the soft segment was approximately one order of magnitude greater than for the interfacial region. T_2 for the soft butadiene phase was smaller than T_2 for the pure rubber, which indicates that copolymerization restricted the mobility of the butadiene. In all cases, less material was found in the styrene phase than would be predicted; however, the approximate stoichiometric amount of material was found in the butadiene phase. Interfacial calculations showed that the interface consisted predominantly of butadiene segments, therefore a substantial amount of styrene must be dissolved in the butadiene. The thickness of the interface was calculated as 20 Å, which agrees roughly with SAXS results on similar systems [127, 128].

NMR can be used to look at the two phases and the interface of a TPE through deuterium labeling. Spiess *et al.* [129, 130] analyzed a series of model polyurethanes based on a monodisperse piperazine hard segment shown in Fig. 11. The synthesis was very carefully controlled so that only specific units in the hard segment were labeled. The area of the narrow component relative to a broad NMR signal was used to quantify the fractional amount of piperazine units that were mobile, which was termed the motionally averaged component (φ_{MA}). The motionally averaged component depended on the position of the piperazine unit in the hard segment, as shown in Fig. 11. Based on studies with materials containing only single piperazine units, the premature rise of

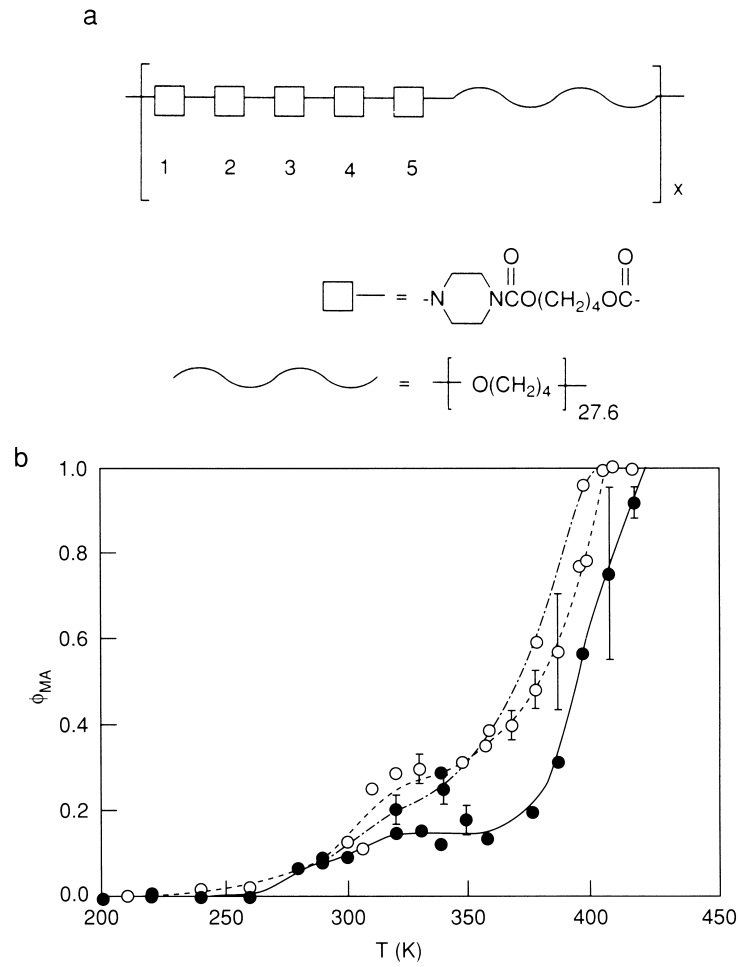

FIGURE 11 (a) Structure of piperazine-based polyurethanes. Deuterium labeling was only on piperazine units 1 and 5, or only on rings 2 and 4, or only on ring 3. (b) Fraction of motionally averaged material φ_{MA} as a function of temperature. ● piperazine at the center (third ring), ◊ at the second and fourth ring, ○ at the outer (first and fifth ring).

the motionally averaged component of the three curves between 250°K and 300°K was assigned to piperazine units dissolved in the hard segment. Based on this assumption, the authors calculated that only 15% of the hard segment was dissolved in the soft segment, while the remaining 85% was contained within the hard segment domains.

The quadropolar characteristic of deuterium was used to study molecular motions in 4GT–PTMO where the two interior carbons on the PTMO were replaced with deuterium [131]. Previous ^{13}C NMR experiments by the

same author [132, 133] showed that the 4GT groups could be thought of as molecular anchors because the motions of these groups occurred on a much slower time scale. The shape of the NMR curve after a series of pulses was used to follow three-bond types of motion by the methylene sequences in PTMO. An activation energy of 5.8 kcal/mol was calculated for the motion, which is slightly greater than one C–C bond rotation in butane (3.7 kcal/mol). Six different trans-gauche conformational transitions were presented and based on NMR data; four of these possibilities were eliminated so that only two remained, as shown in Fig. 12. The authors argued that both of the remaining mechanisms may contribute to the observed motion.

A number of relaxation times were measured on MDI–BD–PTMO polyurethanes and a MDI–PTMO commercial polyurethane that is chain extended with ethylene diamine (ED) in order to differentiate the interfacial, hard segment, and soft segment phases [134–136]. It was shown that T_1(C) and $T_{1\rho}$(C) measurements distinguish between hard segments dissolved in the soft phase and hard segments in the hard phase for the BD chain extended material, while $T_{1\rho}$(C) measurements for the ED chain extended material can distinguish between carbonyls located in all three regions. Eleven percent of the urethane groups were dissolved in the soft segment in the 7:6:1 MDI–BD–PTMO material, while only 20% of the MDI units were crystalline. In the ED material, it was found that 50% of the hard segments were able to move as free rotors, which suggests that the degree of phase separation is poorer in this material than in the MDI/BD material. Since poly(urethaneureas) generally show better phase separation than polyurethanes [137], this result was probably due to effects such as sample preparation method and starting materials. Variable temperatures were studied using a polymethylene adipate soft segment instead of PTMO, and it was shown that the mobile phase component of the hard segment increases with increasing temperature. The amount of increase depended on the composition of the polyurethane, which the authors attributed to the imperfection of the hard domains [138].

IV. PROPERTIES AND EFFECT OF STRUCTURE

A. General Characteristics

Table III lists the properties of some typical thermoplastic elastomers and other common rubbery polymer materials. TPEs generally extend to high elongations without failure and have a high tensile stress at break, i.e., they are extremely tough. As mentioned earlier a thermoplastic elastomer should return to its initial shape after the removal of the stress. The range of extensibilities where a TPE will recover its original shape after stress is removed will generally not be as large as for conventional crosslinked rubbers. At high elongations upon the removal of stress, TPEs will often maintain some

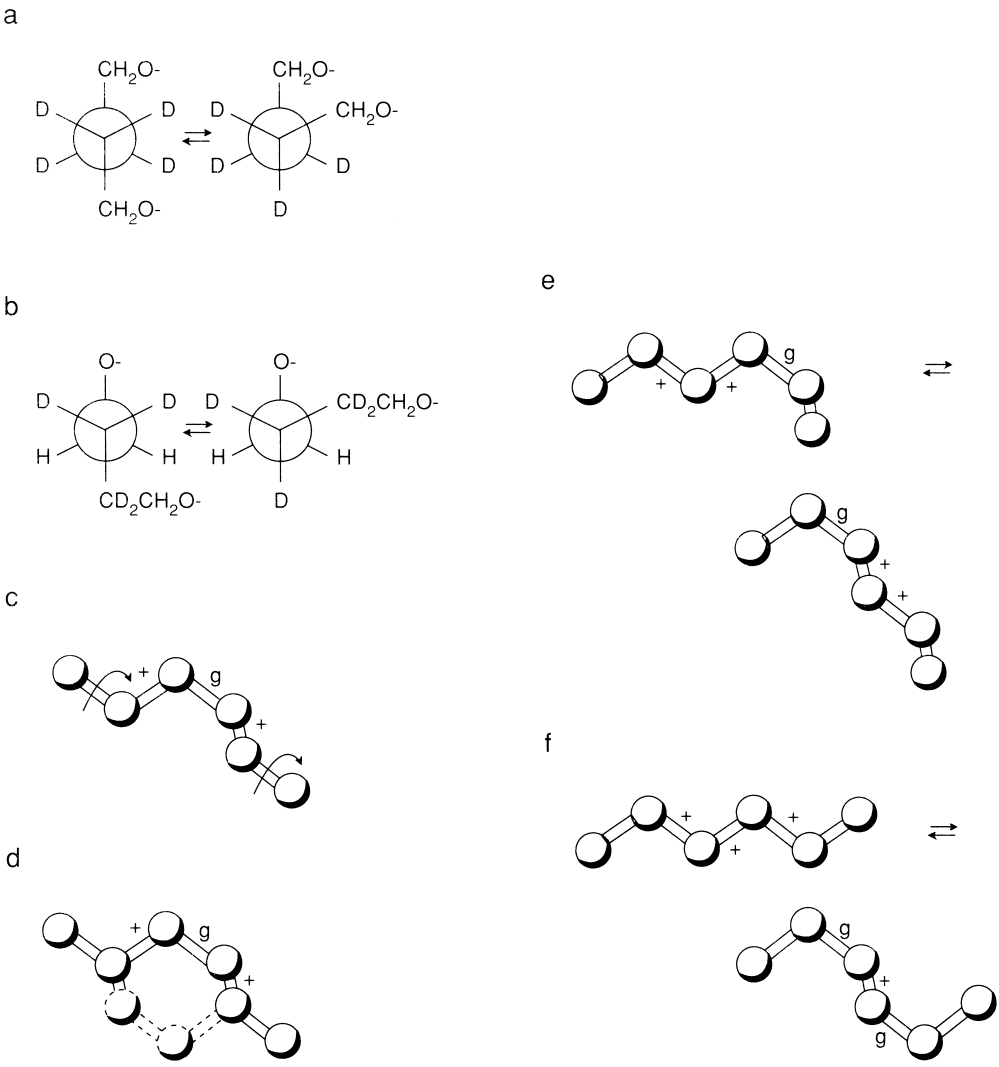

FIGURE 12 Possible mechanisms for PTMO trans-gauche conformational changes in 4GT–PTMO. Only (e) and (f) were found to be consistent with NMR results.

residual elongation, termed *permanent set*. As discussed in the section on infrared spectroscopy, the domains can flow under high stress. The toughness of these materials (area under stress–strain curve) is usually many times that of conventional crosslinked rubbers.

The Mullins effect [139], also called stress softening, occurs in most TPEs. If a TPE sample is strained and then released, then less stress will be required

TABLE III Properties of Typical TPEs Relative to Other Rubbery Polymers

Material	Relative cost	Tensile strength at break (MPa)	Tensile strain at break (%)	Service temperature (°C)	Hardness (Shore A)
Styrene–butadiene rubber	1	15 (reinforced)	500 (reinforced)	high	35–100
Natural rubber	1	30 (reinforced)	500 (reinforced)	high	30–100
Silicone	1.2	5 (reinforced)	150	high	40–100
Polyethylene	1	10	high	–10–50	100
Fluorinated elastomer	1.5	10	200	high	50–90
SBS	2	25	800	–20–80	50–90
Polypropylene–EPM blend	1.5	20	500	0–110	70
Polyurethane	6	50	600	–20–80	50–100
Copolyester	7	40	600	–40–150	>100
Ionomer	5	15	500	–20–100	50–90

to strain the sample a second time. This effect is generally quantified by the hysteresis energy, which is the difference in the areas under the stress–strain curve for a loading cycle followed by an unloading cycle. The Mullins effect can lead to heat buildup in a material, which is undesired in most applications. However, the ability of a TPE to dissipate energy is related to its strength and toughness.

Fracture of a polymer involves initiation, slow crack growth, and catastrophic crack propagation. The extreme toughness in thermoplastic elastomers is due to the inhibition of catastrophic failure from slow crack growth rather than the prevention of initiation or prevention of slow crack growth. Table IV lists the mechanisms that can strengthen two phase materials. The hard domains in TPEs act as both filler and intermolecular tie points. Hard domains are effective fillers if the volume fraction exceeds 0.2, their size is less than 100 nm, and the softening temperature is well above the test temperature [140]. The filler effect is one key for the extreme toughness inherent in most TPEs. Another key is the interface between the hard and soft segments; in polymer blends [141], it has been hypothesized that the strongest materials result from two polymers on the edge of miscibility. These results suggest that broad interfacial zones lead to improved properties in two-phase block copolymers.

Due to the dual filler and crosslinking nature of the hard domains in TPEs, the molecular deformation process is entirely different than the Gaussian network theories used in the description of conventional rubbers. Chain

TABLE IV Strengthening Processes in Polymers[43]

Matrix	Dissipation of energy near crack tip
	Strain-induced crystallization
	Orientation processes
Filler particles	Increased dissipation of energy
	Deflection and bifurcation of cracks
	Cavitation
	Deformation of domains

entanglements, which serve as effective crosslinks, play an important role in governing TPE behavior. The stress–strain results of most TPEs have been described by the empirical Mooney–Rivlin equation:

$$\sigma = \left(\frac{\rho RT}{M_c} + \frac{2C_2}{\lambda} \right) \left(\lambda - \frac{1}{\lambda^2} \right) \tag{13}$$

where σ is the stress (force/unit area), R is the universal gas constant, T is the absolute temperature, λ is the extension ratio, and M_c is the average molecular weight between crosslinks. C_2 is an empirical constant that depends on the material. Stress-strain and swelling measurements have shown that M_c is closer to the molecular weight between entanglements than the soft segment length in SBS [142]. The filler effect is quantified by the Guth–Smallwood equation:

$$\frac{E_F}{E} = (1 + 2.5\phi + 14.1\phi^2) \tag{14}$$

where E_F/E is the ratio of the moduli for the filled and unfilled elastomer and φ is the volume fraction of filler. Combination of these two equations gives reasonable values for M_c in SBS copolymers; however, objections have been raised to using this analysis [143–145]. More complicated theories have been proposed to explain the stress–strain behavior of thermoplastic elastomers [146–148].

The general tensile behavior of TPEs as the temperature changes is shown in Fig. 13. TPEs become more rigid as the temperature nears the soft segment T_g, and a discontinuous change in brittleness will occur at this temperature. Normally, the soft segment T_g is never reached in service, i.e., this temperature is far below room temperature. As the temperature rises in a typical TPE, the modulus and strength decrease slightly due to softening of the hard domains. At the hard segment dissolution temperature, the modulus will decrease dramatically, and the material can no longer be used as a thermoplastic elastomer. The two-phase structure may persist in the melt however. The precise temperature of the dissolution depends on the nature of the hard block. Plasticizers or other additives may be added to reduce the softening temperature; however, these materials will also tend to disrupt the domain structure.

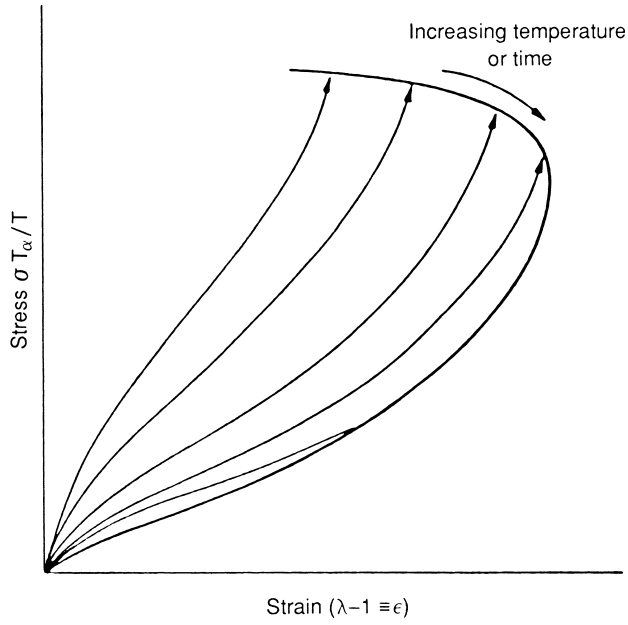

FIGURE 13 Effect of temperature and draw rate on the stress–strain curve of thermoplastic elastomers. δ is stress, T_o is some reference temperature, T is the test temperature, λ is the draw ratio, and ε is the strain. (From Petrovic and Ferguson [15].)

The chemical resistance of many TPEs is poor compared to that of conventional rubbers. Polyurethanes, copolyesters, and copolyamides are very susceptible to oxidation, especially at elevated temperatures. Antioxidants and other additives are added to commercial products to improve the chemical resistance of these materials. Carbon black can be added to improve stability to UV light if the color of the material is unimportant. Hydrolytic stability is poor for the polyester-based polyurethanes and the copolyamides because the ester linkage can be attacked by water. For all TPEs, certain organic solvents can degrade these materials if one or both of the blocks will dissolve in the particular solvent. The resistance to many common oils and greases is high for the more polar TPEs.

B. Mechanical Properties

Because the structures of TPEs are diverse, the influence of structure on mechanical properties may not be universal for all materials. Nevertheless, some general characteristics do hold for most TPEs, and these traits will be highlighted in this section.

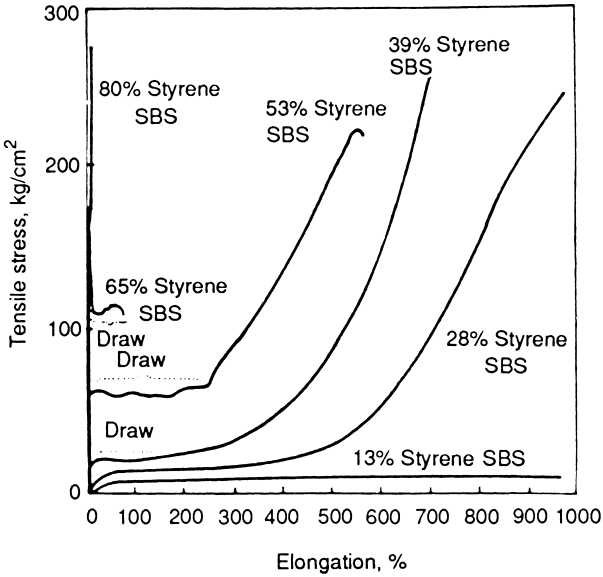

FIGURE 14 Tensile properties of SBS as a function of styrene content.

The relative amount of hard and soft segment influences the mechanical behavior of TPEs. As the hard segment content increases, the material will change from a flexible rubber to a tough, rigid plastic. This is illustrated in Fig. 14, which shows tensile curves for SBS as a function of styrene content. Similar data has been presented for 4GT–PTMO copolyesters and polyurethanes. TPEs also show a qualitative change in the shape of tensile curves as the hard phase changes from discrete to continuous. The yield point at approximately 40% styrene content has been interpreted as evidence of a continuous polystyrene phase; usually the existence of a yield point in a TPE implies a continuous hard phase. Altering the relative amounts of hard and soft segments in a material can be accomplished either through changing the hard segment length, soft segment length, or both. The effect of segment length has been investigated at constant relative amounts of hard and soft segment. In the styrene–diene triblock copolymers, the tensile properties do not depend on segment lengths as long as the polystyrene is of sufficient molecular weight to form strong hard domains (>8000) [149]. However, the molecular weight of the blocks will influence the kinetics of phase separation in styrene–diene systems, which can in turn affect the mechanical properties.

In polyurethanes, copolyesters, and copolyamides, the molecular weight of each block is a key factor in determining the mechanical properties of the material. Soft segment block lengths between 1000 and 5000 have been found to produce materials with optimum properties. Below this value, the

materials are unable to adequately phase separate. Lower molecular weights also inhibit the ability of the soft segment to strain crystallize, which provides an important strengthening mechanism. Finally, lower molecular weight soft segments at a constant overall soft segment content requires short hard domains, which can severely reduce hard domain crystallization. Higher soft-segment molecular weights introduce practical problems. Since these materials are synthesized industrially in the bulk (without solvent), high molecular weight soft segments result in extremely high viscosities during polymerization, which leads to mixing and pumping difficulties as well as problems in achieving high conversions. Also, higher molecular weight blocks promote phase separation, which will reduce fractional conversion. Since all step-growth polymerizations require high fractional conversions in order to achieve high molecular weights, high molecular weight segments are used with difficulty. The effect of hard segment block length is also important. Longer hard segment blocks generally lead to better phase separation and better properties. However, at the same relative hard segment fraction, longer hard segment blocks contribute to difficulties in synthesis. Some of these difficulties can be overcome with solution polymerization methods, which may or may not lend themselves to commercial scale synthesis.

The overall molecular weight can be altered in TPEs. The overall molecular weight, as long as it is greater than some threshold value, has little effect on the mechanical properties. Two important cases can occur where the overall molecular weight is important. If soft segments in multiblock copolymers are used and have low functionality, then the resulting molecular weight distribution will be quite broad, and the properties will be reduced substantially [150]. Most industrially important soft segments have a functionality near 2, so this effect is usually not important. However, of more importance, especially in polyurethanes, is the possibility of side reactions that can lead to network formation. A small amount of crosslinking can actually improve the properties [151], which is presumed to occur through strengthening of the hard domain. Large amounts of crosslinking are undesired since crosslinking can inhibit phase separation and increase the brittleness of the TPE.

The effect of hard and soft segment polydispersity has been investigated in different polyurethanes [25, 152, 153]. Soft segment polydispersity does not significantly alter the mechanical properties, while materials with monodisperse hard segments have a higher modulus and increased tensile strength. An important underlying assumption of these studies is that the soft-segment molecular weight distribution is unaffected by synthesis, which was recently proven to be the case using a novel analytical technique [154]. The improved mechanical properties can be attributed to improved phase separation as shown in synchrotron SAXS studies [155]; better packing of the hard segments may also be playing a role.

A parameter that can be easily changed, which can have a dramatic effect on the properties, involves the constituents of the TPE. In SBS triblock poly-

mers, this includes changing the center block to isoprene or the end blocks to α-methyl styrene. In the first case, the mechanical properties are unaffected except that in SBS the tensile strength depends on the styrene content, while in SIS the tensile strength does not vary with styrene content. Substitution of α-methyl styrene leads to a tougher polymer, which is at least partially due to the higher glass transition (160°C vs. 100°C) of the new endblock. Even though T_g for isoprene and butadiene differ substantially, no corresponding effect due to the different glass transition temperature is found in the mechanical properties of the TPEs [156]. This difference emphasizes the importance of the hard phase in determining the mechanical properties of the material.

For the segmented block copolymers such as the polyurethanes or copolyesters, the composition of the hard segment or the soft segment can also easily be changed. Changing hard segment type will change the crystallinity of the hard phase. For example, copolyesters can be produced using a mixture of tetramethylene terephthalate and another diacid, such as tetramethylene isophthalate, rather than just pure tetramethylene terephthalate. As shown by Witsiepe [17], the ultimate properties of the mixed hard segment material are better if the total hard segment content is low, with little effect on hardness or stiffness. The disadvantage of using mixed acids is that crystallization is limited and proceeds much more slowly. In polyurethanes, symmetric diisocyanates produce stronger TPEs. The presence of substituents on the aromatic ring tends to reduce the tensile properties of polyurethanes. In BD–polyester polyurethanes, the following diisocyanates give tensile strengths according to the following: MDI > hexane diisocyanate > isophorone diisocyanate > toluene diisocyanate (TDI) [157].

Soft segment type also plays an important role in the physical properties of multiblock copolymers. Soft segments that strain crystallize produce tougher materials with higher tensile strengths and tear resistance [158]. Since incorporation into a block copolymer reduces crystallization kinetics and slightly lowers the melting temperature, the unstrained elastomer may not contain any soft segment crystallites. Upon deformation, crystallization may occur, which will cause a large permanent set in the material. An upturn in the tensile curve at high elongations is often taken as evidence of crystallization, but WAXS provides the most direct and conclusive evidence. Soft segments that strain crystallize generally have a melting point slightly above the service temperature, and higher soft segment molecular weights favor strain crystallization. PTMO and polycaprolactone are two common soft segments that can strain crystallize.

Soft segment type also influences the driving force for phase separation. However, improved phase separation does not necessarily lead to improved properties, since both polyether [55] and polybutadiene soft segments generally show more complete phase separation than polyesters, yet the polyester-based materials have better mechanical properties. The most likely explanation for this result is poor interfacial adhesion in well-phase-separated systems [159].

C. Thermal and Chemical Properties

The response to changes in thermal or chemical environment is largely the result of the underlying chemical structure of the material. As discussed in the introduction, lack of resistance to chemical or thermal stimuli limit the use of TPEs, especially as compared to conventional rubbers. Unfortunately it is difficult, if not impossible, to modify thermal and chemical characteristics substantially. The use of small amounts of antioxidants or fillers can improve these properties somewhat, but the overuse of these materials can result in a large change in mechanical behavior.

The sensitivity to hydrolysis is a key issue in many applications. The ester bond in 4GT–PTMO copolymers is sensitive to hydrolysis; however, it is fairly protected since most of the ester is contained in a crystalline structure. The addition of a small amount (1–2%) of a hindered aromatic polycarbodiimide substantially increases the lifetime of this material in the presence of hot water or steam [160]. Polyurethanes are susceptible to hydrolytic attack, especially those with polyester soft segments. However, polyester soft segment polyurethanes are generally more resistant to oils, organic solvents, and thermal degradation. Ionomers will swell when exposed to water; in fact, a commercial hydrated perfluorosulfonic ionomer (Nafion) is used as a membrane separator in chlor–alkali cells. Styrene–diene copolymers and polyolefin TPEs are insensitive to water.

The ability of a TPE to withstand variations in temperature depends almost entirely on the chemical structure. The maximum service temperature is usually about 40°C below the hard segment glass transition or melting temperature. Because of hysteresis, excessive heat buildup can occur during use so that the local temperature of the material can be much higher than the nominal temperature. Changing the maximum service temperature involves changing the structure of the hard block. Using α-methyl styrene in styrene–diene triblock copolymers or ethylene diamine chain extenders in polyurethanes can extend the service temperature in these TPEs substantially. The minimum service temperature is usually about 10°C above the soft segment T_g. Below this temperature, the material will become brittle. If the soft segment can crystallize, then low temperatures can cause crystallization and a corresponding increase in stiffness and brittleness. Using a mixed or copolymer soft segment will eliminate this problem, but at a cost of reducing strain-induced crystallization at higher temperatures.

V. THERMODYNAMICS OF PHASE SEPARATION

This section will present the theoretical framework and understanding about the thermodynamics of phase separation in block copolymers. Most theories consider four factors that influence the phase separation of block copoly-

mers: (1) the Flory–Huggins interaction parameter χ, (2) the overall degree of polymerization N, (3) architectural constraints such as the number of blocks and linear vs. starblock polymers, and (4) the weight fraction f of one component. The thermodynamic theories are conveniently divided into three cases: the strong segregation limit (SSL), the weak segregation limit (WSL), and the intermediate segregation region (ISR). In the SSL, the equilibrium state of the material consists of relatively pure phases of A separated from relatively pure phases of B. In the WSL, the two phases are intimately mixed. The ISR is essentially a region that arises because of finite molecular weight; in the case of infinite molecular weight no ISR exists. Whether the ISR should be considered as part of thermodynamic phase space is questionable.

The transition between the WSL and the SSL is termed the order–disorder transition (ODT), which is also called the microphase separation transition (MST). The analogous transition in small molecules is the solid-to-liquid transition. The reader should be aware of the order–order transition (OOT), which is a shift of morphology from one type to another (e.g., spheres to cylinders), that can occur with changes in temperature in anionically synthesized block copolymers at very specific block lengths [161]. If the ODT temperature is below the hard segment T_g or T_m, then the material is one phase above the hard segment dissolution temperature. If the ODT temperature is above the hard segment T_g or T_m, then the material will exist as a two-phase melt. The phase state of a TPE above the dissolution temperature has a substantial effect on the rheological properties since one-phase mixtures have a viscosity much smaller than two-phase mixtures.

A great deal of effort has been spent on developing theories for diblock or triblock copolymers, much of which has been driven by the measurement of phase diagrams, which in turn provide good tests of theories. It should be noted that the rigorous application of these theories to TPEs used in commercial applications is limited, since in nearly all systems some arrest due to slow kinetics occurs. The most rigorous theories were developed for monodisperse block lengths, e.g., anionically polymerized TPEs. In some cases these theories have been extended to multiblock copolymers that have a distribution of block sizes. Further, amorphous systems have had a significantly larger focus on them than crystalline systems.

In the WSL, the chain configuration is unperturbed; e.g., R_g scales as $N^{1/2}$. However, the probability of finding an A or a B segment at a distance r from a particular point does not only depend on f, it also depends on whether the original point sits on an A or B segment. If the original point lies on an A segment, then at short distances the probability is much higher of finding another A segment and at distances comparable to the chain's radius of gyration, the probability is higher of finding a B segment. This concept is called the correlation hole effect [162]. At extremely large distances, the probability of finding an A segment reduces to the volume fraction of A segments in the WSL. The chains generally do not assume their unperturbed conformation in

the SSL. The probability of finding a segment at a distance r depends strongly on the type of morphology and can also have a directional dependence, whereas in the WSL the probability is isotropic.

The theoretical development of Helfand and Wasserman [163–167] contains all the necessary ingredients for a complete description of phase separation in the strong segregation limit; in fact, the theory has been modified slightly so that the results are considered to be quantitatively reliable [168]. Three energetic contributions are included in this theory: (1) confinement entropy loss due to a concentration of AB joints to the interface, (2) conformational entropy loss due to extended chains, and (3) enthalpy due to mixing of A and B segments. An expression is written for a function that is proportional to the probability density that a chain with N segments has one end at r_0 and another at r. The resultant equation is identical to the form for the time-dependent diffusion equation where the differential with respect to time is replaced by a differential with respect to segment. The remainder of the development involves solving this equation with the appropriate boundary conditions. Complete analytical solutions have not been derived, but numerical solutions to the equations have been calculated. This theory was originally developed for diblock copolymers and has been extended to triblock systems.

The interfacial thickness (t) was predicted to be approximately equal to the following:

$$t = 0.816a\chi^{1/2} \tag{15}$$

where a is the statistical segment length. This equation predicts that the interfacial thickness is independent of molecular weight. In the limit as $N \to \infty$, the domain spacing D was found through numerical analysis to scale as:

$$D \sim aN^{9/14}\chi^{1/7} \tag{16}$$

In this limit, the confinement entropy of a junction is insignificant compared to the stretching entropy of the chain. Numerical predictions of the predicted periodicity have been made for diblock and triblock copolymers for the cylindrical, spherical, and lamellar morphologies. In general, the agreement between the theoretical predictions and the experimentally observed results have been good for cylindrical and lamellar systems, while not as good for spherical systems. Because spheres are isolated, changes in domain size can only occur by transport of segments through an incompatible matrix, which provides a substantial diffusional resistance to changes in morphology. Hence, the morphology tends to not change once it is formed, and the agreement between theory and experiment is poor [169]. Numerical procedures were given for predicting the phase diagram including calculation of the underlying morphology (spheres, cylinders, etc.) as a function of composition. The underlying morphology type was predicted to be almost temperature independent.

Numerous studies were completed on block copolymers in the SSL long before a theory of the detail inherent in the Helfand and Wasserman approach

existed. In the WSL, experiments have been driven by the mean-field theories originally outlined by Leibler for diblock copolymers with monodisperse blocks [170]. This method uses the random phase approximation [171] (RPA) to calculate the free energy in terms of an order parameter $\psi(r)$ which describes the average deviation from the uniform distribution at any point r. The thermodynamic state of the material was found to depend only on χN and f, just as in the Helfand and Wasserman approach. Only three two-phase morphologies are predicted from this model: body-centered-cubic packed (bcc) spheres, hexagonally-closest-packed (hcp) cylinders, and lamellae. Since χ depends on temperature, the morphology can be changed from spheres to cylinders or lamellae simply by changing temperature, in contrast with the Helfand and Wasserman theory, which predicts the underlying morphology is independent of temperature. A critical point (second-order transition) is predicted at $\chi N = 10.495$ for the symmetric diblock copolymer, which also corresponds to the minimum χN that divides the ordered and disordered state. Since the point of demixing for two homopolymers of identical molecular weight is $\chi N = 2$, the joining of two individual chains at the ends means that the individual chains need to be over 2.5 times as long in the diblock copolymer than in the homopolymers to phase separate.

Leibler's theory outlined an experimental method for testing its conclusions. The structure factor for scattering of radiation by the disordered phase was given by:

$$\frac{1}{S(q)} = \frac{F\left[(qR_g)^2, f\right]}{N} - 2\chi \tag{17}$$

where F is a dimensionless function that is related to the Debye correlation function of a Gaussian chain. A Lorentzian peak is predicted for the disordered phase. The position of the peak maximum at q^* does not change with temperature. The periodicity of the concentration fluctuations is given by $2\pi/q^*$, which is approximately the radius of gyration of the chain. The height of the peak is a function of temperature because of changes in χ. Generally, χ has been found to depend on temperature according to the following:

$$\chi = \frac{A}{T} + B \tag{18}$$

where A and B are empirically determined constants. According to the above analysis, a plot of 1/peak intensity in SAXS or SANS experiments vs. reciprocal temperature should be linear when the polymer is in the disordered state. Deviation from linearity will mark the order–disorder transition temperature, while an extrapolation to zero intensity will allow the calculation of the spinodal decomposition temperature. The ODT according to this theory can also be determined from the temperature where q^* changes as a function of temperature since q^* is predicted to be independent of temperature in the disordered state.

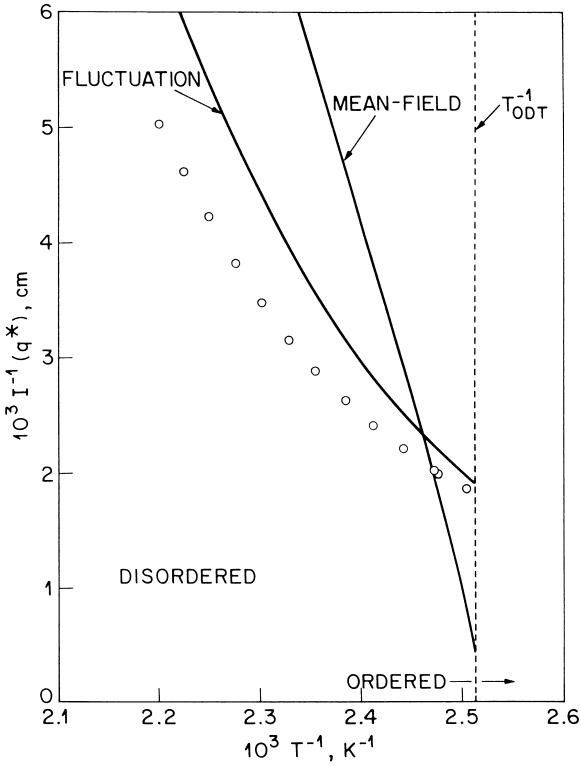

FIGURE 15 Comparison of 1/SANS peak intensity vs. inverse temperature for PEP–PEE diblock copolymer and comparison to theory.

The WSL theory developed by Leibler has been shown to be incorrect because of deviations from the fundamental underlying mean-field assumption. Figure 15 shows experimental results for a poly(ethylene-propylene/ethylethylene) (PEP–PEE) diblock copolymer that has been fit to the predictions of the Leibler theory without any adjustable parameters, since the ODT and χ were calculated from rheological measurements [172]. This mean-field theory does not qualitatively describe the behavior of this material. Other experiments have indicated that the RPA approximation [173] and the Gaussian coil assumption [174, 175] are inaccurate near the ODT.

In the original analysis, it was understood that this theory should not be applied near the critical point. Mean-field theories ignore concentration fluctuations at distances other than $q = q^*$. Near the critical point, concentration fluctuations on very large length scales become increasingly important. A modification to this theory that includes concentration fluctuations has been developed [176]. A critical point is not predicted by the fluctuation theory, rather a

first-order phase transition is predicted for all compositions. A molecular weight dependence is found for χN, which delineates the ordered from the disordered phase shown below for the symmetric diblock copolymer:

$$\chi N = 10.495 + 41.022 N^{-1/3} \tag{19}$$

The minimum χN value corresponding to the disordered phase still occurs at $f = \frac{1}{2}$. The fluctuation theory predicts an ODT at a slightly lower temperature than the Leibler theory. The lamellar and hcp cylinder phases are directly accessible from the disordered state, which seems to be confirmed by experiment, rather than having to pass through the bcc sphere phase as in the Leibler theory. The rather simple structure factor presented in Eq. (17) is retained; however, χ is replaced with a χ_{eff} that depends on temperature, composition, and molecular weight in a complicated manner. At temperatures slightly above the ODT, a partially ordered morphology is predicted. Figure 15 also compares the results of experiment with the fluctuation theory without any adjustable parameters. The qualitative shape of the experimental data is described better by the fluctuation theory; however, quantitative agreement is still not found.

The previously discussed theories were developed for monodisperse diblock copolymers, which are not TPEs. However, Leibler's mean-field theory has been extended to include polydispersity [177] and to include triblock, star, and graft copolymers [178, 179]. In the former case, polydispersity corrections tend to lower χN corresponding to the ODT. As would be expected from the analogy between blends and diblocks, triblocks will phase separate at higher χN values than the corresponding diblocks. This theory predicts a monotonic increase in the critical value of χN as the symmetry of the triblock increases, to a maximum of about 18 for the symmetric triblock. Surprisingly, the minimum χN value that separates the order and disordered regions in triblocks does not necessarily correspond to the critical point.

The development of the mean-field theory for triblocks is very similar to the approach followed by Leibler. A second parameter, τ, defines the asymmetry of the triblock. If the block copolymer is labeled ABA, then starting at the center of the B block, τ is the fraction of A units going in one direction along the chain divided by the overall number of A units in the copolymer. By convention, τ is always less than 0.5, so $\tau = 0$ defines a diblock copolymer, while $\tau = 0.5$ is a symmetric triblock. f is defined as the overall fraction of A units in the triblock copolymer. For all τ values, a critical point is predicted at a certain composition and χN. The critical point does not occur at $f = 0.5$ like in the case of symmetric materials, rather the copolymer composition at the critical point is a function of τ. The ordered phase following the ODT is bcc spheres followed by hcp cylinders and finally lamellae except at the critical point. The same experimental methods and analysis that are used for diblock copolymers can also be used for triblocks. q^* seems to be weakly temperature dependent, and the qualitative shape of the scattering curve is different

because of an upturn at low q [180]. The difference in the ODT temperature between the diblock PEE–PEP and the triblock PEP–PEE–PEP was 72°C, which is near 61°C predicted from the mean-field theories [181].

VI. THERMOPLASTIC ELASTOMERS AT SURFACES

A. General Characteristics

The two phases of TPEs also will affect applications that are sensitive to surface or interfacial properties. Generally, the fraction of a component at an interface can be substantially different than the overall bulk fraction. The presence of an interface introduces another thermodynamic consideration that can also alter the morphology that exists in the bulk of the sample. The compositional and morphological variation depends on the processing conditions that were used to generate the surface, as well as the nature of the other surface. The energetic driving force for these variations is a desire to minimize interfacial energy. The primary parameter that characterizes the interfacial characteristics of a material is the surface tension or surface energy.

Although the two terms are often used interchangeably, strictly speaking the two are not identical. The surface tension is defined as:

$$\gamma = \left(\frac{\partial A}{\partial \Omega} \right)_{V,T,N_i} \tag{20}$$

where A is the Helmholtz free energy of the entire system, Ω is the interfacial energy, V is the system volume, T is temperature, and N_i is the number of moles of the ith component. This derivative is defined such that the surrounding medium is a vacuum. A higher surface tension means a stronger opposition to the formation of a larger surface area. The expression for surface energy is identical except the change in the Helmholtz free energy of the surface replaces the Helmholtz free energy of the system. For relatively deformable polymers, the difference between the two expressions is small and is usually ignored [182]. Surface tension is experimentally measured either from polymer melts or from contact angle experiments. The former requires extrapolation to the solid, while the latter cannot be measured directly and must be calculated from semiempirical equations. However, the values calculated from the two methods usually agree well [183]. The Polymer Handbook lists surface energies for many segments commonly found in TPEs. Most polymers have surface energies in the range 30–45 dyn/cm at room temperature. Exceptions to this simple generalization are fluorine- and silicon-containing polymers, which have significantly lower surface energies.

This section describes analytical methods that are used to characterize the atomic composition or morphology at TPE surfaces. Measurement of surface composition in TPEs can suffer from one major drawback. Since the soft phase

is mobile at room temperature, the surface composition can change depending on the medium in which the measurement is being made. Many analytical methods are performed in ultra high vacuum (UHV), which is not a normal atmosphere for TPE applications. Typically the difference in a TPE surface exposed to UHV or exposed to air is small; however, a significant difference will exist if the surface is exposed to a liquid such as water. Different strategies have been devised to help overcome this problem, and some of these will be discussed in this section. Analytical methods for surface composition also require a very clean surface to give quantitative results. Small amounts of additives normally present in commercial materials may also significantly alter the surface composition [184]. Finally, some methods can alter the surface during measurement.

Another extremely important parameter of any surface technique is the depth of penetration (d_p), which is a characteristic distance from the surface that the measurement will probe. Table V gives approximate depths of penetration for the methods discussed in this section for measurement of TPE surfaces. Since Table V shows that the depth of penetration varies widely, the change in composition can be monitored from the surface almost continuously to thousands of angstroms. Alternatively, some methods discussed in this section measure the morphology near the surface. Studies of TPE surfaces are less numerous than investigations of bulk properties, which in general speaks to the relative lack of importance of the surface properties of TPEs for most applications. However, exceptions to the latter generalization definitely exist, for example in the medical device area.

B. Studies of Surfaces

1. Scanning Electron Microscopy (SEM)

In SEM, electrons are reflected from the surface, and detection is done on the same side of the surface as the source; in TEM, the electrons pass through the sample and are detected on the other side. SEM is done under UHV conditions, generally 10^{-7} – 10^{-9} torr. Probably the most common use of SEM in

TABLE V Depths of Penetration for Surface-Sensitive Analytical Methods

Method	Depth of penetration
Attenuated total internal reflection	1,000–10,000 Å
X-ray photoelectron spectroscopy	10–100 Å
Static secondary ion mass spectrometry	1–10 Å
Dynamic secondary ion mass spectrometry	Varies
Neutron reflectivity	Varies
Atomic force microscopy	Surface

polymer science is to examine fracture surfaces. The morphology of a fracture surface gives details about the fracture mechanism. In TPEs, SEM is not appropriate for determining whether interphase or intraphase fracture occurs, for example; the domains are too small and the large amount of phase mixing may also play a role as well.

In well-phase-separated systems, i.e., anionically synthesized block copolymer cast from solution, information about composition at the surface can be obtained by microtoming perpendicular to the surface and then directing electrons parallel at the just-cut surface. The top (or bottom) of the image contains information about the composition at the free surface. An excellent study on a lamellar SI diblock copolymer with 52% styrene that was cast from toluene [185] showed that generally the lamellae oriented parallel to the air–polymer interface in agreement with earlier studies [186, 187] and studies of other copolymer systems [188, 189]. A micrograph of SI diblocks with lamellae parallel to the interface is shown in Fig. 16. The lower surface energy component polyisoprene (dark component in Fig. 16) was always located at the interface between the polymer and the vacuum. Some micrographs showed perpendicular orientation of the lamellae relative to the surface as also shown in Fig. 16. However, a thin polyisoprene layer is still at the air–polymer inter-

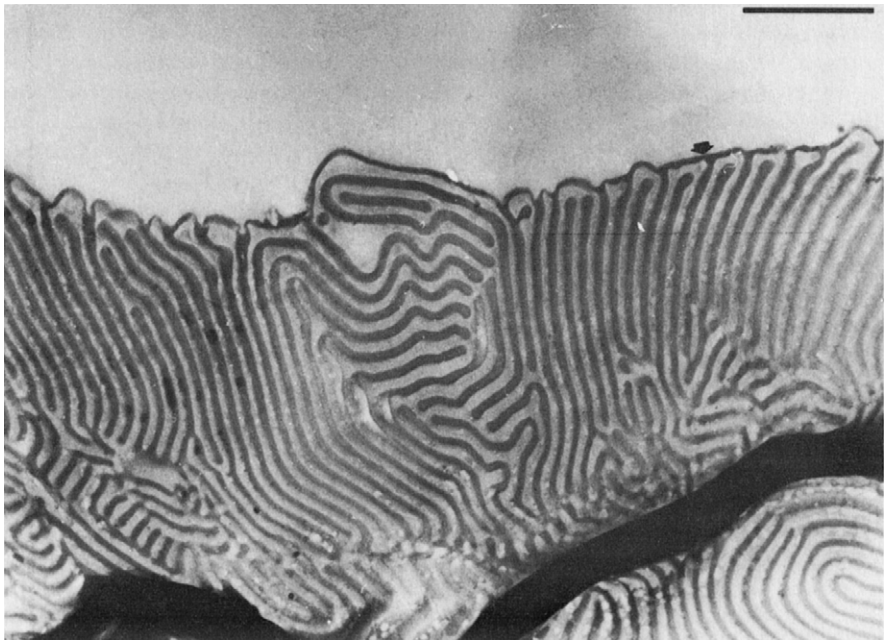

FIGURE 16 Electron micrographs of SI diblock copolymer (MW = 524,000 g/mol, 52% styrene) at a free surface. (a) Lamellae oriented parallel to surface. (b) Lamellae oriented perpendicular to surface.

face in this micrograph, i.e., the lower surface energy component was located at the interface. A very similar system, except with a crystallizable block, did not show the same behavior, i.e., the surface composition depended on the orientation of the crystallites [190]. This type of interaction at a surface can be used in anionically synthesized block copolymers to give very unique morphologies on a surface when very thin films are cast from solution [191, 192].

2. Attenuated Total Internal Reflection Infrared Spectroscopy (ATR)

In ATR, a beam of infrared light is totally reflected inside a specially cut infrared transparent material that has a high index of refraction. Typical materials used for ATR prisms are Ge, Si, and ZnSe. Because the index of refraction differs between the polymer and the prism, an evanescent wave penetrates the polymer if it intimately contacts the prism. The infrared radiation will interact with molecular vibrations in the same manner as in conventional infrared spectroscopy. The amplitude of the evanescent wave decays exponentially from the surface, so the depth of penetration is arbitrarily taken as the point where the amplitude decays to 1/e (37%) of its initial value. The depth of penetration depends on the ratio of the refractive indexes between the polymer and the prism, the angle of incidence, and frequency of radiation in the following manner [193]:

$$d_p = \frac{1}{2\pi v\left[\sin^2\theta - \left(\frac{n_2}{n_1}\right)^2\right]^{1/2}} \tag{21}$$

where v is the frequency, n_2 and n_1 are the refractive index of the polymer and prism respectively, and θ is the angle of incidence of the infrared wave. The dependence of the depth of penetration is not as simple as the above relationship suggests because the refractive indices also have a frequency dependence. For nonisotropic materials, d_p also depends on the direction of the electric field vector of the radiation relative to the surface of the prism. ATR spectroscopy is a very versatile technique and can theoretically be used in almost any medium. The latter capability has made ATR a very important method for the characterization of TPEs used in the medical device area.

Although ATR has been used to quantify the variation in composition at the surface in TPEs [194], a related utility is its ability to monitor *in situ* processes such as reaction injection molding [195] (RIM) and protein adsorption on to a polyurethane substrate [196]. In the latter, the effect of shear rate on the kinetics of protein adsorption and desorption from phosphate buffered saline (PBS) was studied in a specially designed flow cell. A very thin film of the commercial MDI–ED–PTMO polyurethane Biomer was cast from solution onto a Ge ATR prism. The thickness of the film was less than the penetration depth so the protein concentration could be monitored after the infrared absorption of the polymer and PBS was subtracted. The study found that

increasing the wall shear rate does not affect the rate of protein adsorption, but the desorption rate is slowed. In later studies using essentially the same apparatus [197], spectral changes corresponding to protein conformational changes were followed as the protein absorbed to a polyurethane substrate.

3. X-ray Photoelectron Spectroscopy (XPS)

XPS (also termed electron spectroscopy for chemical analysis) takes place in a vacuum and is able to quantify the relative amount of atomic constituents on the surface of a material. With the exception of hydrogen and helium, any chemical element can be identified, and XPS is also sensitive to chemical bonding effects. In XPS, a surface is irradiated with low-energy x-rays (usually aluminum or magnesium K_α), which results in the ejection of core level electrons. Qualitatively, the depth of penetration is limited by inelastic scattering of the ejected photoelectron as it travels toward the surface. Quantitatively, d_p is an extremely complicated function that depends on the energy of x-rays and the structure of the material; typical depths of penetration in a polymer are on the order of a few Ångstroms. The number of ejected photoelectrons that reach the detector corresponding to a particular distance from the surface decays exponentially as the distance increases. d_p is defined where the number of ejected electrons reaches 37% of its initial value and is proportional to $\cos\theta$, where θ is the angle of emission with respect to the sample normal.

The most common use of XPS on TPEs has been to quantify the fractions of each phase at the surface. By varying the emission angle, the composition can be probed at different depths of penetration. XPS studies have consistently shown that the low surface energy component will predominate at a free surface. Even a small difference in surface energy provides a strong driving force for surface enrichment of the lower energy component. The effect of evaporation rate and overall molecular weight was studied in symmetric poly(methyl methacrylate–b–styrene) (PMMA-S) cast from toluene. The surface energy difference between these two components is less than 1 dyne/cm. The amount of polystyrene at the surface was greater for the slowly evaporated film. The fraction of polystyrene at the surface increased as the overall molecular weight increased and reached a constant value of approximately 90% polystyrene at the surface when the overall degree of polymerization was approximately 1000 [198]. A later study on annealed films of these same materials showed that the polystyrene layer completely covered the surface when the degree of polymerization was greater than approximately 2500 [199]. In both studies, the surface excess of polystyrene Φ_{PS} was found to obey the following relationship:

$$\Phi_{PS} = a - bN^{-1/2} \tag{22}$$

where a and b are empirical constants. This functional form was agrees with the mean-field theory of block copolymers at surfaces developed by Fredrickson [200] and the constants were given a physical interpretation

regarding the surface energy differences and the ability of the surface to modify the energetic interactions between the two polymers. The surface excess of polystyrene was also found to decrease with increasing temperature, which agrees with qualitative expectations [201].

Ultra-high vacuum is required to perform XPS, which is a major disadvantage of this technique. As mentioned earlier, samples can show substantially different surface compositions in UHV than under normal conditions, especially if the material is immersed in a liquid, e.g., blood-contacting applications. Recent techniques that utilize freeze-drying and measurements at temperatures lower than the glass transition of the soft segment have been devised in order to quantify the surface composition at liquid interfaces. In a number of different polyurethanes, the low surface energy component was in excess when spectra were collected under normal conditions while the high energy component was in excess when the freeze-drying method was used [202]. This generalization held whether the low energy surface component was the soft or hard segment. This study illustrates surface rearrangement that can occur in any study of polymer surfaces.

4. Secondary Ion Mass Spectroscopy (SIMS)

When a surface is bombarded with a beam of high energy primary ions, atomic collisions between the beam and the solid cause the ejection of secondary ions, which can be characterized using a mass spectrometer. These secondary ions provide information on the atomic and molecular species present at the surface. The ions O_2^+, O^-, and Ar^+ are generally used for SIMS analysis, with the first ion being the most common. SIMS experiments are characterized as either dynamic or static. In static SIMS, the ion beam currents are low (less than $5\,nA/cm^2$) so that the surface etches very slowly. The depth of penetration for static SIMS is approximately 10 A. Beam currents are much higher for dynamic SIMS and successive layers are etched away rapidly during the test. This method eventually produces a pit in the sample due to this etching process. Atomic species can be quantitatively characterized as a function of distance from the surface if the relationship between the etching rate can be measured. In SIMS experiments, the sample surface can become charged because most polymers are nonconductive, and this charge must be removed during the experiment. UHV conditions are required for SIMS experiments.

SIMS is extremely sensitive, even to the part per billion range, and is used widely in the semiconductor industry. SIMS and XPS are complementary since they provide very similar information [203], but the depth resolution of static SIMS is substantially higher than XPS. However, the quantitative use of SIMS in polymer science is currently not as well developed as XPS. SIMS has been used to study the surface of polyurethanes [204, 205] and PMMA-S lamellar diblocks [206]. In the latter study, dynamic SIMS was used to show that the lamellae aligned parallel to the surface after annealing. The thickness of the layer nearest the free surface as well as near the polymer–substrate surface

was shown to be approximately $\frac{1}{2}$ the thickness of the interior layers. The experimental data were fit with a model that included the lamellar period of the block copolymer, and the results were compared with SAXS results from the same material.

5. Atomic Force Microscopy

The concept of atomic force microscopy is extremely simple. Essentially a very small probe (50–100 nm in size) is rastered over a surface such that the force between the surface and the probe is maintained constant; for studies of TPEs normally tapping mode is used, which means that a vertical oscillation is superimposed on the rastering. Essentially, the deflection of the probe is measured as a function of position. The interaction between the probe and the surface is not well understood, but the AFM pattern does not seem to be very sensitive to probe characteristics. The resolution of AFM is in the 1 nm range. A primary advantage of AFM is the scanning range, which allows for the investigation of variations in surface roughness and free surface characteristics over a large lateral area.

Different TPEs imaged using AFM include polyurethanes [207, 208], polypropylene-based thermoplastic elastomers [209], copolyamides [210], and anionically synthesized block copolymers [211, 212]. Not only can one visualize topographical differences, the AFM can also distinguish between hard and soft segments, and hence can determine the shape of these regions at the interface. The contrast is provided by the difference in modulus of the hard and soft segments; this difference allows AFM to distinguish between the two components. Alternatively, the sample can be heated and imaged simultaneously to explore changes in morphology as the system softens [213]. In systems where crystallization is the main driving force toward phase separation, the resulting AFM is qualitatively identical to AFMs from normal semicrystalline polymers. In systems where this is not the case, e.g., polyurethanes, the morphology can be very different. For example, on a system with a monodisperse distribution of hard-domain lengths, such as the spherulitic hard-domain superstructure, the orientation of the chain axis is the same as in normal spherulitic structures, i.e., in a direction tangential to the radius, but no chain folding occurs, as shown in Fig. 17 [214].

VII. RHEOLOGY AND PROCESSING

Chapters 5 and 6 consider the rheology of rubbers in some detail. The theoretical development and characterization techniques outlined in those chapters apply equally well to TPEs. However, there are fundamental differences in the response to stress between a conventional rubber and a TPE. Of course the biggest dissimilarity is that a TPE will flow at higher temperatures while a crosslinked rubber will not. Some of the similarities and differences between

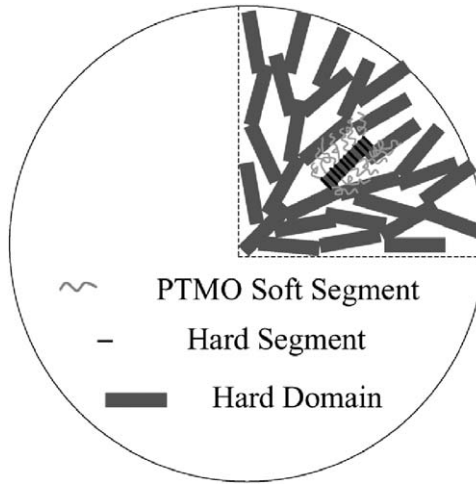

FIGURE 17 Schematic model for a polyurethane with monodisperse hard segment lengths showing spherulitic structure of hard domains and the orientation of chain segments within the arms of the spherulite.

the two types of materials will be discussed in this section. Also, the processing methods used for TPEs will also be introduced; the processing methods for these materials are no different than for any other thermoplastic, and the interested reader can consult monographs on the subject [215, 216].

At service temperature and frequency, the solid-state rheological properties of a TPE and a conventional rubber are similar, although at large strains the former will generally have some permanent set, while the latter will not. Only by changing the temperature and/or the frequency do substantial differences between the two emerge. If the temperature is lowered or the frequency raised, the qualitative response of the two materials is still very similar. Both materials become more resistant to stress until a temperature is reached that corresponds to the T_g of the soft segment in a TPE or the rubbery matrix in a conventional rubber. Below this temperature, both a conventional rubber and a TPE will behave as a one-phase brittle glassy polymer. As the temperature is raised, the two materials show qualitatively different behavior. In a conventional rubber, the material will continue to behave as an elastomer until the degradation temperature is reached. In a TPE, the hard domains will eventually weaken and flow, which allows the material to be processed as a conventional thermoplastic. The processing characteristics will be intimately related to the ODT temperature since the viscosity is substantially lower above the ODT.

More specifically, the dynamic mechanical properties are significantly different in TPEs vs. conventional elastomers. The WLF equation (see Chapter 5) does not generally apply to TPEs since two phases make the material

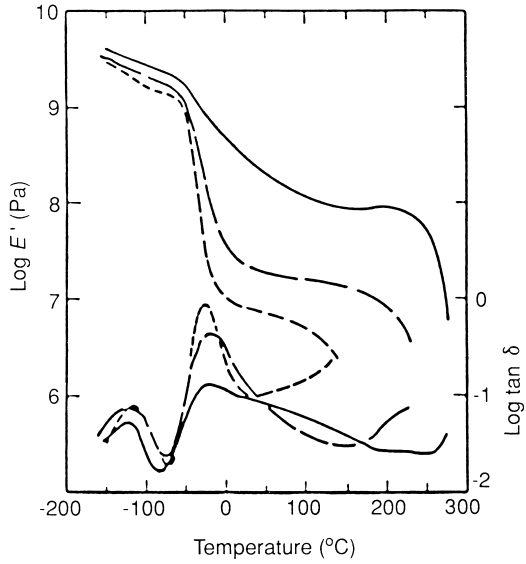

FIGURE 18 Storage modulus (E′) and tan delta (E′/E″) vs. temperature for MDI–ED–PTMO (MW = 1000) polyurethaneureas. The molar ratio of the components MDI–ED–PCL is (——) 3:2:1; (– –) 2:1:1; (----) 1.3:0.3:1.

rheologically complex. Dynamic mechanical experiments are used as a macroscopic characterization of phase separation since a more highly phase separated material will have a larger temperature difference between the soft and hard segment transitions and a flatter plateau modulus. Figure 18 [217] shows E′ and tan δ for a series of polyurethaneureas as a function of increasing hard segment content that demonstrates the forementioned behavior in the more highly phase separated higher hard segment materials. Figure 18 also exhibits the general features common to all dynamic mechanical measurements of TPEs, a soft segment glass transition temperature below room temperature and a hard segment dissolution temperature above room temperature. The normal operating region of a TPE is the flat plateau region between the two transition temperatures. As suggested by the diagram, one can shift the upper transition temperature by increasing phase mixing, which is usually accomplished by reducing the length of the hard segments.

Rheological measurements can also supply a measure of the ODT temperature independent of scattering measurements. In this method, the storage and loss moduli are measured as a function of frequency at different temperatures above and below the MST. One strain level should be used for these experiments since it has been shown that below the ODT, the dynamical mechanical properties are highly strain dependent. The WLF equation is then

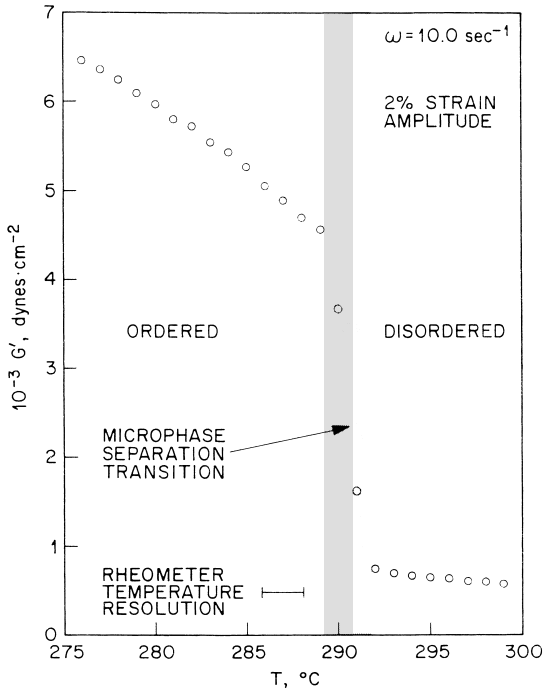

FIGURE 19 Temperature of G', the shear storage modulus, at a frequency of 1.6 Hz for the diblock copolymer PEP–PEE. The ODT temperature was calculated as 291 ± 1°C.

used to collapse all of the data onto one curve in a modulus vs. reduced frequency plot, if the frequency is high enough. The frequency at which the curves begin to diverge marks the critical frequency (w_c) of the material. The critical frequencies are not necessarily identical for the storage and loss moduli, but generally differ by less than an order of magnitude. After finding w_c, a storage or loss modulus is measured as a function of temperature at constant frequency, which is significantly below the critical frequency. The temperature at which a discontinuity occurs in the modulus marks the ODT temperature, as shown in Fig. 19. The authors recommend using the storage modulus because the discontinuity is sharper. This method relies on the different behavior of the storage and loss moduli at low frequencies for the disordered and ordered systems. For the disordered system, the behavior is identical to normal terminal behavior in one-phase materials, i.e., $G' \sim w^2$ and $G'' \sim w$, while in the ordered system, the dependency depends on the morphology and orientation of the material; for a macroscopically unoriented lamellar system, $G' \sim G'' \sim w^{0.5}$.

The viscosity of a TPE depends heavily on whether the system is above or below the ODT temperature. For example, in styrene–diene triblock

systems, commercially important materials have ODT temperatures above a reasonable processing temperature; therefore, melt viscosities are usually orders of magnitude higher in the block copolymer than in the homopolymers of the same molecular weight. Typical values at high shear rates are 10^4 poise, which can increase orders of magnitude as the shear rate is decreased.

Generally, TPEs are processed identically to any other thermoplastic, i.e., injection molding, extrusion, calendaring, etc. Some TPEs, for example ionomers, tend to adhere to surfaces, so special equipment and techniques may be necessary to remove an injection-molded part. The processing temperature must be higher than the hard segment dissolution temperature, but even two-phase melts can generally be handled with conventional equipment. The viscosities of TPEs above the ODT are rather low in comparison to other thermoplastics, because of the low overall molecular weights. In fact, in some one-phase materials with low overall molecular weights such as the copolyesters, blow molding cannot be utilized because of low viscosities [218]. The resultant morphology and properties of the material depend heavily on the processing method.

Reaction injection molding (RIM) is a specialized technique very popular in polyurethane manufacture. Two streams, one containing the diisocyanate and the other containing the diols, are mixed by impingement mixing at high pressures. Normally high pressure piston pumps are needed to provide the high pressures as well as the strict metering required. The diisocyanate may have already been reacted with some polyol prior to impingement mixing, which would correspond to a prepolymer method discussed earlier. The mixed material is quickly allowed to flow into the closed mold, but the flow is always regulated to be laminar. The material is cured for a short time, resulting in a finished part.

VIII. APPLICATIONS

As stated previously, styrene–diene triblock copolymers are the most important category of thermoplastic elastomer. Unlike most other TPEs, they can be blended with large quantities of additives without a drastic effect on properties. In almost all applications, the actual triblock copolymer content is less than 50%. Oils are used as a processing aid and do not result in a significant loss of properties if the polystyrene domains are not plasticized. For this reason, napthalenic oils are preferred. The use of inert fillers such as clays or chalks reduce the cost of the final material. Unlike conventional rubbers, inert fillers do not have a substantial effect on the mechanical properties of TPEs. Thermoplastics such as polyethylene or polypropylene are also used to improve the solvent resistance and can increase the upper service temperature. Polystyrene homopolymer is used as a processing aid, which also increases the hard phase weight fraction and causes the material to stiffen.

KRATON Polymers, the world's largest single producer of styrene–diene block copolymers, produces four types of compounds. SBS compounds are found in shoe soles and as property modifiers for asphalt. In this latter application, the block copolymer is a minor component (~10%) and improves the flexibility at low temperature and increases the softening temperature of the asphalt. SIS materials are employed almost exclusively as adhesives while SEBS triblock copolymers are used as structural materials. The polystyrene content tends to be low in pressure-sensitive adhesives in order to produce a material with more tack; although with hot melt adhesives tack may be undesirable and a harder product is appropriate. The absence of a double bond in SEBS copolymers substantially improves its resistance to UV light and high temperatures, allowing SEBS to be substituted for SIS or SBS in applications where this resistance is necessary. Finally, through postsynthesis processing with maleic anhydride, acid groups are introduced to the SEBS, which improves adhesion to a variety of substrates. These maleated materials are often used in composites, i.e., a polymer containing an inorganic filler.

Applications for TPOs, polyurethanes, copolyesters, and copolyamides are substantially different than for the triblock copolymers. Only small amounts of additives are used in these materials since large amounts of any additive tend to substantially reduce the mechanical properties of these materials. The applications for these multiblock copolymers take advantage of their abrasion resistance, tear strength, and toughness. The TPOs are marginally more expensive then the commodity thermoplastics; however, the segmented block copolymers are substantially more expensive and hence the application must require the improved mechanical properties to justify the increased cost. In the automobile industry, TPEs are used in both interior and exterior parts. For example, TPEs are used in boots and bearings for joints and some tubing as well as exterior bumpers and some paneling. Other industrial uses include hoses, gears, and cables.

Although not a large volume market, the medical device area has certainly been a very important user of TPEs. One very visible application is the use of polyurethanes in angioplasty devices. Polyurethanes (as well as polyamides and polyesters) comprise the balloon material that is expanded to increase the increase the size of opening for blood flow within an artery. Further application of polyurethane TPEs in medical devices can be found in a monograph on this subject by one of the authors of this review [219].

A very visible consumer product group for TPEs has been in sporting goods. Footwear, including ski boots and soccer shoes, often contain a substantial fraction of TPE. Athletic shoe soles are an especially large application for TPEs. Athletic equipment such as skis and golf ball covers are an area where TPEs are used. Polyurethanes are used for track and field surfaces. Finally, TPEs are beginning to be used in outdoor equipment such as tents because of their low permeability to water coupled with their inherent toughness.

REFERENCES

1. "Thermoplastic Elastomers—2nd Edition," Market Research Report by Freedonia Group, 2003.
2. http://www.kraton.com
3. http://www.dupont-dow.com/Products/Engage/engage.asp
4. http://www.santoprene.com/home.html
5. http://www.dow.com/engineeringplastics/prod/na/pel.htm
6. http://plastics.dupont.com/NASApp/myplastics/Mediator?id=75
7. http://www.atofinachemicals.com/techpol/pebax
8. http://www.dupont.com/packaging/products/surlyn.html
9. K. Uhlig, "Discovering Polyurethanes," Hanser, Munich, 1999.
10. M. Szycher, "Handbook of Polyurethanes," CRC Press, Boca Raton, FL, 1999.
11. D. Randall and S. Lee (Eds.), "The Polyurethanes Book," Wiley, New York, 2003.
12. G. Oertel (Ed.), "Polyurethane Handbook: Chemistry–Raw Materials–Processing–Application–Properties," Hanser Publishers, New York, 1994.
13. D. J. Lyman, *Journal of Polymer Science* **45**, 49 (1960).
14. W. Meckel, W. Goyert, and W. Wieder, in "Thermoplastic Elastomers—2nd Edition," G. Holden, N. R. Legge, R. P. Quirk, and H. E. Schroeder (Eds.), Hanser Publishers, New York, 1996, Chap. 2.
15. Z. S. Petrovic and J. Ferguson, *Progress in Polymer Science* **16**, 695 (1991).
16. C. Hepburn, "Polyurethane Elastomers," Applied Science Publishers, New York, 1982, Chap. 1.
17. W. K. Witsiepe, *ACS Advances in Chemistry Series* **129**, 29 (1973).
18. G. K. Hoeschele, *Chimia* **28**, 544 (1974).
19. R. G. Nelb and A. T. Che, in "Thermoplastic Elastomers—2nd Edition," G. Holden, N. R. Legge, R. P. Quirk, and H. E. Schroeder (Eds.), Hanser Publishers, New York, 1996, Chap. 9.
20. M. Morton, "Anionic Polymerization: Principles and Practice," Academic Press, New York, 1983.
21. A. Noshay and J. E. McGrath, "Block Copolymers," Academic Press, New York, 1977, Chap. 6.
22. C. W. Lantman, W. J. MacKnight, and R. D. Lundberg, *Annual Review of Material Science* **19**, 295 (1989).
23. D. C. Lee, T. A. Speckhard, A. D. Sorenson, and S. L. Cooper, *Macromolecules* **19**, 2383 (1986).
24. N. Aust and G. Gobec, *Macromolecular Materials and Engineering* **286**, 119 (2001).
25. C. D. Eisenbach, T. Heinemann, A. Ribbe, and E. Stadler, *Angewandte Makromolekulare Chemie* **202**, 221 (1992).
26. H. Suzuki and H. Ono, *Bulletin of the Chemical Society of Japan* **43**, 682 (1970).
27. H. Suzuki and H. Ono, *Bulletin of the Chemical Society of Japan* **43**, 687 (1970).
28. Y. Löcsei, O. Facosko, and R. F. Pape, *Polymer Bulletin* **9**, 81 (1983).
29. S. A. Dombrowski, I. Goodman, and A. F. Johnson, *Makromol. Chem.*, *Rapid Commun.* **7**, 274 (1986).
30. A. Kaji and M. Murano, *Polymer Journal* **22**, 1065 (1990).
31. D. J. Yontz and S. L. Hsu, *Macromolecules* **33**, 8415 (2000).
32. H. K. Frensdorff, *Macromolecules* **4**, 369 (1971).
33. E. Sorta and L. A. Melis, *Polymer* **19**, 1153 (1978).
34. T. A. Speckhard, J. A. Miller, and S. L. Cooper, *Macromolecules* **19**, 1550 (1986).
35. T. A. Speckhard, J. A. Miller, and S. L. Cooper, *Macromolecules* **19**, 1558 (1986).
36. T. A. Speckhard, J. G. Homan, J. A. Miller, and S. L. Cooper, *Polymer* **28**, 758 (1987).
37. T. A. Speckhard, J. G. Homan, J. A. Miller, and S. L. Cooper, *Polymer* **28**, 768 (1987).
38. F. S. Bates and G. H. Fredrickson, *Annual Review of Physical Chemistry* **41**, 525 (1990).

39. G. H. Fredrickson and F. S. Bates, *Annual Review of Materials Research* **26**, 501, (1996).
40. T. P. Lodge, *Macromolecular Chemistry and Physics* **204**, 265 (2003).
41. I. W. Hamley (Ed.), "Developments Block Copolymer Science and Technology," Wiley, West Sussex, 2004.
42. I. W. Hamley, "The Physics of Block Copolymers," Oxford University Press, Oxford, 1998.
43. T. L. Smith, *Journal of Polymer Science-Polymer Physics Edition* **12**, 1825 (1974).
44. S. Chen, T. Cao, and Y. Jin, *Polymer Comm.* **28**, 314 (1987).
45. C. Li and S. L. Cooper, *Polymer* **31**, 3 (1990).
46. J. A. Laurer and K. I. Winey, *Macromolecules* **31**, 9106, (1998).
47. K. I. Winey, J. Laurer, and B. P. Kirkmeyer, *Macromolecules* **33**, 507, (2000).
48. B. P. Kirkmeyer, A. Taubert, J. S. Kim, and K. I. Winey, *Macromolecules* **35**, 2648 (2002).
49. M. M. Coleman, J. F. Graf, and P. C. Painter, "Specific Interactions and the Miscibility of Polymer Blends," Technomic Publishing Company, Lancaster, PA, 1991, Chap. 3.
50. M. A. Harthcock, *Polymer* **30**, 1234 (1989).
51. N. Luo, D. N. Wang, and S. K. Yang, *Polymer* **37**, 3045 (1996).
52. C. S. P. Sung and N. S. Schneider, *Macromolecules* **8**, 68 (1975).
53. R. W. Seymour, G. M. Estes, and S. L. Cooper, *Macromolecules* **3**, 579 (1970).
54. J. L. Sormana and J. C. Meredith, *Macromolecules* **37**, 2186 (2004).
55. V. W. Srichatrapimuk and S. L. Cooper, *Journal of Macromolecular Science-Physics* **B15**, 267 (1978).
56. J. T. Koberstein, I. Gancarz, and T. C. Clarke, *Journal of Polymer Science: Part B: Polymer Physics* **24**, 2487 (1986).
57. N. Luo, D. N. Wang, and S. K. Ying, *Macromolecules* **30**, 4405 (1997).
58. M. M. Coleman, D. J. Skrovanek, S. E. Howe, and P. C. Painter, *Macromolecules* **18**, 302 (1985).
59. D. J. Skrovanek, S. E. Howe, P. C. Painter, and M. M. Coleman, *Macromolecules* **18**, 1676 (1985).
60. D. J. Skrovanek, P. C. Painter, and M. M. Coleman, *Macromolecules* **19**, 699 (1986).
61. M. M. Coleman, D. J. Skrovanek, and P. C. Painter, *Makromolecular Chemisty*, *Macromolecular Symposia* **5**, 21 (1986).
62. M. M. Coleman, K. H. Lee, D. J. Skrovanek, and P. C. Painter, *Macromolecules* **19**, 2149 (1986).
63. H. Janik, B. Palys, and Z. S. Petrovic, *Macromolecular Rapid Communications* **24**, 265 (2003).
64. C. W. Myers and S. L. Cooper, *Journal of Applied Spectroscopy* **48**, 72 (1994).
65. R. W. Seymour, A. E. Allegrezza Jr., and S. L. Cooper, *Macromolecules* **6**, 896 (1973).
66. A. E. Allegrezza Jr., R. W. Seymour, H. N. Ng, and S. L. Cooper, *Polymer* **15**, 433 (1974).
67. C. B. Wang and S. L. Cooper, *Macromolecules* **16**, 775 (1983).
68. A. Lilaonitkul, J. West, and S. L. Cooper, *Journal of Macromolecular Science-Physics* **B12**, 563 (1976).
69. H. W. Siesler, *Polymer Bulletin* **9**, 471 (1983).
70. J. R. Schoonover, D. G. Thompson, J. C. Osborn, E. B. Orler, D. A. Wrobleski, A. L. Marsh, H. C. Wang, and R. A. Palmer, *Polymer Degradation and Stability* **74**, 87 (2001).
71. D. K. Graff, H. C. Wang, R. A. Palmer, and J. R. Schoonover, *Macromolecules* **32**, 7147 (1999).
72. W. L. Bragg, "The Crystalline State," Macmillan, New York, 1933.
73. L. E. Alexander, "X-ray Diffraction Methods in Polymer Science," Krieger Publishing Company, Malabar, FL, 1985.
74. I. H. Hall and M. G. Pass, *Polymer* **17**, 807 (1976).
75. I. J. Desborough and I. J. Hall, *Polymer* **18**, 825 (1977).
76. R. J. Cella, *Journal of Polymer Science* **C42**, 727 (1973).
77. M. A. Vallance and S. L. Cooper, *Macromolecules* **17**, 1208 (1984).
78. G. Perego, M. Cesari and R. Vitali, *Journal of Applied Polymer Science* **29**, 1157 (1984).
79. E. V. Konyukhova, V. M. Neverov, S. N. Chvalun, and Y. K. Godovsky, *Polymer Science Series A* **46**, 61 (2004).
80. G. R. Hatfield, Y. Guo, W. E. Killinger, R. A. Andrejak, and P. M. Roubicek, *Macromolecules* **26**, 6350 (1993).

81. Y. C. Yu and W. H. Jo, *Journal of Applied Polymer Science* **54**, 585 (1994).
82. Y. C. Yu and W. H. Jo, *Journal of Applied Polymer Science* **56**, 895 (1995).
83. Y. C. Yu and W. H. Jo, *Journal of Applied Polymer Science* **64**, 2155 (1997).
84. J. P. Sheth, J. Xu, and G. L. Wilkes, *Polymer* **44**, 743 (2003).
85. S. Warner, *Journal of Elastomers and Plastics* **22**, 166 (1990).
86. R. M. Briber and E. L. Thomas, *Journal of Macromolecular Science-Physics* **B22**, 509 (1983).
87. R. M. Briber and E. L. Thomas, *Journal of Polymer Science-Polymer Physics Edition* **23**, 1915 (1985).
88. J. Blackwell, M. R. Nagarajan, and T. B. Hoitink, *Polymer* **23**, 950 (1982).
89. C. D. Eisenbach and E. Stadler, *Colloid and Polymer Science* **273**, 352 (1995).
90. H. W. Starkweather, *Journal of Applied Polymer Science* **25**, 139 (1980).
91. E. N. Kresge, *Journal of Applied Polymer Science: Appl. Polym. Symp.* **39**, 37 (1984).
92. A. Guinier and G. Fournet, "Small-Angle Scattering of X-rays," John Wiley and Sons, New York, 1955.
93. J. S. Pederson, *Advances in Colloid and Interface Science* **70**, 171 (1997).
94. O. Glatter and O. Kratky (Eds.), "Small Angle X-ray Scattering," Academic Press, New York, 1982.
95. H. Brumberger (Ed.), "Modern Aspects of Small-Angle Scattering," Kluwer, New York, 1995.
96. W. Ruland, *Journal of Applied Crystallography* **4**, 70 (1971).
97. C. G. Vonk, *Journal of Applied Crystallography* **6**, 81 (1973).
98. R. Séguéla and J. Prud'homme, *Macromolecules* **11**, 1007 (1978).
99. R. Séguéla and J. Prud'homme, *Macromolecules* **14**, 197 (1981).
100. R. Séguéla and J. Prud'homme, *Macromolecules* **21**, 635 (1988).
101. T. Pakula, K. Saijo, H. Kawai, and T. Hashimoto, *Macromolecules* **18**, 1294 (1985).
102. T. Pakula, K. Saijo, and T. Hashimoto, *Macromolecules* **18**, 2037 (1985).
103. S. Polizzi, P. Bösecke, N. Stribeck, H. G. Zachmann, R. Zietz, and R. Bordeianu, *Polymer* **31**, 639 (1990).
104. Z. Ophir and G. L. Wilkes, *J. Polym. Sci.: Polym. Phys. Ed.* **18**, 1469 (1980).
105. D. Tyagi, J. E. McGrath, and G. L. Wilkes, *Polymer Engineering and Science* **26**, 1371 (1986).
106. R. J. Roe, *Journal of Applied Crystallography* **15**, 182 (1982).
107. R. Bonart and E. H. Muller, *Journal of Macromolecular Science-Physics.* **B10**, 345 (1974).
108. J. T. Koberstein and R. S. Stein, *Journal of Polymer Science-Polymer Physics Edition* **21**, 2181 (1983).
109. R. A. Phillips, J. M. McKenna, and S. L. Cooper, *Journal of Polymer Science Part B-Polymer Physics* **32**, 791 (1994).
110. R. A. Phillips and S. L. Cooper, *Macromolecules* **28**, 5734 (1995).
111. R. A. Phillips and S. L. Cooper, *Journal of Polymer Science Part B-Polymer Physics* **34**, 737 (1996).
112. D. G. Ballard, J. Schelten, and G. Wignall, *European Polymer Journal* **9**, 965 (1973).
113. J. P. Cotton, D. Decker, H. Benôit, B. Farnoux, J. Higgins, G. Jannink, R. Ober, C. Picot, and J. des Cloiseaux, *Macromolecules* **7**, 862 (1974).
114. S. N. Jahshan and G. C. Summerfield, *Journal of Polymer Science-Polymer Physics Edition* **18**, 2415 (1980).
115. A. R. Rennie, R. C. Oberthur, "Practical Small Angle Neutron Scattering," Taylor and Francis, New York, 1994.
116. J. Higgins and H. Benoit, "Polymers and Neutron Scattering," Clarendon Press, London, 1994.
117. B. J. Gabrys, "Applications of Neutron Scattering to Soft Condensed Matter," Taylor and Francis, New York, 2000.
118. S. Naylor, N. J. Terrill, G. E. Yu, S. Tanodekaew, W. Bras, S. M. King, C. Booth, A. J. Ryan, *Polymer International* **44**, 371 (1997).
119. J. A. Miller, S. L. Cooper, C. C. Han, and G. Pruckmayr, *Macromolecules* **17**, 1063 (1984).
120. J. A. Miller, G. Pruckmayr, E. Epperson, and S. L. Cooper, *Polymer* **25**, 1915 (1985).
121. S. L. Cooper and J. A. Miller, *Rubber Chemistry and Technology* **58**, 899 (1985).

122. S. L. Cooper, J. A. Miller, and J. G. Homan, *Journal of Applied Crystallography* **21**, 692 (1988).
123. H. Hasegawa, T. Hashimoto, H. Kawai, T. P. Lodge, E. J. Amis, C. J. Glinka, and C. C. Han, *Macromolecules* **18**, 67 (1985).
124. H. Hasegawa, H. Tanaka, T. Hashimoto, and C. C. Han, *Macromolecules* **20**, 2120 (1987).
125. R. W. Richards, G. Welsh, *European Polymer Journal* **31**, 1197 (1995).
126. H. Tanaka and T. Nishi, *Journal of Chemical Physics* **82**, 4326 (1985).
127. T. Hashimoto, M. Shibayama, and H. Kawai, *Macromolecules* **13**, 1237 (1980).
128. T. Hashimoto, M. Shibayama, and H. Kawai, *Macromolecules* **13**, 1660 (1980).
129. J. A. Kornfield, H. W. Spiess, H. Nefzger, H. Hayen, and C. D. Eisenbach, *Macromolecules* **24**, 4787 (1991).
130. A. D. Meltzner, H. W. Spiess, C. D. Eisenbach, and H. Hayen, *Macromolecules* **25**, 993 (1992).
131. L. W. Jelinski, J. J. Dumais, and A. K. Engel, *Macromolecules* **16**, 492 (1983).
132. L. W. Jelinski, *Macromolecules* **14**, 1341 (1981).
133. L. W. Jelinski, J. J. Dumais, P. I. Watnick, K. A. Engel, and M. D. Sefcik, *Macromolecules* **16**, 409 (1983).
134. D. T. Okamoto, S. L. Cooper, and T. W. Root, *Macromolecules* **25**, 1068 (1992).
135. D. T. Okamoto, S. L. Cooper, and T. W. Root, *Macromolecules* **25**, 3301 (1992).
136. D. T. Okamoto, E. M. O'Connell, S. L. Cooper, and T. W. Root, *Journal of Polymer Science, Part B Polymer Physics* **31**, 1163 (1993).
137. C. S. P. Sung, C. B. Hu, and C. S. Wu, *Macromolecules* **13**, 111 (1980).
138. N. J. Clayden, C. Nijs, and G. Eeckhaut, *Macromolecules* **31**, 7820 (1998).
139. L. Mullins, *J. Phys. Chem.* **54**, 239 (1950).
140. T. L. Smith, in "Encyclopedia of Materials Science and Engineering," M. B. Bever (Ed.), Pergamon Press, New York, 1986, p. 1341.
141. D. R. Paul, *Polym. Mater. Sci. Eng.* **50**, 1 (1984).
142. G. Holden, E. T. Bishop, and N. R. Legge, *Journal of Polymer Science* **26**, 37 (1969).
143. D. J. Meier, *Polymer Preprints* **14**, 280 (1973).
144. R. J. Gaylord and D. J. Lohse, *Polymer Engineering and Science* **18**, 359 (1978).
145. R. J. Gaylord, in "Multiphase Polymers," S. L. Cooper and G. M. Estes (Eds.), ACS Advances in Chemistry Series 176, Washington, D.C., 1979, Chap. 12.
146. J. K. Bard and C. I. Chung, in "Thermoplastic Elastomers," G. Holden, N. R. Legge, and H. E. Schroeder (Eds.), Section 1, Hanser Publishers, New York, 1987, Chap. 12.
147. H. Veenstra, P. C. J. Verkooijen, B. J. J. van Lent, J. van Dam, A. P. de Boer, and A. P. H. J. Nijhof, *Polymer* **41**, 1817 (2000).
148. D. J. Read, P. I. C. Teixeira, R. A. Duckett, J. Sweeney, and T. C. B. McLeish, *European Physical Journal E* **8**, 15 (2002).
149. G. Holden and N. R. Legge, in "Thermoplastic Elastomers—2nd Edition," G. Holden, N. R. Legge, R. P. Quirk, and H. E. Schroeder (Eds.), Hanser Publishers, New York, 1996, Chap. 3.
150. T. A. Speckhard and S. L. Cooper, *Rubber Chemistry and Technology* **59**, 405 (1986).
151. W. Nierzwicki, *Journal of Applied Polymer Science* **30**, 761 (1985).
152. L. L. Harrell, *Macromolecules* **2**, 607 (1976).
153. J. A. Miller, S. B. Lin, K. K. S. Hwang, K. S. Wu, P. E. Gibson, and S. L. Cooper, *Macromolecules* **18**, 32 (1985).
154. J. T. Mehl, R. Murgasova, X. Dong, D. M. Hercules, and H. Nefzger, *Analytical Chemistry* **72**, 2490, (2000).
155. D. J. Blundell, G. Eeckhaut, W. Fuller, A. Mahendrasingam, and C. Martin, *Polymer* **43**, 5197 (2002).
156. M. Morton, in "Thermoplastic Elastomers—2nd Edition," G. Holden, N. R. Legge, R. P. Quirk, and H. E. Schroeder (Eds.), Hanser Publishers, New York, 1996, Chap. 4.
157. M. V. Pandya, D. D. Deshpande, and D. G. Hundiwale, *Journal of Applied Polymer Science* **32**, 4959 (1986).
158. L. Morbitzer and H. Hespe, *Journal of Applied Polymer Science* **16**, 2697 (1972).

159. N. S. Schneider and W. Matton, *Polymer Engineering and Science* **19**, 1122 (1979).
160. M. Brown, G. K. Hoeschele, and W. K. Witsiepe (to DuPont), U.S. Patent 3,835,098 (September 10, 1974).
161. S. Sakarai, S. Okamoto, and K. Sakurai, in "Developments in Block Copolymer Science and Technology," I. W. Hamley (Ed.), Wiley, West Sussex, 2004.
162. P. G. DeGennes, "Scaling Concepts in Polymer Physics," Cornell University Press, Ithaca, NY, 1979.
163. E. Helfand, *Macromolecules* **8**, 552 (1975).
164. E. Helfand and Z. R. Wasserman, *Macromolecules* **9**, 879 (1976).
165. E. Helfand and Z. R. Wasserman, *Macromolecules* **11**, 960 (1978).
166. E. Helfand and Z. R. Wasserman, *Macromolecules* **13**, 994 (1980).
167. E. Helfand, in "Developments in Block Copolymers," I. Goodman (Ed.), Applied Science, New York, 1982, Chap. 4.
168. M. D. Whitmore, in "Encyclopedia of Materials: Science and Technology," Elsevier Science, Oxford, 2001.
169. R. J. Meier, in "Thermoplastic Elastomers—2nd Edition," G. Holden, N. R. Legge, R. P. Quirk, and H. E. Schroeder (Eds.), Hanser Publishers, New York, 1996, Chap. 11.
170. L. Leibler, *Macromolecules* **13**, 1602 (1980).
171. P. G. DeGennes, *J. Phys. (Paris)* **31**, 235 (1970).
172. F. S. Bates, J. H. Rosedale, and G. H. Fredrickson, *Journal of Chemical Physics* **92**, 6255 (1990).
173. B. Stühn and F. Stickel, *Macromolecules* **25**, 5306 (1992).
174. F. S. Bates and M. A. Hartney, *Macromolecules* **18**, 2478 (1985).
175. B. Holzer, A. Lehmann, B. Stühn, and M. Kowalski, *Polymer* **32**, 1935 (1991).
176. G. H. Fredrickson and E. Helfand, *Journal of Chemical Physics* **87**, 697 (1987).
177. L. Leibler and H. Benoit, *Polymer* **22**, 195 (1981).
178. M. Olvera de la Cruz and I. C. Sanchez, *Macromolecules* **19**, 2501 (1986).
179. A. M. Mayes and M. Olvera de la Cruz, *Journal of Chemical Physics* **91**, 7228 (1989).
180. J. T. Koberstein, T. P. Russell, D. J. Walsh, and L. Pottick, *Macromolecules* **23**, 877 (1990).
181. M. D. Gehlsen, K. Almdal, and F. S. Bates, *Macromolecules* **25**, 939 (1992).
182. M. D. Lelah and S. L. Cooper, "Polyurethanes in Medicine," CRC Press, Boca Raton, FL, 1986.
183. S. Wu, in "Polymer Handbook," J. Brandrup and E. H. Immergut (Eds.), John Wiley and Sons, New York, 1989.
184. B. J. Tyler, B. D. Ratner, D. G. Castner, and D. Briggs, *J. Biomed. Mater. Res.* **26**, 273 (1992).
185. H. Hasegawa and T. Hashimoto, *Macromolecules* **18**, 590 (1985).
186. T. Hashimoto, A. Todo, H. Itoi, and H. Kawai, *Macromolecules* **10**, 377 (1977).
187. T. Hashimoto, M. Shibayama, and H. Kawai, *Macromolecules* **13**, 1237 (1980).
188. S. H. Anastasiadis, T. P. Russell, S. K. Satija, and C. F. Majkrzak, *Journal of Chemical Physics* **92**, 5677 (1990).
189. X. Chen, J. A. Gardella Jr., and P. L Kumler, *Macromolecules* **25**, 6631 (1992).
190. H. Hasegawa and T. Hashimoto, *Polymer* **33**, 475 (1992).
191. R. A. Segalman, K. E. Schaefer, G. H. Fredrickson, E. J. Kramer, and S. Magonov, *Macromolecules* **36**, 4498 (2003).
192. M. J. Fasolka and A. M. Mayes, *Annual Review of Materials Research* **31**, 323 (2001).
193. H. Ishida, *Rubber Chemistry and Technology* **60**, 497 (1987).
194. C. S. P. Sung and C. B. Hu, in "Multiphase Polymers," S. L. Cooper and G. M. Estes (Eds.), Advances in Chemistry Series, 176, American Chemical Society, Washington, D. C., 1980.
195. H. Ishida and C. Scott, *Journal of Polymer Engineering* **6**, 201 (1986).
196. W. G. Pitt and S. L. Cooper, *Biomaterials* **7**, 340 (1986).
197. T. A. Giroux and S. L. Cooper, *Journal of Colloid and Interface Science* **146**, 179 (1991).
198. P. F. Green, T. M. Christensen, T. P. Russell, and R. Jérôme, *Macromolecules* **22**, 2189 (1989).
199. P. F. Green, T. M. Christensen, T. P. Russell, and R. Jérôme, *Journal of Chemical Physics* **92**, 1478 (1990).

200. G. H. Fredrickson, *Macromolecules* **20**, 2535 (1987).
201. P. F. Green, T. M. Christensen, and T. P. Russell, *Macromolecules* **24**, 252 (1991).
202. T. Kajiyama and A. Takahara, *J. Biomat. App.* **6**, 42 (1991).
203. L. Sabbatini and P. G. Zambonin, *Journal of Electron Spectroscopy and Related Phenomena* **81**, 285 (1996).
204. Y. Deslandes, G. Pleizier, D. Alexander, and P. Santerre, *Polymer* **39**, 2361 (1998).
205. A. G. Shard, M. C. Davies, S. J. B. Tendler, D. E. Jackson, P. N. Lan, E. Schacht, and M. D. Purbrick, *Polymer* **36**, 775 (1995).
206. G. Coulon, T. P. Russell, V. R. Deline, and P. F. Green, *Macromolecules* **22**, 2581 (1989).
207. A. Aneja and G. L.Wilkes, *Polymer* **44**, 7221 (2003).
208. K. Gisselfalt and B. Helgee, *Macromolecular Materials and Engineering* **288**, 265 (2003).
209. H. Schonherr, W. Wiyatno, J. Pople, C. W. Frank, G. G. Fuller, A. P. Gast, and R. M. Waymouth, *Macromolecules* **35**, 2654 (2002).
210. J. Krijgsman, D. Husken, and R. J. Gaymans, *Polymer* **44**, 7573 (2003).
211. B. K. Annis, D. W. Schwark, J. R. Reffner, E. L. Thomas, and B. Wunderlich, *Makromol. Chem.* **193**, 2589 (1992).
212. A. Knoll, R. Magerle, and G. Krausch, *Macromolecules* **34**, 4159 (2001).
213. C. Vasilev, H. Heinzelmann, and G. Reiter, *Journal of Polymer Science Part B-Polymer Physics* **42**, 1312 (2004).
214. J. T. Garrett, C. A. Siedlecki, and J. Runt, *Macromolecules* **34**, 7066 (2001).
215. T. Osswald, "Polymer Processing Fundamentals," Hanser Publishers, New York, 1998.
216. P. J. Corish, "Concise Encyclopedia of Polymer Processing & Applications," Elsevier, New York, 1991.
217. C. B. Wang and S. L. Cooper, *Macromolecules* **16**, 775 (1983).
218. R. K. Adams and G. K. Hoeschele, in "Thermoplastic Elastomers—2nd Edition," G. Holden, N. R. Legge, R. P. Quirk, and H. E. Schroeder (Eds.), Hanser Publishers, New York, 1996, Chap. 8.
219. N. M. K. Lemba, K. A. Woodhouse, and S. L. Cooper, "Polyurethanes in Biomedical Applications," CRC Press, Boca Raton, FL, 1997.
220. R. Bonart, *Polymer* **20**, 1389 (1970).
221. M. Matsuo, *Jpn. Plast.* **2**, 6 (1968).
222. J. Dlugosz, A. Keller, and E. Pedemonte, *Kolloid Z. Z. Polym.* **242**, 1125 (1970).

14 Tire Engineering

BRENDAN RODGERS AND WALTER WADDELL
ExxonMobil Chemical Company
Houston, Texas

I. INTRODUCTION

In human history, the wheel is considered one of the most important inventions, because it found use in a wide range of applications such as transportation vehicles, construction equipment, and internal parts of machinery. Like most inventions, the wheel was a development of earlier devices such as rollers, dating to the Bronze age over 5000 years ago, used to move heavy objects. Wheeled vehicles were recorded in Sumeria in 3500 BC, Assyria in 3000 BC, and central Europe toward 1000 BC. Four-wheeled wagons using a swiveling front axle for steering were recorded in 1500 BC.

With the introduction of swifter horses from the Asiatic Steppes into Mesopotamia, the cart was adapted for military applications. The spoked wheel was introduced and then given its first "tire," consisting of first a leather and then copper and iron binding to prevent damage to the wooden wheel frame.

The next most important event was probably in 1846 when Thompson was granted a patent for an elastomeric air tube, to be fixed onto a wheel to reduce the power to haul a carriage, make motion easier, and reduce noise. This concept was much refined in the 1880s when the first pneumatic tire was developed for use on tricycles.

The discovery of vulcanization by Charles Goodyear in 1839 and the industrialization of Europe and North America enabled the tire to evolve from a rubberized canvas covering a rubber tube to a complex fabric, steel, and elastomeric composite.

This is a revision of the work published in *Science and Technology of Rubber, Second Edition*, 1994.

II. TIRE TYPES AND PERFORMANCE

In terms of both volume production and consumer awareness, pneumatic tires fall into essentially nine categories which are based on vehicle application. There are tires for racing vehicles, passenger vehicles, and light trucks where gross vehicle weights typically do not exceed 7250 kg. In such tires, significant quantities of fabric are used as a reinforcement. Larger tires such as those for heavy trucks, farm and agricultural vehicles, earthmoving equipment, and large aircraft tend to comprise both steel wire and fabric reinforcements. Finally there are a range of specialty tires which include those used on fork lift trucks, light aircraft, light construction equipment, and golf cars.

Regardless of the design or application of the tire, all pneumatic tires must fulfill a fundamental set of functions:

1. Provide load-carrying capacity
2. Provide cushioning and dampening
3. Transmit driving and braking torque
4. Provide cornering force
5. Provide dimensional stability
6. Resist abrasion
7. Generate steering response
8. Have low rolling resistance
9. Provide minimum noise and minimum vibration
10. Be durable throughout the expected life span

Dampening characteristics, elastic properties of rubber, and unique deformability and recovery combine to make tires the only product which satisfies all of these functions.

Essentially three performance parameters govern a tire's functions. These are (1) vehicle mission profile; (2) mechanical properties and performance such as wear resistance and casing durability; and (3) esthetics, comfort, and behavioral characteristics such as vehicle steering precision.

The mechanical properties of a tire describe the tire's characteristics in response to the application of load, torque, and steering input, resulting in the generation of external forces and deflection. Such mechanical properties are interrelated, and thus a design decision affecting one factor will influence the other factors, either positively or negatively. The result is a complex set of forces acting on a rolling tire on a vehicle (Fig. 1).

The tire axis system is the center of the tire–road surface contact shown in Fig. 1. The x axis is the intersection of the wheel plane with the road plane and with the positive direction forward. The z axis is perpendicular to the road plane with a positive direction downward. Thus, the normal force exerted by the tire is positive downward, and the vertical load reaction, which is the road pushing on the tire, is considered negative. The y axis is in the road plane and is directed so as to make the system right handed and orthogonal. This repre-

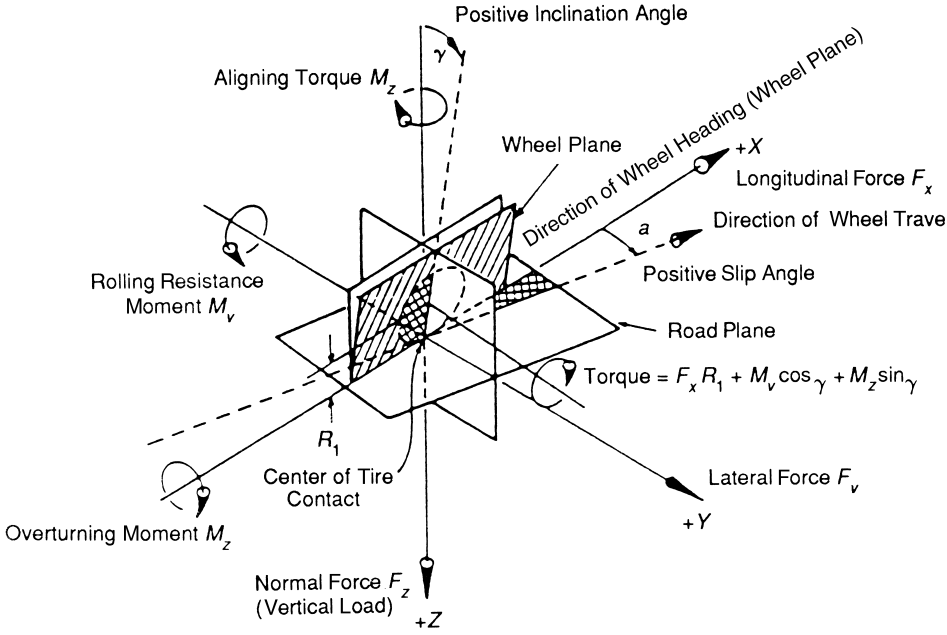

FIGURE 1 Tire forces and moments acting at the center of tire contact. (Reprinted with permission. © 1988 from SAE's 34th Buckendale Lecture. Society of Automotive Engineers, Inc.)

sentation of the tire axis system corresponds closely to the vehicle axis system when the tire is in the right front position of an automobile. In this case, the vehicle would be undergoing a left turn with positive self-aligning torque (M_z) and negative lateral force vector. The forces acting on a tire can thus be broken down into three fundamental vectors: the vertical forces control vehicle esthetics and comfort, the lateral forces impact vehicle control, and the longitudinal or forward forces control performance such as rolling resistance (Fig. 2).

III. BASIC TIRE DESIGN

A tire is essentially a cord–rubber composite. Tires have plies of reinforcing cords extending transversely from bead to bead, on top of which is a belt located below the tread. The belt cords have low extensibility and are made of steel and fabric depending on the tire application. The belt cords are at a relatively low angle, between 12° and 25°, and serve as restrictions to the 90° casing plies.

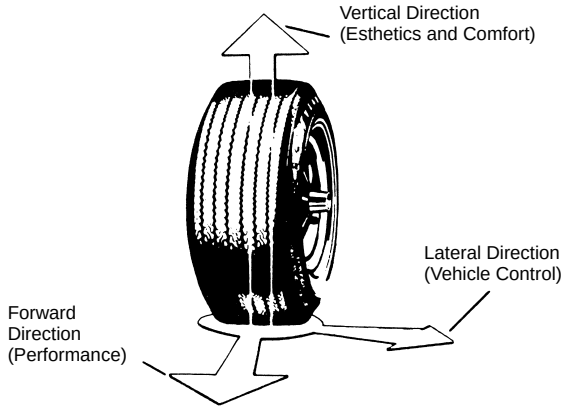

FIGURE 2 Tire functions.

A. Tire Construction

A range of specialized components are found in a tire, which serve to ensure that the product meets its intended design and performance requirements. For example, high-performance passenger tires can have a nylon overlay, also called a cap ply, located over the belt package. Nylon overlays restrict and control tire growth resulting from centrifugal forces created at high speeds. The ply turnup, which describes the manner in which the body ply wraps around the bead wire and turns up the sidewall, anchors the body ply to the bead bundle and further reinforces the lower sidewall region. A toe guard, which is a nylon-reinforced rubber component, protects the bead toe from tearing during mounting and dismounting. Above the toe guard, the chafer further protects the bead area from abrading against the rim flange during use (Fig. 3).

B. Tire Components

A tire is an assembly of a series of parts or subassemblies, each of which has a specific function in the service and performance of the product. Figure 4 illustrates the key components of a truck tire. The following are the parts of a tire:

Tread	The wear resistance component of the tire in contact with the road. It must also provide traction, wet skid, and good cornering characteristics with minimum noise generation and low heat buildup. Tread components can consist of blends of natural rubber, polybutadiene (BR), and styrene–butadiene rubber (SBR), compounded with carbon black, silica, oils, and vulcanizing chemicals.
Tread shoulder	Upper portion of the sidewall; affects tread heat dissipation and tire cornering properties.

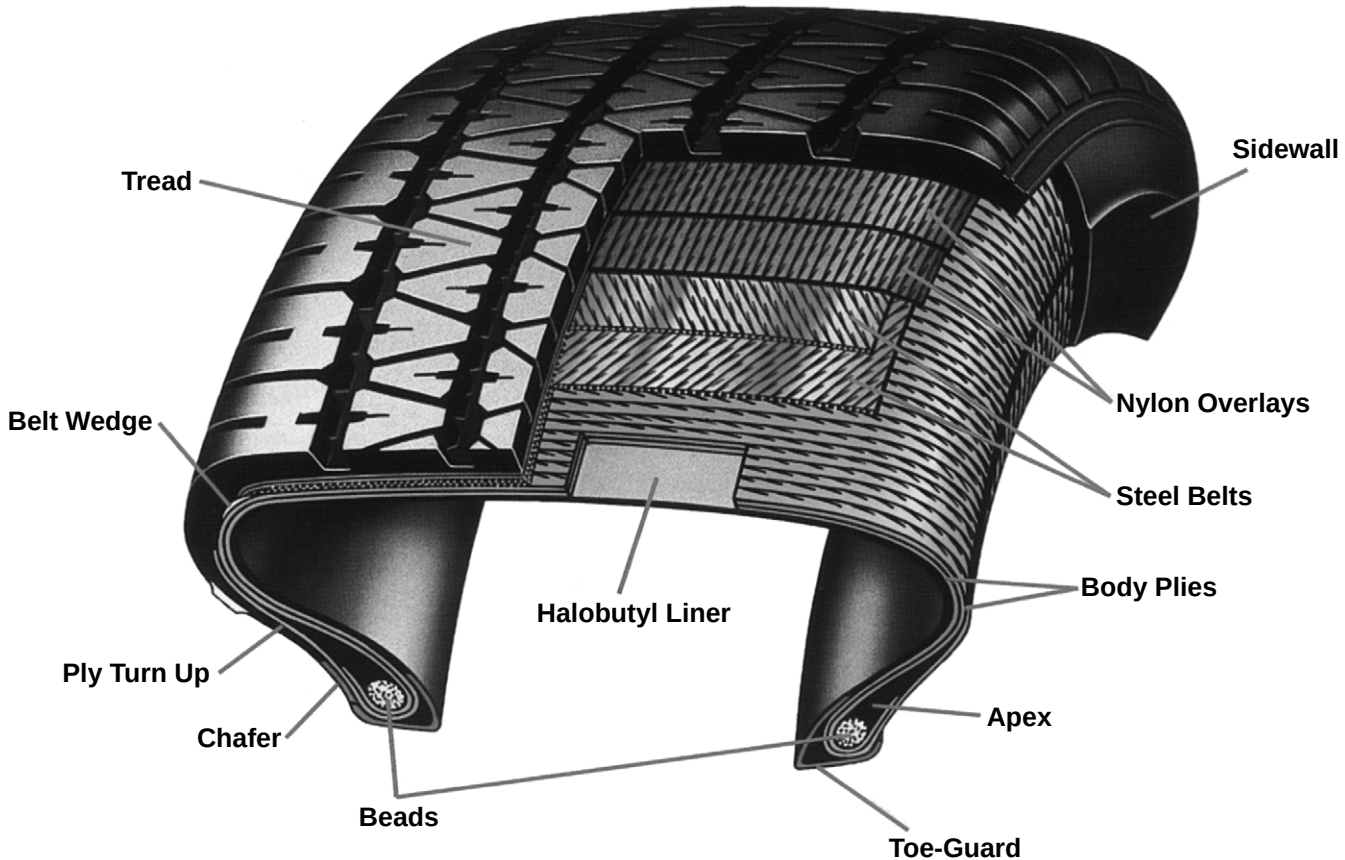

FIGURE 3 Cross-section of a high-performance passenger tire (see color insert).

Tread base	Also termed the cushion; the rubber compound used to ensure good adhesion between belts and tread, heat dissipation, and low rolling resistance.
Sidewall	Protects the casing from side scuffing, controls vehicle–tire ride characteristics, and assists in tread support. Sidewall compounds consist of natural rubber, SBR, and BR along with carbon black and a series of oils and organic chemicals.
Curb guard	A protrusion of rubber sidewall running circumferentially around the tire to protect it from scuffing on curbs.
Beads	Nonextensible steel wire loops which anchor the plies and also lock the tire onto the wheel assembly so that it will not slip or rock on the rim.
Bead area components	Include the apex or bead filler; the chafer, which protects the wire bead components; the chipper which protects the lower sidewall; and the flipper, which helps hold the bead in place.
Plies	Textile or steel cords extending from bead to bead and thereby serving as the primary reinforcing material in the tire casing.
Belts	Layers of textile or steel wire lying under the tread and serving to stiffen the casing, thereby allowing improved wear performance and handling response, better damage resistance, and protection of the ply cords from road hazards.
Shoulder belt wedge	High-adhesive rubber compound in the shoulder region between the belts and casing; improves tread wear and durability.
Liner	Butyl rubber or halogenated derivatives of such polymers which retains the compressed air inside the tire.

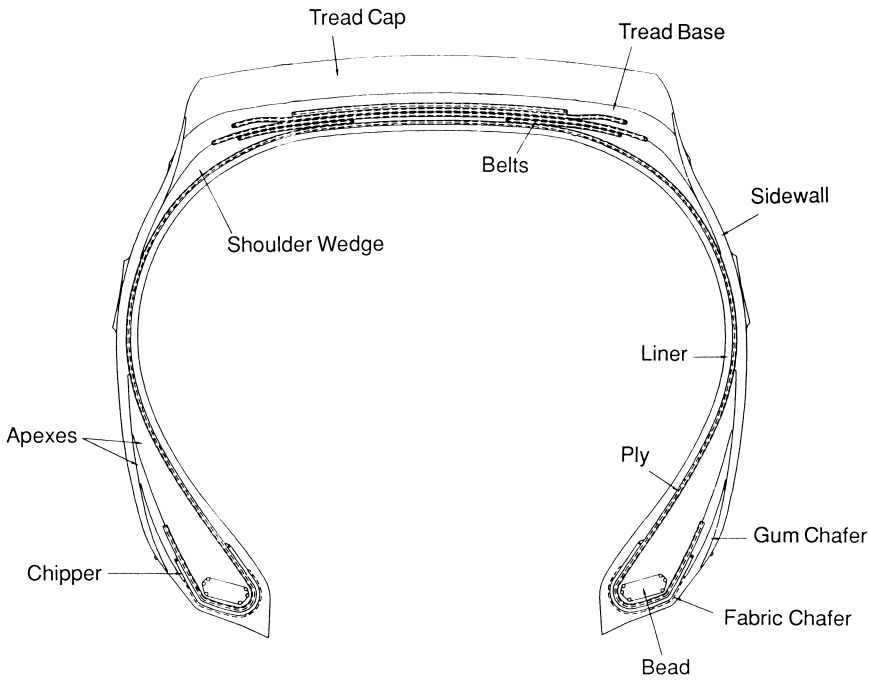

FIGURE 4 Components of a radial truck tire.

IV. TIRE ENGINEERING

In essence, a tire is a composite of complex elastomer formulations, fibers, textiles, and steel cord. The term *tire structure* defines the number, location, and dimensions of the various components used in its composition. The primary components that govern the performance of a tire are the casing plies, bead construction, belts, sidewall, inner liner, and tread. Chafers, flippers, and overlays, which are strips of rubberized fabric located in the bead and crown area, of the tire are termed *secondary components* because they protect the primary components by minimizing stress concentrations [1, 2].

A. Tire Nomenclature and Dimensions

Terminology used to describe tire and rim dimensions is explained in Fig. 5. These dimensions are commonly used throughout the tire industry to describe size, growth, and wheel well clearance factors in addition to computation of variables such as load capacity and revolutions per unit distance traveled [3, 4, 5]. In addition, the following definitions should be noted:

Aspect ratio — A numerical term which expresses the relationship between tire section height and cross-section width. An aspect ratio of 70 indicates the tire section is approximately 70% as high as it is wide.

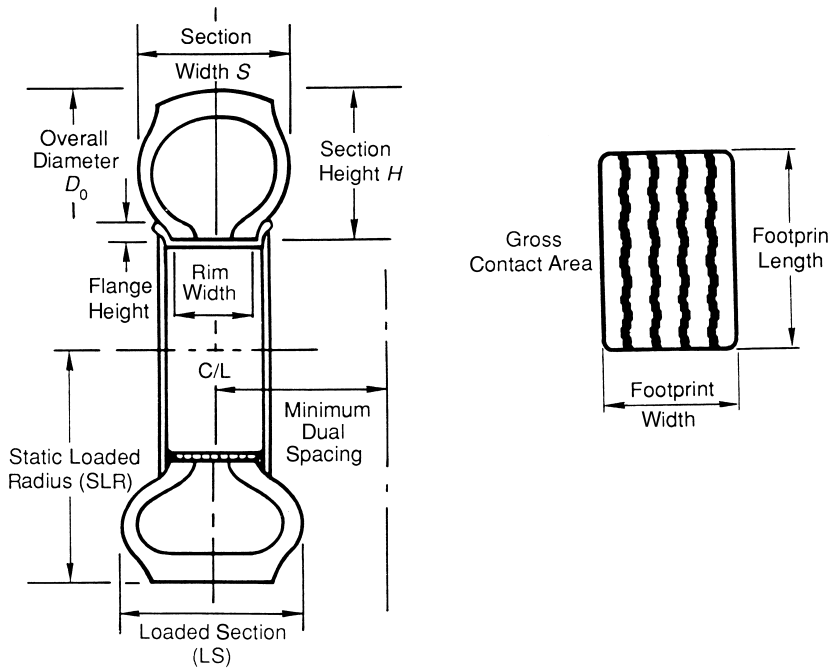

FIGURE 5 Tire and rim dimensions.

Cord angle	Angle of the cord path to the centerline the tire; the predominant factor affecting the tire shape or contour. In radial tires the cord angle is 90°.
Overall diameter	Unloaded diameter of a new tire–rim combination.
Section width	Width of a new tire section excluding side ribs, lettering, and decorations.
Static loaded radius	Distance from the road surface to the horizontal centerline of the rim.
Minimum dual spacing	Minimum dimension recommended from rim centerline to rim centerline for optimum performance of a dual-wheel installation.
Footprint length	Length of a loaded footprint.
Footprint width	Width of the loaded footprint.
Gross contact area	Total area under the loaded footprint.
Net contact area	Area of the tread, excluding voids, under the loaded footprint. Also abbreviated as the percent net-to-gross.
Asymmetrical	Tire design in which the tread pattern on one side of the centerline differs from that on the other side.
Load rating	Maximum load a tire is rated to carry for a given usage at a specified inflation. The "Load Range" is also used to define the load-carrying capability of a tire. Load ranges are specified in Tire & Rim Association tables. Table I illustrates load values for a single mounted 11R24.5 heavy-duty truck tire.

Three basic tire size designations are used:

1. Conventional-size tires used on flat base rims, normally tube-type tires
2. Conventional-size tires used on 15° rims or tubeless
3. Metric sizes also used on 15° rims; tubeless

In addition, the letter "R" in a size designation indicates "radial," "D" or (—) is bias, and "ML" indicates the tire is for mining and logging applications. The letter "P" denotes passenger vehicle tire, and "LT" is light truck.

For example, the tire size designation "LT 235/75R15" has the following meaning:

LT	Light truck
235	Approximate section width in millimeters when mounted on the proper rim
75	Aspect ratio
R	Radial construction
15	Nominal rim diameter in inches

A heavy-duty truck tire would typically have the size designation of 11R24.5 for a conventional tubeless tire; a low-profile metric tire typically could be sized 295/75R22.5. For the conventional tire,

11	Nominal section diameter in inches
R	Radial construction
24.5	Rim diameter in inches

Such conventional-size tires have a standard aspect ratio of 80. The initial step in designing a tire is determination of the required size. Size determination is governed by rim dimensions, wheel well envelope, service load, service speed, and inflation. For a metric heavy-duty truck tire these factors are related by the equation

TABLE I Tire and Rim Association Load Values for a Single Mounted Radial Medium Truck Tire [3]

Load range requirement	Ply rating	Example of tire size	Loaded tire limit (lbs)	Inflation pressure
F	12	295/75R22.5	5,070	90
G	14	295/75R22.5	5,780	100
H	16	295/75R22.5	6,610	120
H	16	285/75R24.5	6,780	120
J	18	385/65R22.5	9,370	120
L	20	425/65R22.5	11,400	120

TABLE II European Tire and Rim Technical Organization ETRTO Load Index Numerical Code for Tire Load Carrying Capability [4]

Load index	Load carrying capability (Kg)
144	2800
145	2900
146	3000
149	3250
152	3550
155	3875
160	4500

$$L = (6.075 \times 10^{-5}) K \times P^{0.7} \times S_{\mathrm{d}}^{1.1} (D_{\mathrm{r}} + S_{\mathrm{d}}) \tag{1}$$

where L = load at 100 kph (kg); P = pressure (kPa); S_{d} = dimensional factor, section width adjusted for aspect ratio; D_{r} = rim diameter; and K = constant dependent on vehicle speed. Using equations such as (1), developed by the Tire & Rim Association, the tire engineer can determine the optimum tire size for a specific application. Normally, load requirements are known so Eq. (1) can thus be used to calculate required service pressure. This process is then used in size and load range selection. Tire industry standards are used extensively in the design process [5, 6]. Load specification are tabulated in Tables I and II.

B. Tire Mold Design

Tire mold design initially begins with determination of the inflated dimensions of the required tire size. By use of inflated tire and growth characteris-

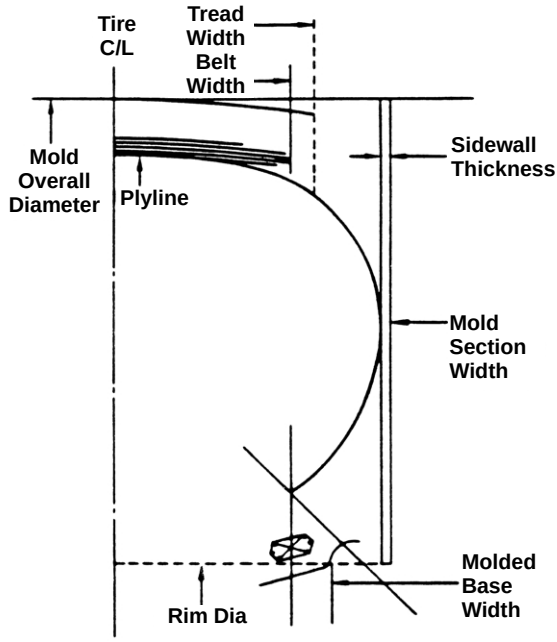

FIGURE 6 Plyline boundaries.

tics of the tire, preliminary plyline and mold dimensions are computed (Fig. 6). Once the mold boundary dimensions, location of the plyline, and tread width and depth are known, the contours of the tread, shoulder, sidewall, and bead components can be established. These dimensions and contours are developed using computer-aided engineering techniques (Fig. 7).

The primary interest in designing a tire lies in the belt area, bead area, and belt and ply cord tension. As radial tires contain multiple belts, these layups must be viewed as a package. The stiffness of the radial tire belt package is a function of belt wire angles, wire gauge, belt gauge, and compound stiffness. Figure 8 illustrates a four-belt configuration of a radial truck tire. As an empirical guide, an increase in the stiffness of the belt package, while maintaining belt width, will improve tread wear performance.

The stiffness of a tire belt package can be quantified by determination of the "Gough stiffness" (S), which is a measure of the in-plan bending stiffness of the rigid belt wire, cord, and rubber compound laminate. High radial tire belt rigidity and crown stiffness can significantly improve tire tread wear through provision of a solid foundation for the tread compound [7, 8]. Elaborating, Gough determined that a simple beam model of tire construction features could be used to predict relative tread wear performance. Using both shearing and bending moments in the computation, an empirical equation was derived defining the stiffness parameter S for a simple laminate

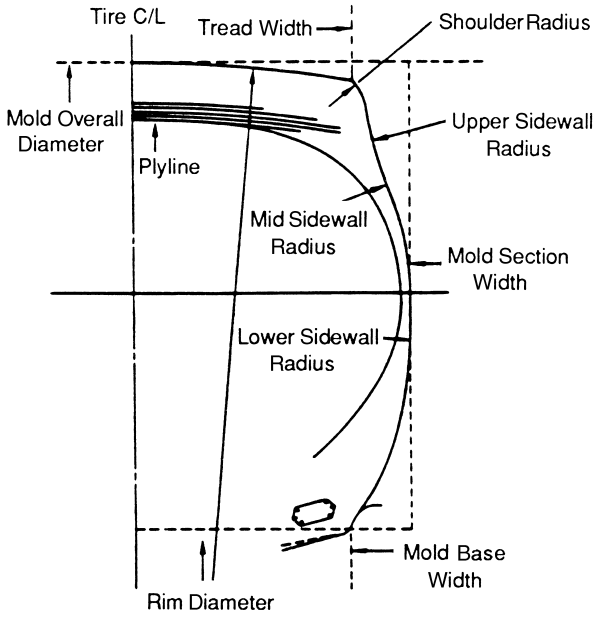

FIGURE 7 CADAM-developed mold cavity.

$$S = P/d \tag{2}$$

where load, P, is the force applied to the crown area layup or laminate to give a deflection d.

In a tire, Gough stiffness is a function of the circumferential modulus and shear modulus of the composite.

$$S = (E \times G)/(C_1 \times E) + (C_2 \times G) \tag{3}$$

where S = Gough stiffness, E = circumferential modulus of the cord–rubber laminate, G = shear modulus of the cord–rubber laminate, C_1 = constant dependent on the tire size, and C_2 = constant dependent on the tire size. In essence, Eq. (3) can be simplified to a model consisting of a simple supported beam of length L with elastic constants E and G deflected distance d by force P as

$$S = PL^3/48EI + 2PL/8AG \tag{4}$$

where A is the in-plane cross-sectional area to which the force P is applied, and I is the moment of inertia of the beam.

Computer analysis of the effect of the belt angle on Gough stiffness of the four-belt layup is illustrated in Fig. 8(b).

For a right/right/left/right belt configuration, the belt angle (θ) of the second and third belts was varied from 10° to 26°. Computation of an optimum belt layup will permit achievement of the required Gough stiffness.

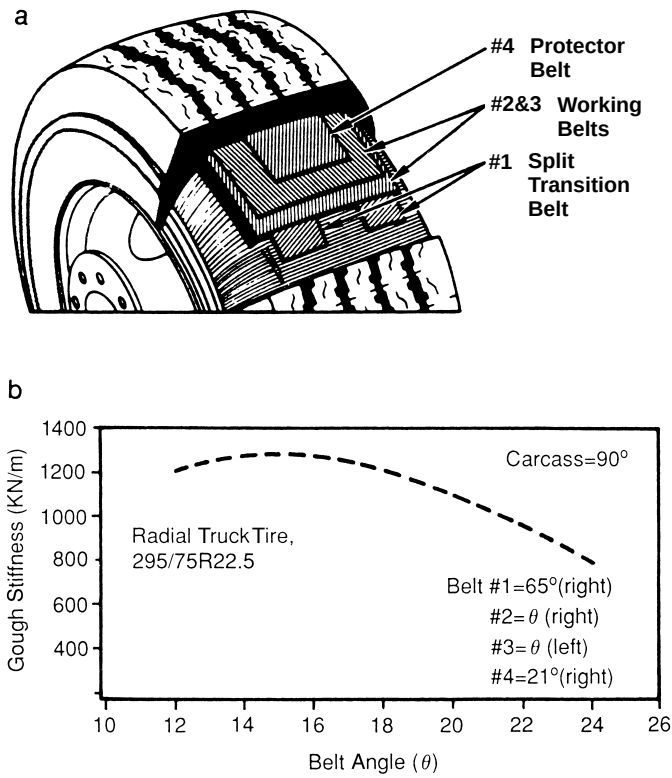

FIGURE 8 (a) Typical four-belt layup for a truck tire. (b) Impact of Gough stiffness.

Structural mechanical calculations such as finite-element analysis (FEA) are used to analyze both the inflated and loaded deflected shapes of a tire cross-section and the resulting stress–strain relationships in the belt area. Such studies permit both quantitative analysis and qualitative comparisons of the range of belt configuration options. Figure 9 shows a heavy-duty truck tire in the loaded and unloaded states. The density of grids is designed so as to preserve the essential features of the tire cross-section geometry while maintaining the total number of grid points.

In an analysis of the belt package, three conditions can be evaluated which allow computation of the range of strain energy densities, i.e., inflated tire condition, loaded tire condition 180° away from the footprint, and loaded tire condition at the center of the footprint. Figure 10 illustrates these three conditions. It shows that the strain energy density in megapascals in an inflated tire is similar to that in a load tire 180° away from the footprint. At the center of the footprint in a loaded condition, however, the strain energy density at the belt edge has increased from the range 0.01–0.27 MPa to 0.05–0.51 MPa. These high-strain areas correspond to typical failure-sensitive regions in actual tires.

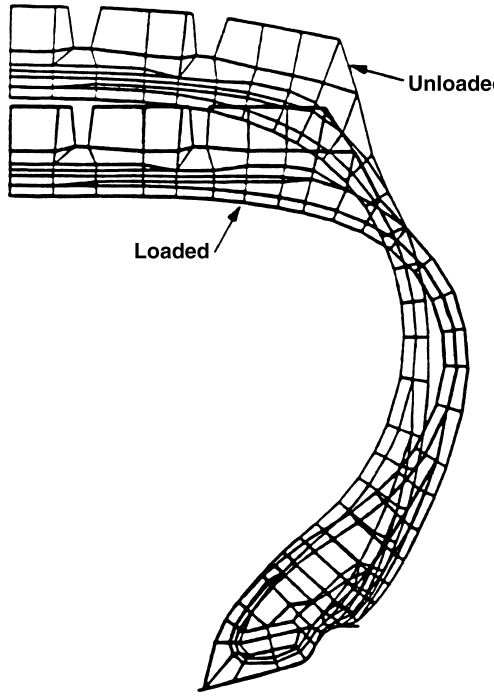

FIGURE 9 Finite-element structure of a heavy-duty truck tire.

Similar to the belt area of the tire, the bead region also lends itself to finite-element analysis. Switching grid details to the bead enables analysis of the ply end strains on inflation as well as in a loaded state as the tire makes a complete revolution. By viewing Fig. 11, it is possible to evaluate strains caused by tire inflation and cyclic deformation via FEA quantitatively, whereas without such tools, tire building and testing are required.

C. Cord Tension

The selection of cord materials for belt and plies in a tire and the associated physical locations lend themselves to further FEA analysis. If one takes an inflated nonbelted tire, the ply cords, whether they are in a single-ply casing or multiple-bias-ply construction, will assume a configuration which minimizes strain within the composite. The resulting cord path is termed the *neutral contour*. Belted tires introduce a restriction to the inflated diameter of the tire, and the neutral contour or plyline of such systems is consequently altered.

The plyline is determined as shown in Fig. 12. The principles of plyline determination were developed by Purdy, a pioneer mathematician

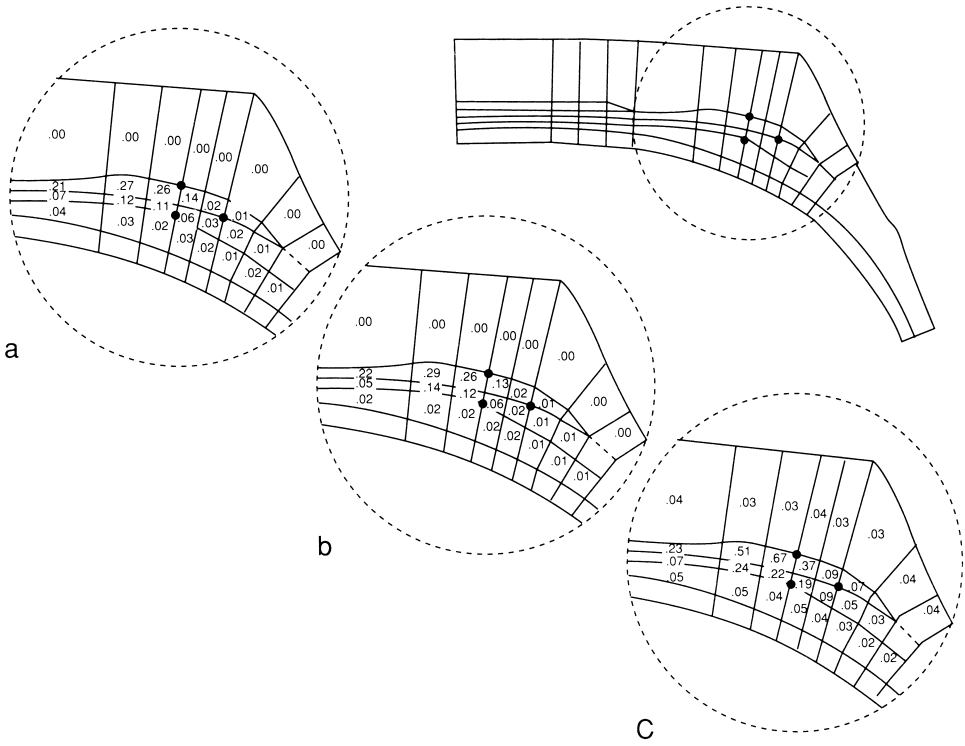

FIGURE 10 Finite-element analysis of belt area showing strain energy density (in MPa). (a) Inflation. (b) Loaded 180° away from footprint. (c) Loaded at center of footprint.

who derived the basic mathematical equations for cord path and tire properties [9].

Typical inflated cord tension plots for a truck tire are shown in Fig. 13. In an unloaded state the cord tension for the belts tends to be at the tire centerline, and the ply tension is greatest at the point corresponding to the sidewall location; however, on application of a load to the inflated tire and consequent deflection, the cord tensions increase at the belt edges away from the centerline and also in the bead zone. As reviewed earlier, these two regions tend to be the failure zones in a tire construction (Fig. 14).

D. Tread Design Patterns

The tread pattern influences the ability of the tire to transmit driving forces, braking, and lateral forces while operating on a broad range of highway and off-road surfaces. The design of a tread pattern is essentially the separation or division of a smooth tread into smaller elements or blocks. These ele-

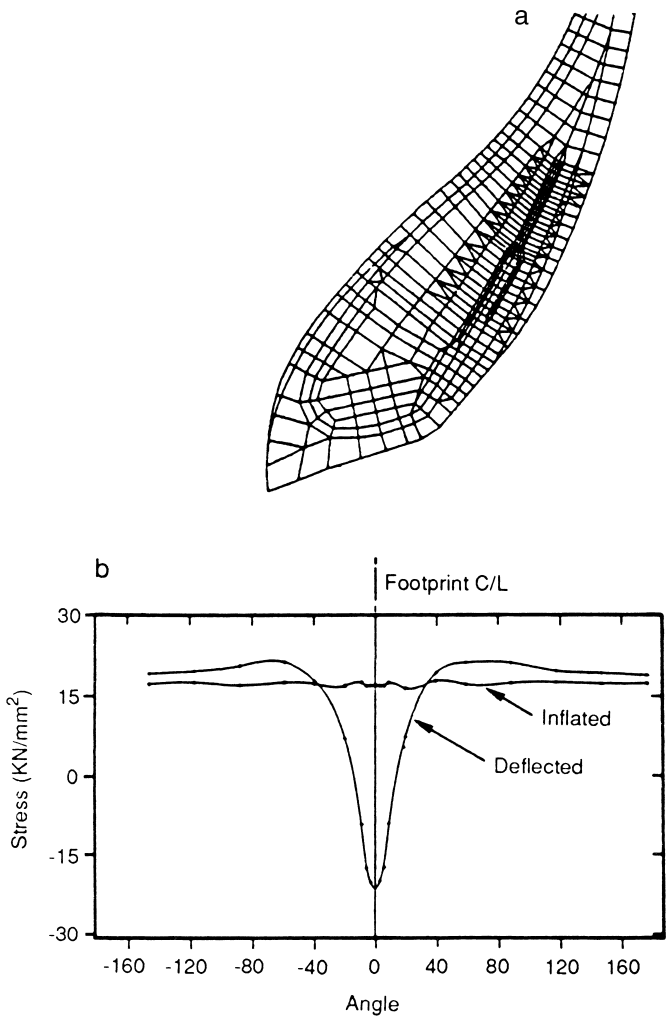

FIGURE 11 (a) Finite-element analysis of a bead region. (b) Ply end stress versus rotation from the center of footprint.

ments are arranged in a repetitive pattern of voids, ribs, lugs, slots, and grooves. The pattern is first described in terms of length, width, percentage of void of the various elements, and angles. The tread elements are then arranged to give the tread traction characteristics, optimized ratio of net-to-gross contact area, and minimum noise creation [1, 10, 11].

For a truck tire, tread patterns can be classified into five basic types (Fig. 15):

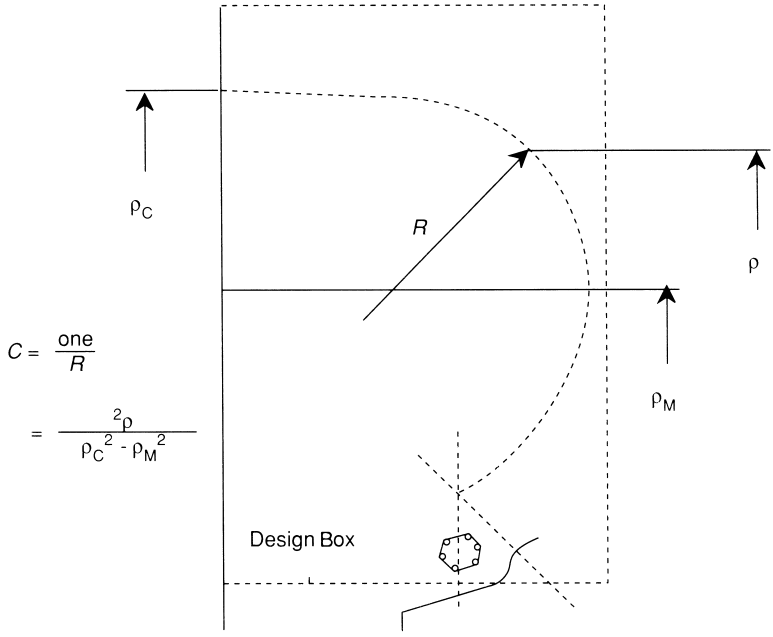

FIGURE 12 Plyline definition. Purdy's equation defines ideal inflated or "natural" shape for "thin-film" structure. C = curvature of the plyline, ρ_c = radius from the center of the axle to the center of the plyline or tire centerline, and ρ_M = radius from the center of the axle to the center plyline width.

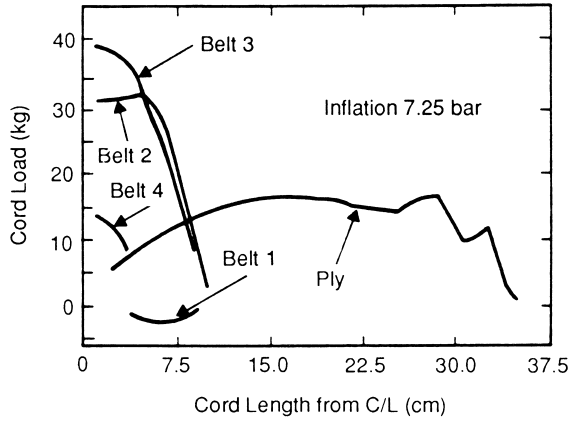

FIGURE 13 Inflated tire unloaded.

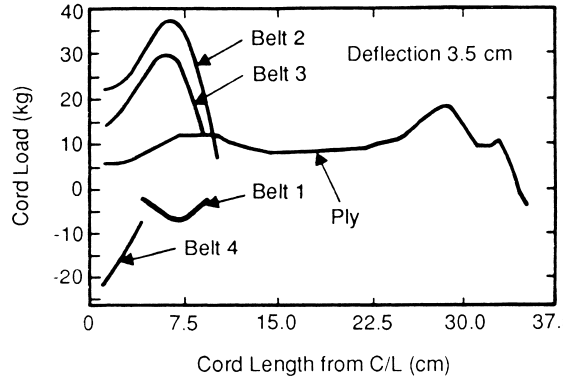

FIGURE 14 Inflated tire loaded and deflected.

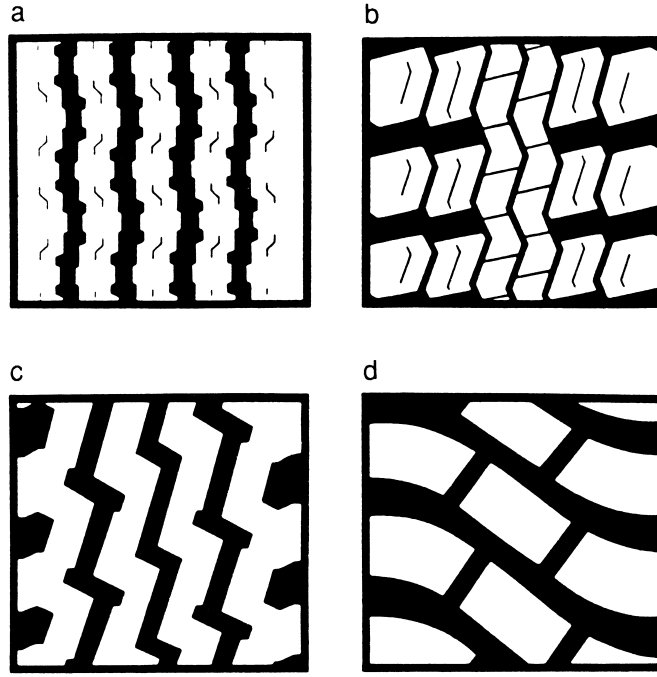

FIGURE 15 Basic tread patterns: (a) highway rib; (b) highway rib/lug design; (c) on/off highway (mixed service); (d) off highway.

1. Highway rib
2. Highway rib/lug combination, where the rib can be either inboard or outboard in the shoulder area (the lugs will be correspondingly opposite to the ribs, outboard or inboard)
3. Highway lug design
4. On/off highway (special service)
5. Off highway

Rib designs with design elements principally in the circumferential direction are the most common type of tread pattern and show overall good service for all-wheel-position summer service. On heavy trucks, they are used nearly exclusively on steer and trailer axles because of their lateral traction and uniform wear characteristics. Rib/lug combinations tend to find use on all-season tires, which require a balance of good tread wear, traction, and wet skid. On heavy-duty truck drive axles, where forward traction is a prime requirement and where fast tread wear occurs as a result of torque-induced slip, the highway lug design is required. For off-highway service conditions the tread pattern assumes a staggered joint lateral circumferential direction for both lateral and forward traction. Grooves tend to be larger and deeper, with the rib walls angled to prevent stone retention.

The ratio of net contact to gross tread surface area decreases as wet traction becomes more important. Tables III and IV illustrate the net-to-gross percentage for various tire tread patterns.

A number of additional terms are used to describe a tread pattern:

Groove amplitude	In staggered groove designs the distance the groove pattern oscillates about the central direction which the groove follows. It is analogous to a sine wave.
Sipes	Small individual tread voids, generally added to a tread design to improve traction characteristics.
Pitch length	Length of each repeating unit in a tread pattern. Variable pitch lengths in a tread design can be used to minimize noise. Pitch would be analogous to the wavelength of a sine wave.
Blade	A protrusion in a curing mold that forms part of the tread design. The protrusion forms a corresponding depression in the finished tire.
Stone ejection rib	Portion of the tread rib designed to throw off stones with the aid of normal tire flexing. Located up to 75% down in the tread grooves to prevent small stones from locking down at the base of the grooves where they cannot be ejected.

V. TIRE MATERIALS

Tire engineering is the study of the stresses created within a tire and includes such factors as straining of components while the tire is being built, the tire stresses while mounted on a wheel of a moving loaded vehicle, quantification of such stresses, and minimization of such stresses through effective distribution of load and proper selection of materials. Consequently, tire tech-

TABLE III Net-to-Gross Contact Area with Nature of Service[1,8]

Type of service	% Net to gross	Relative tread depth	Traction handling	Wear
Highway steer tires	70–75	+ +	+	+ + +
Highway drive axle tire	70–80	+ + +	+ +	+ + + +
Highway trailer tires	75–85	+	+	+ + + +
On/off road (mixed service)	60–70	+ + +	+ + +	+ +
Off highway	55–65	+ + + + +	+ + +	++

TABLE IV Automobile Tire Tread Pattern Classes

Category	Design	Application	Net-to-gross pavement contact area	Vehicle handling comfort
1	Central solid rib, outer rib block configuration	High mileage	High	+ + + + +
2	All block	All season	Medium–high	+ + + +
3	Block–rib	Traction	Medium	+ + +
4	Central groove outboard blocks	Traction, high performance	Low–medium	+ + +
5	Direction —Asymmetric —Symmetrical	High performance	Low–medium	+ +

nology groups tend to be multidisciplinary teams consisting of mechanical engineers, computer scientists, chemical engineers, chemists, and mathematicians. To understand tire engineering, it is necessary to have knowledge of the function of each of the types of materials used in a tire structure. This could be considered essentially in two aspects: the tire reinforcing system and rubber compounding.

A. Tire Reinforcement

A tire is a textile–steel–rubber composite; the steel and textile cords reinforce the rubber and are the primary load-carrying structures within the tire. Because of the performance demands of fatigue resistance, tensile strength, durability, and resilience, seven principal materials have been found suitable for tire application: cotton, rayon, nylon, polyester, steel, fiberglass, and aramid; the latter three materials find primary usage in the tire crown or belt region.

The science of tire reinforcement employs a specialized terminology which the tire engineer must understand:

Brass weight	Typically 3.65 gms/kg of cable; brass coat thickness is of the order of 0.3 microns.
Breaking strength	Tensile strength.
Cord	Structure consisting of two or more strands when used as plied yarn or an end product.
Denier	The weight of cord expressed in grams per 9000 meters.
EPI	Ends of cord per inch width of fabric.
Fibers	Linear macromolecules orientated along the length of the fiber axis.
Filaments	Smallest continuous element of textile, or steel, in a strand.
Filling	Light threads that run right angles to the warp (also referred to as the "pick") that serves to hold the fabric together.
LASE	Load at a specified elongation or strain.
Length of lay	Axial distance an element or strand requires to make a 360° revolution in a cord.
Ply twisting	Twisting of the tire yarn onto itself the required number of turns per inch; two or more spools of twisted yarn are then twisted again into a cord: for example, if two 840-denier nylon cords are twisted together, an 840/2 nylon cord construction is formed; if three 1300-denier polyester cords are twisted together, they give a 1300/3 cord construction.
Rivit	Distance between cords in a fabric; high rivit typically describes a fabric with a low EPI.
Tenacity	Cord strength, frequently expressed in grams per denier.
Tex	Cord weight expressed in grams per 1000 meters.
Twist	Number of turns per unit length in a cord or yarn; direction of twist can be either clockwise ("S" twist) or counterclockwise ("Z" twist); twist imparts durability and fatigue resistance to the cord, though tensile strength can be reduced.
Warp	Cords in a tire fabric that run lengthwise.
Weft	Cords in a fabric running crosswise.
Yarn	Assembly of filaments.

Fibers and steel cord are the primary reinforcement and load-carrying material in the tire. It is thus appropriate to review the properties of such materials for application in tires.

B. Steel Cord

Steel wire used in tires are of various configurations, but all are brass-coated wire strands wrapped together to give cords of different characteristics, depending on the application. Steel tire cord is manufactured from high-carbon-steel rod which is first drawn down to a diameter of approximately 1.2 mm. A brass plating is then added to the wire before a final drawing to 0.15–0.40 mm. These filaments are next stranded to form a cord construction which is designed and optimized for a specific service requirement [12].

TABLE V Composition of Steel Tire Cord

Element	Composition (%)	Function
Carbon	0.65	Strength
Chromium	0.05	Strength
Copper	0.02	Strength
Manganese	0.60	Deoxidation
Silicon	0.25	Deoxidation
Sulfur	0.03	Machinability

Steel tire cord is manufactured from high-quality steel which is necessary because of the performance demands to which tires are subjected. The composition of a typical steel cord is illustrated in Table V. The key mechanical properties governing a steel cord or wire are its tensile strength, elongation, and bending stiffness. A tire cord construction is normally defined by the structure, the length of lay, and the direction of lay. The full description of a steel cord is given by

$$(N \times F) \times D + (N \times F) \times D + (F \times D) \tag{5}$$

where N = number of strands, F = number of filaments, and D = nominal diameter of filaments (in millimeters).

An example of a steel cord specification would therefore take the form

$$(1 \times 4) \times 0.175 + (6 \times 4) \times 0.175 + (1 \times 0.15) \tag{6}$$

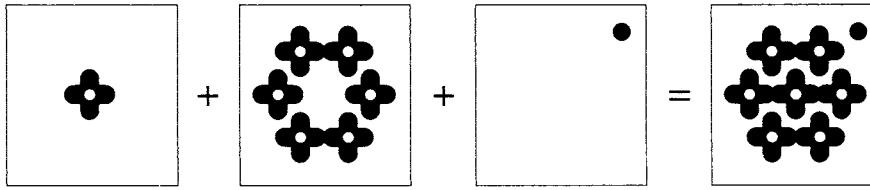

When N or F equals 1, the nomenclature system allows their exclusion. Thus, (6) is reduced to

$$4 \times 0.175 + (6 \times 4) \times 0.175 + 0.15 \tag{7}$$

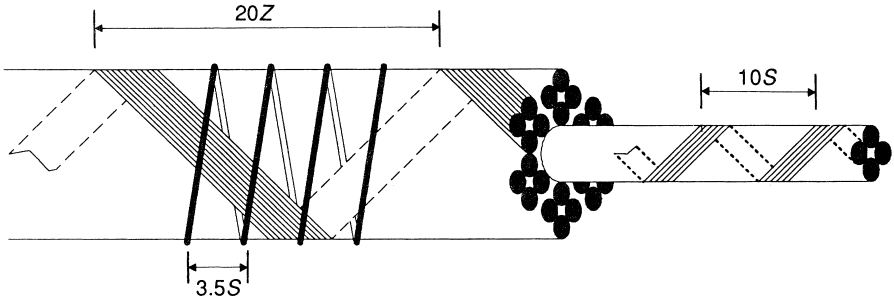

FIGURE 16 Length of lay and direction of lay. (Courtesy of Bekaert Corporation.)

TABLE VI Design of a Tire Cord

Design parameter	Design factor
Stiffness	Number of strands in cord, gauge
Strength	Gauge, number of strands in cord, steel rod composition
Fatigue	Filament gauge
Elongation	Twist, lay

A number of additional conventions are used in defining a steel tire cord:

1. If the diameter D is the same for two or more parts in a sequence, then the diameter is specified only at the end of the sequence.
2. The diameter of the spiral wrap is specified separately.
3. When the innermost strand or wire is identical to the adjacent strand or wire, the definition of the wire can be further simplified by specifying only the sum of the identical components. Then (7) becomes

$$7 \times 4 \times 0.175 + 0.15 \tag{8}$$

4. The sequence or order in a wire designation follows the sequence of manufacture. The length of lay and direction of lay for the cord in (8) can be described as illustrated in Fig. 16.

A number of empirical guidelines govern the construction of a wire for use in tires. For example, if the wire is used in a ply rather than in belts, it will undergo a greater amount of flexing. Hence fatigue performance will be important. If application is in belts, then stiffness becomes a primary design parameter. Thus, key design properties can be specified and are highlighted in Table VI.

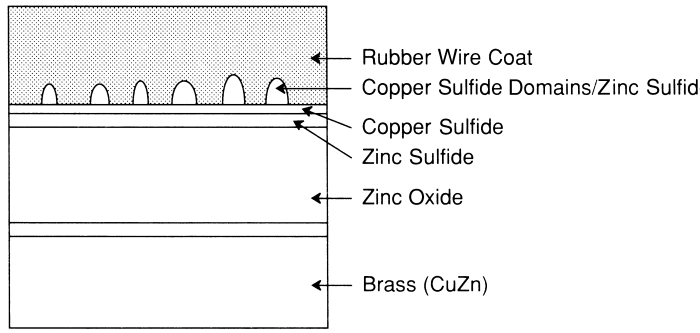

FIGURE 17 Interfacial copper sulfide film in rubber–brass bonding. (From Gough [7].)

The thicker a cord is, the stiffer it will be. Thinner cords tend to show better fatigue resistance. Heavier cords tend to find use in the larger tires such as heavy-duty truck tires and tires for earthmoving equipment.

Wire finds application in tire reinforcement in tire belts, heavy-duty tire plies (e.g., in large truck tires), beads, and chippers (which protects the bead from wheel rim damage).

C. Mechanism of Rubber: Brass Wire Adhesion

The thin coating of brass on the steel cord is the primary adhesive used in steel-to-rubber bonding. The quality of this bonding system built up during vulcanization of, for example, a radial tire will influence the performance of the steel ply or steel belt in the tire and, ultimately, the durability of the product. Though the mechanism of bond formation in rubber–steel cord adhesion is very complex, a brief review of the current understanding of wire to rubber adhesion is presented.

Natural rubber typically used in wire coat compounds forms a strong bond with brass as a result of the formation of an interfacial copper sulfide (CuS) film during vulcanization. Copper sulfide domains are created on the surface of the brass film during the vulcanization reaction. Such domains have a high specific surface area and grow within the wire coat compound before the viscous polymer phase is crosslinked into a elastomeric network. Thus the polymer molecules become locked into the crystalline copper sulfide lattice (Fig. 17). Important factors governing this bonding are formation of copper sulfide, cohesive strength, adhesion to the brass substrate, and rate of secondary corrosion reactions underneath the copper sulfide film.

Zinc sulfide and iron sulfide do not bond because they do not grow rapidly enough during vulcanization, do not form porous domains, and thus cannot interlock with the polymer. As the primary requirement is the formation of a

copper sulfide domain before the initiation of crosslinking, reduction of compound scorch time, consequently, can adversely affect bond formation.

Mechanical stability of the copper sulfide domains is essential to retain long-term durability of the rubber-to-wire adhesion. However, corrosion of the wire–rubber adhesive bond is catalyzed by Zn^{2+} ions that diffuse through the interfacial CuS layer. This will eventually result in an excess of either ZnS or $ZnO/Zn(OH)_2$. Under dry conditions, this process is slow. Nevertheless, Zn^{2+} will migrate to the surface with a consequent drop in mechanical interlocking of the CuS domains and rubber followed by adhesion loss.

Migration of Zn^{2+} ions is a function of the electrical conductivity of the brass coating. Addition of Co^{2+} or Ni^{2+} ions will reduce this conductivity.

Cobalt salts in the wire coat compound act to accelerate the vulcanization rate of high-sulfur compounds which wire coat compounds can be. The increase in crosslink density increases the pullout force of the wire in the rubber. More important, cobalt salts form Co^{2+} ions at the interface of the brass surface during vulcanization, and this will affect copper sulfide formation.

Differences in efficiencies between cobalt adhesion promoters is due to the ease with which Co^{2+} ions can be formed. For example, zinc or brass reacts more easily with cobalt boron decanoate complexes than with cobalt naphthenate or stearate. The Co^{2+} and Co^{3+} ions are incorporated into the ZnO film before the sulfide film has been built up. Both di- and trivalent cobalt ions reduce the electrical conductivity of the ZnO lattice, thereby reducing the diffusion of Zn^{2+} ions through the semiconducting film.

Diffusion of metallic copper domains to the surface following oxidation by $R—S_x$ is not affected, as Cu^{2+} ions migrate along grain boundaries of the ZnO layer. Thus if a cobalt salt is used, formation of copper sulfide at the cord surface will be accelerated, whereas ZnS generation will be hindered (Fig. 18). This review is necessarily brief, and the reader is encouraged to consult additional references for further detail on the chemistry of rubber–brass adhesion [13, 14].

D. Rayon

The first synthetic fiber for tires was rayon. Cellulose is initially treated with sodium hydroxide to form an alkali cellulose. It is then shredded and allowed to age in air where it is oxidized and undergoes molecular weight reduction to enable subsequent spinning operations. Treatment with carbon disulfide produces cellulose xanthate which is then dissolved in sodium hydroxide to form viscose. The material undergoes further hydrolysis and is then fed into spinnerets to produce the fiber. This fiber is passed through a bath of sulfuric acid and sodium sulfate where the viscose fibers are further coagulated.

Washing, bleaching, and twisting into cords follow. The rayon fibers can be drawn or stretched up to 100% of their original length to enable crystalline orientation to produce a high-tenacity rayon suitable for tires.

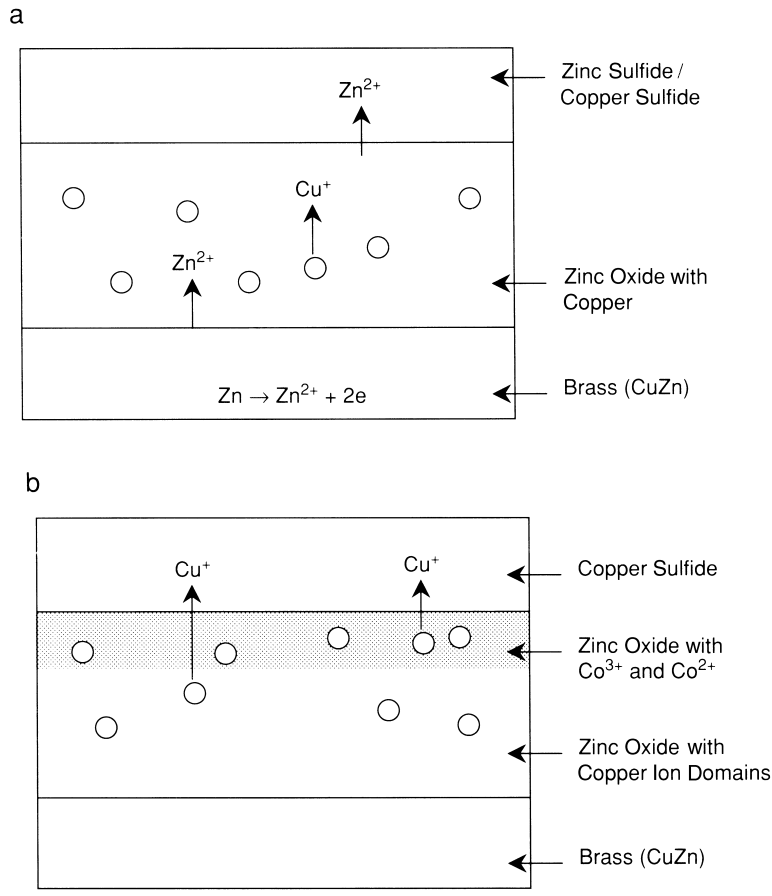

FIGURE 18 Copper sulfide formation at low cobalt concentration. (a) Absence of cobalt allows formation of zinc sulfide. (b) Cobalt ions in zinc oxide film hinder zinc ion migration and zinc sulfide formation.

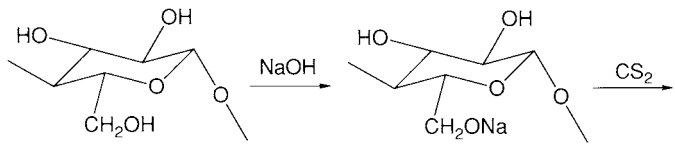

Cellulose Alkali cellulose (9)

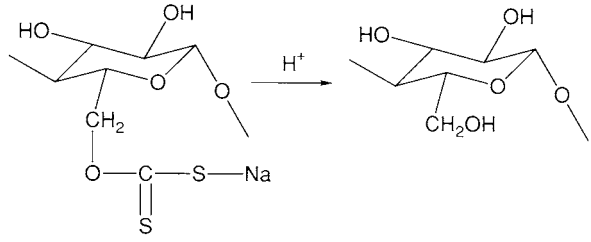

Cellulose xanthate Regenerated cellulose (9)

E. Nylon

Nylon is a polyamide polymer characterized by the presence of amide groups—(CO—NH)—in the main polymer chain. A wide variety of nylon polymers are available but only two have found application in tires: nylon 6,6 and nylon 6.

Nylon 6,6 is produced from a condensation reaction between adipic acid and hexamethylenediamine,

$$\underset{\text{Hexamethylenediamine}}{H_2N-(CH_2)_6-NH_2} + \underset{\text{Adipic acid}}{HOOC-(CH_2)_4-COOH} \longrightarrow \underset{\text{Nylon 6,6 polymer chain}}{+NH-(CH_2)_6-NH-CO-(CH_2)_4-CO+_n} \quad (10)$$

The "6,6" in the polymer designation denotes the six carbon atoms of hexamethylenediamine and the six carbons of adipic acid. Nylon 6 is produced from caprolactam by a ring-opening polymerization. As caprolactam

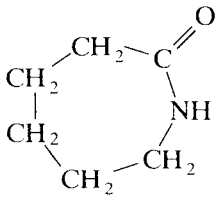

Caprolactam

$$\longrightarrow [-NH-(CH_2)_5-CO-NH-(CH_2)_5-CO-]_n$$

Nylon 6 polymer chain (11)

contains six carbon atoms and only one monomer are used, the polymer is thus designated nylon 6.

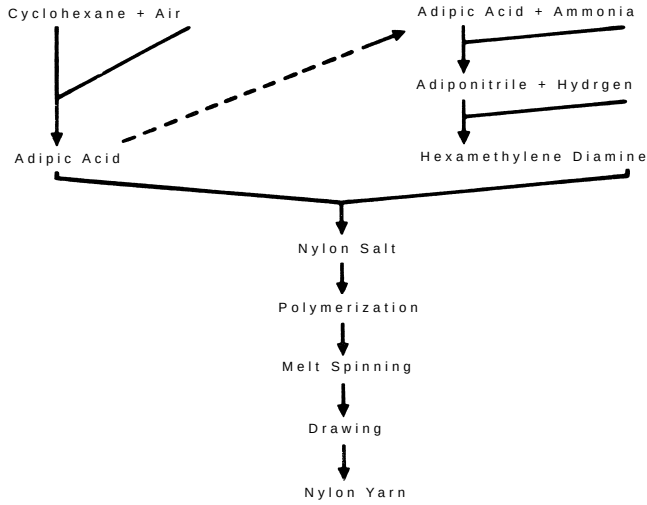

FIGURE 19 Nylon 6,6 manufacture.

After the polymerization stage, the material is passed through a spinneret to form filaments, cooled, and then twisted to form a yarn. This is then drawn by up to 500% to orient the polymer chains, create polymer crystallite zones, and increase tensile strength (Fig. 19).

F. Polyester

Like nylon, a range of polyesters are available commercially for use in tires. Polyethylene terephthalate (PET) is the most important. Also, like nylon, polyester is formed by a condensation polymerization but with the monomers ethylene glycol and dimethyl terephthalate.

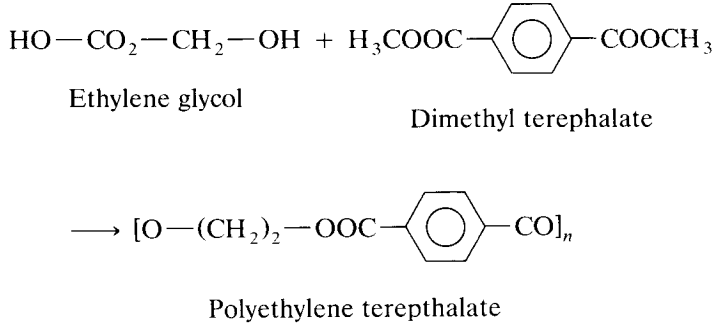

(12)

The polymerized material is then extruded through a spinneret to form filaments about 0.025 mm in diameter. These filaments are cooled, spun into a yarn, and drawn to give the required orientation and crystallinity.

TABLE VII Fiberglass Cord Composition

Silicon dioxide	53%
Calcium oxide	21%
Aluminum oxide	15%
Boron oxide	9%
Magnesium oxide	0.30%
Other oxides	1.7%

G. Fiberglass

Like steel wire, fiberglass is an inorganic fiber and is essentially a lime–alumina–borosilicate glass (Table VII). It is manufactured by blending sand, clay, limestone, and borax, melting the blend at 3000°F, and drawing the filaments of glass through a platinum–rhodium filter. The filaments are then treated with an adhesive precoat and compiled into a yarn with a low twist.

H. Aramid

Another class of fibers which finds application in tires is the aramids. Kevlar is the trade name of the polymer which has found most extensive use among the aramids. Aramid is like nylon in that it contains the amide bond—(CO—NH)—but is produced by copolymerizing terephthalic acid used in polyester and *p*-phenylenediamine. Hence this aromatic polyamide is termed *aramid*.

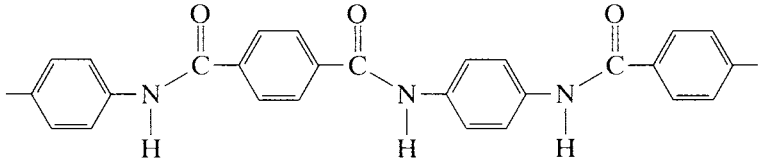

(13)

Table VIII illustrates the evolution of the range of reinforcement materials which have been used in tires.

I. Tire Cord Construction

To use the range of fibers for tire applications, the yarns must be twisted and processed into cords. First, yarn is twisted on itself to give a defined number of turns per inch, i.e., ply twisting. Two or more spools of twisted yarn are then twisted into a cord. Generally the direction of twist is opposite that of the yarn; this is termed a *balanced twist*. There are a number of reasons for twist in a tire cord:

TABLE VIII Trends in Reinforcements

Time	Cord
1900–1956	Cotton
1939–1975	Rayon
1950 to date	Nylon
1965 to date	Polyester
1970 to date	Steel cord
1975–1985	Fiberglass
1980 to date	Aramid
1990 to date	Hybrid cords

1. Twist imparts durability and fatigue resistance to the cord, though tensile strength can be reduced.
2. Without twist, the compressive forces would cause the cord outer filaments to buckle.
3. Increasing twist in a cord further reduces filament buckling by increasing the extensibility of the filament bundle.

Durability reaches a maximum and then begins to decrease with increasing twist. This can be explained by considering the effect of stresses on the cord as the twist increases. As twist increases, the helix angle (the angle between the filament axis and cord axis) increases (Fig. 20). Thus tension stresses normal to the cord axis result in greater-force parting filaments. The reason for the reduction in strength is also evident in this figure. As cord twist increases, the force in the direction of the yarn axis increases, causing a lower overall breaking strength.

In addition to twist, the cord size may be varied to allow for different applications (Table IX). Generally three-ply cords have the best durability. After cable twisting, the cords are woven into a fabric using small fill threads. These threads are also referred to as *picks*. This weaving process introduces an additional construction variable, i.e., the number of cords per inch or EPI (ends per inch) that are woven into the fabric. High-end-count fabric gives greater plunger strength or penetration resistance. Low-end-count fabrics have more rivet (distance between cords) and give better separation resistance because of the greater rubber penetration around the cords.

J. Fabric Processing

The most critical stage in preparing a cord or fabric for use in tires is fabric treatment, which consists of applying an adhesive under controlled conditions of time, temperature, and tension. This process gives the fabric the following properties:

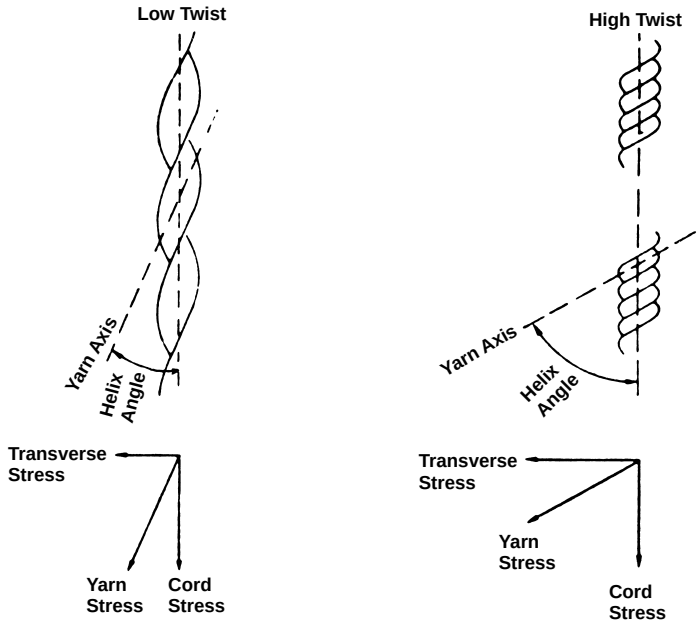

FIGURE 20 Cord geometry.

TABLE IX Tire Cord Applications

Fiber type	Tenacity (strength) (g·Den)	Ultimate elongation (%)	Modulus (g·Den)	Relative durability	Tire applications
Rayon	5.0	16	50	300	Passenger
Nylon	9.0	19	32	1200	Truck tires, off-road
Polyester	6.5	18	65	400	Passenger, truck, farm
Fiberglass	9.0	4.8	260	5	Passenger
Wire	3.8	2.5	200	3	Truck, off-road
Aramid	20.1	4	350	400	Passenger

1. Adhesion for bonding to rubber
2. Optimization of the physical properties of strength, durability, growth, and elongation of the cord for tire application
3. Stabilization of the fabric
4. Equalization of differences resulting from the source of supply of the fiber

Processing consists of passing the fabric through a series of zones which can be viewed as follows:

TABLE X Relation of Cord Properties to Processing Tensions and Temperature

Cord property	Change effected by first increase in		Change effected by second increase in	
	Tension time	Temperature	Tension time	Temperature
Tensile strength	Slightly decrease	Decrease	Slightly decrease	Decrease
Loaded at specified elongation (5%)	Decrease	Decrease	Decrease	Decrease
Ultimate elongation	Increase	Increase	Increase	Increase
Shrinkage	Decrease	Decrease	Decrease	Decrease
Rubber coverage	Increase	Increase	Increase	Increase
Fatigue	Decrease	Decrease	Decrease	Decrease
SCEF	Decrease	Decrease	Decrease	Decrease
Voids	Decrease	Decrease	Decrease	Decrease

1. Adhesive application zone or first dip zone
2. First drying zone
3. First heat treatment zone
4. Second dip zone
5. Second drying zone and then heat treatment zone
6. Final cooling zone

To obtain optimum cord properties of strength, growth, shrinkage, and modulus, specific temperatures and tensions are set at various exposure times within the fabric processing unit. The temperature and tensions in part determine the ratio of crystalline and amorphous areas within the fiber and the orientation of the crystallites, which in turn determine the physical properties of the cord. For example, polyester, when heated, tends to revert to its unorientated form, and the cord shrinks. Stretching the cord in the first heating zone and then allowing the cord to relax in a controlled manner in the second heat treatment zone, i.e., stretch relaxation, will control shrinkage.

Another variable is increase in processing temperature which can decrease cord tensile strength and modulus but will improve fatigue life. The general relationship between cord properties and processing temperatures and tensions is illustrated in Table X.

Note that not all cord properties behave similarly with varying processing conditions. It is thus necessary to determine the processing conditions that optimize cord properties for the desired tire end use. When two or more diametrically opposite properties have to be optimized, more complex mathematical methods must be used.

Wire and fiberglass, being high-modulus inorganic belt cords, are not processed like textile cords. Steel cord is brass plated at the foundry and, thus,

can be used directly at the calendars. Glass yarn is treated with adhesive dip and then used directly in the weaving operation.

K. Function of Adhesive

There are three aspects to adhesion of tire cord to the elastomer treatment: molecular, chemical, and mechanical. Molecular bonding is due to absorption of adhesive chemicals from the adhesive dip or elastomer coating onto the fiber surface by diffusion and could be described by hydrogen bonding and van der Waals forces. Chemical bonding is achieved through chemical reactions between the adhesive and the fabric and rubber, i.e., crosslinking and resin network formation. Mechanical adhesion is a function of the quality of coverage of the cord by the rubber coat compound. The greater the coverage, the better the adhesion.

The fiber properties of primary importance to adhesion are reactivity, surface characteristics, and finish. Rayon has many reactive hydroxyl groups. Nylon is less reactive but contains highly polar amide linkages. Polyester is relatively inert. Thus an adhesive system must be designed for each type of fiber.

Regardless of the fiber, each adhesive system must conform to a rigid set of requirements:

1. Rapid rate of adhesion formation
2. Compatibility with many types of compounds
3. No adverse effect on cord properties
4. Heat resistance
5. Aging resistance
6. Good tack
7. Mechanical stability

The adhesive bond between the rubber and cord is achieved during the tire vulcanization cycle. The rate of adhesive formation should give maximum adhesion at the point of pressure release in the cure cycle.

L. Rubber Compounding

The principles of compounding were reviewed earlier in this text and cover the fundamental characteristics of polymers, filler systems, and the basics of vulcanization in the context of compound development for tire applications. A compound formulation consists of four basic components: the polymer network, the filler or particulate reinforcing system, the stabilizer system, and the vulcanization system (Fig. 21). In addition a series of secondary materials such as resins, processing oils, and short fiber reinforcements may be included in a formula [15, 16, 17].

Elastomers used in radial tires are basically of four types:

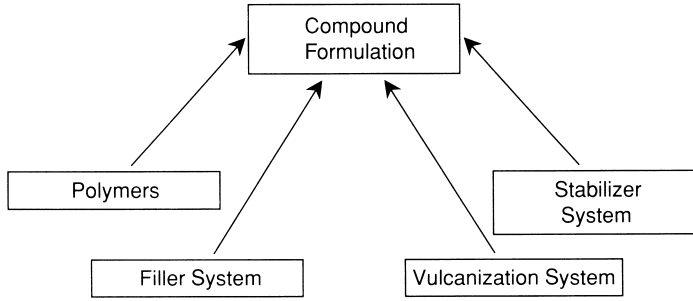

FIGURE 21 Basic compound components.

1. Natural rubber
2. Styrene–butadiene copolymer
3. Polybutadiene
4. Butyl rubber (polyisobutylene with approximately 2% isoprene) and halogenated butyl rubber

Carbon blacks, clays, and silicas constitute the filler or compound reinforcement system. Optimization of these materials in a formulation depends on the application for which the component is intended, e.g., tread, sidewall.

The stabilizer system or antioxidant system protects the compounds from aging and oxidation and improves the long-term durability of the tire.

Design of the vulcanization system is probably the most challenging aspect in designing a compound formulation for application in a tire. Knowledge of accelerator activity, reaction kinetics, and nature of the resulting crosslink network is important in constructing such systems.

VI. TIRE TESTING

Having developed a tire construction for a defined service requirement, the tire engineer must now subject the design to a series of test [3, 4]. This testing falls into two performance categories:

1. Mechanical characteristics of the tire
   - Load deflection of a vertically loaded mounted tire, load-carrying capacity, and load rating
   - Steering properties such as aligning torque, cornering characteristics, and tire lateral and tangential stiffness
   - Traction and wet skid performance
   - Rolling resistance, which affects vehicle fuel economy
   - Noise

2. Durability
   - Tread wear, which encompasses slow wear rates, fast wear rate, and uniformity of wear
   - Casing fatigue resistance
   - Tire heat buildup under loaded dynamic conditions
   - Chipping, cutting, and tearing resistance of the tread and sidewall

This testing is broken down into three phases: tire laboratory testing, proving grounds, and commercial evaluation.

A. Laboratory Testing

Laboratory testing of tires is preceded by testing of raw materials. For compounds such as the tread, sidewall, wire coat compound, and liner, such tests would include determination of the kinetics of vulcanization, tensile strength, tear strength, resilience, and dynamic properties (e.g., storage modulus and loss modulus). Reinforcements such as the ply cord are similarly tested for tensile strength, but also creep behavior, stability (shrink behavior), and fatigue resistance. Much of the physical testing of compounds in a modern laboratory is done by robotics. Compounds are vulcanized under defined conditions, and samples are cut out depending on the type of testing to be done. Robots then load the samples onto test equipment, and the data generated are collected by computer for the test engineer to access.

Materials that meet the appropriate physical property targets are then used in tire building. Testing of these tires depends on the application for which the tire was designed. It is thus appropriate to introduce another series of definitions:

Balance	Weight distribution around the circumference of a tire; poor balance is due to components having irregular dimensions. Balance can also be affected by irregular component splice widths and poor application of component parts.
Conicity	Tendency of a tire to pull a vehicle to one side or another; it is caused by off-centered or misplaced components during the tire building process.
Cornering coefficient	Lateral force divided by the vertical load at a defined slip angle. Stiffer tread compounds would tend to improved cornering coefficient.
Force variation	Periodic variation in normal vertical force of a loaded free-rolling tire, which repeats with every revolution.
Harmonic	Periodic or rhythmic force variations occurring in a sinusoidal manner around tire. One phase is described as the 1st harmonic. When two phases are noted, it is described as a 2nd harmonic. Lateral force variation 1st harmonic is typically due to a tread splice. Radial harmonic may be due to irregular placement of the belt layup.
Lateral force	Side force that is exerted by a tire as it rotates under a load.
Lateral force coefficient	The lateral force divided by the vertical load.

Lateral force variation	Change in force from one side of the tire to the other as it rotates under a load. It may cause the tire to wobble and is due to irregular tire component dimensions. Lateral force variation is a summation of the lateral 1st, 2nd, 3rd, etc., harmonic.
Lateral runout	Difference between the maximum and minimum measurements parallel to the spin axis at the widest point of each tire sidewall when the tire is mounted on a wheel.
Radial runout	Difference between the maximum and minimum measurements on the tread surface and in a plane perpendicular to the spin axis while the tire is mounted on a wheel. It is a measure of the out-of-roundness of the tire. It can also be termed "Centerline Runout."
Radial force	Force acting on a tire perpendicular to the centerline of rotation or direction of axle. It is caused by heavy tire component splices and will increase radial force. Soft spots in the tire, such as those due to stretched ply cords, cause a decrease in radial force.
Radial force variation	Summation of the radial 1st, 2nd, 3rd, etc., harmonic. It is the change in radial force as the tire is rotated. Radial force variation will cause the vehicle to have a rough ride (as if on a poor surfaced road).
Rolling resistance	Resistance of a tire to rolling. It has a direct impact on vehicle fuel economy and is influenced most by compound hysteretic properties.
Runout	Differential between the maximum and minimum lateral or radial forces.
Self-aligning torque	Stabilizing reaction to slip angle that helps the tire and vehicle to return to neutral conditions at the completion of a maneuver.
Slip angle	Angle between the vehicle's direction of travel and the direction in which the front wheels are pointing.
Speed rating	Alphabetic ratings that define the design speed capability of the tire. The letter is incorporated into the size description of the tire, for example a 195/75SR14 has a speed rating of "S." Tables of speed ratings and corresponding alphabetic designations are published by the Tire & Rim Association (Table XI).
Uniformity	Measure of the tire's ability to run smoothly and vibration free; sometimes measured as tire balance, radial force variation, or lateral force variation.

The laboratory equipment designed to test the aforementioned tire properties are based mostly on a steel flywheel with the appropriate monitoring devices such as transducers and infrared temperature monitors. Data are collected directly into computers for real-time analysis and downloading to the tire engineer's work station. Many of these flywheels are also computer controlled so as to simulate service conditions. For example, aircraft tires can undergo a complete cycle of taxi, takeoff, and landing.

B. Proving Grounds

The most definitive method of determining the behavior of a tire is to examine its performance when subjected to road testing. Proving ground testing allows all types of tires such as passenger car, truck, earthmover, and farm to be tested under closely monitored conditions. An industry proving ground will generally have the following test tracks and road courses available:

TABLE XI Tire Speed Ratings

Speed symbol	Maximum speed (kph)	Typical application
D	50	Farm tractors
L	120	Commercial truck
M	130	Commercial truck
S	180	Passenger cars & light trucks
T	190	Passenger
H	210	Luxury passenger cars
V	240	High-performance cars
Z	270	High-performance sports cars
W	Above 270	Super-high-performance cars

1. High-speed tracks, either circular or oval
2. Interstate highway simulation
3. Gravel and unimproved roads
4. Cobblestone
5. Cutting, chipping, and tearing courses
6. Wet and dry skid pads, serpentine and slalom courses for esthetics, and handling tests
7. Tethered tracks for farm tire durability
8. Glass roads for footprint monitoring

For example the 7250-acre Goodyear Proving Grounds in Texas contain a 5-mile high-speed circle, 8 miles of simulated interstate highway, gravel and rock courses for a range of tire type testing, skid pads with spray equipment, and a glass road facility for tire footprint observations and evaluation of water dispersion.

C. Commercial Evaluation

When a new tire design meets the performance targets identified in the laboratory and proving grounds, commercial evaluation is the next stage in the product development cycle. For truck tires for highway service, a quantity of tires will be placed with a commercial fleet, and their performance will be monitored continuously. Data collected from such tests include tread wear, uniformity of wear, casing durability, and driver assessment. Tires are placed with a range of commercial fleets in both short-haul and long-distance service. The collected data are then entered into computers for detailed analysis, calculation of regression equations, and performance evaluation. Customer input is one of the key parameters in such studies.

VII. TIRE MANUFACTURING

The manufacture of tires consists of six basic processes:

1. Mixing elastomers, carbon blacks, and chemicals to form the rubber compound
2. Processing the fabrics and steel cord and coating them with rubber at the calendaring operation
3. Extruding treads, sidewalls, and other rubber components
4. Assembling components on the tire building machine
5. Curing the tire under heat and pressure
6. Finishing, making the final inspection, and shipping

The processes involved in the tire manufacturing operation are illustrated in Fig. 22.

A. Compound Processing

Polymers are first broken down in an internal mixer where, in addition to the polymer, a peptizer may also be added. This stage is essentially a polymer molecular weight reduction phase. After initial breakdown of the polymer, carbon black, rubber chemicals, and oils can be added to the polymer at intervals to complete the compound formulation. Polymer breakdown and mixing generally occur at a high temperature, up to 180°C.

Compounds may also be mixed on open mills, but this takes considerably more time, batch weights are lower, and it is thus less efficient than use of internal mixers.

Degree of breakdown with both types of equipment is dependent on the "friction ratio" or the difference between the operating speeds of the front and back rolls (or rotors, for internal mixers). In addition, clearance, conditions of the rotor surfaces, pressure, and speed influence breakdown.

The mixing operation is designed to obtain uniform dispersion of all the compounding materials in a formulation. For every batch there is a defined mix period, temperature, mill or mixing speed, and sequence of material addition. Though the general guidelines on compound preparation for both mill mixing and internal mixers are similar, mill mixing has been replaced by internal mixers because of efficiency, automation, quality, and uniformity. For example, internal mixers can be computer controlled, allowing monitoring of power consumption, mix times, and batch drop temperatures and control of temperature gradients through a mixing compound at any point in the mix cycle.

The sequence of addition in an internal mixer is typically (1) polymers and peptizer; (2) plasticizers, most carbon black or silica, and oils; (3) balance of fillers and antioxidants; and (4) vulcanization system components.

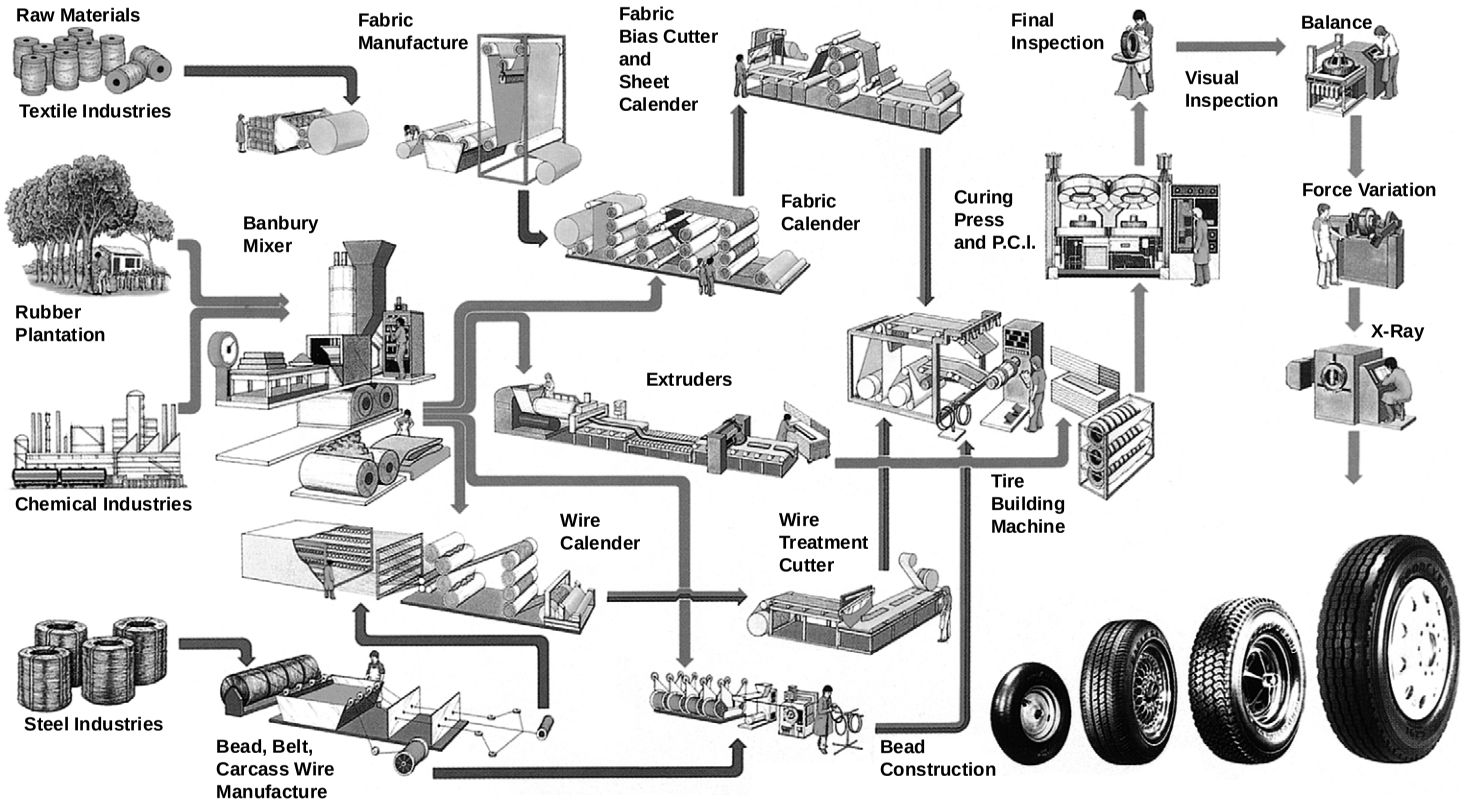

FIGURE 22 The tire manufacturing process (see color insert).

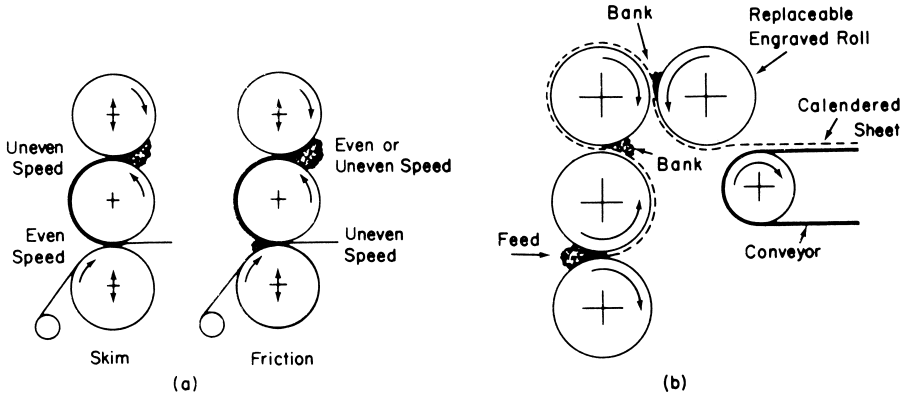

FIGURE 23 (a) Applying rubber to fabrics. (b) Profiling by means of a four-roll engraving calendar.

Construction of a mix cycle is governed by a set of empirical rules:

1. Keep high-tack resins separate from dry powders.
2. Hold batch drop temperatures above the softening point of hard resins.
3. Contain liquids to prevent leakage.
4. Make use of the shear properties of rubber to accelerating mixing.
5. Avoid scorch and subsequent formation of cured particles and crumb.

These five guidelines are adhered to by reducing internal friction through the use of plasticizers, adequate breakdown of the rubber, holding of the curing system ingredients to the final stage of the mix cycle, and use of master batches where possible. After mixing, compounds can either be sheeted and water cooled or passed into pelletizer and then air cooled.

B. Calendaring

Calendaring is the forming operation in which the rubber compound is sheeted or spread evenly onto fabric. The calendar is a heavy-duty machine equipped with three or more chrome-plated steel rolls that revolve in opposite directions (Fig. 23). The rolls are heated with steam or circulated water; the gearing allows the rollers to operate at variable speeds like the mill rolls. Fabric or wire is passed through the calendar rolls, and compound is applied above and below to fully cover the material.

The amount of compound deposited onto a fabric or steel cord is determined by the distance between rollers and is monitored by Beta Gauges. Each cord is insulated on all sides with rubber. The finished treatment or calendared steel cord sheet is cut to length and angle for tire building. Key compound requirements in calendaring operations are minimum shrinkage, optimum tack

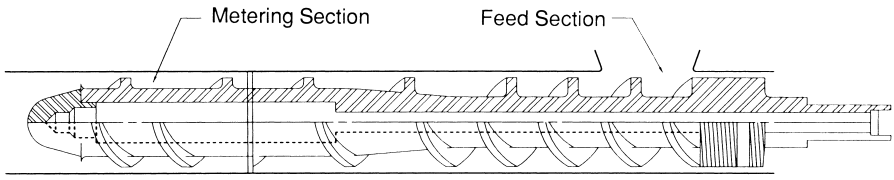

FIGURE 24 Hot feed extruder.

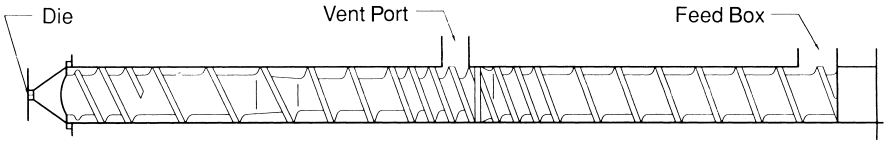

FIGURE 25 Cold feed extruder.

for component-to-component adhesion, and sufficient scorch resistance to enable long dwell times at high processing temperatures.

C. Extrusion

Many of the components of a tire, such as tread, sidewall, and apex, are formed by extrusion of the uncured or "green" rubber. Extruders in a tire manufacturing operation are conventional screw-types systems that fall into two categories:

Hot feed systems	Strips of green compound are fed from warmup mills into a extruder feed box and then into the barrel.
Cold feed systems	Mixed compound is fed directly into the extruder system.

Extruders consist of a barrel into which the material is fed. The mixed compound is then pushed forward by a specially designed screw to a filter system, where any foreign material is removed, and then onto a die, where the required compound profile is produced.

The extruder screw consists of three primary zones: feed zone, compression zone, and metering zone. In the feed zone located under the extruder feed box, the screw flights are well spaced to optimize compound flow. The rubber is passed into a compression zone, where the compound is heated through shear; then into a metering zone, where the compound is further heated to reduce viscosity; and finally into the die for profile formation.

Hot feed extruder systems (Fig. 24) normally have a short barrel and screw with short compression and metering zones because the compound is already hot and has a low viscosity as it enters the feed hopper. Barrel length-to-diameter ratios from 4:1 to 6:1 are typical.

Cold feed extruders (Fig. 25) have much larger length-to-diameter ratios because of the requirements of reducing green compound plasticity, heat

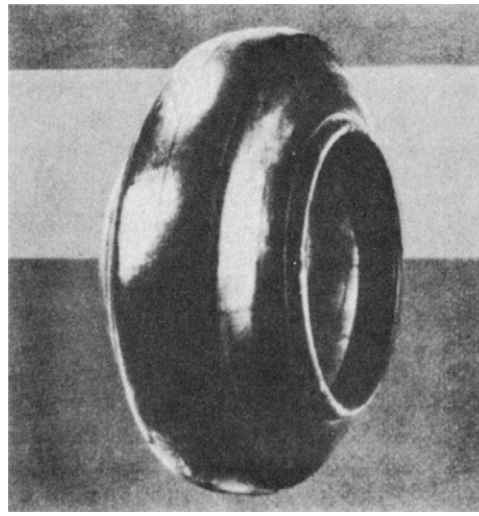

FIGURE 26 Radial green tire.

buildup in the compound, and pressure buildup required to produce the extruded profile. The length-to-diameter ratio is typically 24:1. The modern cold feed extruder is also computer controlled, which enables adjustment of the compound temperature profile through the barrel, pressure control, flow rate, and feed rate. This provides accurate control over die swell, extrudate surface quality, and buildability of the extruded product.

Periodic monitoring of screw flight-to-barrel distances are important to ensure minimum back pressure and compound swirl or turbulence in the flow channel.

D. Tire Building

All tire components, i.e., extruded parts, calendared plies and belts, and beads, are assembled at the tire-building machine. Traditionally, radial tires are built on a flat drum. The initial stage entails application of the inner liner on the cylindrical drum, followed by the ply and any other additional barrier components that the tire engineer has designed into the manufacturing specification. The beads are then positioned and the ply is turned up over them. The structure is transferred to a second-stage machine, where the belts and tread are applied. The building drum is collapsed, and the "green tire" illustrated in Fig. 26 is transferred to the curing or vulcanization presses.

During vulcanization, or curing, the green tire is molded into a high-quality engineered product. In the curing press, the compound flows into the mold shape to give a design to the tread and the desired thickness to the side-

wall. Good flow depends on the plasticity of the uncured stock. To flow, the compound must resist scorching. Flow must be complete before cure begins, or distortion may result. Proper flow is achieved by effective use of compounding fillers, adjustment of acceleration levels, and use of plasticizers.

E. Final Tire Inspection

The manufactured tire must meet the following criteria:

1. All tire components have been successfully processed through the production facility to the tire building machine.
2. The components have come together satisfactorily at the tire building machine without hindering the productivity of the tire building operators.
3. The tire meets the quality and performance goals set by the consumer.

Quality assurance is the last stage in the manufacturing cycle. Here the product is checked to ensure customer satisfaction. Quality checks on a tire include:

1. Buffing and trimming off mold flash from the tire.
2. Visual inspection of each tire for defects.
3. X-ray checks on tires for ply cord spacing and belt layup.
4. Statistical sampling of tires for durability testing, uniformity, and dynamic balancing. This testing includes many of the development tests reviewed earlier such as conicity, radial runout, and lateral force variation.

After the tire passes the quality checks, it is ready for shipment to the warehouse for distribution.

VIII. SUMMARY

In many ways, a tire is an engineering marvel. Geometrically, a tire is a torus. Mechanically, a tire is a flexible, high-pressure container. Structurally, a tire is a high-performance composite built using elastomers, fibers, steel, and a range of organic and inorganic chemicals.

Tire technology is a complex combination of science and engineering that brings together a variety of disciplines. In the development of a tire, knowledge in the areas of tire geometry, dynamic tire behavior, chemistry of component materials, and technology of composite structures is essential. The result is a broad range of products which satisfy vehicle manufacturers as well as end-consumer needs for optimum performance under a variety of service conditions.

REFERENCES

1. T. L. Ford and F. S. Charles, "Heavy Duty Truck Tire Engineering," SAE's 34th L. Ray Buckingdale Lecture, SP729, 1988.
2. J. A. Davison, "Design and Application of Commercial Type Tires," SAE's 15th L. Ray Buckingdale Lecture, SP344, 1969.
3. The Tire & Rim Association, Inc. Year Book, 175 Montrose West Ave., Suite 150, Copley, OH 44321.
4. European Tyre and Rim Technical Organization, Standards Manual, 32/2 Avenue Brugmann—B1060 Brussels, Belgium.
5. Engineering Data Book, "Over-The-Road Truck Tires," The Goodyear Tire & Rubber Company, 2001.
6. F. J. Kovac, "Tire Technology," 5th ed., The Goodyear Tire & Rubber Company, 1978.
7. V. E. Gough, *Rubber Chem. Technol.* **44**, 988 (1968).
8. S. K. Clark, "Mechanics of Pneumatic Tires," U.S. Department of Transportation, Washington, D.C., 1982.
9. J. E. Purdy, "Mathematics Underlying the Design of Pneumatic Tires," 2nd ed., Hiney Printing, Akron, OH, 1970.
10. J. W. Fitch, "Motor Truck Engineering Handbook," 4th ed., Society of Automotive Engineers, Warrendale, PA, 1994.
11. W. H. Waddell, M. B. Rodgers, and D. S. Tracey, "Tire Applications of Elastomers, Part 1. Treads," Rubber Division Meeting, Grand Rapids, MI, Paper H, 2004.
12. Bekaert Corporation, Steel Cord Catalogue, Akron, OH, 1991.
13. W. J. van Ooij, *Rubber Chem. Technol.* **57**, 421 (1984).
14. J. Duddey, in "Rubber Compounding, Chemistry and Applications," Marcel Dekker Inc., New York, 2004.
15. B. Rodgers and W. H. Waddell, Rubber Compounding, in "Kirk-Othmer Encyclopedia of Chemical Technology," 5th ed., John Wiley & Sons, New York, 2004.
16. H. Long, "Basic Compounding and Processing of Rubber," Rubber Division, American Chemical Society, Lancaster Press, Lancaster, PA, 1985.
17. K. C. Baranwal and H. S. Stephens, "Basic Elastomer Technology," Rubber Division, American Chemical Society, Akron, OH, 2001.

15 Recycling of Rubbers

AVRAAM I. ISAYEV
Institute of Polymer Engineering
The University of Akron
Akron, Ohio

I. INTRODUCTION

Manufacturing of tire and other rubber products involves vulcanization process, an irreversible reaction between the elastomer, sulfur, and other chemicals producing crosslinks between the elastomer molecular chains and leading to the formation of a three-dimensional chemical network. The crosslinked elastomers are solid, insoluble, and infusible thermoset materials. This makes the direct reprocessing and recycling of used tires and waste rubbers impossible. Therefore, the environmental problems caused by used tires and other waste rubber products have become serious in recent years. In fact, Charles Goodyear, who invented the sulfur vulcanization process more than 150 years ago [1], was also the first to initiate efforts to recycle cured rubber wastes through a grinding method [2]. Even after so many years of efforts in recycling, the development of a suitable technology to utilize waste rubbers is an important issue facing the rubber industry.

According to a recent survey of the Scrap Tire Management Council of the Rubber Manufacturers Association, approximately 281 million scrap tires were generated in the United States in 2001 alone [3]. The market for scrap tires is consuming about 77.6% of that total amount [3] while the rest is added to an existing stockpile of an estimated 300 million scrap tires located around the United States [4]. These stockpiled tires create serious fire dangers and provide breeding grounds for rodents, snakes, mosquitoes, and other pests, causing health hazards and environmental problems [5]. Moreover, the major use of scrap tires in the United States is to generate the so-called tire-derived

Science and Technology of Rubber, Third Edition

energy by burning used tires. However, burning tires may create a danger of air pollution [6]. About 53% of the consumed scrap tires were burned in 2001, and only 19% of the total consumed amount was turned into ground tire rubber (GRT), which is the initial material for the tire rubber recycling processes [4]. Also, the management of other waste rubbers has become a growing problem in the rubber industry since over 150,000 tons or more of rubber are scrapped from the production of non-tire goods in the form of runners, trim, and pads [7].

Waste tires and rubbers, being made of high quality rubbers, represent a large potential source of raw material for the rubber industry. The main reasons for the low-scale current application of tire and rubber recycling include the following: more stringent requirements for quality of rubber articles, and hence for that of reclaimed rubber; the substitution of other materials for raw rubber (e.g., plastics in some cases); rising costs of recovery from tires and rubber waste due to the more stringent regulations for environmental protection; a comparatively high labor input into reclaim production; and, as a result of all this, the high cost of reclaimed rubber [8]. However, the increasing legislation restricting landfills is demanding the search for economical and environmentally sound methods of recycling discarded tires and waste rubbers. Recent aggressive policies of the automotive industry are aimed at increasing the use of recycled plastic and rubber materials [9–11]. This may serve as an example of the growing industrial demand for such technologies.

The main objective of this chapter is to provide the up-to-date account on recycling of used tires and waste rubbers including existing methods and emerging technologies of grinding, reclaiming, and devulcanization, and also the possibility for recycled rubber utilization into products. Rubber devulcanization is a process in which the scrap rubber or vulcanized waste product is converted, using mechanical, thermal, or chemical energy, into the state in which it can be mixed, processed, and vulcanized again [12]. Strictly speaking, devulcanization in sulfur-cured rubber can be defined as the process of cleaving, totally or partially, poly-, di-, and monosulfidic crosslinks formed during the initial vulcanization [13]. Devulcanization of peroxide- and resin-cured rubber can be defined as the process of cleaving carbon–carbon or other, stronger crosslinks. However, in the present concept, devulcanization is defined as a process that causes the breakup of the chemical network along with the breakup of the macromolecular chains [14].

A number of methods [11, 13–17] have been applied in an attempt to solve the problem and to find more effective ways of tire rubber recycling and waste rubber utilization. These methods include retreading, reclaiming, grinding, pulverization, microwave and ultrasonic processes, pyrolysis, and incineration. Processes for utilization of recycled rubber are also being developed, including the use of reclaimed rubber to manufacture rubber products and thermoplastic–rubber blends and the use of GRT to modify asphalt and cement.

II. RETREADING OF TIRE

Retreading is one way to recycle. Also, it saves energy. It takes about 83 liters of oil to manufacture one new truck tire whereas a retread tire requires only about 26 liters. The cost of a retread tire can be from 30 to 50% less than a new tire [17, 18]. Approximately 24.2 million retreaded tires were sold in North America in 2001, with sales totaling more than $2 billion. Mostly medium- and heavy-duty truck tires, off-the-road vehicles, and aircraft tires were retreaded [18]. However, high labor costs and the potential for tougher safety regulations may hurt the retreading business [17].

III. RECYCLING OF RUBBER VULCANIZATES

A. Reclaiming Technology

Reclaiming is a procedure in which the scrap tire rubber or vulcanized rubber waste is converted, using mechanical and thermal energy and chemicals, into a state in which it can be mixed, processed, and vulcanized again. The principle of the process is devulcanization [12]. In devulcanization, it is assumed that the cleavage of intermolecular bonds of the chemical network, such as carbon–sulfur and/or sulfur–sulfur bonds, takes place, with further shortening of the chains occuring [14].

Many different reclaiming processes [8, 13, 15–17, 19–22] have been applied through the years in an attempt to solve the problem of rubber recycling. Generally, ground rubber scrap is, in most cases, the feedstock for the devulcanization step. Warner [13] and recently Adhikari *et al*. [23] and Isayev [24] presented reviews of the existing literature that is relevant to various methods of devulcanization.

Reclaiming is the most important process in rubber recycling. Many different reclaiming processes [7, 8, 14, 23–32] have been used through the years depending on scrap characteristics and economics. Generally, ground rubber scrap is, in most cases, the feedstock for the reclaiming. The pan process, digester process (either wet or dry), and mechanical or reclaimator processes are currently the common processes used for reclaiming.

The digester process [7, 8, 13, 24–27, 29–32] uses a steam vessel equipped with a paddle agitator for continuous stirring of the crumb rubber while steam is being applied. The wet process may use caustic and water mixed with the rubber crumb, while the dry process uses steam only. If necessary, various reclaiming oils may be added to the mixer in the vessel. The dry digester has the advantage of less pollution being generated and was adopted after the Clean Air and Water Act was enacted.

A mechanical or reclaimator process [25, 32–34] has been used for the continuous reclaiming of whole tire scrap. Fine rubber crumb (typically 30

mesh) mixed with various reclaiming oils is subjected to high temperature with intense mechanical working in a modified extruder for reclaiming the rubber scrap.

Scrap rubber containing natural and synthetic rubbers can be reclaimed by digester process with the use of reclaiming oil having molecular weight between 200 and 1000 and consisting of benzene, alkyl benzene, and alkylate indanes. The composition of this reclaiming oil and the improved digester process using such reclaiming oil has been patented [35].

Recently, a new technology for the devulcanization of sulfur-cured scrap elastomers was reported [36] using a material termed "Delink" [37]. Such technique of devulcanization was designated as Delink process. In this process, 100 parts of 40-mesh or finer crumb is mixed with 2 to 6 parts of Delink reactant in an open two-roll mixing mill. Delink reactant is a proprietary material, and its nature and composition was not disclosed.

A simple process for reclaiming of rubber with a vegetable product that is a renewable resource material (RRM) was developed [38–40]. The major constituent of RRM is diallyl disulfide. Other constituents of RRM are different disulfides, monosulfides, polysulfides, and thiol compounds.

It is known that sulfur-vulcanized Natural Rubber (NR) can be completely recycled at 200 to 225°C by using diphenyldisulphide [41]. Recently, the efficiacy of various disulphides as recycling agents for NR and EPDM vulcanizates were reported [42]. While complete devulcanization was observed on sulfur-cured NR at 200°C, a decrease in crosslink density of 90% was found when EPDM sulfur vulcanizates with diphenyldisulphide were heated to 275°C in a closed mold for 2 hours. At the same time, EPDM cured by peroxide showed a decrease in crosslink density of about 40% under the same conditions.

Another chemical method was recently proposed [43]. It is based on the use of 2-butanol solvent as a devulcanizing agent for sulfur-cured rubber under high temperature and pressure. It is claimed that the molecular weight of the rubber is retained, and its microstructure is not significantly altered during the devulcanization process. However, the process is extremely slow and requires separation of the devulcanized rubber from the solvent.

In addition to the use of organic chemicals, rubbers can be devulcanized by means of inorganic compounds. Discarded tires and tire factory waste were devulcanized by desulfurization of suspended rubber vulcanizate crumb (10 to 30 mesh) in a solvent such as toluene, naphtha, benzene, cyclohexane, etc., in presence of sodium [44]. The alkali metal cleaves mono-, di-, and polysulfidic crosslinks of the swollen and suspended vulcanized rubber crumb at around 300°C in absence of oxygen. However, this process may not be economical because the process involves swelling of the vulcanized rubber crumb in an organic solvent where the metallic sodium in molten condition should reach the sulfidic crosslink sites in the rubber crumb. Also, the solvent may cause pollution and be hazardous. A technology was also proposed to reclaim

powder rubbers using an iron oxide phenyl hydrazine based catalyst [45] and a copper (I) chloride-tributyl amine catalyst [46].

Depending on the specification of the finished products, fillers may be added to the devulcanized product before further processing. The devulcanized rubber from each process is then strained and refined as dictated by the specification of the finished product before being powdered, baled, sheeted, or extruded into the finished form.

Chemical reclaiming process is a possible method for devulcanizing the vulcanized network through the use of chemical agents that attack the C–S or S–S bonds. However, this process of devulcanization is very slow and creates further problems with the removal of the solvents, and additional waste is generated in the form of sludges. Also, some processes require elaborate chemical process techniques, therefore handling and safety become a concern.

B. Surface Treatment

Surface treatment technology [47–49] uses a solvent to treat (devulcanize) the surface of rubber crumb particles of sizes within about 20 to 325 meshes. It is a variation of earlier disclosed technology [43]. The process is carried out at a temperature range of between 150 and 300°C at a pressure of at least 3.4 MPa in the presence of a solvent selected from the group consisting of alcohols and ketones. Among various solvents, the 2-butanol exhibited the best ability to devulcanize sulfur-cured styrene–butadiene rubber (SBR). Duration of the process is above 20 minutes.

Reported data on surface devulcanization experiments were obtained by treating small amounts of rubber crumb in the gas chromatography column. The solvent suitable for this process should have a critical temperature in the range of about 200 to 350°C. The process produces slurry of the surface devulcanized rubber crumb that has to be separated from the solvent. It is claimed that in this process a preferential breakage of S–S and C–S bonds takes place with little breakage of the main chains. The obtained surface modified rubber crumb was subjected to vulcanization as obtained and also in blends with virgin rubber. The vucanizates exhibited a good retention of mechanical properties in blends with virgin rubber. However, this process has been tested on a small laboratory scale.

C. Grinding and Pulverization Technology

Use of waste rubber in a vulcanized state most often requires reduction of particle size and/or surface area. One of the most widely used methods for doing this with scrap tires and rubber wastes is a grinding process. This method was invented and put forward by Goodyear about 150 years ago [2]. Presently, there are three methods of grinding waste rubber: ambient grinding, cryogenic grinding, and wet-ambient grinding [50–52]. There are a number of ways to

reduce tires. The primary reduction of whole tires down to a manageable form is done using the guillotine, the cracker mill, the high-impact hammer mill, and the rotary shear shredder. Vulcanized scrap rubber is first reduced to a 5-by-5-cm^2 or 2.5-by-2.5-cm^2 chip. Then a magnetic separator and a fiber separator (cyclone) remove all the steel and polyester fragments. This can then be further reduced using an ambient ground mill or ground into fine particles while frozen using cryogenic grinding [8].

A method for obtaining fine-mesh rubber is cooling scrap tires in liquid nitrogen below their glass transition temperature and then pulverizing the brittle material in a hammer mill. Cryogenically ground rubber has a much finer particle size, varying from 30 to 100 mesh. But for inexpensive rubbers such as tire rubbers, the process is not economical because of the amount of liquid nitrogen or other cryogen liquids needed to freeze the rubber [25]. However, the process may be economical for expensive rubbers such as fluorocarbon rubbers. Little or no heat is generated in the process; this results in less degradation of the rubber. In addition, the most significant feature of the process is that almost all fiber or steel is liberated from the rubber, resulting in a yield of usable product and little loss of rubber [7].

Because of the high cost of cryogenic size reduction at liquid nitrogen temperature, mechanical size reduction by chopping and grinding is used often. The ambient process often uses a conventional high-powered rubber mill set at close nip. The vulcanized rubber is sheared and ground into small particles. Using this relatively inexpensive method, it is common to produce 10- to 30-mesh material and relatively large crumb. In addition, multiple grinds can be used to further reduce the particle size. Ambient grinding produces an irregular-shaped particle with many small hairlike appendages that attach to the virgin rubber matrix, producing an intimate bonded mixture [32]. The lower particle limit for the process is the production of 40-mesh material. The process, however, generates a significant amount of heat. Excess heat can degrade the rubber, and if not cooled properly, combustion can occur upon storage.

Other suggested recycling processes include mechanical and thermomechanical methods, which only comminute the vulcanizates in rubber and do not devulcanize them. A process using a wet grinding method to achieve a crumb fineness of approximately 200 mesh has been reported [53]. When this product, which had a much higher surface-to-mass ratio, was devulcanized, no chemicals and only minimal heating and mechanical processing were required. Wet or solution process grinding may yield the smallest particle size, ranging from 400 to 500 mesh. The advantage of fine particle wet ground rubber is that it allows good processing, producing relatively smooth extrudates and calendered sheets [53].

The pulverization techniques for rubbers are also being developed based on the concept of polymer pulverization originally proposed for plastics. The

process manufactures polymer powder using a twin-screw extruder imposing compressive shear on the polymer at specific temperatures that depend on the polymer [54]. Based on this method, the solid-state shear extrusion pulverization method of rubber waste was also proposed [55, 56]. The obtained rubber particles were fluffy and exhibited unique elongated shape.

Recently, this process was further developed to carry out pulverization of rubbers in a single screw extruder to obtain particles varied in size from 40 to 1700 μm [57–60]. A schematic diagram of the pulverization technique based on a single screw extruder is shown in Figs. 1(a) and 1(b) [57]. As indicated in Fig. 1(a), the extruder consists of three zones: feeding (Zone 1), compression (Zone 2), and pulverization (Zone 3). The screw is a square pitched with the compression zone having a uniform taper to create a compression ratio of 5. The water-cooling channel is located in the barrel in order to remove the heat generated by the pulverization of rubber. Experimental studies showed that during the pulverization of vulcanized scrap rubber in the extruder, due to friction, a significant amount of heat is generated, leading to partial degradation of the rubber [57]. The rubber granulates are fed into the hopper of the extruder and conveyed into the compression zone, where they are subjected to high compressive shear. Under simultaneous action of this compressive shear and torsion due to the screw rotation, granulates are pulverized and emerge from the pulverization zone as rubber powder having a smaller particle size. Surface oxidation of the rubber particles and initiation of agglomeration of a fraction of the produced particles may take place. The produced particles exhibit irregular shapes with rough surfaces and have a porous structure. The crosslink density and gel fraction of the particles are reduced in comparison with those of the initial rubber granulates. This would indicate the occurrence of partial devulcanization. Due to this effect, the particles obtained in this process can be molded into products after an exposure to high heat and high pressure for a period of at least 1 hour [61, 62]. Table I shows the dependence of the elongation at break, ε_b, tensile strength, σ_b, and crosslink density, ν, of compression-molded slabs of the original rubber vulcanizate and the vulcanizates prepared from particles of size in the range 250 to 425 μm obtained by solid-state shear extrusion pulverization from discarded by-product of natural rubber (SMR-20) vulcanizates. Approximate composition of the rubber compound was about 54 wt% of SMR-20, 27 wt% carbon black (SRF), 11 wt% aromatic oil, and 8 wt% vulcanizing ingredients. Molding temperature and pressure were 157°C and 5.11 MPa, respectively. Slab F1, produced without adding sulfur curatives, exhibited the best failure properties among all slabs produced from the rubber powder. In Sample F1 oil, vulcanizing residue and the sol fraction of the rubber were removed by toluene extraction. This, according to the authors, enhanced particle bonding, leading to improvement of the failure properties. On the other hand, the slabs F2 and F3 produced by adding sulfur curatives to particles showed inferior failure properties than

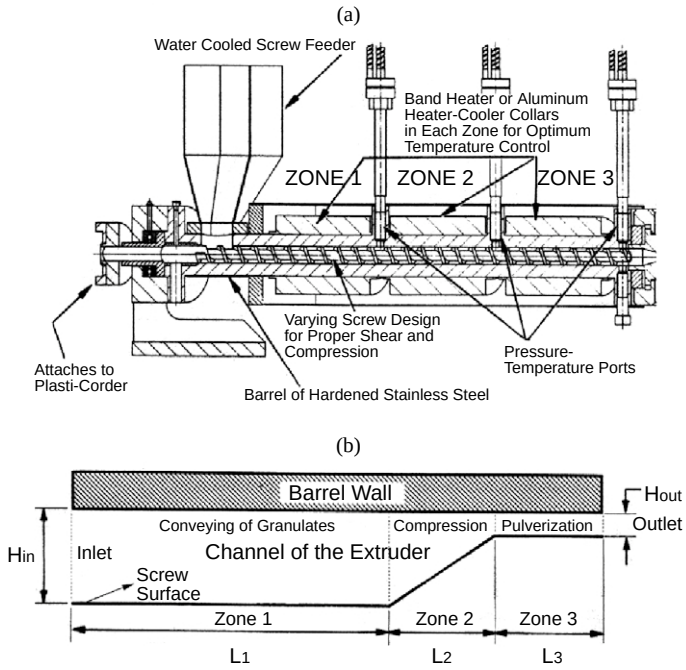

FIGURE 1 Schematic diagram of (a) the single-screw extruder for pulverization of rubbers and (b) geometry of the screw channel with variable depth. (From Bilgili *et al.* [57].)

TABLE I Properties of the Slabs of Pulverized Rubber Waste [62]

	Revulcanizing system				
Slab code	**Sulfur (phr)**	**TBBS (phr)**	**ε_b (%)**	**σ_b (MPa)**	**ν (mol/m^3)**
F1	—	—	360	10.3	50.4
F2	1.0	0.5	350	7.0	73.9
F3	1.0	—	320	8.2	69.5
Original	—	—	470	16.5	66.9

those of slab F1 due to less particle bonding at increased crosslink density during the revulcanization. Furthermore, the slabs F1–F3 showed failure properties inferior to the original slab indicating the inadequacy of compression molding of rubber particles to achieve the properties of the original vulcanizate.

The particles obtained by other grinding processes can also be compression molded into slabs by means of high-pressure, high-temperature sintering

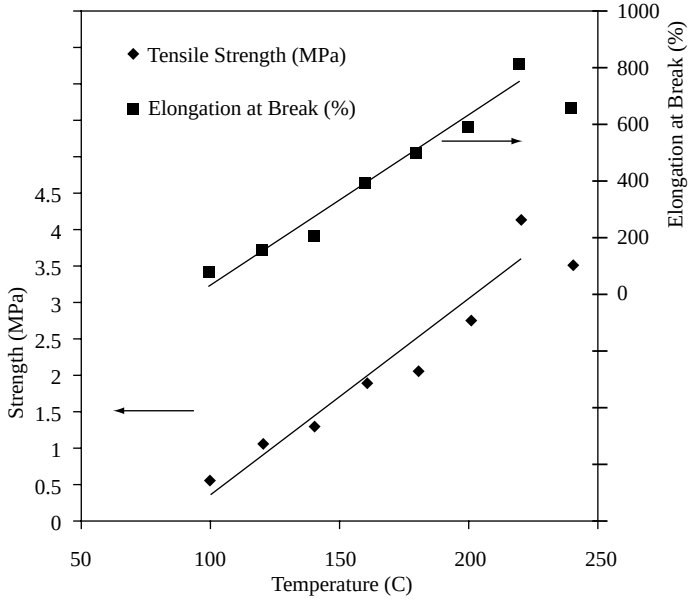

FIGURE 2 Effect of the molding temperature on the mechanical properties of NR–SBR slab compression molded from particles of 80 meshes for 1 hour at pressure of 8.5 MPa. (From Morin *et al.* [63].)

as shown in Morin *et al*. [63] and Tripathy *et al*. [64]. In particular, in these papers, rubber particles of several rubbers, obtained by various grinding methods, were compression molded into slabs with and without an addition of various acids and chemicals. The effect of time, pressure, and temperature on mechanical properties of sintered slabs was studied. In particular, Fig. 2 shows the effect of molding temperature on mechanical properties of NR–SBR slab compression molded from particles of 80 mesh for 1 hour at pressure of 8.5 MPa [63]. It clearly shows the importance of the molding temperature. Below approximately 80°C, this process does not work. The highest tensile strength of about 4 MPa was achieved with the sufficiently high elongation at break (about 800%). The mechanism of consolidation of particles in this process is the result of the breakup of bonds into radicals that cross the particle interface and react with other radicals and thus create a chemical bond across the interface. The authors explained that the inferior properties of the sintered NR particle slabs in comparison with the original one was due to the energetics between void propagation and strain-induced crystallization. Less energy is required to generate voids in the sintered slabs than in the original slab, and this does not allow one to achieve a strain-induced crystallization in the sintered slabs.

D. Devulcanization Technology

1. Microwave Method

Microwave technology has also been proposed to devulcanize waste rubber [15, 65]. This process applies the heat very quickly and uniformly on the waste rubber. The method employs the application of a controlled amount of microwave energy to devulcanize a sulfur-vulcanized elastomer, containing polar groups or components, to a state in which it could be compounded and revulcanized to useful products, such as hoses, requiring significant physical properties. On the basis of the relative bond energies of carbon–carbon, carbon–sulfur, and sulfur–sulfur bonds, it was presumed that the scission of the sulfur–sulfur and sulfur–carbon crosslinks actually occurred. However, the material to be used in the microwave process must be polar enough to accept energy at a rate sufficient to generate the heat necessary for devulcanization. This method is a batch process and requires expensive equipment.

Recently, thermogravimetry was employed to study the changes occurring in rubber vulcanizates during devulcanization carried out by microwave treatment [66]. The degree of degradation of the polymer chains in response to microwave treatment was obtained, allowing the establishment of conditions of devulcanization in order to obtain the best properties of rubber devulcanizates for reuse in rubber processing.

2. Ultrasonic Method

Numerous publications in recent literature are devoted to the study of the effect of ultrasound on polymer solutions [67–72] and on polymer melts during extrusion [73–78]. Significant efforts have also been made to understand the mechanism of the effect of ultrasound on fluids [79, 80] and degradation of polymer in solution [81].

The application of ultrasonic waves to the process of devulcanizing rubber is an attractive field of study. Most references indicate that rubber is vulcanized by ultrasound rather than devulcanized. Rubber devulcanization by using ultrasonic energy was first discussed in Okuda and Hatano [82]. It was a batch process in which a vulcanized rubber was devulcanized at 50 kHz ultrasonic waves after treatment for 20 minutes. The process claimed to break down carbon–sulfur bonds and sulfur–sulfur bonds, but not carbon–carbon bonds. The properties of the revulcanized rubber were found to be very similar to those of the original vulcanizates.

Recently, a novel continuous process has been developed for devulcanization of rubbers as a suitable way to recycle used tires and waste rubbers [83–119]. This technology is based on the use of high-power ultrasounds. The ultrasonic waves of certain levels, in the presence of pressure and heat, can quickly break up the three-dimensional network in crosslinked rubber. The process of ultrasonic devulcanization is very fast, simple, efficient, and solvent and chemical free. Devulcanization occurs at the order of a second and may

lead to the preferential breakage of sulfidic crosslinks in vulcanized rubbers. The process is also suitable for decrosslinking of the peroxide-cured rubbers and plastics. A schematic diagram of the various devulcanization reactors suitable to carry out this process is shown in Fig. 3. Initially, the so-called coaxial devulcanization reactor (see Fig. 3[a]) was developed in our laboratory. The reactor consists of a single screw rubber extruder and an ultrasonic die attachment. A cone-shaped die and the ultrasonic horn have sealed inner cavities for running water for cooling. The shredded rubber is fed into the extruder by a feeder with adjustable output. Thus, the rubber flow rate in the process is controlled by the feed rate. An ultrasonic power supply, an acoustic converter, booster, and a cone-tipped horn are used. The horn vibrates longitudinally with a frequency of 20 kHz and various amplitudes. The ultrasonic unit is mounted onto the extruder flange. The convex tip of the horn matches the concave surface of the die so that the clearance between the horn and the die is uniform. The clearance is controlled. The rubber flows through the clearance and under the action of ultrasonic waves, propagating perpendicular to the flow direction, and it is devulcanized. The die plate and the horn are cooled with tap water.

Later, the barrel (see Fig. 3[b]) and the grooved barrel (see Fig. 3[c]) ultrasonic reactors were developed. In the barrel reactor, two ultrasonic water-cooled horns of rectangular cross-sections were inserted into the barrel through two ports. Two restrictors made of bronze were placed in the barrel. These restrictors blocked the flow of rubber and forced the rubber to flow through the gap created between the rotating screw and the tip of the horn. In the devulcanization section, the larger diameter provided the converging flow of the rubber to the devulcanization zone. The latter may enhance the devulcanization process. In the grooved barrel ultrasonic reactor, two helical channels were made on the barrel surface (grooved barrel). Rubber flows into the helical channel and passes through the gap created between the rotating shaft and the tip of the horns, where devulcanization takes place.

Under the license from the University of Akron for the ultrasonic devulcanization technology, NFM Co. of Massillon, Ohio, has built a prototype of the machine for ultrasonic devulcanization of tire and rubber products [120, 121]. It was reported that retreaded truck tires containing 15 wt% and 30 wt% of ultrasonically devulcanized carbon-black-filled SBR had passed the preliminary dynamic endurance test [121].

Extensive studies on the ultrasonic devulcanization of rubbers and some preliminary studies on ultrasonic decrosslinking of crosslinked plastics were carried out [83–122]. It was shown that this continuous process allows one to recycle various types of rubbers and thermosets. As a most desirable consequence, ultrasonically devulcanized rubber becomes soft, therefore making it possible for this material to be reprocessed, shaped, and revulcanized in very much the same way as the virgin rubber. This new technology has been used successfully in the laboratory to devulcanize a ground tire rubber (GRT)

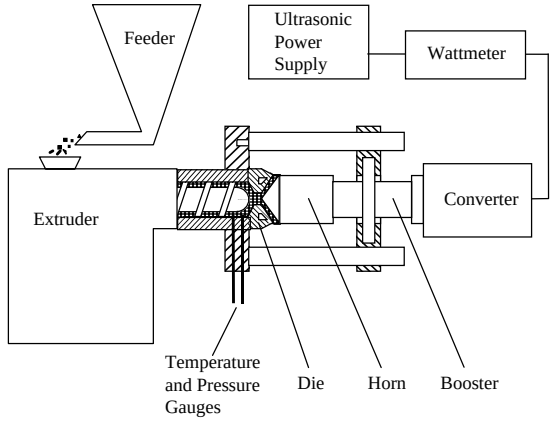

(a)

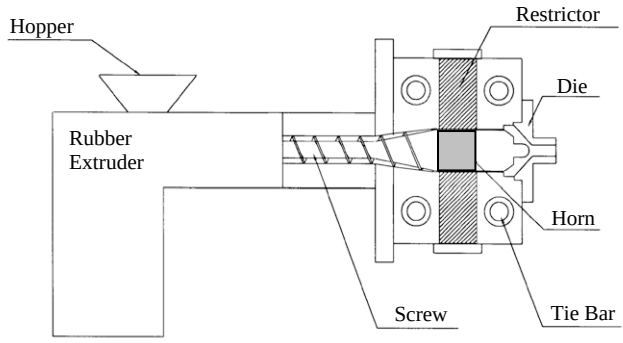

(b)

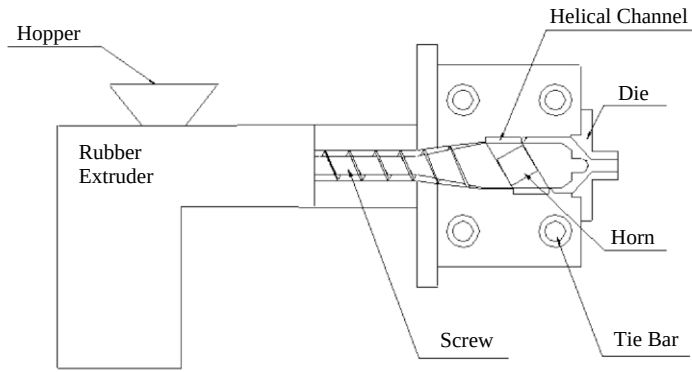

(c)

FIGURE 3 Schematic diagram of (a) coaxial reactor, (b) barrel reactor, and (c) grooved barrel reactor built for devulcanization of rubbers.

[85, 86, 90, 102, 105, 120], unfilled and filled NR [99, 103], guayule rubber [122], unfilled and filled SBR [87, 93, 95–97, 99], unfilled and filled peroxide-cured silicone rubber [98, 100, 104, 111–113, 115], unfilled and filled EPDM and EPDM roofing membrane [110, 117], unfilled polyurethane [116], unfilled resin-cured butyl rubber [118], used tire curing bladder [119], fluoroelastomer, ethylene vinyl acetate foam, and crosslinked polyethylene [83, 84]. After revulcanization, rubber samples exhibit good mechanical properties, which in some cases are comparable to or exceeding those of virgin vulcanizates [95, 100, 110].

Ultrasonic devulcanization studies were concerned with finding the effect of processing parameters such as the pressure, power consumption, die gap, temperature, flow rate, and ultrasonic amplitude on devulcanization; structural changes occurring in various rubbers; rheological properties and curing kinetics of devulcanized rubbers; mechanical properties of revulcanized rubbers; and the effect of design of the devulcanization reactor. Figure 4 shows the entrance pressure of devulcanization zone vs. amplitude of ultrasound at a flow rate of 0.63 g/s, and the entrance pressure of devulcanization zone vs. flow rate at the amplitude of 10 μm and clearance of 2 mm during devulcanization of GRT. The entrance pressure of the devulcanization zone was substantially reduced as the amplitude of ultrasound was increased. Ultrasound facilitated the flow of rubber through the gap not only because of reduction of the friction in the presence of ultrasonic waves but also because of the devulcanization taking place as GRT particles entered the devulcanization zone. The barrel reactor showed a higher pressure in the devulcanization zone than the coaxial reactor, and the grooved barrel reactor showed the lowest pressure at low amplitude of ultrasound and a flow rate of 0.63 g/s. The barrel reactor had a converging zone before the devulcanization zone. The GRT flow was essentially blocked by the restrictor of the devulcanization zone at low amplitude of ultrasound. However, at the ultrasound amplitude of 10 μm, the entrance pressure of the devulcanization zone for the coaxial and barrel reactors was almost the same due to a reduction of restrictor effect at high amplitude. The highest flow rate achieved in the barrel and grooved barrel reactors was 6.3 g/s. The devulcanized sample of flow rate of 6.3 g/s for the coaxial reactor could not be obtained due to an overload of the ultrasonic generator. Furthermore, in the grooved barrel reactor, at a flow rate of 6.3 g/s, the gap size needed to be increased to 3.5 mm, and ultrasonic amplitude needed to be decreased to 6 μm due to an overload of the ultrasound unit. It was natural that the entrance pressure of the devulcanization zone rises with increasing flow rate as indicated in Fig. 4 for all three reactors. Nevertheless, at a high flow rate the barrel reactor had lower entrance pressure at the devulcanization zone than that of the other reactors at the ultrasound amplitude of 10 μm. The difference in die characteristics (pressure vs. flow rate) among the three reactors having the devulcanization zone thickness of 2 mm was possibly related to the difference in power consumption and the difference in shearing conditions. In the

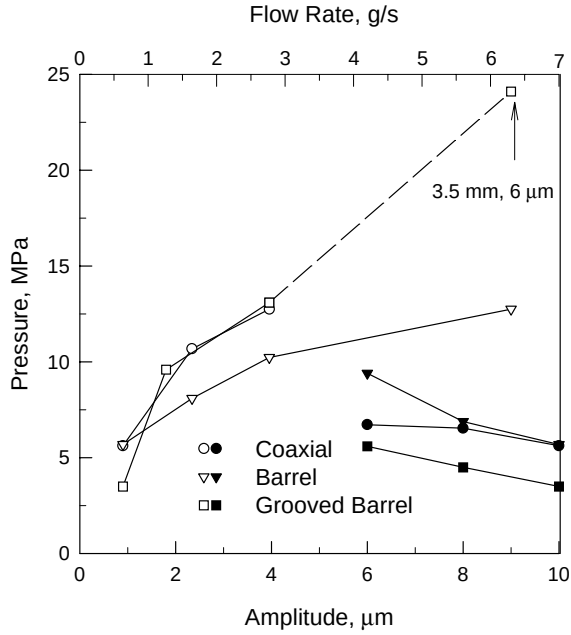

FIGURE 4 The entrance pressure of devulcanization zone of different reactors vs. amplitude of ultrasound at a flow rate of 0.63 g/s, and the entrance pressure of devulcanization zone vs. flow rate at the amplitude of 10 μm and clearance of 2 mm during devulcanization of GRT.

barrel and grooved barrel reactor, the GRT in the devulcanization zone was subjected to a pressure and drag flow while in the coaxial reactor to a pressure flow alone.

The comparison of stress–strain behavior of the vulcanizates prepared from devulcanized GRT produced by the three reactors at the maximum flow rate is shown in Fig. 5. The revulcanized sample obtained from the barrel reactor, having a flow rate of 6.3 g/s, shows a tensile strength of 8.7 MPa, elongation at break of 217%, and modulus at 100% elongation of 2.6 MPa. In addition, the revulcanized sample obtained from the grooved barrel reactor having, a flow rate of 6.3 g/s, shows the tensile strength of 8.3 MPa, the elongation at break of 184%, and modulus at 100% elongation of 3.3 MPa. The output of the barrel and grooved barrel reactors was higher than that of the coaxial reactor. In addition, the mechanical properties of the sample obtained using the barrel reactor at the higher flow rate, which could not be achieved in the coaxial reactor, were higher. These properties met the higher level of specification made for tire reclaim [7]. The samples showing inferior performance were considered overtreated. The overtreatment meant a higher degree of devulcanization along with a significant degradation of the backbone molecular chains. The overtreated samples were usually softer and stickier.

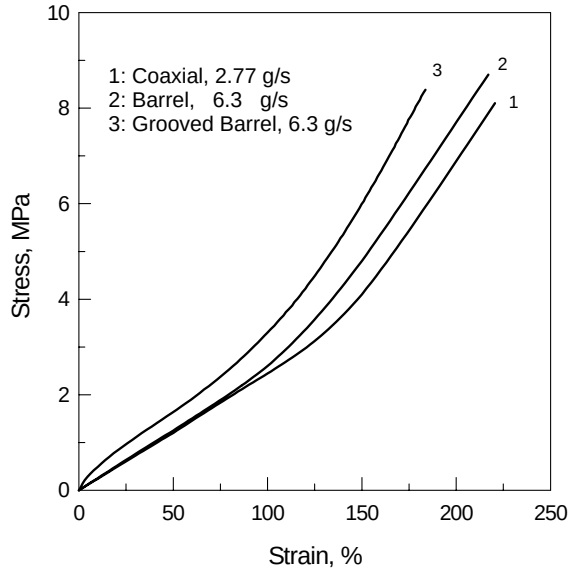

FIGURE 5 The stress–strain curves of the vulcanizates prepared from devulcanized GRT produced by the three reactors at the maximum flow rate as shown.

It is believed that the process of ultrasonic devulcanization is based on a phenomenon called cavitation. In this case, acoustic cavitation occurs in a solid body. This is in contrast to the cavitation typically known to occur in liquids in the regions subjected to rapidly alternating pressures of high amplitude generated by high-power ultrasonics [123]. During the negative half of the pressure cycle, the liquid is subjected to a tensile stress, and during the positive half cycle, it experiences a compression. Any bubble present in the liquid will thus expand and contract alternately. The bubble can also collapse suddenly during the compression. This sudden collapse is known as cavitation and can result in almost instantaneous release of a comparatively large amount of energy. The magnitude of the energy released in this way depends on the value of the acoustic pressure amplitude and, hence, the acoustic intensity.

Although the presence of bubbles facilitates the onset of cavitation, it can also occur in gas-free liquids when the acoustic pressure amplitude exceeds the hydrostatic pressure in the liquid. For a part of the negative half of the pressure cycle, the liquid is in a state of tension. Where this occurs, the forces of cohesion between neighboring molecules are opposed, and voids are formed at weak points in the structure of the liquid. These voids grow in size and then collapse in the same way gas-filled bubbles do. Cavitation may be induced in a gas-free liquid by introducing defects, such as impurities, in its lattice structure.

In the case of polymer solutions, it is well known that the irradiation of a solution by ultrasound waves produces cavitation of bubbles [67, 124]. The formation and collapse of the bubble plays an important role in the degradation of polymers in solution. Most of the physical and chemical effects caused by ultrasound are usually attributed to cavitation: the growth and very rapid, explosive collapse of microbubbles as the ultrasound wave propagates through the solution. The intense shock wave radiating from a cavitating bubble at the final stage of the collapse is undoubtedly the cause of the most severe reactions. This shock wave is capable of causing the scission of macromolecules that lie in its path. The degradation arises as a result of the effect of the ultrasound on the solvent. In any medium, cavities, voids, and density fluctuations exist. It is believed that these induce cavitation, leading to molecular rupture. In solid polymers, the microvoids, present intrinsically, are responsible for cavitation when they are subjected to a hydrostatic pressure in the manner of an impulse. One of the main causes of microvoid generation in polymer materials is the interatomic bond rupture when they are subjected to mechanical and thermal stresses. Extensive studies showing microvoid formation in stressed polymers have been carried out [125].

When applied to rubbers, the cavitation usually corresponds to the effect of formation and unrestricted growth of voids in gas-saturated rubber samples after a sudden depressurization [126, 127]. In general, this has a broader sense and may be understood as the phenomena related to the formation and dynamics of cavities in continuous media [88, 102]. In materials science, for example, it means a fracture mode characterized by formation of internal cavities [128]. In acoustics, the cavitation denotes the phenomena related to the dynamics of bubbles in sonically irradiated liquids [129].

Structural studies of ultrasonically treated rubber show that the breakup of chemical crosslinks is accompanied by the partial degradation of rubber chains [85, 86, 96, 97]. The mechanism of rubber devulcanization under ultrasonic treatment is presently not well understood, unlike the mechanism of the degradation of long-chain polymer in solutions irradiated with ultrasound [124]. Specially, the mechanisms governing the conversion of mechanical ultrasonic energy to chemical energy are not clear. However, it has been shown that devulcanization of rubber under ultrasonic treatment requires local energy concentration, since uniformly distributed ultrasonic energy among all chemical bonds is not capable of rubber devulcanization [88, 89, 130].

It is well known that some amounts of cavities or small bubbles are present in rubber during any type of rubber processing [131]. The formation of bubbles can be nucleated by precursor cavities of appropriate size [126]. The proposed models [88–90, 101, 102] were based on a mechanism of rubber network breakdown caused by cavitation, which is created by high-intensity ultrasonic waves in the presence of pressure and heat. Driven by ultrasound, the cavities pulsate with amplitude depending mostly on the ratio between ambient and ultrasonic pressures (acoustic cavitation).

It is known that, in contrast to plastics, rubber chains break down only when they are fully stretched [132, 133]. An ultrasonic field creates high-frequency extension–contraction stresses in crosslinked media. Therefore, the effects of rubber viscoelasticity have been incorporated into the description of dynamics of cavitation [101, 102]. The devulcanization of the rubber network can occur primarily around pulsating cavities due to the highest level of strain produced by the powerful ultrasound [102].

Generally, cleavage in polymer chains results in the production of macroradicals [134, 135], the existence of which have been confirmed spectroscopically by the use of radical scavengers such as diphenyl picrylhydracyl (DPPH). Obviously, in the absence of scavengers, the macroradicals are free to combine by either disproportionation or combination termination, the former leading to smaller-sized macromolecules while the latter will give a distribution dependent on the size of the combining fragments [136].

It was reported [95] that under some devulcanization conditions the tensile strength of unfilled revulcanized SBR was found to be much higher than that of the original vulcanizate, with elongation at break being practically intact. In particular, Fig. 6 shows the stress–strain curves of unfilled virgin vulcanizates and revulcanized SBR obtained from devulcanized rubbers at various values of ultrasonic amplitudes, A. The devulcanized rubbers were obtained by using the coaxial ultrasonic reactor depicted in Fig. 3(a) at the barrel temperature of 120°C, screw speed of 20 rpm, and flow rate of 0.63 g/s. The ultrasonic horn diameter was 76.2 mm. In contrast to usual findings that the mechanical properties of reclaimed rubber obtained by using different techniques are inferior to those of virgin vulcanizates, the present data are rather unexpected. It was proposed that the improvement in the mechanical properties of revulcanized SBR was primarily due to the extent of nonaffine deformation of the bimodal network that appears in the process of revulcanization of ultrasonically devulcanized rubber. The superior properties of revulcanized rubbers were also observed in the case of unfilled EPDM [110] and silicone [100] rubbers. Unfilled revulcanized NR rubber also shows good properties, with the elongation at break remaining similar to that of the original NR vulcanizates but with the ultimate strength being about 70% of the original NR. Interestingly, the strain-induced crystallization typical for the original NR vulcanizate remained intact in revulcanized NR, as indicated in Fig. 7, where upturn of the stress–strain curves is observed in both the original and revulcanized rubbers. These samples were devulcanized in a coaxial reactor at different flow rates and ultrasonic amplitudes and revulcanized with a recipe consisting of 2.5 phr ZnO, 0.5 phr stearic acid, and 2 phr sulfur.

Fillers play an interesting role in the devulcanization process. Figure 8 shows the stress–strain curves for virgin and devulcanized 35 phr carbon-black-filled NR vulcanizates. Virgin vulcanizates were cured using 5 phr ZnO, 1 phr stearic acid, 1 phr CBS, and 2 phr sulfur. The revulcanization recipe contained 2.5 phr ZnO, 0.5 phr stearic acid, 0.5 CBS, and 2 phr sulfur. The experiments

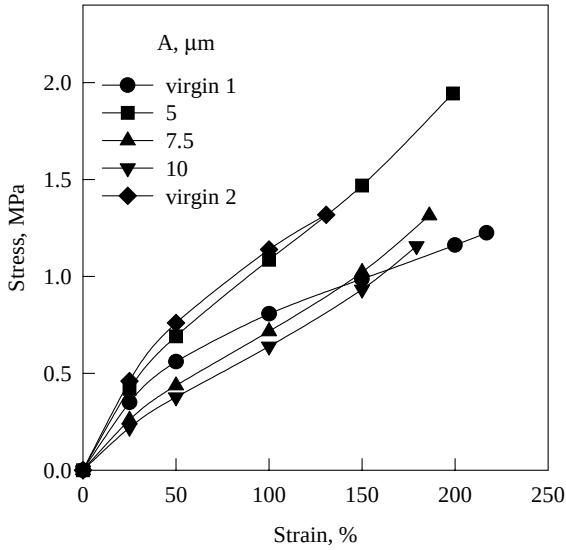

FIGURE 6 The stress–strain curves of unfilled virgin vulcanizates and revulcanized SBR obtained from rubbers devulcanized in coaxial reactor at various values of ultrasonic amplitude.

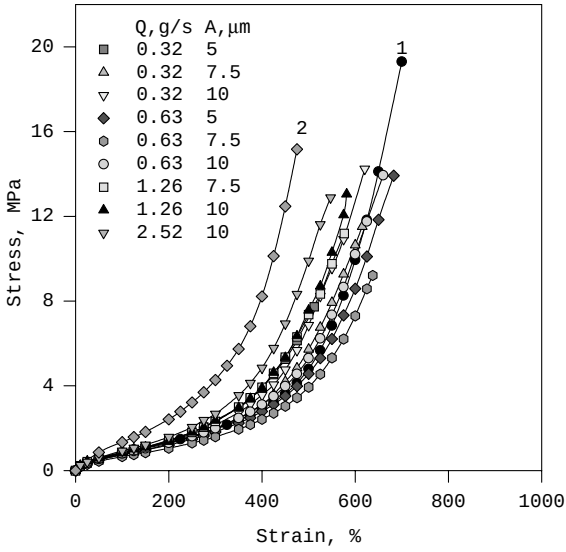

FIGURE 7 The stress–strain curves for unfilled NR vulcanizates prepared from ultrasonically devulcanized NR in coaxial reactor at various flow rates and amplitudes at a die gap of 2.54 mm and a barrel temperature of 120°C.

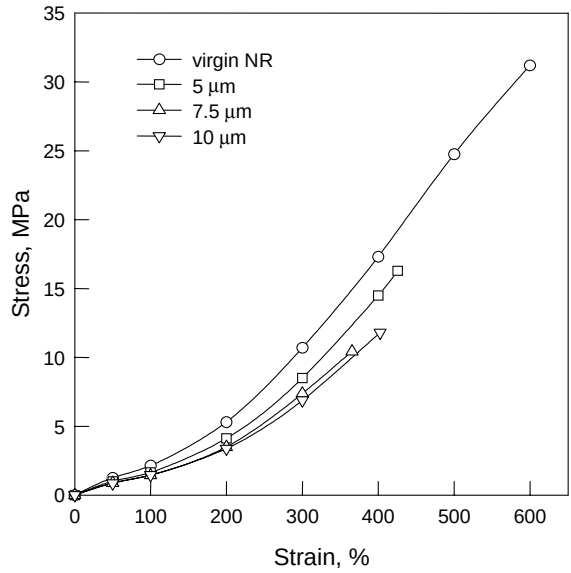

FIGURE 8 The stress–strain curves for 35 phr carbon-black-filled virgin NR and revulcanized NR devulcanized in coaxial reactor at a barrel temperature of 120°C, a gap of 2.54 mm, a flow rate of 0.63 g/s, and various ultrasonic amplitudes.

have shown that upon filling rubbers with carbon black, after devulcanization the mechanical properties of revulcanized rubbers typically deteriorate, with the level of deterioration depending on the devulcanization conditions. This is clearly evident from Fig. 8. It was suggested that ultrasonic devulcanization causes a partial deactivation of filler due to the breakup of the macromolecular chains attached to the surface of carbon black. In many cases, this effect leads to inferior properties of revulcanized carbon-black-filled rubbers. Thus, ultrasonically devulcanized rubber was blended with virgin rubber [137]. The blend vulcanizates indicated significantly improved properties. Also, attempts were made to add a certain amount of a fresh carbon black into the devulcanized rubber. It was shown that the vulcanizates containing a fresh carbon black exhibited better properties than the revulcanized rubber that did not contain an addition of fresh carbon black. However, in some cases, even carbon-black-filled devulcanized rubber shows mechanical properties similar to or better than the original rubber. In particular, this was shown for an EPDM roofing membrane containing carbon black and a significant amount of oil [117]. Apparently, oil plays an important role in the devulcanization process. Possibly, the presence of oil prevents a deactivation of the filler that was observed in vulcanizates not containing oil. But in order to prove this hypothesis, further experiments are required.

Ultrasonic devulcanization also alters revulcanization kinetics of rubbers. It was shown [93] that the revulcanization process of devulcanized SBR was essentially different from that of the virgin SBR. The induction period is shorter or absent for revulcanization of the devulcanized SBR. This is also true for other unfilled and carbon-black-filled rubbers such as GRT, SBR, NR, EPDM, and BR cured by sulfur-containing curative systems, but not for silicone rubber cured by peroxide. It was suggested that a decrease or disappearance of the induction period in the case of the sulfur-cured rubbers is due to an interaction between the rubber molecules chemically modified in the course of devulcanization and unmodified rubber molecules, resulting in crosslinking. It was shown that approximately 85% of the accelerator remained in the ultrasonically devulcanized SBR rubber [93].

Ultrasonically devulcanized rubbers consist of sol and gel. The gel portion is typically soft and has significantly lower crosslink density than that of the original vulcanizate. Due to the presence of sol, the devulcanized rubber can flow and is subjected to shaping. Crosslink density and gel fraction of ultrasonically devulcanized rubbers was found to correlate by a universal master curve [91, 100, 138]. This curve is unique for every elastomer due to its unique chemical structure. Figure 9 presents the normalized gel fraction as a function of normalized crosslink density of devulcanized GRT obtained from three different reactors. The gel fraction and crosslink density of GRT was 0.82 and 9.9×10^{-2} kmol/m^3, respectively. For each reactor, the dependence of gel fraction on crosslink density was described by a unique master curve that was independent of processing conditions such as flow rate (residence time) and amplitude. The unique correlation between gel fraction and crosslink density obtained in the barrel and grooved barrel reactors was shifted toward lower crosslink density than those obtained in the coaxial reactor, indicating a better efficiency of devulcanization. It is considered possible that the additional shearing effect caused by the screw rotation in the barrel and grooved barrel reactors had a positive influence on improving the efficiency of devulcanization.

IV. USE OF RECYCLED RUBBER

A. General Remarks

There are certain technical limitations in the devulcanization of rubbers, and vulcanization is, in fact, not truly reversible [11]. The partial devulcanization of scrap rubber will result in a degradation of physical properties. In many cases, this may limit the amount of substitution levels in high-tech applications such as passenger tires. But it can provide the compounder of less stringent products with an excellent low-cost rubber that can be used as the prime rubber or at very high substitution levels. According to Franta [12], reclaim

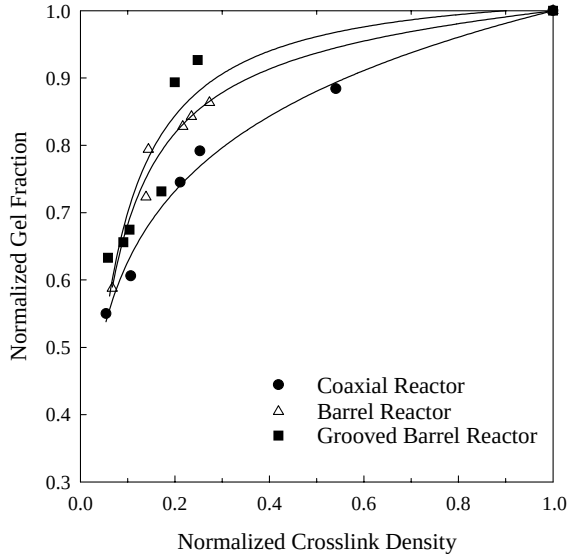

FIGURE 9 Normalized gel fraction vs. normalized crosslink density of devulcanized GRT obtained at various devulcanization conditions using the coaxial, barrel, and grooved barrel reactors.

cannot be used for tread compounds in tires because every addition may decrease their resistance to wear. However, this statement has not been checked in the case of rubber devulcanized without an addition of chemicals. Considerable amounts of reclaim are consumed for carcasses of bias ply tires for cars if the compounds are of NR; for carcasses of radial tires no reclaim is added. On the other hand, reclaim is added to compounds for bead wires, and it may also be added to sidewalls. Within the framework of direct recycling options, a number of applications for GRT outside the rubber industry have been proposed. Such applications include the use as a filler in asphalt for the surface treatment of roads and as a rubberized surface for sport facilities. The ground scrap rubber can be used as fillers in raw material [139–144] and plastic compounds [139, 145]. However, the problem of compatibility with the matrix and size of the filler, as well as the discontinuity at the interface between the two phases, should be considered. Rubber products containing ground rubber have low tensile properties due to insufficient bonding between the ground rubber and the virgin matrix. However, this bonding can be improved in the case of the addition of devulcanized rubber.

B. Use in New Tires

The tire is a complicated composite product consisting of tread, undertread, carcass, inner liner, bead, and sidewall. Many different types of rubber

and carbon-black reinforcement are used in manufacturing tires. Therefore, GRT is a blend of various rubbers and carbon blacks. Accordingly, in using GRT powder and devulcanized GRT in new tire manufacturing, many factors should be considered. Evidently, scrap tire powder can be used as a filler for virgin rubbers, and devulcanized GRT can be used in blends with virgin rubbers. This market consumed approximately 50 million lb of scrap tire rubber in 2001 [3].

Until recently, it was generally understood that only a few percent of ground rubber can be used in new tires. The Scrap Tire Management Council reports that 5% of recycled tire rubber is used in an original equipment tire for the Ford Windstar [3]. Although no other information on the amount of devulcanized rubber used in new tires is available in open literature, a possibility exists for the use of up to 10 wt% of recycled tire rubber in new tire compounds [17]. Recently, it was reported that actual road tests of a truck tire containing 10 wt% of the devulcanized rubber in the tread exhibited tread wear behavior almost equal to that for the standard type with the new rubber compound [146]. The increase in the amount of recycled rubber in tires is growing, but it is likely that results will not be available for a number of years.

C. Rubber/Recycled Rubber Blends

The rubber particles from scrap tires can be incorporated into a virgin rubber as a filler. However, in this case, the compatibility with the matrix is a significant issue. Rubber products containing ground rubber typically have lower tensile properties due to insufficient bonding between the ground rubber and the virgin matrix. The effect of GRT particles of different sizes incorporated in a NR compound on its mechanical properties was reported [147]. Table II shows the tensile strength, elongation at break, and tear strength before and after aging for a virgin vulcanizate and vulcanizates containing GRT particles of various sizes. The vulcanizates A, B, C, and D contained 30 phr of GRT particles of sizes in the range of 650–450 μm, 300–215 μm, 205–160 μm, and 150–100 μm, respectively. The control sample was the virgin NR vulcanizate. The curing recipe contained 6 phr ZnO, 0.5 phr stearic acid, 3.5 phr sulfur, and 0.5 phr MBT. Incorporation of GRT in a NR compound decreased the physical properties of the vulcanizate, with the effect being larger in the case of large particles. However, the NR vulcanizate containing GRT exhibited better properties retention upon aging. It was shown that smaller particles contain less the amount of rubber but higher the amount of fillers and metals.

Recycled tire rubber in the form of large crumb particles is also used for making prepackaged pour-in-place surfacing product [148]. GRT is combined with premixed polyurethane to produce a soft, pliable energy-absorbing rubber surface for playground and other recreational surfaces and is intended for placing over compacted gravel, concrete, or asphalt.

TABLE II Properties of GRT-Filled NR Vulcanizates [147]

Properties	Compound									
	Control		A		B		C		D	
	Before aging	After aging	Before aging	After aging	Before aging	After aging	Before aging	After aging	Before aging	After aging
Tensile strength (MPa)*	14.0	8.8 (63)	2.2	1.6 (71)	4.2	2.5 (60)	7.3	3.3 (45)	8.0	2.5 (31)
Elongation at break (%)	1175	770 (66)	430	230 (53)	620	360 (58)	780	410 (53)	860	400 (47)
Tear strength (kN/m)*	28.2	20.3 (72)	12.4	9.7 (78)	18.5	10.6 (57)	23.8	11.5 (48)	21.2	9.7 (46)
Sol %	2.1	2.2	5.8	6.4	5.2	6.2	4.9	6.0	4.3	6.6
% increase in sol after aging	—	4.8	—	10.3	—	19.2	—	22.4	—	53.5

*Values in parentheses show the % retention of properties after aging at 100°C for 36 h.

In recycling of rubbers, it is customary to add various proportions of ground rubbers to the virgin material. Therefore, blends of both filled and unfilled ground and ultrasonically devulcanized rubbers with virgin rubber have been prepared. The mechanical properties of blends of unfilled Polyurethane (PUR) virgin and devulcanized rubber have been measured [149]. Curatives were added in the blends of devulcanized rubber based on the total rubber, while for blends of ground rubber curatives were added based on virgin rubber content. Figure 10 shows the tensile properties of the two types of blends of PUR [149]. From a comparison of these two figures, it is quite apparent that the blends of the devulcanized samples (see Fig. 10[a]) have better tensile properties compared to the blends of ground samples (see Fig. 10[b]). For the latter, only at a ground concentration of 25%, the tensile properties are similar to that of the original, whereas for the former, the properties are superior to the original at this concentration and comparable at concentrations of 50%. It may be thought that ultrasonic devulcanization causes a better bonding of the devulcanized rubber to the virgin rubber in the blends than in the case of ground-virgin blends.

Ultrasonically devulcanized and ground-carbon black (CB)–filled NR was blended with virgin CB-filled material. Figure 11 gives the tensile strength of these NR–NR blends containing 35 phr CB [137]. The blends of devulcanized

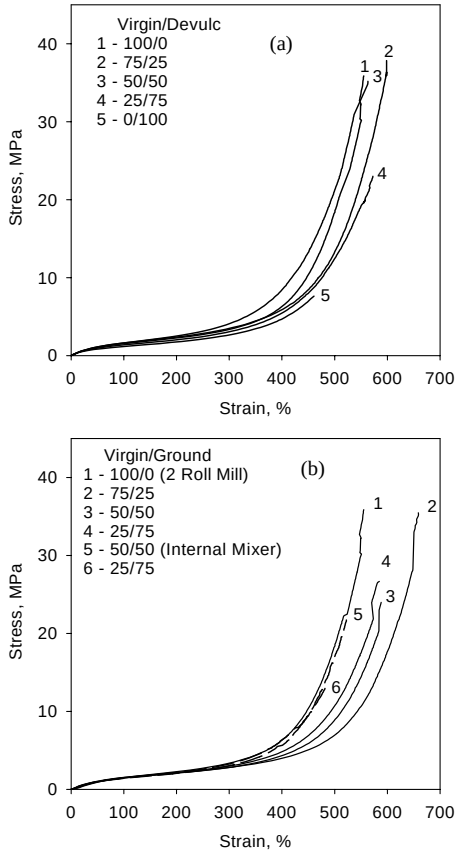

FIGURE 10 Stress vs. strain curves of (a) vulcanized blends of virgin and devulcanized sample, and (b) ground and virgin sample. The conditions of devulcanization are a flow rate of 1.26 g/s, a gap size of 3 mm, an amplitude of 7.5 μm, and a barrel temperature of 120°C using the coaxial reactor.

NR and virgin NR have much better tensile properties than blends with fully cured ground rubber. As the proportion of the virgin NR in the blends of devulcanized NR was increased, the mechanical properties progressively increased at or above the rule of mixture. Therefore, the mechanical properties of these kinds of blends can be improved significantly by ultrasonic devulcanization of ground vulcanizates. The modulus at 100% strain of NR–NR blends containing 35 phr CB was measured [137]. Blends of devulcanized and virgin NR showed a little drop in the modulus, while the modulus of ground and virgin NR was reduced. It is thought that this was due to the migration of curatives; the blends of ground rubber and virgin rubber prepared using curatives for virgin rubber are likely to exhibit reduced modulus. The blends of

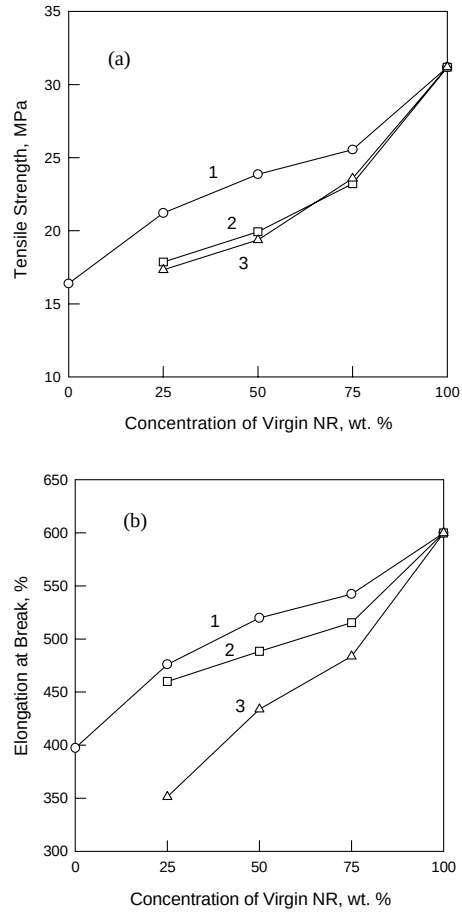

FIGURE 11 (a) Tensile strength and (b) elongation at break of 35 phr CB-filled virgin and devulcanized NR blends: (1) curatives were added to total rubber content; (2) blends of ground NR vulcanizates and virgin NR; curatives were added to virgin rubber; and (3) blends of ground NR vulcanizates and virgin NR; curatives were added to the total rubber content. NR was devulcanized at a flow rate of 0.63 g/s, a gap size of 2.54 mm, an amplitude of 5 μm, and a barrel temperature of 120°C, using the coaxial reactor.

ground rubber and virgin rubber with curatives added based on total rubber content show higher modulus. However, they indicated lower tensile strength and elongation of break due to excess of curatives.

D. Thermoplastic–Recycled Rubber Blend

The technology of polymer blending has emerged as a useful tool in tailoring polymers to the needs of the end users. An exciting development

in blending is the introduction of thermoplastic elastomers (TPEs) based on plastic–rubber blends. These TPEs are becoming increasingly important because of their elastomeric properties and easy processability of the blends and their lower cost.

The blending of waste rubber with thermoplastics is important from the point of view of both disposal of waste and the reduction in the product cost. More attention has been focused on compounding ground tire rubber (GRT) with thermoplastics, which can be subsequently remelted and shaped into a wide range of molded and extruded products [150, 151]. The mechanical properties of such compounds depend on the concentration of GRT, polymer matrix type, and adhesion between the GRT and the polymer matrix, as well as the particle size and their dispersion and interaction between the GRT and the matrix [152]. Generally, adhesion between the GRT and the polymer matrix and the size of the GRT particles are the two major factors controlling the mechanical properties of such composites. Also, dynamic vulcanization techniques can be used to improve the properties of the blends of ultrasonically devulcanized GRT and thermoplastics [153–156]. Dynamic vulcanization is the process of vulcanizing the elastomer during its melt mixing with the molten plastic [157].

The use of GRT, instead of virgin elastomers, however, results in significant deterioration in the mechanical properties of these composites. It was reported [158–160] that the GRT has a detrimental effect on most of the physical properties of cured rubber, the extent of deterioration increasing with the amount and size of the GRT. There have been several investigations with the aim of improving the adhesion between the GRT and the polymer matrix.

The effects of various compatibilizers to promote the adhesion of polyethylene (PE)–GRT blends were studied [139, 161–163]. The authors reported that it was possible to achieve a partial recovery of the same properties through a melt blending process where each component was first conditioned with compatibilizers of similar structure before the actual blending was carried out [150]. Among the various compatibilizers, epoxydized natural rubber [163], ethylene-co-acrylic acid copolymer [139, 161, 162], and ethylene-co-glycidyl methacrylate polymer [150, 162] were found to be effective in improving the impact properties of PE–GRT composites. It was also reported that smaller GRT particle size results in a small increase in the impact property of the composite and has a greater influence on the melt processability of the composites. The percent improvement in the impact energy for linear low-density polyethylene (LLDPE) and the composites prepared from them was greater than that for the corresponding high-density polyethylene (HDPE) composites. It was also suggested that the low polarity and/or low crystallinity of the matrix polymer appeared to favor the compatibility with GRT [152].

Modification of GRT particle surface has been studied to improve the compatibility of GRT and polymer. The polymeric surface modification can be

carried out by chemical treatments like chromic acid etching [164] and thermal oxidation [165], or by mechanical means. Use of maleic anhydride-grafted and chlorinated GRT, respectively, improved physical properties of GRT–EPDM–acrylated high-density polyethylene and GRT–polyvinyl chloride blends [166, 167]. It was found [168] that surface treatment of ground rubber with a matrix of unsaturated curable polymer and a curing agent could also improve the performance of the blends. The effect of cryogenically ground rubber (CGR) (approximately 250 microns) from old tires on some mechanical properties of an unsaturated polyester resin was investigated [169]. Composites made from silane-treated ground rubber showed better mechanical properties than composite made from untreated CGR. However, the particle size of the ground rubber was apparently too large to produce a toughening effect on the filled materials.

High-energy treatments including plasma [170, 171], corona discharge, and electron-beam radiation [151] were used to modify the surface of GRT. The oxidation on the surface of GRT generated by chemical and physical treatment, such as occurs in plasma and autoclave in oxygen atmosphere, was shown to improve adhesion between GRT and polyamide in the blend [170]. An epoxy resin compounded with tire rubber particles modified by plasma surface treatment was also studied [172]. An improvement in mechanical properties of the resulting material over those containing the untreated rubber was observed. The effects of corona discharge treatment of GRT on the impact property of the thermoplastic composite containing the GRT were investigated [162]. X-ray photoelectron spectroscopy analysis showed that the corona discharge treatment of GRT increased the oxygen-containing groups on the ground rubber surface. In some composites, it has been found that treated GRT marginally improved the impact property of the composites. However, prolonged times of treatment and higher power inputs for corona discharge of GRT reduced the impact strength of the composites.

The phenolic resin cure system and maleic anhydride grafted PP compatibilizer significantly improved mechanical properties of PP–ultrasonically devulcanized GRT blends prepared by dynamic vulcanization [153]. Also, a new ultrasonic reactor was built, and an improvement in the efficiency of the process and better properties of PP–GRT blends were achieved while carrying ultrasonic treatment during extrusion in this reactor [154]. In the reactor, two horns were placed in a slit die attached to a plastic extruder. Mechanical properties of PP–GRT, PP–devulcanized GRT (DGRT), and PP–revulcanized GRT (RGRT) that mixed in proportion of 40:60 are shown in Table III. Comparison indicates that the tensile strength, Young's modulus, and elongation at break of the blend prepared by this reactor under certain conditions are higher than those obtained earlier [153]. Also, properties of PP–RGRT at 10 μm are higher than those of PP–GRT at 10 μm. Evidently, the ultrasonic treatment of PP–GRT blends led to a certain level of compatibilization at the interface between the plastic and rubber phases. This was due to mechanochemical

TABLE III The Mechanical Properties of PP–GRT, PP–DGRT, and PP–RGRT Blends [154]

Blend		Tensile strength, MPa	Young's modulus, MPa	Elongation at break, %
PP–GRT		6.7	116	16.6
PP–DGRT	2 horns, 5 μm	6.6	98	21.5
	2 horns, 7.5 μm	6.5	100	20.6
	2 horns, 10 μm	5.15	102	7.6
	1 horn, 5 μm	6.9	110	19.3
	1 horn, 7.5 μm	6.6	104	17.4
	1 horn, 10 μm	7.0	116	21.0
	earlier work [150]	5.2	108	20.7
PP–RGRT	2 horns, 5 μm	6.7	109	13.2
	2 horns, 7.5 μm	6.7	110	13.3
	2 horns, 10 μm	5.9	111	7.0
	1 horn, 5 μm	6.4	110	11.8
	1 horn, 7.5 μm	6.6	110	13.3
	1 horn, 10 μm	7.2	122	14.8
	earlier work [150]	6.7	110	18.0

reactions induced by ultrasound at the interface. In addition, GRT was blended with ultrasonically devulcanized GRT with HDPE using a Brabender internal mixer and a twin-screw extruder [152]. These blends were dynamically vulcanized in these mixers. Also, HDPE and GRT blends mixed earlier by using a twin-screw extruder were passed through the ultrasonic devulcanization extruder and subsequently dynamically vulcanized by means of the internal mixer and the twin-screw extruder. The blends mixed by using the twin-screw extruder prior to devulcanization were found to have better tensile properties and impact strength than any other blends. Rheological properties of these blends were also studied.

Novel blends of GRT and recycled HDPE from used milk containers were studied and patented [173, 174]. The effects of GRT particle size and concentration on mechanical and rheological properties were determined. The blend systems were optimized by a soft rubber–plastic binder produced from a mixture of HDPE and EPDM, wherein EPDM is dynamically vulcanized during its mixing with the HDPE. It was concluded that the softening of the HDPE binder provides compositions of improved ultimate mechanical properties.

E. Concrete Modified by Recycled Rubber

Production of rubber-filled concrete compositions is an area in which further expansion of GRT usage is possible [175–182]. The advantages of using GRT in the cement–concrete structure are an increased crack, freeze–thaw, and impact resistance; shock wave absorption; reduced heat conductivity; and increased resistance to acid rain. However, an addition of rubber particles to concrete has shown to reduce the compressive and flexural strength. Concerning the effect of the size of rubber particles on the compressive strength, the results are contradictory. According to Topcu [183] and Eldin *et al*. [184], the compressive strength of concrete was lowered upon an addition of coarse-graded rubber particles while increased with an addition of the fine-graded particles. In contrast, tests [185] have shown opposite results. This contradiction can possibly be explained by the difference in rubber source, the geometry of the particles, and the way in which the particles were prepared.

The influence of the shape of rubber particles on mechanical properties, workability, and chemical stability of rubber-filled cement was studied [175]. The composite containing rubber shred was able to bridge the crack and to prevent catastrophic failure of the specimen, while the composite containing granular rubber particles was unable to bridge the crack. The pull-out test indicated poor interfacial bonding between the granular rubber particles and the matrix. In fact, many studies in this area indicated that the interface between the rubber and cement is weak. Attempts to improve the interface were made by washing the rubber particles [176, 180, 181]. Some improvement has been achieved by washing the particles with water [180], with water and carbon tetrachloride mixture, and with water and latex mixture [186], leading to an enhanced adhesion in rubber-filled cement. Several surface modifications have also been proposed, including the treatment of rubber with sulfuric acid and nitric acid to chemically oxidize rubber and introduce polar groups. Contrary to expectation, the treatment with nitric acid led to a decrease of the strength of the composite [181]. On the other hand, the treatment with sulfuric acid improved the adhesion of rubber to concrete [187]. Using a combination of chemical and surface probing techniques, it was shown that the hydrophilicity of the rubber surface is greatly improved by acid or base treatment [188, 189]. The rubber surface is typically hydrophobic. This is due to the fact that rubber typically contains zinc stearate that diffuses to the surface and causes hydrophobicity. By acid treatment, zinc stearate can be hydrolyzed to stearic acid. Treating the rubber with base, the zinc ions are converted into sodium ions of NaOH. These conversions create the soluble sodium stearate. It was also found [190] that addition of rubber particles to the mortar led to a decrease in their compressive and flexural strengths due to pull out of particles. However, the treatment of rubber particles before mixing with a bifunctional silane-coupling agent, such as gamma mercapto trimethoxy, improved

the interface and led to increased ductility [190]. It is suggested that this research be expanded to find the effects of the type of coupling agent on the adhesion and the fracture behavior of the rubber-filled cement paste, mortar, and concrete. These materials can be utilized in highway pavement overlays, sidewalks, medians, sound barriers, and other transportation nonstructural uses.

F. Asphalt Modified by Recycled Rubber

Asphalt can be blended with tire rubber to modify the properties of the asphalt. This remains the largest single market for ground rubber. In 2001, an estimated 220 million lb, or approximately 12 million tires, were used in the United States [3]. Mostly, these were consumed in California, Arizona, and Florida. However, other states are beginning to recognize the benefits of the modified asphalt [3]. It was reported that the asphalt industry can absorb up to 40% of scrap tires [191].

Utilization of scrap tire rubber in asphalt has advantages in the performance of roads and their longevity. These include enhanced ductility, crack resistance, skid resistance, and noise reduction. Disadvantages of the rubber-modified asphalt are its cost and a possibility of toxic emissions into the air. Tests indicated that rubber-modified asphalt increases the cost of road construction by about 50% in comparison with conventional asphalt [192]. The requirement for an additional step of hot mixing during processing of the rubber–asphalt mix may possibly cause toxic emissions into the air.

Two processes are used in preparing the rubberized asphalt: dry and wet process. In both processes, the GRT particle size ranges from 6.35 mm to 40 mesh. In the wet process, asphalt is blended with GRT particles and then added into the hot mix. In the dry process, GRT is mixed with aggregate, and the resulting mix is blended with asphalt.

Asphalt blended with GRT has been used for quite some time. Depending on the type of tire, the composition of GRT may include different rubbers. These crosslinked rubbers are mostly immiscible in bitumen. The blends show an improvement in basic asphalt properties as well as in rubberlike characteristics. The blend is thought of as a dispersion of undissolved swollen rubber particles acting as an elastic aggregate within asphalt, modified by the portion of the rubber particles that have dissolved.

The blending of GRT with asphalt was begun in the 1960s by McDonald, who developed and patented a patching material consisted of 25 wt% scrap and asphalt blended at 375°F for 20 minutes [193]. MacDonald continued his work by expanding it to actual road pavement test sections as a seal coat, and in 1968, Sahmaro Petroleum and Asphalt conducted application of a blend of GRT and asphalt as a binder for hot premix. The hot premix is a mixture of stone aggregate, sand, and the tire-asphalt binder all premixed in a batch- or drum-type mixer. This material is then applied as a carpet on top of the road

by a paving machine, followed by a steel roller used to compact the material [194]. Thereafter, many variations of this basic process of hot premix with the blend of GRT and asphalt as the binder have been proposed; most of them involve replacing stone aggregate with GRT. However, this method does not truly modify the asphalt binder. Thus, the process of blending GRT and asphalt before preparing a mixture is the most efficient in improving properties. Typical use levels range from 15 to 30 wt% [195].

A limited amount of work has been done on the characterization of the blends of GRT and asphalt. Blends are typically mixed at temperatures of 300 to 400°C for a period of 0.5 to 2 hours. The mix increases in viscosity and has a consistency of slurry with discernable rubber particles spread throughout. At room temperatures, the resulting composition is a tough rubbery elasticlike material. This mixing period is often referred to as reaction or digestion time. It was suggested [195] that the elastic quality of the blend is caused by the mechanical action of the undissolved rubber particles performing as a completely elastic aggregate within asphalt, which is modified by a portion of the rubber particles that have dissolved. According to Roberts and Lytton [193], the mixing time of 2 hours, as opposed to times of 0.5 and 1 hour, significantly improves elastic recovery, while increasing the mixing time reduces the amount of solid rubber in the mixture and increases both high and low molecular weight fractions of dissolved rubber in the asphalt [196]. This brings up a very interesting point for further investigation: whether the increase in asphalt-soluble-rubber fractions that occurs with longer mixing times can be attributed to elastic properties. The addition of GRT at 10, 20, and 30 wt% levels has significantly increased the softening points and strain recovery over the base asphalt, with a viscosity increase of similar magnitude for all three blends [197].

Rheological properties as affected by asphalt composition, rubber dissolution, and temperature were studied [198]. Rubber content, rubber particle size, and base asphalt composition were found to be the main factors affecting the rheology of the asphalt–rubber binder. By controlling these variables, binders with improved cracking resistance and rutting resistance can be produced. Finally, scrap tires, used as a crumb rubber modifier for asphalt, improve paving performance and safety by being an excellent and cost-effective modifier for the highway pavement industry [199].

G. Use of Crumb Rubber in Soil

The patented soil amendment method of using tire crumb can decrease the negative impacts associated with compaction [200]. The resiliency of the turf is not a direct factor of the elastic nature of rubber but rather the result of increased aeration [201]. Surface hardness characteristics were evaluated [202]. Crumb rubber significantly reduced soil hardness, soil shear strength, and water content [203].

H. Products Made from Recycled Rubber

Compounds containing devulcanized or ground tire rubbers can be used by various manufacturers to make a variety of rubber products. In particular, these compounds can be used or already are used for the production of shoe heels and soles, tubes, conveyor belts, technical rubber moldings, automobile floor mats, and flaps, livestock stall mattresses, playground and track surfacing, railroad track crossing, lower layers of floor coverings, various molded and extruded profiles, sealing plates, battery boxes, and other hard rubber goods. Since tire rubber is typically black, it therefore cannot be used for light and colored compounds unless additional measures have been taken to change the color. Obviously, for every such use, the recycled tire rubber must undergo extensive testing.

V. PYROLYSIS AND INCINERATION OF RUBBER

A. Recovery of Hydrocarbon Liquid and Carbon Black

One method suitable for use in recycling used tires is pyrolysis [204, 205]. Pyrolysis is the thermal decomposition of rubbers in the absence of air and oxygen to produce oils and gases for reuse by petrochemical industries. Carbon black and other solid content remaining after pyrolysis can be used as fillers. Pyrolysis is typically carried out in boilers, autoclaves, rotary kilns, screw conveyors, and fluidized beds. Also, hydrogenation has been performed using a tubing bomb reactor [206]. Research activities in tire rubber pyrolysis to recovery hydrocarbon liquid and carbon black were quite extensive in the 1960s and 1970s and led to plant construction for the pyrolysis of scrap tires in the 1970s [207]. Since then, significant studies have been carried out on tire pyrolysis concerning the evolution of volatile [208] and the utilization of oil and carbon black [209, 210]. However, these attempts proved to be economically unsuccessful due to the low price of crude oil. Also, pyrolysis plants are believed to produce toxic waste as a by-product of operation [211].

During the last 20 years, significant research has been carried out and various pyrolysis processes have been developed [212–214]. However, despite this progress, pyrolysis of scrap tires is done on a limited scale. This is mainly due to the absence of a wide market for the oil and the carbon black derived by means of the pyrolysis process.

B. Tire-Derived Fuel

Tire rubber can be transformed into energy via the incineration method. This process is advocated by a number of the major tire and rubber companies and also by the major utility companies. Tire-derived fuel can be in the

form of rubber chips containing or not containing the inherent wire. The nominal size of the chips is usually about 5 to 10 cm. The larger the size, the greater the content of the wire and the less likely it is to be able to be handled and metered. Scrap tires are used as a fuel supplement for coal or gas in kilns for manufacturing Portland cement, lime, and steel. This reduces by 25% the amount of coal consumption by cement industries. Scrap tires are also burned to generate electricity. Tire-derived fuel may reduce sulfur emissions of power plants and may improve the combustion efficiency by adjusting proper stoichiometry in combination with various coals, wood wastes, and household garbage. The consumption of tire-derived fuel was 115 million scrap tires in the United States in 2001 [3]. However, in burning rubber for fuel, valuable rubber materials are lost. In fact, 60,000 BTU of energy is consumed to make 1 lb of synthetic tire rubber [215]. In contrast, caloric value recovery by burning is 13,000 to 16,000 BTU per pound of rubber, which is not much higher than that of burning much cheaper coal. Moreover, the burning of tires for energy may lead to air pollution [216].

VI. CONCLUDING REMARKS

Waste tires and rubber present a problem of international significance. The present work describes some routes available to solve this problem. Numerous technologies are being developed. Among them, in addition to the well-known grinding techniques, are continuous pulverization methods based on a single- or twin-screw extruder that may serve as a possible route to supply rubber powder as a feedstock for various present and future devulcanization and recycling technologies. These include reclaiming, surface treatment, ultrasonic devulcanization, and utilization of rubber particles for making composites with other materials. Some success has been achieved in development of ultrasonic technology, which is considered one of the promising methods, making devulcanized rubbers suitable for making rubber products from 100% recycled rubber as well as for adding to virgin rubber, virgin and recycled plastics, asphalt, concrete, and cement. Equipment has to be developed that is capable of achieving high enough output to make the process economically feasible. The major challenge in industrial implementation of this process is the development of a high-power ultrasonic generator capable of continuously operating under high pressure and high temperature. Clearly, there is also a lack of scientific understanding of the various processes governing the recycling of rubbers. Development of science-based technologies and processes for rubber recycling, and the use of recycled rubbers in varied end-products, would significantly reduce worldwide energy consumption, provide renewable rubbers from scrap tires and rubber waste, and lead to less pollution of the environment.

ACKNOWLEDGMENTS

This work is supported in part by grant DMI-0084740 from the National Science Foundation. The authors wish to express their appreciation to Professor E. D. von Meerwall and former graduate students and associates Drs. J. Chen, W. Feng, S. Ghose, C. K. Hong, V. Yu Levin, S. H. Kim, J. S. Oh, S. E. Shim, A. Tukachinsky, V. V. Yashin, J. S. Yun, S. P. Yushanov, Mr. B. Diao, Mr. M. Tapale, and Mr. D. Schworm, whose contributions during the last decade made this work possible.

REFERENCES

1. C. Goodyear, inventor, U.S. Patent 3,633 (1844).
2. C. Goodyear, inventor, U.K. Patent 2,933 (1853).
3. U.S. Scrap Tire Markets 2001, Scrap Tire Management Council.
4. Scrap Tire Stockpile Abatement, May 2002, Rubber Manufacturers Association.
5. R. H. Snyder, "Scrap Tyres: Disposal and Reuse," Society of Automotive Engineers, Inc., Warrendale, PA, 1998.
6. P. Hous, H. Bartelds, and E. Smit, *Rubber World* **212**, 36 (1995).
7. W. Klingensmith and K. Baranwal, *Rubber World* **218**, 41 (1998).
8. V. M. Makarov and V. F. Drozdovski, "Reprocessing of Tyres and Rubber Wastes," Ellis Horwood, New York, 1991.
9. *Scrap Tire News*, **13**, 2, 6 (1999).
10. *Scrap Tire News*, **13**, 6, 7 (1999).
11. J. Pryweller, *European Rubber Journal* **181**, 17 (1999).
12. I. Franta (Ed.), "Elastomers and Rubber Compounding Materials," Elsevier, New York, 1989.
13. W. C. Warner, *Rubber Chem. Technol* **67**, 559 (1994).
14. C. P. Rader (Ed.), "Plastic, Rubber and Paper Recycling," American Chemical Society, Washington, D.C., 1995.
15. S. R. Fix, *Elastomerics* **112**, 38 (1980).
16. P. P. Nicholas, *Rubber Chem. Technol.* **55**, 1499 (1982).
17. M. Myhre and D. A. MacKillop, *Rubber Chem. Technol.* **75**, 429 (2002).
18. Fact Sheet, Tire Retread Information Bureau (2002).
19. A. A. Phadke, A. K. Bhattacharya, S. K. Chakraborty, and S. K. De, *Rubber Chem. Technol.* **56**, 726 (1983).
20. B. Siuru, *Scrap Tire News* **11**, 14 (1997).
21. A. Accetta and J. M. Vergnaud, *Rubber Chem. Technol.* **55**, 961 (1982).
22. D. De, S. Maiti, and B. Adhikari, *J. Appl. Polym. Sci.* **73**, 2951 (1999).
23. B. Adhikari, D. De, and S. Maiti, *Prog. Polym. Sci.* **25**, 909 (2000).
24. A. I. Isayev, in "Rubber Technologist's Handbook," J. R. White and S. K. De (Eds.), RAPRA, Shawbury, U.K., 2001, Chap. 15, pp. 511–547.
25. B. D. LaGrone, *Conservation and Recycling* **9**, 359 (1986).
26. B. Bowers, D. Barber, and R. Allinger, Oct., 1986, Paper #82 presented at the meeting of the ACS Rubber Division, Atlanta, GA.
27. K. Knoerr, Oct., 1995, Paper #5 presented at the ACS Rubber Division Meeting, Cleveland, OH.
28. P. M. Lewis, *NR Technology* **17**, 57 (1986).
29. R. Schaefer, Oct., 1986, Paper #79 presented at the ACS Rubber Division Meeting, Atlanta, GA.
30. R. Schaefer and R. Berneking, Oct., 1986, Paper #80 presented at the ACS Rubber Division Meeting, Atlanta, GA.
31. E. M. Solov'ev, V. B. Pavlov, and N. S. Enikolopov, *Intern. Polym. Sci. Technol.* **14**, 10 (1987).

32. J. A. Szilard, "Reclaiming Rubber and Other Polymers," Noyes Data Corporation, London, 1973.
33. W. Kongensmith, *Rubber World* **203**, 16 (1991).
34. J. J. Leyden, *Rubber World* **203**, 28 (1991).
35. J. G. Bryson, U.S. Patent 4,148,763 (1979).
36. R. Kohler and J. O'Neill, *Rubber World* **216**, 32, 34 (1997).
37. B. C. Sekhar and V. A. Kormer, European Patent Application, EP 0 690 091 A1 (1995).
38. D. De, B. Adhikari, and S. Maiti, *J. Polym Material* **14**, 333 (1997).
39. D. De, S. Maiti, and B. Adhikari, *Kautchuk Gummi Kunststoffe* **53**, 346 (2000).
40. D. De, A. K. Ghosh, S. Maiti, and B. Adhikari, *Polym. Recycling* **4**, 15 (1999).
41. K. Knorr, *Kautchuk Gummi Kunststoffe* **47** 1, 54 (1994).
42. M. A. L. Verbruggen, L. van der Does, J. W. M. Noordermeer, M. van Duin, and H. J. Manuel, *Rubber Chem. Technol.* **72**, 731 (1999).
43. L. K. Hunt and R. R. Kovalak, inventors, Assignee Goodyear Tire and Rubber Company, U.S. Patent 5,891,926 (1999).
44. R. D. Myers, P. Nicholson, J. B. MacLeod, and M. E. Moir, U.S. Patent, 5,602,186 (1997).
45. N. Kawabata, B. Okuyama, and S. Yamashita, *J. Appl Polym Sci.* **26**, 1417 (1981).
46. N. Kawabata, T. Murakami, and S. Yamashita, *Nippon Gomu Kyokaishi* **52**, 768 (1979).
47. D. A. Benko and R. N. Beers, inventors, Assignee Goodyear Tire and Rubber Company, U.S. Patent 5,380,269 (2002).
48. D. A. Benko and R. N. Beers, inventors, Assignee Goodyear Tire and Rubber Company, U.S. Patent 6,387,965 (2002).
49. D. A. Benko and R. N. Beers, inventors, Assignee Goodyear Tire and Rubber Comapny, U.S. Patent 6,462,099 (2002).
50. A. A. Hershaft, *Environ. Sci. Technol.* **6**, 412 (1972).
51. A. A. Hershaft, *Elastomerics* **109**, 39 (1977).
52. A. Ratcliffe, *Chem. Eng.* **79**, 62 (1972).
53. J. Lynch and B. LaGrone, "Ultrafine Crumb Rubber," Paper #37 presented at a meeting of the Rubber Division, ACS, Atlanta, GA, October 1986.
54. N. S. Enikolopian, *Pure Appl. Chem.* **57**, 1707 (1985).
55. K. Khait and J. M. Torkelson, *Polym. Plast. Technol. Eng.* **38**, 445 (1999).
56. K. Khait, Paper #24 presented at the ACS Rubber Division Meeting, Chicago, IL, 1994.
57. E. Bilgili, H. Arastoopour, and B. Bernstein, *Rubber Chem. Technol.* **73**, 340 (2000).
58. E. Bilgili, B. Berstein, H. Arastoopour, *AIChE Symp. Ser.* **95**, 83 (1999).
59. E. Bilgili, H. Arastoopour, and B. Bernstein, *Powder Technol.* **115**, 265 (2001).
60. E. Bilgili, H. Arastoopour, and B. Bernstein, *Powder Technol.* **115**, 277 (2001).
61. H. Arastoopour, D. A. Schocke, B. Bernstein, and E. Bilgili, U.S. Patent 5,904,885 (1999).
62. E. Bigili, A. Dybek, H. Arastoopour, and B. Bernstein, *J. Elast. Plastics* **35**, 235 (2003).
63. J. E. Morin, D. E. Williams, and R. J. Farris, *Rubber Chem. Technol.* **75**, 955 (2002).
64. A. R. Tripathy, J. E. Morin, D. E. Williams, S. J. Eyles, and R. J. Farris, *Macromol.* **35**, 4616 (2002).
65. D. S. Novotny, R. L. Marsh, F. C. Masters, and D. N. Tally, U.S. Patent 4,104,205 (1978).
66. T. Kleps, M. Piaskiewicz, and W. Parasiewicz, *J. Thermal Analysis Calorimetry* **60**, 271 (2000).
67. A. M. Basedow and K. Ebert, *Adv. Polym. Sci.* **22**, 83 (1987).
68. G. J. Price, in "Advances in Sonochemistry," T. J. Mason (Ed.), JAI Press Ltd., Greenwich, CT, Vol. 1, 1990, p. 231.
69. G. J. Price, D. J. Norris, and P. J. West, *Macromolecules* **25**, 6447 (1992).
70. G. Schmid and O. Rommel, *Z. Elektrochem* **45**, 659 (1939).
71. G. Schmid, *Physik. Z.* **41**, 326 (1940).
72. H. H. G. Jellinek and G. White, *J. Polymer Sci.* **7**, 21 (1951).
73. A. I. Isayev, C. Wong, and X. Zeng, *SPE ANTEC Tech. Papers* **33**, 207 (1987).
74. A. I. Isayev, C. Wong, and X. Zeng, *Adv. Polym. Technol.* **10**, 31 (1990).

75. A. I. Isayev, Proceeding of the 23rd Israel Conference on Mechanical Engineering, Technion, Haifa, Paper #5.2.3, 1990.
76. A. I. Isayev and S. Mandelbaum, *Polym. Eng. Sci.* **31**, 1051 (1991).
77. S. L. Peshkovsky, M. L. Friedman, A. I. Tukachinsky, G. V. Vinogradov, and N. S. Enikolopian, *Polym. Compos* **4**, 126 (1983).
78. R. Garcia Ramirez and A. I. Isayev, *SPE ANTEC Tech. Papers* **37**, 1084 (1991).
79. K. S. Suslick, *Scientific American* **260**, 80 (1989).
80. K. S. Suslick, S. J. Doctycz, and E. B. Flint, *Ultrasonics* **28**, 280 (1990).
81. G. Gooberman, *J. Polymer Sci.* **42**, 25 (1960).
82. M. Okuda and Y. Hatano, Japanese patent application 62,121,741 (1987).
83. A. I. Isayev, inventor, Assignee the University of Akron, U.S. Patent 5,258,413 (1993).
84. A. I. Isayev and J. Chen, inventors, Assignee the University of Akron, U.S. Patent 5,284,625 (1994).
85. A. I. Isayev, J. Chen, and A. Tukachinsky, *Rubber Chem. Tech.* **68**, 267 (1995).
86. A. Tukachinsky, D. Schworm, and A. I. Isayev, *Rubber Chem. Tech.* **69**, 92 (1996).
87. V. Yu Levin, S. H. Kim, A. I. Isayev, J. Massey, and E. von Meerwall, *Rubber Chem. Technol.* **69**, 104 (1996).
88. A. I. Isayev, S. P. Yushanov, and J. Chen, *J. Appl. Polym. Sci.* **59**, 803 (1996).
89. A. I. Isayev, S. P. Yushanov, and J. Chen, *J. Appl. Polym. Sci.* **59**, 815 (1996).
90. A. I. Isayev, S. P. Yushanov, D. Schworm, and A. Tukachinsky, *Plast. Rubber and Compos. Process. and Appl.* **25**, 1 (1996).
91. S. P. Yushanov, A. I. Isayev, and V. Y. Levin, *J. Polym. Sci.: Part B: Polymer Physics* **34**, 2409 (1996).
92. A. I. Isayev, S. P. Yushanov, S. H. Kim, and V. Yu Levin, *Rheol. Acta* **35**, 616 (1996).
93. V. Yu Levin, S. H. Kim, and A. I. Isayev, *Rubber Chem. Technol.* **70**, 120 (1997).
94. S. T. Johnston, J. Massey, E. von Meerwall, S. H. Kim, V. Yu Levin, and A. I. Isayev, *Rubber Chem. Tech.* **70**, 183 (1997).
95. A. I. Isayev, S. H. Kim, and V. Yu. Levin, *Rubber Chem. Tech.* **70**, 194 (1997).
96. V. Yu Levin, S. H. Kim, and A. I. Isayev, *Rubber Chem. Tech.* **70**, 641 (1997).
97. S. P. Yushanov, A. I. Isayev, and S. H. Kim, *Rubber Chem. Technol.* **71**, 168 (1998).
98. B. Diao, A. I. Isayev, V. Yu Levin, and S. H. Kim, *J. Appl. Polym. Sci.* **69**, 2691 (1998).
99. M. Tapale and A. I. Isayev, *J. Appl. Polym. Sci.* **70**, 2007 (1998).
100. B. Diao, A. I. Isayev, and V. Yu Levin, *Rubber Chem. Technol.* **72**, 152 (1999).
101. V. V. Yashin and A. I. Isayev, *Rubber Chem. Technol.* **72**, 741 (1999).
102. V. V. Yashin and A. I. Isayev, *Rubber Chem. Technol.* **73**, 325 (2000).
103. C. K. Hong and A. I. Isayev, *J. Appl. Polym. Sci.* **79**, 2340 (2001).
104. S. E. Shim and A. I. Isayev, *Rubber Chem. Tech.* **74**, 303 (2001).
105. J. Yun, J. S. Oh, and A. I. Isayev, *Rubber Chem. Technol.* **74**, 317 (2001).
106. A. I. Isayev, in "Rubber Technologist's Handbook," J. R.White and S. K. De (Eds.), RAPRA Technology Ltd., U.K., 2001.
107. A. I. Isayev, in "Encyclopedia of Materials: Science and Technology," K. H. J. Buschow (Ed.), Elsevier, Amsterdam, Vol. 3, 2001.
108. C. K. Hong and A. I. Isayev, *Rubber Chem. Technol.* **75**, 617 (2002).
109. C. K. Hong and A. I. Isayev, *Rubber Chem. Technol.* **75**, 133 (2002).
110. J. Yun and A. I. Isayev, *Rubber Chem. Technol.* **76**, 253 (2003).
111. S. E. Shim, S. Ghose, and A. I. Isayev, *Polymer* **43**, 5535 (2002).
112. S. E. Shim, J. C. Parr, E. von Meerwall, and A. I. Isayev, *J. Phys. Chem. B* **106**, 12072 (2002).
113. S. E. Shim, A. I. Isayev, and E. von Meerwall, *J. Polym. Sci.: Part B: Polym. Phys.* **41**, 454 (2003).
114. J. Yun, A. I. Isayev, S. H. Kim, and M. Tapale, *J. Appl. Polym. Sci.* **88**, 434 (2003).
115. S. E. Shim, and A. I. Isayev, *J. Appl. Polym. Sci.* **88**, 2630 (2003).
116. S. Ghose and A. I. Isayev, *J. Appl. Polym. Sci.* **88**, 980 (2003).

117. J. Yun and A. I. Isayev, *Polym. Eng. Sci.* **43**, 809 (2003).
118. W. Feng and A. I. Isayev, *J. Appl. Polym. Sci.* (in press).
119. W. Feng and A. I. Isayev, Paper presented at the ACS Rubber Division Meeting, Columbus, OH, October 2004.
120. T. Boron, P. Roberson, and W. Klingensmith, *Tire Technology International* **96**, 82 (1996).
121. T. Boron, W. Klingensmith, C. Forest, and S. Shringarpurey, 156th Meeting of the ACS Rubber Division, Orlando, FL, 1999, Paper #136.
122. E. A. Gonzalez de Los Santas, F. Sorieno-Corral, Ma J. Lozano Gonzalez, and R. Cedillo-Garcia, *Rubber Chem. Technol.* **72**, 854 (1999).
123. J. Blitz, "Fundamentals of Ultrasonics," 2nd ed., Butterworth, London, 1967, Chap. 8.
124. K. S. Suslick, "Ultrasound: Its Chemical, Physical and Biological Effects," VCH, New York, 1988.
125. S. N. Zhurkov, V. A. Zakrevskii, V. E. Korsukov, and V. S. Kuksenko, 1972, *Soviet Physics Solid State* **13**, 1680 (1972).
126. A. N. Gent and D. A. Tompkins, *J. Appl. Phys.* **40**, 2520 (1969).
127. A. N. Gent, *Rubber Chem. Technol.* **63**, G49 (1990).
128. M. B. Bever (Ed.), "Encyclopedia of Materials Science and Engineering," Pergamon Press, Oxford, Vol. 4, 1986, p. 2934.
129. F. R. Young, "Cavitation," McGraw-Hill Co., London, 1989, Chap. 2.
130. A. I. Isayev, J. Chen, and S. P. Yushanov, in "Simulation of Materials Processing: Theory, Methods and Application," S. F. Shen and P. Dawson (Eds.), Balkema, Rotterdam, 1995, pp. 77–85.
131. A. I. Kasner and E. A. Meinecke, *Rubber Chem. Technol.* **69**, 424 (1996).
132. A. J. Kinloch and R. J. Young, "Fracture Behavior of Polymers," Applied Science Publishers, London, 1983.
133. H. H. Kausch, "Polymer Fracture," Springer-Verlag, Berlin, 1987.
134. M. Tabata and J. Sohma, *Chem. Phys. Lett.* **73**, 178 (1980).
135. M. Tabata and J. Sohma, *Eur. Polym. J.* **16**, 589 (1980).
136. J. P. Lorimer, in "Chemistry with Ultrasound," T. J. Mason (Ed.), Elsevier, New York, 1990, Chap. 4.
137. C. K. Hong and A. I. Isayev, *J. Mater. Sci.* **37**, 385 (2002).
138. A. P. Yushanov, A. I. Isayev, and S. H. Kim, *Rubber Chem. Technol.* **71**, 168 (1998).
139. P. Rajalingam and W. E. Baker, *Rubber Chem. Technol.* **65**, 908 (1992).
140. N. P. Chopey, *Chem. Eng.* **80**, 54 (1973).
141. D. Gibala and G. R. Hamed, *Rubber Chem. Technol.* **67**, 636 (1994).
142. D. Gibala, K. Laohapisitpanich, D. Thomas, and G. R. Hamed, *Rubber Chem. Technol.* **69**, 115 (1996).
143. R. H. Wolk, *Rubber Age* **104**, 103 (1973).
144. A. N. Theodore, R. A. Pett, and D. Jackson, *Rubber World* **218**, 23 (1998).
145. H. J. Radusch, T. Luepke, S. Poltersdorf, and E. Laemmer, *Kautschuk Gummi* **43**, 767 (1990).
146. K. Fukumori, M. Matsushita, H. Okamoto, N. Sato, Y. Suzuki and K. Takeuchi, *JSAE Review* **23**, 259 (2002).
147. A. K. Naskar, P. K. Pramanik, R. Mukhopadhyay, S. K. De, and A. K. Bhowmick, *Rubber Chem. Technol.* **73**, 902 (2000).
148. *Scrap Tire News* **15**, No. 10, Oct. 2001, pp. 1–3.
149. S. Ghose and A. I. Isayev, *Polym. Eng. Sci.* **44**, 794 (2003).
150. J. R. M. Duhaime and W. E. Baker, *Plast. Rubb. Comp. Proc. Appl.* **15**, 87 (1991).
151. P. Rajalingam, J. Sharpe, and W. E. Baker, *Rubber Chem. Technol.* **66**, 664 (1993).
152. R. D. Deanin and S. M. Hashemiolya, *Polym. Mater. Sci. Eng.* **57**, 212 (1987).
153. T. Luo and A. I. Isayev, *J. Elastomers and Plastics* **30**, 133 (1998).
154. J. S. Oh and A. I. Isayev, *Rubber Chem. Tech.* **75**, 617 (2002).
155. C. K. Hong and A. I. Isayev, *J. Elast. and Plast.* **33**, 47 (2001).

156. H. Michael, H. Scholz, and G. Mennig, *Kautchuk Gummi Kunststoffe* **52** 510 (1999).
157. A. Y. Coran and R. P. Patel, in "Thermoplastic Elastomers," 2nd ed., G. Holden, N. R. Legge, R. Quirk, and H. E. Schroeder (Eds.), Hanser Publishers, New York, 1996.
158. N. C. Hilyward, S. G. Tong, and K. Harrison, *Plast. Rubb. Proc. Appl.* **3**, 315 (1983).
159. A. A. Phadke, S. K. Chakraborty, and S. K. De, *Rubber Chem. Technol.* **57**, 19 (1984).
160. A. A. Phadke and S. K. De, *Polym. Eng. Sci.* **26**, 1079 (1986).
161. K. Oliphant and W. E. Baker, *Polym. Eng. Sci.* **33**, 166 (1993).
162. P. K. Pramanik and W. E. Baker, *J. Elast. Plast.* **27**, 253 (1995).
163. P. K. Pramanik and W. E. Baker, *Plast. Rubb. Comp. Proc. Appl.* **24**, 229 (1995).
164. D. Briggs, *Surf. Interface Anal.* **2**, 107 (1980).
165. D. Briggs, *Euro. Polym. J.* **14**, 1 (1978).
166. A. K. Naskar, S. K. De, and A. K. Bhowmick, *J. Appl. Polym. Sci.* **84**, 370 (2002).
167. A. K. Naskar, A. K. Bhowmick, and S. K. De, *J. Appl. Polym. Sci.* **84**, 622 (2002).
168. F. J. Stark Jr., A. Leigton, and D. Wagner, *Rubber World* **188**, 36 (1983).
169. E. L. Rodriguez, *Polym. Eng. Sci.* **28**, 1455 (1988).
170. A. Chidambaram and K. Min, *SPE ANTEC Tech. Papers* **40**, 2927 (1994).
171. R. H. Campbell and R. W. Wise, *Rubber Chem. Technol.* **37**, 635 (1964).
172. Z. Xu, N. S. Losure, and S. D. Gardner, *J. Avd. Mater.* **30**, 11 (1998).
173. A. Y. Coran and F. Howard, U.S. Patent 5,889,119 (1999).
174. F. Howard and A. Y. Coran, Paper presented at the ITEC, September, Akron, OH, 2000.
175. D. Raghavan, H. Huynh, and C. F. Ferraris, *J. Mater. Sci.* **33**, 1745 (1998).
176. D. Raghavan, K. Tratt, and R. P. Wool, *Mater. Research Soc. Sym.* **344**, 177 (1994).
177. H. Goldstein, *Civ. Eng.* **65**, 60 (1995).
178. N. N. Eldin and A. B. Senouci, *ASCE J. Const. Eng. Mgmt.* **188**, 561 (1992).
179. N. N. Eldin and A. B. Senouci, *Cem. Concr. Agg.* **15**, 74 (1993).
180. N. N. Eldin and A. B. Senouci, *ASCE J. Mater. Civ. Eng.* **5**, 478 (1993).
181. B. I. Lee, L. Burnett, T. Miller, B. Postage, and J. Cuneo, *J. Mater. Sci. Lett.* **12**, 967 (1993).
182. F. Shutov, G. Ivanov, H. Arastoopour, and S. Volfson, *Polym. Mater. Sci. Eng.* **67**, 404 (1992).
183. I. B. Topcu, *Cement Concrete Research* **25**, 304 (1995).
184. N. N. Eldin and A. B. Senouci, *Cement Concrete Compos.* **16**, 287 (1994).
185. N. A. Ali, A. D. Amos, and M. Roberts, in Proceed. Intern. Conf. Concrete 2000, University of Dundee, U.K., 2000, pp. 379–390.
186. H. Rostami, J. Lepore, T. Silverstram, and I. Zandi, Proceed. Intern. Conf. Concrete 2000, Dundee, U.K., 1993, pp. 391–399.
187. J. A. Lepore and M. W. Tantala, In Proceed. Concr. Inst. Australia, Concrete 97, 1997, pp. 623–627.
188. N. Segre and I. Joekes, *Cement Concrete Research* **30**, 1421 (2000).
189. N. Segre, P. J. M. Monteiro, and G. Sposito, *J. Coll. Interface Sci.* **248**, 521 (2002).
190. D. Raghavan, *J. Appl. Polym. Sci.* **77**, 934 (2000).
191. Anonymous, *Biocycle* **34**, 9 (1993).
192. J. L. McQuillen Jr., H. B. Takallou, R. G. Hicks, and D. Esch, *ASCE J. Transport. Eng.* **114**, 259 (1988).
193. F. L. Roberts and R. L. Lytton, *Transportation Research Record* **115**, 216 (1987).
194. R. H. Renshaw, "Rubber in Roads," Plastics and Rubber Institute, South African Section, S. Africa, 1985, p. 1.
195. H. B. Takallou and M. B. Takallou, *Elastomerics* **123**, 19 (1991).
196. I. S. Schuller, Ph.D. Dissertation, Texas A&M University, 1991.
197. H. Al-Abdual-Wahhab and G. Al-Amri, *J. Mater. Civil Eng.* **3**, 189 (1991).
198. T. C. Billiter, R. R. Davison, C. J. Glover, and J. A. Bullin, *Petrol. Sci. Technol.* **15**, 205 (1997).
199. M. Rouse, *Rubber World*, p. 23, May (1995).
200. R. C. Malmgren, N. Parviz, P. N. Soltanpour, and J. E. Cipra, U.S. Patent 5,014,562 (1991).
201. G. Logsdon, *Biocycle* **31**, 44, 84 (1990).
202. J. N. Rogers III and D. V. Waddington, *Agronomy J.* **84**, 203 (1992).

203. P. H. Groenevelt and P. E. Grunthal, *Soil and Tillage Res.* **47**, 169 (1998).
204. M. Moore, *Crain's Tire Business* **9**, 15 (1991).
205. W. Kaminsky and H. Sinn, in "Book Recycling and Recovery of Plastics," J. Brandrup, M. Bittner, W. Michaeli, and G. Menges (Eds.), Hanser Publishers, Munich, 1996.
206. A. M. Mastral, R. Murillo, M. S. Callen, and T. Garcia, *Resources Conserv. Recycling* **29**, 263 (2000).
207. S. Kawakami, K. Inoue, H. Tanaka, and T. Sakai, in "Thermal Conversion of Solid Wastes and Biomass," J. L. Jones and S. B. Radding (Eds.), Symposium Series 130, ACS Publishers, Washington, D.C., 1980.
208. J. A. Conesa, A. Fullana, and R. Font, *Energy Fuel* **14**, 409 (2000).
209. C. Roy, A. Chaala, and H. Darmstadt, *J. Anal. Appl. Pyrol.* **51**, 201 (1999).
210. M. R. Beck and W. Klingensmith, *ACS Sympos. Series* **609**, 254 (1995).
211. J. D. Osborn, *Rubber World* p. 34, May (1995).
212. W. Kaminsky and C. Mennerich, *J. Anal. Appl. Pyrolysis* **58**, 803 (2001).
213. P. T. William, *Chem. Review* **12**, 17 (2002).
214. P. T. William and A. J. Brindle, *J. Anal. Appl. Pyrolysis* **67**, 143 (2003).
215. P. T. William and F. Ferrer, *Resources Conserv. Recycling* **19**, 221 (1997).
216. A. M. Mastral, M. S. Callen, R. Murillo, and T. Garcia, *Environ. Sci. Technol.* **33**, 4155 (1999).

Index